

Second Edition

RENEWABLE AND EFFICIENT ELECTRIC POWER SYSTEMS

Gilbert M. Masters

IEEE
IEEE PRESS

WILEY

Contents

Title Page

Copyright Page

Dedication

Preface

Chapter 1: The U.S. Electric Power Industry

- 1.1 ELECTROMAGNETISM: THE TECHNOLOGY BEHIND ELECTRIC POWER
- 1.2 THE EARLY BATTLE BETWEEN EDISON AND WESTINGHOUSE
- 1.3 THE REGULATORY SIDE OF ELECTRIC UTILITIES
- 1.4 ELECTRICITY INFRASTRUCTURE: THE GRID
- 1.5 ELECTRIC POWER INFRASTRUCTURE: GENERATION
- 1.6 FINANCIAL ASPECTS OF CONVENTIONAL POWER PLANTS
- 1.7 SUMMARY
- REFERENCES
- PROBLEMS

Chapter 2: Basic Electric and Magnetic Circuits

- 2.1 INTRODUCTION TO ELECTRIC CIRCUITS
- 2.2 DEFINITIONS OF KEY ELECTRICAL QUANTITIES
- 2.3 IDEALIZED VOLTAGE AND CURRENT SOURCES
- 2.4 ELECTRICAL RESISTANCE
- 2.5 CAPACITANCE
- 2.6 MAGNETIC CIRCUITS
- 2.7 INDUCTANCE
- 2.8 TRANSFORMERS
- PROBLEMS

Chapter 3: Fundamentals of Electric Power

3.1 EFFECTIVE VALUES OF VOLTAGE AND CURRENT
3.2 IDEALIZED COMPONENTS SUBJECTED TO SINUSOIDAL VOLTAGES
3.3 POWER FACTOR
3.4 THREE-WIRE, SINGLE-PHASE RESIDENTIAL WIRING
3.5 THREE-PHASE SYSTEMS
3.6 SYNCHRONOUS GENERATORS
3.7 TRANSMISSION AND DISTRIBUTION
3.8 POWER QUALITY
3.9 POWER ELECTRONICS
3.10 BACK-TO-BACK VOLTAGE-SOURCE CONVERTER
REFERENCES
PROBLEMS

Chapter 4: The Solar Resource
4.1 THE SOLAR SPECTRUM
4.2 THE EARTH'S ORBIT
4.3 ALTITUDE ANGLE OF THE SUN AT SOLAR NOON
4.4 SOLAR POSITION AT ANY TIME OF DAY
4.5 SUN PATH DIAGRAMS FOR SHADING ANALYSIS
4.6 SHADING ANALYSIS USING SHADOW DIAGRAMS
4.7 SOLAR TIME AND CIVIL (CLOCK) TIME
4.8 SUNRISE AND SUNSET
4.9 CLEAR-SKY DIRECT-BEAM RADIATION
4.10 TOTAL CLEAR-SKY INSOLATION ON A COLLECTING SURFACE
4.11 MONTHLY CLEAR-SKY INSOLATION
4.12 SOLAR RADIATION MEASUREMENTS
4.13 SOLAR INSOLATION UNDER NORMAL SKIES
4.14 AVERAGE MONTHLY INSOLATION
REFERENCES
PROBLEMS

Chapter 5: Photovoltaic Materials and Electrical Characteristics
5.1 INTRODUCTION
5.2 BASIC SEMICONDUCTOR PHYSICS
5.3 PV MATERIALS
5.4 EQUIVALENT CIRCUITS FOR PV CELLS

5.5 FROM CELLS TO MODULES TO ARRAYS
5.6 THE PV *I–V* CURVE UNDER STANDARD TEST CONDITIONS
5.7 IMPACTS OF TEMPERATURE AND INSOLATION ON *I–V* CURVES
5.8 SHADING IMPACTS ON *I–V* CURVES
5.9 MAXIMUM POWER POINT TRACKERS
REFERENCES
PROBLEMS

Chapter 6: Photovoltaic Systems
6.1 INTRODUCTION
6.2 BEHIND-THE-METER GRID-CONNECTED SYSTEMS
6.3 PREDICTING PERFORMANCE
6.4 PV SYSTEM ECONOMICS
6.5 OFF-GRID PV SYSTEMS WITH BATTERY STORAGE
6.6 PV-POWERED WATER PUMPING
REFERENCES
PROBLEMS

Chapter 7: Wind Power Systems
7.1 HISTORICAL DEVELOPMENT OF WIND POWER
7.2 WIND TURBINE TECHNOLOGY: ROTORS
7.3 WIND TURBINE TECHNOLOGY: GENERATORS
7.4 POWER IN THE WIND
7.5 WIND TURBINE POWER CURVES
7.6 AVERAGE POWER IN THE WIND
7.7 ESTIMATING WIND TURBINE ENERGY PRODUCTION
7.8 WIND FARMS
7.9 WIND TURBINE ECONOMICS
7.10 ENVIRONMENTAL IMPACTS OF WIND TURBINES
REFERENCES
PROBLEMS

Chapter 8: More Renewable Energy Systems
8.1 INTRODUCTION
8.2 CONCENTRATING SOLAR POWER SYSTEMS
8.3 WAVE ENERGY CONVERSION

8.4 TIDAL POWER
8.5 HYDROELECTRIC POWER
8.6 PUMPED-STORAGE HYDRO
8.7 BIOMASS FOR ELECTRICITY
8.8 GEOTHERMAL POWER
REFERENCES
PROBLEMS

Chapter 9: Both Sides of the Meter
9.1 INTRODUCTION
9.2 SMART GRID
9.3 ELECTRICITY STORAGE
9.4 DEMAND SIDE MANAGEMENT
9.5 ECONOMICS OF ENERGY EFFICIENCY
9.6 COMBINED HEAT AND POWER SYSTEMS
9.7 COGENERATION TECHNOLOGIES
9.8 FUEL CELLS
REFERENCES
PROBLEMS

Appendix A: Energy Economics Tutorial
A.1 SIMPLE PAYBACK PERIOD
A.2 INITIAL (SIMPLE) RATE OF RETURN
A.3 THE TIME VALUE OF MONEY AND NET PRESENT VALUE
A.4 INTERNAL RATE OF RETURN
A.5 NET PRESENT VALUE WITH FUEL ESCALATION
A.6 IRR WITH FUEL ESCALATION
A.7 ANNUALIZING THE INVESTMENT
A.8 LEVELIZED BUSBAR COSTS
A.9 CASH-FLOW ANALYSIS

Appendix B: Useful Conversion Factors

Appendix C: Sun-Path Diagrams

Appendix D: Hourly Clear-Sky Insolation Tables

Appendix E: Monthly Clear-Sky Insolation Tables

Appendix F: Shadow Diagrams

Appendix G: Solar Insolation Tables by City

Index

RENEWABLE AND EFFICIENT ELECTRIC POWER SYSTEMS

Second Edition

GILBERT M. MASTERS

IEEE PRESS

WILEY

Copyright © 2013 by John Wiley & Sons, Inc. All rights reserved

Published by John Wiley & Sons, Inc., Hoboken, New Jersey
Published simultaneously in Canada

No part of this publication may be reproduced, stored in a retrieval system, or transmitted in any form or by any means, electronic, mechanical, photocopying, recording, scanning, or otherwise, except as permitted under Section 107 or 108 of the 1976 United States Copyright Act, without either the prior written permission of the Publisher, or authorization through payment of the appropriate per-copy fee to the Copyright Clearance Center, Inc., 222 Rosewood Drive, Danvers, MA 01923, (978) 750-8400, fax (978) 750-4470, or on the web at www.copyright.com. Requests to the Publisher for permission should be addressed to the Permissions Department, John Wiley & Sons, Inc., 111 River Street, Hoboken, NJ 07030, (201) 748-6011, fax (201) 748-6008, or online at http://www.wiley.com/go/permission.

Limit of Liability/Disclaimer of Warranty: While the publisher and author have used their best efforts in preparing this book, they make no representations or warranties with respect to the accuracy or completeness of the contents of this book and specifically disclaim any implied warranties of merchantability or fitness for a particular purpose. No warranty may be created or extended by sales representatives or written sales materials. The advice and strategies contained herein may not be suitable for your situation. You should consult with a professional where appropriate. Neither the publisher nor author shall be liable for any loss of profit or any other commercial damages, including but not limited to special, incidental, consequential, or other damages.

For general information on our other products and services or for technical support, please contact our Customer Care Department within the United States at (800) 762-2974, outside the United States at (317) 572-3993 or fax (317) 572-4002.

Wiley also publishes its books in a variety of electronic formats. Some content that appears in print may not be available in electronic formats. For more information about Wiley products, visit our web site at www.wiley.com.

Library of Congress Cataloging-in-Publication Data:

Masters, Gilbert M.
Renewable and efficient electric power systems / Gilbert M. Masters. – Second edition.
pages cm
"Published simultaneously in Canada"–Title page verso.
Includes bibliographical references.
ISBN 978-1-118-14062-8 (cloth)
1. Electric power systems–Energy conservation. 2. Electric power systems–Electric losses.
3. Renewable energy sources. 4. Energy consumption. I. Title.
TK1005.M33 2013
621.31–dc23
2012048449

ISBN: 9781118633519

To the students who continue to motivate and inspire me

PREFACE

This book provides a solid, quantitative, practical introduction to a wide range of renewable energy systems. For each topic, the theoretical background is introduced, practical engineering considerations associated with designing systems and predicting their performance are provided, and methods to evaluate the economics of these systems are presented. While more attention is paid to the fastest growing, most promising, wind and solar technologies, the book also introduces tidal and wave power, geothermal, biomass, hydroelectric power, and electricity storage technologies. Both supply-side and demand-side technologies are blended in the final chapter, which introduces the coming smart grid.

The book is intended for a mixed audience of engineering and other technology-focused individuals. The course I teach at Stanford, for example, has no prerequisites. About half the students are undergraduate and half are graduate students. Almost all are from engineering and natural science departments, with a growing number of business students. The book has been designed to encourage self-teaching by providing numerous, completely worked examples throughout. Nearly every topic that lends itself to quantitative analysis is illustrated with such examples. Each chapter ends with a set of problems that provide added practice for the student, which should also facilitate the preparation of homework assignments by the instructor.

This new edition has been completely rewritten, updated and reorganized. A considerable amount of new material is presented, both in the form of new topics as well as greater depth in some areas. New topics include wave and tidal power, pumped storage, smart grid, and geothermal power. The section on fundamentals of electric power is strengthened to make this book a much better bridge to advanced courses in power in electrical engineering departments. This includes an introduction to phasor notation, more emphasis on reactive power as well as real power, more on power converter and inverter electronics, and more material on generator technologies. Renewable energy systems have become mainstream technologies and are now, literally, big business. Throughout this edition, more depth has been provided on the financial analysis of large-scale conventional and renewable energy projects.

The book consists of three major sections:

I. Background material on the electric power industry (Chapters 1, 2, 3).

II. Focus on photovoltaics (PVs) and wind power systems (Chapters 4, 5, 6, 7).

III. Other renewables, energy efficiency, and the smart grid (Chapters 8 and 9)

I. BACKGROUND (Chapters 1, 2, 3): The context for renewable energy systems is provided by an introduction to the electric power industry (Chapter 1), including conventional power plant technologies, the regulatory and operational sides of the grid itself, along with financial aspects such as levelized cost of generation. For users who are new to basic electrical components and circuits, or who need a quick review, Chapter 2 provides sufficient coverage to allow any technical student to come up to speed quickly on those fundamentals.

While many students already have some electricity background and can skip Chapter 2,

most have not had a course on electric power, which is the subject of Chapter 3. In fact, it is my impression that many engineering schools that de-emphasized electric power in the past are experiencing a new surge of interest in this field. Chapter 3 provides non-electrical-engineering students the background essential for success in more advanced electrical power courses.

II. PHOTOVOLTAICS AND WIND POWER (Chapters 4, 5, 6, 7): These chapters are the heart of the book. Chapter 4 covers the solar resource, including solar angles, shading problems, clear-sky solar intensity, direct and indirect portions of solar irradiation (important distinctions for concentrating solar technologies), and how to work with real hour-by-hour, typical meteorological year (TMY) solar data for a given location.

Chapter 5 introduces photovoltaic (PV) materials and the electrical characteristics of cells, modules, and arrays. With this background, students can appreciate the dramatic impacts of shading on PV performance as well as how modern electronics can help mitigate those impacts.

Chapter 6 is on PV systems, including sizing, and predicting performance for grid-connected, utility-scale and net-metered rooftop systems, as well as off-grid stand-alone systems with battery storage. Grid-connected systems dominate the market today, while off-grid systems, including microgrid systems, are beginning to have significant impacts in emerging economies where electricity is a scarce commodity. Considerable attention is paid to the economics of all PV systems.

Chapter 7 provides an extensive analysis of wind power systems, including statistical characterizations of wind resources, emerging wind power technologies, and combining the two to predict turbine performance. Wind power currently dominates the renewables market, with billions of dollars of investment money flowing into that sector, so considerable attention is paid in this chapter to the financial analysis of such investments.

III. OTHER RENEWABLES AND THE SMART GRID (Chapters 8, 9): Chapter 8 introduces concentrating solar power systems, including their potential to include thermal storage to provide truly dispatchable electric power. Two emerging ocean power technologies are described: tidal power and wave power. These show considerable promise in part because their variable power outputs are somewhat more predictable than those for wind and solar systems. Hydroelectric power, including micro-hydro systems (again for emerging economies), and pumped storage systems to provide backup power for other variable renewables are described. Finally, biomass for electricity and geothermal systems are introduced.

Chapter 9 is titled “Both Sides of the Meter” and describes the range of issues encountered when variable renewables interact with demand-responsive loads. It begins with the smart grid, including advanced metering infrastructure, technologies that will provide better control of the grid, and interactions with loads that can be controlled to accommodate variations in supply-side resources. The role of electricity storage, including battery storage in electric vehicles, is introduced. Demand-side management, more efficient use of electricity, fuel cells, and other combined heat and power systems are all critical components in balancing our future supply/demand equation.

Finally, the book includes a number of appendices, including Appendix A, a brief energy-economics tutorial. The others provide assorted useful data for system analysis.

This book has been in the making for over four decades, beginning with the impact that

Denis Hayes and Earth Day 1970 had in shifting my career from semiconductors and computer logic into environmental engineering. Then it was Amory Lovins' groundbreaking paper "The Soft Energy Path: The Road Not Taken?" (Foreign Affairs, 1976) that focused my attention on the relationship between energy and environment and the important roles that renewables and efficiency must play in meeting the coming challenges. The penetrating analyses of Art Rosenfeld at the University of California, Berkeley, and the astute political perspectives of Ralph Cavanagh at the Natural Resources Defense Council have been constant sources of guidance and inspiration. These and other trailblazers have illuminated the path, but it has been the challenging, committed, enthusiastic students in my Stanford classes who have kept me invigorated, excited, and energized over the years, and I am deeply indebted to them for their stimulation and friendship. Finally, I owe a special debt of gratitude to my long-time friend and colleague, Jane Woodward, for her generosity and support, which enables me to keep on trucking in this field that I love.

I specifically want to thank a number of individuals who have provided help with specific sections of this new edition. Professor Nick Jenkins of Cardiff University elevated my understanding of power systems with the courses he taught at Stanford. Doctoral students (now graduated) Eric Stoutenburg, Elaine Hart, and Mike Dvorak gave me helpful insights into wind, tidal, and wave power. Design guidelines provided by Eric Youngren from Solar Nexus International have helped ground me in the realities of off-grid PV systems. Two students, Robert Conroy and Adam Raudonis, developed the shadow diagram website that I used for Appendix F. My old friend, now at Sunpower, Bob Redlinger, has been my guru for the financial and business aspects of renewables. The sharp eyes of Fred Zeise, who has saved me from numerous embarrassments with his careful checking of the manuscript, are greatly appreciated. Finally, I raise my glass, as we have done almost every evening for four decades, to my wife, Mary, who helps the sun rise every day of my life.

GILBERT M. MASTERS

Stanford University
April, 2013

CHAPTER 1

THE U.S. ELECTRIC POWER INDUSTRY

Little more than a century ago, there were no motors, lightbulbs, refrigerators, air conditioners, or any of the other electrical marvels that we think of as being so essential today. Indeed, nearly 2 billion people around the globe still live without the benefits of such basic energy services. The electric power industry has since grown to be one of the largest enterprises in the world. It is also one of the most polluting of all industries, responsible for three-fourths of U.S. sulfur oxides (SO_x) emissions, one-third of our carbon dioxide (CO_2) and nitrogen oxides (NO_x) emissions, and one-fourth of particulate matter and toxic heavy metals.

The electricity infrastructure providing power to North America includes over 275, 000 mi of high voltage transmission lines and 950, 000 MW of generating capacity to serve a customer base of over 300 million people. While its cost has been staggering—over $1 trillion—its value is incalculable. Providing reliable electricity is a complex technical challenge that requires real-time control and coordination of thousands of power plants to move electricity across a vast network of transmission lines and distribution networks to meet the exact, constantly varying, power demands of those customers.

While this book is mostly concerned with the alternatives to large, centralized power systems, we need to have some understanding of how these conventional systems work. This chapter explores the history of the utility industry, the basic systems that provide the generation, transmission, and distribution of electric power, and some of the regulatory issues that govern the rules that control the buying and selling of electric power.

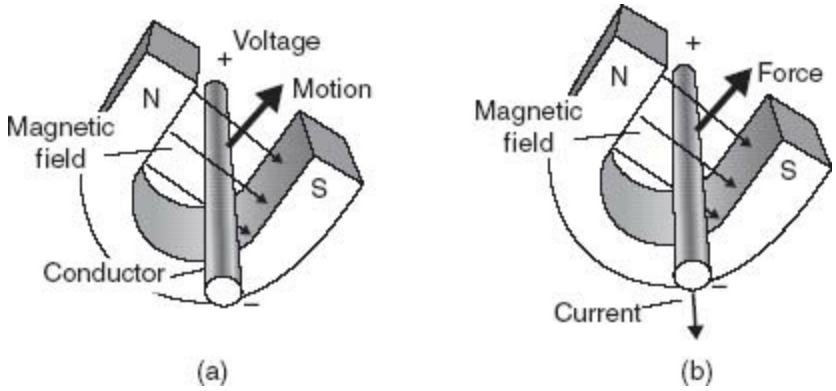
1.1 ELECTROMAGNETISM: THE TECHNOLOGY BEHIND ELECTRIC POWER

In the early nineteenth century, scientists such as Hans Christian Oersted, James Clerk Maxwell, and Michael Faraday began to explore the wonders of electromagnetism. Their explanations of how electricity and magnetism interact made possible the development of electrical generators and motors—inventions that have transformed the world.

Early experiments demonstrated that a voltage (originally called an *electromotive force*, or *emf*) could be created in an electrical conductor by moving it through a magnetic field as shown in Figure 1.1a. Clever engineering based on that phenomenon led to the

development of direct current (DC) dynamos and later to alternating current (AC) generators. The opposite effect was also observed; that is, if current flows through a wire located in a magnetic field, the wire will experience a force that wants to move the wire as shown in Figure 1.1b. This is the fundamental principle by which electric motors are able to convert electric current into mechanical power.

FIGURE 1.1 Moving a conductor through a magnetic field creates a voltage (a). Sending current through a wire located in a magnetic field creates a force (b).

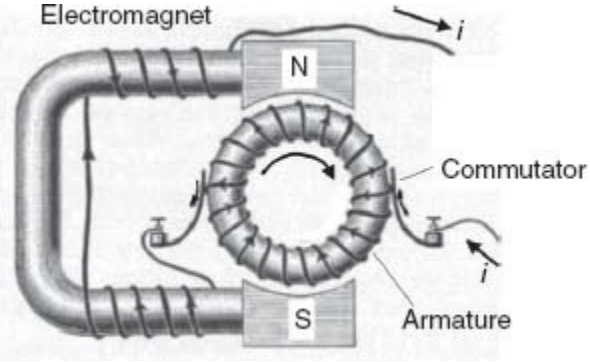


Note the inherent symmetry of the two key electromagnetic phenomena. Moving a wire through a magnetic field causes a current to flow, while sending a current through a wire in a magnetic field creates a force that wants to move the wire. If this suggests to you that a single device could be built that could act as a generator if you applied force to it, or act as a motor if you put current into it, you would be absolutely right. In fact, the electric motor in today's hybrid electric vehicles does exactly that. In normal operation, the electric motor helps power the car, but when the brakes are engaged, the motor acts as a generator, slowing the car by converting the vehicle's kinetic energy into electrical current that recharges the vehicle's battery system.

A key to the development of electromechanical machines, such as motors and generators, was finding a way to create the required magnetic fields. The first *electromagnet* is credited to a British inventor, William Sturgeon, who, in 1825, demonstrated that a magnetic field could be created by sending current through a number of turns of wire wrapped around a horseshoe-shaped piece of iron. With that, the stage was set for the development of generators and motors.

The first practical DC motor/generator, called a dynamo, was developed by a Belgian, Zénobe Gramme. His device, shown in Figure 1.2, consisted of a ring of iron (the *armature*) wrapped with wire, which was set up to spin within a stationary magnetic field. The magnetic field was based on Sturgeon's electromagnet. The key to Gramme's invention was his method of delivering DC current to and from the armature using contacts (called a *commutator*) that rubbed against the rotating armature windings. Gramme startled the world with his machines at a Vienna Exposition in 1873. Using one dynamo to generate electricity, he was able to power another, operating as a motor, three-quarters of a mile away. The potential to generate power at one location and transmit it through wires to a distant location, where it could do useful work, stimulated imaginations everywhere. An enthusiastic American writer, Henry Adams, in a 1900 essay called “The Dynamo and the Virgin” even proclaimed the dynamo as “a moral force” comparable to European cathedrals.

FIGURE 1.2 Gramme's "electromotor" could operate as a motor or as a generator.



1.2 THE EARLY BATTLE BETWEEN EDISON AND WESTINGHOUSE

While motors and generators quickly found application in factories, the first major electric power market developed around the need for illumination. Although many others had worked on the concept of electrically heating a filament to create light, it was Thomas Alva Edison who, in 1879, created the first workable incandescent lamp. Simultaneously he launched the Edison Electric Light Company, which was a full-service illumination company that provided not only the electricity but also the lightbulbs themselves. In 1882, his company began distributing power primarily for lights, but also for electric motors, from his Pearl Street Station in Manhattan. This was to become the first investor-owned utility in the nation.

Edison's system was based on DC, which he preferred in part because it not only provided flicker-free light, but also because it enabled easier speed control of DC motors. The downside of DC, however, was that in those days it was very difficult to change the voltage from one level to another—something that became simple to do in AC after the invention of the transformer in 1883. As we will show later, power line losses are proportional to the square of the current flowing through them, while the power delivered is the product of current and voltage. By doubling the voltage, for example, the same power can be delivered using half the current, which cuts power line losses by a factor of four. Given DC's low voltage transmission constraint, Edison's customers had to be located within just a mile or two of a generating station.

Meanwhile, George Westinghouse recognized the advantages of AC for transmitting power over greater distances and, utilizing AC technologies developed by Tesla, launched the Westinghouse Electric Company in 1886. Within just a few years, Westinghouse was making significant inroads into Edison's electricity market and a bizarre feud developed between these two industry giants. Rather than hedge his losses by developing a competing AC technology, Edison stuck with DC and launched a campaign to discredit AC by condemning its high voltages as a safety hazard. To make the point, Edison and his assistant, Samuel Insull, began demonstrating its lethality by coaxing animals, including dogs, cats, calves, and eventually even a horse, onto a metal plate wired to a 1000-V AC generator and then electrocuting them in front of the local press (Penrose, 1994). Edison and other proponents of DC continued the campaign by promoting the idea that capital

punishment by hanging was horrific and could be replaced by a new, more humane approach based on electrocution. The result was the development of the electric chair, which claimed its first victim in 1890 in Buffalo, NY (also home of the nation's first commercially successful AC transmission system).

The advantages of high voltage transmission, however, were overwhelming and Edison's insistence on DC eventually led to the disintegration of his electric utility enterprise. Through buyouts and mergers, Edison's various electricity interests were incorporated in 1892 into the General Electric Company, which shifted the focus from being a utility to manufacturing electrical equipment and end-use devices for utilities and their customers.

One of the first demonstrations of the ability to use AC to deliver power over large distances occurred in 1891 when a 106 mi, 30, 000 -V transmission line began to carry 75 kW of power between Lauffen and Frankfurt, Germany. The first transmission line in the United States went into operation in 1890 using 3.3 kV lines to connect a hydroelectric station on the Willamette River in Oregon to the city of Portland, 13 mi away. Meanwhile, the flicker problem for incandescent lamps with AC was resolved by trial and error with various frequencies until it was no longer a noticeable problem. Surprisingly, it was not until the 1930s that 60 Hz finally became the standard in the United States. Some countries had by then settled on 50 Hz, and even today, some countries, such as Japan, use both.

1.3 THE REGULATORY SIDE OF ELECTRIC UTILITIES

Edison and Westinghouse launched the electric power industry in the United States, but it was Samuel Insull who shaped what has become the modern electric utility by bringing the concepts of regulated utilities with monopoly franchises into being. It was his realization that the key to making money was to find ways to spread the high fixed costs of facilities over as many customers as possible. One way to do that was to aggressively market the advantages of electric power, especially, for use during the daytime to complement what was then the dominant nighttime lighting load. In previous practices, separate generators were used for industrial facilities, street lighting, street cars, and residential loads, but Insull's idea was to integrate the loads so that he could use the same expensive generation and transmission equipment on a more continuous basis to satisfy them all. Since operating costs were minimal, amortizing high fixed costs over more kilowatt-hour sales results in lower prices, which creates more demand. With controllable transmission line losses and attention to financing, Insull promoted rural electrification, further extending his customer base.

With more customers, more evenly balanced loads, and modest transmission losses, it made sense to build bigger power stations to take advantage of economies of scale, which also contributed to decreasing electricity prices and increasing profits. Large, centralized facilities with long transmission lines required tremendous capital investments; to raise such large sums, Insull introduced the idea of selling utility common stock to the public.

Insull also recognized the inefficiencies associated with multiple power companies competing for the same customers, with each building its own power plants and stringing

its own wires up and down the streets. The risk of the monopoly alternative, of course, was that without customer choice, utilities could charge whatever they could get away with. To counter that criticism, he helped establish the concept of regulated monopolies with established franchise territories and prices controlled by *public utility commissions* (PUCs). The era of regulation had begun.

1.3.1 The Public Utility Holding Company Act of 1935

In the early part of the twentieth century, as enormous amounts of money were being made, utility companies began to merge and grow into larger conglomerates. A popular corporate form emerged, called a *utility holding company*. A holding company is a financial shell that exercises management control of one or more companies through ownership of their stock. Holding companies began to purchase each other and by 1929, 16 holding companies controlled 80% of the U.S. electricity market, with just three of them owning 45% of the total.

With so few entities having so much control, it should have come as no surprise that financial abuses would emerge. Holding companies formed pyramids with other holding companies, each owning stocks in subsequent layers of holding companies. An actual operating utility at the bottom found itself directed by layers of holding companies above it, with each layer demanding its own profits. At one point, these pyramids were sometimes ten layers thick. When the stock market crashed in 1929, the resulting depression drove many holding companies into bankruptcy causing investors to lose fortunes. Insull became somewhat of a scapegoat for the whole financial fiasco associated with holding companies and he fled the country amidst charges of mail fraud, embezzlement, and bankruptcy violations, charges for which he was later cleared.

In response to these abuses, Congress created the *Public Utility Holding Company Act of 1935* (PUHCA) to regulate the gas and electric industries and prevent holding company excesses from reoccurring. Many holding companies were dissolved, their geographic size was limited, and the remaining ones came under control of the newly created Securities and Exchange Commission (SEC).

While PUHCA had been an effective deterrent to the previous holding company financial abuses, recent changes in utility regulatory structures, with their goal of increasing competition, led many to say it had outlived its usefulness and it was repealed as part of the Energy Policy Act of 2005.

1.3.2 The Public Utility Regulatory Policies Act of 1978

With the country in shock from the oil crisis of 1973 and with the economies of scale associated with ever larger power plants having pretty much played out, the country was drawn toward energy efficiency, renewable energy systems, and new, small, inexpensive gas turbines (GTs). To encourage these systems, President Carter signed the Public Utility Regulatory Policies Act of 1978 (PURPA).

There were two key provisions of PURPA, both relating to allowing independent power producers (IPPs), under certain restricted conditions, to connect their facilities to the utility-owned grid. For one, PURPA allows certain industrial facilities and other customers to build and operate their own, small, on-site generators while remaining connected to the

utility grid. Prior to PURPA, utilities could refuse service to such customers, which meant self-generators had to provide all of their own power, all of the time, including their own redundant, backup power systems. That virtually eliminated the possibility of using efficient, economical on-site power production to provide just a portion of a customer's needs.

PURPA not only allowed grid interconnection but it also required utilities to purchase electricity from certain *qualifying facilities* (QFs) at a "just and reasonable price." The purchase price of QF electricity was to be based on what it would have cost the utility to generate the power itself or to purchase it on the open market (referred to as the *avoided cost*). This provision stimulated the construction of numerous renewable energy facilities, especially in California, since PURPA guaranteed a market, at a good price, for any electricity generated.

PURPA, as implemented by the Federal Energy Regulatory Commission (FERC), allowed interconnection to the grid by *Qualifying Small Power Producers* or *Qualifying Cogeneration Facilities*, both are referred to as QFs. Small power producers were less than 80 MW in size that used at least 75% wind, solar, geothermal, hydroelectric, or municipal waste as energy sources. Cogenerators were defined as facilities that produced both electricity and useful thermal energy in a sequential process from a single source of fuel, which may be entirely oil or natural gas.

PURPA not only gave birth to the electric side of the renewable energy industry, it also enabled clear evidence to accrue which demonstrated that small, on-site generation could deliver power at considerably lower cost than the retail rates charged by utilities. Competition had begun.

1.3.3 Utilities and Nonutilities

Electric utilities traditionally have been given a monopoly franchise over a fixed geographical area. In exchange for that franchise, they have been subject to regulation by State and Federal agencies. Most large utilities were vertically integrated; that is, they owned generation, transmission, and distribution infrastructure. After PURPA along with subsequent efforts to create more competition in the grid, most utilities now are just distribution utilities that purchase wholesale power, which they sell to their retail customers using their monopoly distribution system.

The roughly 3200 utilities in the United States can be subdivided into one of four categories of ownership—investor-owned utilities, federally owned, other publicly owned, and cooperatively owned.

Investor-owned utilities (IOUs) are privately owned with stock that is publicly traded. They are regulated and authorized to receive an allowed rate of return on their investments. IOUs may sell power at wholesale rates to other utilities or they may sell directly to retail customers.

Federally owned utilities produce power at facilities run by entities such as the Tennessee Valley Authority (TVA), the U.S. Army Corps of Engineers, and the Bureau of Reclamation. The Bonneville Power Administration, the Western, Southeastern, and Southwestern Area Power Administrations, and the TVA, market and sell power on a nonprofit basis mostly to Federal facilities, publicly owned utilities and cooperatives, and

certain large industrial customers.

Publicly owned utilities are state and local government agencies that may generate some power, but which are usually just distribution utilities. They generally sell power at a lower cost than IOUs because they are nonprofit and are often exempt from certain taxes. While two-thirds of the U.S. utilities fall into this category, they sell only a few percent of the total electricity.

Rural electric cooperatives were originally established and financed by the Rural Electric Administration in areas not served by other utilities. They are owned by groups of residents in rural areas and provide services primarily to their own members.

Independent Power Producers (IPPs) and Merchant Power Plants are privately owned entities that generate power for their own use and/or for sale to utilities and others. They are distinct in that they do not operate transmission or distribution systems and are subject to different regulatory constraints than traditional utilities. In earlier times, these nonutility generators (NUGs) had been industrial facilities generating on-site power for their own use, but they really got going during the utility restructuring efforts of the 1990s when some utilities were required to sell off some of their power plants.

Privately owned power plants that sell power onto the grid can be categorized as IPPs or merchant plants. IPPs have pre-negotiated contracts with customers in which the financial conditions for the sale of electricity are specified by power purchase agreements (PPAs). Merchant plants, on the other hand, have no predefined customers and instead sell power directly to the wholesale spot market. Their investors take the risks and reap the rewards. By 2010, some 40% of the U.S. electricity was generated by IPPs and merchant power plants.

1.3.4 Opening the Grid to NUGs

After PURPA, the Energy Policy Act of 1992 (EPAct) created additional competition in the electricity generation market by opening the grid to more than just the QFs identified in PURPA. A new category of access was granted to *exempt wholesale generators* (EWGs), which can be of any size, using any fuel, and any generation technology, without the restrictions and ownership constraints that PURPA and PUHCA imposed. EPAct allows EWGs to generate electricity in one location and sell it anywhere else in the country using someone else's transmission system to wheel their power from one location to another.

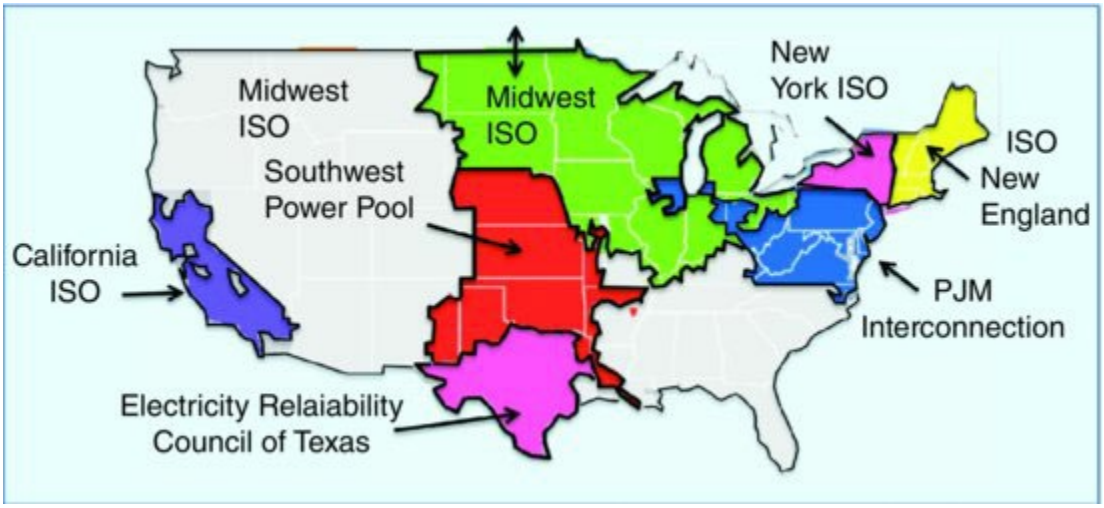
While the 1992 EPAct allowed IPPs and merchant plants to gain access to the transmission grid, problems arose during periods when the transmission lines were being used to near capacity. In these and other circumstances, the IOUs that owned the lines favored their own generators, and NUGs were often denied access. In addition, the regulatory process administered by the FERC was initially cumbersome and inefficient. To eliminate such deterrents, the FERC issued Order 888 in 1996, which had as a principal goal the elimination of anticompetitive practices in transmission services by requiring IOUs to publish nondiscriminatory tariffs that applied to all generators.

Order 888 also encouraged the formation of *independent system operators* (ISOs), which are nonprofit entities established to control the operation of transmission facilities owned by traditional utilities. Later, in 1999, the FERC issued Order 2000, which broadened its efforts to break up vertically integrated utilities by calling for the creation of *regional*

transmission organizations (RTOs). RTOs can follow the ISO model in which the ownership of the transmission system remains with the utilities, with the ISO being there to provide control of the system's operation, or they would be separate transmission companies that would actually own the transmission facilities and operate them for a profit. The goal has been for ISOs and RTOs to provide independent, unbiased transmission operation that would ensure equal access to the power grid for both utility and new, NUGs.

There are now seven ISO/RTOs in the United States (Fig. 1.3), which together serve two-thirds of the U.S. electricity customers. They are nonprofit entities that provide a number of services, including the coordination of generation, loads, and available transmission to help maintain system balance and reliability, administering tariffs that establish the hour-by-hour wholesale price of electricity, and monitoring the market to help avoid manipulation and abuses. In other words, these critical entities manage not only the flow of actual electrical power through the grid; they also manage the information about power flows as well as the flow of money between power plants and transmission owners, marketers, and buyers of power.

FIGURE 1.3 These seven ISO/RTOs deliver two-thirds of the U.S. electricity.



1.3.5 The Emergence of Competitive Markets

Prior to PURPA, the accepted method of regulation was based on monopoly franchises, vertically integrated utilities that owned some or all of their own generation, transmission, and distribution facilities, and consumer protections based on a strict control of rates and utility profits. In the final decades of the twentieth century, however, the successful deregulation of other traditional monopolies such as telecommunications, airlines, and the natural gas industry, provided evidence that introducing competition in the electric power industry might also work there. While the disadvantages of multiple systems of wires to transmit and distribute power continue to suggest they be administered as regulated monopolies, there is no inherent reason why there should not be competition between generators who want to put power onto those wires. The whole thrust of both PURPA and EPAct was to begin the opening up of that grid to allow generators to compete for customers, thereby hopefully driving down costs and prices.

In the 1990s, California's electric rates were among the highest in the nation—especially

for its industrial customers—which led to an effort to try to reduce electricity prices by introducing competition among generation sources. In 1996, the California Legislature passed Assembly Bill (AB) 1890. AB 1890 had a number of provisions, but the critical ones included:

a. To reduce their control of the market, the three major IOUs, Pacific Gas and Electric (PG&E), Southern California Edison (SCE), and San Diego Gas and Electric (SDG&E), which accounted for three-fourths of California's supply, were required to sell off most of their generation assets. About 40% of California's installed capacity was sold off to a handful of NUGs including Mirant, Reliant, Williams, Dynergy, and AES. The thought was that new players who purchased these generators would compete to sell their power, thereby lowering prices.

b. All customers would be given a choice of electricity suppliers. For a period of about 4 years, large customers who stayed with the IOUs would have their rates frozen at the 1996 levels, while small customers would see a 10% reduction. Individual rate payers could choose non-IOU providers if they wanted to, and this "customer choice" was touted as a special advantage of deregulation. Some providers, for example, offered elevated percentages of their power from wind, solar, and other environmentally friendly sources as "green power."

c. Utilities would purchase wholesale power on the market, which, due to competition, was supposed to be comparatively inexpensive. The hope was that with their retail rates frozen at the relatively high 1996 levels, and with dropping wholesale prices in the new competitive market, there would be extra profits left over that could be used to pay off those costly stranded assets—mostly nuclear power plants.

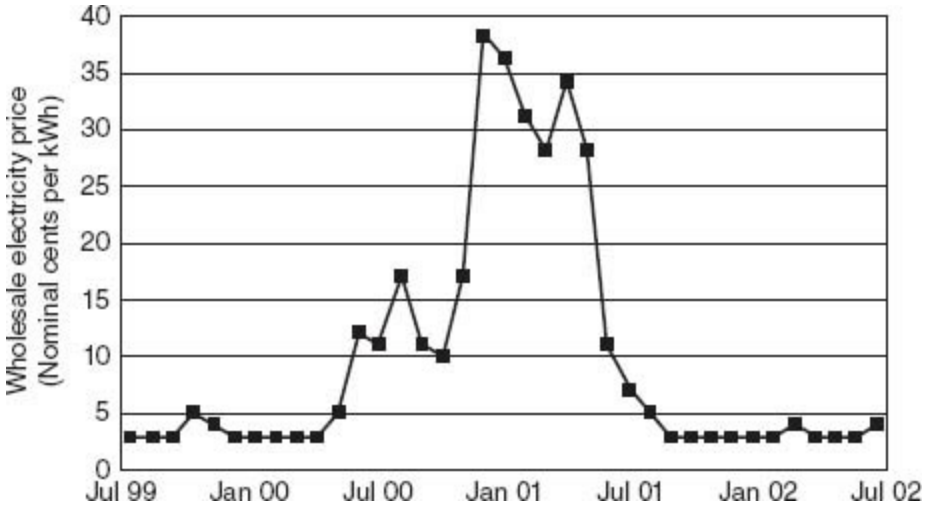
d. The competitive process was set up so that each day there would be an auction run by an ISO in which generators would submit bids indicating the hour-by-hour price at which they were willing to provide power on the following day. The accumulation of the lowest bids sufficient to meet the projected demands would then be allowed to sell their power at the price that the highest accepted bidder received. Any provider who bid too high would not sell power the next day. So if a generator bid $10/MWh (1 ¢/kWh) and the market clearing price was $40/MWh, that generator would get to sell power at the full $40 level. This was supposed to encourage generators to bid low so they would be assured of the ability to sell power the next day.

On paper, it all sounded pretty good. Competition would cause electricity prices to go down and customers could choose providers based on whatever criteria they liked, including environmental values. As wholesale power prices dropped, utilities with high, fixed retail rates could make enough extra money to pay off old debts and start fresh.

For 2 years, up until May 2000, the new electricity market seemed to be working with wholesale prices averaging about $30/MWh (3 ¢/kWh). Then, in the summer of 2000, it all began to unravel (Fig. 1.4). In August 2000, the wholesale price was five times higher than it had been in the same month in 1999. During a few days in January 2001, when demand is traditionally low and prices normally drop, the wholesale price spiked to the astronomical level of $1500/MWh. By the end of 2000, Californians had paid $33.5 billion for electricity, nearly five times the $7.5 billion spent in 1999. In just the first month and a half of 2001, they spent as much as they had in all of 1999.

FIGURE 1.4 California wholesale electricity prices during the crisis of 2000–2001.

Reproduced with permission from Bachrach et al. (2003).



What went wrong? Factors that contributed to the crisis included higher-than-normal natural gas prices, a drought that reduced the availability of imported electricity from the Pacific Northwest, reduced efforts by California utilities to pursue customer energy efficiency programs in the deregulated environment, and, some argue, insufficient new plant construction. But, when California had to endure rolling blackouts in January 2001, a month when demand is always far below the summer peaks and utilities normally have abundant excess capacity, it became clear that none of the above arguments were adequate. Clearly, the IPPs had discovered they could make a lot more money manipulating the market, in part by withholding supplies, than by honestly competing with each other.

The energy crisis finally began to ease by the summer of 2001 after the FERC finally stepped in and instituted price caps on wholesale power, the Governor began to negotiate long-term contracts, and the state's aggressive energy-conservation efforts began to pay off. Those conservation programs, for example, are credited with cutting the June, 2001, California energy demand by 14% compared with the previous June.

In March 2003, the FERC issued a statement concluding that California electricity and natural gas prices were driven higher because of widespread manipulation and misconduct by Enron and more than 30 other energy companies during the 2000–2001 energy crisis. In 2004, audio tapes were released that included Enron manipulators joking about stealing money from those “dumb grandmothers” in California. By 2005, Dynergy, Duke, Mirant, Williams, and Reliant had settled claims with California totaling $2.1 billion—a small fraction of the estimated $71 billion that the crisis is estimated to have cost the state.

While the momentum of the 1990s toward restructuring was shaken by the California experience, the basic arguments in favor of a more competitive electric power industry remain attractive. As of 2011, there were 14 states, mostly in the Northeast, that operate retail markets in which customers may choose alternative power suppliers. Those customers that choose not to participate in the market continue to purchase retail from their historical utility. Meanwhile, eight other states have suspended their efforts to create this sort of retail competition, including California.

A capsule summary of the most significant technological and regulatory developments that have shaped today's electric power systems is presented in Table 1.1.

TABLE 1.1 Chronology of Major Electricity Milestones

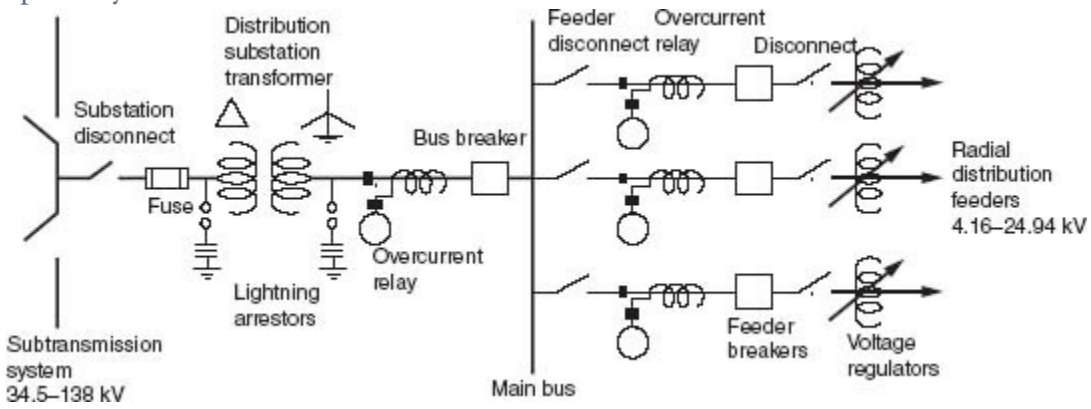
Year	Event
1800	First electric battery (A. Volta)
1820	Relationship between electricity and magnetism confirmed (H.C. Oersted)
1821	First electric motor (M. Faraday)
1826	Ohm's law (G.S. Ohm)
1831	Principles of electromagnetism and induction (M. Faraday)
1832	First dynamo (H. Pixil)
1839	First fuel cell (W. Grove)
1872	Gas turbine patent (F. Stulze)
1879	First practical incandescent lamp (T.A. Edison and J. Swan, independently)
1882	Edison's Pearl Street Station opens
1883	Transformer invented (L. Gaulard and J. Gibbs)
1884	Steam turbine invented (C. Parsons)
1886	Westinghouse Electric formed
1888	Induction motor and polyphase AC systems (N. Tesla)
1889	Impulse turbine patent (L. Pelton)
1890	First single-phase AC transmission line (Oregon City to Portland)
1891	First three-phase AC transmission line (Germany)
1903	First successful gas turbine (France)
1907	Electric vacuum cleaner and washing machines
1911	Air conditioning (W. Carrier)
1913	Electric refrigerator (A. Goss)
1935	Public Utility Holding Company Act (PUHCA)
1936	Boulder dam completed
1962	First nuclear power station (Canada)
1973	Arab oil embargo, price of oil quadruples
1978	Public Utility Regulatory Policies Act (PURPA)
1979	Iranian revolution, oil price triples; Three Mile Island nuclear accident
1983	Washington Public Power Supply System $2.25 billion nuclear reactor bond default
1986	Chernobyl nuclear accident (USSR)
1990	Clean Air Act amendments introduce tradeable SO_2 allowances
1992	National Energy Policy Act (EPAct): market-based competition begins
1996	California begins restructuring
2001	Restructuring collapses in California; Enron and PG&E bankruptcy
2003	Great Northeast power blackout: 50 million people lose power
2005	Energy Policy Act of 2005 (EPAct05): revisits PUHCA, PURPA, strengthens FERC
2008	Tesla all-electric roadster introduced
2011	Fukushima nuclear reactor meltdown

1.4 ELECTRICITY INFRASTRUCTURE: THE GRID

Electric utilities, monopoly franchises, large central power stations, and long transmission lines have been the principal components of the prevailing electric power paradigm since the days of Insull. Electricity generated at central power stations is almost always three-phase, AC power at voltages that typically range from about 14 to 24 kV. At the site of generation, transformers step up the voltage to long-distance transmission line levels, typically in the range of 138–765 kV. Those voltages may be reduced for regional distribution using subtransmission lines that carry voltages in the range of 34.5–138 kV.

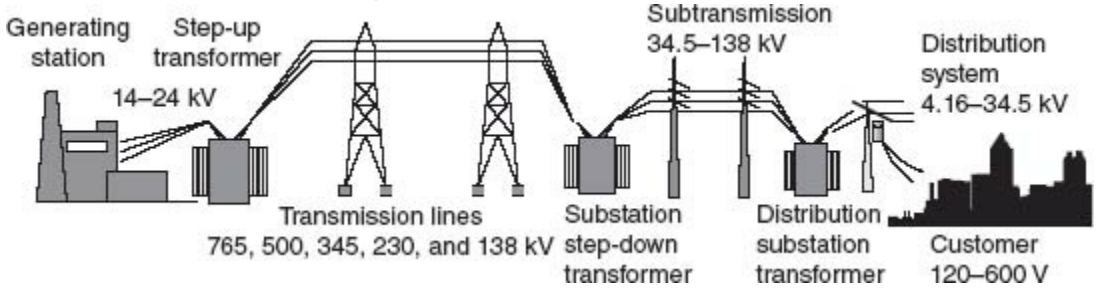
When electric power reaches major load centers, transformers located in distribution-system substations step down the voltage to levels typically between 4.16 and 34.5 kV range, with 12.47 kV being the most common. Feeder lines carry power from distribution substations to the final customers. An example of a simple distribution substation is diagrammed in Figure 1.5. Note the combination of switches, circuit breakers, and fuses that protect key components and which allow different segments of the system to be isolated for maintenance or during emergency *faults* (short circuits) that may occur in the system. Along those feeder lines on power poles or in concrete-pad-mounted boxes, transformers again drop voltage to levels suitable for residential, commercial, and industrial uses.

FIGURE 1.5 A simple distribution station. For simplification, this is drawn as a *one-line diagram*, which means a single conductor on the diagram corresponds to the three lines in a three-phase system.



A sense of the overall utility generation, transmission, and distribution system is shown in Figure 1.6.

FIGURE 1.6 Simplified power generation, transmission, and distribution system.

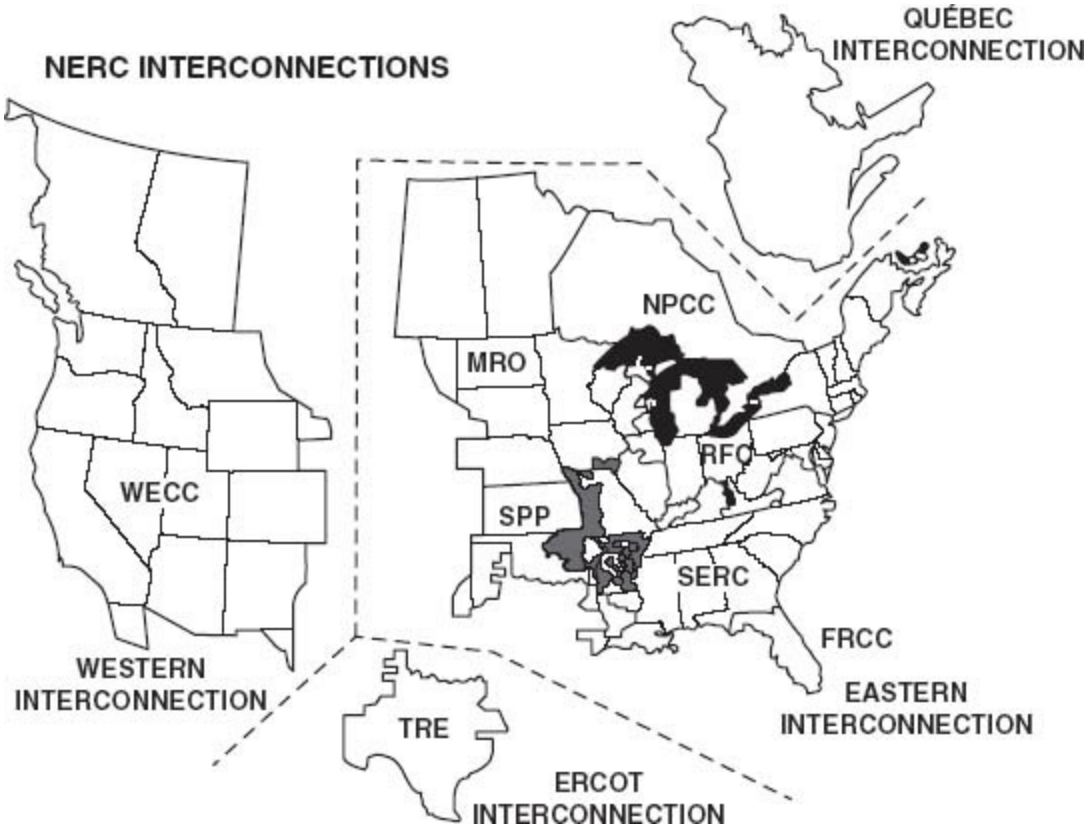


1.4.1 The North American Electricity Grid

The system in Figure 1.6 suggests a rather linear system with one straight path from sources to loads. In reality, there are multiple paths that electric currents can take to get from generators to end users. Transmission lines are interconnected at switching stations and substations, with lower voltage "subtransmission" lines and distribution feeders extending into every part of the system. The vast array of transmission and distribution (T&D) lines is called a power "grid." Within a grid, it is impossible to know which path electricity will take as it seeks out the path of least resistance to get from generator to load.

As Figure 1.7 shows, the U.S. portion of the North American power grid actually consists of three separate interconnection grids—the Eastern Interconnect, the Western Interconnect, and Texas, which is virtually an electric island with its own power grid. Within each of these interconnection zones, everything is precisely synchronized so that every circuit within a given interconnect operates at exactly the same frequency. Interconnections between the grids are made using high voltage DC (HVDC) links, which consist of *rectifiers* that convert AC to DC, a connecting HVDC transmission line between the interconnect regions, and *inverters* that convert DC back to AC. The advantage of a DC link is that problems associated with exactly matching AC frequency, phase, and voltages from one interconnect to another are eliminated in DC. HVDC links can also connect various parts of a single grid, as is the case with the 3000 MW Pacific Intertie (also called Path 65) between the Pacific Northwest and Southern California. Quite often national grids of neighboring countries are linked this way as well (such as the Québec interconnection).

FIGURE 1.7 The U.S. portion of the North American power grid consists of three separate interconnect regions—the Western, Eastern, and ERCOT (Texas) interconnections. Also shown are the eight regions governed by the North American Electric Reliability Corporation (NERC).



Also shown in Figure 1.7 are the eight regional councils that make up the North American Electric Reliability Corporation (NERC). NERC has the responsibility for overseeing operations in the electric power industry and for developing and enforcing mandatory reliability standards. Its origins date back to the great Northeast Blackout of 1965, which left 30 million people without power. Those councils are listed in Table 1.2.

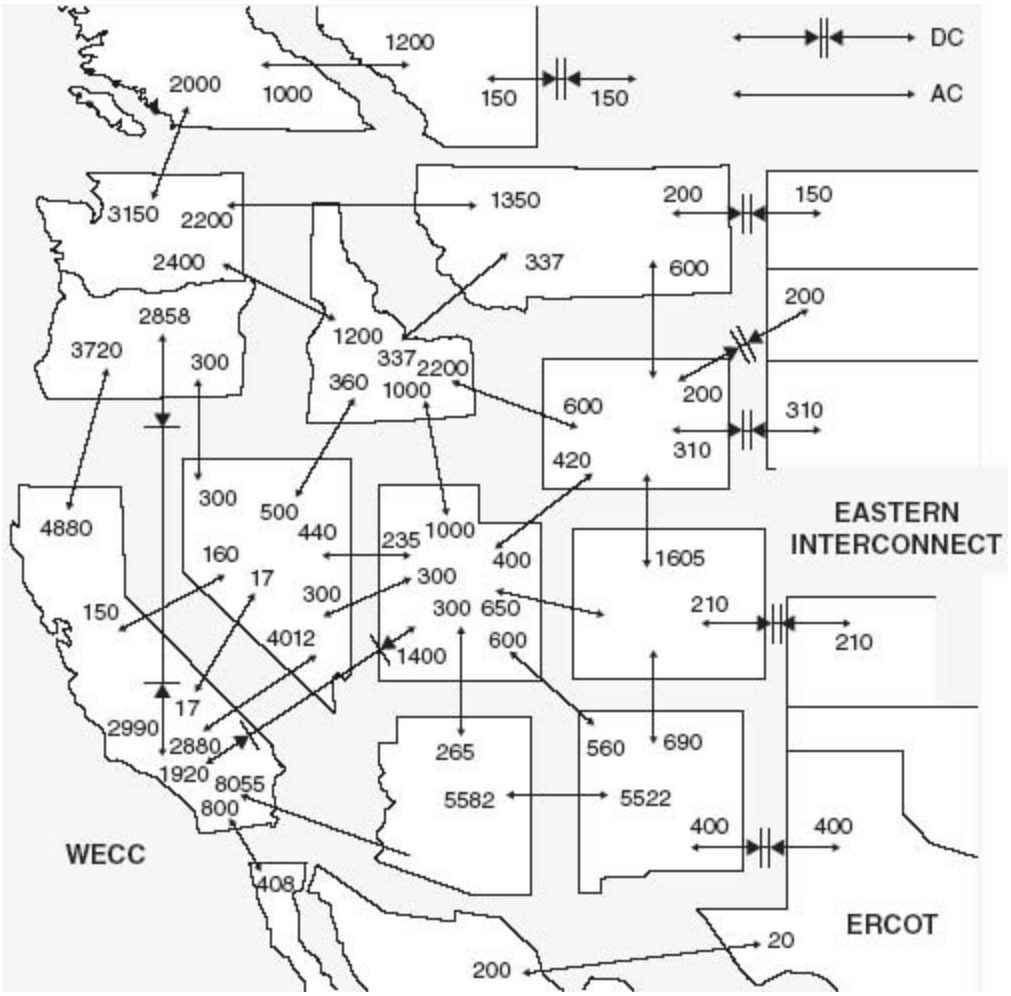
TABLE 1.2 NERC Regional Reliability Councils

	Council Name	Capacity (MW)	Coal (%MWh)
FRCC	Florida Reliability Coordinating Council	53,000	19
MRO	Midwest Reliability Organization	51,000	51
NPCC	Northeast Power Coordinating Council	71,000	9
RFC	Reliability First Corporation	260,000	50
SERC	Southeastern Reliability Corporation	215,000	33
SPP	Southwest Power Pool RE	57,000	33
TRE (ERCOT)	Texas Reliability Entity	81,000	19
WECC	Western Electricity Coordinating Council	179,000	18

Source: EIA/DOE, 2008.

The Western Electricity Coordinating Council (WECC) covers the 12 states west of the Rockies and the Canadian provinces of British Columbia and Alberta. A map showing the interstate transmission corridors within WECC is shown in Figure 1.8. Also, note the relatively modest transmission capabilities of the HVDC connections between the Western interconnection, the Eastern, and the Texas interconnect.

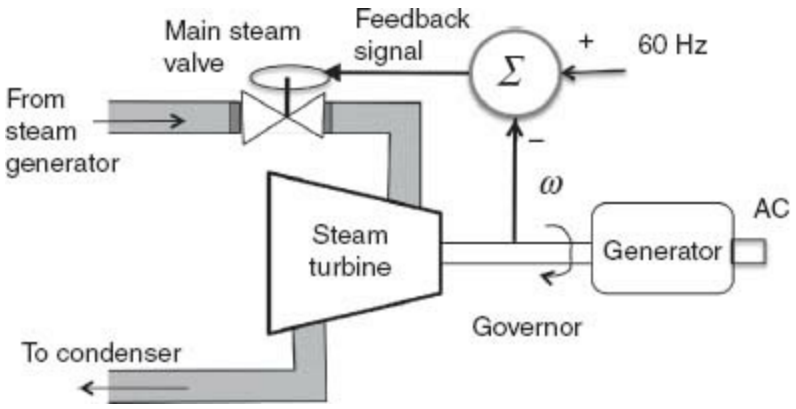
FIGURE 1.8 WECC nonsimultaneous interstate power transmission capabilities (MW). From Western Electricity Coordinating Council Information Summary, 2008.



1.4.2 Balancing Electricity Supply and Demand

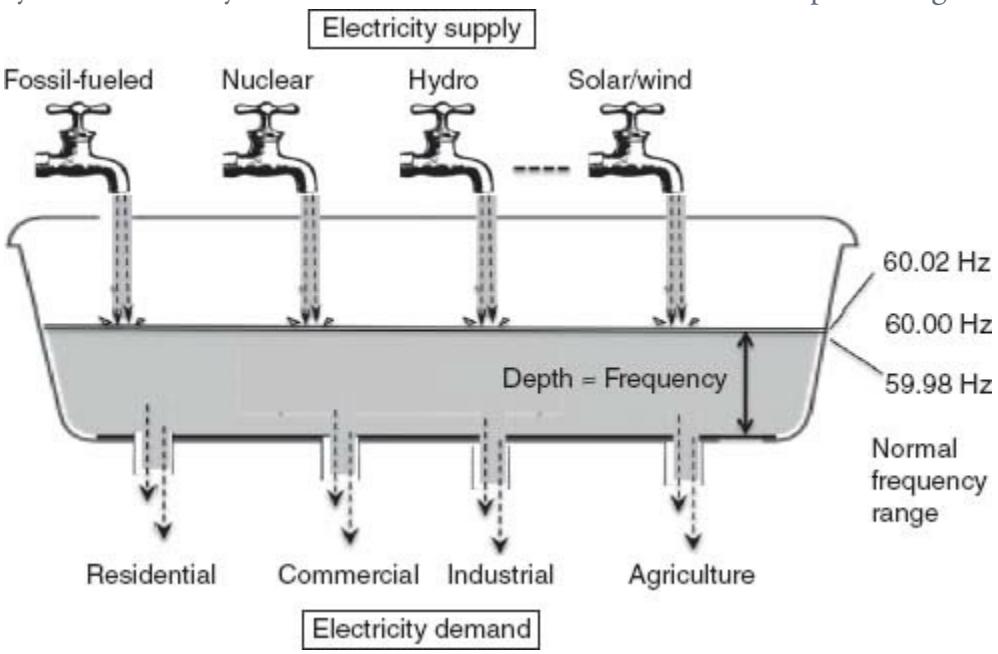
Managing the power grid is a constant struggle to balance power supply with customer demand. If demand exceeds supply, turbine generators, which can be very massive, slow down just a bit, converting some of their kinetic energy (inertia) into extra electrical power to help meet the increased load. Since the frequency of the power generated is proportional to the generator's rotor speed, increasing load results in a drop in frequency. If this is a typical power plant, it takes a few seconds for a governor (Fig. 1.9) to increase torque to bring it back up to speed. Similarly, if demand decreases, turbines speed up a bit before they can be brought back under control. Managing that system balance is the job of roughly 140 Control-Area Balancing Authorities located throughout the grid. Among those are the seven ISOs and RTOs described earlier.

FIGURE 1.9 Frequency is often automatically controlled with a governor that adjusts the torque from the turbine to the generator.



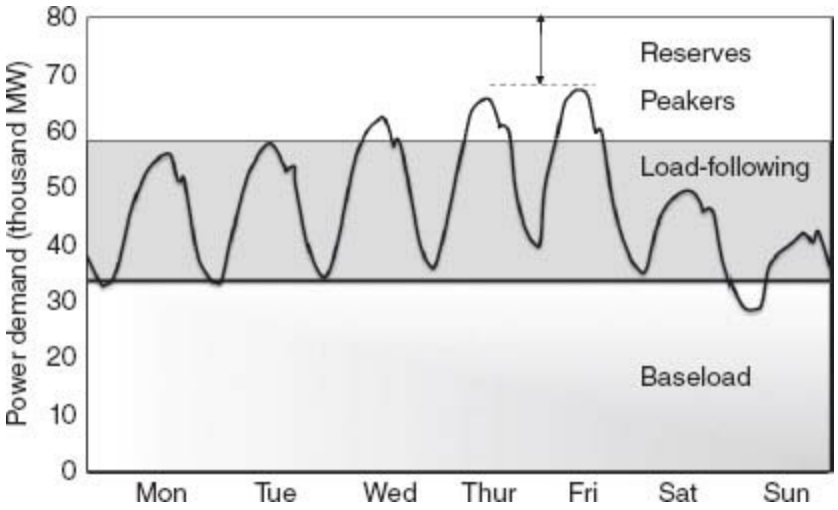
The simple analogy shown in Figure 1.10 suggests thinking of electricity supply as being a set of nozzles delivering water to a bathtub that is constantly being drained by varying amounts of consumer demand. Using the water level to represent grid frequency, the goal is to keep the water at a nearly constant level corresponding to grid frequencies that typically are in the range of about 59.98–60.02 Hz. If the frequency drops below about 59.7 Hz emergency measures, such as shedding loads (blackouts) may be called for to prevent damage to the generators.

FIGURE 1.10 A simple analogy for a grid operating as a load-following system in which the supply is continuously varied to maintain a constant water level representing frequency.



On a gross, hour-by-hour, day-by-day scale, a utility's power demand looks something like that shown in Figure 1.11. There is a predictable diurnal variation, usually rising during the day and decreasing at night, along with reduced demand on the weekends compared to weekdays.

FIGURE 1.11 Example of weekly load fluctuations.



Not all power plants can respond to changing loads to the same extent or at the same rates. Ramp rates (how fast they can respond) as well as marginal operational costs (mostly fuel related) can determine which plants get dispatched first. Some plants, such as nuclear reactors, are designed to run continuously at close to full power; so they are sometimes described as "must-run" plants. The intermittency aspect of renewables means they are normally allowed to run whenever the wind is blowing or the sun is shining since they have almost zero marginal costs. When the power available from renewables plus nuclear exceeds instantaneous demand, it is the renewables that usually have to be curtailed.

Most fossil-fueled plants, along with hydroelectric facilities, can easily be slowly ramped up and down to track the relatively smooth, predictable diurnal changes in load. These are load-following intermediate plants. Some small, cheap to build, but expensive to run, plants, sometimes referred to as *peakers*, are mostly used only a few tens of hours per year to meet the highest peak demands. Some plants are connected to the grid, but deliver no power until they are called upon, such as when another plant suddenly trips off line. These fall into the category of spinning reserves.

Finally, there are small, fast-responding plants that may purposely be run at something like partial output to track the second-by-second changes in demand. These provide what is referred to as *regulation* services, or *frequency regulation*, or *automatic generation control* (AGC) for the grid. They can provide *regulation up* power, which means they increase power when necessary, and/or, they can provide *regulation down* power, which means they can decrease power to follow decreasing loads. They are paid a monthly fee per megawatt of regulation up or regulation down services that they provide, whether or not they are ever called upon to do so.

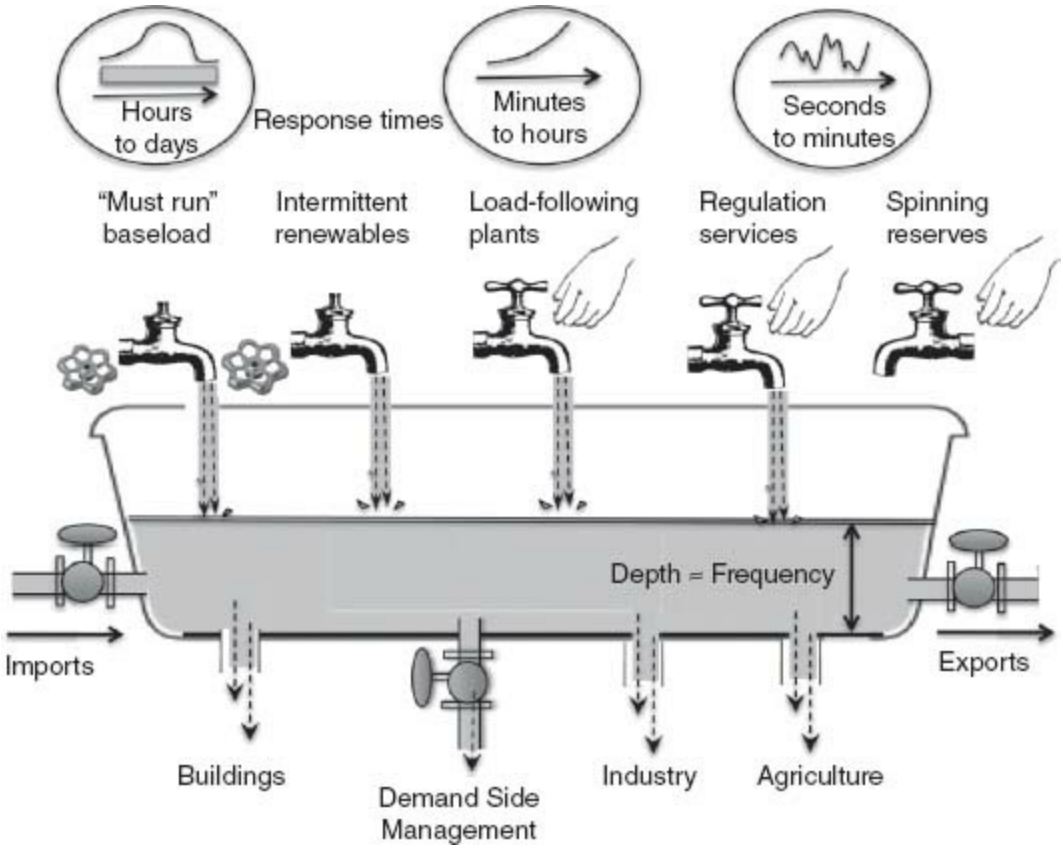
If transmission is available, ISOs, RTOs, and other grid balancing authorities can also import power from adjacent systems or deliver power to them.

All of the above methods of changing power plant outputs to track changing loads are the dominant paradigm for maintaining balance on the grid. Newly emerging *demand response* (DR) approaches are changing that paradigm by bringing the ability of customers to control their own power demands into play. Especially, if given a modest amount of advanced notice, and some motivation to do so, building energy managers can control demand on those critical peak power days by dimming lights, adjusting thermostats, precooling buildings, shifting loads, and so forth. Another approach, referred to as *demand dispatch*, involves automating DR in major appliances such as refrigerators and electric

water heaters by designing them to monitor, and immediately respond to, changes in grid frequency. So, for example, when frequency drops, the fridge can stop making ice, and the water heater can delay heating, until frequency recovers. All of these potential ways to control loads are often referred to as being *demand-side management*, or DSM.

Figure 1.12 extends the "bathtub" analogy to incorporate all of these approaches to keep the grid balanced.

FIGURE 1.12 A more complicated bathtub analogy that incorporates the roles that different kinds of power plants provide as well as the potential for demand response.



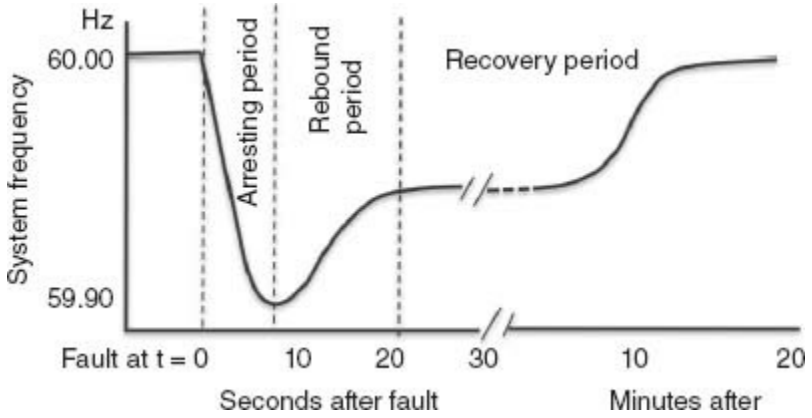
1.4.3 Grid Stability

During normal operations, the grid responds to slight imbalances in supply and demand by automatically adjusting the power delivered by its generation facilities to bring system frequency back to acceptable levels. Small variations are routine; however, large deviations in frequency can cause the rotational speed of generators to fluctuate, leading to vibrations that can damage turbine blades and other equipment. Power plant pumps delivering cooling water and lubrication slow down as well. Significant imbalances can lead to automatic shutdowns of portions of the grid, which can affect thousands of people. When parts of the grid shut down, especially when that occurs without warning, power that surges around the outage can potentially overload other parts of the grid causing those sections to go down as well. Avoiding these calamitous events requires fast-responding, automatic controls supplemented by fast operator actions.

When a large conventional generator goes down, demand suddenly, and significantly, exceeds supply causing the rest of the interconnect region to almost immediately experience

a drop in grid frequency. The inertia associated with all of the remaining turbine/generators in the interconnect region helps control the rate at which frequency drops. In addition, conventional frequency regulation systems, which are already operating, ramp up power to try to compensate for the lost generation. If those are insufficient, frequency control reserves will automatically be called up. If everything goes well, as is suggested in Figure 1.13, within a matter of seconds frequency rebounds to an acceptable level, which buys time for grid operators to dispatch additional power from other generators. It may take 10 min or so for those other resources to bring the system back into balance at the desired 60 Hz.

FIGURE 1.13 After a sudden loss of generation, automatic controls try to bring frequency to an acceptable level within seconds. Operator-dispatched power takes additional time to completely recover. From Eto et al., 2010.

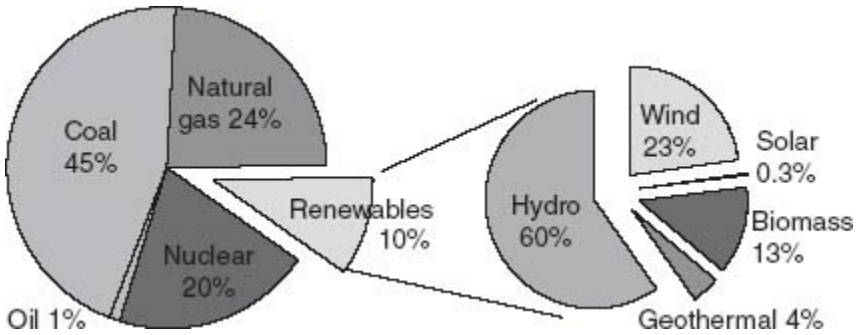


Most often, major blackouts occur when the grid is running at near capacity, which for most of the United States occurs during the hottest days of summer when the demand for air conditioning is at its highest. When transmission line currents increase, resistive losses (proportional to current squared) cause the lines to heat up. If it is a hot day, especially with little or no wind to help cool the lines, the conductors expand and sag more than normal and are more likely to come in contact with underlying vegetation causing a short-circuit (i.e., a *fault*). Perhaps surprisingly, one of the most common triggers for blackouts on those hot days results from insufficient attention having been paid to simple management of tree growth within transmission-line rights-of-way. In fact, the August 2003 blackout that hit the Midwest and Northeastern parts of the United States, as well as Ontario, Canada, was initiated by this very simple phenomenon. That blackout caused 50 million people to be without power, some for as long as four days, and cost the United States roughly $4–10 billion.

1.4.4 Industry Statistics

As shown in Figure 1.14, 70% of the U.S. electricity is generated in power plants that burn fossil fuels—coal, natural gas, and oil—with coal being the dominant source. Note that oil is a very minor fuel in the electricity sector, only about 1%, and that is almost all residual fuel oil—literally the bottom of the barrel—that has little value for anything else. That is, petroleum and electricity currently have very little to do with each other. However that may change as we begin to more aggressively electrify the transportation sector.

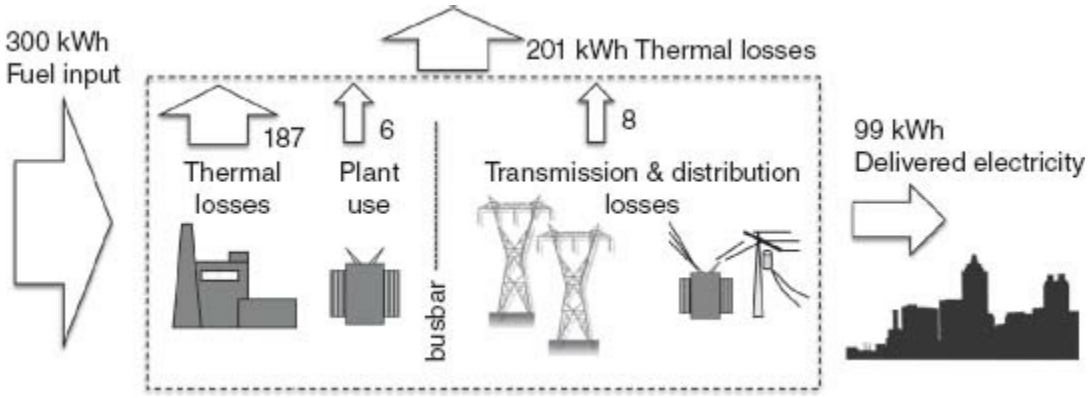
FIGURE 1.14 Energy sources for U.S. electricity in 2010 (based on EIA Monthly Energy Review, 2011).



About 20% of our electricity comes from nuclear power plants and the remaining 10% comes from a handful of renewable energy systems—mostly hydroelectric facilities. That is, close to one-third of our power is generated with virtually no direct carbon emissions (there are, still, emissions associated with the embodied energy associated with building those plants). Wind and solar plants in 2010 accounted for only about 2.5% of the U.S. electricity, but that fraction is growing rapidly.

Only about one-third of the energy content of fuels used to generate electricity ends up being delivered to end-use customers. The missing two-thirds is made up of thermal losses at the power plant (which will be described more carefully later), electricity used to help run the plant itself (much of that helps control emissions), and losses in T&D lines. As Figure 1.15 illustrates, if we imagine starting with 300 units of fuel energy, close to 200 are lost along the way and 100 are delivered to customers in the form of electricity, which leads to a very convenient 3:2:1 ratio for estimating energy flows in our power systems.

FIGURE 1.15 Only about one-third of the energy content of fuels ends up as electricity delivered to customers (losses shown are based on data in the 2010 EIA *Annual Energy Review*).

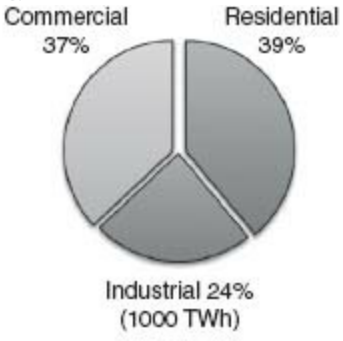


Three-fourths of U.S. electricity that makes it to customers is used in residential and commercial buildings, with an almost equal split between the two. The remaining one-fourth powers industrial facilities. A breakdown of the way electricity is used in buildings is presented in Figure 1.16. A quick glance shows that for both residential and commercial buildings, lighting and space cooling are the most electricity-intensive activities. Those two are important not only because they are significant in total energy (about 30% of total kWh sold) but also because they are the principal drivers of the peak demand for power, which for many utilities occurs in the mid-afternoon on hot, sunny days. It is the peak load

that dictates the total generation capacity that must be built and operated.

FIGURE 1.16 End uses for U.S. electricity. Cooling and lighting are especially important both in terms of total electricity consumption, and in their role in driving peak demand (data based on *EIA Building Energy Databook*, 2010).

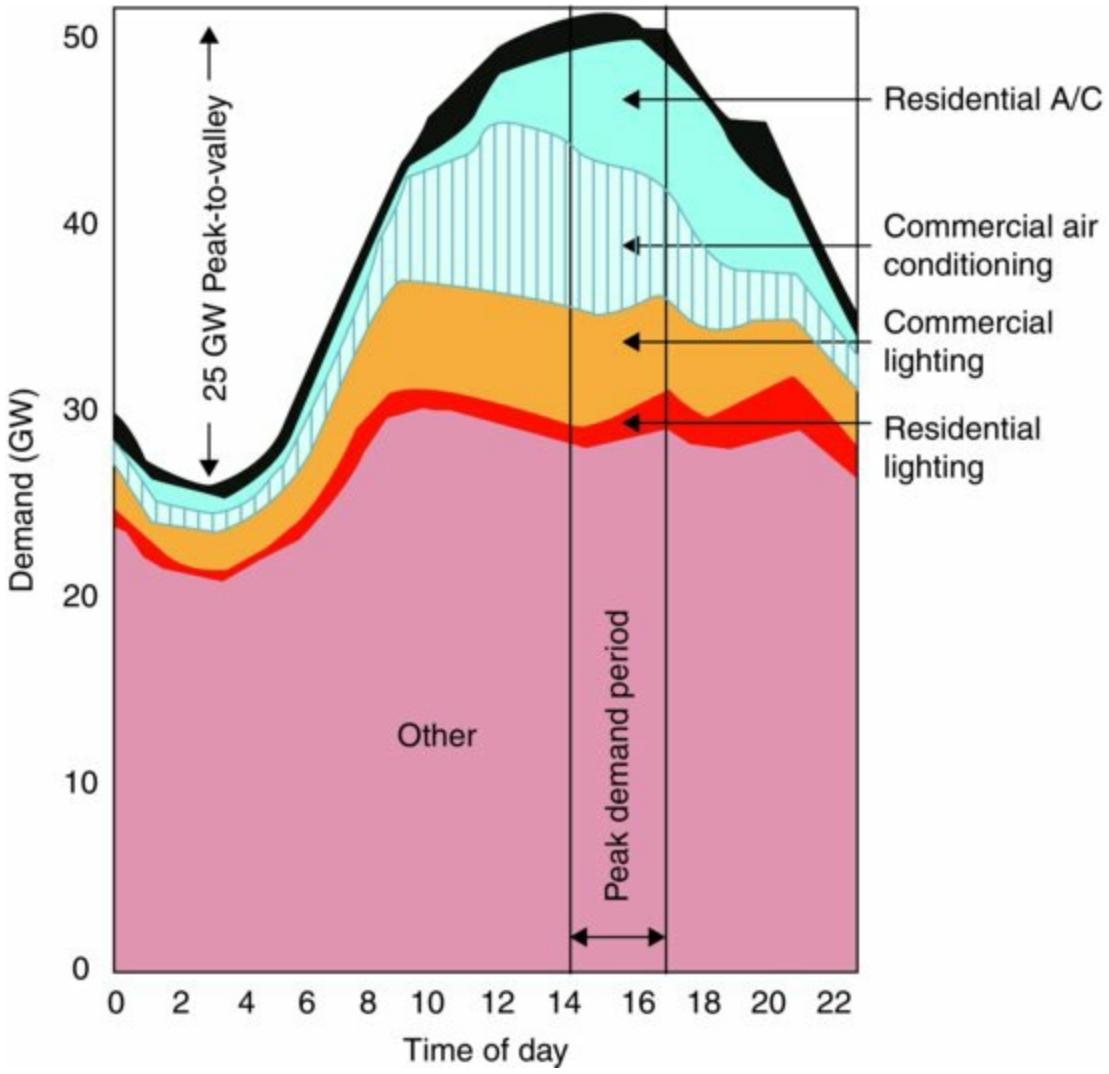
Commercial	Percentage
Lighting	26%
Space cooling	15%
Ventilation	13%
Refrigeration	10%
Electronics	7%
Computers	5%
Space heating	5%
Water heating	2%
Cooking	1%
Other	17%
TOTAL (TWh)	1500



Residential	Percentage
Space cooling	22%
Lighting	14%
Water heating	9%
Refrigeration	9%
Space heating	9%
Electronics	7%
Wet cleaning	6%
Computers	4%
Cooking	2%
Other	18%
TOTAL (TWh)	1600

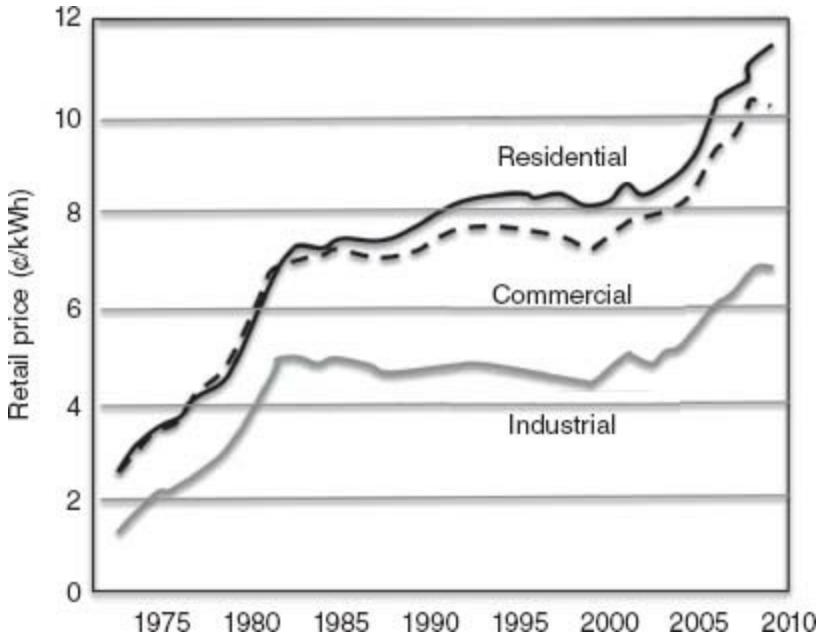
As an example of the impact of lighting and air conditioning on the peak demand for power, Figure 1.17 shows the California power demand on a hot, summer day. As can be seen, the diurnal rise and fall of demand is almost entirely driven by air conditioning and lighting. Better buildings with greater use of natural daylighting, more efficient lamps, increased attention to reducing afternoon solar gains, greater use of natural-gas-fired absorption air conditioning systems, load shifting by using ice made at night to cool during the day, and so forth, could make a significant difference in the number and type of power plants needed to meet those peak demands. The tremendous potential offered by building-energy efficiency and DR will be explored later in the book.

FIGURE 1.17 The load profile for a peak summer day in California (1999) showing that lighting and air conditioning account for almost all of the daytime rise. Adapted from Brown and Koomey (2002).



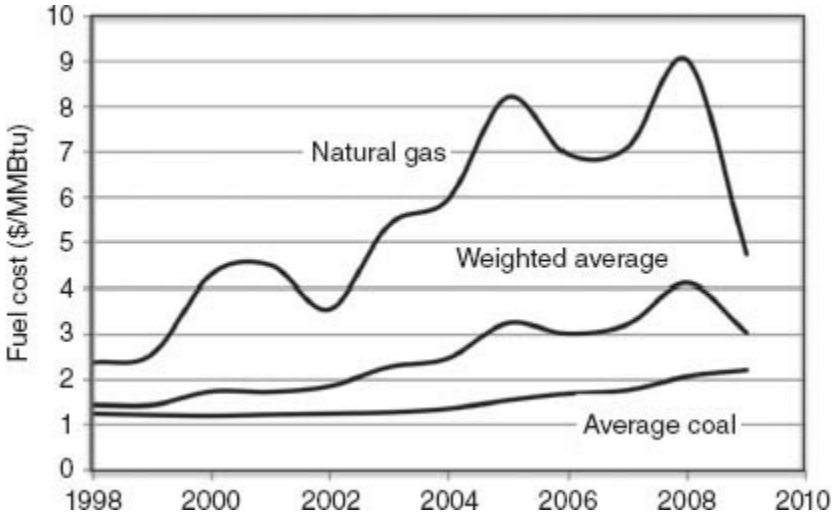
The "peakiness" of electricity demand caused by daytime-building-energy use is one of the reasons the price of electricity delivered to residential and commercial customers is typically about 50% higher than that for industrial facilities (Fig. 1.18). Industrial customers, with more uniform energy demand, can be served in a large part by less expensive, base-load plants that run more or less continuously. The distribution systems serving utilities are more uniformly loaded, reducing costs, and certainly the administrative costs to deal with customer billing and so forth are less. They also have more political influence.

FIGURE 1.18 Average U.S. retail prices for electricity (1973–2010). Note prices are not adjusted for inflation. From *EIA Annual Energy Review* (2010).



It is interesting to note the sharp increases in prices that occurred in the 1970s and early 1980s, which can be attributed to increasing fuel costs associated with the spike in OPEC oil prices in 1973 and 1979, as well as the huge increase in spending for nuclear power plant construction during that era. For the following two decades, the retail prices of electricity were quite flat, basically just rising in parallel with the average inflation rate. Then, as Figure 1.19 shows, at the turn of the twenty-first century, fuel prices and hence electricity once again began a rapid rise. Within a decade, coal prices doubled while natural gas prices quadrupled, then dramatically fell by 50%. The volatility in natural gas makes it very difficult to make long-term investment decisions about what kind of power plants to build.

FIGURE 1.19 Weighted average fossil fuel costs for U.S. power plants, 1998–2009. Data from *EIA Electric Power Annual*, 2010.



1.5 ELECTRIC POWER INFRASTRUCTURE:

GENERATION

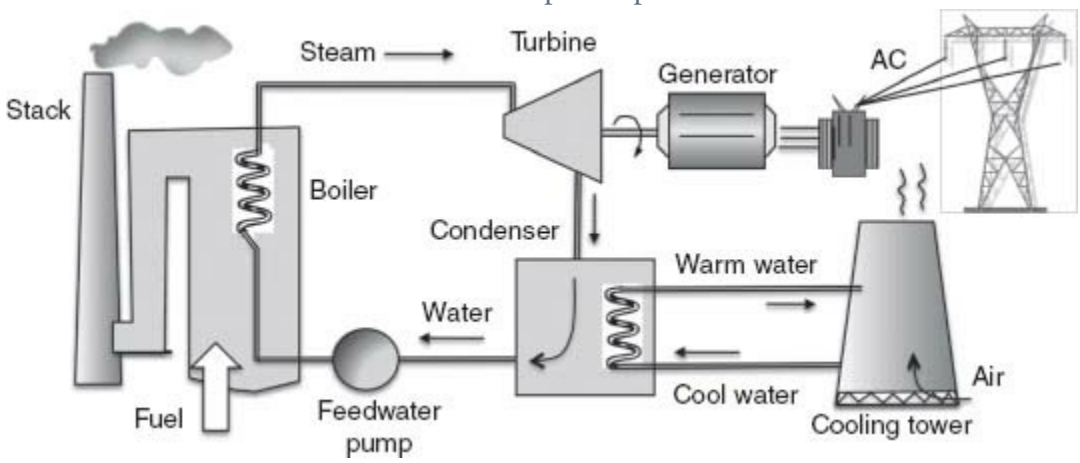
Power plants come in a wide range of sizes, run on a variety of fuels, and utilize a number of different technologies to convert fuels into electricity. Most electricity today is generated in large, central stations with power capacities measured in hundreds or even thousands of megawatts (MW). A single, large nuclear power plant, for example, generates about 1000 MW, also described as 1 gigawatt (GW). The total generation capacity of the United States is equivalent to about 1000 such power plants—that is, 1000 GW or 1 terrawatt (TW). With siting and permitting issues being so challenging, power plants are often clustered together into what is usually referred to as a *power station*. For example, the Three Gorges hydroelectric power station in China consists of 26 individual turbines, and the Fukushima Daiichi nuclear power station in Japan had six individual reactors.

About 90% of the U.S. electricity is generated in power plants that convert heat into mechanical work. The heat may be the result of nuclear reactions, fossil fuel combustion, or even concentrated sunlight focused onto a boiler. Utility-scale thermal power plants are based on either (a) the *Rankine cycle,* in which a working fluid is alternately vaporized and condensed, or (b) the *Brayton cycle,* in which the working fluid remains a gas throughout the cycle. Most *base-load* thermal power plants, which operate more or less continuously, are Rankine cycle plants in which steam is the working fluid. Most *peaking* plants, which are brought on line as needed to cover the daily rise and fall of demand, are gas turbines based on the Brayton cycle. The newest generation of thermal power plants use both cycles and are called combined-cycle plants.

1.5.1 Basic Steam Power Plants

The basic steam cycle can be used with any source of heat, including combustion of fossil fuels, nuclear fission reactions, or concentrated sunlight onto a boiler. The essence of a fossil-fuel-fired steam power plant is diagrammed in Figure 1.20. In the steam generator, fuel is burned in a firing chamber surrounded by a boiler that transfers heat through metal tubing to the working fluid. Water circulating through the boiler is converted to high pressure, high temperature steam. During this conversion of chemical to thermal energy, losses on the order of 10% occur due to incomplete combustion and loss of heat up the stack.

FIGURE 1.20 Basic fuel-fired, steam electric power plant.



High pressure steam is allowed to expand through a set of turbine wheels that spin the turbine and generator shaft. For simplicity, the turbine in Figure 1.20 is shown as a single unit, but for increased efficiency it may actually consist of two or sometimes three turbines in which the exhaust steam from a higher pressure turbine is reheated and sent to a lower pressure turbine, and so forth. The generator and turbine share the same shaft allowing the generator to convert the rotational energy of the shaft into electrical power that goes out onto the transmission lines for distribution. A well-designed turbine may have an efficiency approaching 90%, while the generator may have a conversion efficiency even higher than that.

The spent steam is drawn out of the last turbine stage by the partial vacuum created in the condenser as the cooled steam undergoes a phase change back to the liquid state. The condensed steam is then pumped back to the boiler to be reheated, completing the cycle.

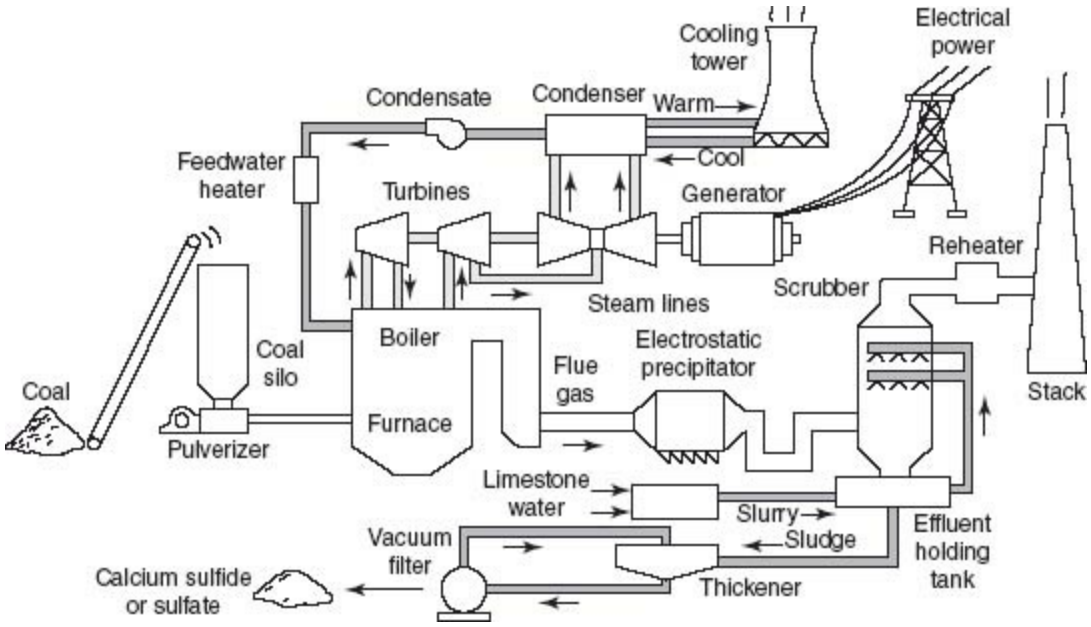
The heat released when the steam condenses is transferred to cooling water, which circulates through the condenser. Usually, cooling water is drawn from a river, lake or sea, heated in the condenser, and returned to that body of water, in which case the process is called *once-through cooling*. The more expensive approach shown in Figure 1.20 involves use of a cooling tower, which not only requires less water but it also avoids the thermal pollution associated with warming up a receiving body of water. Water from the condenser heat exchanger is sprayed into the tower and the resulting evaporation transfers heat directly into the atmosphere (see Example 1.1).

1.5.2 Coal-Fired Steam Power Plants

Coal-fired power plants built before the 1960s were notoriously dirty. Fortunately, newer plants have effective, but expensive, emission controls that significantly decrease toxic emissions (but do little to control climate-changing CO_2 emissions). Unfortunately, many of those old plants are still in operation.

Figure 1.21 shows some of the complexity that emission controls add to coal-fired steam power plants. Flue gas from the boiler is sent to an electrostatic precipitator (ESP), which adds a charge to the particulates in the gas stream so they can be attracted to electrodes that collect this fly ash. Fly ash is normally buried, but it has a much more useful application as a replacement for cement in concrete. In fact, for every ton of fly ash used in concrete, roughly 1 ton of CO_2 emissions are avoided.

FIGURE 1.21 Typical coal-fired power plant using an electrostatic precipitator for particulate control and a limestone-based SO_2 scrubber.



Next, a flue gas desulfurization (FGD, or *scrubber*) system sprays a limestone slurry over the flue gases, precipitating the sulfur to form a thick calcium sulfite sludge that must be dewatered and either buried in landfills or reprocessed into useful gypsum. As of 2010, less than half of the U.S. coal plants had scrubbers.

Not shown in Figure 1.21 are emission controls for nitrogen oxides, NO_x. Nitrogen oxides have two sources. Thermal NO_x is created when high temperatures oxidize the nitrogen (N_2) in air. Fuel NO_x results from nitrogen impurities in fossil fuels. Some NO_x emission reductions have been based on careful control of the combustion process rather than with external devices such as scrubbers and precipitators. More recently, *selective catalytic reduction* (SCR) technology has proven effective. The SCR in a coal station is similar to the catalytic converters used in cars to control emissions. Before exhaust gases enter the smokestack, they pass through the SCR where anhydrous ammonia reacts with nitrogen oxide and converts it to nitrogen and water.

Flue gas emission controls are not only very expensive, accounting for upward of 40% of the capital cost of a new coal plant, but they also drain off about 5% of the power generated by the plant, which lowers overall efficiency.

The thermal efficiency of power plants is often expressed as a *heat rate*, which is the thermal input (Btu or kJ) required to deliver 1 kWh of electrical output (1 Btu/kWh = 1.055 kJ/kWh) at the busbar. The smaller the heat rate, the higher the efficiency. In the United States, heat rates are usually expressed in Btu/kWh, which results in the following relationship between it and thermal efficiency, η.

$$\text{Heat rate (Btu/kWh)} = \frac{3412\ \text{Btu/kWh}}{\eta} \tag{1.1}$$

Or, in SI units,

$$\text{Heat rate (kJ/kWh)} = \frac{1\ \text{(kJ/s)/kW} \times 3600\ \text{s/h}}{\eta} = \frac{3600\ \text{kJ/kWh}}{\eta} \tag{1.2}$$

While Edison's first power plants in the 1880s had heat rates of about 70, 000 Btu/kWh (≈5% efficient), the average pulverized coal (PC) steam plant operating in the United States

today has an efficiency of 33% (10, 340 Btu/kWh). These plants are referred to as being subcritical in that the steam contains a two-phase mixture of steam and water at temperatures and pressures around 1000°F and 2400 lbf/in^2 (540°C, 16 MPa). With new materials and technologies, higher temperatures and pressures are possible leading to greater efficiencies. Power plants operating above 1000°F/3200 lbf/in^2 (540°C/22 MPa), called *supercritical* (SC) plants, have heat rates between 8500 and 9500 Btu/kWh. *Ultra-supercritical* (USC) plants operate above 1100°F/3500 lbf/in^2 (595°C/24 MPa) with heat rates of 7600–8500 Btu/kWh.

Example 1.1 Carbon Emissions and Water Needs of a Coal-Fired Power Plant. Consider an average PC plant with a heat rate of 10, 340 Btu/kWh burning a typical U.S. coal with a carbon content of 24.5 kgC/GJ (1 GJ = 10^9 J). About 15% of thermal losses are up the stack and the remaining 85% are taken away by cooling water.

a. Find the efficiency of the plant.

b. Find the rate of carbon and CO_2 emissions from the plant in kg/kWh.

c. If CO_2 emissions eventually are taxed at $10 per metric ton (1 metric ton = 1000 kg), what would be the additional cost of electricity from this coal plant (¢/kWh)?

d. Find the minimum flow rate of *once-through* cooling water (gal/kWh) if the temperature increase in the coolant returned to the local river cannot be more than 20°F.

e. If a cooling tower is used instead of once-through cooling, what flow rate of water (gal/kWh) taken from the local river is evaporated and lost. Assume 144 Btu are removed from the coolant for every pound of water evaporated.

Solution

a. From Equation 1.1, the efficiency of the plant is

$$\eta = \frac{3412\ \text{Btu/kWh}}{10{,}340\ \text{Btu/kWh}} = 0.33 = 33\%$$

b. The carbon emission rate would be

$$\text{C emission rate} = \frac{24.5\ \text{kgC}}{10^9\text{J}} \times \frac{10{,}340\ \text{Btu}}{\text{kWh}} \times \frac{1055\ \text{J}}{\text{Btu}} = 0.2673\ \text{kgC/kWh}$$

Recall, that CO_2 has a molecular weight of 12 + 2 × 16 = 44; so

$$\text{CO}_2\ \text{emission rate} = \frac{0.2673\ \text{kgC}}{\text{kWh}} \times \frac{44\ \text{gCO}_2}{12\ \text{gC}} = 0.98\ \text{kg CO}_2\text{/kWh}$$

This is a handy rule of thumb, that is, 1 kWh from a coal plant releases close to 1 kg of CO_2.

c. At $10/t of CO_2, the value of savings is

$$0.98\,\text{kg CO}_2\text{/kWh} \times \$10/1000\,\text{kg} = \$0.0098/\text{kWh} \approx 1¢/\text{kWh}$$

That suggests another handy rule of thumb. That is, for every $10/t CO_2 tax, add about a penny per kWh to the cost of coal-fired electricity.

d. With 67% of the input energy wasted and 85% of that being removed by the cooling water, the coolant flow rate needed for a 20°F rise will be

$$\text{Cooling water} = \frac{0.85 \times 0.67 \times 10{,}340 \text{ Btu/kWh}}{1 \text{ Btu/lb°F} \times 20\text{°F} \times 8.34 \text{ lb/gal}} = 35.3 \text{ gal } H_2O/\text{kWh}$$

(Note we have used the specific heat of water as 1 Btu/lb°F.)

e. With cooling coming from evaporation in the cooling tower,

$$\text{Make up water} = \frac{0.67 \times 0.85 \times 10{,}340 \text{ Btu/kWh}}{144 \text{ Btu/lb} \times 8.34 \text{ lb/gal}} = 4.9 \text{ gal/kWh}$$

So, to avoid thermal pollution in the river, you need to permanently remove about 5 gal of water per kWh generated.

The above example developed a couple of simple rules of thumb for coal plants based on per unit of electricity generated. Other simple generalizations can be developed based on the annual electricity generated. The annual energy delivered by a power plant can be described by its rated power (P_R), which is the power it delivers when operating at full capacity, and its capacity factor (CF), which is the ratio of the actual energy delivered to the energy that would have been delivered if the plant ran continuously at full rated power. Assuming rated power in kW, annual energy in kWh, and 24 h/d × 365 days/yr = 8760 h in a year, the annual energy delivered by a power plant is thus given by

$$\text{Annual energy (kWh/yr)} = P_R(\text{kW}) \times 8760 \text{ h/yr} \times \text{CF} \quad (1.3)$$

Another way to interpret the CF is to think of it as being the ratio of average power to rated power over a year's time.

For example, the average coal-fired power plant in the United States has a rated power of about 500 MW and an average CF of about 70%. Using Equation 1.3, the annual energy generated by such a plant would be

(1.4)

$$\text{Annual energy} = 500{,}000 \text{ kW} \times 8760 \text{ h/yr} \times 0.70 = 3.07 \times 10^9 \text{ kWh/yr}$$

Using the assumptions in Example 1.1, it was shown that a typical power plant emits 0.98 kg CO_2/kWh, which means our generic 500 MW plant emits almost exactly 3×10^9 kg (3 million metric tons) of CO_2 per year.

Similar, but more carefully done calculations than those presented above have led to a newly proposed energy-efficiency unit, called the *Rosenfeld*, in honor of Dr. Arthur Rosenfeld (Koomey et al., 2010). Dr. Rosenfeld is credited with advocating the description of the benefits of technologies that save energy (e.g., better refrigerators, lightbulbs, etc.) in terms of power plants that do not have to be built rather than in the less intuitive terms of billions of kWh saved.

The *Rosenfeld* is based on savings realized by not building a 500 MW, 33% efficient, coal-fired power plant, operating with a CF of 70%, sending power through a T&D system with 7% losses. One Rosenfeld equals an energy savings of 3 billion kWh/yr and an annual carbon reduction of 3 million metric tons of CO_2. As an example, since 1975 refrigerators have gotten 25% bigger, 60% cheaper, and the new ones use 75% less energy, resulting in an annual savings in the United States of about 200 billion kWh/yr. In Rosenfelds, that is equivalent to having eliminated the need for 200/3 = 67 500-MW coal-fired power plants

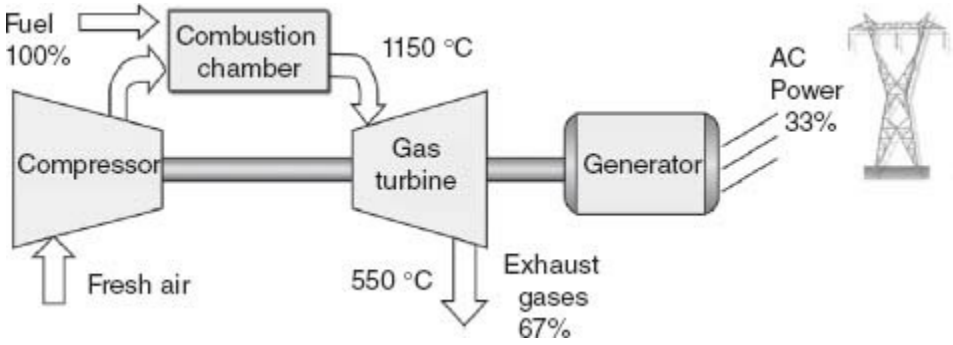
and 200 million metric tons of CO_2 per year that is not pumped into our atmosphere.

1.5.3 Gas Turbines

The characteristics of characteristics of gas turbines (GTs), also known as combustion turbines (CTs), for electricity generation are somewhat complementary to those of the steam turbine generators just discussed. Steam power plants tend to be large, coal-fired units that operate best with fairly fixed loads. They tend to have high capital costs, largely driven by required emission controls, and low operating costs since they so often use low-cost boiler fuels such as coal. Once they have been purchased, they are cheap to operate; so they usually are run more or less continuously. In contrast, GTs tend to be natural-gas-fired, smaller units, which adjust quickly and easily to changing loads. They have low capital costs and relatively high fuel costs, which means they are the most cost-effective as peaking power plants that run only intermittently. Historically, both steam and gas turbine plants have had similar efficiencies, typically in the low 30% range.

A basic simple-cycle GT driving a generator is shown in Figure 1.22. In it, fresh air is drawn into a compressor where spinning rotor blades compress the air, elevating its temperature and pressure. That hot, compressed air is mixed with fuel, usually natural gas, though LPG, kerosene, landfill gas, or oil are sometimes used, and burned in the combustion chamber. The hot exhaust gases are expanded in a turbine and released to the atmosphere. The compressor and the turbine share a connecting shaft, so that a portion, typically more than half, of the rotational energy created by the spinning turbine is used to power the compressor.

FIGURE 1.22 Basic simple-cycle gas turbine and generator.



Gas turbines have long been used in industrial applications and as such were designed strictly for stationary power systems. These *industrial gas turbines* tend to be large machines made with heavy, thick materials whose high thermal capacitance and moment of inertia reduces their ability to adjust quickly to changing loads. They are available in a range of sizes from hundreds of kilowatts to hundreds of megawatts. For the smallest units they are only about 20% efficient, but for turbines over about 10 MW they tend to have efficiencies of around 30%.

Another style of gas turbine takes advantage of the billions of dollars of development work that went into designing lightweight, compact engines for jet aircraft. The thin, light, superalloy materials used in these *aeroderivative turbines* enable fast starts and quick acceleration, so they easily adjust to rapid load changes and numerous startup/shutdown events. Their small size makes it easy to fabricate the complete unit in the factory and ship

it to a site, thereby reducing the field installation time and cost. Aeroderivative turbines are available in sizes ranging from a few kilowatts up to about 50 MW. In their larger sizes, they achieve efficiencies exceeding 40%.

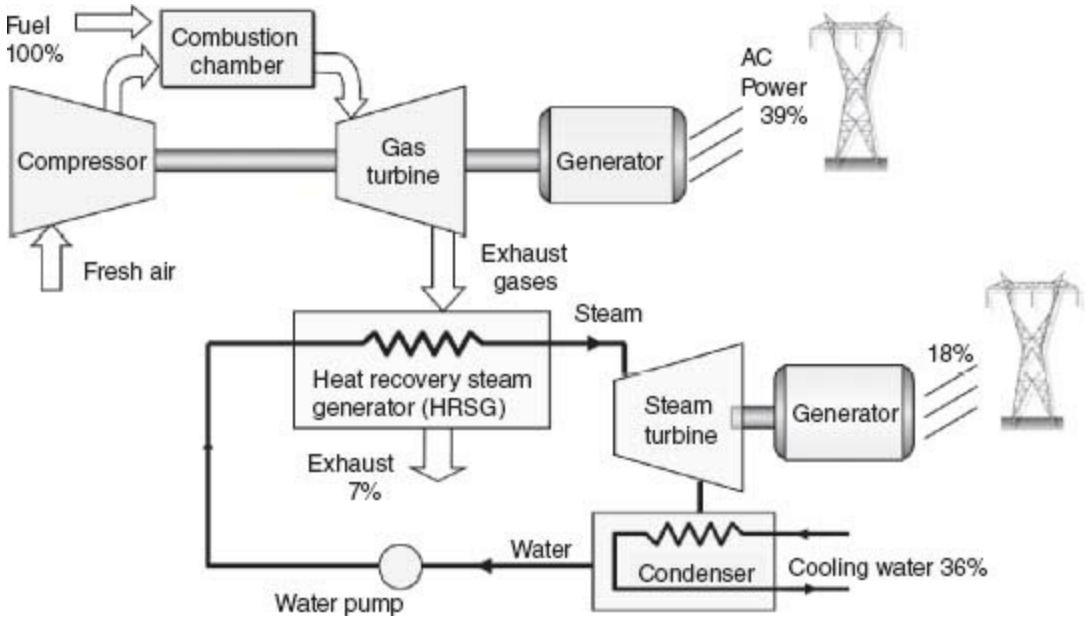
One way to increase the efficiency of gas turbines is to add a heat exchanger, called a heat recovery steam generator (HRSG) to capture some of the waste heat from the turbine. Water pumped through the HRSG turns to steam, which is injected back into the airstream coming from the compressor. The injected steam displaces a portion of the fuel heat that would otherwise be needed in the combustion chamber. These units, called steam-injected gas turbines (STIG), can have efficiencies approaching 45%. Moreover, the injected steam reduces combustion temperatures, which helps control NO_x emissions. They are considerably more expensive than simple GTs due to the extra cost of the HRSG and the care that must be taken to purify the incoming feedwater.

1.5.4 Combined-Cycle Power Plants

Note the temperature of the gases exhausted into the atmosphere in the simple-cycle GT shown in Figure 1.22 is over 500°C. Clearly that is a tremendous waste of high quality heat that could be captured and put to good use. One way to do so is to pass those hot gases through a heat exchanger to boil water and make steam. The heat exchanger is called an HRSG and the resulting steam can be put to work in a number of applications, including industrial process heating or water and space heating for buildings. Of course, such *combined heat and power* (CHP) applications are viable only if the GT is located very close to the site where its waste heat can be utilized. Such CHP systems will be considered in a later chapter.

A more viable alternative is to use the steam generated in an HRSG to power a second-stage steam turbine to generate more electricity as shown in Figure 1.23. Working together, such natural-gas-fired, combined-cycle power plants (NGCCs) have heat rates of 6300–7600 Btu/kWh (45–54% efficiency). New ones being proposed may reach 60%. If the decline in natural gas prices and rise in coal prices shown in Figure 1.19 provides any indication of the future, coupled with the lower carbon emissions when natural gas is used, these NGCC plants will provide stiff competition for the next generation of supercritical or ultra-supercritical coal plants being proposed.

FIGURE 1.23 Combined-cycle power plants have achieved efficiencies approaching 60%.



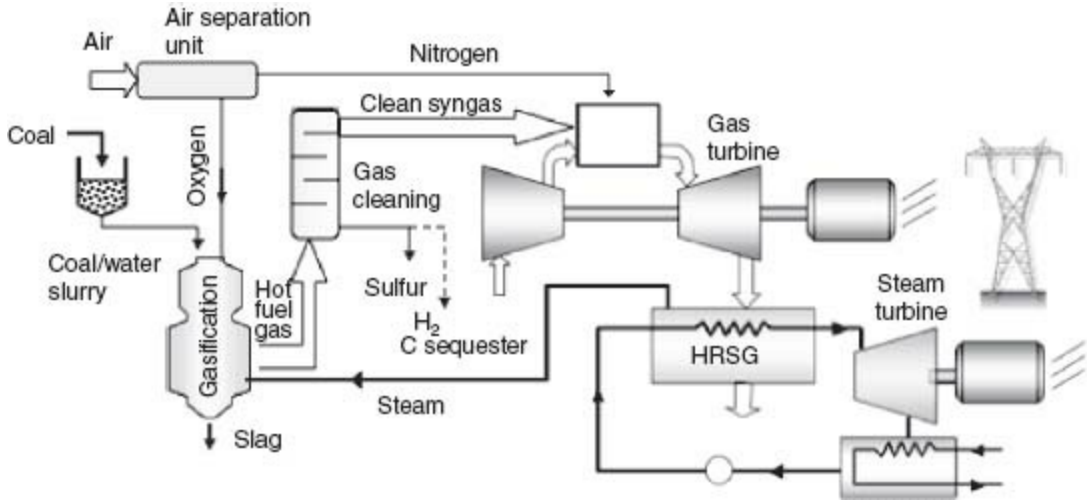
1.5.5 Integrated Gasification Combined-Cycle Power Plants

With combined-cycle plants achieving such high efficiencies, and with natural gas being an inherently cleaner fuel, the trend in the United States has been away from building new coal-fired power plants. Coal, however, is a much more abundant fuel than natural gas, but in its conventional, solid form, it cannot be used in a gas turbine. Erosion and corrosion of turbine blades due to impurities in coal would quickly ruin a gas turbine. However, coal can be processed to convert it into a synthetic gas, which can be burned in what is called an *integrated gasification, combined-cycle* (IGCC) power plant.

Gas derived from coal, called "town gas, " was popular in the late 1800s before the discovery of large deposits of natural gas. One hundred years later, coal's air pollution problems prompted the refinement of technologies for coal gasification. Several gasification processes have been developed, primarily in the Great Plains Gasification Plant in Beulah, ND, in the 1970s and later in the 100 MW Cool Water project near Barstow, CA, in the 1980s.

As shown in Figure 1.24, the essence of an IGCC consists of bringing a coal-water slurry into contact with steam to form a fuel gas consisting mostly of carbon monoxide (CO) and hydrogen (H_2). The fuel gas is cleaned up, removing most of the particulates, mercury and sulfur, and then burned in the GT. Air used in the combustion process is first separated into nitrogen and oxygen. The nitrogen is used to cool the GT and the oxygen is mixed with the gasified coal, which helps increase combustion efficiency. Despite energy losses in the gasification process, by taking advantage of combined-cycle power generation, an IGCC should be able to burn coal with an overall thermal efficiency of perhaps 40%. This is considerably higher than the conventional PC plants, about the same as SC plants, but below the efficiency of USC plants.

FIGURE 1.24 An integrated gasification, combined-cycle (IGCC) power plant.



An advantage of IGCC, relative to SC plants, is that the CO_2 produced by the process is in a concentrated, high pressure gas stream, which makes it easier to separate and capture than is the case for ordinary low pressure flue gases. If a carbon sequestration technology could be developed to store that carbon in perpetuity, it might be possible to envision a future with carbon-free, high efficiency, coal-fired power plants capable of supplying clean electricity for several centuries into the future.

IGCC plants are more expensive than pulverized coal and they have trouble competing economically with NGCC plants. As of 2010, there were only five coal-based IGCC plants in the world; two of which were in the United States. The potential for future natural gas prices to rise, coupled with the possibility of a future cost for carbon emissions and the potential to remove and sequester carbon from the syngas before it is burned have kept the interest in IGCC plants alive. Their future, however, is quite uncertain.

1.5.6 Nuclear Power

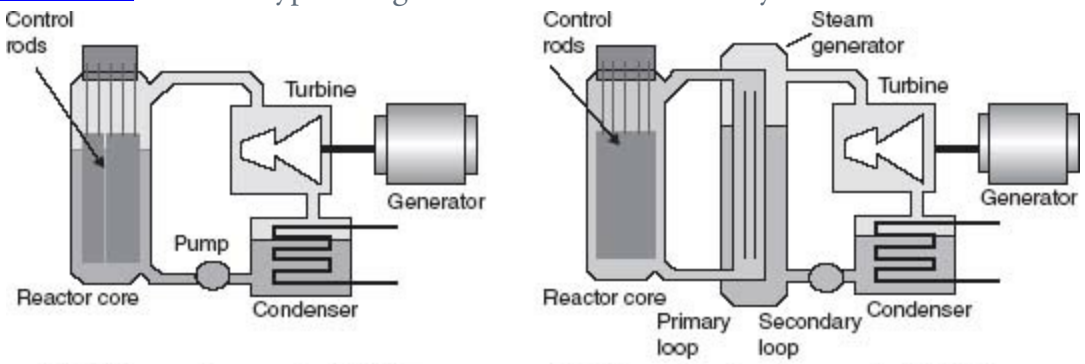
Nuclear power has had a rocky history, leading it from its glory days in the 1970s as a technology thought to be "too cheap to meter, " to a technology that in the 1980s some characterized as "too expensive to matter." The truth is probably somewhere in the middle. If the embodied carbon associated with construction is ignored, reactors do have the advantage of being essentially a carbon-free source of electric power, so climate concerns are helping nuclear power begin to enjoy a resurgence of interest. After the 2011 Japanese meltdowns at Fukushima, whether a new generation of cheaper, safer reactors can overcome public misgivings over safety, where to bury radioactive wastes, and how to keep plutonium from falling into the wrong hands, remains to be seen.

The essence of the nuclear reactor technology is basically the same simple steam cycle described for fossil-fueled power plants. The main difference is the heat is created by nuclear reactions instead of fossil fuel combustion.

Light Water Reactors: Water in a reactor core not only acts as the working fluid, it also serves as a *moderator* to slow down the neutrons ejected when uranium fissions. In *light water reactors* (LWRs), ordinary water is used as the moderator. Figure 1.25 illustrates the two principal types of LWRs—(a) *boiling water reactors* (BWRs), which make steam by boiling water within the reactor core itself and (b) *pressurized water reactors* (PWRs) in which a separate heat exchanger, called a steam generator, is used. PWRs are more

complicated, but they can operate at higher temperatures than BWRs and hence are somewhat more efficient. PWRs can be somewhat safer since a fuel leak would not pass any radioactive contaminants into the turbine and condenser. Both types of reactors are used in the United States, but the majority are PWRs.

FIGURE 1.25 The two types of light water reactors commonly used in the United States.



(a) Boilling water reactor (BWR) (b) Pressurized water reactor (PWR)

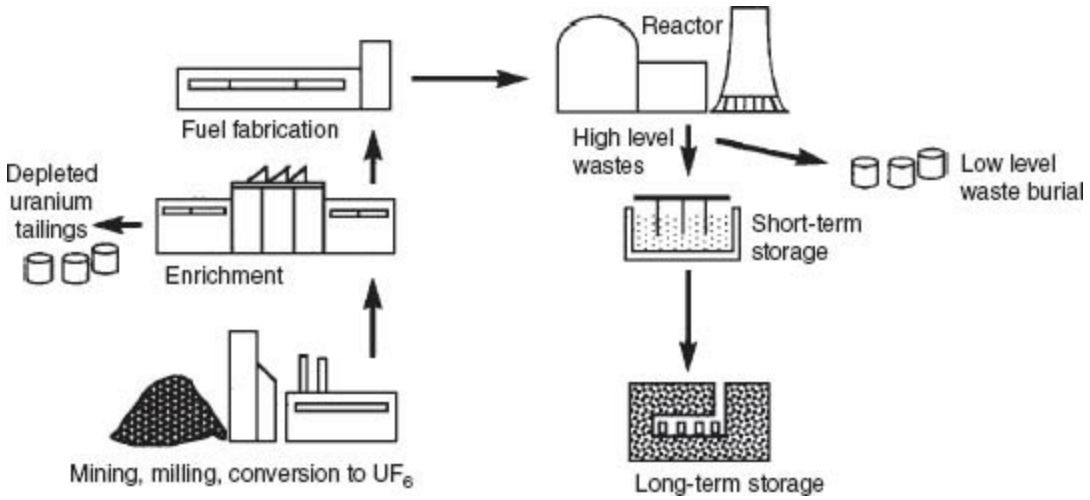
Heavy Water Reactors: Reactors commonly used in Canada use heavy water; that is, water in which some of the hydrogen atoms are replaced with deuterium (hydrogen with an added neutron). The deuterium in heavy water is more effective in slowing down neutrons than ordinary hydrogen. The advantage in these Canadian deuterium reactors (commonly called CANDU) is that ordinary uranium as mined, which contains only 0.7% of the fissile isotope U-235, can be used without the enrichment that LWRs require.

High Temperature, Gas-Cooled Reactors (HTGR): HTGRs use helium as the reactor core coolant rather than water, and in some designs it is helium itself that drives the turbine. These reactors operate at considerably higher temperatures than conventional water-moderated reactors, which means their efficiencies can be higher—upward of 45% rather than the 33% that typifies LWRs.

There are two HTGR concepts under development—the Prismatic Fuel Modular Reactor (GT-MHR) based on German technology and the Modular Pebble Bed Reactor (MPBR) which is being developed in South Africa. Both are based on microspheres of fuel, but differ in how they are configured in the reactor. The MPBR incorporates the fuel microspheres in carbon-coated balls ("pebbles") roughly 2 in in diameter. One reactor will contain close to half a million such balls. The advantage of a pebble reactor is that it can be refueled continuously by adding new balls and withdrawing spent fuel balls without having to shut down the reactor.

The Nuclear Fuel "Cycle": The costs and concerns for nuclear fission are not confined to the reactor itself. Figure 1.26 shows current practice from mining and processing of uranium ores, to enrichment that raises the concentration of U-235, to fuel fabrication and shipment to reactors. Highly radioactive spent fuel removed from the reactors these days sits on-site in short-term storage facilities while we await a longer-term storage solution such as the underground federal repository that had been planned for Yucca Mountain, Nevada. Eventually, after 40 years or so, the reactor itself will have to be decommissioned and its radioactive components will also have to be transported to a secure disposal site.

FIGURE 1.26 A once-through fuel system for nuclear reactors.



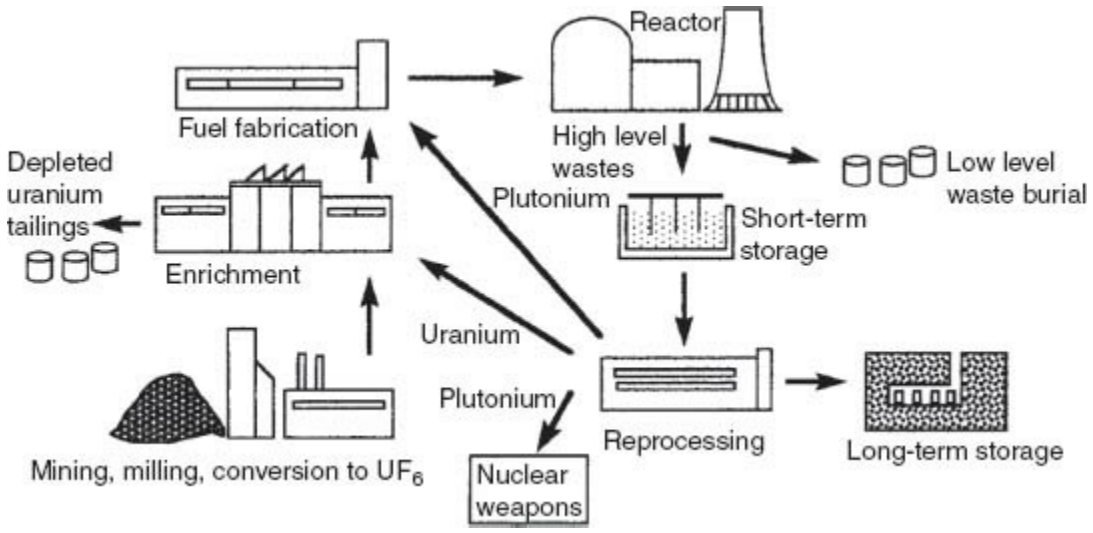
Reactor wastes contain not only the fission fragments formed during the reactions, which tend to have half-lives measured in decades, but also include some radionuclides with very long half-lives. Of major concern is plutonium, which has a half-life of 24, 390 years. Only a few percent of the uranium atoms in reactor fuel is the fissile isotope U-235, while essentially all of the rest is U-238, which does not fission. Uranium-238 can, however, capture a neutron and be transformed into plutonium as the following reactions suggest.

$$(1.5)\ {}^{238}_{92}\mathrm{U} + n \rightarrow {}^{239}_{92}\mathrm{U} \xrightarrow{\beta} {}^{239}_{93}\mathrm{Np} \xrightarrow{\beta} {}^{239}_{94}\mathrm{Pu}$$

This plutonium, along with several other long-lived radionuclides, makes nuclear wastes dangerously radioactive for tens of thousands of years, which greatly increases the difficulty of providing safe disposal. Removing the plutonium from nuclear wastes before disposal has been proposed as a way to shorten the decay period but that introduces another problem. Plutonium not only is radioactive and highly toxic, it is also the critical ingredient in the manufacture of nuclear weapons. A single nuclear reactor produces enough plutonium each year to make dozens of small atomic bombs and some have argued that if the plutonium is separated from nuclear wastes, the risk of illicit diversions for such weapons would cause an unacceptable risk.

On the other hand, plutonium is a fissile material, which, if separated from the wastes, can be used as a reactor fuel (Fig. 1.27). Indeed, France, Japan, Russia, and the United Kingdom have reprocessing plants in operation to capture and reuse that plutonium. In the United States, however, Presidents Ford and Carter considered the proliferation risk too high and commercial reprocessing of wastes has ever since not been allowed.

FIGURE 1.27 Nuclear fuel cycle with reprocessing.



1.6 FINANCIAL ASPECTS OF CONVENTIONAL POWER PLANTS

A very simple model of power plant economics takes all of the costs and puts them into two categories—fixed costs and variable costs. Fixed costs are monies that must be spent even if the power plant is never turned on; they include such things as capital costs, taxes, insurance, property taxes, corporate taxes, and any fixed operations and maintenance (O&M) costs that will be incurred even when the plant is not operated. Variable costs are the added costs associated with actually running the plant. These are mostly fuel plus variable operations and maintenance costs.

1.6.1 Annualized Fixed Costs

To keep our analysis simple means ignoring many details which are more easily considered with a spreadsheet approach described in Appendix A. For example, a distinction can be made between "overnight" (or "instant") construction costs versus total installed cost (or "all-in cost"). The former refers to what it would cost to build the plant if no interest is incurred during construction, that is, if you could build the whole thing overnight. The installed cost is the overnight cost plus finance charges associated with capital during construction. The difference can be considerable for projects that take a long time to construct, which is an important distinction that needs to be made when comparing large conventional plants having long lead times versus smaller distributed generation.

A first cut at annualizing fixed costs is to lump all of its components into a single total that can then be multiplied by *fixed charge rate (FCR).* The FCR accounts for interest on loans and acceptable returns for investors (both of which depend on the perceived risks for the project and on the type of ownership), fixed operation and maintenance (O&M) charges, taxes, and so forth. Since FCR depends primarily on the cost of capital, it varies as interest rates change. With rated power of the plant P_R and a capital cost expressed in the usual way ($/kW)

$$\text{Annual fixed costs (\$/yr)} = P_R\ \text{(kW)} \times \text{Capital cost (\$/kW)} \times \text{FCR (\%/yr)} \tag{1.6}$$

Another complication is associated with the potentially ambiguous definition of the rated capacity of a power plant, P_R. It normally refers to the power delivered at the busbar connection to the grid, which means it includes on-site power needs as well as the transformer that raises the voltage to grid levels, but does not include the losses in getting the power to consumers. To do a fair comparison between a small, distributed generation system with no T&D losses versus a central power plant hundreds of miles away from loads, that distinction can be significant.

As described earlier, there are three types of ownership to be considered—investor owned utilities (IOUs), publicly owned utilities (POUs), and privately owned merchant plants. Merchant plants and IOUs are financed with a mix of loans (debt) and money provided by investors (equity). POUs are financed entirely with debt. Debt rates tend to be considerably below the returns expected by investors, so there are advantages to using high fractions of conventional loans subject to constraints set by lending agencies. As might be expected from the estimates of financing rates and investor participation shown in Table 1.3, merchant plants tend to be the most expensive since they have higher financing costs. Least expensive are POU plants since they have the lowest financing costs and are also exempt from a number of the taxes that other ownership structures must contend with.

TABLE 1.3 Example Capital-Cost Default Values

Ownership	Capital Structure		Cost of Capital		Weighted Average Cost of Capital (WACC) (%)
	Equity (%)	Debt (%)	Equity Rate (%)	Debt Rate (%)	
Merchant (fossil fuel)	60	40	12.50	7.50	10.50
Merchant (nonfossil)	40	60	12.50	7.50	9.50
Investor-owned utility (IOU)	50	50	10.50	5.00	7.75
Publicly owned utility (POU)	0	100	0.00	4.50	4.50

We can annualize debt and equity by taking a weighted average and then treating that as a single loan interest rate that is to be repaid in equal annual payments. Annual payments A ($/yr) on a loan of P ($) with interest rate i (%/yr) paid over a term of n years can be calculated using the following *capital recovery factor* (*CRF*).

$$A(\$/\text{yr}) = P(\$) \cdot \text{CRF}(\%/\text{yr}) \quad \text{where } CRF = \frac{i(1+i)^n}{[(1+i)^n - 1]} \tag{1.7}$$

Most of the FCR in Equation 1.6 can be estimated using the above CRF. The rest of the FCR is made up of insurance, property taxes, fixed O&M, and corporate taxes. The California Energy Commission adds about 2 percentage points to the CRF to account for these factors. Merchant and IOU plants need to add another 3–4 percentage points to their CRF to cover their corporate taxes, which is another way that POUs that pay no corporate taxes have an advantage (CEC, 2010).

Annual fixed costs are often expressed with units of $/yr-kW of rated power.

Example 1.2 Annual Fixed Costs for an NGCC Plant. Consider a natural-gas fired, combined cycle power plant with a total installed cost of $1300/kW. Assume this is an IOU with 52% equity financing at 11.85% and 48% debt at 5.40% with investments

"booked" on a 20-year term. Add 2% of the capital cost per year to account for insurance, property taxes, variable O&M, and another 4% for corporate taxes. Find the annual fixed cost of this plant ($/yr-kW).

Solution. First, find the weighted average cost of capital.

$$\text{Average cost of capital} = 0.52 \times 11.85\% + 0.48 \times 5.40\% = 8.754\%$$

Using Equation 1.7 with this interest rate and a 20-year term gives

$$\text{CRF} = \frac{0.08754\,(1+0.08754)^{20}}{\left[(1+0.08754)^{20}-1\right]} = 0.10763/\text{yr} = 10.763\%/\text{yr}$$

Adding the other charges gives a total FCR of

$$\begin{aligned}\text{FCR} &= 10.763\%\ (\text{finance}) + 2\%\ (\text{fixed O\&M, insurance, etc.}) + 4\%\ (\text{taxes})\\ &= 16.763\%\end{aligned}$$

From Equation 1.6, the annual fixed cost of the plant per kW of rated power would be

$$\text{Annual fixed cost} = \$1300/\text{kW} \times 0.16763/\text{yr} = \$218/\text{yr-kW}$$

1.6.2 The Levelized Cost of Energy (LCOE)

The variable costs, which also need to be annualized, depend on the annual fuel demand, the unit cost of fuel, and the O&M rate for the actual operation of the plant.

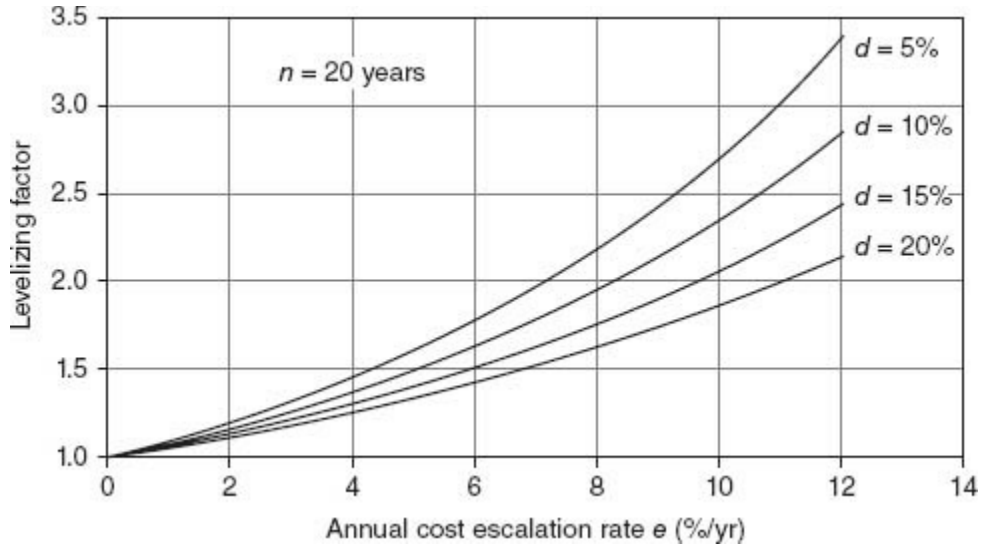
$$\text{Variable costs (\$/yr)} = [\text{Fuel} + \text{O\&M}]\ \$/\text{kWh} \times \text{Annual energy (kWh/yr)} \tag{1.8}$$

Annual energy delivered depends on the rated power of the plant and its capacity factor.

$$\text{Annual energy (kWh/yr)} = P_R\ (\text{kW}) \times 8760\ \text{hr/yr} \times \text{CF} \tag{1.9}$$

The cost of fuel is often expressed in dollars per million Btu ($/MMBtu) at current prices. Since fuel costs are so volatile (e.g., Fig. 1.19), estimating the levelized cost of fuel over the life of the economic analysis is a challenge. One approach, described more carefully in Appendix A, introduces a levelizing factor (LF), which depends on an estimate of the fuel price escalation rate and the owner's discount factor. Figure 1.28 shows, for example, that if fuel escalates at a nominal 5%/yr and if future costs are discounted at a 10% rate (e.g., $1.10 cost a year from now has a discounted cost today of $1.00), the LF is about 1.5.

FIGURE 1.28 Levelizing factors for a 20-year term as a function of the escalation rate of annual costs with the owner's discount rate as a parameter. The derivation of this figure is provided in Appendix A.



The annualized fuel cost is thus

(1.10)
$$\text{Fuel (\$/yr)} = \text{Energy (kWh/yr)} \times \text{Heat rate (Btu/kWh)} \times \text{Fuel cost (\$/Btu)} \times \text{LF}$$

The other important component of annual cost is the operations and maintenance (O&M) cost associated with running the plant. Those are often expressed in $/kWh.

Combining the annual fixed cost and the annualized variable cost, divided by the annual kWh generated gives the levelized cost of energy.

(1.11)
$$\text{LCOE (\$/kWh)} = \frac{[\text{Annual fixed cost} + \text{Annual variable cost}]\ (\$/\text{yr})}{\text{Annual output (kWh/yr)}}$$

or, on a per kW of rated power basis, LCOE can be written as

(1.12)
$$\text{LCOE (\$/kWh)} = \frac{[\text{Annual fixed cost} + \text{Annual variable cost}]\ (\$/\text{kW-yr})}{8760\ \text{h/yr} \times \text{CF}}$$

Example 1.3 LCOE for an NGCC Plant. The levelized fixed cost of the NGCC plant in Example 1.2 was found to be $218/yr-kW. Suppose natural gas now costs $6/MMBtu and in the future it is projected to rise at 5%/yr. The owners have a 10% discount factor. Annual O&M adds another 0.4 ¢/kWh. If its heat rate is 6900 Btu/kWh and the plant has a 70% CF, find its LCOE.

Solution. Using Equation 1.9 with an assumed 1 kW of rated power, the annual energy delivered per kW of rated power is

$$\text{Annual energy} = 1\ \text{kW} \times 8760\ \text{h/yr} \times 0.70 = 6132\ \text{kWh/yr}$$

From Figure 1.28 the levelizing factor for fuel is 1.5. From Equation 1.10, the annualized fuel cost per kW is

$$\text{Annual fuel cost (per kW)} = 6132\ \text{kWh/yr} \times 6900\ \text{Btu/kWh} \times \$6/10^6\ \text{Btu} \times 1.5 = \$381/\text{yr}$$

Annual O&M adds another $0.004/kWh × 6132 kWh/yr = $25/yr

$$\text{Total variable costs (per kW)} = \$381 + \$25 = \$406/\text{yr}$$

Adding the $218/yr-kW for annualized fixed costs gives a total

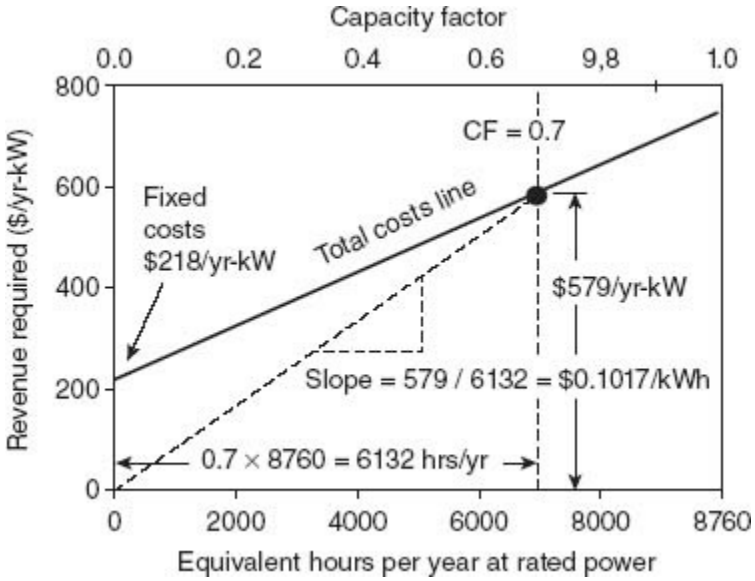
$$\text{Total annualized costs} = (\$218 + \$406)\ \$/\text{yr-kW}$$

Using Equation 1.12, the total levelized cost is therefore

$$\text{LCOE} = \frac{\$218/\text{yr-kW} + \$406/\text{yr-kW}}{8760\ \text{h/yr} \times 0.70} = \$0.1017/\text{kWh} = 10.17¢/\text{kWh}$$

The LCOE results derived in Example 1.3 were based on a particular value of capacity factor. As shown in Figure 1.29, it is very straightforward, of course, to vary CF and see how it affects LCOE. If we reinterpret capacity factor to have it represent the equivalent number of hours per year of plant operation at rated power, then the slope of a line drawn from the origin to a spot on the total costs line is equal to the LCOE. Clearly, the average cost increases as CF decreases, which helps explain why peaking power plants that operate only a few hours each day have such a high average cost of electricity.

FIGURE 1.29 A graphical presentation of Examples 1.2 and 1.3. The average cost of electricity is the slope of a line drawn from the origin to the revenue curve that corresponds to the capacity factor.



1.6.3 Screening Curves

Some technologies, such as coal and nuclear plants, tend to be expensive to build and cheap to operate, so they make sense only if they run most of the time. Others, such as combustion turbine (CT), are just the opposite—cheap to build and expensive to operate, so they are better suited as peakers. An economically efficient power system will include a mix of power plant types appropriate to the amount of time those plants actually are in operation.

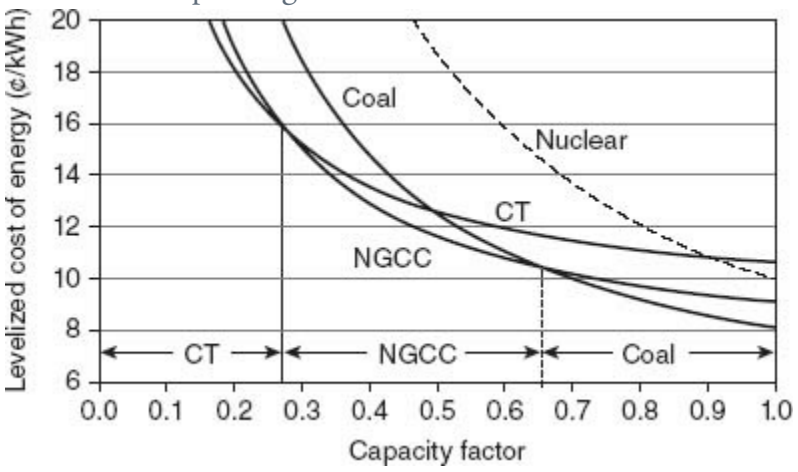
Example 1.3 laid out the process for combining various key cost parameters to create an estimate of the levelized cost of electricity as a function of the CF. Based on the assumptions shown in Table 1.4, the LCOE for four types of power plants are compared—a simple-cycle CT, a pulverized coal plant, a combined-cycle plant, and a new nuclear power plant. These are referred to as *screening curves*. As can be seen, for this example, CT is the least expensive option as long as it runs with a CF < 0.27, which means it is the best

choice for a peaker plant that operates only a few hours each day (in this case about 6.5 h/d). The coal plant is most cost-effective when it runs with CF > 0.65 (almost 16 h/d), which makes it a good base-load plant. The combined-cycle plant fits in the middle and is a good intermediate, load-following plant.

TABLE 1.4 Assumptions Used to Generate Figure 1.30

Technology	Fuel	Capital Cost ($/kW)	Heat Rate (Btu/kWh)	Variable O&M (¢/kWh)	Fuel Price ($/MMBtu)	Fuel Levelization	FCR
Pulverized coal-steam	Coal	2300	8750	0.40	2.50	1.5	0.167
Combustion turbine	Gas	990	9300	0.40	6.00	1.5	0.167
Combined cycle	Gas	1300	6900	0.40	6.00	1.5	0.167
Nuclear	U-235	4500	10,500	0.40	0.60	1.5	0.167

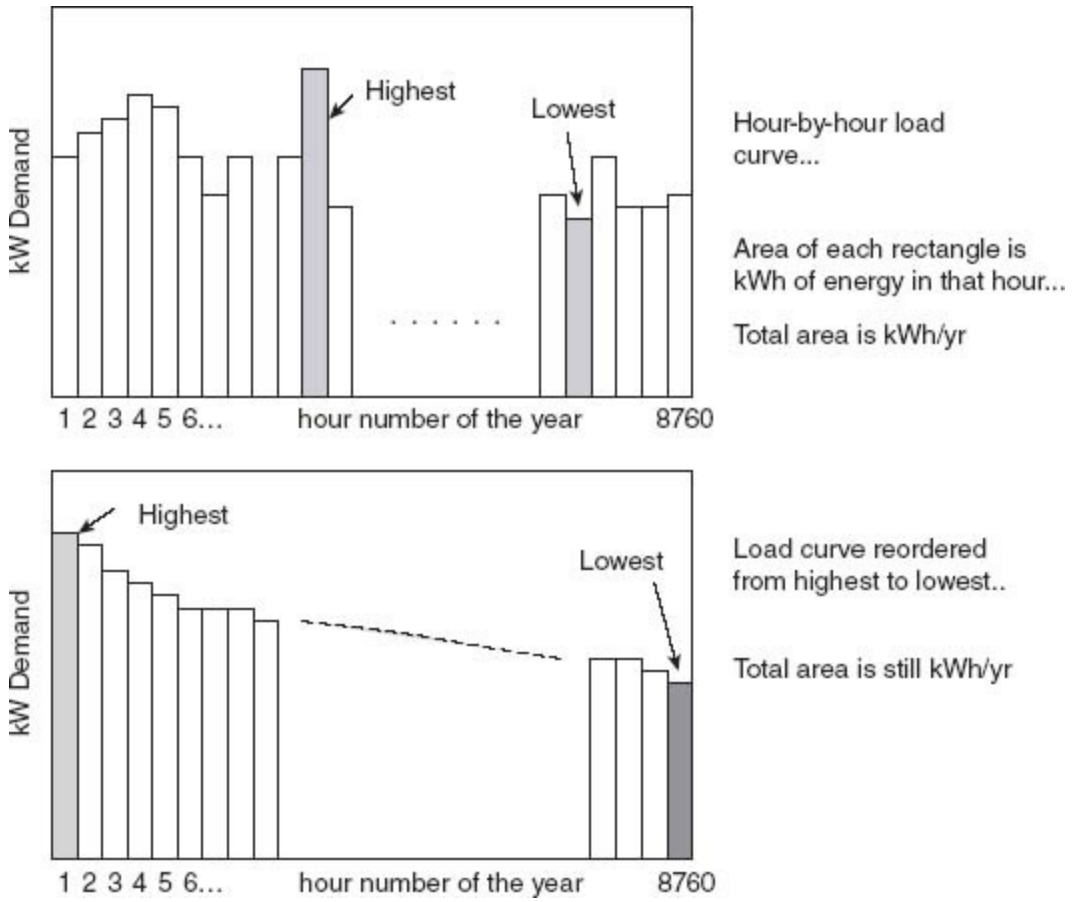
FIGURE 1.30 Screening curves for coal-steam, combustion turbine, combined-cycle, and nuclear plants based on assumptions given in Table 1.4.



1.6.4 Load Duration Curves

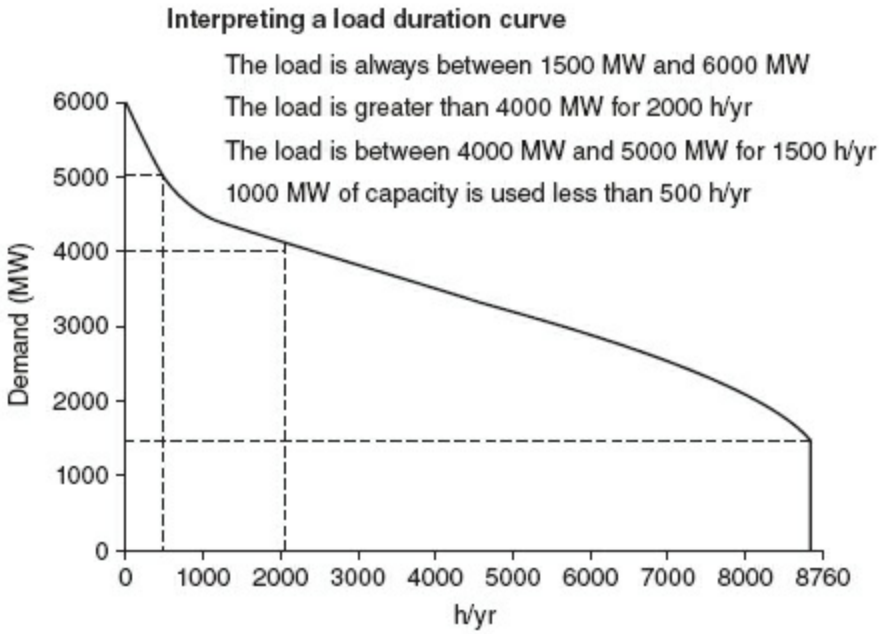
We can imagine a load versus time curve, such as those shown in Figures 1.12 and 1.31, as being a series of one-hour power demands arranged in chronological order. Each slice of the load curve has a height equal to the power (kW) and a width equal to the time (1 h); so its area is kWh of energy used in that hour. As suggested in Figure 1.31, if we rearrange those vertical slices, ordering them from the highest kW demand to the lowest through an entire year of 8760 hours, we get something called a *load duration curve*. The area under the load duration curve is the total kWh of electricity used per year.

FIGURE 1.31 A load duration curve is simply the hour-by-hour load curve rearranged from chronological order into an order based on magnitude. The area under the curve is the total kWh/yr.



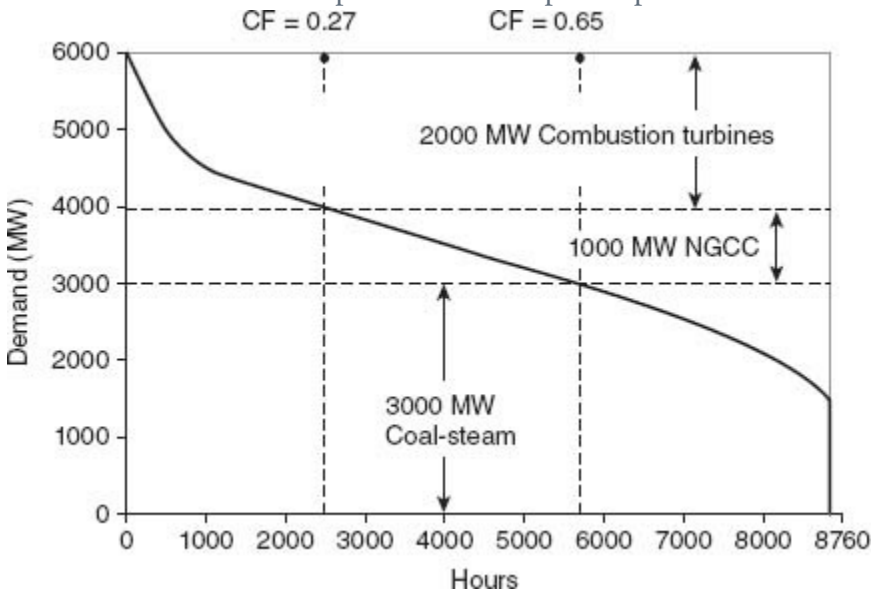
A smooth version of a load duration curve is shown in Figure 1.32. Note the *x*-axis is still measured in hours, but now a different way to interpret the curve presents itself. The graph tells how many hours per year the load (MW) is equal to or above a particular value. For example, in the figure, the load is always above 1500 MW and below 6000 MW. It is above 4000 MW for 2500 h each year, and it is above 5000 MW for only about 500 h/yr. That means it is between 4000 MW and 5000 MW for about 2000 h/yr. It also means that 1000 MW of generation, 16.7% is in use less than 500 h/yr and sits idle for 94% of the time. In California, 25% of generation capacity is idle 90% of the time.

FIGURE 1.32 Interpreting a load duration curve.



By entering the crossover points from the resource screening curves (Fig. 1.30) into the load duration curve, it is easy to come up with a first-order estimate of the optimal mix of power plants. For example, the crossover between combustion turbines and combined-cycle plants in Figure 1.30 occurs at a CF of about 0.27, which corresponds to 0.27 × 8760 = 2500 h of operation (at rated power), while the crossover between combined cycle and coal-steam is at CF = 0.65 (5700 h). Putting those onto the load duration curve helps identify the number of MW of each kind of power plant this utility should have. As shown in Figure 1.30, coal plants are the cheapest option as long as they operate for more than 5700 h/yr. The load duration curve (Fig. 1.33) indicates that the demand is at least 3000 MW for 5700 hours. Therefore, we should have 3000 MW of base-load, coal-steam plants in the mix.

FIGURE 1.33 Plotting the crossover points from screening curves (Fig. 1.30) onto the load duration curve to determine an optimum mix of power plants.

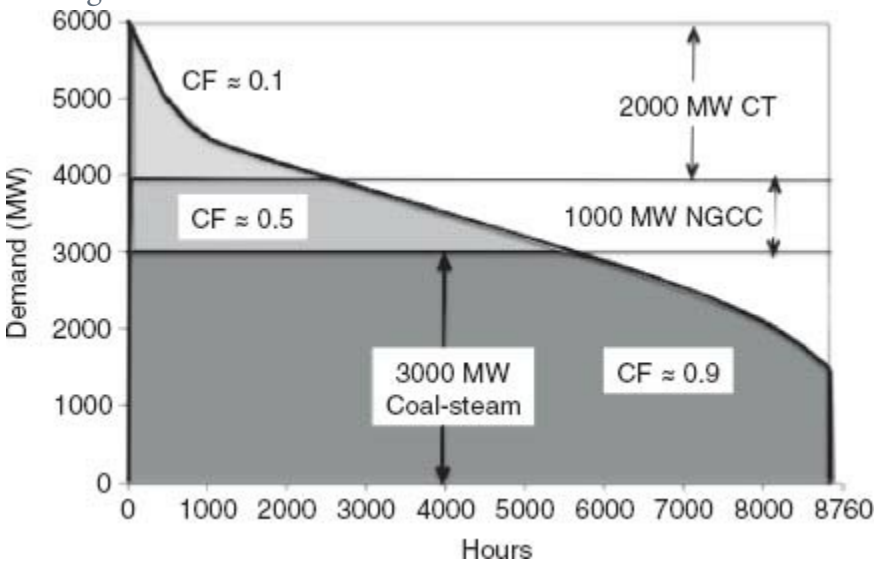


Similarly, combustion turbines are the most effective if they operate less than 0.27 CF or

less than 2500 h/yr. Similarly, combined-cycle plants need to operate at least 2500 h/yr and less than 5700 h to be the most cost-effective. The screening curve tells us that 1000 MW of these intermediate plants would operate within that range. Finally, since CTs are the most cost-effective if they operate less than CF 2500 h/yr (CF, 0.27) and the load duration curve tells us the demand is between 4000and 6000 MW for 2500 h, the mix should contain 2000 MW of peaking CTs.

The generation mix shown on a load duration curve allows us to find the average capacity factor for each type of generating plant in the mix, which will determine the average cost of electricity for each type. Figure 1.34 shows rectangular horizontal slices corresponding to the energy that would be generated by each plant type if it operated continuously. The shaded portion of each slice is the energy actually generated. The ratio of shaded area to total rectangle area is the CF for each. The base-load coal plants operate with a CF of about 0.9, the intermediate-load combined-cycle plants operate with a CF of about 0.5, and the peaking combustion turbines have a CF of about 0.1.

FIGURE 1.34 The fraction of each horizontal rectangle that is shaded is the capacity factor for that portion of generation facilities.



Mapping those capacity factors onto the screening curves in Figure 1.30 indicates new coal plants delivering electricity at 8.6 ¢/kWh, the NGCC plants at 11.6 ¢/kWh, and the CTs delivering power at 27.7 ¢/kWh. The peaker plant electricity is so much more expensive in part because they have a lower efficiency while burning the more expensive natural gas, but mostly because their capital cost is spread over so few kilowatt-hours of output since they are used so little.

Using screening curves for generation planning is merely a first cut at determining what a utility should build to keep up with changing loads and aging existing plants. Unless the load duration curve already accounts for a cushion of excess capacity, called the *reserve margin*, the generation mix just estimated would have to be augmented to allow for plant outages, sudden peaks in demand, and other complicating factors.

The process of selecting which plants to operate at any given time is called *dispatching*. Since costs already incurred to build power plants (sunk costs) must be paid no matter what, it makes sense to dispatch plants in the order of their operating costs, from the lowest to the highest. Hydroelectric plants are a special case since they must be operated with

multiple constraints, including the need for water supply, flood control, and irrigation, as well as insuring proper flows for downstream ecosystems. Hydro is especially useful as a dispatchable source backup to other intermittent renewable energy systems.

1.6.5 Including the Impact of Carbon Costs and Other Externalities

With such a range of generation technologies to choose from, how should a utility, or society in general, make decisions about which ones to use? An economic analysis is of course the central basis for comparison. Costs of construction, fuel, O&M, and financing are crucial factors. Some of these can be straightforward engineering and accounting estimates and others, such as the future cost of fuel and whether there will be a carbon tax and if so, how much and when, require something akin to a crystal ball. Even if these cost estimates can all be agreed upon, there are other additional *externalities*, that the society must bear that are not usually included in such calculations, such as health care and other costs of the pollution produced. Other complicating factors include the vulnerability we expose ourselves to with large, centralized power plants, transmission lines, pipelines, and other infrastructure that may fail due to natural disasters, such as hurricanes and earthquakes, or less natural ones, due to terrorism or war.

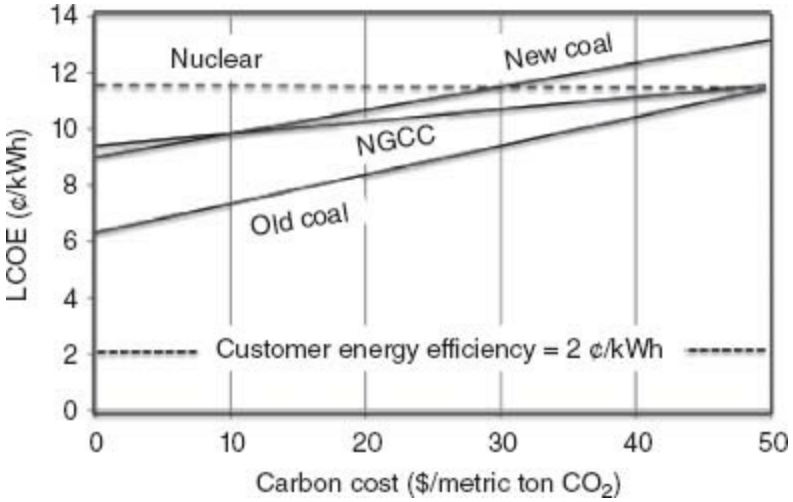
As concerns about climate change grow, there is increasing attention to the importance of carbon emissions from power plants. The shift from coal-fired power plants to more efficient plants powered by natural gas can greatly reduce those emissions. Reductions result from the increased efficiency that many of these plants have, especially, compared with the existing coal plants, as well as the lower carbon intensity of natural gas. As shown in Table 1.5, combined-cycle gas plants emit less than half as much carbon as coal plants.

TABLE 1.5 Assumptions for Calculating Carbon Emissions. Carbon Intensity Based on EIA Data. Efficiency Is Based on HHV of Fuels.

Technology	Heat Rate (Btu/kWh)	Efficiency (%)	Fuel (kg C/GJ)	Emissions (kg C/kWh)	Emissions (kg CO_2/kWh)
New coal	8750	39.0	24.5	0.23	0.83
Old coal	10,340	33.0	24.5	0.27	0.98
CT	9300	36.7	13.7	0.13	0.49
NGCC	6900	49.4	13.7	0.10	0.37

At some point, carbon emissions will no longer be cost-free (already the case outside of the United States). As Figure 1.35 suggests, nuclear plants and gas-fired combined-cycle plants would be cost-competitive with already built coal plants if emissions were to be priced at around \$50/t of CO_2. The figure also provides a rough estimate of the cost of carbon savings through energy efficiency measures on the customer's side of the meter.

FIGURE 1.35 Impact of carbon cost on LCOE (plotted for equal CF = 0.85 and assumptions given in Table 1.5).



Epstein et al. (2011) estimate that the life cycle cost of coal and its associated waste streams exceeds $300 billion per year in the United States alone. Accounting for these damages, they estimate that these externalities add between 9.5 and 26.9 ¢/kWh, with a best estimate of almost 18 ¢/kWh, to the cost of coal-based electricity, making even current coal plants far more expensive than wind, solar, and other forms of nonfossil fuel power generation.

1.7 SUMMARY

The focus of this chapter has been on developing a modest understanding of how the current electricity industry functions. We have seen how it evolved from the early days of Edison and Westinghouse into the complex system that has served our needs remarkably well over the past century or so. That system, however, is beginning a major transformation from one based primarily on fossil fuels, with their adverse environmental impacts and resource limitations, into a more distributed system that emphasizes efficient use of energy coupled with more widely distributed generation based primarily on renewable energy sources. It is moving from a load-following system into one in which supply and demand will be balanced by a combination of generation response and demand response. Both sides of the meter will have to play active roles, not only to control costs, but also to address critical questions that arise when higher and higher fractions of supply come from intermittent renewables.

In other words, hopefully enough groundwork has been laid to motivate the rest of this book.

REFERENCES

Bachrach, D., Ardema, M., and A. Leupp (2003). *Energy Efficiency Leadership in California: Preventing the Next Crisis*, Natural Resources Defense Council, Silicon Valley Manufacturing Group, April.

Brown, R.E., and J. Koomey (2002). *Electricity Use in California: Past Trends and Present Usage Patterns*, Lawrence Berkeley National Labs, LBL-47992, Berkeley, CA.

California Energy Commission (2010). *Cost of generation model user's guide.* CEC-200-2010-002.

Epstein, P.R., Buonocore, J.J., Eckerle, K., Hendryx, M., Stout III, B.M., Heinberg, R., Clapp, R.W., May, B., Reinhart, N.L., Ahern, M.M., Doshi, S.K., and L. Glustrom (2011). *Full Cost Accounting for the Life Cycle of Coal.* R. Constanza, K. Limburg, and I. Kubiszewski, (eds.), Ecological Economics Reviews. Annals of The New York Academy of Sciences, vol 1219, pp. 73–98.

Eto, J.H., Undrill, J., Mackin, P., Illian, H., Martinez, C., O'Malley, M., and Coughlin, K (2010). *Use of frequency response metrics to assess the planning and operating requirements for reliable integration of variable renewable generation*, Lawrence Berkeley National Labs, LBNL-4142E, Berkeley, CA.

Koomey, J., Akbari, H., Blumstein, C., Brown, M., Brown, R., Calwell, C., Carter, S., Cavanagh, R., Chang, A., and Claridge, D., et al. (2010). Defining a standard metric for electricity savings. *Environmental Research Letters*, vol 5. no.1, p. 014017.

Penrose, J.E. (1994). Inventing electrocution. *Invention and Technology.* Spring, pp. 35–44.

PROBLEMS

1.1 A combined-cycle, natural gas, power plant has an efficiency of 52%. Natural gas has an energy density of 55, 340 kJ/kg and about 77% of the fuel is carbon.

a. What is the heat rate of this plant expressed as kJ/kWh and Btu/kWh?

b. Find the emission rate of carbon (kg C/kWh) and carbon dioxide (kg CO_2/kWh). Compare those with the average coal plant emission rates found in Example 1.1.

1.2 In a reasonable location, a photovoltaic array will deliver about 1500 kWh/yr per kW of rated power.

a. What would its CF be?

b. One estimate of the maximum potential for rooftop photovoltaics (PVs) in the United States suggests as much as 1000 GW of PVs could be installed. How many "Rosenfeld" coal-fired power plants could be displaced with a full build out of rooftop PVs?

c. Using the Rosenfeld unit, how many metric tons of CO_2 emissions would be avoided per year?

1.3 For the following power plants, calculate the added cost (¢/kWh) that a $50 tax per metric ton of CO_2 would impose. Use carbon content of fuels from Table 1.5.

a. Old coal plant with heat rate 10, 500 Btu/kWh.

b. New coal plant with heat rate 8500 Btu/kWh.

c. New IGCC coal plant with heat rate 9000 Btu/kWh.

d. NGCC plant with heat rate 7000 Btu/kWh.

e. Gas turbine with heat rate 9500 Btu/kWh.

1.4 An average pulverized coal power plant has an efficiency of about 33%. Suppose a new ultra-supercritical (USC) coal plant increases that to 42%. Assume coal burning

emits 24.5 kg C/GJ.

a. If CO_2 emissions are eventually taxed at $50 per metric ton, what would the tax savings be for the USC plant ($/kWh)?

b. If coal that delivers 24 million kJ of heat per metric ton costs $40/t what would be the fuel savings for the USC plant ($/kWh)?

1.5 The United States has about 300 GW of coal-fired power plants that in total emit about 2 Gt of CO_2/yr while generating about 2 million GWh/yr of electricity.

a. What is their overall capacity factor?

b. What would be the total carbon emissions (Gt CO_2/yr) that could result if all of the coal plants were replaced with 50%-efficient NGCC plants that emit 13.7 kgC/GJ of fuel?

c. Total U.S. CO_2 emissions from all electric power plants is about 5.8 Gt/yr. What percent reduction would result from switching all the above coal plants to NGCC?

1.6 Consider a 55%-efficient, 100-MW, NGCC merchant power plant with a capital cost of $120 million. It operates with a 50% capacity factor. Fuel currently costs $3/MMBtu and current annual O&M is 0.4 ¢/kWh. The utility uses a levelizing factor LF = 1.44 to account for future fuel and O&M cost escalation (see Example 1.3).

The plant is financed with 50% equity at 14% and 50% debt at 6%. For financing purposes, the "book life" of the plant is 30 years. The FCR, which includes insurance, fixed O&M, corporate taxes, and so on, includes an additional 6% on top of finance charges.

a. Find the annual fixed cost of owning this power plant ($/yr).

b. Find the levelized cost of fuel and O&M for the plant.

c. Find the LCOE.

1.7 The levelizing factors shown in Figure 1.28 that allow us to account for fuel and O&M escalations in the future are derived in Appendix A and illustrated in Example A.5.

a. Find the LF for a utility that assumes its fuel and O&M costs will escalate at an annual rate of 4% and which uses a discount factor of 12%.

b. If natural gas now costs $4/MMBtu, use the LF just found to estimate the life cycle fuel cost ($/kWh) for a power plant with a heat rate of 7000 Btu/kWh.

1.8 Consider the levelizing factor approach derived in Appendix A as applied to electricity bills for a household. Assume the homeowner's discount rate is the 6%/yr interest rate that can be obtained on a home equity loan, the current price of electricity is $0.12/kWh, and the time horizon is 10 years.

a. Ignoring fuel price escalation (e = 0), what is the 10-year levelized cost of electricity ($/kWh)?

b. If fuel escalation is the same as the discount rate (6%), what is the levelizing factor and the levelized cost of electricity?

c. With a 6% discount rate and 4% electricity rate increases projected into the future, what is the levelizing factor and the LCOE?

1.9 Consider the levelizing factor approach derived in Appendix A as applied to electricity

bills for a household. Assume the homeowner's discount rate is the 5%/yr interest rate that can be obtained on a home equity loan, the current price of utility electricity is $0.12/kWh, price escalation is estimated at 4%/yr, and the time horizon is 20 years.

a. What is the levelized cost of utility electricity for this household ($/kWh) over the next 20 years?

b. Suppose the homeowner considers purchasing a rooftop photovoltaic (PV) system that costs $12, 000 and delivers 5000 kWh/yr. Assume the only costs for those PVs are the annual loan payments on a $12, 000, 5%, 20-year loan that pays for the system (we are ignoring tax benefits associated with the interest portion of the payments). Compare the LCOE ($/kWh) for utility power versus these PVs.

1.10 Using the representative power plant heat rates, capital costs, fuels, O&M, levelizing factors and fixed charge rates given in Table 1.4, compute the cost of electricity from the following power plants. For each, assume an FCR of 0.167/yr.

a. Pulverized coal-steam plant with CF = 0.70.

b. Combustion turbine with CF = 0.20.

c. Combined-cycle natural gas plant with CF = 0.5.

d. Nuclear plant with CF = 0.85.

e. A wind turbine costing $1600/kW with CF = 0.40, O&M $60/yr-kW, LF = 1.5, FCR = 0.167/yr.

1.11 Consider the following very simplified load duration curve for a small utility.

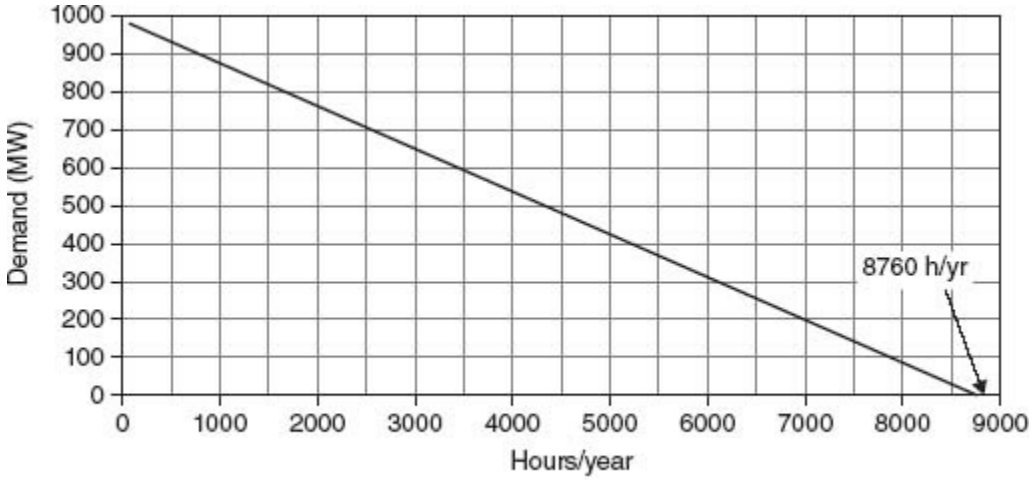


FIGURE P1.11

a. How many hours per year is the load less than 200 MW?

b. How many hours per year is the load between 200 MW and 600 MW?

c. If the utility has 600 MW of base-load coal plants, what would their average capacity factor be?

d. Find the energy delivered by the coal plants.

1.12 Suppose the utility in Problem 1.11 has 400 MW of combustion turbines operated as peaking power plants.

a. How much energy will these turbines deliver (MWh/yr)?

b. If these peakers have the "revenue required" curve shown below, what would the

selling price of electricity from these plants (¢/kWh) need to be?

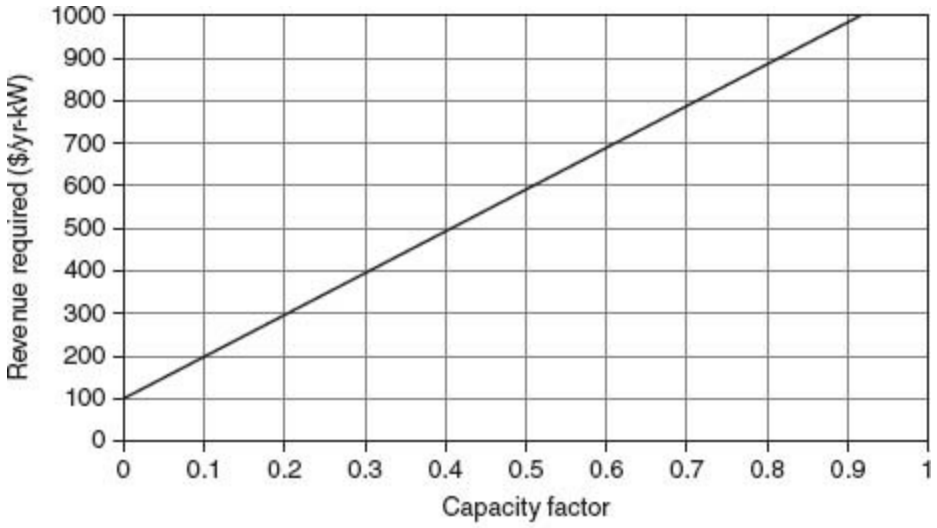
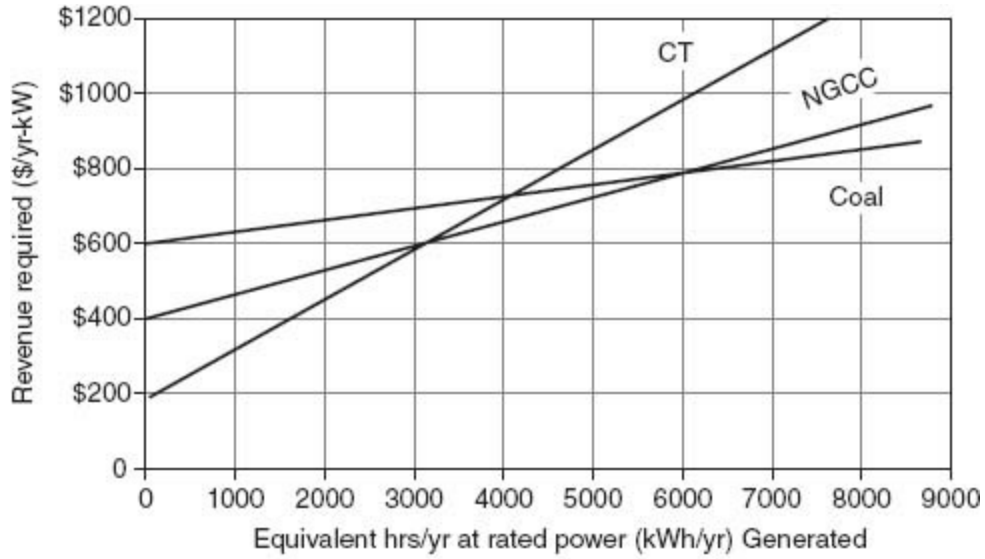


FIGURE P1.12

1.13 As shown below, on a per kW of rated power basis, the costs to own and operate a CT, an NGCC, and a coal plant have been determined to be:

$$\text{CT (\$/yr)} = \$200 + \$0.1333 \times \text{h/yr}$$
$$\text{NGCC (\$/yr)} = \$400 + \$0.0666 \times \text{h/yr}$$
$$\text{Coal (\$/yr)} = \$600 + \$0.0333 \times \text{h/yr}$$

Also shown is the load duration curve for an area with a peak demand of 100 GW.



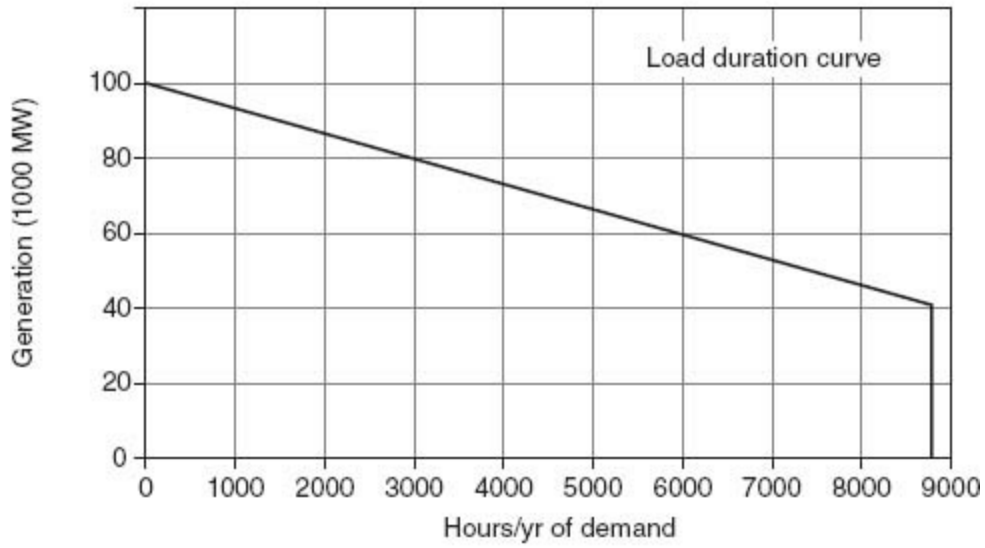


FIGURE P1.13

a. How many MW of each type of plant would you recommend?

b. What would be the capacity factor for the NGCC plants?

c. What would be the average cost of electricity from the NGCC plants?

d. What would be the average cost of electricity from the CT plants?

e. What would be the average cost of electricity from the coal plants?

1.14 The following table gives capital costs and variable costs for coal plants, NGCC plants, and natural-gas-fired CTs.

	Coal	NGCC	CT
Capital cost ($/kW)	2000	1200	800
Variable cost (¢/kWh)	2.0	4.0	6.0

This is a municipal utility with a low fixed charge rate of 0.10/yr for capital costs. Its load duration curve is shown below.

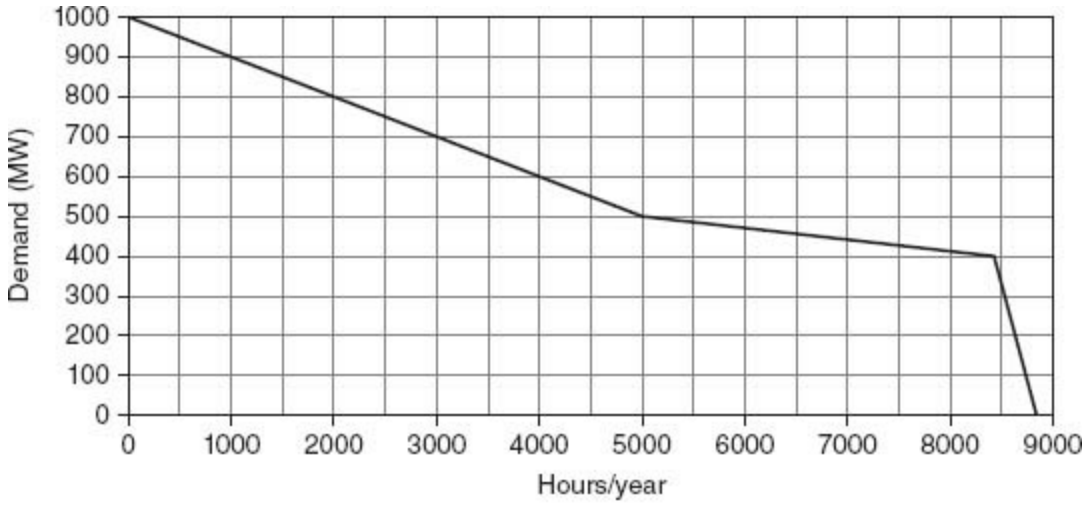


FIGURE P1.14

a. On a single graph, draw the screening curves (Revenue required $/yr-kW vs. h/yr) for the three types of power plants (like Figure 1.29).

b. For a least-cost system, what is the maximum number of hours a CT should operate, the minimum number of hours the coal plant should operate, and the range of hours the NGCC plants should operate. You can do this algebraically or graphically.

c. How many MW of each type of power plant would you recommend?

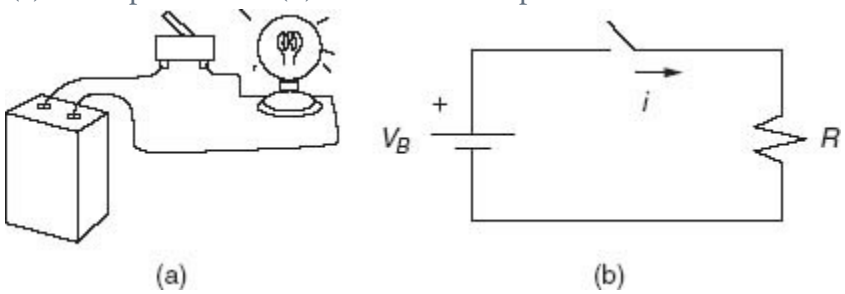
CHAPTER 2

BASIC ELECTRIC AND MAGNETIC CIRCUITS

2.1 INTRODUCTION TO ELECTRIC CIRCUITS

In elementary physics classes, you undoubtedly have been introduced to the fundamental concepts of electricity and how real components can be put together to form an electrical circuit. A very simple circuit, for example, might consist of a battery, some wire, a switch, and an incandescent lightbulb as shown in Figure 2.1. The battery supplies the energy required to force electrons around the loop, heating the filament of the bulb, and causing the bulb to radiate a lot of heat and some light. Energy is transferred from a *source*, the battery, to a *load*, the bulb. You probably already know that the *voltage* of the battery and the electrical *resistance* of the bulb have something to do with the amount of *current* that will flow in the circuit. From your own practical experience you also know that no current will flow until the switch is closed. That is, for a circuit to do anything, the loop has to be completed so that electrons can flow from the battery to the bulb and then back again to the battery. And finally, you probably realize that it does not matter much whether there is one foot of wire connecting the battery to the bulb, or 2 ft; but that it probably would matter if there is a mile of wire between itself and the bulb.

FIGURE 2.1 (a) A simple circuit. (b) An idealized representation of the circuit.



Also shown in Figure 2.1 is a model made up of *idealized* components. The battery is modeled as an ideal source that puts out a constant voltage, V_B, no matter what amount of current, i, is drawn. The wires are considered to be perfect conductors that offer no resistance to current flow. The switch is assumed to be open or closed. There is no arcing of current across the gap when the switch is opened, nor is there any bounce to the switch as it makes contact on closure. The lightbulb is modeled as a simple resistor, R, that never changes its value, no matter how hot it becomes or how much current is flowing through it.

For most purposes, the idealized model shown in Figure 2.1b is an adequate

representation of the circuit; that is, our prediction of the current that will flow through the bulb whenever the switch is closed will be sufficiently accurate that we can consider the problem solved. There may be times, however, when the model is inadequate. The battery voltage, for example, may drop as more and more current is drawn, or as the battery ages. The lightbulb's resistance may change as it heats up, and the filament may have a bit of inductance and capacitance associated with it as well as resistance so that when the switch is closed, the current may not jump instantaneously from zero to some final, steady-state value. The wires may be undersized, and some of the power delivered by the battery may be lost in the wires before it reaches the load. These subtle effects may or may not be important, depending on what we are trying to find out and how accurately we must be able to predict the performance of the circuit. If we decide they are important, we can always change the model as necessary and then proceed with the analysis.

The point here is simple. The combinations of resistors, capacitors, inductors, voltage sources, current sources, and so forth, that you see in a circuit diagram are merely models of real components that comprise a real circuit, and a certain amount of judgment is required to decide how complicated the model must be before sufficiently accurate results can be obtained. For our purposes, we will be using very simple models in general, leaving many of the complications to more advanced textbooks.

2.2 DEFINITIONS OF KEY ELECTRICAL QUANTITIES

We shall begin by introducing the fundamental electrical quantities that form the basis for the study of electric circuits.

2.2.1 Charge

An atom consists of a positively charged nucleus surrounded by a swarm of negatively charged electrons. The charge associated with one electron has been found to be 1.602×10^{-19} coulombs; or, stated the other way around, one coulomb can be defined as the charge on 6.242×10^{18} electrons. While most of the electrons associated with an atom are tightly bound to the nucleus, good conductors, like copper, have *free electrons* that are sufficiently distant from their nuclei that their attraction to any particular nucleus is easily overcome. These conduction electrons are free to wander from atom to atom, and their movement constitutes an electric current.

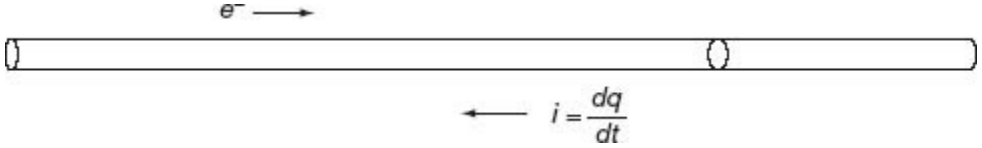
2.2.2 Current

In a wire, when one coulomb's worth of charge passes a given spot in one second, the current is defined to be one ampere (A), named after the nineteenth-century physicist André-Marie Ampère. That is, current i is the net rate of flow of charge q past a point, or through an area:

$$i = \frac{dq}{dt} \tag{2.1}$$

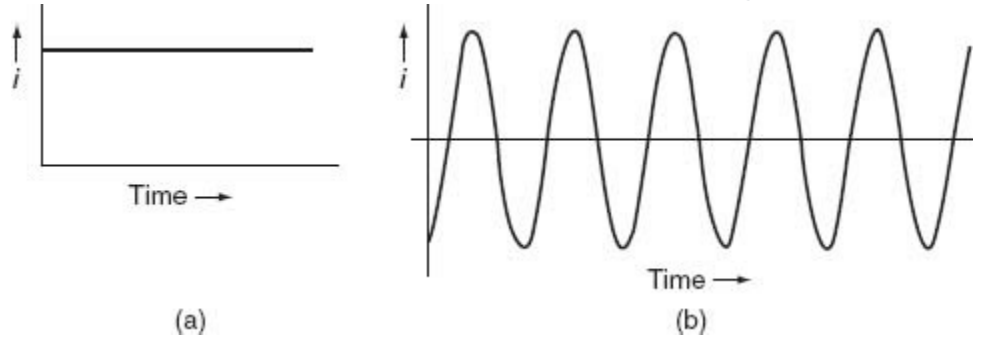
In general, charges can be negative or positive. For example, in a neon light, positive ions move in one direction and negative electrons move in the other. Each contributes to current, and the total current is their sum. By convention, the direction of current flow is taken to be the direction that positive charges would move, whether or not positive charges happen to be in the picture. Thus, in a wire, electrons moving to the right constitute a current that flows to the left, as shown in Figure 2.2.

FIGURE 2.2 By convention, negative charges moving in one direction constitutes a positive current flow in the opposite direction.



When charge flows at a steady rate in one direction only, the current is said to be *direct current*, or DC. A battery, for example, supplies direct current. When charge flows back and forth sinusoidally, it is said to be *alternating current*, or AC. In the United States, the AC electricity delivered by the power company has a frequency of 60 cycles/s, or 60Hz. Examples of AC and DC are shown in Figure 2.3.

FIGURE 2.3 (a) Steady-state direct current (DC). (b) Alternating current (AC).



Using some basic physical properties of the conductor in which current flows, along with the Avogadro constant (6.023×10^{23} atoms/mol) and the charge on an electron, we can easily calculate the average *drift velocity* at which electrons move down a wire as they carry current through a circuit. With so many free electrons available in a wire, they do not have to drift very fast to carry large amounts of current.

$$\text{Drift velocity (m/s)} = \frac{i(\text{coulombs/s})}{n(\text{electrons/m}^3) \cdot q(\text{coulombs/electron}) \cdot A(\text{m}^2)} \quad (2.2)$$

Example 2.1 How Fast do Electrons Move in a Wire? A 12-gage copper household wire has a cross-sectional area of 3.31×10^{-6} m^2. The density of copper is 8.95 g/m^3, its atomic weight is 63.55 g/mol, and each atom has one electron in the conduction band. Estimate the average drift velocity of electrons in the wire when it carries 20 A.

Solution. This is mostly just a question of keeping track of units to make them all properly cancel:

$$n = \frac{6.023 \times 10^{23} \text{ atoms}}{\text{mol}} \times \frac{1 \text{ electron}}{\text{atom}} \times \frac{\text{mol}}{63.55 \text{ g}} \times \frac{8.95 \text{ g}}{\text{cm}^3} \times \frac{10^6 \text{ cm}^3}{\text{m}^3}$$
$$= 8.48 \times 10^{28} \text{ electrons/m}^3$$

For a current of 20 A (20 C/s), Equation 2.2 gives us

$$\text{Drift} = \frac{20\ \text{C/s}}{8.48 \times 10^{28}\ (\text{electrons/m}^3) \times 1.602 \times 10^{-19}\ (\text{C/electron}) \times 3.31 \times 10^{-6}\ \text{m}^2}$$

$$\text{Drift} = 0.00044\ \text{m/s} = 1.6\ \text{m/h}$$

Example 2.2 shows how slowly electrons move along a wire: roughly 1 in/min. With typical household current, they reverse direction 60 times a second, which means they barely move at all. Indeed, the electrons that help make toast in the morning are electrons that came with the toaster when you bought it.

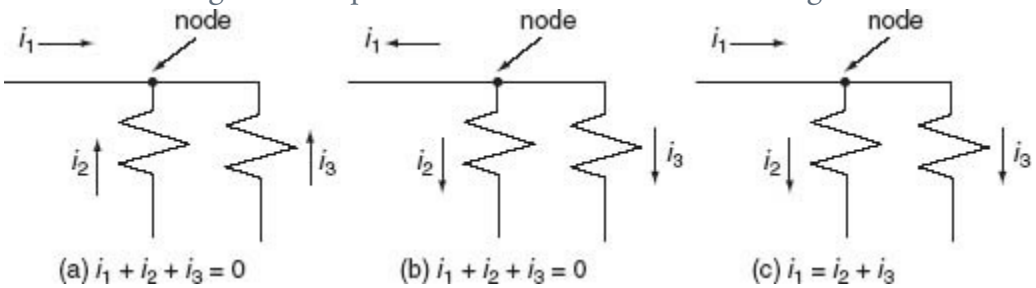
Meanwhile, even though the bulk rate at which electrons travel is very slow, the wave of energy that flows down a power line as one electron collides with, and energizes, adjacent electrons travels at nearly the speed of light.

2.2.3 Kirchhoff's Current Law

Two of the most fundamental properties of circuits were established experimentally a century-and-a-half ago by a German professor, Gustav Robert Kirchhoff (1824–1887). The first property, known as Kirchhoff's current law (KCL), states that *at every instant of time the sum of the currents flowing into any node of a circuit must equal the sum of the currents leaving the node*, where a node is any spot where two or more wires are joined. This is a very simple, but powerful concept. It is intuitively obvious once you assert that current is the flow of charge, and that charge is conservative—neither created nor destroyed as it enters a node. Unless charge somehow builds up at a node, which it does not, then the rate at which charge enters a node must equal the rate at which charge leaves the node.

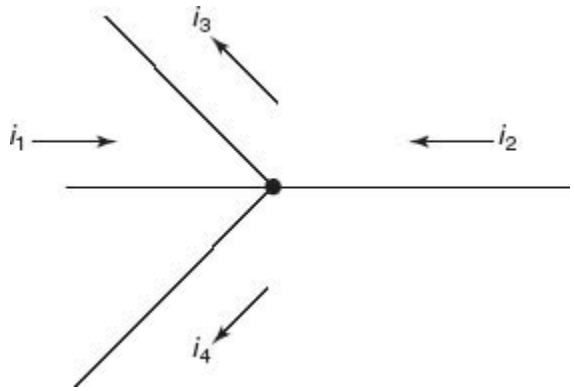
There are several alternative ways to state KCL. The most commonly used statement says that the sum of the currents into a node is zero as shown in Figure 2.4a, in which case some of those currents must have negative values while some have positive values. Equally valid would be the statement that the sum of the currents leaving a node must be zero as shown in Figure 2.4b (again some of these currents need to have positive values and some negative). Finally, we could say that the sum of the currents entering a node equals the sum of the currents leaving a node (Fig. 2.4c). These are all equivalent as long as we understand what is meant about the direction of current flow when we indicate it with an arrow on a circuit diagram. Current that actually flows in the direction shown by the arrow is given a positive sign. Currents that actually flow in the opposite direction have negative values.

FIGURE 2.4 Illustrating various ways that KCL can be stated. (a) The sum of the currents into a node equals zero. (b) The sum of the currents leaving the node is zero. (c) The sum of the currents entering a node equals the sum of the currents leaving the node.



Note that you can draw current arrows in any direction that you want—that much is arbitrary—but having once drawn the arrows, you must then write KCL in a manner that is consistent with your arrows, as has been done in Figure 2.4. The algebraic solution to the circuit problem will automatically determine whether or not your arrows were correct.

Example 2.2 Using Kirchhoff's Current Law. A node of a circuit is shown with current direction arrows chosen arbitrarily. Having picked those directions, $i_1 = -5\text{A}$, $i_2 = 3\text{A}$, and $i_3 = -1\text{A}$. Write an expression for KCL and solve for i_4.



Solution. By Kirchhoff's current law,

$$i_1 + i_2 = i_3 + i_4$$
$$-5 + 3 = -1 + i_4$$

so that,

$$i_4 = -1\text{A}$$

That is, i_4 is actually 1 A flowing into the node. Note that i_2, i_3, and i_4 are all entering the node, and i_1 is the only current that is leaving the node.

2.2.4 Voltage

Electrons will not flow through a circuit unless they are given some energy to help send them on their way. That "push" is measured in volts, where voltage is defined to be the amount of energy (w, in joules) given to a unit of charge,

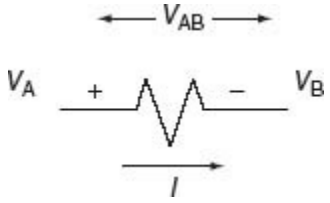
$$V = \frac{dw}{dq} \tag{2.3}$$

A 12-V battery therefore gives 12 J of energy to each coulomb of charge that it stores. Note that the charge does not actually have to move for voltage to have meaning. Voltage describes the potential for charge to do work.

While currents are measured *through* a circuit component, voltages are measured *across* components. Thus, for example, it is correct to say that current through a battery is 10 A, while the voltage across that battery is 12 V. Other ways to describe the voltage across a component include whether the voltage rises across the component or drops. Thus, for example, for the simple circuit in Figure 2.1, there is a voltage rise across the battery and voltage drop across the lightbulb.

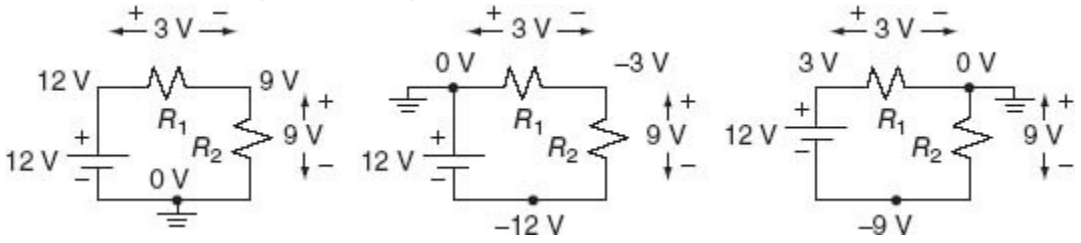
Voltages are always measured with respect to something. That is, the voltage of the positive terminal of the battery is "so many volts" with respect to the negative terminal; or the voltage at a point in a circuit is some amount with respect to some other point. In Figure 2.5, current through a resistor results in a voltage drop from point A to point B of V_{AB} volts. V_A and V_B are the voltages at each end of the resistor, measured with respect to some other point.

FIGURE 2.5 The voltage drop from point A to point B is V_{AB}, where $V_{AB} = V_A - V_B$.



The reference point for voltages in a circuit is usually designated with a *ground* symbol. While many circuits are actually grounded—that is, there is a path for current to flow directly into the earth—some are not (such as the battery, wires, switch, and bulb in a flashlight). When a ground symbol is shown on a circuit diagram, you should consider it to be merely a reference point at which the voltage is defined to be zero. Figure 2.6 points out how changing the node labeled as ground changes the voltages at each node in the circuit, but does not change the voltage drop across each component.

FIGURE 2.6 Moving the reference node around (ground) changes the voltages at each node, but does not change the voltage drop across each component.



2.2.5 Kirchhoff's Voltage Law

The second of Kirchhoff's fundamental laws states that *the sum of the voltages around any loop of a circuit at any instant is zero*. This is known as Kirchhoff's voltage law (KVL). Just as was the case for Kirchhoff's current law, there are alternative, but equivalent, ways of stating KVL. We can, for example, say that the sum of the voltage rises in any loop equals the sum of the voltage drops around the loop. Thus in Figure 2.6, there is a voltage rise of 12 V across the battery and a voltage drop of 3 V across R_1 and a drop of 9 V across R_2. Note that for this to be true, it does not matter which node was labeled ground. Just as was the case with KCL, we must be careful about labeling and interpreting the signs of voltages in a circuit diagram in order to write the proper version of KVL. A plus (+) sign on a circuit component indicates a reference direction under the assumption that the potential at that end of the component is higher than the voltage at the other end. Again, as long as we are consistent in writing KVL, the algebraic solution for the circuit will automatically take care of signs.

Kirchhoff's voltage law has a simple mechanical analog in which mass is analogous to

charge and elevation is analogous to voltage. If a weight is raised from one elevation to another, it acquires potential energy equal to the change in elevation times its weight. Similarly, the potential energy given to charge is equal to the amount of charge times the voltage to which it is raised. If you decide to take a day hike, in which you start and finish the hike at the same spot, you know that no matter what path was taken, when you finish the hike the sum of the increases in elevation has to have been equal to the sum of the decreases in elevation. Similarly, in an electrical circuit, no matter what path is taken, as long as you return to the same node at which you started, KVL provides assurance that the sum of voltage rises in that loop will equal the sum of the voltage drops in the loop.

2.2.6 Power

Power and *energy* are two terms that are often misused. Energy can be thought of as the ability to do work, and has units such as joules or Btu. Power, on the other hand, is the *rate* at which energy is generated, or used, and therefore has rate units such as joules/s or Btu/h. There is often confusion about the units for electrical power and energy. Electrical power is measured in watts, which is a rate (1 J/s = 1 W), so electrical energy is watts multiplied by time—for example, watt-hours. Be careful not to say "watts per hour, " which is incorrect (even though you will see this all too often in newspapers or magazines).

When a battery delivers current to a load, power is generated by the battery and dissipated by the load. We can combine Equations 2.1 and 2.3 to find an expression for instantaneous power supplied, or consumed, by a component of a circuit:

$$p = \frac{dw}{dt} = \frac{dw}{dq} \cdot \frac{dq}{dt} = vi \tag{2.4}$$

Equation 2.4 tells us that the power supplied at any instant by a source, or consumed by a load, is given by the current through the component times the voltage across the component. When current is given in amperes, and voltage in volts, the units of power are *watts* (W). Thus, a 12-V battery delivering 10 A to a load is supplying 120 W of power.

2.2.7 Energy

Since power is the rate at which work is being done, and energy is the total amount of work done, energy is just the integral of power.

$$w = \int p\,dt \tag{2.5}$$

In an electrical circuit, energy can be expressed in terms of joules (J) where 1 watt-second = 1 joule. In the electric power industry, the units of electrical energy are more often given in watt-hours, or for larger quantities kilowatt-hours (kWh) or megawatt-hours (MWh). Thus, for example, a 100-W computer that is operated for 10 h will consume 1000 Wh, or 1 kWh of energy. A typical household in the United States uses approximately 950 kWh/mo, which means, on average (720 h/mo), it uses about 1.3 kW of power.

2.2.8 Summary of Principal Electrical Quantities

The key electrical quantities already introduced and the relevant relationships between

these quantities are summarized in Table 2.1.

TABLE 2.1 Key Electrical Quantities and Relationships

Electrical Quantity	Symbol	Unit	Abbreviation	Relationship
Charge	q	Coulomb	C	$q = \int i dt$
Current	i	Ampere	A	$i = dq/dt$
Voltage	v	Volt	V	$v = dw/dq$
Power	p	Joule/second or watt	J/s, W	$p = dw/dt$
Energy	w	Joule or watt-hour	J, Wh	$w = \int p\, dt$

Since electrical quantities vary over such a large range of magnitudes, you will often find yourself working with very small quantities or very large quantities. For example, the voltage created by your TV antenna may be measured in millionths of a volt (microvolts, μV), while the power generated by a large power station may be measured in billions of watts, or gigawatts (GW). The total generation capacity of all of U.S. power plants is about 1000 GW, or 1 terawatt (TW). To describe quantities that may take on such extreme values, it is useful to have a system of prefixes that accompany the units. The most commonly used prefixes in electrical engineering are given in Table 2.2.

TABLE 2.2 Common Prefixes

Small Quantities			Large Quantities		
Quantity	Prefix	Symbol	Quantity	Prefix	Symbol
10^{-3}	milli	m	10^{3}	kilo	k
10^{-6}	micro	μ	10^{6}	mega	M
10^{-9}	nano	n	10^{9}	giga	G
10^{-12}	pico	p	10^{12}	tera	T

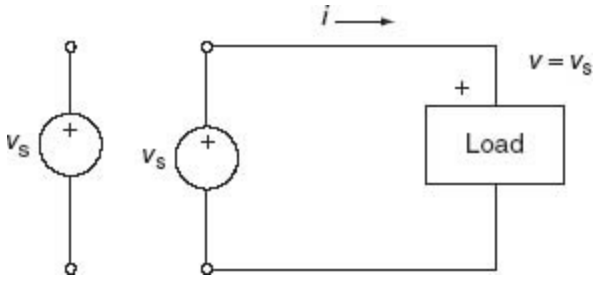
2.3 IDEALIZED VOLTAGE AND CURRENT SOURCES

Electric circuits are made up of a relatively small number of different kinds of circuit *elements*, or *components*, which can be interconnected in an extraordinarily large number of ways. At this point in our discussion, we will concentrate on the idealized characteristics of these circuit elements, realizing that real components resemble, but do not exactly duplicate, the characteristics that we describe here.

2.3.1 Ideal Voltage Source

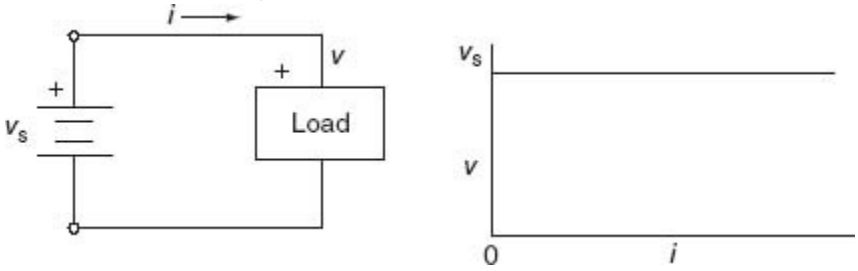
An ideal voltage source is one that provides a given, known voltage v_s, no matter what sort of load it is connected to. That is, regardless of the current drawn from the ideal voltage source, it will always provide the same voltage. Note that an ideal voltage source does not have to deliver a constant voltage; for example, it may produce a sinusoidally varying voltage—the key is that voltage is not a function of the amount of current drawn. A symbol for an ideal voltage source is shown in Figure 2.7.

FIGURE 2.7 A constant voltage source delivers v_s no matter what current the load draws. The quantity v_s can vary with time and still be ideal.



A special case of an ideal voltage source is an ideal battery that provides a constant DC output, as shown in Figure 2.8. A real battery approximates the ideal source; but as current increases, the output drops somewhat. To account for that drop, quite often the model used for a real battery is an ideal voltage source in series with the internal resistance of the battery.

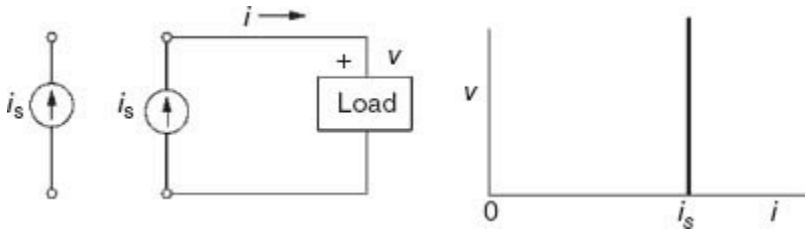
FIGURE 2.8 An ideal DC voltage.



2.3.2 Ideal Current Source

An ideal current source produces a given amount of current i_s, no matter what load it sees. As shown in Figure 2.9, a commonly used symbol for such a device is circle with an arrow indicating the direction of current flow. While a battery is a good approximation to an ideal voltage source, there is nothing quite so familiar that approximates an ideal current source. Some transistor circuits come close to this ideal and are often modeled with idealized current sources.

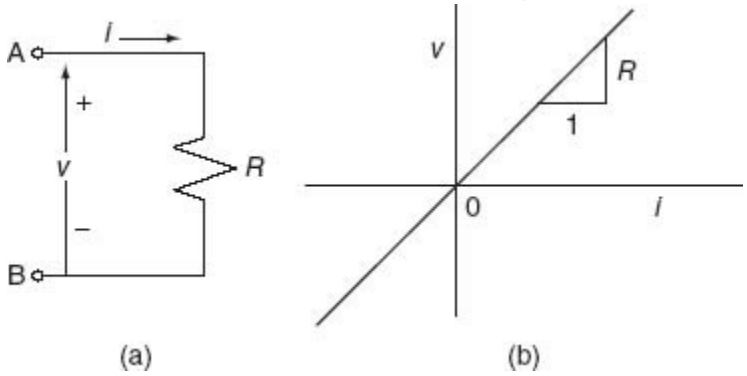
FIGURE 2.9 The current produced by an ideal current source does not depend on the voltage across the source.



2.4 ELECTRICAL RESISTANCE

For an ideal *resistance* element, the current through it is directly proportional to the voltage drop across it, as shown in Figure 2.10.

FIGURE 2.10 (a) Symbol for an ideal resistor. (b) Voltage–current relationship.



2.4.1 Ohm's Law

The equation for an ideal resistor is given in Equation 2.6 in which v is in volts, i is in amperes, and the constant of proportionality is resistance R, measured in ohms (Ω). This simple formula is known as *Ohm's law* in honor of the German physicist, Georg Ohm, whose original experiments led to this incredibly useful and important relationship.

$$v = Ri \tag{2.6}$$

Note that voltage v is measured across the resistor. That is, it is the voltage at point A with respect to the voltage at point B. When current is in the direction shown, the voltage at A with respect to B is positive, so it is quite common to say there is a *voltage drop* across the resistor.

An equivalent relationship for a resistor is given in Equation 2.7, where current is given in terms of voltage and the proportionality constant is conductance G, with units of siemens (S). In older literature, the unit of conductance was mhos (ohms spelled backwards).

$$i = Gv \tag{2.7}$$

By combining Equations 2.4 and 2.6, we can easily derive the following equivalent relationships for power dissipated by the resistor:

$$p = vi = i^2R = \frac{v^2}{R} \tag{2.8}$$

Example 2.3 Power to an Incandescent Lamp. The current–voltage relationship for an incandescent lamp is nearly linear, so it can quite reasonably be modeled as a simple resistor. Suppose such a lamp has been designed to consume 60 W when it is connected to a 12-V DC power source. What is the resistance of the filament, and what amount of current will flow? If the actual voltage is only 11 V, how much energy would it consume over a 100-h period?

Solution. From Equation 2.8,

$$R = \frac{v^2}{p} = \frac{12^2}{60} = 2.4\ \Omega$$

and from Ohm's law:

$$i = v/R = 12/2.4 = 5\ \text{A}$$

Connected to an 11-V source, the power consumed would be

$$p = \frac{v^2}{R} = \frac{11^2}{2.4} = 50.4\,\text{W}$$

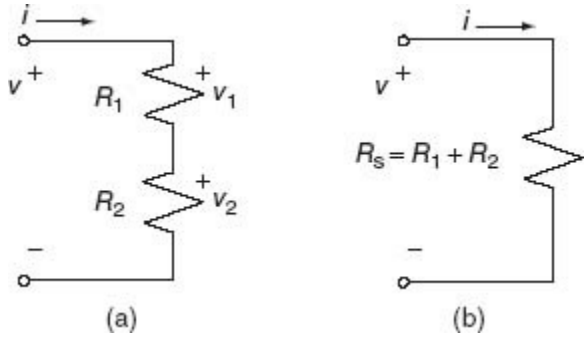
Over a 100-h period, it would consume

$$w = pt = 50.4\ \text{W} \times 100\ \text{h} = 5040\ \text{Wh} = 5.04\ \text{kWh}$$

2.4.2 Resistors in Series

We can use Ohm's law and Kirchhoff's voltage law to determine the equivalent resistance of resistors wired in *series* (so the same current flows through each one) as shown in Figure 2.11.

FIGURE 2.11 R_s is equivalent to resistors R_1 and R_2 in series.



For R_s to be equivalent to the two series resistors, R_1 and R_2, the voltage–current relationships must be the same. That is, for the circuit in Figure 2.11a

(2.9) $v = v_1 + v_2$

and from Ohm's law,

(2.10) $v = iR_1 + iR_2$

For the circuit in Figure 2.11b to be equivalent, the voltage and current must be the same

(2.11) $v = iR_s$

By equating Equations 2.10 and 2.11, we conclude that

(2.12) $R_s = R_1 + R_2$

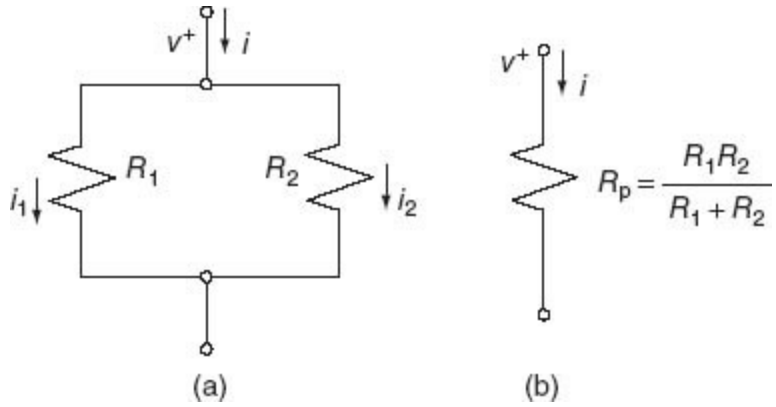
And, in general, for *n*-resistances in series the equivalent resistance is

(2.13) $R_s = R_1 + R_2 + \cdots + R_n$

2.4.3 Resistors in Parallel

When circuit elements are wired together as in Figure 2.12, so that the same voltage appears across each of them, they are said to be in *parallel*.

FIGURE 2.12 Equivalent resistance of resistors wired in parallel.



To find the equivalent resistance of two resistors in parallel, we can first incorporate Kirchhoff's current law followed by Ohm's law:

$$i = i_1 + i_2 = \frac{v}{R_1} + \frac{v}{R_2} = \frac{v}{R_p} \tag{2.14}$$

so that

$$\frac{1}{R_1} + \frac{1}{R_2} = \frac{1}{R_p} \quad \text{or} \quad G_1 + G_2 = G_p \tag{2.15}$$

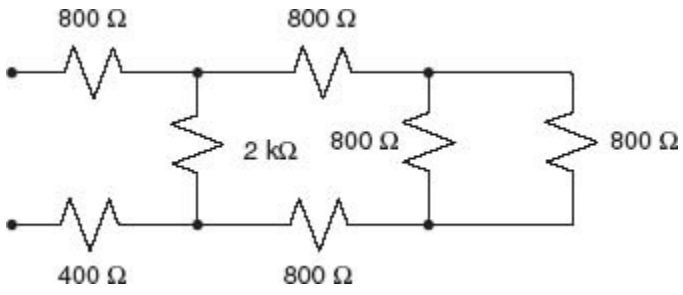
Note that one reason for introducing the concept of conductance is that the conductance of a parallel combination of n resistors is just the sum of the individual conductances.

For two resistors in parallel, the equivalent resistance can be found from Equation 2.15 to be

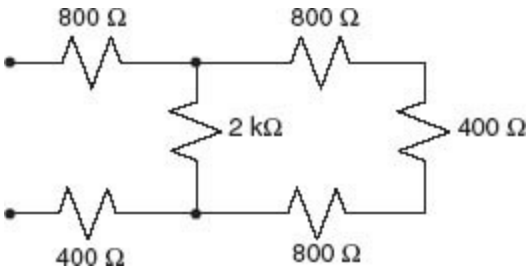
$$R_p = \frac{R_1 R_2}{R_1 + R_2} \tag{2.16}$$

Note that when R_1 and R_2 are of equal value, the resistance of the parallel combination is just one-half that of either one. Also, you might note that the parallel combination of two resistors always has a lower resistance than either one of those resistors.

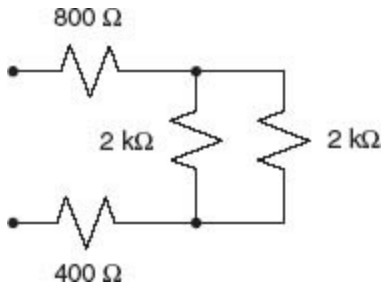
Example 2.4 Analyzing a Resistive Circuit. Find the equivalent resistance of the following network.



Solution. While this circuit may look complicated, you can actually work it out in your head. The parallel combination of the two 800 Ω resistors on the right end is 400 Ω, leaving the following equivalent:



The three resistors on the right end are in series, so they are equivalent to a single resistance of 2 kΩ (= 800 Ω + 400 Ω + 800 Ω). The network now looks like the following:

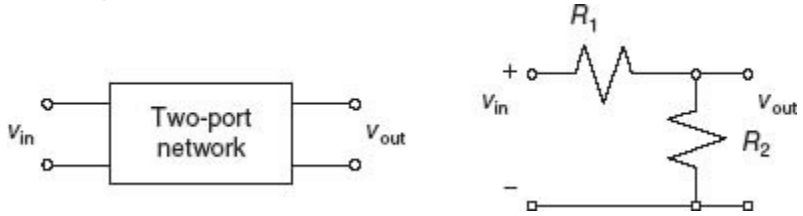


The two 2-kΩ resistors combine to 1 kΩ, which is in series with the 800 Ω and 400 Ω resistors. The total resistance of the network is thus 800 Ω + 1 kΩ + 400 Ω = 2.2 kΩ

2.4.4 The Voltage Divider

A voltage divider is a deceptively simple, but surprisingly useful and important circuit. It is our first example of a two-port network. Two-port networks have a pair of input wires and a pair of output wires, as shown in Figure 2.13.

FIGURE 2.13 A voltage divider is an example of a two-port network.

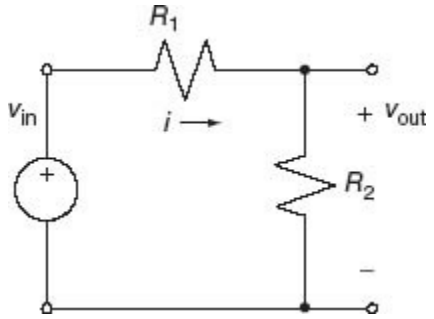


The analysis of a voltage divider is a straightforward extension of Ohm's law and what we have learned about resistors in series.

As shown in Figure 2.14, when a voltage source is connected to the voltage divider, an amount of current flows equal to

$$i = \frac{v_{in}}{R_1 + R_2} \tag{2.17}$$

FIGURE 2.14 A voltage divider connected to an ideal voltage source.

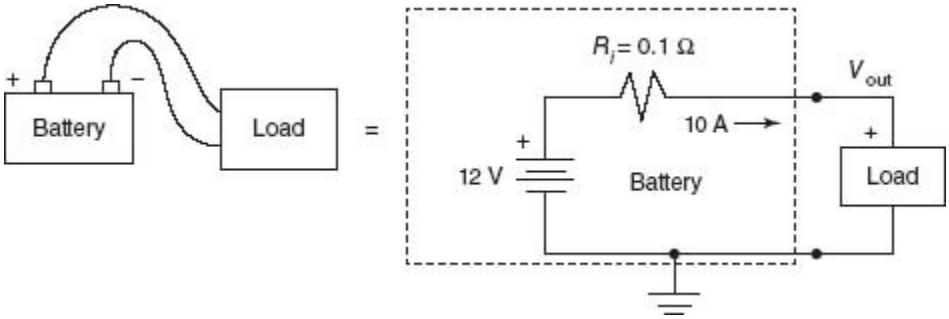


Since $v_{out} = iR_2$, we can write the following voltage divider equation:

$$v_{out} = v_{in}\left(\frac{R_2}{R_1 + R_2}\right) \quad (2.18)$$

Equation 2.18 is so useful that it is well worth committing to memory.

Example 2.5 Analyzing a Battery as a Voltage Divider. Suppose an automobile battery is modeled as an ideal 12-V source in series with a 0.1 Ω internal resistance.



a. What would the battery output voltage drop to when 10 A is delivered?

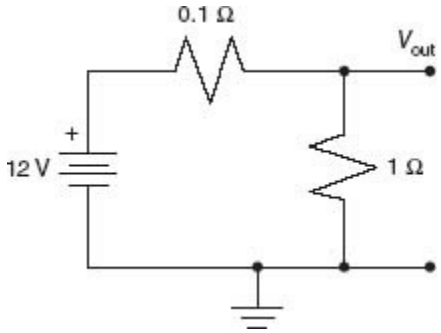
b. What would be the output voltage when the battery is connected to a 1-Ω load?

Solution

a. With the battery delivering 10 A, the output voltage drops to

$$V_{out} = V_B - IR_i = 12 - 10 \times 0.1 = 11\ \text{V}$$

b. Connected to a 1-Ω load, the circuit can be modeled as shown below:



We can find V_{out} from the voltage divider relationship (Eq. 2.18):

$$V_{out} = V_{in}\left(\frac{R_2}{R_1 + R_2}\right) = 12\left(\frac{1.0}{0.1 + 1.0}\right) = 10.91\ \text{V}$$

2.4.5 Wire Resistance

In many circumstances, connecting wire is treated as if it is perfect—that is, it has no resistance—so there is no voltage drop in those wires. In circuits delivering a fair amount of power, however, that assumption may lead to serious errors. Stated another way, an important part of the design of power circuits is choosing heavy enough wire to transmit that power without excessive losses. If connecting wire is too small, power is wasted and, in extreme cases, conductors can get hot enough to cause a fire hazard.

The resistance of wire depends primarily on its length, diameter, and the material of which it is made. Equation 2.19 describes the fundamental relationship for resistance (Ω):

$$R = \rho \frac{l}{A} \tag{2.19}$$

where ρ is the resistivity of the material, l is the wire length, and A is the wire cross-sectional area.

With l in meters (m) and A in m^2, units for resistivity ρ in the SI system are Ω-m (in these units copper has $\rho = 1.724 \times 10^{-8}$ Ω-m). The units often used in the United States, however, are tricky (as usual) and are based on areas expressed in *circular mils* (cmil). One circular mil is the area of a circle with diameter 0.001 in (1 mil = 0.001 in). So how can we determine the cross-sectional area of a wire (in circular mils) with diameter d (mils)? That is the same as asking how many 1-mil-diameter circles can fit into a circle of diameter d mils.

$$A = \frac{\frac{\pi}{4} d^2 \text{ sq mil}}{\frac{\pi}{4} 1^2 \text{ sq mil/cmil}} = d^2 \text{ cmil} \tag{2.20}$$

Example 2.6 From Mils to Ohms. The resistivity of annealed copper at 20°C is 10.37 Ω-cmils/ft. What is the resistance of 100 ft of wire with diameter 80.8 mils (0.0808 in)?

Solution

$$R = \rho \frac{l}{A} = 10.37 \text{ Ω-cmil/ft} \cdot \frac{100 \text{ ft}}{(80.8)^2 \text{ cmil}} = 0.1588 \text{ Ω}$$

Electrical resistance of wire also depends somewhat on temperature (as temperature increases, greater molecular activity interferes with the smooth flow of electrons, thereby increasing resistance). As to materials, copper is preferred, but aluminum, being cheaper, is sometimes used by professionals, but never in home-wiring systems. Aluminum under pressure slowly deforms, which eventually loosens connections. That, coupled with high-resistivity oxide that forms overexposed aluminum, can cause high enough i^2R losses to pose a fire hazard.

There is also a phenomenon, called the *skin effect*, which causes wire resistance to increase with frequency. At higher frequencies, the inherent inductance in the core of the conductor causes current to flow less easily in the center of the wire than along the outer edge of a conductor, thereby increasing the average resistance of the entire conductor. At 60 Hz, for example, most of the current flows in just the outer one-third of an inch of wire, which means the phenomenon is unimportant for household wiring, but can be quite important

for utility-scale power.

Wire size in the United States with diameter less than about 0.5 in is specified by its American Wire Gage (AWG) number. The AWG numbers are based on wire resistance, with larger AWG numbers corresponding to higher resistance and hence smaller diameter. Conversely, smaller AWG means larger diameter and lower resistance. Ordinary house wiring is usually No. 12 AWG, which is roughly the diameter of the lead in an ordinary pencil. The largest wire designated with an AWG number is 0000, which is usually written 4/0, with a diameter of 0.460 in. For heavier wire, which is usually stranded (made up of many individual wires bundled together), the size is specified in the United States in thousands of circular mills (kcmil). For example, 1000 kcmil stranded copper wire for utility transmission lines is 1.15 in in diameter and has a resistance of 0.076 Ω/mi. In countries using the metric system, wire size is simply specified by its diameter in millimeters. Table 2.3 gives some values of wire resistance, in ohms per 100 ft, for various gages of copper wire at 68°F. Also given is the maximum allowable current for copper wire clad in the most common insulation.

TABLE 2.3 Characteristics of Copper Wire (Same as old 1.3)

Wire Gage (AWG No.)	Diameter (in)	Area (cmils)	Ohms per 100 ft[a]	Max Current (A)
000	0.4096	168,000	0.0062	195
00	0.3648	133,000	0.0078	165
0	0.3249	106,000	0.0098	125
2	0.2576	66,400	0.0156	95
4	0.2043	41,700	0.0249	70
6	0.1620	26,300	0.0395	55
8	0.1285	16,500	0.0628	40
10	0.1019	10,400	0.0999	30
12	0.0808	6530	0.1588	20
14	0.0641	4110	0.2525	15

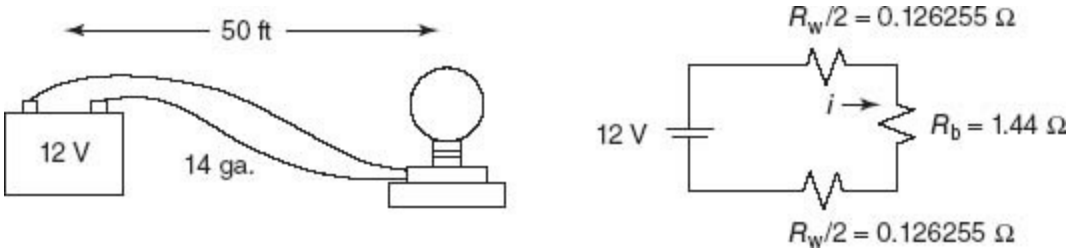
[a]DC, at 68°F.

Example 2.7 Wire Losses. Suppose an ideal 12-V battery is delivering current to a 12-V, 100-W incandescent lightbulb. The battery is 50 ft from the bulb and No. 14 copper wire is used. Find the power lost in the wires and the power delivered to the bulb.

Solution. The resistance, R_b, of a bulb designed to use 100 W when it is supplied with 12 V can be found from Equation 2.8:

$$p = \frac{v^2}{R} \quad \text{so} \quad R_b = \frac{v^2}{p} = \frac{12^2}{100} = 1.44\ \Omega$$

From Table 2.3, 50 ft of 14-gage wire has 0.2525 Ω/100 ft, so since we have 50 ft of wire to the bulb and 50 ft back again, the wire resistance is R_w = 0.2525 Ω. The circuit is as follows:



From Ohm's law, the current flowing in the circuit is

$$i = \frac{v}{R_{tot}} = \frac{12\text{ V}}{(0.12625 + 0.12625 + 1.44)\,\Omega} = 7.09\text{ A}$$

So, the power delivered to the lightbulb is

$$p_b = i^2 R_b = (7.09)^2 \times 1.44 = 72.4\text{ W}$$

and the power lost in the wires is

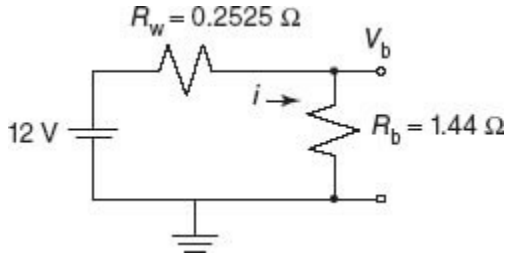
$$p_w = i^2 R_w = (7.09)^2 \times 0.2525 = 12.7\text{ W}$$

Note that our bulb is receiving only 72.4 W instead of 100 W, so it will not be nearly as bright. Also note that the battery is delivering

$$p_{battery} = 72.4 + 12.7 = 85.1\text{ W}$$

of which, quite a bit, about 15%, is lost in the wires (12.7/85.1 = 0.15).

Alternate Solution: Let us apply the concept of a voltage divider to solve this problem. We can combine the wire resistance going to the load with the wire resistance coming back, resulting in the simplified circuit model shown below:



Using Equation 2.18, the voltage delivered to the load (the lightbulb) is

$$v_{out} = v_{in}\left(\frac{R_2}{R_1 + R_2}\right) = 12\left(\frac{1.44}{0.2525 + 1.44}\right) = 10.21\text{ V}$$

The 1.79 V difference between the 12 V supplied by the battery and the 10.21 V that actually appears across the load is referred to as the *voltage sag.*

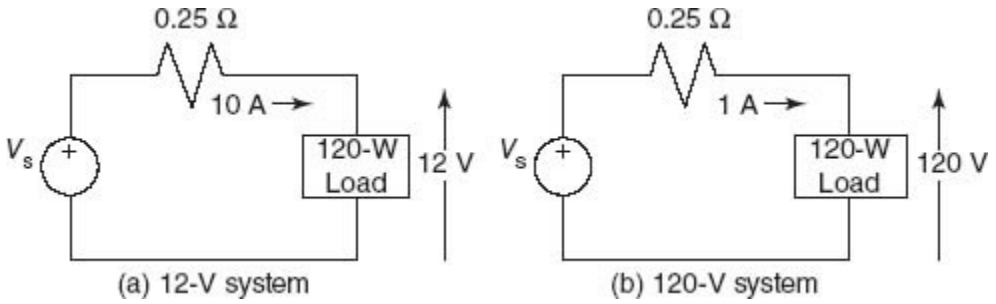
Power lost in the wires is thus

$$p_w = \frac{v_w^2}{R_w} = \frac{(1.79)^2}{0.2525} = 12.7\text{ W}$$

Example 2.7 illustrates the importance of the resistance of the connecting wires. We would probably consider 15% wire loss to be unacceptable, in which case we might want to increase the wire size (but larger wire is more expensive and harder to work with). If feasible, we could take the alternative approach to wire losses, which is to increase the supply voltage. Higher voltages require less current to deliver a given amount of power.

And, less current means less i^2R power loss in the wires as the following example demonstrates.

Example 2.8 Raising Voltage to Reduce Wire Losses. Suppose a load that requires 120 W of power is located 50 ft from a generator. The load can be designed to operate at 12 V or 120 V. Using No. 14 wire, find the voltage sag and power losses in the connecting wire for each voltage.



Solution. There are 100 ft of No. 14 wire (to the load and back) with total resistance of 0.2525 Ω (Table 2.3).

At 12 V: To deliver 120 W at 12 V requires a current of 10 A, so the voltage sag in the 0.2525-Ω wire carrying 10 A is

$$v_{\text{sag}} = iR = 10 \text{ A} \times 0.2525 \ \Omega = 2.525 \text{ V}$$

The power loss in the wire is

$$p = i^2R = (10)^2 \times 0.2525 = 25.25 \text{ W}$$

That means the generator must provide 25.25 + 120 = 145.25 W at a voltage of 12 + 2.525 = 14.525 V. Wire losses are 25.25/145.25 = 0.174 = 17.4% of the power generated. Such high losses are generally unacceptable.

At 120 V: The current required to deliver 120 W is only 1 A, which means the voltage drop in the connecting wire is only

$$\text{Voltage sag} = iR = 1 \text{ A} \times 0.2525 \ \Omega = 0.2525 \text{ V}$$

The power loss in the wire is

$$p_w = i^2R = (1)^2 \times 0.2525 = 0.2525 \text{ W } (1/100^{\text{th}} \text{that of the 12-V system})$$

The source must provide 120 W + 0.2525 W = 120.2525 W, of which the wires will lose only 0.21%.

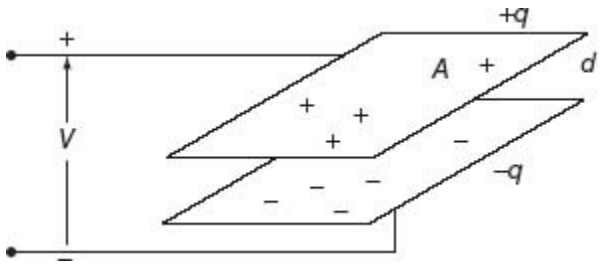
Note that i^2R power losses in the wires are 100 times larger in the 12-V circuit, which carries 10 A, than they are in the 120-V circuit carrying only 1 A. That is, increasing the voltage by a factor of 10 causes line losses to decrease by a factor of 100, which is why electric power companies transmit their power at such high voltages.

2.5 CAPACITANCE

Capacitance is a parameter in electrical circuits that describes the ability of a circuit component to store energy in an electrical field. Capacitors are discrete components that

can be purchased at the local electronics store, but the capacitance effect can occur whenever conductors are in the vicinity of each other. A capacitor can be as simple as two parallel conducting plates (Fig. 2.15), separated by a nonconducting dielectric such as air or even a thin sheet of paper.

FIGURE 2.15 A capacitor can consist of two parallel, charged plates separated by a dielectric.



If the surface area of the plates is large compared to their separation, the capacitance is given by

$$C = \varepsilon \frac{A}{d} \quad \text{farads} \tag{2.21}$$

where C is capacitance (farads, F), ε is permittivity (F/m), A is the area of one plate (m^2), and d is the separation distance (m).

Example 2.9 Capacitance of Two Parallel Plates. Find the capacitance of two 0.5 m^2 parallel conducting plates separated by 0.001 m of air with permittivity 8.8×10^{-12} F/m.

Solution

$$C = 8.8 \times 10^{-12}\ \text{F/m} \cdot \frac{0.5\ \text{m}^2}{0.001\ \text{m}} = 4.4 \times 10^{-9}\ \text{F} = 0.0044\ \mu\text{F} = 4400\ \text{pF}$$

Note that even with the quite large plate area in the example, the capacitance is a very small number. In practice, to achieve large surface area in a small volume, many capacitors are assembled using two flexible sheets of conductor, separated by a dielectric and rolled into a cylindrical shape with connecting leads attached to each plate.

Capacitance values in electronic circuits are typically in the microfarad (10^{-6} F = μF) to picofarad (10^{-12} = pF) range. Capacitors used in utility power systems are much larger and are typically in the millifarad range. Later, we will see how a different unit of measure, the volt-ampere-reactive (VAR), will be used to characterize the size of large, power-system capacitors.

While Equation 2.21 can be used to determine the capacitance from physical characteristics, of greater importance is the relationship between voltage, current, and capacitance. As suggested in Figure 2.15, when charge q builds up on the plates of a capacitor, a voltage v is created across the capacitor. This leads to the fundamental definition of capacitance, which is that capacitance is equal to the amount of charge required to create a 1-V potential difference between the plates.

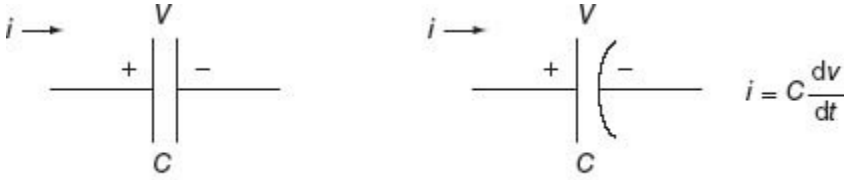
$$C(\text{farads}) = \frac{q\ (\text{coulombs})}{v\ (\text{volts})} \tag{2.22}$$

Since current is the rate at which charge is added to the plates, we can rearrange Equation 2.22 and then take the derivative to get

$$i = \frac{dq}{dt} = C\frac{dv}{dt} \tag{2.23}$$

The circuit symbol for a capacitor is usually drawn as two parallel lines, as shown in Figure 2.16a, but you may also encounter the symbol shown in Figure 2.16b. Sometimes, the term *condenser* is used for capacitors, as is the case in automobile ignition systems.

FIGURE 2.16 Two symbols for capacitors.

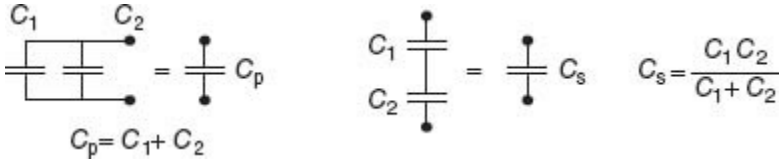


From the defining relationship between current and voltage (Eq. 2.23), it can be seen that if voltage is not changing, then current into the capacitor has to be zero. That is, under DC conditions, the capacitor appears to be an open circuit, through which no current flows.

$$\text{DC}: \quad \frac{dv}{dt} = 0, \; i = 0, \qquad \text{⫫} = \text{¦ open circuit} \tag{2.24}$$

Kirchhoff's current and voltage laws can be used to determine that the capacitance of two capacitors in parallel is the sum of their capacitances and the capacitance of two capacitors in series is equal to the product of the two over the sum, as shown in Figure 2.17.

FIGURE 2.17 Capacitors in series and capacitors in parallel.



Another important characteristic of capacitors is their ability to store energy in the form of an electric field created between the plates. Since power is the rate of change of energy, we can write that energy is the integral of power:

$$w_c = \int p\,dt = \int vi\,dt = \int vC\frac{dv}{dt}dt = C\int v\,dv$$

So, we can write that the energy stored in the electric field of a capacitor is

$$w_c = \frac{1}{2}Cv^2 \tag{2.25}$$

One final property of capacitors is that the *voltage across a capacitor cannot be changed instantaneously*. To change voltage instantaneously, charge would have to move from one plate, around the circuit, and back to the other plate in zero time. To see this conclusion mathematically, write power as the rate of change of energy,

$$p = \frac{dw}{dt} = \frac{d}{dt}\left(\frac{1}{2}Cv^2\right) = Cv\frac{dv}{dt} \tag{2.26}$$

and then note that if voltage could change instantaneously, dv/dt would be infinite, and it would therefore take infinite power to cause that change, which is impossible. Thus, the conclusion that voltage cannot change instantaneously. An important practical application of this property will be seen when we look at rectifiers that convert AC to DC. Capacitors resist rapid changes in voltages and are used to smooth the DC voltage produced from such DC power supplies. In power systems, capacitors have a number of other uses that will be explored in the next chapter.

2.6 MAGNETIC CIRCUITS

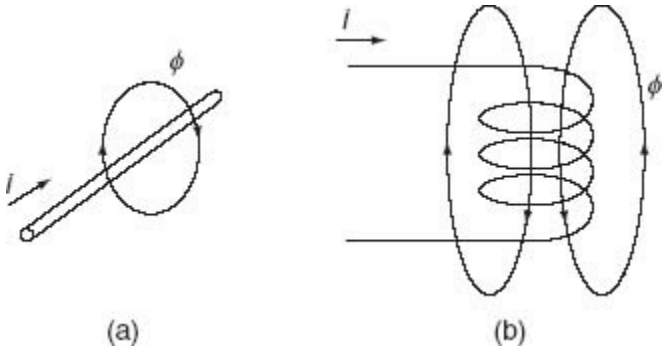
Before we can introduce inductors and transformers, we need to understand the basic concept of electromagnetism. The simple notions introduced here will be expanded in later chapters when electric power quality (especially harmonic distortion), motors and generators, and fluorescent ballasts are covered.

2.6.1 Electromagnetism

Electromagnetic phenomena were first observed and quantified in the early nineteenth century, most notably, by three European scientists: Hans Christian Oersted, André-Marie Ampère, and Michael Faraday. Oersted observed that a wire carrying current could cause a magnet suspended nearby to move. Ampère, in 1825, demonstrated that a wire carrying current could exert a force on another wire carrying current in the opposite direction. And Faraday, in 1831, discovered that current could be made to flow in a coil of wire by passing a magnet close to the circuit. These experiments provided the fundamental basis for the development of all electromechanical devices, including, most importantly, motors and generators.

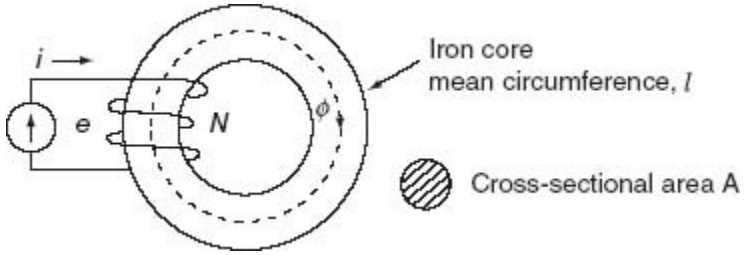
What those early experiments established was that electrical current flowing along a wire creates a magnetic field around the wire, as shown in Figure 2.18a. That magnetic field can be visualized by showing lines of magnetic flux, which are represented with the symbol ϕ. The direction of that field can be determined using the "right-hand rule" in which you imagine wrapping your right hand around a wire, with your thumb pointing in the direction of current flow. Your fingers then show the direction of the magnetic field. The field created by a coil of wire is suggested in Figure 2.18b.

FIGURE 2.18 A magnetic field is formed around a conductor carrying current.



Consider an iron core wrapped with N turns of wire carrying current i as shown in Figure 2.19. The magnetic field formed by the coil will take the path of least resistance—which is through the iron—in much the same way that electric current stays within a copper conductor. In essence, the iron is to a magnetic field what a wire is to current.

FIGURE 2.19 Current in the N-turn winding around an iron core creates a magnetic flux ϕ. An electromotive force (voltage) e is induced in the coil proportional to the rate of change of flux.



What Faraday discovered is that current flowing through the coil not only creates a magnetic field in the iron, but it also creates a voltage across the coil that is proportional to the rate of change of magnetic flux ϕ in the iron. That voltage is called an electromotive force, or emf, and is designated by the symbol e. Assuming all of the magnetic flux ϕ links all of the turns of the coil, we can write the following important relationship, which is known as *Faraday's law of electromagnetic induction*:

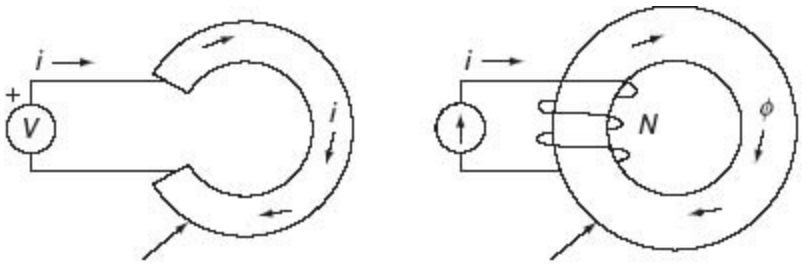
$$e = N\frac{d\phi}{dt} \tag{2.27}$$

The sign of the induced emf is always in a direction that opposes the current that created it, a phenomenon referred to as *Lenz's law*.

2.6.2 Magnetic Circuits

Magnetic phenomena are described using a fairly large number of terms that are often, at first, somewhat difficult to keep track of. One approach that may help is to describe analogies between electrical circuits, which are usually more familiar, and corresponding magnetic circuits. Consider the electrical circuit shown in Figure 2.20a, and the analogous magnetic circuit shown in Figure 2.20b. The electrical circuit consists of a voltage source, v, sending current, i, through an electrical load with resistance, R. The electrical load consists of a long wire of length, l, cross-sectional area, A, and conductance, ρ.

FIGURE 2.20 Analogous electrical and magnetic circuits.



(a) Electrical circuit (b) Magnetic circuit

The resistance of the electrical load is given by Equation 2.19. The current flowing in the electrical circuit is given by Ohm's law.

$$R = \rho \frac{l}{A} \tag{2.19}$$

In the magnetic circuit of Figure 2.20b, the driving force, analogous to voltage, is called the *magnetomotive force* (mmf), designated by $\mathcal{F}$. The magnetomotive force is created by wrapping N turns of wire, carrying current, i, around a toroidal core. By definition, the magnetomotive force is the product of *current x turns*, and has units of *ampere-turns* (A-t).

$$\text{Magnetomotive force (mmf)}\ \mathcal{F} = Ni\ \text{(ampere-turns)} \tag{2.28}$$

The response to that mmf (analogous to current in the electrical circuit) is the creation of magnetic flux ϕ, which has SI unit of *webers* (Wb). The magnetic flux is proportional to the mmf driving force and inversely proportional to a quantity called *reluctance* $\mathcal{R}$, which is analogous to electrical resistance, resulting in the "Ohm's Law" of magnetic circuits given by

$$\mathcal{F} = \mathcal{R}\phi \tag{2.29}$$

From Equation 2.29, we can ascribe units for reluctance $\mathcal{R}$ as ampere-turns per weber (A-t/Wb).

Reluctance depends on the dimensions of the core as well as its materials:

$$\text{Reluctance} = \mathcal{R} = \frac{l}{\mu A}\ \text{(A-t/Wb)} \tag{2.30}$$

Note the similarity between Equation 2.30 and the equation for resistance given in Equation 2.19.

The parameter in Equation 2.30 that indicates how readily the core material accepts magnetic flux is the material's *permeability* μ, with units of webers per ampere-turn-meter (Wb/A-t-m). The vast majority of materials do not respond to magnetic fields and their permeability is very close to that of free space

$$\text{Permeability of free space}\quad \mu_0 = 4\pi \times 10^{-7}\ \text{Wb/A-t-m} \tag{2.31}$$

Materials are often characterized by their *relative permeability*, μ_r, which for easily magnetized materials may be in the range of hundreds to hundreds of thousands for rare-earth magnets.

$$\text{Relative permeability } \mu_r = \frac{\mu}{\mu_0} \tag{2.32}$$

As will be noted later, however, the relative permeability is not a constant for a given material: it varies with the magnetic field intensity. In this regard, the magnetic analogy deviates from its electrical counterpart and so must be used with some caution.

The most common materials that readily accept magnetic flux, that is *ferromagnetic materials*, are principally iron, cobalt, and nickel. When alloyed with certain *rare-earth* elements, especially Nd (neodymium) and Sm (samarium), extremely powerful magnets can be produced. Neodymium magnets ($Nd_2Fe_{14}B$) are the strongest and are now commonly used in cordless power tools, some motors, computer hard drives, and audio speakers. Samarium–cobalt magnets ($SmCo_5$) are not as strong, but handle higher temperatures better. Rare-earth magnets are becoming extremely attractive for wind turbine generators and electric vehicle motors.

Another important quantity of interest in magnetic circuits is the *magnetic flux density*, *B*. As the name suggests, it is simply the "density" of flux given by the following:

$$\text{Magnetic flux density } B = \frac{\phi}{A} \text{ Wb/m}^2 \text{ or teslas (T)} \tag{2.33}$$

The final magnetic quantity that we need to introduce is the *magnetic field intensity*, *H*. Referring back to the simple magnetic circuit shown in Figure 2.20b, the magnetic field intensity is defined as the magnetomotive force (mmf) per unit length around the magnetic loop. With *N* turns of wire carrying current, *i*, the mmf created in the circuit is *Ni* ampere-turns. With *l* representing the mean path length for the magnetic flux, the magnetic field intensity is therefore:

$$\text{Magnetic field intensity } H = \frac{Ni}{l} \text{ A-t/m} \tag{2.34}$$

An analogous concept in electric circuits is the electric field strength, which is voltage drop per unit of length. In a capacitor, for example, the intensity of the electric field formed between the plates is equal to the voltage across the plates divided by the spacing between the plates.

Finally, if we combine Equations 2.28, 2.20, 2.30, 2.33, and 2.34, we arrive at the following relationship between magnetic flux density *B* and magnetic field intensity *H*:

$$B = \mu H \tag{2.35}$$

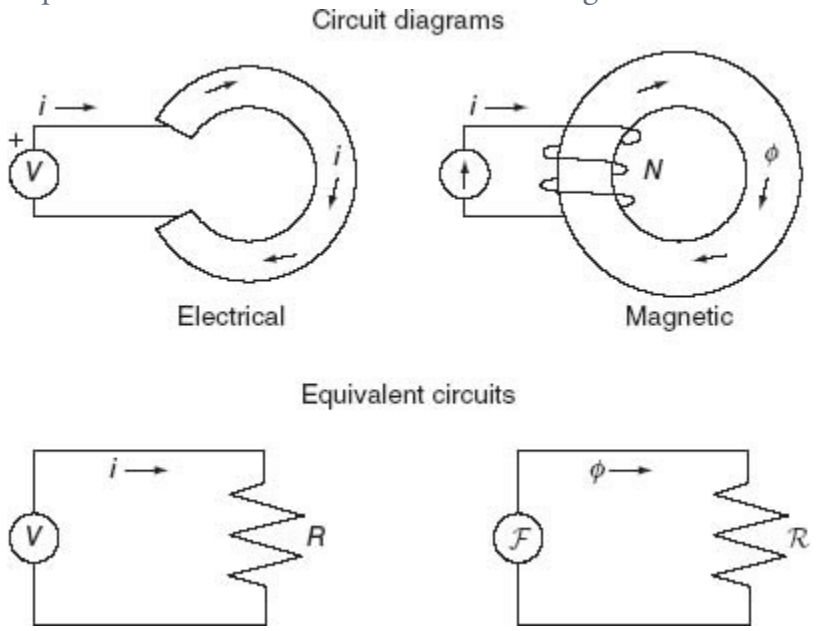
Returning to the analogies between the simple electrical circuit and magnetic circuit shown in Figure 2.20, we can now identify equivalent circuits, as shown in Figure 2.21, along with the analogs shown in Table 2.4.

TABLE 2.4 Analogous Electrical and Magnetic Circuit Quantities

Electrical	Magnetic	Magnetic Units
Voltage *v*	Magnetomotive force $\mathcal{F} = Ni$	Amp-turns
Current *i*	Magnetic flux ϕ	Webers Wb
Resistance *R*	Reluctance $\mathcal{R}$	Amp-turns/Wb
Conductivity 1/ρ	Permeability μ	Wb/A-t-m
Current density *J*	Magnetic flux density *B*	Wb/m^2 = teslas (T)

Electric field E	Magnetic field intensity H	Amp-turns/m

FIGURE 2.21 Equivalent circuits for the electrical and magnetic circuits are shown.



2.7 INDUCTANCE

Having introduced the necessary electromagnetic background, we can address inductance. Inductance is, in some sense, a mirror image of capacitance. While capacitors store energy in their electric field, inductors store energy in a magnetic field. While capacitors prevent voltage from changing instantaneously, inductors, as we shall see, prevent current from changing instantaneously.

2.7.1 Physics of Inductors

Consider a coil of wire carrying some current creating a magnetic field within the coil. As shown in Figure 2.22, if the coil has an air core, the flux can pretty much go where it wants to, which leads to the possibility that much of the flux will not link all of the turns of the coil. To help guide the flux through the coil, so that flux leakage is minimized, the coil might be wrapped around a ferromagnetic bar or ferromagnetic core as shown in Figure 2.23. The lower reluctance path provided by the ferromagnetic material also greatly increases the flux ϕ.

FIGURE 2.22 A coil with an air core will have considerable leakage flux.

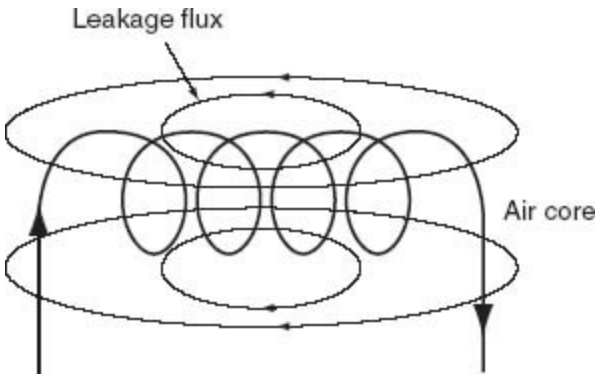
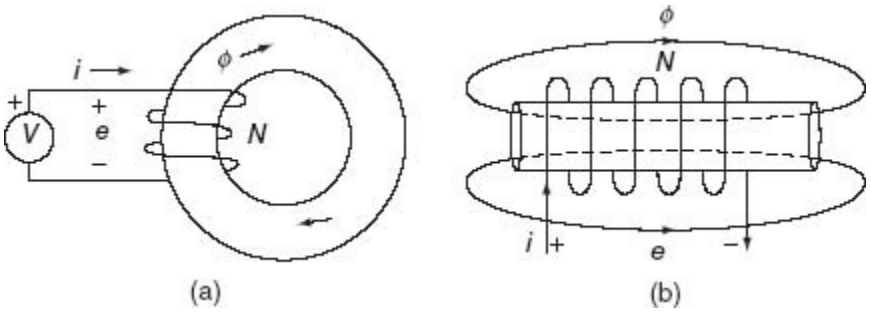


FIGURE 2.23 Flux can be increased and leakage reduced by wrapping the coils around a ferromagnetic material that provides a lower reluctance path. The flux will be much higher using the core (a) rather than the rod (b).



We can easily analyze the magnetic circuit in which the coil is wrapped around the ferromagnetic core in Figure 2.23a. Assume all of the flux stays within the low reluctance pathway provided by the core, and apply Equation 2.29.

$$\phi = \frac{Ni}{\mathcal{R}} \tag{2.36}$$

From Faraday's law (Eq. 2.27), changes in magnetic flux create a voltage e, called the electromotive force (emf), across the coil equal to $N\,(d\phi/dt)$

Substituting Equation 2.36 into Equation 2.27 gives

$$e = N\frac{d}{dt}\left(\frac{Ni}{\mathcal{R}}\right) = \frac{N^2}{\mathcal{R}}\frac{di}{dt} = L\frac{di}{dt} \tag{2.37}$$

where inductance L has been introduced and defined as

$$\text{Inductance } L = \frac{N^2}{\mathcal{R}} \quad \text{henries (H)} \tag{2.38}$$

Note in Figure 2.23a that a distinction has been made between e, the emf voltage induced across the coil, and v, a voltage that may have been applied to the circuit to cause the flux in the first place. If there are no losses in the connecting wires between the source voltage and the coil, then $e = v$ and we have the final defining relationship for an inductor:

$$v = L\frac{di}{dt} \tag{2.39}$$

As given in Equation 2.38, inductance is inversely proportional to reluctance $\mathcal{R}$. Recall that the reluctance of a flux path through air is much greater than the reluctance if it passes through a ferromagnetic material. That tells us if we want a large inductance, the flux needs to pass through materials with high permeability (not air).

Example 2.10 Inductance of a Core-and-Coil. Find the inductance of a core with effective length l = 0.1 m, cross-sectional area A = 0.001 m^2, and relative permeability μ somewhere between 15, 000 and 25, 000. It is wrapped with N = 10 turns of wire. What is the range of inductance for the core?

Solution. When the core's permeability is 15, 000 times that of free space, it is

$$\mu_{\text{core}} = \mu_r \mu_0 = 15{,}000 \times 4\pi \times 10^{-7} = 0.01885 \text{ Wb/A-t-m}$$

so its reluctance is

$$\mathcal{R} = \frac{l}{\mu_{\text{core}} A} = \frac{0.1 \text{ m}}{0.01885 \text{ (Wb/A-t-m)} \times 0.001 \text{ m}^2} = 5305 \text{ A-t/Wb}$$

and its inductance is

$$L = \frac{N^2}{\mathcal{R}} = \frac{10^2}{5305} = 0.0188 \text{ H} = 18.8 \text{ mH}$$

Similarly, when the relative permeability is 25, 000 the inductance is

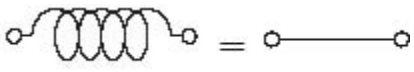
$$L = \frac{N^2}{\mathcal{R}} = \frac{N^2 \mu_r \mu_0 A}{l} = \frac{10^2 \times 25{,}000 \times 4\pi \times 10^{-7} \times 0.001}{0.1}$$
$$= 0.0314 \text{ H} = 31.3 \text{ mH}$$

The point of Example 2.10 is that the inductance of a coil of wire wrapped around a solid core can be quite variable given the imprecise value of the core's permeability. Its permeability depends on how hard the coil is driven by mmf, so you cannot just pick up an off-the-shelf inductor like this and know what its inductance is likely to be. The trick to getting a more precise value of inductance, given the uncertainty in permeability, is to sacrifice some amount of inductance by building a small air gap into the core. Another approach is to get the equivalent of an air gap by using a powdered ferromagnetic material in which the spaces between particles of material act as the air gap. The air gap reluctance, which is determined strictly by geometry, is large compared to the core reluctance so the impact of core permeability changes is minimized.

2.7.2 Circuit Relationships for Inductors

From the defining relationship between voltage and current for an inductor (Eq. 2.39), we can note that when current is not changing with time the voltage across the inductor is zero. That is, for DC conditions, an inductor looks the same as a short-circuit, zero-resistance wire:

$$\text{DC: } v = L\frac{di}{dt} = L \cdot 0 = 0 \quad \text{(2.40)}$$



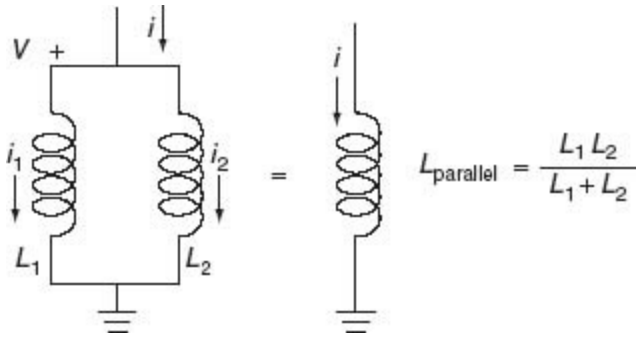
When inductors are wired in series, the same current flows through each one so the voltage drop across the pair is simply:

$$v_{\text{series}} = L_1\frac{di}{dt} + L_2\frac{di}{dt} = (L_1 + L_2)\frac{di}{dt} = L_{\text{series}}\frac{di}{dt} \quad \text{(2.41)}$$

where L_{series} is the equivalent inductance of the two series inductors. That is,

$$L_{\text{series}} = L_1 + L_2 \quad \text{(2.42)}$$

FIGURE 2.24 Two inductors in parallel.



Consider Figure 2.24 for two inductors in parallel. The total current flowing is the sum of the currents.

(2.43) $$i_{\text{parallel}} = i_1 + i_2$$

The voltages are the same across each inductor so we can use the integral form of Equation 2.39 to get

(2.44) $$\frac{1}{L_{\text{parallel}}}\int v\,dt = \frac{1}{L_1}\int v\,dt + \frac{1}{L_2}\int v\,dt$$

Dividing out the integral gives us the equation for inductors in parallel:

(2.45) $$L_{\text{parallel}} = \frac{L_1 L_2}{L_1 + L_2}$$

Just as capacitors store energy in their electric fields, inductors also store energy, but this time it is in their magnetic fields. Since energy w is the integral of power p, we can easily set up the equation for energy stored:

(2.46) $$w_{\text{L}} = \int p\,dt = \int vi\,dt = \int \left(L\frac{di}{dt}\right) i\,dt = L\int i\,\text{d}i$$

This leads to the following equation for energy stored in an inductor's magnetic field:

(2.47) $$w_{\text{L}} = \frac{1}{2}Li^2$$

If we use Equation 2.47 to learn something about the power dissipated in an inductor, we get

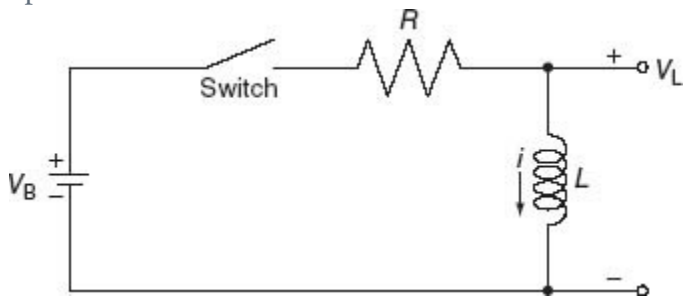
(2.48) $$p = \frac{dw}{dt} = \frac{d}{dt}\left(\frac{1}{2}Li^2\right) = Li\frac{di}{dt}$$

From Equation 2.48, we can deduce another important property of inductors: *the current through an inductor cannot be changed instantaneously!* For current to change instantaneously, di/dt would be infinite, which (Eq. 2.48) tells us would require infinite power, which is impossible. It takes time for the magnetic field, which is storing energy, to collapse. Inductors, in other words, make current act like it has inertia.

Now wait a minute. If current is flowing in the simple circuit containing an inductor, resistor, and switch as shown in Figure 2.25, why can't you just open the switch and cause the current to stop instantaneously? Surely, it does not take infinite power to open a switch. The answer is that the current has to keep going for at least a short interval just after opening the switch. To do so, current momentarily must jump the gap between the contact

points as the switch is opened. That is, the switch "arcs" and you get a little spark. Too much arc and the switch can be burned out.

FIGURE 2.25 A simple R–L circuit with a switch.



We can develop an equation that describes what happens when an open switch in the R–L circuit of Figure 2.25 is closed. Doing so gives us a little practice with Kirchhoff's voltage law. The voltage rise due to the battery must equal the voltage drop across the resistance plus inductance:

$$V_B = iR + L\frac{di}{dt} \tag{2.49}$$

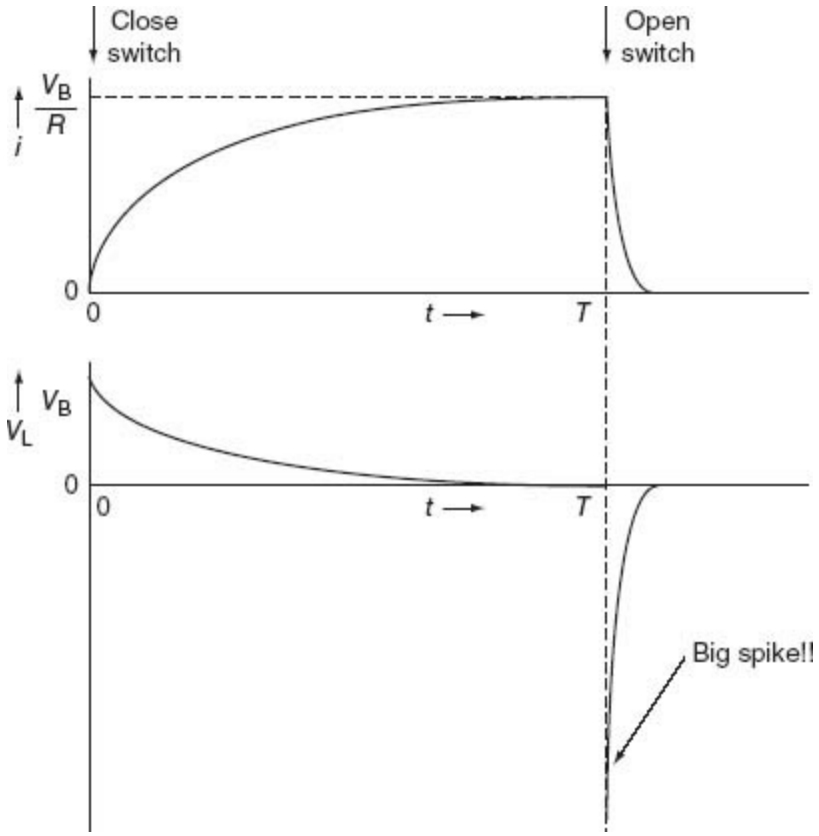
Without going through the details, the solution to Equation 2.49, subject to the initial condition that $i = 0$ at $t = 0$, is

$$i = \frac{V_B}{R}\left(1 - e^{-\frac{R}{L}t}\right) \tag{2.50}$$

Does this solution look right? At $t = 0$, $i = 0$, so that is alright. At $t = \infty$, $i = V_B/R$. That seems alright too since eventually the current reaches a steady state, DC value, which means the voltage drop across the inductor is zero ($v_L = L\ di/dt = 0$). At that point, all of the voltage drop is across the resistor, so current is $I = V_B/R$. The quantity L/R in the exponent of Equation 2.50 is called the *time constant*, T.

We can sketch out the current flowing in the circuit of Figure 2.25 along with the voltage across the inductor as we go about opening and closing the switch (Fig. 2.26). If we start with the switch open at $t = 0^-$ (where the minus suggests just before $t = 0$), the current will be zero and the voltage across the inductor, v_L will be 0 (since $v_L = L\ di/dt$ and $di/dt = 0$).

FIGURE 2.26 Opening a switch at $t = T$ produces a large spike of voltage across the inductor.



At $t = 0$, the switch is closed. At $t = 0^+$ (just after the switch closes), the current is still zero since it cannot change instantaneously. With zero current, there is no voltage drop across the resistor ($v_R = iR = 0$), which means the entire battery voltage appears across the inductor ($v_L = V_B$). Note there is no restriction on how rapidly inductor voltage can change, so an instantaneous jump is allowed. Current climbs after the switch is closed until DC conditions are reached at which point $di/dt = 0$ so $v_L = 0$ and the entire battery voltage is dropped across the resistor. Current i asymptotically approaches V_B/R.

Now, at time $t = T$, open the switch. Current quickly, but not instantaneously, drops to zero (by arcing). Since the voltage across the inductor is $v_L = L\, di/dt$, and di/dt (the slope of current) is a very large negative quantity, v_L shows a precipitous, downward spike as shown in Figure 2.26. This large spike of voltage can be much, much higher than the little voltage provided by the battery.

In other words, with just an inductor, a battery, and a switch, we can create a very large voltage spike as we open the switch. This peculiar property of inductors is used to advantage in an automobile ignition system to cause spark plugs to ignite the gasoline in the cylinders of your engine. In your ignition system, a switch opens (it used to be the points inside your distributor, now it is a transistorized switch) creating a spike of voltage that is further amplified by a transformer coil to create a voltage of tens of thousands of volts—enough to cause an arc across the gap in your car's spark plugs. The other important application of this voltage spike is to use it to start the arc between electrodes of a fluorescent lamp.

2.8 TRANSFORMERS

When Thomas Edison created the first electric utility in 1882, he used DC to transmit power from generator to load. Unfortunately, at the time, it was not possible to change DC voltages easily from one level to another, which meant transmission was at the relatively low voltages of the DC generators. As we have seen, transmitting power at low voltage means high currents must flow, resulting in large i^2R power losses in the wires as well as high voltage drops between power plant and loads. The result was that power plants had to be located very close to loads. In those early days, it was not uncommon for power plants in cities to be located only a few blocks apart.

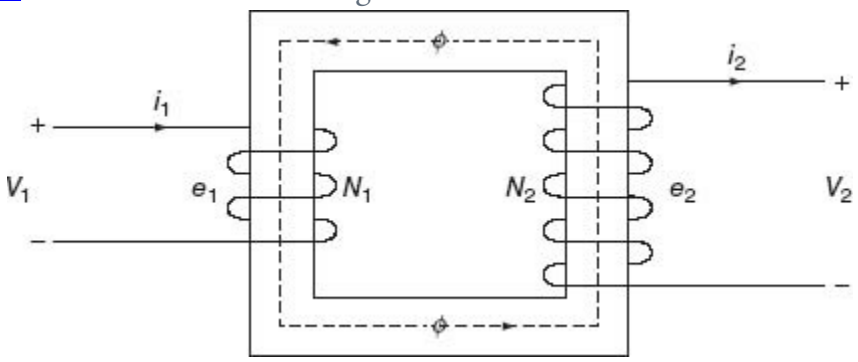
In a famous battle between two giants of the time, George Westinghouse solved the transmission problem by introducing AC generation using transformers to boost the voltage entering transmission lines, and transformers to reduce the voltage back down to safe levels at the customer's site. Edison lost the battle but never abandoned DC—a decision that soon led to the collapse of his electric utility company.

It would be hard to overstate the importance of transformers in modern electric power systems. Transmission line power losses are proportional to the square of current, and inversely proportional to the square of voltage. Raising voltages by a factor of 10 lowers line losses by a factor of 100. Modern systems generate voltages in the range of 12–25 kV. Transformers boost that voltage to hundreds of thousands of volts for long-distance transmission. At the receiving end, transformers drop the transmission line voltage to perhaps 4–35 kV at electrical substations for local distribution. Other transformers then drop the voltage to safe levels for home, office, and factory use.

2.8.1 Ideal Transformers

A simple transformer configuration is shown in Figure 2.27. Two coils of wire are wound around a magnetic core. As shown, the primary side of the transformer has N_1 turns of wire carrying current i_1, while the secondary side has N_2 turns carrying i_2.

FIGURE 2.27 An idealized two-winding transformer.



If we assume an ideal core with no flux leakage, then the magnetic flux ϕ linking the primary windings is the same as the flux linking the secondary. From Faraday's law, we can write

$$e_1 = N_1 \frac{d\phi}{dt} \tag{2.51}$$

and

$$e_2 = N_2 \frac{d\phi}{dt} \quad (2.52)$$

Continuing the idealization of the transformer, if there are no wire losses, then the voltage on the incoming wires, v_1 is equal to the emf e_1, and on the output wires v_2 equals e_2. Dividing Equation 2.52 by Equation 2.51 gives

$$\frac{v_2}{v_1} = \frac{e_2}{e_1} = \frac{N_2\,(\mathrm{d}\phi/\mathrm{d}t)}{N_1\,(\mathrm{d}\phi/\mathrm{d}t)} \quad (2.53)$$

Before canceling out the $\mathrm{d}\phi/\mathrm{d}t$, note that we can only do so if $\mathrm{d}\phi/\mathrm{d}t$ is not equal to zero. That is, the following fundamental relationship for transformers (Eq. 2.54) is not valid for DC conditions.

$$v_2 = \left(\frac{N_2}{N_1}\right) v_1 = (\text{turns ratio}) \cdot v_1 \quad (2.54)$$

The quantity in the parenthesis is called the *turns ratio*. If voltages are to be raised, then the turns ratio needs to be greater than 1; to lower voltages, it needs to be less than 1.

Does Equation 2.54, which says we can easily increase the voltage from primary to secondary, suggests we are getting something for nothing? The answer is, as might be expected, no. While Equation 2.54 suggests an easy way to raise AC voltages, energy still must be conserved. If we assume our transformer is perfect—that is, it has no energy losses of its own—then power going into the transformer on the primary side must equal power delivered to the load on the secondary side. That is,

$$v_1 i_1 = v_2 i_2 \quad (2.55)$$

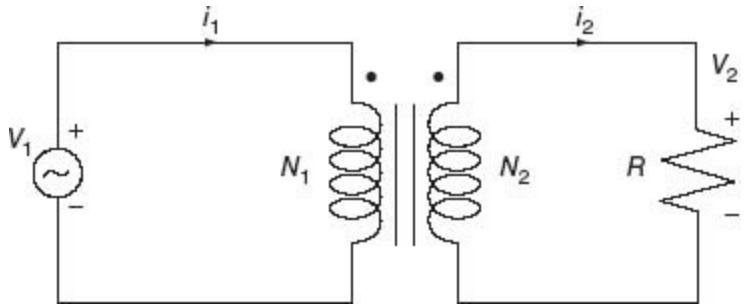
Substituting Equation 2.54 into Equation 2.55 gives

$$i_2 = \left(\frac{v_1}{v_2}\right) i_1 = \left(\frac{N_1}{N_2}\right) i_1 \quad (2.56)$$

What Equation 2.56 shows is that if we increase the voltage on the secondary side of the transformer (to the load), we correspondingly reduce the current to the load. For example, bumping the voltage up by a factor of 10 reduces the current delivered by a factor of 10. On the other hand, decreasing the voltage by a factor of 10 increases the current 10-fold on the secondary side.

Another important consideration in transformer analysis is what a voltage source "sees" when it sends current into a transformer that is driving a load. For example, in Figure 2.28 a voltage source, transformer, and resistive load are shown. The symbol for a transformer shows a couple of parallel bars between the windings, which is meant to signify that the coil is wound around a metal (steel) core (not an air core). The dots above the windings indicate the polarity of the windings. When both dots are on the same side (as in Figure 2.28), a positive voltage on the primary produces a positive voltage on the secondary.

FIGURE 2.28 A resistance load being driven by a voltage source through a transformer.



Back to the question of the equivalent load seen by the input voltage source for the circuit of Figure 2.28. If we call that load R_{in}, then we have

(2.57) $$v_1 = R_{in} i_1$$

Rearranging Equation 2.57 and substituting in Equations 2.55 and 2.56 gives

(2.58) $$R_{in} = \left(\frac{v_1}{i_1}\right) = \frac{(N_1/N_2)\,v_2}{(N_2/N_1)\,i_2} = \left(\frac{N_1}{N_2}\right)^2 \cdot \frac{v_2}{i_2} = \left(\frac{N_1}{N_2}\right)^2 R$$

where $v_2/i_2 = R$ is the resistance of the transformer load.

As far as the input voltage source is concerned, the load it sees is the resistance on the secondary side of the transformer divided by the square of the turns ratio. This is referred to as a resistance transformation (or more generally an *impedance* transformation).

Example 2.11 Some Transformer Calculations. A 120- to 240-V step-up transformer is connected to a 100-Ω load.

a. What is the turns ratio?

b. What resistance does the 120-V source see?

c. What is the current on the primary side and on the secondary side?

Solution

a. The turns ratio is the ratio of the secondary voltage to the primary voltage:

$$\text{Turns ratio} = \frac{N_2}{N_1} = \frac{v_2}{v_1} = \frac{240\ \text{V}}{120\ \text{V}} = 2$$

b. The resistance seen by the 120-V source is given by Equation 2.58:

$$R_{in} = \left(\frac{N_1}{N_2}\right)^2 R = \left(\frac{1}{2}\right)^2 \cdot 100 = 25\ \Omega$$

c. The primary side current will be

$$i_{\text{primary}} = \frac{v_1}{R_{in}} = \frac{120\ \text{V}}{25\ \Omega} = 4.8\ \text{A}$$

On the secondary side, current will be

$$i_{\text{secondary}} = \frac{v_2}{R_{\text{load}}} = \frac{240\ \text{V}}{100\ \Omega} = 2.4\ \text{A}$$

Note that power is conserved:

$$v_1 \cdot i_1 = 120\ \text{V} \cdot 4.8\ \text{A} = 576\ \text{W}$$

$$v_2 \cdot i_2 = 240\ \text{V} \cdot 2.4\ \text{A} = 576\ \text{W}$$

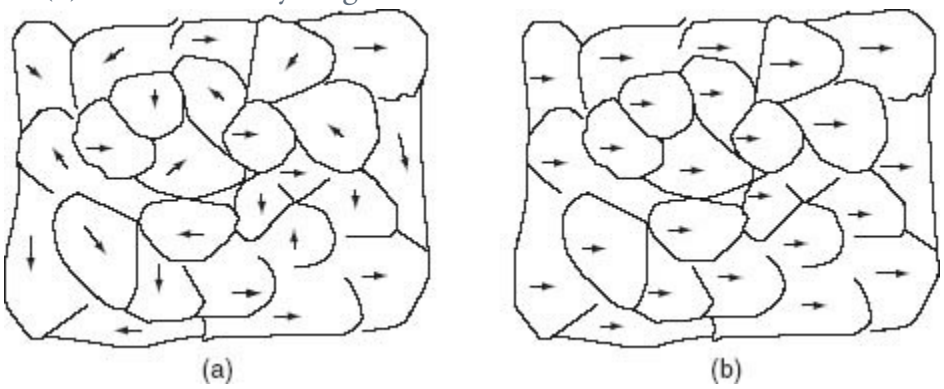
2.8.2 Magnetization Losses

Up to this point, we have considered a transformer to have no losses of any sort associated with its performance. We know, however, that real windings have inherent resistance so that when current flows there will be voltage and power losses. There are also losses associated with the magnetization of the core, which will be explored now.

The orientation of atoms in ferromagnetic materials (principally iron, nickel, and cobalt, as well as some rare-earth elements) is affected by magnetic fields. This phenomenon is described in terms of unbalanced spins of electrons, which causes the atoms to experience a torque, called a *magnetic moment*, when exposed to a magnetic field.

Ferromagnetic metals exist in a crystalline structure with all of the atoms within a particular portion of the material arranged in a well-organized lattice. The regions in which the atoms are all perfectly arranged are called subcrystalline *domains*. Within each magnetic domain, all of the atoms have their spin axes aligned with each other. Adjacent domains, however, may have their spin axes aligned differently. The net effect of the random orientation of domains in an unmagnetized ferromagnetic material is that all of the magnetic moments cancel each other and there is no net magnetization. This is illustrated in Figure 2.29a.

FIGURE 2.29 Representation of the domains in an (a) unmagnetized ferromagnetic material and (b) one that is fully magnetized.

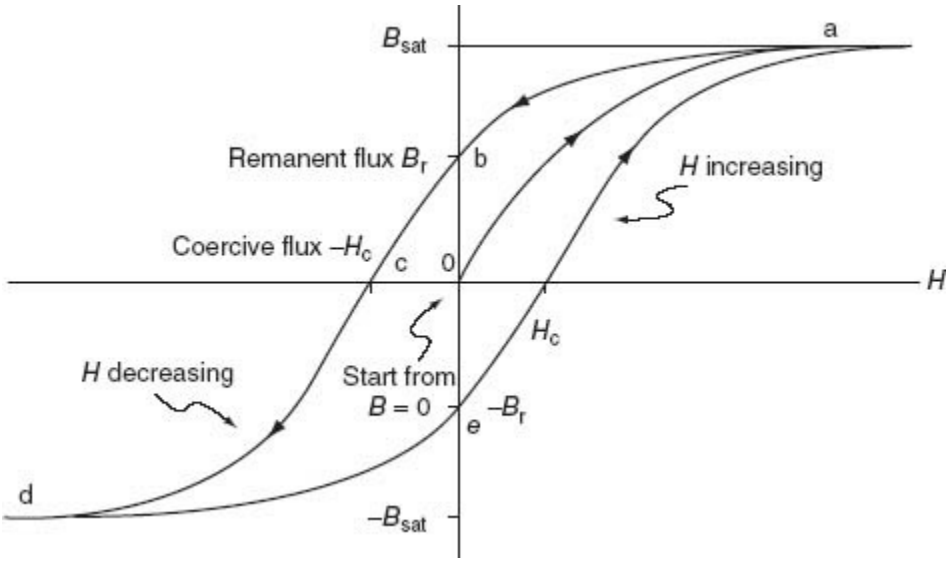


When a strong magnetic field H is imposed on the domains, their spin axes begin to align with the imposed field, eventually reaching saturation as shown in Figure 2.27b. After saturation is reached, increasing the magnetizing force causes no increase in flux density, B. This suggests that the relationship between magnetic field H and flux density B will not be linear, as was implied in Equation 2.35, and in fact will exhibit some sort of S-shaped behavior. That is, permeability μ is not constant.

Figure 2.30 illustrates the impact that the imposition of a magnetic field H on a ferromagnetic material has on the resulting magnetic flux density B. The field causes the magnetic moments in each of the domains to begin to align. When the magnetizing force H is eliminated, the domains relax, but do not return to their original random orientation, leaving a remnant flux B_r; that is, the material becomes a "permanent magnet." One way to demagnetize the material is to heat it to a high enough temperature (called the *Curie temperature*) that the domains once again take on their random orientation. For iron, the Curie temperature is 770°C, which is about the same as that for samarium–cobalt magnets. For neodymium magnets, the Curie temperature is relatively low (300–400°C), but their

lower cost and higher magnetization makes them the most commonly used.

FIGURE 2.30 Cycling an imposed mmf on a ferromagnetic material produces a hysteresis loop.



Consider what happens to the *B–H* curve as the magnetic domains are cycled back and forth by an imposed AC magnetomotive force. On the *B–H* curve of Figure 2.30, the cycling is represented by the path o–a followed by the path a–b. If the field is driven somewhat negative, the flux density can be brought back to zero (point c) by imposing a *coercive force*, H_c; forcing the applied mmf even more to negative brings us to point d. Driving the mmf back in the positive direction takes us along path d–e–a.

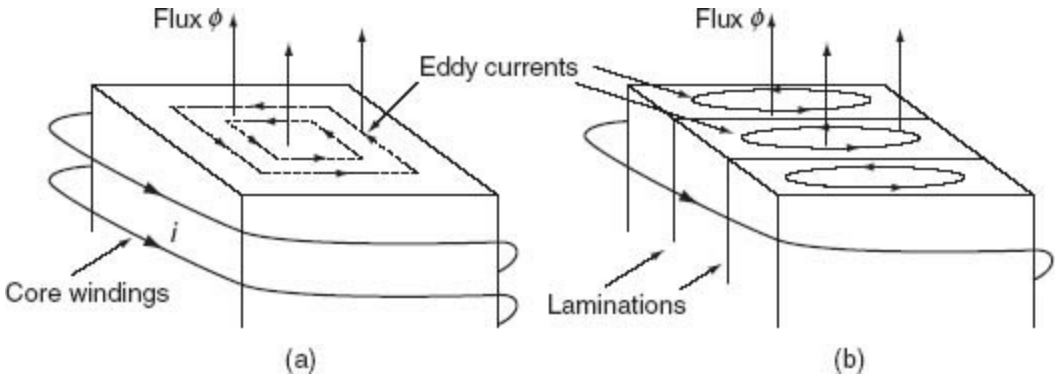
The phenomenon illustrated in the *B–H* curve is called hysteresis. Cycling a magnetic material causes the material to heat up; in other words, energy is being wasted. It can be shown that the energy dissipated as heat in each cycle is proportional to the area contained within the hysteresis loop. Each cycle through the loop creates an energy loss, therefore the rate at which energy is lost, which is power, is proportional to the frequency of cycling and the area within the hysteresis loop. That is, we can write an equation of the sort

$$\text{Power loss due to hysteresis} = k_1 f \tag{2.59}$$

where k_1 is just a constant of proportionality and f is the frequency.

Another source of core losses is caused by small currents, called *eddy currents*, that are formed within the ferromagnetic material as it is cycled. Consider a cross section of core with magnetic flux ϕ aligned along its axis as shown in Figure 2.31a. We know from Faraday's law that anytime a loop of electrical conductor has varying magnetic flux passing through it, there will be a voltage (emf) created in that loop proportional to the rate of change of ϕ. That emf can create its own current in the loop. In the case of our core, the ferromagnetic material is the conductor, which we can think of as forming loops of conductor wrapped around flux, creating the eddy currents shown in the figure.

FIGURE 2.31 Eddy currents in a ferromagnetic core result from changes in flux linkages: (a) A solid core produces large eddy current losses. (b) Laminating the core yields smaller losses.



To analyze the losses associated with eddy currents, imagine the flux as a sinusoidal, time-varying function

(2.60) $\phi = \sin(\omega t)$

The emf created by changing flux is proportional to dϕ/dt

(2.61) $$e = k_2 \frac{d\phi}{dt} = k_2\,\omega\cos(\omega t)$$

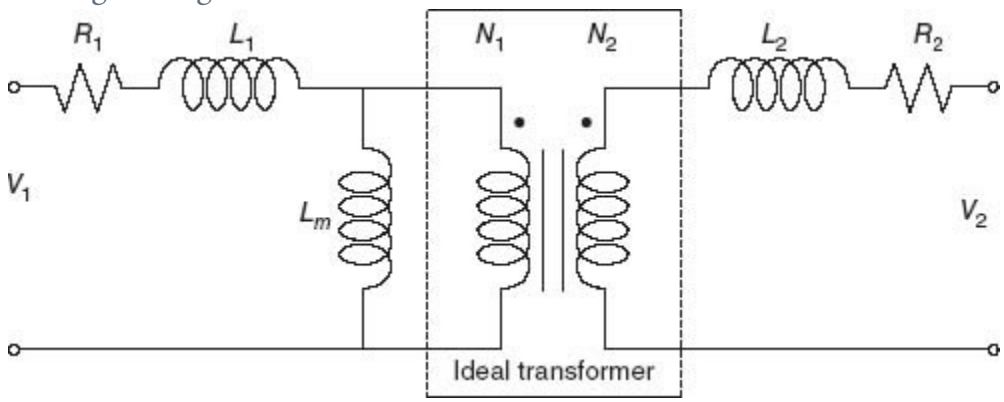
where k_2 is just a constant of proportionality. The power loss in a conducting "loop" around this changing flux is proportional to voltage squared over loop resistance:

(2.62) $$\text{Eddy current power loss} = \frac{e^2}{R} = \frac{1}{R}\cdot[k_2\omega\cos(\omega t)]^2$$

Equation 2.62 suggests that power loss due to eddy currents is inversely proportional to the resistance of the "loop" through which the current is flowing. To control power losses, therefore, there are two approaches: (1) increase the electrical resistance of the core material and (2) make the loops smaller and tighter. Tighter loops have more resistance (since resistance is inversely proportional to the cross-sectional area through which current flows) and they contain less flux ϕ (emf is proportional to the rate of change of flux, not flux density).

Real transformer cores are designed to control both causes of eddy current losses. Steel cores, for example, are alloyed with silicon to increase resistance; also, high resistance magnetic ceramics, called ferrites, are used instead of conventional alloys. To make the loops smaller, cores are usually made up of many thin, insulated, laminated layers as shown in Figure 2.31b.

FIGURE 2.32 A model of a real transformer accounts for winding resistances, leakage fluxes, and magnetizing inductance.



The second, very important conclusion from Equation 2.62 is that eddy current losses are proportional to frequency squared.

(2.63) Power loss due to eddy currents $= k_3 f^2$

Later, when we consider harmonics in power circuits, we will see that some loads cause currents consisting of multiples of the fundamental 60-Hz frequency. The higher frequency harmonics can lead to transformer core burnouts due to the eddy current dependence on frequency squared.

A real transformer can be modeled using a circuit consisting of an idealized transformer with added idealized resistances and inductors as shown in Figure 2.32. Resistances R_1 and R_2 represent the resistances of the primary and secondary windings. L_1 and L_2 represent the inductances associated with primary and secondary leakage fluxes that pass through air instead of core material. Inductance L_m, the *magnetizing inductance*, allows the model to show current in the primary windings even if the secondary is an open circuit with no current flowing.

PROBLEMS

2.1 A source is connected through a switch to a load that is a resistor, a capacitor, or an inductor. At t = 0, the switch is closed and current delivered to the load results in the voltage shown below. What is the circuit element and what is its magnitude?

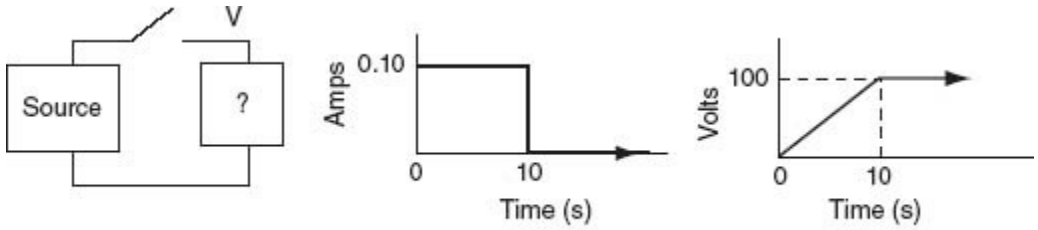


FIGURE P2.1

2.2 A voltage source produces the square wave shown below. The load, which is an ideal resistor, capacitor, or inductor, draws current as shown below.

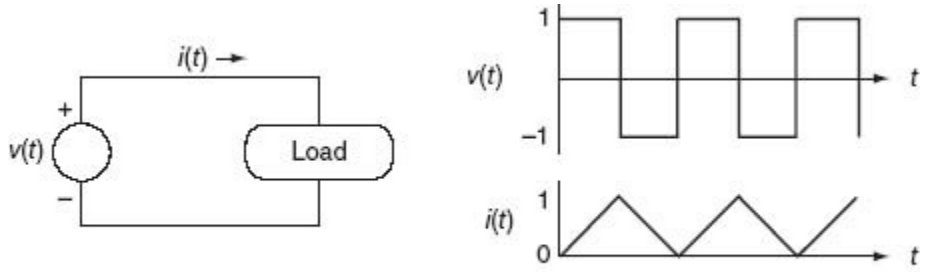


FIGURE P2.2

a. Is the "load" a resistor, a capacitor, or an inductor?

b. Sketch the power delivered to the load versus time.

c. What is the average power delivered to the load?

2.3 A source supplies voltage $v\ (\text{volts}) = 10\sqrt{2}\cos \omega t$ to a 5-Ω resistive load.

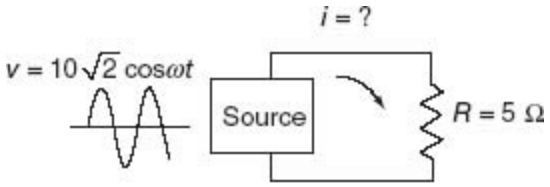


FIGURE P2.3

a. Write an expression for the current (amps) delivered to the load.

b. Write an expression for the power delivered to the load.

c. Sketch a graph of power versus time. What is the average power (W) delivered to the load?

2.4 Suppose your toaster has 14-gage wire inside and, to simplify the analysis, suppose we approximate the normal 60-Hz sinusoidal current flowing through that wire with a square wave carrying ± 10 A. Using a drift-velocity calculation, find the average back-and-forth distance those electrons travel.

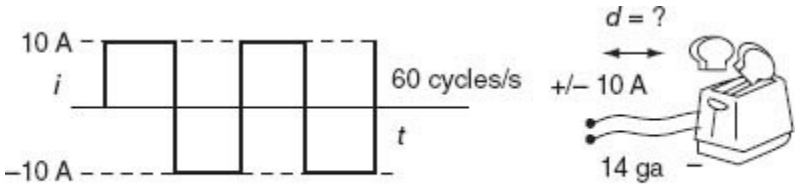


FIGURE P2.4

2.5 As is the case for all metals, the resistance of copper wire increases with temperature in an approximately linear manner that can be expressed as

$$R_n = R_n\,[1 + \alpha\,(T_2 - T_1)]$$

where α = 0.00393/°C. How hot do copper wires have to get to cause their resistance to increase by 10% over their value at 20°C?

2.6 A 52-gal electric water heater is designed to deliver 4800 W to an electric-resistance heating element in the tank when it is supplied with 240 V (it does not matter if this is AC or DC).

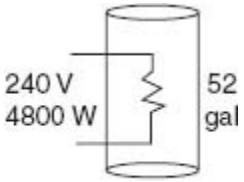


FIGURE P2.6

a. What is the resistance of the heating element?

b. How many watts would be delivered if the element is supplied with 208 V instead of 240 V?

c. Neglecting any losses from the tank, how long would it take for 4800 W to heat the 52 gal of water from 60°F to 120°F? The conversion between kilowatts of electricity and Btu/hr of heat is given by 3412 Btu/h = 1 kW. Also, one Btu heats 1 lb of water by 1°F and 1 gal of water weighs 8.34 lbs.

d. If electricity costs $0.12/kWh, what is the cost of a 15-gal, 110°F shower if the cold-water supply temperature is 60°F?

2.7 Suppose an automobile battery is modeled as an ideal 12-V battery in series with an internal resistance of 0.01 Ω as shown in (a) below.

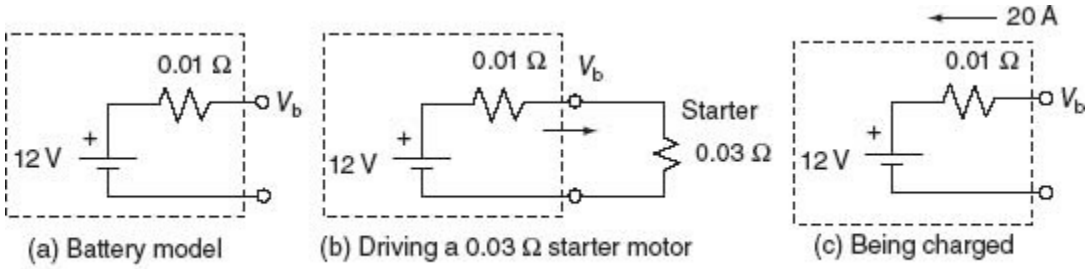


FIGURE P2.7

a. What current will be delivered when the battery powers a 0.03-Ω starter motor, as in (b)? What will the battery output voltage be?

b. Compare the power delivered by the battery to the starter with the power lost in the battery's internal resistance. What percentage is lost in the internal resistance?

c. To recharge the battery, what voltage must be applied to the battery in order to deliver a 20 A charging current as in (c)?

d. Suppose the battery needs another 480 Wh of energy to be fully charged, which could be achieved with a quick-charge of 80 A for 0.5 h (80 A × 0.5 h × 12 V = 480 Wh) or a trickle charge of 10 A for 4 h. Compare Wh of energy lost in the internal resistance of the battery for each charging scheme.

e. Automobile batteries are often rated in terms of their cold-cranking amperes (CCA), which is the number of amperes they can provide for 30 s at 0°F while maintaining an output voltage of at least 1.2 V per cell (7.2 V for a 12-V battery). What would be the CCA for the above battery (assuming the idealized 12-V source still holds)?

2.8 A photovoltaic (PV) system is delivering 15 A of current through 12-gage wire to a battery 80 ft away.

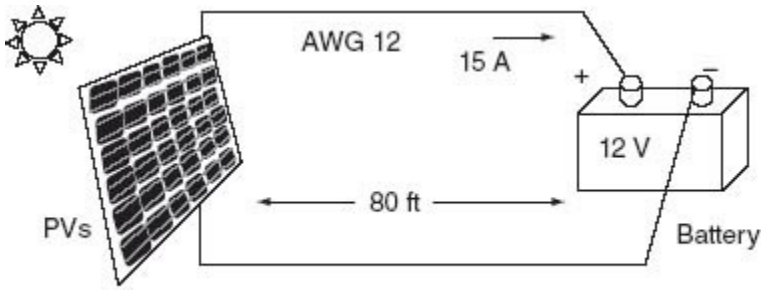


FIGURE P2.8

a. Find the voltage drop in the wires.

b. What fraction of the power delivered by the PVs is lost in the connecting wires?

c. Using Table 2.3 as a guide, what wire size would be needed to keep wire losses to less than 5% of the PV power output? (Assume the PVs will continue to keep the current at 15 A, which by the way, is realistic).

2.9 Consider the problem of using a low-voltage system to power your little cabin. Suppose a 12-V system powers a pair of 60-W lightbulbs (wired in parallel). The distance between these loads and the battery pack is 50 ft.

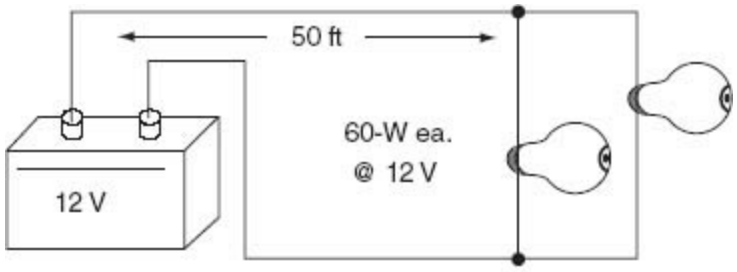


FIGURE P2.9

a. Since these bulbs are designed to use 60 W at 12 V, what would be the (filament) resistance of each bulb?

b. What would be the current drawn by two such bulbs if each receives a full 12 V?

c. Of the gages shown in Table 2.3, what gage wire should be used if it is the minimum size that will carry the current?

d. Find the equivalent resistance of the two bulbs plus the wire resistance to and from the battery. Both lamps are turned on (in this and subsequent parts).

e. Find the current delivered by the battery with both lamps turned on.

f. Find the power delivered by the battery.

g. Find the power lost in the connecting wires in watts and as a percentage of battery power.

h. Find the power delivered to the lamps in watts and as a percentage of their rated power.

2.10 Suppose the system in Problem 2.9 is redesigned to work at 24 V with 12-gage wire and two 24-V 60-W bulbs. What percentage of the battery power is now lost in the wires?

2.11 Suppose the lighting system in a building draws 20 A (AC or DC; it does not matter) and the lamps are, on the average, 100 ft from the electrical panel. Table 2.3 suggests that 12-gage wire meets code, but you want to consider the financial merits of wiring the circuit with bigger 10-gage wire. Suppose the lights are on 2500 h/yr and electricity costs $0.10/kWh.

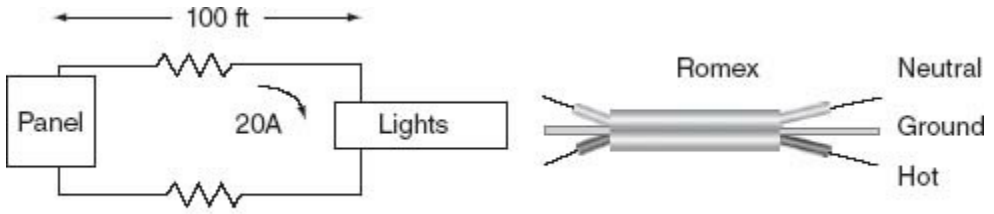


FIGURE P2.11

a. Find the energy savings per year (kWh/yr) that would result from using 10-gage instead of 12-gage wire.

b. Suppose 12-gage Romex (two conductors, each 100-ft long, plus a ground wire that carries no current, in a tough insulating sheath) costs $50/100 ft, and 10-gage Romex costs $70/100 ft. What would the "simple payback" period (first cost divided by annual savings) be when utility electricity costs $0.10/kWh?

c. An effective way to evaluate energy efficiency projects is by calculating the annual

cost associated with conservation and dividing it by the annual energy saved. This is the *Cost of Conserved Energy* (CCE) and is described more carefully in Appendix A. CCE is defined as follows

$$\text{CCE} = \frac{\text{annual cost of saved electricity (\$/yr)}}{\text{annual electricity saved (kWh/yr)}} = \frac{\Delta P \cdot \text{CRF}(i, n)}{\text{kWh/yr}}$$

where ΔP is the extra cost of the conservation feature (heavier duty wire in this case), and CRF is the capital recovery factor (which equals your annual loan payment on \$1 borrowed for n years at interest rate i).

What would be the "cost of conserved energy" CCE (¢/kWh) if the building (and wiring) is being paid for with a 7%, 20-year loan with CRF = 0.0944/yr. How does that compare with the cost of electricity that you do not have to purchase from the utility at 10¢/kWhr?

2.12 *Thevenin's theorem* says that the output of any circuit consisting of resistors and ideal voltage sources can be modeled as a voltage source in series with a resistance. Suppose the Thevenin equivalent of a circuit consists of a 12-V source in series with a 6-Ω resistance.

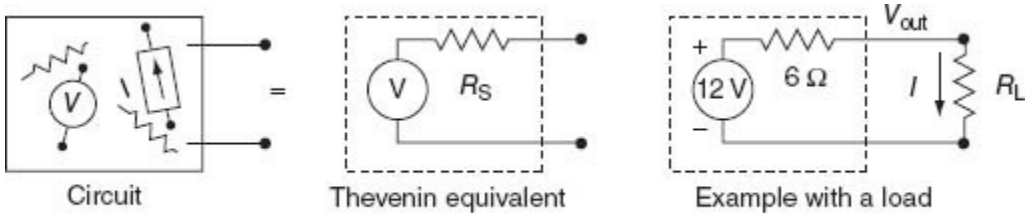


FIGURE P2.12

a. What is the output voltage with an infinite load so no current flows (called the open-circuit voltage, V_{OC})?

b. What is the output current when the terminals are shorted together (called the short-circuit current, I_{SC}).

c. Write an equation for the output current I as a function of the output voltage V_{out}. Draw a graph of I versus V_{out} (as the load changes).

d. Using the equation found in (c), determine the location (I, V) on the graph at which the maximum power will be delivered to a load. This is called the *maximum power point* and you will see it a lot in the chapters on photovoltaics. Show that point on your I–V graph from part (c).

e. What load resistance will result in the circuit delivering maximum power to the load? How much power would that be?

2.13 When circuits involve a source and a load, the same current flows through each one, and the same voltage appears across both. A graphical solution can therefore be obtained by simply plotting the current–voltage (I–V) relationship for the source onto the same axes that the I–V relationship for the load is plotted, and then finding the crossover point where both are satisfied simultaneously. This is an especially powerful technique when the relationships are nonlinear, as will be the case for the analysis of photovoltaic systems.

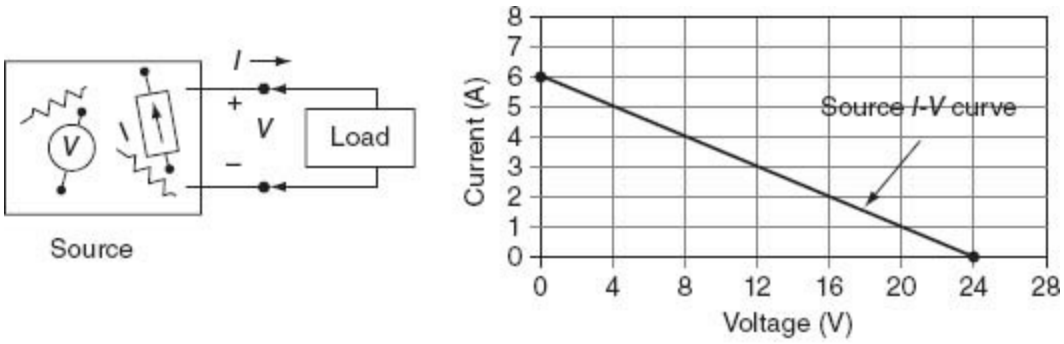


FIGURE P2.13

Consider the following *I–V* curve for a source delivering power to a load. For the following loads, plot their *I–V* curves onto the *I–V* curve for the source shown and at the crossover points note the current, voltage, and power delivered to the load.

a. The load is a simple 2-Ω resistor. Find *I*, *V*, and *P*.

b. The load is an ideal battery that is always at 12 V no matter what current.

c. The source is charging a battery that is modeled as an ideal 12-V battery in series with a 2-Ω internal series resistance.

2.14 Suppose a photovoltaic (PV) module consists of 40 individual cells wired in series, (a). In some circumstances, when all cells are exposed to the sun, it can be modeled as a series combination of forty 0.5-V ideal batteries, (b). The resulting graph of current versus voltage would be a straight, vertical 20-V line as shown in (c).

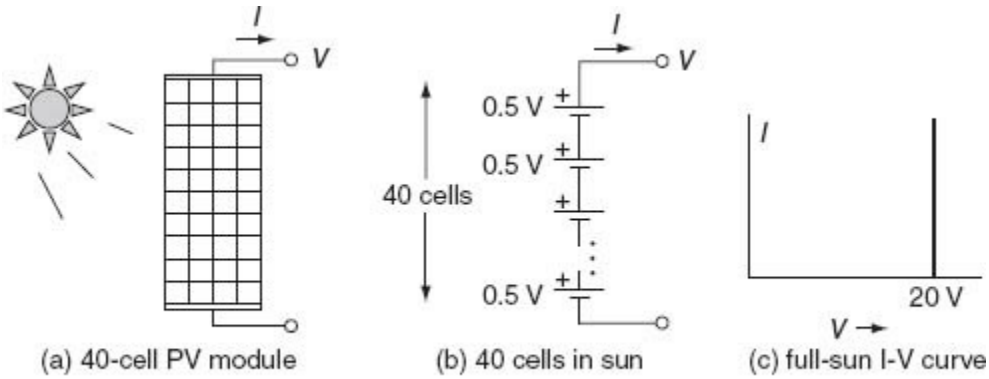


FIGURE P2.14

a. When an individual cell is shaded, it looks like a 5-Ω resistor instead of a 0.5-V battery, as shown in (d). Draw the *I–V* curve for the PV module with one cell shaded.

b. With two cells shaded, as in (e), draw the *I–V* curve for the PV module on the same axes as you have drawn the full-sun and 1-cell shaded *I–V* lines.

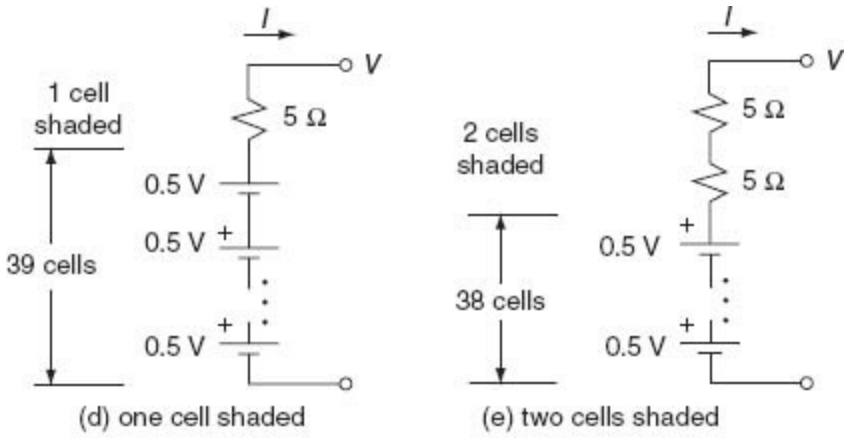


FIGURE P2.14A

2.15 If the photovoltaic (PV) module in Problem 2.14 is connected to a 5-Ω load, find the current, voltage, and power delivered to the load under the following circumstances. Comment on the power lost due to shading.

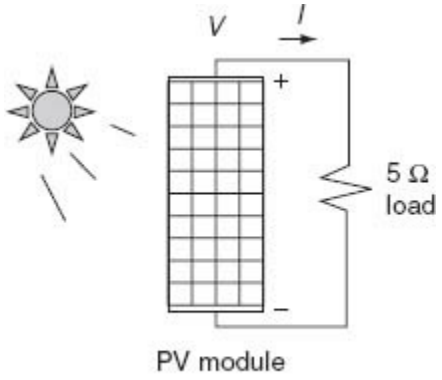


FIGURE P2.15

a. Every cell in the PV module is in the sun.

b. One cell is shaded.

c. Two cells are shaded.

2.16 The core-and-coil inductor in Example 2.10 had an inductance that varied from 18.8 to 31.3 mH when the material's relative permeability ranged from 15, 000 to 25, 000. To avoid that uncertainty, it is common to add an air gap in the core so that its reluctance is the series sum of air gap and core reluctances.

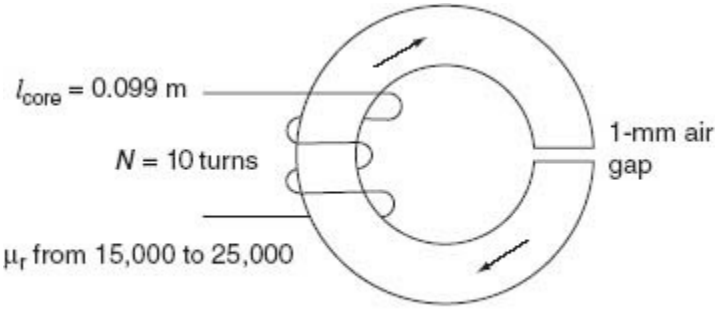


FIGURE P2.16

Find the range of inductance that would result if the core in that example is built with a 0.001-m air gap.

CHAPTER 3

FUNDAMENTALS OF ELECTRIC POWER

3.1 EFFECTIVE VALUES OF VOLTAGE AND CURRENT

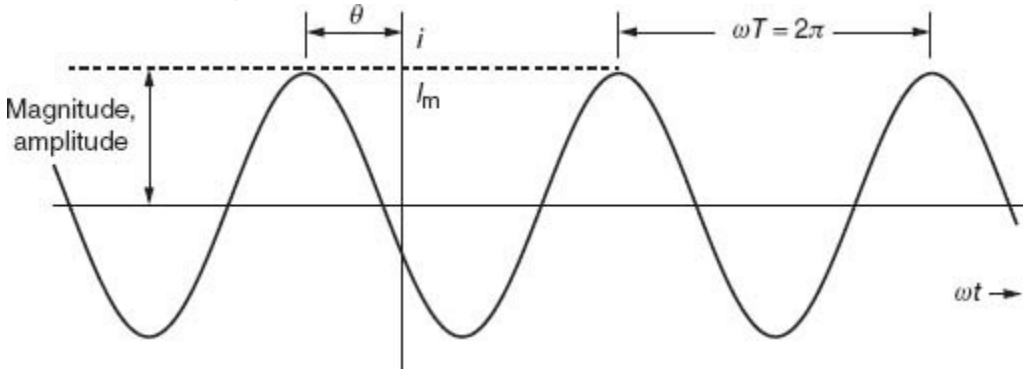
When voltages are nice, steady, DC, it is intuitively obvious what is meant when someone says, for example, "this is a 9-V battery." But what does it mean to say the voltage at the wall outlet is 120-V AC? Since it is AC, the voltage is constantly changing, so just what is it that the "120-V" refers to?

First, let us describe a simple sinusoidal current:

(3.1) $$i = I_m \cos(\omega t + \theta)$$

where i is the current, a function of time; I_m is the magnitude, or amplitude, of the current; ω = angular frequency (radians/s); and θ is the phase angle (radians). Note conventional notation uses lowercase letters for time-varying voltages or currents (e.g., i and v), while capitals are used for quantities that are constants (or parameters), (e.g., I_m or V_{rms}). Also note that we just as easily could have described the current with a sine function instead of cosine. A plot of Equation 3.1 is shown in Figure 3.1.

FIGURE 3.1 Illustrating the nomenclature for a sinusoidal function.



The frequency ω in Equation 3.1 is expressed in radians per second. Equally common is to express the frequency f in hertz (Hz), which are "cycles per second." Since there are 2π radians per cycle, we can write

(3.2) $$\omega = 2\pi \text{ (radians/cycle)} \cdot f \text{ (cycle/s)} = 2\pi f$$

The sinusoidal function is periodic--that is, it repeats itself--so we can also describe it using its period, T:

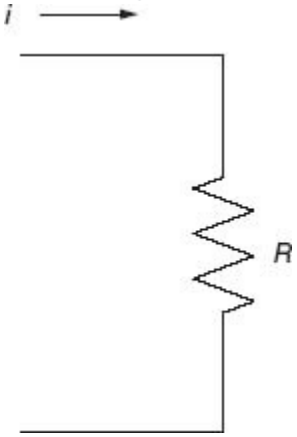
(3.3) $T = 1/f$

Thus, the sinusoidal current can have the following equivalent representations:

$$i = I_m \cos(\omega t + \theta) = I_m \cos(2\pi f t + \theta) = I_m \cos\left(\frac{2\pi}{T}t + \theta\right) \quad (3.4)$$

Suppose we have a portion of a circuit, consisting of a current i passing through a resistance R as shown in Figure 3.2.

FIGURE 3.2 A time-varying current i through a resistance R.



The instantaneous power dissipated by the resistor is

(3.5) $p = i^2 R$

In Equation 3.5, power is given a lowercase symbol to indicate it is a time-varying quantity. The average value of power dissipated in the resistance is given by

(3.6) $P_{avg} = (i^2)_{avg} R = (I_{eff})^2 R$

In Equation 3.6 an effective value of current, I_{eff}, has been introduced. The advantage of defining the effective value this way is that the resulting equation for average power dissipated looks very similar to the instantaneous power described by Equation 3.5. This leads to a definition of the effective value of current given below:

(3.7) $I_{eff} = \sqrt{(i^2)_{avg}} = I_{rms}$

The effective value of current is the square root of the mean value of current squared. That is, it is the root-mean-squared (rms) value of current. The definition given in Equation 3.7 applies to any current function, be it sinusoidal or otherwise.

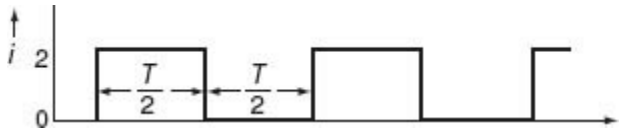
To find the rms value of a function, we can always work it out formally using the following:

$$I_{rms} = \sqrt{(i^2)_{avg}} = \sqrt{\frac{1}{T}\int_0^T i^2(t)dt} \quad (3.8)$$

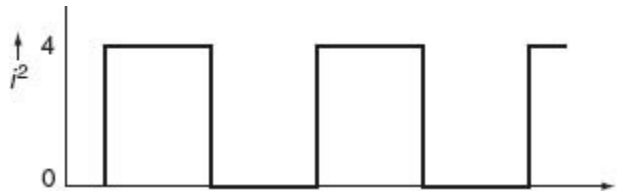
Oftentimes, however, it is easier to simply graph the square of the function and determine the average by inspection, as the following example illustrates.

Example 3.1 rms Value of a Square Wave. Find the rms value of a square-wave current

that jumps back and forth from 0 to 2 A as shown below:



Solution. We need to find the square root of the average value of the square of the current. The waveform for current squared is:



The average value of current squared is 2 by inspection (half the time it is zero, half the time it is 4):

$$I_{\text{rms}} = \sqrt{(i^2)_{\text{avg}}} = \sqrt{2}\ \text{A}$$

Let us derive the rms value for a sinusoid by using the simple graphical procedure. If we start with a sinusoidal voltage

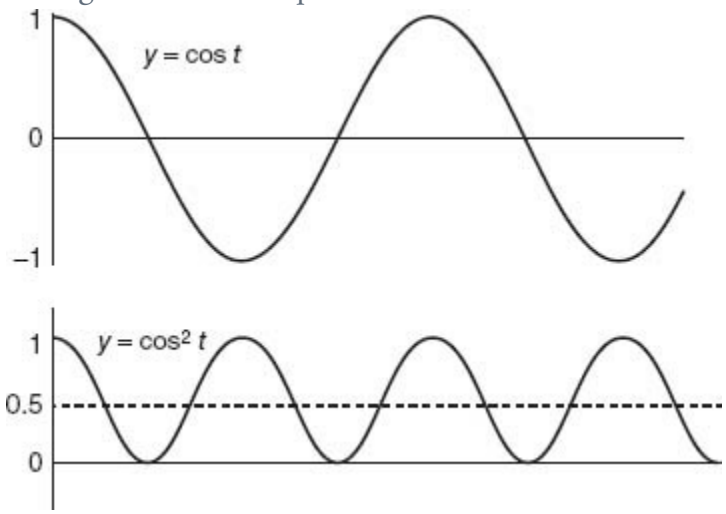
(3.9) $$v = V_{\text{m}} \cos \omega t$$

The rms value of voltage is

(3.10) $$V_{\text{rms}} = \sqrt{(v^2)_{\text{avg}}} = \sqrt{(V_{\text{m}}^2 \cos^2 \omega t)_{\text{avg}}} = V_{\text{m}} \sqrt{(\cos^2 \omega t)_{\text{avg}}}$$

Since we need to find the average value of the square of a sine wave, let us graph $y = \cos^2 \omega t$ as has been done in Figure 3.3.

FIGURE 3.3 The average value of the square of a sinusoid is 1/2.



By inspection of Figure 3.3, the mean value of $\cos^2 \omega t$ is 1/2. Therefore, using Equation 3.10, the rms value of a sinusoidal voltage is

$$V_{rms} = V_m\sqrt{\frac{1}{2}} = \frac{V_m}{\sqrt{2}} \quad (3.11)$$

This is a very important result:

The rms value of a sinusoid is the amplitude divided by the square root of 2.

Note this conclusion applies only to sinusoids! When an AC current or voltage is described (e.g., 120 V, 10 A), the values specified are always the rms values.

Example 3.2 Wall Outlet Voltage. Find an Equation like 3.1 for the 120-V, 60-Hz voltage delivered to your home.

Solution. From Equation 3.11, the amplitude (magnitude, peak value) of the voltage is

$$V_m = \sqrt{2}V_{rms} = 120\sqrt{2} = 169.7 \text{ V}$$

The angular frequency ω is

$$\omega = 2\pi f = 2\pi 60 = 377 \text{ rad/s}$$

The waveform is thus

$$v = 169.7 \cos 377t$$

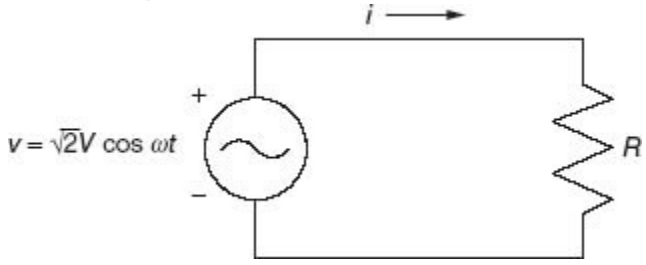
It is conventional practice to treat the incoming voltage as having zero phase angle, so that all currents will have phase angles measured relative to that reference voltage.

3.2 IDEALIZED COMPONENTS SUBJECTED TO SINUSOIDAL VOLTAGES

3.2.1 Ideal Resistors

Consider the response of an ideal resistor to excitation by a sinusoidal voltage as shown in Figure 3.4.

FIGURE 3.4 A sinusoidal voltage imposed on an ideal resistance.



The voltage across the resistance is the same as the voltage supplied by the source:

$$v = V_m \cos \omega t = \sqrt{2}V_{rms} \cos \omega t = \sqrt{2}V \cos \omega t \quad (3.12)$$

Note the three ways that the voltage has been described: using the amplitude of the voltage V_m, the rms value of voltage V_{rms}, and the symbol V which, in this context, means the rms value. *We will consistently use current I or voltage V* (capital letters, without subscripts) to mean the rms values of that current or voltage.

The current that will pass through a resistor with the above voltage imposed will be

$$i = \frac{v}{R} = \frac{V_m}{R}\cos\omega t = \frac{\sqrt{2}V_{rms}}{R}\cos\omega t = \frac{\sqrt{2}V}{R}\cos\omega t \quad (3.13)$$

Since the phase angle of the resulting current is the same as the phase angle of the voltage (zero), they are said to be *in phase* with each other. The rms value of current is therefore:

$$I_{rms} = I = \frac{I_m}{\sqrt{2}} = \frac{\sqrt{2}V/R}{\sqrt{2}} = \frac{V}{R} \quad (3.14)$$

Note how simple the result is: the rms current I is equal to the rms voltage V divided by the resistance R. We have, in other words, a very simple AC version of Ohm's law:

$$V = RI \quad (3.15)$$

where V and I are rms quantities.

Now let us look at the average power dissipated in the resistor.

$$P_{avg} = (vi)_{avg} = \left[\sqrt{2}V\cos\omega t \cdot \sqrt{2}I\cos\omega t\right]_{avg} = 2VI(\cos^2\omega t)_{avg} \quad (3.16)$$

The average value of $\cos^2\omega t$ is 1/2. Therefore,

$$P_{avg} = 2VI \cdot \frac{1}{2} = VI \quad (3.17)$$

In a similar way, it is easy to show the expected alternative formulas for average power are also true:

$$P_{avg} = VI = I^2R = \frac{V^2}{R} \quad (3.18)$$

Note how the AC problem has been greatly simplified by using rms values of current and voltage. You should also note that the power given in Equation 3.18 is the *average* power and not some kind of rms value. Since AC power is always interpreted to be average power, the subscript in P_{avg} is not usually needed.

Example 3.3 AC Power for a Light Bulb. Suppose a conventional incandescent light bulb uses 60 W of power when it is supplied with a voltage of 120 V. Modeling the bulb as a simple resistance, find that resistance as well as the current that flows. How much power would be dissipated if the voltage drops to 110 V?

Solution. Using Equation 3.18, we have

$$R = \frac{V^2}{P} = \frac{(120)^2}{60} = 240\ \Omega$$

$$\text{and} \quad I = \frac{P}{V} = \frac{60}{120} = 0.5\ \text{A}$$

When the voltage sags to 110 V, the power dissipated will be

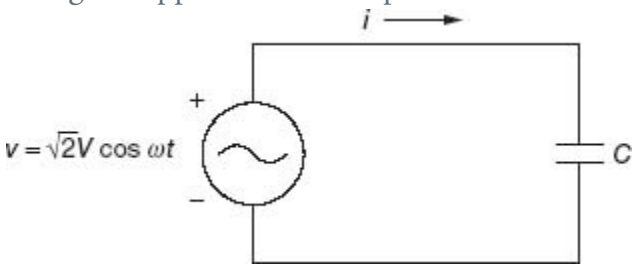
$$P = \frac{V^2}{R} = \frac{(110)^2}{240} = 50.4\ \text{W}$$

3.2.2 Idealized Capacitors

Recall the defining equation for a capacitor, which says that current is proportional to the

rate of change of voltage across the capacitor. Suppose we apply an AC voltage of V volts (rms) across a capacitor, as shown in Figure 3.5.

FIGURE 3.5 An AC voltage V, applied across a capacitor.



The resulting current through the capacitor will be

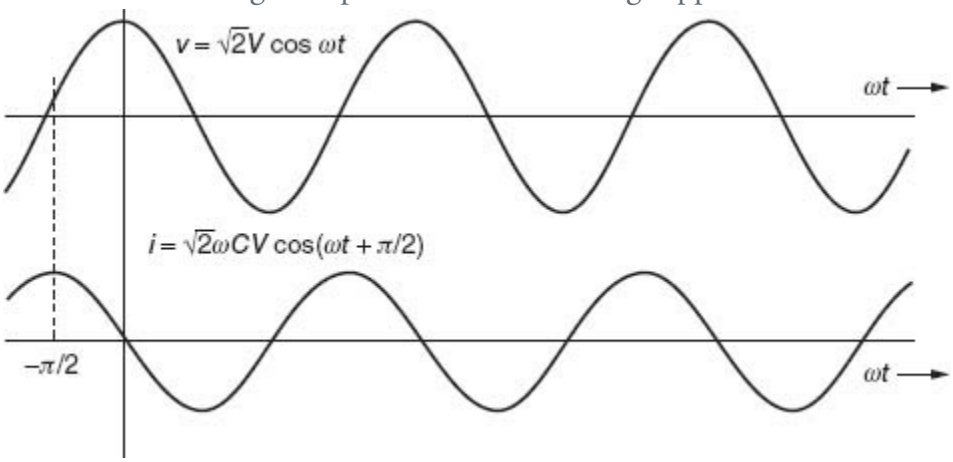
$$i = C\frac{\mathrm{d}v}{\mathrm{d}t} = C\frac{d}{dt}\left(\sqrt{2}V\ \cos\omega t\right) = -\omega C\sqrt{2}V\ \sin\omega t \tag{3.19}$$

If we apply the trigonometric identity that $\sin x = -\cos(x + \pi/2)$, we get

$$i = \sqrt{2}\omega CV\cos\left(\omega t + \frac{\pi}{2}\right) \tag{3.20}$$

There are several things to note about Equation 3.20. For one, the current waveform is a sinusoid of the same frequency as the voltage waveform. Also note that there is a 90° phase shift ($\pi/2$ radians) between the voltage and current. The current is said to be *leading* the voltage by 90°. That the current leads the voltage should make some intuitive sense since charge must be delivered to the capacitor before it shows a voltage. The graph in Figure 3.6 also suggests the idea that the current peaks 90° before the voltage peaks.

FIGURE 3.6 Current through a capacitor leads the voltage applied to it.



Finally, writing Equation 3.20 in terms of Equation 3.1 gives

$$i = \sqrt{2}\omega CV\cos\left(\omega t + \frac{\pi}{2}\right) = I_{\mathrm{m}}\cos(\omega t + \theta) = \sqrt{2}I\cos(\omega t + \theta) \tag{3.21}$$

which says that the rms current I is given by

$$I = \omega\ C\ V \tag{3.22}$$

and the phase angle between current and voltage is

$$\theta = \pi/2 \tag{3.23}$$

That is, the current leads the voltage by $\pi/2$ radians, or 90°. Rearranging Equation 3.22

gives

$$V = \left(\frac{1}{\omega C}\right) I \tag{3.24}$$

Equation 3.24 is beginning to look like an AC version of Ohm's law for capacitors in which we relate the rms values of voltage V and current I with a simple function of capacitance and frequency. The quantity that connects them is called the *capacitive reactance*, X_C, with units of ohms.

$$\text{Capacitive reactance } X_C = \frac{1}{\omega C} \text{ ohms} \tag{3.25}$$

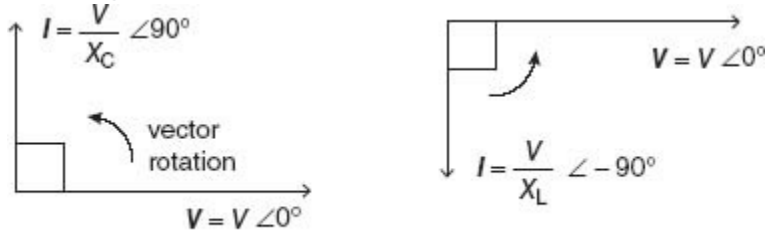
What Equations 3.24 and 3.25 miss, however, is that 90° phase angle difference between the two rms scalars V and I. In fact, the term reactance is used, instead of resistance, to remind us that there is a 90° phase shift to contend with.

A simple way to introduce the phase angle is shown in Equation 3.26. Note current is now written in bold face, which means it has a magnitude and an angle associated with it.

$$\boldsymbol{I}_C = \frac{V}{X_C} \angle 90° \tag{3.26}$$

Figure 3.7a shows a representation of Equation 3.26 as two orthogonal vectors with the voltage vector being assumed to have a zero phase angle. Imagining these vectors rotating (counterclockwise) helps make it clear that current in a capacitor leads voltage across the capacitor by 90°. These rotating vectors are called *phasors*.

FIGURE 3.7 Phasor diagrams for a capacitor (a) and an inductor (b).



(a) Capacitor (b) Inductor

Equation 3.26 can also be written as a voltage vector 90° behind current

$$\boldsymbol{V}_C = X_C \boldsymbol{I} \angle -90° \tag{3.27}$$

Example 3.4 Current in a Capacitor. A 120-V, 60-Hz AC source sends current to a 10-μF capacitor (Fig. 3.5). Find the reactance of the capacitor, the rms value of current in the circuit, and a time-domain equation for current.

Solution. From Equation 3.25, the capacitive reactance is

$$X_C = \frac{1}{\omega C} = \frac{1}{2\pi \cdot 60 \cdot 10 \times 10^{-6}} = 265\ \Omega$$

The rms value of current is

$$I = \frac{V}{X_C} = \frac{120}{265} = 0.452\ \text{A}$$

The complete equation for current is

$$i = \sqrt{2} \cdot 0.452 \cos\left(2\pi \cdot 60 + \frac{\pi}{2}\right) = 0.639 \cos\left(377t + \frac{\pi}{2}\right)$$

Also of interest is the average power dissipated by a capacitor subjected to a sinusoidal voltage. Since instantaneous power is the product of voltage and current, we can write:

(3.28) $$p = vi = \sqrt{2}V \cos \omega t \cdot \sqrt{2}I \cos \omega t \left(\omega t + \frac{\pi}{2}\right)$$

Using the trigonometric identity: $\cos A \cdot \cos B = \frac{1}{2}[\cos(A + B) + \cos(A - B)]$ gives

(3.29) $$p = 2VI \cdot \frac{1}{2}\left\{\cos\left(\omega t + \omega t + \frac{\pi}{2}\right) + \cos\left[\omega t - \left(\omega t + \frac{\pi}{2}\right)\right]\right\}$$

since $\cos(-\pi/2) = 0$, this simplifies to

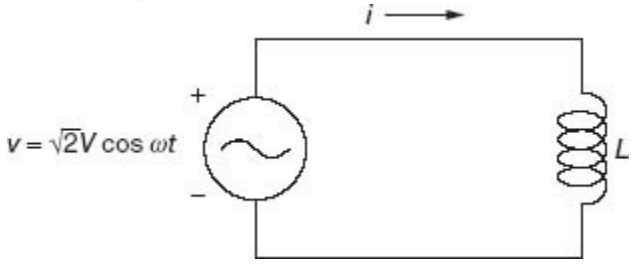
(3.30) $$p = VI \cos\left(2\omega t + \frac{\pi}{2}\right)$$

Since the average value of a sinusoid is zero, Equation 3.30 tells us that *the average power dissipated by a capacitor is zero*.

(3.31) $$\text{Capacitor: } P_{\text{avg}} = 0$$

Some of the time the capacitor is absorbing power (charging) and some of the time it is delivering power (discharging), but for an ideal capacitor with no energy gained or lost during the cycle, the average power is zero.

FIGURE 3.8 A sinusoidal voltage across an ideal inductor.



3.2.3 Idealized Inductors

A sinusoidal voltage applied across an inductor is shown in Figure 3.8. We have to find the current through the inductor. Starting with the fundamental relationship for inductors,

(3.32) $$v = L\frac{di}{dt}$$

and then solving for current:

(3.33) $$i = \int di = \int \frac{v}{L} dt = \frac{1}{L} \int v dt$$

and inserting the equation for applied voltage

(3.34) $$i = \frac{1}{L} \int \sqrt{2}V \cos \omega t \, dt = \frac{\sqrt{2}V}{L} \int \cos \omega t \, dt = \frac{\sqrt{2}V}{\omega L} \sin \omega t$$

Applying the trigonometric relationship $\sin \omega t = \cos(\omega t - \pi/2)$ gives

$$i = \left(\frac{1}{\omega L}\right)\sqrt{2}V\cos\left(\omega t - \frac{\pi}{2}\right) = \sqrt{2}I\cos(\omega t + \theta) \quad (3.35)$$

Equation 3.35 tells us that (1) the current through the inductor has the same frequency ω as the applied voltage, (2) the current *lags* behind the voltage by an angle θ = $-\pi/2$, and (3) the rms value of current is

$$I = \left(\frac{1}{\omega L}\right)V \quad (3.36)$$

Rearranging Equation 3.36 gives us something that again looks like an AC version of Ohm's law, this time for inductors:

$$V = (\omega L)I \quad (3.37)$$

where V and I are rms values. The connection between them is called the *inductive reactance,* X_L, with units of ohms.

$$\text{Inductive reactance } X_L = \omega L \text{ ohms} \quad (3.38)$$

Just as we did for an ideal capacitor, we can treat current through an inductor as a vector I, this time with a lagging phase angle (current lags voltage) of –90° (Fig. 3.7b).

$$\boldsymbol{I} = \frac{V}{X_L}\angle -90° \quad (3.39)$$

$$\text{or} \quad \boldsymbol{V} = IX_L\angle 90° \quad (3.40)$$

Equation 3.40 indicates that the voltage vector is 90° ahead of the current. For an inductor, you have to supply some voltage before current flows; for a capacitor, you need to supply current before voltage builds up. One way to remember which is which, is with the memory aid:

"*ELI the ICE man*"

That is, for an inductor L, voltage E (as in emf) comes before current I, while for a capacitor C, current I comes before voltage E.

Finally, let us take a look at the power dissipated by an inductor:

$$p = vi = \sqrt{2}V\cos\omega t \cdot \sqrt{2}V\cos\left(\omega t - \frac{\pi}{2}\right) \quad (3.41)$$

Using the same trigonometric manipulations shown in Equations 3.29 and 3.30, it is easy to show that the average power dissipated in an inductor is zero.

So, an inductor is exactly analogous to a capacitor in that it absorbs energy while current is increasing, storing that energy in its magnetic field, then it returns that energy when the current drops and the magnetic field collapses. *The net power dissipated when an inductor is subjected to an AC voltage is zero.*

3.2.4 Impedance

Analyzing simple circuits consisting of R, L, and C components driven by sinusoidal voltages can get pretty tedious if we stick with an approach based on manipulating trigonometric functions. In some circumstances, however, solutions based on simple vector diagrams can suffice. As circuits get more complicated, it is well worth the time to learn to manipulate complex algebraic functions in which numbers can have both real and

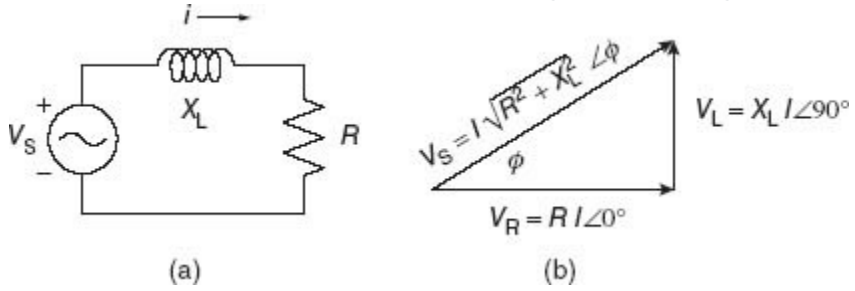
imaginary components.

Let us begin with the vector analysis approach. Consider the simple R–L circuit shown in Figure 3.9a. We can write Kirchhoff's voltage law for the loop as

(3.42) $$V_S\angle\phi = RI\angle 0° + X_L I\angle 90°$$

which is expressed as a vector diagram in Figure 3.9b.

FIGURE 3.9 Analysis of a simple R–L circuit (a), using a vector diagram (b).



The hypotenuse in Figure 3.9b is easy to find from the geometry of the triangle:

(3.43) $$V_S = I\sqrt{R^2 + X_L^2}\ \angle\phi \qquad \text{where } \phi = \tan^{-1}\left(\frac{X_L}{R}\right)$$

This, again, looks somewhat like a version of Ohm's law, but this time the connection between V and I is a quantity known as *impedance* Z. Impedance has units of ohms and it is a vector in that it has a magnitude and an angle.

(3.44) $$\mathbf{Z} = \sqrt{R^2 + X_L^2}\angle \tan^{-1}\left(\frac{X_L}{R}\right)$$

Example 3.5 Circuit Analysis Using Vectors. Suppose an AC generator is modeled as a 120-V, 60-Hz voltage source in series with its own internal inductance of 0.01 H. If it delivers power to a 12-Ω resistive load, find the following:

a. The rms current flowing in the circuit.

b. The voltage and power delivered to the load.

c. The voltage drop across the internal inductance.

Solution

a. Figure 3.9 sets up the solution. Using Equation 3.38 the reactance of the inductor is

$$X_L = \omega L = 2\pi \cdot 60 \cdot 0.01 = 3.77\ \Omega$$

Using Equation 3.44, the impedance is

$$\mathbf{Z} = \sqrt{12^2 + 3.77^2}\angle \tan^{-1}\left(\frac{3.77}{12}\right) = 12.52$$

To find rms current I, we do not need the phase angle, so from Equation 3.43

$$I = \frac{V}{Z} = \frac{120}{12.58} = 9.54\ \text{A}$$

b. The voltage and power delivered to the load resistance is

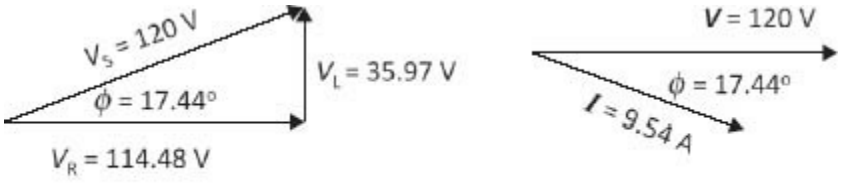
$$V = IR = 9.54 \times 12 = 114.48\ \text{V}$$

$$P = I^2 R = (9.54)^2 \times 12 = 1092\ \text{W}$$

c. The voltage drop across the internal inductance is

$$V_L = X_L I = 3.77 \times 9.54 = 35.97 \text{ V}$$

Two ways to present the results of this analysis are shown below. If you consider the phasor diagram to be vectors rotating in a counterclockwise direction, then it is clear that the current is lagging behind the voltage.



(a) Voltage triangle (b) Phasor diagram

Example 3.5 showed how a simple AC circuit can be easily analyzed without the complications associated with trigonometric functions. For more difficult circuits, however, engineers prefer a far more powerful approach in which vectors are represented in the complex plane. While a more thorough introduction to complex algebra can be found in any elementary circuits book, we can do the necessary manipulations without much background as long as you do not worry too much about the theory behind the process.

The starting point for complex algebra is a symbol j which represents the square root of −1 (mathematicians use i to designate such an imaginary number, but to avoid confusion with current, electrical engineers use j). Algebraically, then

(3.45) $$j = \sqrt{-1} \qquad j^2 = -1 \qquad j^3 = -j \qquad j^4 = 1$$

A simple interpretation of j is that it rotates a scalar quantity counterclockwise by 90°. So, for example, when a rotational operator j is attached to a capacitive or inductive reactance (a scalar), those quantities become impedances with both magnitude and angle. The quantity j^2 then acts like two 90° shifts, which is like turning a vector around giving it a minus sign. For example,

(3.46) $$\mathbf{Z}_\text{L} = \omega L \angle 90° = j\omega L = jX_\text{L}$$

(3.47) $$\mathbf{Z}_\text{C} = \frac{1}{\omega C}\angle -90° = \frac{1}{j\omega C} \cdot \frac{j}{j} = -j\frac{1}{\omega C} = -jX_\text{C}$$

Voltage, current, and impedance quantities involving magnitudes and angles (bold-face type) can be manipulated using the following guidelines.

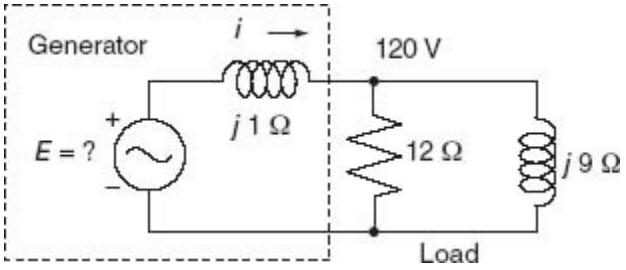
(3.48a) Multiplication: $$\mathbf{Z}_1 \cdot \mathbf{Z}_2 = \mathrm{Z}_1\angle\phi_1 \cdot \mathrm{Z}_2\angle\phi_2 = \mathrm{Z}_1\mathrm{Z}_2\angle(\phi_1 + \phi_2)$$

(3.48b) Division: $$\frac{\mathbf{Z}_1}{\mathbf{Z}_2} = \frac{\mathrm{Z}_1\angle\phi_1}{\mathrm{Z}_2\angle\phi_2} = \frac{\mathrm{Z}_1}{\mathrm{Z}_2}\angle(\phi_1 - \phi_2)$$

(3.48c) Rectangular to polar: $$\mathbf{Z} = A + jB = \sqrt{A^2 + B^2}\angle \tan^{-1}\left(\frac{B}{A}\right)$$

(3.48d) Polar to rectangular: $$\mathbf{Z} = Z\angle\phi = Z\cos\phi + jZ\sin\phi$$

Example 3.6 Generator Delivering Power to a Load. A generator is modeled as source of emf E delivering current i through its own internal inductive impedance of j 1 Ω. The goal is to provide 120 V to the R–L load shown below.



Find the voltage E that the generator must provide.

Solution. First let us find the impedance of the load:

$$\mathbf{Z}_{\text{Load}} = \frac{\mathbf{Z}_{\text{R}} \cdot \mathbf{Z}_{\text{L}}}{\mathbf{Z}_{\text{R}} + \mathbf{Z}_{\text{L}}} = \frac{12 \cdot j9}{12 + j9}$$

One way to simplify this is to multiply the numerator and denominator by the complex conjugate of the denominator (and noting that $j^2 = -1$)

$$\mathbf{Z}_{\text{Load}} = \frac{j108}{12 + j9} \times \frac{(12 - j9)}{(12 - j9)} = \frac{972 + j1296}{144 + 81} = 4.32 + j5.76$$

In polar form this is

$$\mathbf{Z}_{\text{Load}} = \sqrt{4.32^2 + 5.76^2} \angle \tan^{-1}\left(\frac{5.76}{4.32}\right) = 7.2 \angle 53.1^\circ\ \Omega$$

Using the voltage divider concept described for resistors in Chapter 2 gives

$$\boldsymbol{V}_{\text{Load}} = \boldsymbol{E}_{\text{Generator}} \cdot \frac{\mathbf{Z}_{\text{Load}}}{\mathbf{Z}_{\text{Total}}}$$

$$\mathbf{Z}_{\text{Total}} = j1 + 4.32 + j5.76 = 4.32 + j6.76$$

$$= \sqrt{4.32^2 + 6.76^2} \angle \tan^{-1}\left(\frac{6.76}{4.32}\right) = 8.02 \angle 57.42^\circ\ \Omega$$

Let us assume the 120 V supplied to the load has a reference angle of 0°.

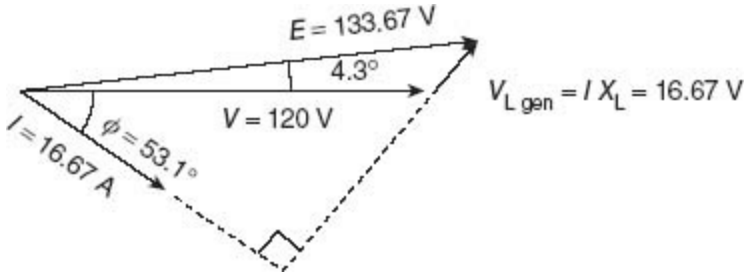
$$\boldsymbol{E}_{\text{Gen}} = 120 \angle 0^\circ \left(\frac{\mathbf{Z}_{\text{Total}}}{\mathbf{Z}_{\text{Load}}}\right) = 120 \angle 0^\circ \left(\frac{8.02 \angle 57.42^\circ}{7.2 \angle 53.13^\circ}\right) = 133.67 \angle 4.29^\circ\ \text{V}$$

Current delivered by the generator would be

$$\boldsymbol{I}_{\text{Gen}} = \frac{\boldsymbol{E}_{\text{Gen}}}{\mathbf{Z}_{\text{Total}}} = \frac{133.67 \angle 4.29^\circ}{8.02 \angle 57.42^\circ} = 16.67 \angle -53.13^\circ\ \text{A}$$

In the above example, the generator must develop an emf of 133.67 V and it must lead the 120 V delivered to the load by 4.29°. Current through the generator lags the 120 V by 53.13°. Current through the generator's internal inductance is 90° out of phase with the 16.67-V drop across that inductor. Kirchhoff's voltage law is played out nicely in the phasor diagram for this quite important system. As shown in Figure 3.10, the 120 V delivered to the load, plus the voltage drop across the internal reactance of the generator (IX_{L}), equals the emf E produced by the generator.

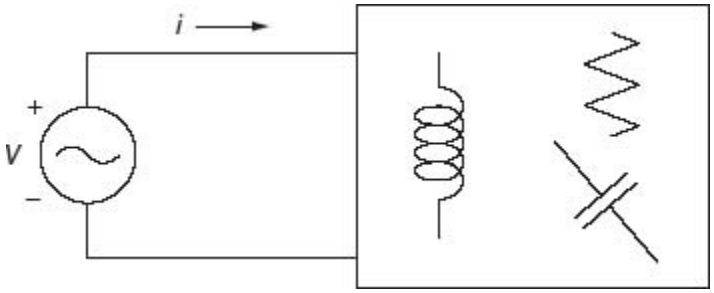
FIGURE 3.10 A phasor diagram for a generator delivering power to a load (Example 3.6).



3.3 POWER FACTOR

Those rather tedious derivations for the impact of AC voltages applied to idealized resistors, capacitors and inductors have led to three simple, but important conclusions. One is that the currents flowing through any of these components will have the same AC frequency as the source of the voltage that drives the current. Another is that there can be a phase shift between current and voltage. And finally, resistive elements are the only components that dissipate any net energy. Let us put these ideas together to analyze the generalized black box of Figure 3.11.

FIGURE 3.11 A black box of ideal resistors, capacitors, and inductors.



The black box contains any number of idealized resistors, capacitors, and inductors, wired up any which way. The voltage source driving this box of components has rms voltage V and we will arbitrarily assign it a phase angle of $\phi = 0$.

(3.49) $$v = \sqrt{2}V \cos \omega t$$

Since the current delivered to the black box has the same frequency as the voltage source that drives it, we can write the following generalized current response as

(3.50) $$i = \sqrt{2}I \cos(\omega t + \phi)$$

The instantaneous power supplied by the voltage source, and dissipated by the circuit in the box, is

(3.51) $$p = vi = \sqrt{2}V \cos \omega t \cdot \sqrt{2}I \cos(\omega t + \phi) = 2VI\,[\cos \omega t \cdot \cos(\omega t + \phi)]$$

Once again, applying the identity $\cos A \cdot \cos B = \frac{1}{2}[\cos(A + B) + \cos(A - B)]$, gives

(3.52) $$p = 2VI \left\{ \frac{1}{2} [\cos(\omega t + \omega t + \phi)] + \cos(\omega t - \omega t - \phi) \right\}$$

so

(3.53) $$p = VI\cos(2\omega t + \phi) + VI\cos(-\phi)$$

The average value of the first term in Equation 3.53 is zero, and using cos x = cos $(-x)$ lets us write that the average power dissipated in the black box is given by

(3.54) $$P_{avg} = VI\cos(\phi) = VI \times PF$$

Equation 3.54 is an important result. The power expressed by Equation 3.54 tells us the rate at which real work can be done by whatever is inside the black box. The quantity cos ϕ, is called the *power factor* (PF).

$$\text{Power factor} = \text{PF} = \cos\phi$$

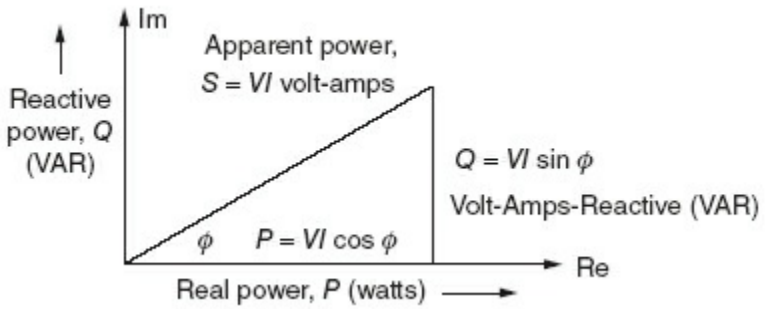
(3.55)

Why is power factor important? With an "ordinary" watt-hour meter on the premises, a utility customer usually pays only for watts of real power used within their factory, business, or home. The utility, on the other hand, has to cover the i^2R resistive power losses in the transmission and distribution wires that bring that power to the customer. When a customer has voltage and current way out of phase—that is, the power factor is considerably below 1.0—more current is drawn than is necessary to do the job, which translates into more i^2R power losses on the utility's side of the meter, more i R voltage drop in utility power lines, and more potential overheating of transformers for both customers and utilities.

3.3.1 The Power Triangle

Equation 3.54 sets up an important concept, called the *power triangle*. As shown in Figure 3.12, the hypotenuse of the power triangle is the product of rms volts V times rms amperes I. This leg is called the *apparent power*, S, and it has units of volt-amperes (VA). Those volt-amperes are resolved into the horizontal leg, $P = VI$ cos ϕ, which is *real power* in watts. Remember it is only watts of real power that can actually do any work. The vertical side of the triangle, $Q = VI$ sin ϕ, is called *reactive power* and has units of VAR (which stands for volt-amps-reactive). Reactive VAR power is associated with inductance and capacitance, which means it refers to voltages and currents being out of phase with each other by 90°. Reactive power is incapable of doing any net work; energy absorbed in one half of a cycle is returned, unchanged, in the other half of the cycle.

FIGURE 3.12 Showing apparent power S (volt-amperes) resolved into reactive power Q (VAR) and real power P (watts).



Using our operator j to refer to a 90° phase shift, we can write the following equation for

apparent power

$$S = VI\cos\phi + jVI\sin\phi = P + jQ \tag{3.56}$$

Based on the notation in Equation 3.56, the horizontal axis in Figure 3.12 is referred to as the *real axis* (Re) and the vertical axis is the *imaginary axis* (Im).

With so many quantities to keep track of, it may be helpful to make the following summarization of P and Q in resistors, inductors, and capacitors:

1. Resistors absorb real power $P_R = V^2/R$ watts, but their reactive power $Q_R = 0$.
2. Inductors absorb zero real power, $P_L = 0$ W, but absorb reactive power $Q_L = V^2/X_L$ VARS. Inductors cause *lagging* power factors.
3. Capacitors absorb zero real power, $P_C = 0$ W, but deliver positive reactive power $Q_C = V^2/X_C$ VARS. Capacitors cause *leading* power factors.

When we get to a description of power generators, we will see that they must be designed to provide as much P and Q as are needed by whatever loads to which they are delivering power.

Example 3.7 Power Triangle for a Motor. An 85-% efficient, 240-V, 60-Hz, single-phase induction motor draws 25 A of current while delivering 3.5 kW of useful work to its shaft. Draw its power triangle.

Solution. Delivering 3.5 kW of power at 85% efficiency means the electrical power input is

$$\text{Real electrical power} \quad P_{in} = \frac{3.5\text{ kW}}{0.85} = 4.12\text{ kW}$$

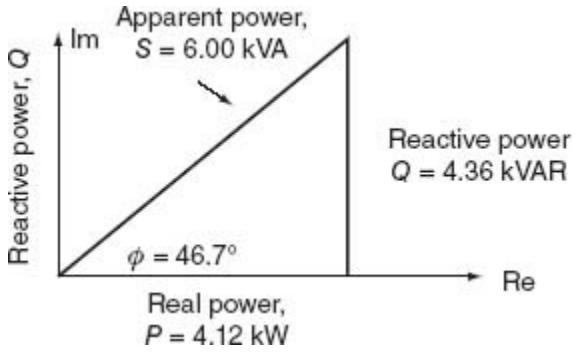
$$\text{Apparent power } S = 25\text{ A} \times 240\text{ V} = 6000\text{ VA} = 6.00\text{ kVA}$$

$$\text{Power factor PF} = \frac{\text{Real power}}{\text{Apparent power}} = \frac{4.12\text{ kW}}{6.00\text{ kW}} = 0.69$$

$$\text{Phase angle } \phi = \cos^{-1} 0.69 = 46.7°$$

$$\text{Reactive power} = Q = S\sin\phi = 6.00 \quad \sin 46.7° = 4.36\text{ kVAR}$$

The power triangle is therefore:



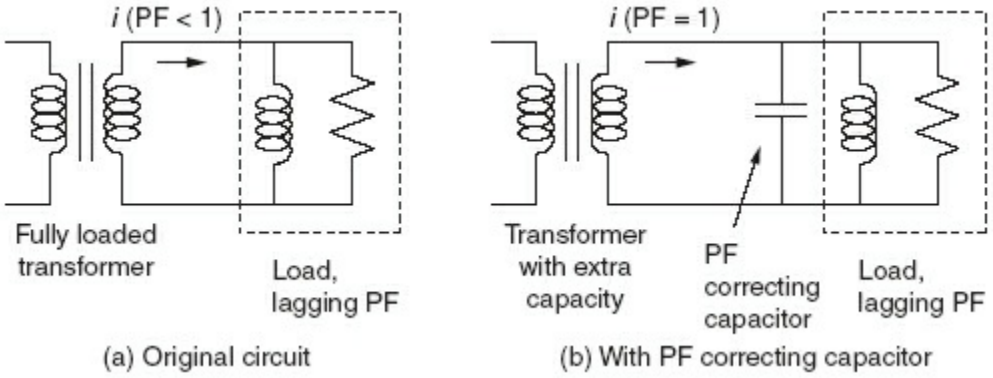
3.3.2 Power Factor Correction

Utilities are very concerned about customers who draw excessive amounts of reactive power—that is, customers with poor power factors. As has already been mentioned, reactive power increases line losses for the utility, but does not result in any more kilowatt-hours (kWh) of energy sales to the customer. To discourage poor power factors, utilities will either charge customers a penalty based on how low the power factor is, or they will charge not only for kWh of energy, but also for kVAR of reactive power.

Many large customers have loads that are dominated by electric motors, which are highly inductive. It has been estimated that lagging power factor, mostly caused by induction motors, is responsible for as much as one-fifth of all grid losses in the United States, equivalent to about 1.5% of total national power generation, and costing several billion dollars per year. Another reason for concern about power factor is that transformers (on both sides of the meter) are rated in kVA, not kW, since it is heating caused by current flow that causes them to fail. By correcting power factor, a transformer can deliver more real power to the loads. This can be especially important if loads are projected to increase to the point where existing transformers would no longer be able to handle the load without overheating and potentially burning out. Power factor correction can sometimes avoid the need for additional transformer capacity.

The question is, how can the power factor be brought closer to a perfect 1.0? The typical approach is fairly intuitive—namely, if the load is highly inductive, which most are, then try to offset that by adding capacitors as is suggested in Figure 3.13. The idea is for the capacitor to provide the current that the inductance needs rather than having that come from the transformer. The capacitor, in turn gets its current from the inductance. That is, the two reactive elements, capacitor and inductance, oscillate, sending current back and forth to each other.

FIGURE 3.13 Correcting power factor for an inductive load by adding a parallel capacitor.



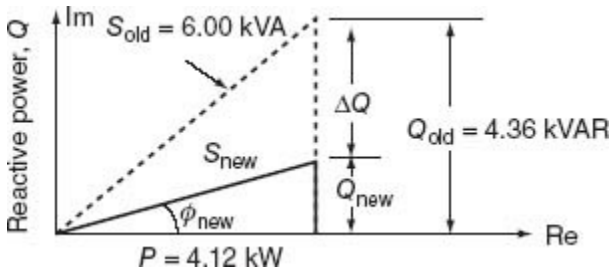
Capacitors used for power factor compensation are rated by the volt-amperes-reactive (VAR) that they supply at the system's voltage. When rated in these units, sizing a power factor correcting capacitor is quite straightforward and is based on the kVAR of a capacitor offsetting some or all of the kVAR in the power triangle. There are times, however, when the actual value of capacitance is needed. The relationship between Q_C (VAR), capacitive reactance, X_C, and capacitance, C, can be found from the following.

$$Q_C = \frac{V^2}{X_C} = \frac{V^2}{(1/\omega C)} = \omega C V^2 \quad (3.57)$$

Note, by the way, that the VAR rating of a capacitor depends on the square of the voltage. For example, a 100-VAR capacitor at 120 V would be a 400-VAR reactance at 240 V. That is, the VAR rating itself is meaningless without knowing the voltage at which the capacitor will be used.

Example 3.8 Improving Power Factor by Adding Capacitive Reactance. The 240-V, 60-Hz motor in Example 3.7 had a lagging power factor of 0.69, which is not very good. How much capacitance needs to be added to improve PF to 0.95? Express the answer in VARs, ohms, and farads.

Solution. It helps to begin by drawing the before-and-after power triangle:



The original phase angle needs to change from 46.7° to

$$\cos \phi_{new} = \frac{P}{S} = \text{PF} = 0.95$$

$$\phi_{new} = \cos^{-1}(0.95) = 18.19°$$

So maintaining the original P = 4.12 kW, the new Q needs to be

$$Q_{new} = P \tan \phi_{new} = 4.12 \tan 18.19° = 1.35 \text{ kVAR}$$

The added capacitive reactance needs to change Q by

$$\Delta Q = 4.36 - 1.35 = 3.01 \text{ kVAR}$$

Using Equation 3.57

$$X_C = \frac{V^2}{Q} = \frac{240^2}{3010} = 19.1\ \Omega$$

$$\text{and} \quad C = \frac{Q}{\omega V^2} = \frac{3010}{2\pi \cdot 60 \cdot 240^2} = 0.000139 \text{ F} = 139\ \mu\text{F}$$

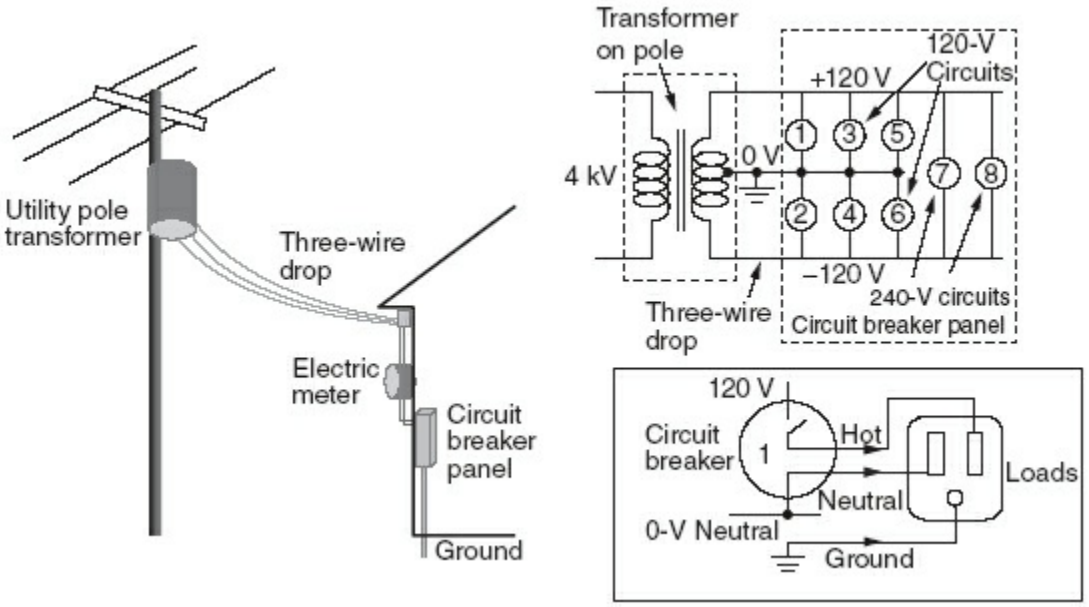
3.4 THREE-WIRE, SINGLE-PHASE RESIDENTIAL WIRING

The wall receptacle at home provides single-phase, 60-Hz power at a nominal voltage of about 120 V (actual voltages are usually in the range of 110–125 V). Such voltages are

sufficient for typical, low power applications such as lighting, electronic equipment, toasters, and refrigerators. For appliances that requires higher power, such as electric clothes dryers or electric space heaters, special outlets in your home provide power at a nominal 240 V. Running high power equipment on 240 V rather than 120 V cuts current in half, which cuts i^2R heating of wires to one-fourth. That allows easy-to-work-with, 12-gage wire to be used in a household, both for 120-V and 240-V applications. So, how is that 240 V provided?

Somewhere nearby, usually on a power pole or in a pad-mounted rectangular box, there is a transformer that steps down the voltage from the utility distribution system at typically 4.16 kV (though sometimes as high as 34.5 kV) to the 120/ 240 V household voltage. Figure 3.14 shows the basic three-wire, single-phase service drop to a home, including the transformer, electric meter, circuit-breaker panel box, and an individual breaker.

FIGURE 3.14 Three-wire, single-phase, power drop, including the wiring in the breaker box to feed 120 V and 240 V circuits in the house.



As shown in Figure 3.14, by grounding the center tap of the secondary side of the transformer (the neutral, white wire), the top and bottom ends of the windings are at the equivalent of +120 V and –120 V. The voltage difference between the two "hot" sides of the circuit (red and black wires) is 240 V. Note the inherent safety advantages of this configuration: at no point in the home's wiring system is the voltage more than 120 V higher than ground.

The ±120-V lines are 120 V (rms) with a 180° phase angle between them. In fact, it would be reasonable to say this is a two-phase system (but nobody does). There are a number of ways to demonstrate the creation of 240 V across the two hot leads coming into a circuit. One is using algebra, which is modestly messy:

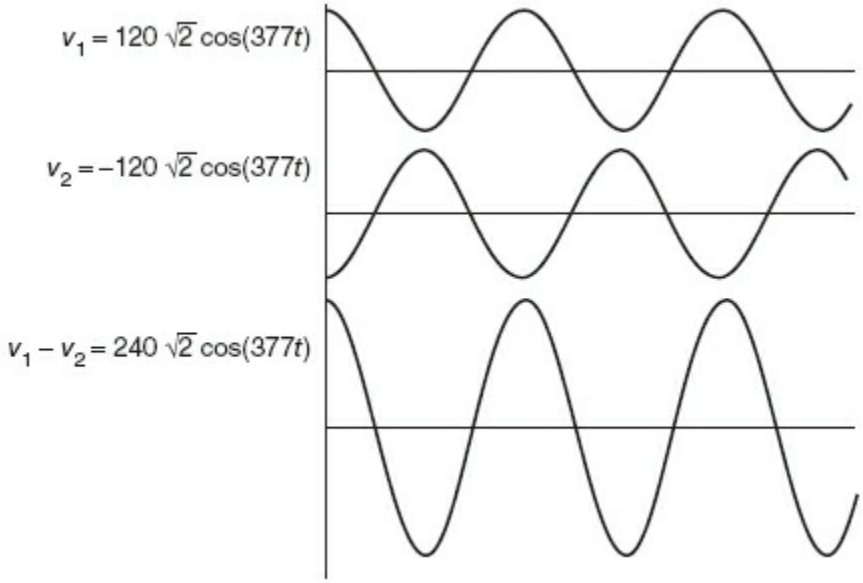
$$v_1 = 120\sqrt{2}\cos(2\pi \cdot 60t) = 120\sqrt{2}\cos 377t \tag{3.58}$$

$$v_2 = 120\sqrt{2}\cos(377t + \pi) = -120\sqrt{2}\cos 377t \tag{3.59}$$

(3.60) $$v_1 - v_2 = 240\sqrt{2}\cos 377t$$

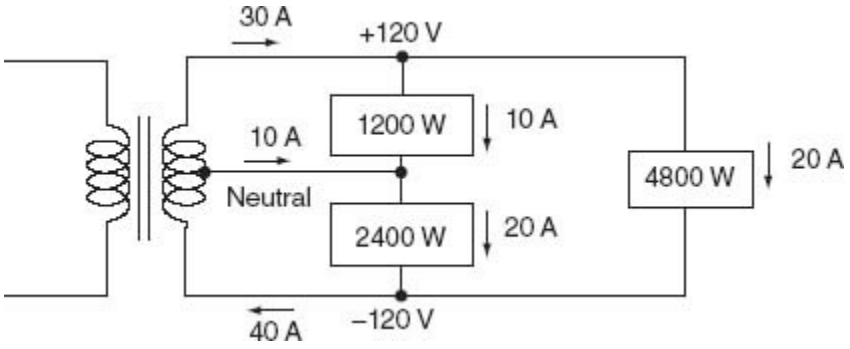
A second approach is to actually draw the waveforms, as has been done in Figure 3.15.

FIGURE 3.15 Waveforms for ±120 V and the difference between them creating 240 V.



Example 3.9 Currents in a Single-Phase, Three-Wire System. A three-wire, 120/240-V system supplies a residential load of 1200 W at 120 V on phase A, 2400 W at 120 V on phase B, and 4800 W at 240 V. The power factor for each load is 1.0. Find the currents in each of the three legs.

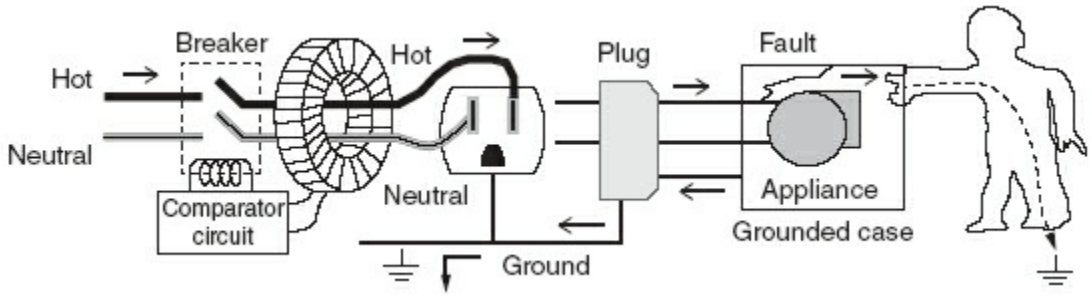
Solution. The 1200-W load at 120 V draws 10 A; the 2400-W load draws 20 A; and the 4800-W 240-V load draws 20 A. A simple application of Kirchhoff's current law results in the following diagram. Note the sum of the currents at each node equals zero; also note the currents are rms values that we can add directly since they each have current and voltage in phase.



Electricity, of course, can be dangerous. Risk is especially high in bathrooms and kitchens where there is greater danger of grounding oneself in a puddle of water. In those rooms, building codes require *ground-fault interrupter* (GFI) wall outlets (Fig. 3.16). In normal GFI operation, all current from the hot line, through the appliance, is returned through the neutral wire. None goes through the ground wire. With equal hot and neutral currents passing through a toroidal coil, their magnetic fields cancel. If, however, there is

leakage or a short between the hot wire and the case of an appliance, current in the neutral line will slow or stop, which means the magnetic fields of the hot and neutral lines will no longer cancel. That results in a spike of magnetic flux that is detected in a comparator circuit, which sends a signal to immediately open the breaker.

FIGURE 3.16 A ground fault interrupter (GFI) protects against dangerous faults by opening a breaker when unequal currents in the hot wire and neutral line are sensed.



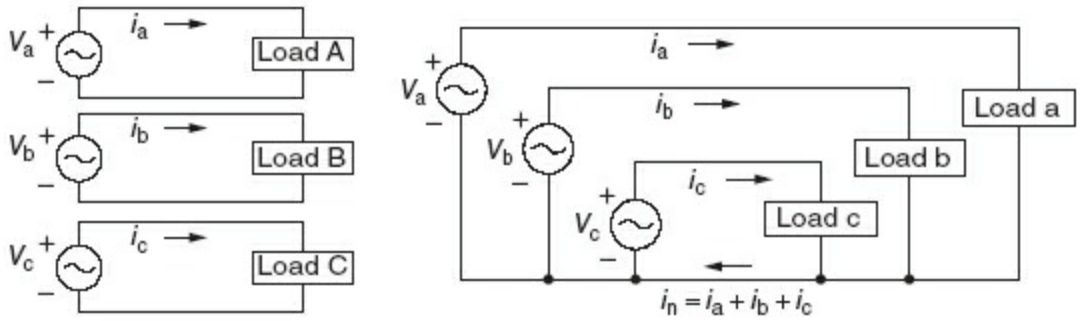
3.5 THREE-PHASE SYSTEMS

Commercial electricity is almost always produced with three-phase synchronous generators, and it is also almost always sent on its way along three-phase transmission lines. There are several good reasons why three-phase circuits are so common. For one, three-phase generators are much more efficient in terms of power per unit of mass and they operate much smoother, with less vibration, than single-phase generators. Another advantage is that three-phase currents in motor and generator stators create a rotating magnetic field that makes these machines spin in the right direction and at the right speed. Finally, three-phase transmission and distribution systems use their wires much more efficiently.

3.5.1 Balanced, Wye-Connected Systems

To understand the advantages of three-phase transmission lines, begin by comparing the three independent, single-phase circuits in Figure 3.17a with the circuit shown in Figure 3.17b. The three generators are the same in each case, so the total power delivered has not changed, but in Figure 3.17b, they are all sharing the same wire to return current to the generators. That is, by sharing the "neutral" return wire, only four wires are needed to transmit the same power as the six wires needed in the three single-phase circuits. That would seem to sound like a nice savings in transmission wire costs.

FIGURE 3.17 By combining the return wires for the circuits in (a), the same power can be sent using four wires instead of six (b). But it would appear the return wire could carry much more current than the supply lines.



(a) Three separate circuits (b) Combined use of the neutral line

The potential problem with combining the neutral return wires for the three circuits in Figure 3.17b is that we now have to size the return wire to handle the sum of the individual currents. So, maybe we have not gained much after all in terms of saving money on the transmission cables. The key to making that return wire oversizing problem disappear is to be more clever in our choice of generators. Suppose each generator develops the same voltage, but does so 120° out of phase with the other two generators, so that

$$v_a = V\sqrt{2}\cos(\omega t) \qquad \boldsymbol{V}_a = V\angle 0° \tag{3.61}$$

$$v_b = V\sqrt{2}\cos(\omega t - 120°) \qquad \boldsymbol{V}_b = V\angle -120° \tag{3.62}$$

$$v_c = V\sqrt{2}\cos(\omega t + 120°) \qquad \boldsymbol{V}_c = V\angle 120° \tag{3.63}$$

Sizing the neutral return wire (Fig. 3.17b) means we need to look at currents flowing in each phase of the circuit so that we can add them up. The simplest situation to analyze occurs when each of the three loads are exactly the same so that the currents are all the same except for their phase angles. When that is the case, the three-phase circuit is said to be *balanced*. With balanced loads, the currents in each phase can be expressed as

$$i_a = I\sqrt{2}\cos(\omega t) \qquad \boldsymbol{I}_a = I\angle 0° \tag{3.64}$$

$$i_b = I\sqrt{2}\cos(\omega t - 120°) \qquad \boldsymbol{I}_b = I\angle -120° \tag{3.65}$$

$$i_c = I\sqrt{2}\cos(\omega t + 120°) \qquad \boldsymbol{I}_c = I\angle 120° \tag{3.66}$$

The current flowing in the neutral wire is therefore

$$i_n = i_a + i_b + i_c = I\sqrt{2}[\cos(\omega t) + \cos(\omega t - 120) + \cos(\omega t + 120°)] \tag{3.67}$$

This looks messy, but something great happens when you apply some trigonometry. Recall the identity:

$$\cos A \cdot \cos B = \frac{1}{2}[\cos(A + B) + \cos(A - B)] \tag{3.68}$$

so that

$$\cos \omega t \cdot \cos(120^\circ) = \frac{1}{2}[\cos(\omega t + 120) + \cos(\omega t - 120^\circ)]$$

(3.69)

Substituting Equation 3.69 into Equation 3.67 gives

$$i_n = I\sqrt{2}[\cos \omega t + 2\cos(\omega t) \cdot \cos(120^\circ)]$$

(3.70)

But cos (120°) = −1/2, so that

$$i_n = I\sqrt{2}[\cos \omega t + 2\cos(\omega t) \cdot (-1/2)] = 0$$

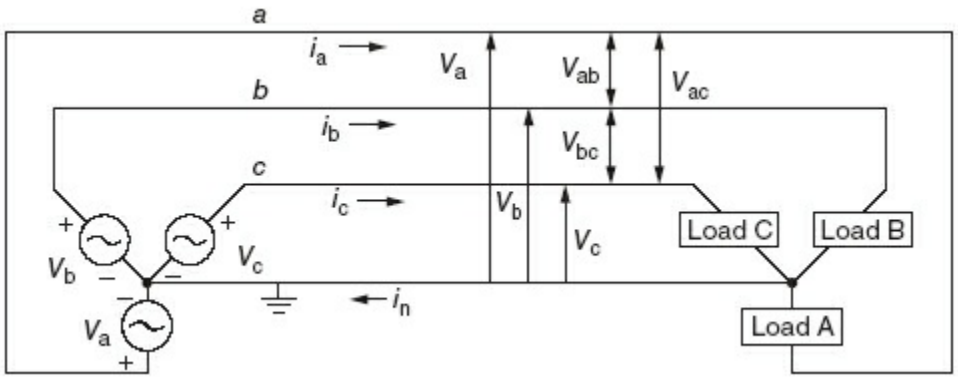
(3.71)

Now, we can see a perhaps startling conclusion: for a balanced three-phase circuit, there is no current in the neutral wire; in fact, for a balanced three-phase circuit, we do not even need the neutral wire! Referring back to Figure 3.17, what we have done is to go from six transmission cables for three separate, single-phase circuits, to just three transmission cables (of the same size) for a balanced three-phase circuit. In three-phase transmission lines, the neutral conductor is quite often eliminated or, if it is included at all, it will be a much smaller conductor designed to handle only modest amounts of current when loads are unbalanced.

While the algebra suggests transmission lines can do without their neutral cable, the story is different for three-phase loads. For three-phase *loads* (as opposed to three-phase transmission lines), the practice of undersizing neutral lines in wiring systems in buildings has in the past had unexpected, dangerous consequences. As we will see later in this chapter, when loads include more and more computers, copy machines, and other electronic equipment, harmonics of the fundamental 60-Hz current are created, and those harmonics do not cancel out the way the fundamental frequency did in Equation 3.71. The result is that undersized neutral lines in buildings can end up carrying much more current than expected, which can cause dangerous overheating and fires. Those same harmonics also play havoc on transformers in buildings as we shall see.

Figure 3.17b has been redrawn in its more conventional format in Figure 3.18. As drawn, the configuration is referred to as a three-phase, four-wire, *wye-connected* or *star-connected* circuit. Later we will briefly look at another wiring system that creates circuits in which the connections form a *delta* rather than a wye.

FIGURE 3.18 A four-wire, wye-connected, three-phase circuit, showing source and load.



Example 3.10 An Unbalanced Three-Phase System. A small, rural power grid has a very unbalanced three-phase, wye-connected distribution system. The three phases have currents

$$\boldsymbol{I}_a = 100\angle 0^\circ \text{ A} \qquad \boldsymbol{I}_b = 80\angle -120^\circ \text{ A} \qquad \boldsymbol{I}_c = 40\angle 120^\circ \text{ A}$$

Find the current in the neutral wire.

Solution. Let us solve this using our phasor notation:

$$\boldsymbol{I}_a = 100$$

$$\boldsymbol{I}_b = 80\,[\cos(-120^\circ) + j\sin(-120^\circ)] = -40 - j69.28$$

$$\boldsymbol{I}_c = 40\,[\cos(120^\circ) + j\sin(120^\circ)] = -20 + j34.64$$

so $I_n = I_a + I_b + I_c = 100 - 40 - 20 + j(-69.28 + 34.64) = 40 - j34.64$

$$\boldsymbol{I}_n = \sqrt{40^2 + (-34.64)^2}\angle \tan^{-1}\left(-\frac{34.64}{40}\right) = 52.91\angle -40.9^\circ \text{ A}$$

And the phasor diagram looks like:

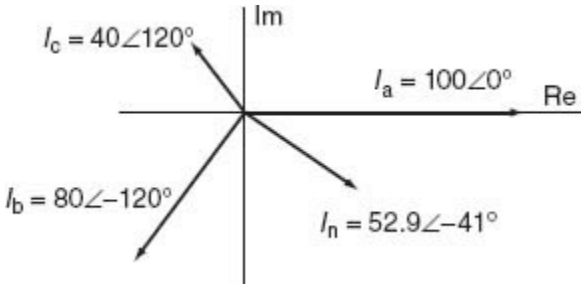


Figure 3.18 shows the specification of various voltages within a three-phase, wye-connected system. The voltages measured with respect to the neutral wire, that is, V_a, V_b, and V_c, are called *phase voltages.* Voltages measured between the phases themselves, for example, the voltage at "a" with respect to the voltage at "b" is labeled V_{ab}. These voltages, V_{ab}, V_{ac}, and V_{bc}, are called *line voltages*. When the voltage on a transmission line or transformer is specified, it is always the line voltages that are being referred to.

Let us develop the relationship between phase voltages and line voltages. To help define a sign convention, let us be a bit more precise about phase voltages with subscripts that remind us they are with respect to the neutral (e.g., V_{an} is the voltage of phase "a" with respect to the neutral "n." For example, the line-to-line voltage between line a and line b:

$$\boldsymbol{V}_{ab} = \boldsymbol{V}_{an} + \boldsymbol{V}_{nb} = -\boldsymbol{V}_{na} + \boldsymbol{V}_{nb} \tag{3.72}$$

For a balanced system, each phase voltage has the same magnitude, call it V_{phase}. So we can write

$$\boldsymbol{V}_{na} = \boldsymbol{V}_{phase}\angle 0^\circ \tag{3.73}$$

$$\boldsymbol{V}_{nb} = \boldsymbol{V}_{phase}\angle -120^\circ \tag{3.74}$$

$$\boldsymbol{V}_{nc} = \boldsymbol{V}_{phase}\angle 240^\circ = \boldsymbol{V}_{phase}\angle 120^\circ \tag{3.75}$$

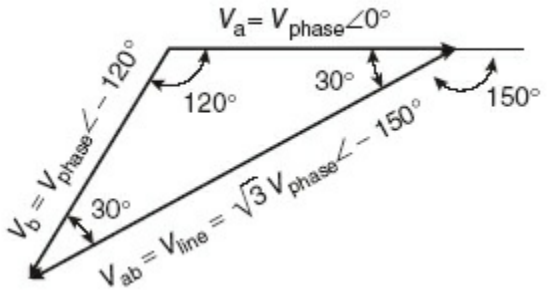
Substituting Equations 3.73 and 3.74 into Equation 3.72 gives line voltage V_{ab}

$$\begin{aligned} \boldsymbol{V}_{ab} &= -V_{phase}\angle 0^\circ + V_{phase}\angle -120^\circ \\ &= -V_{phase} + V_{phase}\left[\cos(-120^\circ) - j\sin 120^\circ\right] \end{aligned} \tag{3.76}$$

$$= V_{phase}\left(-\frac{3}{2} - j\frac{\sqrt{3}}{2}\right) = \sqrt{3}V_{phase}\angle -150^\circ \tag{3.77}$$

A vector diagram of this result is shown in Figure 3.19.

FIGURE 3.19 Vector diagram showing the origin of $V_{line} = \sqrt{3}V_{phase}$.



Since the above derivation applies to all three phases, we can write the general and important relationship between phase voltages V_{phase} and line voltages V_{line}

$$V_{line} = \sqrt{3}V_{phase} \quad \text{(valid for wye connection)} \tag{3.78}$$

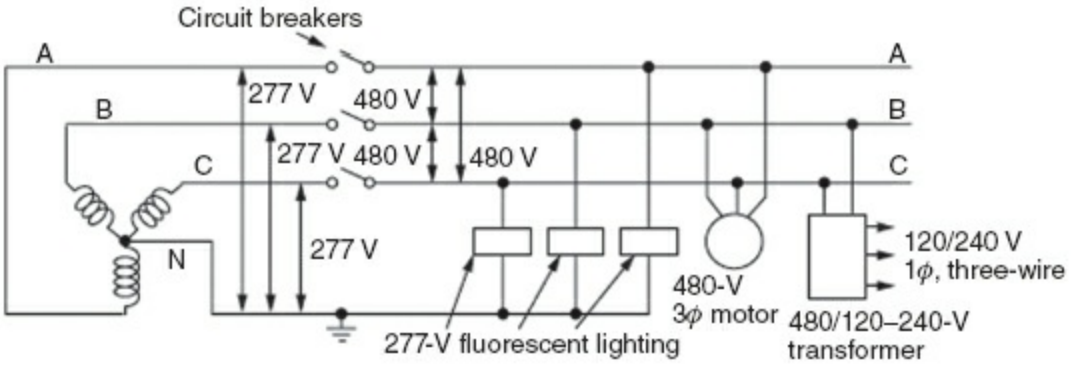
That factor of $\sqrt{3}$ appears over and over again in three-phase calculations (in much the same way that $\sqrt{2}$ shows up so often in single-phase equations).

To illustrate Equation 3.78, the most widely used four-wire, three-phase service to buildings provides power at a line voltage of 208 V. With the neutral wire serving as the reference voltage, that means the phase voltages are

$$V_{phase} = \frac{V_{line}}{\sqrt{3}} = \frac{208\text{ V}}{\sqrt{3}} = 120\text{ V} \tag{3.79}$$

For relatively high power demands, such as large motors, a line voltage of 480 V is often provided, which means the phase voltage is V_{phase} = 480/$\sqrt{3}$ = 277 V. The 277-V phase voltages, for example, are often used in large commercial buildings to power fluorescent lighting systems. A wiring diagram for a 480/277-V system, which includes a single-phase transformer to convert the 480-V line voltage into 120-V/240-V power is shown in Figure 3.20.

FIGURE 3.20 Example of a three-phase, 480-V, large-building wiring system that provides 480-V, 277-V, 240-V and 120-V service. The voltage supply is represented by three coils, which are the three windings on the secondary side of the three-phase transformer serving the building.



To find the power delivered in a balanced, three-phase system, we need to consider all three kinds of power: apparent power S (VA), real power P (watts), and reactive power Q (VAR). Recalling that a three-phase circuit is, in essence, just three separate single-phase circuits, the total apparent power is just three times the apparent power in each phase:

$$S_{3\phi} = 3V_{\text{phase}}I_{\text{phase}} \quad \text{(VA)} \tag{3.80}$$

Similarly, the reactive power is

$$Q_{3\phi} = 3V_{\text{phase}}I_{\text{phase}}\sin\phi \quad \text{(VARs)} \tag{3.81}$$

where ϕ is the phase angle between phase current and voltage, which is assumed to be the same for all three phases since this is a balanced load. Finally, the real power in a balanced three-phase circuit is given by

$$P_{3\phi} = 3V_{\text{phase}}I_{\text{phase}}\cos\phi \quad \text{(watts)} \tag{3.82}$$

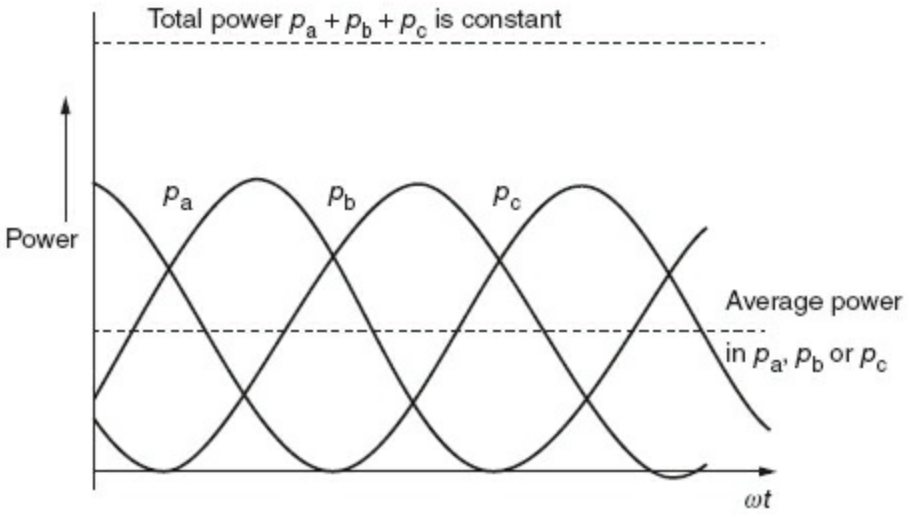
Using Equation 3.78, while realizing that phase current and line current are the same thing, allows us to rewrite S, Q, and P in terms of line voltages and currents:

(3.83)

$$S_{3\phi} = \sqrt{3}\,V_{\text{line}}I_{\text{line}}, \quad Q_{3\phi} = \sqrt{3}\,V_{\text{line}}I_{\text{line}}\sin\phi, \quad \text{and } P_{3\phi} = \sqrt{3}\,V_{\text{line}}I_{\text{line}}\cos\phi$$

While Equations 3.82 and 3.83 give an average value of real power, it can be shown algebraically that in fact the real power delivered is a constant that does not vary with time. The sketch shown in Figure 3.21 shows how the summation of the power in each of the three legs leads to a constant total. That constant level of power is responsible for one of the advantages of three-phase power—that is, the smoother performance of motors and generators. For single-phase systems, instantaneous power varies sinusoidally leading to rougher motor/generator operation.

FIGURE 3.21 The sum of the three phases of power in balanced delta and wye loads is a constant, not a function of time.



Example 3.11 Correcting the Power Factor in a Three-Phase Circuit. Suppose a shop has a three-phase, star-connected 480-V transformer delivering power to an 80-kW motor with a rather poor power factor PF of 0.5 (Fig. 3.20).

a. Find the total apparent power S, reactive power Q, and the individual line current needed by this motor.

b. How many kVA in the transformer would be freed up if the power factor is improved to 0.9?

Solution

a. Before PF correction, with P = 80 kW the apparent power S can be found from

$$S = \frac{P}{\cos\phi} = \frac{P}{\text{PF}} = \frac{80}{0.5} = 160 \text{ kVA}$$

To find reactive power, we first need the phase angle

$$\phi = \cos^{-1} \text{PF} = \cos^{-1}(0.5) = 60°$$

$$Q = S \sin\phi = 160 \sin(60°) = 138.6 \text{ VAR}$$

Using Equation 3.83 we can get line current

$$I_{\text{line}} = \frac{S}{\sqrt{3}V_{\text{line}}} = \frac{160{,}000}{480\sqrt{3}} = 192.5 \text{ A}$$

b. After correcting the power factor to 0.9, the resulting apparent power is now

$$S = \frac{P}{\text{PF}} = \frac{80}{0.9} = 88.9 \text{ kVA}$$

The reduction in demand from the transformer is

$$\Delta S = 160 - 88.9 = 71.1 \text{ kVA}$$

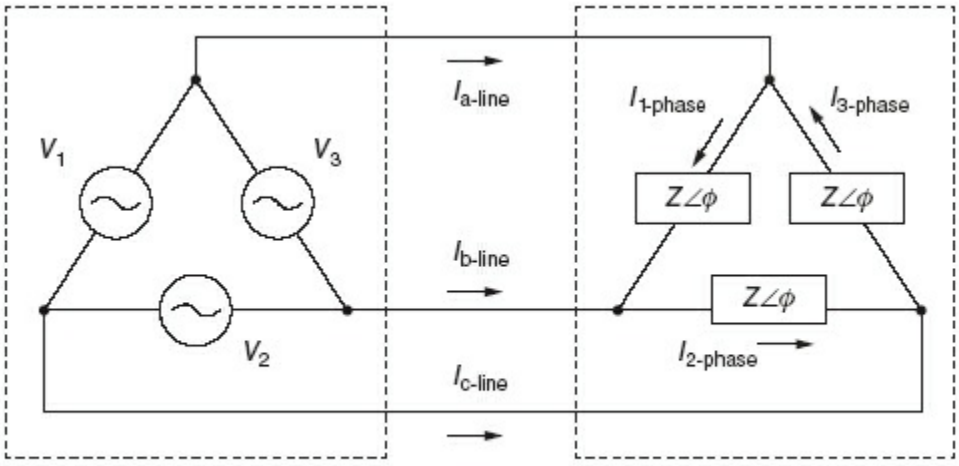
Power factor adjustment not only reduces line losses but, as the above example illustrates, it also makes possible a smaller, less-expensive transformer. In a transformer, it is the heat given off as current runs through the windings that determines its rating. Transformers are rated by their voltage and their kVA limits, and not by the kW of real power delivered to their loads. In the above example, power factor correction reduced the kVA needed from 160 to 88.9 kVA—a reduction of 44%. That reduction could be used to accommodate

future growth in factory demand without needing to buy a new, bigger transformer; or perhaps, when the existing transformer needs replacement, a smaller one could be purchased.

3.5.2 Delta-Connected, Three-Phase Systems

So far we have dealt only with three-phase circuits that are wired in the wye-(or star) configuration, but there is another way to connect three-phase generators, transformers, transmission lines, and loads. The *delta* connection uses three wires and has no inherent ground or neutral line (though oftentimes, one of the lines is grounded). The wiring diagrams for delta-connected sources and loads are shown in Figure 3.22.

FIGURE 3.22 Three-phase balanced delta source and load.



(a) Three-phase balanced delta source

(b) Three-phase balanced delta load

A summary of the key relationships between currents and voltages for wye-connected and delta-connected three-phase systems is presented in Table 3.1. Note the expressions *S*, *P*, and *Q* are the same for both wye- and delta-connected systems.

TABLE 3.1 Summary of Wye- and Delta-Connected Current, Voltage, and Power Relationships. Note *P*, *S*, and *Q* are the Same for Both Systems

Quantity	Wye-Connected	Delta-Connected
Current (rms)	$I_{\text{line}} = I_{\text{phase}}$	$I_{\text{line}} = \sqrt{3} I_{\text{phase}}$
Voltage (rms)	$V_{\text{line}} = \sqrt{3} V_{\text{phase}}$	$V_{\text{line}} = V_{\text{phase}}$
Real power (kW)	$P_{3\phi} = 3\ V_{\text{phase}} I_{\text{phase}} \cos\phi = \sqrt{3}\, V_{\text{line}} I_{\text{line}} \cos\phi$	
Apparent power (VA)	$S_{3\phi} = 3 V_{\text{phase}} I_{\text{phase}} = \sqrt{3} V_{\text{line}} I_{\text{line}}$	
Reactive power (VAR)	$Q_{3\phi} = 3 V_{\text{phase}} I_{\text{phase}} \sin\phi = \sqrt{3} V_{\text{line}} I_{\text{line}} \sin\phi$	

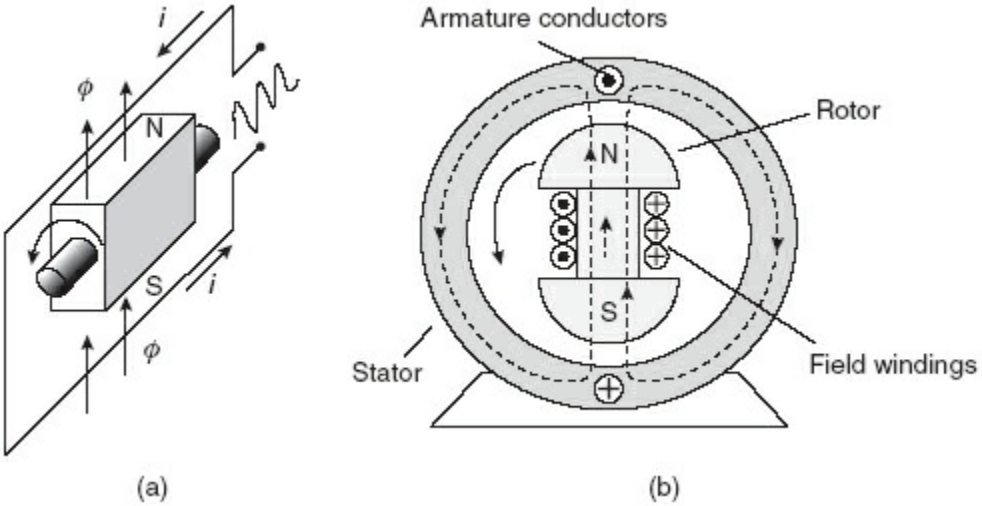
3.6 SYNCHRONOUS GENERATORS

With the exception of minor amounts of electricity generated using internal combustion

engines, fuel cells, or photovoltaics, the electric power industry is based on some energy source forcing a fluid (steam, combustion gases, water, or air) to pass through turbine blades, causing a shaft to spin. The function of the generator, then, is to convert the rotational energy of the turbine shaft into electricity.

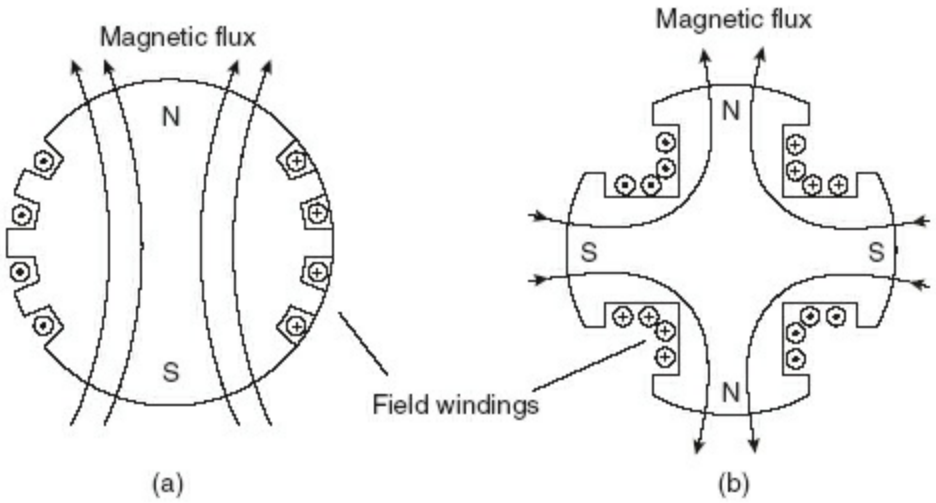
Electric generators are all based on the fundamental concepts of electromagnetic induction developed by Michael Faraday in 1831. Faraday discovered that moving a conductor through a magnetic field induces an electromagnetic force (emf), or voltage, across the wire. A generator, very simply, is an arrangement of components designed to cause relative motion between a magnetic field and the conductors in which the emf is to be induced. Those conductors, out of which flows electric power, form what is called the *armature*. Most large generators have the armature windings fixed in the stationary portion of the machine (called the *stator*) and the necessary relative motion is caused by rotating the magnetic field (Fig. 3.23a).

FIGURE 3.23 The rotor's magnetic field can be created with a permanent magnet (a) or current through field windings (b). The windings indicate current flow into the page with a "+" and current out of the page with a dot (the + is meant to resemble the feathers of an arrow moving away from you; the dot is the point of the arrow coming toward you).



The magnetic field in the rotor of a generator can be created using a permanent magnet, as suggested in Figure 3.23a, but for most generators, the field windings are fed, or *excited*, by an external source that sends DC current through brushes and slip rings into conductors affixed to the rotor (Fig. 3.23b). Field windings may be imbedded into slots that run along the length of a round rotor as shown in Figure 3.24a or they may be wound around what are called *salient poles*, as shown in Figure 3.24b. Salient pole rotors are less expensive to fabricate and are often used in slower-spinning hydroelectric generators, but most thermal plants use round rotors, which are better able to handle the centrifugal forces and resulting stresses associated with higher speeds.

FIGURE 3.24 Field windings on (a) two-pole, round rotor; (b) four-pole, salient rotor.



Both round and salient pole rotors may be wound with a range of numbers of magnetic poles. Adding more poles allows the generator to spin more slowly while still producing a desired frequency for its output power. In general, rotor speed N as a function of number of poles p and output frequency required f is given by

$$N(\text{rpm}) = \frac{1 \text{ revolution}}{(p/2) \text{ cycles}} \times \frac{f \text{ cycles}}{\text{s}} \times \frac{60 \text{ s}}{\text{min}} = \frac{120f}{p} \tag{3.84}$$

While the United States uses 60 Hz exclusively for power, Europe and parts of Japan use 50 Hz. Table 3.2 provides a convenient summary of rotor speeds required for a synchronous generator to deliver power at 50 Hz and at 60 Hz. Permanent magnet generators, with large numbers of poles, are beginning to look attractive as a way to do away with high maintenance gear boxes in large, slow-speed wind turbines.

TABLE 3.2 *Shaft Rotation (rpm) as a Function of Number of Poles and Desired Output Frequency*

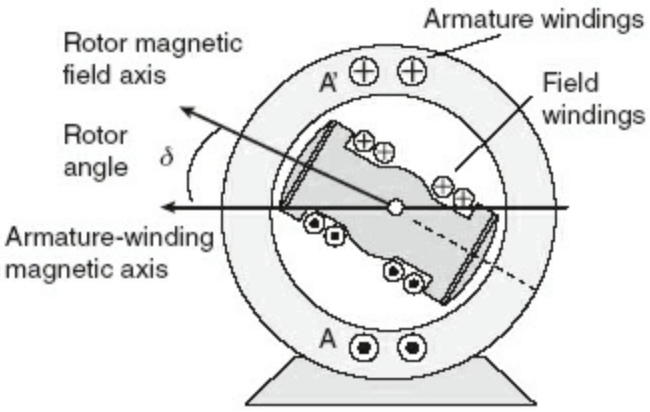
Poles p	50 Hz rpm	60 Hz rpm
2	3000	3600
4	1500	1800
6	1000	1200
8	750	900
10	600	720
12	500	600

3.6.1 The Rotating Magnetic Field

Virtually all, large, conventional power plants rely on three-phase, grid-connected, synchronous generators to convert mechanical torque into electrical power. To understand these generators, we must deal with the interactions between two fields—one created by current in the armature windings and one created on the rotor. Figure 3.25 shows a salient-pole rotor and its magnetic field axis along with the magnetic axis for a single phase of armature windings. Note the armature designations A and A′ which refer to coils in a single winding—that is, they are connected together around the back of the generator. When

armature current is in the positive portion of its AC cycle, it shows up as a "dot" in the A wires and a "+" in the A′ wire, meaning current is going away from you in A′ and coming toward you in A. In the negative portion of its cycle, the "dot" and "+" indicators would switch to A′ and A, respectively.

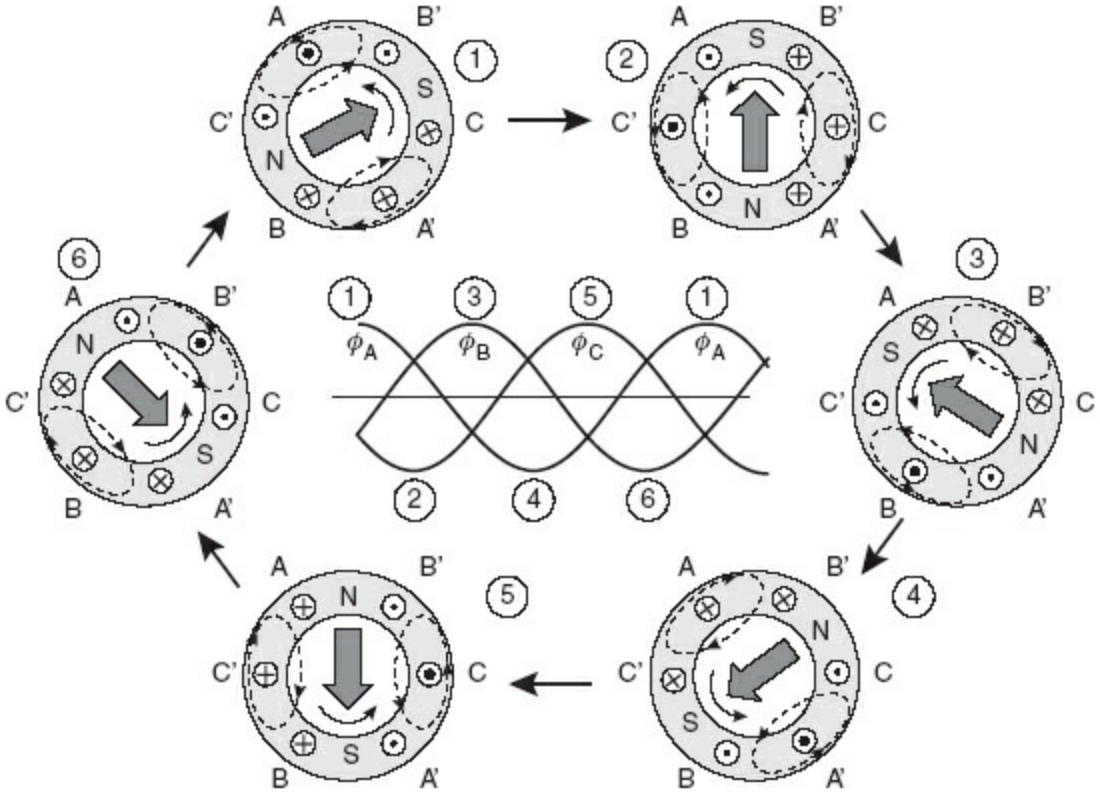
FIGURE 3.25 Showing the interaction between magnetic fields created by the exciter field on the rotor and currents in a single phase of armature windings.



If there is no load on the generator—that is, if it is not delivering any power, the rotor and armature magnetic fields will line up, one on top of the other. In general, however, there will be an angle, δ, between the two magnetic fields.

Since we are describing a grid-connected generator, it is absolutely essential that the rotor spin at exactly the same speed as every other generator on the grid. To make that happen, the armature has three sets of windings to take three-phase power from the grid. Those currents flowing through the stator windings create the effect of a rotating magnetic field inside the generator as shown in Figure 3.26. The rotor then, with its own magnetic field, locks onto that rotating armature field forcing the rotor to spin at precisely the desired speed.

FIGURE 3.26 The rotating magnetic field created by three-phase armature currents.



So now with the rotor spinning at the correct frequency, the machine can either act as a motor or as a generator. As a motor, if you tried to slow down the shaft, the machine would convert electrical power into increased torque on the shaft to keep it spinning at the same speed. The magnetic field of the rotor would fall a little bit behind the stator's rotating magnetic field.

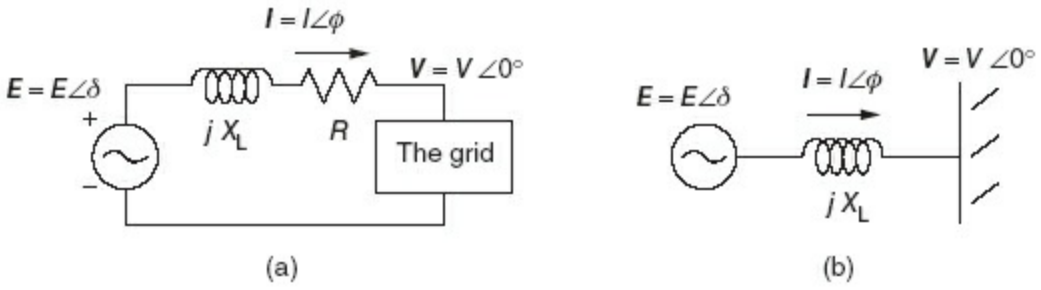
As a generator, when electrical power needs to be delivered, it comes from the mechanical torque provided by whatever is driving the generator (usually a turbine). The rotor spins at the same speed, but now the rotor's magnetic field pushes a little bit ahead of the rotating stator field. As more power is required, the angle between the two fields, called the rotor angle or the power angle δ increases.

3.6.2 Phasor Model of a Synchronous Generator

As the generator shaft spins, the rotor induces an emf E as it passes over each of the three armature windings. Meanwhile, the grid is providing its own voltage V onto those same three windings. Both E and V have the same 60-Hz frequency, but they are out of phase with each other with E leading V by the rotor power angle δ. A simple equivalent circuit of the generator itself consists of a voltage source E sending current I to the grid through an inductive reactance X_L and winding resistance R (Fig. 3.27a). Figure 3.27b shows two simplifications. One is based on the assumption that the reactance in the armature is far larger than its resistance—enough so that R can be ignored. The other is to assume the grid can be represented by what is often referred to as an "infinite busbar" with a constant voltage V and an assumed reference angle of zero.

FIGURE 3.27 Equivalent circuit of a generator feeding power to the grid. (a) Including

armature resistance. (b) Simplified connection to an infinite busbar.



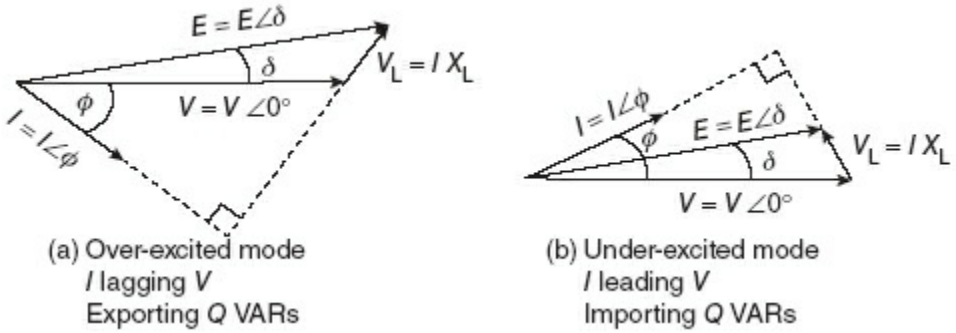
Perhaps the easiest way to interpret the equivalent circuit is with the phasor diagrams shown in Figure 3.28, which give us several keys to understanding the output of a synchronous generator:

1. The emf E created when the rotor swings by armature windings is directly proportional to the rotor's magnetic field, which is directly proportional to the field current. That is, the length of the phasor E is determined by the amount of field current.
2. Increasing field current can cause I to lag V, which exports VARs (the *over-excited* mode, Fig. 3.28a). Decreasing field current can cause I to lead V, which imports VARs (the *under-excited* mode, Fig. 3.28b).
3. Real power and reactive power delivered are

$$P = VI\cos\phi \text{ (W)} \quad \text{and} \quad Q = VI\sin\phi \text{ (VAR)} \tag{3.85}$$

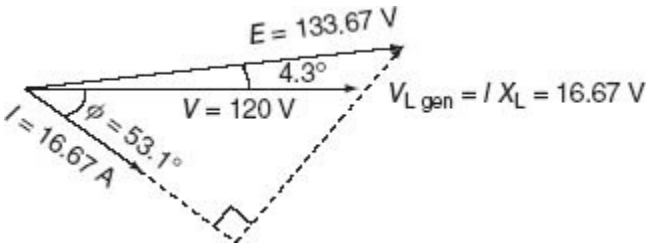
4. The power angle δ between E and V is determined by the torque applied by the turbine. Increasing torque, increases δ. Increasing δ in the over-excited mode (Fig. 3.28a) increases P and decreases the amount of Q exported to the grid. Increasing δ in the under-excited mode decreases P and increases imported Q (Fig. 3.28b).

FIGURE 3.28 Phasor diagrams for a grid-connected, three-phase, synchronous generator in which ϕ is the power factor angle and δ is the rotor angle.



The beauty of the synchronous generator is the operator has independent control of P and Q. By varying torque delivered to the generator shaft, real power P delivered can be changed. By varying current to the rotor's field windings, Q can be adjusted. There are bounds, of course, on the range of P and Q that can be delivered. The amount of Q that can be exported, for example, may be constrained by the maximum current that the rotor can tolerate. The amount of P that can be delivered is limited by the torque available on the shaft as well as the current capacity of the armature.

Example 3.12 A Generator Exporting P and Q. In Example 3.6, the following phasor diagram was found for an over-excited generator delivering power to a load with an inductive/resistive impedance.



Find the amount of P and Q exported to this load and the power factor.

Solution. Using Equation 3.85, it is easy to find

$$P = VI\cos\phi = 120 \times 16.67 \cos 53.1^\circ = 1200 \text{ W}$$

$$Q = VI\sin\phi = 120 \times 16.67 \sin 53.1^\circ = 1600 \text{ VAR}$$

And power factor is

$$\text{PF} = \cos\phi = \cos 53.1^\circ = 0.6 \quad \text{which is pretty low.}$$

3.7 TRANSMISSION AND DISTRIBUTION

As described in Chapter 1, the traditional model of transmission and distribution (T&D) includes high voltage lines that carry bulk power over long distances, followed by a complex mesh of substations and distribution lines that deliver power to customers. That model is evolving into one in which more and more distributed generation (DG) sources are imbedded into the distribution system itself. Some of the implications of this evolution will be described in this section.

3.7.1 Resistive Losses in T&D

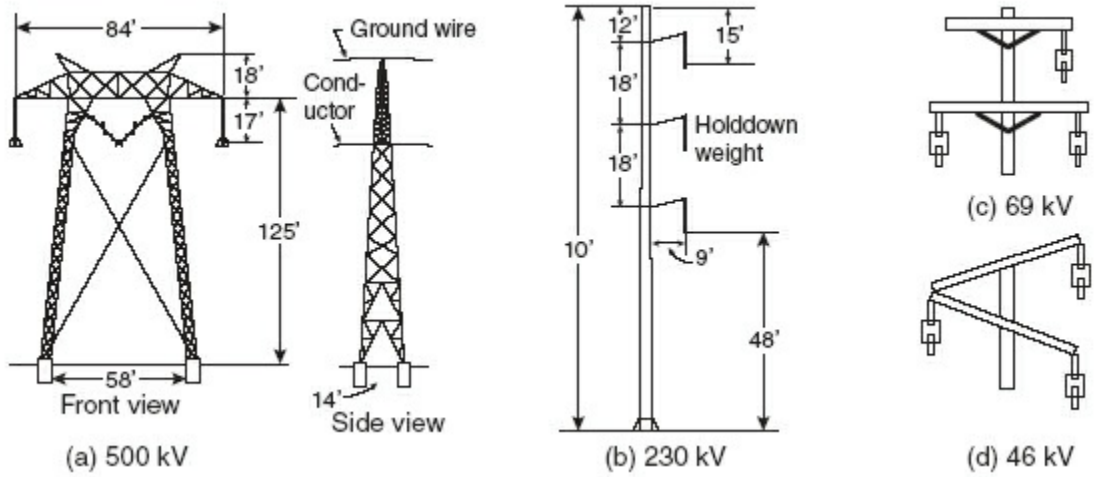
The physical characteristics of T&D lines depend very much on the voltages that they carry. Cables carrying higher voltages must be spaced further apart from each other and from the ground to prevent arcing from line to line. As power levels increase, more current must be carried, so to control losses thicker conductors are required. Table 3.3 lists the most common voltages in use in the United States along with their usual designation as being transmission, subtransmission, distribution, or utilization voltages.

TABLE 3.3 Nominal Standard T&D System Voltages

Transmission (kV)	Subtransmission (kV)	Distribution (kV)	Utilization (V)
765	138	24.94	600
500	115	22.86	480
345	69	13.8	240
230	46	13.2	208
161	34.5	12.47	120
		8.32	
		4.16	

Figure 3.29 shows examples of towers used for various representative transmission and subtransmission voltages. Note the 500-kV tower has three suspended connections for the three-phase current, but it also shows a fourth, ground wire above the entire structure. That ground wire not only serves as a return path in case the phases are not balanced, but it also provides a certain amount of lightning protection.

FIGURE 3.29 Examples of transmission towers: (a) 500 kV; (b) 230-kV steel pole; (c) 69-kV wood tower; (d) 46-kV wood tower.



Overhead transmission lines are usually uninsulated, stranded aluminum or copper wire that is often wrapped around a steel core to add strength (Fig. 3.30). The resistance of such cable is of obvious importance due to the i^2R power losses in the wires as they may carry hundreds of amperes of current. Examples of cable resistances, diameters, and current-carrying capacity are shown in Table 3.4.

TABLE 3.4 Conductor Characteristics[a]

Conductor Material	Outer Diameter (in)	Resistance (Ω/mi)	Ampacity (A)
ACSR	0.502	0.7603	315
ACSR	0.642	0.4113	475
ACSR	0.858	0.2302	659
ACSR	1.092	0.1436	889
ACSR	1.382	0.0913	1187
Copper	0.629	0.2402	590
Copper	0.813	0.1455	810
Copper	1.152	0.0762	1240
Aluminum	0.666	0.3326	513
Aluminum	0.918	0.1874	765
Aluminum	1.124	0.1193	982

[a]Resistances at 75°C conductor temperature and 60 Hz, ampacity at 25°C ambient, and 2-ft/s wind velocity.
Source: Data from Bosela (1997).

Example 3.13 Transmission Line Losses. Consider a 40-mi long, three-phase, 230-kV (line-to-line) transmission system using 0.502-in-diameter ACSR cable. The line supplies a three-phase, wye-connected, 100-MW load with a 0.90 power factor. Find the power losses in the transmission line and its efficiency. What savings would be achieved if the power factor could be corrected to 1.0?

Solution. From Table 3.4, the cable has 0.7603-Ω/mi resistance, so each line has resistance

$$R = 40 \text{ mi} \times 0.7603 \ \Omega/\text{mi} = 30.41 \ \Omega$$

The phase voltage from line to neutral is given by Equation 3.78

$$V_{\text{phase}} = \frac{V_{\text{line}}}{\sqrt{3}} = \frac{230 \text{ kV}}{\sqrt{3}} = 132.79 \text{ kV}$$

The 100 MW of real power delivered is three times the power delivered in each phase. From Equation 3.82

$$P = 3V_{\text{phase}} I_{\text{phase}} \times \text{Power Factor} = 100 \times 10^6 \text{ W}$$

Solving for the phase current (same as the line current) gives

$$I_{\text{phase}} = \frac{100 \times 10^6}{3 \times 132,790 \times 0.90} = 278.9 \text{ A}$$

Checking Table 3.4, this is less than the 315 A the cable is rated for (at 25°C).

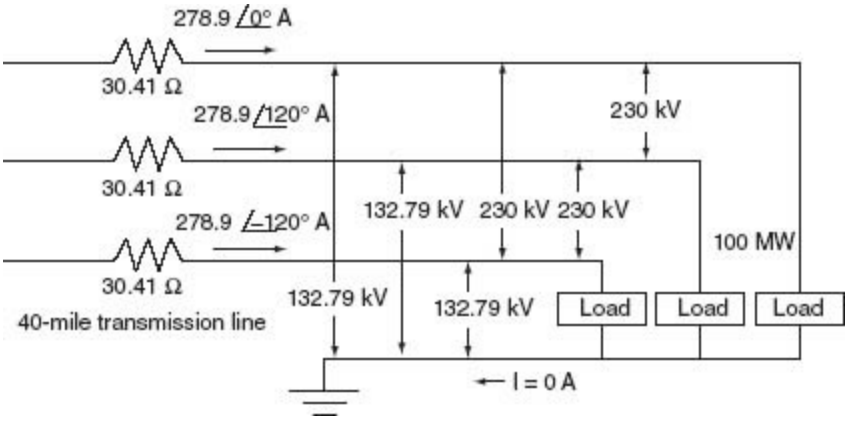
The total line losses in the three phases is therefore

$$P = 3I^2R = 3 \times (278.9)^2 \times 30.41 = 7.097 \times 10^6 \text{ W} = 7.097 \text{ MW}$$

The overall efficiency of the transmission line is therefore

$$\text{Efficiency} = \frac{\text{Power delivered}}{\text{Input power}} = \frac{100}{100 + 7.097} = 0.9337 = 93.37\%$$

That is, there are 6.63% losses in the transmission line. The figure below summarizes the calculations.

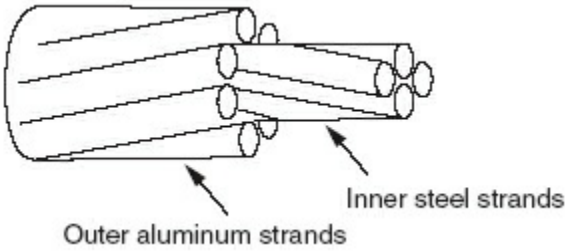


Using Equation 3.82, if the power factor could be corrected to 1.0, the line losses would be reduced to

$$P_{\text{loss}} = 3\,(I_{\text{line}})^2\,R_{\text{line}} = 3\left(\frac{100 \times 10^6/3 \text{ W/line}}{132{,}790 \text{ V} \cdot \text{PF} = 1}\right)^2 \cdot 30.41\ \Omega = 5.75 \text{ MW}$$

which is 19% reduction in line losses.

FIGURE 3.30 Aluminum conductor with steel reinforcing (ACSR).



Those line losses, such as described in the previous example, cause wires to heat up. Moreover, as copper or aluminum wires heat up their resistance increases by about 4% for each 10°C of heating, which increases the I^2R heating even more. On hot, windless days, when air conditioners drive up peak power demands, wires expand and sag, which increases the likelihood of arcing or shorting out. Many major blackouts have occurred with the grid running at near capacity during the hottest days of summer when sagging lines arced to trees within transmission line rights-of-way.

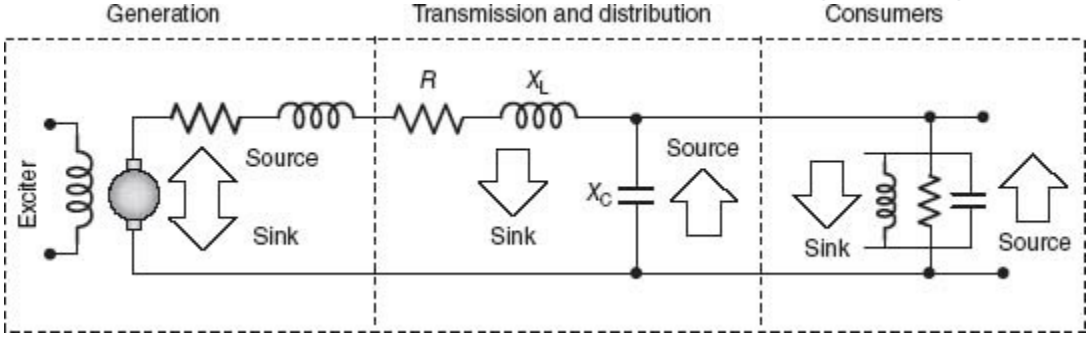
3.7.2 Importance of Reactive Power *Q* in T&D Systems

Back in Chapter 1, we described the delicate balance that must be maintained between the instantaneous power P delivered into the grid by generators and the instantaneous power demanded by loads (including losses in transmission and distribution). Even slight differences between supply and demand affect system frequency, which must be kept within very tight bounds to keep the grid stable. When that concept was introduced, we had not yet mentioned the complications associated with reactive power, Q. For grid stability, both P and Q must be balanced.

Figure 3.31 suggests that sources and sinks for Q occur across the entire grid. Starting with generation, the workhorses are synchronous generators. As just described, a key

advantage of synchronous generators is the ease with which reactive power Q can be controlled. By adjusting its field current, a generator can either deliver Q or absorb Q depending on that moment's reactive power demands from the grid.

FIGURE 3.31 Sources and sinks for reactive power Q occur throughout the grid.



At the opposite end of the figure, loads themselves may serve as sources or sinks of reactive power. However, since a very high fraction of customer loads are driven by the inductive reactance of electric motor windings, customer loads are primarily sinks for Q. That is, they demand power that most often has current lagging behind voltage.

Between power plants and actual customer loads are transmission and distribution (T&D) lines, which have their own impacts on overall P and Q balancing. Transmission and distribution lines, with their inherent resistive, capacitive, and inductive properties, can be either a source or a sink for reactive power.

While line resistance impacts P through I^2R power losses, it has no impact on Q, so let us focus on inductance and capacitance. The inductance of lines is mostly a function of the spacing between conductors and the length of the line. Since X_L increases with line length, that voltage drop can become very significant with long lines. Once a line is in place, however, the inductive reactance is a given quantity that does not vary with current. It causes current to lag behind voltage, so it is a sink for Q.

The reactive capacitance of lines X_C is in parallel with the lines, as shown in Figure 3.31. That means capacitance increases with line length, but reactance ($X_C = 1/\omega C$) decreases. Longer lines, therefore, divert more and more current through X_C, so less current actually makes it to the load. That diverted current, equal to the following, is called the line's *charging current*:

$$\text{Charging current } I_C = \frac{V_{phase}}{X_C} \tag{3.86}$$

Since capacitance is a function of the permittivity of the dielectric as well as the spacing between conductors, coaxial cables, with closely spaced lines separated by high permittivity insulators, have even smaller capacitive reactance per unit of length than those suspended in air from towers. The charging current needs of coaxial cables, often used for underground or undersea applications, can greatly restrict their length.

Now, put the impacts of T&D capacitive and inductive reactances together. While line inductance causes current to lag voltage, line capacitance shifts the phase angle in the other direction. That is, inductance acts as a sink for Q while capacitance acts as a source.

$$\text{Reactive power source: } Q_C = \frac{V^2}{X_C} = \omega C V^2 \quad (3.87)$$

$$\text{Reactive power sink: } Q_L = I^2 X_L = \omega L I^2 \quad (3.88)$$

As Equations 3.87 and 3.88 suggest, this balancing act between transmission line Q_C and Q_L is complicated by the fact that Q_C, which depends on voltage, is fairly constant, while Q_L, which depends on load current, shows a dramatic diurnal variation. Under low current, light-demand conditions, transmission can act as a net source of Q, while during heavy demand periods it becomes a sink. That suggests that synchronous generators during peak demand times often need to operate as sources of reactive power, but during light load conditions, they may need to be adjusted to absorb excessive reactive power.

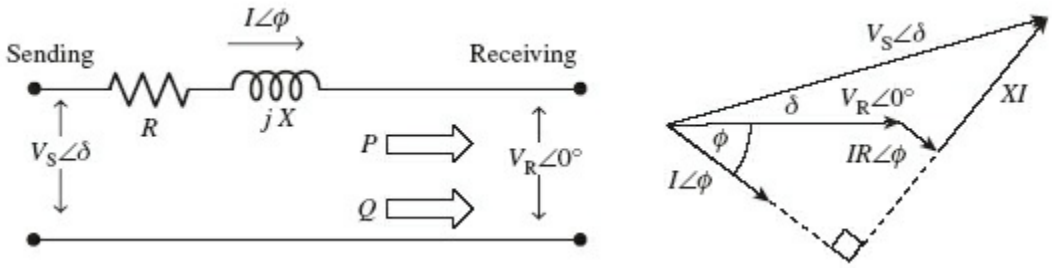
3.7.3 Impacts of P and Q on Line Voltage Drop

The P and Q components of apparent power S not only have to be balanced, but they also are important determinants of voltage along the line. As apparent power (VA) is delivered to loads, the resistive properties of the lines will cause IR voltage drops that vary with demand, but what the implications are for inductive and capacitive properties is less obvious. As it turns out, reactive power Q, sent down transmission lines to loads, usually has more impact on line voltage than does the actual power P.

Note the inductive reactance in Figure 3.31 is in series with the line resistance. Even though no net power is lost in the inductance, its IX_L voltage drop can be significant, especially when lines are heavily loaded. While inductive reactance causes line voltage to drop, those capacitive charging currents mentioned above tend to raise voltage especially along lightly loaded lines with little inductive drop.

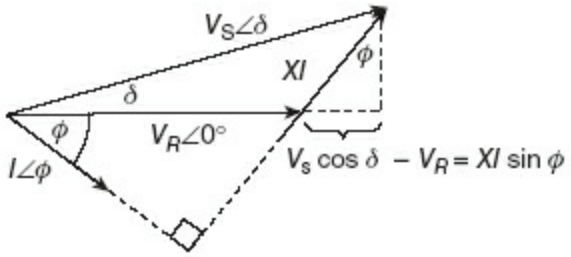
A simple question to ask is what is the magnitude of the voltage change between a source and a load when P and Q are delivered down a transmission line modeled as a series combination of inductance and resistance (Fig. 3.32).

FIGURE 3.32 Voltage drop across a transmission line delivering P and Q.



The vector diagram in Figure 3.32 has been drawn assuming the load is inductive, that is, it absorbs Q. To simplify the analysis of this fairly complex diagram, let us first assume we can separate the impact of reactance X from resistance R. The vector diagram for the circuit with just X now simplifies to that shown in Figure 3.33.

FIGURE 3.33 Voltage drop in the line due to just inductive reactance.



From Figure 3.33, we can write

$$V_S \cos\delta - V_R = XI \sin\phi \tag{3.89}$$

From the definition of Q delivered

$$Q = V_R I \sin\phi \tag{3.90}$$

we can write

$$V_S \cos\delta - V_R = \frac{XQ}{V_R} \tag{3.91}$$

Neglecting R and assuming the angle δ is small enough that cos δ ≈ 1, then we get the following important approximation:

$$\Delta V = V_S - V_R = \frac{XQ}{V_R} \tag{3.92}$$

Equation 3.92 tells us that if we can neglect line resistance, the voltage loss in a transmission or distribution line is directly proportional to the amount of reactive power Q being delivered to the load. It is especially appropriate for high voltage transmission lines for which line reactance X is much greater than line resistance R (see Table 3.5).

TABLE 3.5 Example Transmission Line Parameters

kV	Typical X/R ratio
500	19.8
230	9.6
138	6.2
46	2.7
13.2	1.5
4.16	1.2
Source: Based on Ferris and Infield (2008).	

If we separately address the impact of $V = IR$ losses in the line, we get

$$\Delta V_R = IR = \frac{(V_R I)R}{V_R} = \frac{PR}{V_R} \tag{3.93}$$

Even though the voltage drops through R and X are at different angles, an often-used

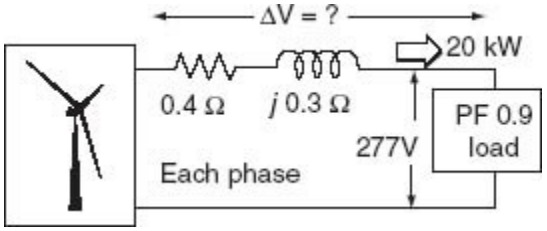
approximation is based on simply adding Equations 3.92 and 3.93 to provide the following estimate of the magnitude of voltage drop in a line delivering P and Q:

$$\Delta V = \frac{PR + QX}{V_R} \tag{3.94}$$

Note that Equation 3.94 was derived assuming the load is absorbing VARs. If the load is a source of Q instead of a sink, then the sign of Q in Equation 3.94 should be negative.

Example 3.14 Estimating Voltage Drop in a Power Line. A small renewable energy system wants to deliver 60 kW of three-phase power at 480 V (277-V phase voltage) to a load with a 0.9 lagging power factor. If each phase has inductive reactance X = 0.3 Ω and resistance R = 0.4 Ω, what voltage needs to be supplied by the source to each phase of the line?

Solution. Each of the three phases delivers P = 20 kW at 277 V, so we can draw the following circuit for each phase of the system:



To find Q, we need the phase angle of the load

$$\phi = \cos^{-1}(\text{PF}) = \cos^{-1}(0.9) = 25.842°$$

$$\text{So} \quad Q = P\tan\phi = 20{,}000\tan(25.842°) = 9686 \text{ VAR}$$

$$\text{Using (3.94)}, \Delta V = \frac{PR + QX}{V_R} = \frac{20{,}000 \times 0.4 + 9686 \times 0.3}{277} = 39.4 \text{ V}$$

So the phase-to-neutral source voltage should be about 277 + 39.4 ≈ 316 V.

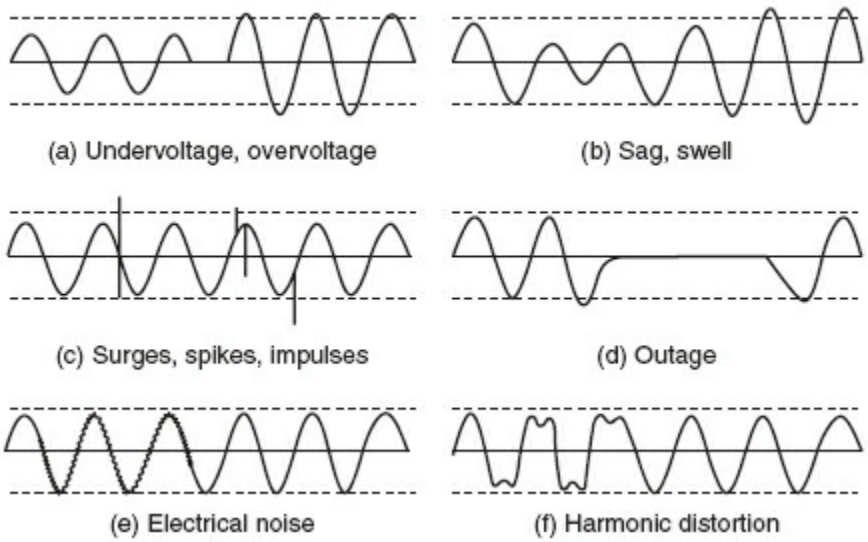
Example 3.14 points out how high Q loads can force the generation source to deliver power at a considerably higher voltage than what the last load along the power line requires. As a result, if there are intermediate loads along the way, which might also want some of that power, they could be exposed to damaging overvoltages. This overvoltage concern is particularly acute for many wind farms located in rural areas that deliver power over long, high impedance, lines. In such circumstances, overvoltage may actually limit the amount of distributed generation that connecting distribution lines can accommodate.

3.8 POWER QUALITY

Utilities have long been concerned with a set of current and voltage irregularities, which are lumped together and referred to as *power quality* issues. Figure 3.34 illustrates some of these irregularities. Voltages that rise above, or fall below, acceptable levels, and do so for more than a few seconds, are referred to as undervoltages and overvoltages. When those

abnormally high or low voltages are momentary occurrences lasting less than a few seconds, such as might be caused by a lightning strike or a car ramming into a power pole, they are called sag and swell incidents. Transient surges or spikes lasting from a few microseconds to milliseconds are often caused by lightning strikes, but can also be caused by the utility switching power on or off somewhere else in the system. Downed power lines can blow fuses or trip breakers resulting in power interruptions or outages.

FIGURE 3.34 Power quality problems.



Power interruptions of even very short duration, sometimes as short as a few cycles, or voltage sags of 30% or so, can bring the assembly line of a factory to a standstill when programmable logic controllers reset themselves and adjustable speed drives on motors malfunction. Restarting such lines can cause delays and wastage of damaged product, with the potential to cost hundreds of thousands of dollars per incident. Outages in digital economy businesses can be even more devastating.

While most of the power quality problems shown in Figure 3.34 are caused by disturbances on the utility side of the meter, two of the problems are caused by the customers themselves. As shown in Figure 3.34e, when circuits are not well grounded, a continuous, jittery voltage "noise" appears on top of the sinusoidal signal. The last problem illustrated in Figure 3.34f is harmonic distortion, which shows up as a continuous distortion of the normal sine wave. Solutions to power quality problems lie on both sides of the meter. Utilities have a number of technologies including filters, high energy surge arrestors, fault current limiters, and dynamic voltage restorers that can be deployed. Customers can invest in uninterruptible power supplies (UPS), voltage regulators, surge suppressors, filters, and various line conditioners. Products can be designed to be more tolerant of irregular power and they can be designed to produce fewer irregularities themselves.

3.8.1 Introduction to Harmonics

Loads that are modeled using our basic components of resistance, inductance, and capacitance, when driven by sinusoidal voltage and current sources, respond with smooth sinusoidal currents and voltages of the same frequency throughout the circuit. As we shall

see, however, nonlinear electronic components such as diodes that allow current to flow in only one direction and transistors that act as on/off switches can create serious waveform distortions called harmonics. Harmonic distortion can cause a surprising number of problems ranging from blown circuit breakers, to computer malfunctions, transformer failures, and even fires caused by overloaded neutral wires in three-phase circuits. Ironically, essentially everything digital contributes to the problem and at the same time it is those digital devices that are the most sensitive to the distortions they create.

To understand harmonic distortion, and its effects, we need to review the somewhat messy mathematics of periodic functions. Any periodic function can be represented by a Fourier series made up of an infinite sum of sines and cosines with frequencies that are multiples of the fundamental (e.g., 60 Hz) frequency. Frequencies that are multiples of the fundamental are called harmonics; for example, the third harmonic for a 60-Hz fundamental is 180 Hz.

The definition of a periodic function is that $f(t) = f(t + T)$, where T is the period. The Fourier series, or harmonic analysis, of any periodic function can be represented by

$$f(t) = \left(\frac{a_0}{2}\right) + a_1 \cos \omega t + a_2 \cos 2\omega t + a_3 \cos 3\omega t + \cdots$$

$$+ b_1 \sin \omega t + b_2 \sin 2\omega t + b_3 \sin 3\omega t + \cdots \tag{3.95}$$

where $\omega = 2\pi f = 2\pi/T$. The coefficients can be found from

$$a_n = \frac{2}{T} \int_0^T f(t) \cos n\omega t \, dt, \quad n = 0, 1, 2 \ldots \tag{3.96}$$

and

$$b_n = \frac{2}{T} \int_0^T f(t) \sin n\omega t \, dt, \quad n = 1, 2, 3 \ldots \tag{3.97}$$

Under special circumstances, the series in Equation 3.95 simplifies. For example, when there is no DC component to the waveform (average value = 0), the first term, a_0, drops out:

$$a_0 = 0: \quad \text{when average value, DC} = 0 \tag{3.98}$$

For functions with symmetry about the y-axis, the series contains only cosine terms. That is,

$$\text{cosines only:} \quad \text{when } f(t) = f(-t) \tag{3.99}$$

For the series to contain only sine terms, it must satisfy the relation

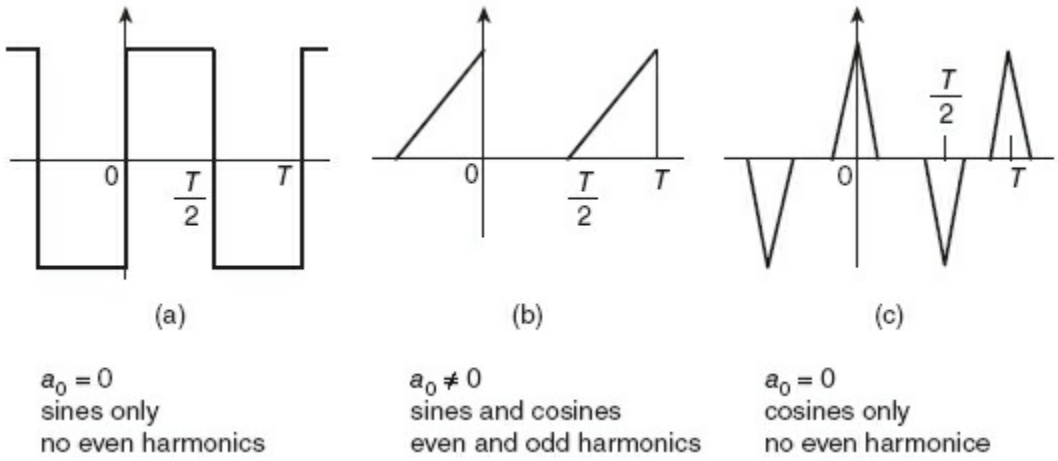
$$\text{sines only:} \quad \text{when } f(t) = -f(-t) \tag{3.100}$$

Finally, when a function has what is called *half-wave symmetry,* it contains no even harmonics. That is,

$$\text{no even harmonics:} \quad \text{when } f\left(t+\frac{T}{2}\right) = -f(t) \tag{3.101}$$

Examples of these properties are illustrated in Figure 3.35.

FIGURE 3.35 Examples of periodic functions, with indications of special properties of their Fourier series representations.



Example 3.15 Harmonic Analysis of a Square Wave. Find the Fourier series equivalent of the square wave in Figure 3.35a, assuming it has a peak value of 1 V.

Solution. We know by inspection, using Equations 3.91–3.98 that the series will have only sines, with no even harmonics. Therefore, all we need are the even coefficients b_n from Equation 3.97

$$b_n = \frac{2}{T}\int_0^T f(t)\sin n\omega t\, dt = \frac{2}{T}\left[\int_0^{T/2} 1\cdot \sin n\omega t\, dt + \int_{T/2}^{T}(-1)\sin n\omega t\, dt\right]$$

Recall the integral of a sine is the cosine with a sign change, so

$$b_n = \frac{2}{n\omega T}\left\{(-1)\left[\cos n\omega\frac{T}{2} - \cos n\omega\cdot 0\right] + \cos n\omega T - \cos n\omega\frac{T}{2}\right\}$$

Substituting $\omega = 2\pi f = 2\pi/T$ gives

$$b_n = \frac{1}{n\pi}(-2\cos n\pi + 1 + \cos 2n\pi)$$

Since this is half-wave symmetric, there are no even harmonics; that is, n is always an odd number. For odd values of n,

$$\cos n\pi = \cos\pi = -1 \quad \text{and} \quad \cos 2n\pi = \cos 0 = 1$$

That makes for a nice, simple solution:

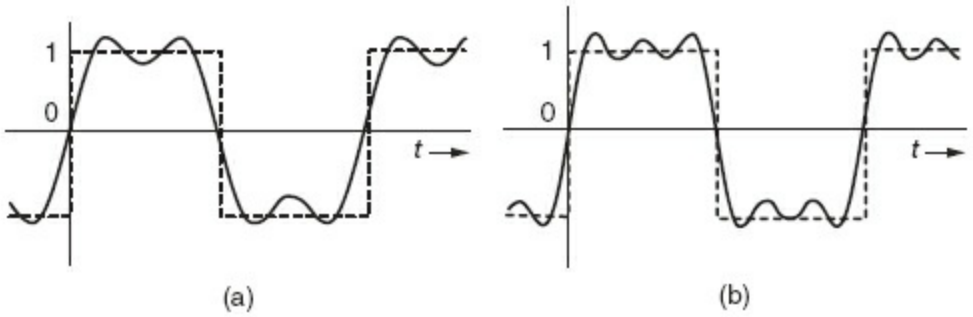
$$b_n = \frac{4}{n\pi} \quad \text{where } n = 1, 3, 5, 7\ldots$$

So the series representation of the square wave with an amplitude of 1 is

$$f(t) = \frac{4}{\pi}\left(\sin\omega t + \frac{1}{3}\sin 3\omega t + \frac{1}{5}\sin 5\omega t + \cdots\right)$$

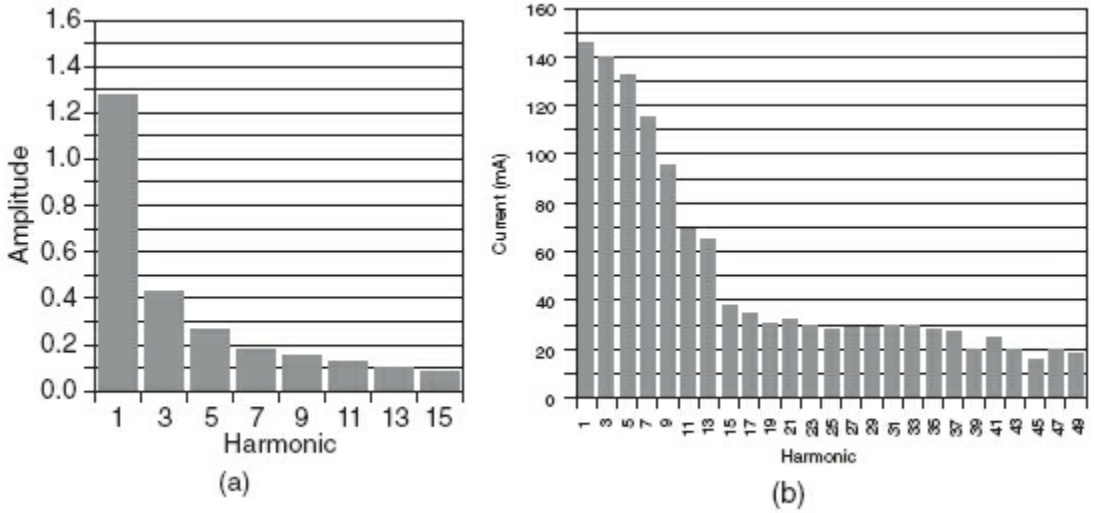
To show how quickly the Fourier series for the square wave begins to approximate reality, Figure 3.36 shows the sum of the first two terms of the series and the sum of the first three terms, along with the square wave that it is approximating. Adding more terms, of course, will make the approximation more and more accurate.

FIGURE 3.36 Showing the sum of the first two terms (a) and first three terms (b) of the Fourier series for a square wave, along with the square wave that it is approximating.



The first few terms in the harmonic analysis of the square wave derived in Example 3.15 along with an actual harmonic spectrum for an early electronically ballasted compact fluorescent lamp (CFL) are shown in Figure 3.37. Note how far the harmonics extend for the CFL.

FIGURE 3.37 Showing harmonic spectrum for (a) the square wave analyzed in Example 3.15 and (b) an early electronically ballasted 18-W compact fluorescent lamp.



3.8.2 Total Harmonic Distortion

While the Fourier series description of the harmonics in a periodic waveform contains all of the original information in the waveform, it is relatively awkward to work with. There are several simpler quantitative measures that can be developed that are more easily used. For example, suppose we start with a series representation of a current waveform that is symmetric about the *y*-axis:

$$i = \sqrt{2}(I_1 \cos \omega t + I_2 \cos 2\omega t + I_3 \cos 3\omega t + \cdots)$$

(3.102)

where I_n is the rms value of the current in the nth harmonic. The rms value of current is therefore

(3.103)

$$I_{\text{rms}} = \sqrt{(i^2)_{\text{avg}}} = \sqrt{\left[\sqrt{2}(I_1 \cos \omega t + I_2 \cos 2\omega t + I_3 \cos 3\omega t + \cdots)\right]^2_{\text{avg}}}$$

After a fair amount of algebraic manipulation of Equation 3.103, the final result is simple and intuitive:

$$I_{\text{rms}} = \sqrt{I_1^2 + I_2^2 + I_3^2 \ldots}$$

(3.104)

So, the rms value of current when there are harmonics is just the square root of the sum of the squares of the individual rms values for each frequency. While this was presented here for just a sum of cosines, it holds for the general case in which the sum involves cosines and sines.

In the United States, the most commonly used measure of distortion is called the *total harmonic distortion* (THD), which is defined as

$$\text{THD} = \frac{\sqrt{I_2^2 + I_3^2 + I_4^2 \ldots}}{I_1}$$

(3.105)

Note that since THD is a ratio, it does not matter whether the currents in Equation 3.105 are expressed as peak values of rms values. When they are rms values, we can recognize THD to be the ratio of the rms current in all frequencies except the fundamental, divided by the rms current in the fundamental. When no harmonics are present, the THD is zero. When there are harmonics, there is no particular limit to THD and it is often above 100%.

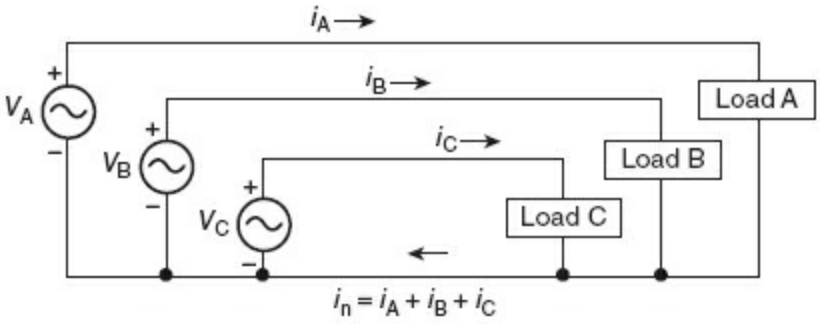
3.8.3 Harmonics and Overloaded Neutrals

We know from Section 3.5.1 that current in the neutral line of a balanced, three-phase, four-wire, wye-connected system (Fig. 3.38), with no harmonics, is zero.

(3.106)

$$i_n = i_A + i_B + i_C = \sqrt{2} I_{\text{phase}} [\cos \omega t + \cos(\omega t + 120°) + \cos(\omega t - 120°)] = 0$$

FIGURE 3.38 Showing the neutral line current in a four-wire, three-phase, wye-connected circuit.



The question now is what happens when there are harmonics in the phase currents? As we shall see, even if the loads are balanced, harmonics have the potential to cause unexpectedly high, and potentially dangerous, currents to flow in the neutral line.

Suppose each phase carries exactly the same current (shifted by 120° of course), but now there are third harmonics involved. That is,

$$\begin{aligned} i_A &= \sqrt{2}\,[I_1 \cos \omega t + I_3 \cos 3\omega t] \\ i_B &= \sqrt{2}\,\{I_1(\cos \omega t + 120°) + I_3 \cos [3(\omega t + 120°)]\} \\ i_C &= \sqrt{2}\,\{I_1(\cos \omega t - 120°) + I_3 \cos [3(\omega t - 120°)]\} \end{aligned} \tag{3.107}$$

Now, since the currents in the fundamental frequency add to zero, the sum of the three phase currents in Equation 3.107 becomes

$$i_n = \sqrt{2}\,[I_3 \cos 3\omega t + I_3 \cos (3\omega t + 360°) + I_3 \cos (3\omega t - 360°)] \tag{3.108}$$

But since $\cos(3\omega t \pm 360°) = \cos 3\omega t$, and the fundamental currents have already dropped out, the total current in the neutral line simplifies to

$$i_n = 3\sqrt{2} I_3 \cos 3\omega t \tag{3.109}$$

In terms of rms values,

$$I_n = 3I_3 \tag{3.110}$$

That is, the rms current in the neutral line is three times the rms current in each line's third harmonic. There is considerable likelihood, therefore, that harmonics can actually cause the neutral to carry even more current than the phase conductors.

The same argument about harmonics adding in the neutral applies to all of the harmonic numbers that are multiples of 3 (since $3 \times n \times 120° = n360° = 0°$). That is, the 3rd, 6th, 9th, 12th… harmonics all add to the neutral current in an amount equal to three times their phase-current harmonics. For currents that show half-wave symmetry, there are no even harmonics, so the only harmonics that appear on the neutral line for balanced loads of this sort will be 3rd, 9th, 15th, 21st, … etc. These harmonics, divisible by 3, are called *triplen* harmonics.

Note, by the way, that harmonics not divisible by 3 cancel out in the neutral wire in just the same way that the fundamental cancels.

Example 3.16 Neutral Line Current. A four-wire, wye-connected balanced load has phase currents described by the following harmonics:

Harmonic	f (Hz)	rms Current (A)
1	60	100
3	180	50
5	300	20
7	420	10
9	540	8
11	660	4
13	780	2

a. Find the THD in the phase current.

b. Find the rms current flowing in the neutral wire and compare it to the rms phase currents.

Solution

a. Using Equation 3.105, we can easily find the THD in the phase currents:

$$\text{THD} = \frac{\sqrt{50^2 + 20^2 + 10^2 + 8^2 + 4^2 + 2^2}}{100} = 0.555 = 55.5\%$$

b. Only the harmonics divisible by 3 will contribute to neutral line current, so that means all we need to consider are the third and ninth harmonics.

Assuming the fundamental is 60 Hz, the harmonics contribute

Third harmonic: $3 \times 50 = 150$ A at 180 Hz

Ninth harmonic: $3 \times 8 = 24$ A at 540 Hz.

The rms current is the square root of the sum of the squares of the harmonic currents, so the neutral wire will carry

$$I_n = \sqrt{150^2 + 24^2} = 152 \text{ A}$$

The rms current in each phase will be

$$I_{\text{phase}} = \sqrt{100^2 + 50^2 + 20^2 + 10^2 + 8^2 + 4^2 + 2^2} = 114 \text{ A}$$

Note in the above example that the neutral line, rather than having zero current (as it would be without harmonics), actually carries one-third more current than the phase lines! Before we had so many electronic loads in buildings that create most of our harmonics, building codes in the United States allowed smaller neutral wires than the phase conductors, which led to the potential for dangerous overheating in older buildings. It has only been since the mid-1980s that the building code has required the neutral wire to be a full-size conductor.

3.8.4 Harmonics in Transformers

Recall from Chapter 2 that cyclic magnetization of ferromagnetic materials causes magnetic domains to flip back-and-forth. With each cycle, there are hysteresis losses in the magnetic material, which heat the core at a rate that is proportional to frequency.

$$\text{Power loss due to hysteresis} = k_1 f \tag{3.111}$$

Also recall that sinusoidal variations in flux within a magnetic core induce circulating currents within the core material itself. To help minimize these currents, silicon alloyed steel cores or powdered ceramics, called ferrites, are used to increase the resistance to current formation. Also, by laminating the core, currents have to flow in smaller spaces, which also increases the path resistance. The important point is that those currents are proportional to the rate of change of flux and therefore the heating caused by those i^2R losses are proportional to frequency squared:

$$\text{Power losses due to eddy currents} = k_2 f^2 \tag{3.112}$$

Since harmonic currents in the windings of a transformer can have rather high frequencies and since core losses depend on frequency—especially eddy-current losses, which are dependent on the square of frequency—harmonics can cause transformers to overheat. Even if the overheating does not immediately burn out the transformer, the durability of transformer-winding insulation is very dependent on temperature so harmonics can shorten transformer lifetime.

Concern over harmonic distortion—especially when voltage distortion from one facility (e.g., a building) can affect loads of other customers on the same feeder—has led to the establishment of a set of THD limits set forth by the Institute for Electrical and Electronic Engineers (IEEE) known as the IEEE Standard 519-1992.

3.9 POWER ELECTRONICS

Earlier, we described the epic struggle between Edison and Westinghouse in the early days of electric power. Edison lost that battle because his DC voltages could not easily be bumped up or down to take advantage of the benefits of high voltage transmission of power. Westinghouse, the proponent of AC, had transformers to perform those tasks so his power could easily be transported long distances from power plants to customers with minimal losses along the way. These days, we have solid-state electronic devices that allow us to go from AC to DC, from DC to AC, and from one DC voltage to another DC voltage. We will look at these *power converters*, along with other power conditioning transformations, in this section.

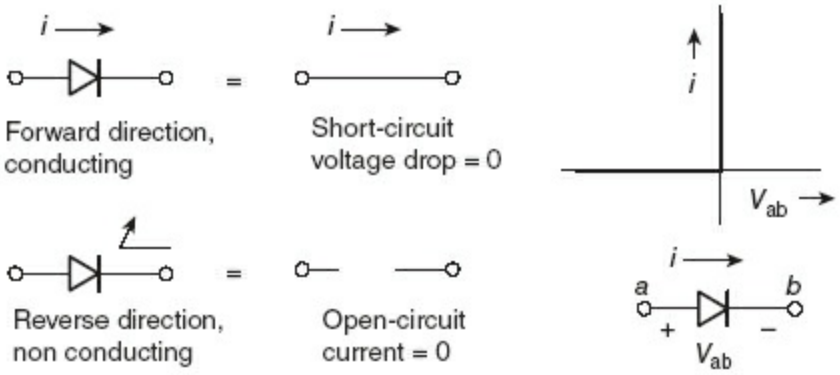
3.9.1 AC-to-DC Conversion

A device that converts AC into DC is called a *rectifier*. When a rectifier is equipped with a *filter* to help smooth the output, the combination of rectifier and filter is usually referred to as a *DC power supply*. In the opposite direction, a device that converts DC into AC is called an *inverter*.

The key component in rectifying an AC voltage into DC is a *diode*. A diode is basically a one-way street for current: It allows current to flow relatively unimpeded in one direction, but it blocks current flow in the opposite direction. In the forward direction, an ideal diode looks just like a zero-resistance, short circuit so that the voltage at both diode terminals is

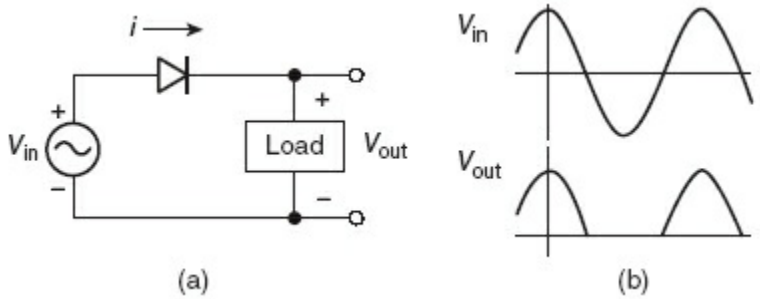
the same. In the reverse direction, no current flows and the ideal diode acts like an open circuit. Figure 3.39 summarizes the characteristics of an ideal diode, including its current versus voltage relationship. Real diodes, as opposed to the ideal ones shown in the figure, will be described much more carefully later in the book when photovoltaics are presented.

FIGURE 3.39 Characteristics of an ideal diode. In the forward direction, it acts like a short circuit; in the reverse direction, it appears to be an open circuit.



The simplest rectifier is comprised of just a single diode placed between the AC source voltage and the load as shown in Figure 3.40. On the positive stroke of the input voltage, the diode is forward biased, current flows, and the full input voltage appears across the load. When the input voltage goes negative, however, current wants to go in the opposite direction, but it is prevented from doing so by the diode. No current flows, so there is no voltage drop across the load, leading to the output voltage waveform shown in Figure 3.40b.

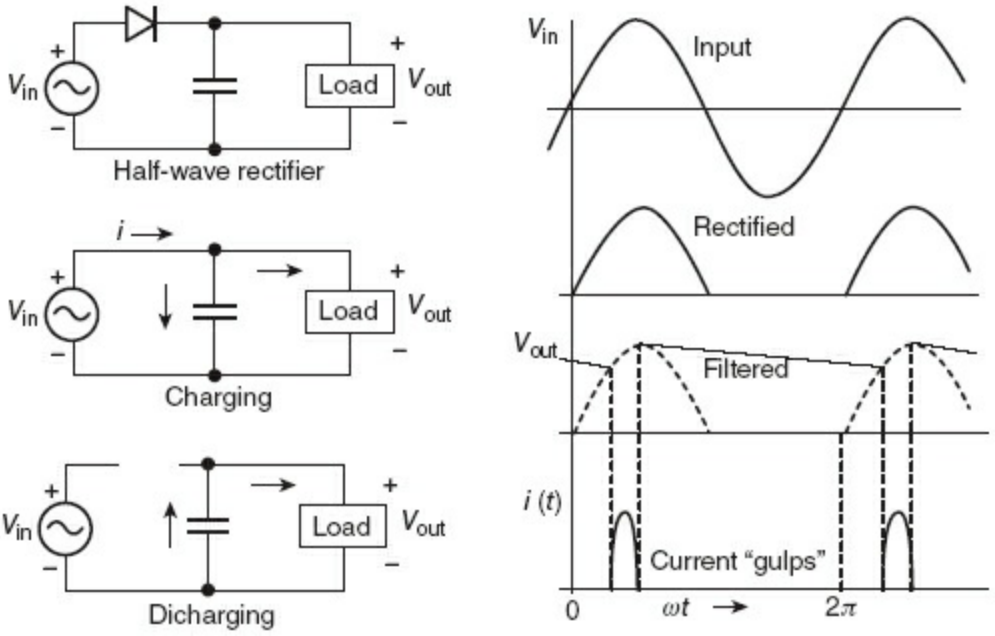
FIGURE 3.40 A half-wave rectifier: (a) The circuit. (b) The input and output voltages.



While the output voltage waveform in Figure 3.40b does not look very much like DC, it does have an average value that is not zero. The DC value of a waveform is defined to be the average value, so the waveform does have a DC component, but it also has a bunch of wiggles, called *ripple*, in addition to its DC level. The purpose of a filter is to smooth out those ripples. The simplest filter is just a big capacitor attached to the output, as shown in Figure 3.41. During the last portion of the upswing of input voltage, current flows through the diode to the load and capacitor and charges the capacitor. Once the input voltage starts to drop, the diode cuts off and the capacitor then discharges sending current through the load. The resulting output voltage is greatly smoothed compared to the rectifier without the capacitor. Note how current flows from the input source only for a short while in each cycle and does so very close to the times when the input voltage peaks.

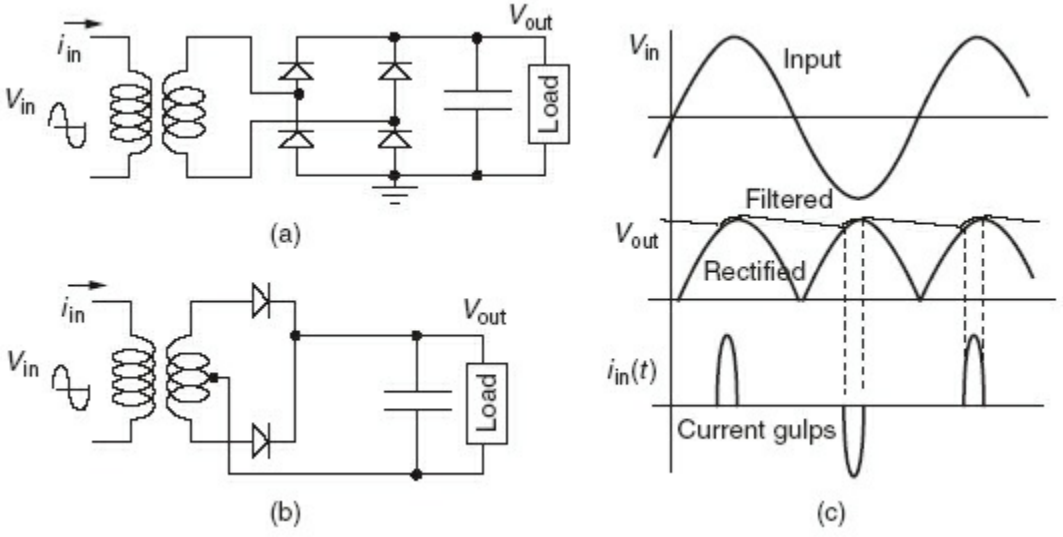
FIGURE 3.41 A half-wave rectifier with capacitor filter showing the gulps of current that

occur during the brief periods when the capacitor is charging.



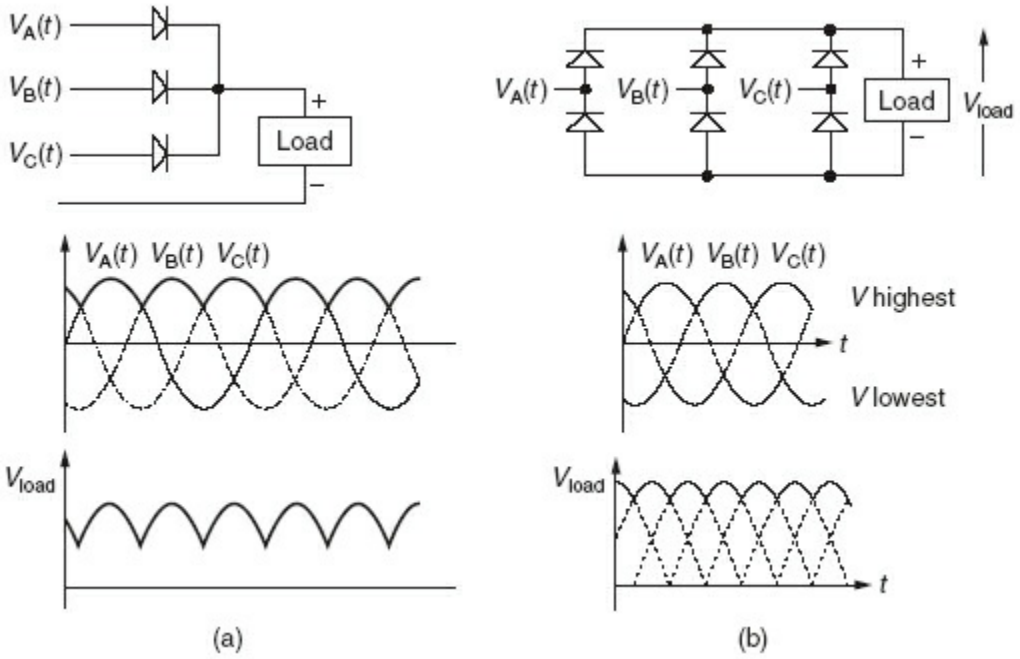
The ripple on the output voltage can be further reduced by using a full-wave rectifier instead of the half-wave version described above. Two versions of power supplies incorporating full-wave rectifiers are shown in Figure 3.42: one is shown using a center-tapped transformer with just two diodes; the other uses a four-diode bridge rectifier. The transformers drop the voltage to an appropriate level. The capacitors smooth the full-wave-rectified output for the load. Both of these full-wave rectifiers produce voltage waveforms with two positive humps per cycle as shown. This means that the capacitor filter is recharged twice per cycle instead of once, which smoothes the output voltage considerably. Note that there are now two gulps of current from the source: one in the positive direction and one in the negative direction. These current gulps are highly nonlinear, which lead to the extensive harmonics shown in Figure 3.37b.

FIGURE 3.42 Full-wave rectifiers with capacitor filters showing gulps of current drawn from the supply. (a) A four-diode, bridge rectifier. (b) A two-diode, center-tapped transformer rectifier.



Three-phase circuits also use the basic diode rectification idea to produce a DC output. Figure 3.43a shows a three-phase, half-wave rectifier. At any instant the phase with the highest voltage will forward bias its diode, transferring the input voltage to the output. The result is an output voltage that is considerably smoother than a single-phase, full-wave rectifier.

FIGURE 3.43 (a) Three-phase, half-wave rectifier. (b) Three-phase, full-wave rectifier.



The three-phase, full-wave rectifier shown in Figure 3.43b is better still. The voltage at any instant that reaches the output is the difference between the highest of the three input voltages and the lowest of the three-phase voltages. It therefore has a higher average voltage than the three-phase, half-wave rectifier, and it reaches its peak values with twice the frequency, resulting in relatively low ripple even without a filter. For very smooth DC outputs, an inductor (sometimes called a "choke") is put in series with the load to act as a smoothing filter.

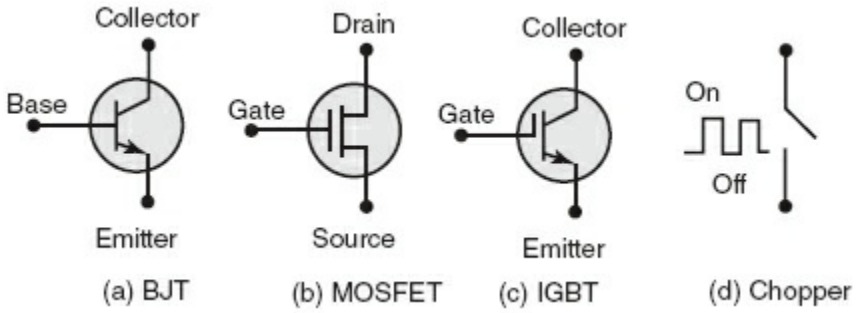
3.9.2 DC-to-DC Conversions

The transformer has been the traditional technology used to convert from one voltage to another, but they only work with AC signals. With the development of power transistors, it has become relatively easy now to perform the equivalent voltage changes in DC.

For our purposes, transistors are just three-terminal devices that can act as electrically controllable on/off switches. When the switch is closed, the device offers very little resistance to current flow between two of its terminals. Current flow stops when the switch is opened. The opening and closing of the switch is controlled by the third terminal. The switch itself is usually a bipolar junction transistor (BJT), a metal-oxide-semiconductor field-effect transistor (MOSFET), or a combination of the two called an insulated-gate bipolar transistor (IGBT). The rising star of these is the IGBT, which has many desirable features including simple voltage-controlled switching, high power and current capabilities, and fast switching times. Figure 3.44 shows some of the symbols for these devices,

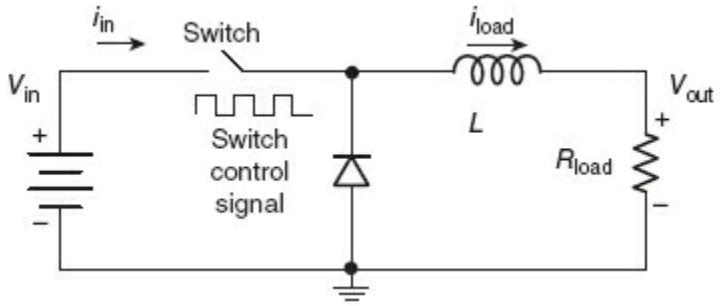
including one that represents a simple switch, often called a *chopper*.

FIGURE 3.44 Symbols for various transistor switches.



Actual DC-to-DC voltage conversion circuits are quite complex (see for example, *Power Electronics*, M. H. Rashid, 2004), but we can get a basic understanding of their operation by studying briefly the simple *buck converter* depicted in Figure 3.45.

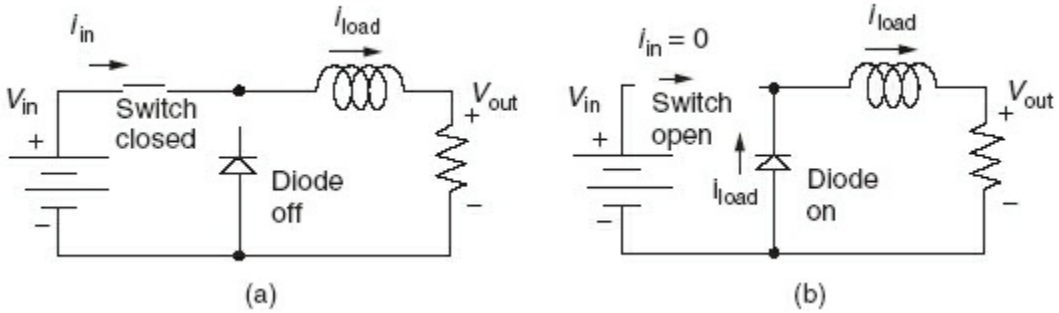
FIGURE 3.45 A DC-to-DC, step-down, voltage converter—sometimes called a *buck converter*.



In Figure 3.45 the rectified, incoming (high) voltage is represented by an idealized DC source of voltage V_{in}. There is also a chopper switch that allows that DC input voltage to be either (a) connected across the diode so that it can deliver current to the inductor and load or (b) disconnected from the circuit entirely. The switch itself is a transistor with its on/off control accomplished with associated digital circuitry not shown here. That voltage control is a signal that we can think of as having a value of either 0 or 1. When the control signal is 1, the switch is closed (short circuit); when it is 0, the switch is open.

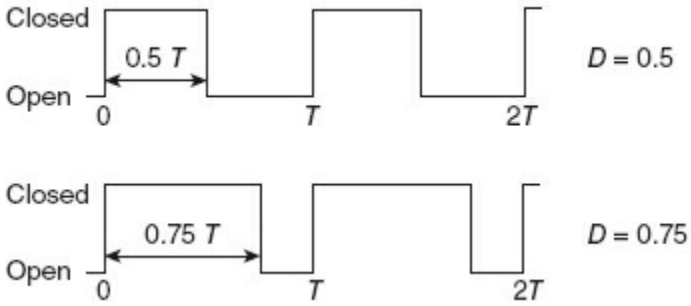
The basic idea behind the buck converter is that by rapidly opening and closing the switch, short bursts of current are allowed to flow through the inductor to the load (here represented by a resistor). With the switch closed, the diode is reverse-biased (open circuit) and current flows directly from the source to the load (Fig. 3.46a). When the switch is opened, as in Figure 3.36b, the inductor keeps the current flowing through the load resistor and diode (remember, inductors act as "current momentum" devices—we cannot instantaneously start or stop current through one). If the switch is flipped on and off with high enough frequency, the current to the load does not have much of a chance to build up or decay; that is, it is fairly constant, producing a DC voltage on the output.

FIGURE 3.46 The buck converter with (a) switch closed and (b) switch open.



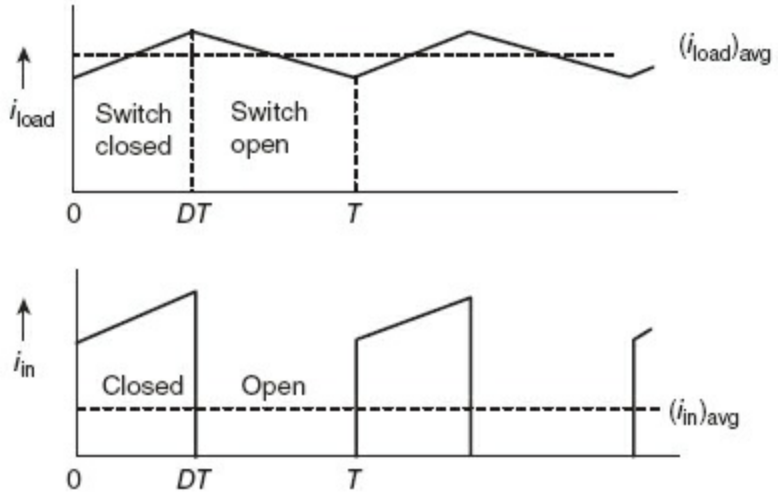
The remaining feature to describe in the buck converter is the relationship between the DC input voltage V_{in}, and the DC output voltage, V_{out}. It turns out that the relationship is a simple function of the *duty cycle* of the switch. The duty cycle, D, is defined to be the fraction of the time that the control voltage is a "1" and the switch is closed. Figure 3.47 illustrates the duty cycle concept.

FIGURE 3.47 The fraction of the time that the switch in a DC-to-DC buck converter is closed is called the duty cycle, D. Two examples are shown.



We can now sketch the current through the load and the current from the source, as has been done in Figure 3.48. When the switch is closed, the two currents are equal and rising. When the switch is open, the input current immediately drops to zero and the load current begins to sag. If the switching rate is fast enough, and they are designed that way, the rising and falling of these currents is essentially linear so they appear as straight lines in the figure. With T representing the period of the switching circuit, then within each cycle the switch is closed DT seconds.

FIGURE 3.48 When the switch is closed, the input and load currents are equal and rising; when it is open, the input drops to zero and the load current sags.



We are now ready to determine the relationship between input voltage and output voltage in the switching circuit. Start by using Figure 3.48 to determine the relationship between average input current and average output current. While the switch is closed, the areas under the input current and load current curves are equal:

$$(i_{in})_{avg} \cdot T = (i_{load})_{avg} \cdot DT \quad \text{so} \quad (i_{in})_{avg} = D \cdot (i_{load})_{avg} \tag{3.113}$$

We will use an energy argument to determine the voltage relationship. Begin by writing the average power delivered to the circuit by the input voltage source:

$$(P_{in})_{avg} = (V_{in} \cdot i_{in})_{avg} = V_{in}(i_{in})_{avg} = V_{in} \cdot D \cdot (i_{load})_{avg} \tag{3.114}$$

The average power into the circuit equals the average power dissipated in the switch, diode, inductor, and load. If the diode and switch are ideal components, they dissipate no energy at all. Also, we know the average power dissipated by an ideal inductor as it passes through its operating cycle is also zero. That means the average input power equals the average power dissipated by the load. The power dissipated by the load is given by

$$(P_{load})_{avg} = (V_{out} \cdot i_{load})_{avg} = (V_{out})_{avg} \cdot (i_{load})_{avg} \tag{3.115}$$

Equating (3.114) and (3.115) gives

$$V_{in} \cdot D \cdot (i_{load})_{avg} = (V_{out})_{avg} \cdot (i_{load})_{avg} \tag{3.116}$$

which results in the relationship we have been looking for:

$$(V_{out})_{avg} = D \cdot V_{in} \tag{3.117}$$

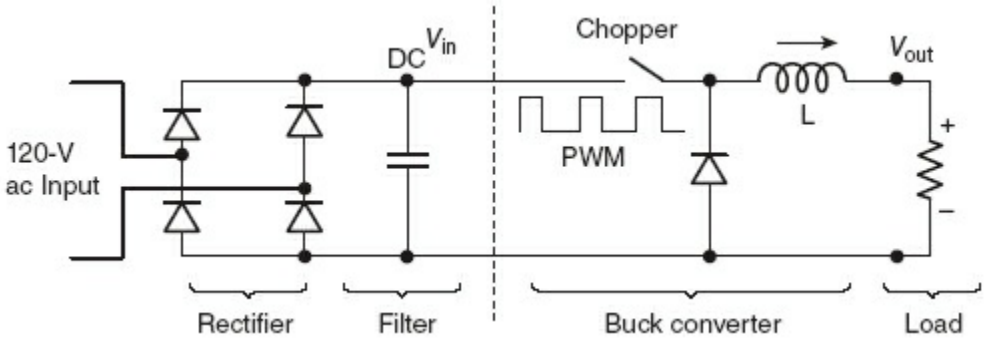
So, the only parameter that determines the DC-to-DC, buck converter step-down voltage is the duty cycle of the switch.

As long as the switching cycle is fast enough, the load will be supplied with a very precisely controlled DC voltage. The buck converter is essentially, then, a DC step-down transformer. Since the output voltage is determined by the width of the "on" pulses, this control approach is referred to as *pulse-width modulation* (PWM) and the circuits

themselves are referred to as *switching* or *switch-mode* converters.

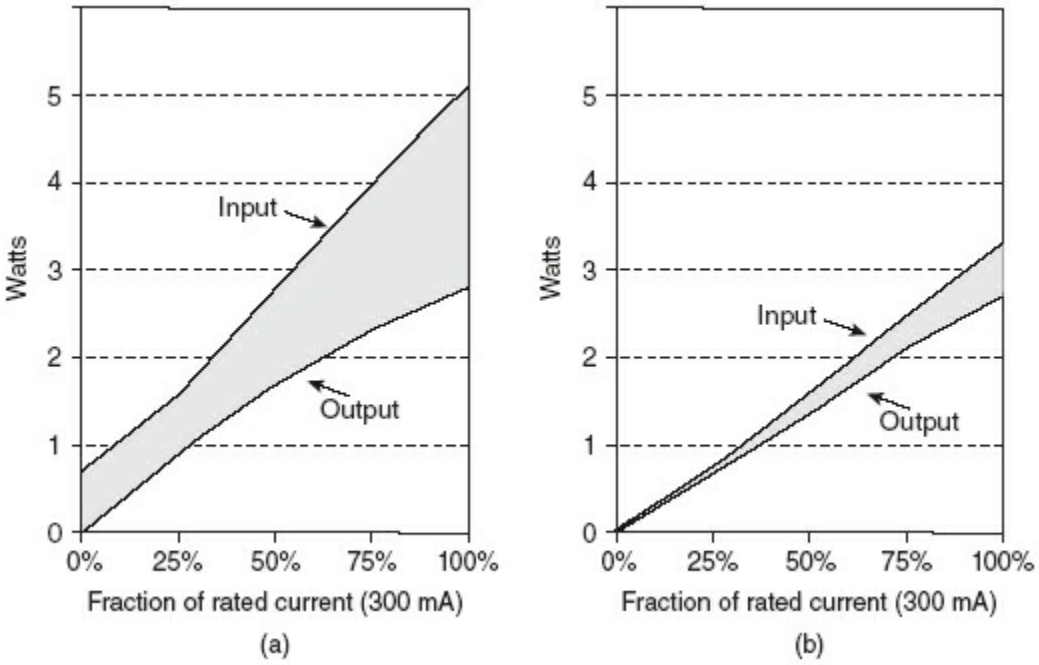
One of the most important uses of buck converters is for power supplies that convert typical 120-V AC voltage into the low voltage DC needed in virtually every electronic product. As shown back in Figure 3.42, traditional power supplies (sometimes referred to as "linear" systems) rely on a conventional transformer to drop the voltage before rectification and filtering. Switch-mode converters eliminate that transformer by rectifying the incoming power at its original voltage and then dropping that voltage with a buck converter (Fig. 3.49).

FIGURE 3.49 A (simplified) switch-mode power supply using a buck converter.



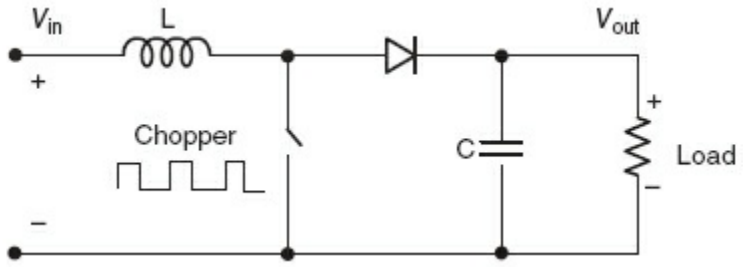
Linear power supplies typically operate in the 50–60% range of energy efficiency, while switching power supplies are over 80% efficient. Figure 3.50 provides an example comparing the efficiencies of a 9-V linear power supply for a cordless phone versus one incorporating a switch-mode supply. The switching supply is far more efficient throughout the range of currents drawn. Also note that the linear supply continues to consume power even when the device is delivering no power at all to the load. The wasted energy that occurs when appliances are apparently turned off, but continue to consume power, or when the appliance is not performing its primary function, is referred to as standby power (or sometimes power *vampires*). A typical US household has roughly 20 such appliances that together consume about 500 kWh/yr in standby mode. That 5–8% of all residential electricity costs about $4 billion per year (Meier, 2010).

FIGURE 3.50 Power consumed by 9-V linear (a) and switch-mode power supplies (b) for a cordless phone. From Calwell and Reeder (2002).



While a buck converter steps DC voltages down, the analogous circuit shown in Figure 3.51 is a DC-to-DC *boost converter* that steps up voltages. When the switch is closed, current flows from the source through the inductor and the switch, building up current in the inductor. When the switch is opened, the inductor provides a shot of current through the diode to the capacitor and load. Because of the inductor's current momentum property, it can send that current through the diode even if the voltage across the capacitor is higher than the input voltage. The charged capacitor helps hold the voltage across the load when the chopper switch closes again.

FIGURE 3.51 A boost converter steps up DC voltages.



An analysis similar to the one shown above for the buck converter results in the following relationship between the input and output voltages as a function of the duty cycle D of the chopper.

$$(V_{out})_{avg} = \frac{1}{1 - D} \cdot V_{in} \tag{3.118}$$

From Equation 3.118, we see that the output voltage can be stepped up by varying the duty cycle. The minimum voltage, equal to the input voltage, results when the switch is left open ($D = 0$). As the duty cycle increases, the switch stays closed longer, the current in the inductor builds up, and the output voltage increases with each burst of this increased

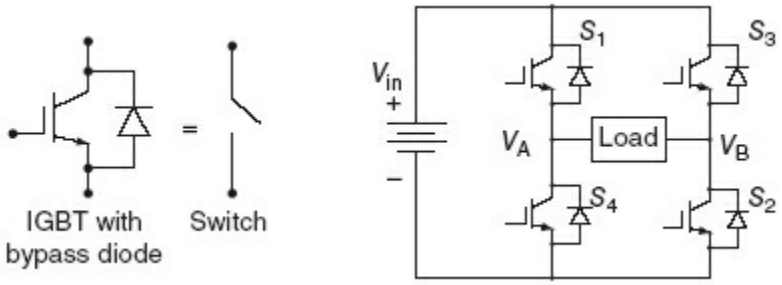
current. However, as Equation 3.118 suggests, leaving the switch closed ($D = 1$) is not feasible since the input source cannot provide infinite current.

3.9.3 DC-to-AC Inverters

DC-to-AC inverters have improved over time as more and more powerful transistor switches have been developed along with more sophisticated control systems. They range from very basic, low power, single-phase inverters that yield a simple square wave, to sophisticated utility-scale devices that produce sinusoidal outputs with full power factor control.

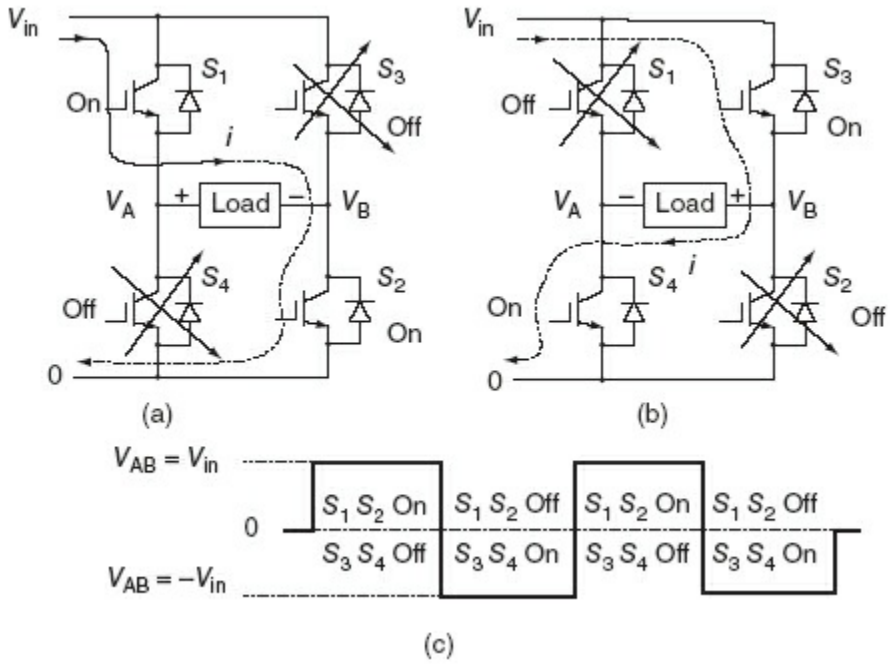
Figure 3.52 shows a basic inverter circuit consisting of four, controllable, transistorized switches. In this case, they are shown as IGBTs with added parallel diodes to provide a bypass path for transient currents. These switches are voltage-controlled, so the inverter is often called a *voltage-source converter* (VSC).

FIGURE 3.52 A simple single-phase DC-to-AC inverter.



One pair of switches, S_1 and S_2, work together; that is, both are closed (on) or open (off) at the same time. Similarly S_3 and S_4 is another pair with opposite schedules. As shown in Figure 3.53, when S_1 and S_2 are on (and S_3 and S_4 are off), the full input voltage V_{in} appears across the load. When the pairs of switches are inverted, the output voltage V_{AB} becomes V_{in}. That is, a square wave with amplitude V_{in} is created. This is not only a very crude approximation to a desired smooth sinusoidal output, but as Example 3.15 illustrated it has rather terrible harmonics.

FIGURE 3.53 Showing current flow when (a) S_1 and S_2 are on and S_3 and S_4 are off, (b) after switching on/off signals and (c) the resulting square-wave output.



A widely adopted variation on the simple four-switch inverter uses pulse-width modulation to control the switches, which greatly improves the output waveform. The idea of PWM is to combine a sinusoidal modulating wave of whatever output frequency is needed with a much higher-frequency carrier wave (Fig. 3.54). Those waveforms are fed into a comparator that puts out a signal to turn on S_1 and S_2 as long as the modulating wave is greater than the carrier. A digital inverter flips that 1 or 0 to automatically turn off S_3 and S_4 when the other two switches are turned on.

FIGURE 3.54 Switch driver for pulse-width modulation (PWM). Based on Jenkins et al. *Distributed Generation* (2010).

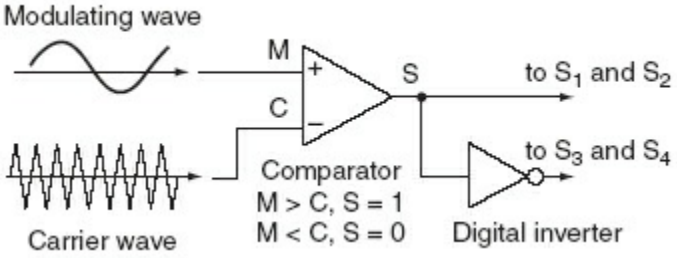
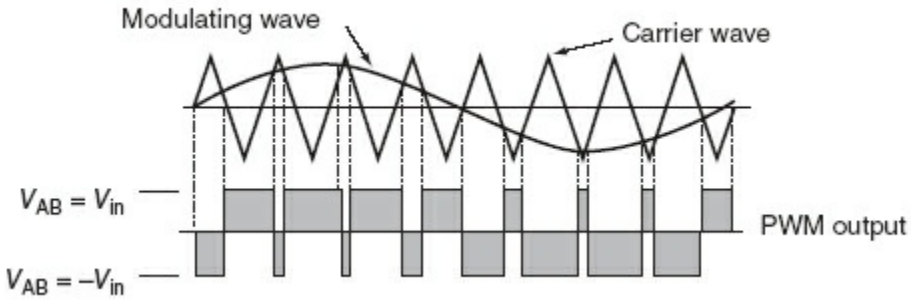


Figure 3.55 shows the modulating wave and carrier wave together along with the PWM output that results. As can be seen, the output V_{AB} is either equal to plus-or-minus the DC value of V_{in}. A Fourier analysis of the PWM rectangles would show a strong fundamental at the modulating frequency, a series of very small harmonics, and another sizeable harmonic at the carrier frequency (see for example, P. Klein, *Elements of Power Electronics*, 1997). Since the carrier frequency is quite high, relatively speaking, it is easy to filter out that harmonic. Either the inherent inductance of the output load or some purposeful inductance added to the output can smooth the waveform yielding an almost pure sinusoid whose frequency, amplitude, and power factor are easily controllable.

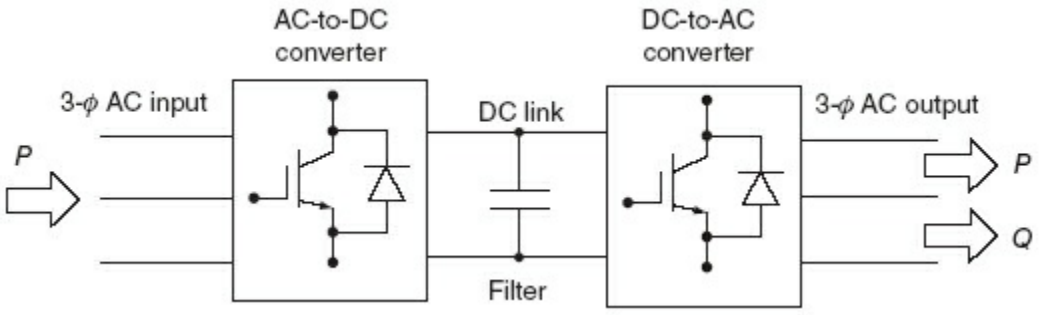
FIGURE 3.55 The raw PWM output consists of the sequence of voltage rectangles.



3.10 BACK-TO-BACK VOLTAGE-SOURCE CONVERTER

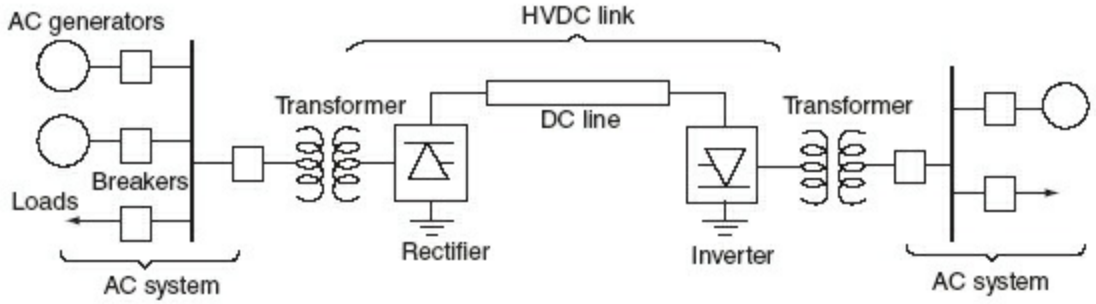
There are many important circumstances when an AC source with its own frequency and voltage needs to be matched to a load with different frequency, phase angle, and voltage requirements. For example, the only way to control the rotational speed of an induction motor is to vary the frequency of its incoming power—something that is easy to do with a back-to-back voltage-source converter (VSC). As shown in Figure 3.56, such a converter has an AC-to-DC input stage, followed by a DC link that may include some filtering, and ending with a DC-to-AC inverter. As suggested in the figure, with careful design the output voltage, power factor, and frequency can be controlled. That is, it can act very much like a synchronous inverter capable of delivering both real power P and reactive power Q to its loads.

FIGURE 3.56 Simplified schematic of a back-to-back voltage converter delivering both real power P and reactive power Q.



One of the most important uses of back-to-back voltage converters is to connect different power grids together using high voltage direct current (HVDC) lines. An HVDC link requires converters at both ends of the DC transmission line, each capable of acting either as a rectifier or as an inverter to allow power flow in either direction. A simple one-line drawing of an HVDC link is shown in Figure 3.57. HVDC lines offer the most economic form of transmission over very long distances—that is, distances beyond about 500 mi or so. For these longer distances, the extra costs of converters at each end can be more than offset by the reduction in transmission line and tower costs.

FIGURE 3.57 A one-line diagram of a DC link between AC systems. The inverter and rectifier can switch roles to allow bidirectional power flow.



REFERENCES

Bosela, T.R. (1997). *Introduction to Electrical Power System Technology*, Prentice Hall, Upper Saddle River, NJ.

Calwell, C., and T Reeder (2002). *Power Supplies: A Hidden Opportunity for Energy Savings*, Ecos Consulting, May.

Ferris, L., and D. Infield (2008). *Renewable Energy in Power Systems.* Wiley, Hoboken, NJ.

Jenkins, N., Ekanayake, J.B., and G. Strbac (2010). *Distributed Generation*, The Institute of Engineering and Technology Press, Stevenage, UK.

Meier, A. (2002). *Reducing Standby Power: A Research Report*, Lawrence Berkeley National Labs, April.

PROBLEMS

3.1 Inexpensive inverters often used a "modified" square wave approximation to a sinusoid. For the following voltage waveform, what would be the rms value of voltage?

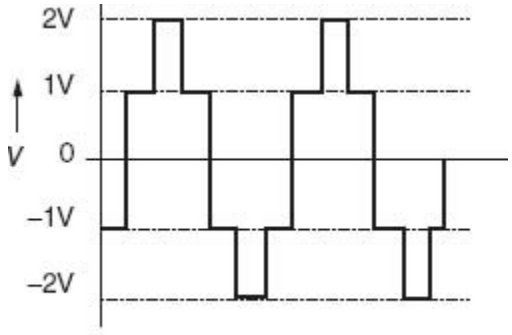


FIGURE P3.1

3.2 Find the rms value of voltage for the sawtooth waveform shown below.

Recall from calculus how you find the average value of a periodic function:

$$\bar{f}(t) = \frac{1}{T}\int_0^T f(t)\mathrm{d}t$$

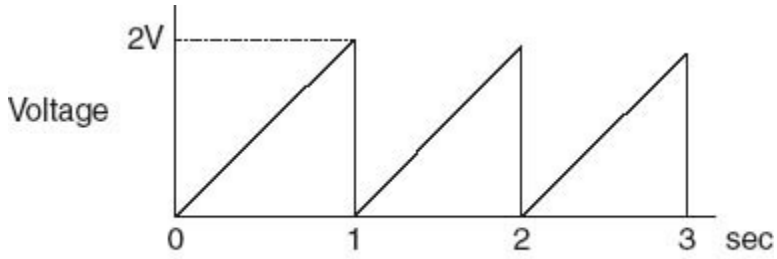


FIGURE P3.2

3.3 A load connected to a 120-V AC source draws "gulps" of current (e.g., Fig. 3.42) approximated by narrow rectangular pulses of amplitude 10 A as shown below. The connecting wire between source and load has a resistance of 1 Ω.

Sketch the resulting voltage waveform V_{OUT} across the load, labeling any significant values.

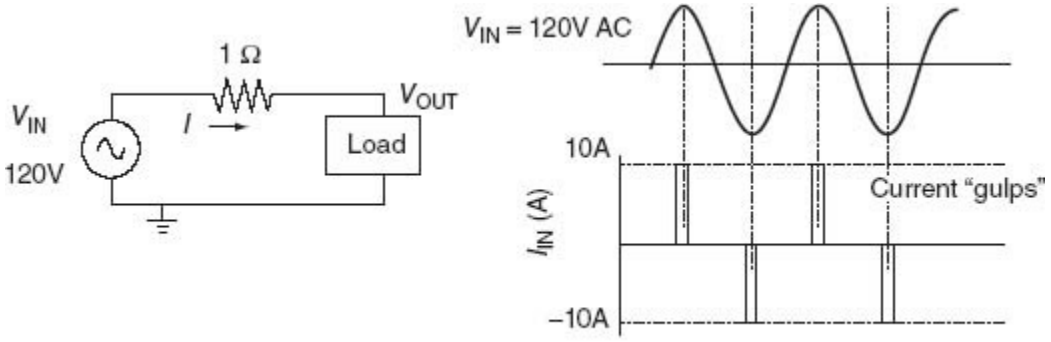


FIGURE P3.3

3.4 Currents can flow through transmission lines even if the rms voltage at each end of the line is the same. Consider the following simple circuit consisting of two 120-V sources with differing phase angles connected by a line with 10-Ω resistance. Describe the current using phasor notation $\boldsymbol{I} = I\angle\phi$ and as a function of time $i = \sqrt{2}I\cos(\omega t + \phi)$. What is the rms value of current?

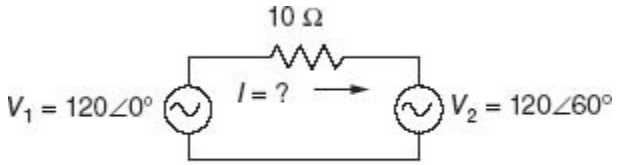


FIGURE P3.4

3.5 Consider the following 120-V, 60-Hz circuit,

a. What is the reactance and the impedance of the inductor?

b. Express the impedance of the combination of R and L in both polar $Z = Z\angle\phi$ and rectangular $Z = a + jb$ form.

c. What is the current expressed as a phasor and as a function of time.

d. What is the power factor?

e. What is the output voltage expressed as a phasor and as a function of time.

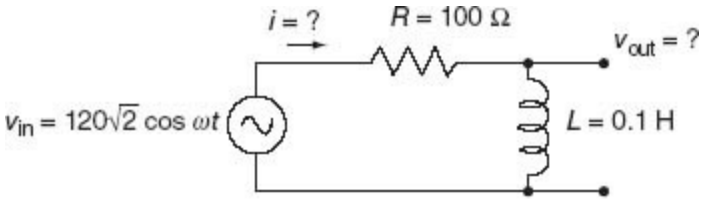


FIGURE P3.5

3.6 A 120-V, 60-Hz source supplies current to a 1-μF capacitor, a 7.036-H inductor, and a 1-Ω resistor, all wired in parallel.

a. Find the reactances (Ω) for the capacitor and for the inductor.

b. Find the rms current through each of the three load components.

c. Express the impedance of each in polar form $Z = Z\angle\phi$ and rectangular form Z = a + jb.

d. Write the currents through each of the three components in the form of phasors, $I = I_{\text{rms}}\angle\phi$ and in complex notation I = a + jb.

e. Find the total current delivered by the source, expressed in phasor I_{Tot} notation. What is the rms value of total current?

f. What is the power factor?

g. Write the total current in the time domain $i = \sqrt{2}I\cos(\omega t + \phi)$.

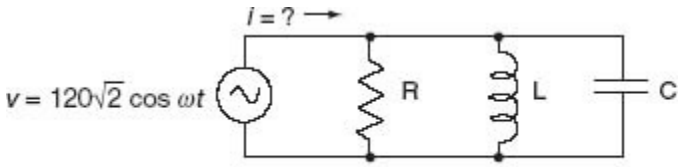


FIGURE P3.6

3.7 Repeat Problem (3.3) but this time have the 120-V, 60-Hz source supply current to a 30-μF capacitor, a 0.2-H inductor, and a 100-Ω resistor, all wired in parallel.

a. Find the reactances (Ω) for the capacitor and for the inductor.

b. Find the rms current through each of the three load components.

c. Express the impedance of each in polar form $Z = Z\angle\phi$ and rectangular form Z = a + jb.

d. Write the currents through each of the three components in the form of phasors, $I = I_{\text{rms}}\angle\phi$ and in complex notation I = a + jb.

e. Find the total current delivered by the source, expressed in phasor I_{Tot} notation. What is the rms value of total current?

f. What is the power factor?

g. Write the total current in the time domain $i = \sqrt{2}I\cos(\omega t + \phi)$

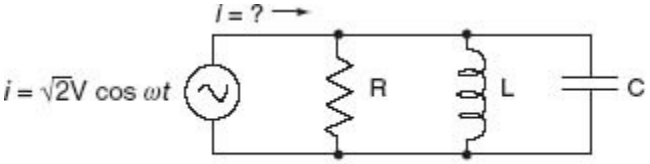


FIGURE P3.7

3.8 A 277-V supply delivers 50 A to a single-phase electric motor. The motor windings

cause the current to lag behind the voltage by 30°. Find the power factor and draw the power triangle showing real power P(kW), reactive power Q(kVAR), and the apparent power S(kVA).

3.9 A 120-V AC supply delivers power to a load modeled as a 5-Ω resistance in series with a 3-Ω inductive reactance. Find the active, reactive, and apparent power consumption of the load along with its power factor. Draw its power triangle.

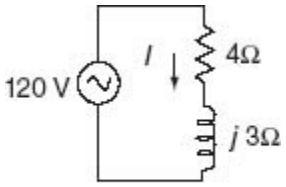


FIGURE P3.9

3.10 A transformer rated at 1000 kVA is operating near capacity as it supplies a load that draws 900 kVA with a power factor of 0.70.

a. How many kW of real power is being delivered to the load?

b. How much additional load (in kW of real power) can be added before the transformer reaches its full rated kVA (assume the power factor remains 0.70).

c. How much additional power (above the amount in a) can the load draw from this transformer without exceeding its 1000 kVA rating if the power factor is corrected to 1.0?

3.11 Suppose a motor with power factor 0.5 draws 3600 W of real power at 240 V. It is connected to a transformer located 100 ft away.

a. Use Table 2.3 to pick the minimum wire gage that could be used to connect the transformer to the motor.

b. What power loss will there be in those wires?

c. Draw a power triangle for the wire and motor combination using the real power of motor plus wires and reactive power of the motor itself.

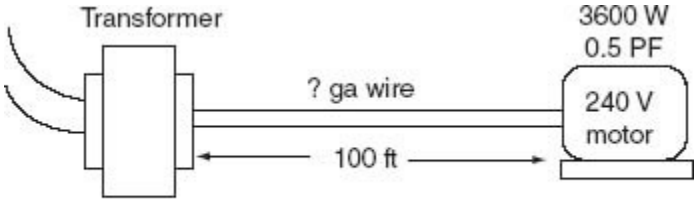


FIGURE P3.11

3.12 Suppose a utility charges its large industrial customers $0.08/kWh for energy plus $10/mo per peak kVA (demand charge). Peak kVA means the highest level drawn by the load during the month. If a customer uses an average of 750 kVA during a 720-h month, with a 1000-kVA peak, what would be their monthly bill if their power factor (PF) is 0.8? How much money could be saved each month if their real power is the same but their PF is corrected to 1.0?

3.13 Consider a synchronous generator driven by a microturbine that delivers power to a strong, balanced, three-phase, wye-connected, 208-V grid (that 208 V is the line voltage). As shown, we will analyze it as if it consists of three separate single-phase circuits.

a. What is the phase voltage ($V_{PHASE,\ GRID}$) for the grid?

b. The following vector (phasor) diagram for one of the phases shows the way the generator is currently operating. Its field current is creating an emf (E_{GEN}) of 130 V at a power angle δ = 6.9°. The current I_L delivered to the grid has a phase angle of 30° lagging with respect to the grid. The inductive reactance of the generator armature (stator) windings is X_L = 0.5 Ω, which means the voltage drop across that inductance is $V_L = I_L X_L = 0.5\ I_L$. And, of course, current through the inductance lags the voltage across the inductance by 90° (ELI the ICE man).

Under the above conditions, find the following:

b1. The current I_L through the inductive reactance (this means you need to solve the above triangle).

b2. The real power P (W) delivered to the grid by this phase.

b3. The reactive power Q (VAR) delivered to the grid by this phase.

b4. Find the total real power P, reactive power Q, and apparent power S, delivered by the all three phases of the three-phase generator.

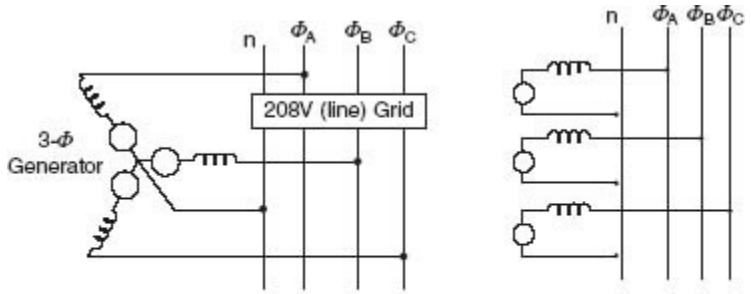


FIGURE P3.13a

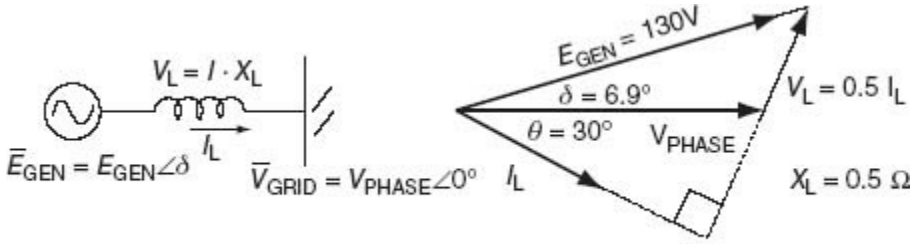


FIGURE P3.13b

3.14 A small wind turbine is trying to deliver 30 kW of real power through a 480-V (277-V phase voltage), three-phase power line to a load having a 0.95 lagging power factor. The power line phase has an impedance of 0.05 + j 0.1 Ω. What voltage does the turbine have to provide at its end of the power line?

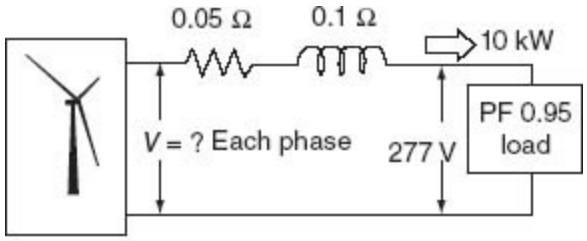


FIGURE P3.14

3.15 The current waveform for a half-wave rectifier with a capacitor filter looks something like the following:

Since this is a periodic function, it can be represented by a Fourier series:

$$i(t) = \left(\frac{a_0}{2}\right) + \sum_{n=1}^{\infty} a_n \cos(n\omega t) + \sum_{m=1}^{\infty} b_m \sin(m\omega t)$$

Which of the following assertions are true and which are false?

a. The value of a_0 is zero.

b. There are no sine terms in the series.

c. There are no cosine terms in the series.

d. There are no even harmonics in the series.

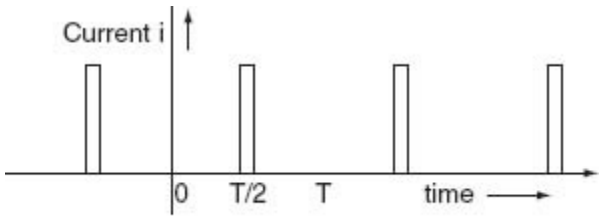


FIGURE P3.15

3.16 Consider a balanced three-phase system with phase currents shown below.

$$i_a = 5\sqrt{2}\cos\omega t + 4\sqrt{2}\cos(3\omega t)$$
$$i_b = 5\sqrt{2}\cos(\omega t + 120°) + 4\sqrt{2}\cos[3(\omega t + 120°)]$$
$$i_c = 5\sqrt{2}\cos(\omega t - 120°) + 4\sqrt{2}\cos[3(\omega t - 120°)]$$

a. What is the rms value of the current in each phase?

b. What is the THD in each of the phase currents?

c. What is the current in the neutral as a function of time $i_n(t)$?

d. What is the rms value of the current in the neutral line? Compare it to the individual phase currents.

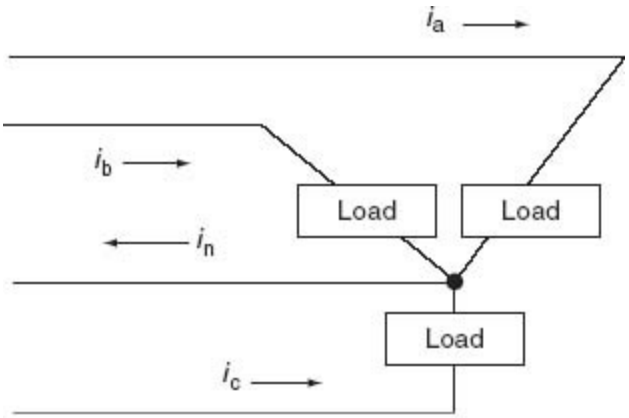


FIGURE P3.16

3.17 Consider a wye-connected balanced three-phase load with each phase having the currents and harmonics shown below.

Harmonic	rms Current (A)
1	9.2
3	8.1
5	6.4
7	4.3
9	2.7
11	2

a. Find the rms current in each phase.

b. Find the THD in each phase.

c. Find the rms current in the neutral line.

d. Make a graph of the phase current versus time.

$$i = \sqrt{2}\,(I_1 \cos 377t + I_3 \cos 3 \cdot 377t + \cdots I_{11} \cos 11 \cdot 377t)$$

CHAPTER 4

THE SOLAR RESOURCE

The source of energy that keeps our planet at just the right temperature, powers our hydrologic cycle, creates our wind and weather, and provides our food and fiber is a relatively insignificant yellow dwarf star some 93 million miles away. Powering our sun are thermonuclear reactions in which hydrogen atoms fuse together to form helium. In the process, about 4 billion kilograms of mass per second are converted into energy as described by Einstein's famous relationship $E = mc^2$. This fusion has been continuing reliably for the past 4 or 5 billion years and is expected to continue for another 4 or 5 billion years.

To design and analyze solar systems that will convert some of that sunlight into electricity, we need to work our way through a fairly straightforward, though complicated looking, set of equations to predict where the sun is in the sky at any time of day as well as its intensity.

4.1 THE SOLAR SPECTRUM

Every object emits radiant energy in an amount that is a function of its temperature. The usual way to describe how much radiation an object emits is to compare it to a theoretical abstraction called a *blackbody*. A blackbody is defined to be a perfect emitter as well as a perfect absorber. As a perfect emitter, it radiates more energy per unit of surface area than any real object at the same temperature. As a perfect absorber, it absorbs all radiation that impinges upon it; that is, none is reflected and none is transmitted through it. The wavelengths emitted by a blackbody depend on its temperature as described by *Planck's law*:

$$E_\lambda = \frac{3.74 \times 10^8}{\lambda^5 \left[\exp\left(\frac{14{,}400}{\lambda T}\right) - 1\right]} \tag{4.1}$$

where E_λ is the emissive power per unit area of a blackbody (W/m^2/μm), T is the absolute temperature of the body (K), and λ is the wavelength (μm).

The area under Planck's curve between any two wavelengths is the power emitted between those wavelengths, so the total area under the curve is the total radiant power emitted. That total is conveniently expressed by the *Stefan–Boltzmann law of radiation*:

$$E = \sigma A T^4 \tag{4.2}$$

where E is the total blackbody emission rate (W), σ is the Stefan–Boltzmann constant (5.67

$\times 10^{-8}$ W/m^2/K), T is the absolute temperature of the blackbody (K), and A is the surface area of the blackbody (m^2).

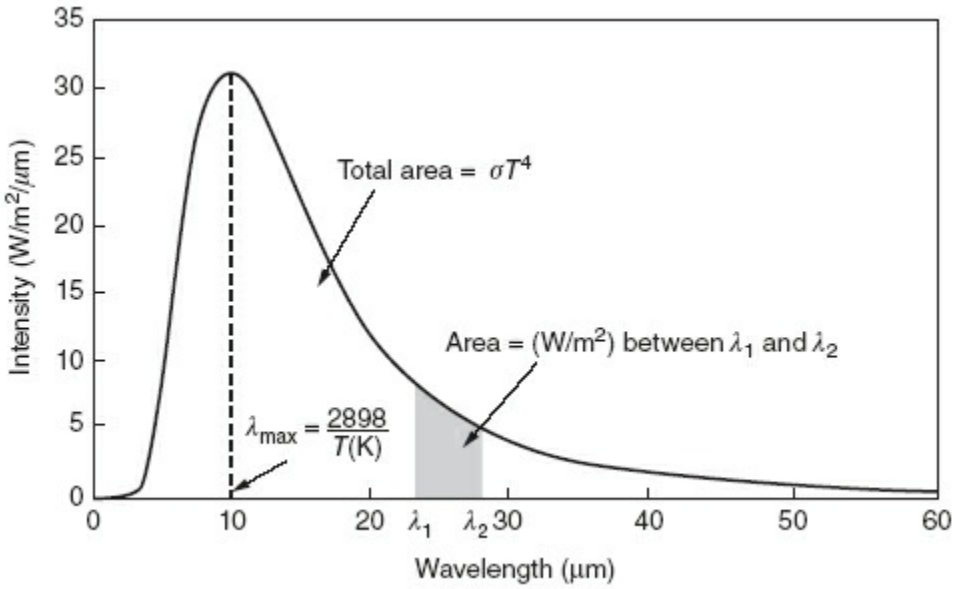
Another convenient feature of the blackbody radiation curve is given by *Wien's displacement rule*, which tells us the wavelength at which the spectrum reaches its maximum point:

$$\lambda_{max}(\mu m) = \frac{2898}{T(K)} \quad (4.3)$$

where the wavelength is in microns (μm) and the temperature is in kelvins (K).

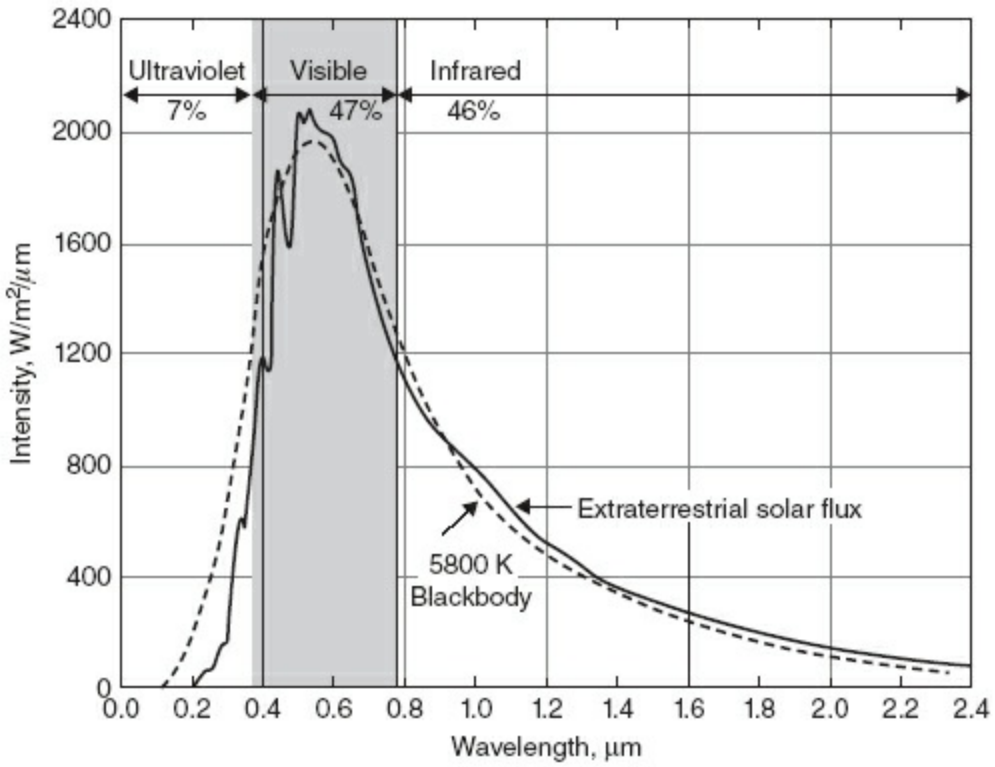
An example of these key attributes of blackbody radiation is shown in Figure 4.1.

FIGURE 4.1 The spectral emissive power of the earth modeled as a 288 K blackbody.



While the interior of the sun is estimated to have a temperature of around 15 million kelvins, the radiation that emanates from the sun's surface has a spectral distribution that closely matches that predicted by Planck's law for a 5800 K blackbody. Figure 4.2 shows the close match between the actual solar spectrum and that of a 5800 K blackbody. The total area under the blackbody curve has been scaled to equal 1.37 kW/m^2, which is the solar insolation (from incident solar radiation) just outside the earth's atmosphere, also described as irradiation. Also shown are the areas under the actual solar spectrum that corresponds to wavelengths within the ultraviolet (7%), visible (47%), and infrared (46%) portions of the spectrum. The visible spectrum, which lies between the ultraviolet (UV) and infrared (IR), ranges from 0.38 μm (violet) to 0.78 μm (red).

FIGURE 4.2 The extraterrestrial solar spectrum compared with a 5800 K blackbody.



Example 4.1 The Earth's Spectrum. Consider the earth to be a blackbody with average surface temperature 15°C and area equal to 5.1×10^{14} m^2. Find the rate at which energy is radiated by the earth and the wavelength at which maximum power is radiated. Compare this peak wavelength with that for a 5800 K blackbody (the sun).

Solution. Using Equation 4.2, the earth radiates

$$E = \sigma A T^4 = (5.67 \times 10^{-8}\text{W/m}^2/\text{K}^4) \times (5.1 \times 10^{14}\text{m}^2) \times (15 + 273\ \text{K})^4$$

$$= 2.0 \times 10^{17}\ \text{W}$$

The wavelength at which the maximum power is emitted is given by Equation 4.3:

$$\lambda_{\max}(\text{earth}) = \frac{2898}{T(\text{K})} = \frac{2898}{288} = 10.1\ \mu\text{m}$$

For the 5800 K sun,

$$\lambda_{\max}(\text{sun}) = \frac{2898}{5800} = 0.5\ \mu\text{m}.$$

It is worth noting that earth's atmosphere reacts very differently to the much longer wavelengths emitted by the earth's surface (Fig. 4.1) than it does to the short wavelengths arriving from the sun (Fig. 4.2). This difference is the fundamental factor responsible for the greenhouse effect.

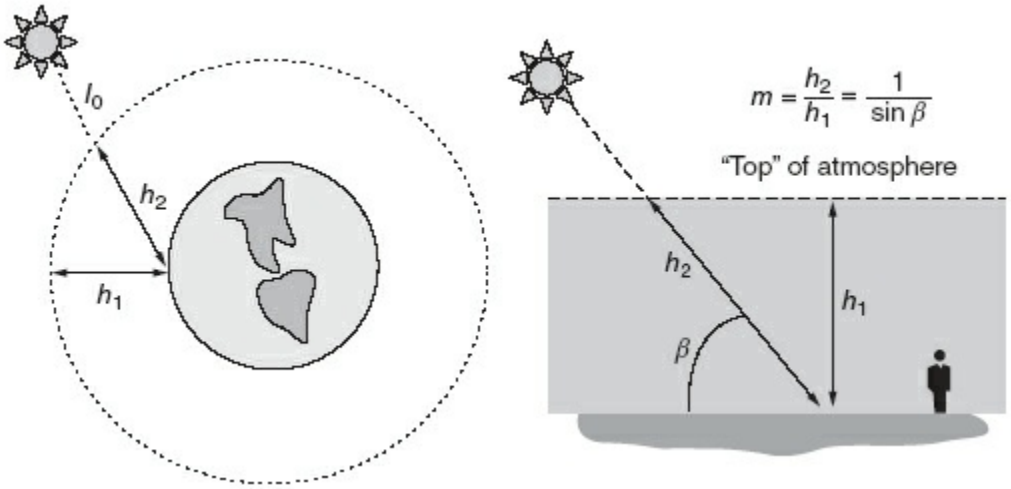
As solar radiation makes its way toward the earth's surface, some is absorbed by various constituents in the atmosphere giving the terrestrial spectrum an irregular, bumpy shape. The terrestrial spectrum also depends on how much atmosphere the radiation has to pass through to reach the surface. The length of the path h_2 taken by the sun's rays as they pass

through the atmosphere, divided by the minimum possible path length h_1, which occurs when the sun is directly overhead, is called the *air mass ratio*, *m*. As shown in Figure 4.3, under the simple assumption of a flat earth (valid for altitude angles greater than about 10°), the air mass ratio can be expressed as

$$\text{Air mass ratio } m = \frac{h_2}{h_1} = \frac{1}{\sin \beta} \tag{4.4}$$

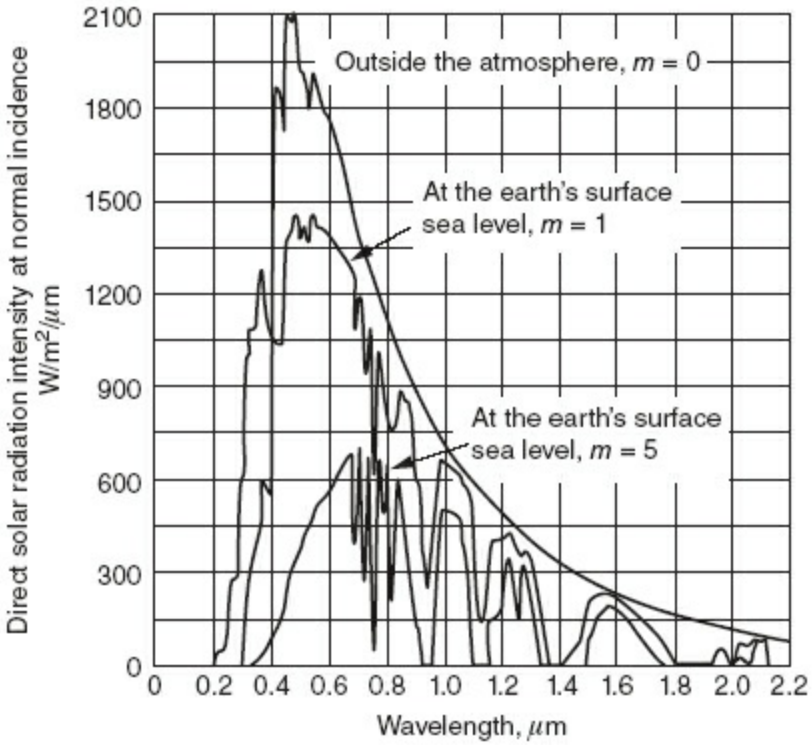
where h_1 is the path length through the atmosphere with the sun directly overhead, h_2 is the path length through the atmosphere to reach a spot on the surface, and β is the altitude angle of the sun (see Fig. 4.3). Thus, an air mass ratio of 1 (designated "AM1") means the sun is directly overhead. By convention, AM0 means no atmosphere; that is, it is the extraterrestrial (ET) solar spectrum. Often, an air mass ratio of 1.5 is assumed for an average solar spectrum at the earth's surface. With AM1.5, 2% of the incoming solar energy is in the UV portion of the spectrum, 54% is in the visible, and 44% is in the IR.

FIGURE 4.3 The air mass ratio *m* is a measure of the amount of atmosphere the sun's rays must pass through to reach the earth's surface. For the sun directly overhead, *m* = 1.



The impact of the atmosphere on incoming solar radiation for various air mass ratios is shown in Figure 4.4. As sunlight passes through more atmosphere, less energy arrives at the earth's surface and the spectrum shifts toward longer wavelengths.

FIGURE 4.4 Solar spectrum for extraterrestrial (*m* = 0), for sun directly overhead (*m* = 1), and at the surface with the sun low in the sky, *m* = 5. From Kuen et al. (1998), based on *Trans. ASHRAE*, vol. 64 (1958) p. 50.



4.2 THE EARTH'S ORBIT

The earth revolves around the sun in an elliptical orbit, making one revolution every 365.25 days. The eccentricity of the ellipse is small and the orbit is, in fact, quite nearly circular. The point at which the earth is nearest the sun, the perihelion, occurs on January 2, at which point it is a little over 147 million kilometers away. At the other extreme, the aphelion, which occurs on July 3, the earth is about 152 million kilometers from the sun. This variation in distance is described by the following relationship

$$d = 1.5 \times 10^8 \left\{1 + 0.017 \sin\left[\frac{360\,(n - 93)}{365}\right]\right\} \text{ km} \tag{4.5}$$

where n is the *day number*, with January 1 as day 1 and December 31 being day number 365. Table 4.1 provides a convenient list of day numbers for the first day of each month. *It should be noted that Equation 4.5 and all other equations developed in this chapter involving trigonometric functions use angles measured in degrees, not radians.*

TABLE 4.1 Day Numbers for the First Day of Each Month

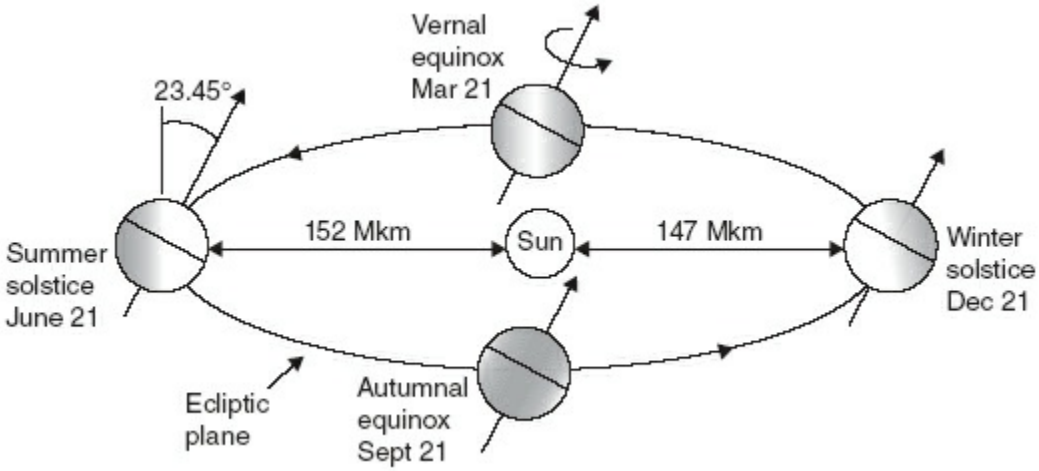
January	$n = 1$	July	$n = 182$
February	$n = 32$	August	$n = 213$
March	$n = 60$	September	$n = 244$
April	$n = 91$	October	$n = 274$
May	$n = 121$	November	$n = 305$
June	$n = 152$	December	$n = 335$

Each day, as the earth rotates about its own axis, it also moves around the ellipse. If the earth were to spin only 365° in a day then after 6 months, our clocks would be off by 12 h

—that is, at noon on day 1 it would be the middle of the day, but 6 months later noon would occur in the middle of the night. To keep it synchronized, the earth needs to rotate one extra turn each year, which means in a 24-h day the earth actually rotates 360.99°, which is a little surprising to most of us.

As shown in Figure 4.5, the plane swept out by the earth in its orbit is called the ecliptic plane. The earth's spin axis is currently tilted 23.45° with respect to the ecliptic plane and that tilt is, of course, what causes our seasons. On March 21 and September 21, a line from the center of the sun to the center of the earth passes through the equator and everywhere on earth we have 12 h of daytime and 12 h of darkness, hence the term *equinox* (equal day and night). On December 21, the winter *solstice* in the Northern Hemisphere, the inclination of the North Pole reaches its highest angle away from the sun (23.45°), while on June 21, the opposite occurs. By the way, for convenience we are using the 21st day of the month for the solstices and equinoxes even though the actual days vary slightly from year to year.

FIGURE 4.5 The tilt of the earth's spin axis with respect to the ecliptic plane is what causes our seasons. "Winter" and "Summer" are designations for the solstices in the Northern Hemisphere.



For solar energy applications, the characteristics of the earth's orbit are considered to be unchanging, but over longer periods of time, measured in thousands of years, orbital variations are extremely important as they significantly affect climate. The shape of the orbit oscillates from elliptical to more nearly circular with a period of 100, 000 years (*eccentricity*). The earth's tilt angle with respect to the ecliptic plane fluctuates from 21.5° to 24.5° with a period of 41, 000 years (*obliquity*). Finally, there is a 23, 000-year period associated with the *precession* of the earth's spin axis. This precession determines, for example, where in the earth's orbit a given hemisphere's summer occurs. Changes in the orbit affect the amount of sunlight striking the earth as well as the distribution of sunlight both geographically and seasonally. Those variations are thought to be influential in the timing of the coming and going of ice ages and interglacial periods. In fact, careful analysis of the historical record of global temperatures does show a primary cycle between glacial episodes of about 100, 000 years, mixed with secondary oscillations with periods of 23, 000 years and 41, 000 years that match these orbital changes. This connection between orbital variations and climate were first proposed in the 1930s by an astronomer, Milutin Milankovitch, and the orbital cycles are now referred to as *Milankovitch oscillations*. Sorting

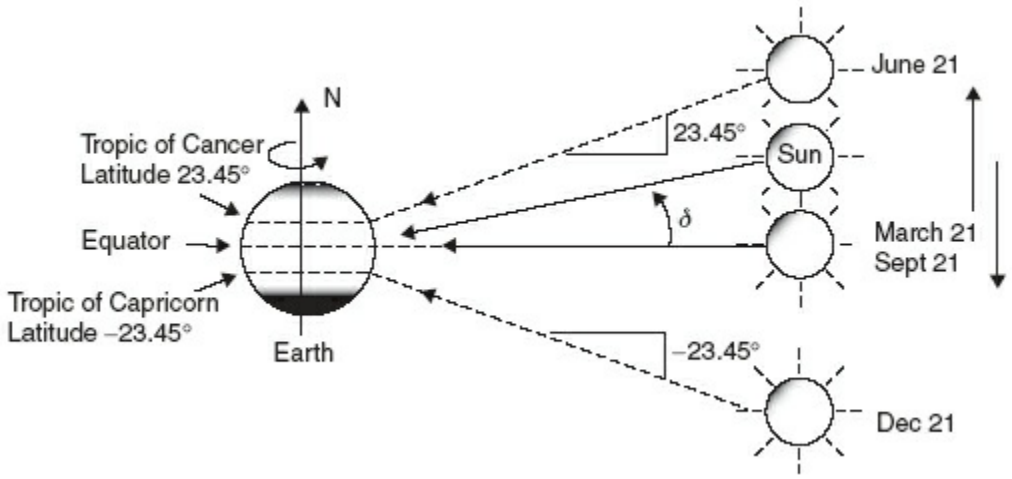
out the impact of human activities on climate from those caused by natural variations such as the Milankovitch oscillations is a critical part of the current climate change discussion.

4.3 ALTITUDE ANGLE OF THE SUN AT SOLAR NOON

We all know the sun rises in the east and sets in the west and reaches its highest point sometime in the middle of the day. In many situations, it is quite useful to be able to predict exactly where in the sky the sun will be at any time, at any location, on any day of the year. Knowing that information we can, for example, design an overhang to allow the sun to come through a window to help heat a house in the winter while blocking the sun in the summer. In the context of photovoltaics, we can, for example, use knowledge of solar angles to help pick the best tilt angle for our modules to expose them to the greatest insolation and we can figure out how to prevent one row of modules from shading another.

While Figure 4.5 correctly shows the earth revolving around the sun, it is a difficult diagram to use when trying to determine various solar angles as seen from the surface of the earth. An alternative (and ancient!) perspective is shown in Figure 4.6, in which the earth is fixed, spinning around its north–south axis; the sun sits somewhere out in space slowly moving up and down as the seasons progress. On June 21 (the summer solstice), the sun reaches its highest point, and a ray drawn to the center of the earth at that time makes an angle of 23.45° with the earth's equator. On that day, the sun is directly over the Tropic of Cancer at latitude 23.45°. At the two equinoxes, the sun is directly over the equator. On December 21, the sun is 23.45° below the equator, which defines the latitude known as the Tropic of Capricorn.

FIGURE 4.6 An alternative view with a fixed, spinning earth and a sun that moves up and down. The angle between the sun and the equator is called the solar declination δ.



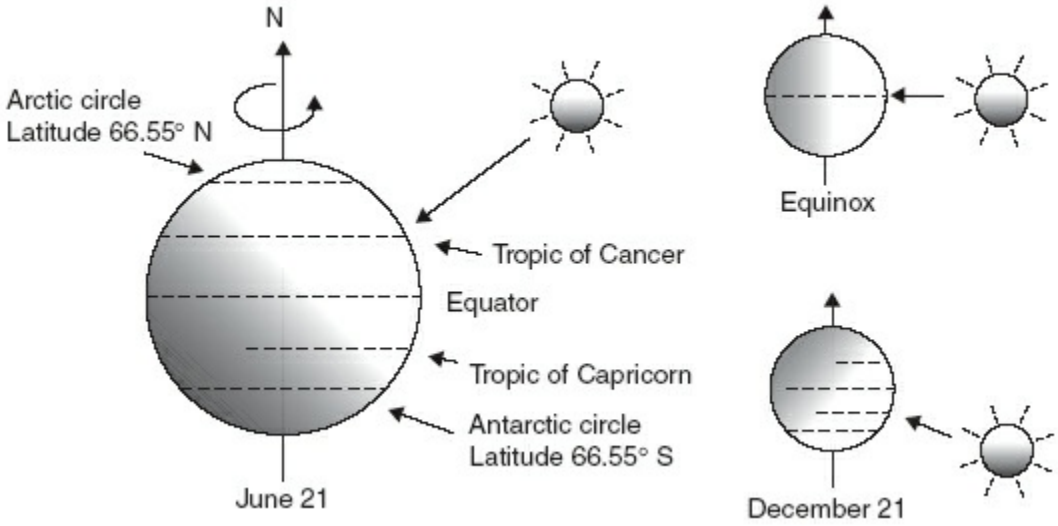
As shown in Figure 4.6, the angle formed between the plane of the equator and a line drawn from the center of the sun to the center of the earth is called the solar declination, δ. It varies between the extremes of ±23.45° and a simple sinusoidal relationship that assumes a 365-day year and which puts the spring equinox on day n = 81 provides a very good

approximation. Exact values of declination, which vary slightly from year to year, can be found in the annual publication *The American Ephemeris and Nautical Almanac*.

$$\delta = 23.45 \sin\left[\frac{360}{365}(n - 81)\right] \tag{4.6}$$

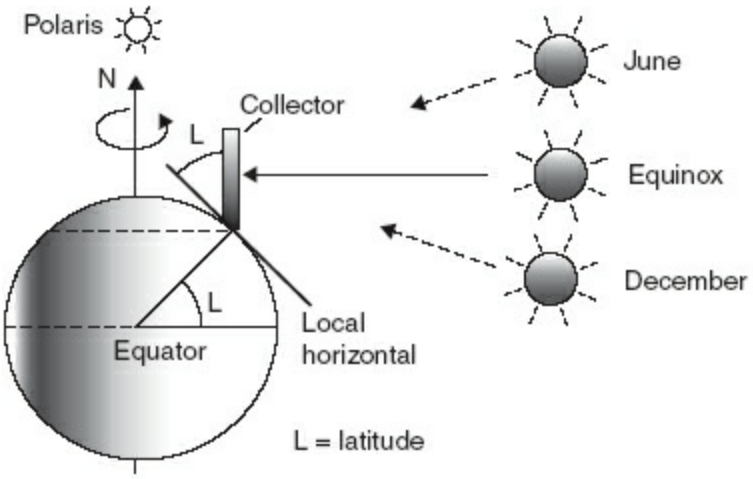
While Figure 4.6 does not capture the subtleties associated with the earth's orbit, it is entirely adequate for visualizing various latitudes and solar angles. For example, it is easy to understand the seasonal variation of daylight hours. As suggested in Figure 4.7, during the summer solstice, all of the earth's surface above latitude 66.55° N (90–23.45°) basks in 24 h of daylight, while in the southern hemisphere below latitude 66.55° S it is continuously dark. Those latitudes, of course, correspond to the Arctic and Antarctic Circles.

FIGURE 4.7 Defining the earth's key latitudes is easy with the simple version of the earth–sun system.



It is also easy to use Figure 4.6 to gain some intuition into what might be a good tilt angle for a solar collector. Figure 4.8 shows a south-facing collector on the earth's surface that is tipped up at an angle equal to the local latitude, L. As can be seen, with this tilt angle, the collector is parallel to the axis of the earth. During an equinox, at *solar noon* when the sun is directly over the local meridian (line of longitude), the sun's rays will strike the collector at the best possible angle, that is, they are perpendicular to the collector face. At other times of the year, the sun is a little high or a little low for normal incidence, but on the average it would seem to be a good tilt angle.

FIGURE 4.8 A south-facing collector tipped up to an angle equal to its latitude is perpendicular to the sun's rays at solar noon during the equinoxes.



Solar noon is an important reference point for almost all solar calculations. In the northern hemisphere, at latitudes above the Tropic of Cancer, solar noon occurs when the sun is due south of the observer. South of the Tropic of Capricorn, in Australia and New Zealand for example, it is when the sun is due north. And in the tropics, the sun may be either due north, due south, or directly overhead at solar noon.

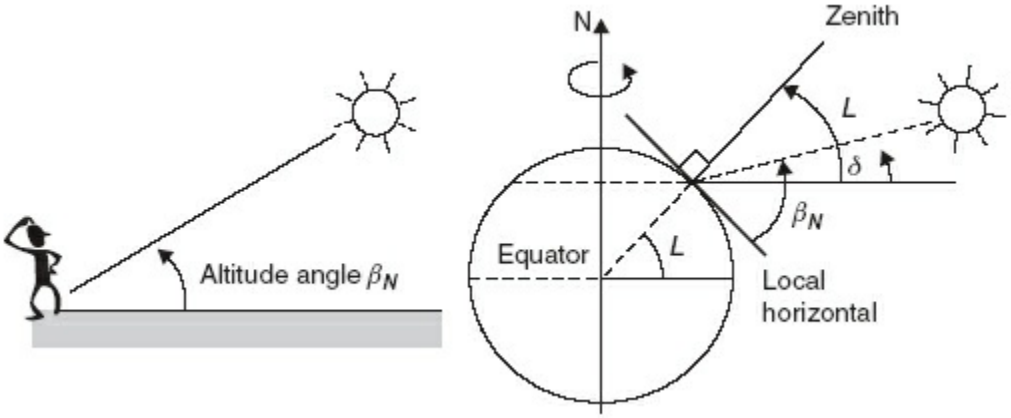
On the average, facing a collector toward the equator (for most of us in the Northern Hemisphere that means facing it south) and tilting it up at an angle equal to the local latitude is a good rule-of-thumb for annual performance. Of course, if you want to emphasize winter collection you might want a slightly higher angle, and vice versa for increased summer efficiency.

Having drawn the earth–sun system as shown in Figure 4.6 also makes it easy to determine a key solar angle, namely the *altitude angle* β_N of the sun at solar noon. The altitude angle is the angle between the sun and the local horizon directly beneath the sun. From Figure 4.9, we can write down the following relationship by inspection:

$$\beta_N = 90^\circ - L + \delta \tag{4.7}$$

where L is the latitude of the site. Notice in the figure the term *zenith* is introduced, which refers to an axis drawn directly overhead at a site.

FIGURE 4.9 The altitude angle of the sun at solar noon.



Example 4.2 Tilt Angle of a PV Module. Find the optimum tilt angle for a south-facing

photovoltaic module in Tucson (latitude 32.1°) at solar noon on March 1.

Solution. From Table 4.1, March 1st is the 60th day of the year so the solar declination (Eq. 4.6) is

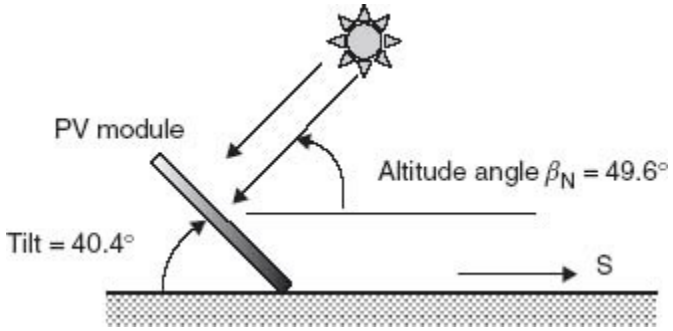
$$\delta = 23.45 \sin\left[\frac{360}{365}(n-81)\right] = 23.45° \sin\left[\frac{360}{365}(60-81)°\right] = -8.3°$$

which, from Equation 4.7, makes the altitude angle of the sun equal to

$$\beta_N = 90 - L + \delta = 90 - 32.1 - 8.3 = 49.6°$$

The tilt angle that would make the sun's rays perpendicular to the module at noon would therefore be

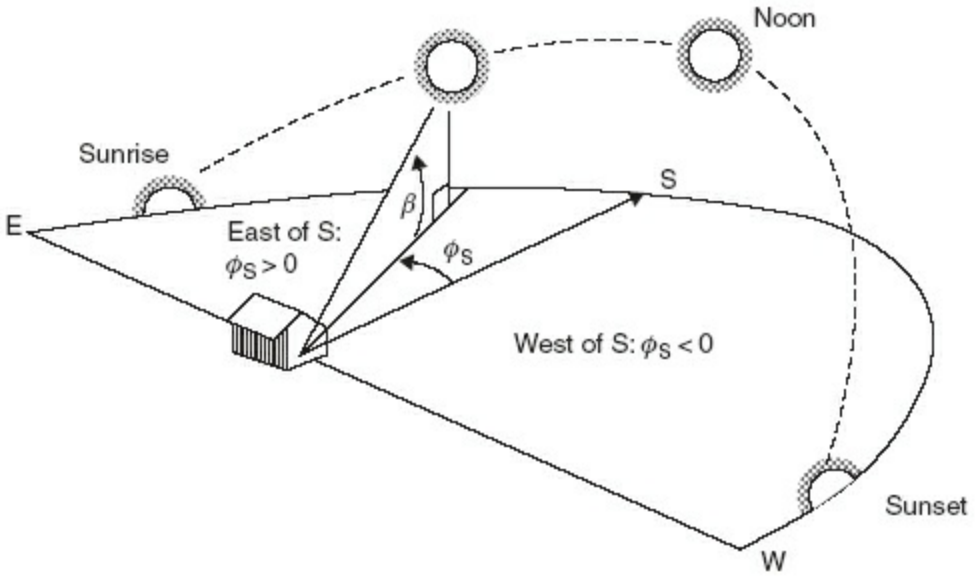
$$\text{Tilt} = 90 - \beta_N = 90 - 49.6 = 40.4°$$



4.4 SOLAR POSITION AT ANY TIME OF DAY

The location of the sun at any time of the day can be described in terms of its altitude angle β and its azimuth angle ϕ_S as shown in Figure 4.10. By the usual convention in solar work, azimuth angles in the Northern Hemisphere are measured in degrees off of due south, while in the Southern Hemisphere they are measured relative to due north. *By convention, the azimuth angle is positive in the morning with the sun in the east and negative in the afternoon with the sun in the west.* The subscript "s" in the azimuth angle helps us remember that this is the azimuth angle of the sun. Later, we will introduce another azimuth angle for the solar collector and a different subscript "c" will be used.

FIGURE 4.10 The sun's position can be described by its altitude angle β and its azimuth angle ϕ_S. By convention, the azimuth angle is considered to be positive before solar noon.



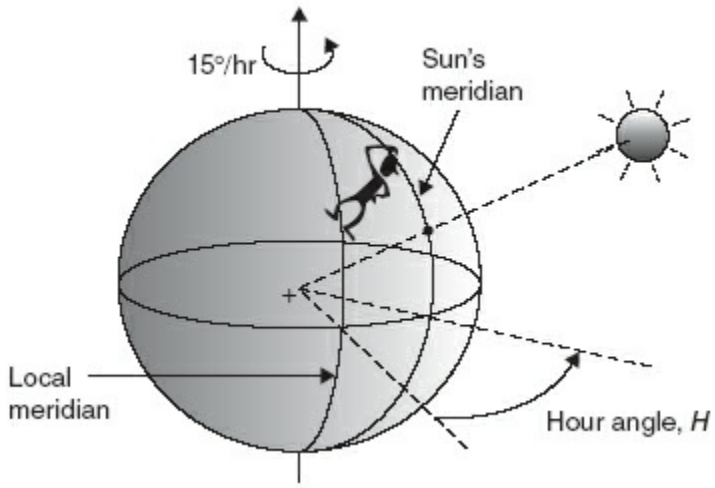
The azimuth and altitude angles of the sun depend on the latitude, day number, and most importantly on the time of the day. For now, we will express time as the number of hours before or after solar noon. Thus, for example, 11:00 A.M. *solar time* (ST) is 1 h before the sun crosses your local meridian (due south for most of us). Later we will learn how to make the adjustment between ST and local clock time (CT). The following two equations allow us to compute the altitude and azimuth angles of the sun. For a derivation see, for example, Kuen et al. (1998):

$$\sin \beta = \cos L \cos \delta \cos H + \sin L \sin \delta \tag{4.8}$$

$$\sin \phi_S = \frac{\cos \delta \sin H}{\cos \beta} \tag{4.9}$$

Notice that time in these equations is expressed by a quantity called the *hour angle*, *H*. The hour angle is the number of degrees that the earth must rotate before the sun will be directly over your local meridian (line of longitude). As shown in Figure 4.11, at any instant, the sun is directly over a particular line of longitude, called the sun's meridian. The difference between the local meridian and the sun's meridian is the hour angle, with positive values occurring in the morning before the sun crosses the local meridian.

FIGURE 4.11 The hour angle is the number of degrees the earth must turn before the sun is directly over the local meridian. It is the difference between the sun's meridian and the local meridian.



Considering the earth to rotate 360° in 24 h, or 15°/h, the hour angle can be described as follows:

$$\text{Hour angle } H = \left(\frac{15^\circ}{\text{hour}}\right) \cdot (\text{hours before solar noon}) \tag{4.10}$$

Thus, the hour angle H at 11:00 A.M. ST would be +15° (the earth needs to rotate another 15°, or 1 h, before it is solar noon). In the afternoon, the hour angle is negative so, for example, at 2:00 P.M. ST H would be –30°.

There is a slight complication associated with finding the azimuth angle of the sun from Equation 4.9. During spring and summer in the early morning and late afternoon, the magnitude of the sun's azimuth is liable to be more than 90° away from south (that never happens in the fall and winter). Since the inverse of a sine is ambiguous, sin x = sin (180 – x), we need a test to determine whether to conclude the azimuth is greater than or less than 90° away from south. Such a test is

$$\text{if } \cos H \geq \frac{\tan\delta}{\tan L} \quad \text{then } |\phi_S| \leq 90^\circ \quad \text{otherwise } |\phi_S| > 90^\circ \tag{4.11}$$

Example 4.3 Where is The Sun? Find the altitude angle and azimuth angle for the sun at 3:00 P.M. solar time in Boulder, Colorado (latitude 40°) on the summer solstice.

Solution. Since it is the solstice we know, without computing, that the solar declination δ is 23.45°. Since 3:00 P.M. is 3 h after solar noon, from Equation 4.10:

$$H = \left(\frac{15^\circ}{\text{h}}\right) \cdot (\text{hour before solar noon}) = \frac{15^\circ}{\text{h}} \cdot (-3\text{ h}) = -45^\circ$$

Using Equation 4.8, the solar altitude angle is

$$\sin\beta = \cos L \cos\delta \cos H + \sin L \sin\delta$$
$$= \cos 40^\circ \cdot \cos 23.45^\circ \cdot \cos(-45^\circ) + \sin 40^\circ \cdot \sin 23.45^\circ = 0.7527$$
$$\beta = \sin^{-1}(0.7527) = 48.8^\circ$$

From Equation 4.9, the azimuth angle is

$$\sin \phi_S = \frac{\cos \delta \sin H}{\cos \beta}$$

$$= \frac{\cos 23.45° \cdot \sin(-45°)}{\cos 48.8°} = -0.9848$$

But the arcsine is ambiguous and two possibilities exist:

$$\phi_S = \sin^{-1}(-0.9848) = -80° \quad (80° \text{ west of south}) \quad \text{or}$$

$$\phi_S = 180 - (-80) = 260° \quad (100° \text{ west of south})$$

To decide which of these two options is correct, we apply Equation 4.11:

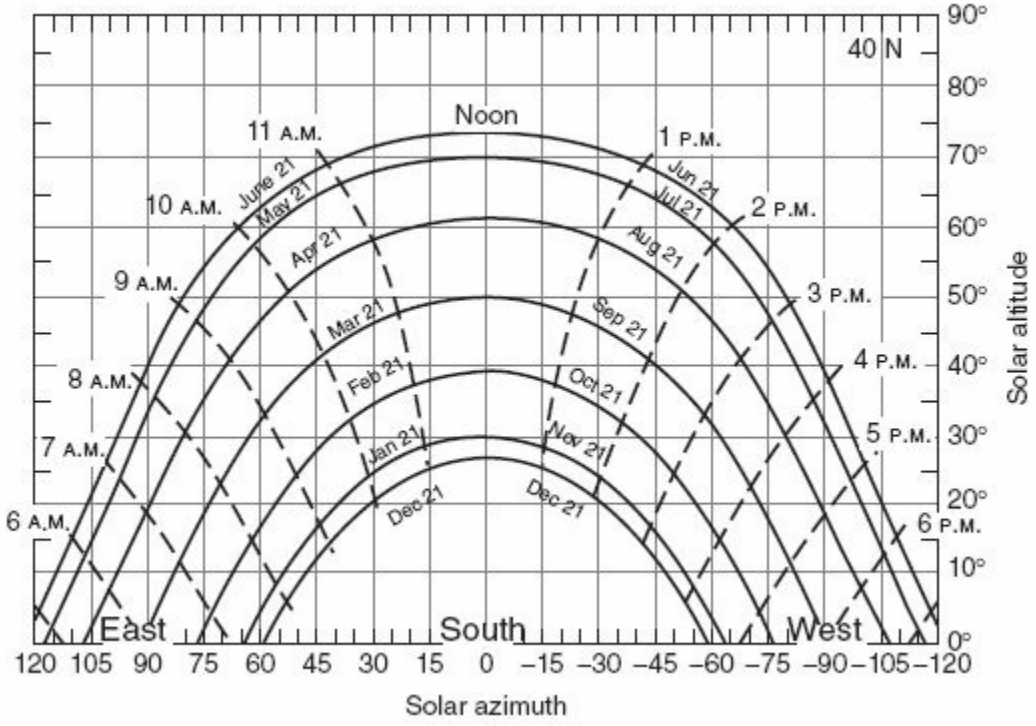
$$\cos H = \cos(-45°) = 0.707 \quad \text{and} \quad \frac{\tan \delta}{\tan L} = \frac{\tan 23.45°}{\tan 40°} = 0.517$$

Since $\cos H \geq \dfrac{\tan \delta}{\tan L}$ we conclude that the azimuth angle is

$$\phi_S = -80° \quad (80° \text{ west of south})$$

Solar altitude and azimuth angles for a given latitude can be conveniently portrayed in graphical form, an example of which is shown in Figure 4.12. Similar sun path diagrams for other latitudes are given in Appendix C. As can be seen, in the spring and summer, the sun rises and sets slightly to the north and our need for the azimuth test given in Equation 4.11 is apparent; at the equinoxes, it rises and sets precisely due east and due west (everywhere on the planet); during the fall and winter, the azimuth angle of the sun is never greater than 90°.

FIGURE 4.12 A sun path diagram showing solar altitude and azimuth angles for 40° latitude. Diagrams for other latitudes are in Appendix C. Similar charts for any location can be generated at http://solardat.uoregon.edu/SunChartProgram.html.



4.5 SUN PATH DIAGRAMS FOR SHADING ANALYSIS

Not only do sun path diagrams, such as that shown in Figure 4.12, help to build one's intuition into where the sun is at any time, they also have a very practical application in the field when trying to predict shading patterns at a site—a very important consideration for photovoltaics, which are very shadow sensitive. The concept is simple. What is needed is a sketch of the azimuth and altitude angles for trees, buildings, and other obstructions along the southerly horizon that can be drawn on top of a sun path diagram. Sections of the sun path diagram that are covered by the obstructions indicate periods of time when the sun will be behind the obstruction and the site will be shaded.

There are several site-assessment products available on the market that make the superposition of obstructions onto a sun path diagram pretty quick and easy; some even allow you to use your cell phone GPS and camera to instantly see shading impacts. You can do a fine job, however, with a simple compass, plastic protractor, and a plumb-bob, but the process requires a little more effort. The compass is used to measure azimuth angles of obstructions, while the protractor and plumb-bob measure altitude angles.

Begin by tying the plumb-bob onto the protractor so that when you sight along the top edge of the protractor the plumb-bob hangs down and provides the altitude angle of the top of the obstruction. Figure 4.13 shows the idea. By standing at the site and scanning the southerly horizon, the altitude angles of major obstructions can be obtained reasonably quickly and quite accurately. The azimuth angles of obstructions, which go along with their altitude angles, are measured using a compass. Remember, however, that a compass points to magnetic north rather than true north; this difference, called the magnetic declination or deviation, must be corrected for. In the United States, that deviation ranges anywhere from about 16° E in Seattle (the compass points 16° east of true north) to 17° W at the northern tip of Maine.

FIGURE 4.13 A site survey can be made using a simple compass, protractor, and plumb-bob. The example shows the compass correction for San Francisco.

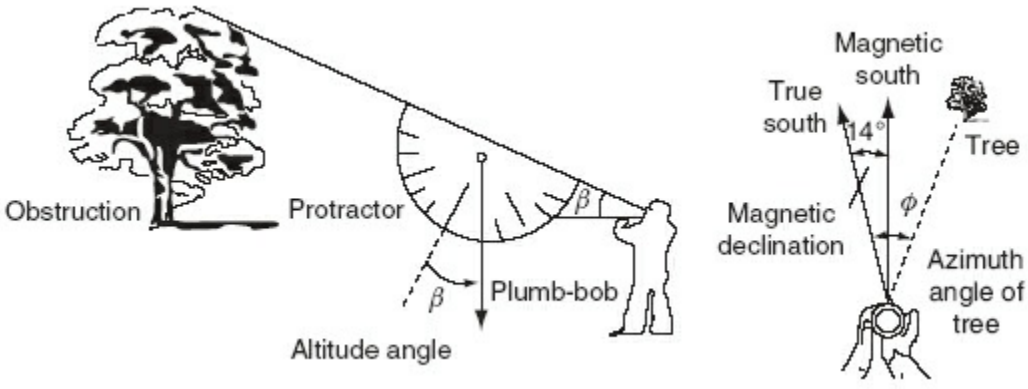
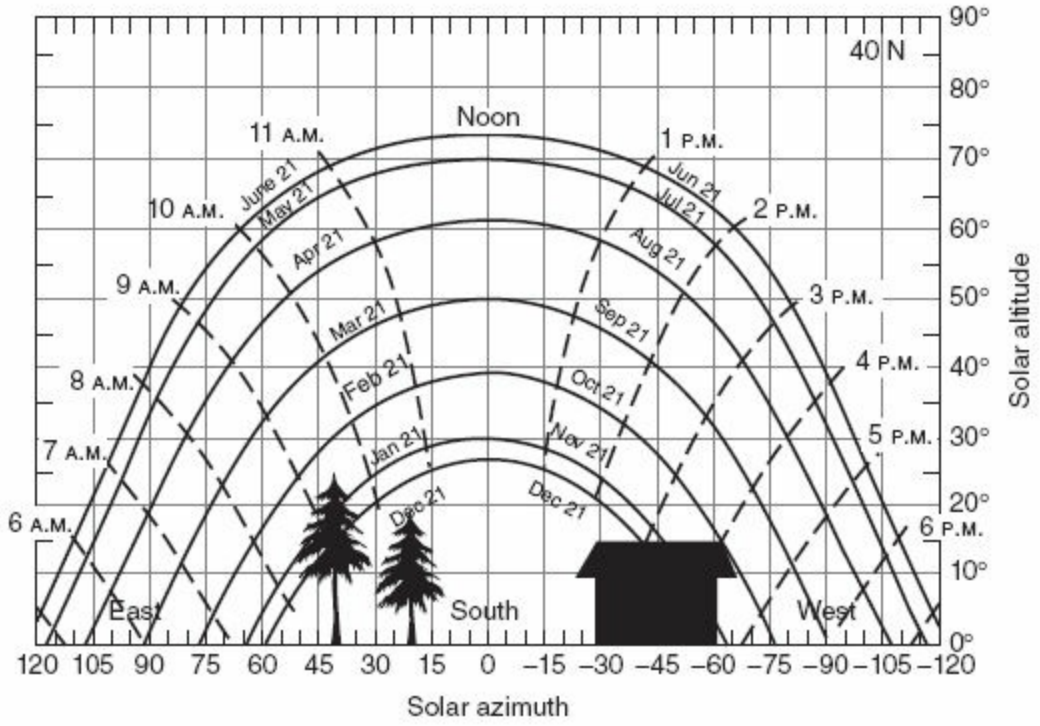


Figure 4.14 shows an example of how the sun path diagram, with a superimposed sketch of potential obstructions, can be interpreted. The site is a proposed solar house with a couple of trees to the southeast and a small building to the southwest. In this example, the site receives full sun all day long from February through October. From November through January, about one hour's worth of sun is lost from around 8:30 A.M. to 9:30 A.M., and

the small building shades the site after about 3 o'clock in the afternoon.

FIGURE 4.14 A sun path diagram with superimposed obstructions makes it easy to estimate periods of shading at a site.



When obstructions plotted on a sun path diagram are combined with hour-by-hour insolation information, an estimate can be obtained of the energy lost due to shading. Table 4.2 shows an example of the hour-by-hour insolations available on a clear day in January at 40° latitude for south-facing collectors with fixed tilt angle, or for collectors mounted on 1-axis or 2-axis tracking systems. Later in this chapter, the equations that were used to compute this table will be presented, and in Appendix D, there is a full set of such tables for a number of latitudes.

TABLE 4.2 Hour-by-Hour (W/m^2) and Daylong (kWh/m^2) Clear Sky Insolation at 40° Latitude in January for Tracking and Fixed, South-Facing Collectors[a]

	Tracking		Fixed, South-Facing Tilt Angles						
Solar Time	One-axis	Two-axis	0	20	30	40	50	60	90
7, 5	0	0	0	0	0	0	0	0	0
8, 4	439	462	87	169	204	232	254	269	266
9, 3	744	784	260	424	489	540	575	593	544
10, 2	857	903	397	609	689	749	788	803	708
11, 1	905	954	485	722	811	876	915	927	801
12	919	968	515	761	852	919	958	968	832
$kWh/m^2/d$	6.81	7.17	2.97	4.61	5.24	5.71	6.02	6.15	5.47

[a]A complete set of tables is in Appendix D.

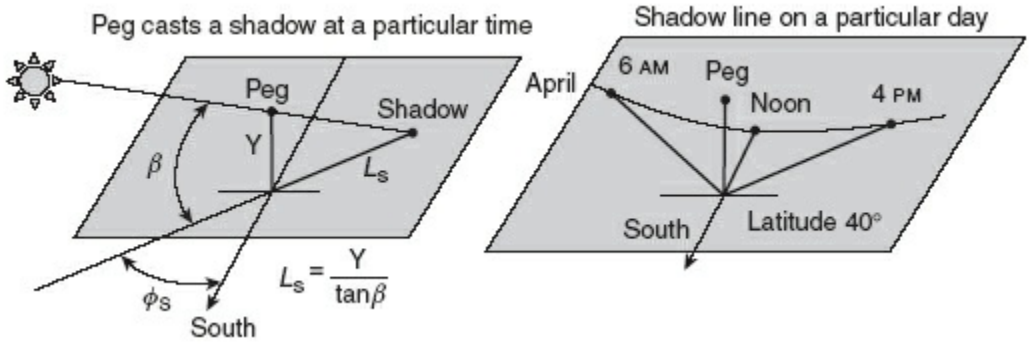
Example 4.4 Loss of Insolation Due to Shading. Estimate the insolation available on a clear day in January on a south-facing collector at 40° latitude with a fixed, 30° tilt angle at the site having the sun path and obstructions diagram shown in Figure 4.14.

Solution. With no obstructions, Table 4.2 indicates that the panel would be exposed to 5.24 kWh/m^2/d. The sun path diagram shows loss of about 1 h of sun at around 9:00 A.M., which eliminates about 0.49 kWh. An hour's worth of sun is also lost around 4 P.M., which drops roughly another 0.20 kWh. The remaining insolation is roughly

$$\text{Insolation} \approx 5.24 - 0.49 - 0.20 = 4.55 \approx 4.6 \text{ kWh/m}^2\text{/d}$$

Note it has been assumed that the insolations shown in Table 4.2 are appropriate averages covering the half hour before and after the hour. Given the crudeness of the obstruction sketch (to say nothing of the fact that the trees are likely to grow anyway), a more precise assessment is not warranted.

FIGURE 4.15 The start of a shadow diagram for a particular day of the year at a particular location.



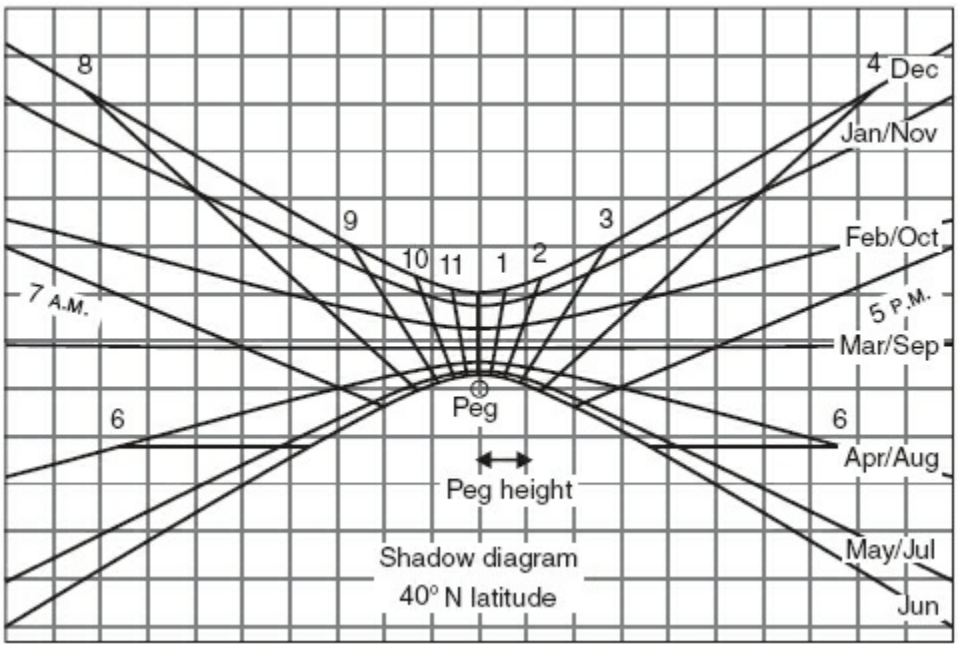
4.6 SHADING ANALYSIS USING SHADOW DIAGRAMS

In setting up a solar field, it is important to design the array so that collectors do not shade each other. A simple graphical approach to doing so is based on an analysis of the shadows cast by a vertical peg. Assuming horizontal ground, we can use Equations 4.8 and 4.9 to predict the length of the peg's shadow, and the shadow's azimuth angle, at any particular location and time of day. As shown in Figure 4.15, if we trace out the shadow tip through that day we get a single tip-of-the-shadow line.

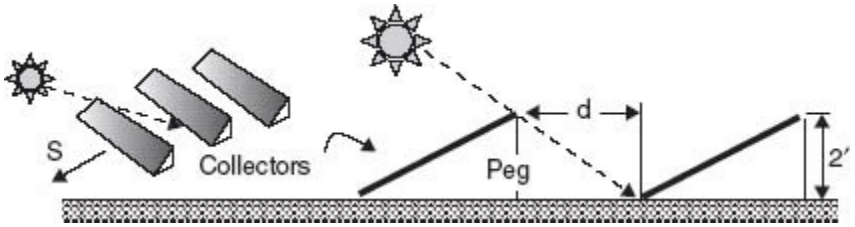
By mapping out those shadow lines, month-by-month, a shadow diagram such as the one shown in Figure 4.16 can be generated for any given latitude. The key to being able to develop quantitative information from such a diagram is to make the spacing of grid lines on the shadow diagram to be the same as the height of our imaginary peg. Thus, for example, the tip of the shadow cast by a vertical peg at 4:00 P.M. in December is about six peg-heights north of the peg and eight peg-heights to the east. The following example illustrates how useful this can be in spacing rows of solar collectors.

FIGURE 4.16 A shadow diagram drawn for 40° N latitude. Curves are drawn for the 21st

of each month. Similar diagrams by R. Conroy and A. Raudonis are included in Appendix F and are available at http://stanford.edu/group/shadowdiagram/.



Example 4.5 Spacing For Rows of Collectors. Long rows of solar collectors lined up along an east–west direction are located in a spot at 40° N latitude. The backs of the solar racks are 2 ft high.



a. Use the shadow diagram in Figure 4.16 to decide how far apart the rows should be placed to assure no shading from one row to another anytime between 9:00 A.M. and 3:00 P.M.

b. Using Equations 4.8 and 4.9, what would the spacing be to avoid shading between 8:00 A.M. and 4:00 P.M.?

Solution

a. Imagine a 2-ft-high peg at the back edge of a row of collectors as shown above. Clearly, the worst day, with the longest north–south shadows is the winter solstice, December 21st. From Figure 4.16 the longest shadow toward the north at 9:00 A.M. or 3:00 P.M. is close to three pegs long (3 squares back). With each peg being 2 ft high, the separation distance should be about

$$d = 2 \text{ ft/peg} \times 1 \text{ peg/square} \times 3 \text{ squares to the north} = 6 \text{ ft of separation}$$

b. From Equation 4.8, using the solstice declination of δ = −23.45° and an hour angle H = 60° (4 h before solar noon):

$$\begin{aligned}\beta &= \sin^{-1}(\cos L \cos\delta \cos H + \sin L \sin\delta)\\ &= \sin^{-1}[\cos 40^\circ \cos(-23.45^\circ)\cos 60^\circ + \sin 40^\circ \sin(-23.45^\circ)]\\ &= 5.485^\circ\end{aligned}$$

So, from Figure 4.15, the length of the shadow at that time is

$$L_S = \frac{Y}{\tan\beta} = \frac{2\text{ ft}}{\tan 5.485^\circ} = 20.8\text{ ft}$$

From Equation 4.9, the azimuth angle of the shadow is

$$\phi_S = \sin^{-1}\left(\frac{\cos\delta \cdot \sin H}{\cos\beta}\right)$$

$$\phi_S = \sin^{-1}\left[\frac{\cos(-23.45^\circ)\cdot \sin 60^\circ}{\cos 5.485^\circ}\right] = 52.95^\circ$$

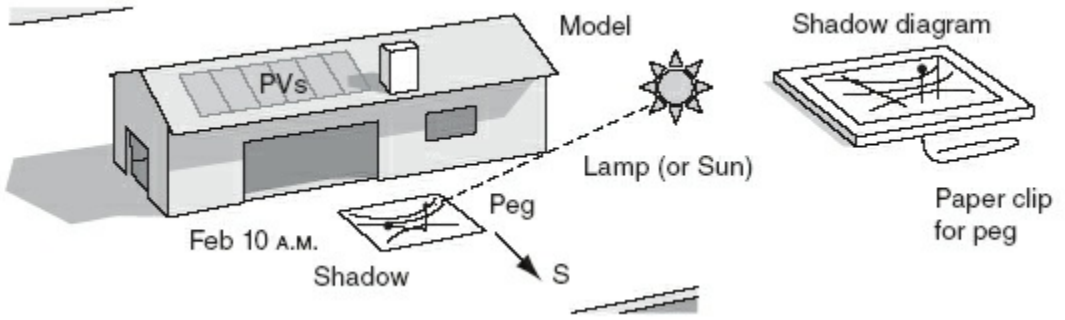
Since it is winter, we do not need to check to see if the azimuth is greater than 90°. The north–south distance behind the 2 ft back of the modules is

$$d = L_S \cos\phi = 20.8\cos(52.95^\circ) = 12.5\text{ ft}$$

We could have gotten this much more easily by just counting squares in the shadow diagram. Also note that spacing has gone from 6 ft to over 12 ft just to capture a modest amount of early morning and late afternoon sunlight during just a couple of winter months.

These shadow diagrams are very handy when working with physical models. As suggested in Figure 4.17, begin by fixing an actual peg onto the diagram (a paperclip works well) with height equal to one square. Mount this shadow and peg onto the base of your model. Using an artificial lamp, or the sun itself, make the peg cast a shadow such that the shadow tip lands on the month and time of day of interest. The lamp will then show the correct shadows for that time on the model itself.

FIGURE 4.17 Using a shadow diagram with a physical model helps predict shading problems. Note the shading on the PV array from the chimney.



4.7 SOLAR TIME AND CIVIL (CLOCK) TIME

For most solar work, it is common to deal exclusively in solar time (ST), where everything is measured relative to solar noon (when the sun is on our line of longitude). There are

occasions, however, when local time, called civil time, or clock time (CT), is needed. There are two adjustments that must be made in order to connect local CT and ST. The first is a longitude adjustment that has to do with the way in which regions of the world are divided into time zones. The second is a little fudge factor that needs to be thrown in to account for the uneven way in which the earth moves around the sun.

Obviously, it just would not work for each of us to set our watches to show noon when the sun is on our own line of longitude. Since the earth rotates 15°/h (4 minutes per degree), for every degree of longitude between one location and another, clocks showing solar time would have to differ by 4 min. The only time two clocks would show the same time would be if they both were due north/south of each other.

To deal with such longitude complication, the earth is nominally divided into 24, 1-h time zones, with each time zone ideally spanning 15° of longitude. Of course, geopolitical boundaries invariably complicate the boundaries from one zone to another (China, for example, though it covers five normal time zones, has only a single standard time). The intent is for all clocks within the time zone to be set to the same time. Each time zone is defined by a *local time meridian* located, ideally, in the middle of the zone, with the origin of this time system passing through Greenwich, England, at 0° longitude. Time zones around the world are expressed as positive or negative offsets from what used to be called Greenwich Mean Time (GMT), but what is now more precisely defined as Coordinated Universal Time (UTC). The local time meridians for the United States, as well as UTC offsets are given in Table 4.3.

TABLE 4.3 *Local Time Meridians for U.S. Standard Time Zones (Degrees West of Greenwich) and UTC Offsets*

Time Zone	LT Meridian	UTC Time
Eastern	75°	UTC – 5:00
Central	90°	UTC – 6:00
Mountain	105°	UTC – 7:00
Pacific	120°	UTC – 8:00
Eastern Alaska	135°	UTC – 9:00
Hawaii	150°	UTC – 10:00

The longitude correction between local clock time and solar time is based on the time it takes for the sun to travel between the local time meridian and the observer's line of longitude. If it is solar noon on the local time meridian, it will be solar noon 4 min later for every degree that the observer is west of that meridian. For example, San Francisco, at latitude 122°, will have solar noon 8 min after the sun crosses the 120° local time meridian for the Pacific Time Zone.

The second adjustment between solar time and local clock time is the result of the earth's elliptical orbit, which causes the length of a *solar day* (solar noon to solar noon) to vary throughout the year. As the earth moves through its orbit, the difference between a 24-h day and a solar day changes following an expression known as the *equation of time*, E:

$$E = 9.87 \sin 2B - 7.53 \cos B - 1.5 \sin B \text{ (minutes)} \quad (4.12)$$

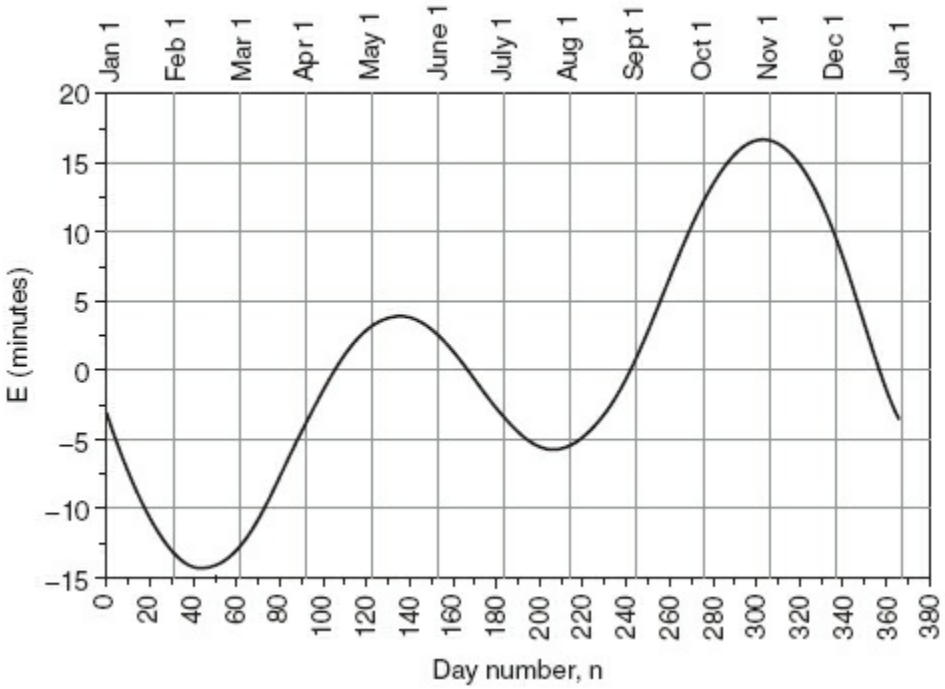
where

$$B = \frac{360}{364}(n - 81) \text{ (degrees)}$$

(4.13)

As before, n is the day number. A graph of Equation 4.12 is given in Figure 4.18.

FIGURE 4.18 The equation of time adjusts for the earth's tilt angle and noncircular orbit.



Putting together the longitude correction and the equation of time gives us the final relationship between local standard clock time and solar time.

$$+\frac{4 \text{ min}}{\text{degree}}(\text{Local Time Meridian} - \text{Local longitude})^\circ + E(\text{min})$$

(4.14)

When daylight savings time is in effect, 1 h must be added to the local clock time ("Spring ahead, Fall back").

Example 4.6 Solar Time to Local Time. Find Eastern Daylight Time for solar noon in Boston (longitude 71.1° W) on July 1st.

Solution. From Table 4.1, July 1 is day number n = 182. Using Equations 4.12–4.14 to adjust for local time, we obtain

$$B = \frac{360}{364}(n - 81) = \frac{360}{364}(182 - 81) = 99.89^\circ$$

$$E = 9.87 \sin 2B - 7.53 \cos B - 1.5 \sin B$$

$$= 9.87 \sin[2 \cdot (99.89)] - 7.53 \cos(99.89) - 1.5 \sin(99.89) = -3.5 \text{ min}$$

For Boston at longitude 71.1° in the Eastern Time Zone with local time meridian 75°

$$\text{CT} = \text{ST} - 4(\text{min}/^\circ)(\text{local time meridian} - \text{local longitude}) - E(\text{min})$$

$$\text{CT} = 12{:}00 - 4\,(75 - 71.1) - (-3.5) = 12{:}00 - 12.1\,\text{min}$$

$$= 11{:}47.9\ \text{A.M. EST}$$

To adjust for Daylight Savings Time, add 1 h, so solar noon will be at about 12:48 P.M. EDT.

4.8 SUNRISE AND SUNSET

A sun path diagram, such as was shown in Figure 4.12, can be used to locate the azimuth angles and approximate times of sunrise and sunset. A more careful estimate of sunrise/sunset can be found from a simple manipulation of Equation 4.8. At sunrise and sunset, the altitude angle β is zero so we can write

$$\sin\beta = \cos L \cos\delta \cos H + \sin L \sin\delta = 0 \tag{4.15}$$

$$\cos H = -\frac{\sin L \sin\delta}{\cos L \cos\delta} = -\tan L \tan\delta \tag{4.16}$$

Solving for the hour angle at sunrise, H_{SR}, gives

$$H_{SR} = \cos^{-1}(-\tan L \tan\delta) \quad (+ \text{ for sunrise}) \tag{4.17}$$

Note in Equation 4.17 that since the inverse cosine allows for both positive and negative values, we need to use our sign convention, which requires the positive value to be used for sunrise (and the negative for sunset).

Since the earth rotates 15°/h, the hour angle can be converted to time of sunrise or sunset using

$$\text{Sunrise (geometric)} = 12{:}00 - \frac{H_{SR}}{15^\circ/\text{h}} \tag{4.18}$$

Equations 4.15–4.18 are geometric relationships based on angles measured to the center of the sun, hence the designation *geometric sunrise* in Equation 4.18. They are perfectly adequate for any kind of normal solar work, but they will not give you exactly what you will find in the newspaper for sunrise or sunset. The difference between weather service sunrise and our geometric sunrise (Eq. 4.18) is the result of two factors. The first deviation is caused by atmospheric refraction, which bends the sun's rays making the sun *appear* to rise about 2.4 min sooner than geometry would tell us, and set 2.4 min later. The second is that the weather service definition of sunrise and sunset is the time at which the upper limb (top) of the sun crosses the horizon, while ours is based on the center crossing the horizon.

Example 4.7 Sunrise in Boston. Find the time at which geometric sunrise will occur in Boston (latitude 42.3°) on July 1st (n = 182).

Solution. From Equation 4.6, the solar declination is

$$\delta = 23.45 \sin\left[\frac{360}{365}(n - 81)\right] = 23.45 \sin\left[\frac{360}{365}(182 - 81)\right] = 23.1°$$

From Equation 4.17, the hour angle at sunrise is

$$H_{SR} = \cos^{-1}(-\tan L \cdot \tan \delta) = \cos^{-1}(-\tan 42.3° \cdot \tan 23.1°) = 112.86°$$

From Equation 4.18, solar time of geometric sunrise is

$$\begin{aligned}\text{Sunrise (geometric)} &= 12{:}00 - \frac{H_{SR}}{15°/\text{h}} \\ &= 12{:}00 - \frac{112.86°}{15°/\text{h}} = 12{:}00 - 7.524\ \text{h} \\ &= 4{:}28.6\ \text{A.M. (solar time)}\end{aligned}$$

From Example 4.6, on this date, in Boston, local clock time is 12.1 min earlier than solar time, so sunrise will be at

$$\text{Sunrise} = 4{:}28.6 - 12.1\ \text{min} = 4{:}16\ \text{A.M. Eastern Standard Time}$$

It turns out that actual sunrise, accounting for refraction and use of the upper limb of the sun, will be about 5 min earlier. There is a convenient website for finding sunrise and sunset times on the web at http://aa.usno.navy.mil/data/docs/RS_OneDay.html.

With so many angles to keep track of, it may help to summarize the terminology and equations for them all in one spot, which has been done in Box 4.1.

4.9 CLEAR-SKY DIRECT-BEAM RADIATION

Solar flux striking a collector will be a combination of *direct beam* radiation that passes in a straight line through the atmosphere to the receiver, *diffuse* radiation that has been scattered by molecules and aerosols in the atmosphere, and *reflected* radiation that has bounced off the ground or other surfaces in front of the collector

BOX 4.1 Summary of Solar Angles

δ	=	solar declination
n	=	day number
L	=	latitude
β	=	solar altitude angle, β_N = angle at solar noon
H	=	hour angle
H_{SR}	=	sunrise hour angle
ϕ_S	=	solar azimuth angle (+ before solar noon, – after)
ϕ_C	=	collector azimuth angle (+ east of south, – west of south)
ST	=	solar time

CT	=	civil, or clock time
E	=	equation of time
Σ	=	collector tilt angle
θ	=	incidence angle between sun and collector face

$$\delta = 23.45 \sin\left[\frac{360}{365}(n - 81)\right] \tag{4.6}$$

$$\beta_N = 90^\circ - L + \delta \tag{4.7}$$

$$\sin\beta = \cos L \cos\delta \cos H + \sin L \sin\delta \tag{4.8}$$

$$\sin\phi_S = \frac{\cos\delta \sin H}{\cos\beta} \tag{4.9}$$

$$\text{if } \cos H \geq \frac{\tan\delta}{\tan L} \quad \text{then} |\phi_S| \leq 90^\circ \quad \text{otherwise } |\phi_S| > 90^\circ$$

$$\text{Hour angle } H = \left(\frac{15^\circ}{\text{h}}\right) \cdot (\text{Hours before solar noon}) \tag{4.10}$$

$$E = 9.87 \sin 2B - 7.53 \cos B - 1.5 \sin B \text{ (min)} \tag{4.12}$$

$$B = \frac{360}{364}(n - 81) \tag{4.13}$$

(4.14)

$$\text{Solar Time (ST)} = \text{Clock Time (CT)} + \frac{4\,\text{min}}{\text{degree}} (\text{Local Time Meridian} - \text{Local longitude})^\circ + E(\text{min})$$

$$H_{SR} = \cos^{-1}(-\tan L \tan\delta) \quad (+ \text{ for sunrise}) \tag{4.17}$$

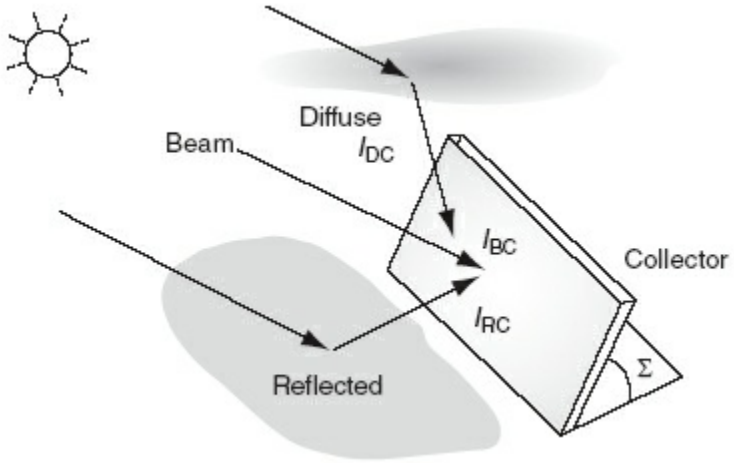
(Fig. 4.19). The preferred units, especially in solar-electric applications, are watts (or kilowatts) per square meter. Other units involving British Thermal Units, kilocalories, and langleys may also be encountered. Conversion factors between these units are given in Table 4.4.

TABLE 4.4 Conversion Factors for Various Insolation Units

1 kW/m^2	316.95 Btu/h/ft^2
	1.433 langley/min
1 kWh/m^2	316.95 Btu/ft^2
	85.98 langleys
	3.60 × 10^6 J/m^2
1 Langley	1 cal/cm^2
	41.856 kJ/m^2

	0.01163 kWh/m^2
	3.6878 Btu/ft^2

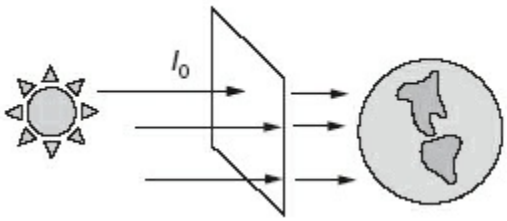
FIGURE 4.19 Solar radiation striking a collector I_C is a combination of direct beam I_{BC}, diffuse I_{DC}, and reflected I_{RC}.



Solar collectors that focus sunlight usually operate on just the beam portion of the incoming radiation since those rays are the only ones that arrive from a consistent direction. Most photovoltaic systems, however, do not use focusing devices so all three components—beam, diffuse, and reflected—can contribute to energy collected. The goal of this section is to be able to estimate the rate at which just the beam portion of solar radiation passes through the atmosphere and arrives at the earth's surface on a clear day. Later, the diffuse and reflected radiation will be added to the clear day model. And finally, procedures will be presented that will enable more realistic average insolation calculations for specific locations based on empirically derived data for certain given sites.

The starting point for a clear-sky radiation calculation is with an estimate of the extraterrestrial (ET) solar insolation, I_0, that passes perpendicularly through an imaginary surface just outside of the earth's atmosphere as shown in Figure 4.20. This insolation depends on the distance between the earth and the sun, which varies with the time of year. It also depends on the intensity of the sun, which rises and falls with a fairly predictable cycle. During peak periods of magnetic activity on the sun, the surface has large numbers of cooler, darker regions called *sunspots*, which in essence block solar radiation, accompanied by other regions, called *faculae*, that are brighter than the surrounding surface. The net effect of sunspots that dim the sun, and faculae that brighten it, is an increase in solar intensity during periods of increased numbers of sunspots. Sunspot activity seems to follow an 11-year cycle with the most recent peaks occurring in 2001 and 2013. Sunspot variations can change extraterrestrial insolation by a few tenths of a percent.

FIGURE 4.20 The extraterrestrial solar flux.



Ignoring sunspots, one expression that is used to describe the day-to-day variation in extraterrestrial solar insolation is the following:

$$I_0 = \text{SC} \cdot \left[1 + 0.034 \cos\left(\frac{360\,n}{365}\right)\right] \ (\text{W/m}^2) \tag{4.19}$$

where SC is called the *solar constant,* and n is the day number. The solar constant is an estimate of the average annual extraterrestrial insolation, with 1367 W/m^2 currently being the most commonly accepted value.

As the beam passes through the atmosphere, a good portion of it is absorbed by various gases in the atmosphere or scattered by air molecules or particulate matter. In fact, over a year's time less than half of the radiation that hits the top of the atmosphere reaches the earth's surface as direct beam. On a clear day, however, with the sun high in the sky, beam radiation at the surface can exceed 70% of the extraterrestrial flux.

Attenuation of incoming radiation is a function of the distance that the beam has to travel through the atmosphere, which is easily calculable, as well as factors such as dust, air pollution, atmospheric water vapor, clouds, and turbidity, which are not so easy to account for. A commonly used model treats attenuation as an exponential decay function

$$I_B = A\, e^{-km} \tag{4.20}$$

where I_B is the beam portion of the radiation reaching the earth's surface (normal to the rays), A is an "apparent" extraterrestrial flux, and k is a dimensionless factor called the *optical depth*. The air mass ratio m was introduced in Equation 4.4 under the assumption of a "flat earth, " but a more carefully derived relationship that accounts for the spherical nature of our atmosphere is the following:

$$\text{Air mass ratio } m = \sqrt{(708 \sin\beta)^2 + 1417} - 708 \sin\beta \tag{4.21}$$

where β is the altitude angle of the sun.

Table 4.5 gives values of A and k that are used in the American Society of Heating, Refrigerating and Air-conditioning Engineers (ASHRAE) Clear Day Solar Flux Model. This model is based on empirical data collected by Threlkeld and Jordan (1958) for a moderately dusty atmosphere with atmospheric water vapor content equal to the average monthly values in the United States. Also included is a diffuse factor, C, that will be introduced later.

TABLE 4.5 Optical Depth k, Apparent Extraterrestrial Flux, A, and the Sky Diffuse Factor C for the 21st Day of Each Month

Month	Jan	Feb	Mar	Apr	May	Jun	Jul	Aug	Sep	Oct	Nov	Dec
A (W/m^2)	1230	1215	1186	1136	1104	1088	1085	1107	1151	1192	1221	1233
k	0.142	0.144	0.156	0.180	0.196	0.205	0.207	0.201	0.177	0.160	0.149	0.142
C	0.058	0.060	0.071	0.097	0.121	0.134	0.136	0.122	0.092	0.073	0.063	0.057

Source: From ASHRAE (1993).

For computational purposes, it is handy to have an equation to work with rather than a table of values. Close fits to the values of optical depth k and apparent extraterrestrial flux A given in Table 4.5 are as follows:

$$A = 1160 + 75 \sin\left[\frac{360}{365}(n - 275)\right] \text{ (W/m}^2\text{)} \tag{4.22}$$

$$k = 0.174 + 0.035 \sin\left[\frac{360}{365}(n - 100)\right] \tag{4.23}$$

where again n is the day number.

Example 4.8 Direct Beam Radiation at the Surface of the Earth. Find the direct beam solar radiation normal to the sun's rays at solar noon on a clear day in Atlanta (latitude 33.7°) on May 21. Use Equations 4.22 and 4.23 to see how closely they approximate Table 4.5.

Solution. Using Table 4.1 to help, May 21 is day number 141. From Equation 4.22, the apparent extraterrestrial flux, A is

$$A = 1160 + 75 \sin\left[\frac{360}{365}(n - 275)\right]$$

$$= 1160 + 75 \sin\left[\frac{360}{365}(141 - 275)\right] = 1104 \text{ W/m}^2$$

(which agrees with Table 4.5).

From Equation 4.23, the optical depth is

$$k = 0.174 + 0.035 \sin\left[\frac{360}{365}(n - 100)\right]$$

$$= 0.174 + 0.035 \sin\left[\frac{360}{365}(141 - 100)\right] = 0.197$$

(which is very close to the value given in Table 4.5).

From Equation 4.6, the solar declination on May 21 is

$$\delta = 23.45 \sin\left[\frac{360}{365}(141 - 81)\right] = 20.14°$$

From Equation 4.7, the altitude angle of the sun at solar noon is

$$\beta_N = 90° - L + \delta = 90 - 33.7 + 20.1 = 76.4°$$

The air mass ratio (Eq. 4.21) is

$$m = \sqrt{(708 \sin\beta)^2 + 1417} - 708 \sin\beta$$

$$= \sqrt{(708 \sin 76.4°)^2 + 1417} - 708 \sin 76.4° = 1.029$$

Finally, using Equation 4.20, the predicted value of clear-sky beam radiation at the earth's surface is

$$I_B = Ae^{-km} = 1104e^{-0.197 \times 1.029} = 902 \text{ W/m}^2$$

TABLE 4.6 Hour-by-Hour Clear-Sky Insolation (W/m2) for June 21 at Latitude 40° Including 0.2 Reflectance. Similar Tables for Other Months and Latitudes, Without Reflectance, are Given in Appendix D

Solar Time	Tracking		Tilt Angles, Latitude 40°						
	One-axis	Two-axis	0	20	30	40	50	60	90
6, 6	496	542	189	130	97	62	60	58	51
7, 5	706	764	387	333	295	250	199	146	84
8, 4	816	878	572	541	506	459	400	334	109
9, 3	877	939	731	726	696	649	586	510	220
10, 2	910	973	853	870	846	800	734	650	318
11, 1	924	989	929	961	940	895	828	740	381
12	928	993	955	992	973	928	860	771	403
kWh/m²/d	10.39	11.16	8.28	8.12	7.73	7.16	6.48	5.64	2.73

4.10 TOTAL CLEAR-SKY INSOLATION ON A COLLECTING SURFACE

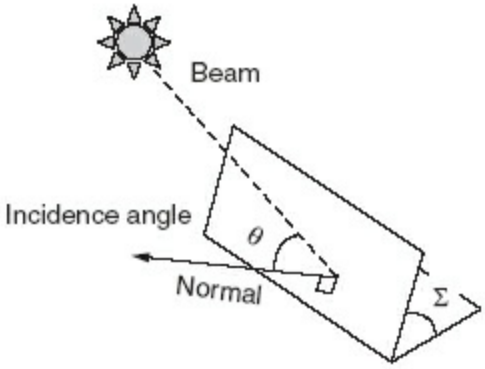
Reasonably accurate estimates of the clear-sky direct beam insolation are easy enough to work out and the geometry needed to determine how much of that will strike a collector surface is straightforward. It is not so easy to account for the diffuse and reflected insolation, but since that energy bonus is a relatively small fraction of the total, even crude models are usually acceptable.

4.10.1 Direct Beam Radiation

The translation of direct beam radiation I_B (normal to the rays) into beam insolation striking a collector face I_{BC} is a simple function of the angle of incidence θ between a line drawn normal to the collector face and the incoming beam radiation (Fig. 4.21). It is given by

$$I_{BC} = I_B \cos\theta \quad (4.24)$$

FIGURE 4.21 The incidence angle θ between a normal to the collector face and the incoming solar beam radiation.



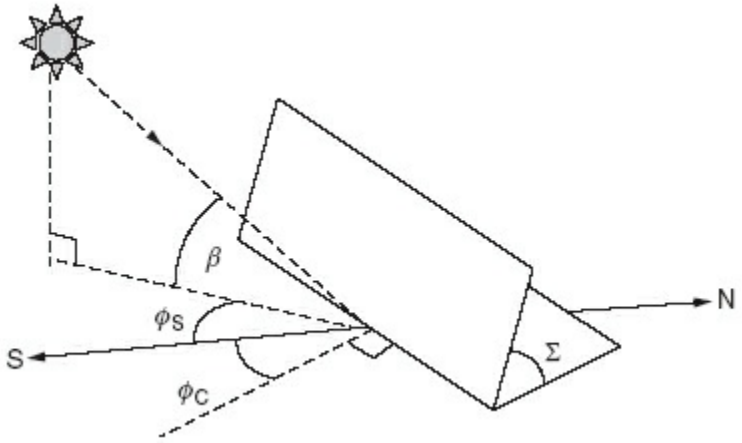
For the special case of beam insolation on a horizontal surface I_{BH},

$$I_{BH} = I_B \cos(90° - \beta) = I_B \sin\beta \tag{4.25}$$

The angle of incidence θ will be a function of the collector orientation and the altitude and azimuth angles of the sun at any particular time. Figure 4.22 introduces these important angles. The solar collector is tipped up at an angle Σ and faces in a direction described by its azimuth angle ϕ_C (measured relative to due south, *with positive values in the easterly direction and negative values toward the west*). The incidence angle is given by

$$\cos\theta = \cos\beta\cos(\phi_S - \phi_C)\sin\Sigma + \sin\beta\cos\Sigma \tag{4.26}$$

FIGURE 4.22 Illustrating the collector azimuth angle ϕ_C and tilt angle Σ along with the solar azimuth angle ϕ_S and altitude angle β. Azimuth angles are positive in the southeast direction, and negative in the southwest.



Example 4.9 Beam Insolation on a Collector. In Example 4.8, at solar noon in Atlanta (latitude 33.7°) on May 21, the altitude angle of the sun was found to be 76.4° and the clear-sky beam insolation was found to be 902 W/m^2. Find the beam insolation at that time on a collector that faces 20° toward the southeast if it is tipped up at a 52° angle.

Solution. Using Equation 4.26, the cosine of the incidence angle is

$$\cos\theta = \cos\beta\cos(\phi_S - \phi_C)\sin\Sigma + \sin\beta\cos\Sigma$$

$$= \cos 76.4° \cdot \cos(0 - 20°) \cdot \sin 52° + \sin 76.4° \cdot \cos 52° = 0.7725$$

From Equation 4.24, the beam radiation on the collector is

$$I_{BC} = I_B \cos\theta = 902\ \text{W/m}^2 \cdot 0.7725 = 697\ \text{W/m}^2$$

4.10.2 Diffuse Radiation

The diffuse radiation on a collector is much more difficult to estimate accurately than it is for the beam. Consider the variety of components that make up diffuse radiation as shown in Figure 4.23. Incoming radiation can be scattered from atmospheric particles and moisture, and it can be reflected by clouds. Some is reflected from the surface back into the sky and scattered again back to the ground. The simplest models of diffuse radiation assume it arrives at a site with equal intensity from all directions; that is, the sky is considered to be *isotropic*. Obviously, on hazy or overcast days the sky is considerably brighter in the vicinity of the sun, and measurements show a similar phenomenon on clear days as well, but these complications are often ignored.

The model developed by Threlkeld and Jordan (1958), which is used in the ASHRAE Clear Day Solar Flux Model, suggests that diffuse insolation on a horizontal surface I_{DH} is proportional to the direct beam radiation I_B no matter where in the sky the sun happens to be

$$I_{DH} = I_B C \tag{4.27}$$

where C is a sky diffuse factor. Monthly values of C are given in Table 4.5, and a convenient approximation is as follows

$$C = 0.095 + 0.04 \sin\left[\frac{360}{365}(n - 100)\right] \tag{4.28}$$

Applying Equation 4.27 to a full day of clear skies typically predicts that about 15% of the total horizontal insolation on a clear day will be diffuse.

What we would like to know is how much of that horizontal diffuse radiation strikes a collector so that we can add it to the beam radiation. As a first approximation, it is assumed that diffuse radiation arrives at a site with equal intensity from all directions. That means the collector will be exposed to whatever fraction of the sky the face of the collector points to, as shown in Figure 4.24. When the tilt angle of the collector Σ is zero, that is the panel is flat on the ground, the panel sees the full sky and so it receives the full horizontal diffuse radiation, I_{DH}. When it is a vertical surface, it sees half the sky and is exposed to half of the horizontal diffuse radiation, and so forth. The following expression for diffuse radiation on the collector, I_{DC} is used when the diffuse radiation is idealized in this way.

$$I_{DC} = I_{DH}\left(\frac{1 + \cos\Sigma}{2}\right) = I_B C\left(\frac{1 + \cos\Sigma}{2}\right) \tag{4.29}$$

FIGURE 4.23 Diffuse radiation can be scattered by atmospheric particles and moisture or reflected from clouds. Multiple scatterings are possible.

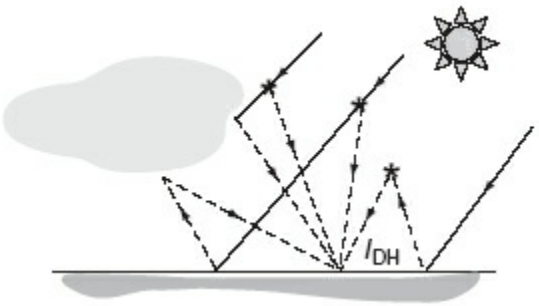
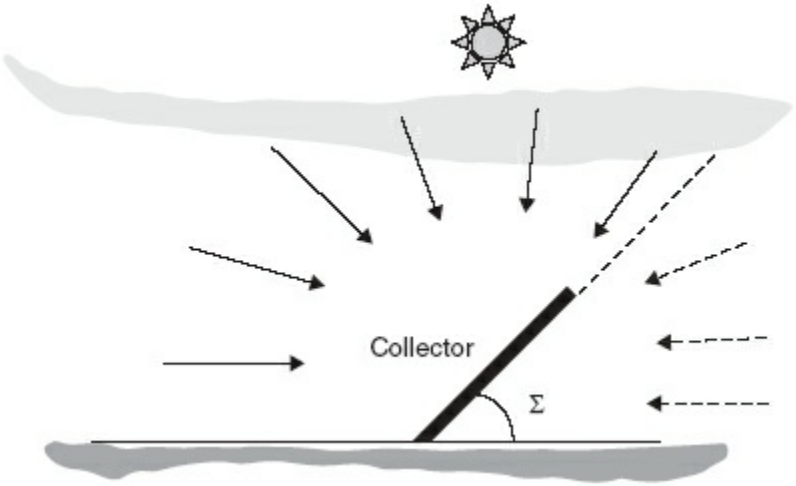


FIGURE 4.24 Diffuse radiation on a collector assumed to be proportional to the fraction of a hemispherical sky that the collector "sees."



Example 4.10 Diffuse Radiation on a Collector. Continue Example 4.9 and find the diffuse radiation on the panel. Recall it is solar noon in Atlanta on May 21st (n = 141), the collector faces 20° toward the southeast and is tipped up at a 52° angle. The clear-sky beam insolation was found to be 902 W/m^2.

Solution. Start with Equation 4.28 to find the diffuse sky factor, C

$$C = 0.095 + 0.04 \sin\left[\frac{360}{365}(n - 100)\right]$$

$$= 0.095 + 0.04 \sin\left[\frac{360}{365}(141 - 100)\right] = 0.121$$

And from Equation 4.29, the diffuse energy striking the collector is

$$I_{DC} = I_B C\left(\frac{1 + \cos\sum}{2}\right)$$

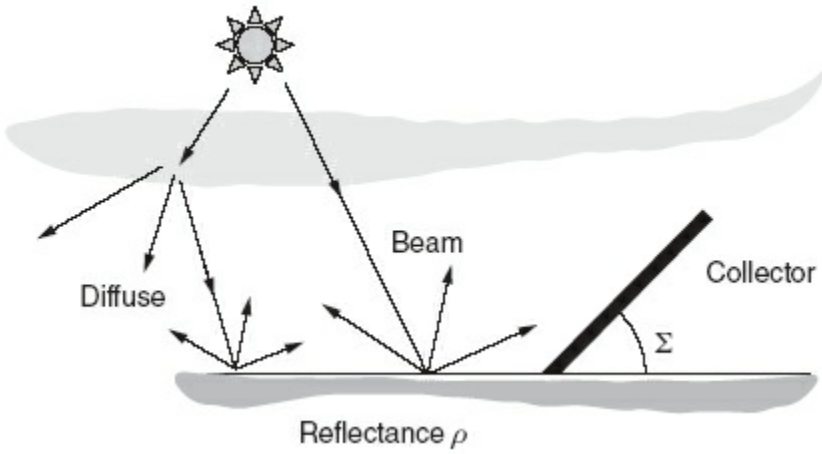
$$= 902 \times 0.121\left(\frac{1 + \cos 52°}{2}\right) = 88 \text{ W/m}^2$$

Added to the total beam insolation found in Example 4.9 of 697 W/m^2, gives a total beam plus diffuse on the collector of 785 W/m^2.

4.10.3 Reflected Radiation

The final component of insolation striking a collector results from radiation that is reflected by surfaces in front of the panel. This reflection can provide a considerable boost in performance, as for example on a bright day with snow or water in front of the collector, or it can be so modest that it might as well be ignored. The assumptions needed to model reflected radiation are considerable and the resulting estimates are very rough indeed. The simplest model assumes a large, horizontal area in front of the collector, with a reflectance ρ that is diffuse, and that it bounces the reflected radiation in equal intensity in all directions, as shown in Figure 4.25. Clearly this is a very gross assumption, especially if the surface is smooth and bright.

FIGURE 4.25 The ground is assumed to reflect radiation with equal intensity in all directions.



Estimates of ground reflectance range from about 0.8 for fresh snow to about 0.1 for a bituminous-and-gravel roof, with a typical default value for ordinary ground or grass taken to be about 0.2. The amount reflected can be modeled as the product of the total horizontal radiation (beam I_{BH} plus diffuse I_{DH}) times the ground reflectance ρ. The fraction of that ground-reflected energy that will be intercepted by the collector depends on the slope of the panel Σ, resulting in the following expression for reflected radiation striking the collector I_{RC}:

$$I_{RC} = \rho\,(I_{BH} + I_{DH})\left(\frac{1-\cos\Sigma}{2}\right) \tag{4.30}$$

For a horizontal collector (Σ = 0), Equation 4.30 correctly predicts no reflected radiation on the collector; for a vertical panel, it predicts that the panel "sees" half of the reflected radiation, which also is appropriate for this simple model.

Substituting expressions 4.25 and 4.27 into 4.30 gives the following for reflected radiation on the collector:

$$I_{RC} = \rho I_H\left(\frac{1-\cos\Sigma}{2}\right) = I_B\rho\,(C+\sin\beta)\left(\frac{1-\cos\Sigma}{2}\right) \tag{4.31}$$

Example 4.11 Reflected Radiation Onto a Collector. Continue Examples 4.9 and 4.10 and find the reflected radiation on the panel if the reflectance of the surfaces in front of the panel is 0.2. Recall it is solar noon in Atlanta on May 21, the altitude angle of the sun β is 76.4°, the collector faces 20° toward the southeast and is tipped up at a 52° angle, the Diffuse Sky Factor C is 0.121, and the clear-sky beam insolation is 902 W/m^2.

Repeat the calculation with snow on the ground having reflectance 0.8.

Solution. From Equation 4.31, the clear-sky reflected insolation on the collector is

$$I_{RC} = I_B \rho (C + \sin\beta)\left(\frac{1 - \cos\Sigma}{2}\right)$$

$$= 0.2 \cdot 902 \text{ W/m}^2 (0.121 + \sin 76.4°)\left(\frac{1 - \cos 52°}{2}\right) = 38 \text{ W/m}^2$$

The total insolation on the collector is therefore

$$I_C = I_{BC} + I_{DC} + I_{RC} = 697 + 88 + 38 = 823 \text{ W/m}^2$$

Of that total, 84.7% is direct beam, 10.7% is diffuse, and only 4.6% is reflected. The reflected portion is modest and is often ignored.

With the higher 0.8 reflectance value,

$$I_{RC} = 0.8 \cdot 902 \text{ W/m}^2 (0.121 + \sin 76.4°)\left(\frac{1 - \cos 52°}{2}\right) = 152 \text{ W/m}^2$$

So total insolation is now 937 W/m^2, a 14% increase with snow on the ground.

While these clear-sky calculations look tedious, they are easily converted into a simple spreadsheet, such as the one shown in Figure 4.26.

FIGURE 4.26 A straightforward spreadsheet to calculate clear-sky insolation. Data entries correspond to Examples 4.8–4.11.

CLEAR SKY INSOLATION CALCULATOR			Month	n
Day number n	141	ENTER	1-Jan	1
Latitude (°)	33.7	ENTER (+ for Northern Hemisphere)	1-Feb	32
Collector azimuth φc (°)	20	ENTER (+ is East of local meridian)	1-Mar	60
Collector tilt Σ(°)	52	ENTER	1-Apr	91
Solar time ST (24 hr)	12	ENTER	1-May	121
Hour angle H	0	H = 15°/hr x (12-ST) (4.10)	1-Jun	152
Declination δ (°)	20.14	δ = 23.45sin(360/365(n-81)) (4.7)	1-Jul	182
Altitude angle β (°)	76.44	β = ASIN((cosL cosδ cosH+sinL sinδ) (4.8)	1-Aug	213
Air mass ratio m	1.03	m = ((708*sinβ)^2+1417)^05-708*sinβ (4.21)	1-Sep	244
A (W/m^2)	1104	A = 1160 + 75 sin(360/365(n-275)) (4.22)	1-Oct	274
k	0.197	k = 0.174 + 0.035sin(360/365(n-100)) (4.23)	1-Nov	305
Ib (W/m^2)	902	Ib = A exp(-k m) (4.21)	1-Dec	335
Solar azimuth > 90°?	NO	"NO" if cosH > tanδ/tanL (4.11)		
Solar azimuth φs (°)	0.00	if("NO",Φs = Asin(cosδ sinH/cosβ),180-Asin(cosδ sinH/cosβ)) (4.9)		
Ibc (W/m^2)	697	Ibc = Ib *(cosβ cos(Φs -Φc) sin(Σ)+sinβ cos (Σ)) (4,24, 4.26)		
C	0.121	C = 0.095 + 0.04sin(360/365(n-100)) (4.28)		
Idc (W/m^2)	88	Idc = C Ib (1+cos Σ)/2 (4.29)		
Reflectance ρ	0.2	ENTER: None = 0, default = 0.2, snow = 0.8		
Irc (W/m^2)	38	Irc = ρ Ib (C+sinβ)(1-cosΣ)/2 (4.31)		
Insolation Ic (W/m^2)	823	Ic = I bc+ Idc + Irc		

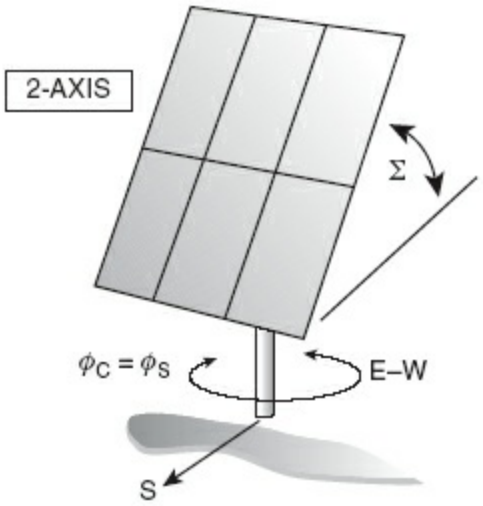
LOCAL TIME CONVERTER:		
Longitude	84.4	ENTER
Local Time Meridian	75	ENTER
B	59.34	B = 360/364(n-81) (4.13)
Eqn of time E (min)	3.53	E = 9.87sin2B - 7.53cosB -1.5sinB (4.12)
Add for CT (min)	34.07	CT - ST = - 4(LTM - LL) - E (4.14)
Clock Time (hr)	12:34 PM	CT = TIME(Hr,Min,0)

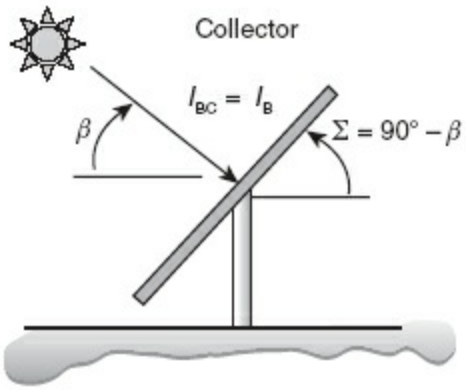
4.10.4 Tracking Systems

Thus far, the assumption has been that the collector is permanently attached to a surface that does not move. In many circumstances, however, racks that allow the collector to track the movement of the sun across the sky are quite cost effective. Trackers are described as being either *two-axis trackers*, which track the sun both in the azimuth and altitude angles so the collectors are always pointing directly at the sun, or *single-axis trackers*, which track only one angle or the other.

Calculating the beam plus diffuse insolation on a two-axis tracker is quite straightforward (Fig. 4.27). The beam radiation on the collector is the full insolation I_B normal to the rays calculated using Equation 4.21. The diffuse and reflected radiation are found using Equations 4.29 and 4.31 with a collector tilt angle equal to the complement of the solar altitude angle; that is, $\Sigma = 90° - \beta$.

FIGURE 4.27 Two-axis tracking angular relationships.





Two-axis tracker:

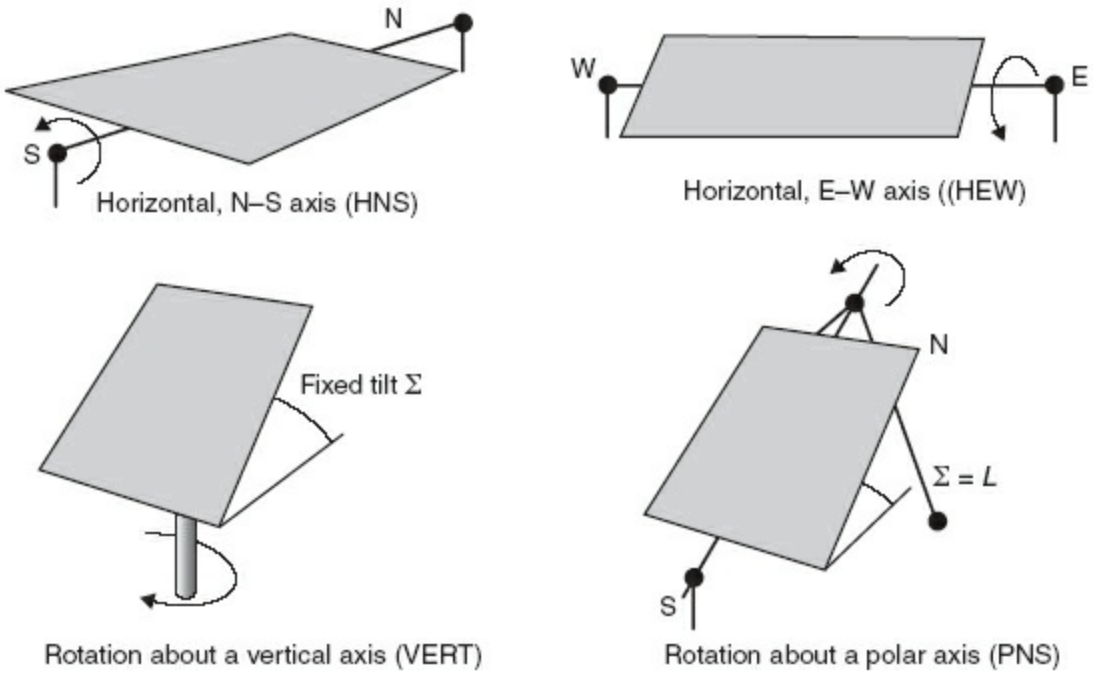
(4.32) $$I_{BC} = I_B$$

(4.33) $$I_{DC} = I_B C \left[\frac{1 + \sin\beta}{2}\right]$$

(4.34) $$I_{RC} = I_B \rho(\sin\beta + C)\left[\frac{1 - \sin\beta}{2}\right]$$

Four ways to do single-axis tracking for solar collectors are shown in Figure 4.28. Two approaches rotate the collectors along a horizontal axis, with either a north–south or an east–west orientation. The other two have a fixed tilt angle; one rotates about a vertical axis and the other about a tilted axis.

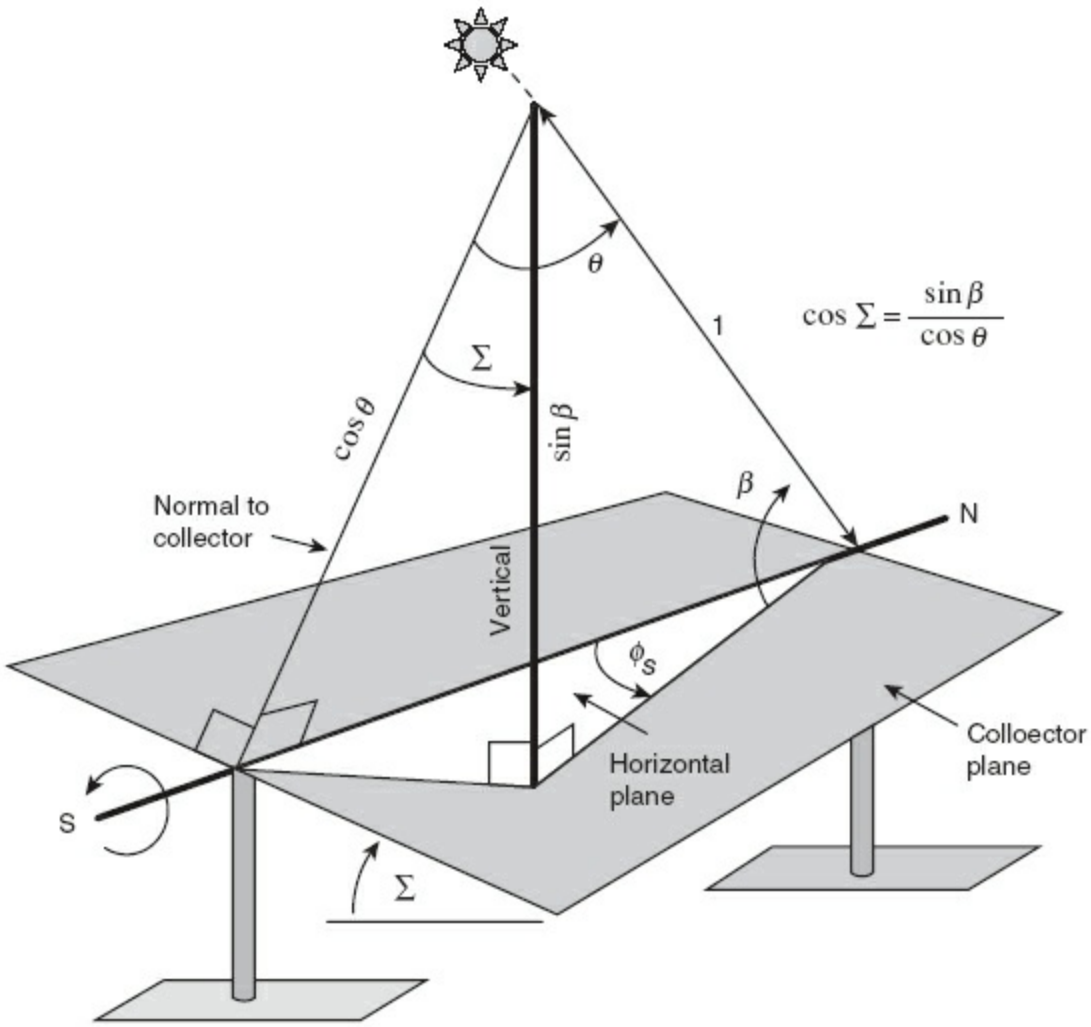
FIGURE 4.28 Four ways to do single-axis tracking.



A geometric analysis for clear-sky radiation on the horizontal, north–south (HNS) axis configuration is shown in Figure 4.29. From the figure, it is relatively easy to derive the tilt angle for the collector as a function of the solar altitude angle β and the incidence angle between sunlight and a normal to the collector, θ:

$$\Sigma = A \cos\left(\frac{\sin\beta}{\cos\theta}\right) \tag{4.35}$$

FIGURE 4.29 Deriving the optimum tilt for a horizontal, north–south oriented, single-axis tracker.



Using the tilt angle from Equation 4.35, the incidence angle between this HNS collector and the incoming beam radiation (Eq. 4.36) provided by Boes (1979), and the diffuse and reflected relationships in Equations 4.33 and 4.34 allow us to write the HNS insolations as *Horizontal, North-South single-axis tracker (HNS):*

$$\cos\theta = \sqrt{1 - (\cos\beta \cos\phi_S)^2} \tag{4.36}$$

$$I_{DC} = I_B C \left[\frac{1 + (\sin\beta / \cos\theta)}{2}\right] \tag{4.37}$$

$$I_{RC} = I_B \rho (C + \sin\beta) \left[\frac{1 - (\sin\beta / \cos\theta)}{2}\right] \tag{4.38}$$

Similar equations for all four of the tracking configurations shown in Figure 4.28 are summarized in Box 4.2.

Example 4.12 Insolation on a Single-Axis Tracker. Continue previous examples and find the insolation on a hoizontal north-south axis tracker at solar noon on May 21 in Atlanta (latitude 33.7°). Take advantage of the calculations already done as shown in the

spreadsheet in Figure 4.26.

Solution. Start with the beam portion of the incident solar radiation, $I_{BC} = I_B \cos \theta$. From Equation 4.36, along with the altitude angle of the sun $\beta = 76.44°$ from Figure 4.26, and the fact that the sun's azimuth angle ϕ_S at solar noon is just 0° gives

$$\text{HNS: } \cos\theta = \sqrt{1 - (\cos\beta \cos\phi_S)^2} = \sqrt{1 - (\cos 76.44 \cdot \cos 0)^2} = 0.972$$

Since I_B was already found to be 902 W/m^2, the beam insolation on the collector is

$$I_{BC} = I_B \cos\theta = 902 \times 0.972 = 877 \text{ W/m}^2$$

Using Equation 4.37, along with the sky diffuse factor $C = 0.121$ from Figure 4.26, gives

$$I_{DC} = I_{DH}\left[\frac{1 + (\sin\beta/\cos\theta)}{2}\right] = I_B C\left[\frac{1 + (\sin\beta/\cos\theta)}{2}\right]$$

$$= 902 \times 0.121\left[\frac{1 + \sin 76.44/0.972}{2}\right] = 109 \text{ W/m}^2$$

And finally, from Equation 4.38, the reflected radiation (assuming a reflectance factor ρ of 0.20) is

$$I_{RC} = \rho I_H\left[\frac{1 - (\sin\beta/\cos\theta)}{2}\right] = I_B\rho\,(C + \sin\beta)\left[\frac{1 - (\sin\beta/\cos\theta)}{2}\right]$$

$$= 902 \times 0.20(0.121 + \sin 76.44)\left[\frac{1 - \sin 76.44/0.972}{2}\right] = 0$$

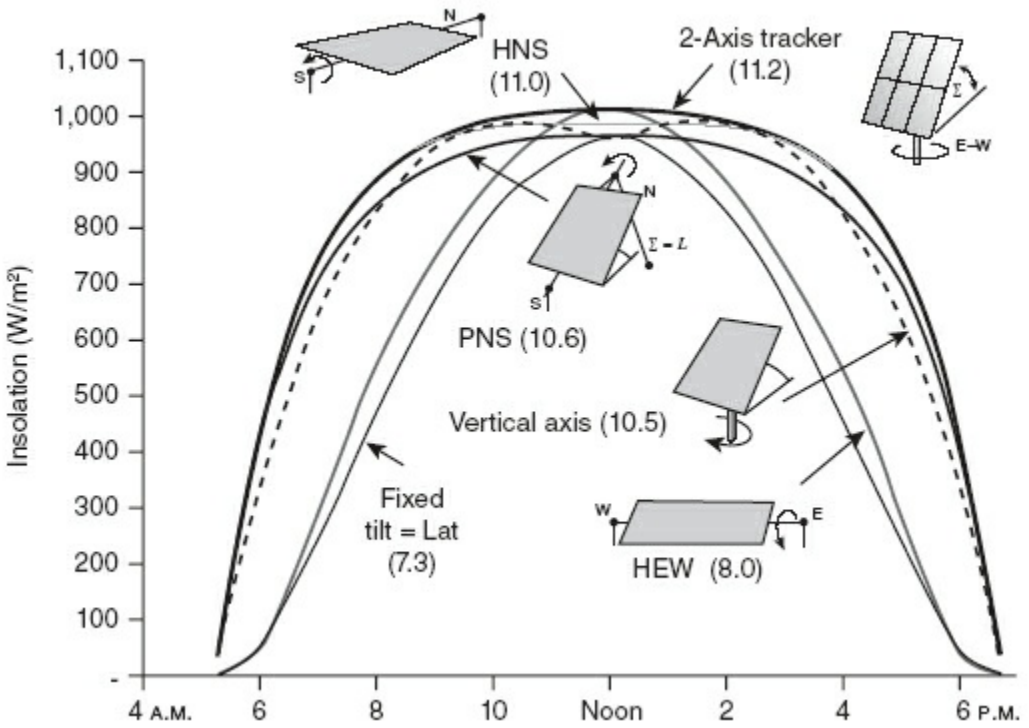
The radiation reflected from the ground onto the collector face is negligible since the collector is pointing straight up toward the sky at solar noon.

Total radiation on the tracker is therefore

$$I_C = I_{BC} + I_{DC} + I_{RC} = 877 + 109 + 0 = 986 \text{ W/m}^2$$

The above process, repeated hour-by-hour for all five trackers, along with a south-facing polar tilt fixed collector, produces the results shown in Figure 4.30. Included in the figure are total kWh/m^2/d of solar insolation for each collector. Later we will see that those units can also be interpreted as being the equivalent of hours per day of full sunshine. Thus the fixed array would be exposed to the equivalent of 7.3 h of full sun on a clear day in Atlanta, while the two-axis tracker sees 11.2 h of sun; that is a 53% improvement. The HNS collector (11.0 h of full sun) and the vertical-axis collector (10.5 h) do almost as well as the full, more expensive, double-axis tracking system. The single-axis, east–west collector (8.0 h) is hardly better than a fixed array, which means this east–west approach is unlikely to be used.

FIGURE 4.30 Comparing clear-sky insolation striking various trackers and fixed a fixed tilt collector on May 21, latitude 33.7° (Atlanta). Numbers in parentheses are kWh/m^2/d.



To assist in keeping this whole set of clear-sky insolation relationships straight, Box 4.2 offers a helpful summary of nomenclature and equations. And, obviously, working with these equations is tedious until they have been put onto a spreadsheet. Or, for most purposes it is sufficient to look up values in a table, and if necessary, do some interpolation. In Appendix D, there are tables of hour-by-hour clear-sky insolation for various tilt angles and latitudes, an example of which is given here in Table 4.6.

TABLE 4.7 Daily and Annual Clear-Sky Insolation (Beam Plus Diffuse) for Various Fixed-Orientation Collectors, Along with One- and Two-Axis Trackers

Daily Clear-Sky Insolation (kWh/m²) Latitude 40° N																				
Azim:	S							SE/SW						E, W					Tracking	
Tilt:	0	20	30	40	50	60	90	20	30	40	50	60	90	20	30	40	50	60	90	One-axis	Two-axis
Jan	3.0	4.6	5.2	5.7	6.0	6.2	5.5	4.1	4.5	4.7	4.9	4.9	4.0	2.9	2.8	2.7	2.6	2.4	1.7	6.8	7.2
Feb	4.2	5.8	6.3	6.6	6.8	6.7	5.4	5.3	5.6	5.7	5.7	5.5	4.2	4.1	3.9	3.7	3.5	3.3	2.2	8.2	8.3
Mar	5.8	6.9	7.2	7.3	7.1	6.8	4.7	6.5	6.6	6.6	6.4	6.0	4.1	5.5	5.3	5.0	4.6	4.3	2.8	9.5	9.5
Apr	7.2	7.7	7.7	7.4	6.9	6.2	3.3	7.5	7.4	7.1	6.6	6.1	3.7	6.9	6.6	6.2	5.7	5.2	3.3	10.3	10.6
May	8.1	8.0	7.7	7.1	6.4	5.5	2.3	8.0	7.6	7.2	6.5	5.8	3.2	7.7	7.3	6.8	6.2	5.5	3.5	10.2	11.0
Jun	8.3	8.1	7.6	7.0	6.2	5.2	1.9	8.0	7.6	7.1	6.4	5.6	3.0	7.8	7.4	6.9	6.3	5.6	3.4	9.9	11.0
Jul	8.0	7.9	7.6	7.0	6.3	5.5	2.2	7.9	7.5	7.1	6.4	5.7	3.2	7.6	7.2	6.7	6.1	5.5	3.4	10.0	10.7
Aug	7.1	7.5	7.5	7.2	6.7	6.0	3.2	7.3	7.2	6.9	6.5	5.9	3.6	6.7	6.4	6.0	5.5	5.0	3.2	9.8	10.1
Sept	5.6	6.7	6.9	7.0	6.9	6.5	4.5	6.3	6.4	6.3	6.1	5.8	4.0	5.4	5.2	4.9	4.5	4.1	2.7	9.0	9.0
Oct	4.1	5.5	6.0	6.3	6.4	6.4	5.1	5.0	5.3	5.4	5.4	5.2	4.0	3.9	3.7	3.6	3.3	3.1	2.1	7.7	7.8
Nov	2.9	4.5	5.1	5.5	5.8	5.9	5.3	3.9	4.3	4.6	4.7	4.7	3.9	2.8	2.7	2.6	2.5	2.3	1.6	6.5	6.9
Dec	2.5	4.1	4.7	5.2	5.5	5.7	5.2	3.6	3.9	4.2	4.4	4.4	3.8	2.4	2.3	2.2	2.1	2.0	1.4	6.5	6.5
Total	2029	2352	2415	2410	2342	2208	1471	2231	2249	2216	2130	1997	1357	1938	1848	1738	1612	1467	960	3167	3305

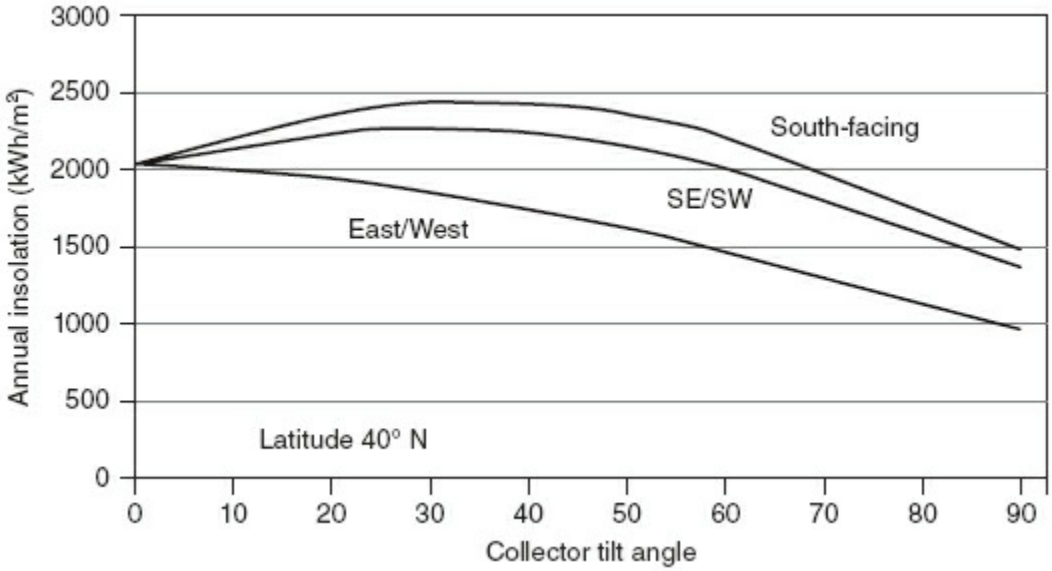
Tables for other latitudes are in Appendix E.

4.11 MONTHLY CLEAR-SKY INSOLATION

The instantaneous insolation equations just presented can be tabulated into daily, monthly, and annual values that, even though they are just clear-sky values, provide considerable

insight into the impact of collector orientation. For example, Table 4.7 presents monthly and annual clear-sky insolation on collectors with various azimuth and tilt angles, as well as for 1- and 2-axis tracking mounts, for latitude 40° N. They have been computed as the sum of just the beam plus diffuse radiation, which ignores the usually modest reflective contribution. Similar tables for other latitudes are given in Appendix E. When plotted, as has been done in Figure 4.31, it becomes apparent that *annual* performance is relatively insensitive to wide variations in collector orientation for nontracking systems. For this latitude, the annual insolation for south-facing collectors varies by less than 10% for collectors mounted with tilt angles ranging anywhere from 10° to 60°. And, only a modest degradation is noted for panels that do not face due south. For a 45° collector azimuth angle (southeast, southwest), the annual insolation available drops by less than 10% in comparison with south-facing panels at similar tilt angles.

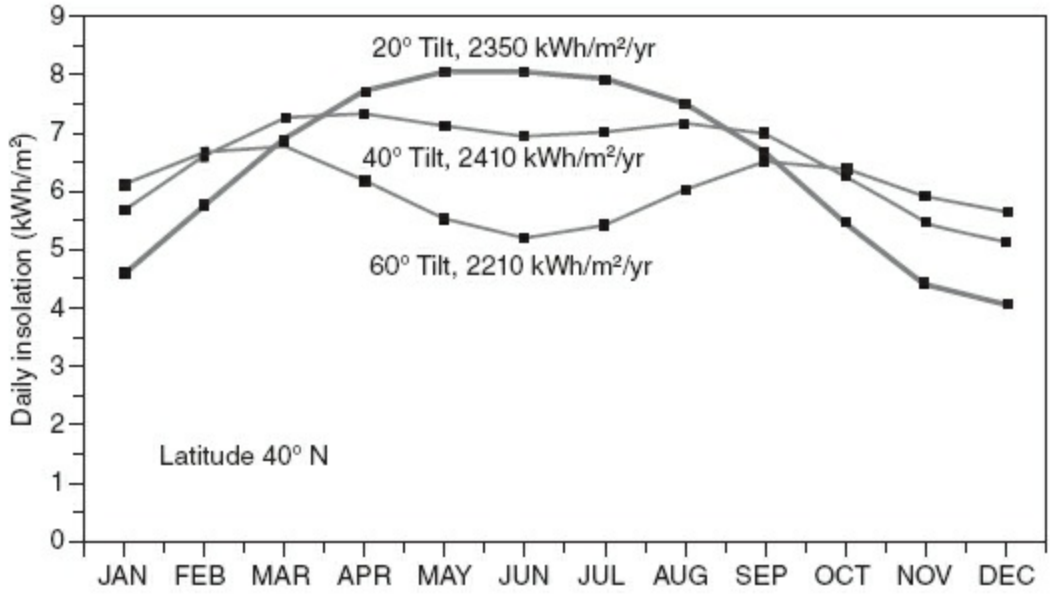
FIGURE 4.31 Annual insolation, assuming all clear days, for collectors with varying azimuth and tilt angles. Annual amounts vary only slightly over quite a range of collector tilt and azimuth angles.



While Figure 4.31 seems to suggest orientation is not critical, remember that it has been plotted for *annual insolation* without regard to monthly distribution. For a grid-connected photovoltaic system, for example, that may be a valid way to consider orientation. Deficits in the winter are automatically offset by purchased utility power, and any extra electricity generated during the summer can simply go back onto the grid. For a stand-alone PV system, however, where batteries or a generator provide backup power, it is quite important to try to smooth out the month-to-month energy delivered to minimize the size of the backup system needed in those low-yield months.

A graph of monthly insolation, instead of the annual plots given in Figure 4.31, shows dramatic variations in the pattern of monthly solar energy for different tilt angles. Such a plot for three different tilt angles at latitude 40°, each having nearly the same annual insolation, is shown in Figure 4.32. As shown, a collector at the modest tilt angle of 20° would do well in the summer, but deliver very little in the winter, so it would not be a very good angle for a stand-alone PV system. At 40° or 60°, the distribution of radiation is more uniform and would be more appropriate for such systems.

FIGURE 4.32 Daily clear-sky insolation on south-facing collectors with varying tilt angles. Even though they all yield roughly the same annual energy, the monthly distribution is very different.



BOX 4.2 Summary of Clear-Sky Solar Insolation Equations

I_0	=	extraterrestrial solar insolation
m	=	air mass ratio
I_B	=	beam insolation at the earth's surface = I_{DNI}
A	=	apparent extraterrestrial solar insolation
k	=	atmospheric optical depth
C	=	sky diffuse factor
I_{BC}	=	beam insolation on collector
θ	=	incidence angle
Σ	=	collector tilt angle
I_H	=	insolation on a horizontal surface = I_{GHI}
I_{DH}	=	diffuse insolation on a horizontal surface = I_{DHI}
I_{DC}	=	diffuse insolation on collector
I_{RC}	=	reflected insolation on collector
ρ	=	ground reflectance
I_C	=	insolation on collector

$$I_0 = 1370\left[1 + 0.034\cos\left(\frac{360n}{365}\right)\right] \tag{4.19}$$

$$m = \sqrt{(708\sin\beta)^2 + 1417} - 708\sin\beta \tag{4.21}$$

(4.20) $$I_B = Ae^{-km}$$

$$A = 1160 + 75 \sin\left[\frac{360}{365}(n - 275)\right] \ (\mathrm{W/m^2})$$
(4.22)

$$k = 0.174 + 0.035 \sin\left[\frac{360}{365}(n - 100)\right]$$
(4.23)

(4.24) $$I_{BC} = I_B \cos\theta \quad \text{(for all orientations)}$$

$$I_C = I_{BC} + I_{DC} + I_{RC}$$

Fixed orientation:

(4.26) $$\cos\theta = \cos\beta \cos(\phi_S - \phi_C) \sin\Sigma + \sin\beta \cos\Sigma$$

$$C = 0.095 + 0.04 \sin\left[\frac{360}{365}(n - 100)\right]$$
(4.28)

$$I_{DC} = I_{DH}\left(\frac{1 + \cos\Sigma}{2}\right) = I_B C\left(\frac{1 + \cos\Sigma}{2}\right)$$
(4.29)

$$I_{RC} = \rho I_H\left(\frac{1 - \cos\Sigma}{2}\right) = I_B \rho\,(C + \sin\beta)\left(\frac{1 - \cos\Sigma}{2}\right)$$
(4.31)

Two-axis tracking:

$$\cos\theta = 1$$

$$I_{DC} = I_{DH}\left(\frac{1 + \sin\beta}{2}\right) = I_B C\left(\frac{1 + \sin\beta}{2}\right)$$
(4.33)

$$I_{RC} = \rho I_H\left(\frac{1 - \sin\beta}{2}\right) = I_B \rho\,(C + \sin\beta)\left(\frac{1 - \sin\beta}{2}\right)$$
(4.34)

One-axis, horizontal, north-south (HNS):

(4.36) $$\cos\theta = \sqrt{1 - (\cos\beta \cos\phi_S)^2}$$

$$I_{DC} = I_{DH}\left[\frac{1 + (\sin\beta/\cos\theta)}{2}\right] = I_B C\left[\frac{1 + (\sin\beta/\cos\theta)}{2}\right]$$
(4.37)

(4.38)

$$I_{RC} = \rho I_H\left[\frac{1 - (\sin\beta/\cos\theta)}{2}\right] = I_B \rho\,(C + \sin\beta)\left[\frac{1 - (\sin\beta/\cos\theta)}{2}\right]$$

One-axis, horizontal, east–west (HEW):

(4.39) $$\cos\theta = \sqrt{1 - (\cos\beta \sin\phi_S)^2}$$

$$I_{DC} = I_{DH}\left[\frac{1+(\sin\beta/\cos\theta)}{2}\right] = I_B C\left[\frac{1+(\sin\beta/\cos\theta)}{2}\right] \quad (4.40)$$

(4.41)

$$I_{RC} = \rho I_H\left[\frac{1-(\sin\beta/\cos\theta)}{2}\right] = I_B\rho\,(C+\sin\beta)\left[\frac{1-(\sin\beta/\cos\theta)}{2}\right]$$

One-axis, polar mount, north–south (PNS)

$$\cos\theta = \cos\delta \quad (4.42)$$

$$I_{DC} = I_{DH}\left[\frac{1+\sin(\beta-\delta)}{2}\right] = I_B C\left[\frac{1+\sin(\beta-\delta)}{2}\right] \quad (4.43)$$

(4.44)

$$I_{RC} = \rho I_H\left[\frac{1-\sin(\beta-\delta)}{2}\right] = I_B\rho\,(C+\sin\beta)\left[\frac{1-\sin(\beta-\delta)}{2}\right]$$

One-axis, vertical mount: tilt = Σ (VERT):

$$\cos\theta = \sin(\beta+\Sigma) \quad (4.28)$$

$$I_{DC} = I_{DH}\left(\frac{1+\cos\Sigma}{2}\right) = I_B C\left(\frac{1+\cos\Sigma}{2}\right) \quad (4.29)$$

$$I_{RC} = \rho I_H\left[\frac{1-\cos\Sigma}{2}\right] = I_B\rho\,(C+\sin\beta)\left[\frac{1-\cos\Sigma}{2}\right] \quad (4.31)$$

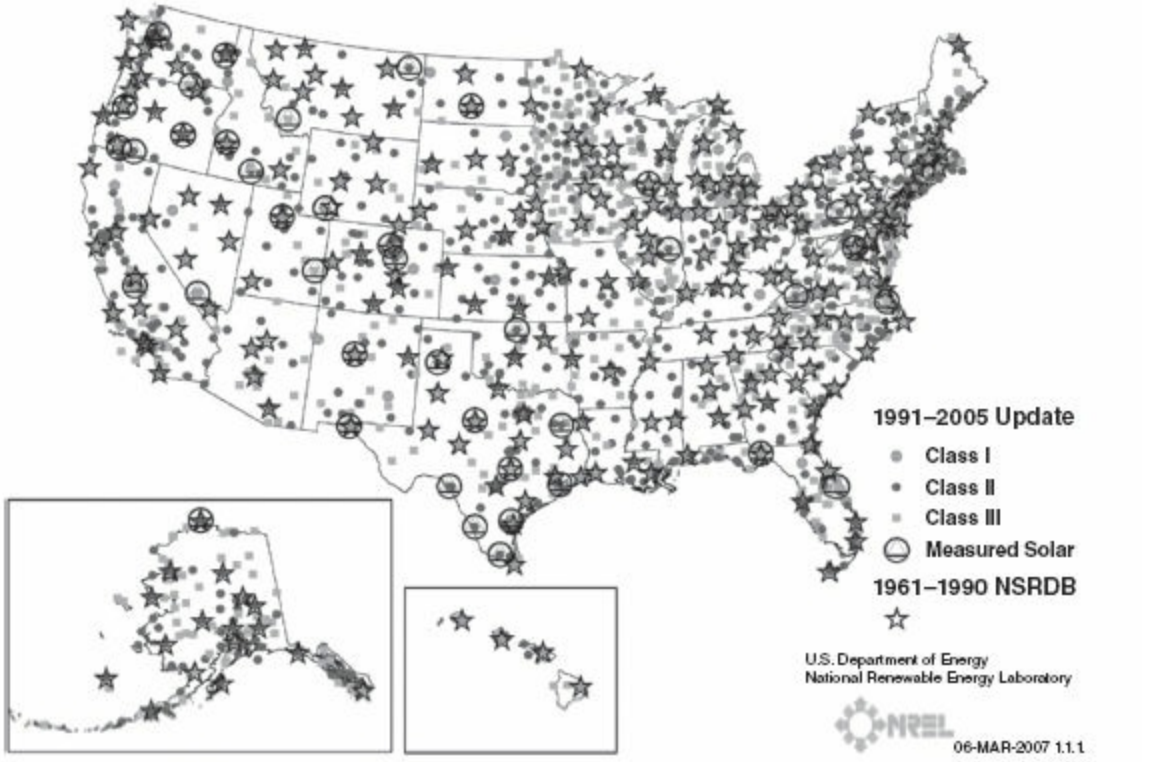
4.12 SOLAR RADIATION MEASUREMENTS

Creation of solar energy databases began in earnest in the United States in the 1970s by the National Oceanic and Atmospheric Administration (NOAA) and later by the National Renewable Energy Laboratory (NREL). In 1995, NREL established the original National Solar Radiation Data Base (NSRDB) for 239 sites in the United States. Of these, only 56 were primary stations for which long-term solar measurements had been made, while data for the remaining 183 sites were based on estimates derived from models incorporating meteorological data such as cloud cover. The World Meteorological Organization (WMO), through its World Radiation Data Center in Russia, continues to compile data for hundreds of other sites around the world. Later, models based on satellite imagery from the Geostationary Operational Environment Satellite (GOES) were developed that compared radiation reflected off the top of clouds with measured irradiance on the earth's surface. Extensions of those models now allow satellite data to be used to create irradiance estimates on an hour-by-hour basis over a 10-km grid for all 50 states.

The 1991–2005 NSRDB contains 1454 sites subdivided into three classifications. Class I Stations have a complete period of record (all hours 1991–2005) for solar and key meteorological fields and have the highest quality solar-modeled data (221 sites). Class II (637 sites) and Class III stations (596 sites) have lower quality datasets. A map of these

stations is shown in Figure 4.33.

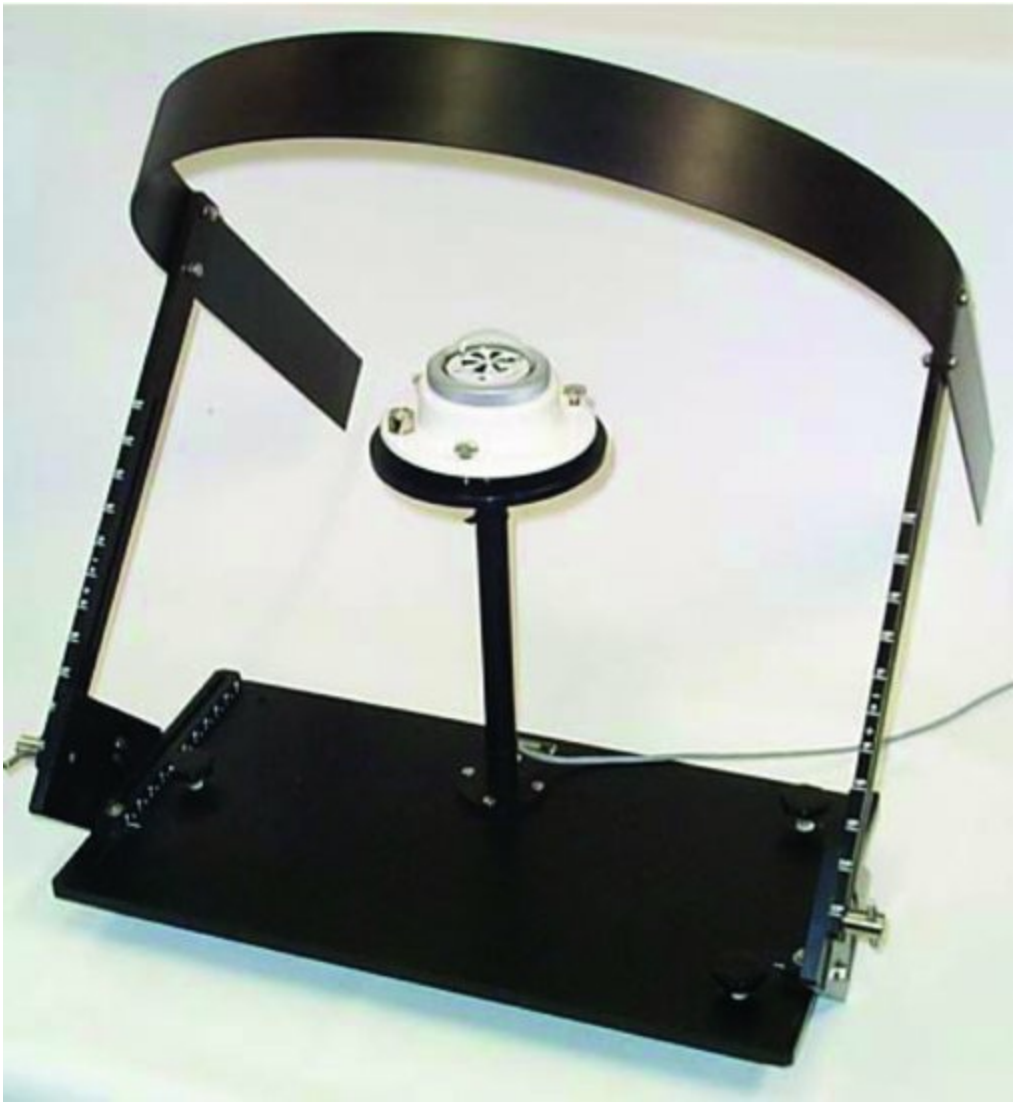
FIGURE 4.33 Map showing the original 239 National Solar Radiation Data Base (NSRDB) stations augmented with newer sites. From NREL (1998).



There are two principle types of devices used to measure solar radiation at the earth's surface. The most widely used instrument, called a *pyranometer* measures the total radiation arriving from all directions, including both direct and diffuse components. That is, it measures all of the radiation that is of potential use to a solar collecting system. The other device, called a *pyrheliometer*, looks at the sun through a narrow, collimating tube, so it measures only the direct beam radiation. Data collected by pyrheliometers are especially important for focusing collectors since their solar resource is pretty much restricted to just the beam portion of incident radiation.

Pyranometers and pyrheliometers can be adapted to obtain other useful data. For example, as shall be seen in the next section, the ability to sort out the direct from the diffuse is a critical step in the conversion of measured insolation on a horizontal surface into estimates of radiation on tilted collectors. By temporarily affixing a shade ring to block the direct beam, a pyranometer can be used to measure just diffuse radiation (Fig. 4.34). By subtracting the diffuse from the total the beam portion can then be determined. In other circumstances, it is important to know not only how much radiation the sun provides, but also how much it provides within certain ranges of wavelengths. For example, newspapers now routinely report on the UV portion of the spectrum to warn us about skin cancer risks. That sort of data can be obtained by fitting pyranometers or pyrheliometers with filters to allow only certain wavelengths to be measured.

FIGURE 4.34 Pyranometer with a shade ring to measure diffuse radiation.



The most important part of a pyranometer or pyrheliometer is the detector that responds to incoming radiation. The most accurate detectors use a stack of thermocouples, called a thermopile, to measure how much hotter a black surface becomes when exposed to sunlight. The most accurate of these incorporate a sensor surface that consists of alternating black and white segments (Fig. 4.35). The thermopile measures the temperature difference between the black segments, which absorb sunlight, and the white ones, which reflect it, to produce a voltage that is proportional to insolation. Other thermopile pyranometers have sensors that are entirely black and the temperature difference is measured between the case of the pyranometer, which is close to ambient, and the hotter, black sensor.

FIGURE 4.35 A thermopile-type, black-and-white pyranometer (a) and a Li-Cor silicon-cell pyranometer (b).



(a) (b)

The alternative approach uses a photodiode sensor that sends a current through a calibrated resistance to produce a voltage proportional to insolation. These pyranometers are less expensive but are also less accurate than those based on thermopiles. Unlike thermopile sensors, which measure all wavelengths of incoming radiation, photoelectric sensors respond to only a limited portion of the solar spectrum. The most popular devices use silicon photosensors, which means any photons with longer wavelengths than their band-gap of 1.1 μm do not contribute to the output. Photoelectric pyranometers are calibrated to produce very accurate results under clear skies, but if the solar spectrum is altered, as for example when sunlight passes through glass or clouds, they will not be as accurate as a pyranometer that uses a thermopile sensor. And, they do not respond accurately to artificial light.

4.13 SOLAR INSOLATION UNDER NORMAL SKIES

Thus far, we have considered only clear-sky solar radiation, which obviously has limited practical value. Of greater importance is estimating the radiation that will be seen on a collector under more realistic conditions.

In this section, two approaches will be described. The first converts hourly beam and diffuse solar radiation data provided by the NSRDB into hour-by-hour estimates of insolation on a collector surface. With 8760 h/yr to manipulate, this does not lend itself to simple hand calculations, though it is an easy task when done on a computer. The second starts with more basic data—monthly measured average horizontal irradiation—and converts those into estimated monthly insolation on a south-facing collector surface.

4.13.1 TMY Insolation on a Solar Collector

The NSRDB provides the starting point for creation of what is called a *typical meteorological year* (TMY) database of location-specific hour-by-hour insolation and weather data. These data are selected to represent the range of weather phenomena likely to be encountered for the location, while maintaining the yearlong averages that the original data provide. The third iteration of TMY data (referred to as TMY3) can be downloaded

from the NREL website (http:// rredc.nrel.gov/solar/old_data/nsrdb/1991-2005/tmy3/).

TMY insolation data provide hour-by-hour estimates of both normal (perpendicular) and horizontal (relative to the earth's surface) extraterrestrial irradiation (ETRN and ETR), Global Horizontal Irradiance (GHI), Direct Normal Irradiance (DNI), and Diffuse Horizontal Irradiance (DHI) as well as wind, temperature, humidity, illuminance, and precipitation. These data are important for renewable energy systems, but also they are fundamental to modeling the performance of building energy systems.

Using equations already developed, it is quite straightforward to convert terrestrial DNI and DHI data into hourly irradiation onto any of the tracking or fixed-orientation solar collector configurations shown in Figure 4.30. The following equations form the basis for the analysis:

$$I_{BC} = I_B \cos\theta = \text{DNI} \cos\theta \tag{4.48}$$

$$I_{DC} = I_{DH}\left(\frac{1+\cos\Sigma}{2}\right) = \text{DHI}\left(\frac{1+\cos\Sigma}{2}\right) \tag{4.49}$$

$$I_{RC} = \rho I_{BH}\left(\frac{1-\cos\Sigma}{2}\right) = \text{GHI}\cdot\rho\left(\frac{1-\cos\Sigma}{2}\right) \tag{4.50}$$

The two quantities that need to be worked out are the incidence angle factor, cos θ, and something related to the collector tilt angle Σ. Box 4.2 already shows how those factors were dealt with under clear-sky conditions for the fixed collector orientation as well as the range of tracking options.

Example 4.13 Converting TMY data to Collector Irradiance. Return to the Atlanta example that we have already worked on (Latitude 33.7°, May 21 n = 141, solar noon, tilt Σ = 52°, collector azimuth ϕ_C = 20° to the southeast, solar altitude β = 76.44°, solar azimuth ϕ_S = 0°) for which we found the total clear-sky insolation to be 823 W/m^2.

The TMY data for Atlanta, May 21 show GHI = 880 W/m^2, DNI = 678 W/m^2, and DHI = 242 W/m^2. Find the insolation on the collector. Repeat the calculation for a single-axis tracker with north–south orientation (HNS).

Solution. From Equation 4.26 in Box 4.2

$$\cos\theta = \cos\beta\cos(\phi_S - \phi_C)\sin\Sigma + \sin\beta\cos\Sigma$$
$$= \cos 76.44^\circ \cos(0 - 20^\circ)\sin 52^\circ + \sin 76.44^\circ \cos 52^\circ = 0.772$$

Fixed orientation:

From Equation 4.48: $I_{BC} = \text{DNI}\cos\theta = 678 \times 0.772 = 524\ \text{W/m}^2$

From Equation 4.49:

$$I_{DC} = \text{DHI}\left(\frac{1+\cos\Sigma}{2}\right) = 242\left(\frac{1+\cos 52^\circ}{2}\right) = 195\ \text{W/m}^2$$

From Equation 4.50:

$$I_{RC} = \text{GHI}\cdot\rho\left(\frac{1-\cos\Sigma}{2}\right) = 880 \times 0.2\left(\frac{1-\cos 52^\circ}{2}\right) = 34\ \text{W/m}^2$$

Total insolation: I_C = 524 + 195 + 34 = 753 W/m^2

Horizontal north-south orientation:

For the HNS collector, use Equations 4.36–4.38 from Box 4.2 to give

$$\cos\theta = \sqrt{1-(\cos\beta\cos\phi_S)^2} = \sqrt{1-(\cos 76.44^\circ\cos 0^\circ)^2} = 0.972$$

$$I_{BC} = \text{DNI}\cos\theta = 678 \times 0.972 = 659\ \text{W/m}^2$$

$$I_{DC} = \text{DHI}\left[\frac{1+(\sin\beta/\cos\theta)}{2}\right] = 242\left[\frac{1+(\sin 76.44^\circ/0.972)}{2}\right]$$
$$= 242\ \text{W/m}^2$$

This should make sense since at solar noon an HNS is parallel to the ground so all of DHI lands on the collector face.

$$I_{RC} = \rho\cdot\text{GHI}\left[\frac{1-(\sin\beta/\cos\theta)}{2}\right] = 0.2 \times 880\left[\frac{1-(\sin 76.44/0.972)}{2}\right]$$
$$= 0\ \text{W/m}^2$$

(Again, with the collector parallel to the ground, there is no reflection)

Total insolation (HNS): $I_C = 659 + 242 + 0 = 901\ \text{W/m}^2$

The slight discrepancy between measured GHI = 880 Wh/hm^2 and our calculated value of 901 W/m^2 can be explained by the fact that GHI is measured over a full hour's time, while our value is an instantaneous value at the peak time of solar noon.

Obviously, all of these equations are tedious, but they are not hard to transfer into simple spreadsheets. Figure 4.36 shows one spreadsheet implementation that suggests how TMY data might be coupled with Box 4.2 equations to estimate hour-by-hour insolation onto collectors.

FIGURE 4.36 Converting TMY data into hourly insolation onto a collector surface. Data correspond to Examples 4.8–4.13. TMY data are for Atlanta.

Day number n		141	ENTER			
Latitude L		33.7	ENTER			
Collector azimuth ϕ_C		20	ENTER			
Collector tilt Σ		52	ENTER			
Declination δ (°)		20.14	$\delta = 23.45\sin(360/365\ (n\text{-}81))$			
Reflectance ρ		0.2	ENTER			

TMY Time	TMY GHI	TMY DNI	TMY DHI	β (4.8)	ϕ_S (4.9)	cosθ (4.26)	I_C (W/m²)
5.00	0	0	0	−0.64	114.92	0.000	–
6.00	11	13	10	11.01	106.97	0.159	11
7.00	109	303	55	23.15	99.49	0.374	162
8.00	317	667	64	35.56	91.83	0.558	436
9.00	425	329	237	48.02	82.97	0.697	437
10.00	567	339	319	60.17	70.67	0.783	545
11.00	865	830	151	71.00	48.27	0.808	826
12.00	880	678	242	76.44	0.00	0.772	753
13.00	864	577	303	71.00	−48.27	0.677	669
14.00	842	608	265	60.17	−70.67	0.530	568
15.00	897	718	269	48.02	−82.97	0.339	495
16.00	539	405	235	35.56	−91.83	0.120	259
17.00	470	418	185	23.15	−99.49	0.000	168
18.00	321	519	110	11.01	−106.97	0.000	101
19.00	126	340	57	−0.64	−114.92	0.000	51

4.14 AVERAGE MONTHLY INSOLATION

Historically, most of the long-term collected site-specific data have been insolation measured on a horizontal surface. One approach to convert these older data into expected radiation on a tilted surface depends on sorting out what portion of the total measured horizontal insolation $\bar{I}_H$ is diffuse $\bar{I}_{DH}$ and what portion is direct beam, $\bar{I}_{BH}$.

$$\bar{I}_H = \bar{I}_{DH} + \bar{I}_{BH} \tag{4.51}$$

Once that decomposition has been estimated, adjusting the resulting horizontal radiation into diffuse and reflected radiation on a collecting surface is straightforward and uses equations already presented. Similar steps can be made to deal with beam radiation.

Procedures for decomposing total horizontal insolation into its diffuse and beam components begin by defining a clearness index K_T, which is the ratio of the average horizontal insolation at the site $\bar{I}_H$ to the extraterrestrial insolation on a horizontal surface above the site and just outside the atmosphere, $\bar{I}_0$.

$$\text{Clearness index } K_T = \frac{\bar{I}_H}{\bar{I}_0} \tag{4.52}$$

Usually the clearness index is based on a monthly average and Equation 4.52 can either be computed daily, and those values averaged over the month, or a day in the middle of the month can be used to represent the average monthly condition. A high clearness index corresponds to clear skies in which most of the radiation will be direct beam while a low one indicates overcast conditions having mostly diffuse insolation.

The average daily extraterrestrial insolation on a horizontal surface $\bar{I}_0$ (kWh/m^2/d) can be calculated by averaging the product of the radiation normal to the rays (Eq. 4.19) times the sine of the solar altitude angle (Eq. 4.8) from sunrise to sunset, resulting in

$$\bar{I}_0 = \left(\frac{24}{\pi}\right) \text{SC} \left[1 + 0.034 \cos\left(\frac{360n}{365}\right)\right] (\cos L \cos\delta \sin H_{SR} + H_{SR} \sin L \sin\delta) \tag{4.53}$$

where H_{SR} is the sunrise hour angle (Eq. 4.17) in radians. The extraterrestrial solar constant (SC) used here will be 1.37 kW/m^2.

A number of attempts to correlate clearness index and the fraction of horizontal insolation that is diffuse have been made, including Liu and Jordan (1961) and Collares-Pereira and Rabl (1979). The Liu and Jordan correlation for the horizontal diffuse fraction is as follows:

$$\frac{\bar{I}_{DH}}{\bar{I}_H} = 1.390 - 4.027 K_T + 5.531 K_T^2 - 3.108 K_T^3 \tag{4.54}$$

From Equation 4.54, the diffuse portion of horizontal insolation can be estimated. Then, using Equations 4.29 and 4.30 as if they are average values, the diffuse and reflected radiation on a tilted collector surface are

$$\bar{I}_{DC} = \bar{I}_{DH} \left(\frac{1 + \cos\Sigma}{2}\right) \tag{4.55}$$

and

$$\bar{I}_{RC} = \rho \bar{I}_H \left(\frac{1 - \cos\Sigma}{2}\right) \tag{4.56}$$

where Σ is the collector slope with respect to the horizontal. Equations 4.55 and 4.56 are sufficient for our purposes, but it should be noted that more complex models that do not require the assumption of an isotropic sky are available (Perez et al., 1990).

Average beam radiation on a horizontal surface can be found by subtracting the diffuse portion $\bar{I}_{DH}$ from the total $\bar{I}_H$. To convert the horizontal beam radiation into beam on the collector $\bar{I}_{BC}$, begin by combining Equation 4.25

$$I_{BH} = I_B \sin\beta \tag{4.25}$$

with Equation 4.24

$$I_{BC} = I_B \cos\theta \tag{4.24}$$

to get

$$I_{BC} = I_{BH}\left(\frac{\cos\theta}{\sin\beta}\right) = I_{BH} R_B \tag{4.57}$$

where θ is the incidence angle between the collector and beam, and β is the sun's altitude angle. The quantity in the parentheses is called the *beam tilt factor* R_B.

Equation 4.57 is correct on an instantaneous basis, but since in this section we are working with monthly averages, what is needed is an average value for the beam tilt factor. In the Liu and Jordan procedure, the beam tilt factor is estimated by simply averaging the value of cos θ over those hours of the day in which the sun is in front of the collector and dividing that by the average value of sin β over those hours of the day when the sun is above the horizon. For south-facing collectors at tilt angle Σ, a closed-form solution for those averages can be found and the resulting average beam tilt factor becomes

$$\bar{R}_B = \frac{\cos(L-\Sigma)\cos\delta\sin H_{SRC} + H_{SRC}\sin(L-\Sigma)\sin\delta}{\cos L\cos\delta\sin H_{SR} + H_{SR}\sin L\sin\delta} \tag{4.58}$$

where H_{SR} is the sunrise hour angle (in radians) given in Equation 4.17

$$H_{SR} = \cos^{-1}(-\tan L\tan\delta) \tag{4.17}$$

and H_{SRC} is the sunrise hour angle for the collector (when the sun first strikes the collector face, θ = 90°):

$$H_{SRC} = \min\left\{\cos^{-1}(-\tan L\tan\delta),\quad \cos^{-1}[-\tan(L-\Sigma)\tan\delta]\right\} \tag{4.59}$$

Recall L = latitude, Σ = collector tilt angle, and δ = solar declination.

To summarize the approach, once the horizontal insolation has been decomposed into beam and diffuse components, it can be recombined into the insolation striking a collector using the following

$$\bar{I}_C = \left(1-\frac{\bar{I}_{DH}}{\bar{I}_H}\right)\cdot\bar{R}_B + \bar{I}_{DH}\left(\frac{1+\cos\Sigma}{2}\right) + \rho\bar{I}_H\left(\frac{1-\cos\Sigma}{2}\right) \tag{4.60}$$

where $\bar{R}_B$ can be found for south-facing collectors using Equation 4.58.

Example 4.14 Average Monthly Insolation on a Tilted Collector. Average horizontal

insolation in Oakland, California (latitude 37.73° N) in July is 7.32 kWh/m^2/d. Estimate the insolation on a 30° tilt angle, south-facing collector. Assume ground reflectivity of 0.2.

Solution. Begin by finding mid-month declination and sunrise hour angle for July 16 (day number n = 197):

$$\delta = 23.45 \sin\left[\frac{360}{365}(n - 81)\right] = 23.45 \sin\left[\frac{360}{365}(197 - 81)\right] = 21.35° \tag{4.6}$$

$$H_{SR} = \cos^{-1}(-\tan L \tan\delta)$$

$$= \cos^{-1}(-\tan 37.73° \tan 21.35°) = 107.6° = 1.878 \text{ radians} \tag{4.17}$$

Using a solar constant of 1.37 kW/m^2, the ET horizontal insolation from Equation 4.53 is

$$\bar{I}_0 = \left(\frac{24}{\pi}\right) SC\left[1 + 0.034\cos\left(\frac{360n}{365}\right)\right](\cos L \cos\delta \sin H_{SR} + H_{SR} \sin L \sin\delta)$$

$$= \left(\frac{24}{\pi}\right) 1.37\left[1 + 0.034\cos\left(\frac{360 \cdot 197}{365}\right)^\circ\right](\cos 37.73 \cos 21.35° \sin 107.6°$$

$$+ 1.878 \sin 37.73° \sin 21.35°) = 11.34 \text{ kWh/m}^2\text{/d}$$

From Equation 4.52, the clearness index is

$$K_T = \frac{\bar{I}_H}{\bar{I}_0} = \frac{7.32 \text{ kWh/m}^2\text{/d}}{11.34 \text{ kWh/m}^2\text{/d}} = 0.645$$

From Equation 4.54, the fraction diffuse is

$$\frac{\bar{I}_{DH}}{\bar{I}_H} = 1.390 - 4.027K_T + 5.531K_T^2 - 3.108K_T^3$$

$$= 1.390 - 4.027(0.645) + 5.531(0.645)^2 - 3.108(0.645)^3 = 0.259$$

So, the diffuse horizontal radiation is

$$\bar{I}_{DH} = 0.259 \cdot 7.32 = 1.90 \text{ kWh/m}^2\text{/d}$$

The diffuse radiation on the collector is given by Equation 4.55

$$\bar{I}_{DC} = \bar{I}_{DH}\left(\frac{1 + \cos\Sigma}{2}\right) = 1.90\left(\frac{1 + \cos 30°}{2}\right) = 1.77 \text{ kWh/m}^2\text{/d}$$

The reflected radiation on the collector is given by Equation 4.56

$$\bar{I}_{RC} = \rho\bar{I}_H\left(\frac{1 - \cos\Sigma}{2}\right) = 0.2 \cdot 7.32\left(\frac{1 - \cos 30°}{2}\right) = 0.10 \text{ kWh/m}^2\text{/d}$$

From Equation 4.51, the beam radiation on the horizontal surface is

$$\bar{I}_{BH} = \bar{I}_H - \bar{I}_{DH} = 7.32 - 1.90 = 5.42 \text{ kWh/m}^2\text{/d}$$

To adjust this for the collector tilt, first find the sunrise hour angle on the collector from Equation 4.59

$$H_{SRC} = \min\left\{\cos^{-1}(-\tan L \tan\delta),\quad \cos^{-1}[-\tan(L-\Sigma)\tan\delta]\right\}$$

$$= \min\left\{\cos^{-1}(-\tan 37.73^\circ \tan 21.35^\circ),\right.$$

$$\left.\cos^{-1}[-\tan(37.73-30)^\circ \tan 21.35^\circ]\right\}$$

$$= \min\{107.6^\circ, 93.0^\circ\} = 93.0^\circ = 1.624 \text{ radians}$$

The beam tilt factor (Eq. 4.58) is thus

$$\bar{R}_B = \frac{\cos(L-\Sigma)\cos\delta \sin H_{SRC} + H_{SRC}\sin(L-\Sigma)\sin\delta}{\cos L \cos\delta \sin H_{SR} + H_{SR}\sin L \sin\delta}$$

$$= \frac{\cos(37.73-30)^\circ \cos 21.35^\circ \sin 93^\circ + 1.624 \sin(37.73-30)^\circ \sin 21.35^\circ}{\cos 37.73^\circ \cos 21.35^\circ \sin 107.6^\circ + 1.878 \sin 37.73^\circ \sin 21.35^\circ}$$

$$= 0.893$$

So the beam insolation on the collector is

$$\bar{I}_{BC} = \bar{I}_{BH}\bar{R}_B = 5.42 \cdot 0.893 = 4.84 \text{ kWh/m}^2\text{/d}$$

Total insolation on the collector is thus

$$\bar{I}_C = \bar{I}_{BC} + \bar{I}_{DC} + \bar{I}_{RC} = 4.84 + 1.77 + 0.10 = 6.7 \text{ kWh/m}^2\text{/d}$$

Clearly, with calculations that are this tedious it is worth spending the time to set up a spreadsheet such as the one shown in Figure 4.37 or, better still, use precomputed data available on the web or from publications such as the *Solar Radiation Data Manual for Flat-Plate and Concentrating Collectors* (NREL, 1994). An example of the sort of data available from NREL is shown in Table 4.8. Average total radiation data are given for south-facing collectors with various fixed tilt angles as well as for the polar-axis, north–south tracker (PNS) and the two-axis tracker. In addition, the ranges of insolation for each month are presented, which, along with the figure, gives a good sense of how variable insolation has been during the period in which the actual measurements were made. Also included are values for just the direct beam portion of radiation for concentrating collectors that cannot focus diffuse radiation. The direct-beam data are presented for horizontal collectors in which the tracking rotates about a north–south axis (HNS) or an east–west axis (HES) as well as for the PNS mount.

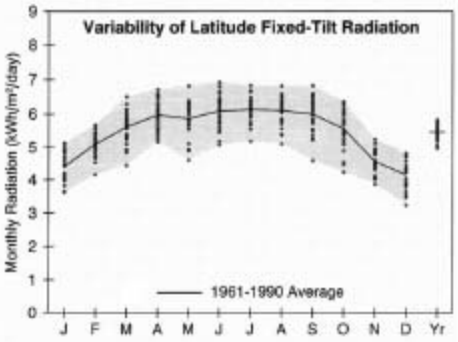
TABLE 4.8 Average Solar Radiation for Boulder, CO (kWh/m^2/d) for Various Collector Configurations

Boulder, CO

WBAN NO. 94018

LATITUDE: 40.02° N
LONGITUDE: 105.25° W
ELEVATION: 1634 meters
MEAN PRESSURE: 836 millibars

STATION TYPE: Primary



Solar Radiation for Flat-Plate Collectors Facing South at a Fixed Tilt (kWh/m²/day), Uncertainty ±9%

Tilt (°)		Jan	Feb	Mar	Apr	May	June	July	Aug	Sept	Oct	Nov	Dec	Year
0	Average	2.4	3.3	4.4	5.6	6.2	6.9	6.7	6.0	5.0	3.8	2.6	2.1	4.6
	Min/Max	2.1/2.7	2.8/3.5	3.7/5.0	4.8/6.1	5.1/7.2	5.7/7.8	5.6/7.4	5.2/6.6	4.0/5.5	3.1/4.2	2.3/2.8	1.9/2.3	4.3/4.8
Latitude -15	Average	3.8	4.6	5.4	6.1	6.2	6.6	6.6	6.3	5.9	5.1	4.0	3.5	5.4
	Min/Max	3.2/4.4	3.8/5.1	4.3/6.2	5.3/6.8	4.9/7.3	5.5/7.6	5.6/7.4	5.3/7.1	4.6/6.7	4.0/5.8	3.4/4.6	2.8/4.1	4.9/5.7
Latitude	Average	4.4	5.1	5.6	6.0	5.9	6.1	6.1	6.1	6.0	5.6	4.6	4.2	5.5
	Min/Max	3.6/5.1	4.2/5.7	4.4/6.5	5.2/6.7	4.6/6.8	5.1/6.9	5.2/6.8	5.1/6.8	4.6/6.8	4.2/6.4	3.9/5.2	3.2/4.8	5.0/5.8
Latitude +15	Average	4.8	5.3	5.6	5.6	5.2	5.2	5.3	5.5	5.8	5.7	4.8	4.5	5.3
	Min/Max	3.9/5.6	4.3/5.9	4.4/6.5	4.8/6.2	4.1/6.0	4.4/5.9	4.5/5.9	4.6/6.2	4.4/6.6	4.2/6.5	4.1/5.6	3.5/5.3	4.8/5.6
90	Average	4.5	4.6	4.3	3.6	2.8	2.6	2.7	3.2	4.0	4.6	4.4	4.3	3.8
	Min/Max	3.6/5.4	3.7/5.2	3.5/5.0	3.0/4.0	2.3/3.1	2.2/2.8	2.3/2.9	2.7/3.6	3.1/4.6	3.4/5.3	3.7/5.1	3.4/5.2	3.4/4.1

Solar Radiation for 1-Axis Tracking Flat-Plate Collectors with a North-South Axis (kWh/m²/day), Uncertainty ±9%

Axis Tilt (°)		Jan	Feb	Mar	Apr	May	June	July	Aug	Sept	Oct	Nov	Dec	Year
0	Average	3.7	4.9	6.2	7.6	8.2	9.1	9.0	8.2	7.1	5.7	4.0	3.3	6.4
	Min/Max	3.0/4.4	4.1/5.5	4.6/7.4	6.2/8.7	6.2/10.0	7.4/10.9	7.1/10.2	6.7/9.3	5.3/8.3	4.2/6.6	3.4/4.4	2.6/3.9	5.7/6.9
Latitude -15	Average	4.8	5.9	7.0	8.1	8.4	9.1	9.1	8.6	7.9	6.7	5.0	4.4	7.1
	Min/Max	3.8/5.6	4.8/6.7	5.1/8.4	6.6/9.2	6.3/10.2	7.4/10.9	7.1/10.3	7.0/9.8	5.8/9.2	4.8/7.8	4.2/5.7	3.3/5.2	6.2/7.6
Latitude	Average	5.2	6.2	7.2	8.0	8.1	8.8	8.7	8.4	7.9	7.1	5.5	4.9	7.2
	Min/Max	4.2/6.2	5.1/7.1	5.2/8.6	6.6/9.2	6.1/9.9	7.1/10.4	6.8/10.0	6.8/9.6	5.8/9.3	5.0/8.2	4.6/6.3	3.6/5.8	6.3/7.8
Latitude +15	Average	5.5	6.4	7.1	7.7	7.7	8.2	8.2	8.0	7.8	7.1	5.7	5.2	7.1
	Min/Max	4.4/6.6	5.2/7.3	5.2/8.6	6.3/8.9	5.8/9.4	6.6/9.8	6.4/9.3	6.5/9.2	5.6/9.1	5.0/8.3	4.8/6.6	3.8/6.2	6.1/7.6

Solar Radiation for 2-Axis Tracking Flat-Plate Collectors (kWh/m²/day), Uncertainty ±9%

Tracker		Jan	Feb	Mar	Apr	May	June	July	Aug	Sept	Oct	Nov	Dec	Year
2-Axis	Average	5.6	6.4	7.2	8.1	8.5	9.4	9.2	8.6	8.0	7.1	5.7	5.3	7.4
	Min/Max	4.5/6.7	5.2/7.3	5.2/8.6	6.7/9.3	6.4/10.4	7.6/11.1	7.2/10.5	7.0/9.8	5.8/9.3	5.1/8.3	4.8/6.6	3.9/6.3	6.5/8.0

Direct Beam Solar Radiation for Concentrating Collectors (kWh/m²/day), Uncertainty ±8%

Tracker		Jan	Feb	Mar	Apr	May	June	July	Aug	Sept	Oct	Nov	Dec	Year
1-Axis, E-W Horiz Axis	Average	3.5	3.7	3.7	4.0	4.2	5.0	4.9	4.5	4.4	4.3	3.6	3.4	4.1
	Min/Max	2.3/4.6	2.8/4.5	2.1/4.8	2.9/5.0	2.9/5.7	3.5/6.4	3.8/6.1	3.4/5.4	2.8/5.5	2.5/5.2	2.7/4.7	2.0/4.3	3.4/4.5
1-Axis, N-S Horiz Axis	Average	2.6	3.4	4.2	5.3	5.6	6.6	6.5	6.0	5.4	4.3	2.8	2.3	4.6
	Min/Max	1.6/3.4	2.5/4.2	2.2/5.7	3.6/6.4	3.8/7.6	4.8/8.5	4.8/8.1	4.5/7.1	3.4/6.7	2.4/5.3	2.2/3.6	1.3/3.0	3.7/5.1
1-Axis, N-S Tilt=Latitude	Average	3.9	4.5	5.0	5.6	5.5	6.2	6.2	6.1	6.0	5.5	4.1	3.6	5.2
	Min/Max	2.5/5.1	3.4/5.5	2.7/6.6	3.8/6.8	3.7/7.5	4.5/8.0	4.6/7.7	4.6/7.3	3.8/7.6	3.1/6.7	3.1/5.3	2.0/4.6	4.2/5.7
2-Axis	Average	4.1	4.6	5.0	5.7	5.8	6.8	6.7	6.3	6.1	5.6	4.3	4.0	5.4
	Min/Max	2.7/5.4	3.5/5.7	2.7/6.6	3.9/6.9	4.0/7.9	4.9/8.7	4.9/8.3	4.8/7.5	3.8/7.6	3.2/6.8	3.3/5.6	2.2/5.0	4.3/6.0

Note: Additional tables are in Appendix G.
Source: From NREL (1994).

FIGURE 4.37 An example spreadsheet to determine monthly insolation estimates from measured horizontal insolation (data correspond to Example 4.14).

Average Monthly Insolation Calculator		
Day number n	197	ENTER
Latitude L (°)	37.79	ENTER (+ for Northern Hemisphere)
Collector azimuth φc (°)	20	ENTER (+ for East of local meridian)
Collector tilt Σ (°)	30	ENTER
Total Horizontal avg I_H (kWh/m2/d)	7.92	ENTER Monthly average
Reflectance ρ	0.2	ENTER: None = 0, default = 0.2, snow = 0.8
Solar Constant SC (kW/m^2)	1.37	Assumed
Mid-mo Declination δ	21.35	δ=23.45sin[(360/365)(n-81)]
Sunrise hour angle H_{SR} (rad)	1.878	H_{SR} =ACOS(-tanL tanδ)+C10+C10
E.T. horizintal insolation I_o avg (kWh/m2/d)	11.34	I_o avg = (24/π)SC[1+0.034cos(360n/365)](cosLcosδsinHSR+HSRsinLsinδ)
Clearness Index K_T	0.645	$KT = I_{H,AVG} / I_{O,AVG}$
Diffuse fraction	0.259	$I_{DH}/I_o = 1.390-0.4027K_T + 5.591\ K_T^2 - 3.108K_T^3$
Diffuse horizontal (kWh/m2/d)	1.90	$I_{DH,AVG} = I_H \times (I_{DH}/I_H)$
Diffuse on collector (kWh/m2/d)	1.77	$I_{DC} = I_{DH}(1+\cos\Sigma)/2$
Reflected on collector (kWh/m2/d)	0.10	$I_{RC} = \rho\ I_{H,AVG}(1-\cos\Sigma)/2$
Horizontal beam insolation, I_{BH} (kWh/m2/d)	5.42	$I_{BH} = I_H - I_{DH}$
Sunrise hour angle on collector H_{SRC} (rad)	1.62	H_{SRC} = min(Acos(-tanLtanδ), Acos(-tan(L-Σ)tanδ)
Beam tilt factor R_B	0.899	$R_B = [\cos(L-\Sigma)\cos\delta\sin H_{SRC} + H_{SRC}\sin(L-\Sigma)\sin\delta]/(\cos L\cos\delta\sin H_{SR} + H_{SR}\sin L\sin\delta)$
Beam insolation on collector I_{BC} (kWh/m2/d)	4.84	$I_{BC} = I_{BH} R_B$
Total collector insolation (kWh/m2/d)	6.7	$I_C = I_{BC} + I_{DC} + I_{RC}$

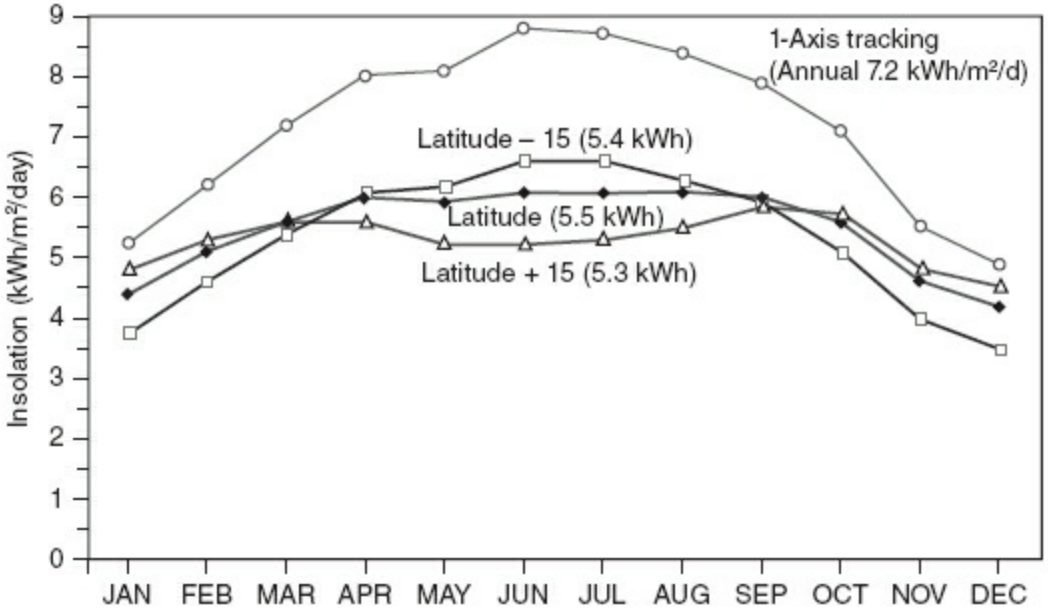
Solar data from the NREL Solar Radiation Manual have been reproduced in Appendix G, a sample of which is shown in Table 4.9

TABLE 4.9 Sample of the Solar Data (kWh/m^2/d) from Appendix G

	Los Angeles, CA: Latitude 33.93° N												
Tilt	Jan	Feb	Mar	Apr	May	June	Jul	Aug	Sept	Oct	Nov	Dec	Year
Lat − 15	3.8	4.5	5.5	6.4	6.4	6.4	7.1	6.8	5.9	5.0	4.2	3.6	5.5
Lat	4.4	5.0	5.7	6.3	6.1	6.0	6.6	6.6	6.0	5.4	4.7	4.2	5.6
Lat + 15	4.7	5.1	5.6	5.9	5.4	5.2	5.8	6.0	5.7	5.5	5.0	4.5	5.4
90	4.1	4.1	3.8	3.3	2.5	2.2	2.4	3.0	3.6	4.2	4.3	4.1	3.5
1-Axis (Lat)	5.1	6.0	7.1	8.2	7.8	7.7	8.7	8.4	7.4	6.6	5.6	4.0	7.0
Temp (°C)	18.7	18.8	18.6	19.7	20.6	22.2	24.1	24.8	24.8	23.6	21.3	18.8	21.3

Radiation data for Boulder are plotted in Figure 4.38. As was the case for clear-sky graphs presented earlier, there is little difference in annual insolation for fixed, south-facing collectors over a wide range of tilt angles, but the seasonal variation is significant. The boost associated with single-axis tracking is large, about 30%.

FIGURE 4.38 Insolation on south-facing collectors in Boulder, CO, at tilt angles equal to the latitude and latitude ± 15°. Values in parentheses are annual averages (kWh/m^2/d). The one-axis tracker with tilt equal to the latitude delivers 30% more annual energy. Data from NREL (1994).



Maps of the seasonal variation in horizontal solar radiation around the world are easily found online. These provide a rough indication of the solar resource and are useful when more specific local data are not conveniently available. The units in these figures are average kWh/m^2/d of insolation, but there is another way to interpret them. On a bright, sunny day with the sun high in the sky, the insolation at the earth's surface is roughly 1 kW/m^2. In fact, that convenient value, 1 kW/m^2, is defined to be *1-sun of insolation*. That means, for example, an average daily insolation of say 5.5 kWh/m^2 is equivalent to 1 kW/m^2 (1-sun) for 5.5 h; that is, it is the same as 5.5 h of full sun. The units on these radiation maps can therefore be thought of as "hours of full sun." As will be seen in the next chapters on photovoltaics, the hours-of-full-sun approach is central to the analysis and design of PV systems.

REFERENCES

The American Ephemeris and Nautical Almanac, published annually by the Nautical Almanac Office, U.S. Naval Observatory, Washington, D.C.

ASHRAE, (1993), *Handbook of Fundamentals*, American Society of Heating, Refrigeration and Air Conditioning Engineers, Atlanta.

Boes, E.C. (1979). *Fundamentals of Solar Radiation.* Sandia National Laboratories, SAND79-0490, Albuquerque, NM.

Collares-Pereira, M., and A. Rabl (1979). The Average Distribution of Solar Radiation–Correlation Between Diffuse and Hemispherical, *Solar Energy*, vol. 22, pp. 155–166.

Liu, B.Y.H., and R.C. Jordan (1961). Daily Insolation on Surfaces Tilted Toward the Equator, *Trans. ASHRAE*, vol. 67, pp. 526–541.

Kuen, T.H., Ramsey, J.W., and J.L. Threlkeld, (1998), *Thermal Environmental Engineering*, 3rd ed., Prentice-Hall, Englewood Cliffs, NJ.

NREL, (1994). *Solar Radiation Data Manual for Flat-Plate and Concentrating Collectors*,

NREL/TP-463-5607, National Renewable Energy Laboratory, Golden, CO.

NREL, (2007). *National Solar Radiation Database 1991–2005 Update: User's Manual*, NREL/TP-581-41364, National Renewable Energy Laboratory, Golden, CO.

Perez, R., Ineichen, P., Seals, R., Michalsky, J., and R. Stewart (1990). Modeling Daylight Availability and Irradiance Components from Direct and Global Irradiance, *Solar Energy*, vol. 44, no. 5, pp. 271–289.

Threlkeld, J.L., and R.C. Jordan (1958). Direct solar radiation available on clear days. *ASHRAE Transactions*, vol. 64, pp. 45.

PROBLEMS

4.1 Consider the design of a "light shelf" for the south side of an office building located at a site with latitude 30°. The idea is that the light shelf should help keep direct sunlight from entering the office. It also bounces light up onto the ceiling to distribute natural daylight more uniformly into the office.

As shown, the window directly above the light shelf is 2-ft high and the window directly below is 4 ft. What should the dimensions X_1 and X_2 be to be sure that no direct sunlight ever enters the space at solar noon?

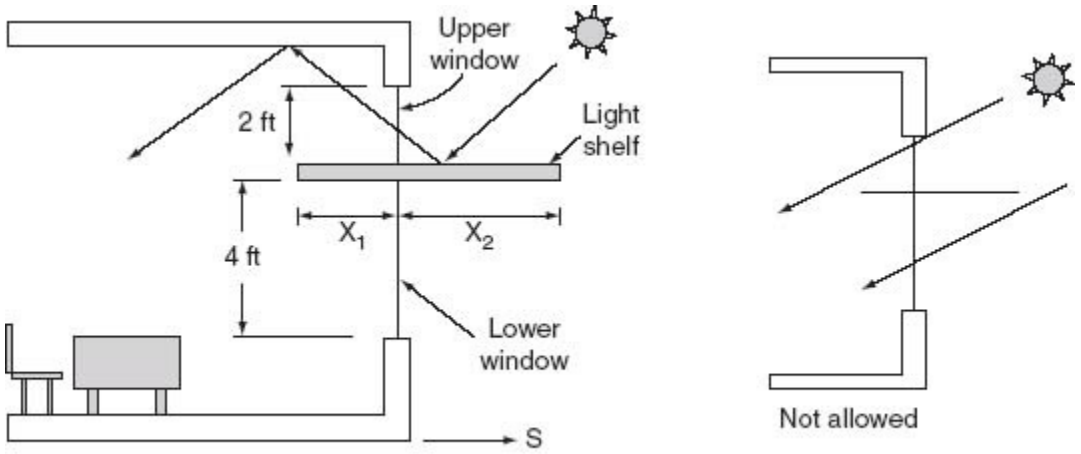


FIGURE P4.1

4.2 Rows of buildings with photovoltaics covering vertical south-facing walls need to have adequate spacing to assure one building does not shade the collectors on another.

a. Using the shadow diagram for 30°N in Appendix F, roughly what ratio of separation distance (*d*) to building height (*H*) would assure no shading anytime between 8:00 A.M. and 4:00 P.M.?

b. If the spacing is such that $d = H$, during what months will the rear building receive full solar exposure.

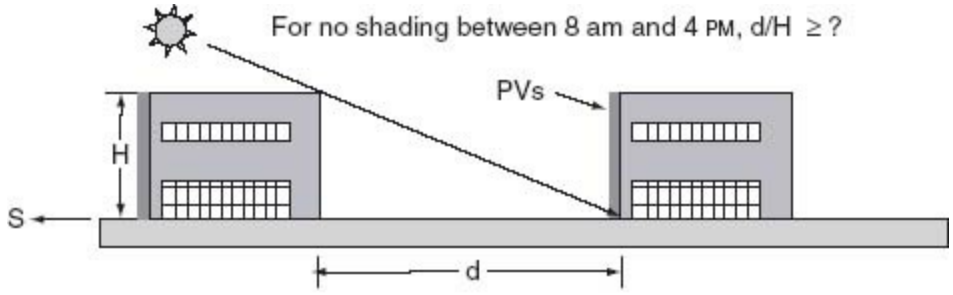


FIGURE P4.2

4.3 Consider the challenge of designing an overhang to help shade a south-facing, sliding-glass patio door. You would like to shade the glass in the summer to help control air-conditioning loads, and you would also like the glass to get full sun in the winter to help provide passive solar heating of the home.

Suppose the slider has a height of 6.5 ft, the interior ceiling height is 8 ft, and the local latitude is 40°.

a. What should be the overhang projection *P* to shade the entire window at solar noon during the solstice in June?

b. With that overhang, where would the shade line, *Y*, be at solar noon on the winter solstice?

c. The shadow distance *Y* for a south-facing window when it is not solar noon is given by

$$Y = \frac{P \tan \beta}{\cos \phi_S}$$

Will the bottom of the shadow on the solstice still entirely shade the window at 10:00 A.M.?

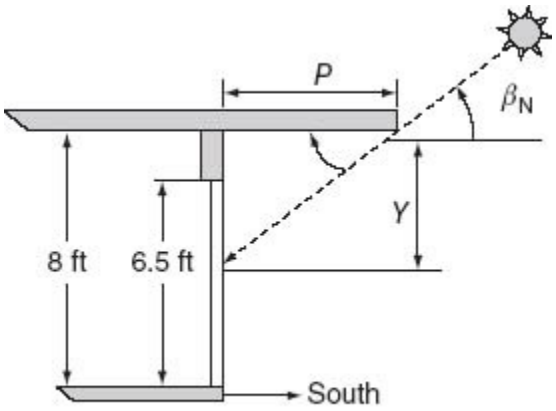


FIGURE P4.3

4.4 Suppose you are concerned about how much shading a tree will cause for a proposed photovoltaic system. Standing at the site with your compass and plumb-bob, you estimate the altitude angle of the top of the tree to be about 30° and the width of the tree to have azimuth angles that range from about 30° to 45° west of south. Your site is at latitude 32°.

Using a sun path diagram (Appendix C), describe the shading problem the tree will pose (approximate shaded times each month).

4.5 Suppose you are concerned about a tall thin tree located 100 ft from a proposed PV site. You do not have a compass or protractor and plumb-bob, but you do notice that an

hour before solar noon on June 21 it casts a 30-ft shadow directly toward your site. Your latitude is 32° N.

a. How tall is the tree?

b. What is its azimuth angle with respect to your site?

c. Using an appropriate sun path diagram from Appendix C, roughly what are the first and last days in the year when the shadow will land on the site?

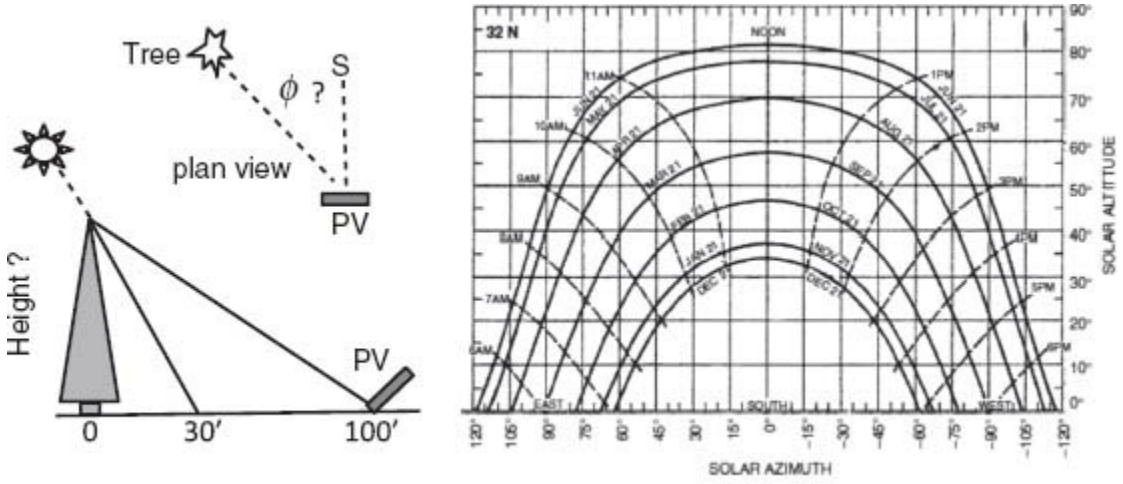


FIGURE P4.5

4.6 Using Figure 4.18, what is the greatest difference between local standard time and solar time for the following locations? At approximately what date would that occur?

a. San Francisco, CA (longitude 122°, Pacific Time Zone)

b. Boston, MA (longitude 71.1°, Eastern Time Zone)

c. Boulder, CO (longitude 105.3°, Mountain Time Zone)

d. Greenwich, England (longitude 0°, local time meridian 0°)

4.7 Calculate the following for (geometric) sunrise in Seattle, latitude 47.63°, longitude 122.33° W (in the Pacific Time Zone), on the summer solstice (June 21st).

a. Find the azimuth angle of sunrise relative to due south.

b. Find the time of sunrise expressed in solar time.

c. Find the local time of sunrise. Compare it to the website http://aa.usno.navy.mil/data/docs/RS_OneDay.html. Why do they differ?

4.8 Suppose it is the summer solstice, June 21 (n = 172) and weather service says sunrise is 4:11 A.M. Pacific Standard Time (PST) and sunset is at 8:11 P.M. If we ignore the differences between geometric and weather service sunrise/sunset times, we can use our equations to provide a rough estimate of local latitude and longitude.

a. Estimating solar noon as the midway point between sunrise and sunset, at what clock time will it be solar noon?

b. Use Equations 4.12–4.14 to estimate your local longitude.

c. Use Equation 4.17 to estimate your local latitude.

4.9 A south-facing collector at latitude 40° is tipped up at an angle equal to its latitude. Compute the following insolations for January 1st at solar noon:

a. The direct beam insolation normal to the sun's rays.

b. Beam insolation on the collector.

c. Diffuse radiation on the collector.

d. Reflected radiation with ground reflectivity 0.2.

4.10 Create a "clear-sky insolation calculator" for direct, diffuse, and reflected radiation using the spreadsheet shown in Figure 4.26 as a guide. Confirm that it gives you 859 W/m^2 under the following conditions: August 1, 30° latitude, tilt 40°, southwest facing (–45°), 3:00 P.M. ST, reflec-tance 0.2.

Use the calculator to compute clear-sky insolation under the following conditions (times are solar times):

a. January 1, latitude 40°, horizontal insolation, solar noon, reflectance = 0

b. March 15, latitude 20°, south-facing collector, tilt 20°, 11:00 A.M., $\rho = 0.2$.

c. July 1, latitude 48°, south–east collector (azimuth 45°), tilt 20°, 2:00 P.M., $\rho = 0.3$.

4.11 The following table shows TMY data (W/m^2) for Denver (latitude 39.8°) on July 1 ($n = 182$, $\delta = 23.12°$). Calculate the expected irradiation on the following collector surfaces. Notice answers are given for some of them to help check your work.

a. South-facing, fixed 40° tilt, reflectance 0.2, solar noon.

b. South-facing, fixed 30° tilt, reflectance 0.2 solar noon (Ans: 1024 W/m^2).

c. Horizontal, north–south axis, tracking collector (HNS), reflectance 0.2, at 11:00 A.M. ST.

d. Horizontal north–south axis, tracking collector (HNS), reflectance 0.2, at solar noon. (Ans: 1006 W/m^2).

e. Two-axis tracker, reflectance 0.2, at solar noon.

f. Two-axis tracker, reflectance 0.2, at 11:00 A.M. ST. (Ans. 1029 W/m^2).

g. One-axis tracker, vertical mount (VERT), tilt = 30° at 11:00 A.M. ST, reflectance 0.2. (Ans: 1019 W/m^2).

h. One-axis tracker, vertical mount (VERT), tilt = 30° at solar noon, reflectance 0.2.

TABLE P4.11

TMY Time	TMY GHI	TMY DNI	TMY DHI
5.00	–	–	–
6.00	42	334	40
7.00	273	608	68
8.00	476	744	93
9.00	667	820	114
10.00	825	864	128
11.00	938	889	138
12.00	998	901	143
13.00	1000	901	143
14.00	944	890	138
15.00	835	866	129
16.00	637	677	172
17.00	455	608	134
18.00	172	51	154
19.00	67	104	49

4.12 Download TMY3 data for Mountain View (Moffett Field, latitude 37.4°), CA from the NREL website (http://rredc.nrel.gov/solar/old_data/nsrdb/1991-2005/tmy3). The raw data are in CSV format. By opening the CSV file in Excel, you can convert it to normal rows and columns of data. Be sure to save it then as an Excel file.

a. Use TMY3 to find the irradiation on a south-facing photovoltaic module with a fixed 18° tilt angle on September 21 (equinox) at solar noon. Assume 0.2 reflectance.

b. Compare that to clear-sky irradiation on that module.

4.13 In Example 4.13, the average irradiation in September on a 30° fixed-tilt, south-facing collector in Oakland (latitude 37.73°, horizontal insolation 7.32 kWh/m^2/d, reflectivity 0.2) was estimated to be 6.7 kWh/m^2/d. Repeat that calculation if the collector tilt angle is only 10°.

CHAPTER 5

PHOTOVOLTAIC MATERIALS AND ELECTRICAL CHARACTERISTICS

5.1 INTRODUCTION

A material or device that is capable of converting the energy contained in photons of light into an electrical voltage and current is said to be *photovoltaic*. A photon with short enough wavelength and high enough energy can cause an electron in a photovoltaic material to break free of the atom that holds it. If a nearby electric field is provided, those electrons can be swept toward a metallic contact where they can emerge as an electric current. The driving force to power photovoltaics comes from the sun and it is interesting to note that the rate at which the surface of the earth receives solar energy is something like 6000 times our total energy demand.

The history of PVs began in 1839 when a 19-year-old French physicist, Edmund Becquerel, was able to cause a voltage to appear when he illuminated a metal electrode in a weak electrolyte solution. Almost 40 years later, Adams and Day were the first to study the PV effect in solids. They were able to build cells made of selenium that were 1–2% efficient. Selenium cells were quickly adopted by the emerging photography industry for photometric light meters; in fact, they are still used for that purpose today.

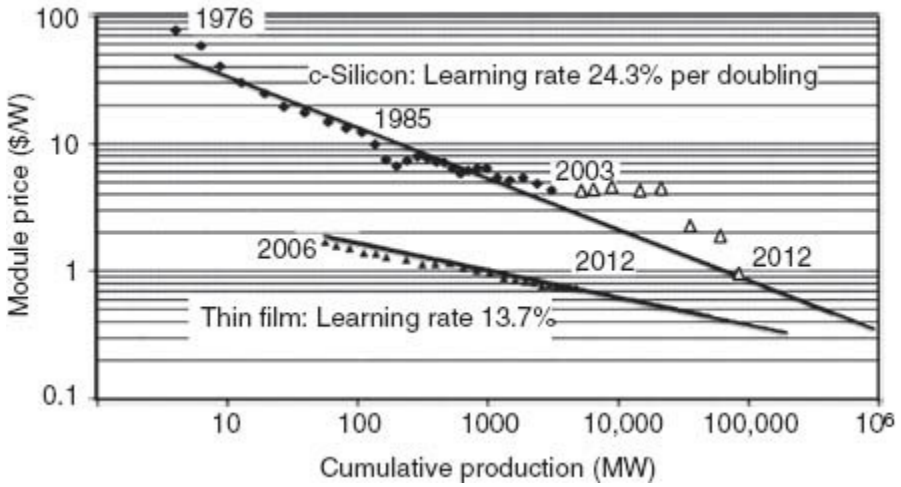
As part of his development of quantum theory, Albert Einstein published a theoretical explanation of the PV effect in 1904, which led to a Nobel Prize in 1923. About the same time, in what would turn out to be a cornerstone of modern electronics in general, and PVs in particular, a Polish scientist by the name of Jan Czochralski, began to develop a method to grow perfect crystals of silicon. By the 1940s and 1950s, the Czochralski process began to be used to make the first generation of single-crystal silicon photovoltaics, and that technique continues to dominate the PV industry today.

In the 1950s, there were several attempts to commercialize PVs, but their cost was prohibitive. The real emergence of PVs as a practical energy source came in 1958 when they were first used in space for the Vanguard I satellite. For space vehicles, cost is much less important than weight and reliability, and solar cells have ever since played an important role in providing onboard power for satellites and other space craft. Spurred on by the emerging energy crises of the 1970s, the development work supported by the space program began to pay off back on the ground. By the 1980s, higher efficiencies and lower costs brought PVs closer to reality and they began to find application in many off-grid terrestrial applications such as pocket calculators, off-shore buoys, highway lights, signs and emergency call boxes, rural water pumping, and small home systems. By the early part of the twenty-first century, however, growth in PV system installations accelerated rapidly at both ends of the scale; from a few tens of watts for off-grid cell phone charging and home

solar systems in developing countries to hundreds of megawatt utility scale systems in sunny areas across the globe.

PV costs continued to decline until about 2003, when the industry began to experience a shortage of a key raw material, polysilicon. That bottleneck was broken a few years later and costs quickly resumed their downward trend as shown in Figure 5.1. As will be described later in this chapter, crystal-silicon-based PVs (c-Si) have traditionally dominated the market, but more recently, thin-film PVs have been challenging that dominance. Figure 5.1 shows what are referred to as *experience curves* for both c-Si and thin-film module costs. The straight lines fitted to the data indicate that c-Si costs have decreased by 24.3% for every doubling of production (called the *learning rate*), while for the relatively new thin-film technologies, the decline has been at 13.7% per doubling.

FIGURE 5.1 Photovoltaic module costs and cumulative production for both crystal silicon (c-Si) and thin-film technologies (Based on NREL data, 2012).



With rapidly declining module costs, attention has shifted toward the other cost components of installed systems. In 2010, the U.S. Department of Energy (DOE) created its SunShot program, which has the goal of making complete systems cost competitive with conventional generation by 2020, and to do so without subsequent subsidies. That translates to installed costs of $1/Wp for utility scale systems, $1.25/Wp for commercial rooftop PV, and $1.50/Wp for residential rooftop systems. The Wp designation, by the way, refers to the peak DC power delivered under idealized, standard test conditions (STCs) that will be described later.

5.2 BASIC SEMICONDUCTOR PHYSICS

Photovoltaics use semiconductor materials to convert sunlight into electricity. The technology for doing so is very closely related to the solid-state technologies used to make transistors, diodes, and all of the other semiconductor devices that we use so much of these days. The starting point for most of the world's current generation of PV devices, as well as almost all semiconductors, is pure crystalline silicon. Silicon is in the fourth column of the periodic table, which is referred to as Group IV (Table 5.1). Germanium is another Group IV element and it is also used as a semiconductor in some electronics. Other elements that

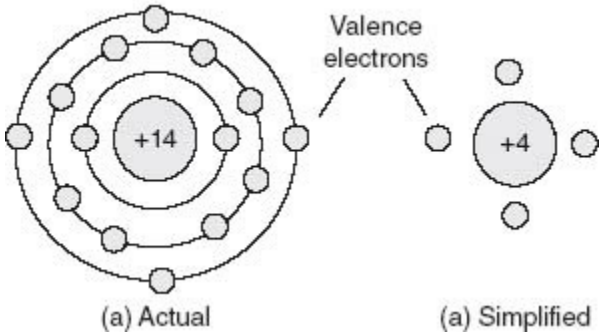
play important roles in PVs are boldfaced. As we will see, boron and phosphorus, from Groups III and V, are added to silicon to make most electronic devices, including PVs. Gallium and arsenic are used in GaAs solar cells, cadmium and tellurium are used in CdTe cells, and copper, indium, and selenium are used in CIS cells.

TABLE 5.1 A Portion of the Periodic Table with the Most Important Elements for Photovoltaics Highlighted

I	II	III	IV	V	VI
		5 B	6 C	7 N	8 O
		13 Al	**14 Si**	**15 P**	16 S
29 Cu	30 Zn	**31 Ga**	32 Ge	**33 As**	**34 Se**
47 Ag	**48 Cd**	**49 In**	50 Sn	51 Sb	**52 Te**

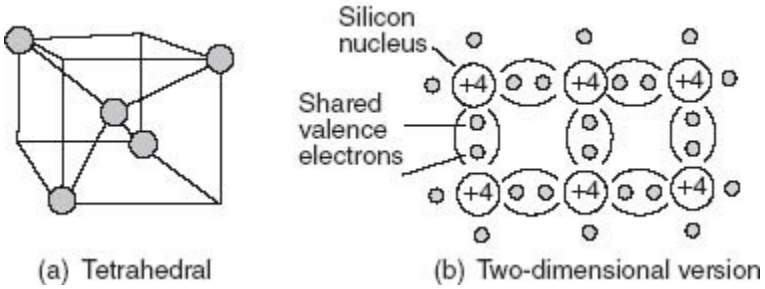
Silicon has 14 protons in its nucleus and so it has 14 orbital electrons as well. As shown in Figure 5.2a, its outer orbit contains four valence electrons—that is, it is tetravalent. Those valence electrons are the only ones that matter in electronics, so it is common to draw silicon as if it has a +4 charge on its nucleus and four tightly held valence electrons, as shown in Figure 5.2b.

FIGURE 5.2 Silicon has 14 protons and 14 electrons as in (a). A convenient shorthand is drawn in (b), in which only the four outer electrons are shown, spinning around a nucleus with a +4 charge.



In pure crystalline silicon, each atom forms covalent bonds with four adjacent atoms in the three-dimensional tetrahedral pattern shown in Figure 5.3a. For convenience, that pattern is drawn as if it were all in a plane, as in Figure 5.3b.

FIGURE 5.3 Crystalline silicon forms a three-dimensional, tetrahedral structure (a); but it is easier to draw it as a two-dimensional flat array (b).



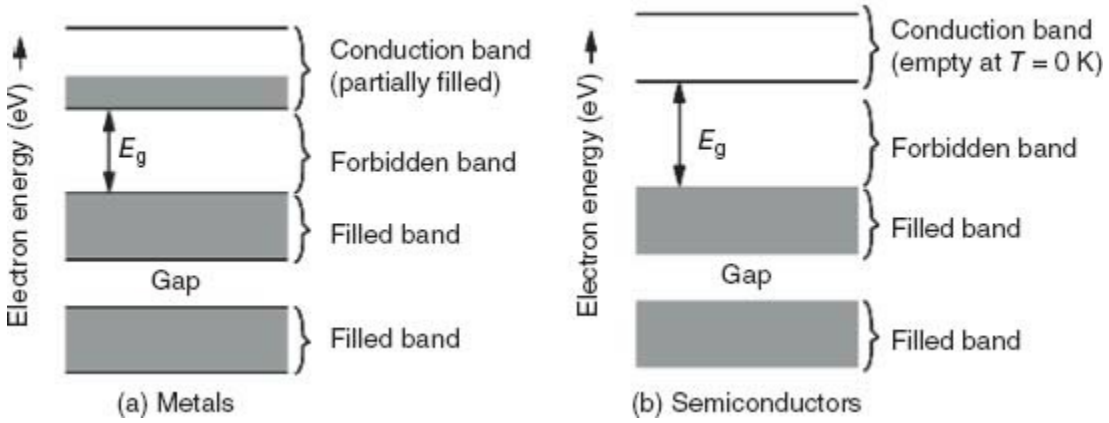
5.2.1 THE BAND-GAP ENERGY

At absolute zero temperature, silicon is a perfect electrical insulator. There are no electrons

free to roam around as there are in metals. As the temperature increases, some electrons will be given enough energy to free themselves from their nuclei, making them available to flow as electric current. The warmer it gets, the more electrons there are to carry current, so its conductivity increases with temperature (in contrast to metals, where conductivity decreases). That change in conductivity, it turns out, can be used to advantage to make very accurate temperature measurement sensors called *thermistors*. Silicon's conductivity at normal temperatures is still very low and so it is referred to as a semiconductor. As we will see, by adding minute quantities of other materials, the conductivity of pure (intrinsic) semiconductors can be greatly improved.

Quantum theory describes the differences between conductors (metals) and semiconductors (e.g., silicon) using energy band diagrams such as those shown in Figure 5.4. Electrons have energies that must fit within certain allowable energy bands. The top energy band is called the conduction band, and it is electrons within this region that contribute to current flow. As shown in Figure 5.4, the conduction band for metals is partially filled, but for semiconductors at absolute zero temperature, the conduction band is empty. At room temperature, only about one out of 10^{10} electrons in silicon exists in the conduction band.

FIGURE 5.4 Energy bands for (a) metals and (b) semiconductors. Metals have partially filled conduction bands, which allow them to carry electric current easily. Semiconductors at absolute zero temperature have no electrons in the conduction band, which makes them insulators.

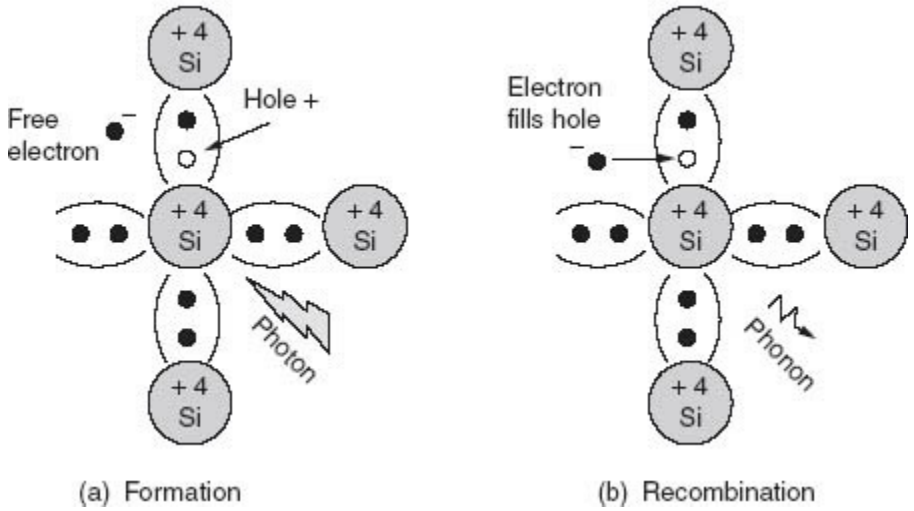


The gaps between allowable energy bands are called forbidden bands, the most important of which is the gap separating the conduction band from the highest filled band below it. The energy that an electron must acquire to jump across the forbidden band into the conduction band is called the *band-gap energy*, designated E_g. The units for band-gap energy are usually electron volts (eV), where one electron volt is the energy that an electron acquires when its voltage is increased by 1 V ($1\ \text{eV} = 1.6 \times 10^{-19}$ J).

The band-gap energy (E_g) for silicon is 1.12 eV, which means an electron needs to acquire that much energy to free itself from the electrostatic force that ties it to its own nucleus; that is, to jump into the conduction band. Where might that energy come from? We already know that a small number of electrons get that energy thermally. For PVs, the energy source is photons of electromagnetic energy from the sun. When a photon with more than 1.12 eV of energy is absorbed by a solar cell, a single electron may jump to the

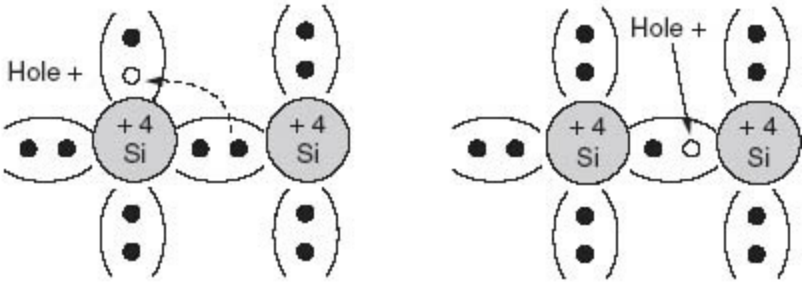
conduction band. When it does so, it leaves behind a nucleus with a +4 charge that now has only three electrons attached to it. That is, there is a net positive charge, called a *hole*, associated with that nucleus as shown in Figure 5.5a. Unless there is some way to sweep the electrons away from the holes, they will eventually recombine, obliterating both the hole and the electron as in Figure 5.5b. When recombination occurs in what are called *direct* band-gap materials, the energy that had been associated with the electron in the conduction band will be released as a photon, which is the basis for light-emitting diodes (LEDs). Silicon, however, is an *indirect* band-gap material, which means recombination emits energy in the form of lattice vibrations, called phonons, rather than light.

FIGURE 5.5 A photon with sufficient energy can create a hole–electron pair as in (a). Unless they are separated, the electron will likely recombine with a hole (b).



It is important to note that not only are the negatively charged electrons in the conduction band free to roam around in the crystal, but the positively charged holes left behind can also move as well. As shown in Figure 5.6, a valence electron in a filled energy band can easily move to fill a hole in a nearby atom, without having to change energy bands. Having done so, the hole, in essence, moves to the nucleus from which the electron originated. This is analogous to a student leaving her seat to get a drink of water. A roaming student (electron) and a seat (hole) are created. Another student already seated might decide he wants that newly vacated seat, so he gets up and moves, leaving his seat behind. The empty seat appears to move around just the way a hole moves around in a semiconductor. The important point here is that electric current in a semiconductor can be carried not only by negatively charged electrons, but also by positively charged holes that can move around as well.

FIGURE 5.6 When a hole is filled by a nearby valence electron, the positively charged hole appears to move.



(a) An electron moves to fill the hole (b) The hole has moved

So, photons with enough energy create hole–electron pairs in a semiconductor. Photons can be characterized by their wavelengths or their frequency as well as by their energy; the three are related by the following:

(5.1) $c = \lambda\nu$

where c is the speed of light (3×10^8 m/s), ν is the frequency (hertz), λ is the wavelength (m), and

(5.2) $$E = h\nu = \frac{hc}{\lambda}$$

where E is the energy of a photon (J) and h is Planck's constant (6.626×10^{-34} J·s).

Example 5.1 Photons to Create Hole–Electron Pairs in Silicon. What maximum wavelength can a photon have to create hole–electron pairs in silicon? What minimum frequency is that? Silicon has a band-gap of 1.12 eV and 1 eV = 1.6×10^{-19} J.

Solution. From Equation 5.2, the wavelength must be less than:

$$\lambda \leq \frac{hc}{E} = \frac{6.626 \times 10^{-34}\text{J} \cdot \text{s} \times 3 \times 10^8\text{m/s}}{1.12\text{ eV} \times 1.6 \times 10^{-19}\text{J/eV}} = 1.11 \times 10^{-6}\text{m} = 1.11\ \mu\text{m}$$

and from Equation 5.1, the frequency must be at least

$$\nu \geq \frac{c}{\lambda} = \frac{3 \times 10^8\text{m/s}}{1.11 \times 10^{-6}\text{m}} = 2.7 \times 10^{14}\text{ Hz}$$

For a silicon PV cell, photons with wavelength greater than 1.11 μm have energy $h\nu$ less than the 1.12 eV band-gap energy needed to excite an electron. None of those photons create hole–electron pairs capable of carrying current, so all of their energy is wasted. It just heats the cell. On the other hand, photons with wavelengths shorter than 1.11 μm have more than enough energy to excite an electron. Since (at least for conventional solar cells) one photon can excite only one electron, any extra energy above the 1.12 eV needed is also dissipated as waste heat in the cell. The band-gaps for other important PV materials, gallium arsenide (GaAs), cadmium telluride (CdTe), copper indium diselenide ($CuInSe_2$), copper gallium diselenide ($CuGaSe_2$), amorphous silicon (a-Si), and conventional crystal silicon are shown in Table 5.2. All of these materials will be described more carefully later in the chapter.

TABLE 5.2 Band-Gap and Cut-off Wavelength Above Which Electron Excitation Does Not Occur

Quantity	Si	a-Si	CdTe	$CuInSe_2$	$CuGaSe_2$	GaAs
Band-gap (eV)	1.12	1.7	1.49	1.04	1.67	1.43
Cut-off wavelength (μm)	1.11	0.73	0.83	1.19	0.74	0.87

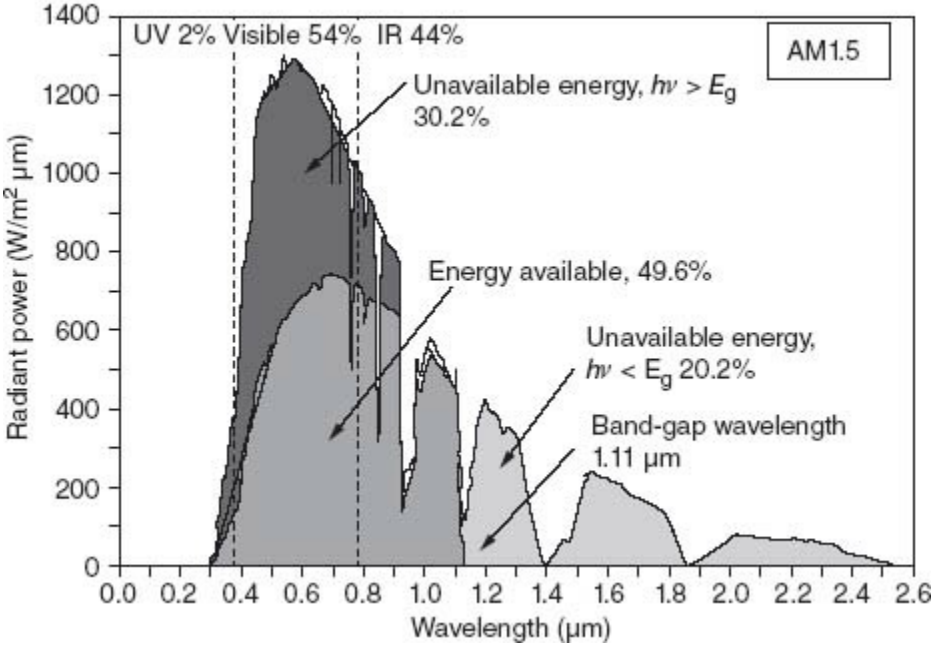
5.2.2 Band-Gap Impact on PV Efficiency

The two phenomena relating to photons with energies above and below the band-gap establish a maximum theoretical efficiency for a solar cell. To explore this constraint, we need to introduce the solar spectrum.

As was described in the last chapter, the surface of the sun emits radiant energy with spectral characteristics that well match those of a 5800 K blackbody. Just outside of the earth's atmosphere, the average radiant flux is about 1.37 kW/m^2, an amount known as the solar constant. As solar radiation passes through the atmosphere, some is absorbed by various constituents in the atmosphere, so that by the time it reaches the earth's surface the spectrum is significantly distorted.

The amount of solar energy reaching the ground, as well as its spectral distribution, depends very much on how much atmosphere it has had to pass through to get there. Recall that the length of the path taken by the sun's rays through the atmosphere to reach a spot on the ground, divided by the path length corresponding to the sun directly overhead, is called the *air mass ratio*, *m*. Thus, an air mass ratio of 1 (designated "AM1") means the sun is directly overhead. By convention, AM0 means no atmosphere; that is, it is the extraterrestrial solar spectrum. For most PV work, an air mass ratio of 1.5, corresponding to the sun being 42° above the horizon, is assumed to be the standard. The solar spectrum at AM1.5 is shown in Figure 5.7. For an AM1.5 spectrum, 2% of the incoming solar energy is in the ultraviolet (UV) portion of the spectrum, 54% is in the visible, and 44% is in the near infrared (IR).

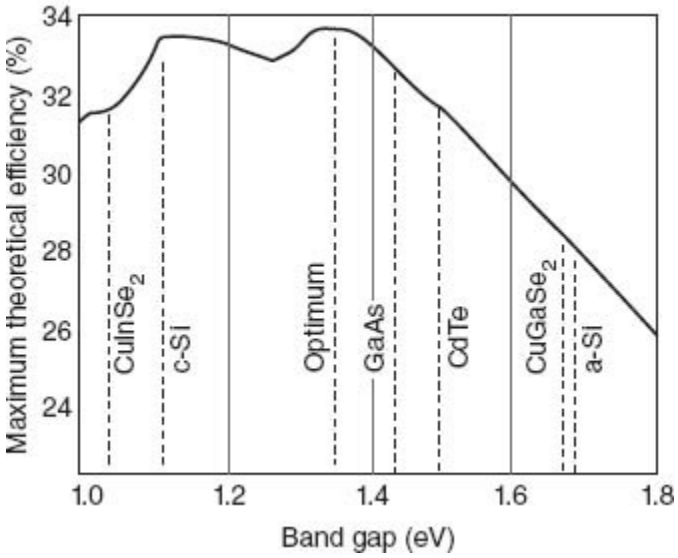
FIGURE 5.7 Solar spectrum at AM1.5 showing impact of unusable energy by crystal silicon PV cells. Photons with wavelengths longer than 1.11 μm do not have enough energy to excite electrons (20.2% of the incoming solar energy); those with shorter wavelengths cannot use all of their energy, which accounts for another 30.2% unavailable. Spectrum is based on ERDA/NASA (1977).



We can now make a simple estimate of the upper bound on the efficiency of a silicon solar cell. We know the band-gap for silicon is 1.12 eV, corresponding to a wavelength of 1.11 μm, which means any energy in the solar spectrum with wavelengths longer than 1.11 μm cannot send an electron into the conduction band. And, any photons with wavelength less than 1.11 μm, waste their extra energy. If we know the solar spectrum, we can calculate the energy loss due to these two fundamental constraints. Figure 5.7 shows the results of this analysis, assuming a standard air mass ratio AM1.5. As is presented there, 20.2% of the energy in the spectrum is lost due to photons having less energy than the band-gap of silicon ($h\nu < E_g$), and another 30.2% is lost due to photons with $h\nu > E_g$. The remaining 49.6% represents the maximum possible fraction of the sun's energy that could be collected with a silicon solar cell. That is, the constraints imposed by silicon's band-gap limit the efficiency of silicon to just under 50%.

There are other fundamental constraints to PV efficiency, most importantly black-body radiation losses and recombination. Cells in the sun get hot, which means their surfaces radiate energy proportional to the fourth power of their temperature. This accounts for something on the order of 7% loss. The recombination constraint is related to slow-moving holes that stack up in the cell making it more difficult for electrons to pass through without falling back into a hole. These hole-saturation effects can account for another 10% or so of losses. The solar spectrum, black-body radiation, and recombination constraints were first evaluated by William Shockley and Hans Queisser back in 1961 resulting in what is now known as the *Shockley–Queisser limit* of 33.7% for the maximum efficiency of a single-junction PV under normal (unenhanced) sunlight (Shockley and Queisser, 1961). Figure 5.8 shows this limit as a function of the band-gap of the semiconductor material.

FIGURE 5.8 The Shockley–Queisser limit for the maximum possible solar cell efficiency (single-junction, unenhanced insolation) as a function of band-gap.

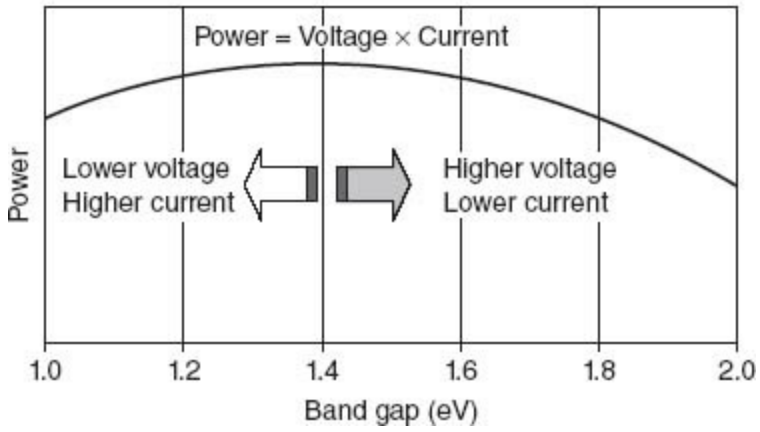


Even this simple discussion gives some insight into the trade-off between choosing a PV material that has a small band-gap versus one with a large band-gap. With a smaller band-gap, more solar photons have the energy needed to excite electrons, which is good since it creates the charges that will enable current to flow. However, a small band-gap means more photons have surplus energy above the threshold needed to create hole–electron pairs, which wastes their potential. High band-gap materials have the opposite combination. A high band-gap means fewer photons have enough energy to create the current-carrying electrons and holes, which limits the current that can be generated. On the other hand, a high band-gap gives those charges a higher voltage with less left over surplus energy.

Another way to think about the impact of band-gap is to realize that it is a measure of the energy given to a unit of charge, which is voltage. That is, the bigger the band-gap, the higher the voltage created in the cell when exposed to sunlight. On the other hand, a higher band-gap means fewer electrons will have enough energy to jump the gap, which means less current can be created by the cell. Since power is the product of current and voltage, there must be some middle-ground band-gap, usually estimated to be between 1.2 and 1.6 eV, which will result in the highest power and efficiency.

Finally, it is important to note that the band-gap of a semiconductor material is temperature dependent. As temperature rises, valence electrons acquire a bit more kinetic energy which decreases the energy that a photon needs to have to send them into the conduction band. The result is a decrease in the band-gap. As we shall see when PV current versus voltage curves are introduced, as PV temperature increases, their open-circuit voltage drops and their short-circuit current rises, which is consistent with Figure 5.9.

FIGURE 5.9 Maximum efficiency of photovoltaics as a function of their band-gap.

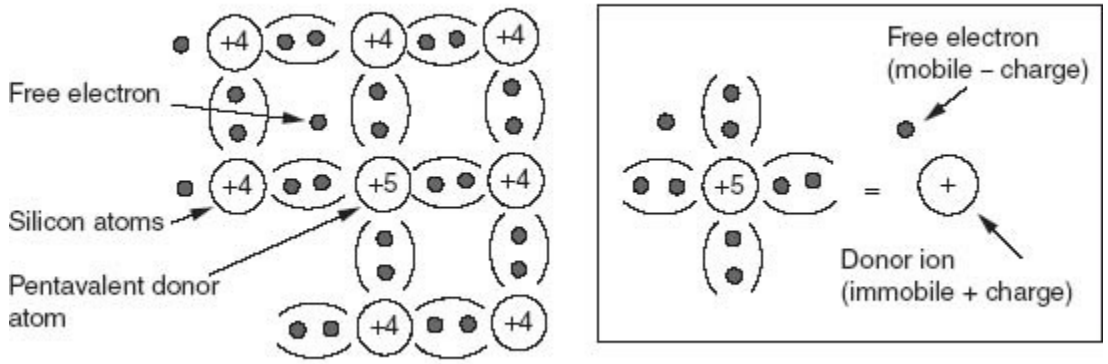


5.2.3 The p–n Junction

As long as a solar cell is exposed to photons with energies above the band-gap energy, hole–electron pairs will be created. The problem is, of course, that those electrons can fall right back into a hole causing both charge carriers to disappear. To avoid that recombination, electrons in the conduction band must continuously be swept away from holes. In PVs that is accomplished by creating a built-in electric field within the semiconductor itself that pushes electrons in one direction and holes in the other. To create the electric field, two regions are established within the crystal. Using silicon as our example, on one side of the dividing line separating the regions, pure (intrinsic) silicon is purposely contaminated with very small amounts of a trivalent element from column III of the periodic table; on the other side, pentavalent atoms from column V are added.

Consider the side of the semiconductor that has been doped with a pentavalent element such as phosphorus. Only about one phosphorus atom per 1000 silicon atoms is typical. As shown in Figure 5.10, an atom of the pentavalent impurity forms covalent bonds with four adjacent silicon atoms. Four of its five electrons are now tightly bound, but the fifth electron is left on its own to roam around the crystal. When that electron leaves the vicinity of its donor atom, there will remain a +5 donor ion fixed in the matrix, surrounded by only four negative valence electrons. That is, each donor atom can be represented as a single, fixed, immobile positive charge plus a freely roaming negative charge as shown in Figure 5.10b. Pentavalent, that is, +5, elements donate electrons to their side of the semiconductor so they are called *donor* atoms. Since there are now negative charges that can move around the crystal, a semiconductor doped with donor atoms is referred to as an *n-type material*.

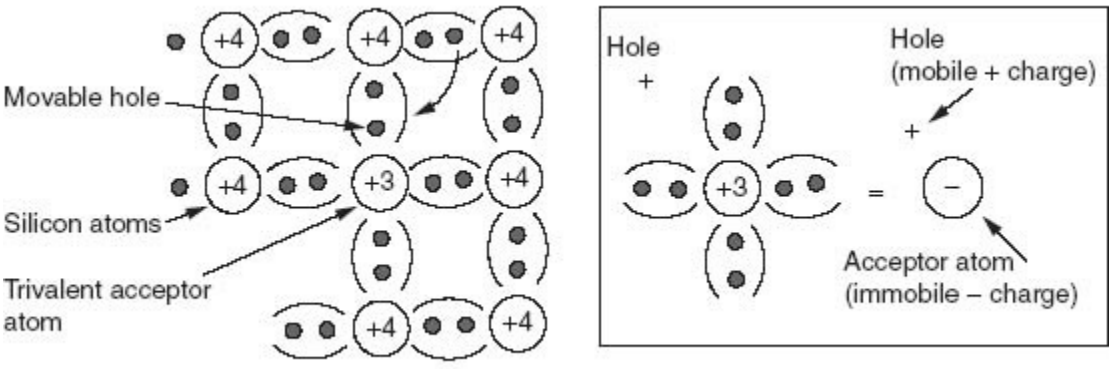
FIGURE 5.10 An n-type material. (a) The pentavalent donor. (b) The representation of the donor as a mobile, negative charge with a fixed, immobile positive charge.



(a) The donor atom in Si crystal (b) Representation of the donor atom

On the other side of the semiconductor, silicon is doped with a trivalent element such as boron. Again the concentration of dopants is small, something on the order of one boron atom per 10 million silicon atoms. These dopant atoms fall into place in the crystal, forming covalent bonds with the adjacent silicon atoms as shown in Figure 5.11. Since each of these impurity atoms has only three electrons, only three of the covalent bonds are filled, which means a positively charged hole appears next to its nucleus. An electron from a neighboring silicon atom can easily move into the hole, so these impurities are referred to as *acceptors* since they accept electrons. The filled hole now means there are four negative charges surrounding a +3 nucleus. All four covalent bonds are now filled creating a fixed, immobile net negative charge at each acceptor atom. Meanwhile, each acceptor has created a positively charged hole that is free to move around in the crystal, so this side of the semiconductor is called a *p-type* material.

FIGURE 5.11 In a p-type material, trivalent acceptors contribute mobile, positively charged holes while leaving immobile, negative charges in the crystal lattice.

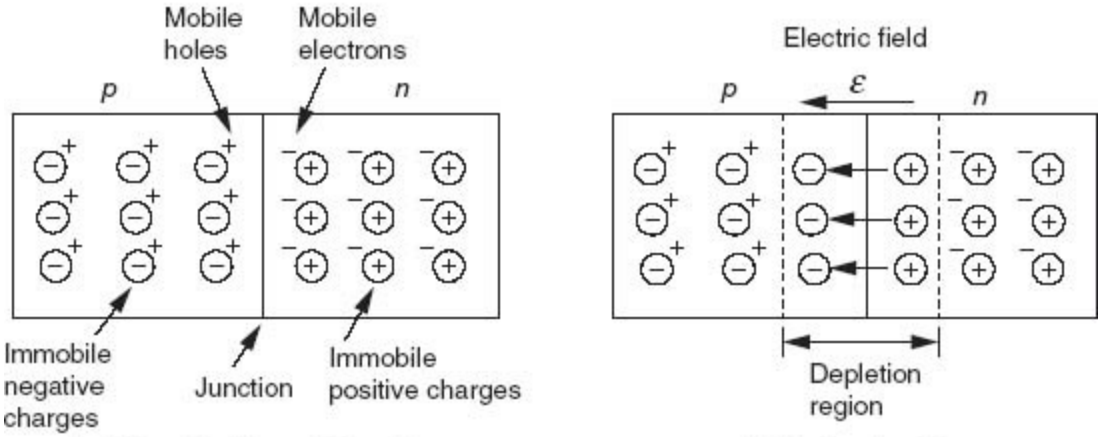


(a) An acceptor atom in Si crystal (b) Representation of the acceptor atom

Now, suppose we imagine putting an n-type material next to a p-type material forming a junction between them. In the n-type material, mobile electrons drift by diffusion across the junction. In the p-type material, mobile holes drift by diffusion across the junction in the opposite direction. As depicted in Figure 5.12, when an electron crosses the junction, it fills a hole leaving an immobile, positive charge behind in the n-region, while it creates an immobile, negative charge in the p-region. These immobile charged atoms in the *p* and *n* regions create an electric field that works against the continued movement of electrons and holes across the junction. As the diffusion process continues, the electric field countering

that movement increases until eventually (actually, almost instantaneously) all further movement of charged carriers across the junction stops.

FIGURE 5.12 (a) When a p–n junction is first formed there are mobile holes in the p-side and mobile electrons in the n-side. (b) As they migrate across the junction, an electric field builds up that opposes, and quickly stops, that diffusion.

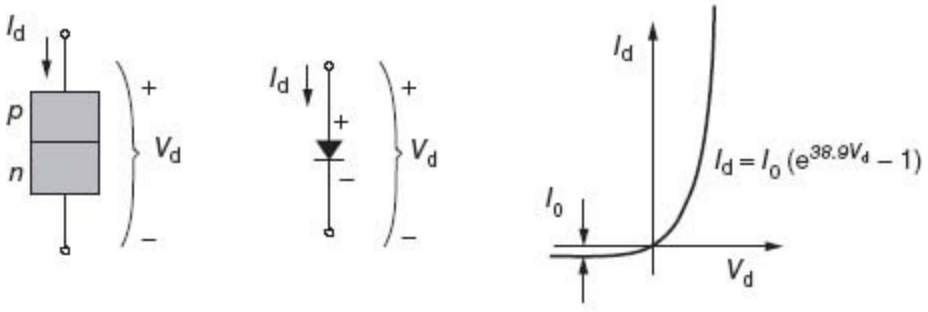


The exposed immobile charges creating the electric field in the vicinity of the junction form what is called a *depletion region*, meaning that the mobile charges are depleted—gone—from this region. The width of the depletion region is only about 1 μm and the voltage across it is perhaps 1 V, which means the field strength is about 10, 000 V/cm! Following convention, the arrows representing an electric field in Figure 5.12b start on a positive charge and end on a negative charge. The arrow, therefore, points in the direction that the field would push a positive charge, which means it holds the mobile positive holes in the p-region (while it repels the electrons back into the n-region).

5.2.4 The p–n Junction Diode

Anyone familiar with semiconductors will immediately recognize that what has been described thus far is just a common, conventional p–n junction diode, the characteristics of which are presented in Figure 5.13. If we were to apply a voltage V_d across the diode terminals, forward current would flow easily through the diode from the p-side to the n-side; but if we try to send current in the reverse direction, only a very small ($\approx 10^{-12}$ A/cm^2) reverse saturation current I_0 will flow. That reverse saturation current is the result of thermally generated carriers with the holes being swept into the p-side and the electrons into the n-side. In the forward direction, the voltage drop across the diode is only a few tenths of a volt.

FIGURE 5.13 A p–n junction diode allows current to flow easily from the p-side to the n-side, but not in reverse. (a) p–n junction; (b) its symbol; (c) its characteristic curve.



(a) *p–n* junction diode (b) Symbol for real diode (c) Diode characteristic curve

The symbol for a real diode is shown here as a blackened triangle with a bar; the triangle suggests an arrow, which is a convenient reminder of the direction in which current flows easily. The triangle is blackened to distinguish it from an "ideal" diode. Ideal diodes have no voltage drop across them in the forward direction and no current at all flows in the reverse direction.

The voltage–current characteristic curve for the p–n junction diode is described by the following Shockley diode equation:

$$I_d = I_0 \left(e^{qV_d/kT} - 1\right) \tag{5.3}$$

where I_d is the diode current in the direction of the arrow (A), V_d is the voltage across the diode terminals from the p-side to the n-side (V), I_0 is the reverse saturation current (A), q is the electron charge (1.602×10^{-19} C), k is Boltzmann's constant (1.381×10^{-23} J/K), and T is the junction temperature (K).

Substituting the above constants into the exponent of Equation 5.3 gives

$$\frac{qV_d}{kT} = \frac{1.602 \times 10^{-19}}{1.381 \times 10^{-23}} \cdot \frac{V_d}{T\,(\mathrm{K})} = 11{,}600 \frac{V_d}{T\,(\mathrm{K})} \tag{5.4}$$

A junction temperature of 25°C is often used as a standard, which results in the following diode equation:

$$I_d = I_0 \left(e^{38.9V_d} - 1\right) \quad (\text{at } 25°\text{C}) \tag{5.5}$$

Example 5.2 A p–n Junction Diode. Consider a p–n junction diode at 25°C with a reverse saturation current of 10^{-9} A. Find the voltage drop across the diode when it is carrying the following:

a. no current (open-circuit voltage)

b. 1 A

c. 10 A

Solution

a. In the open-circuit condition, $I_d = 0$, so from Equation 5.5 $V_d = 0$.

b. With $I_d = 1$ A, we can find V_d by rearranging Equation 5.5:

$$V_d = \frac{1}{38.9} \ln\left(\frac{I_d}{I_0} + 1\right) = \frac{1}{38.9} \ln\left(\frac{1}{10^{-9}} + 1\right) = 0.532 \text{ V}$$

c. With I_d = 10 A,

$$V_d = \frac{1}{38.9} \ln\left(\frac{10}{10^{-9}} + 1\right) = 0.592 \text{ V}$$

Note how little the voltage drop changes as the diode conducts more and more current, changing by only about 0.06 V as the current increased by a factor of 10. Often in normal electronic circuit analysis, the diode voltage drop when it is conducting current is assumed to be nominally about 0.6 V, which is quite in line with the above results.

While the Shockley diode Equation 5.3 is appropriate for our purposes, it should be noted that in some circumstances, it is modified with an "ideality factor" A, which accounts for different mechanisms responsible for moving carriers across the junction. The resulting equation is then

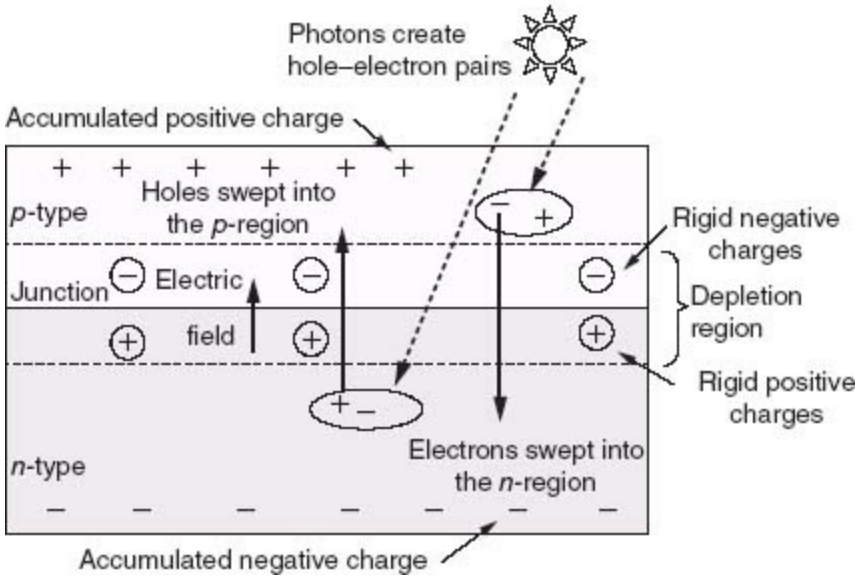
$$I_d = I_0 \left(e^{qV_d/AkT} - 1\right) \quad (5.6)$$

where the ideality factor A is 1 if the transport process is purely diffusion, and $A \approx 2$ if it is primarily recombination in the depletion region.

5.2.5 A Generic PV Cell

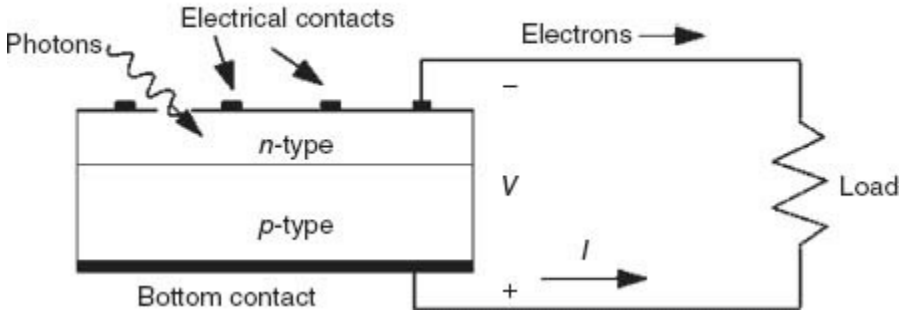
Let us consider what happens in the vicinity of a p–n junction when it is exposed to sunlight. As photons are absorbed, hole–electron pairs may be formed. If these mobile charge carriers reach the vicinity of the junction, the electric field in the depletion region will push the holes into the p-side and the electrons into the n-side as shown in Figure 5.14. The p-side accumulates holes and the n-side accumulates electrons, which creates a voltage that can be used to deliver current to a load.

FIGURE 5.14 When photons create hole–electron pairs near the junction, the electric field in the depletion region sweeps holes into the p-side and electrons into the n-side of the cell.



If electrical contacts are attached to the top and bottom of the cell, electrons will flow out of the n-side into the connecting wire, through the load and back to the p-side as shown in Figure 5.15. Since wire cannot conduct holes, it is only the electrons that actually move around the circuit. When they reach the p-side, they recombine with holes completing the circuit. By convention, positive current flows in the opposite direction to electron flow so the current arrow in the figure shows current going from the p-side to the load and back into the n-side.

FIGURE 5.15 Electrons flow from the n-side contact, through the load, and back to the p-side where they recombine with holes. Conventional current *I* is in the opposite direction.



5.3 PV MATERIALS

There are a number of ways to categorize PVs. In rather rough terms, first-generation solar cells are relatively thick (e.g., 200 μm) single p–n-junction-based semiconductors. Second-generation cells are mostly thin-film PVs, where "thin" means something like 1–10 μm. And, finally, so-called third-generation PVs include multijunction tandem cells, quantum dots, and technologies capable of creating more than one hole–electron pair per photon. Some of these are capable of exceeding the Shockley–Queisser theoretical efficiency limits.

While silicon used to dominate the PV industry, there is emerging competition from thin films made of compounds of two or more elements. Referring back to the portion of

the periodic table of the elements shown in Table 5.1, recall that silicon is in the fourth column, and it is referred to as a Group IV element. PV properties similar to those obtained with Group IV elements can be achieved by pairs of elements from the third and fifth columns (called III-V materials) or pairs from the second and sixth columns (II-VI materials). As examples, gallium, which is a Group III element, paired with arsenic, which is Group V, can be used to make gallium arsenide (GaAs) PVs while cadmium (Group II) and tellurium (Group VI) are combined to form CdTe ("cad-telluride") cells.

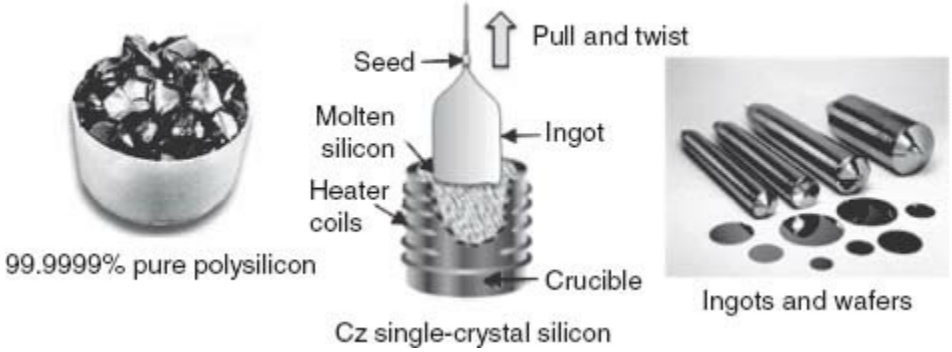
5.3.1 Crystalline Silicon

Silicon is the second most abundant element on earth, comprising approximately 20% of the earth's crust. Pure silicon almost immediately forms a layer of SiO_2 on its surface when exposed to air, so it exists in nature mostly in SiO_2-based minerals such as quartzite or in silicates such as mica, feldspars, and zeolites.

The raw material for silicon-based PVs and other semiconductors could be common sand, but it is usually naturally purified, high quality silica or quartz (SiO_2) from mines. Silica processing starts with a high temperature arc furnace that uses carbon to reduce silica to a metallurgical-grade silicon, somewhat better than 99% pure. Upgraded metallurgical-grade silicon (UMG-Si) is becoming a competitor for the much more highly purified silicon needed for the most efficient single crystal Silicon (sc-Si) photovoltaics. This 99.9999% semiconductor-grade polycrystalline silicon (referred to as poly-Si or just "poly") has the appearance of rock-like chunks of a multifaceted shiny metal.

The most commonly used technique for forming sc-Si from a crucible of molten poly is the Czochralski, or Cz, method (Fig. 5.16a), in which a small seed of solid, crystalline silicon about the size of a pencil is dipped into the vat and then slowly withdrawn using a combination of pulling and rotating. As it is withdrawn, the molten silicon atoms bond with atoms in the crystal and then solidify (freeze) in place. At a pull rate of about 50 mm/h, it takes around 30 h to grow a 1.5 m long cylindrical ingot or "boule" of sc-Si. By adding proper amounts of a dopant to the melt, the resulting ingot can be fabricated as an n- or p-type material. Usually the dopant is boron and the ingot is therefore a p-type semiconductor. An alternative to the Czochralski method is called the float zone (FZ) process, in which a solid ingot of silicon is locally melted and then solidified by a radio frequency (RF) field that passes slowly along the ingot.

FIGURE 5.16 The Czochralski method for growing sc-Si.



After the cylindrical ingot is formed, it must then be sliced or sawn to form thin *wafers*.

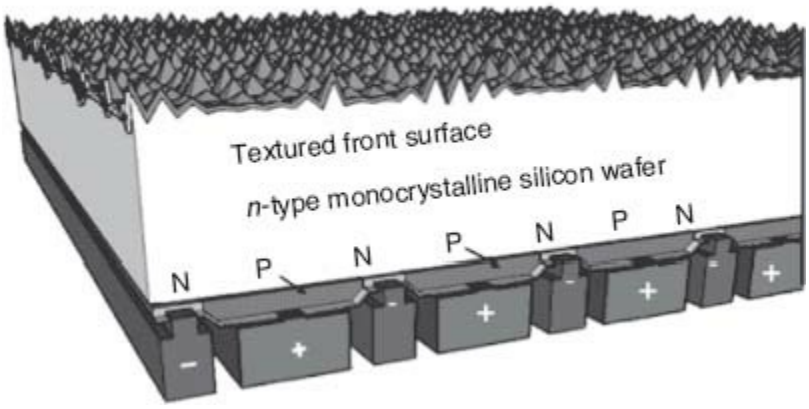
In this step, as much as 20% of the silicon ends up as sawdust, known as *kerf*. The wafers are then etched to remove some of the surface damage and to expose the microscopic crystalline structure at the top of the cell. The surface is made up of a jumble of four-sided pyramids, which helps reflect light down into the crystal. After polishing, the wafers are ready to be doped to make the p–n junction.

During the above wafer fabrication, the crystalline silicon is usually doped with acceptor atoms making it p-type throughout its thickness. To form the junction, a thin 0.1–0.5 μm n-type layer is created by diffusing enough donor atoms into the top of the cell to overwhelm the already existing acceptors. For most sc-Si, the donor atoms are phosphorus from phosphine gas (PH_3) and the acceptors are boron (from diborane, B_2H_3).

Since silicon is naturally quite reflective to solar wavelengths, some sort of surface treatment is required to reduce those losses. An antireflection (AR) coating of some transparent material such as silicon nitride is applied. These coatings tend to readily transmit the green, yellow, and red light into the cell, but some of the shorter-wavelength blue light is reflected, which gives the cells their characteristic dark blue color.

The next step is the attachment of electrical contacts to the cell. The underside of the cell is usually a full metal contact, typically aluminum. The top contacts are usually a grid of fingers and busbars printed onto the front surface using silver paste that is then fired at high temperature to bond to the cell. That coverage, of course, reduces the amount of sunlight reaching the junction and hence reduces the overall cell efficiency. For some types of cells with a glass superstrate, it is possible to replace those wires with a top layer of a transparent conducting oxide (TCO), such as tin oxide (SnO_2), deposited onto the underside of the glass. The best way to avoid grid wire loss is to eliminate front side metallization altogether and cleverly put all of the contacts as well as the junctions themselves on the underside of the cell as shown in Figure 5.17. SunPower's rear-contact cells have achieved efficiencies over 24%.

FIGURE 5.17 Rear-contact solar cell junctions and wire contacts on the back side of the cell.



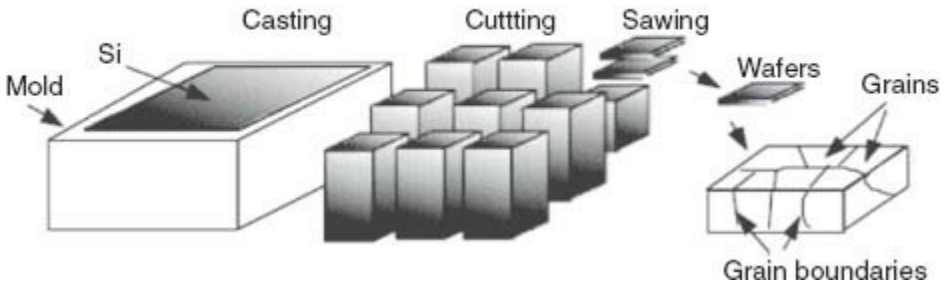
With the cost of sliced and polished wafers being a significant fraction of the cost of PVs, attempts have been made to find other ways to fabricate crystalline silicon. Several such technologies are based on growing crystalline silicon that emerges as a long, thin, continuous ribbon from the silicon melt. The ribbons can then be scribed and broken into rectangular cells without the wastefulness of sawing an ingot and without the need for

separate polishing steps.

Another way to avoid the costly Czochralski processes is based on carefully cooling and solidifying a crucible of molten metallurgic-grade silicon, yielding a large, solid rectangular ingot. Since these ingots may be quite large, on the order of 40 × 40 × 40 cm and weighing over 100 kg, the ingot needs to be cut into smaller, more manageable blocks, which are then sliced into silicon wafers using either saw or wire-cutting techniques. Sawing can waste a significant fraction of the ingot, but since this casting method is itself cheaper and it utilizes less expensive, less pure silicon than the Cz process, the waste is less important.

Casting silicon in a mold and then carefully controlling its rate of solidification results in an ingot that is not a single, large crystal. Instead, it consists of many regions, or grains, that are individually crystalline and which tend to have grain boundaries that run perpendicularly to the plane of the cell. Defective atomic bonds at these boundaries increase recombination and diminish current flow resulting in cell efficiencies that tend to be a few percentage points below Cz cells. Those grain boundaries also provide a distinctive physical appearance to multicrystalline cells since reflection off each grain region is slightly different. Figure 5.18 illustrates the casting, cutting, slicing, and grain boundary structure of these multicrystalline silicon (mc-Si) cells.

FIGURE 5.18 Casting, cutting, and sawing of silicon results in wafers with individual grains of crystalline silicon separated by grain boundaries.



The PV technologies described thus far result in individual, thick cells that must be wired together to create modules with the desired voltage and current characteristics. This wiring is done with automated soldering machines that connect the cells in series—that is, with the front of one cell connected to the back of the next. After soldering, the cells are laminated into a sandwich of materials that offer structural support as well as weather protection. The upper surface is tempered glass and the cells are encapsulated in two layers of ethylene vinyl acetate (EVA). Finally, the back is covered with sheets of polymer that prevent moisture penetration.

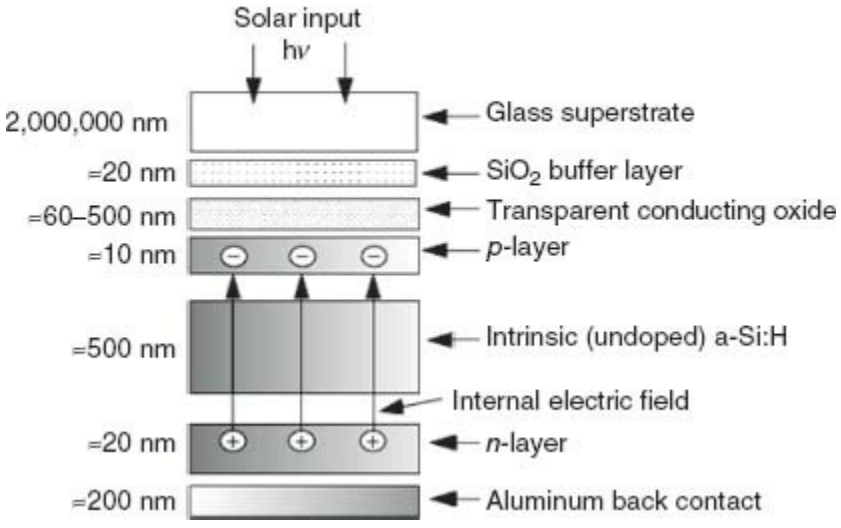
5.3.2 Amorphous Silicon

Conventional crystalline silicon technologies require considerable amounts of expensive material with additional complexity and costs needed to wire individual cells together. An alternative technology is based on amorphous (glassy) silicon (a-Si); that is, silicon in which there is very little order to the arrangement of atoms. Since it is not crystalline, the organized tetrahedral structure in which one silicon atom bonds to its four adjacent neighbors in a precisely defined manner does not apply. While almost all of the atoms do

form bonds with four other silicon atoms, there remain numerous "dangling bonds" where nothing attaches to one of the valence electrons. These dangling-bond defects act as recombination centers so that photogenerated electrons recombine with holes before they can travel very far. The key to making a-Si into a decent PV material was first discovered, somewhat by accident, in 1969, by a British team that noted a glow when silane gas SiH_4 was bombarded with a stream of electrons (Chittick et al., 1969). That led to their critical discovery that by alloying amorphous silicon with hydrogen, the concentration of defects could be reduced by about three orders of magnitude. The concentration of hydrogen atoms in these alloys is roughly one atom in 10 so their chemical composition is approximately $Si_{0.9}H_{0.1}$. Moreover, the silicon–hydrogen alloy that results, designated as a-Si:H, is easily doped to make n-type and p-type materials for solar cells.

So, how can a p–n junction be formed in an amorphous material with very little organization among its atoms? Figure 5.19 shows a cross-section of a simple a-Si:H cell that uses glass as the supporting superstrate. On the underside of the glass a buffer layer of SiO_2 may be deposited in order to prevent subsequent layers of atoms from migrating into the glass. Next comes the electrical contact for the top of the cell, which is usually a transparent conducting oxide such as tin oxide, indium tin oxide, or zinc oxide. The actual p–n junction, whose purpose is of course to create the internal electric field in the cell to separate holes and electrons, consists of three layers consisting of the p-layer and n-layer separated by an undoped (intrinsic) region of a-Si:H. As shown, the p-layer is only 10-nm thick, the intrinsic, or i-layer is about 500 nm, and the n-layer is about 20 nm. Note the electric field created between the rigid positive charges in the n-layer and the rigid negative charges in the p-layer spans almost the full depth of the cell. That means light-induced hole–electron pairs created almost anywhere within the cell will be swept across the intrinsic layer by the internal field. These amorphous silicon PVs are referred to as *p-i-n* cells.

FIGURE 5.19 Cross-section of an amorphous silicon p-i-n cell. The example thicknesses are in nanometers (10^{-9} m) and are not drawn to scale.

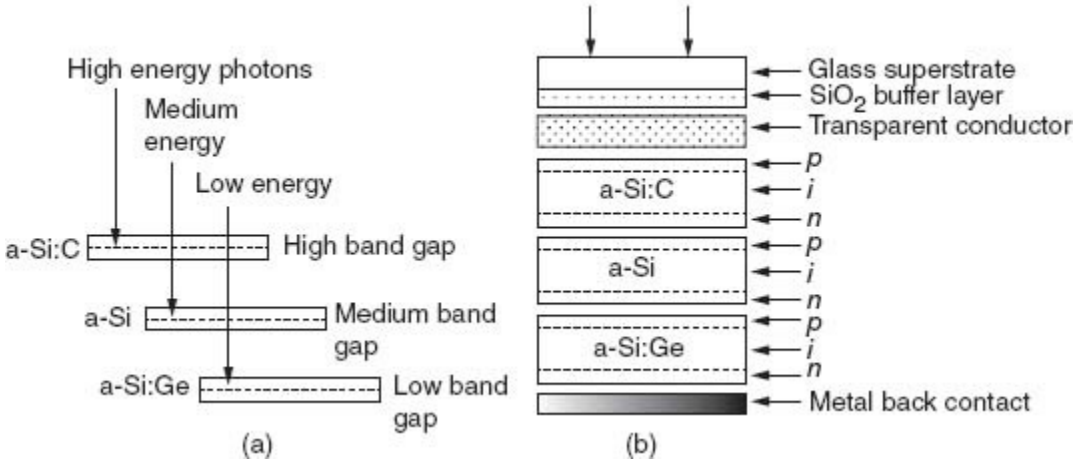


The band-gap of a-Si:H is 1.75 eV, which is quite a bit higher than the 1.1 eV for crystalline silicon. Recall that higher band-gaps increase voltage at the expense of lower

currents (a smaller fraction of solar photons have sufficient energy to create hole–electron pairs). Since power is the product of voltage and current, there will be some optimum band-gap for a single-junction cell, which will theoretically result in the most efficient device. As was shown in Figure 5.8, that optimum band-gap is about 1.35 eV. So crystalline silicon has a band-gap somewhat too low, while a-Si has one too high to be optimum. As it turns out, however, amorphous silicon has the handy property that alloys made with other Group IV elements will cause the band-gap to change. As a general rule, moving up a row in the periodic table increases band-gap, while moving down a row decreases band-gap. Referring to the portion of the periodic table given in Table 5.1, this rule would suggest that carbon (directly above silicon) would have a higher band-gap than silicon, while germanium (directly below silicon) would have a lower band-gap. To lower the 1.75 eV band-gap of amorphous silicon toward the 1.35 eV optimum, that suggests an alloy of silicon with the right amount of germanium (forming a-Si:H:Ge) can help improve cell efficiency.

The above discussion on a-Si alloys leads to an even more important opportunity, however. When a-Si is alloyed with carbon, for example, the band-gap can be increased (to about 2 eV), and when alloyed with germanium the gap will be reduced (to about 1.3 eV). That suggests that multijunction PV devices can be fabricated by layering p–n junctions of different alloys. The idea behind a multijunction cell (also known as a *tandem* cell) is to create junctions with decreasing band-gaps as photons penetrate deeper and deeper into the cell. As shown in Figure 5.20a, the top junction should capture the most energetic photons while allowing photons with less energy to pass through to the next junction below, and so forth. In Figure 5.20b, an amorphous silicon, three-junction PV device is shown in which the cell takes advantage of the ability of germanium and carbon to increase or decrease the a-Si:H band-gap.

FIGURE 5.20 Multijunction (tandem) amorphous silicon solar cells can be made by alloying a-Si:H (band-gap ≈ 1.75 eV) with carbon a-Si:C in the top layer (≈ 2.0 eV) to capture the highest energy (blue) photons and germanium a-Si:Ge (≈ 1.3 eV) in the bottom layer to capture the lowest energy (red) photons.



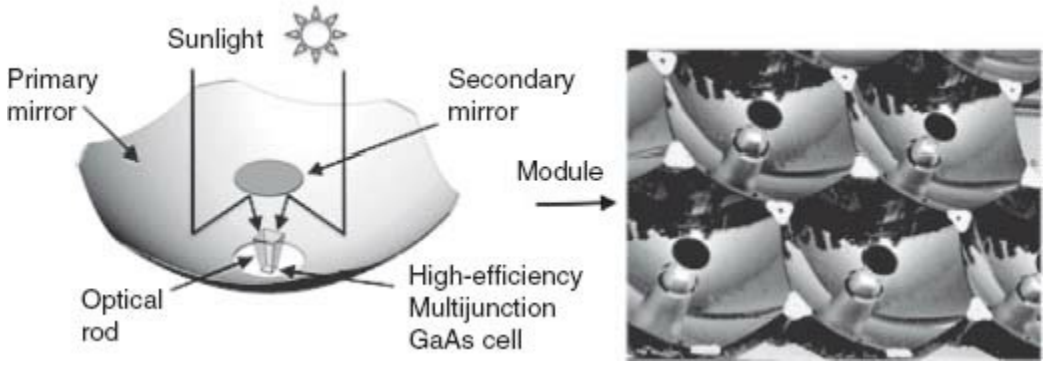
5.3.3 Gallium Arsenide

Gallium arsenide is an example of what are referred to as compound semiconductors in

which the basic crystalline structure is made up of a mixture of elements. The crystals are grown using an epitaxial process in which thin layers of material are grown one on top of the other. Each layer can be doped appropriately to create p- and n-type materials as well as to provide multijunction, high efficiency performance. As shown in Figure 5.8, the GaAs band-gap of 1.43 eV is quite near the optimum value so it may not be surprising to discover that GaAs cells are among the very most efficient, single-junction and multijunction PVs made today. In fact, the theoretical maximum efficiency of single-junction GaAs solar cells, without solar concentration, is a very high 29%, and with concentration it is all the way up to 39% (Bube, 1998). As of 2012, multijunction GaAs cells had already achieved 29% one-sun efficiency and over 43% efficiencies in concentrated sunlight.

In contrast to silicon cells, the efficiency of GaAs is relatively insensitive to increasing temperature, which helps them perform better than Si under concentrated sunlight. They are also less affected by cosmic radiation, and as thin films they are lightweight, which gives them an advantage in space applications. On the other hand, gallium is much less abundant in the earth's crust and it is a very expensive material. When coupled with the much more difficult processing required to fabricate GaAs cells, they have been too expensive in the past for most ordinary single-junction, one-sun, flat-plate applications. However, they are enjoying somewhat of a renaissance now with multijunction cells under concentrated sunlight (Fig. 5.21). By combining cheap sunlight-concentrating optics with expensive per unit of area, but very small in size, GaAs cells, overall cost effectiveness is quite comparable to other PV systems.

FIGURE 5.21 Multijunction GaAs cells used in a tracking, concentrating collector system (From SolFocus).

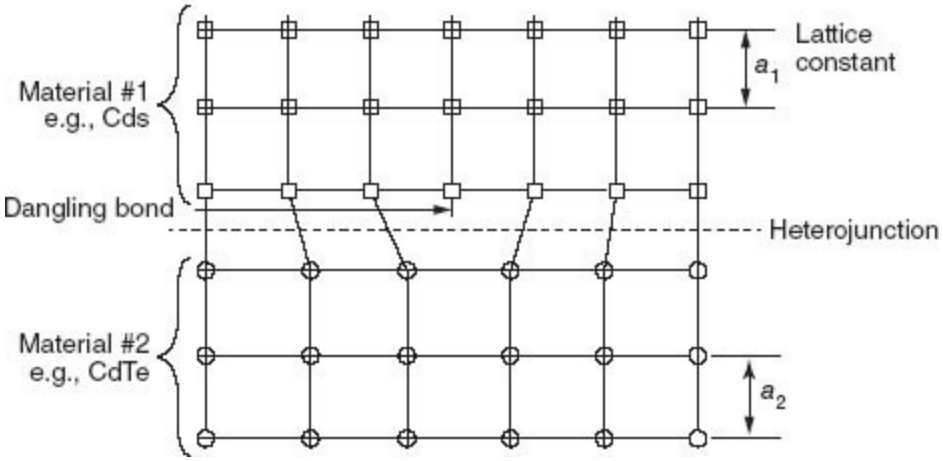


5.3.4 Cadmium Telluride

Cadmium telluride (CdTe) is the most successful example of a II-VI PV compound. Although it can be doped in both p-type and n-type forms, it is most often used as the p-layer in cells for which the n-layer is an entirely different material. When different materials make up the two sides of the junction, the cells are called heterojunction cells (as distinct from single-material homojunction cells). One difficulty associated with heterojunctions is the mismatch between the size of the crystalline lattice of the two materials, which leads to dangling bonds as shown in Figure 5.22. One way to sort out the best materials to use for the n-layer of CdTe cells is based on the mismatch of their lattice dimensions as expressed by their *lattice constants* (the a_1, a_2 dimensions shown in Fig. 5.22). The compound that is

most often used for the n-layer is cadmium sulfide (CdS), which has a relatively modest lattice mismatch of 9.7% with CdTe.

FIGURE 5.22 The mismatch between heterojunction materials leads to dangling bonds as shown.



The band-gap for CdTe is 1.44 eV, which puts it very close to the optimum for terrestrial cells. Thin-film laboratory cells using the n-CdS/p-CdTe heterojunction have efficiencies over 17% and production modules are reaching efficiencies over 12%. While this is considerably lower than crystalline silicon, they more readily lend themselves to mass production manufacturing and since they are thin film they need far less raw material. They have become, therefore, less expensive on a dollar-per-watt basis. When area constraints are not an issue, their lower efficiency, but cheaper cost, makes them economically competitive with silicon.

One aspect of CdS/CdTe cells that needs to be considered carefully is the potential hazard to human health and the environment associated with cadmium. Cadmium is a very toxic substance and it is categorized as a probable human carcinogen. As is the case for most PV technologies, special precautions need to be taken during the manufacturing process. Once the cells, and the cadmium they contain, are sealed between the two glass plates that are standard in current modules, the likelihood of exposure is considered highly unlikely even in the event of a fire.

5.3.5 Copper Indium Gallium Selenide

The goal in exploring compounds made up of a number of elements is to find combinations with band-gaps that approach the optimum value while minimizing inefficiencies associated with lattice mismatch. Copper indium selenide, $CuInSe_2$, better known as "CIS, " is a *ternary* compound consisting of one element, copper, from the first column of the periodic table, another from the third column, indium, along with selenium from the sixth column. It is therefore referred to as a I-III-VI material. A simplistic way to think about this complexity is to imagine that the average properties of Cu (Group I) and In (Group III) are somewhat like those of an element from the second column (Group II), so the whole molecule might be similar to a II-VI compound such as CdTe.

CIS cells have a band-gap of 1.0 eV, which is considerably below the ideal band-gap of

about 1.4 shown in Figure 5.8. When gallium is used as the ternary compound instead of indium, the resulting compound has a band-gap of 1.7 eV, which is above the ideal. With the substitution of gallium for some of the indium in the CIS material, the relatively low band-gap of CIS is increased and efficiency is improved. This is consistent with our interpretation of the periodic table in which band-gap increases for elements in higher rows of the table (Ga is above In). By blending the two, it is, in principle, possible to provide whatever band-gap between 1.0 and 1.7 that might be desired. The result, written as $CuIn_xGa_{(1-x)}Se_2$ where the "x" and "$(1 - x)$" refer to the relative percentages of indium and gallium, is referred to as a copper indium gallium selenide (CIGS) cell. They use a very thin layer of cadmium sulfide (CdS) for their n-type layer. Laboratory efficiencies of 20% and commercial modules with 14% efficiency make CIGS currently more efficient than CdTe; moreover, they use considerably less cadmium than CdTe.

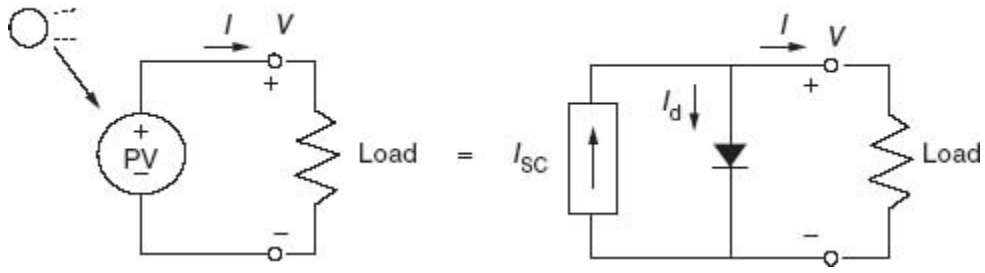
5.4 EQUIVALENT CIRCUITS FOR PV CELLS

It is very handy to have some way to model the behavior of individual solar cells and combinations of them in modules and arrays. Engineers like to characterize real electrical devices in terms of equivalent circuits made up of discrete idealized components as a way to help predict performance. Just remember these are idealized representations and there are no discrete resistors, for example, sitting somewhere inside a solar cell.

5.4.1 The Simplest Equivalent Circuit

A simple equivalent circuit model for a PV cell consists of a real diode in parallel with an ideal current source as shown in Figure 5.23. The ideal current source delivers current in proportion to the solar flux to which it is exposed.

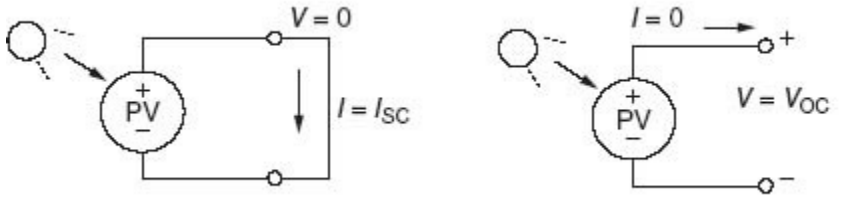
FIGURE 5.23 A simple equivalent circuit for a PV cell consists of a current source driven by sunlight in parallel with a real diode.



There are two conditions of particular interest for the actual PV and for its equivalent circuit. As shown in Figure 5.24, they are (1) the current that flows when the terminals are shorted together (the short-circuit current, I_{SC}) and (2) the voltage across the terminals when the leads are left open (the open-circuit voltage, V_{OC}). When the leads of the equivalent circuit for the PV cell are shorted together, no current flows in the (real) diode since $V_d = 0$, so all of the current from the ideal source flows through the shorted leads.

Since that short-circuit current must equal I_{SC}, the magnitude of the ideal current source itself must be equal to I_{SC}.

FIGURE 5.24 Two important parameters for photovoltaics are the short-circuit current I_{SC} and the open-circuit voltage V_{OC}.



(a) Short-circuit current (b) Open-circuit voltage

Now we can write a voltage and current equation for the equivalent circuit of the PV cell shown in Figure 5.23. Start with

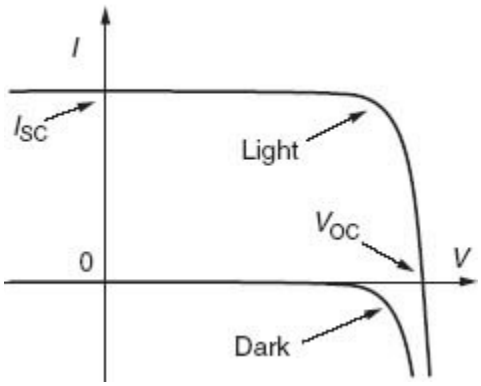
$$I = I_{SC} - I_d \tag{5.7}$$

and then substitute Equation 5.3 into Equation 5.7 to get

$$I = I_{SC} - I_0\left(e^{qV/kT} - 1\right) \tag{5.8}$$

It is interesting to note that the second term in Equation 5.8 is just the diode equation with a negative sign. That means a plot of Equation 5.8 is just I_{SC} added to the diode curve of Figure 5.13c turned upside-down. Figure 5.25 shows the current–voltage relationship for a PV cell when it is dark (no illumination) and light (illuminated) based on Equation 5.8.

FIGURE 5.25 Photovoltaic current–voltage relationship for "dark" (no sunlight) and "light" (an illuminated cell). The dark curve is just the diode curve turned upside down. The light curve is the dark curve plus I_{SC}.



When the leads from the PV cell are left open, $I = 0$ and we can solve Equation 5.8 for the open-circuit voltage V_{OC}:

$$V_{OC} = \frac{kT}{q}\ln\left(\frac{I_{SC}}{I_0} + 1\right) \tag{5.9}$$

And at 25°C, Equations (5.8) and (5.9) simplify to

(5.10) $$I = I_{SC} - I_0\left(e^{38.9V} - 1\right)$$

and

(5.11) $$V_{OC} = 0.0257 \ln\left(\frac{I_{SC}}{I_0} + 1\right)$$

In both of these equations, short-circuit current, I_{SC}, is directly proportional to solar irradiation, which means we can now quite easily plot sets of PV current–voltage curves for varying sunlight. Also, quite often laboratory specifications for the performance of PVs are given per square centimeter of junction area, in which case the currents in the above equations are written as current densities. Both of these points are illustrated in the following example.

Example 5.3 The *I–V* Curve for a PV Cell. Consider a 150 cm^2 PV cell with reverse saturation current $I_0 = 10^{-12}$ A/cm^2. In full sun, it produces a short-circuit current of 40 mA/cm^2 at 25°C. What would be the short-circuit current and open-circuit voltage in full sun and again for 50% sun. Plot the resulting *I–V* curves.

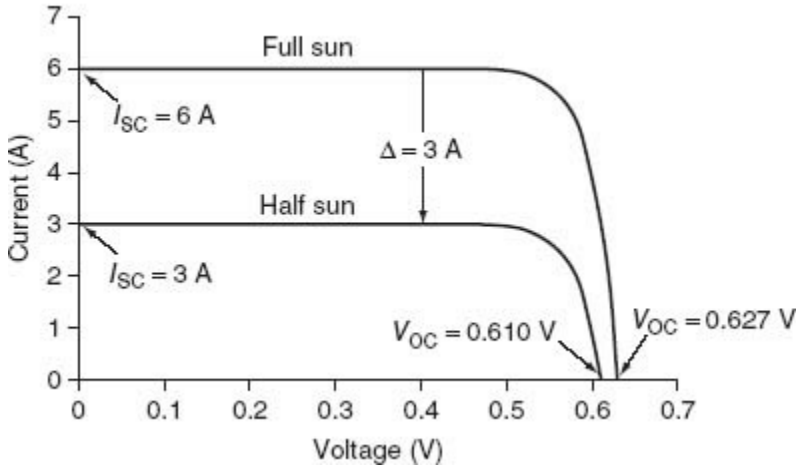
Solution. The reverse saturation current $I_0 = 10^{-12}$ A/cm^2 × 150 cm^2 = 1.5 × 10^{-10} A. At full sun short-circuit current, I_{SC}, is 0.040 A/cm^2 × 150 cm^2 = 6.0 A. From Equation 5.11, the open-circuit voltage for a single cell is

$$V_{OC} = 0.0257 \ln\left(\frac{I_{SC}}{I_0} + 1\right) = 0.0257 \ln\left(\frac{6.0}{1.5 \times 10^{-10}} + 1\right) = 0.627 \text{ V}$$

Since short-circuit current is proportional to solar intensity, at half sun I_{SC} = 3 A and the open-circuit voltage is

$$V_{OC} = 0.0257 \ln\left(\frac{3.0}{1.5 \times 10^{-10}} + 1\right) = 0.610 \text{ V}$$

Plotting Equation 5.10 gives us the following. Note that the half-sun curve is just the full-sun curve shifted downward by 3 A.



5.4.2 A More Accurate Equivalent Circuit for a PV Cell

Most often, a more complex PV equivalent circuit than the one shown in Figure 5.23 is needed. For example, consider the impact of shading on a string of cells wired in series (Fig. 5.26 shows two such cells). If any cell in the string is in the dark (shaded), it produces no current. In our simplified equivalent circuit for the shaded cell, the current through that cell's current source is zero and its diode is back biased so it does not pass any current either (other than a tiny amount of reverse saturation current). That means the simple equivalent circuit suggests that no power will be delivered to a load if any of its cells are shaded. While it is true that PV modules are very sensitive to shading, the situation is not quite as bad as that. So, we need a more complex model if we are going to be able to deal with realities such as the shading problem.

FIGURE 5.26 The simple equivalent circuit of a string of cells in series suggests that virtually no current can flow to the load if any cell is in the dark (shaded). A more complex model can deal with this problem.

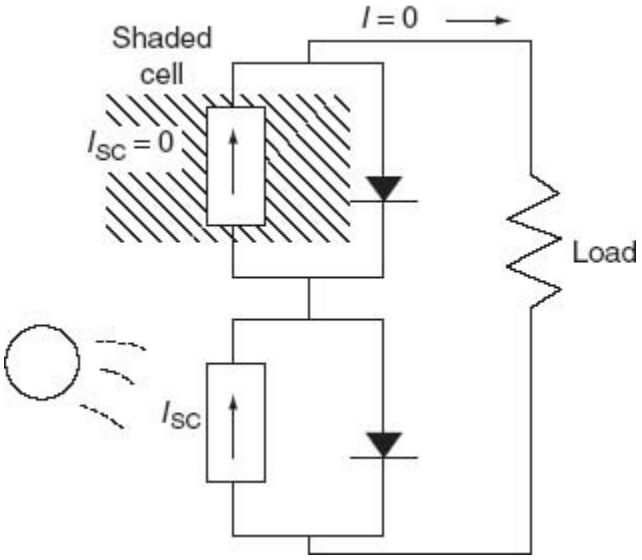


FIGURE 5.27 The simple PV equivalent circuit with an added parallel resistance.

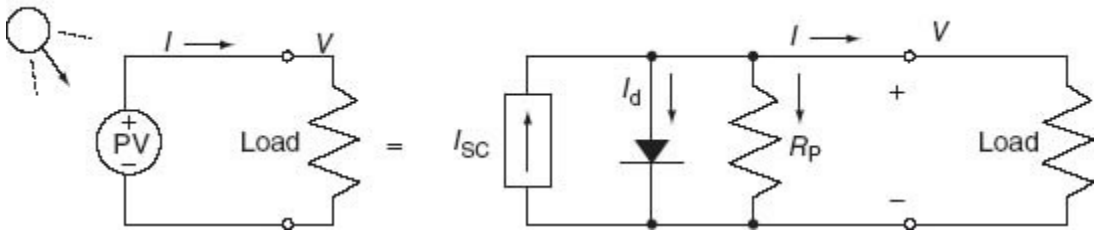


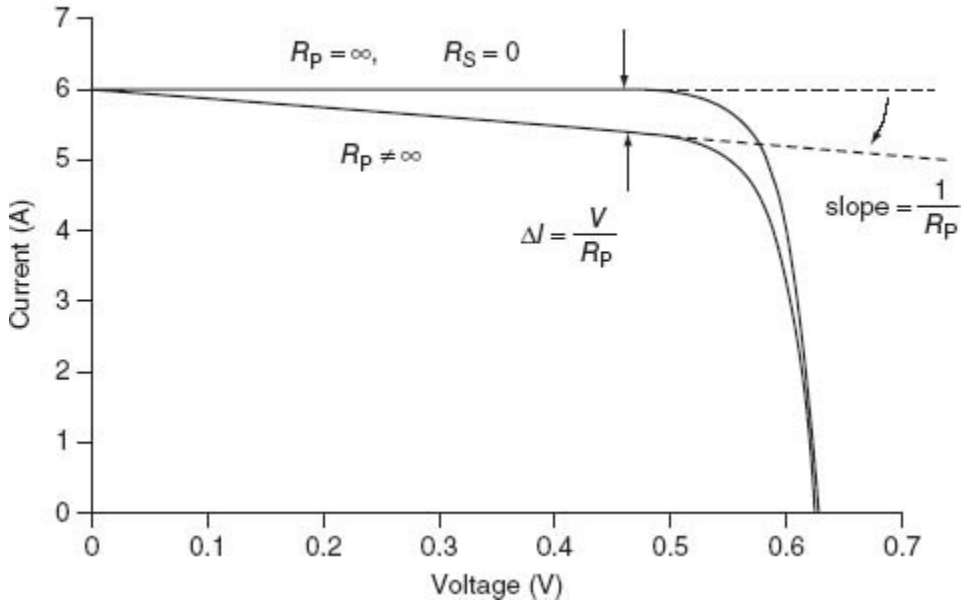
Figure 5.27 shows a PV equivalent circuit that includes some parallel leakage resistance R_P. The ideal current source I_{SC} powered by the sun in this case delivers current to the diode, the parallel resistance, and the load:

$$I = (I_{SC} - I_d) - \frac{V}{R_P} \tag{5.12}$$

The term in the parentheses of Equation 5.12 is the same current that we had for the simple model. So, what Equation 5.12 tells us is that at any given voltage, the parallel

leakage resistance causes load current for the ideal model to be decreased by V/R_P as is shown in Figure 5.28.

FIGURE 5.28 Modifying the idealized PV equivalent circuit by adding parallel resistance causes the current at any given voltage to drop by V/R_P.



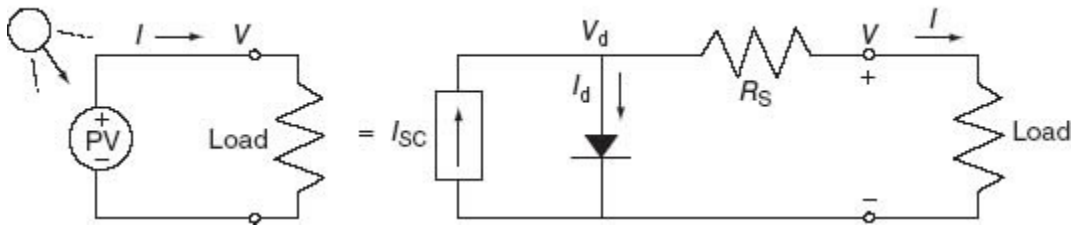
For a cell to have less than 1% losses due to its parallel resistance, R_P should be greater than about

$$R_P > \frac{100 V_{OC}}{I_{SC}} \tag{5.13}$$

For a large cell, I_{SC} might be around 6 A and V_{OC} about 0.6 V, which says its parallel resistance should be greater than about 10 Ω.

An even better equivalent circuit will include series resistance as well as parallel resistance. Before we can develop that model, consider Figure 5.29 in which the original PV equivalent circuit has been modified to include only some series resistance, R_S. Some of this might be contact resistance associated with the bond between the cell and its wire leads, and some might be due to the resistance of the semiconductor itself.

FIGURE 5.29 A PV equivalent circuit with series resistance.



To analyze Figure 5.29, start with the equation for the simple equivalent circuit (Eq. 5.8)

(5.8) $$I = I_{SC} - I_d = I_{SC} - I_0\left(e^{qV_d/kT} - 1\right)$$

and then add the impact of R_S,

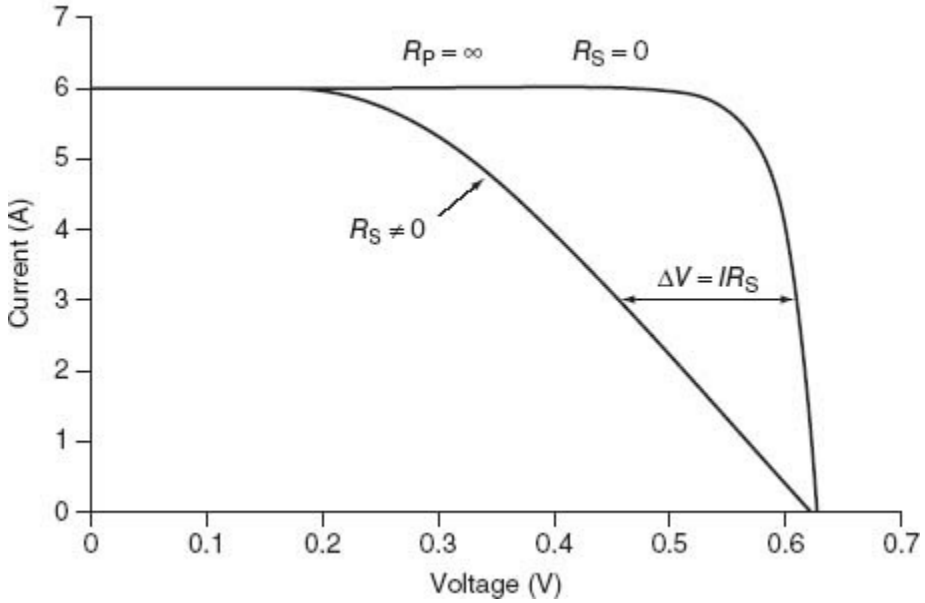
(5.14) $$V_d = V + IR_S$$

to give

(5.15) $$I = I_{SC} - I_0\left\{\exp\left[\frac{q}{kT}(V + IR_S)\right] - 1\right\}$$

Equation 5.15 can be interpreted as the original PV I–V curve with the voltage at any given current shifted to the left by $\Delta V = IR_S$ as shown in Figure 5.30.

FIGURE 5.30 Adding series resistance to the PV equivalent circuit causes the voltage at any given current to shift to the left by $\Delta V = IR_s$.



For a cell to have less than 1% losses due to the series resistance, R_S will need to be less than about

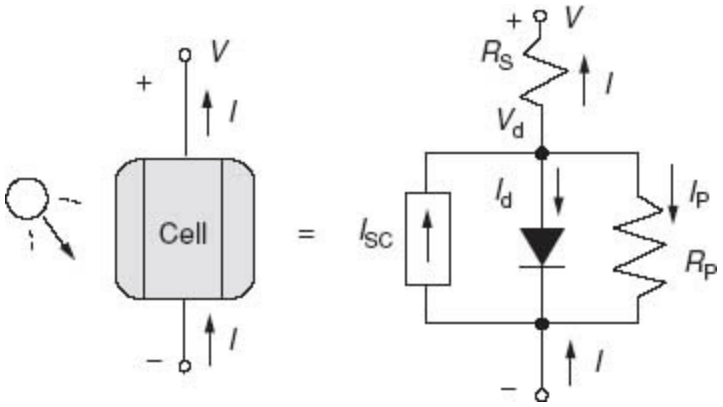
(5.16) $$R_S < \frac{0.01\,V_{OC}}{I_{SC}}$$

which, for a large cell with I_{SC} = 6 A and V_{OC} = 0.6 V, would be less than 0.001 Ω.

Finally, let us generalize the PV equivalent circuit by including both series and parallel resistances as shown in Figure 5.31. We can write the following equation for current and voltage

(5.17) $$I = I_{SC} - I_0\left\{\exp\left[\frac{q}{kT}(V + IR_S)\right] - 1\right\} - \left(\frac{V + IR_S}{R_P}\right)$$

FIGURE 5.31 A more complex equivalent circuit for a PV cell includes both parallel and series resistances. The shaded diode reminds us this is a "real" diode rather than an ideal one.



Unfortunately, Equation 5.17 is a complex equation for which there is no explicit solution for either voltage V or current I. A spreadsheet solution, however, is fairly straightforward and has the extra advantage of enabling a graph of I versus V to be obtained easily. The approach is based on incrementing values of diode voltage, V_d, in the spreadsheet. For each value of V_d, corresponding values of current I and voltage V can easily be found. Example 5.4 shows how this can be done.

Using the sign convention shown in Figure 5.31 and applying Kirchhoff's current law to the node above the diode, we can write

$$I_{SC} = I + I_d + I_P \tag{5.18}$$

Rearranging and substituting the Shockley diode Equation 5.5 at 25°C gives

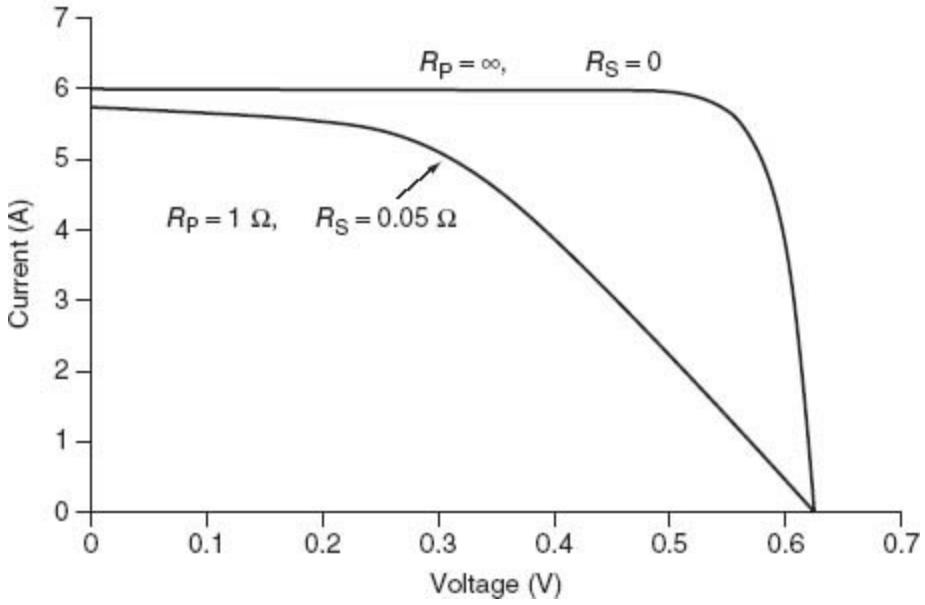
$$I = I_{SC} - I_0\left(e^{38.9V_d} - 1\right) - \frac{V_d}{R_P} \tag{5.19}$$

For each value of V_d in the spreadsheet, current I can be found from Equation 5.19. Voltage across an individual cell then can be found from

$$V = V_d - IR_S \tag{5.20}$$

A plot of Equation 5.17 obtained this way for an equivalent circuit with R_S = 0.05 Ω and R_P = 1 Ω is shown in Figure 5.32. As might be expected, the graph combines features of Figures 5.28 and 5.30.

FIGURE 5.32 Series and parallel resistances in the PV equivalent circuit decrease both voltage and current delivered. To improve cell performance, high R_P and low R_S are needed.

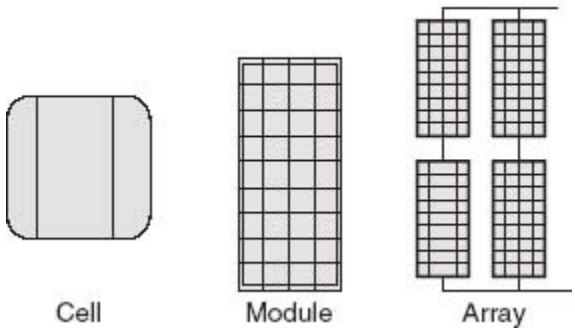


5.5 FROM CELLS TO MODULES TO ARRAYS

Since an individual cell produces only about 0.5 V, it is a rare application for which just a single cell is of any use. Instead, the basic building block for PV applications is a *module* consisting of a number of pre-wired cells in series, all encased in tough, weather-resistant packages. A typical module from a few years ago had 36 cells in series and since they were often used for 12-V battery charging, they were often designated as "12-V modules" even though they are capable of delivering much higher voltages than that. As the market has shifted toward larger and larger systems, 72-, 96-, and 128-cell modules are now quite common. More cells per module means fewer modules and fewer interconnections between them, which is a major advantage for larger-scale PV systems.

Multiple modules, in turn, can be wired in series to increase voltage and in parallel to increase current, the product of which is power. An important element in PV system design is deciding how many modules should be connected in series and how many in parallel to deliver whatever energy is needed. Such combinations of modules are referred to as an *array*. Figure 5.33 shows this distinction between cells, modules, and arrays.

FIGURE 5.33 Photovoltaic cells, modules, and arrays.

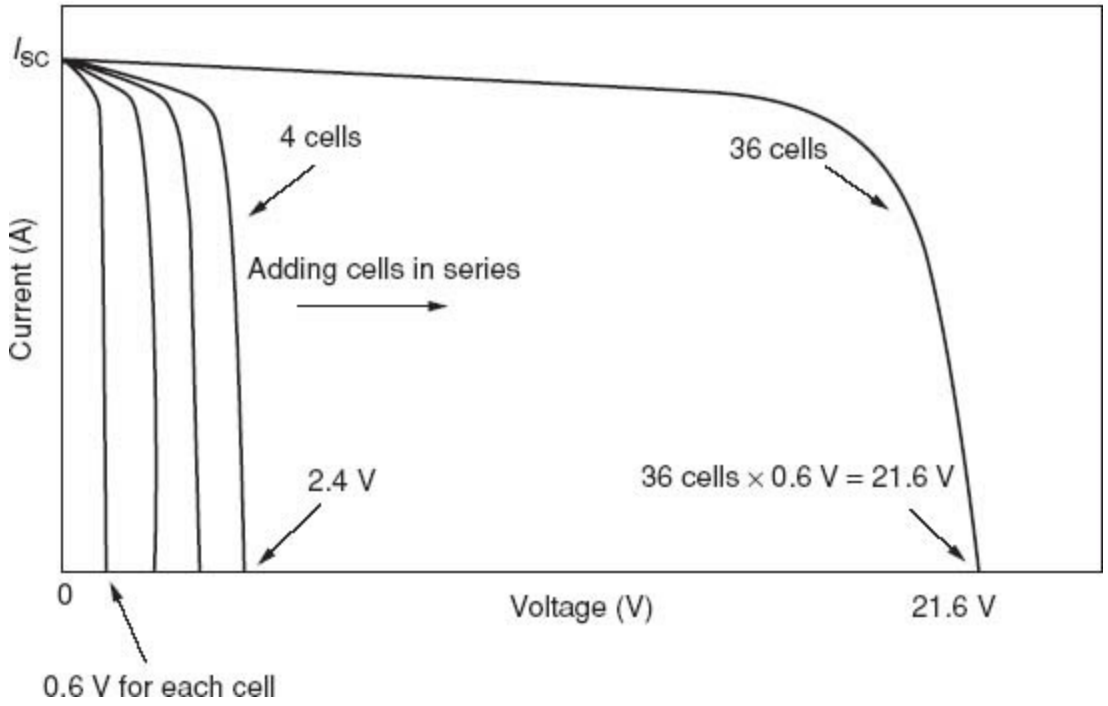


5.5.1 From Cells to a Module

When PVs are wired in series, all the cells carry the same current, and at any given current, their voltages add as shown in Figure 5.34. That means we can continue the spreadsheet solution of Equations 5.19 and 5.20 to find an overall module voltage V_{module} by multiplying Equation 5.20 by the number of cells in the module n.

$$V_{module} = n\,(V_d - IR_S) \tag{5.21}$$

FIGURE 5.34 For cells wired in series, their voltages at any given current add. This figure is for a module with 36 cells.



Example 5.4 Voltage and Current From a PV Module. A PV module is made up of 72 identical cells, all wired in series. With 1-sun insolation (1 kW/m^2), each cell has short-circuit current I_{SC} = 6.0 A and at 25°C, its reverse saturation current is $I_0 = 5 \times 10^{-11}$ A. Parallel resistance R_P = 10.0 Ω and series resistance R_S = 0.001 Ω.

a. Find the voltage, current, and power delivered when the diode voltage in the equivalent circuit for each cell is 0.57 V.

b. Set up a spreadsheet for I and V of the entire module and present a few lines of output show how it works.

Solution

a. Using V_d = 0.57 V in Equation 5.19 along with the other data gives current

$$I = I_{SC} - I_0\left(e^{38.9V_d} - 1\right) - \frac{V_d}{R_P}$$

$$= 6.0 - 5 \times 10^{-11}\left(e^{38.9\times0.57} - 1\right) - \frac{0.57}{10.0} = 5.73 \text{ A}$$

Under these conditions, Equation 5.21 gives the voltage produced by the 72-cell module:

$$V_{module} = n\left(V_d - IR_S\right) = 72\left(0.57 - 5.73 \times 0.001\right) = 40.63 \text{ V}$$

Power delivered is therefore

$$P(\text{Watts}) = V_{module}\, I = 40.63 \text{ V} \times 5.73 \text{ A} = 232.8 \text{ W}$$

A spreadsheet might look something like the following:

Daily Clear-Sky Insoation (kWh/m^2)														Latitude 30° N							
Azimuth:		South						SE, SW						East, West						Tracking	
Tilt:	0	20	30	40	50	60	90	20	30	40	50	60	90	20	30	40	50	60	90	1-Axis	2-Axis
Jan	4.31	5.92	6.47	6.83	7.00	6.95	5.64	5.38	5.68	5.82	5.79	5.63	4.22	4.11	3.91	3.71	3.43	3.15	2.06	7.90	8.33
Feb	5.48	6.81	7.20	7.37	7.32	7.07	5.12	6.35	6.53	6.53	6.36	6.04	4.22	5.24	5.02	4.73	4.38	4.01	2.63	9.26	9.39
Mar	6.67	7.48	7.57	7.44	7.09	6.54	3.87	7.13	7.11	6.90	6.53	6.01	3.79	6.36	6.04	5.63	5.21	4.70	2.98	9.97	9.97
Apr	7.66	7.77	7.50	7.03	6.35	5.50	2.23	7.65	7.37	6.93	6.36	5.64	3.16	7.29	6.90	6.44	5.89	5.26	3.27	10.24	10.51
May	8.15	7.74	7.20	6.51	5.64	4.61	1.27	7.77	7.32	6.72	6.03	5.21	2.65	7.75	7.33	6.80	6.18	5.51	3.36	10.03	10.77
Jun	8.23	7.63	7.01	6.25	5.31	4.24	1.00	7.72	7.20	6.56	5.82	4.98	2.43	7.82	7.38	6.83	6.19	5.52	3.32	9.74	10.72
July	8.04	7.63	7.10	6.41	5.55	4.54	1.27	7.66	7.21	6.62	5.93	5.12	2.60	7.65	7.23	6.70	6.09	5.43	3.29	9.78	10.53
Aug	7.48	7.59	7.32	6.85	6.20	5.37	2.20	7.46	7.19	6.75	6.18	5.49	3.06	7.12	6.74	6.28	5.73	5.11	3.16	9.81	10.09
Sept	6.51	7.26	7.33	7.19	6.84	6.31	3.72	6.93	6.90	6.68	6.31	5.80	3.64	6.21	5.89	5.49	5.06	4.56	2.88	9.50	9.50
Oct	5.29	6.56	6.92	7.09	7.05	6.80	4.95	6.12	6.29	6.28	6.11	5.80	4.05	5.05	4.84	4.55	4.20	3.84	2.50	8.76	8.88
Nov	4.22	5.77	6.30	6.65	6.81	6.77	5.49	5.25	5.54	5.67	5.64	5.48	4.10	4.02	3.83	3.62	3.34	3.07	2.00	7.64	8.05
Dec	3.86	5.52	6.12	6.54	6.76	6.79	5.71	4.97	5.31	5.50	5.53	5.42	4.19	3.69	3.52	3.34	3.11	2.86	1.90	7.39	7.95
kWh/m^2/yr	2310	2545	2555	2497	2368	2172	1289	2445	2423	2341	2207	2025	1280	2200	2088	1951	1790	1613	1015	3346	3489

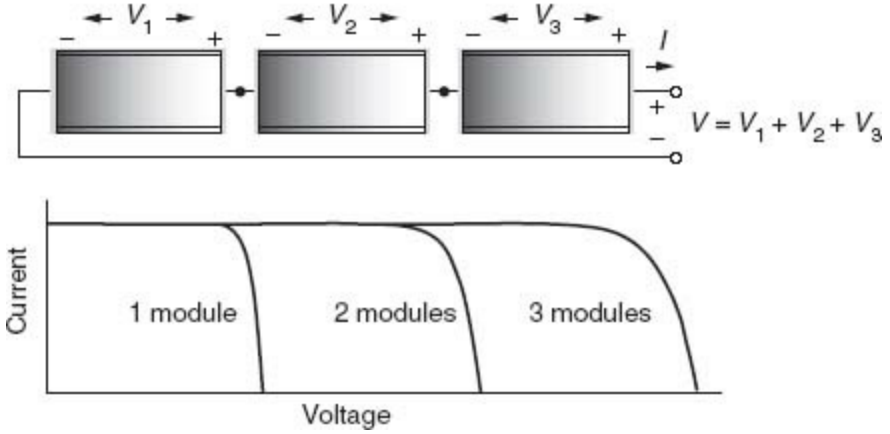
Note that we have found the maximum power point (MPP) for this module, which is at I = 5.73 A, V = 40.627 V, and P = 232.8 W. This could be described as a 233-W module. It would be easy to draw the entire I–V curve from this spreadsheet.

5.5.2 From Modules to Arrays

Modules can be wired in series to increase voltage, and in parallel to increase current. Arrays are made up of some combination of series and parallel modules to increase power. In general, modules are first arrayed in a series string to build up voltage to as high as safety concerns will allow before paralleling those strings to increase power. This strategy helps reduce I^2R power loss in connecting wires.

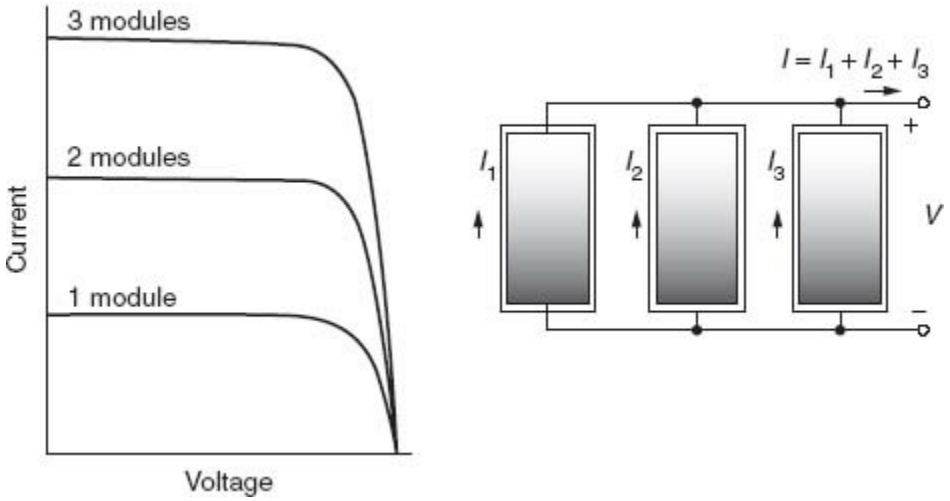
For a string of modules in series, the I–V curves are simply added along the voltage axis. That is, at any given current (which flows through each of the modules), the total voltage of the string is just the sum of the individual module voltages as is suggested in Figure 5.35.

FIGURE 5.35 For modules in series, at any given current the voltages add.



For modules in parallel, the same voltage is across each module and the total current is the sum of the currents. That is, at any given voltage, the *I–V* curve of the parallel combination is just the sum of the individual module currents at that voltage. Figure 5.36 shows the *I–V* curve for three modules in parallel.

FIGURE 5.36 For modules in parallel, at any given voltage the currents add.



When high power is needed, the array will usually consist of a combination of series and parallel modules for which the total *I–V* curve is the sum of the individual module *I–V* curves. Figure 5.37 shows how the *I–V* curves for individual modules stack up for an array consisting of two parallel strings with three modules per string. Figure 5.38 shows one way to arrange multiple strings into a large array.

FIGURE 5.37 The total *I–V* curve of an array consisting of two strings of three modules each.

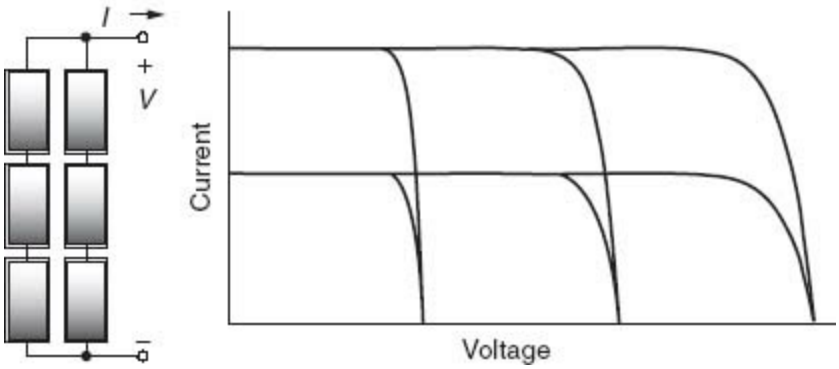
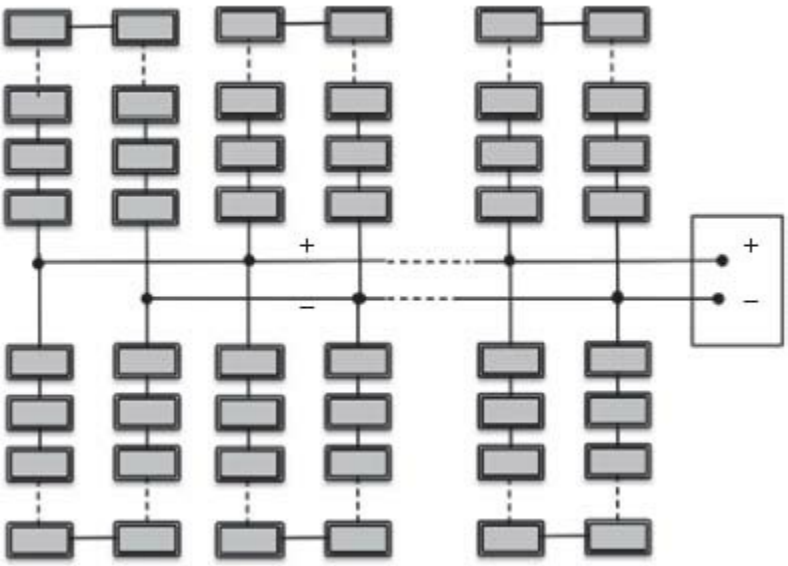


FIGURE 5.38 Multiple strings in parallel for large power arrays.



5.6 THE PV *I–V* CURVE UNDER STANDARD TEST CONDITIONS

Consider, for the moment, a single PV module that you want to connect to some sort of a load (Fig. 5.39). For example, the load might be a DC motor driving a pump or it might be a battery. Before the load is connected, the module sitting in the sun will produce an open-circuit voltage V_{OC}, but no current will flow. If the terminals of the module are shorted together (which does not hurt the module at all, by the way), the short-circuit current I_{SC} will flow, but the output voltage will be zero. In both cases, since power is the product of current and voltage, no power is delivered by the module and no power is received by the load. When the load is actually connected, some combination of current and voltage will result and power will be delivered. To figure out how much power, we have to consider the *I–V* characteristic curve of the module as well as the *I–V* characteristic curve of the load.

FIGURE 5.39 No power is delivered when the circuit is open (a) or shorted (b). When the load is connected, the same current flows through the load and module and the same

voltage appears across them (c).

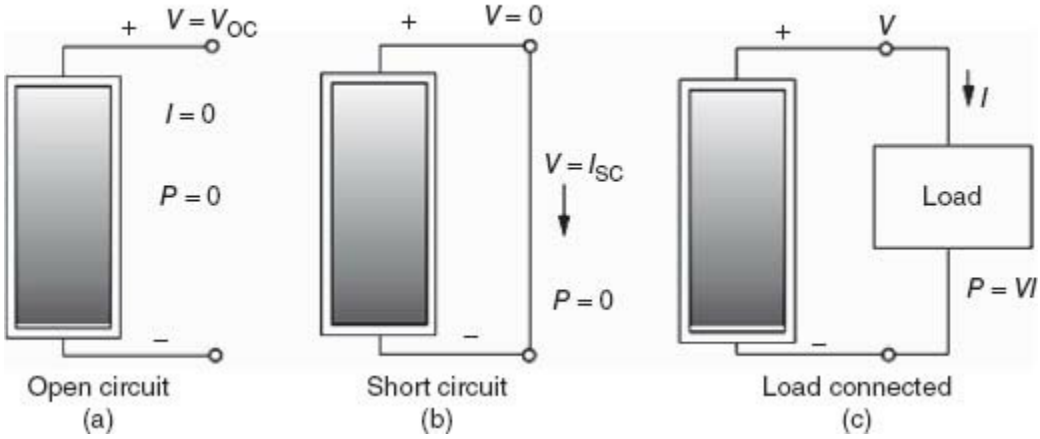
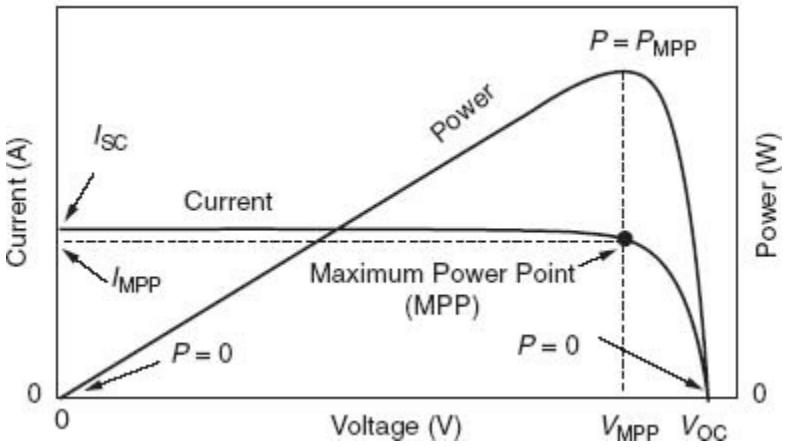


Figure 5.40 shows a generic *I–V* curve for a PV module, identifying several key parameters including the open-circuit voltage V_{OC} and the short-circuit current I_{SC}. Also shown is the product of voltage and current, that is, power delivered by the module. At the two ends of the *I–V* curve, the output power is zero since either current or voltage is zero at those points. The MPP is that spot near the knee of the *I–V* curve at which the product of current and voltage reaches its maximum. The power, voltage, and current at the MPP are usually designated as P_{MPP}, V_{MPP}, and I_{MPP}, respectively, with the understanding that these are values obtained under well-defined idealized test conditions to be described later.

FIGURE 5.40 The *I–V* curve and power output for a PV module. If drawn under standard test conditions, the MPP identifies the rated voltage V_R, current I_R, and power P_R for the module.

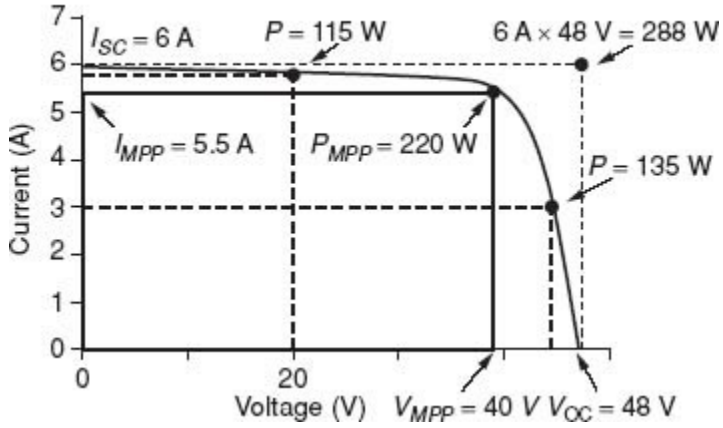


Another way to visualize the location of the MPP is by imagining trying to find the biggest possible rectangle that will fit beneath the *I–V* curve. As shown in Figure 5.41, the sides of the rectangle correspond to current and voltage, so its area is power. Another quantity that is often used to characterize module performance is the *fill factor* (FF). The fill factor is the ratio of the power at the MPP to the product of V_{OC} and I_{SC}, so FF can be visualized as the ratio of two rectangular areas, as is suggested in Figure 5.41. The best commercial solar cells have FF over 70%, which from our discussion of the equivalent circuit of cells, indicates they have reasonably high parallel resistances and low series

resistance.

$$\text{Fill factor} = \frac{\text{Power at the maximum power point}}{V_{OC} \cdot I_{SC}} = \frac{V_{MPP} \cdot I_{MPP}}{V_{OC} \cdot I_{SC}} \tag{5.22}$$

FIGURE 5.41 The maximum power point (MPP) corresponds to the biggest rectangle that can fit beneath the *I–V* curve. The fill factor (FF) is the ratio of the area (power) at MPP to the area formed by a rectangle with sides V_{OC} and I_{SC}.



The fill factor for the module shown in Figure 5.41 is

$$\text{Fill factor} = \frac{40\text{V} \times 5.5\text{A}}{48\text{V} \times 6\text{A}} = \frac{220\text{W}}{288\text{W}} = 0.76$$

Since PV *I–V* curves shift all around as the amount of insolation changes and as the temperature of the cells varies, standard test conditions (STCs) have been established to enable fair comparisons of one module to another. Those test conditions include a solar irradiance of 1 kW/m^2 (1 sun) with spectral distribution shown in Figure 5.7, corresponding to an air mass ratio of 1.5 (AM1.5). The standard cell temperature for testing purposes is 25°C (it is important to note that 25° is cell temperature, not ambient temperature). Manufacturers always provide performance data under these operating conditions—some examples of which are shown in Table 5.3. The key parameter for a module is its STC rated power P_{MPP}. Usually the DC watts produced under STCs are referred to as *peak watts*, W_p.

TABLE 5.3 Examples of PV Module Performance Data Under Standard Test Conditions (1 kW/m^2, AM1.5, 25°C Cell Temperature)

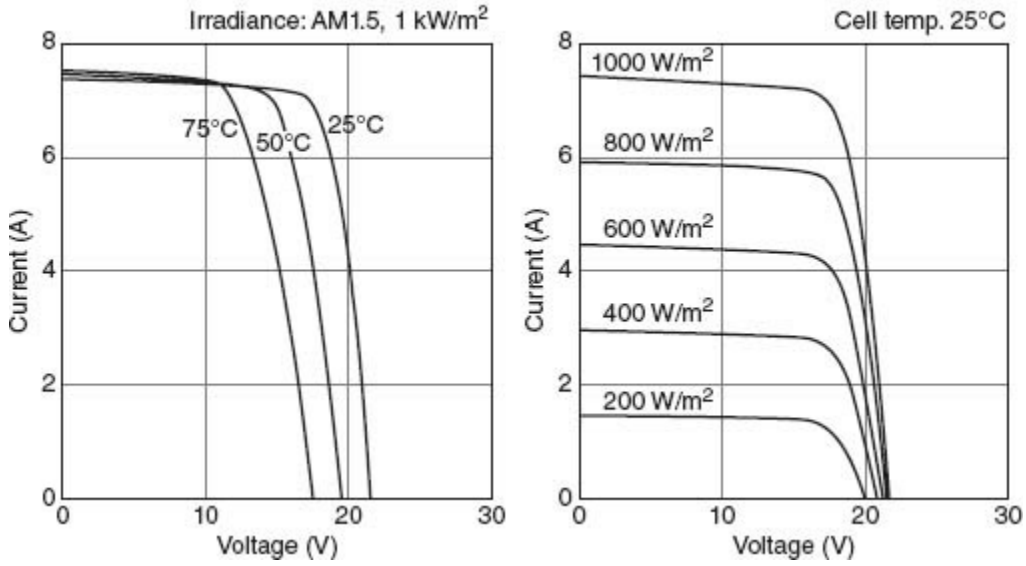
Manufacturer	SunPower	Yingli	First Solar	NanoSolar	Sharp
Model	E20/435	YGE 245	FS Series 3	Utility 230	NS-F135G5
Material	c-Si	mc-Si	CdTe	CIGS	a-Si
Panel efficiency	20.1%	15.6%	12.2%	11.6%	9.6%
Rated power P_{MPP} (W_p)	435	245	87.5	230	135
Rated voltage V_{MPP} (V)	72.9	30.2	49.2	40.2	47
Rated current I_{MPP} (A)	5.97	8.11	1.78	6	2.88
Open-circuit voltage V_{OC} (V)	85.6	37.8	61	50.7	61.3
Short-circuit current I_{SC} (A)	6.43	8.63	1.98	6.7	3.41
NOCT (°C)	45	46	45	47	45
Temp. Coeff. of P_{max} (%/K)	−0.38	−0.45	−0.25	−0.39	−0.24
Temp. Coeff. V_{OC} (%/K)	−0.27	−0.33	−0.27	−0.30	−0.30
Temp. Coeff. I_{SC}(%/K)	0.05	0.06	0.04	0.00	0.07
Dimensions (m)	2.07 × 1.05	1.65 × 0.99	1.20 × 0.60	1.93 × 1.03	1.40 × 1.00
Weight (kg)	25.4	26.8	15	34.7	26

The table also shows some parameters related to temperature. Later we will learn how to adjust rated power to account for temperature effects as well as see how to adjust it to give us an estimate of the actual AC power that the module and inverter combination will deliver.

5.7 IMPACTS OF TEMPERATURE AND INSOLATION ON *I–V* CURVES

Manufacturers will often provide *I–V* curves that show how the curves shift as insolation and cell temperatures change (Fig. 5.42). Note as insolation drops, short-circuit current drops in direct proportion. Cutting insolation in half, for example, drops I_{SC} by half. As Example 5.3 illustrated, the entire *I–V* curve shifts downward as insolation drops, which causes a modest reduction in V_{OC} as well.

FIGURE 5.42 Current–voltage characteristic curves under various cell temperatures and irradiance levels for a Kyocera KC120-1 PV module.



As can be seen in Figure 5.42, as PVs get hotter, the open-circuit voltage decreases by a considerable amount while the short-circuit current increases only very slightly. PVs, perhaps surprisingly, therefore perform better on cold, clear days than hot ones. Table 5.3 includes some temperature impacts for the five different PV technologies. For example, the Yingli multicrystalline silicon module shows a drop in P_{MPP} of about 0.45% for each degree Celsius that cell temperature increases, while the FirstSolat CdTe module only decreases by 0.25%/K. On a watt-by-watt basis, that gives a performance benefit to CdTe in hot climates.

Given this significant shift in performance as cell temperature changes, it should be quite apparent that temperature needs to be included in any estimate of PV system performance.

Cells vary in temperature not only because ambient temperatures change, but also because insolation on the cells changes. Since only a small fraction of the insolation hitting a module is converted to electricity and carried away, most of that incident energy is absorbed and converted to heat. To help system designers account for changes in cell performance with temperature, it is now standard practice for manufacturers to provide an indicator called the nominal operating cell temperature (NOCT). The NOCT is the expected cell temperature in a module when ambient is 20°C, solar irradiation is 0.8 kW/m^2, and wind speed is 1 m/s. To account for other ambient conditions, the following expression may be used:

$$T_{cell} = T_{amb} + \left(\frac{\text{NOCT} - 20^\circ}{0.8}\right) \cdot S \tag{5.23}$$

where T_{cell} is cell temperature (°C), T_{amb} is ambient temperature, and S is solar insolation (kW/m^2).

Example 5.5 Impact of Cell Temperature on Power for a PV Module. Estimate cell temperature, open-circuit voltage, and maximum power output for the Yingli module in Table 5.3 under conditions of 1-sun insolation and ambient temperature 30°C.

Solution. Using Equation 5.23 with S = 1 kW/m^2 and NOCT = 46°C from the table, cell temperature is estimated to be

$$T_{cell} = T_{amb} + \left(\frac{\text{NOCT} - 20^\circ}{0.8}\right) \cdot S = 30 + \left(\frac{46 - 20}{0.8}\right) \cdot 1 = 62.5^\circ\text{C} \quad (145^\circ\text{F})$$

From Table 5.3, for this module at the standard temperature of 25°C, V_{OC} = 37.8 V. Since V_{OC} drops by 0.33%/°C, the new V_{OC} will be about

$$V_{OC} = 37.8\,[1 - 0.0033\,(62.5 - 25)] = 33.1 \text{ V}$$

With maximum power expected to drop about 0.45%/°C, this 245-W module at its MPP will deliver

$$P_{max} = 245\,[1 - 0.0045\,(62.5 - 25)] = 204 \text{ W}$$

which is a rather significant drop of 17% from its rated power.

When the NOCT is not given, another approach to estimating cell temperature is based on the following:

$$T_{\text{cell}} = T_{\text{amb}} + \gamma \left(\frac{\text{Insolation}}{1\ \text{kW/m}^2} \right) \tag{5.24}$$

where γ is a proportionality factor that depends somewhat on wind speed and how well ventilated the modules are when installed. Typical values of γ range between 25°C and 35°C; that is, in 1-sun of insolation, cells tend to be 25–35°C hotter than their environment.

5.8 SHADING IMPACTS ON *I–V* CURVES

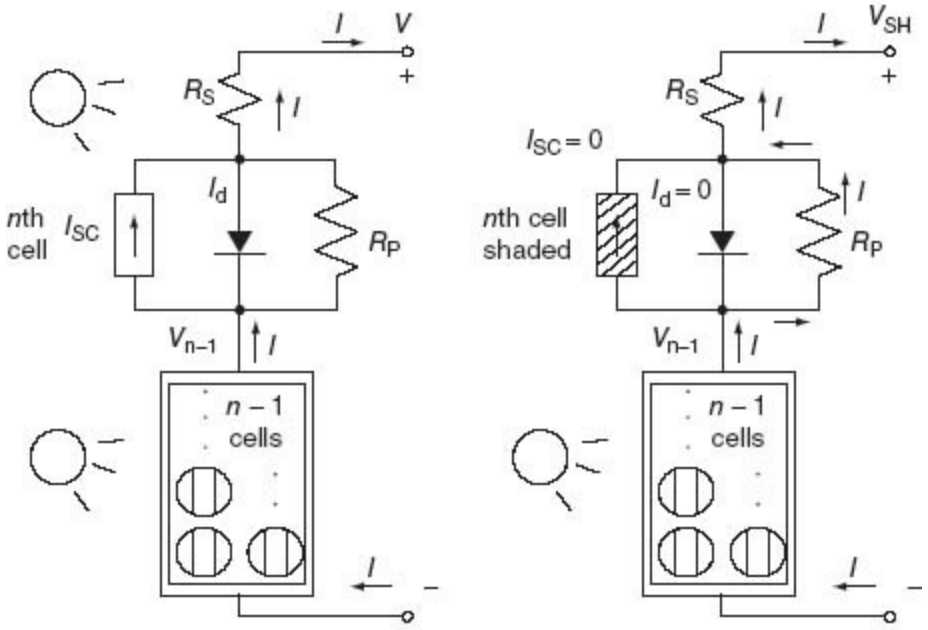
Unlike solar thermal systems, PVs are especially sensitive to even small amounts of shading. When even just a single cell is shaded, the output of the entire module can be dramatically reduced. And, since most arrays consist of strings of modules, a single module with even a small fraction of its area in the shade can compromise the performance of an entire string.

Mitigation measures to deal with shading issues have focused in the past on special bypass and blocking diodes to help current flow around shaded cells, but new, more sophisticated electronic measures can now help address this important issue.

5.8.1 Physics of Shading

To help understand this important phenomenon, consider Figure 5.43 in which an n-cell module with current I and output voltage V has one cell separated from the others (shown as the top cell, though it can be any cell in the module). The equivalent circuit of the top cell has been drawn using Figure 5.31, while the other $(n - 1)$ cells in the string are shown as just a module with current I and output voltage V_{n-1}.

FIGURE 5.43 A module with n cells in which all of the cells are in the sun (a) or in which the top cell is completely shaded (b).



In Figure 5.43a, all of the cells are in the sun and since they are in series, the same current I flows through each of them. In Figure 5.43b, however, the top cell is shaded and its current source I_{SC} has been reduced to zero. The voltage drop across R_P as current flows through it causes the diode to be reverse biased, so the diode current is also (essentially) zero. That means the entire current flowing through the module must travel through both R_P and R_S in the shaded cell on its way to the load. That means the top cell, instead of adding to the output voltage, actually reduces it.

Consider the case when the bottom n – 1 cells still have full sun and still carry their original current I so they will still produce their original voltage V_{n-1}. That means the output voltage V_{SH} with one cell shaded will drop to

$$V_{SH} = V_{n-1} - I\,(R_P + R_S) \tag{5.25}$$

With all n cells in the sun and carrying I, the output voltage was V so the voltage of the bottom n – 1 cells will be

$$V_{n-1} = \left(\frac{n-1}{n}\right) V \tag{5.26}$$

Combining Equations 5.25 and 5.26 gives

$$V_{SH} = \left(\frac{n-1}{n}\right) V - I\,(R_P + R_S) \tag{5.27}$$

The drop in voltage ΔV at any given current I caused by the shaded cell is given by

$$\Delta V = V - V_{SH} = V - \left(1 - \frac{1}{n}\right) V + I\,(R_P + R_S) \tag{5.28}$$

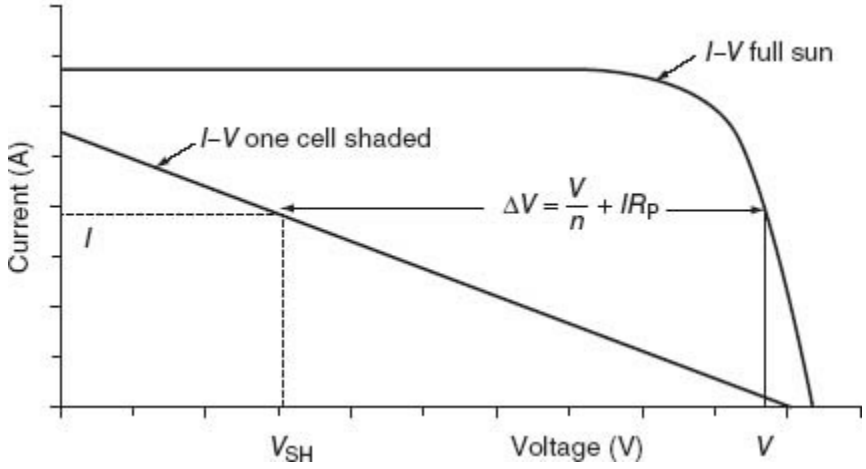
$$\Delta V = \frac{V}{n} + I\,(R_P + R_S) \tag{5.29}$$

Since the parallel resistance R_P is orders of magnitude greater than the series resistance R_S, Equation 5.29 simplifies to

$$\Delta V \cong \frac{V}{n} + I \cdot R_P \tag{5.30}$$

At any given current, the *I–V* curve for the module with one shaded cell drops by ΔV. The huge impact this can have is illustrated in Figure 5.44.

FIGURE 5.44 Effect of shading one cell in an n-cell module. At any given current, module voltage drops from V to $V - \Delta V$.



Example 5.6 Impacts of Shading on a PV Module. The 72-cell PV module described in Example 5.4 had a parallel resistance per cell of R_P = 10.0 Ω and a series resistance R_S of 0.001 Ω. In full sun and at current I = 5.73 A, the output voltage of the module was found to be V = 40.63 V. If one cell is shaded, find the following if somehow the same 5.73 A is forced to flow through the module.

a. The module output voltage.

b. Power dissipated in the shaded cell.

Solution

a. From Equation 5.29, the drop in module voltage will be

$$\Delta V = \frac{V}{n} + I\,(R_P + R_S) = \frac{40.63}{72} + 5.73 \times (10.0 + 0.001) = 57.87 \text{ V}$$

(obviously, we could have ignored R_S).

The module output voltage will now be 40.63 – 57.87 = –17.24 V

(Yes, this is possible. For example, if this module with one shaded cell is part of a string of modules and the good ones are trying to drive 5.73 A through the whole string, then it would be better to completely remove that shaded module from the string than to leave it in place!)

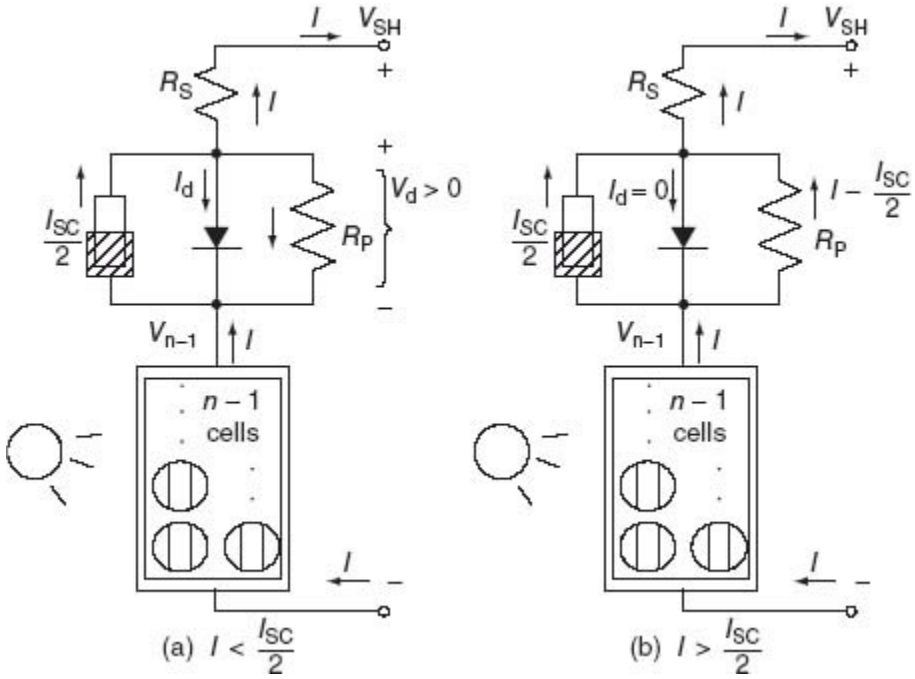
b. Since that 5.73 A flows through both R_S and R_P, the power dissipated in that shaded cell will be

$$P = I^2 (R_P + R_S) = (5.73)^2 (10.0 + 0.001) = 69.7 \text{ W}$$

All of that power dissipated in the shaded cell is converted to heat, which can cause a local hot spot that may permanently damage the plastic laminates enclosing the cell.

Consider now, the case of partial shading on an individual cell in an otherwise fully sunny module. Figure 5.45 shows two circumstances in which a single cell is experiencing 50% shading dropping its short-circuit current to half of what it would be in full sun, $I_{SC}/2$. If the current to the cell I from the rest of the module is less than $I_{SC}/2$, some current will still flow through the diode and the cell will still contribute a slightly reduced, but positive voltage to the entire module.

FIGURE 5.45 With one cell half-shaded, its equivalent circuit diode still conducts as long as current I from the rest of the module is less than $I_{SC}/2$ (a). Once I exceeds $I_{SC}/2$, the diode shuts off and I passes through R_P and R_S, which can result in very large voltage drops in that cell (b).



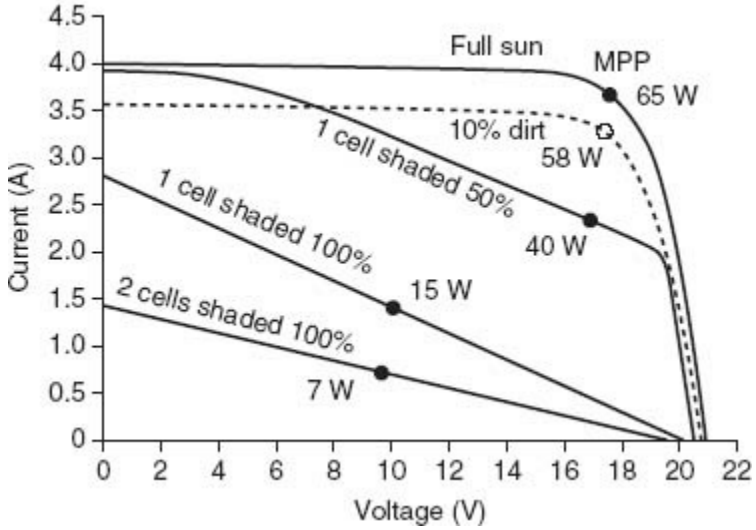
On the other hand, if I is greater than $I_{SC}/2$, then current equal to the difference between the two will be diverted through the parallel resistance R_P. The resulting voltage drop across R_P causes the diode to become reverse biased so it shuts off and no longer carries any current. Analogous to Equation 5.30, the total voltage loss to the entire module, because this single cell has been partially shaded, is

$$\Delta V = \frac{V}{n} + \left(I - \frac{I_{SC}}{2}\right) R_P \tag{5.31}$$

The resulting I–V curve for an example module with 50% shading on one cell is shown

in Figure 5.46. The figure also shows curves for one cell completely shaded and two cells completely shaded. The MPPs identified in the figure show almost 75% drop in power from 65 W, with no shading, to 40 W with just one cell half-shaded. With an entire cell shaded, the drop is over 75%. Also note how one fully shaded cell will produce negative voltages for the entire module if other modules in a string drive more than about 2.8 A through the shaded module. This is similar to what was demonstrated in Example 5.6.

FIGURE 5.46 Showing the difference in *I–V* curves for individual cells being shaded and also for uniformly distributed dirt (dashed) on a module. The dots show power at the MPPs.



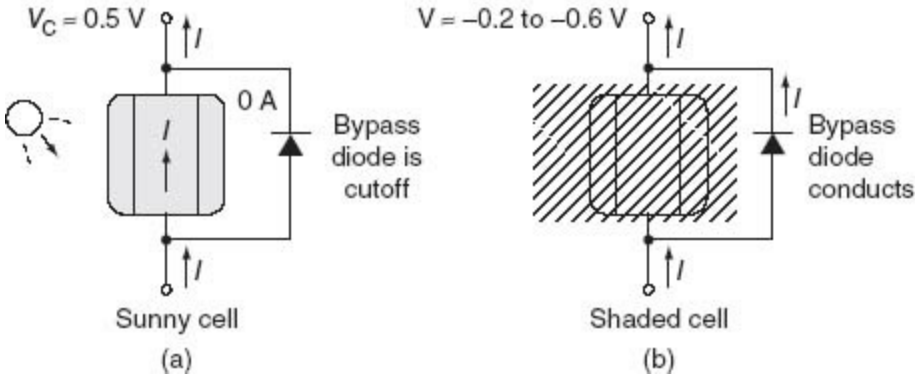
Finally, Figure 5.46 also illustrates the difference between uniformly distributed dirt on a module versus the more startling impact of individual cells being covered by shading or clumps of debris. When modules get dirty, the *I–V* curve shifts downward just the way it would if the sun were a bit less intense. As shown in the figure, a 10% uniform sun blockage by dirt lowers the MPP by a similar fraction.

5.8.2 Bypass Diodes and Blocking Diodes for Shade Mitigation

As we have seen, each cell at its MPP adds about 0.5 V to the output of a module when it is in the sun. If a cell is shaded, however, it can drop the voltage by a considerable amount. One way to imagine solving that voltage-drop problem would be to add a *bypass diode* across each cell as is suggested in Figure 5.47. When a solar cell is in the sun, there is a voltage rise across the cell so the bypass diode is cut off and no current flows through it—it is as if the diode is not even there. When the solar cell is shaded, however, the drop that would occur if the cell conducted any current would turn on the bypass diode, diverting the current flow through that diode. An ordinary bypass diode, when it conducts, drops about 0.6 V. Special Schottky diodes drop just a few tenths of a volt. So, the bypass diode controls the voltage drop across the shaded cell, limiting it to a relatively modest 0.2–0.6 volts instead of the rather large drop that may occur without it (in Example 5.6, the shaded cell lost over 17 V).

FIGURE 5.47 Mitigating the shade problem with a bypass diode. In the sun (a), the bypass diode is cut off and all the normal current goes through the solar cell. In shade (b),

the bypass diode conducts current around the shaded cell allowing just the diode drop of about 0.6 V to occur.



While providing a bypass diode across every cell in a module is feasible, the usual approach is for the manufacturer to provide just a few diodes, with each one covering a certain number of cells within the module (Fig. 5.48). Figure 5.49 shows how those diodes can still provide two-thirds, 43 W, of the full-sun power when one cell is completely shaded. Without the diodes, the maximum power for this module with one shaded cell would have been only 15 W.

FIGURE 5.48 Three bypass diodes, each covering one-third of the cells in a module.

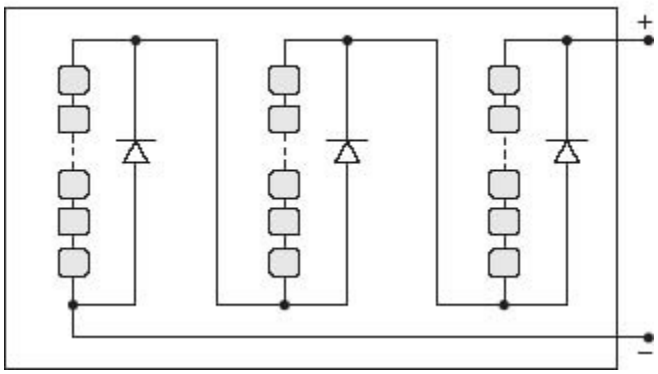
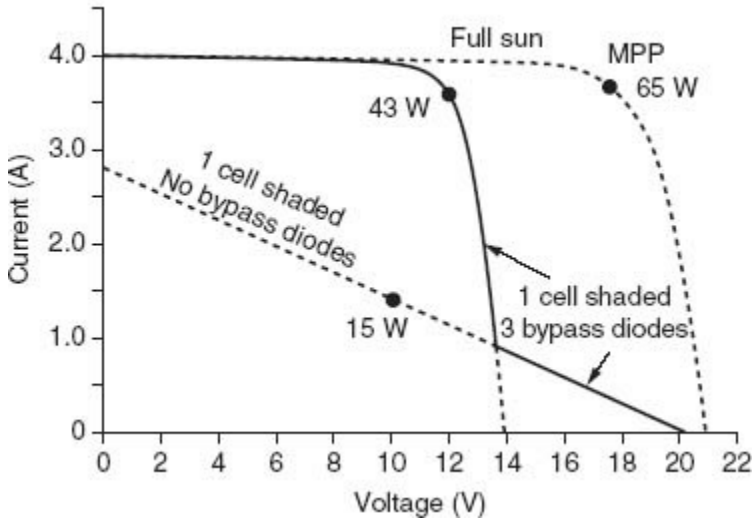
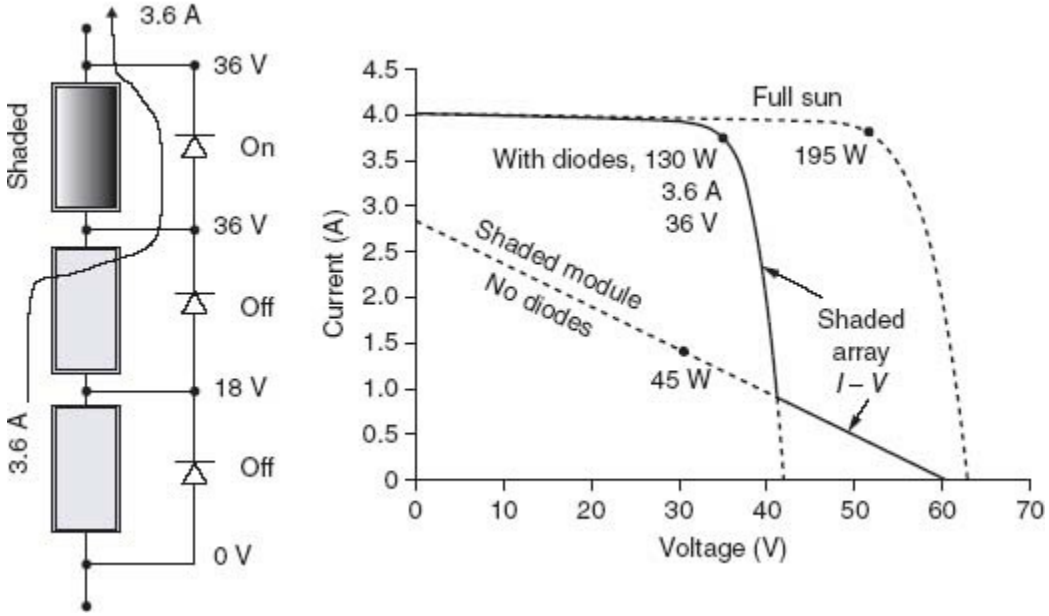


FIGURE 5.49 A module with three bypass diodes with one cell shaded. Without the diodes only 15 W would be generated compared to the 43 W provided with diodes.



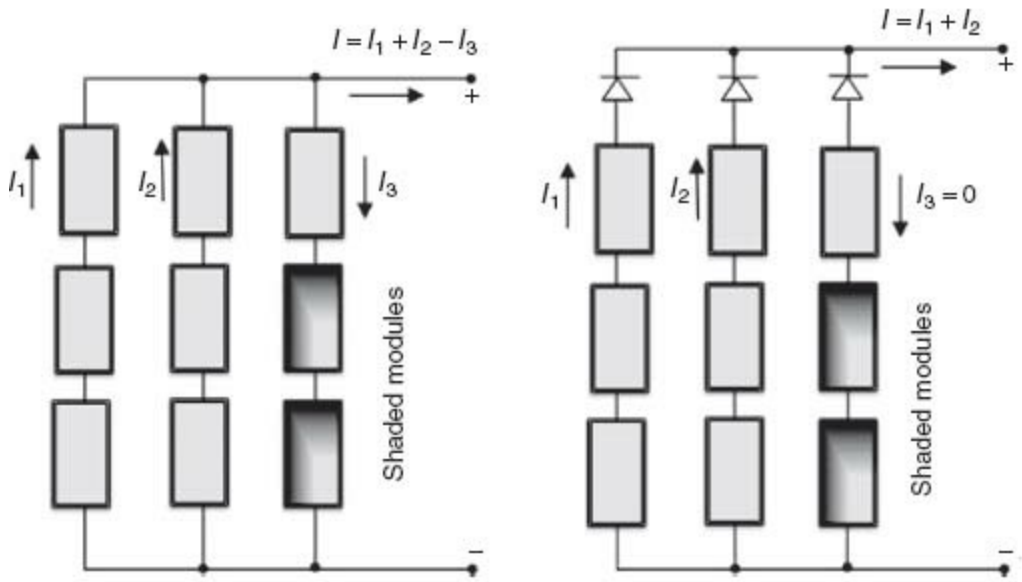
Just as cells are wired in series to increase module voltage, modules can be wired in series strings to increase array voltage. And, just a single cell can drag down the current within a module, a few shaded cells in a single module can drag down the power delivered by the entire string in an array. The benefit already demonstrated for a bypass diodes within a module also applies to a diodes applied across each module in a string. The example in Figure 5.50 shows current being diverted around a shaded module, which allows the string to preserve two-thirds of its potential power output. Without the diodes, three-fourths of the power output would have been lost.

FIGURE 5.50 Showing the ability of bypass diodes to mitigate shading problems in a string of modules.



Bypass diodes help current go around a shaded or malfunctioning module within a string. This not only improves the string performance, but also prevents hot spots from developing in individual shaded cells. When strings of modules are wired in parallel, a similar problem may arise when one of the strings is not performing well. Instead of supplying current to the array, a malfunctioning or shaded string can withdraw current from the rest of the array. By placing *blocking diodes* (also called *isolation diodes*) at the top of each string as shown in Figure 5.51, the reverse current drawn by a shaded string can be prevented.

FIGURE 5.51 Blocking diodes prevent reverse current from flowing down malfunctioning or shaded strings.



(a) Without blocking diodes (b) With blocking diodes

5.9 MAXIMUM POWER POINT TRACKERS

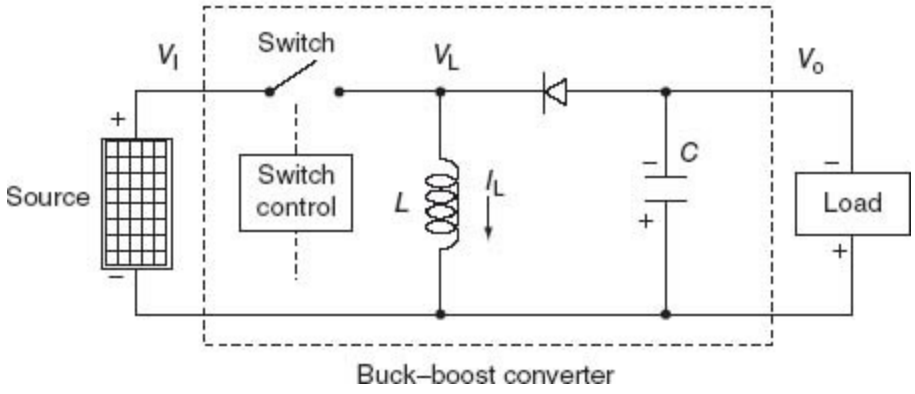
Solar irradiance, ambient temperature, and shading all have impact on the shape of PV *I–V* curves. Ideally, given the cost of PV systems, you would like to keep your expensive PVs operating at their optimum point on these shifting *I–V* curves. In most cases, this means incorporating a *maximum power point tracker* (MPPT) as part of the system. For some simple applications, such as directly coupled PV water-pumping or small-scale battery charging systems, the extra cost and complexity of MPPTs may not be justified and they are often omitted.

5.9.1 The Buck–Boost Converter

There are some very clever, quite simple, circuits that are at the heart of MPPTs as well as a number of other important power devices. The key is to be able to convert DC voltages from one level to another—something that was very difficult to do efficiently before high power, field-effect transistors (FETs) became available in the 1980s and insulated-gate bipolar transistors (IGBTs) in the 1990s. At the heart of these modern *switched-mode* DC-to-DC converters is one of these transistors used as a simple ON-OFF switch that either allows current to pass through it or the current is blocked.

A *boost converter* is a commonly used circuit to step up DC voltage while a *buck converter* is often used to step down voltage, both of which were described in Section 3.9.2 of this book. There are a number of other DC-to-DC converter schemes, including the circuit of Figure 5.52, which is called a *buck–boost converter*. A buck–boost converter is capable of raising or lowering a DC voltage from its source to whatever DC voltage is needed by the load. The transistor switch flips on and off at a rapid rate (on the order of 20 kHz) under control of some sensing and logic algorithm to be described in the next section.

FIGURE 5.52 A buck–boost converter used as part of a maximum power point tracker.



To analyze the buck–boost converter, we have to go back to first principles. Conventional DC or AC circuit analysis does not help much and instead the analysis is based on an energy balance for the magnetic field of the inductor. Basically there are two situations to consider: the circuit with the switch closed and the circuit with the switch open.

When the switch is closed, the input voltage V_i is applied across the inductor, driving current I_L through the inductor. All of the source current goes through the inductor since the diode blocks any flow to the rest of the circuit. During this portion of the cycle, energy is being added to the magnetic field in the inductor as current builds up. If the switch stayed closed, the inductor would eventually act like a short circuit and the PVs would deliver short-circuit current at zero volts.

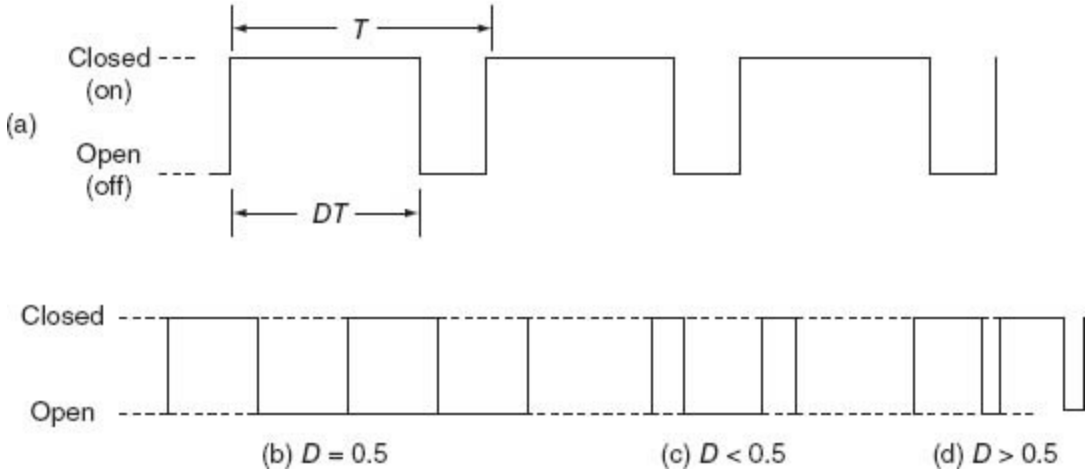
When the switch is opened, current in the inductor continues to flow as the magnetic field begins to collapse (remember current through an inductor cannot be changed instantaneously—to do so would require infinite energy). Inductor current now flows through the capacitor, the load and the diode. Inductor current charging the capacitor provides a voltage (with a polarity reversal) across the load that will help keep the load powered after the switch closes again.

If the switch is cycled quickly enough, the current through the inductor does not have a chance to drop much while the switch is open before the next jolt of current from the source. With a fast enough switch and a large enough inductor, the circuit can be designed to have nearly constant inductor current, which is our first important insight into how this circuit works: inductor current is essentially constant. Similarly, with a fast switching speed, the voltage across the capacitor does not have a chance to drop much, while the switch is closed, before the next jolt of current from the inductor charges it back up again. Capacitors, recall, cannot have their voltage change instantaneously so if the switch is cycling fast enough and the capacitor is sized large enough, the output voltage across the capacitor and load is nearly constant. We now have our second insight into this circuit: output voltage V_o is essentially constant (and opposite in sign to V_i).

Finally, we need to introduce the duty cycle of the switch itself. This is what controls the relationship between the input and output voltages of the converter. The duty cycle D ($0 < D < 1$) is the fraction of the time that the switch is closed, as illustrated in Figure 5.53. This variation in the fraction of time the switch is in one state or the other is referred to as *pulse–width modulation* (PWM).

FIGURE 5.53 The duty cycle D is the fraction of the time the switch is closed (a).

Examples: (b) 50% duty cycle; (c) $D < 0.5$; and (d) $D > 0.5$.



For this simple description, all of the components in the converter will be considered to be ideal. As such, the inductor, diode and capacitor do not consume any net energy over a complete cycle of the switch. Therefore, the average power into the converter is equal to the average power delivered by the converter; that is, it has 100% efficiency. Real converters have efficiencies in the high 90% range, so this is not a bad assumption.

Now focus on the inductor. While the switch is closed, from time $t = 0$ to $t = DT$, the voltage across the inductor is a constant V_i. The average power put into the magnetic field of the inductor is given by

$$\bar{P}_{L,\,\text{in}} = \frac{1}{T}\int_0^{DT} V_i I_L \mathrm{d}t = \frac{1}{T} V_i \int_0^{DT} I_L \mathrm{d}t \tag{5.32}$$

Under the assumption that inductor current is constant, that means power into the inductor is

$$\bar{P}_{L,\,\text{in}} = \frac{1}{T} V_i I_L \int_0^{DT} \mathrm{d}t = V_i I_L D \tag{5.33}$$

When the switch opens, the inductor's magnetic field begins to collapse, returning the energy it just acquired. The diode conducts, which means that the voltage across the inductor V_L is the same as the voltage across the load V_o. The average power delivered during this part of the cycle (from $t = DT$ to $t = T$) is therefore

$$\bar{P}_{L,\,\text{out}} = \frac{1}{T}\int_{DT}^{T} V_L I_L \mathrm{d}t = \frac{1}{T}\int_{DT}^{T} V_o I_L \mathrm{d}t \tag{5.34}$$

With good design, both V_o and I_L are essentially constant, so average power from the inductor is

$$\bar{P}_{L,\,\text{out}} = \frac{1}{T} V_o I_L (T - DT) = V_o I_L (1 - D) \tag{5.35}$$

Over a complete cycle, average power into the inductor plus average power out of the

inductor is zero. So, from Equations 5.33 and 5.35, we get

$$\frac{V_o}{V_i} = -\left(\frac{D}{1-D}\right) \tag{5.36}$$

Equation 5.36 is pretty interesting. It tells us we can bump DC voltages up or down (there is also a sign change) just by varying the duty cycle of the buck–boost converter. Longer duty cycles allow more time for the capacitor to charge up and less time for it to discharge, so the output voltage increases as D increases. For a duty cycle of 1/2, the output voltage is the same as the input voltage. A duty cycle of 2/3 results in a doubling of voltage, while D = 1/3 cuts voltage in half. As the following example illustrates a DC-to-DC converter is the DC analog of a conventional AC transformer for which the turns ratio is in essence controlled by the duty cycle.

Example 5.7 Duty Cycle for a MPPT. Under certain ambient conditions, a particular PV module has its maximum power point at V_m = 30 V and I_m = 6 A. What duty cycle should be provided to a buck–boost converter if the module is to deliver 12 V to charge a battery? How many amperes would be delivered to the battery? If the ambient were to cool off some without a change in insolation, should the duty cycle be increased or decreased?

Solution. The converter must drop the PV voltage of 30 V down to the desired 12 V. Using Equation 5.36 and ignoring the sign change (just switch the terminals on the battery):

$$\frac{12}{30} = \left(\frac{D}{1-D}\right) = 0.4$$

solving

$$D = 0.4 - 0.4D$$

$$D = \frac{0.4}{1.4} = 0.286$$

Since we will assume a 100% efficient converter, input power equals output power so that

$$V_{PV} \cdot I_{PV} = V_{Battery} \cdot I_{Battery}$$

$$I_{Battery} = \frac{30V \cdot 6A}{12V} = 15A$$

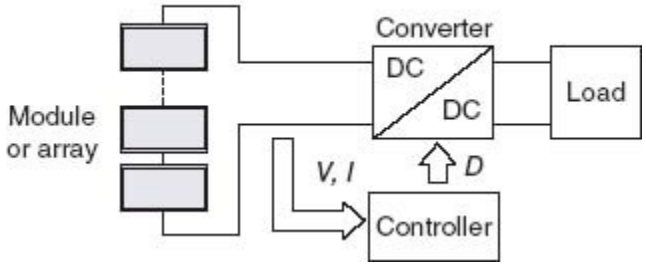
With cooler temperatures, the PV voltage at the MPP increases somewhat (e.g., see Fig. 5.35) so the duty cycle D should be decreased a bit.

5.9.2 MPPT Controllers

An actual MPPT needs some way to know how to adjust the duty cycle of its DC-to-DC converter to keep the PV array voltage on its MPP, which means it needs a control unit. A simple version of an MPPT, consisting of a DC-to-DC converter and control system is

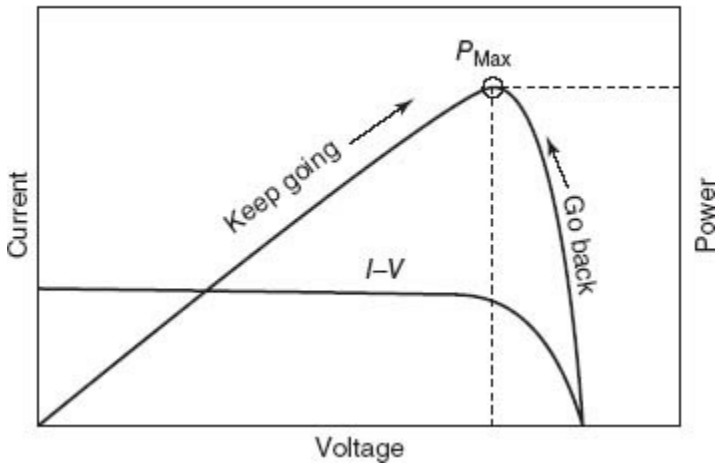
shown in Figure 5.54. The PV source may be a single module or it could be an entire array. The controller senses the current and voltage being delivered by the PVs and, using any of a number of possible control approaches, adjusts the converter to best match the desired output to the load.

FIGURE 5.54 A simple block diagram of an MPPT system.



There are literally dozens of methods that can be used to enable controllers to achieve the goal of maximum power point tracking (e.g., Esram and Chapman, 2007). Some are conceptually simple, such as the fractional open-circuit voltage method in which the voltage is set at a fixed value equal to some percentage of the measured V_{OC}. Others, such as those referred to as hill-climbing or perturb-and-observe approaches involve algorithms that adjust the PV voltage and see whether the change made increases or decreases the power delivered. Recall the typical *I–V* and power curves shown in Figure 5.55 (without the complications of shading). If, for example, a perturbation that increases the voltage increases the power delivered, then the voltage will continue to be increased until it no longer does so. Similarly, if the perturbation decreases output power, then the next adjustment should be in the opposite direction.

FIGURE 5.55 Hill-climbing or perturb-and-observe approaches to find the MPP.



Another technique, referred to as the *incremental conductance* method is based on the fact that the slope of the power versus voltage curve is zero at the MPP.

$$\text{At the MPP: } \frac{dP}{dV} = 0 \tag{5.37}$$

Since the fundamental definition of power is $P = IV$, we can write

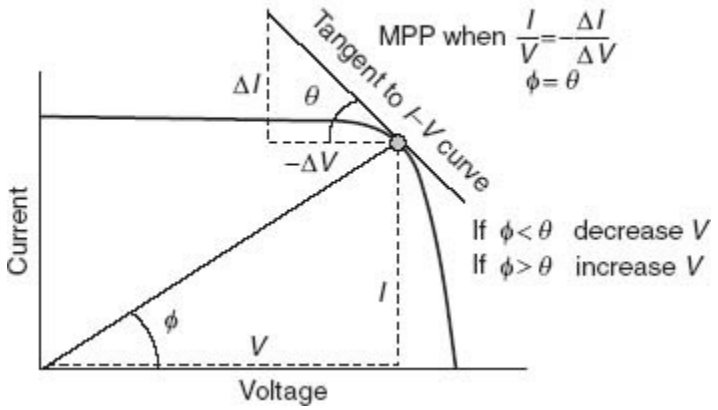
$$\frac{dP}{dV} = I\frac{dV}{dV} + V\frac{dI}{dV} = I + V\frac{dI}{dV} \approx I + V\frac{\Delta I}{\Delta V} \quad (5.38)$$

where we are approximating the differentials with finite changes ΔI and ΔV. Substituting Equation 5.38 into Equation 5.37 tells us that

$$\text{At the MPP}: \frac{\Delta I}{\Delta V} = -\frac{I}{V} \quad (5.39)$$

The ratio of I/V, called the instantaneous conductance, is based on measurements of PV current and voltage taken at fixed increments of time. The ratio $\Delta I/\Delta V$, called the incremental conductance, refers to changes that might have occurred in I and V during one of those time steps. Figure 5.56 shows one interpretation of these conductances on a PV I–V curve. The instantaneous conductance is the slope of a line drawn from the origin to the operating point. The incremental conductance is the negative slope of the I–V curve at that same operating point. From Figure 5.56, at the MPP the angles formed by the two slopes are equal. We could imagine, therefore, that the MPP can be found by incrementing the duty cycle of the converter until the ratio of the incremental changes ΔV and ΔI equals I/V; that is, until the angles ϕ and θ are equal.

FIGURE 5.56 Interpreting the incremental conductance MPP method. The MPP corresponds to the spot where angle φ equals the angle θ.

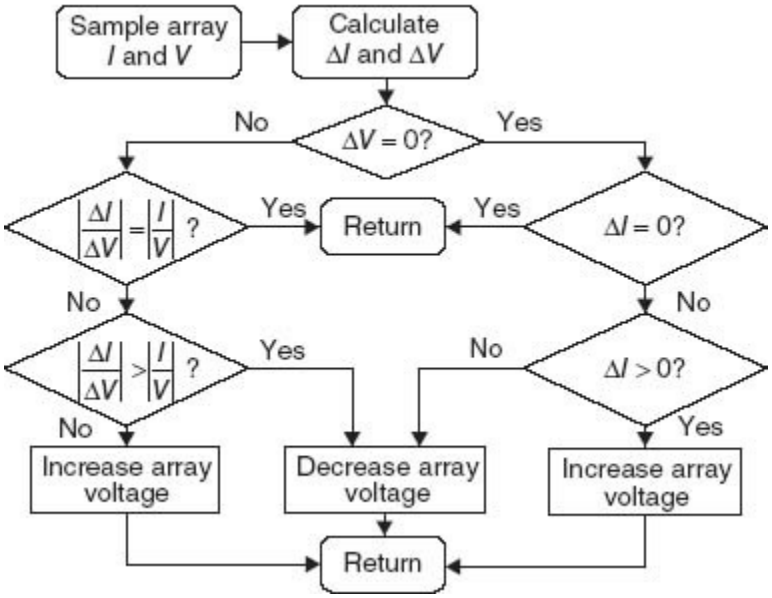


Having located the MPP, the duty cycle of the converter remains fixed until subsequent I and V measurements indicate that a change is needed. That change may be the result of temperature or insolation shifts in the I–V curve, which move the MPP. For example, if insolation increases, the MPP will move somewhat to the right. At the next time step, the sensors will indicate an increase in current ΔI, but until the duty cycle changes, ΔV is still zero. That increase in insolation has moved the MPP to the right so the PV voltage needs to increase; that is, the duty cycle needs to increase.

Duty cycle adjustments can also be motivated by changes in the desired load voltage, for example, when the voltage of a battery rises during charging. If the duty cycle has not changed, then the array voltage will also rise, moving it to the right of the MPP so the duty cycle should therefore be decreased. The algorithm shown in Figure 5.57 summarizes how

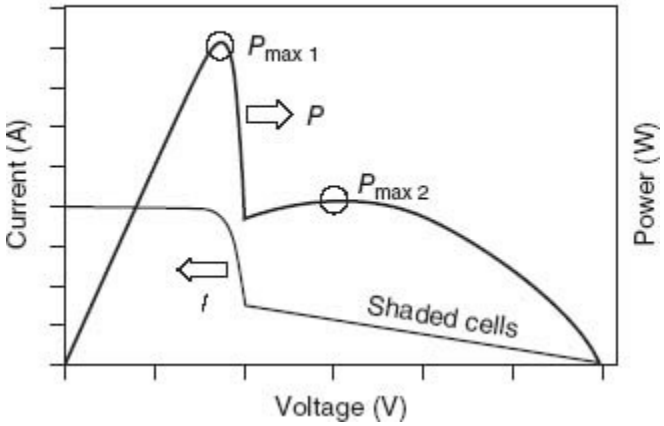
measurements of I and V, along with calculations of ΔI and ΔV from one time step to another, can be used to adjust the array voltage.

FIGURE 5.57 An incremental conductance algorithm to direct the controller how to adjust the duty cycle of a DC-to-DC converter.



For complex I–V curves, such as can occur when shading impacts cause bypass diodes to turn on within an individual module or along a string of modules, there may be multiple local power-maximum points. An example, similar to the curves demonstrated in Figure 5.50, is shown in Figure 5.58. Most of the MPP methods need an initial stage to start the tracking process at something close to the correct local maximum to avoid being trapped onto a false MPP.

FIGURE 5.58 Shaded cells or modules with bypass diodes can create multiple MPPs.



REFERENCES

Bube RH. *Photovoltaic Materials.* London: Imperial College Press; 1998.

Esram T, Chapman PL. Comparison of photovoltaic array maximum power point tracking techniques. *IEEE Transactions on Energy Conversion* 2007;22: 439–449.

ERDA/NASA. Terrestrial photovoltaic measurement procedures. Cleveland, OH: NASA; 1977. Report nr ERDA/NASA /1022-77/16, NASA TM 73702.

PROBLEMS

5.1 The experience curve shown in Figure 5.1 is based on the following equation:

$$C(t) = C(0)\left[\frac{N(t)}{N(0)}\right]^K \quad \text{where } K = \frac{\ln(1 - \text{LR})}{\ln 2}$$

where $C(t)$ is the unit cost at time t, $C(0)$ is the unit cost at time $t = 0$, $N(t)$ is the cumulative production by time t, and LR is the learning ratio, which is the fractional decrease in cost per doubling of cumulative production.

a. From Figure 5.1, let $t = 0$ be the time at which PV production costs were about \$30/W, cumulative production to that point was about 10 MW, and the subsequent learning curve showed a 24.3% decline in costs per doubling of production. What would a continuation of this learning curve suggest the c-Si module price would be after 1 million megawatts of cumulative production would have been achieved?

b. With 2012, c-Si modules costing \$0.90/W and cumulative production to that point having been 100, 000 MW, what would have been the learning rate over the period between 10 and 100, 000 MW?

c. An easy way to determine the learning ratio LR from real data is to start with the log of both sides of the basic equation

$$\ln C(t) = \ln[C(0)] + K \ln\left[\frac{N(t)}{N(0)}\right]$$

Using the following data, plot ln($C(t)$ versus ln[N(t)/N(0)], fit a straight line. The slope of that line is K. Use it to find LR.

$N(t)$	$C(t)$
10	10.0
50	8.0
250	5.0
1400	4.0
6000	2.4
31, 000	2.0

5.2 For the simple equivalent circuit of a 0.017 m^2 PV cell shown below, the reverse saturation current is $I_0 = 4 \times 10^{-11}$ A and at an insolation of 1-sun the short-circuit current is $I_{SC} = 6.4$ A. At 25°C, find the following:

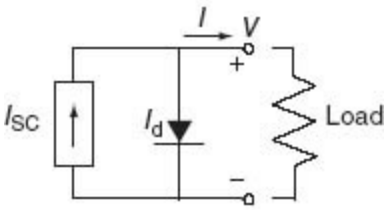


FIGURE P5.2

a. The open-circuit voltage.

b. The load current and output power when the output voltage is $V = 0.55$ V.

c. The efficiency of the cell at $V = 0.55$ V.

5.3 Suppose the equivalent circuit for the PV cell in Problem 5.2 includes a parallel resistance of $R_P = 10\ \Omega$. At 25°C, with an output voltage of 0.57 V, find the following:

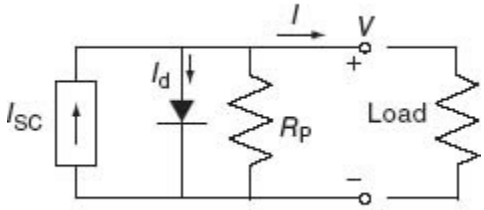


FIGURE P5.3

a. The load current and the power delivered to the load.

b. The efficiency of the cell.

5.4 The following figure shows two *I–V* curves. Both have zero series resistance. One is for a PV cell with an equivalent circuit having an infinite parallel resistance. For the other, what is the parallel resistance in its equivalent circuit?

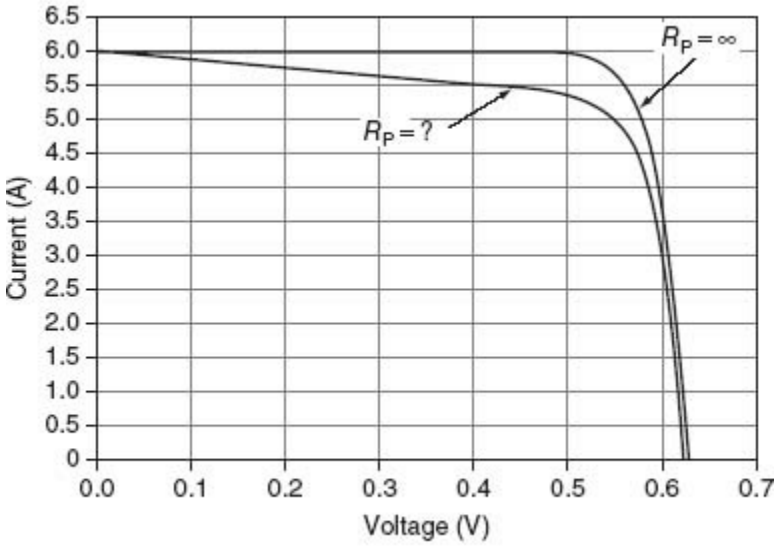


FIGURE P5.4

5.5 The following figure shows two *I–V* curves. Both have equivalent circuits with infinite parallel resistances. One circuit includes a series resistance while the other one does not. What is the series resistance for the cell that has one?

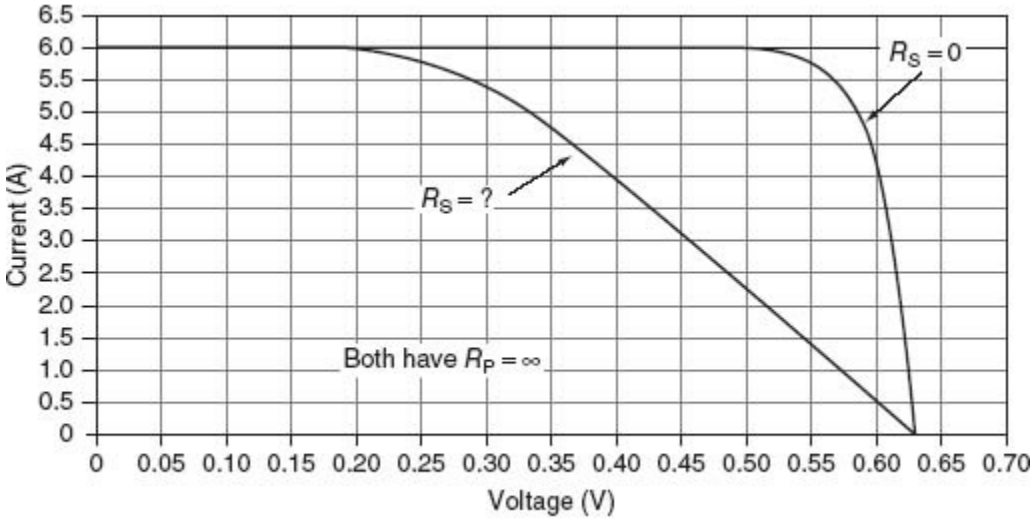


FIGURE P5.5

5.6 Recreate the spreadsheet that was started in Example 5.4 for a 72-cell, 233-W PV module for which the equivalent circuit of each cell has both series (0.001 Ω) and parallel resistances (10.0 Ω).

a. From your spreadsheet, what is the current, voltage, and power delivered when the diode voltage V_d is 0.4 V?

b. Plot the entire *I–V* curve for this module.

5.7 Consider how you might make a simple, cheap pyranometer out of a single small (e.g., 1 cm^2) PV cell along with a precision load resistor. The PV cell has the following *I–V* curve and the goal is for the digital multimeter (DMM, with infinite input resistance), when set on its millivolt DC scale, to give you direct readings of insolation.

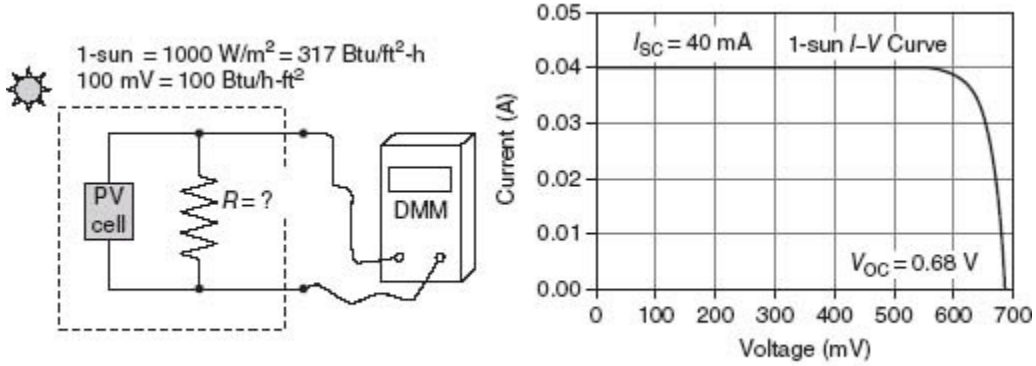


FIGURE P5.7

a. Find the load resistance that the pyranometer needs if the goal is to have the output of the DMM on a millivolt (mV) scale provide insolation readings directly in Btu/ft^2/h (full sun = 1 kW/m^2 = 317 Btu/ft^2/h = 317 mV).

Sketch the *I–V* curve with your load resistance superimposed onto it. Show the PV-curve at both 1-sun and 1/2-sun insolation.

b. Suppose you want the mV reading to be W/m^2. What resistance would work (but only for modest values of insolation). Draw an *I–V* curve with this resistor on it and make a crude estimate of the range of insolations for which it would be relatively

accurate.

5.8 A 4-module array has two south-facing modules in series exposed to 1000 W/m^2 of insolation, and two west-facing modules exposed to 500 W/m^2. The 1-sun *I–V* curve for a single module with its MPP at 4A, 40 V is shown below.

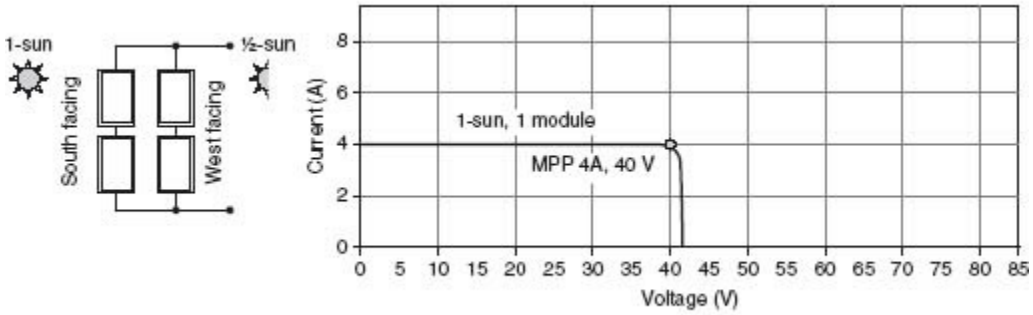


FIGURE P5.8

Draw the *I–V* curve for the 4-module array under these conditions. What is the output power (W) at the array's MPP?

5.9 A 200-W c-Si PV module has NOCT = 45°C and a temperature coefficient for rated power of –0.5%/°C.

a. At 1-sun of irradiation while the ambient is 25°C, estimate the cell temperature and output power.

b. Suppose the module is rigged with a heat exchanger that can cool the module while simultaneously providing solar water heating. How much power would be delivered if the module temperature is now 35°C? What percentage improvement is that?

c. Suppose ambient is the same temperature, but now insolation drops to 0.8 kW/m^2. What percentage improvement in power output would the heat exchanger provide if it still maintains the cell temperature at 35°C?

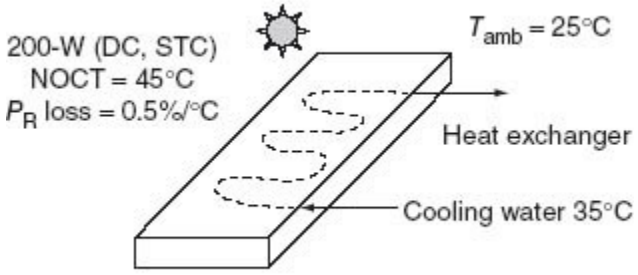


FIGURE P5.9

5.10 Consider this very simple model for cells wired in series within a PV module. Those cells that are exposed to full sun deliver 0.5 V; those that are completely shaded act like 5-Ω resistors. For a module containing 40 such cells, an idealized *I–V* curve with all cells in full sun is as follows.

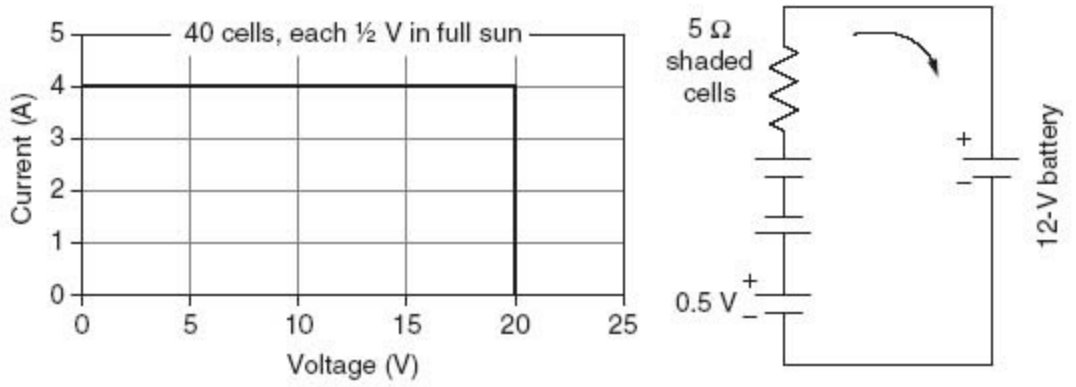


FIGURE P5.10

a. Draw the PV *I–V* curves that will result when one cell is shaded and when two cells are shaded (no battery load).

b. If you are charging an idealized 12-V battery (vertical *I–V* curve), compare the current delivered under these three circumstances (full sun and both shaded circumstances).

5.11 An idealized 1-sun *I–V* curve for a single 80-W module is shown below. For two such modules wired in series, draw the resulting *I–V* curve if the modules are exposed to only 1/2 sun, and one cell, in one of the modules, is shaded. Assume the shaded cell has an equivalent parallel resistance of 10 Ω.

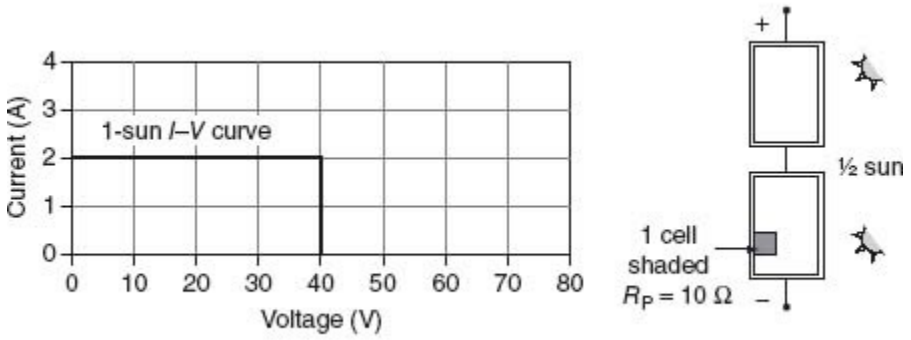


FIGURE P5.11

Sketch the resulting *I–V* curve. How much power would be generated at the MPP?

5.12 The 1-sun *I–V* curve for a 40-cell PV module in full sun is shown below along with an equivalent circuit for a single cell (including its 10 Ω parallel resistance).

An array with two such modules in series has one fully shaded cell in one of the modules. Consider the potential impact of bypass diodes around each of the modules.

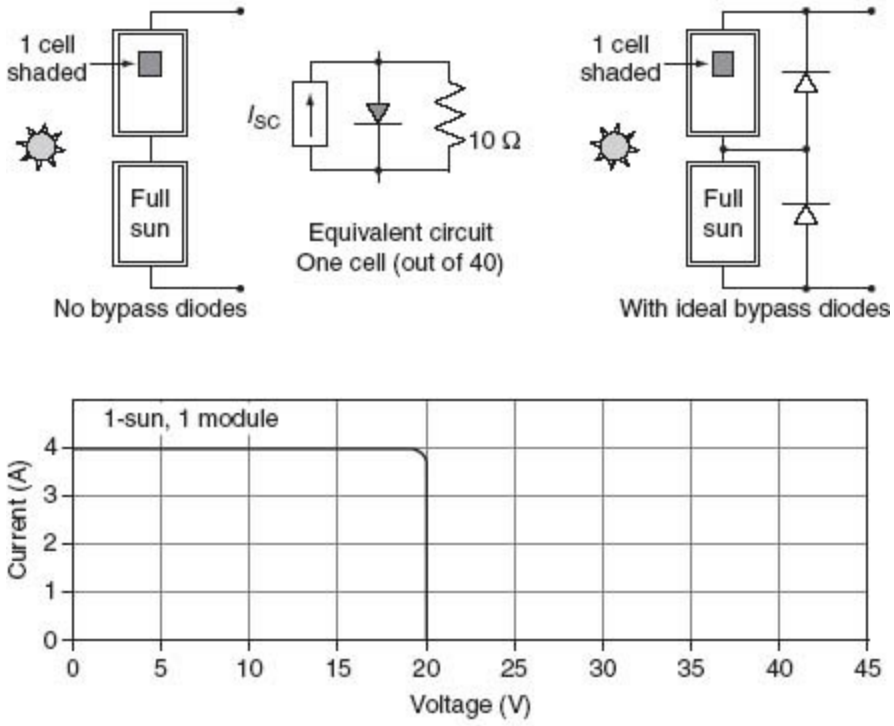


FIGURE P5.12

a. Sketch the 1-sun *I–V* curve for the series combination of modules with one cell shaded but no bypass diodes. Find the power output at the MPP. Compare it to the output when there is no shading.

b. Sketch the 1-sun *I–V* curve when the bypass diodes are included. Estimate the maximum power output now (close is good enough).

5.13 Consider a single 87.5 W, First Solar CdTe module (Table 5.3) used to charge a 12-V battery.

a. What duty cycle should be provided to an MPP, buck–boost converter to deliver 14 V to the battery when the module is working at standard test conditions? How many amperes will it deliver to the battery under those conditions?

b. Suppose ambient temperature is 25°C with 1-sun of insolation. Recalculate the amperes delivered to the battery.

CHAPTER 6

PHOTOVOLTAIC SYSTEMS

6.1 INTRODUCTION

The focus of this chapter is on the analysis and design of photovoltaic (PV) systems in their four most commonly encountered configurations. One dichotomy is based on whether the systems are grid connected or not. Grid-connected systems, in turn, can be broken into two categories based on which side of the electric meter the PVs are placed. Relatively small-scale systems, usually on rooftops, feed power directly to customers on their side of the meter. The grid is used as a backup buffer supply. These "behind-the-meter" systems compete against the retail price of grid electricity, which helps their economics. Systems on the utility side of the meter are generally much larger and their owners sell power into the wholesale electricity market. These systems are more likely to use single- or double-axis tracking systems, with or without concentrated sunlight, than rooftop systems that dominate behind-the-meter systems.

Off-grid systems can also be broken into two categories. One describes stand-alone systems that typically use batteries for energy storage. These range all the way from "pico-scale" PV-powered lanterns and cell phone chargers to larger solar-powered homes, schools, and small businesses, especially in emerging economies around the globe. The other is for loads that are directly connected to the PVs with no intermediate electronics or battery storage. These are mostly water-pumping systems for which water storage replaces the need for electricity storage. Such systems can be exceedingly simple and reliable, but are surprisingly tricky to analyze as we shall see in this chapter.

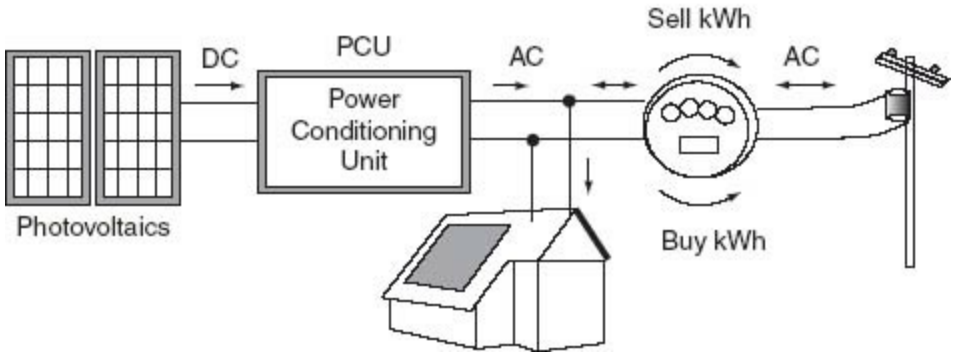
6.2 BEHIND-THE-METER GRID-CONNECTED SYSTEMS

Grid-connected PV systems on the customer's side of the meter have a number of desirable attributes. Compared to utility-scale systems, they avoid land acquisition costs since they are located on the owner's property, and they compete against the much higher retail price of electricity. Compared to off-grid PV systems, they are less expensive since they avoid the cost and inefficiencies, as well as reliability aspects, of batteries and backup generators. Off-grid PV systems, on the other hand, typically compete against much more expensive fuel-fired generators rather than relatively cheap utility power.

6.2.1 Physical Components in a Grid-Connected System

Figure 6.1 shows a simplified diagram of a grid-connected PV system. The customer, in this case, is shown as a single-family residence for which a typical PV system may be rated at something like 1–10 kW of generation capacity. A similar system on a commercial building might have tens of kW to perhaps a megawatt or two of capacity, typically located on rooftops and perhaps in parking lots. While residential and commercial systems are physically similar, the differences in utility rate structures and financial incentives for residential and commercial facilities lead to significantly different economics. In this section, we will deal with the systems.

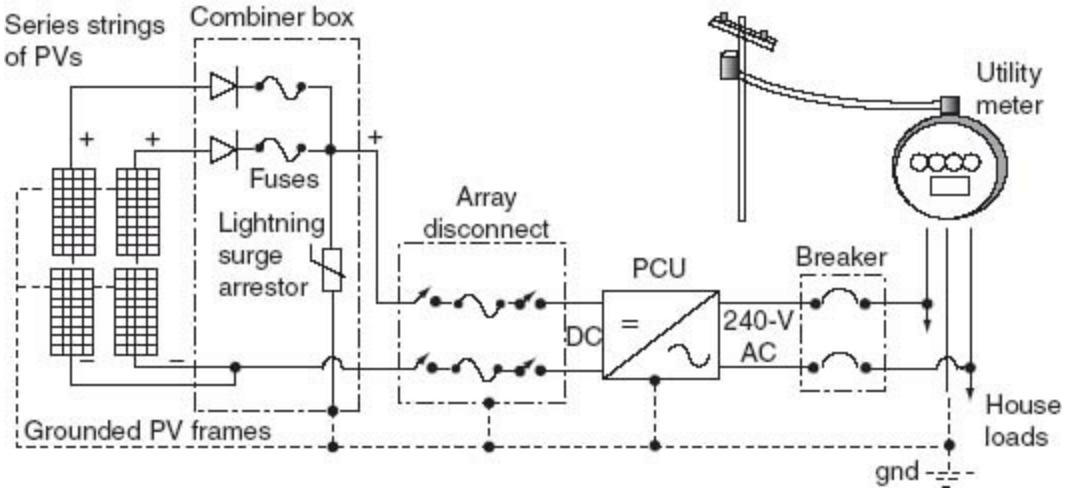
FIGURE 6.1 Simplified grid-connected PV system with net metering.



The PVs in Figure 6.1 deliver DC power to a power-conditioning unit (PCU). The PCU includes a maximum power point tracker (MPPT) to keep the PVs operating at the most efficient point on their *I–V* curve as well as an inverter to convert DC to AC. If the PVs supply less than the immediate demand of the building, the PCU draws supplementary power from the utility grid; so building demand is always satisfied. If, at any moment, the PVs supply more power than is needed, the excess is sent back onto the grid, potentially spinning the electric meter backward building up an energy credit with the utility. The system is relatively simple since failure-prone batteries are not needed for backup power—although, sometimes they may be included if utility outages are problematic.

Some details of the various components in a typical grid-connected, home-size system are shown in Figure 6.2. The system consists of the array itself with leads from each string sent to a combiner box that includes blocking diodes, individual fuses for each string, and usually a lightning surge arrestor. Heavy gauge wire from the combiner box delivers DC power to a fused array disconnect switch, which allows the PVs to be completely isolated from the system. The PCU includes an MPPT, a DC-to-AC inverter, a ground-fault circuit interrupter (GFCI) that shuts the system down if any currents flow to ground, and circuitry to disconnect the PV system from the grid if utility power is lost. The PCU sends AC power, usually at 240 V, through a breaker to the utility service panel. By tying each end of the inverter output to opposite sides of the service panel, 120-V power is delivered to each household circuit.

FIGURE 6.2 Principal components in a grid-connected PV system using a single inverter and a single utility meter.



The PCU must be designed to quickly and automatically drop the PV system from the grid in the event of a utility power outage. When there is an outage, breakers automatically isolate a section of the utility lines in which the fault has occurred, creating what is referred to as an "island." A number of very serious problems may occur if, during such an outage, a self-generator, such as a grid-connected PV system, supplies power to that island.

Most faults are transient in nature, such as a tree branch brushing against the lines, and so utilities have automatic procedures that are designed to limit the amount of time the outage lasts. When there is a fault, breakers trip to isolate the affected lines, and then they are automatically reclosed a second or two later. It is hoped that in the interim the fault clears and customers are without power for just a brief moment. If that does not work, the procedure is repeated with somewhat longer intervals until finally, if the fault does not clear, workers are dispatched to the site to take care of the problem. If a self-generator is still on the line during such an incident, even for less than one second, it may interfere with the automatic reclosing procedure leading to a longer-than-necessary outage. And if a worker attempts to fix a line that has supposedly been disconnected from all energy sources, but it is not, then a serious hazard has been created.

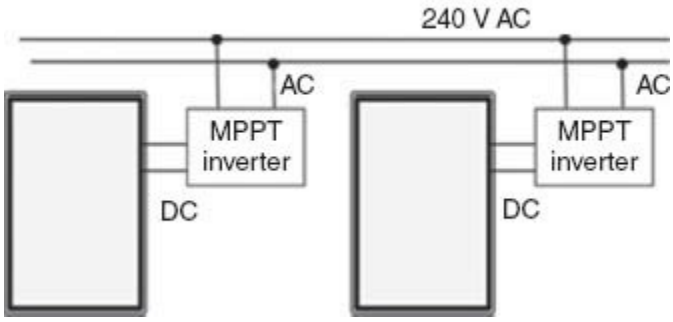
When a grid-connected system must provide power to its owners during a power outage, a small battery backup system may be included. If the users really need uninterruptible power for longer periods of time, the battery system can be augmented with a generator.

6.2.2 Microinverters

An alternative approach to the single inverter system shown in Figure 6.2 is based on each PV module having its own microinverter/MPPT mounted directly onto the backside of the panel (Fig. 6.3). These microinverters offer several significant advantages. With each module having its own MPPT, bypass diodes are no longer needed and the risk of a poorly performing module bringing down an entire string (Section 5.8.2) is eliminated. Similarly, having many small inverters avoids the risk of an inverter malfunction taking down the entire array. Individual inverters also facilitate remote monitoring which can help identify performance issues module by module, and if a module needs to be replaced, it can be individually shut down and safely removed without affecting the rest of the array.

FIGURE 6.3 An alternative to having a single MPPT/inverter for an entire array is to

provide microinverters for each module.

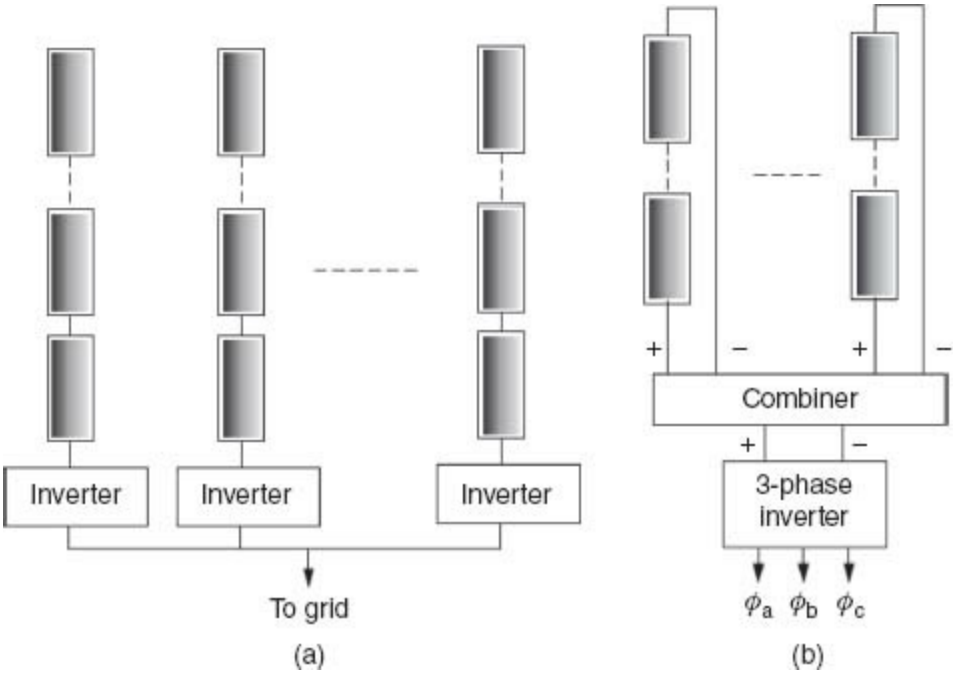


There are some safety advantages to multiple microinverters as well. For example, the array can be wired using conventional AC components at lower voltages than are common in DC systems. AC circuit breakers can be safer and cheaper than their DC counterparts because they are designed to disconnect during the zero-crossing of AC current. With DC there is no zero-crossing and, as we learned in Section 2.7.2, current momentum caused by inductance means it cannot be stopped instantaneously and trying to do so can cause a potentially dangerous arc. Codes now often require special arc-fault circuit interrupters for DC wiring to avoid the risk of fires. Finally, the ability to disconnect modules at the breaker box, or even remotely, reduces the danger of PVs still being energized during emergencies when firefighters, for example, might have to be up on the roof.

Having AC modules also makes fitting an array to an irregular roof surface-–especially one that has potential shading problems—much easier since the designer is not constrained to parallel strings with equal numbers of modules per string. Each module is totally independent and can be put anywhere. In fact, a customer's system can easily be expanded as loads change or as budgets allow.

The above advantages come at a cost. A single inverter may be significantly cheaper than a large number of microinverters—especially for larger arrays. For such systems, strings of PV modules may be tied into inverters in a manner analogous to the individual inverter/module concept (Fig. 6.4a). By doing so, the system is modularized making it easier to service portions of the system without taking the full system offline. Expensive DC cabling is also minimized making the installation potentially cheaper than a large, central inverter. Large, central inverter systems providing three-phase power to the grid are also an option (Fig. 6.4b). Details of how such inverters work were described in Chapter 3.

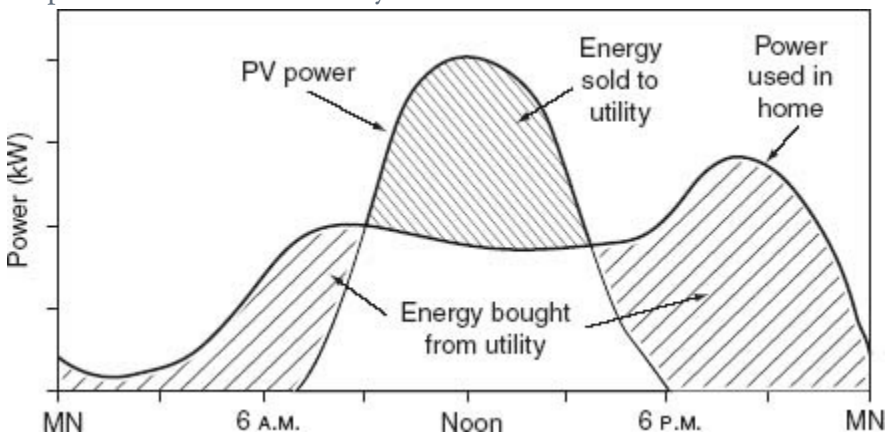
FIGURE 6.4 Larger grid-connected systems may use an individual inverter for each string (a), or may incorporate a large, central inverter system to provide three-phase power (b).



6.2.3 Net Metering and Feed-In Tariffs

The system shown in Figure 6.1, with its single electric meter that spins in both directions, is an example of a *net metering* billing arrangement with the local utility. As shown in Figure 6.5, whenever the PV system delivers more power than the home needs at that moment, the excess spins the electric meter backward, building up a credit with the utility. At other times, when demand exceeds that supplied by the PVs, the grid provides supplementary power. The customer's monthly electric bill is only for the net amount of energy that the PV system is unable to supply.

FIGURE 6.5 During the day, any excess power from the array is sold to the utility; at night, power is purchased from the utility.



In its simplest form, net metering requires no new equipment since essentially all electricity meters run in either direction. The financial accounting, on the other hand, can be rather complex. For example, in an effort to encourage customers to shift their loads away from peak demand times, some offer residential time-of-use (TOU) rates. For many utilities, the peak demand occurs on hot, summer afternoons when air conditioners are humming and less cost-effective reserve power plants are put on line, so it makes sense for

them to try to charge more during those times. Conversely, at night when there is idle capacity, rates can be significantly lower. Customers with PVs who chose TOU rates may be able to sell power to the utility at a higher price during the day than they pay to buy it back at night.

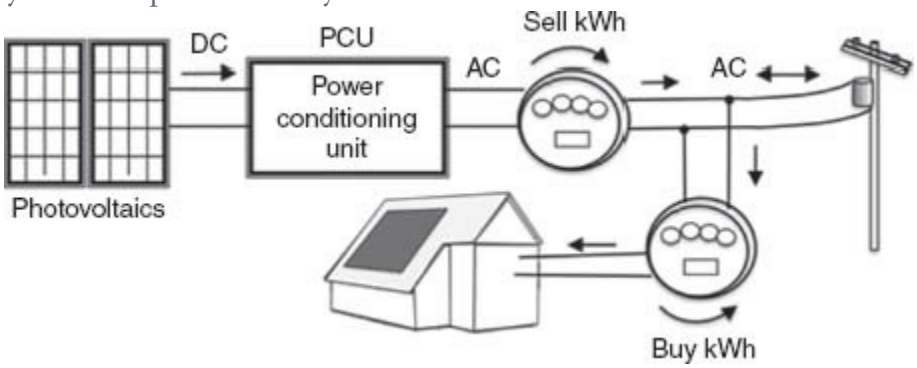
Table 6.1 illustrates an example in which a PV system provides all of the electricity needed by a household during a bright summer month. If a flat-rate structure were chosen, the household bill would be zero for that month. By signing up for TOU rates, however, the net bill would have the utility owing the customer $24 for that month. Utilities often allow negative kWh sales to a customer over a given time period, but they usually true up their books in such a way that makes sure the utility never ends up owing the customer money over an entire year.

TABLE 6.1 TOU Energy and Dollar Calculations for an Example PV System that Provides 100% of Electricity Demand for an Example Month in the Summer

Period	Time	Rate ($/kWh)	PV Delivers (kWh/mo)	Household Demand (kWh/mo)	Net Utility Usage (kWh/mo)	Bill with Solar and TOU ($/mo)
Partial peak	Morning	0.17	400	300	−100	(17.00)
Peak	Afternoon	0.27	500	400	−100	(27.00)
Off peak	Evening	0.10	100	300	200	20.00
Total			1000	1000	0	(24.00)

It is also possible to use a two-meter system, one to measure all of the power generated by the PVs and the other to measure all of the power used in the building (Fig. 6.6). That allows separate rates to be created for each in what is called a *feed-in tariff*. This approach to renewables, which started in Europe, has begun to be offered by utilities in the United States as well. Feed-in tariffs can be designed to encourage adoption of PVs by guaranteeing at the outset a generous price for all electricity generated by the customer's system. This greatly reduces the uncertainty about the value of the PVs, which makes them that much easier to finance. Each year the utility has the ability to adjust the tariff for all new customers, so that as the cost of new systems decreases over time so can the tariff.

FIGURE 6.6 A two-meter system allows a feed-in tariff to provide separate rates for power generated by PVs and power used by customers.



6.3 PREDICTING PERFORMANCE

PV modules are rated under standard test conditions (STCs) that include a solar irradiance of 1 kW/m^2 (called "1-sun"), a cell temperature of 25°C, and an air mass ratio of 1.5 (AM1.5). Under these laboratory conditions, module outputs are thus often referred to as "watts STC" or just "peak watts" (Wp). Out in the field, modules are subject to very different conditions and their outputs will vary significantly from the STC rated power that the manufacturer specifies. Insolation is not always 1-sun, modules get dirty, and cells are typically 20–40°C hotter than the surrounding air. Unless it is very cold outside, or it is not a very sunny day, cells will usually be much hotter than the 25°C at which they are rated.

6.3.1 Nontemperature-Related PV Power Derating

A simple way to deal with the goal of converting STC ratings into expected AC power delivered under real field conditions is to introduce a derating factor:

$$P_{AC} = P_{DC,STC} \times \text{Derate factor} \tag{6.1}$$

To that end, Sandia National Laboratory has created a performance evaluation model called the Solar Advisor Model (SAM) that is the basis for a now commonly used online PV performance calculator called PVWATTS. PVWATTS is readily available on the National Renewable Energy Laboratory (NREL) website. Their calculator provides a number of estimates of factors that can contribute to an overall derate factor, including default values that can be modified by users to suit their own circumstances. Table 6.2 presents their estimates.

TABLE 6.2 PVWATTS Derate Factors for DC-STC to AC Power Ratings (Not Including Temperature Impacts)

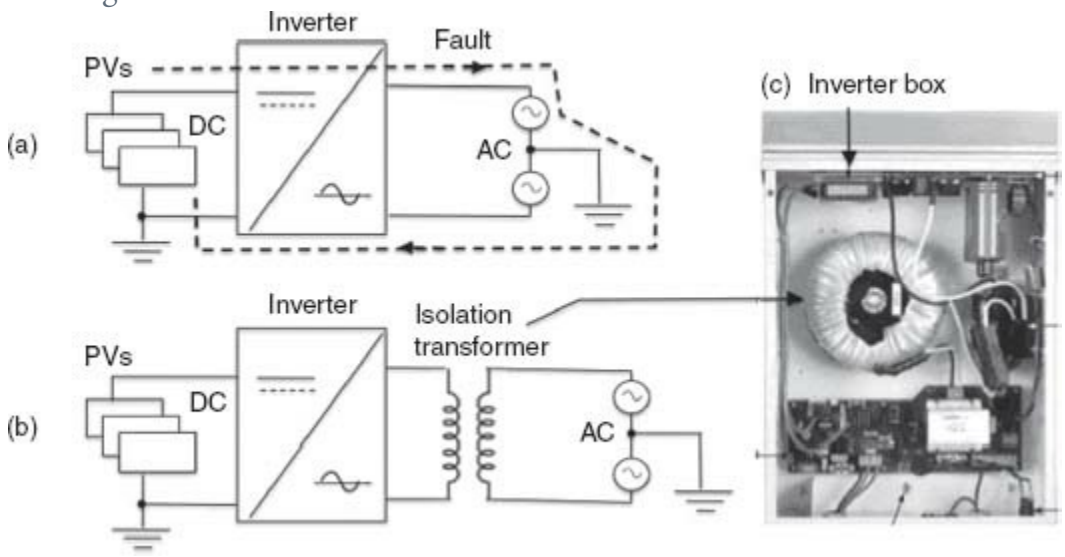
Item	PVWATTS Default	Range
PV module nameplate DC rating	0.95	0.80–1.05
Inverter and Transformer	0.92	0.88–0.98
Module mismatch	0.98	0.97–0.995
Diodes and connections	1.00	0.99–0.997
DC wiring	0.98	0.97–0.99
AC wiring	0.99	0.98–0.993
Soiling	0.95	0.30–0.995
System availability	0.98	0.00–0.995
Shading	1.00	0.00–0.995
Sun tracking	1.00	0.95–1.00
Age	1.00	0.70–1.00
Total derate factor without NOCT	0.770	

A few clarifications to Table 6.2 are in order. The PV module nameplate DC rating refers to the fact that modules coming off the assembly line may all have the same manufacturer nameplate rating, but not all of them may produce that much power even under standard test conditions in the field. A separate but related entry, designated as "Age, " allows users to try to account for the long-term decrease in module efficiency. Studies suggest degradation rates on the order of 0.5%/yr may be likely for crystal silicon (c-Si.)

Newer thin-film modules have improved and are now expected to age at a similar rate to c-Si (Jordan et al., 2011; Marion et al., 2005).

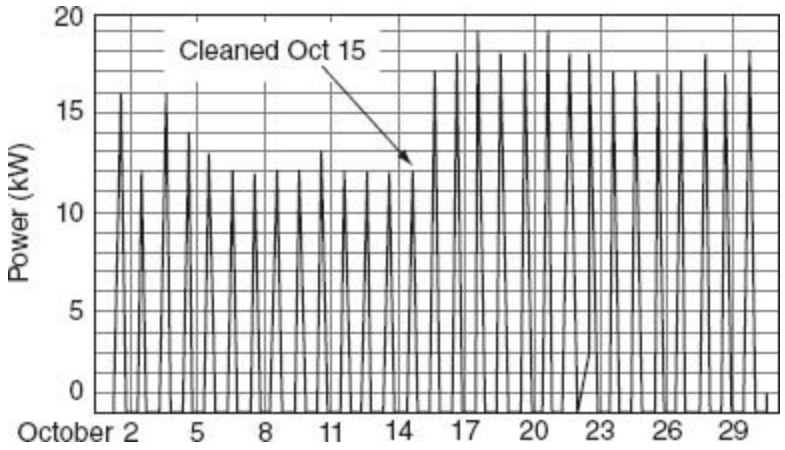
Inverter efficiency is usually very high as long as it operates with relatively high load factors. For safety, most systems include an isolation transformer to prevent fault currents from the DC side of the system to be passed onto the AC grid (Fig. 6.7). These transformers not only contribute to losses, but also are expensive and take up a fair amount of room inside the inverter box. Transformers can be avoided by not grounding the DC portion of the system, which is common in Europe, but is still under consideration in the United States.

FIGURE 6.7 Isolation transformers prevent fault currents from passing from the DC side of the system onto the AC grid connection (a) Showing fault; (b) the isolation transformer; (c) illustrating the size of the transformer.



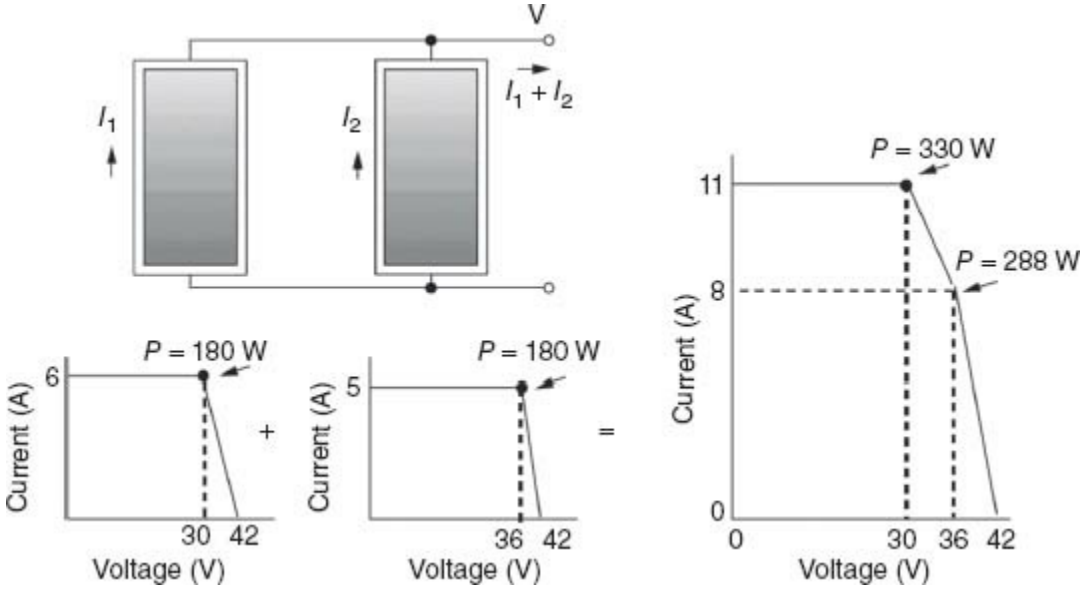
The soiling derate is highly variable depending on rainfall, collector tilt, sources of soiling (including snow), and whether or not periodic washing occurs. Figure 6.8 shows an example of a washing experiment that was conducted in early fall on a nearly horizontal array located in an open field on the edge of the Stanford campus. California summers are characterized by having virtually zero rainfall and the array had never been washed before. After the long summer, the 20-kW array was producing about 12 kW at midday. After washing, the peak output increased by almost 50%.

FIGURE 6.8 A washing experiment conducted in early fall 2008 on a 20-kW nearly horizontal array on the edge of the Stanford campus.



Module mismatch accounts for slight differences in *I–V* curves even though modules may deliver the same power under standard test conditions. For example, Figure 6.9 shows two mismatched 180-W modules wired in parallel. They each have the same rated output, but their somewhat idealized *I–V* curves have been drawn so that one produces 180 W at 30 V and the other does so at 36 V. As shown, the sum of their *I–V* curves shows the maximum power of the combined modules is only 330 W instead of the 360 W that would be expected if their *I–V* curves were identical. Note that if microinverters were used, there would be no module mismatch for this example.

FIGURE 6.9 Illustrating the loss due to mismatched modules. Each module is rated at 180 W but the parallel combination yields only 330 W at MPP.

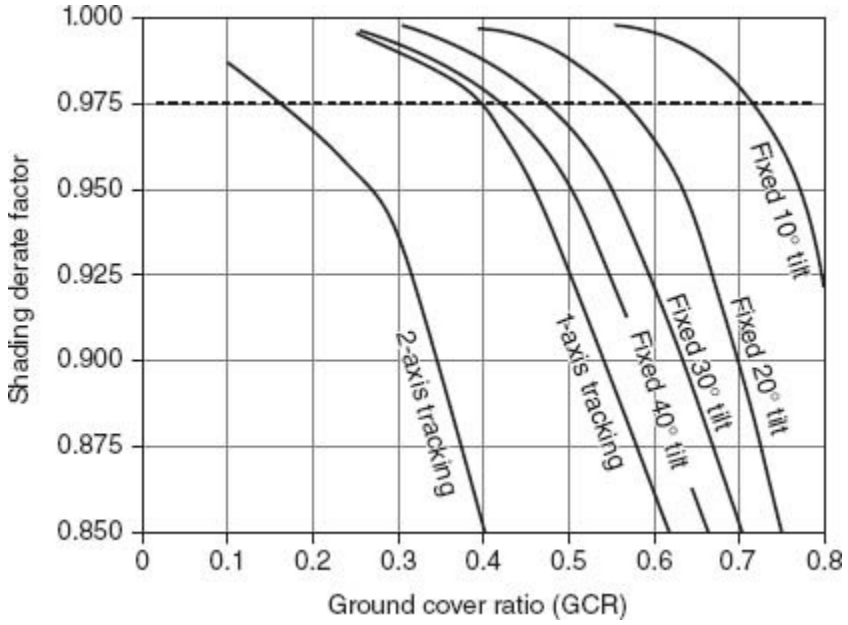


Shading losses can be the result of nearby obstructions or debris on the panels, but it can also be caused by one collector shading another during certain parts of the day. When there are area constraints, which is often the case on buildings in general, and especially if the roof is flat, which is the case on many commercial buildings, a design decision must be made between horizontal collectors that can fill the space with no shading versus rows of tilted collectors, which may cause shading from one row to another. The tilted collector option can use fewer collectors to get the job done and stacking them in the rows eliminates future access problems if modules need attention.

In Section 4.6, shadow diagrams were used to help predict shading problems. A different

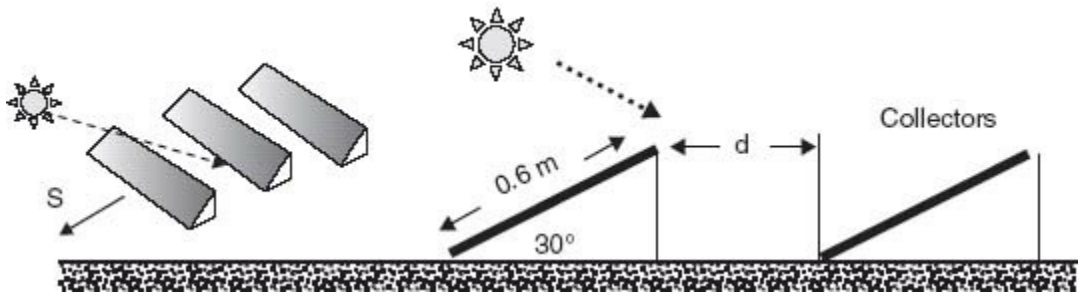
approach is provided by Figure 6.10, in which shading derate factors for various array configurations are plotted versus a quantity called the ground cover ratio (GCR). The GCR is the ratio of the area of the PVs themselves to the total ground area. Smaller GCR means collectors are spaced further apart so shading is reduced and the derate factor is improved. The PVWATTS website from which this figure was taken indicates that industry practice is to optimize the use of space by configuring the PV system for a GCR that corresponds to a shading derate factor of 0.975 (2.5% loss). Example 6.1 illustrates its use.

FIGURE 6.10 Shading derate factors for various collector configurations. The dashed line suggests an optimum derate of 0.975 (from PVWATTS website).



Example 6.1 Optimum Spacing of Rows of PVs. The CdTe modules described in Table 5.3 have dimensions of 1.2 × 0.6 m. Using Figure 6.10 and the recommended 0.975 derate factor, what should be the collector spacing between rows if the 1.2-m dimension is on the bottom and these south-facing collectors have a 30° tilt angle.

Solution. Begin with a sketch of the geometry.



From Figure 6.10, it looks like GCR should be about 0.47 to give us a derate factor of 0.975. Just using a per-unit of distance along the collector row and the definition of the GCR gives

$$\text{GCR} = \frac{\text{Collector area } A_C}{\text{Total ground area } A_{\text{Tot}}} = \frac{0.6 \times 1}{(0.6\cos 30^\circ + d) \times 1} = 0.47$$

$$0.47 \times 0.6\cos\ 30^\circ + 0.47d = 0.6$$

$$\text{Spacing } d = \frac{0.6 - 0.2442}{0.47} = 0.76 \text{ m}$$

6.3.2 Temperature-Related PV Derating

Note that PVWATTS derate estimates do not include the very important loss due to cells operating at temperatures above the STC reference temperature of 25°C. That is because PVWATTS uses location-specific typical meteorological year (TMY), hour-by-hour estimates of insolation and ambient temperature to account for losses due to elevated cell temperatures. Recall from Section 4.13.1, how TMY data can be used to find hourly insolation on modules. Hourly cell temperature can be estimated from that insolation along with TMY ambient temperatures and the normal operating cell temperature (NOCT) provided by manufacturers (Section 5.7). NOCT, which is based on an assumed irradiation S of 0.8 kW/m^2 and an assumed ambient temperature of 20°C, can be adjusted for actual conditions using Equation 5.23

$$T_{\text{cell}} = T_{\text{amb}} + \left(\frac{\text{NOCT} - 20^\circ\text{C}}{0.8\ \text{kW/m}^2}\right) \cdot S(\text{kW/m}^2) \quad (6.2)$$

Using cell temperature estimates calculated from TMY data and Equation 6.2, coupled with the module's temperature coefficient of P_{max}, it is easy to compute hourly NOCT derate factors as the following example illustrates.

Example 6.2 Using TMY Data to Estimate Hourly NOCT Derate Factors. In Example 4.13, calculations based on Atlanta TMY data indicated that 753 W/m^2 would strike a collector at 52° tilt angle, 20° azimuth angle on May 21 at noon. At that time, TMY ambient temperature is 25.6°C. Find the temperature derate factor at noon for the single-crystal silicon (sc-Si) module in Table 5.3 (NOCT = 45°C, temperature coefficient of P_{max} = –0.38%/°C).

Solution. From (6.2)

$$T_{\text{cell}} = T_{\text{amb}} + \left(\frac{\text{NOCT} - 20^\circ\text{C}}{0.8\ \text{kW/m}^2}\right) \cdot S(\text{kW/m}^2)$$

$$T_{\text{cell}} = 25.6 + \left(\frac{45 - 20}{0.8}\right) \cdot 0.753 = 49.1^\circ\text{C}$$

Since the temperature coefficient is based on a comparison with the STC cell temperature of 25°C, the degradation of P_{max} will be

$$\text{Decrease in } P_{\text{max}} = 0.38\%/^\circ\text{C} \cdot (49.1 - 25^\circ\text{C}) = 9.16\%$$

That translates to a noon temperature derate factor of

$$\text{NOCT derate} = 1 - 0.0916 = 0.908$$

That is, a 9.2% decrease in performance.

Table 6.3 extends the calculations shown in Example 6.2 to show a full day's worth of temperature derate factors. Notice a few hours in the morning, with cool temperatures and not much insolation, have cells below 25°C; so during those hours, the cells perform better than they would under STCs (i.e., derates are above 1.0).

TABLE 6.3 Hourly NOCT Derate Factors for Atlanta, May 21, Example 6.2

TMY Time	Insolation I_C (kW/m^2)	T_{amb} (°C)	T_{cell} (°C)	NOCT Derate	Effective I_C (kW/m^2)
5.00		16.1	16.1	1.034	
6.00	0.011	16.1	16.4	1.033	0.011
7.00	0.162	16.7	21.8	1.012	0.164
8.00	0.436	18.3	31.9	0.974	0.425
9.00	0.437	20.0	33.7	0.967	0.423
10.00	0.545	21.7	38.7	0.948	0.516
11.00	0.826	23.3	49.1	0.908	0.750
12.00	0.753	25.6	49.1	0.908	0.684
13.00	0.669	26.1	47.0	0.916	0.613
14.00	0.568	25.6	43.4	0.930	0.529
15.00	0.495	26.1	41.6	0.937	0.464
16.00	0.259	26.7	34.8	0.963	0.249
17.00	0.168	26.7	31.9	0.974	0.163
18.00	0.101	25.6	28.8	0.986	0.100
19.00	0.051	23.9	25.5	0.998	0.051
Total	5.480				5.141
		Daily NOCT derate factor = 0.938			

The question arises as to how to find a total daylong derate. Since the point of derate factors is to account for reductions in energy delivered caused by factors such as temperature, it makes sense to care more about derates when insolation is high since a given derate will cause more energy to be lost during those hours. The final column in Table 6.3 is the product of that hour's derate times the insolation during that hour. By totaling the raw insolation column and the effective insolation column after the derates have been applied, we get before and after total kWh/m^2 of insolation. The ratio of the two, in this case 0.938, is the overall daylong temperature derate factor. Over a day's time, we have lost the equivalent of 6.2% of the insolation, which translates directly into 6.2% loss in energy delivered by the PVs.

The example shown in Table 6.3 was derived for a day with an average daytime temperature of 23°C. Cell temperature effects on this pleasant spring day will give a derating factor of 0.938, which means it will cut PV production by 6.2%. In the winter, when it is colder, the temperature derate impact will be less; in the summer, it will more. This 0.938 might, in fact, be a pretty good estimate for the entire year, but to confirm that would require a full 365-day analysis. We will leave that to solar calculators such as PVWATTS (in fact, working backward through PVWATTS suggests their overall, yearlong

temperature derate for Atlanta is 0.920, which is an 8.0% loss).

There is another very useful solar calculator online; this one is from the California Energy Commission (CEC). The CEC calculator supports the California Solar Initiative (CSI) by helping consumers figure out the PV incentives offered by the three major investor-owned utilities in California. The CSI approach begins by adjusting the DC, STC rated power of modules to predict their output under what are called PVUSA test conditions (PTC), which are defined as 1-sun irradiance in the plane of the array, 20°C ambient temperature and a windspeed of 1 m/s. The financial incentives are based on module DC, PTC ratings, inverter efficiency, and the location and orientation of the array. Since users enter the actual modules and inverters being considered, the CSI calculator provides direct comparisons of the predicted performance of the major system components.

6.3.3 The "Peak-Hours" Approach to Estimate PV Performance

Predicting performance is a matter of combining the characteristics of the major components—the PV array and the power conditioning unit—with local insolation and temperature data. After having adjusted DC power under STC to expected AC from the PCU using an appropriate derate factor, the next key thing to evaluate is the amount of sunlight available at the site. Chapter 4 was devoted to developing equations for clear-sky insolation, and tables of values are given in Appendix D and E for clear skies. In Appendix G, there are tables of estimated average insolations for a number of locations in the United States.

If the units for daily, monthly, or annual average insolation are specifically kWh/m^2/d, then there is a very convenient way to interpret that number. Since 1-sun of insolation is defined as 1 kW/m^2, we can think of an insolation of say 5.6 kWh/m^2/d as being the same as 5.6 h/d of 1-sun or 5.6 h of "peak sun." So, if we know the AC power delivered by an array under 1-sun insolation (P_{AC}), we can simply multiply that rated power by the number of hours of peak sun to get daily kWh delivered.

To see whether this simple approach is reasonable, consider the following analysis. We can write the energy delivered in a day's time as

$$\text{Energy (kWh/d)} = \text{Insolation}\left(\frac{\text{kWh/m}^2}{\text{day}}\right) \cdot A(\text{m}^2) \times \bar{\eta} \tag{6.3}$$

where A is the area of the PV array and $\bar{\eta}$ is the average system efficiency over the day.

When exposed to 1-sun of insolation, we can write for AC power from the system

$$P_{AC}(\text{kW}) = \left(\frac{1\ \text{kW}}{\text{m}^2}\right) \cdot A(\text{m}^2) \times \eta_{1\text{-sun}} \tag{6.4}$$

where $\eta_{1\text{-sun}}$ is the system efficiency at 1-sun. Combining Equations 6.3 and 6.4 gives

$$\text{Energy (kWh/d)} = P_{AC}(\text{kW})\left[\frac{\text{Insolation (kWh/m}^2\text{/d)}}{1\ \text{kW/m}^2}\right] \cdot \left(\frac{\bar{\eta}}{\eta_{1\text{-sun}}}\right) \tag{6.5}$$

If we assume that the average efficiency of the system over a day's time is the same as the

efficiency when it is exposed to 1-sun, then the energy collected is what we hoped it would be

$$\text{Energy (kWh/d)} = P_{AC}(\text{kW}) \cdot (\text{h/d of "peak sun"}) \tag{6.6}$$

The key assumption in Equation 6.6 is that the system efficiency remains pretty much constant throughout the day. The main justification is that these grid-connected systems have MPPTs that keep the operating point near the knee of the *I–V* curve all day long. Since power at the maximum point is nearly directly proportional to insolation, system efficiency should be reasonably constant. Cell temperature also plays a role, but it is less important. Efficiency might be a bit higher than average in the morning, when it is cooler and there is less insolation, but all that will do is make Equation 6.6 slightly conservative.

Combining Equation 6.1 with Equation 6.6 gives us a way to do simple calculations to estimate annual energy production from a PV array. With the help of PVWATTS, it can also give us a bit more insight into that elusive overall derate factor when it includes temperature effects.

$$\text{Energy (kWh/yr)} = P_{DC,STC} \times \text{Derate factor} \times (\text{h/d of "peak sun"}) \times 365\ \text{d/yr} \tag{6.7}$$

Typical values for the overall derate factor in the range of 0.70–0.75 seem appropriate, with the lower end of the range applying to hotter climate areas.

Example 6.1 Annual Energy Using the Peak-Sun Approach. A south-facing, 5-kW (DC, STC) array in Atlanta, GA, has a tilt angle equal 18.65° (L–15) for which PVWATTS estimates the annual insolation is 5.12 kWh/m^2/d.

a. Using the peak hours approach estimate the annual energy that will be delivered. This is a relatively warm climate area so let us assume an overall derate factor of 0.72.

b. Then, use the PVWATTS online calculator to compare results. From that result, determine the value of the overall annual derate factor that works in Equation 6.7. With 0.77 being the default nonthermal derate factor, what would be the derate for temperature alone?

c. What improvement would be realized if modules had microinverters that eliminate the module mismatch derate and which also replace the PVWATTS 2% derate DC wiring losses with 1% AC wiring loss?

Solution

a. From Equation 6.7, our estimate is

$$\text{Energy} = 5\ \text{kW} \times 0.72 \times 5.12\ \text{h/d} \times 365\ \text{d/yr} = 6727\ \text{kWh/yr}$$

b. PVWATTS for zip code 30303 using the 0.77 derate factor for everything but temperature, gives 6624 kWh/yr.

The overall derate factor including thermal impacts that PVWATTS must be using is

$$\text{kWh/yr} = P_{\text{DC,STC}} \times \text{Overall derate} \times (\text{h/d peak sun}) \times 365 \text{ d/yr}$$

$$\text{Overall derate} = \frac{6624 \text{ kWh/yr}}{5 \text{ kW} \times 5.12 \text{ h/d} \times 365 \text{ d/yr}} = 0.709$$

Since PVWATTS uses 0.77 as the derate for everything but temperature, that suggests

$$\text{Temperature derate} = \frac{\text{Overall derate}}{\text{Default } 0.77} = \frac{0.709}{0.77} = 0.921 \text{ or about } 7.9\% \text{ loss.}$$

c. Adjusting the defaults in Table 6.2 changes module mismatch from 0.98 to 1.0 and using AC instead of DC wiring changes their loss factor from 0.98 to 0.99. The 0.77 nonthermal derating then becomes

$$\begin{aligned}\text{New derate value} &= 0.95 \times 0.92 \times 1.0 \times 1.0 \times 0.99 \times 0.99 \times 0.95 \times 0.98 \\ &= 0.798\end{aligned}$$

So the total derate with microinverters including our newly found temperature impact is

$$\text{Total derate} = 0.921 \times 0.798 = 0.735$$

So our new peak-hour estimate of annual energy using microinverters is

$$\text{Energy} = 5 \text{ kW} \times 0.735 \times 5.12 \text{ h/d} \times 365 = 6838 \text{ kWh/yr}$$

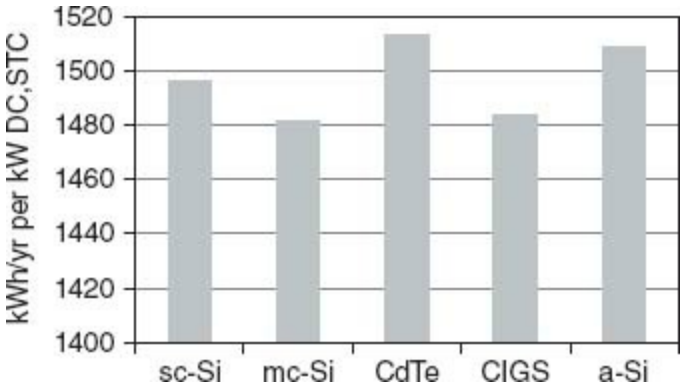
That is a boost of 6838 – 6624 = 214 kWh/yr, about 3.2% over the default PVWATTS estimate.

Some time ago, Scheuermann et al. (2002) measured 19 PV systems in California and found the actual derate between 0.53 and 0.70. On the other hand, early monitoring of NREL's net-zero energy Research Support Facility (RSF) in Golden, CO, resulted in a much better total derate factor of 0.84 (Blair et al., 2012). Over time, there has been a general trend toward more efficient components, better maintenance, and greater care during installation that is showing up in better derate factors.

6.3.4 Normalized Energy Production Estimates

With online calculators readily available, we can easily derive performance data for different PV technologies in different locations. One handy way to make such comparisons is by using manufacturer-provided $P_{\text{DC, STC}}$ ratings to normalize the predicted kWh/yr system outputs. For example, Figure 6.11 shows the normalized outputs of the five Table 5.3 collectors that we have been using for examples. Note, however, that the scale emphasizes what are relatively small differences; between the worst and the best it is only 2%.

FIGURE 6.11 Normalized outputs by PV technology for the modules in Table 5.3 for Palo Alto, CA, tilt angle 38°, 94.5%-efficient inverter, using the CA CSI calculator.



The normalized outputs in Figure 6.11 for the five technologies can be explained quite well by using the temperature deratings under NOCT conditions:

$$\text{Power loss} = P_{DC,STC} \cdot \text{Temperature coefficient } (\%/°C) \cdot (\text{NOCT} - 25)°C \tag{6.8}$$

$$\text{sc-Si} = \frac{0.38\%}{°C} \cdot (45 - 25)°C = 7.6\%$$

$$\text{mc-Si} = \frac{0.45\%}{°C} \cdot (46 - 25)°C = 9.4\%$$

$$\text{CdTe} = \frac{0.25\%}{°C} \cdot (45 - 25)°C = 5.0\%$$

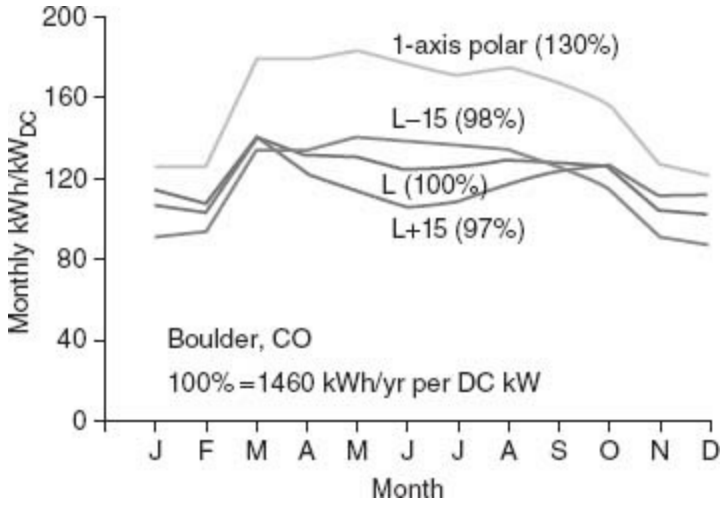
$$\text{CIGS} = \frac{0.40\%}{°C} \cdot (47 - 25)°C = 8.8\%$$

$$\text{a-Si} = \frac{0.24\%}{°C} \cdot (45 - 25)°C = 4.8\%$$

Note how these temperature impacts alone suggest slightly better (per kW_{DC}) performance might be expected from cadmium telluride (CdTe) and triple-junction amorphous silicon (a-Si) technologies than the others, which seems to be confirmed by the examples shown in Figure 6.11.

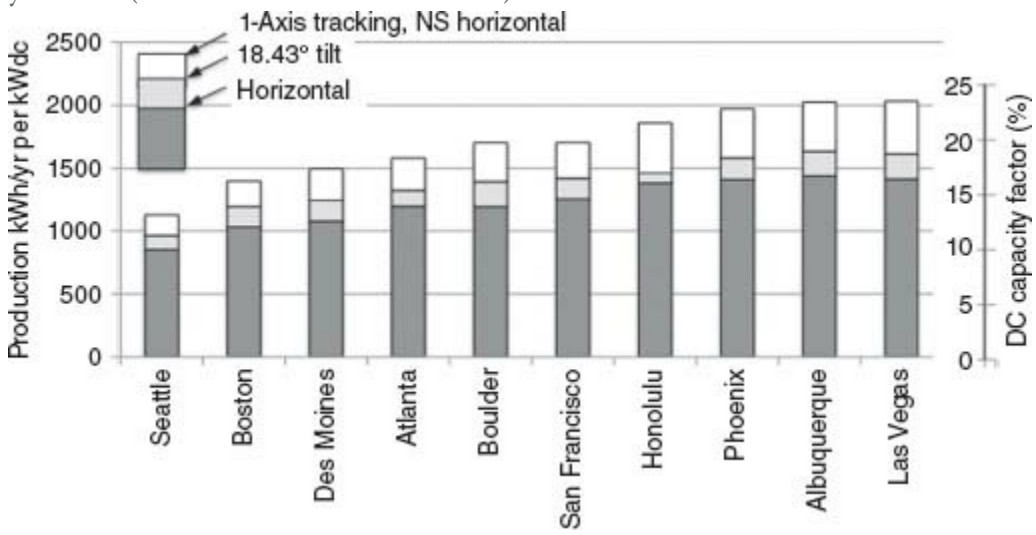
Figure 6.12 presents monthly, normalized energy production for an example location (Boulder, CO) as a way to point out that the tilt angle for net-metered PVs is not particularly important on an annual kWh basis. The difference in performance between an L–15 tilt angle (latitude minus 15°) and L+15 is only a couple of percent. In fact, the reduction at a standard 4-in-12 roof pitch of 18.43° is only 5%. With TOU rates, shallow-pitched, net-metered systems can more than offset those losses by selling more electricity in the summers when it is more valuable. Note, by the way, the sizeable 30% improvement in kWh with single-axis tracking. Two-axis tracking is only 6% better than single-axis tracking.

FIGURE 6.12 Comparing monthly energy production for fixed-tilt arrays and single-axis tracking. The percentages are annual totals relative to a fixed tilt equal to the local latitude (L).



Normalized expected energy productions for a number of U.S. cities are shown in Figure 6.13. The configurations chosen are most representative of residential and commercial installations (horizontal arrays, arrays pitched at a typical 4-in-12 roof slope (18.43°), and horizontal single-axis tracking arrays). For typical roof pitch, south-facing collectors in areas with good, 5.5 full-sun h/d will deliver about 1500 kWh/yr of AC energy per $kW_{DC, STC}$.

FIGURE 6.13 Normalized electricity production for a range of U.S. cities. Fixed arrays at typical 4-in-12 roof pitch, horizontal, and 1-axis tracking with horizontal NS axis. Also DC capacity factors (from PVWATTS calculator).



6.3.5 Capacity Factors for PV Grid-Connected Systems

A simple way to present the energy delivered by any electric power generation system is in terms of its rated AC power P_{AC} and its capacity factor (CF). As described in Section 1.6.2, capacity factor over a period of time, usually 1 year, is the ratio of the energy actually delivered to the energy that would have been delivered if the system ran at full rated power all the time. It can also be thought of as the ratio of average power to rated power.

The normal governing equation for annual performance of power plants in terms of CF is based on the annual AC rating of the plant:

$$\text{Energy (kWh/yr)} = P_{AC}(\text{kW}) \cdot \text{CF} \cdot 8760\ (\text{h/yr}) \tag{6.9}$$

where 8760 is the product of 24 h/d × 365 d/yr. Monthly or daily capacity factors are similarly defined.

For PVs, it is a common practice to describe performance in terms of their DC capacity factor

$$\text{Energy (kWh/yr)} = P_{DC,STC}(\text{kW}) \cdot \text{CF}_{DC} \cdot 8760\ (\text{h/yr}) \tag{6.10}$$

Combining this with the "peak-hours" approach to delivered energy

$$\text{Energy (kWh/yr)} = P_{DC}(\text{kW}) \cdot (\text{Derate}) \cdot (\text{h/d full sun}) \cdot 365\ \text{days/yr} \tag{6.11}$$

leads to the following description of a DC capacity factor

$$\text{DC capacity factor } (\text{CF}_{DC}) = \frac{\text{h/d of "peak sun"}}{24\ \text{h/d}} \times \text{Derate factor} \tag{6.12}$$

For normalized PV outputs with units of kWh/yr per $\text{KW}_{\text{DC, STC}}$ (Eq. 6.10) leads to another way to express DC capacity factors:

$$\text{CF}_{DC} = \frac{(\text{kWh/yr})/\text{kW}_{DC,STC}}{8760\ \text{h/yr}} \tag{6.13}$$

Figure 6.13 shows the DC capacity factors for those selected cities.

6.3.6 Some Practical Design Considerations

With the utility there to provide energy storage and backup power, sizing grid-connected systems is not nearly as critical as it is for stand-alone systems. Sizing can be more a matter of how much unshaded area is conveniently available on the building coupled with the customer's budget. Oversizing with net-metered systems can be an issue since the utility may not be willing to pay for any excess energy.

With solar calculators such as PVWATTS and the CSI readily available online, sizing the number of modules needed to meet design goals is quite straightforward. For a paper-and-pencil analysis, or preparing your own spreadsheet to play with, sizing can begin with establishing a kWh/yr target, followed by a simple calculation of the peak watts of DC PV power needed and the collector area required. Or it can start with the area available, from which you can work backward to determine the kWh/yr that can be produced and the peak watts that will make it happen.

At this point, the design begins to be determined by the modules and inverter chosen. Unless the chosen modules have their own microinverters, the array will consist of parallel strings of modules, with the number of modules in a string determined by maximum voltages allowed by code as well as the input voltages needed by the inverter.

Example 6.4 System Sizing in Silicon Valley, CA. Size a PV system to supply 5000 kWh/yr to a home in Silicon Valley. Do the calculations by hand-making assumptions as needed. Test the final design using the CSI calculator (Zip code 94305).

Solution. Assume the roof is south facing with a 4-in-12 pitch (18.43° tilt). PVWATTS

estimates 5.32 kWh/m^2/d of insolation. It is a relatively cool region, so let us assume a derate factor of 0.75. Then, using Equation 6.11

$$P_{DC}(\text{kW}) = \frac{\text{Energy (kWh/yr)}}{(\text{Derate}) \cdot (\text{h/d full sun}) \cdot 365\ \text{day/yr}}$$

$$= \frac{5000\ \text{kWh/yr}}{0.75 \times 5.32\ \text{h/d} \times 365\ \text{d/yr}} = 3.43\ \text{kW}$$

Let us assume top quality c-Si modules with 19% efficiency. Using STCs, the PVs need to deliver 3.43 kW, so the area required can be found from

$$P_{DC,STC} = 1\ \text{kW/m}^2 \times A\ (\text{m}^2) \times \eta$$

$$A = \frac{3.43\ \text{kW}}{1\ \text{kW/m}^2 \times 0.19} = 18.05\ \text{m}^2$$

Having confirmed that there is sufficient area on the roof, suppose we pick a SunPower 240-W module with the following key STC characteristics:

Peak power	240 W
Rated voltage V_{MPP}	40.5 V
Open-circuit voltage V_{OC}	48.6 V
Short-circuit current I_{SC}	6.3 A
Temperature coefficient of power	–0.38%/K
Temperature coefficient of V_{OC}	–0.27%/K
Temperature coefficient of I_{SC}	–0.05%/K
NOCT	45°C
Dimensions	1.56 m × 0.798 m = 1.245 m^2/module

We are going to need about 3.43 kW/0.240 kW = 14.3 modules. Before we decide on 14 or 15 modules, let us consider the number of modules per string. To do that, we need an example inverter. Let us try the SunPower 5000 with the following important characteristics:

Maximum power	5000 W
MPP tracking voltage range	250–480 V
Range of input operating voltage	250–600 V
PV start voltage	300 V
Maximum DC input current	21 A
Maximum input short circuit current	36 A

Start with the inverter MPP tracking voltage range of 250–480 V. At 40.5 V per module that suggests a range of 250 V/40.5 V = 6.2 to 480 V/40.5 V = 11.9 modules per string.

We need to see how that changes with temperature. Suppose the coldest daytime temperature that might be expected is –5°C, which is 30° colder than the 25° STC temperature. When it is cold, voltage increases, so at that cell temperature we might expect

the MPP voltage to be

$$V_{MPP} = 40.5\ \text{V} \cdot [1 - 0.0027(-5 - 25)] = 43.8\ \text{V}$$

which means we need fewer than 480 V/43.8 V = 10.9 modules per string to stay in the MPP bounds.

The National Electrical Code restricts all voltages on residential systems in one- and two-family dwellings to no more than 600 V, which is also the inverter limit, so we need to check that constraint. On the coldest day, the maximum module V_{OC} will be

$$V_{OC} = 48.6\ \text{V} \cdot [1 - 0.0027(-5 - 25)] = 52.5\ \text{V}$$

which tells us we need fewer than 600 V / 52.5 V = 11.4 modules per string. So, the two cold weather tests suggest no more than 10 modules per string.

Now we need to test conditions when it is as hot as might be expected. Assuming the hottest day is 40°C with insolation 1 kW/m^2/d, then the highest cell temperature and MPP voltage will be

$$T_{cell} = T_{amb} + \left(\frac{\text{NOCT} - 20}{0.8}\right) \cdot S = 40 + \left(\frac{45 - 20}{0.8}\right) \cdot 1 = 71.3°\text{C}$$

$$V_{MPP}(\text{hot}) = 40.5\ \text{V} \cdot [1 - 0.0027(71.3 - 25)] = 35.4\ \text{V}$$

With only 35.4 V and the need to have at least 250 V for the inverter MPPT, that says we need at least 250 V/35.4 V = 7 modules per string.

So, the conclusion is something between 7 and 10 modules per string will satisfy the inverter constraints. Since we decided we needed about 14.3 modules to meet the load, we could be pretty close to our goal by using two strings of seven modules each. With only two strings, each having short circuit current of 6.3 A, means we are well below 31 A maximum current to this inverter.

When this 14 module (3.36 kW$_{DC}$) system was tested on the CSI solar calculator, their result was 4942 kWh/yr. Using our simple peak-hours approach with a 0.75 derate factor would have predicted the system would deliver

$$14 \times 0.24\ \text{kW} \times 5.32\ \text{h/d} \times 365\ \text{d/yr} \times 0.75 = 4893\ \text{kWh/d}$$

which is very close to the result found using the CSI calculator.

6.4 PV SYSTEM ECONOMICS

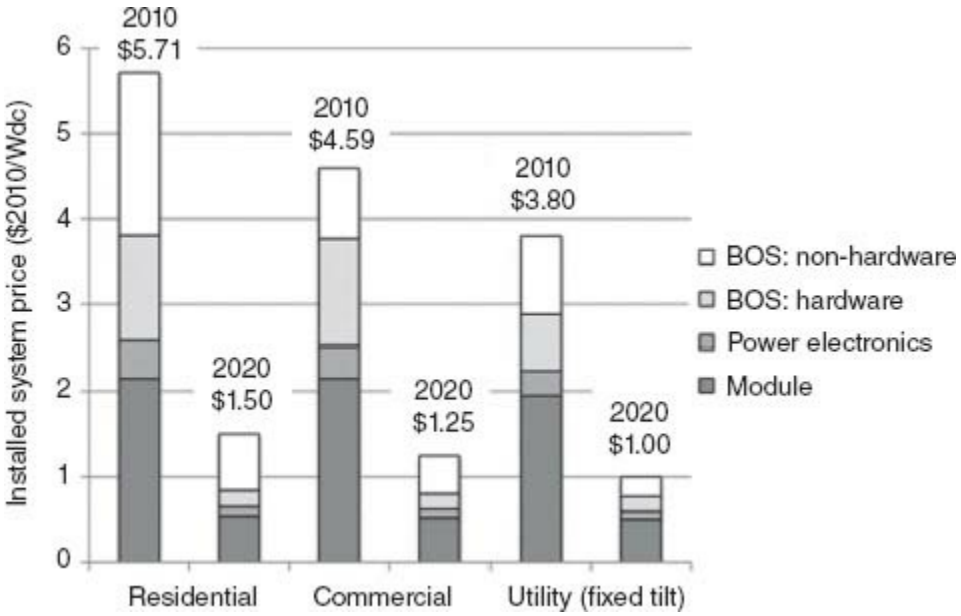
We now have the tools to allow us to estimate the energy delivered by grid-connected PV systems, so the next step is to explore their economic viability. System sizing is pretty similar for both residential and commercial buildings, but their economics differ for several reasons, including some economies-of-scale advantages for larger systems, but more importantly, differences in the economic incentives to each, and differences in the value of the utility power being displaced. Utility-scale systems competing against wholesale power costs are different still, and will be covered in a later section. See Appendix A for a review of some of the basic economic concepts that will be utilized in this section.

6.4.1 PV System Costs

The most important inputs to any economic analysis of a PV system are the initial cost of the system and the amount of energy it will deliver each year. Whether the system is economically viable depends on other factors—most especially, the price of the energy displaced by the system, whether there are any tax credits or other economic incentives, and how the system is to be paid for. A detailed economic analysis will include estimates of operation and maintenance costs, future costs of utility electricity, loan terms and income tax implications if the money is to be borrowed or personal discount rates if the owner purchases it outright, system lifetime, costs or residual value when the system is ultimately removed, and so forth.

Begin with the installed cost of the system. For individual buyers, it is total dollars for their system that matters, but when an overall snapshot of the industry is being presented it is a common practice to describe installed costs in dollars per watt of DC peak power. Figure 6.14 gives us some reference points to help calibrate ourselves to system prices in the recent past and goals for the near future. The 2020 targets shown are those called for in the U.S. Department of Energy's SunShot program, which calls for an overall reduction in the cost of PV power to the point where it can directly compete with incumbent electricity technologies without subsidies.

FIGURE 6.14 Estimated 2010 prices for residential and commercial PV systems before incentives, along with SunShot goals for 2020. Redrawn from Goodrich et al. (2012) (NREL).

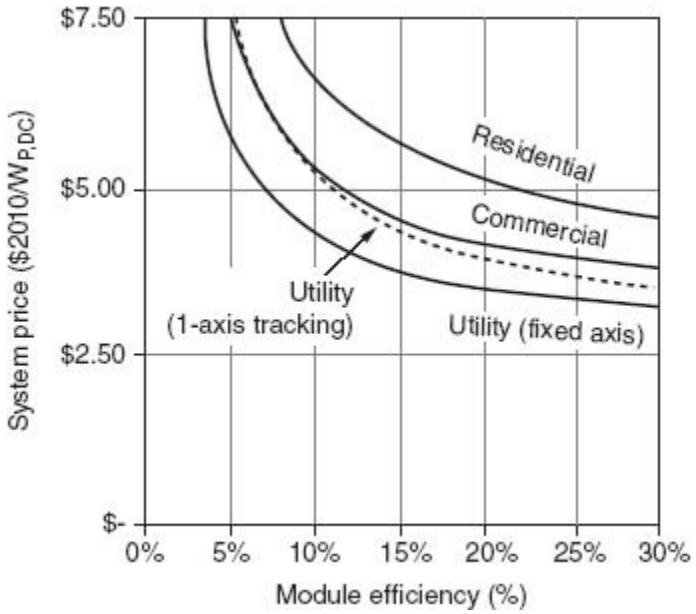


As shown in Figure 6.14, the 2010 estimated total installed selling price for residential systems in the United States in 2010 was $5.71 per peak DC watt. That was the cost to consumers before any tax incentives or utility rebates were applied. Broken down into categories, 38% was for the modules, 8% for power electronics (mostly the inverter), 22% for noninverter wiring and mounting hardware, and 33% was for the nonhardware balance of systems (BOS). This latter category includes permits, labor, overhead, and profit. The 2020 target is a 75% reduction to $1.50/Wp. Note the commercial prices are modestly lower ($4.59 in 2010 and $1.25 in 2020) with most of that advantage being gained on the

nonhardware BOS costs that go with economies of scale. The utility-scale systems in Figure 6.14 are for nontracking, fixed-tilt arrays. Note how it is the reduced cost of the hardware BOS that accounts for much of their 2010 advantage over commercial systems.

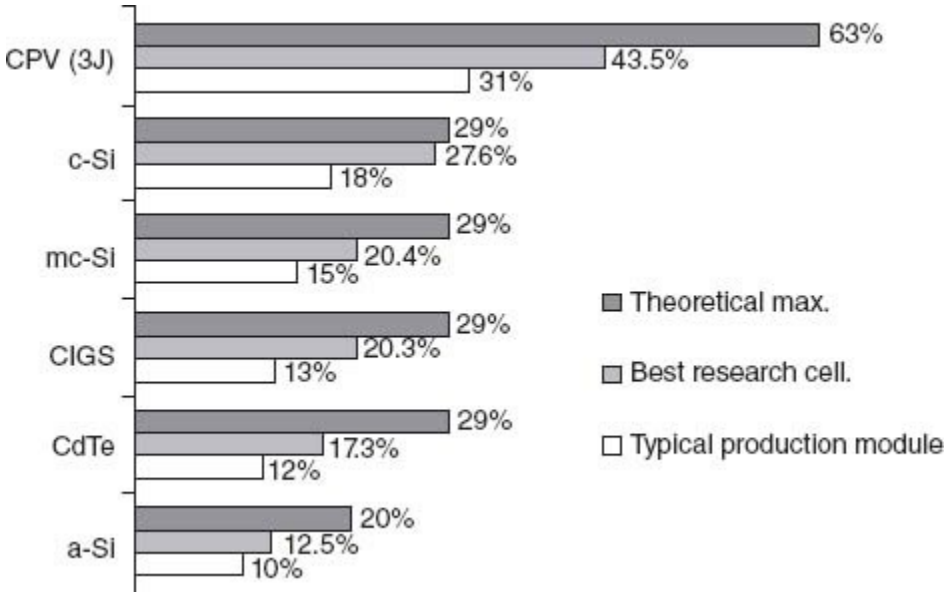
An interesting question arises with PVs located on buildings rather than in open fields where utility-scale systems are installed. When there are area constraints, module efficiency takes on additional importance since the above analysis indicates that roughly two-thirds of system prices are relatively fixed and must be paid for with the kilowatt-hours generated by the modules. In these circumstances, the additional cost of high-efficiency modules can usually be justified by the extra energy they generate. Figure 6.15 shows an NREL sensitivity analysis of the impact of module efficiency on system prices assuming equal $/Wp PV cost.

FIGURE 6.15 Sensitivity of installed PV system price to module efficiency (with equal $/Wp module prices). Redrawn from Goodrich et al. (2012) (NREL).



Significant decreases in module cost and increases in module efficiency are important parts of the SunShot scenario for 2020. Figure 6.16 summarizes the current efficiency status of competing PV technologies along with their theoretical maximum possible efficiencies. sc-Si is closer to its ultimate limit than the others, which suggests there is no much more room for improvement there. It seems likely most future system price reductions will have to come from the nonhardware BOS costs.

FIGURE 6.16 Production, laboratory, and theoretical maximum PV module efficiencies (from NREL, 2012 SunShot Update).



6.4.2 Amortizing Costs

A simple way to estimate the cost of electricity generated by a PV system is to imagine taking out a loan to pay for the system and then using annual payments divided by annual kWh delivered to give $/kWh. If an amount of money, or principal, P ($) is borrowed over a period of n (years) at an interest rate of i (decimal fraction/year), then the annual loan payments, A ($/yr) will be

$$A = P \cdot \mathrm{CRF}(i, n) \tag{6.14}$$

where CRF(i, n) is the capital recovery factor given by

$$\mathrm{CRF}(i, n) = \frac{i(1+i)^n}{(1+i)^n - 1} \tag{6.15}$$

A short table of capital recovery factors is provided in Table 6.4. These are the conventional per-year values

TABLE 6.4 Capital Recovery Factors

Term	2%	3%	4%	5%	6%	7%	8%	9%	10%
5	0.2122	0.2184	0.2246	0.2310	0.2374	0.2439	0.2505	0.2571	0.2638
10	0.1113	0.1172	0.1233	0.1295	0.1359	0.1424	0.1490	0.1558	0.1627
15	0.0778	0.0838	0.0899	0.0963	0.1030	0.1098	0.1168	0.1241	0.1315
20	0.0612	0.0672	0.0736	0.0802	0.0872	0.0944	0.1019	0.1095	0.1175
25	0.0512	0.0574	0.0640	0.0710	0.0782	0.0858	0.0937	0.1018	0.1102
30	0.0446	0.0510	0.0578	0.0651	0.0726	0.0806	0.0888	0.0973	0.1061

Equations 6.14 and 6.15 were written as if the loan payments are made only once each year. They are easily adjusted to find monthly payments by dividing the annual interest rate i by 12 and multiplying the loan term n by 12 leading to the following:

$$\text{CRF (monthly)} = \frac{(i/12)[1+(i/12)]^{12n}}{[1+(i/12)]^{12n}-1} \tag{6.16}$$

Example 6.5 Cost of PV Electricity for the Silicon Valley House. The 3.36 kW_{DC} PV system designed in Example 6.4 delivers 4942 kWh/yr. Suppose the system cost is the 2010 residential average of \$5.71/W_{DC} (without incentives). If the system is paid for with a 4.5%, 30-year loan, what would be its cost of electricity? If the SunShot goal of \$1.50/W is achieved, what would the cost be?

Solution. The system will cost \$5.71/W × 3360 W = \$19, 186.

The capital recovery factor (CRF) for this loan would be

$$\text{CRF}(i,n) = \frac{i(1+i)^n}{(1+i)^n-1} = \frac{0.045(1.045)^{30}}{(1.045)^{30}-1} = 0.06139/\text{yr}$$

So the annual payments would be

$$A = P \cdot \text{CRF}(i,n) = \$19{,}186 \times 0.06139 = \$1177.80/\text{yr}$$

The cost per kWh is therefore

$$\text{Cost of electricity} = \frac{\$1066.42/\text{yr}}{4942\ \text{kWh/yr}} = \$0.238/\text{kWh}$$

At the SunShot goal of \$1.50/W, the cost would be

$$\text{Cost of electricity} = \frac{\$1.50/\text{W} \times 3360\ \text{W} \times 0.06139/\text{yr}}{4942\ \text{kWh/yr}} = \$0.062/\text{kWh}$$

That is considerably below the \$0.116/kWh average 2012 U.S. residential price.

A significant factor that was ignored in the cost calculation of Example 6.5 is the impact of the income tax benefit that goes with a home loan. Interest on such loans is tax deductible, which means a person's gross income is reduced by the loan interest, and it is only the resulting net income that is subject to income taxes. The tax benefit that results depends on the marginal tax bracket (MTB) of the homeowner, which is defined for 2012 federal income tax in Table 6.5. For example, a married couple earning \$120, 000 per year is in the 25% MTB, which means a one-dollar tax deduction reduces their income tax by 25 cents. The value of the tax deduction will be even greater when it reduces the homeowner's state income tax as well. For example, the same taxpayer in California would be in the 32% MTB when both state and federal taxes are considered.

TABLE 6.5 Federal Income Tax Brackets for 2012

	Married Filing Jointly	Single
10% bracket	\$0–\$17, 400	\$0–\$8700
15% bracket	\$17, 400–\$70, 700	\$8700–\$35, 350
25% bracket	\$70, 700–\$142, 700	\$35, 350–\$85, 650

29% bracket	$142, 700–$217, 450	$85, 650–$178, 650
33% bracket	$217, 450–$388, 350	$178, 650–$388, 350
35% bracket	Over $388, 350	Over $388, 350

During the first years of a long-term loan, almost all of the annual payments will be interest, with very little left to reduce the principal, while the opposite occurs toward the end of the loan. That means the tax benefit of interest payments varies from year to year. For our purposes, we will assume loan payments are made once a year at the end of the year. For example, in the first year, interest is owed on the entire amount borrowed and the tax benefit is

$$\text{First-year tax benefit} = i \times P \times \text{MTB} \tag{6.17}$$

In addition to the tax benefit of deductible interest, there may be local, state, and federal incentives as well as rebates provided by electric utilities. Since these are so variable and location specific, the only one we will mention here is the long-standing 30% federal renewable energy tax credit. Realize that tax credits and tax deductions are quite different incentives. A tax credit is much more valuable since it reduces the buyer's tax burden by the full amount of the credit while a tax deduction reduces it by the product of the deduction times the MTB.

Example 6.6 Cost of PV Electricity Including Tax Benefits. The 3.36-kW_{DC} PV system for the house in Silicon Valley costs $19, 186 and delivers 4942 kWh/yr. The homeowner finances the net cost of the system after receiving a 30% federal tax credit using a 4.5%, 30-year loan. If the homeowner is in the 25% MTB, what is the cost of PV electricity in the first year?

Solution. The capital cost of the system after the 30% tax credit is

$$P = \$19,186(1 - 0.30) = \$13,430$$

The CRF for the loan is still 0.06139/yr, so the loan payments will be

$$A = P \cdot \text{CRF}(i, n) = \$13,430 \times 0.06139 = \$824.49/\text{yr}$$

During the first year, the owner has use of $13, 430 for a full year without yet paying any interest. So at the end of the first year, the interest owed is

$$\text{First-year interest} = 0.045 \times \$13,430 = \$604.35$$

After making that first $824.49 payment, $604.35 of which is interest, the loan principal is reduced by only $824.49 – $604.35 = $220.14.

The first-year tax savings based on the tax-deductible interest portion of the payment is

$$\text{First-year tax savings} = 0.25 \times \$604.35 = \$151.09$$

The net cost of the PV system in that first year will therefore be

$$\text{First-year cost of PV} = \$824.49 - \$151.09 = \$673.40$$

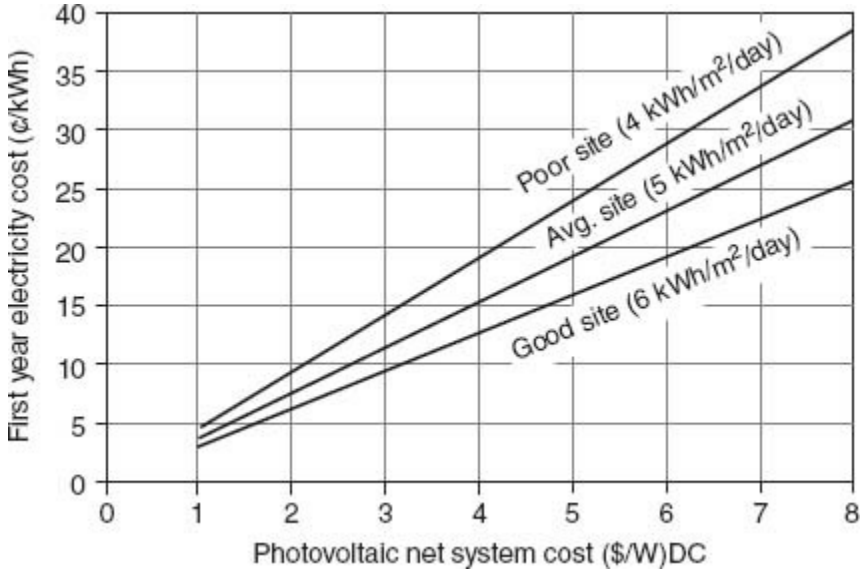
which means the first-year cost of electricity is

$$\text{First-year cost of PV electricity} = \frac{\$673.40/\text{yr}}{4942\ \text{kWh/yr}} = \$0.136/\text{kWh}$$

This is not much more than the 2012 $0.116/kWh average price of electricity in the United States.

Figure 6.17 shows the way the above calculations play out when insolation and capital cost are treated as parameters.

FIGURE 6.17 First-year cost of electricity with net system cost (after rebates) and panel insolation as parameters. Assumptions: 5%, 30-year loan, 25% MTB, 0.75 derate factor.



6.4.3 Cash Flow Analysis

The analysis in Example 6.6 covered only the first year of the PV investment. A straightforward cash flow analysis, however, easily accounts for complicating factors such as PV performance degradation, utility price escalation, declining tax-deductible interest over time, periodic maintenance costs, and disposal or salvage value of the equipment at the end of its lifetime.

Table 6.6 shows portions of a spreadsheet version of a 30-year cash flow analysis for the Silicon Valley PV system described in Examples 6.4–6.6. New inputs include an annual PV performance degradation of 0.5%/yr and a utility price increase of 3%/yr, with both starting at the end of the first year. Note the net cash flow during the first year shows a loss of $49.95 since the net cost of the loan ($623.26) is greater than the utility savings ($573.30). In the 30th year, there is a positive $413.37 cash flow.

TABLE 6.6 Cash Flow Analysis for the Silicon Valley PV System

Rated DC power (kW_{DC})	3.36	ENTER			
Insolation ($kWh/m^2/d$ = h/d)	5.32	ENTER			
Derating	0.7575	ENTER			
First-year production (kWh/yr)	4942				
System degradation (%/yr)	0.5%	ENTER			
Cost before incentives ($/Wp)	$5.71	ENTER			
System cost	$19,185.60				
Rebates (30% default)	$5755.68				
Final cost ($) and ($/Wp)	$13,429.92	$4.00			
Down payment	$1000.00	ENTER			
Loan principal	$12,429.92				
Loan interest (%/yr)	4.5%	ENTER			
Loan Term (yr)	30	ENTER			
CRF (*i*,*n*)/yr	0.06139				
Annual payments ($/yr)	$763.09				
Marginal tax bracket (MTB)	25%	ENTER			
Nominal discount rate	5.0%	ENTER			
First-year utility price ($/kWh)	$0.116	ENTER			
Utility	3.0%	ENTER			
Year	0	1	2	...	30
Payment ($/yr)	$1000.00	$763.09	$763.09		$763.09
Interest ($/yr)		$559.53	$550.18		$32.86
Delta balance		$203.75	$212.91	...	$730.23
Loan balance	$12,429.92	$12,226.17	$12,013.26	...	$(0.00)
Tax savings on interest ($/yr)		$139.84	$137.54		$8.22
Net cost of PV		$623.26	$625.55		$754.88
PV kWh generated (kWh/yr)		4942	4918	...	4274
Utility price ($/kWh)		$0.116	$0.119		$0.273
Utility cost without PVs		$573.30	$587.55	...	$1168.24
Net cash flow ($/yr)	$(1000.00)	$(49.95)	$(38.00)		$413.37
Internal rate of return (IRR)	7.37%				
Net present value (NPV)	$623.45				

There are also two financial measures included in the spreadsheet. One is a cumulative net present value (NPV) calculation and the other is an evaluation of the 30-year internal rate of return (IRR) on the owner's solar investment. Both of these terms are described more carefully in Appendix A, but for now just a simple explanation will be provided. Also, they are both standard functions in Excel so you can easily let your spreadsheet compute these important results.

A present value calculation takes into account the time value of money, that is, the fact that one dollar ten years from now is not as good as having one dollar in your pocket today. A *present worth* or *present value* calculation accounts for this distinction. Imagine having P dollars today that you can invest at an interest rate d. A year from now you would have $P(1 + d)$ dollars in your account; n years from now you would have a future amount of money $F = P(1 + d)^n$ dollars in the account. This means a future amount of money F should be equivalent to having P in our pocket today, where

$$P = \frac{F}{(1+d)^n} \tag{6.18}$$

When converting a future value F into a present worth P the interest term d in Equation 6.18 is referred to as a discount rate. The discount rate can be thought of as the interest rate that could have been earned if the money had been put into the best alternative investment available. For example, in our Table 6.6 spreadsheet, the PV system is projected to save $413.37 in utility bills in the 30th year, so with our discount rate of 5%/yr the present

worth of that savings would be

$$P = \frac{F}{(1+d)^n} = \frac{\$413.37}{(1+0.05)^{30}} = \$95.64 \quad (6.19)$$

That is, the savings way out in the 30th year is like putting $95.64 into the owner's pocket today. For our spreadsheet in Table 6.6, the cumulative NPV is a net positive $623.45.

The second financial summary introduced in our spreadsheet is an internal rate of return (IRR). The IRR is perhaps the most persuasive measure of the value of an energy efficiency or renewable energy project since it allows the energy investment to be directly compared with the return that might be obtained for any other competing investment. One simple definition is that the IRR is the discount rate that makes the NPV of the energy investment equal to zero. For our spreadsheet example, in which the owner put in $1000 as a down payment plus a few tens of dollars during the first few years while the system was losing money, the IRR is a respectable 7.37%. That is, the potential buyer of this system would need to find some alternative investment that would earn better than 7.37% to be equivalent to his or her investment in this solar system.

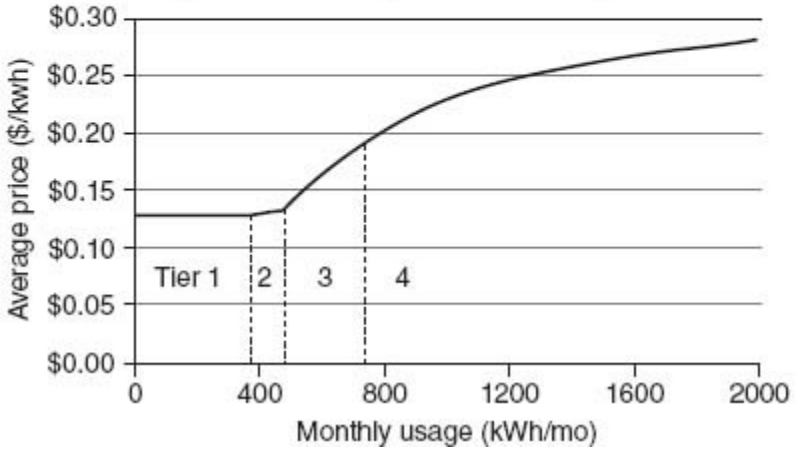
6.4.4 Residential Rate Structures

So far, our analysis has treated utility costs as if they are a simple $/kWh fee along with some future escalation rate. The reality is much more complicated. Electric rates vary considerably, depending not only on the utility itself, but also on the electrical characteristics of the specific customer purchasing the power. The rate structure for a residential customer will typically include a basic fee to cover costs of billing, meters, and other equipment, plus an energy charge based on the number of kilowatt-hours of energy used. Commercial and industrial customers are usually billed not only for energy (kilowatt-hours) but also for the peak amount of power that they use (kilowatts). That *demand charge* for power ($/mo/kW) is the most important difference between the rate structures designed for small customers versus large ones. Large industrial customers may also pay additional fees if their power factor, that is, the phase angle between the voltages supplied and the currents drawn, is outside of certain bounds.

Consider the example residential rate structure shown in Figure 6.18 for one of California's major investor-owned utilities. Note that it includes four tiers based on monthly kWh consumed and also note that the rates increase with increasing demand. This is an example of what is called an *inverted block rate structure*, designed to discourage excessive consumption. Not that long ago, the most common structures were based on *declining block rates*, which made electricity cheaper as the customer's demand increased. The figure shows 365 kWh/mo as the baseline consumption. Actually, that value depends on season and location as well as the home's heating and cooling system. Clearly, this rate structure provides far more financial incentive to invest in a solar system for customers who consume larger amounts of electricity.

FIGURE 6.18 Example of a standard summer residential rate schedule for a California utility. Average consumption for this utility is in Tier 3 (from PG&E E-1, 2012).

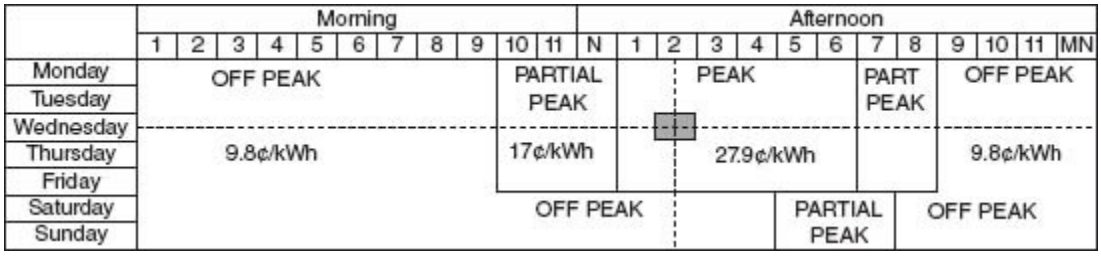
Tier 1 baseline	Tier 2 (101–130% of baseline)	Tier 3 (131–200% of baseline)	Tier 4 (Over 200% of baseline)
e.g. 1st 365 kWh	366–475	475–730	>731 kWh/mo
$0.1285	$0.1460	$0.2956	$0.3356



While the standard rate structure in Figure 6.18 does discourage excessive consumption, it does not address the peak demand issue. A kilowatt-hour used at midnight is priced the same as a kilowatt-hour used in the middle of a hot, summer afternoon when all of the utility's plants may be running at full capacity. In an effort to encourage customers to shift their loads away from peak demand times, many utilities are beginning to offer residential TOU rates.

Figure 6.19 presents an example of the Tier 1 residential summer TOU rate schedule for the same utility shown in Figure 6.18. For comparison, the standard rate is $0.146/kWh, no matter when the energy is used. For the TOU schedule, during off-peak times electricity is only $0.098/kWh, but during peak demands, it is $0.279/kWh. The incentive is certainly there to shift loads whenever possible off of the peak demand period. The other interesting, and tricky, thing to consider is the potential advantages associated with signing up for TOU rates with a net-metered PV system. Selling electricity to the utility at peak rates and buying it back at night-rates can increase the economic viability of PVs. A careful calculation would need to be made to determine whether the TOU rate or the regular residential rate schedule would be most appropriate for an individual homeowner considering PVs.

FIGURE 6.19 An example of time-of-use (TOU) rate schedule. The intersection of the dotted lines suggests how a homeowner might know the rates at 2:00 P.M. on a Wednesday.



With TOU rate structures, prices vary seasonally and by time of day following a

predetermined pricing schedule. New dynamic rate structures being introduced take advantage of the ability of smart meters to record electric usage in short time intervals, which creates the potential for time-varying electricity prices. These dynamic rate structures include real-time pricing (RTP) and critical peak pricing (CPP). With RTP, prices vary hourly following the wholesale electricity market conditions. With CPP, customers sign up for a reduced rate for all but a few unscheduled "events." During these CPP events, which are allowed to occur only a limited number of times each year, the price of electricity jumps to a predetermined, very high rate. CPP programs are justified by the cost savings associated with not having to build, and only occasionally operate, peaking power plants.

Table 6.7 shows an example of proposed CPP rate schedule. As designated, CPP events would occur between 4:00 P.M. and 7:00 P.M. on no more than 12 summer days per year, for a total of no more than 36 h. Customers who choose this option will be notified of a CPP event one day in advance. In exchange they receive lower off-peak rates.

TABLE 6.7 A Proposed Critical Peak Pricing Rate Schedule ($/kWh)[a]

Schedule	Off Peak (Base Usage) ($)	Off Peak (Above Base) ($)	Peak ($)	Event ($)
TOU	0.0846	0.1660	0.2700	
TOU + CPP	0.0721	0.1411	0.2700	0.7500

[a]Sacramento Municipal Utility District (SMUD), 2012.

6.4.5 Commercial and Industrial Rate Structures

The rate structures that apply to commercial and industrial customers usually include a monthly demand charge based on the highest amount of power drawn by the facility. That demand charge may be especially severe if the customer's peak corresponds to the time during which the utility has its maximum demand since at those times the utility is running its most expensive peaking power plants.

In the simplest case, the demand charge is based on the peak demand in a given month, usually averaged over a 15-minute period, no matter what time of day it occurs. When TOU rates apply, there may be a combination of demand charges that apply to different time periods as well as the seasons. For the rate structure shown in Table 6.8, one charge applies to the maximum demand no matter what time it is reached and the others are time-period specific. As Example 6.7 points out, these demand charges are additive.

TABLE 6.8 Electricity Rate Structure Including Monthly Demand Charges

Energy ($/kWh)	Off Peak	Partial Peak	Peak
Summer	$0.0698	$0.0950	$0.1336
Winter	$0.0727	$0.0899	
Demand ($/kW/mo)	**Maximum**	**Partial peak**	**Peak**
Summer	$11.85	$3.41	$14.59
Winter	$11.85	$0.21	

Example 6.7 Impact of Demand Charges. During a summer month, a small commercial

building is billed for the following energy and peak demands using the rate structure given in Table 6.8. The maximum peak for the month is 100 kW.

	Off Peak	Partial Peak	Peak
Energy (kWh/mo)	18,000	8000	12,000
Peak demand (kW)	60	80	100

a. Compute the monthly bill.

b. Suppose a 20-kW_{DC} PV system shaves the off-peak, partial-peak, and peak energy loads by 700, 600, and 1400 kWh/mo, respectively. Suppose too, it drops the peak demand by 15 kW during the peak and partial-peak periods. Compute the resulting dollar savings on the utility bill. How much does that work out to per kWh of PV?

Solution

a. Looking at the three time periods, the maximum demand at any time during the month must be 100 kW, which will be charged out at \$11.85/kW = \$1185.

In addition, separate demand charges apply during the peak and partial-peak periods:

$$\text{Peak and partial peak demand} = 80\ \text{kW} \times \$3.41 + 100\ \text{kW} \times \$14.59 = \$1732$$

$$\text{Total demand charge} = \$1185 + \$1732 = \$2917$$

$$\text{Energy} = 18{,}000 \times \$0.0698 + 8000 \times \$0.0950 + 12{,}000 \times \$0.1336 = \$3620$$

$$\text{Total bill} = \$3619 + \$2917 = \$6536\ (44\%\ \text{of which is demand charges})$$

b. With PVs the savings will be

$$\text{Demand savings} = 15\ \text{kW} \times (\$11.85 + \$3.41 + \$14.59) = \$443$$

$$\text{Energy \$ savings} = 700 \times \$0.0698 + 600 \times \$0.0950 + 1400 \times \$0.1336 = \$275$$

$$\text{Total savings} = \$443 + \$275 = \$718\ (62\%\ \text{is demand savings})$$

Total energy delivered by the PVs = 700 + 600 + 1400 = 2700 kWh

$$\text{PV savings} = \frac{\$718}{2700\ \text{kWh}} = \$0.266/\text{kWh}$$

The demand charge in the rate schedule shown in Table 6.8 applies to the peak demand for each particular month in the year. The revenue derived from demand charges for a single month with especially high demand may not be sufficient for the utility to pay for the peaking power plant they had to build to supply that load. To address that problem, some utilities have a ratchet adjustment built into the demand charges. For example, the monthly demand charges may be ratcheted to a level of perhaps 80% of the annual peak demand. That is, if a customer reaches a highest annual peak demand of 1000 kW, then for every month of the year the demand charge will be based on consumption of at least 0.80 × 1000 kW = 800 kW. This can lead to some rather extraordinary penalties for customers who add a few kilowatts to their load right at the time of their annual peak, and conversely, it provides considerable incentive to reduce their highest peak demand.

6.4.6 Economics of Commercial-Building PV Systems

The economics of a behind-the-meter PV system for larger customers differs considerably from that of a residential system. Figure 6.14 showed the capital cost advantage of larger systems and Example 6.7 showed how ignoring demand charges will miss a major attribute of their cost-effectiveness. In addition, there are significant tax advantages that go with these systems.

Businesses are allowed to depreciate their capital investments by writing off the expenditures, which means they get to deduct those costs from their profits before paying corporate taxes. Renewable energy systems can be depreciated using a depreciation scheduled called the Modified Accelerated Cost Recovery System (MACRS). Under MACRS, photovoltaic systems are eligible for the depreciation schedule shown in Table 6.9. If a 30% tax credit is taken, then the amount that can be depreciated is reduced by half of that 30%. The table works out the MACRS financial gain, for an example $100, 000 PV system. Between the 30% tax credit and the accelerated depreciation, the net effective system cost is reduced by almost 57%.

TABLE 6.9 MACRS Depreciation Schedule

Investment			$100,000	
30% Investment Tax Credit (ITC)			30,000	
Depreciable basis			85,000	Inv – 50% × ITC
Corporate tax rate			35%	
Corporate discount rate			6%	
Year	MACRS	Depreciation	Tax Savings	Present Value
0	20.00%	$17,000	$ 5,950	$ 5,950
1	32.00%	$27,200	$ 9,520	$ 8,981
2	19.20%	$16,320	$ 5,712	$ 5,084
3	11.52%	$ 9,792	$ 3,427	$ 2,878
4	11.52%	$ 9,792	$ 3,427	$ 2,715
5	5.76%	$ 4,896	$ 1,714	$ 1,281
Totals	100%	$85,000	$29,750	$26,887
Effective Net System Cost (Inv – ITC – MACRS):				$43,113

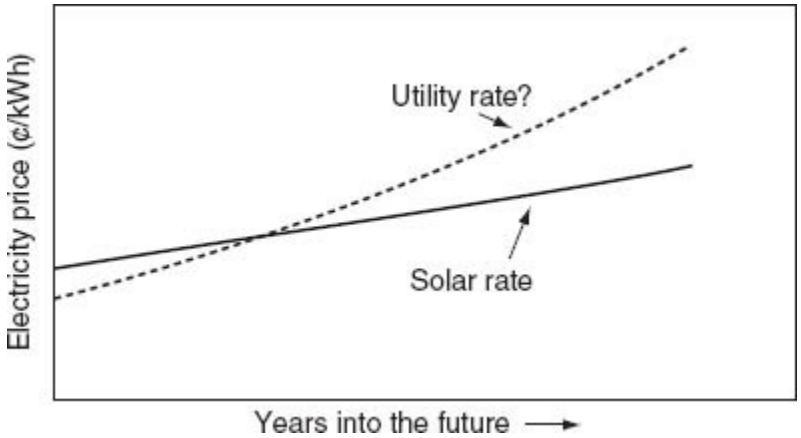
While time-of-use rates with demand charges attempt to capture the true cost of utility service, they are still relatively crude since they only differentiate between relatively large blocks of time (e.g., peak, partial peak, and off peak) and they typically only acknowledge two seasons: summer and nonsummer. The ideal rate structure would be one based on real-time pricing (RTP) in which the true cost of energy is reflected in rates that change throughout the day, each and every day. With RTP, there would be no demand charges, just energy charges that might vary, for example, on an hourly basis.

Some utilities now offer day-ahead, hour-by-hour, real-time pricing for large customers. When a customer knows that tomorrow afternoon the price of electricity will be high, they can implement appropriate measures to respond to that high price. With the price of electricity more accurately reflecting the real, almost instantaneous, cost of power, it is hoped that market forces will encourage the most efficient management of demand.

6.4.7 Power Purchase Agreements

Residential customers cannot depreciate their systems the way businesses can, nonprofit organizations cannot take advantage of tax credits, and many investors do not owe enough taxes to have credits pay off quickly enough. For these and other reasons, many photovoltaic systems are now being installed using third-party financing in which an outside entity contracts to finance, install, and maintain systems on the premises of their customers. In exchange, the customer signs a repayment agreement that specifies the price of electricity generated by the system over the term of the contract. It is not uncommon for these power purchase agreements (PPAs) to start with a slightly higher unit price for solar power than what the utility offers, but the assumption is that over time it will result in net savings for the host (Fig. 6.20).

FIGURE 6.20 An example of PPA in which the initial solar rate is higher than the utility rate.



From the customer's perspective, these PPAs provide a hedge against uncertain future utility price increases and, of course, they help "green" the customer's brand. They require no capital expenditures by the customer and since the host pays only for the kilowatt-hours actually generated, it is the PPA provider who has the incentive to properly operate and maintain the system. From the provider's perspective, they get the tax credits, depreciation allowances, utility rebates, a steady revenue stream, and they may be able to sell the renewable energy credits (RECs) and potential future carbon credits as well.

6.4.8 Utility-Scale PVs

Utility-scale PV systems have economies-of-scale advantages over smaller behind-the-meter systems (Fig. 6.14), but they have the disadvantage of having to compete in the wholesale electricity market where the price is often one-third that of retail rates.

Power purchase agreements are common, but now the customer is a utility rather than a building owner. To account for the variable value of electricity sold during different times of day, many of these PPAs include a generation time-of-delivery (TOD) factor. The original contract includes an agreed upon PPA base rate, which is then adjusted on an hour-by-hour basis using TOD factors such as the ones shown in Table 6.10.

TABLE 6.10 Time-of-Delivery Factors

Season	Period	Definition	Factor
Summer	On Peak	WDxH, noon–6:00 P.M.[a]	3.13
June–	Mid-Peak	WDxH, 8:00 A.M.–noon, 6–11:00 P.M.	1.35
September	Off Peak	All other times	0.75
Winter	Mid-Peak	WDxH, 8:00 A.M.–9:00 P.M.	1.00
October–	Off Peak	WDxH, 6–8:00 A.M., 9:00 P.M.–midnight	0.83
May	Off Peak	WE/H, 6:00 A.M.–midnight[b]	0.83
	Super-Off-Peak	Midnight–6:00 A.M.	0.61

[a]WDxH is defined as weekdays except holidays.
[b]WE/H is defined as weekends and holidays.
(Southern California Edison, 2010).

Example 6.8 Applying TOD Factors for a Utility-Scale PV Plant. A 1000-kW_{DC}, 30° fixed tilt, PV system at 40° latitude has a PPA with a base rate of $0.10/kWh that is subject to the TOD factors of Table 6.10. Assuming a derate factor of 0.75, find the revenue earned for the noon hour on a clear weekday in June. For the month of June, assume all clear days consisting of 22 weekdays and 8 weekend days; find the average price that will be paid for the energy delivered.

Solution. From the hour-by-hour clear-sky insolation values given in Appendix D, the irradiance at noon on the array will be 960 W/m^2. Assuming that is a good average for the hour, the energy delivered for the noon hour will be

$$\text{Energy (noon)} = P_{DC}(\text{kW}) \cdot \text{Insolation (h full sun)} \cdot \text{Derate}$$

$$= 1000\ \text{kW} \times 0.960\ \text{h} \times 0.75 = 720\ \text{kWh}$$

Noon on a weekday has a TOD of 3.13, so the revenue earned for that hour will be

$$\text{Revenue} = 720\ \text{kWh} \times 3.13 \times \$0.10/\text{kWh} = \$225.36$$

From a spreadsheet, we can work out the rest of the hourly revenues for both weekdays and weekends:

			Weekdays		Weekends	
Solar Time	Insolation (W/m^2)	kWh/d del	TOD X	Revenue $/d	TOD X	Revenue $/d
6	93	70	0.75	$ 5.23	0.75	$ 5.23
7	289	217	0.75	$ 16.26	0.75	$ 16.26
8	498	374	1.35	$ 50.42	0.75	$ 28.01
9	686	515	1.35	$ 69.46	0.75	$ 38.59
10	834	626	1.35	$ 84.44	0.75	$ 46.91
11	928	696	1.35	$ 93.96	0.75	$ 52.20
12	960	720	3.13	$ 225.36	0.75	$ 54.00
1	928	696	3.13	$ 217.85	0.75	$ 52.20
2	834	626	3.13	$ 195.78	0.75	$ 46.91
3	686	515	3.13	$ 161.04	0.75	$ 38.59
4	498	374	3.13	$ 116.91	0.75	$ 28.01
5	289	217	3.13	$ 67.84	0.75	$ 16.26
6	93	70	1.35	$ 9.42	0.75	$ 5.23
Totals		5712		$1313.96		$428.40

Total revenue for a June month with 22 weekdays and 8 weekend days will be

$$\text{Revenue} = 22 \times \$1313.96 + 8 \times \$428.40 = \$32{,}334.32/\text{mo}$$

The energy collected will be 5712 kWh/d × 30 d/mo = 171, 360 kWh/mo.
So the per kWh average payment will be

$$\text{Average rate} = \frac{\$32{,}334.32/\text{mo}}{171{,}360\ \text{kWh/mo}} = \$0.189/\text{kWh}$$

Under the clear-sky assumptions in Example 6.8, a $0.10/kWh PPA actually provides almost double that in revenue for the owner. This illustrates the importance of generating electricity during the times when it is most needed. Since afternoon power is worth more than morning power, the owners will probably orient the array slightly to the west to emphasize that added value. Those TOD factors also point out the economic disadvantage that wind systems have in regions where the strongest winds are at night.

6.5 OFF-GRID PV SYSTEMS WITH BATTERY STORAGE

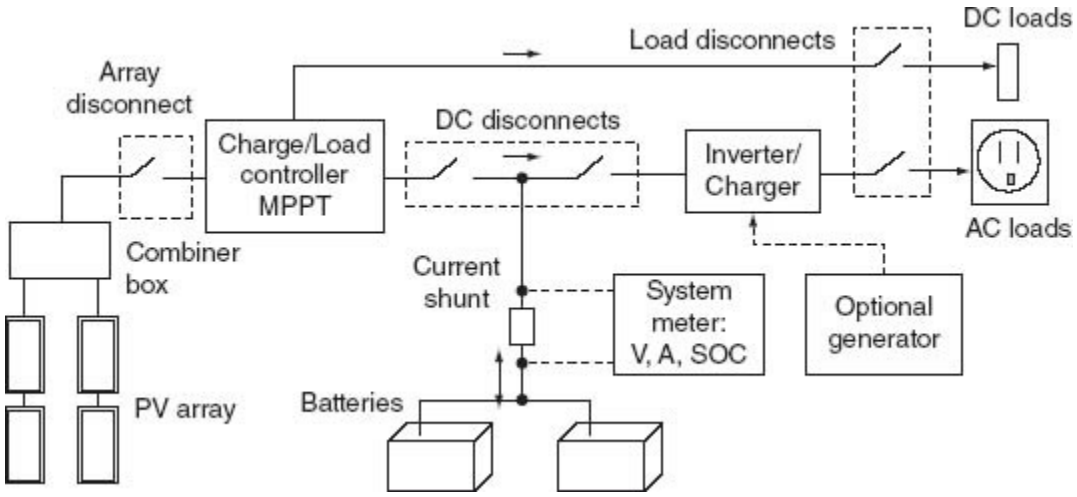
Grid-connected PV systems have a number of desirable attributes. Their relative simplicity can result in high reliability; their MPPT unit assures high PV efficiency; their ability to deliver power to the utility during times of day when it is most valuable increases their economic viability, as does the potential to avoid land costs by installing systems on buildings or parking lots. On the other hand, they have to compete with the relatively low price of utility power, and of course, they are dependent on the grid itself.

When there is no grid available, the competition that PVs face is either the cost of stringing new power lines at tens of thousands of dollars per mile or running noisy, polluting, high maintenance generators burning relatively expensive fuel. For the 1–2 billion people across the globe who currently have little or no access to commercial electricity, having even a little bit of power can transform lives. Even "pico-scale" PV systems with just a few watts of power can replace a kerosene lamp with light-emitting diodes (LEDs), making it possible to read in the evening. A few more watts might let an entrepreneur start a cell phone charging business. Another couple of modules enable lights, a TV, computer, and maybe a few small appliances to be powered. A couple of kilowatts can power a small, modern cabin in the woods and 10 kW will power a room full of computers in a village school as well as a pump for its water supply. String some wires from a modest array on a community center roof and a number of dwellings can be powered with a solar-powered microgrid. Small off-grid solar systems, which used to be a "back-to-the-land" phenomenon in the developed world, are now seen by some to be the market of the future in emerging economies around the globe. Some estimates suggest there are 150 GW of diesel generators out there providing power at over $0.40/kWh that could be replaced with renewables (Bloomberg New Energy Finance, 2012).

6.5.1 Stand-alone System Components

Figure 6.21 identifies a number of important components that make up a basic stand-alone PV system. The system consists of the PV array itself, batteries for storage, a charge controller, an inverter, and a system monitor, along with a number of disconnect switches. A backup generator may or may not be included in the system.

FIGURE 6.21 A "one-line"diagram of the important components in a stand-alone PV system.



The PV array delivers power through its accompanying combiner box to a controller. The controller has three important functions. Its MPPT keeps the PVs operating at their most efficient operating point. Its charge control function protects the batteries by shutting off charging current when they are fully charged and by disconnecting the batteries from the DC loads when it senses a low-voltage condition.

The system meter provides real-time information about the performance of the system. It is not essential, but it is very important. Depending on their capabilities, they can monitor

battery voltage, current being delivered to and from the batteries, and the state of charge (SOC) of the batteries. It may also indicate the accumulated energy flows from the battery system. The diagram shows a current shunt, which is a very precise in-line resistor with a very small resistance. The system meter measures current flows by monitoring the voltage drop across the shunt.

Sometimes, especially with smaller systems, the only loads might be just DC-powered devices, in which case the inverter may not be necessary. In some circumstances, both AC and DC loads may be provided for from the same system. Some systems do so to avoid inverter losses whenever possible by powering as many loads as possible on DC. Quite a range of DC devices are manufactured for boating and recreational vehicles, so they can be quite readily available. Another reason for providing both AC and DC is to allow some high power, low usage devices such as water pumps or shop motors to run on DC, thereby avoiding the need to install an overly large and expensive inverter that will not perform well when only modest loads are supplied. Most inverters have efficiencies over 90% as long as they are not operated well below their rated power, but when an inverter rated at several kW is delivering only 100 W, its efficiency may be more like 60–70%. When no load is present, a good inverter will power down to just a few watts of standby power while it waits for something to be turned on that needs AC. When it senses a load, the inverter powers up and while running uses on the order of 5–20 W of its own. That means standby losses associated with so many of our electronic devices may keep the inverter running continuously, even though no real energy service is being delivered. That much loss for so little gain suggests paying attention to manually shutting down turned-off electronic equipment.

There are other features that can come into play with inverters. An important attribute is a low-voltage disconnect to protect the batteries. Also, as shown in Figure 6.21, some inverters are bidirectional, which means they can also act as battery chargers when a backup AC engine–generator is part of the system. As a charger, it converts AC from the generator into DC to charge the batteries; as an inverter it converts DC from the batteries into AC needed by the load. The charger/inverter unit may include an automatic transfer switch that allows the generator to supply AC loads directly whenever it is running.

Minor, but important, players in these systems are the fuses, circuit breakers, cables, wires and wire terminals, mounting hardware, battery boxes, earth-grounding and lighting-protection systems, and so forth. Unfortunately, far too many systems installed in rural areas have failed prematurely due to lack of attention being paid to these details. For good summaries of lessons learned designing and installing real systems, see, for example, Undercuffler (2010) and Youngren (2011).

Off-grid systems must be designed with great care to assure satisfactory performance. Users must be willing to check and maintain batteries, they must be willing to adjust their energy demands as weather and battery charge vary, they may have to fuel and fix a balky generator, and they must take responsibility for the safe operation of the system. The reward is electricity that is truly valued.

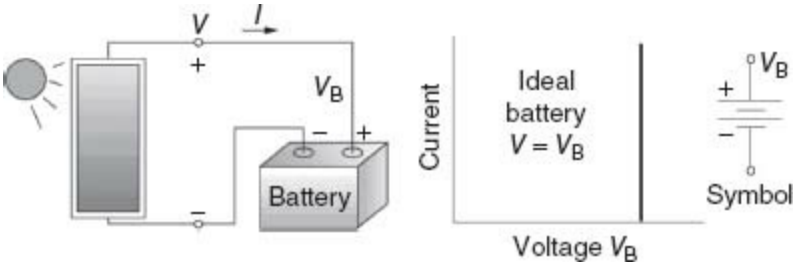
6.5.2 Self-regulating Modules

Figure 6.21 describes an ideal system capable of delivering enough power to handle significant loads. In some circumstances, however, even simpler systems can make great

sense. Staying in DC eliminates the inverter. Directly coupling PVs to the batteries without an MPPT shaves the cost. A simple charge controller to help protect the batteries along with appropriate fuses, breakers, and wiring can complete the system.

Let us analyze the possibility of eliminating the charge controller altogether. Consider the minimal system shown in Figure 6.22 in which a module is directly connected to a battery. Begin by assuming an ideal battery in which the voltage remains constant no matter what its state of charge or the rate at which it is being charged or discharged. That means it will have an *I–V* curve that is simply a straight up-and-down line as shown in the figure.

FIGURE 6.22 An ideal battery has a vertical *I–V* characteristic curve.



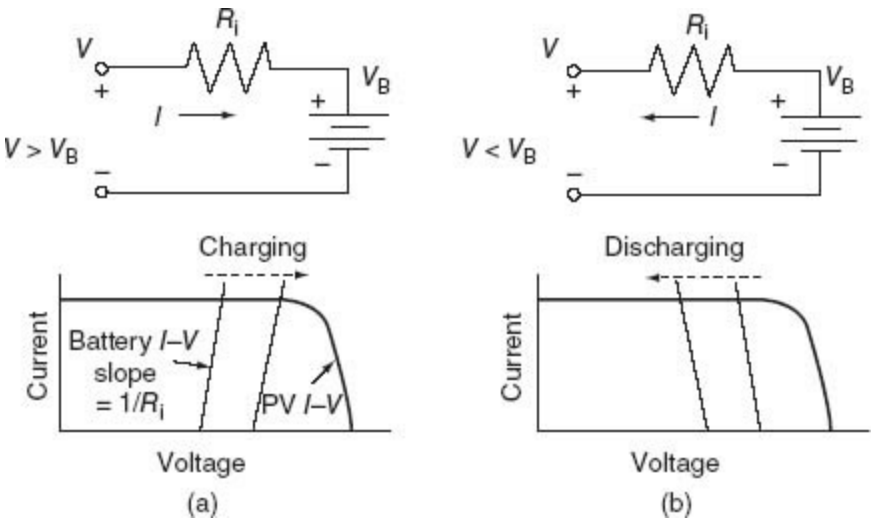
The simple equivalent circuit representation of Figure 6.22 is complicated by a number of factors, including the fact that the open-circuit voltage V_B depends not only on the state of charge, but also on battery temperature and how long it has been resting without any current flowing. For a conventional 12-V, lead–acid battery at 78°F, which has been allowed to rest for a day, V_B ranges from 12.7 V for a fully charged battery to about 11.3 V for one that has only 10% of its charge remaining.

A real battery also has some internal resistance, which is often modeled with an equivalent circuit consisting of an ideal battery of voltage V_B in series with the internal resistance R_i as shown in Figure 6.23. During the charge cycle, with positive current flow into the battery, we can write

(6.20) $$V = V_B + R_i I$$

which plots as a slightly tilted, straight line with slope equal to I/R_i. During charging, the applied voltage needs to be greater than V_B. As the process continues, V_B itself increases so the *I–V* line slides to the right as shown in Figure 6.23a. During discharge, the output voltage of the battery is less than V_B, the slope of the *I–V* line flips, and the *I–V* curve moves back to the left as shown in Figure 6.23b. Even this rendition can be further refined to account for variations in the internal resistance as a function of temperature and state of charge, as well the age and condition of the battery.

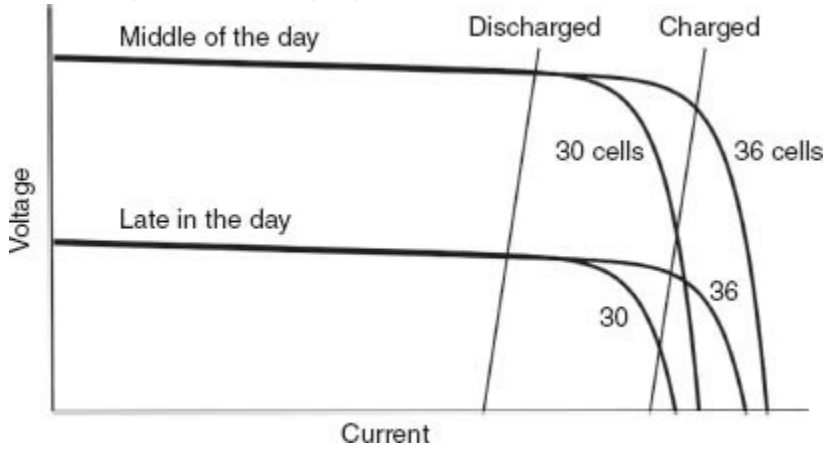
FIGURE 6.23 A real battery can be modeled as an ideal battery in series with its internal resistance, with current flowing in opposite directions during charging (a) and discharging (b). During charging/discharging, the slightly tilted *I–V* curve slides right or left.



The operating point of the battery–PV combination is the spot at which both have the same current and voltage; that is, it is the intersection of the two *I–V* curves. Since both *I–V* curves vary with time, predicting the performance of this simple system can be a challenge. For example, since the *I–V* curve for a battery moves toward the right as the battery gains charge during the day, there is a chance that the PV operating point will begin to slide off the edge of the knee—especially late in the day when warmer temperatures and lower insolation cause the knee itself to move toward the left.

Sliding off the knee in the afternoon may not be a bad thing, however, since current has to be slowed or stopped anyway when a battery reaches full charge. If the PV-battery system has a charge controller, it will automatically prevent overcharging of the batteries. For very small battery charging systems, however, the charge controller can sometimes be omitted if modules with fewer cells in series are used. Such self-regulating modules sometimes have 33, or even 30, cells instead of the usual 36 that normal 12-V battery charging PVs typically have. With 30 cells, V_{MPP} is around 14 V and V_{OC} is about 18 V (compared to the 17 V and 21 V values for a 36-cell module). The idea is to purposely cause the current to drop off as the battery approaches full charge as suggested in Figure 6.24. There is some risk with this approach and since it does not protect against over discharging, a simple and inexpensive charge controller would be preferred.

FIGURE 6.24 A self-regulating PV module with fewer cells offers a risky approach to automatically controlling battery charging.



6.5.3 Estimating the Load

The design process for stand-alone systems begins with an estimate of the loads that are to be provided for. As with all design processes, a number of iterations may be required. On the first pass, the user may try to provide the capability to power anything and everything that normal, grid-connected living allows. Various iterations will follow in which trade-offs are made between more expensive, but more efficient, appliances and devices in exchange for fewer PVs and batteries. Lifestyle adjustments need to be considered in which some loads are treated as essentials that must be provided for and others are luxuries to be used only when conditions allow. A key decision involves whether to use all DC loads to avoid the inefficiencies associated with inverters, or whether the convenience of an all AC system is worth the extra cost, or perhaps a combination of the two is best. Another important decision is whether to include a generator backup system, and if so, what fraction of the load it will have to supply.

Power needed by a load and energy required over time by that load are both important for system sizing. In the simplest case, energy (watt-hours or kilowatt-hours) is just the product of some nominal power rating of the device times the hours that it is in use. The situation is often more complicated, however. For example, an amplifier needs more power when the volume is increased, and many appliances, such as refrigerators and washing machines, use different amounts of power during different portions of their operating cycles. An especially important consideration for household electronic devices—TVs, VCRs, computers, portable phones, and so on—is the power consumed when the device is in its standby or charging modes. Many devices, such as TVs, use power even while they are turned off since some circuits remain energized awaiting the turn-on signal from the remote. Other devices, especially cable and dish video recording boxes tend to consume almost the same amount of power 24 h a day as they update their TV guides and await the shows that you have programmed to record. Consumer electronics now account for about 10% of all U.S. residential electricity and researchers at Lawrence Berkeley National Labs conclude that almost two-thirds of that energy occurs when these devices are not actually being used (Rosen and Meier, 2000). Major appliances and shop tools have another complication caused by the surge of power required to start their electric motors. While that large initial spike does not add much to the energy used by a motor, it has important implications for sizing inverters, wires, fuses, and other ancillary electrical components in the system.

Table 6.11 lists examples of power used by a number of household electrical loads. Some of these are simply watts of power, which can be multiplied by hours of use to get watt-hours of energy. Many of the devices listed in the consumer electronics category show power while they are being used (active) and power consumed the rest of the time (standby), both of which must be considered when determining energy consumption. Refrigerators are also unusual since they are always turned on, but their power demand varies throughout the day. The data given on refrigerator labels are average watt-hours per day based on measurements made with the refrigerator located in a 90°F room. That means they are likely to overstate the actual demand in someone's home—perhaps by as much as 20%. Tables like this one are useful for average values, but the best source of power and energy data are actual measurements that can easily be performed with readily available meters. Another source is the device nameplate itself, but those tend to overstate power

since they are meant to describe maximum demand rather than the likely average. Some nameplates provide only amperage and voltage, and while it is tempting to multiply the two to get power, that can also be an overestimate since it ignores the phase angle, or power factor, between current and voltage.

TABLE 6.11 Power Requirements of Typical Household Loads

Kitchen Appliances	
Refrigerator/freezer: Energy Star 14 cu ft.	300 W, 950 Wh/d
Refrigerator/freezer: Energy Star 19 cu ft.	300 W, 1080 Wh/d
Refrigerator/freezer: Energy Star 22 cu ft.	300 W, 1150 Wh/d
Chest freezer: Energy Star 22 cu ft.	300 W, 1300 Wh/d
Dishwasher (hot dry)	1400 W, 1.5 kWh/load
Electric range burner (small/large)	1200 / 2000 W
Toaster oven	750 W
Microwave oven	1200 W
General Household	
Clothes dryer (gas/electric, 1400 W)	250 W; 0.3 / 3 kWh/load
Washer (w/o H_2O heating/with electric heating)	250 W; 0.3 / 2.5 kWh/load
Furnace fan: $^1/_2$ hp	875 W
Celling fan	100 W
Air conditioner: window, 10, 000 Btu	1200 W
Heater (portable)	1200–1875 W
Compact fluorescent lamp (100 W equivalent)	25 W
Clothes iron	1100 W
Clocks, cordless phones, answering machines	3 W
Hair dryer	1500 W
Consumer electronics (Active/Standby)	
TV: 30–36 in Tube	120 / 3.5 W
TV: 40–49 in Plasma	400 / 2 W
TV: 40–49 in LCD	200 / 2 W
Satellite or cable with DVR (Tivo)	44 / 43 W
Digital cable box (no DVR)	24 / 18 W
DVD, VCR	15 / 5 W
Game console (X-Box)	150 / 1 W
Stereo	50 / 3 W
Modem DSL	5 / 1 W
Printer inkjet	9 / 5 W
Printer laser	130 / 2 W
Tuner AM/FM	10 / 1 W

Computer: Desktop (on/sleep/off)	74 / 21 / 3 W
Computer: Notebook (in use/sleep)	30 / 16 W
Computer monitor LCD	40 / 2 W
Outside	
Power tools, cordless	30 W
Circular saw, 7 1/4 in	900 W
Table saw, 10 in	1800 W
Centrifugal water pump: 50 ft at 10 gal/min	450 W
Submersible water pump: 300 ft at 1.5 gal/min	180 W
Source: Rosen and Meier (2000) with updates from LBL and others.	

Example 6.9 A Modest Household Demand. Estimate the monthly energy demand for a cabin with all AC appliances, consisting of a 19 cu ft refrigerator, six 25-W compact fluorescent lamps (CFLs) used 6 h/d, a 44-in LCD TV turned on 3 h/d and connected to a satellite with digital video recording (DVR), 10 small electric devices using 3 W continuously, a microwave used 12 min/d and a small range burner 1 h/d, a clothes washer that does four loads a week with solar heated water, a laptop computer used 2 h/d, and a 300-ft deep well that supplies 120 gal of water per day.

Solution. Using data from Table 6.11, we can put together the following table of power and energy demands. The total is about 6.3 kWh/d, which is about 2300 kWh/yr.

Appliance	Power (W)	Hours/day	Wh/d	Percentage
Refrigerator, 19 cu ft	300		1080	17%
Range burner (small)	1200	1	1200	19%
Microwave at 12 min/d	1200	0.2	240	4%
Lights (6 at 25 W, 6 h/d)	150	6	900	14%
Clothes washer (4 load/wk at 0.3 kWh)	250		171	3%
LCD TV 3 h/d (on)	200	3	600	10%
LCD TV 21 h/d (standby)	2	21	42	1%
Satellite with DVR	44	3	132	2%
Satellite (standby)	43	21	903	14%
Laptop computer (2 h/d at 30 W)	30	2	60	1%
Assorted electronics (10 at 3 W)	30	24	720	11%
Well pump (120 gal/d at 1.5 gal/min)	180	1.33	240	4%
Total	3566		6288	

We can note several interesting things from this table. For starters, kitchen use accounts for 40% of the total, which is a relatively high fraction due in part to an assumption that it is an all-electric stove. On the other hand, this is a very good refrigerator that uses only about half the energy of an old one. When using PV power, it will almost always make sense to purchase the most efficient appliances available.

Watching TV accounts for 27% of the energy, with 55% of that being standby loads mostly associated with that DVR.

6.5.4 Initial Array Sizing Assuming an MPP Tracker

As should be the case in most design processes, a good start is based on many assumptions that will have to be refined as the design proceeds. Our starting point for array sizing will be based on the assumption that the system includes an MPPT and that the batteries will be sized to carry the load during inclement weather conditions. The first assumption allows us to use the peak-hours approach to system sizing and the second allows us to use average solar insolation values instead of hour-by-hour TMY calculations.

Without the grid, the orientation of the collectors becomes much more important since we cannot carry much, if any, excess power from 1 month to the next. That suggests starting with a fairly steep collector tilt angle to try to bump up the winter insolation and sizing the system based on the worst month of the year.

Example 6.10 Initial Array Sizing for a House in Boulder, CO. Using Appendix G insolation data, size an off-grid array to meet the 6.29 kWh/d load found in Example 6.9. For now, assume an 80% round-trip battery efficiency and make any other appropriate assumptions.

Solution. To get relatively uniform output over the year we will chose south-facing, L+15 tilt angle collectors. From Appendix G, the month with the least insolation is December with 4.5 kWh/m^2/d, or 4.5 h/d of full sun. Let us assume the usual 0.75 derate factor for inverter, dirt, wiring, and so on We will assume all of the PV kW go into and back out of the battery on their way to the load, so we will apply the full 80% round-trip efficiency:

$$6.29\ \text{kWh/d} = P_{\text{DC}}\,(\text{kW}) \cdot 4.5\ \text{h/d} \cdot 0.75 \cdot 0.80$$

$$P_{\text{DC}} = \frac{6.29}{4.5 \times 0.75 \times 0.80} = 2.33\ \text{kW}$$

That takes care of December, but it will mean excess energy for the other months of the year. Repeating the calculation leads to the following monthly results:

	Jan	Feb	Mar	Apr	May	Jun	Jly	Aug	Sep	Oct	Nov	Dec	Annual
Insolation (h/d)	4.8	5.3	5.6	5.6	5.2	5.2	5.3	5.5	5.8	5.7	4.8	4.5	5.3
PV (kWh/d)	6.71	7.41	7.83	7.83	7.27	7.27	7.41	7.69	8.11	7.97	6.71	6.29	2691
Load (kWh/d)	6.29	6.29	6.29	6.29	6.29	6.29	6.29	6.29	6.29	6.29	6.29	6.29	2295
Excess	0.42	1.12	1.54	1.54	0.98	0.98	1.12	1.40	1.82	1.68	0.42	0.00	396

These are average monthly values, which include inclement weather periods during which we hope there is enough storage to carry us through, or else behavioral modifications that will reduce the load appropriately. And there is always the option of a generator backup.

Suppose we change the design criteria to specify that the PVs will cover the average annual load, in which case the rated power of the array would be

$$P_{\text{DC}} = \frac{6.29}{5.3 \times 0.75 \times 0.80} = 1.98\ \text{kW}$$

While this could provide all of the loads on the average, it is unlikely to do so without an excessively large storage system to carry excess from 1 month into a later month with

deficits. Consider the following table of performance for the 1.98-kW system, in which no month-to-month carryover from good months to bad months is counted.

	Jan	Feb	Mar	Apr	May	Jun	Jly	Aug	Sep	Oct	Nov	Dec	Annual
Insolation (h/d)	4.8	5.3	5.6	5.6	5.2	5.2	5.3	5.5	5.8	5.7	4.8	4.5	5.3
PV (kWh/d)	5.72	6.29	6.29	6.29	6.20	6.20	6.29	6.29	6.29	6.29	5.72	5.36	2227
Load (kWh/d)	6.29	6.29	6.29	6.29	6.29	6.29	6.29	6.29	6.29	6.29	6.29	6.29	2295

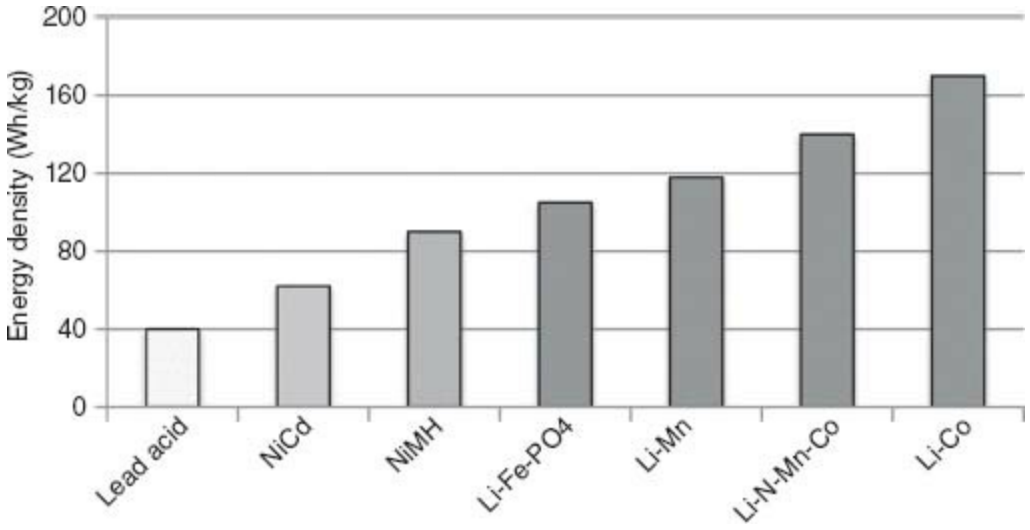
The 1.98-kW system is only 2295 – 2227 = 68 kWh/yr short of meeting the load while saving 2.33 – 1.98 = 0.35 kW of PV costs, which at say $4/W would save about $1400. The marginal cost of those last 68 kWh/yr would be hard to justify, especially if a backup generator becomes part of the system, which suggests the smaller system might provide better value.

As we shall see, when PVs are directly connected to batteries without an MPP tracker, the simple "peak-hour" approach for estimating the interaction between generation and loads no longer applies. To explore that, we need to learn more about batteries.

6.5.5 Batteries

Stand-alone systems obviously need some method to store energy gathered during good times to be able to use it during the bad. Depending on scale, a number of technologies are available now, or will be in the near future. Possible storage systems include flow batteries, compressed air, pumped storage, flywheels, and electrolysis of water to make hydrogen for fuel cells. For simple off-grid systems, however, it is still the lowly battery that makes the most sense today. And, among the many possible battery technologies, it is the familiar lead–acid battery that continues to be the workhorse of PV systems. The main competitor to conventional lead–acid batteries are various rapidly emerging lithium-ion technologies that power most of today's electric vehicles. The far greater energy density (Wh/kg) of lithium batteries is much more important for vehicles than for stationary applications, but as their costs decrease, they will likely become the battery of choice for off-grid PV systems as well in the near future. Figure 6.25 shows how much more energy can be packed into small packages with various lithium-ion battery technologies.

FIGURE 6.25 Lead–acid batteries are bigger and heavier than their emerging competition, but they remain the least costly option (from Battery University website, 2012).



In addition to energy storage, batteries provide several other important energy services for PV systems, including the ability to provide surges of current that are much higher than the instantaneous current available from the array, as well as the inherent and automatic property of controlling the output voltage of the array so that loads receive voltages that are within their own range of acceptability.

6.5.6 Basics of Lead–Acid Batteries

Lead–acid batteries date back to the 1860s when inventor Raymond Gaston Planté fabricated the first practical cells made with corroded lead-foil electrodes and a dilute solution of sulfuric acid and water. Automobile SLI batteries (starting, lighting, ignition) have been highly refined to perform their most important task, which is to start your engine. To do so, they have to provide short bursts of very high current (400–600 A). Once the engine has started, its alternator quickly recharges the battery, which means under normal circumstances the battery is almost always at or near full charge. SLI batteries are not designed to withstand deep discharges, and in fact will fail after only a few complete discharge cycles. That makes them inappropriate for most PV systems, in which slow, but deep, discharges are the norm. If they must be used, as is sometimes the case in developing countries where they may be the only batteries available, daily discharges of less than about 25% can yield several hundred cycles, or a year or two of operation at best.

In comparison with SLI batteries, deep discharge batteries have thicker plates, which are housed in bigger cases that provide greater space both above and beneath the plates. Greater space below allows more debris to accumulate without shorting out the plates, and greater space above lets there be more electrolyte in the cell to help keep water losses from exposing the plates. Thicker plates and larger cases mean these batteries are big and heavy. A single 12-V deep discharge battery can weigh several hundred pounds. They are designed to be discharged repeatedly by 80% of their capacity without harm, although such deep discharges result in a lower lifetime number of cycles. A deep-cycle, lead–acid battery can be cycled several thousand times with daily discharges of 25% or less of its rated capacity, which would give it a lifetime on the order of 10 years. That lifetime could be cut in half with 50% daily discharges, which suggests the battery bank in a PV system should be designed to store at least 4 or 5 days worth of energy demand to minimize deep cycling and prolong battery life.

To understand some of the subtleties in sizing battery systems, we need a basic understanding of their chemistry. Very simply, an individual cell in a lead–acid battery consists of a positive electrode made of lead dioxide (PbO_2) and a negative electrode made of a highly porous, metallic lead (Pb) structure, both of which are completely immersed in a sulfuric acid electrolyte. Thin lead plates are structurally very weak and would not hold up well to physical abuse unless alloyed with a strengthening material. Automobile SLI batteries use calcium for strengthening, but calcium does not tolerate discharges of more than about 25% very well. Deep discharge batteries use antimony instead, and so are often referred to as lead–antimony batteries.

One way to categorize lead–acid batteries is based on whether they are sealed or not. Conventional vehicle batteries are flooded, which means the plates are submerged in a weak solution of sulfuric acid and water. Toward the end of a charging cycle, voltage may rise enough to cause electrolysis, which releases potentially dangerous hydrogen and oxygen gases while it removes water from the battery. Flooded batteries are vented to allow these gases to escape and they require access to the cells to maintain proper water level over the plates.

Sealed batteries, on the other hand, have special valves to minimize gas releases by internally recycling those gases within the battery itself, hence the name valve-regulated lead–acid (VRLA) batteries. Chargers for sealed batteries need to be designed to avoid overvoltages, which are the source of battery outgassing. The electrolyte in sealed batteries may take the form of a gel or as an absorbent glass mat (AGM). They are a bit more expensive, but eliminating the need for water maintenance, along with their ability to be oriented in any direction without spillage, makes them a common choice for PV systems.

The chemical reactions taking place while a lead–acid battery discharges are as follows:

(6.21) Positive plate: $PbO_2 + 4H^+ + SO_4^{2-} + 2e^- \rightarrow PbSO_4 + 2H_2O$

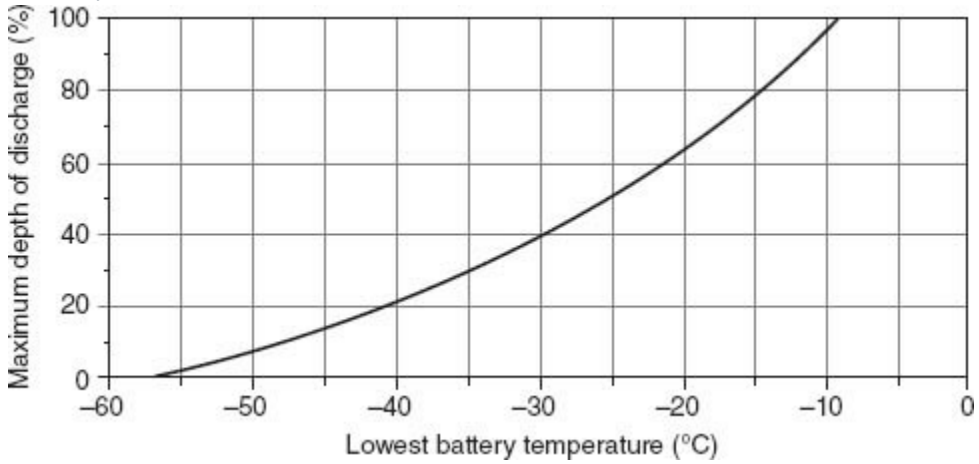
(6.22) Negative plate: $Pb + SO_4^{2-} \rightarrow P_bSO_4 + 2e^-$

It is, by the way, simpler to refer to the terminals by their charge (positive or negative) rather than as the anode and cathode. Strictly speaking, the anode is the electrode at which oxidation occurs, which means during discharge the anode is the negative terminal, but during charging it is the positive terminal.

As can be seen from Equation 6.22, during discharge electrons are released at the negative electrode, which then flow through the load to the positive plate where they enter into the reaction given by Equation 6.21. The key feature of both reactions is that sulfate ions (SO_4^{2-}) that start out in the electrolyte when the battery is fully charged, end up being deposited onto each of the two electrodes as lead sulfate ($PbSO_4$) during discharge. That lead sulfate, which is an electrical insulator, blankets the electrodes leaving less and less active area for the reactions to take place. As the battery approaches its fully discharged state, the cell voltage drops sharply while its internal resistance rises abruptly. Meanwhile, during discharge, the specific gravity of the electrolyte drops as sulfate ions leave solution, providing an accurate indicator of the battery's state of charge. The battery is more vulnerable to freezing in its discharged state since the antifreeze action of the sulfuric acid is diminished when there is less of it present. A fully discharged lead–acid battery will freeze at around −8°C (17°F), while a fully charged one will not freeze until the electrolyte drops below −57°C (−71°F). In very cold conditions, concern for freezing may limit the

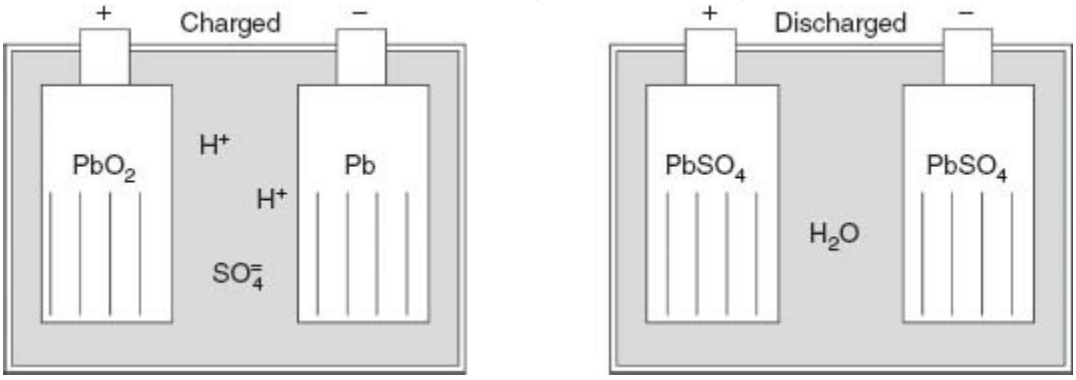
maximum allowable depth of discharge, as shown in Figure 6.26.

FIGURE 6.26 Concern for battery freezing may limit the allowable depth of discharge of a lead–acid battery.



The opposite reactions occur during charging. Battery voltage and specific gravity rise, while freeze temperature and internal resistance drops. Sulfate is removed from the plates and re-enters the electrolyte as sulfate ions (Fig. 6.27). Unfortunately, not all of the lead sulfate returns to solution and each battery charge/discharge cycle leaves a little more sulfate permanently attached to the plates. This sulfation is a primary cause of a battery's finite lifetime. The amount of lead sulfate that permanently bonds to the electrodes depends on the length of time that it is allowed to exist, which means for good battery longevity, it is important to keep them as fully charged as possible and to completely charge them on a regular basis. That suggests a generator backup system to top up batteries is an important consideration.

FIGURE 6.27 A lead–acid battery in its charged and discharged states.



As batteries cycle between their charged and partially discharged states, the voltage as measured at the terminals and the specific gravity of the electrolyte changes. While either may be used as an indication of the SOC of the battery, both are tricky to measure correctly. To make an accurate voltage reading, the battery must be at rest, which means at least several hours must elapse after any charging or discharging. Specific gravity is also difficult to measure since stratification of the electrolyte means a sample taken from the liquid above the plates may not be an accurate average value. Since sealed batteries are now more common for PV systems, SOC is most easily estimated by a simple measurement of the at-rest (preferably for at least 6 h), open-circuit battery voltage. The following is an

estimate for the state of charge as a function of the at-rest, open-circuit voltage (V_{OC}) for a 12-V lead–acid battery (based on Trojan Battery Company data):

$$\text{SOC}(\%) = 73.1 \cdot V_{OC} - 833.3 \quad (6.23)$$

For example, if the measured battery voltage is 12 V, the SOC would be

$$\text{SOC}(\%) = 73.1 \times 12 - 833.3 = 44\%$$

while at full charge the voltage would be a bit over 12.7 V.

6.5.7 Battery Storage Capacity

Energy storage in a battery is typically given in units of ampere-hours (Ah) at some nominal voltage and at some specified discharge rate. A lead–acid battery, for example, has a nominal voltage of 2 V per cell (e.g., 6 cells for a 12-V battery) and manufacturers typically specify the ampere-hour capacity at a discharge rate that would drain the battery down over a specified period of time at a temperature of 25°C. For example, a fully charged 12-V battery that is specified to have a 20-h, 200-Ah capacity could deliver 10 A for 20 h, at which point the battery would be considered to be fully discharged. This ampere-hour specification is referred to as a C/20 or 0.05C rate, where the C refers to ampere-hours of capacity and the 20 is hours it would take to deplete. Note how tricky it would be to specify how much energy the battery delivered during its discharge. Energy is volts × amperes × hours, but since voltage varies throughout the discharge period, we cannot just say 12 V × 10 A × 20 h = 2400 Wh. To avoid that ambiguity, almost everything having to do with battery storage capacity is specified in ampere-hours rather than watt-hours.

The ampere-hour capacity of a battery is very much tied to the discharge rate. More rapid drawdown of a battery results in lower ampere-hour capacity, while longer discharge times result in higher ampere-hour capacity. Deep-cycle batteries intended for PV systems are often specified in terms of their 20- or 24-h discharge rate as well as the much longer C/100 rate that is more representative of how they are actually used. Table 6.12 provides some examples of such batteries, including their C/20 rates as well as their voltage and weight.

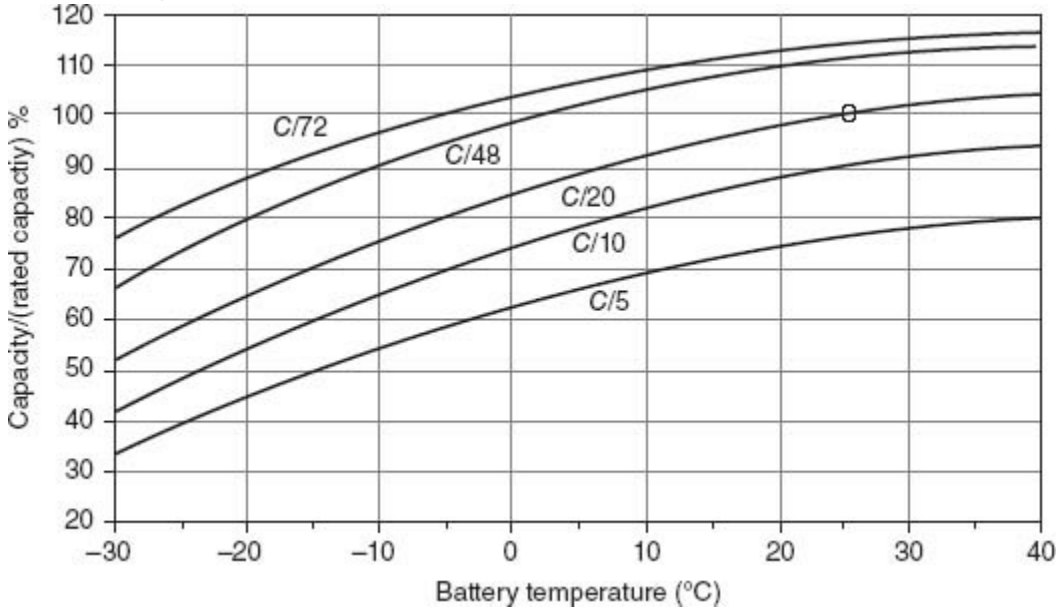
TABLE 6.12 Example Deep-Cycle Lead–Acid Battery Characteristics

Battery	Electrolyte	Voltage	Nominal Ah	Rate (h)	Weight (lbs)
Rolls Surette 4CS-17P	Flooded	4	546	20	128
Trojan T10S-RE	Flooded	6	225	20	67
Concorde PVX 3050T	AGM	6	305	24	91
Fullriver DC260-12	AGM	12	260	20	172
Trojan 5SHP-GEL	Gel	12	125	20	85

The ampere-hour capacity of a battery is not only rate dependent, but it also depends on temperature. Figure 6.28 captures both of these phenomena by comparing capacity under varying temperature and discharge rates to a reference condition of C/20 and 25°C. These curves are approximate for typical deep-cycle lead–acid batteries, but specific data available from the battery manufacturer should be used whenever possible. As shown in the figure, battery capacity decreases dramatically in colder conditions. At −30°C (−22°F), for example, a battery that is discharged at the C/20 rate will have only half of its rated capacity. The

combination of cold temperature effects on battery performance—decreased capacity, decreased output voltage, and increased vulnerability to freezing when discharged—means that lead–acid batteries need to be well protected in cold climates. Nickel–cadmium batteries do not suffer from these cold weather effects, which is the main reason they are sometimes used instead of lead–acids in cold climates. By the way, the apparent improvement in battery capacity at high temperatures does not mean heat is good for a battery. In fact, a rule-of-thumb estimate is that battery life is shortened by 50% for every 10°C above the optimum 25°C operating temperature.

FIGURE 6.28 Lead–acid battery capacity depends on discharge rate and temperature. The capacity percentage ratio is based on a rated capacity at C/20 and 25°C.



Example 6.11 Battery Storage Calculation in a Cold Climate. Suppose batteries located at a remote telecommunication site may drop to –20°C. If they must provide 2 days of storage for a load that needs 500 Ah/d at 12 V, how many ampere-hours of storage should be specified for the battery bank?

Solution. From Figure 6.26, to avoid freezing the maximum depth of discharge at –20°C is about 60%. For 2 days of storage, with a discharge of no more than 60%, the batteries need to store

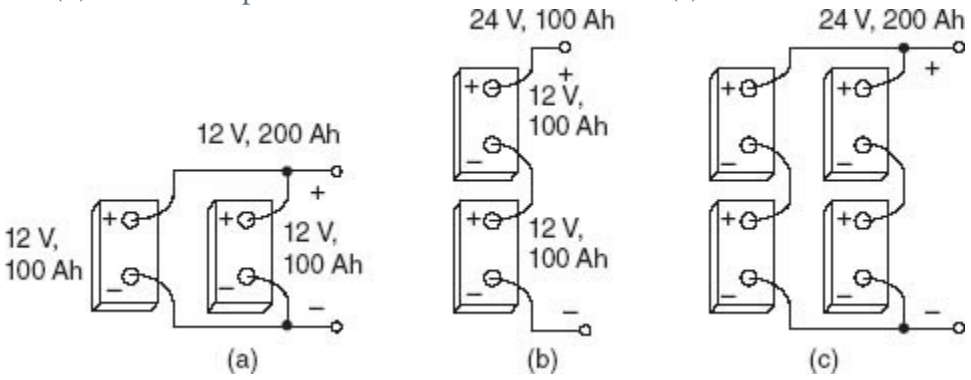
$$\text{Battery storage} = \frac{500\ \text{Ah/d} \times 2\ \text{days}}{0.60} = 1667\ \text{Ah}$$

Since the rated capacity of batteries is likely to be specified at an assumed temperature of 25°C at a C/20 rate, we need to adjust the battery capacity to account for our different temperature and discharge period. From Figure 6.28, the actual capacity of batteries at –20°C discharged over a 48-h period is about 80% of their rated capacity. That means we need to specify batteries with rated capacity

$$\text{Battery storage (25° C, 48-h rate)} = \frac{1667\ \text{Ah}}{0.8} = 2082\ \text{Ah}$$

Battery systems typically consist of a number of batteries wired in series and parallel combinations to achieve the needed ampere-hour capacity and voltage rating. For batteries wired in series, the voltages add, but since the same current flows through each battery, the ampere-hour rating of the string is the same as it is for each battery. For batteries wired in parallel, the voltage across each battery is the same, but since currents add, the ampere-hour capacity is additive. Figure 6.29 illustrates these notions.

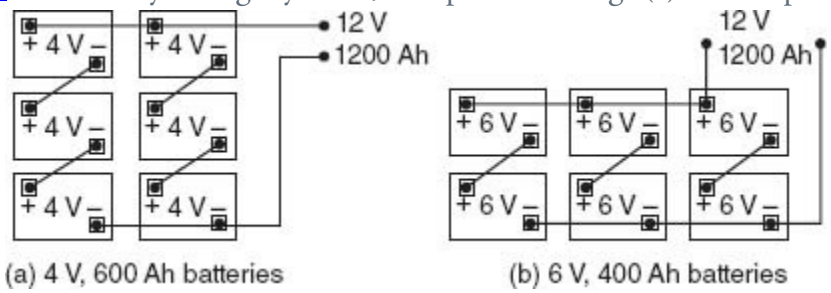
FIGURE 6.29 For batteries wired in parallel, ampere-hours add (a). For batteries in series, voltages add (b). For series/parallel combinations, both add (c).



Since there is no difference in energy stored in the 2-battery, series and parallel example shown in Figure 6.29, the question arises as to which is better. The key difference between the two is the amount of current that flows to deliver a given amount of power. Batteries in series have higher voltage and lower current, which means more manageable wire sizes without excessive voltage and power losses, along with smaller fuses and switches, and slightly easier connections between batteries. So Figure 6.29b is preferred over Figure 6.29a.

Once the system voltage for the battery bank has been determined, with higher being better, then there is a tradeoff between series and parallel combinations of batteries to achieve the desired total ampere-hours of storage. When batteries are wired in parallel, the weakest battery will drag down the voltage of the entire bank, so the most efficient battery configuration is one that has all of the batteries wired in a single series string. However, if a battery fails in a single-string system, the entire bank can go down. For redundancy, then, good practice suggests two parallel strings so that the user is never completely without power. Thus, in the examples shown in Figure 6.30, the configuration in (a) is preferred.

FIGURE 6.30 For battery storage systems, two parallel strings (a) are the preferred option.



6.5.8 Coulomb Efficiency Instead of Energy Efficiency

As mentioned earlier, almost everything having to do with batteries is described in terms of

currents rather than voltage or energy. Battery capacity C is given in ampere-hours rather than watt-hours, charging and discharging is expressed in C/T rates, which are amperes. And, as we shall see, even battery efficiency is more easily expressed in terms of current efficiency rather than energy efficiency. The reason, of course, is that battery voltage is so ambiguous without specifying whether it is a "rest" voltage measured some time after charging or discharging, a voltage during charging, or a voltage during discharge. And even those charging and discharging voltages depend on the rates at which current is entering or leaving the battery as well as the state of charge of the battery, its temperature, age, and general condition.

Imagine charging a battery with a constant current I_C over a period of time ΔT_C during which time applied voltage is V_C. The energy input to the battery is thus

$$E_{in} = V_C I_C \Delta T_C \tag{6.24}$$

Suppose the battery is then discharged at current I_D, voltage V_D over a period of time ΔT_D, delivering energy

$$E_{out} = V_D I_D \Delta T_D \tag{6.25}$$

The energy efficiency of the battery would be

$$\text{Energy efficiency} = \frac{V_D I_D \Delta T_D}{V_C I_C \Delta T_C} \tag{6.26}$$

If we recognize that current (A) × time (h) is Coulombs of charge expressed as Ah

$$\text{Energy efficiency} = \left(\frac{V_D}{V_C}\right)\left(\frac{I_D \Delta T_D}{I_C \Delta T_C}\right) = \left(\frac{V_D}{V_C}\right)\left(\frac{\text{Coulombs out, } Ah_{out}}{\text{Coulombs in, } Ah_{in}}\right) \tag{6.27}$$

The ratio of discharge voltage to charge voltage is called the *voltage efficiency* of the battery, and the ratio of Ah_{out} to Ah_{in} is called the *Coulomb efficiency*.

$$\text{Energy efficiency} = (\text{Voltage efficiency}) \times (\text{Coulomb efficiency}) \tag{6.28}$$

A typical 12-V lead–acid battery might be charged at a voltage of around 14 V and its discharge voltage might be around 12 V. Its voltage efficiency would therefore be

$$\text{Voltage efficiency} = \frac{12\text{ V}}{14\text{ V}} = 0.86 = 86\% \tag{6.29}$$

The Coulomb efficiency is the ratio of coulombs of charge out of the battery to coulombs that went in. If they all do not come back out, where did they go? When a battery approaches full charge, its cell voltage gets high enough to electrolyze water, creating hydrogen and oxygen gases that may be released. Among the negative effects of this *gassing* is loss of some of those charging electrons along with the escaping gases. As long as the battery SOC is low, little gassing occurs and the Coulomb efficiency is nearly 100%, but it can drop below 90% during the final stages of charging. Over a full charge cycle, it is typically 90–95%. As we shall see later, when it comes to sizing batteries, the Coulomb efficiency will be the measure that is most appropriate.

Assuming a 90% Coulomb efficiency, the overall energy efficiency of a lead–acid battery

with 86% voltage efficiency would be about

$$\text{Energy efficiency} = 0.86 \times 0.90 = 0.77 = 77\% \tag{6.30}$$

which is close to a commonly quoted estimate of 75% for lead–acid battery efficiency.

6.5.9 Battery Sizing

Two design decisions have to be made when sizing batteries for a stand-alone system. Instead of working with energy storage in kWh, it is the voltage of the battery bank and the ampere-hour rating of individual batteries in the array that matter.

The voltage of the battery bank has to be matched to the input voltage requirements of the inverter (if there is one) or the loads themselves if it is an all-DC system. To control I^2R wire losses, higher voltages are preferred. Lower currents means smaller gauge wire can be used, which is easier to work and, along with the associated breakers, fuses, and other wiring details, is cheaper. The system voltage for modest loads is usually 12, 24, or 48 V. One guideline that can be used to pick the system voltage is based on keeping the maximum steady-state current drawn below around 100 A, so that readily available electrical hardware and wire sizes can be used. Using this guideline results in the minimum system voltage suggestions given in Table 6.13. Maximum steady-state power that the batteries and inverter have to supply can be estimated by adding the individual power demands of all the loads that might be expected to be operating at the same time. Table 6.11 provided representative values of power for a number of common household devices, which can be used as a starting point in an analysis.

TABLE 6.13 Minimum System Voltages Based on Limiting Current to 100 A

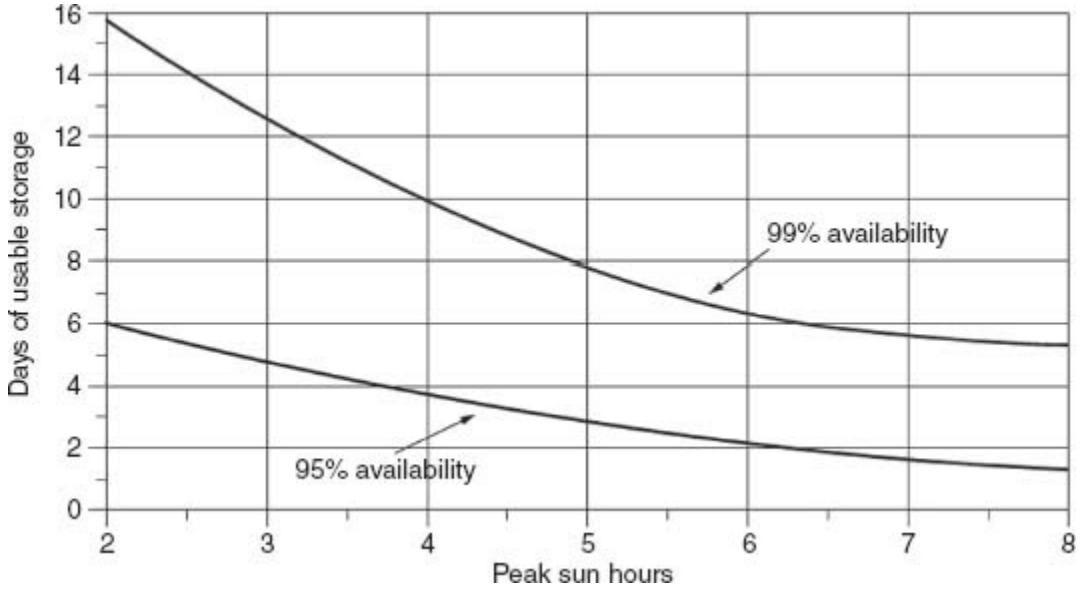
Maximum AC Power	Minimum DC System Voltage
<1200 W	12 V
1200–2400 W	24 V
2400–4800 W	48 V

If good weather could always be counted on, battery sizing might mean simply providing enough storage to carry the load through the night and into the next day until the sun picks up the load once again. The usual case, of course, is one in which there are periods of time when little or no sunlight is available and the batteries might have to be relied on to carry the load for some number of days. During those periods, there may be some flexibility in the strategy to be taken. Some noncritical loads, for example, might be reduced or eliminated, and if a generator is part of the system, a tradeoff between battery storage and generator run times will be part of the design.

Given the statistical nature of weather and the variability of owner responses to inclement conditions, there are no set rules about how best to size battery storage. The key tradeoff will be cost. Sizing a storage system to meet the demand 99% of the time can easily cost triple that for one that meets demand only 95% of the time. As a starting point for estimating the number of days of storage to be provided, consider Figure 6.31, which is based on the excellent guidebook *Stand-Alone Photovoltaic Systems Handbook of Recommended Design Practices* (Sandia, 1995). The graph gives an estimate for days of

battery storage needed to supply a load as a function of the peak sun hours per day in a given month. To account for a range of load criticality, two curves are given: one for loads that must be satisfied during 99% of the 8760 h in a year and one for less-critical loads, for which a 95% system availability is satisfactory.

FIGURE 6.31 Days of battery storage needed for a stand-alone system with 95% and 99% system availability. Peak sun hours are on a month-by-month basis. Based on Sandia Laboratories (1995).



The "usable" description of storage in Figure 6.31 assumes you have already accounted for impacts associated with maximum discharge levels and rates as well as temperature constraints (Figs. 6.26 and 6.28). The relationship between usable storage and nominal, rated storage (at C/20, 25°C) is given by

$$\text{Usable capacity} = \text{Nominal capacity (C/20, 25°C)} \times (\text{MDOD}) \times (\text{T, DR}) \tag{6.31}$$

where

MDOD = Maximum depth of discharge (default: 0.8 for lead–acid, deep discharge batteries, 0.25 for auto SLI; subject to freeze constraints given in Fig. 6.26).

TDR = Temperature and discharge-rate factor (Fig. 6.28)

The following example illustrates the process.

Example 6.12 Battery Sizing for the Off-Grid House in Boulder, CO. The household analyzed in Examples 6.9 and 6.10 has an expected AC demand of 6288 Wh/d. A decision has been made to size the batteries to provide a 95% system availability during an average month of the year. A backup generator will cover the other 5%. The batteries will be kept in a well-ventilated shed whose temperature may reach as low as −10°C. Make appropriate assumptions and design the battery bank.

Solution. We need to estimate both the average and peak loads that the batteries must supply. Since the batteries will deliver power through a charge controller and an inverter, we need to estimate its efficiency. At their peak, inverters have efficiencies in the 90+% range, but with significant fractions of less-than-peak loads, an overall efficiency of more like 85% is reasonable. Let us estimate the controller efficiency at 97%. The DC load is

then

$$\text{Battery DC load} = \frac{\text{Household AC load}}{\text{Inverter efficiency} \times \text{Controller efficiency}} = \frac{6288 \text{ Wh/d}}{0.85 \times 0.97} = 7626 \text{ Wh/d} \quad (6.32)$$

To translate that into ampere-hours of battery capacity, we need to pick a system voltage. A glance at the load described in Example 6.9 shows if everything in the house was turned on at the same time the demand would be about 3.6 kW, which by Table 6.13 suggests we need a 48-V system voltage to keep the peak current below 100 A. With a 48-V system voltage the batteries need to supply

$$\text{Load} = \frac{7398 \text{ Wh/d}}{48 \text{ V}} = 159 \text{ Ah/d at } 48 \text{ V}$$

In Example 6.9, we decided to use an L + 15 tilt angle for which the average monthly insolation is 4.5 kWh/m^2/d (Appendix G), so from Figure 6.31 it looks like a 3-day storage capacity will cover our needs about 95% of the time. So, the usable storage we need is

$$\text{Usable storage} = 159 \text{ Ah/d} \times 3 \text{ days} = 477 \text{ Ah at } 48\text{V}$$

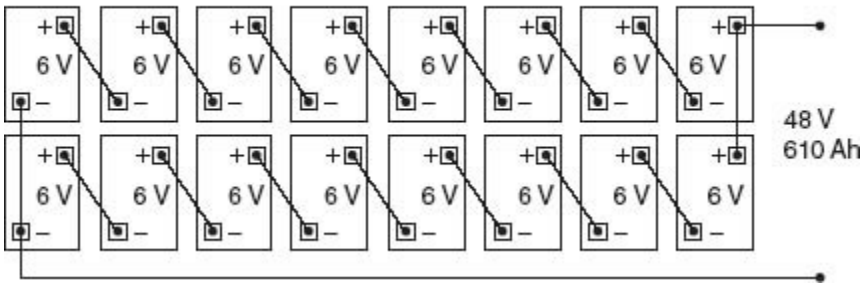
We will pick deep discharge lead–acid batteries that can be routinely discharged by 80%. But, we need to check to see whether that depth of discharge will expose the batteries to a potential freeze problem. From Figure 6.26, at −10°C the batteries could be discharged to over 95% without freezing the electrolyte, so an 80% discharge is acceptable.

Batteries that are nominally rated at C/20 and 25°C will be operated in much colder conditions which degrade storage capacity, but they will be discharged at a much slower rate, which increases capacity. Figure 6.28 suggests that at −10°C and a C/72 rate, which covers the 3 days of no sun that we have designed for, storage capacity would be about 0.97 times the nominal capacity.

Applying the 0.80 factor for maximum discharge and the 0.97 factor for discharge rate and temperature in Equation 6.33 gives

$$\text{Nominal (C/20, 25°C) capacity} = \frac{\text{Usable capacity}}{\text{MDOD} \times (\text{TDR})} = \frac{477 \text{ Ah}}{0.80 \times 0.97} = 615 \text{ Ah at } 48 \text{ V} \quad (6.33)$$

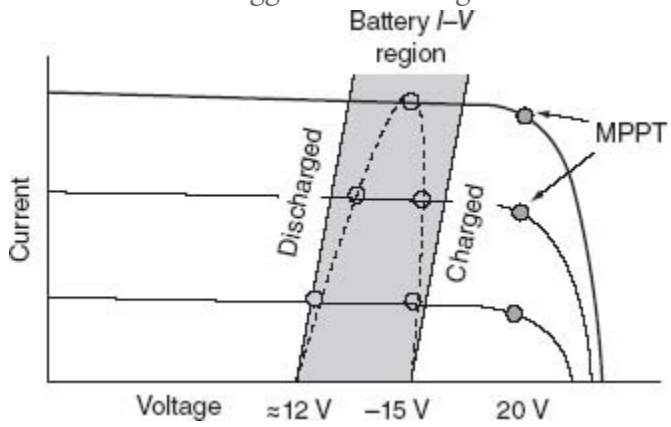
Table 6.12 can help us pick a battery. A single string of 12 of those 4-V, 546-Ah Rolls Surette batteries would be a bit undersized, but the redundancy advantage that goes with two strings suggests we use 16 of the 6-V, 305-Ah Concorde 3050T batteries as shown below.



6.5.10 Sizing an Array with No MPP Tracker

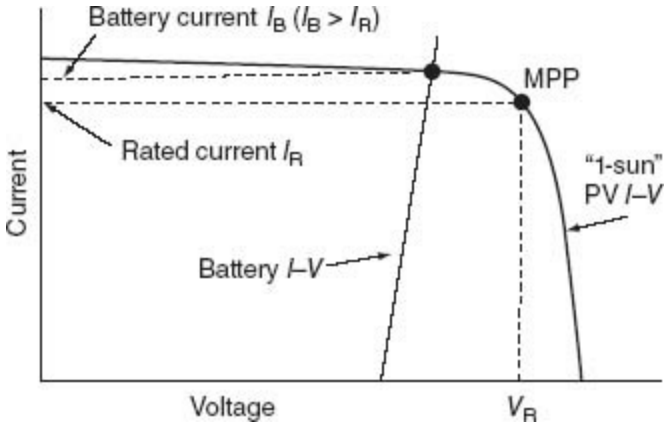
In Section 6.5.4, stand-alone system PV arrays were sized assuming a maximum power point tracker. By including an MPPT, we were able to use the simple "peak-hours" approach to system sizing. When there is no MPP tracker, the operating point is determined by the intersection of the *I–V* curve for the batteries with the *I–V* curve of the PVs. Figure 6.32 suggests the daily path of the operating point, which typically will be well below the knee where an MPPT would operate. Without an MPPT, the something like 20% or so of the potential charging will be lost.

FIGURE 6.32 With PVs directly connected to batteries, the operating point will move around within the shaded area as voltage rises during charging and as insolation changes throughout the day. The dotted line suggests a morning-to-afternoon trajectory.



One way to analyze the performance of PV-to-battery, direct coupling is suggested in Figure 6.33. As shown, during battery charging, the operating point is almost always above the knee of the PV *I–V* curve, which means that charging current will exceed the rated current of the PVs. It is a fairly conservative estimate, therefore, to simply use the rated current of the PVs as an indication of the battery charging current at 1-sun insolation. There are circumstances in which this assumption should be checked, as for example, when a 12-V battery is charged in a high temperature environment with a "self-regulating" PV module having fewer than the usual 36 cells in series. Fewer cells and higher temperatures move the MPP toward the battery *I–V* curve and the conservatism of the rated-current assumption decreases.

FIGURE 6.33 Estimating battery charging at 1-sun to be the rated current of the PVs is a fairly conservative assumption.



A simple sizing procedure is based on the same "peak-hours" approach used for grid-connected systems, except it will be applied to current rather than power. So, for example, an area with 6 kWh/m^2/d of insolation is treated as if it has 6 h/d of 1-sun irradiation. Then, using the rated current I_R at 1-sun times peak hours of sun gives us ampere-hours of current provided to the batteries.

The product of rated current I_R times peak hours of insolation provides a good starting-point estimate for ampere-hours delivered to the batteries. It is common practice to apply a derating factor of about 0.9 to account for dirt and gradual aging of the modules. The temperature and module-mismatch factors that were quite important for grid-connected systems with MPPTs are usually ignored for PV-battery systems since the operating point is so far from the knee those variations are minimal.

Another important aspect of this approach is that it is based on ampere-hours from the PVs into the batteries, and ampere-hours from the batteries to the load. That is, the appropriate battery efficiency measure will be the Coulomb efficiency (Ah_{out}/Ah_{in}) rather than the actual energy efficiency. The current delivered by batteries, to the controller, inverter, and load, is

(6.34)

$$\text{Ah from batteries} = I_R \times \text{Peak sun hours} \times \text{PV derate} \times \text{Coulomb efficiency}$$

Energy delivered through the controller and inverter to satisfy the household load is

(6.35)

$$\text{Watt-hours per day} = \text{Ah/d from batteries} \times \text{System voltage} \times \text{Controller } \eta \times \text{Inverter } \eta$$

Example 6.13 PVs for the Boulder House, Without an MPPT. The Boulder house in Example 6.10 needs 6.29 kWh/d of AC delivered from the inverter. We sized a 1.98-kW$_{DC}$ array to meet the load in an average month with 5.3 kWh/m^2/d insolation. In Example 6.12, we settled on a 48-V system voltage for the batteries.

Assuming a 90% Coulomb efficiency, 0.90 module derate, an 85%-efficient inverter, and a 97%-efficient controller, size the PV array using the peak-hours approach for a system without an MPPT. Pick a collector type from the list given in Table 5.3.

Solution. We will pick a collector based on the need for the array to supply a 48-V battery system. The best match for the 48-V system voltage would be the Yingli 245, with a rated

voltage 30.2 V, so two of those in series would assure the knee is above the 48-V system voltage. All of the other collector options would result in even higher voltages at the knee, which would be excessively wasteful. The Yingli has a rated current of 8.11 A.

From Equations 6.34 and 6.35, the average energy delivered to the load by a series pair of these modules in one string would be

$$\begin{aligned}\text{Energy} &= 8.11\ \text{A} \times 48\ \text{V} \times 5.3\ \text{h/d} \times 0.90 \times 0.90 \times 0.85 \times 0.97 \\ &= 1378\ \text{Wh/d per string}\end{aligned}$$

The number of strings needed to deliver the 6.29-kWh/d load would be

$$\text{Parallel strings} = \frac{6.29\ \text{kWh/d}}{1.378\ \text{kWh/d}} = 4.6\ \text{strings of 2 modules each}$$

Since we sized for an average month, which already means a number of months will be underserved, let us round up to five strings. Energy delivered in the worst month of the year, December, with 4.5 h/d of insolation, the energy delivered would be,

$$\begin{aligned}\text{Energy} &= 5\ \text{strings} \times 8.11\ \text{A} \times 48\ \text{V} \times 4.5\ \text{h/d} \times 0.9 \times 0.9 \times 0.85 \times 0.97 \\ &= 5850\ \text{Wh/d}\end{aligned}$$

which is 93% of the 6.29-kWh/d load in December.

The rated power of the array will be

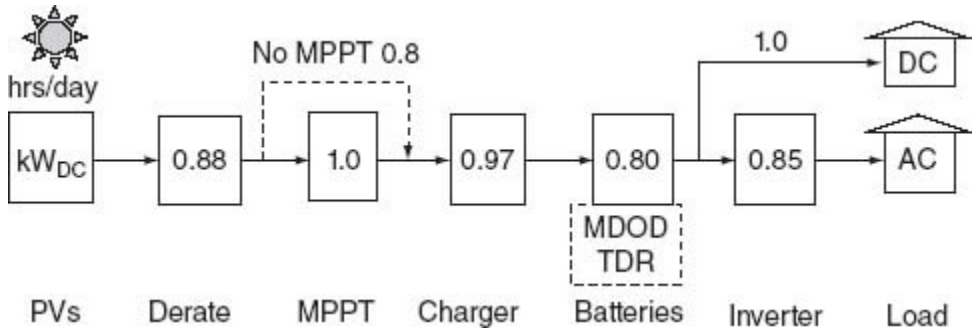
$$P_R = 5\ \text{strings} \times 2\ \text{modules/string} \times 245\ \text{W/module} = 2.45\ \text{kW}_{\text{DC}}$$

In the above example, the design calls for a 2.45-kW array to meet the average load without an MPPT. Using similar design criteria in Example 6.10, we found that a 1.98-kW array would deliver comparable performance with an MPPT. That is, the PV system without an MPPT needs about 20% more PVs than the system with an MPPT. We will use that as a guideline for a 0.80 penalty factor for non-MPPT systems. Doing so will let us create a simple spreadsheet approach that covers both types of off-grid system without having to develop separate procedures.

6.5.11 A Simple Design Template

With all of the accumulated efficiency factors presented thus far, it might help to summarize them in a figure and then incorporate them into a relatively straightforward spreadsheet. Begin with Figure 6.34 in which the flow of power is shown through all of the processes involved in supplying power to a combination of DC and AC loads.

FIGURE 6.34 Power flows in an off-grid PV system. Values are suggested as "typical" parameter estimates.



The suggested parameter values in Figure 6.34 are meant to be "typical" estimates. We will step through each one:

PVs	This analysis is based on a "peak-hours" approach in which all the following factors affect the final energy delivered to both AC and DC loads.
Derate	This 0.88 derate factor is meant to account for dirt, module mismatch, wiring losses, and so on, but not inverter efficiency.
MPPT	If there is an MPPT this factor is 1.0. If not, a value of 0.80 is suggested to account for the operating point of a non-MPPT battery, PV system being well to the left of the knee of the PV *I–V* curve (see Example 6.13).
Charger	This factor accounts for the modest losses in the charge controller.
Batteries	The 0.80 factor is an estimate of the round-trip efficiency of putting energy into a battery and getting it back out again. To the extent that daytime generation goes straight from PVs to the load, bypassing the batteries, this factor could be increased.
MDOD, TDR	The maximum depth of discharge (MDOD) and the TDR are not loss factors, but they are needed to size the battery pack.
Inverter	The 0.85 efficiency is lower than that for a grid-connected system, since much of the time it will be operating well below its optimum point. For DC loads, there is no inverter, so a factor of 1.0 is used.

Table 6.14 presents a spreadsheet approach that incorporates the key design decisions.

TABLE 6.14 An Example Design Template for Off-Grid Systems (Illustrating a System Without an MPPT Including Both AC and DC Loads)

HOUSEHOLD LOADS					
AC Loads	No	W ea.	Watts	h/d	Wh/d
Refrigerator, 19 cu ft	1	300	300		1080
Lights (6 at 25 W, 6 h/d)	6	25	150	6	900
LCD TV 3 h/d (on)	1	200	200	3	600
LCD TV 21 h/d (standby)	1	2	2	21	42
Satellite with DVR	1	3	44	3	132
Satellite (standby)	1	21	43	21	903
Assorted electronics at 3 W ea	10	3	30	24	720
Microwave at 12 min/d	1	1200	1200	0.2	240
Range burner (small)	1	1200	1200	1	1200
Clothes washer (0.25 kW; load/wk at 0.3 kWh)	4	250	250		171
Laptop computer (2 h/d at 30 W)	1	30	30	2	60
Well pump (120 gal/d at 1.5 gal/min)	1	180	180	1.33	240
Other	0		0		0
Total			3566		6288
DC Loads					
Circular saw	1	900	900	0.5	450
Other	0		0		0
Total			900		450

BATTERY DATA		
Days of storage	3.0	Figure 6.31 may help
System voltage	48	Typical 12, 24, 48 V
Maximum current (A)	93	With all loads on at once; try to keep below 100A
Inverter efficiency η	85%	Typical 85%
Battery DC delivery (Ah/d)	9.4	Ah/d = DC Wh/d / System voltage
Battery AC delivery (Ah/d)	154.1	Ah/d = AC Wh/d / System voltage / Inverter efficiency
Battery total delivery (Ah/d)	163.5	Ah/d = DC + AC
Maximum depth of discharge (MDOD)	80%	Typical 80%
Temperature and discharge rate (TDR) adjustment	97%	Figure 6.28
Minimum battery storage (Ah)	652	Ah = (dc+ac Ah/d) × (days) / (MDOD, TDR) / contr eff

PHOTOVOLTAIC DATA		
Design month insolation (kWh/m^2/d = h/d)	5.3	Annual average is reasonable with backup generator
Derate (dirt, mismatch, wiring)	0.88	Typical 0.75; does not include battery losses
MPP impact	0.80	Typical 1.0 with MPPT; 0.8 without MPPT
Charge controller efficiency	97%	Typical 97%
Battery round-trip efficiency	80%	Typical 80%
$P_{DC,STC}$ (kW)	2.71	P_{DC} = Ah/d × V/(h/d × derate × MPP × controller × battery efficiency)

RESULTS													
	Jan	Feb	Mar	Apr	May	Jun	Jly	Aug	Sep	Oct	Nov	Dec	Average
Insolation (h/d)	4.8	5.3	5.6	5.6	5.2	5.3	5.5	5.8	5.8	5.7	4.8	4.5	5.3
Load (kWh/d)	6.74	6.74	6.74	6.74	6.74	6.74	6.74	6.74	6.74	6.74	6.74	6.74	6.74
PV supply (kWh/d)	6.10	6.74	7.12	7.12	6.61	6.74	6.99	7.37	7.37	7.25	6.10	5.72	6.77
%Load (100% max)	91%	100%	100%	100%	98%	100%	100%	100%	100%	100%	91%	85%	97%

It should be easy to reverse-engineer Table 6.14 to create your own spreadsheet. The only modestly tricky part is calculating the month-by-month energy delivered by the PV system once it has been sized. For example, the energy delivered in August without an MPPT by a 2.71-kW$_{DC}$ array exposed to 5.8 kWh/m^2/d of insolation will be

$$\begin{aligned}\text{Energy to batteries} &= 2.71\ \text{kW} \times 5.8\ \text{h/d} \times 0.88\ \text{(derate)} \times 0.80\ \text{(no MPPT)} \\ &\quad \times 0.97\ \text{(controller)} \\ &= 10.73\ \text{kWh/d}\end{aligned}$$

We assume all of that goes through the 80%-efficient batteries before being delivered to the DC and AC loads. With 5.75% of the energy going to DC loads (9.4/163.5 Ah) with no inverter

$$\text{Energy delivered to DC loads} = 10.73\ \text{kWh/d} \times 0.80 \times 5.75\% = 0.49\ \text{kWh/d}$$

The other 94.25% of the power goes through the 85%-efficient inverter for AC loads:

$$\text{Energy to AC loads} = 10.73\ \text{kWh/d} \times 0.80 \times 94.25\% \times 0.85\ (\text{inv})$$
$$= 6.88\ \text{kWh/d}$$

Total energy delivered to loads = 0.49 + 6.88 = 7.37 kWh/d, which is more than was needed in the design, so for that month the percent load is pegged at 100% under the assumption that carryover of extra energy from 1 month to another is unlikely.

6.5.12 Stand-alone PV System Costs

A PV system designed to supply the entire load in the worst season usually delivers much more energy than is needed during the rest of the year. Outside of the tropics, it is not at all unusual for the energy supplied during the best month to be as much as double that of the worst month. After estimating the cost of a system that has been designed to be completely solar, a buyer may very well decide that a hybrid system with most of the load covered by PVs and the remainder supplied by a generator is worth considering. The key to that decision is estimating the relationship between shrinking the PV system and increasing the fraction of the load carried by the generator.

When a generator is included in the system, it is most convenient if is made to be an inverter-charger. That is, one that converts DC from the batteries into AC for the load, as well as converting AC from the generator into DC to charge the batteries. Switching from one mode to the other can be done manually or with an automatic transfer switch in the unit itself. The generator can be sized just to charge the batteries, which is the usual case, or it can be sized large enough to charge batteries and simultaneously run the entire household.

With a hybrid system, the battery storage bank can be smaller since the generator can charge the batteries during prolonged periods of poor weather. One constraint on how small storage can be is to check to be sure that the load cannot discharge the batteries at too fast a rate—certainly no faster than C/5. A nominal 3-day storage system is often recommended since it will avoid discharging too rapidly, while at the same time keeping the number of times the generator has to be fired up to a reasonable level. Finally, the generator should be sized so that it does not charge the batteries too rapidly—again, certainly no faster than C/5.

Generators are somewhat costly, depending on the quality of the machine. They require periodic oil changes, tune-ups, and major overhauls. Home-size generators burn fuel at varying rates and are especially dependent on the fraction of full load at which they operate.

Example 6.14 Fuel Cost for a Diesel Generator. Manufacturer's specifications for a 9.1-kW diesel generator indicate fuel use at full rated power is 4 L/h (1.06 gal/h), while at 50% load it consumes 2.5 L/h (0.66 gal/h). If diesel costs $4/gal ($1.057/L), find the fuel cost per kWh of generation at full and half load.

Solution. The energy efficiency and fuel cost at 100% of rated power and at 50% of rated power will be

$$\text{kWh/gal: Rate (100\% load)} = \frac{9.1\ \text{kW}}{1.057\ \text{gal/h}} = 8.61\ \text{kWh/gal}$$

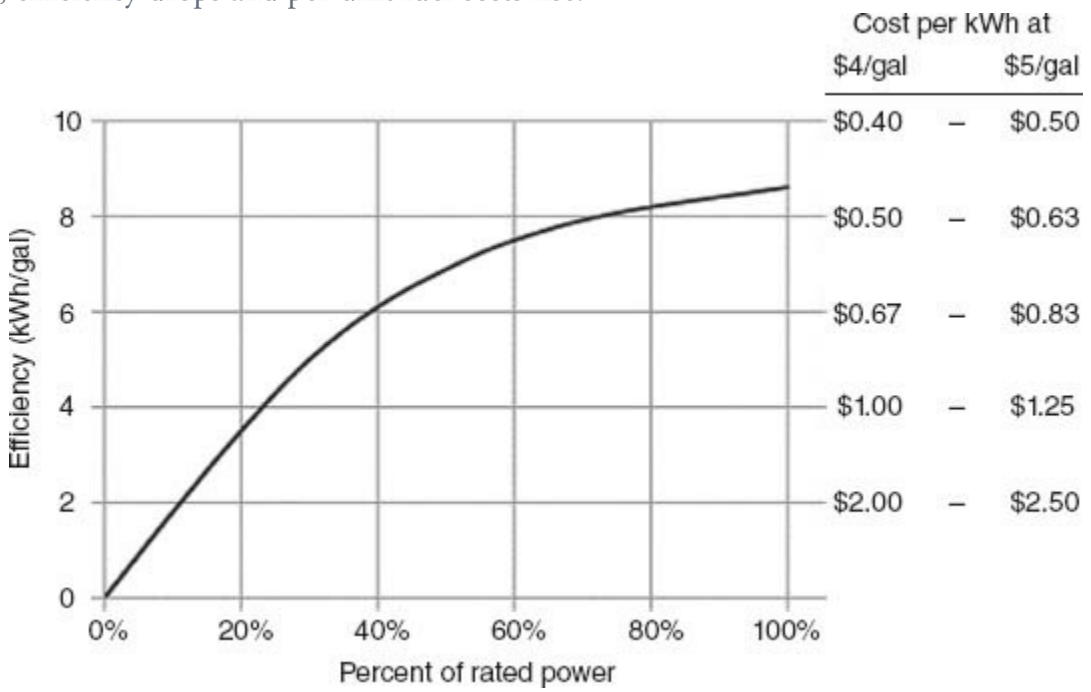
$$\text{Rate (50\% load)} = \frac{9.1 \times 0.5\ \text{kW}}{0.66\ \text{gal/h}} = 6.89\ \text{kWh/gal}$$

$$\text{At \$4/gallon: Cost (100\% load)} = \frac{\$4/\text{gal}}{8.61\ \text{gal/h}} = \$0.46/\text{kWh}$$

$$\text{: Cost (50\% load)} = \frac{\$4/\text{gal}}{6.89\ \text{gal/h}} = \$0.58/\text{kWh}$$

Example 6.14 provides a starting point for estimating the cost of electricity from a standby diesel generator. The full power curve for this particular generator is shown in Figure 6.35, with cost per kWh estimates at fuel costs of $4/gal and $5/gal. As shown, the unit cost is very dependent on the percentage of rated power actually being generated, which points out the importance of proper sizing. As rough guidelines, backup generators produce roughly 5–10 kWh/gal of fuel, which at $4/gal works out to about $0.40–$0.80/kWh.

FIGURE 6.35 Efficiency curve for a 9.1-kW diesel generator. When run at only partial load, efficiency drops and per-unit fuel costs rise.



Given the wide range of uncertainties that accompany the economics of off-grid PV systems, it is difficult to generalize their cost-effectiveness. They may be located a few miles from a major economic center with easy access to sources of quality materials and well-trained labor, or they may be tens or hundreds of miles from such amenities. But despite these difficulties, it may be worthwhile to at least step through an example with some approximate estimates of costs.

Example 6.15 A Rough Cost Analysis for an Off-Grid System. Using the following rough unit-cost estimates, find the cost of electricity for the stand-alone system designed in Table 6.14 (2.71 kWp, 632-Ah battery, 6.77 kWh/d delivered). Assume financing with a 4%, 20-year loan.

PV array cost	$2/Wp
Battery cost	$150/kWh
BOS hardware	$2/Wp
BOS nonhardware	30% of hardware costs

Solution. Using system data from Table 6.14

$$\text{PV array cost} = 2.71\ \text{kWp} \times 1000\ \text{W/kW} \times \$2/\text{Wp} = \$5420$$

$$\text{Battery cost} = \frac{632\ \text{Ah} \times 48\ \text{V}}{1000\ \text{VAh/kWh}} \times \$150/\text{kWh} = \$4550$$

$$\text{BOS hardware cost} = 2710\ \text{Wp} \times \$2/\text{Wp} = \$5420$$

$$\text{BOS nonhardware} = 30\%\ (\$5420 + \$4550 + \$5420) = \$4617$$

$$\text{Total wholesale} = \$5420 + \$4550 + \$5420 + \$4617 = \$20{,}007$$

$$\text{Amortized with a CRF (4\%, 20 years)} = 0.0736/\text{yr (Table 6.4)}$$

$$\text{Cost per kWh} = \frac{\$20{,}007 \times 0.0736/\text{yr}}{6.77\ \text{kWh/d} \times 365\ \text{d/yr}} = \$0.60/\text{kWh}$$

The above analysis, without any incentives, resulted in 60 ¢/kWh PV electricity, which makes it potentially financially competitive with diesel. And, the PV system is certainly a lot cleaner and more user-friendly than diesel.

6.6 PV-POWERED WATER PUMPING

One of the most economically viable PV applications today is water pumping in remote areas. For an off-grid home, a simple PV system can raise water from a well or spring and store it in either a pressurized or an unpressurized tank for domestic use. Water for irrigation, cattle watering, or village water supplies—especially in developing countries—can be critically important and the value of a PV water-pumping system in these circumstances can far exceed its costs.

The simplest PV water-pumping systems consist of just a PV array directly connected to a DC pump. Water that is pumped when the sun is out may be used during those times or it can be stored in a tank for later use. The costs and complexities of batteries, controllers, and inverters can be eliminated, resulting in a system that combines simplicity, low cost, and reliability. On the other hand, matching PVs and pumps in such directly coupled systems (without battery storage) and predicting their daily performance is actually a quite challenging task.

As suggested in Figure 6.36, a simple, directly coupled PV-pump system has an electrical side in which PVs create a voltage V that drives current I through wires to a motor load,

and a hydraulic side in which a pump creates a pressure, H (for *head*) that drives water at some flow rate Q through pipes to some destination. The figure suggests the hydraulic side is a *closed* loop with water circulating back to the pump, but it may also be an *open* system in which water is raised from one level to the next and then released. On the electrical side of the system, the voltage and current delivered at any instant are determined by the intersection of the PV I–V curve and the motor I–V curve. In the hydraulic system, H is analogous to voltage while Q is analogous to current. As shown in Figure 6.37, the intersection between the H–Q curve drawn for the pump itself and the H–Q pressure and flow curve for the load determines the hydraulic operating point. The analogies are also true with regard to power. For both sides of the system, maximum power is delivered to the load at an operating point located on the knee of their respective system curves.

FIGURE 6.36 The electrical characteristics of the PV–motor combination need to be matched to the hydraulic characteristics of the pump and its load.

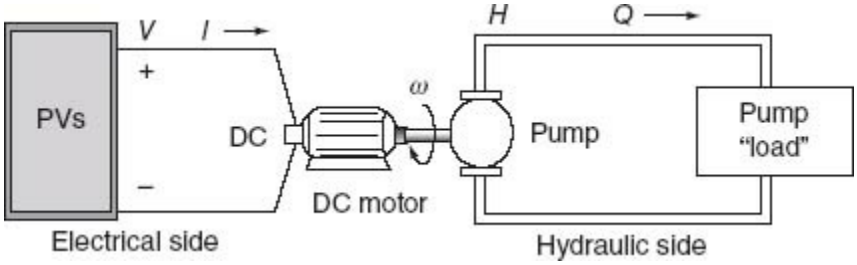
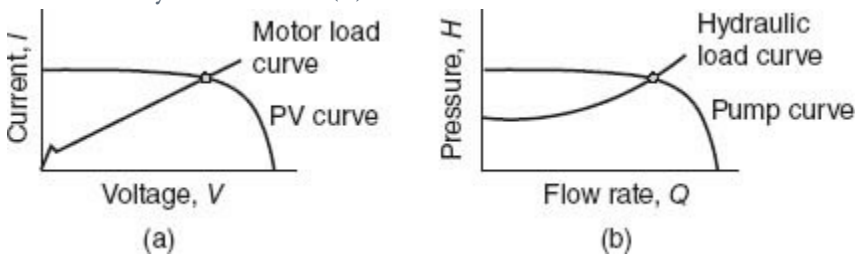


FIGURE 6.37 Showing the analogies between the I–V curves on the electrical side (a) and the H–Q curves on the hydraulic side (b).



While the system in Figure 6.36 could not be simpler, the analysis of how it will operate is rather tricky. The power delivered to the pump motor will vary throughout the day as insolation changes, which means the pump curve on the hydraulic side will vary up and down as well. With both operating points moving around, predicting the amount of water pumped over a day's time becomes a challenge.

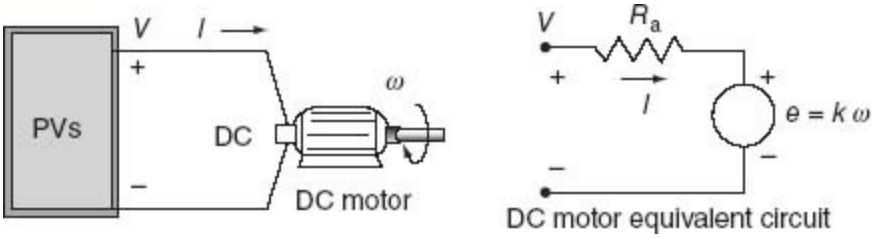
6.6.1 The Electrical Side of the System

Since the electrical system in question is DC, the pump will usually be driven by a DC motor. Most are permanent magnet DC motors, which can be modeled as shown in Figure 6.38. Note as the motor spins, it develops a *back electromotive force* (emf) e, which is a voltage proportional to the speed of the motor (ω) that opposes the voltage supplied by the PVs. From the equivalent circuit, the voltage–current relationship for the DC motor is simply

$$V = IR_a + e = IR_a + k\omega \quad (6.36)$$

where back emf $e = k\omega$ and R_a is the armature resistance.

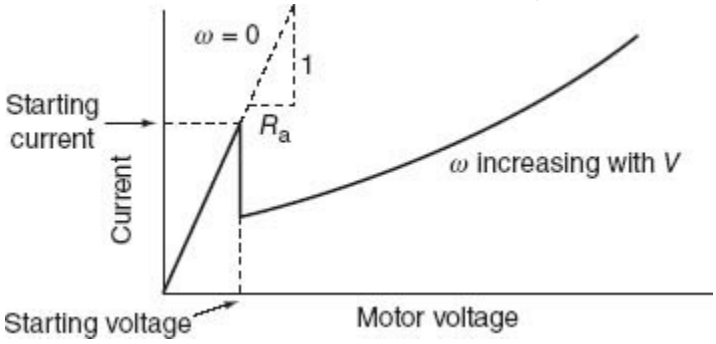
FIGURE 6.38 Electrical model of a permanent magnet DC motor.



A DC motor runs at nearly constant speed for any given applied voltage even though the torque requirement of its load may change. For example, as the torque requirement increases, the motor slows slightly, which drops the back emf and allows more armature current to flow. Since motor torque is proportional to armature current, the slowing motor draws more current, delivers more torque to the load, and regains almost all of its lost speed.

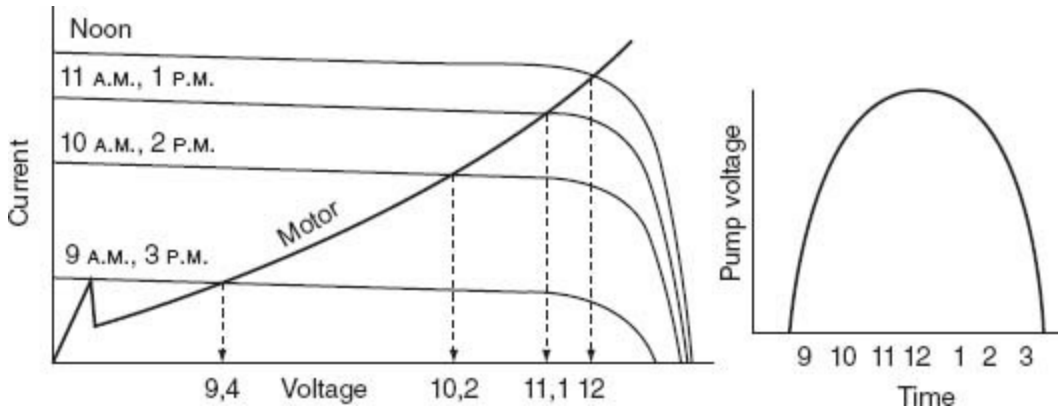
Based on Equation 6.36, the electrical characteristic curve of a DC motor will appear to be something like the one shown in Figure 6.39. Note that at start-up, while $\omega = 0$, the current rises rapidly with increasing voltage until current is sufficient to create enough starting torque to break the motor free from static friction. Once the motor starts to spin, back emf drops the current, and thereafter, I rises more slowly with increasing voltage. Note that if you stall a DC motor while the voltage is way above the starting voltage, the current may be so high that the armature windings can burn out. That is why you should never leave power on a DC motor if the armature is mechanically stuck for some reason.

FIGURE 6.39 Electrical characteristics of a permanent magnet DC motor.



A DC motor I–V curve is superimposed onto a set of hour-by-hour PV I–V curves in Figure 6.40. The mismatch of operating points with the ideal MPP is apparent. Note in this example that the motor does not start until about 9:00 A.M., when insolation and current are finally high enough to overcome static friction. This incurs some morning losses, which could be eliminated with a DC-to-DC converter that would transform the low, morning PV current into high enough current to start the motor sooner. But, that makes the system more complicated than the simple one being described here.

FIGURE 6.40 Superimposing the DC motor curve on hourly PV I–V curves yields hour-by-hour voltages supplied to the pump motor.



6.6.2 Hydraulic Pump Curves

Pumps suitable for PV-powered systems generally fall into one of two categories: *centrifugal* pumps and *positive displacement* pumps. Centrifugal pumps have fast-spinning impellers that literally throw the water out of the pump, creating suction on the input side of the pump, and pressure on the delivery side. When these are installed above the water, they are limited by the ability of atmospheric pressure to push water up into the suction side of the pump—that is, to a theoretical maximum of about 32 ft; in practice, that is more like 20 ft. When the pump is installed below the water line, however, the pump can push water up hundreds of feet. Submersible pumps with waterproof housings for the motor are suspended in a well using the same pipe that the water is pumped through. In this configuration, centrifugal pumps can push water over 1000 vertical feet. One of the disadvantages of centrifugal pumps, however, is that their speedy impellers are susceptible to abrasion and clogging by grit in the water. When powered by PVs, they are also particularly sensitive to changes in solar intensity during the day.

Positive displacement pumps come in several types, including *helical pumps*, which use a rotating shaft to push water up a cavity; *jack pumps*, which have an above-ground oscillating arm that pulls a long drive shaft up and down (like the classic oil-rig pumper); and *diaphragm pumps* that use a rotating cam to open and close valves. The traditional hand pump and wind-powered water pumps are versions of jack pumps. Jack pumps use simple flap valves that work very much like hydraulic diodes. During each upward stroke of the shaft, a flap closes and a gulp of water is carried upward; during the downward stroke, the valve opens and new water enters a chamber to be carried upward on the next stroke. In general, positive displacement pumps pump at slower rates; so they are most useful in low volume applications. They easily handle high heads, however, and they are much less susceptible to gritty water problems than centrifugal pumps. They also are less sensitive to changes in solar intensity. A brief comparison of the two types of pumps is presented in Table 6.15.

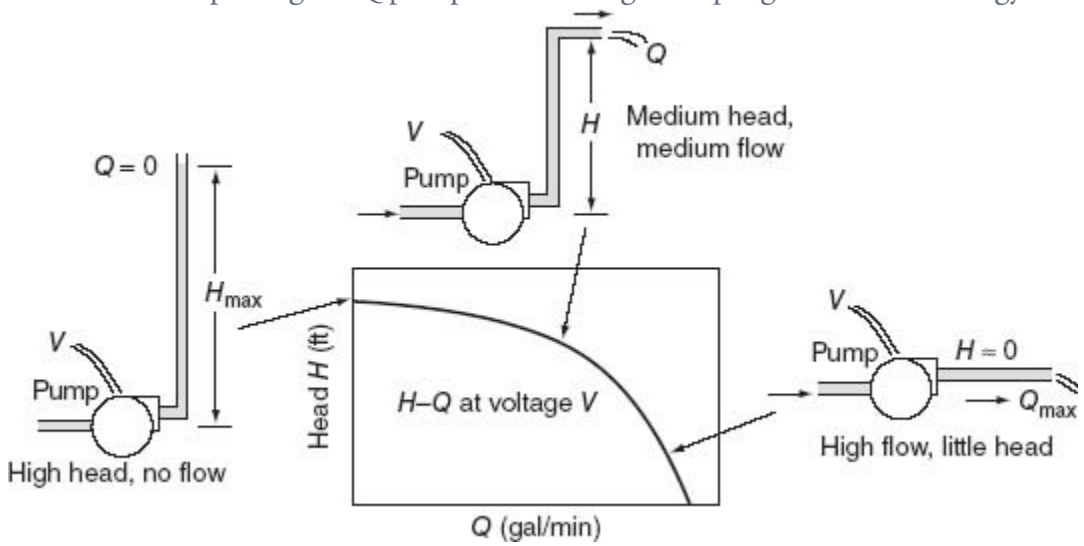
TABLE 6.15 A Comparison Between Centrifugal and Positive Displacement Pumps

Centrifugal	Positive Displacement
High speed impellers	Volumetric movement
Large flow rates	Lower flow rates
Loss of flow with higher heads	Flow rate less affected by head
Low irradiance reduces ability to achieve head	Low irradiance has little effect on head

Potential grit abrasion	Unaffected by grit

The graphical relationship between head and flow is called the *hydraulic pump curve*, illustrated in Figure 6.41. To help understand the shape of the curve, imagine a small centrifugal pump connected to a hose that has one end submerged in a pond. Raising the open end of the hose higher and higher (increasing the head) will result in less and less flow until a point is reached at which there is no flow at all. Similarly, as the open end is lowered, head decreases and flow increases until the hose is flat on the ground and the flow reaches a maximum.

FIGURE 6.41 Interpreting *H–Q* pump curves using a simple garden hose analogy.



Electrical *I–V* curves and hydraulic *Q–H* curves share many similar features. For example, recall that the electrical power delivered by a PV is the product of *I* times *V* and the MPP is at the knee of the *I–V* curve. For the hydraulic side, the power delivered by the pump to the fluid is given by

$$P = \rho HQ \tag{6.37}$$

where ρ is fluid density. In American units,

$$\begin{aligned} P(\mathrm{W}) &= 8.34\ \mathrm{lb/gal} \times H(\mathrm{ft}) \times Q(\mathrm{gal/min}) \times (1\ \mathrm{min}/60\ \mathrm{s}) \\ &\quad \times 1.356\ \mathrm{W/(ft\text{-}lb/s)} \\ P(\mathrm{W}) &= 0.1885 \times H(\mathrm{ft}) \times Q(\mathrm{gal/min}) \end{aligned} \tag{6.38}$$

In SI units,

$$P(\mathrm{W}) = 9.81 \times H(\mathrm{m}) \times Q(\mathrm{L/s}) \tag{6.39}$$

When *Q* is zero, there is no power delivered to the fluid; when the head *H* is zero, there is no power delivered either. Similar to PV curves, the MPP occurs at the spot at which you can fit the biggest rectangle under the *H–Q* curve.

Note the pump curve suggested in Figure 6.41 is a single curve corresponding to a particular voltage applied to the pump. As we have seen, in a directly coupled PV-to-pump system, pump voltage varies throughout the day (Fig. 6.40). Many manufacturers of pumps intended for solar applications will supply pump curves for voltages corresponding to

nominal 12-V module voltages. Figure 6.42 shows an example of a set of pump curves for the Jacuzzi SJ1C11 DC centrifugal pump, which is intended for use with PVs. Individual curves have been given for 15-, 30-, 45-, and 60-V inputs. A typical "12-V" PV module operating near the knee of its *I–V* curve delivers about 15 V, so these pump voltages are meant to correspond to 1, 2, 3, and 4, typical "12-V" PV modules wired in series. Also shown are indications of the efficiency of the pump as a function of flow rate and head. Note that the peak in efficiency (about 44%) occurs along the knee of the pump curves, which is exactly analogous to the case for a PV *I–V* curve.

FIGURE 6.42 Pump curves for the Jacuzzi SJ1C11 pump for various input voltages. Pump efficiencies are also shown, with the peak along the knee of the curves.

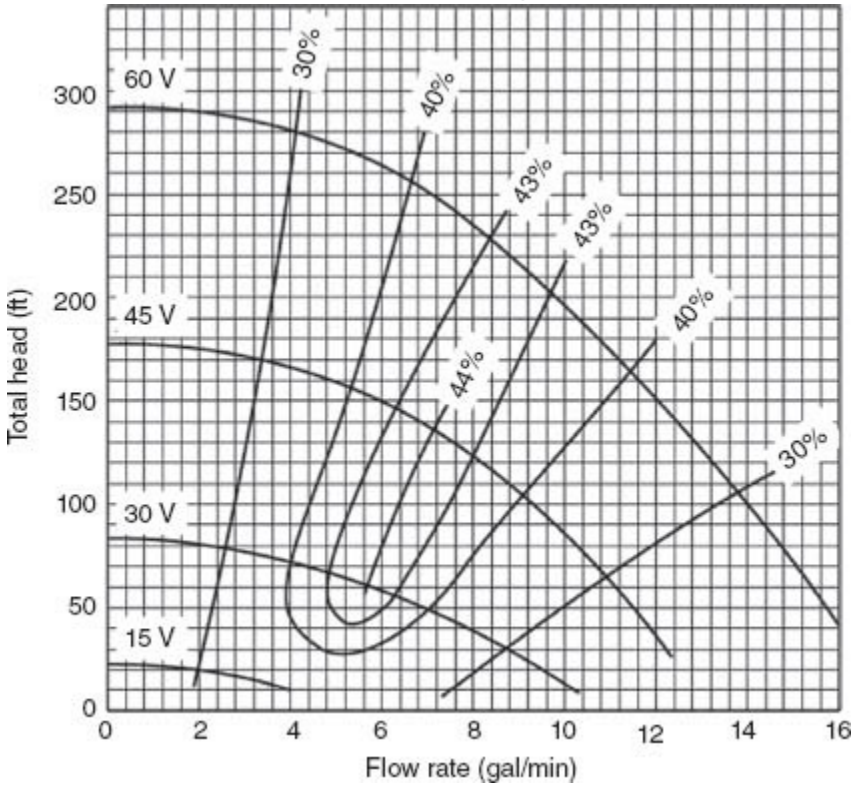


Figure 6.42 has enough information on it to derive the pump *I–V* curve. By selecting various intersection points where pump efficiency and pump voltage lines cross and coupling those data with Equation 6.38, we can create a table of pairs of *I* and *V*. For example, the 30%-efficiency line crosses the 15-V line at Q = 2 gal/min and H = 20 ft. From Equation 6.38

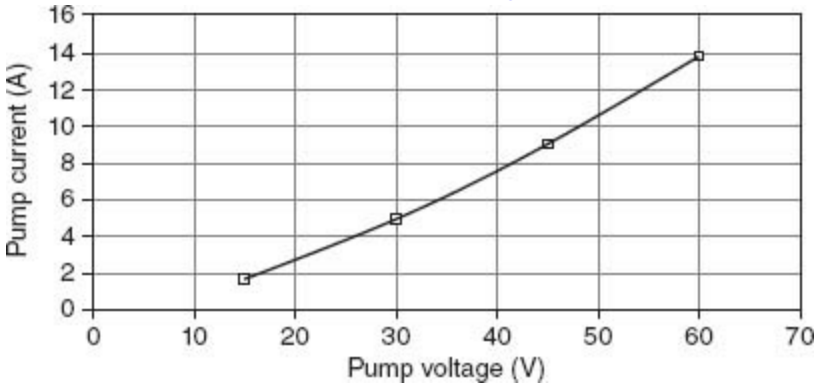
$$P = \frac{0.1885 \times H(\text{ft}) \times Q(\text{gal/min})}{\text{Efficiency}} = \frac{0.1885 \times 20 \times 2}{0.30} = 25 \text{ W}$$

And, from $P = VI$, at 15 V, current is 25 W/15 V = 1.7 A. Table 6.16 shows the data points used to plot the pump *I–V* curve shown in Figure 6.43.

TABLE 6.16 Deriving the Pump *I–V* Curve Using Data From Figure 6.42

V	Gal/min	Head (ft)	Efficiency (%)	P (W)	I (A)
15	2	20	30	25	1.7
30	5.6	62	44	149	5.0
45	6.4	145	43	407	9.0
60	6.8	258	40	827	13.8

FIGURE 6.43 The pump *I–V* curve derived from Figure 6.42.



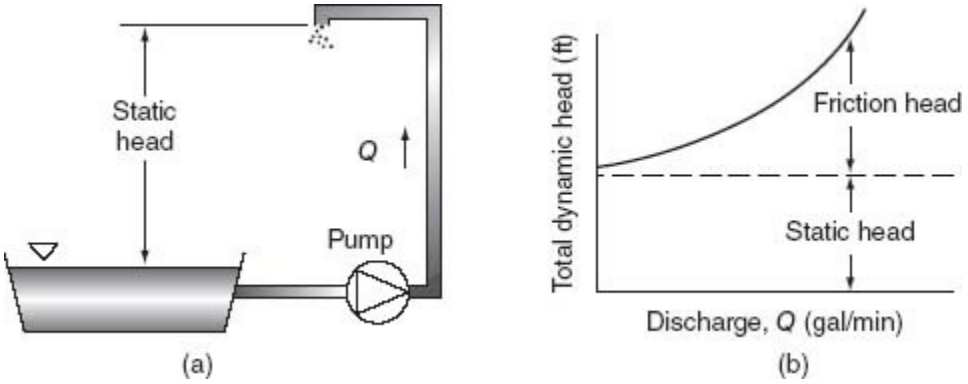
If the *I–V* pump curve just derived in Figure 6.43 is superimposed onto the *I–V* curve for PVs directly connected to the pump, the intersection point determines the voltage delivered to the pump. To determine fluid flow rates, however, we need to introduce the hydraulic side of the system.

6.6.3 Hydraulic System Curves

Figure 6.44 shows an open system in which water is to be raised from one level to the next. The vertical distance between the lower water surface and the elevation of the discharge point is referred to as the *static head* (or gravity head), and in the United States, it is usually given in "feet or inches of water." Head can also be measured in units of pressure, such as pounds per square inch (psi) or Pascals (1 psi = 6895 Pa). To convert between these two equivalent approaches to units, just picture the pressure that a cube of water exerts on its base. For example, a 1-ft cube weighing 62.4 lb would exert a pressure on its 144 square inches of base equal to

$$1 \text{ ft of head} = 62.4 \text{ lb}/144 \text{ in}^2 = 0.433 \text{ psi} \tag{6.40}$$

FIGURE 6.44 An "open" system (a) and the resulting "system curve" (b) showing the static and friction head components.



Conversely, 1 psi = 2.31 ft of water. Typical city water pressure is about 60 psi which corresponds to a column of water roughly 140 ft high.

If the pump is capable of supplying only enough pressure to the column of water to overcome the static head, the water would rise in the pipe and just make it to the discharge point and then stop. In order to create flow, the pump must provide an extra amount of head to overcome friction losses in the piping system. These friction losses rise roughly as the square of the flow velocity (as is suggested in Fig. 6.44). They depend on the roughness of the inside of the pipe and the numbers and types of bends and valves in the system. For example, the pressure drop per 100 ft of plastic water pipe for various flow rates and diameters is presented in Table 6.17. In keeping with U.S. tradition, flow rates are given in gal/min, pipe diameters in inches, and head in feet of water.

TABLE 6.17 Pressure Loss Due to Friction in Plastic Pipe for Various Nominal Tube Diameters[a]

Gal/min	0.5 in	0.75 in	1 in	1.5 in	2 in	3 in
1	1.4	0.4	0.1	0.0	0.0	0.0
2	4.8	1.2	0.4	0.0	0.0	0.0
3	10.0	2.5	0.8	0.1	0.0	0.0
4	17.1	4.2	1.3	0.2	0.0	0.0
5	25.8	6.3	1.9	0.2	0.0	0.0
6	36.3	8.8	2.7	0.3	0.1	0.0
8	63.7	15.2	4.6	0.6	0.2	0.0
10	97.5	26.0	6.9	0.8	0.3	0.0
15		49.7	14.6	1.7	0.5	0.0
20		86.9	25.1	2.9	0.9	0.1

[a]Units are feet of water per 100 ft of tube.

Table 6.18 gives pressure drops of various plumbing fittings expressed as equivalent lengths of pipe. For example, each 2-in 90° elbow (ell) in a plumbing run adds to the pressure drop the same amount as would 5.5 ft of straight pipe. So we can add up all the bends and valves in a pipe run and find what equivalent length of straight pipe would have the same pressure drop.

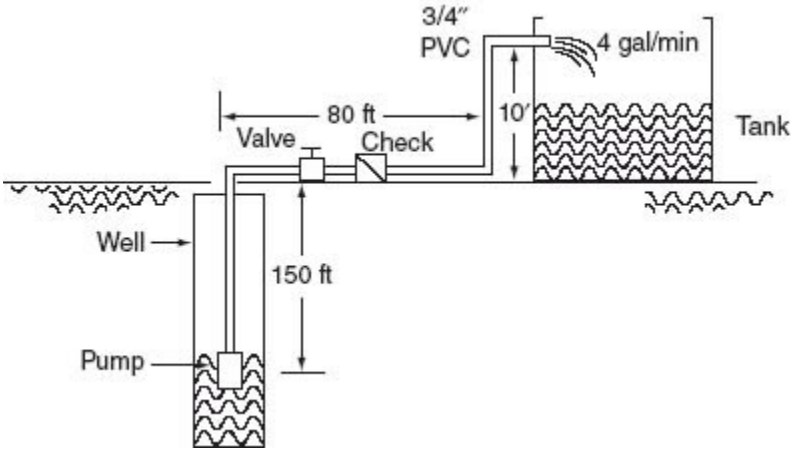
TABLE 6.18 Friction Loss in Valves and Elbows Expressed as Equivalent Lengths of Tube[a]

Fitting	0.5 in	0.75 in	1 in	1.5 in	2 in	3 in
90° ell	1.5	2.0	2.7	4.3	5.5	8.0
45° ell	0.8	1.0	1.3	2.0	2.5	3.8
Long sweep ell	1.0	1.4	1.7	2.7	3.5	5.2
Close return bend	3.6	5.0	6.0	10.0	13.0	18.0
Tee-straight run	1.0	2.0	2.0	3.0	4.0	5.0
Tee-side inlet or outlet	3.3	4.5	5.7	9.0	12.0	17.0
Globe valve, open	17.0	22.0	27.0	43.0	55.0	82.0
Gate valve, open	0.4	0.5	0.6	1.0	1.2	1.7
Check valve: swing	4.0	5.0	7.0	11.0	13.0	20.0

[a]Units are feet of pipe for various nominal pipe diameters.

The sum of the friction head and the static head is known as the *total dynamic head* (*H*).

Example 6.16 Total Dynamic Head for a Well. What pumping head would be required to deliver 4 gal/min from a depth of 150 ft. The well is 80 ft from the storage tank and the delivery pipe rises another 10 ft. The piping is 3/4-in diameter PVC, there are three 90° elbows, one swing-type check valve, and one gate valve in the line.



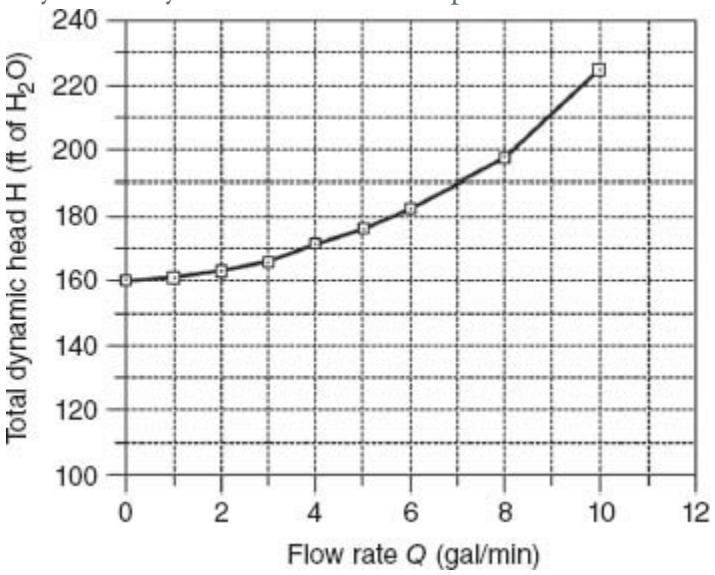
Solution. The total length of pipe is 150 + 80 + 10 = 240 ft. From Table 6.18, the three ells add the equivalent of 3 × 2.0 = 6 ft of pipe; the check valve adds the equivalent of 5 ft of pipe; the gate valve (assuming it is totally open) adds the equivalent of 0.5 ft of pipe. The total equivalent length of pipe is therefore 240 + 6 + 5+ 0.5 = 251.5 ft.

From Table 6.17, 100 ft of 3/4-in pipe at 4 gal/min has a pressure drop of 4.2 ft/100 ft of tube. Our friction-head requirement is therefore 4.2 × 251.5/100 = 10.5 ft of water.

The water must be lifted 150 + 10 = 160 ft (static head). Total head requirement is the sum of static and friction heads, or 160 + 10.5 = 170.5 ft of water pressure.

If the process followed in Example 6.16 is repeated for varying flow rates, a plot of total dynamic head *H* (static plus friction) versus flow rate, called the *hydraulic system curve*, can be derived. The hydraulic system curve for the above example is given in Figure 6.45.

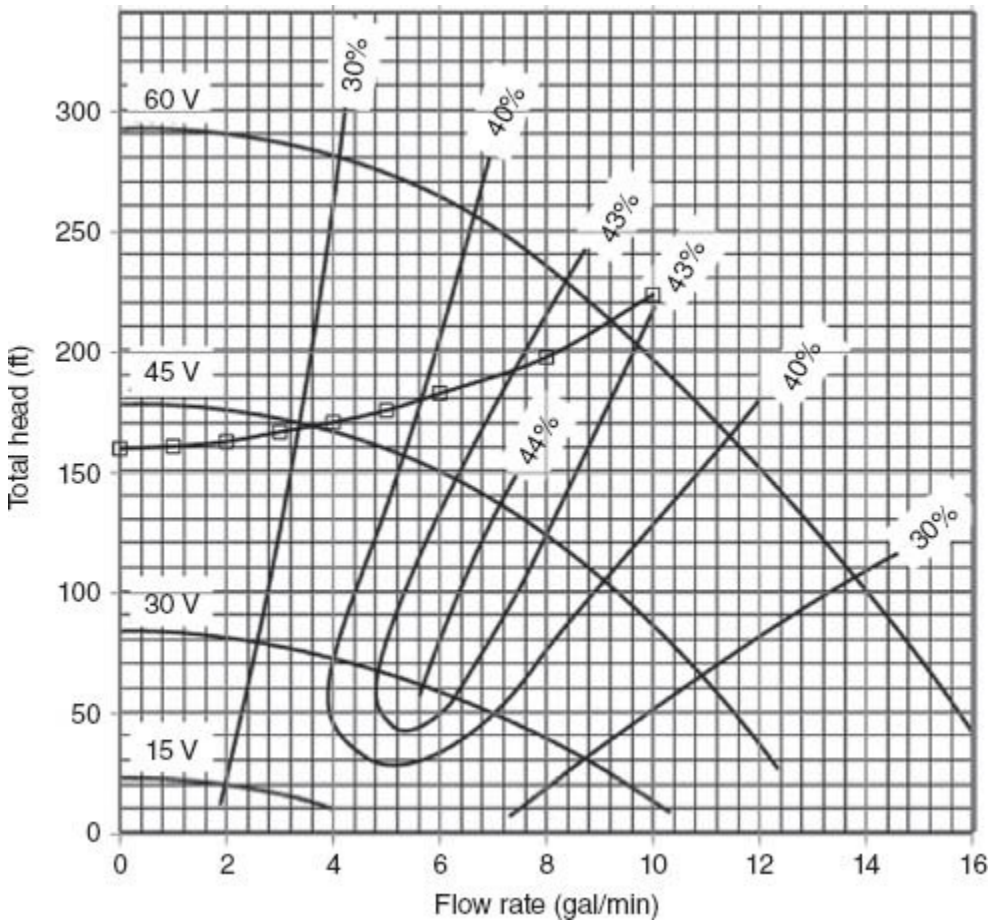
FIGURE 6.45 The hydraulic system curve for Example 6.16.



6.6.4 Putting it All Together to Predict Performance

Just as an *I–V* curve for a PV load is superimposed onto the *I–V* curves for the PVs, so too is the *Q–H* system curve superimposed onto the *Q–H* pump curve to determine the hydraulic operating point. For example, superimposing the system curve of Figure 6.45 onto the pump curves in Figure 6.42 gives us the diagram in Figure 6.46. A glance at the figure tells us a lot. For example, this pump will not deliver any water unless the voltage applied to the pump is at least about 40 V. At 45 V, about 3.2 gal/min would be pumped, while at 60 V the flow would be about 9.2 gal/min.

FIGURE 6.46 The system curve for Example 6.17, 150-ft well, superimposed onto the pump curves for the Jacuzzi SJ1C11. No flow occurs until pump voltage exceeds about 40 V.



What started out to be the very simplest physical combination of a PV module directly connected to a DC pump has turned into a quite complex, but fascinating, process in which a combination of nonlinear curves are laid one on top of another to try to predict hour-by-hour pumping rates. On the electrical side, by superimposing the pump curve onto the time-varying PV *I–V* curves, we can find hour-by-hour voltages delivered to the pump. By superimposing the hydraulic system curve onto the pump curves that vary with voltage, we can find the hour-by-hour pumping rates.

Let us illustrate the process with an example.

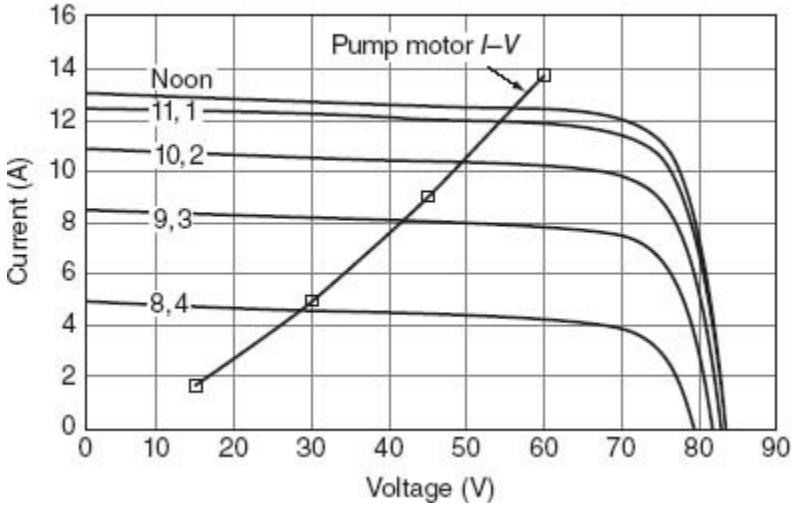
Example 6.17 Estimating Total Gallons Per Day Pumped. Pick a solar collector and use

it to estimate the daily water pumped using the Jacuzzi SJ1C11 pump to deliver water from the 150-ft well analyzed in Example 6.16. The pump *I–V* curve is given in Figure 6.43. Design for a clear day in December at latitude 20° N with a south-facing 20° tilt array.

Solution. Figure 6.46 suggests that we will need a PV array that can deliver at least 40 V for much of the day and a glance at Figure 6.43 says it will need to supply over 8 A during that time. A combination of any of the collectors described in Table 5.3 can be used, but the simplest system will be one with the fewest modules, so let us try the SunPower E20/435 with V_{MPP} = 72.9 V, I_{MPP} = 5.97 A. The voltage is plenty for this task, but we will need two modules in parallel to get into the right current range.

From Appendix D, we get the hourly irradiance values shown below. By scaling the 1-sun short-circuit current for a pair of modules in parallel (I_{SC} = 6.43 A × 2 at 1000 W/m^2), we get the short-circuit currents at each hour. Then, all that we need to do is for each hour slide the 1-sun *I–V* curve down to match the I_{SC} for that hour. Adding the *I–V* curve for the pump motor from Figure 6.43 results in the following figure.

Two Parallel Modules 1-sun I_{SC} = 12.86 A									
Time	8	9	10	11	Noon	1	2	3	4
Insolation W/m^2	393	645	832	949	988	949	332	645	393
I_{SC} @ Insolation	5.1	8.3	10.7	12.2	12.7	12.2	10.7	8.3	5.1



From the figure, we can write down hourly voltages, which when coupled with the hydraulic curves in Figure 6.46 leads to the following table:

Time	8	9	10	11	Noon	1	2	3	4	Total gallons
Voltage	29	42	49	54	57	54	49	42	29	
Gal/min	0	0.5	7.5	7.8	8	7.8	7.5	0.5	0	
Gal/h	0	30	450	468	480	468	450	30	0	2376

So, our final design is two 435-W modules in parallel, directly coupled to the pump that should deliver close to 2400 gal over the course of one clear day.

REFERENCES

Blair N, Dobos A, Sather N. Case studies comparing System Advisor Model (SAM) results to real performance data. In: 2012 World Renewable Energy Forum, Denver. 2012 May 13–17.

Goodrich A, James T, Woodhouse M. Residential, commercial, and utility-scale photovoltaic system prices in the United States: current drivers and cost-reduction opportunities. National Renewable Energy Laboratory; Golden, CO; 2012 Feb. NREL/TP-6A20-53347.

Jordan DC, Smith RM, Osterwald CR, Gelak E, Kurtz SR. Outdoor PV degradation comparison. National Renewable Energy Laboratory; Golden, CO; 2011 Feb. NREL/CP-5200-47704.

Marion B, Adelstein J, Boyle K. Performance parameters for grid-connected photovoltaic systems. In: 31st IEEE photovoltaic specialist conference; Lake Buena Vista, FL; 2005.

Rosen K, Meier A. Energy use of U.S. consumer electronics at the end of the 20th century. Lawrence Berkeley National Labs, Berkeley, CA; 2000. LBNL-46212.

Sandia National Laboratories. *Maintenance and Operation of Stand-alone Photovoltaic Systems.* Albuquerque, NM: US Department of Energy; 1991.

Sandia National Laboratories. *Stand-alone Photovoltaic Systems Handbook of Recommended Practices.* Albuquerque, NM: US Department of Energy; 1995.

Schuermann, K, Boleyn DR, Lily PN, Miller S. Measured output for nineteen residential PV systems: updated analysis of actual system performance and net metering impacts. Proceedings of the 31st American solar energy society annual conference; Reno; 2002.

Youngren E. Shortcut to failure: why whole system integration and balance of systems components are crucial to off-grid PV system sustainability. Solar Nexus International; IEEE Global Humanitarian Technology Conference, Seattle, WA. Oct 30-Nov 1; 2011.

PROBLEMS

6.1 A clean, 1 m^2, 15%-efficient module (STC), has its own 90%-efficient inverter. Its NOCT is 45°C and its rated power degrades by 0.5%/°C above the 25°C STC.

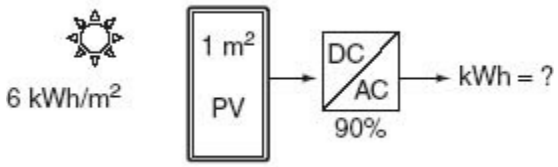


FIGURE P6.1

a. What is the STC rated power of the module?

b. For a day with 6 kWh/m^2 of insolation, find the kWh that it would deliver if it operates at its NOCT temperature. Assume the only deratings are due to temperature and inverter efficiency.

6.2 NREL's PVWATTS website predicts that 5.56 kWh/m^2/d of insolation on a south-facing, 40° tilt array in Boulder, CO, will deliver 1459 kWh/yr of AC energy per $kW_{DC, STC}$ of PV modules.

a. Using the "peak-hours" approach to performance estimation, what overall derate factor (including temperature effects) would yield the same annual energy delivered?

b. Since PVWATTS' derate value of 0.77 includes everything but temperature impacts, what temperature-induced derating needs to be included to make the peak-hours approach predict the same annual energy?

(Overall derate = PVWATTS derate × Temperature derate).

c. Use the PVWATTS website to find the overall annual temperature derate factors for a cold place (Bismarck, ND) and a hot place (Houston, TX). Use the same south-facing, 40° tilt array.

6.3 You are to size a grid-connected PV system to deliver 4000 kWh/yr in a location characterized by 5.5 kWh/m^2/d of insolation on the array.

a. Find the DC, STC rated power of the modules assuming a 0.72 derate factor.

b. Find the PV collector area required if, under standard test conditions, these are 18%-efficient modules.

c. Find the first-year net cost of electricity ($/kWh) if the system costs $4 per peak watt ($4/$W_{DC, STC}$), it is paid for with a 5%, 30-year loan, interest on the loan is tax deductible, and the owner is in a 29% marginal tax bracket.

6.4 The beginning of a financial spreadsheet for a PV system is shown below. Fill in the row for year 2.

TABLE P6.4

Year	Payment	Interest	Delta Balance	Loan Balance	Tax Savings	Net Cost	$/kWh
0				$8000.00			
1	$500.00	$400.00	$100.00	$7900.00	$120.00	$380.00	$0.19000
2	?	?	?	?	?	?	?

6.5 Recreate the cash flow spreadsheet provided in Table 6.6 and see whether you can reproduce those same results.

a. In what year do you first see a positive cash flow?

b. What is the present value of the cash flow in year 14?

c. What NPV do you get when you set the discount rate to be the same as the IRR?

d. Eliminate the down payment and see what happens to the IRR. Then try paying for the whole system with cash. Again, compare IRR and comment.

e. Find the NPV and IRR for a 4-kW system in an area with 5.5-kWh/m^2/d insolation, using a derating of 0.72. Keep everything else the same.

6.6 A grid-connected PV array consisting of sixteen 150-W modules can be arranged in a number of series and parallel combinations: (16S, 1P), (8S, 2P), (4S, 4P), (2S, 8P), (1S, 16P). The array delivers power to a 2500-W inverter. The key characteristics of modules

and inverter are given below.

Using the input voltage range of the inverter MPPT and the maximum input voltage of the inverter as design constraints, what series/parallel combination of modules would best match the PVs to the inverter? Check the result to see whether the inverter maximum input current is satisfied. For this simple check, you do not need to worry about temperatures.

TABLE P6.6

Inverter		Module	
Maximum AC power	2500 W	Rated power $P_{DC,STC}$	150 W
Input voltage range for MPP	250–550 V	Voltage at MPP	34 V
Maximum input voltage	600 V	Open-circuit voltage	43.4 V
Maximum input current	11 A	Current at MPP	4.40 A
		Short-circuit current	4.8 A

6.7 Redo Example 6.4 using the 85.7-W CdTe modules described below and the same Sunny Boy 5-kW inverter to supply about 5000 kWh/yr in an area with 5.32 kWh/m^2/d of insolation. Assume the same 0.75 derate factor.

Module characteristics:

Peak power	87.5 W
Rated voltage V_{MPP}	49.2 V
Open-circuit voltage V_{OC}	61 V
Short-circuit current I_{SC}	1.98 A
Temperature coefficient of power	–0.25%/K
Temperature coefficient of V_{OC}	–0.27%/K
Temperature coefficient of I_{SC}	–0.04%/K
NOCT	45°C

a. What DC-STC power (kW) would be required to provide 5000 kWh/yr?

b. Before worrying about the inverter, how many modules would be required?

c. Using the 600-V maximum allowable voltage on a residential roof, what is the maximum number of modules in a single string if the coldest temperature expected is –5°C? Using this constraint, what is the best number of strings and modules per string?

d. Use the coldest ambient temperature to help determine the maximum number of modules per string need to be sure the MPP stays below the 480 V that the inverter needs for proper tracking.

e. What is the minimum number of modules per string to satisfy the inverter constraint that says it needs at least 250 V to properly maintain MPP tracking. Assume the hottest ambient temperature is 40°C.

f. The maximum allowable DC input current for the inverter is 21 A. What is the maximum number of strings that would be allowed?

g. Using all of these constraints, choose the best combination of strings and number of modules per string to satisfy the design.

6.8 You have four PV modules with identical *I–V* curves (I_{SC} = 1 A, V_{OC} = 20 V) as shown. There are three ways you could wire them up to deliver power to a DC motor (which acts like a 10-Ω load):

Draw the *I–V* curves for all three combinations on the same graph. Which wiring system would be best? Briefly explain your answer.

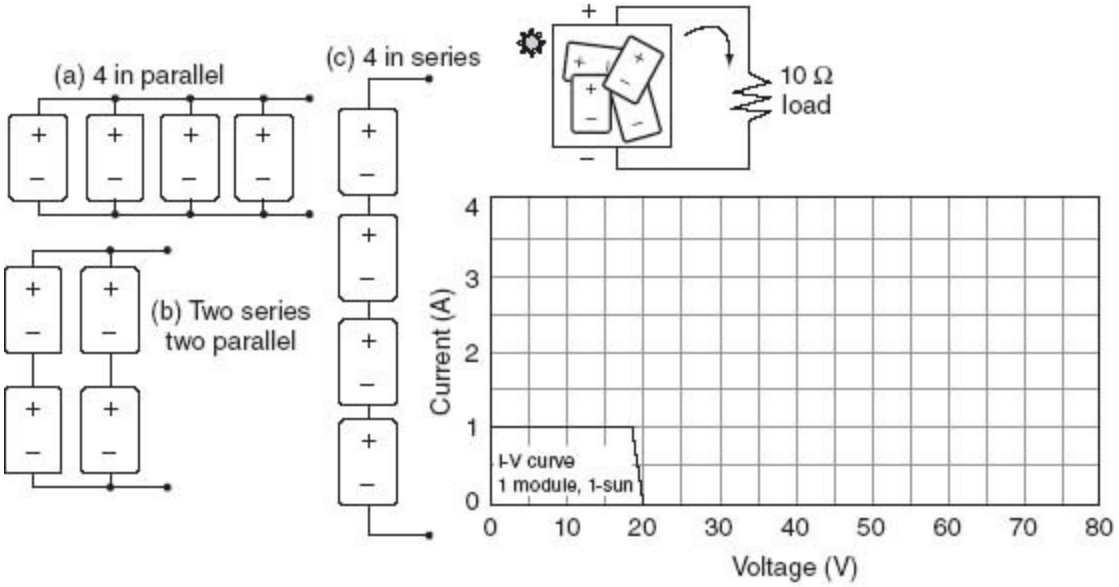


FIGURE P6.8

6.9 The summer TOU rate structure shown in Table 6.7 includes an off-peak energy charge of $0.0846/kWh for usage up to 700 kWh/mo and $0.166/kWh for usage above that base. During the peak demand period, it is a flat $0.27/kWh.

a. What will the customer's bill be for 1000 kWh used off peak and 800 kWh on peak?

b. Suppose the customer signs up for the TOU + CPP rate structure. During 3 days, a critical peak pricing period is announced during which time electricity costs $0.75/kWh. If they use 100 of their 800 peak period kilowatt-hours during that time, what will their bill be that month?

c. Suppose the customer shuts off their power during those CPP periods, what would now be the utility bill?

6.10 A small office building that uses 40, 000 kWh/mo during the summer has a peak demand of 100 kW. An 80-kW PV system is being proposed that will provide 20, 000 kWh/mo. The before and after demand curves are shown in Figure P6.10.

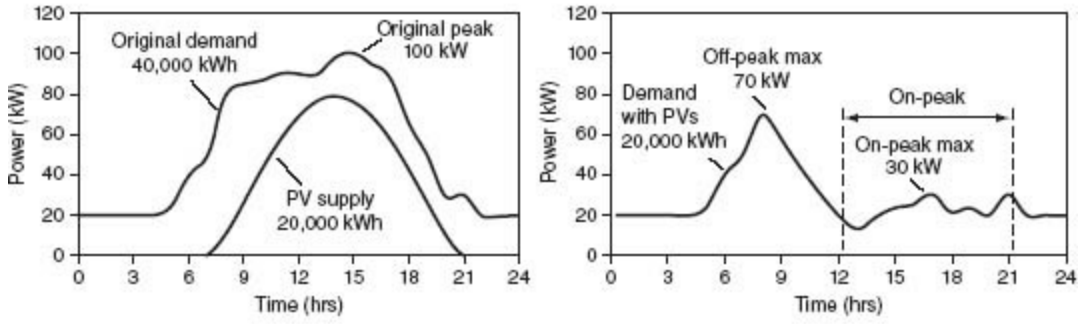


FIGURE P6.10

The utility rate schedule includes demand charges that vary depending on whether the customer has signed up for TOU rates or not. And the TOU rates have a demand charge that varies with on- or off-peak periods.

TABLE P6.10

	Non-TOU Rates ($)	TOU Rates ($)	
Energy charge ($/kWh)	0.06	0.05	
Demand charge ($/mo/kWp)	12.00	14.00	On peak
		5.00	Off peak

a. What would be the utility bill without the PVs when the non-TOU rate schedule has been chosen?

b. Which rate structure would be the best for the customer if they install the PVs. How much money would the PVs save with that rate structure?

6.11 A 100-kW PV system is being proposed for a commercial building in an area with 5.5-kWh/m^2/d insolation. The before tax-credit cost of the system is $5/Wp. Assuming a 0.72 derate factor:

a. What is the annual electricity production that might be expected?

b. What is the MACRS depreciable basis for the system after a 30% tax credit has been taken?

c. For a corporate tax rate of 38% and a discount rate of 7%, find the present value of the MACRS depreciation.

d. What is the effective net system cost after the tax credit and MACRS depreciation? Effective $/kW cost of the system?

6.12 In Example 6.8, the time of day (TOD) factors for a PPA were worked out for a PV array that faces due south. Since those TOD factors favor afternoon generation, consider the following clear-sky hourly insolation values for those same collectors now facing toward the southwest.

Solar Time	Insolation (W/m^2)
6	60
7	92
8	282
9	484

10	670
11	821
12	923
1	967
2	947
3	862
4	716
5	516
6	272

Compare the revenue generated by the south-facing versus southwest-facing collectors under the following conditions:

a. One hour at solar noon on a summer weekday.

b. One week at solar noon in the summer.

c. One week at 3:00 P.M. in the summer.

d. Create a spreadsheet to work out the entire month's revenue to compare to the $32, 334 that a south-facing collector will generate. What is the average PPA price paid per kWh generated?

6.13 Suppose a 12-V battery bank rated at 200 Ah under standard conditions needs to deliver 600 Wh over a 12-h period each day. If they operate at −10°C, how many days of use would they be able to supply?

6.14 Consider the design of a small PV-powered LED flashlight. The PV array consists of eight series cells, each with rated current 0.3 A at 0.6 V. Storage is provided by three series AA batteries that each store 2 Ah at 1.2 V when fully charged. The LED provides full brightness when it draws 0.4 A at 3.6 V.

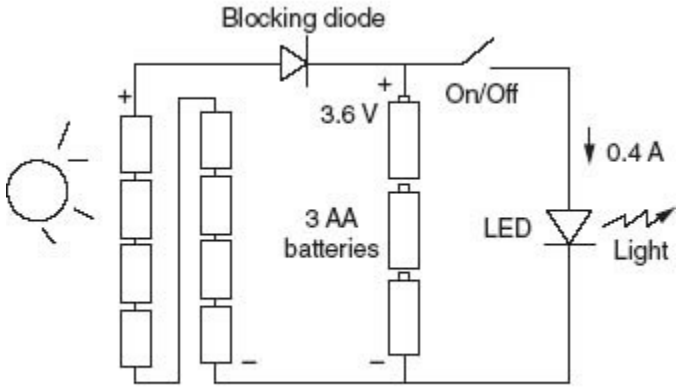


FIGURE P6.14

The batteries have a Coulomb efficiency of 95% and for maximum cycle life can be discharged by up to 80%. Assume the PVs have a 0.90 derating due to dirt and aging.

a. How many hours of light could this design provide each evening if the batteries are fully charged during the day?

b. How many kWh/m^2/d of insolation would be needed to provide the amount of light found in (a)?

c. With 14%-efficient cells, what PV area would be required?

6.15 You are to design a 24-V, all-DC, stand-alone PV system to meet a 2.4 kWh/d demand for a small, isolated cabin. You want to size the PV array to meet the load in a month with average insolation equal to 5.0 kWh/m^2/d.

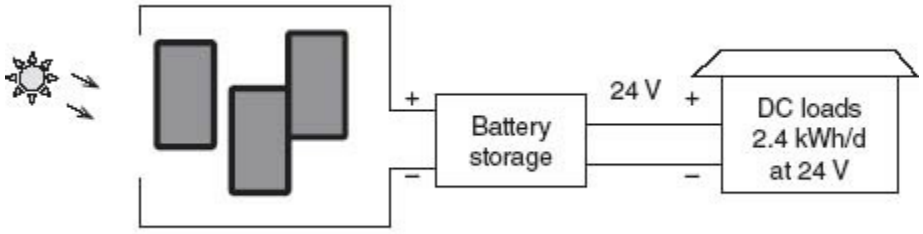


FIGURE P6.15

Your chosen PVs have their 1-sun MPP at V_R = 18 V and I_R = 5 A. Assume a 0.80 derate factor for dirt, wiring, module mismatch (i.e., 20% loss). You will use 200-Ah, 12-V batteries with 100% Coulomb efficiency.

a. How many PV modules are needed (you may need to round up or down)? Sketch your PV array.

b. How many 200-Ah, 12-V, deep-cycle batteries would be required to cover 3 days of no sun if their maximum discharge depth is 75%? Show how you would wire them up.

6.16 Analyze the following simple PV/battery system, which includes four PV modules each with rated current and voltage as shown, and four 160-Ah, 6-V batteries with 90% Coulomb efficiency. An 85%-efficient inverter feeds the AC load. Note there is no MPPT.

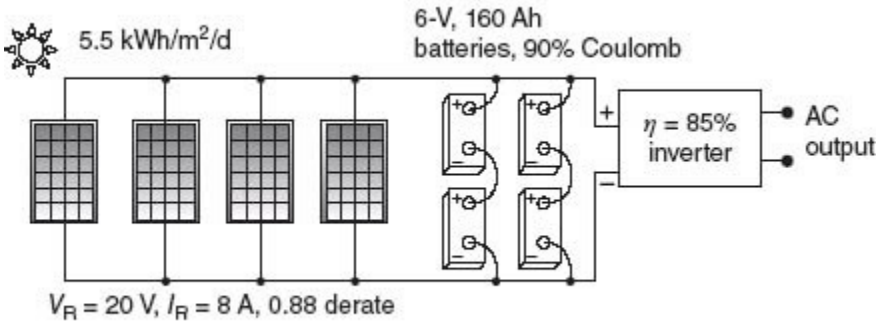


FIGURE P6.16

a. With 5.5 kWh/m^2/d of insolation, and 12% module loss due to dirt, wiring losses, and so on, estimate the kWh/d that would reach the loads (assume all PV current passes through the batteries before it reaches the inverter).

b. If the load requires 1 kWh/d, for how many cloudy days in a row can previously fully charged batteries supply the load with no further PV input? Assume 80% of their ampere-hour capacity is available.

6.17 Suppose the system in Problem 6.16 is redesigned to include an MPPT and a 97%-efficient charge controller. Assuming a typical 80% round-trip energy efficiency for the

batteries and a module derate of 0.88, how many kWh/d would reach the load with the same 5.5 kWh/m^2/d insolation?

6.18 Following the guidelines given in Figure 6.34 for the design of off-grid PV systems, design a system that will deliver an average of 10 kWh/d of AC energy for a house located in a region with average insolation equal to 5 kWh/m^2/d.

a. How many $kW_{DC, STC}$ of PVs should be used?

b. For a 48-V battery system, how many ampere-hours of storage would be needed to provide 3 days worth of energy with no sun? Assume maximum discharge of 80%.

c. Using the cost guidelines provided in Example 6.15, what would be the capital cost of this system?

d. Assuming a 4%, 20-year loan, what would be the cost per kWh?

e. Suppose the diesel generator with efficiency curve shown in Figure 6.35 operates at 70% of rated power while burning diesel that costs $4.50/gal. What is its cost per kWh generated?

6.19 Consider a directly coupled PV pump system with PV *I–V* curves and pump/system *H–Q* curves as shown below. Note that the startup characteristics of the pump motor as it tries to overcome static friction before it can actually start pumping.

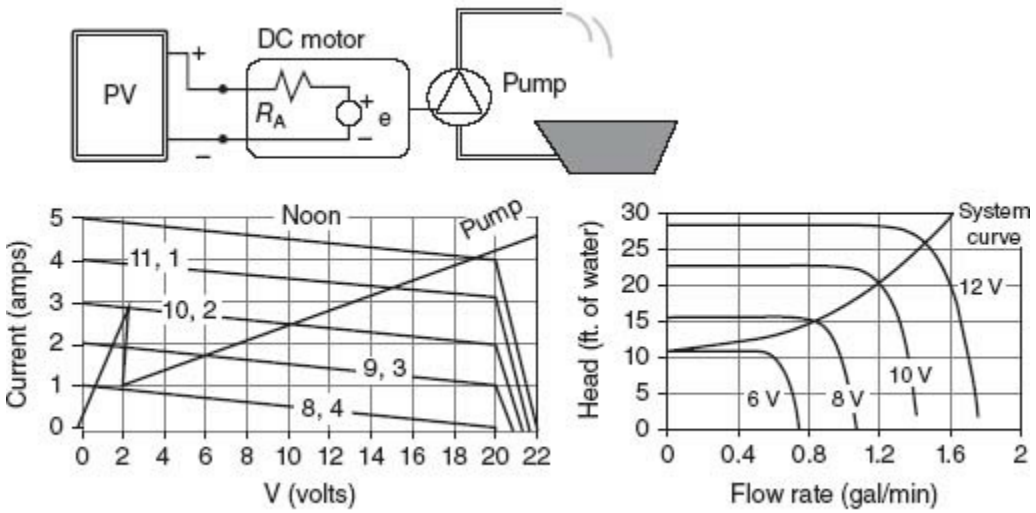


FIGURE P6.19

a. At what time in the morning will the water start to flow?

b. What will the flow rate be a little after 10:00 A.M.?

c. At what time in the afternoon will the flow stop?

d. Assuming the equivalent circuit shown above for the pump motor, what is the motor's armature resistance, R_A?

6.20 A single PV module is directly connected to a DC water pump. The module has 41 cells, each of which has a parallel resistance of 9 Ω. The *I–V* curves for the DC pump motor and the PV module under 1-sun of insolation are shown below. Also shown are the hydraulic *Q–H* curves for the pump and its load.

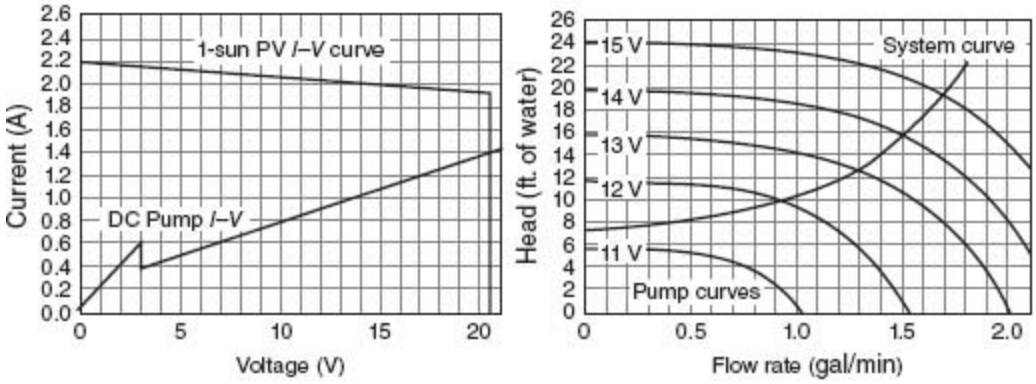


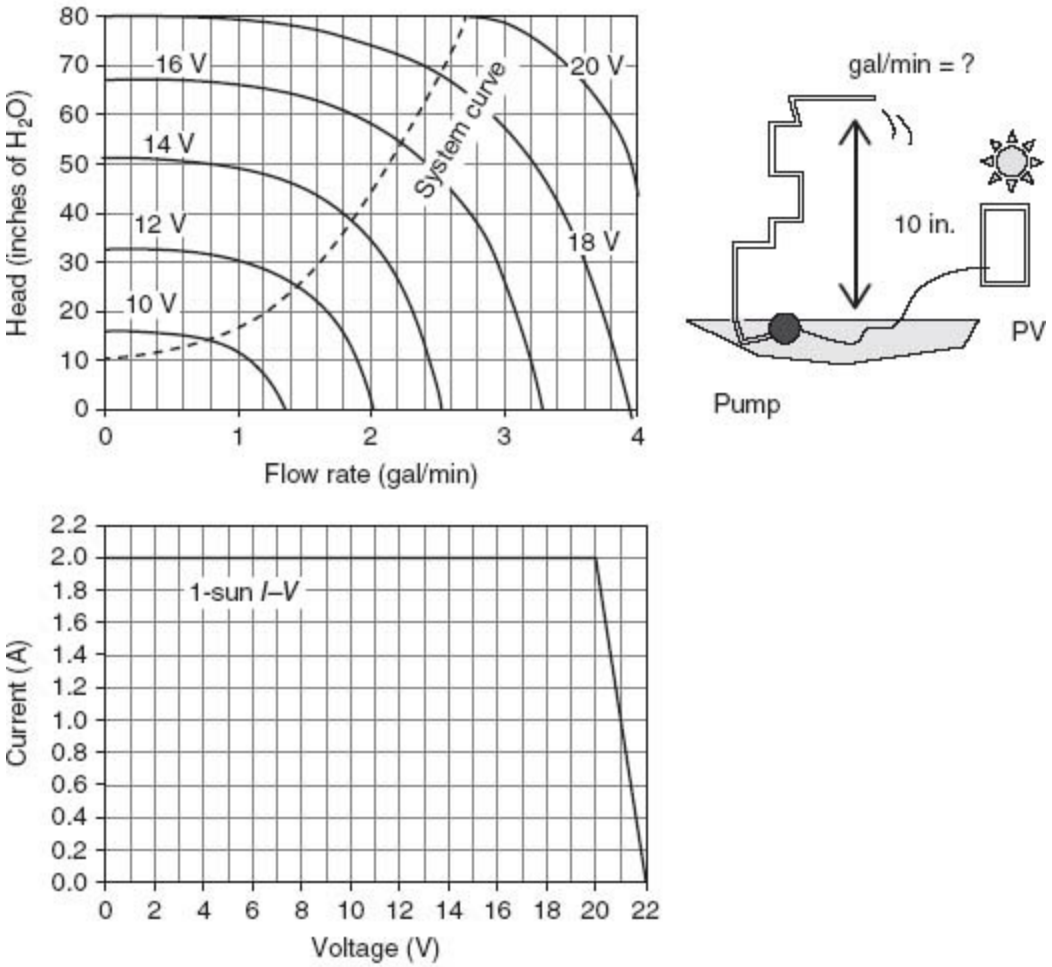
FIGURE P6.20

a. At some time in the morning, the pump is delivering 1.5 gal/min of flow. At that time sketch the PV *I–V* curve. What must the insolation have been at that time?

b. At that time in the morning, what will the flow rate drop to if one cell is completely shaded?

6.21 Suppose you are setting up a little fountain for a pond using a PV-powered DC pump. Shown below are pump curves for various voltages along with a system curve including a static head of 10 in. The PV *I–V* curve and hourly insolations are also shown.

Suppose the electrical characteristics of the pump can be modeled as a simple 10-Ω resistance. Find the hourly flow rates (gal/min) and estimate the total gallons pumped in 1 day (assume insolation is constant over each 1-h interval).



Time	8 A.M.	9	10	11	12	1	2	3	4 P.M.
Insolation (kW/m^2)	0.4	0.5	0.7	0.9	1.0	0.9	0.7	0.5	0.4
gal/min = ?									

FIGURE P6.21

CHAPTER 7

WIND POWER SYSTEMS

7.1 HISTORICAL DEVELOPMENT OF WIND POWER

Wind has been utilized as a source of power for thousands of years for such tasks as propelling sailing ships, grinding grain, pumping water, and powering factory machinery. The world's first wind turbine used to generate electricity was built by a Dane, Poul la Cour, in 1891. It is especially interesting to note that la Cour used the electricity generated by his turbines to electrolyze water, producing hydrogen for gaslights in the local schoolhouse. In that regard, we could say he was a century ahead of his time since the vision that many have for the twenty-first century includes grid-storage systems based on excess photovoltaic and wind power electrolyzing water to make hydrogen that could be used in fuel cells.

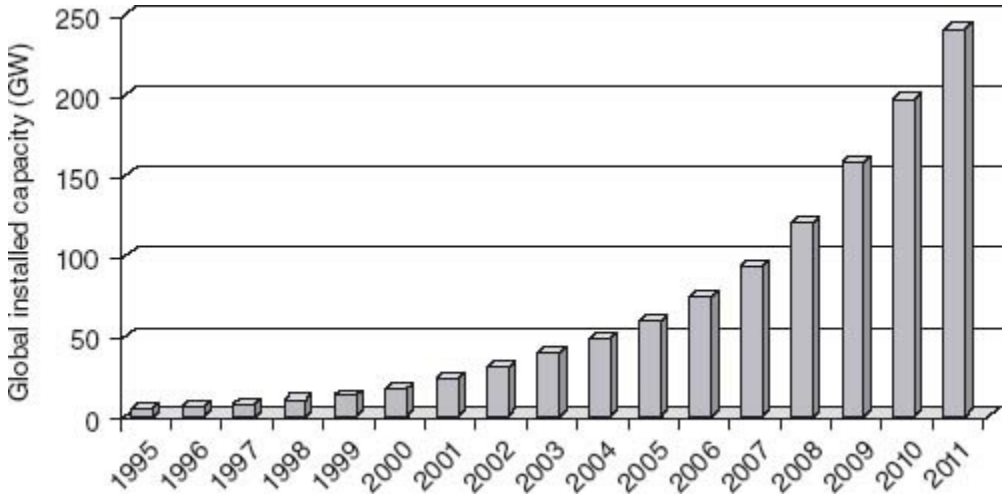
In the United States, the first wind-electric systems were built in the late 1890s, and by the 1930s and 1940s, hundreds of thousands of small-capacity, wind-electric systems were in use in rural areas not yet served by the electricity grid. In 1941, a wind turbine comparable in size to the largest ones in operation at the turn of the century went into operation at Grandpa's Knob in Vermont. Designed to produce 1.25 MW from a 53-m (diameter), two-bladed prop, the unit had withstood winds as high as 50 m/s (115 mph) before it catastrophically failed in 1945 in a modest 12-m/s wind (one of its 8-metric ton blades broke loose and was hurled 200 m away). Subsequent interest in wind systems declined as the utility grid expanded and became more reliable and electricity prices declined.

The oil shocks of the 1970s, which heightened awareness of our energy problems, coupled with substantial financial and regulatory incentives for alternative energy systems, stimulated a renewal of interest in wind power. Within a decade or so, dozens of manufacturers installed thousands of new wind turbines (mostly in California). While many of those machines performed below expectations, the tax credits and other incentives deserve credit for shortening the time required to sort out the best technologies. The wind boom in California was short lived, and when the tax credits were terminated in the mid-1980s, installation of new machines in the United States stopped almost completely for a decade. Since most of the world's wind power sales, up until about 1985, were in the United States, that sudden drop in the market practically wiped out the industry worldwide until the early 1990s.

Meanwhile, wind turbine technology development continued—especially in Denmark, Germany, and Spain—and those countries were ready when sales began to boom in the mid-1990s. As shown in Figure 7.1, the global installed capacity of wind turbines grew by a

factor of ten over the decade from 2002 to 2012. In 2012, wind crossed the 250-GW benchmark, which at the time was about three times the global installed capacity of photovoltaics. The most remarkable change during that decade was the emergence of China, whose installed capacity in just those last 5 years grew from 2.6 GW in 2006 to 63 GW in 2011.

FIGURE 7.1 Global installed capacity of wind turbines grew by a factor of ten over the last decade. From DOE (2012).



Globally, the countries with the most installed wind capacity in 2012 are shown in Figure 7.2. The world leader was China, followed by the United States, Germany, Spain, and India. Also shown are the capacity additions made in 2011, where China clearly dominated the market, accounting for over 40% of total global additions. In the United States, Texas took the lead away from California some years ago and in 2012 had nearly as much capacity as the next three states combined (Iowa, California, and Illinois). Another measure of the rapid progress being made is the fraction of total electricity generated that wind provides in certain regions around the globe. In South Dakota, for example, it was over 20% in 2011, while in Denmark, it was close to 30% (Fig. 7.3).

FIGURE 7.2 Total installed capacity by the beginning of 2012, showing additions made in 2011. From DOE (2012).

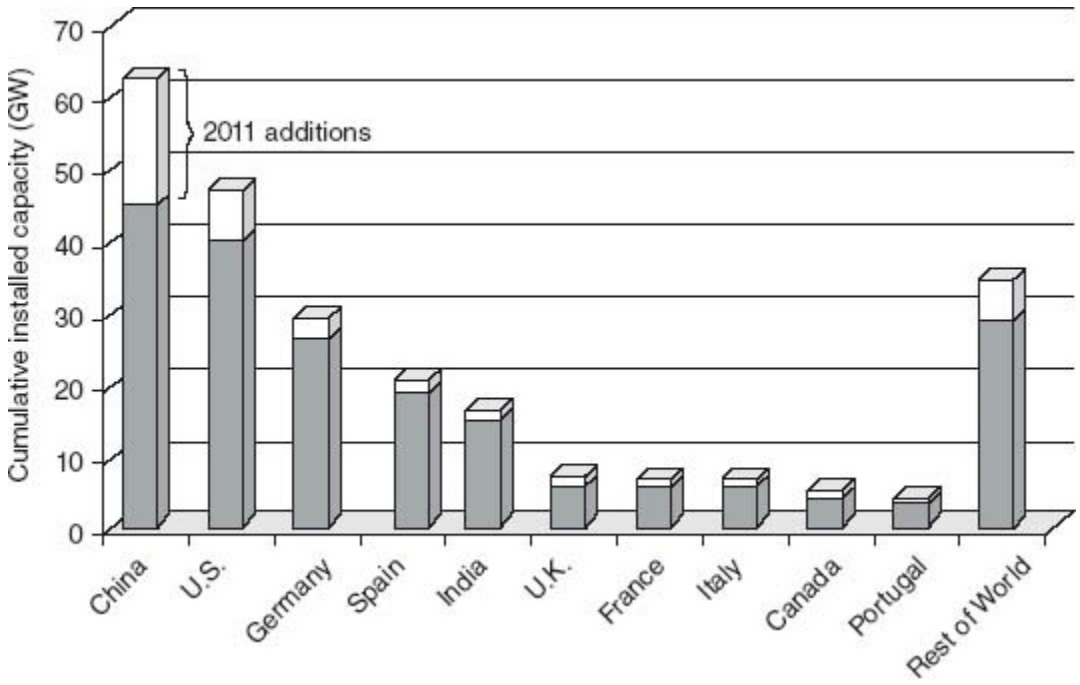
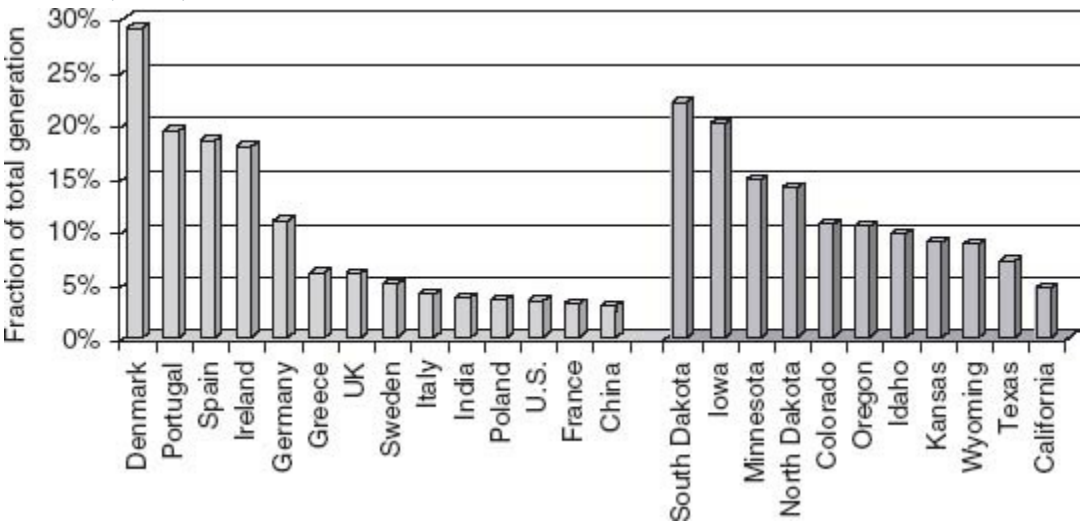


FIGURE 7.3 2011 Fraction of total generation provided by wind in countries and states. From DOE (2012).

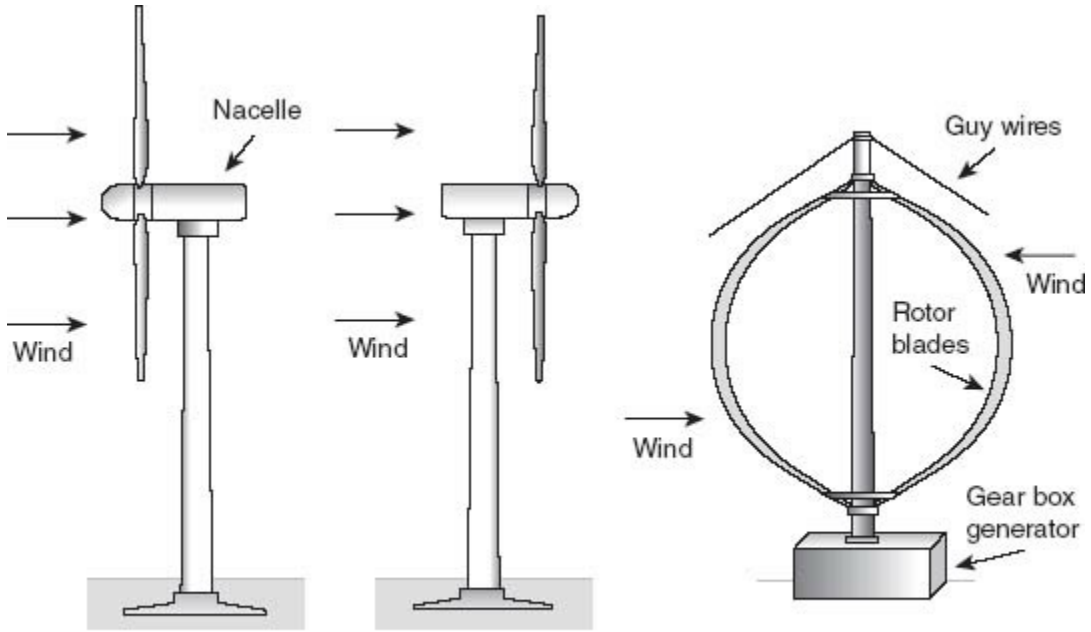


Most early wind turbines were used to grind grain into flour, hence the name "windmill." Strictly speaking, therefore, calling a machine that pumps water or generates electricity a windmill is somewhat of a misnomer. Instead, people are using more accurate, but generally clumsier, terminology: "wind-driven generator, " "wind generator, " "wind turbine, " "wind turbine generator" (WTG), and "wind energy conversion system" (WECS) all are in use. For our purposes, "wind turbine" will suffice even though often we will be talking about system components (e.g., towers, generators, etc.) that clearly are not part of a "turbine."

One way to classify wind turbines is in terms of the axis around which the turbine blades rotate. Almost all large machines are horizontal axis wind turbines (HAWTs), but there are some smaller turbines with blades that spin around a vertical axis (vertical axis wind turbines (VAWTs)). Examples of the two types are shown in Figure 7.4. While virtually all large wind turbines are of the horizontal axis type, there was a period of time when some

HAWTs were upwind machines and some were downwind types. A downwind machine has the advantage of letting the wind itself control the yaw (the left–right motion) so it naturally orients itself correctly with respect to wind direction. They do have a problem, however, with wind shadowing effects of the tower. Every time a blade swings behind the tower it encounters a brief period of reduced wind, which causes the blade to flex. This flexing not only has the potential to lead to blade failure due to fatigue, but also increases blade noise and reduces power output. Upwind turbines on the other hand require somewhat complex yaw control systems to keep the blades facing into the wind. In exchange for that added complexity, however, upwind machines operate more smoothly and deliver more power. Essentially all modern wind turbines are of the upwind type.

FIGURE 7.4 Horizontal axis wind turbines (HAWTs) are either upwind machines (a) or downwind machines (b). Vertical axis wind turbines (VAWTs) accept the wind from any direction (c).



Another fundamental design decision for HAWTs relates to the number of rotating blades. Perhaps the most familiar wind turbine for most people is the multibladed, water-pumping windmill so often seen on old farms. These machines are radically different from those designed to generate electricity. For water pumping, the windmill must provide high starting torque to overcome the weight and friction of the pumping rod that moves up and down in the well. They must also operate in low wind speeds in order to provide nearly continuous water pumping throughout the year. Their multibladed design presents a large area of rotor facing into the wind, which enables both high torque and low speed operation. On the other hand, wind turbines with many blades operate with much lower rotational speed than those with fewer blades. As the revolutions per minute (rpm) of the turbine increases, the turbulence caused by one blade affects the efficiency of the blade that follows. With fewer blades, the turbine can spin faster before this interference becomes excessive, and a faster spinning shaft means generators can be physically smaller in size.

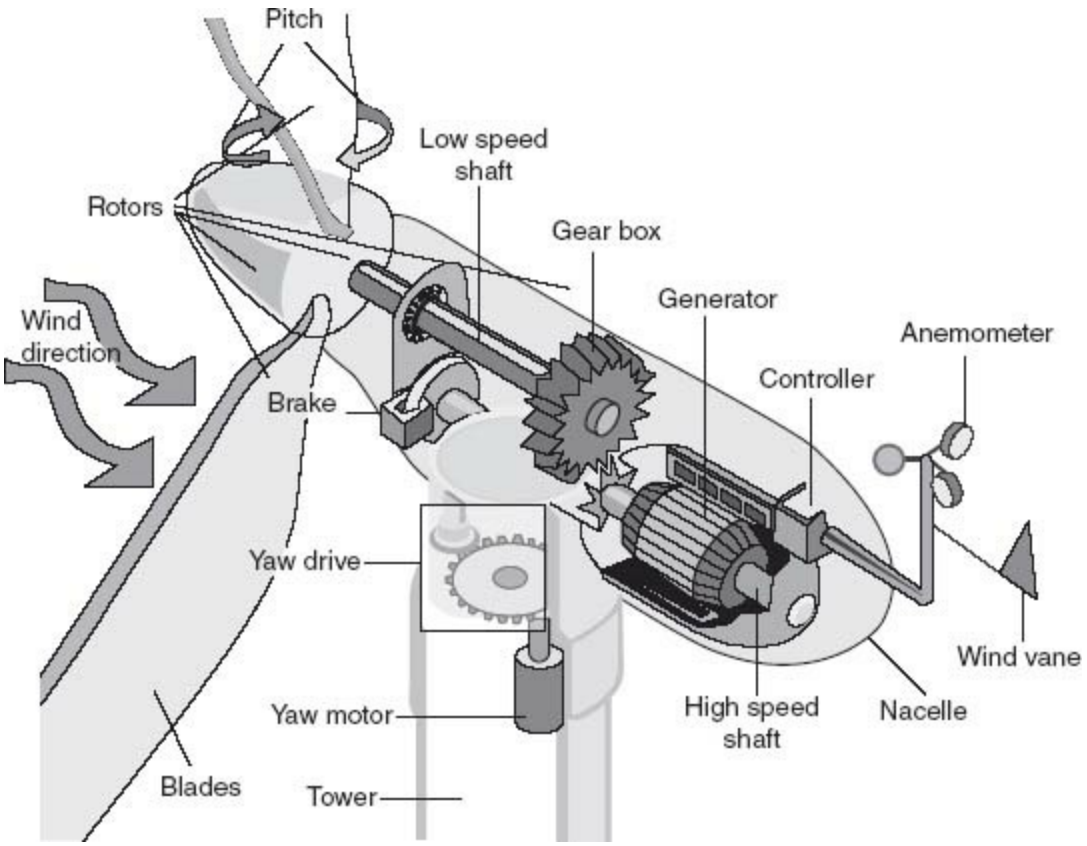
There was a time when two-bladed HAWTs were in competition with three-bladed

turbines. Two-bladed rotors are cheaper to fabricate and easier to hoist up to the nacelle. Also, they spin faster, which leads to reduced generator costs. On the other hand, three-bladed turbines show smoother operation since impacts of tower interference and variation of wind speed with height are more evenly transferred from rotors to the drive shaft. They also tend to be quieter. All large, modern turbines have three blades.

The principal advantage of vertical axis machines, such as the Darrieus rotor shown in Figure 7.4c, is that the heavy generator and gearbox contained in the nacelle can be located down on the ground, where it can be serviced easily. Since the heavy equipment is not perched on top of a tower, the tower itself need not be structurally as strong as that for an HAWT. The tower can be lightened even further when guy wires are used, which is fine for towers located on land but not for offshore installations. Another advantage is that they do not need any kind of yaw control to keep them facing into the wind. The blades on a Darrieus rotor, as they spin around, are almost always in pure tension, which means they can be relatively lightweight and inexpensive since they do not have to handle the constant flexing associated with blades on horizontal-axis machines. The principal disadvantage of vertical-axis turbines, which has led to their demise in larger scales, is that the blades are close to the ground where wind speeds are lower. As we will see later, power in the wind increases as the cube of velocity so ground-level VAWTs miss out on the opportunity to get their turbines higher up into those much more powerful winds. One market in which VAWTs are making some inroads is small-scale turbines generating just a few kilowatts each that can be installed on buildings or in their vicinity.

The key components to a wind energy conversion system are shown in Figure 7.5. The function of the blades is to convert kinetic energy in the wind into rotating shaft power to spin a generator that produces electric power. Usually, that shaft rotation is too slow to directly couple to a generator, so a gearbox transfers power from the low speed shaft to a higher speed shaft that spins the generator. Assuming it is an upwind machine, another gearbox and motor adjust the yaw to keep the blades facing into the wind when generating power, as well as turning the rotors out of the wind when winds are too strong to safely operate the turbine. In those circumstances, a brake engages to lock the blades in place.

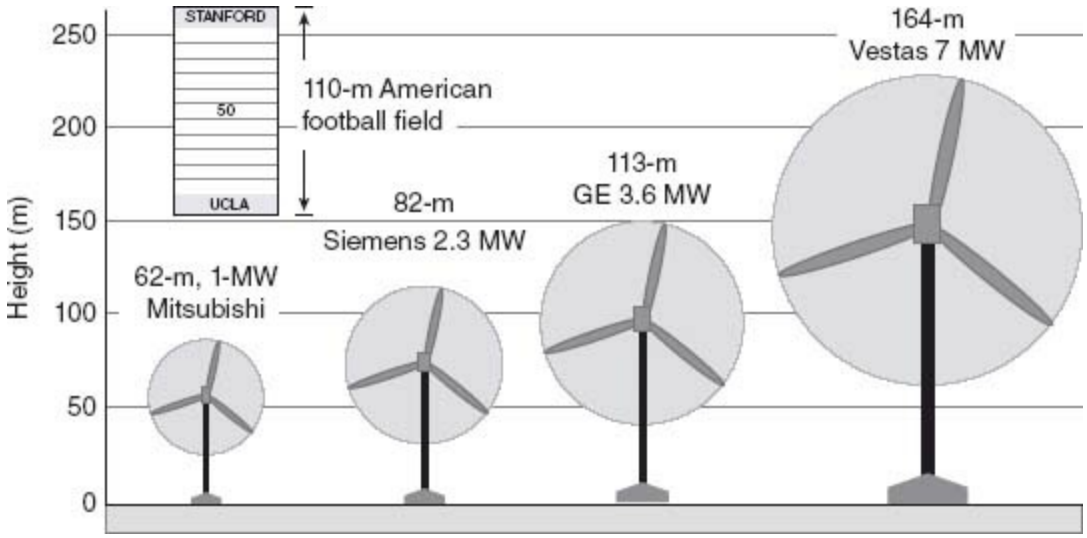
FIGURE 7.5 Principal components of most wind energy conversion systems.



7.2 WIND TURBINE TECHNOLOGY: ROTORS

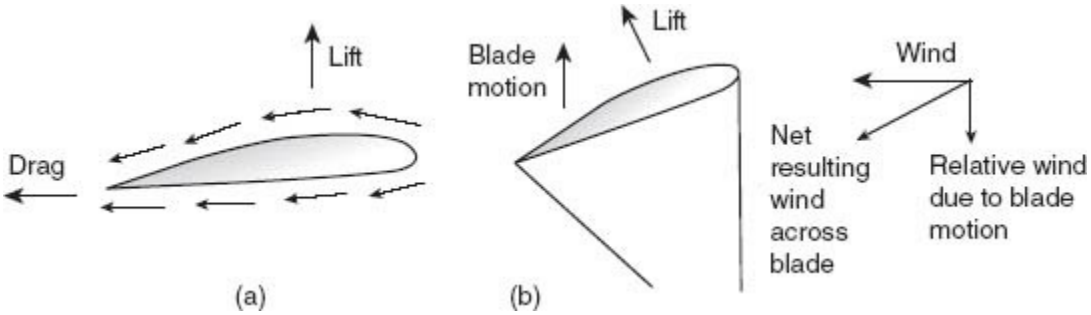
Wind technology has been advancing rapidly during the first decades of the twenty-first century. Not only have turbines gotten much bigger, but also their efficiencies have improved significantly as well. At the turn of the century, most new turbines were rated at roughly 1–2 MW each, had hub heights of 50–80 m, and blade diameters of 80–100 m. As shown in Figure 7.6, a decade or so later the largest machines, designed primarily for the more consistent high winds offshore, were as large as 7 MW with blades over 150 m in diameter. For comparison, an American football field is about 110 m from goal post to goal post.

FIGURE 7.6 Increasing size of wind turbines.



In order to understand some aspects of wind turbine performance, we need a brief introduction to how rotor blades extract energy from the wind. Begin by considering the simple airfoil cross section shown in Figure 7.7a. An airfoil, whether it is the wing of an airplane or the blade of a windmill, takes advantage of Bernoulli's principle to obtain lift. Air moving over the top of the airfoil has a greater distance to travel before it can rejoin the air that took the shortcut under the foil. That means the air on top moves faster causing its pressure to be lower than that under the airfoil, which creates the lifting force that holds an airplane up or that causes a wind turbine blade to rotate.

FIGURE 7.7 The lift in (a) is the result of faster air sliding over the top of the wind foil. In (b), the combination of actual wind and the relative wind due to blade motion creates a resultant that creates the blade lift.

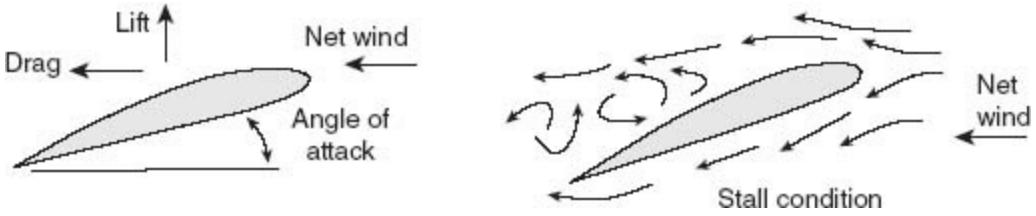


Describing the forces on a wind turbine blade is a bit more complicated than for a simple aircraft wing. A rotating turbine blade sees air moving toward it not only from the wind itself, but also from the relative motion of the blade as it rotates. As shown in Figure 7.7b, the combination of wind and blade motion is like adding two vectors, with the resultant moving across the airfoil at the correct angle to obtain lift that moves the rotor along. Since the blade is moving much faster at the tip than near the hub, the blade must be twisted along its length to keep the angles right.

Up to a point, increasing the angle between the airfoil and the wind (called the angle of attack), improves lift at the expense of increased drag. As shown in Figure 7.8, however, increasing the angle of attack too much can result in a phenomenon known as stall. When a wing stalls, the airflow over the top no longer sticks to the surface and the resulting turbulence destroys lift. When an aircraft climbs too steeply, stall can have tragic results. In

a wind turbine, this can be a good thing.

FIGURE 7.8 Increasing the angle of attack can cause a wing to stall.



Power delivered by a wind turbine increases rapidly with increasing wind speed. At some wind speed, the generator reaches its maximum capacity at which point there must be some way to shed some of the wind's power or else the generator may be damaged. Three approaches are common on large machines: a passive stall-control design, an active pitch-control system, and an active stall-control combination of the two.

For *stall-controlled* machines, the blades are carefully designed to automatically reduce efficiency when winds are excessive. Nothing rotates—as it does in pitch-controlled schemes—and there are no moving parts, so this is referred to as passive control. The aerodynamic design of the blades, especially their twist as a function of distance from the hub, must be very carefully done so that a gradual reduction in lift occurs as the blades rotate faster. This approach is simple and reliable, but it sacrifices some power at lower wind speeds. It has been popular on wind turbines less than about 1 MW in size.

For *pitch-controlled* turbines, an electronic system monitors the generator output power and if it exceeds specifications, the pitch of the turbine blades is adjusted to shed some of the wind. Physically, a hydraulic system slowly rotates the blades about their axes, turning them a few degrees at a time to reduce or increase their efficiency as conditions dictate. The strategy is to reduce the blade's angle of attack when winds are high. Most large turbines rely on this approach for controlling the power output.

The third approach is an *active stall-control* scheme in which the blades rotate just as they do in the active, pitch-control approach. The difference is, however, that when winds exceed the rated wind speed for the generator, instead of reducing the angle of attack of the blades, it is increased to induce stall.

For pitch-controlled and active-stall-controlled machines, the rotor can be stopped by rotating the blades about their longitudinal axis to create a stall. For stall-controlled machines, it is common on large turbines to have spring loaded, rotating tips on the ends of the blades. When activated, a hydraulic system trips the springs, and the blade tips rotate 90° out of the wind stopping the turbine in a few rotor revolutions. If the hydraulic system fails, the springs automatically activate when rotor speed is excessive. Once a rotor has been stopped, by whatever control mechanism, a mechanical brake locks the rotor shaft in place, which is especially important for safety during maintenance.

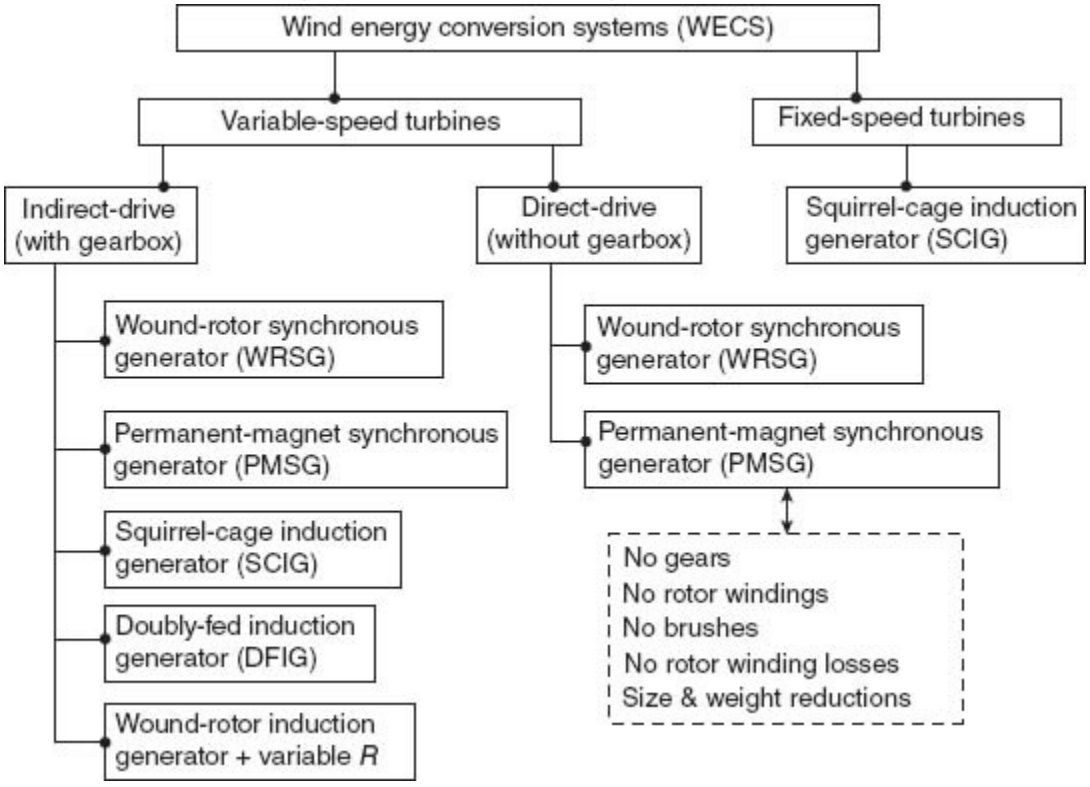
Small, kilowatt size wind turbines can have any of a variety of techniques to spill wind. Passive yaw controls that cause the axis of the turbine to move more and more off the wind as wind speeds increase are common. This can be accomplished by mounting the turbine slightly to the side of the tower so that high winds push the entire machine around the tower. Another simple approach relies on a wind vane mounted parallel to the plane of the blades. As winds get too strong, wind pressure on the vane rotate the machine away from the wind.

7.3 WIND TURBINE TECHNOLOGY: GENERATORS

One way to categorize wind energy systems is by whether their rotors rotate at a fixed or variable speed. As will be demonstrated later, there is a maximum efficiency point for rotors at which the rotation rate of the rotor is optimally matched to the current wind speed. Since wind speeds vary, for maximum efficiency rotor speeds should be variable as well, but that capability comes at a cost. Fixed-speed turbines offer the simplest, least-cost approach to a wind system, but suffer from the inefficiencies associated with not being able to operate the turbine at its maximum power point. In addition, mechanical stresses associated with rapidly changing winds are more severe for fixed-speed turbines, which necessitate sturdier designs.

Figure 7.9 illustrates the range of wind system configurations that are all currently in use. The primary distinguishing characteristics include whether the turbines are fixed or variable speed, whether the generators are synchronous or inductive, and whether there is a gearbox or not. The most advanced system shown is a variable speed turbine, without a gearbox, that uses a permanent magnet synchronous generator (PMSG). These are the biggest, most efficient wind turbines on the market, developed especially for offshore applications.

FIGURE 7.9 System configurations for wind energy systems. Based on Wu et al. (2011).



7.3.1 Fixed-Speed Synchronous Generators

Synchronous generators, which produce almost all of the electric power in the world, were presented in Chapter 3. In that context they were described as being fixed-speed generators since they spin precisely at a precise rotational speed determined by the number of poles on

the rotor p and the frequency f (Hz) of the three-phase armature voltage provided by the grid.

$$N(\text{rpm}) = \frac{120\,f}{p} \tag{7.1}$$

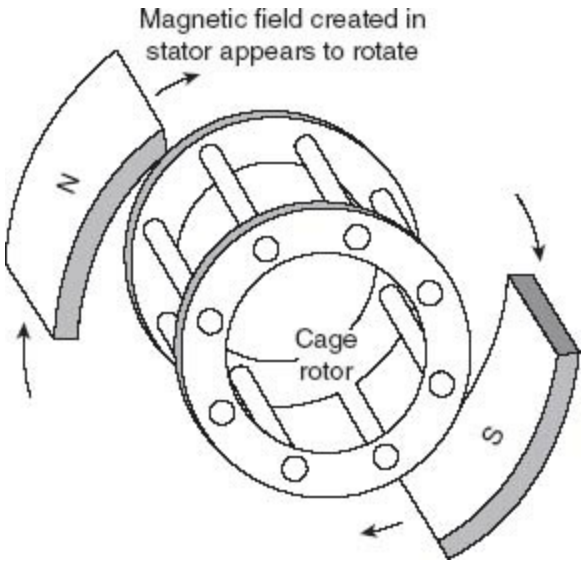
As shown in Figures 3.24 and 3.25, armature currents create a rotating magnetic field within the generator that interacts with a second magnetic field created on the rotor itself. The rotor field can be created either with permanent magnets (PMSG) on the rotor or with a field current delivered through slip rings to windings on the rotor itself. The latter configuration is referred to as having a wound rotor synchronous generator (WRSG).

7.3.2 The Squirrel-Cage Induction Generator

Most of the world's wind turbines use induction generators rather than the synchronous machines just mentioned. In contrast to a synchronous generator (or motor), induction machines do not turn at a fixed speed, so they are often described as *asynchronous* generators. While induction generators are uncommon in power systems other than wind turbines, their counterpart, induction motors, are the most prevalent motors—using almost one-third of all the electricity generated worldwide. In fact, just as is the case for synchronous machines, an induction machine can act as a motor or generator depending on whether shaft power is being put into the machine (generator) or taken out (motor). Both modes of operation—as a motor during start-up and as a generator when the wind picks up—take place in wind turbines with induction generators. Induction generators rely on a rotating magnetic field created in the armature windings, but their speed is allowed to vary somewhat from the fixed speed of the rotating magnetic field.

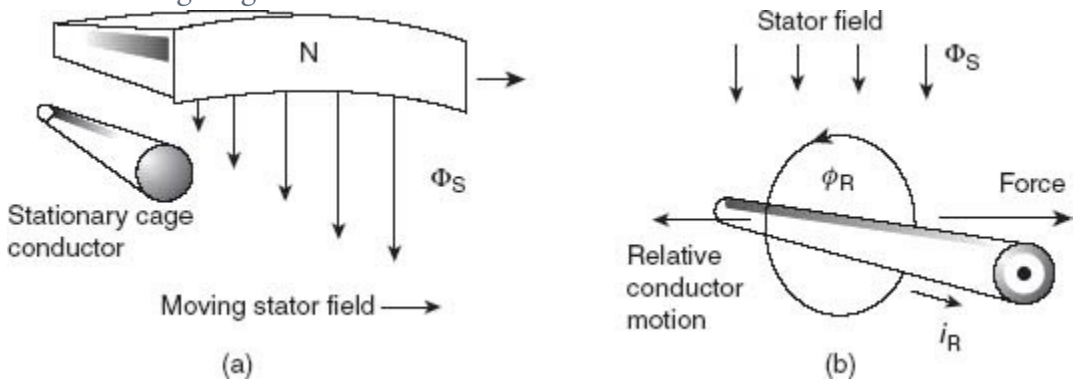
There are two categories of induction machines: those that have wound rotors (wound rotor induction generators (WRIGs)), and those that have what are often called "squirrel"-cage rotors (squirrel-cage induction generators (SCIGs)), or more simply, cage rotors. Cage rotors consist of a number of copper or aluminum bars shorted together at their ends, forming a cage not unlike the one you might have to give your pet rodent some exercise. The cage is then imbedded in an iron core consisting of thin (0.5 mm) insulated steel laminations to help control eddy current losses. The key advantage of SCIGs is that their rotors do not require the exciter, brushes, and slip rings that are needed by WRIGs. Figure 7.10 shows the basic relationship between stator and rotor, which can be thought of as a pair of magnets in the stator spinning around the cage rotor.

FIGURE 7.10 A cage rotor consists of thick, conducting bars shorted at their ends, around which circulates a rotating magnetic field.



To understand how the rotating stator field interacts with the cage rotor, consider Figure 7.11a. The rotating stator field is shown moving toward the right, while the conductor in the cage rotor is stationary. Looked at another way, the stator field can be thought to be stationary and, relative to it, the conductor appears to be moving to the left, cutting lines of magnetic flux as shown in Figure 7.11b. Faraday's law of electromagnetic induction says whenever a conductor cuts flux lines, an electromotive force (emf) will develop along the conductor and, if allowed to, a current will flow. In fact, the cage rotor has thick conductor bars with very little resistance, so lots of current can flow easily. That rotor current, labeled i_R in Figure 7.11b, will create its own magnetic field, which wraps around the conductor. The rotor's magnetic field then interacts with the stator's magnetic field producing a force that attempts to drive the cage conductor to the right. In other words, the rotor wants to spin in the same direction (in this case, clockwise), and at the same speed, as that of the rotating stator field.

FIGURE 7.11 In (a), the stator field moves toward the right while the cage rotor conductor is stationary. As shown in (b), that is equivalent to the stator field being stationary while the conductor moves to the left, cutting the lines of flux. The conductor then experiences a force toward the right that tries to make the rotor want to catch up to the stator's rotating magnetic field.



When the stator of an induction machine is provided with three-phase excitation current and the shaft is connected to a wind turbine, as the wind begins to blow the machine will start operation by motoring up toward its synchronous speed. When the wind speed is

sufficient to force the generator shaft to exceed synchronous speed, the induction machine automatically becomes a three-phase generator delivering electrical power back to its stator windings. The relative speed between the stator magnetic field and the rotor itself is called the slip speed *s*, defined as

$$s = \frac{N_S - N_R}{N_S} = 1 - \frac{N_R}{N_S} \tag{7.2}$$

where N_S is the no-load synchronous speed given by Equation 7.1 and N_R is the rotor speed. Slip is defined to be positive when the rotor is moving at a slower speed than the stator's rotating magnetic field; that is, when the machine is acting as a motor. When the rotor moves faster than the rotating magnetic field, slip is negative, and the machine becomes a generator.

For grid-connected inductance machines, the slip is normally no more than about ±1%, which means, for example, that a 4-pole, 60-Hz generator will spin at about

$$\begin{aligned} N_R &= (1-s)N_S = (1-s).\frac{120\,f}{p} \\ &= [1-(-0.01)].\frac{120 \times 60}{4} = 1818\ \text{rpm} \end{aligned} \tag{7.3}$$

If the gearbox has a 100:1 gear ratio, the turbine blades will be forced to turn at close to 18 rpm.

One approach that has been used to provide some flexibility in the rotation speed of SCIGs is suggested by Equation 7.3. By clever wiring of the stator windings, it is possible to remotely switch the number of poles in the generator. As far as the rotor is concerned, the number of poles in the stator is irrelevant. That is, the stator can have external connections that switch the number of poles from one value to another without needing any change in the rotor. For example, a 60-Hz four-pole generator spins at about 1800 rpm, while one with six poles will spin at about 1200 rpm. A 100:1 gearbox, then, would mean the rotors could spin at either 12 or 18 rpm. This pole-switching approach, by the way, is common in household appliance motors such as those used in washing machines and exhaust fans to give two- or three-speed operation.

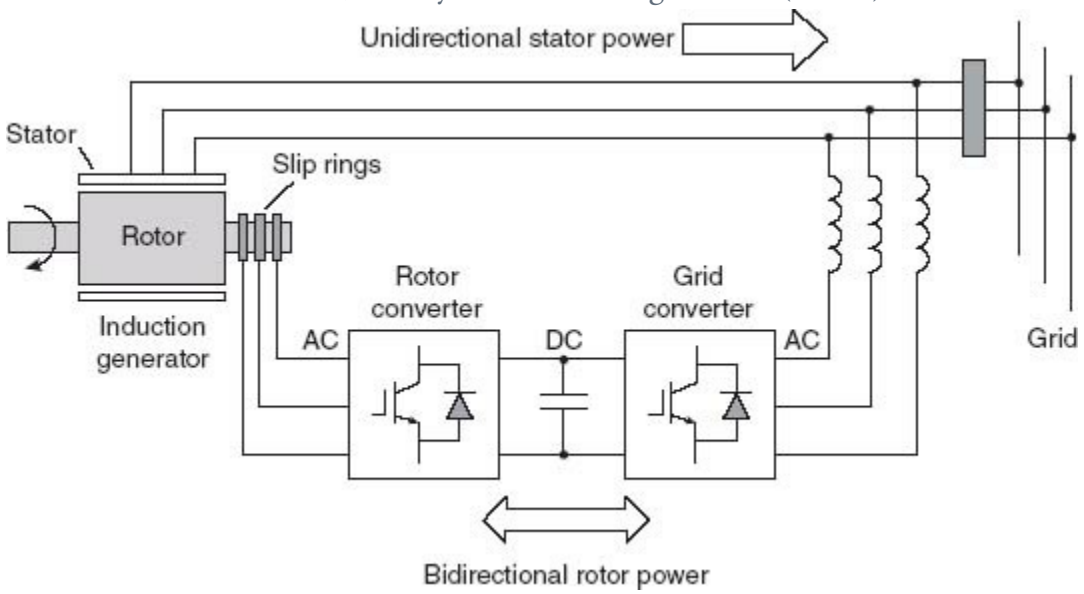
7.3.3 The Doubly-Fed Induction Generator

The cage induction generator, with no electrical connections to the rotor, has the significant advantage of simplicity and robustness. On the other hand, it is pretty much a fixed-speed machine whose rotation rate differs only modestly from that of a synchronous generator. Even that modest variation, though, helps when it comes to absorbing shocks caused by rapidly fluctuating winds.

The added complexity of a wound rotor induction generator, which needs slip rings to energize the rotor, are often more than justified by the additional flexibility in rotor speed control that they can provide. One of the most popular wind turbine configurations is based on what is referred to as a wound-rotor, doubly-fed induction generator (DFIG). As shown in Figure 7.12, the stator part of a DFIG system is conventional. That is, the grid

provides three-phase voltages that create the stator's rotating magnetic field. Power generated in the stator is fed back to the grid in the normal way. The difference is that the rotor is set up to allow bidirectional power flow to or from the grid. When the rotor spins at less than the synchronous frequency (sub-synchronous), the machine acts like a motor, slowing down the turbine and absorbing power from the grid. When it operates in super-synchronous mode, going faster than synchronous speed, power is generated from the rotor itself and sent back to the grid.

FIGURE 7.12 A wound-rotor, doubly-fed induction generator (DFIG).



As shown, the key is a modestly sized back-to-back voltage converter (Section 3.10) that makes it possible to deliver AC voltages to the rotor at the slip frequency. If those voltages oppose the rotor emf, the generator will spin faster and power will be delivered from the rotor to the network (super-synchronous). When they add to rotor emf, power will be absorbed by the rotor and it will run slower (sub-synchronous). The usual range of speed control is from about 40% below synchronous speed up to about 20% above synchronous speed. In addition to speed control, the converters also allow control of both real power P and reactive power Q flows from the stator to the grid independently of the generator's turning speed.

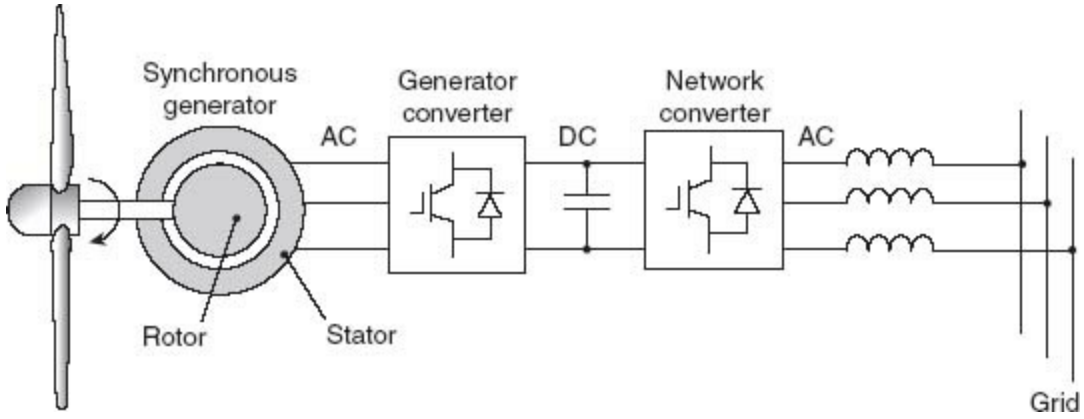
7.3.4 Variable-Speed Synchronous Generators

The DFIG configuration just described uses a relatively small voltage converter, which might be rated at about 30% of the full power of the turbine. And, it is capable of about the same magnitude of speed adjustments.

The next step up is to gain complete control of speed with a full-capacity converter powering a synchronous generator (Fig. 7.13). The generator can be either a wound-rotor type, in which case slip rings and an exciter circuit are needed, or it can be built with a permanent-magnet rotor that avoids those complications. When a PMSG is provided with a large enough number of poles, the gearbox as well can be eliminated. Permanent magnets, however, use rare earth materials such as neodymium, which have some issues of their own. The resource base for rare earth materials, especially in the United States, is an issue of

some concern, as is as the materials' propensity to permanently lose magnetic field strength when exposed to high temperatures.

FIGURE 7.13 A gearless, variable-speed synchronous generator with full-capacity converters.



The gearless configuration shown in Figure 7.13 has considerable impact on the shape of the wind turbine's nacelle. It does not need to be as long since there is no gearbox, but it does need a larger diameter nacelle to be able to house the multi-pole, permanent-magnet generator. The increased sophistication of these systems increases their cost, but decreases their maintenance requirements. They are making their first inroads into the market using very large turbines for use in offshore systems. An example of which is shown in Figure 7.14.

FIGURE 7.14 The GE 4.1-MW, 113-m, direct-drive, permanent-magnet, variable-speed, synchronous generator. Reproduced with permission from General Electric.



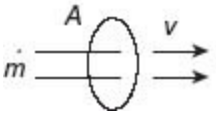
7.4 POWER IN THE WIND

Consider a "packet" of air with mass m moving at a speed v. Its kinetic energy, KE, is given by the familiar relationship:

$$\text{KE} = \frac{1}{2}mv^2 \tag{7.4}$$

Since power is energy per unit time, the power represented by a mass of air moving at

velocity v through area A will be



$$\text{Power through area } A = \frac{\text{Energy}}{\text{Time}} \times \frac{1}{2}\left(\frac{\text{Mass}}{\text{Time}}\right)v^2 \tag{7.5}$$

The mass flow rate $\dot{m}$, through area A, is the product of air density ρ, speed v, and cross-sectional area A:

$$\frac{\text{Mass passing through } A}{\text{Time}} = \dot{m} = \rho A v \tag{7.6}$$

Combining Equation 7.6 with Equation 7.5 gives us an important relationship:

$$P_w = \frac{1}{2}\rho A v^3 \tag{7.7}$$

In SI units, P_w is the power in the wind (watts); ρ is the air density (kg/m^3), which at 15°C and 1 atm is 1.225 kg/m^3; A is the cross-sectional area through which the wind passes (m^2); v is the wind speed normal to A (m/s) (a useful conversion 1 m/s = 2.237 mph). Oftentimes power in the wind is expressed per unit of cross-sectional area (W/m^2), in which case it is referred to as *specific power* or *power density*.

Note that the power in the wind increases as the *cube* of wind speed. That means, for example, that doubling the wind speed increases the power by eightfold. Another way to look at it is that the energy contained in 1 h of 20 mph winds is the same as that contained in 8 h at 10 mph, which is the same as that contained in 64 h (more than two and a half days) of 5 mph wind. Later we will see that most wind turbines are not even turned on in low speed winds without much loss in total energy that could have been delivered.

Equation 7.7 also indicates that wind power is proportional to the swept area of the turbine rotor. For a conventional horizontal axis turbine, the area A is obviously just $A = (\pi/4)D^2$, so wind power is proportional to the square of the blade diameter. Doubling the diameter increases the power available by a factor of four. That simple observation helps explain the economies of scale that go with larger wind turbines. The cost of a turbine increases somewhat in proportion to blade diameter, but power is proportional to diameter squared, so bigger machines have proven to be more cost effective.

Of obvious interest is the energy in a combination of wind speeds. Since Equation 6.4 is a nonlinear relationship between power and wind, we cannot use average wind speed to predict total energy available, as the following example illustrates.

Example 7.1 Don't Just Use Average Wind Speed. Compare the amount of wind energy at 15°C and 1-atm pressure that passes through 1 m^2 of cross-sectional area for the following wind regimes:

a. 100 h of 6 m/s winds (13.4 mph)

b. 50 h at 3 m/s plus 50 h at 9 m/s (i.e., an average wind speed of 6 m/s)

Solution

a. With steady 6 m/s winds, all we have to do is multiply power, given in Equation 7.7, by hours:

$$\text{Energy}\,(6\ \text{m/s}) = \frac{1}{2}\rho A v^3 \Delta t$$

$$= \frac{1}{2} \cdot 1.225\ \text{kg/m}^3 \cdot 1\ \text{m}^2 \cdot (6\ \text{m/s})^3 \cdot 100\ \text{h} = 13{,}230\ \text{Wh}$$

b. With 50 h at 3 m/s

$$\text{Energy}\,(3\ \text{m/s}) = \frac{1}{2} \cdot 1.225\ \text{kg/m}^3 \cdot 1\ \text{m}^2 \cdot (3\ \text{m/s})^3 \cdot 50\ \text{h} = 827\ \text{Wh}$$

And 50 h at 9 m/s contains

$$\text{Energy}\,(9\ \text{m/s}) = \frac{1}{2} \cdot 1.225\ \text{kg/m}^3 \cdot 1\ \text{m}^2 \cdot (9\ \text{m/s})^3 \cdot 50\ \text{h} = 22{,}326\ \text{Wh}$$

for a total of 827 + 22, 326 = 23, 153 Wh

Example 7.1 clearly illustrates the inaccuracy associated with using average wind speeds in Equation 7.7. While both of the wind regimes had the same average wind speed, the combination of 9-m/s and 3-m/s winds (averaging 6 m/s) produces 75% more energy than winds blowing at a steady 6 m/s. Later we will see that, under certain common assumptions about wind speed probability distributions, energy in the wind is typically almost twice the amount that would be found by plugging average wind speed into Equation 7.7.

7.4.1 Temperature and Altitude Correction for Air Density

When wind power data are presented, it is often assumed that the air density is 1.225 kg/m^3; that is, it is assumed that air temperature is 15°C (59°F) and pressure is 1 atm (sea level). Using the ideal gas law, we can easily determine the air density under other conditions.

$$pV = nRT \tag{7.8}$$

where p is the absolute pressure (atm), V is the volume (m^3), n is the mass (mol), R is the ideal gas constant (8.2056×10^{-5}m^3 · atm · K^{-1} · mol^{-1}), and T is absolute temperature (K). Note pressure is in atmospheres, where 1 atm of pressure equals 101.325 kPa (Pa is the abbreviation for Pascals, where 1 Pa = 1 Newton/m^2). One atmosphere also is equal to 14.7 pounds per square inch (psi), so 1 psi = 6.89 kPa. Finally, 100 kPa is called a *bar* and 100 Pa is a millibar, which is the unit of pressure often used in meteorology work.

If we let M.W. stand for the molecular weight of the gas (g/mol), we can write the following expression for air density, ρ:

$$\rho\ (\text{kg/m}^3) = \frac{n(\text{mol}) \cdot \text{M.W.}\ (\text{g/mol}) \cdot 10^{-3}\ (\text{kg/g})}{V\ (\text{m}^3)} \tag{7.9}$$

Since we are working with air, we can easily figure out its equivalent molecular weight by looking at its constituent molecules, which are mostly nitrogen (78.08%), oxygen (20.95%), a little bit of argon (0.93%), carbon dioxide (0.039%), and so forth. Using the constituent molecular weights (N_2 = 28.02, O_2 = 32.00, Ar = 39.95, CO_2 = 44.01) we find

the equivalent molecular weight of air to be

$$\text{M.W.(air)} = 0.781 \times 28.02 + 0.2095 \times 32.00 + 0.0093 \times 39.95 + 0.00039 \times 44.01 = 28.97$$

Combining Equations 7.8 and 7.9 with this value of air's molecular weight gives us the following expression

$$\rho = \frac{p \times \text{M.W.}}{RT} = \frac{p(\text{atm})}{T(\text{K})} \times \frac{28.97\ \text{g/mol} \times 10^{-3}\ \text{kg/g}}{8.2056 \times 10^{-5}\ \text{m}^3 \cdot \text{atm/(K·mol)}}$$

$$\rho(\text{kg/m}^3) = \frac{353.1\ p(\text{atm})}{T(\text{K})} \tag{7.10}$$

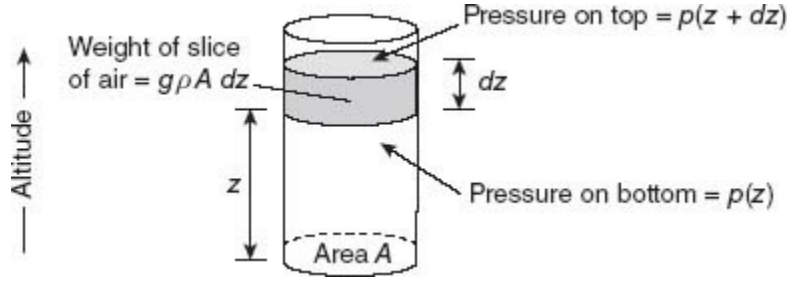
For example, at 1 atm and 30°C, the density of air is

$$\rho = \frac{353.1 \times 1}{30 + 273.15} = 1.165\ \text{kg/m}^3$$

which is a 5% decrease in density compared to the reference 1.225 kg/m^3. Since power is proportional to density, it is also a 5% decrease in power in the wind.

Air density, and hence power in the wind, depends on atmospheric pressure as well as temperature. Since air pressure is a function of altitude, it is useful to have a correction factor to help estimate wind power at sites above sea level.

FIGURE 7.15 A column of air in static equilibrium used to determine the relationship between air pressure and altitude.



Consider a static column of air with cross section A, as shown in Figure 7.15. A horizontal slice of air in that column of thickness dz and density ρ, will have mass ρAdz. If the pressure at the top of the slice due to the weight of the air above it is $p(z + \text{d}z)$, then the pressure at the bottom of the slice, $p(z)$, will be $p(z + \text{d}z)$ plus the added weight per unit area of the slice itself

$$p(z) = p(z + \text{d}z) + \frac{g\rho A\text{d}z}{A} \tag{7.11}$$

where g is the gravitational constant, 9.806 m/s^2. Thus we can write the incremental pressure dp for an incremental change in elevation, dz as

$$\text{d}p = p(z + \text{d}z) - p(z) = -g\rho\text{d}z \tag{7.12}$$

(7.13) That is, $\frac{dp}{dz} = -\rho g$

Substituting Equation 7.10 into Equation 7.13 and including various conversion factors results in

(7.14)

$$\frac{dp}{dz} = -\frac{353.1}{T}\left(\frac{\text{kg}}{\text{m}^3}\right) \times \left(9.806\frac{\text{m}}{\text{s}^2}\right)\left(\frac{\text{atm}}{101{,}325\,\text{Pa}} \times \frac{1\,\text{Pa}}{\text{N/m}^2} \times \frac{1\text{N}}{\text{kg}\cdot\text{m/s}^2}\right) \cdot p$$

(7.15) $$\frac{dp}{dz} = -\left(\frac{0.0342}{T}\right)p$$

Solving Equation 7.15 is complicated by the fact that temperature changes with altitude, typically at the rate of about 6.5°C drop per kilometer of increasing elevation. If, however, we make the simplifying assumption that T is a constant throughout the air column we can easily solve Equation 7.15 while introducing only a slight error.

(7.16) $$p = p_0 \exp\left(-0.0342z/T\right)$$

If let the reference pressure p_0 be the standard 1 atm, and then combine Equation 7.16 with Equation 7.10, we get the following useful density correction for both temperature and altitude

(7.17) $$\rho(\text{kg/m}^3) = \frac{353.1\exp\left(-0.0342\,z/T\right)}{T}$$

where T is in kelvins (K) and z is in meters.

Example 7.2 Combined Temperature and Altitude Correction. Find the power density (W/m^2) in 10 m/s winds at an elevation of 2000 m (6562 ft) and a temperature of 25°C (298.15 K). Compare that to the power density under standard 1-atm and 15°C conditions.

Solution. From Equation 7.17

$$\rho = \frac{353.1\exp\left(-0.0342 \times 2000/298.15\right)}{298.15} = 0.9415\,\text{kg/m}^3$$

And, from Equation 7.7, we get wind power density

$$P/A = \frac{1}{2}\rho v^3 = 0.5 \times 0.9415 \times 10^3 = 470.8\,\text{W/m}^2$$

Under standard conditions

$$P/A = \frac{1}{2}\rho v^3 = 0.5 \times 1.225 \times 10^3 = 612.5\,\text{W/m}^2$$

That is a 23% decrease in power density at the higher elevation and temperature.

7.4.2 Impact of Tower Height

Since power in the wind is proportional to the cube of the wind speed, the economic impact of even modest increases in wind speed can be significant. One way to get the turbine into higher winds is to mount it on a taller tower. In the first few hundred meters above the ground, wind speed is greatly affected by the friction that the air experiences as it moves across the earth's surface. Smooth surfaces, such as a calm sea, offer very little resistance and the variation of speed with elevation is only modest. At the other extreme, surface winds are slowed considerably by high irregularities such as forests and buildings.

One expression that is often used to characterize the impact of the roughness of the earth's surface on wind speed is the following:

$$\left(\frac{v}{v_0}\right) = \left(\frac{H}{H_0}\right)^{\alpha} \tag{7.18}$$

where v is the wind speed at height H, v_0 is the wind speed at height H_0 (often a reference height of 10 m), and α is a friction coefficient sometimes called the Hellman exponent or the shear exponent.

The friction coefficient α is a function of the terrain over which the wind blows. Table 7.1 gives some representative values for rather loosely defined terrain types. Oftentimes, for rough approximations in somewhat open terrain a value of 1/7 (the "one-seventh" rule of thumb) is used for α.

TABLE 7.1 Friction Coefficient for Various Terrain Characteristics

Terrain Characteristics	Friction Coefficient α
Smooth hard ground, calm water	0.10
Tall grass on level ground	0.15
High crops, hedges, and shrubs	0.20
Wooded countryside, many trees	0.25
Small town with trees and shrubs	0.30
Large city with tall buildings	0.40

While the power law given in Equation 7.18 is very often used in the United States, there is another approach that is more common in Europe. This alternative formulation is

$$\left(\frac{v}{v_0}\right) = \frac{\ln(H/l)}{\ln(H_0/l)} \tag{7.19}$$

where l is called the roughness length. Descriptions of some roughness classifications and roughness lengths are given in Table 7.2. Equation 7.19 is preferred by some since it has a theoretical basis in aerodynamics while Equation 7.18 does not. When the atmosphere is thermally neutral (that is, it cools with a gradient of –9.8°C/km) the air flow within the boundary layer theoretically varies logarithmically, starting with a wind speed of zero at a distance above ground equal to the roughness length. In this chapter, we will stick with the exponential expression (Eq. 7.18). Obviously, both the exponential formulation and the logarithmic version only provide a first approximation to the variation of wind speed with

elevation. In reality, nothing is better than actual site measurements.

TABLE 7.2 Roughness Classifications for Use in Equation 7.19

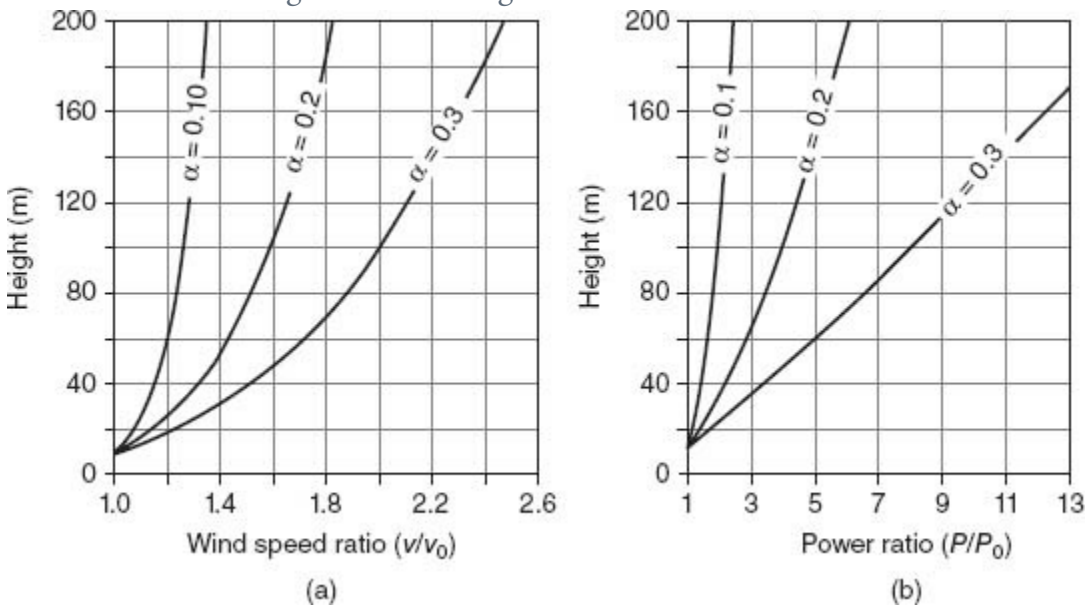
Roughness Class	Description	Roughness Length/(m)
0	Water surface	0.0002
1	Open areas with a few windbreaks	0.03
2	Farm land with some windbreaks more than 1-km apart	0.1
3	Urban districts and farm land with many windbreaks	0.4
4	Dense urban or forest	1.6

Since power in the wind varies as the cube of wind speed, we can rewrite Equation 7.18 to indicate the relative power of the wind at height H versus the power at the reference height of H_0.

$$\frac{P}{P_0} = \left(\frac{1/2\rho A v^3}{1/2\rho A v_0^3}\right) = \left(\frac{v}{v_0}\right)^3 = \left(\frac{H}{H_0}\right)^{3\alpha} \quad (7.20)$$

In Figure 7.16, the ratio of wind power at other elevations to that at 10 m shows the dramatic impact of the cubic relationship between wind speed and power. Even for a smooth ground surface, for instance, for an offshore site, the power doubles when the height increases from 10 to 100 m. For a rougher surface, with friction coefficient α = 0.3, the power increases eightfold at 100 m.

FIGURE 7.16 Increasing wind speed (a) and power ratios (b) with height for various friction coefficients α using a reference height of 10 m.

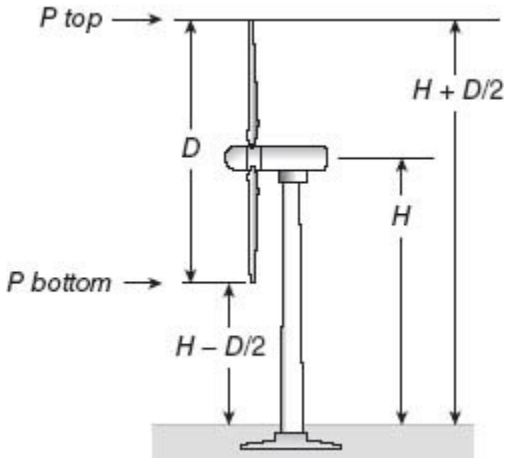


Example 7.3 Impact of Tower Height on Rotor Stress. A wind turbine with a 50-m rotor diameter is to be mounted on either a 50-m tower or an 80-m tower. Assume the usual 1/7th rule of thumb for the shear-friction coefficient.

a. Compare the wind power density at each hub height.

b. For each height, compare the ratio of the power density at the highest point that

the tip of a rotor blade reaches to the lowest point to which it falls.



Solution

a. Using Equation 7.20 with 50-m and 100-m hub heights:

$$\frac{P}{P_0} = \left(\frac{H}{H_0}\right)^{3\alpha} = \left(\frac{80}{50}\right)^{3\times 1/7} = 1.22$$

so there is 22% more power available at the taller hub height.

b. For the 50-m blade at a 50-m hub height, the tip reaches 75 m at its highest point and 25 m at its lowest:

$$\frac{P}{P_0} = \left(\frac{75}{25}\right)^{3\times 1/7} = 1.60$$

The power in the wind at the top of the rotor swing is 60% higher than it is when the tip reaches its lowest point.

At the 80-m hub height, the power ratio from the highest to the lowest point will be

$$\frac{P}{P_0} = \left(\frac{105}{55}\right)^{3\times 1/7} = 1.32$$

Example 7.3 illustrates an important point about the variation in wind speed and power across the face of a spinning rotor. For large machines, when a blade is at its high point, it can be exposed to much higher wind forces than when it is at the bottom of its arc. This variation in stress as the blade moves through a complete revolution can be compounded by the impact of the tower itself on wind speed—especially for downwind machines, which have a significant amount of wind "shadowing" as the blades pass behind the tower. The resulting flexing of a blade can increase the noise generated by the wind turbine and may contribute to blade fatigue, which can ultimately cause blade failure.

7.5 WIND TURBINE POWER CURVES

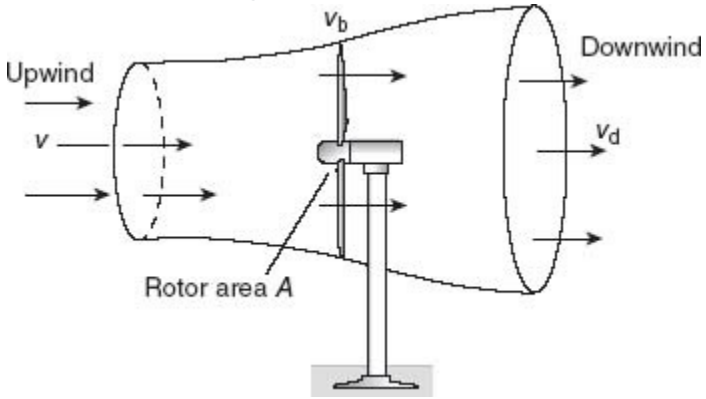
It is interesting to note that a number of energy technologies have certain fundamental constraints that restrict the maximum possible conversion efficiency from one form of

energy to another. For heat engines, it is the Carnot efficiency that limits the maximum work that can be obtained from an engine working between a hot and a cold reservoir. For photovoltaics, it is the band-gap of the material that limits the conversion efficiency from sunlight into electrical energy. For fuel cells, it is the Gibbs free energy that limits the energy conversion from chemical to electrical forms. And now, we will explore the constraint that limits the ability of a wind turbine to convert kinetic energy in the wind to mechanical power.

7.5.1 The Betz Limit

The original derivation for the maximum power that a turbine can extract from the wind is credited to a German physicist, Albert Betz, who first formulated the relationship in 1919. The analysis begins by imagining what must happen to the wind as it passes through a wind turbine. As shown in Figure 7.17, wind approaching from the left is slowed down as a portion of its kinetic energy is extracted by the turbine. The wind leaving the turbine has a lower velocity and its pressure is reduced, causing the air to expand downwind of the machine. An envelope drawn around the air mass that passes through the turbine forms what is called a *stream tube*, as suggested in the figure.

FIGURE 7.17 Approaching wind slows and expands as a portion of its kinetic energy is extracted by the wind turbine, forming the stream tube shown.



So why cannot the turbine extract all of the kinetic energy in the wind? If it did, the air would have to come to a complete stop behind the turbine, which, with nowhere to go, would prevent any more of the wind to pass through the rotor. The downwind velocity, therefore, cannot be zero. Also, it makes no sense for the downwind velocity to be the same as the upwind speed, since that would mean the turbine extracted no energy at all from the wind. That suggests that there must be some ideal slowing of the wind that will result in maximum power extracted by the turbine. What Betz showed was that an ideal wind turbine would slow the wind to one-third of its original speed.

In Figure 7.17, the upwind velocity of the undisturbed wind is v, the velocity of the wind through the plane of the rotor blades is v_b, and the downwind velocity is v_d. The mass flow rate of air within the stream tube is everywhere the same, call it $\dot{m}$. The power extracted by the blades P_b is equal to the difference in kinetic energy between the upwind and downwind air flows:

(7.21) $$P_b = \frac{1}{2}\dot{m}\left(v^2 - v_d^2\right)$$

The easiest spot to determine mass flow rate $\dot{m}$ is at the plane of the rotor where we know the cross-sectional area is just the swept area of the rotor A. The mass flow rate is thus

(7.22) $$\dot{m} = \rho A v_b$$

If we now make the assumption that the velocity of the wind through the plane of the rotor is just the average of the upwind and downwind speeds (Betz' derivation actually shows that this is true), then we can write

(7.23) $$P_b = \frac{1}{2}\rho A\left(\frac{v + v_d}{2}\right)\left(v^2 - v_d^2\right)$$

To help keep the algebra simple, let us define the ratio of downstream to upstream wind speed to be λ:

(7.24) $$\frac{v_d}{v} = \lambda$$

Substituting Equation 7.24 into Equation 7.23 gives

$$P_b = \frac{1}{2}\rho A\left(\frac{v + \lambda v}{2}\right)\left(v^2 - \lambda^2 v^2\right)$$

$$= \frac{1}{2}\rho A v^3 \times \left[\frac{1}{2}(1+\lambda)\left(1-\lambda^2\right)\right]$$

(7.25) $$= \text{Power in the wind} \times \text{Fraction extracted}$$

Equation 7.25 shows us that the power extracted from the wind is equal to the upstream power in the wind multiplied by the quantity in brackets. The quantity in the brackets is therefore the fraction of the wind's power that is extracted by the blades; that is, it is the efficiency of the rotor, usually designated as C_p.

(7.26) $$\text{Rotor efficiency} = C_p = \frac{1}{2}(1+\lambda)\left(1-\lambda^2\right)$$

So our fundamental relationship for the power delivered by the rotor becomes

(7.27) $$P_b = \frac{1}{2}\rho A v^3 \cdot C_p$$

To find the maximum possible rotor efficiency, we simply take the derivative of Equation 7.27 with respect to λ and set it equal to zero:

$$\frac{dC_p}{d\lambda} = \frac{1}{2}\left[(1+\lambda)(-2\lambda) + (1-\lambda^2)\right]$$
$$= \frac{1}{2}\left[(1+\lambda)(-2\lambda) + (1+\lambda)(1-\lambda)\right]$$
$$= \frac{1}{2}(1+\lambda)(1-3\lambda) = 0$$

which has the solution

$$\lambda = \frac{v_d}{v} = \frac{1}{3} \tag{7.28}$$

In other words, the blade efficiency will be a maximum if it slows the wind to one-third of its undisturbed, upstream velocity.

If we now substitute $\lambda = 1/3$ into the equation for rotor efficiency (Eq. 7.26), we find the theoretical maximum blade efficiency is

(7.29)

$$\text{Maximum rotor efficiency} = \frac{1}{2}\left(1+\frac{1}{3}\right)\left(1-\frac{1}{3^2}\right) = \frac{16}{27} = 0.5926 \approx 59.3\%$$

This conclusion—that the maximum theoretical efficiency of a rotor is 59.3%—is called the *Betz efficiency* or sometimes *Betz' law*.

The obvious question is how close are modern wind turbine rotors to the 59.3% Betz limit? Under the best operating conditions, they can approach 80% of that limit, which puts them in the range of about 45–50% efficiency in converting the power in the wind into the power of a rotating generator shaft.

For a given wind speed, rotor efficiency is a function of the rate at which the rotor turns. If the rotor turns too slowly, the efficiency drops off since the blades are letting too much wind pass by unaffected. If the rotor turns too fast, efficiency is reduced as the turbulence caused by one blade increasingly affects the blade that follows. The usual way to illustrate rotor efficiency is to present it as a function of its *tip speed ratio* (TSR). The TSR is the speed at which the outer tip of the blade is moving divided by the wind speed

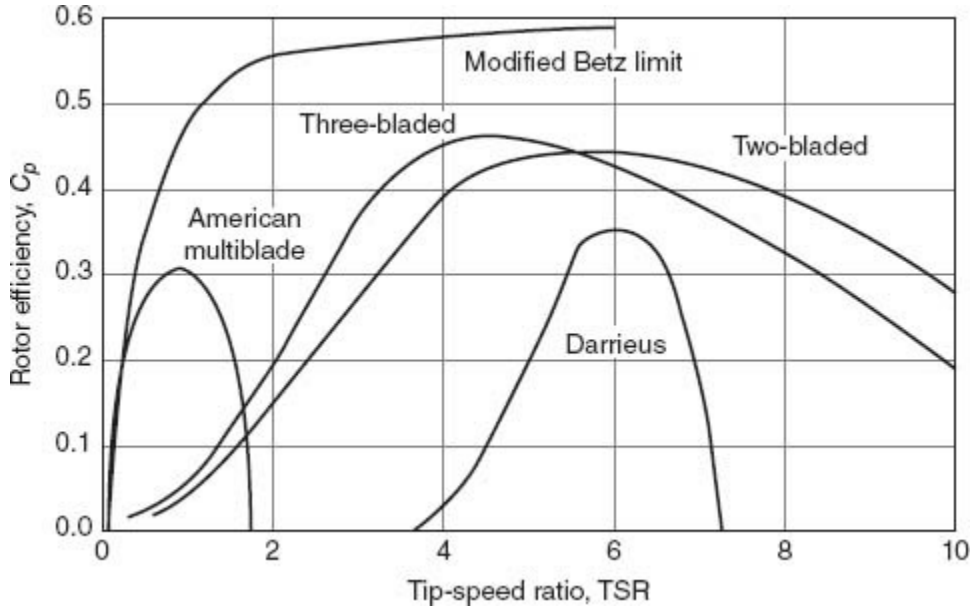
$$\text{Tip speed ratio (TSR)} = \frac{\text{Rotor tip speed}}{\text{Upwind wind speed}} = \frac{\text{rpm} \times \pi D}{60v} \tag{7.30}$$

where rpm is revolutions per minute for the rotor, D is the rotor diameter (m), and v is wind speed (m/s) upwind of the turbine.

A plot of idealized rotor efficiency for various rotor types versus TSR is given in Figure 6.11. The American multiblade spins relatively slowly, with an optimal TSR around 1.0 and maximum efficiency just over 30%. The two- and three-blade rotors spin much faster, with optimum TSR in the 4–6 range and maximum efficiencies of roughly 40–50%. Also shown is a line corresponding to Betz efficiency modified to account for the swirling whirlpool impact that the blades impart on the wind as it passes through the turbines, which Betz did not include, as well as the fact that a slowly turning rotor does not intercept all of the wind, which reduces the maximum possible efficiency to something below the Betz limit.

As shown in Figure 7.18, modern wind turbines operate best when their TSR is in the range of around 4–6, meaning the tip of a blade is moving four to six times the wind speed. Ideally, then, for maximum efficiency, turbine blades should change their speed as the wind speed changes, which is one of the key reasons that the variable-speed generators described in Section 7.3 can be so effective.

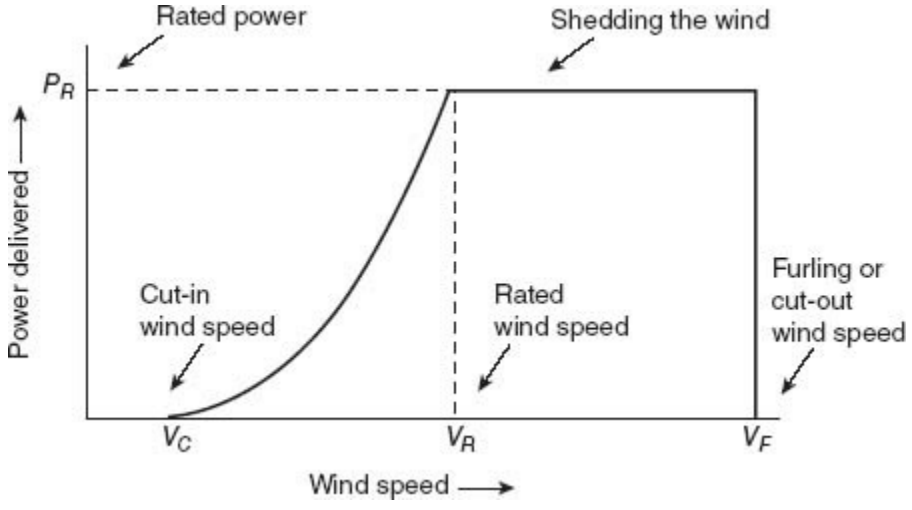
FIGURE 7.18 Rotors with fewer blades reach their optimum efficiency at higher rotational speeds.



7.5.2 Idealized Wind Turbine Power Curve

One of the key pieces of information that manufacturers provide for their wind turbines is a graph showing the relationship between wind speed and electrical power expected from the complete system, including blades, gearbox, and generator. A somewhat idealized power curve is shown in Figure 7.19.

FIGURE 7.19 Idealized power curve. No power is generated at wind speeds below V_C; at wind speeds between V_R and V_F, the output is equal to the rated power of the generator; above V_F the turbine is shut down.



Cut-in wind speed: Low speed winds may not have enough power to overcome friction in the drive train of the turbine, and even if this does happen and the generator is rotating, the electrical power generated may not be enough to offset the power required by the generator field windings. The cut-in wind speed V_C is the minimum needed to generate net power. Since no power is generated at wind speeds below V_C that portion of the wind's energy is wasted. Fortunately, there is not much energy in those low speed winds anyway, so usually not much is lost.

Rated wind speed: As velocity increases above the cut-in wind speed, the power delivered by the generator in the idealized curve rises as the cube of wind speed. When winds reach the rated wind speed V_R, the generator deliverers as much power as it is designed for. Above V_R, there must be some way to shed some of the wind's power or else the generator may be damaged.

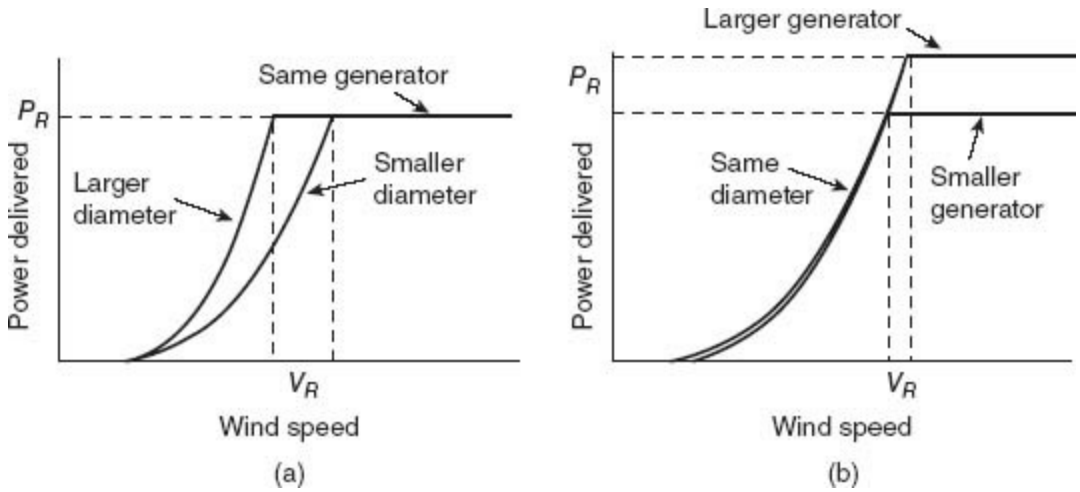
Section 7.2 described three blade-design approaches to shedding power. For pitch-controlled turbines, a hydraulic system slowly rotates the blades about their axes, turning them a few degrees at a time to reduce or increase their efficiency as conditions dictate. The strategy is to reduce the blade's angle of attack when winds are high. For passive stall-controlled machines, the blades are carefully designed to automatically reduce efficiency when winds are excessive. With the active stall control scheme, the blades rotate just as they do in the pitch-control approach, but instead of reducing the blades' angle of attack in high winds, it is increased to induce stall.

Cut-out or furling wind speed: At some point, the wind is so strong that there is real danger to the wind turbine. At this wind speed V_F, called the cut-out wind speed or the furling wind speed ("furling" is the term used in sailing to describe the practice of folding up the sails when winds are too strong), the machine must be shut down. Above V_F mechanical brakes lock the rotor shaft in place, so output power is zero.

7.5.3 Real Power Curves

The idealized power curve of Figure 7.19 provides a convenient framework within which to consider the tradeoffs between rotor diameter and generator size as ways to increase the energy delivered by a wind turbine. As shown in Figure 7.20a, increasing the rotor diameter, while keeping the same generator, shifts the power curve toward the left so that rated power is reached at a lower wind speed. This strategy increases output power for lower speed winds. On the other hand, keeping the same rotor but increasing the generator size allows the power curve to continue upward to the new rated power. For lower speed winds, there is not much change, but in an area with higher wind speeds, increasing the generator rated power is a good strategy.

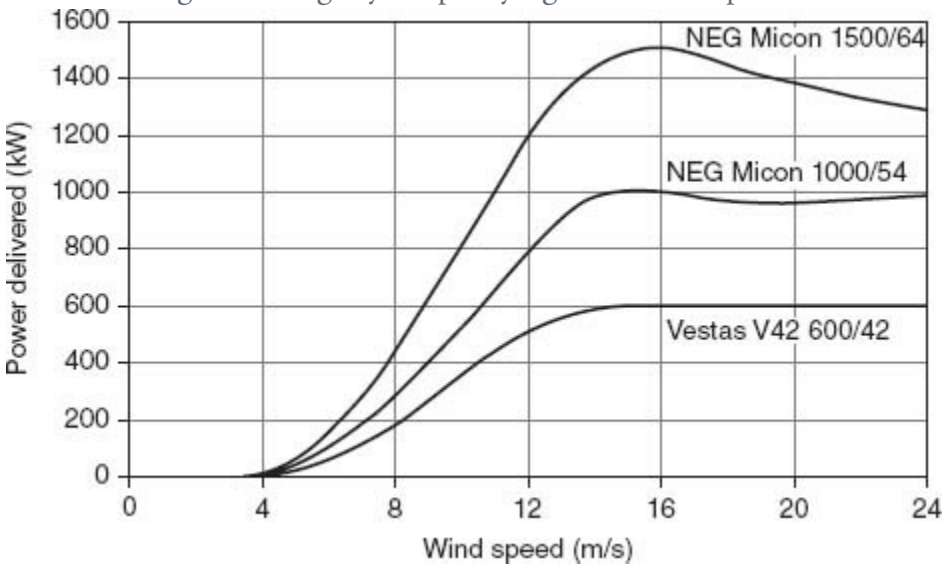
FIGURE 7.20 (a) Increasing rotor diameter reduces the rated wind speed, emphasizing lower speed winds. (b) Increasing the generator size increases rated power, emphasizing higher wind speeds.



Manufacturers often offer a line of turbines with various rotor diameters and generator ratings so that customers can best match the distribution of wind speeds with an appropriate machine. In areas with relatively low wind speeds, a larger rotor diameter may be called for. In areas with relatively high wind speeds, it may be better to increase the generator rating.

Figure 7.21 shows actual power curves for three wind turbines: the NEG Micon (now Vestas) 1500/64, with rated power 1500 kW and rotor diameter 64 m; the NEG Micon 1000/54; and the Vestas V42 600/42. Their resemblance to the idealized power curve is apparent, with most of the discrepancy resulting from the inability of wind-shedding techniques to precisely control output when winds exceed the rated wind speed. This is most pronounced in passive stall-controlled rotors. Note how the rounding of the curve in the vicinity of the rated power makes it difficult to determine what an appropriate value of the rated wind speed V_R should be. As a result, rated wind speed is used less often these days as part of the turbine product literature.

FIGURE 7.21 Showing the ambiguity in specifying rated wind speed for turbines.



Example 7.4 Matching Generators and Rotors. An 82-m, 1.65-MW, fixed-speed wind turbine has a rated wind speed of 13 m/s. It is connected through a gearbox to a 4-pole, 60-

Hz synchronous generator.

a. What gear ratio should the gearbox have if the turbine is designed to turn at 14.4 rpm?

b. What is the tip speed ratio when the winds are blowing at the rated wind speed?

c. What is the overall efficiency of the machine (including rotor, gearbox, generator, etc.) at its rated wind speed?

d. The power curve for this machine indicates that it will deliver half of its rated output in 8 m/s winds. What is its efficiency and TSR at that wind speed?

e. What would be the TSR with 8 m/s winds if the generator could switch from four poles to six?

Solution

a. From Equation 7.1 the generator shaft spins at

$$N = \frac{120f}{p} = \frac{120 \times 60}{4} = 1800\,\text{rpm}$$

So the gear ratio should be

$$\text{Gear ratio} = \frac{\text{Generator speed}}{\text{Rotor speed}} = \frac{1800\,\text{rpm}}{14.4\,\text{rpm}} = 125$$

b. The TSR at the 13 m/s rated wind speed:

$$\text{TSR} = \frac{82\pi\ \text{m/rev} \times 14.4\,\text{rev/min}}{13\,\text{m/s} \times 60\,\text{s/min}} = 4.76$$

c. Overall efficiency at rated wind speed:

Assuming the standard 1.225 kg/m^3 air density, the power in the wind at 13 m/s is

$$P_w = \frac{1}{2}\rho A v_w^3 = \frac{1}{2} \times 1.225 \times \frac{\pi}{4} \times 82^2 \times 13^3 = 7106 \times 10^3\,\text{W}$$

So the overall efficiency of this 1.65 MW machine is

$$\text{Overall efficiency} = \frac{1650\,\text{kW}}{7106\,\text{kW}} = 23.2\%$$

d. Efficiency and TSR at 8 m/s:

$$P_w = \frac{1}{2} \times 1.225 \times \frac{\pi}{4} \times 82^2 \times 8^3 = 1656 \times 10^3\,\text{W}$$

$$\text{Overall effciency} = \frac{0.5 \times 1650\,\text{kW}}{1656\,\text{kW}} = 49.8\%$$

$$\text{TSR} = \frac{82\pi\ \text{m/rev} \times 14.4\,\text{rev/min}}{8\,\text{m/s} \times 60\,\text{s/min}} = 7.7$$

A glance at Figure 7.18 suggests that this TSR is a bit on the high side.

e. Switching from four- to six-pole operation:

$$N = \frac{120f}{p} = \frac{120 \times 60}{6} = 1200\,\text{rpm}$$

With our 125 gear ratio, the turbine would now spin at

$$\text{Rotor} = 1200\,\text{rpm}/125 = 9.6\,\text{rpm}$$

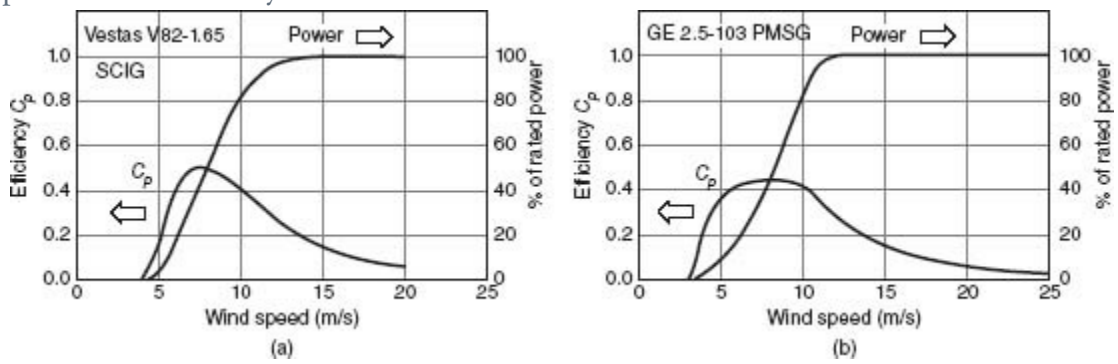
And TSR would be

$$\text{TSR} = \frac{82\pi\ \text{m/rev} \times 9.6\,\text{rev/min}}{8\ \text{m/s} \times 60\ \text{s/min}} = 5.1$$

This looks closer to the optimum range of TSRs.

Example 7.4 outlines the process by which an overall efficiency curve can be generated from a manufacturer's power curve. Figure 7.22 shows power and efficiency curves for two quite different wind turbines. One has a fixed-speed, SCIG and the other is a variable-speed, PMSG design, with a full-capacity power converter. Note how peaked the efficiency curve is for the SCIG, which is a reflection of its limited ability to efficiently deal with variable wind speeds. The PMSG on the other hand has rather consistent efficiency up to its rated wind speed, after which, of course, it spills wind and efficiency declines.

FIGURE 7.22 Power curves and calculated efficiency. (a) Vestas V82-1.65, active-stall, squirrel-cage induction generator (SCIG). (b) GE 2.5-103, permanent-magnet, synchronous generator (PMSG) with full-capacity power converter. Note the different shapes of their efficiency curves.



7.5.4 IEC Wind Turbine Classifications

Wind turbine specifications not only provide data relating to the power curve itself, but also include what sort of wind regimes they have been designed to be able to withstand. The International Electrotechnical Commission (IEC) is a nongovernmental organization that establishes safety standards for a wide range of electric technologies, including wind energy systems.

The IEC 61400 series of standards covers a wide range of safety and performance issues for the wind turbine industry including such things as mechanical loads, acoustics, power quality, construction safety, and so forth. Wind turbines are specified to meet IEC standards within a particular classification scheme that is based on average wind speed, extreme 50-year wind speed and wind gusts, and turbulence intensity. The turbulence intensity is the ratio of the standard deviation of wind speed to the 10-min mean wind

speed. Table 7.3 shows how wind turbine class is organized around these parameters.

TABLE 7.3 IEC 61400-1 Wind Classifications

Wind Turbine Generator Class	I	II	III
V_{avg} Average wind speed at hub height (m/s)	10.0	8.5	7.5
V_{ref} 50-year maximum 10-minute wind speed (m/s)	50	42.5	37.5
V_{e50} 50-year extreme 3-second gusts (m/s)	70	59.5	53.5
Turbulence Class A	16%	16%	16%
Turbulence Class B	14%	14%	14%
Turbulence Class C	12%	12%	12%

Wind turbine manufacturers will typically offer different models of turbines designed for different hub heights and IEC classifications. For example, design loads for an IEC Class IIA turbine will be higher than those for a similar model designed for less challenging Class IIIB conditions. The Class IIIB turbine might have the very same generator, but with a larger rotor, which means it will have a higher capacity factor (CF) and deliver more energy.

7.5.5 Measuring the Wind

The starting point for wind prospecting is to gather enough site data to at least be able to estimate average wind speed. That can most easily be done with a simple cup anemometer, which spins at a rate proportional to the wind speed. Most of the world's long-term wind data are based on just these or similar propeller-type devices. But, with modern turbines, much more detailed wind information is needed to design them for safe operation and to more accurately predict their performance and financial value. Two more advanced types of anemometers are now in common use for modern, utility-scale wind systems. One is based on sonic measurements and the other relies on the Doppler effect (Fig. 7.23).

FIGURE 7.23 Three types of anemometers.



Sonic anemometers send three ultrasonic sound waves across their measurement space and then measure the time differential at which the sounds arrive at opposing sensors. Since the speed of sound increases or decreases depending on whether it is moving with the wind or against it, that time differential makes it possible to calculate both the speed and direction of the wind through which the sound passes. Thus, for example, if there is no wind at all, the sound waves all arrive at the three sensors at the same time. They can collect rapidly changing, real-time wind data, in two or three dimensions, which makes them well suited for turbulence measurements. They can be mounted on meteorological towers (met towers) as well as right on the nacelle of the wind turbine itself.

Ground-mounted, sonic detection and ranging (SODAR) anemometers transmit pulses

of sound into the air. The length of time required for a pulse to bounce off atmospheric particles and make its way back to a receiver provides information on the altitude of the reflecting particles. If the particles are moving, a Doppler effect frequency shift in the received signals will detect that motion. By establishing three sonic cones above the transmitter, a vector analysis of the received signals makes it possible to calculate horizontal and vertical wind speeds as well as the direction. Light detection and ranging (LIDAR) systems are similar but use light instead of sound. SODAR and LIDAR anemometers are most useful for measuring wind speeds at elevations typical of the range intercepted by the swept area of large turbines; that is, from roughly 50–200 m. Most meteorological towers on which more conventional anemometers are typically mounted are usually less than 60 m in height.

7.6 AVERAGE POWER IN THE WIND

Having presented the equations for *power* in the wind and described the essential components of a wind turbine system, it is time to put the two together to determine how much *energy* might be expected from a wind turbine in various wind regimes.

The cubic relationship between power in the wind and wind velocity tells us that we cannot determine the average power in the wind by simply substituting average wind speed into Equation 7.7. We saw that in Example 7.1. We can begin to explore this important characteristic of wind by rewriting Equation 7.7 in terms of average values

$$P_{\text{avg}} = \left(\frac{1}{2}\rho A v^3\right)_{\text{avg}} = \frac{1}{2}\rho A \left(v^3\right)_{\text{avg}} \tag{7.31}$$

In other words, we need to find the average value of the cube of velocity. To do so will require that we introduce some statistics.

7.6.1 Discrete Wind Histogram

We are going to have to work with the mathematics of probability and statistics, which may be new territory for some. To help motivate our introduction to this material, we will begin with some simple concepts involving discrete functions involving wind speeds, then we can move on to more generalized continuous functions.

What do we mean by the average of some quantity? Suppose, for example, we collect some wind data at a site and then want to know how to figure out the average wind speed during the measurement time. The average wind speed can be thought of as the total meters, kilometers, or miles of wind that have blown past the site, divided by the total time that it took to do so. Suppose, for example, that during a 10-h period, there were 3 h of no wind, 3 h at 5 mph, and 4 h at 10 mph. The average wind speed would be

$$v_{avg} = \frac{\text{Miles of wind}}{\text{Total hours}} = \frac{3\,\text{h} \cdot 0\,\text{mile/h} + 3\,\text{h} \cdot 5\,\text{mile/h} + 4\,\text{h} \cdot 10\,\text{mile/h}}{3 + 3 + 4\,\text{h}}$$

$$= \frac{55\,\text{miles}}{10\,\text{h}} = 5.5\,\text{mph} \tag{7.32}$$

By regrouping some of the terms in Equation 7.32, we could also think of this as having no wind 30% of the time, 5 mph 30% of the time, and 10 mph 40% of the time

(7.33)

$$v_{avg} = \left(\frac{3\,\text{h}}{10\,\text{h}}\right) \times 0\,\text{mph} + \left(\frac{3\,\text{h}}{10\,\text{h}}\right) \times 5\,\text{mph} + \left(\frac{4\,\text{h}}{10\,\text{h}}\right) \times 10\,\text{mph} = 5.5\,\text{mph}$$

We could write Equations 7.32 and 7.33 in a more general way as

$$v_{avg} = \frac{\sum_i [v_i \cdot (\text{hours at } v_i)]}{\sum \text{hours}} = \sum_i [v_i \cdot (\text{fraction of hours at } v_i)] \tag{7.34}$$

Finally, if those winds were typical, we could say that the probability that there is no wind is 0.3, the probability that it is blowing 5 mph is 0.3, and the probability it is 10 mph is 0.4. This lets us describe the average value in probabilistic terms

$$v_{avg} = \sum_i [v_i \cdot \text{probability}\,(v = v_i)] \tag{7.35}$$

We know from Equation 7.31 that the quantity of interest in determining average power in the wind is not the average value of v, but the average value of v^3. The averaging process is exactly the same as our simple example above, yielding the following:

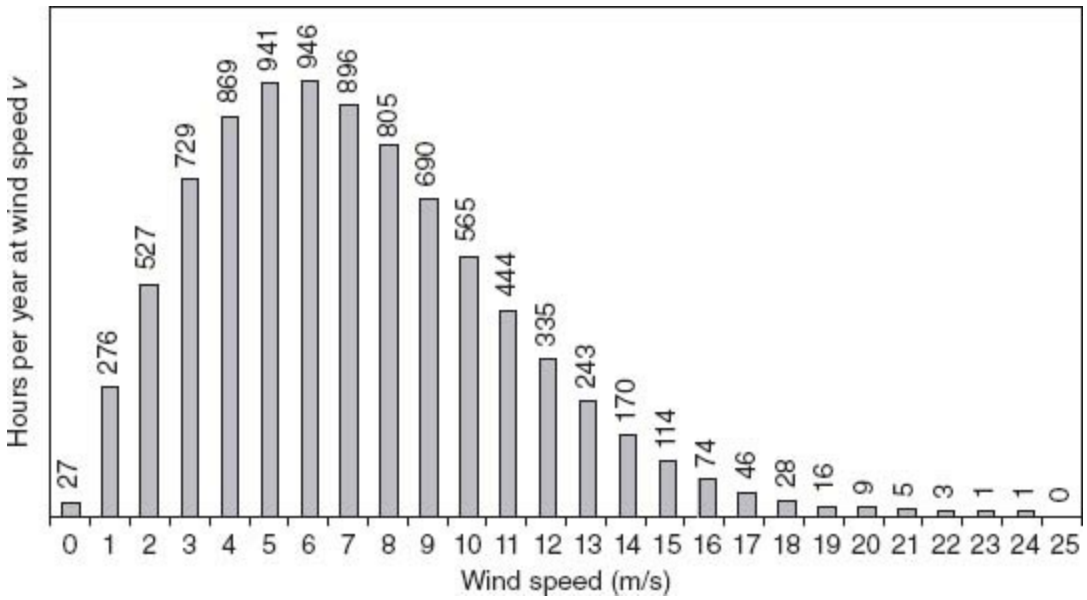
$$(v^3)_{avg} = \frac{\sum_i [v_i^3 \cdot (\text{hours at } v_i)]}{\sum \text{hours}} = \sum_i [v_i^3 \cdot (\text{fraction of hours at } v_i)] \tag{7.36}$$

Or, in probabilistic terms,

$$(v^3)_{avg} = \sum_i [v_i^3 \cdot \text{probability}\,(v = v_i)] \tag{7.37}$$

Now, let us apply Equation 7.37 to figuring out the average power in a wind regime. Begin by imagining that we have an anemometer that accumulates site data on hours per year of wind blowing at 1 m/s (0.5–1.5 m/s), at 2 m/s (1.5–2.5 m/s), and so on. An example table of a histogram of such data is shown in Figure 7.24. The following example shows how to use a spreadsheet approach to figure out the average power in these winds.

FIGURE 7.24 An example of a wind histogram showing hours that the wind blows in each wind speed bracket.



Example 7.5 Average Power in the Wind. Using the data given in Figure 7.24, find the average wind speed and the average power in the wind (W/m^2). Assume the standard air density of 1.225 kg/m^3. Compare the result with that which would be obtained if the average power were miscalculated using just the average wind speed.

Solution. We need to set up a spreadsheet to determine average wind speed v and the average value of v^3. Let us do a sample calculation of one line of a spreadsheet using 805 h/yr at 8 m/s:

$$\text{Fraction of the hours at 8 m/s} = \frac{805\ \text{h/yr}}{24\ \text{h/d} \times 365\ \text{d/yr}} = 0.0919$$

$$[v_8 \cdot (\text{Fraction of the hours at 8 m/s})] = 8 \times 0.0919 = 0.735$$

$$\left[(v_8)^3 \cdot (\text{Fraction of the hours at 8 m/s})\right] = 8^3 \times 0.0919 = 47.05$$

The rest of the spreadsheet to determine average wind power using Equation 7.31 is as follows:

	Daytona Beach, FL						Latitude 29.18° N						
Tilt	Jan	Feb	Mar	Apr	May	Jun	July	Aug	Sept	Oct	Nov	Dec	Year
Lat − 15	3.8	4.5	5.5	6.4	6.4	6.0	5.9	5.8	5.2	4.7	4.1	3.6	5.2
Lat	4.3	4.9	5.7	6.3	6.0	5.5	5.5	5.6	5.3	5.0	4.6	4.1	5.2
Lat + 15	4.6	5.1	5.6	5.9	5.4	4.8	4.9	5.1	5.1	5.1	4.8	4.4	5.1
90	3.9	3.8	3.6	2.9	2.1	1.8	1.9	2.4	3.0	3.6	4.0	3.9	3.1
1-Axis (Lat)	5.2	6.0	7.2	8.3	7.9	7.1	7.1	7.0	6.5	6.1	5.5	4.9	6.6
Temp. (°C)	20.0	20.8	23.8	26.7	29.2	31.1	32.1	31.7	30.4	27.5	24.2	21.3	26.6

	Miami, FL						Latitude 25.80° N						
Tilt	Jan	Feb	Mar	Apr	May	Jun	July	Aug	Sept	Oct	Nov	Dec	Year
Lat − 15	4.1	4.7	5.5	6.2	5.9	5.5	5.7	5.6	5.1	4.7	4.2	3.9	5.1
Lat	4.7	5.2	5.7	6.1	5.6	5.1	5.4	5.5	5.1	5.1	4.7	4.5	5.2
Lat + 15	5.0	5.4	5.6	5.7	5.0	4.5	4.8	5.0	4.9	5.1	4.9	4.9	5.1
90	4.1	3.9	3.4	2.6	1.9	1.6	1.7	2.1	2.7	3.5	3.9	4.1	3.0
1-Axis (Lat)	5.7	6.4	7.2	7.8	7.2	6.3	6.7	6.7	6.2	6.1	5.6	5.4	6.5
Temp. (°C)	24.0	24.7	26.2	28.0	29.6	30.9	31.7	31.7	31.0	29.2	26.9	24.8	28.2

	Tallahassee, FL						Latitude 30.38° N						
Tilt	Jan	Feb	Mar	Apr	May	Jun	July	Aug	Sept	Oct	Nov	Dec	Year
Lat − 15	3.6	4.3	5.2	6.1	6.2	6.0	5.7	5.6	5.3	5.0	4.1	3.4	5.0
Lat	4.0	4.7	5.4	6.0	5.9	5.6	5.4	5.4	5.3	5.4	4.6	4.0	5.1
Lat + 15	4.3	4.9	5.3	5.6	5.2	4.9	4.7	4.9	5.1	5.5	4.8	4.2	5.0
90	3.6	3.7	3.4	2.9	2.2	1.9	2.0	2.4	3.1	4.0	4.0	3.7	3.1
1-Axis (Lat)	4.8	5.8	6.7	7.8	7.7	7.1	6.8	6.8	6.6	6.7	5.5	4.6	6.4
Temp. (°C)	17.2	19.1	23.1	26.9	30.2	32.7	32.9	32.8	31.4	27.5	22.8	18.8	26.3

	Atlanta, GA						Latitude 33.65° N						
Tilt	Jan	Feb	Mar	Apr	May	Jun	July	Aug	Sept	Oct	Nov	Dec	Year
Lat − 15	3.4	4.2	5.1	6.0	6.2	6.3	6.1	5.9	5.3	4.9	3.8	3.2	5.0
Lat	3.8	4.6	5.3	5.8	5.8	5.8	5.7	5.7	5.4	5.2	4.2	3.7	5.1
Lat + 15	4.1	4.7	5.1	5.4	5.2	5.1	5.0	5.2	5.1	5.3	4.9	3.9	4.9
90	3.5	3.7	3.5	3.0	2.4	2.2	2.2	2.7	3.2	4.0	3.8	3.5	3.1
1-Axis (Lat)	4.5	5.5	6.6	7.6	7.7	7.6	7.3	7.2	6.7	6.4	5.0	4.3	6.4
Temp. (°C)	10.2	12.8	17.9	22.6	26.4	29.9	31.1	30.6	27.7	22.6	17.4	12.2	21.8

	Savannah, GA						Latitude 32.13° N						
Tilt	Jan	Feb	Mar	Apr	May	Jun	July	Aug	Sept	Oct	Nov	Dec	Year
Lat − 15	3.5	4.3	5.2	6.1	6.2	6.1	6.0	5.6	5.1	4.8	3.9	3.4	5.0
Lat	4.0	4.7	5.4	6.0	5.8	5.7	5.6	5.4	5.1	5.1	4.4	3.9	5.1
Lat + 15	4.3	4.8	5.3	5.6	5.2	4.9	4.9	5.0	4.9	5.2	4.6	4.2	4.9
90	3.7	3.8	3.6	3.0	2.3	2.0	2.1	2.5	3.0	3.8	3.9	3.7	3.1
1-Axis (Lat)	4.8	5.7	6.8	7.9	7.7	7.4	7.1	6.8	6.3	6.3	5.3	4.5	6.4
Temp. (°C)	15.4	16.9	21.2	25.3	28.9	31.6	32.8	32.1	29.6	25.3	21.1	16.8	24.7

The average wind speed is

$$v_{\text{avg}} = \sum_i [v_i \text{ (Fraction of hours at } v_i)] = 7.0 \text{ m/s}$$

The average value of v^3 is

$$\left(v^3\right)_{\text{avg}} = \sum_i \left[(v_i)^3 \cdot (\text{Fraction of hours at } v_i)\right] = 653.24$$

The average power in the wind on a per unit of area basis is

$$P_{\text{avg}}/A = \frac{1}{2}\rho\left(v^3\right)_{\text{avg}} = 0.5 \times 1.225 \times 653.24 = 400\ \text{W/m}^2$$

If we had miscalculated average power in the wind by using the *average* wind speed of 7 m/s in Equation 7.7 we would have found:

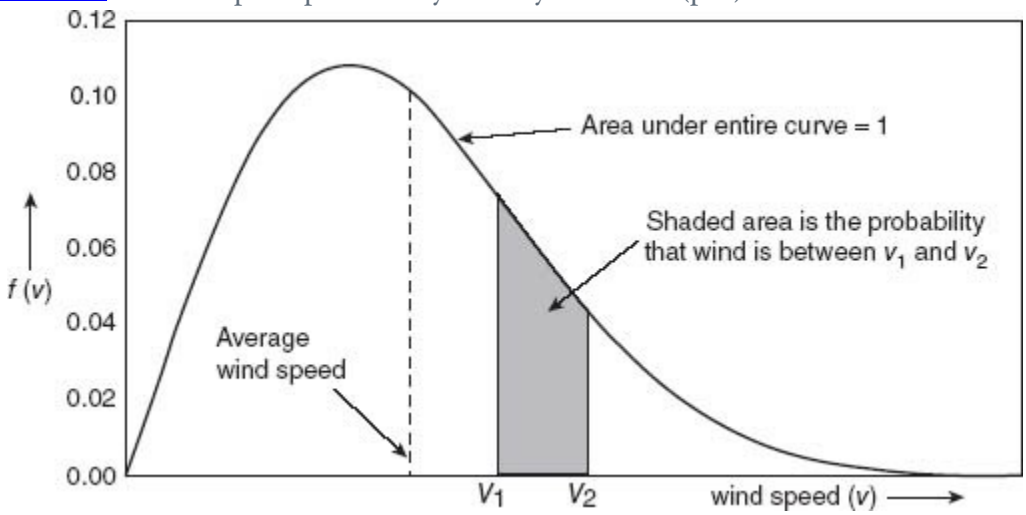
$$P_{\text{avg}}/A(\text{WRONG}) = \frac{1}{2}\rho\left(v_{\text{avg}}\right)^3 = 0.5 \times 1.225 \times 7.0^3 = 210\ \text{W/m}^2$$

In the above example, the ratio of the average wind power calculated correctly using $(v^3)_{\text{avg}}$ to that found when the average velocity is (mis)used, is 400/210 = 1.9. That is, the correct answer is nearly twice as large as the power found when average wind speed is substituted into the fundamental wind power equation (Eq. 7.7). In the next section we will see that this conclusion is always the case when certain probability characteristics for the wind are assumed.

7.6.2 Wind Power Probability Density Functions

The type of information displayed in the discrete wind speed histogram in Figure 7.24 is most often presented as a continuous function, called a probability density function (pdf). The defining features of a pdf, such as that shown in Figure 7.25, are that the area under the curve is equal to unity, and the area under the curve between any two wind speeds equals the probability that the wind is between those two speeds.

FIGURE 7.25 A wind speed probability density function (pdf).



Expressed mathematically,

$f(v)$ = wind speed probability density function

$$\text{Probability}\,(v_1 \le v \le v_2) = \int_{v1}^{v2} f(v)dv \tag{7.38}$$

$$\text{Probability}\,(0 \le v \le \infty) = \int_0^{\infty} f(v)dv = 1 \tag{7.39}$$

If we want to know the number of hours per year that the wind blows between any two wind speeds, simply multiply Equation 7.38 by 8760 h/yr:

$$\text{Hours/yr}\,(v_1 \le v \le v_2) = 8760 \int_{v_1}^{v_2} f(v)dv \tag{7.40}$$

The average wind speed can be found using a pdf in much the same manner as it was found for the discrete approach to wind analysis (Eq. 7.35):

$$v_{\text{avg}} = \int_0^{\infty} v \cdot f(v)dv \tag{7.41}$$

The average value of the cube of velocity, also analogous to the discrete version in Equation 7.36, is

$$(v^3)_{\text{avg}} = \int_0^{\infty} v^3 f(v)dv \tag{7.42}$$

7.6.3 Weibull and Rayleigh Statistics

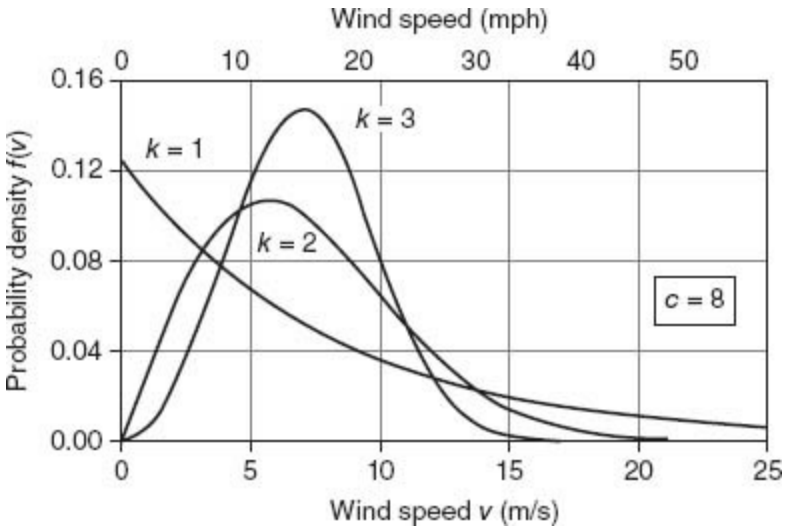
A quite general expression that is often used as the starting point for characterizing the statistics of wind speeds is called the *Weibull probability density function*:

$$f(v) = \frac{k}{c}\left(\frac{v}{c}\right)^{k-1} \exp\left[-\left(\frac{v}{c}\right)^{k}\right] \quad \text{Weibull pdf} \tag{7.43}$$

where k is called the *shape parameter*, and c is called the *scale parameter*.

As the name implies, the shape parameter k changes the look of the pdf. For example, the Weibull pdf with a fixed scale parameter (c = 8) but varying shape parameters k is shown in Figure 7.26. For k = 1, it looks like an exponential decay function; it would probably not be a good site for a wind turbine since most of the winds are at such low speeds. For k = 2, the wind blows fairly consistently, but there are periods during which the winds blow much harder than the more typical speeds bunched near the peak of the pdf. For k = 3, the function resembles the familiar bell-shaped curve, and the site would be one where the winds are almost always blowing and doing so at a fairly constant speed, such as might be expected of trade winds.

FIGURE 7.26 Weibull probability density function with shape parameter k = 1, 2, and 3 (with scale parameter c = 8).



Of the three Weibull pdfs in Figure 7.26, intuition probably would lead us to think the middle one, for which $k = 2$, is the most realistic for a likely wind turbine site; that is, it has winds that are mostly pretty strong, with periods of low wind and some really good, high speed winds as well. In fact, when little detail is known about the wind regime at a site, the usual starting point is to assume $k = 2$. When the shape parameter k is equal to 2, the pdf is given its own name, the *Rayleigh probability density function*.

$$f(v) = \frac{2v}{c^2}\exp\left[-\left(\frac{v}{c}\right)^2\right] \quad \text{Rayleigh pdf} \tag{7.44}$$

There is a direct relationship between scaling factor c and average wind speed $\bar{v}$. Substituting the Rayleigh pdf into Equation 7.41, and referring to a table of standard integrals, results in

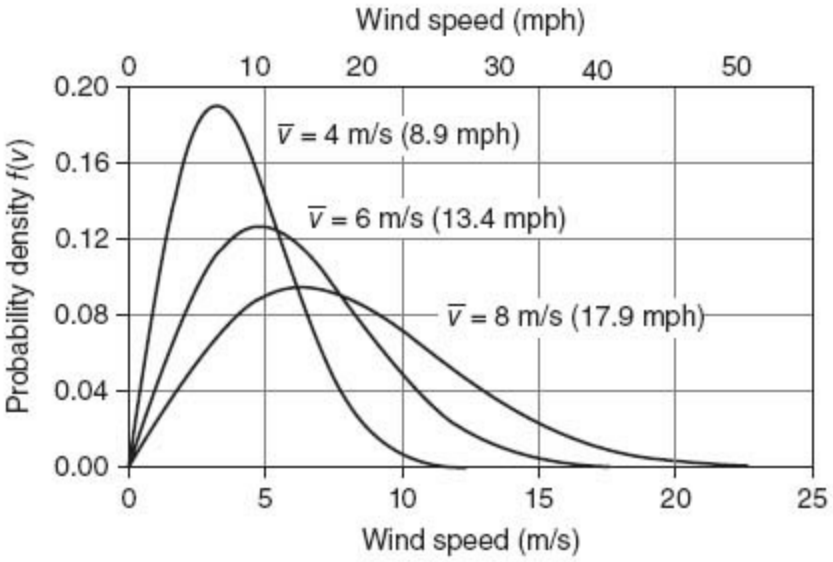
$$\bar{v} = \int_0^\infty v \cdot f(v)\mathrm{d}v = \int_0^\infty 2\left(\frac{v}{c}\right)^2 \exp\left[-\left(\frac{v}{c}\right)^2\right] = \frac{\sqrt{\pi}}{2}c \tag{7.45}$$

Even though Equation 7.45 was derived for Rayleigh statistics, for which $k = 2$, it is quite accurate for a range of shape factors k from about 1.5 to 4 (Johnson, 1985). Substituting Equation 7.45 into Equation 7.44 gives us a more intuitive way to write the Rayleigh pdf in terms of average wind speed $\bar{v}$:

$$f(v) = \frac{\pi v}{2\bar{v}^2}\exp\left[-\frac{\pi}{4}\left(\frac{v}{\bar{v}}\right)^2\right] \tag{7.46}$$

The impact of changing the average wind speed for a Rayleigh pdf is shown in Figure 7.27. As can be seen, higher average wind speeds flatten the curves and shift them toward the right.

FIGURE 7.27 The Rayleigh probability density function with varying average wind speeds.



7.6.4 Average Power in the Wind with Rayleigh Statistics

The starting point for wind prospecting is to gather enough site data to at least be able to estimate average wind speed. That can most easily be done with a simple anemometer such as the one shown in Figure 7.23. Dividing miles or meters of wind by elapsed time gives an average wind speed. These very simple devices measuring average wind speed, coupled with the assumption that the wind speed distribution follows Rayleigh statistics, enables us to make a pretty good estimate of the average power in the wind.

Substituting the Rayleigh pdf (Eq. 7.46) into Equation 7.42 lets us find the average value of the cube of wind speed:

$$(v^3)_{\text{avg}} = \int_0^\infty v^3 \cdot f(v)dv = \int_0^\infty v^3 \cdot \frac{\pi v}{2\bar{v}^2} \exp\left[-\frac{\pi}{4}\left(\frac{v}{\bar{v}}\right)^2\right]dv \tag{7.47}$$

which with the help of a handy table of integrals, gives us the following very important result:

$$(v^3)_{\text{avg}} = \frac{6}{\pi} \cdot \bar{v}^3 \approx 1.91\bar{v}^3 \tag{7.48}$$

Equation 7.48 is very interesting and very useful. It says that if we assume Rayleigh statistics then the average of the cube of wind speed is just 1.91 times the average wind speed cubed. Therefore, assuming Rayleigh statistics, we can rewrite the fundamental relationship for average power in the wind as

$$\bar{P} = \frac{6}{\pi} \cdot \left(\frac{1}{2}\rho A\bar{v}^3\right) \text{ (Rayleigh assumptions)} \tag{7.49}$$

That is, with Rayleigh statistics, *the average power in the wind is equal to the power found at the average wind speed multiplied by 6/π or 1.91.*

Example 7.6 Average Power in the Wind. A 10-m-high anemometer finds the average

wind speed at that height to be 6 m/s. Estimate the average power in the wind at a height of 50 m. Assume Rayleigh statistics, a standard friction coefficient α = 1/7, and standard air density ρ = 1.225 kg/m^3. Repeat for a taller 80-m height.

Solution. We first adjust the winds at 10 m to those expected at 50 m using Equation 7.18:

$$\bar{v}_{50} = \bar{v}_{10}\left(\frac{H_{50}}{H_{10}}\right)^{\alpha} = 6\left(\frac{50}{10}\right)^{1/7} = 7.55\ \text{m/s}$$

So, using Equation 7.49, per unit of area the average power in the wind would be

$$\bar{P} = \frac{6}{\pi} \times \left(\frac{1}{2}\rho A \bar{v}^3\right) = \frac{6}{\pi}\left(\frac{1}{2} \times 1.225 \times 7.55^3\right) = 504\ \text{W/m}^2$$

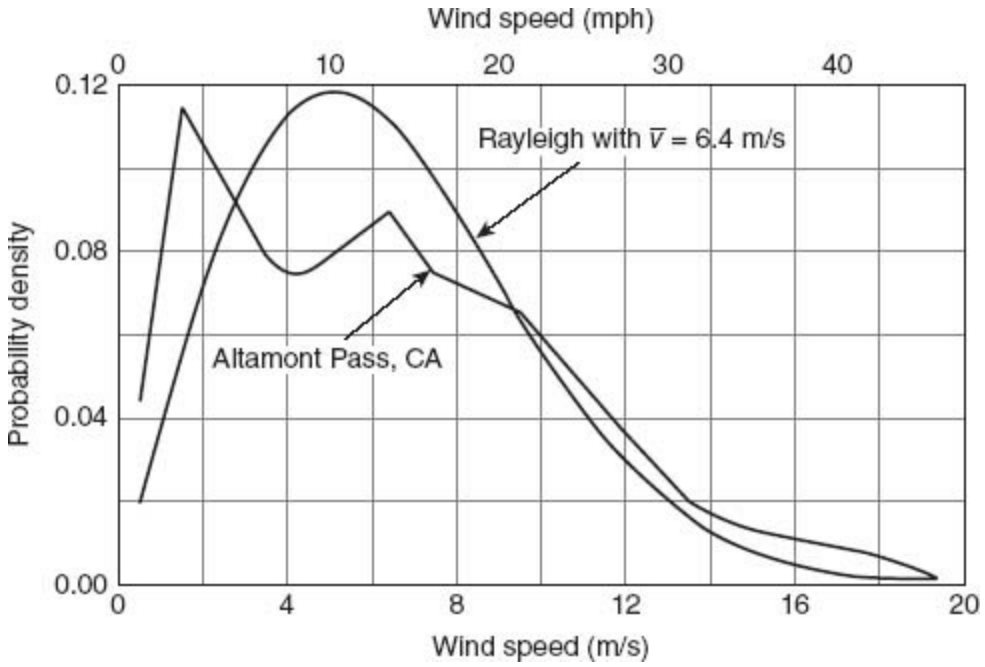
Let us take a slightly different approach to finding the power at 80 m. From Equation 7.20 we can write

$$\bar{P}_{10} = \frac{6}{\pi} \cdot \frac{1}{2} \cdot 1.225 \cdot 6^3 = 252.67\ \text{W/m}^2$$

$$\bar{P}_{80} = \bar{P}_{10}\left(\frac{H_{80}}{H_{10}}\right)^{3\alpha} = 252.67\left(\frac{80}{10}\right)^{3\times 1/7} = 616\ \text{W/m}^2$$

Lest we become too complacent about the importance of gathering real wind data rather than relying on Rayleigh assumptions, consider Figure 7.28, which shows the pdf for winds at one of California's original major wind farms, Altamont Pass. Altamont Pass is located roughly midway between San Francisco (on the coast) and Sacramento (inland valley). In the summer months, rising hot air over Sacramento draws cool surface air through Altamont Pass, creating strong summer afternoon winds, but in the winter there is not much of a temperature difference and the winds are generally very light unless a storm is passing through. The wind speed pdf for Altamont clearly shows the two humps that correspond to not much wind for most of the year, along with very high winds on hot, summer afternoons. For comparison, a Rayleigh pdf with the same annual average 10-m wind speed as Altamont (6.4 m/s) has also been drawn in the figure.

FIGURE 7.28 Probability density function for wind at Altamont Pass, CA., and a Rayleigh pdf with the same average wind speed of 6.4 m/s. From Cavallo et al. (1993).



7.6.5 Wind Power Classifications

The procedure demonstrated in Example 7.6 is commonly used to estimate average wind power density (W/m^2) in a region. That is, measured values of average wind speed using an anemometer located 10 m above the ground are used to estimate average wind speed and power density at a height 50 m above the ground. Rayleigh statistics, a friction coefficient of 1/7, and sea-level air density at 0°C of 1.225 kg/m^3 are assumed. A standard wind power classification scheme based on these assumptions is given in Table 7.4.

TABLE 7.4 Standard Wind Power Classifications[a]

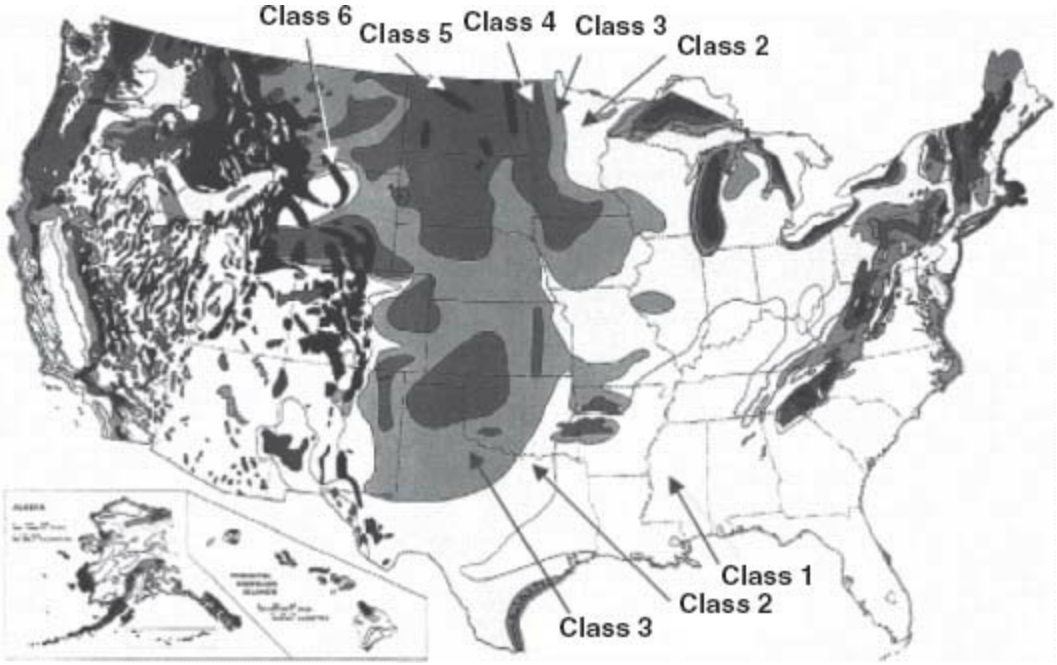
Wind Power Class (50 m)	Average Wind Speed at 10 m (m/s)	Average Wind Speed at 50 m (m/s)	Wind Power Density at 50 m (W/m^2)	Average Wind Speed at 80 m (m/s)	Wind Power Density at 80 m (W/m^2)
1	0–4.4	0–5.5	0–200	0–5.9	0–250
2	4.4–5.1	5.5–6.4	200–300	5.9–6.9	250–380
3	5.1–5.6	6.4–7.0	300–400	6.9–7.5	380–500
4	5.6–6.0	7.0–7.5	400–500	7.5–8.0	500–600
5	6.0–6.4	7.5–8.0	500–600	8.0–8.6	600–750
6	6.4–7.0	8.0–8.8	600–800	8.6–9.4	650–980
7	7.0–9.5	8.8–12	800–2000	9.4–12.8	980–2400

[a]Assumptions include Rayleigh statistics, ground friction coefficient $\alpha = 1/7$, air density 1.225 kg/m^3, 10-m anemometer height and 50-m hub height.

A map of the United States showing contours of equal wind power density at 50-m based on the Table 7.4 assumptions is shown in Figure 7.29. As can be seen, there is a broad band of states stretching from Texas to North Dakota with especially high wind power potential, including large areas with Class 4 or better winds (over 400 W/m^2 at 50 m).

FIGURE 7.29 Average annual wind power density at 50 m elevation. From NREL Wind

Energy Resource Atlas of the United States.



It should be noted that the wind power classifications used in Figure 7.29 were created in the 1980s when the standard hub height for turbines was 50 m. Now that most turbines are at much taller heights, the wind power classifications in which Class 4 winds start at 400 W/m^2 and Class 5 winds start at 500 W/m^2, and so on, have become somewhat ambiguous. At 80 m, for example, the wind power densities in Table 7.4 are roughly one step higher than at 50 m. Should 500 W/m^2 winds at 80 m still be called Class 4 winds? The industry seems to be evolving toward keeping the classification system with a clarification that, for example, says Class 4 winds start at 7 m/s, 400 W/m^2 at 50-m hub height. For other elevations, Equation 7.18 can then be used to adjust the 50-m wind speed to other heights.

7.7 ESTIMATING WIND TURBINE ENERGY PRODUCTION

How much of the energy in the wind can be captured and converted into electricity? The answer depends on a number of factors, including the characteristics of the machine (rotor, gearbox, generator, tower, nearby turbines, controls), the terrain (topography, surface roughness, obstructions) and, of course, the wind regime (speed, height impacts, timing, predictability). It also depends on the motivation behind the question. From a policy perspective, the details of specific turbine characteristics are less important than determining some overall estimates of the potential contributions that the technology might provide. For potential investors, back-of-the envelope calculations to see whether a proposed project merits further investigation may be a sufficient starting point. For engineers, comparing the likely performance of one turbine over another requires a much more carefully done, site-specific analysis.

7.7.1 Wind Speed Cumulative Distribution Function

To predict energy delivered by a wind turbine requires linking the power curve for the machine to a statistical model of the wind regime. Beginning with a probability density function, $f(v)$, recall that the total area under a pdf curve is equal to one, and the area between any two wind speeds is the probability that the wind is between those speeds. Therefore, the probability that the wind is less than some specified wind speed V is given by

$$\text{Probability that } (v \le V) = F(V) = \int_0^V f(v)dv \tag{7.50}$$

The integral $F(V)$ in Equation 7.50 is given a special name: the *cumulative distribution function*. The probability that the wind V is less than 0 is 0, and the probability that the wind is less than infinity is 1, so $F(V)$ has the following constraints:

$$F(V) = \text{probability } v \le V \qquad F(0) = 0 \text{ and } F(\infty) = 1 \tag{7.51}$$

In the field of wind energy, the most important pdf is the Weibull distribution function:

$$f(v) = \frac{k}{c}\left(\frac{v}{c}\right)^{k-1} \exp\left[-\left(\frac{v}{c}\right)^{k}\right] \tag{7.52}$$

The cumulative distribution function for Weibull statistics is therefore

$$F(V) = \text{prob}(v \le V) = \int_0^V \frac{k}{c}\left(\frac{v}{c}\right)^{k-1} \exp\left[-\left(\frac{v}{c}\right)^{k}\right] dv \tag{7.53}$$

This integral looks pretty imposing. The trick to the integration is to make the change of variable:

$$x = \left(\frac{v}{c}\right)^{k} \text{ so that } dx = \frac{k}{c}\left(\frac{v}{c}\right)^{k-1} dv \quad \text{and} \quad F(V) = \int_0^x e^{-x}dx \tag{7.54}$$

which results in

$$F(V) = \text{prob}(v \le V) = 1 - \exp\left[-\left(\frac{V}{c}\right)^{k}\right] \tag{7.55}$$

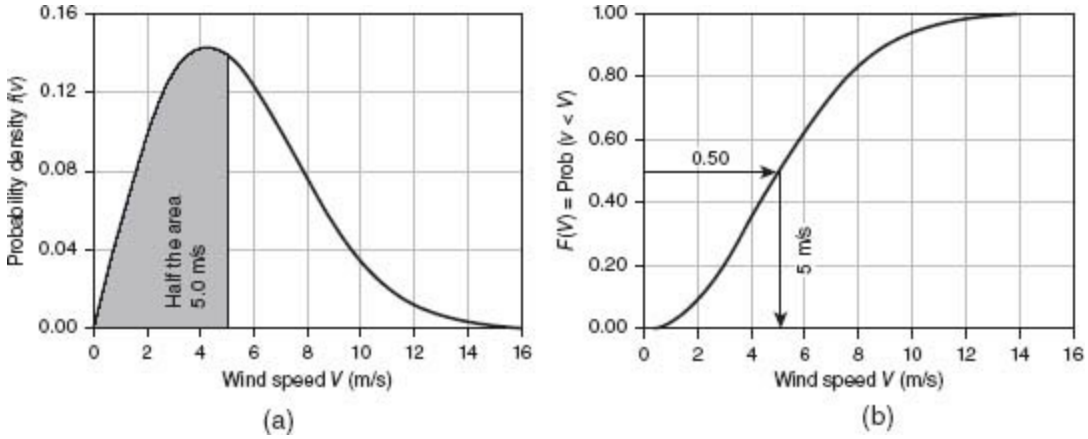
For the special case of Rayleigh statistics, k = 2, and from Equation 7.45 $c = 2\bar{v}/\sqrt{\pi}$, where $\bar{v}$ is the average wind speed, the probability that the wind is less than V is given by

$$F(V) = \text{prob}(v \le V) = 1 - \exp\left[-\frac{\pi}{4}\left(\frac{V}{\bar{v}}\right)^{2}\right] \text{(Rayleigh)} \tag{7.56}$$

A graph of a Weibull pdf $f(v)$ and its cumulative distribution function, $F(V)$ is given in Figure 7.30. The example shown there has k = 2 and c = 6, so it is actually a Rayleigh pdf. The figure shows that half of the time the wind is less than or equal to 5 m/s. That is, half the area under the $f(v)$ curve falls to the left of 5 m/s, and $F(5)$ = 0.5. Note that this does not mean the average wind speed is 5 m/s. In fact, since this example is a Rayleigh pdf, the

average wind speed is given by Equation 7.45: $\bar{v} = c\sqrt{\pi}/2 = 6\sqrt{\pi}/2 = 5.32\,\text{m/s}.$

FIGURE 7.30 An example pdf (a), and its cumulative distribution function (b). In this case, half the time the wind is less than 5 m/s, so half of the area under the pdf is to the left of v = 5 m/s.



Also of interest is the probability that the wind is greater than a certain value:

(7.57) $$\text{prob}(v \geq V) = 1 - \text{prob}(v \leq V) = 1 - F(V)$$

For Weibull statistics, Equation 7.57 becomes

(7.58) $$\text{prob}(v \geq V) = 1 - \left\{1 - \exp\left[-\left(\frac{V}{c}\right)^k\right]\right\} = \exp\left[-\left(\frac{V}{c}\right)^k\right]$$

and for Rayleigh statistics:

(7.59) $$\text{prob}(v \geq V) = \exp\left[-\frac{\pi}{4}\left(\frac{V}{\bar{v}}\right)^2\right] \text{ (Raleigh)}$$

Example 7.7 Linking a Power Curve to Rayleigh Statistics. A 2.1-MW Suzlon S97 wind turbine has a cut-in wind speed v_c = 3.5 m/s, rated wind speed v_R = 11 m/s, and a furling wind speed of v_F = 20 m/s. If this machine is located in Rayleigh winds with an average wind speed of 7 m/s, find the following:

a. How many hours per year is the wind below the cut-in wind speed?

b. How many hours per year will the turbine be shut down due to excessive winds?

c. How many kWh/yr will be generated when the machine is running at rated power?

d. If this turbine in these winds has an overall capacity factor of 38%, what fraction of its annual energy delivered will be provided by winds below the 11 m/s rated wind speed?

Solution

a. Using Equation 7.56, the probability that the wind speed is below cut-in 3.5 m/s is

$$F(V_c) = \text{prob}(v \le V_c) = 1 - \exp\left[-\frac{\pi}{4}\left(\frac{V_c}{\bar{v}}\right)^2\right]$$

$$= 1 - \exp\left[-\frac{\pi}{4}\left(\frac{3.5}{7}\right)^2\right] = 0.178$$

In a year with 8760 h (365 × 24), the number of hours the wind will be less than 3.5 m/s is

$$\text{Hours}(v \le 3.5\,\text{m/s}) = 8760\,\text{h/yr} \times 0.178 = 1562\,\text{h/yr}$$

So, the equivalent of roughly 2 months of the year the turbine will not be generating electricity.

b. Using (7.58), the hours when the wind is higher than V_F = 20 m/s will be

$$\text{Hours}(v \ge V_F) = 8760 \cdot \exp\left[-\frac{\pi}{4}\left(\frac{V_F}{\bar{v}}\right)^2\right]$$

$$= 8760 \cdot \exp\left[-\frac{\pi}{4}\left(\frac{20}{7}\right)^2\right] = 14.4\,\text{h/yr}$$

So, for only a few hours per year would we expect the turbine to be shut down due to excessively strong winds.

c. Assuming its power curve is flat above V_R, the turbine will deliver 2100 kW any time the wind is between V_R = 11 m/s and V_F = 20 m/s. The number of hours that the wind is higher than 11 m/s is

$$\text{Hours}(v \ge 11) = 8760 \cdot \exp\left[-\frac{\pi}{4}\left(\frac{11}{7}\right)^2\right] = 1260\,\text{h/yr}$$

So, the number of hours per year that the winds blow between 11 m/s and 20 m/s is 1260 – 14 = 1246 h/yr. The energy the turbine delivers from those winds will be

$$\text{Energy}(V_R \le v \le V_F) = 2100\,\text{kW} \times 1246\,\text{h/yr} = 2.62 \times 10^6\,\text{kWh/yr}$$

With a 38% CF, the turbine will deliver

$$2100\,\text{kW} \times 8760\,\text{h/yr} \times 0.38 = 6.99 \times 10^6\,\text{kWh/yr}$$

Of that, we expect 2.62 million kWh/yr to be generated in winds above the rated wind speed, so the fraction delivered at winds below that will be

$$\%\text{ of energy from } v < 11\,\text{m/s} = \frac{6.99 - 2.62}{6.99} = 0.625 = 62.5\%$$

7.7.2 Using Real Power Curves with Weibull Statistics

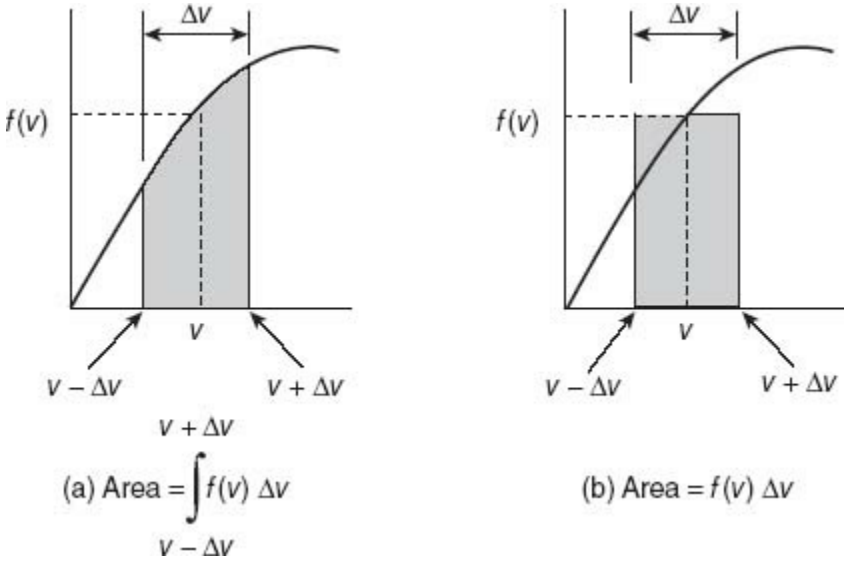
With the power curve in hand, we know the power delivered at any given wind speed. If we combine the power at any wind speed with the hours the wind blows at that speed, we can add up the total kWh of energy produced. If the site has data for hours at each wind speed, those would be used to calculate the energy delivered. Alternatively, when wind data are incomplete, it is customary to assume Weibull statistics with an appropriate shape parameter k, and scale parameter c.

We started the description of wind statistics using discrete values of wind speed and hours per year at that wind speed, then moved on to continuous pdf. It is time to take a step backwards and modify the continuous pdf to estimate hours at discrete wind speeds. With hours at any given speed and turbine power at that speed, we can easily do a summation to find the expected energy that will be delivered.

Suppose we ask, what is the probability that the wind blows at some specified speed v? A statistician will tell you that the correct answer is zero. It never blows at *exactly* v m/s. A more legitimate question is, what is the probability that the wind blows between $v - \Delta v/2$ and $v + \Delta v/2$? On a pdf, that probability is the area under the curve between $v - \Delta v/2$ and $v + \Delta v/2$ as shown in Figure 7.31a. If Δv is small enough, then a reasonable approximation is the rectangular area shown in Figure 7.31b. This suggests that we can make the following approximation:

$$\text{prob}(v - \Delta v/2 \le V \le v + \Delta v/2) = \int_{v-\Delta v/2}^{v+\Delta v/2} f(v)\mathrm{d}v \approx f(v)\Delta v \tag{7.60}$$

FIGURE 7.31 The probability that v is within $v \pm \Delta v/2$ is the shaded area in (a). A reasonable approximation is the shaded area in (b) $f(v)\Delta v$, as long as Δv is relatively small.



While this may look complicated, it really makes life very simple. It says we can conveniently make a continuous pdf discrete by saying the probability that the wind blows at some wind speed V is just $f(V)$, and let the statisticians squirm. The following example lets us check to see if this seems reasonable.

Example 7.8 Discretizing $f(v)$ For a wind site with Rayleigh winds having average speed $\bar{v}$ = 8 m/s, what is the probability that the wind would blow between 6.5 and 7.5 m/s? How does this compare to the pdf evaluated at 7 m/s?

Solution. Using Equation 7.59, we obtain

$$\text{prob}(v > 6.5) = \exp\left[-\frac{\pi}{4}\left(\frac{6.5}{8}\right)^2\right] = 0.59542$$

$$\text{prob}(v > 7.5) = \exp\left[-\frac{\pi}{4}\left(\frac{7.5}{8}\right)^2\right] = 0.50143$$

So, using the correct area under the pdf, the probability that the wind is between 6.5 and 7.5 m/s is

$$\text{prob}(6.5 < v < 7.5) = 0.59542 - 0.50143 = 0.09400$$

Now try the simplification suggested in Figure 7.31b. Using the Rayleigh pdf (Eq. 7.46), the probability density function at 7 m/s is

$$f(v) = \frac{\pi v}{2\bar{v}^2}\exp\left[-\frac{\pi}{4}\left(\frac{v}{\bar{v}}\right)^2\right]$$

Using a 1 m/s increment around v = 7 m/s, the rectangular approximation is

$$\text{prob}(6.5 < v < 7.5) = 1 \times \frac{\pi \cdot 7}{2 \cdot 8^2}\exp\left[-\frac{\pi}{4}\left(\frac{7}{8}\right)^2\right] = 0.09416$$

The approximation 0.09416 is only 0.2% higher than the correct value of 0.09400.

The above example is reassuring. It suggests we can use the pdf evaluated at integer values of wind speed to represent the probability that the wind blows at that speed. Combining power curve data supplied by the turbine manufacturer (examples are given in Table 7.5) with appropriate wind statistics, gives us a straightforward way to estimate annual energy production. This is most easily done using a spreadsheet. Example 7.9 demonstrates the process.

TABLE 7.5 Examples of Wind Turbine Power Specifications

Brand:	Vestas	Vestas	Suzlon	Suzlon	GE	GE	GE	Siemens	Siemens	Vergnet
P_R (kW):	7000	3075	2100	2100	2500	1600	1500	3000	2300	275
D (m):	164	112	97	88	103	100	77	101	101	32
Wind (m/s)	Power (kW)	Power (kW)	Power (kW)	Power (kW)	Power (kW)	Power (kW)	Power (kW)	Power (kW)	Power (kW)	Power (kW)
0	0	0	0	0	0	0	0	0	0	0
1	0	0	0	0	0	0	0	0	0	0
2	0	0	0	0	0	0	0	0	0	0
3	0	20	20	0	10	4	4	60	0	0
4	120	130	80	10	85	60	40	130	100	3
5	480	300	220	130	205	190	120	280	230	18
6	950	550	420	305	400	460	250	480	420	36
7	1630	900	678	540	695	750	420	765	720	58
8	2550	1350	1020	830	1130	1080	640	1175	1100	98
9	3750	1920	1433	1180	1630	1390	920	1650	1530	141
10	5000	2500	1830	1523	2050	1540	1200	2200	2000	189
11	5950	2950	2050	1845	2340	1595	1360	2700	2240	243
12	6695	3060	2090	2040	2480	1620	1450	2900	2300	272
13	6960	3072	2100	2080	2500	1620	1490	2970	2300	275
14	6995	3075	2100	2100	2500	1620	1510	2990	2300	275
15	7000	3075	2100	2100	2500	1620	1510	3000	2300	275
16	7000	3075	2100	2100	2500	1620	1510	3000	2300	275
17	7000	3075	2100	2100	2500	1620	1510	3000	2300	275
18	7000	3075	2100	2100	2500	1620	1510	3000	2300	275
19	7000	3075	2100	2100	2500	1620	1510	3000	2300	275
20	7000	3075	2100	2100	2500	1620	1510	3000	2300	275
21	7000	3075	0	0	2500	1620	1510	3000	2300	0
22	7000	3075	0	0	2500	1620	1510	3000	2300	0
23	7000	3075	0	0	2500	1620	1510	3000	2300	0
24	7000	3075	0	0	2500	1620	1510	3000	2300	0
25	7000	3075	0	0	2500	1620	1510	3000	2300	0

Example 7.9 Annual Energy Delivered Using a Spreadsheet. Suppose a Vestas 112-m wind turbine rated at 3075 kW is installed at a site having Rayleigh wind statistics with an average wind speed of 8 m/s at the hub height.

a. Find the energy generated by 7 m/s winds (actually 6.5–7.5 m/s).

b. Find the total annual energy delivered by this turbine in these winds.

c. From (b), find the overall average efficiency of this turbine in these winds.

d. Find its annual capacity factor in these winds.

Solution

a. From Equation 7.46 in a regime with 8 m/s average wind speed the Rayleigh probability density at 7 m/s is

$$f(v) = \frac{\pi v}{2\bar{v}^2} \exp\left[-\frac{\pi}{4}\left(\frac{v}{\bar{v}}\right)^2\right]$$

$$f(7) = \frac{\pi 7}{2 \cdot 8^2} \exp\left[-\frac{\pi}{4}\left(\frac{7}{8}\right)^2\right] = 0.09416$$

In a year with 8760 h, our estimate of the hours the wind blows at 7 m/s is

$$\text{Hours at 7 m/s} = 8760\ \text{h/yr} \times 0.09416 = 824.9\ \text{h/yr}$$

From Table 7.5, this turbine delivers 900 kW at 7 m/s. So our estimate of the energy delivered by 7 m/s winds is

$$\text{Energy (at 7 m/s)} = 900\ \text{kW} \times 824.9\ \text{h/yr} = 742{,}394\ \text{kWh/yr}$$

b. Portions of the rest of the spreadsheet are given below. The total energy produced is 12.41×10^6 kWh/yr.

	Raleigh, NC						Latitude 35.87° N						
Tilt	Jan	Feb	Mar	Apr	May	Jun	July	Aug	Sept	Oct	Nov	Dec	Year
Lat − 15	3.4	4.1	5.0	5.8	6.0	6.2	6.0	5.7	5.1	4.6	3.7	3.1	4.9
Lat	3.8	4.5	5.2	5.7	5.7	5.7	5.6	5.5	5.2	4.9	4.1	3.6	5.0
Lat + 15	4.1	4.6	5.1	5.3	5.0	4.9	4.9	5.0	5.0	5.0	4.3	3.8	4.8
90	3.6	3.8	3.6	3.1	2.5	2.3	2.4	2.8	3.3	3.8	3.7	3.5	3.2
1-Axis (Lat)	4.5	5.5	6.5	7.5	7.4	7.5	7.2	6.9	6.4	6.0	4.9	4.2	6.2
Temp. (°C)	9.4	11.4	16.7	22.1	25.9	29.4	31.1	30.4	27.3	22.0	17.0	11.5	21.2

	Bismarck, ND						Latitude 46.77° N						
Tilt	Jan	Feb	Mar	Apr	May	Jun	July	Aug	Sept	Oct	Nov	Dec	Year
Lat − 15	3.1	4.0	5.0	5.6	6.1	6.5	6.8	6.4	5.3	4.2	2.9	2.6	4.9
Lat	3.5	4.4	5.2	5.5	5.7	5.9	6.3	6.1	5.4	4.5	3.2	3.0	4.9
Lat + 15	3.7	4.5	5.1	5.1	5.1	5.1	5.5	5.5	5.1	4.5	3.4	3.2	4.7
90	3.7	4.2	4.3	3.7	3.3	3.1	3.4	3.7	3.9	3.9	3.2	3.1	3.6
1-Axis (Lat)	4.0	5.2	6.4	7.3	8.0	8.6	9.2	8.5	7.0	5.5	3.7	3.3	6.4
Temp. (°C)	−18.7	−14.9	−7.9	−0.6	5.7	10.9	13.6	12.2	6.2	0.3	−7.9	−15.9	−1.4

	Omaha, NE						Latitude 41.37° N						
Tilt	Jan	Feb	Mar	Apr	May	Jun	July	Aug	Sept	Oct	Nov	Dec	Year
Lat − 15	3.3	4.0	4.7	5.5	6.0	6.5	6.5	6.1	5.2	4.4	3.2	2.7	4.9
Lat	3.8	4.4	4.9	5.3	5.6	6.0	6.0	5.8	5.3	4.7	3.5	3.2	4.9
Lat + 15	4.1	4.6	4.8	5.0	5.0	5.2	5.3	5.3	5.1	4.7	3.7	3.4	4.7
90	3.9	4.1	3.8	3.2	2.8	2.7	2.8	3.2	3.6	3.9	3.3	3.2	3.4
1-Axis (Lat)	4.5	5.3	6.1	7.0	7.5	8.3	8.3	7.8	6.7	5.7	4.1	3.6	6.3
Temp. (°C)	−1.3	1.7	8.7	16.9	22.7	28.0	30.3	28.9	23.8	17.8	8.7	0.5	15.6

	Albuquerque, NM						Latitude 35.05° N						
Tilt	Jan	Feb	Mar	Apr	May	Jun	July	Aug	Sept	Oct	Nov	Dec	Year
Lat − 15	4.6	5.4	6.3	7.3	7.7	7.8	7.4	7.2	6.6	5.9	4.8	4.3	6.3
Lat	5.3	6.0	6.5	7.2	7.2	7.1	6.9	6.9	6.8	6.5	5.5	5.0	6.4
Lat + 15	5.8	6.2	6.5	6.6	6.3	6.1	6.0	6.3	6.5	6.6	5.9	5.5	6.2
90	5.2	5.1	4.5	3.7	2.8	2.4	2.5	3.2	4.2	5.1	5.2	5.1	4.1
1-Axis (Lat)	6.5	7.5	8.6	9.9	10.3	10.4	9.5	9.3	9.0	8.3	6.8	6.1	8.5
Temp. (°C)	8.2	11.9	16.3	21.6	26.5	32.2	33.6	31.7	27.7	21.7	14.1	8.6	21.2

	Ely, NV						Latitude 39.28° N						
Tilt	Jan	Feb	Mar	Apr	May	Jun	July	Aug	Sept	Oct	Nov	Dec	Year
Lat − 15	4.0	4.7	5.5	6.3	6.6	7.2	7.2	6.9	6.6	5.5	4.1	3.6	5.7
Lat	4.6	5.2	5.7	6.2	6.2	6.6	6.6	6.6	6.7	6.0	4.7	4.3	5.8
Lat + 15	5.0	5.5	5.6	5.7	5.5	5.6	5.7	6.0	6.5	6.1	5.0	4.7	5.6
90	4.8	4.8	4.3	3.6	2.9	2.6	2.8	3.4	4.4	4.9	4.5	4.5	4.0
1-Axis (Lat)	5.5	6.5	7.4	8.4	8.9	9.9	9.9	9.5	9.2	7.7	5.6	5.1	7.8
Temp. (°C)	4.3	6.4	9.1	13.9	19.6	25.7	30.6	29.1	24.0	17.5	9.6	4.8	16.2

c. The average efficiency is the fraction of the wind's energy that is actually converted into electrical energy. Since Rayleigh statistics are assumed, we can use Equation 7.49 to find average power in the wind for a 112-m rotor diameter (assuming the standard value of air density equal to 1.225 kg/m^3):

$$\bar{P} = \frac{6}{\pi}\left(\frac{1}{2}\rho A\bar{v}^3\right)$$
$$= \frac{6}{\pi} \times \frac{1}{2} \times 1.225 \times \frac{\pi}{4}(112)^2 \times 8^3 = 6.045 \times 10^6\ \text{W}$$

In a year with 8760 h, the energy in the wind is

$$\text{Energy in wind} = 8760\,\text{h/yr} \times 6045\,\text{kW} = 52.96 \times 10^6\,\text{kWh}$$

So the average efficiency of this machine in these winds is

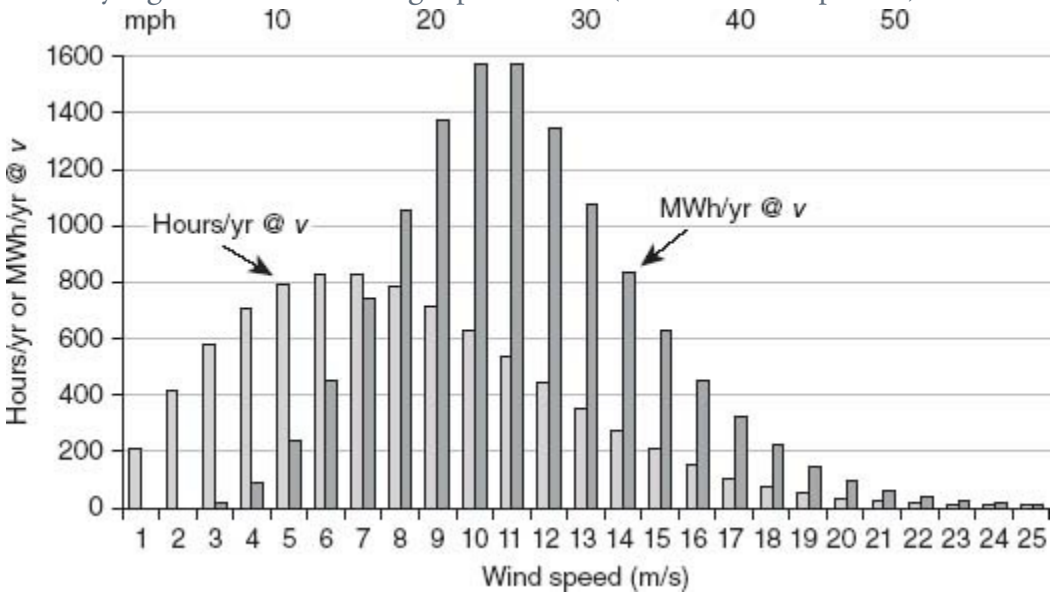
$$\text{Average efficiency} = \frac{12.415 \times 10^6\,\text{kWh/yr}}{52.96 \times 10^6\,\text{kWh/yr}} = 23.4\%$$

d. The CF for this machine in these winds is

$$\text{CF} = \frac{\text{Energy delivered}}{\text{Energy at full power}} = \frac{12.415 \times 10^6\,\text{kWh/yr}}{3075\,\text{kW} \times 8760\,\text{h/yr}} = 0.461 = 46.1\%$$

A histogram of hours per year and MWhr per year at each wind speed for the above example is presented in Figure 7.32. Note how little energy is delivered at lower wind speeds in spite of the large number of hours of wind at those speeds. This is, of course, another example of the importance of the cubic relationship between power in the wind and wind speed.

FIGURE 7.32 Hours per year and MWh per year at each wind speed for the Vestas-112 turbine in Rayleigh winds with average speed 8 m/s (based on Example 7.9).



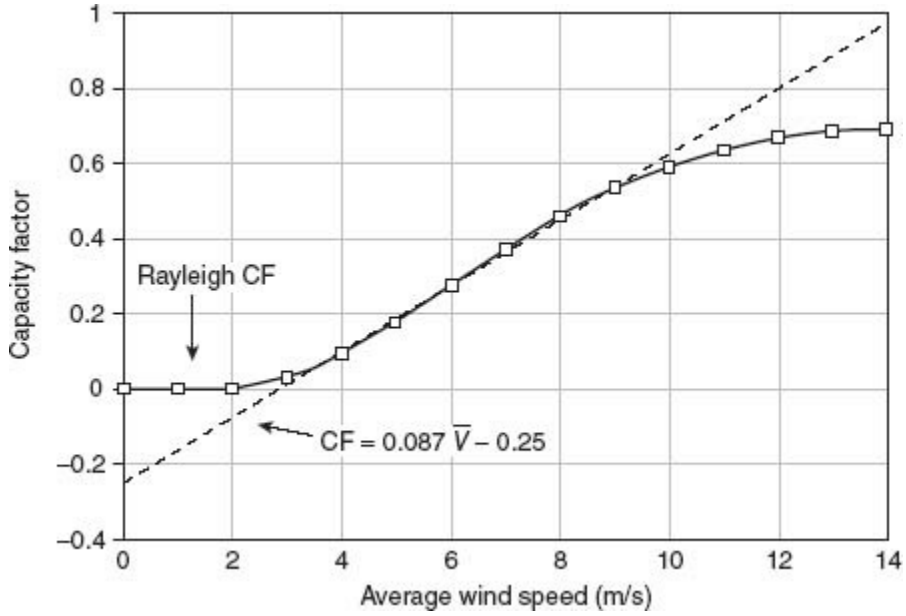
7.7.3 A Simple Way to Estimate Capacity Factors

Example 7.9 showed how turbine power curves can be combined with wind pdfs to estimate delivered energy, and how that can be used to find capacity factors in those winds. In this section, our goal is to find a simpler way to estimate capacity factor when very little

is known about a site and wind turbine.

By repeating the process outlined in Example 7.9, while varying the average wind speed, we can quite easily derive a plot of CF versus average wind speed for any turbine under any pdf. The graph shown in Figure 7.33 shows results of that calculation for the Vestas 112-m wind turbine just analyzed under the assumption of Rayleigh probability statistics. Most good wind sites will have average wind speeds in the range of about 5–9 m/s. Note how linear the CF is between those wind speeds. For winds with higher averages, more and more of the wind is above a turbine's rated wind speed and CF begins to level out and can even drop some. A similar flattening of the curve occurs when the average wind speed is down near the cut-in wind speed and below, since much of the wind produces no electrical power at all.

FIGURE 7.33 Capacity factor (CF) for the Vestas 112-m wind turbine in Example 7.9 assuming Rayleigh statistics. A linear fit to the "sweet spot" of average wind speeds is shown.



The S-shaped curve of Figure 7.33 was derived for a specific turbine operating in winds that follow Rayleigh statistics. As it turns out, all turbines show the same sort of curve with a sweet spot of linearity in the range of average wind speeds that are likely to be encountered in practice. Note how different this conclusion is from what might have been expected by simply considering the power in the wind itself, which increases as the cube of wind speed. It is as if the very nonlinear power in the wind relationship is cancelled out by the very nonlinear turbine power characteristics to give us a wonderfully simple linear relationship between average wind speed and energy produced by a wind turbine.

This suggests the possibility of modeling CF as a linear function of wind speed in that most important 5–10 m/s region. For this particular Vestas-112 turbine the linear fit shown in Figure 7.33 leads to the following:

$$\text{CF} = 0.087\bar{V} - 0.25 \tag{7.61}$$

The rated power P_R of this turbine is 3075 kW and the rotor diameter D is 112 m. The ratio of rated power expressed in kW to the square of rotor diameter expressed in meters,

for this particular turbine just happens to be

$$\frac{P_R}{D^2} = \frac{3075\,\text{kW}}{(112\,\text{m}^2)} = 0.25 \tag{7.62}$$

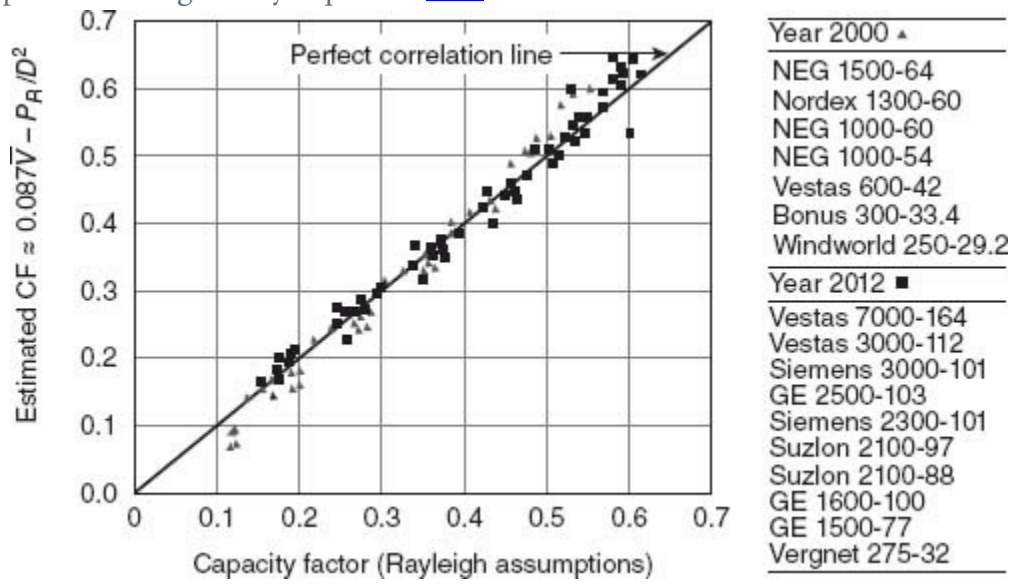
That is an interesting coincidence. For *this particular* wind we can write the CF as

$$\text{CF} = 0.087\bar{V} - \frac{P_R}{D^2}\ \text{(Rayleigh winds)} \tag{7.63}$$

where $\bar{V}$ is the average wind speed (m/s), P_R is the rated power of the turbine (kW), and D is the rotor diameter (m). Note that for Equation 7.63 to work, you must use just those fixed units.

Surprisingly, even though the estimate in Equation 7.63 was derived for a single turbine, it seems to work quite well in many circumstances as a predictor of capacity factor. In the first edition of this book, CFs found using Equation 7.63 for a number of turbines popular in the year 2000 were found to be surprisingly consistent with those determined using Rayleigh assumptions. Turbines are considerably larger now and have more advanced designs as well, but when Equation 7.63 was applied to the 10 modern turbines in Table 7.5, it continued to correlate very well with the approach based on Rayleigh assumptions, especially within the realistic 0.2–0.5 CF range. Figure 7.34 shows the correlations based on those 2000 and 2012 turbines, which cover a range of sizes from 250 kW all the way up to 7000 kW.

FIGURE 7.34 Correlation between capacity factors based on Rayleigh assumptions and the simple estimates given by Equation 7.63.



This simple CF relationship is very handy since it only requires the rated power and rotor diameter for the wind turbine, along with average wind speed, and of course, once CF has been estimated it is easy to calculate the expected annual energy delivered. Again, be careful to use the correct units—P_R in kW, $\bar{V}$ in m/s, and D in m.

$$\text{Annual energy (kWh/yr)} = 8760\,\text{h/yr} \cdot P_R(\text{kW}) \left\{ 0.087\bar{V}(\text{m/s}) - \frac{P_R(\text{kW})}{[D(\text{m})]^2} \right\} \quad (7.64)$$

The question sometimes arises as to whether or not a high CF is a good thing. A high CF means the turbine is deriving much of its energy in the flat, wind-shedding region of the power curve above the rated wind speed. That means power production is relatively stable, which can have some advantages in terms of the interface with the local grid. On the other hand, a high CF means a significant fraction of the wind's energy is not being captured, since the blades are purposely shedding much of the wind to protect the generator. It might be better to have a larger generator to capture those higher speed winds, in which case CF goes down while energy delivered increases. A bigger generator, of course, costs more. In other words, CF itself is not a good indicator of the overall economics for the wind plant.

Example 7.10 Energy Estimate Using the Simple CF Approach. For a site with an average wind speed of 7 m/s, compare the CFs and annual energy delivered by a 100-m rotor connected to either a 2500-kW or a 3000-kW generator.

Solution. For the 2500-kW generator Equations 7.63 and 7.64 give

$$\text{CF} = 0.087\bar{V} - \frac{P_R}{D^2} = 0.087 \times 7 - \frac{2500}{100^2} = 0.359$$

$$\text{Energy} = 8760\,\text{h/yr} \times 2500\,\text{kW} \times 0.359 = 7.9 \times 10^6\,\text{kWh/yr}$$

For the 3000-kW generator:

$$\text{CF} = 0.087\bar{V} - \frac{P_R}{D^2} = 0.087 \times 7 - \frac{3000}{100^2} = 0.309$$

$$\text{Energy} = 8760\,\text{h/yr} \times 3000\,\text{kW} \times 0.309 = 8.1 \times 10^6\,\text{kWh/yr}$$

So even though the 3000-kW generator has a lower capacity factor, it would deliver slightly more energy.

Example 7.10 illustrates the use of Equation 7.63 to make quick first-order estimates of CFs, optimal generator sizing, annual energy production, and potential global estimates of wind potential (e.g., Jacobson and Masters, 2001). Of course, the spreadsheet approach using Weibull pdfs (not just Rayleigh) has a solid theoretical basis and is the preferred method for specific turbines. Also, remember that Equation 7.63 was developed to match today's large turbines, and is likely to overestimate the output of much smaller, less-efficient, residential-scale systems. Also, it might underestimate the more efficient gearless, full-capacity-converter, direct-drive turbines (Fig. 7.13) that are coming in the near future.

One interesting use for Equation 7.64 is to explore combinations of generator sizes with rotor diameters for various wind regimes. Taking the derivative of Equation 7.64 with respect to P_R for a fixed blade diameter, and setting it equal to zero gives

(7.65)

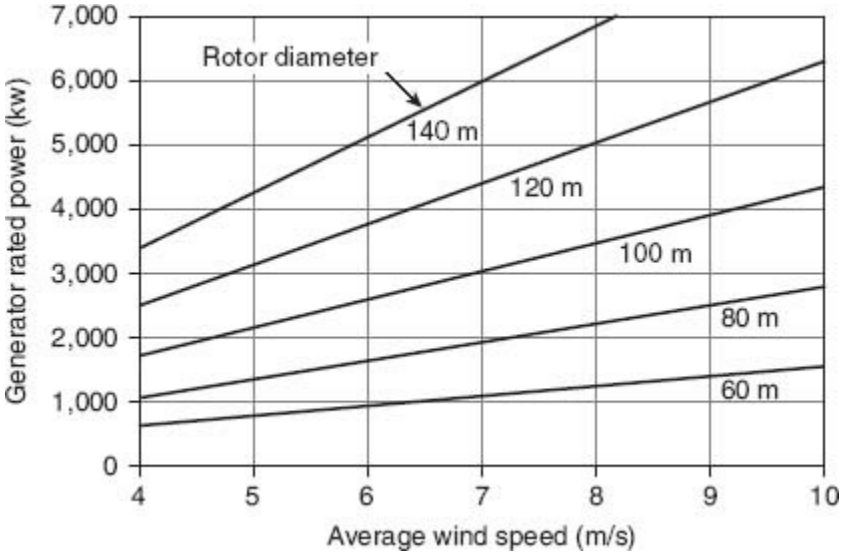
$$\frac{\text{d(Energy)}}{\text{d}P_R} = \frac{d}{dP_R}\left[8760\,P_R\left(0.087\bar{V} - \frac{P_R}{D^2}\right)\right] = 8760\left(0.087\bar{V} - \frac{2P_R}{D^2}\right) = 0$$

Solving for the optimum generator for a given blade diameter results in

$$P_R(\text{kW}) = 0.0435\bar{V}(\text{m/s})[D(\text{m})]^2 \quad (7.66)$$

A plot of this relationship is shown in Figure 7.35. For example, for a site with 7 m/s average wind speeds, a designer might want to do a quick economic comparison between say a wind farm consisting of 2000-kW, 80-m turbines and one based on 3000-kW, 100-m turbines, both of which look "optimal" in this figure. But, for example, putting a 100-m blade on a 2000-kW generator might not be worth pursuing.

FIGURE 7.35 A starting-point sizing guide for combinations of rotors and generators based on the assumptions built into the CF estimates used in Equation 7.64.



There are far too many caveats to stretch the implications of Equation 7.66 much farther, but it is intriguing to see what light it can shed on the idea of an optimum CF. Rearranging Equation 7.66 gives us

$$\frac{P_R}{D^2} = 0.0435\bar{V} \quad (7.67)$$

Putting that back into Equation 7.64 gives an estimate of the optimum CF to be

$$\text{CF} = 0.087\bar{V} - \frac{P_R}{D^2} = 0.087\bar{V} - 0.0435\bar{V} = 0.0435\bar{V} \quad (7.68)$$

For example, most California wind farms are located in regions with roughly 7 m/s winds, for which Equation 7.68 suggests a target CF might be about 0.0435 × 7 = 0.30. In the wind belt running from North Dakota to Texas, 8 m/s is more common for which Equation 7.68 suggests a higher CF of about 0.35 for a target. Both of these CFs are typical for wind farms in those regions of the country (Wiser and Bollinger, 2012).

7.8 WIND FARMS

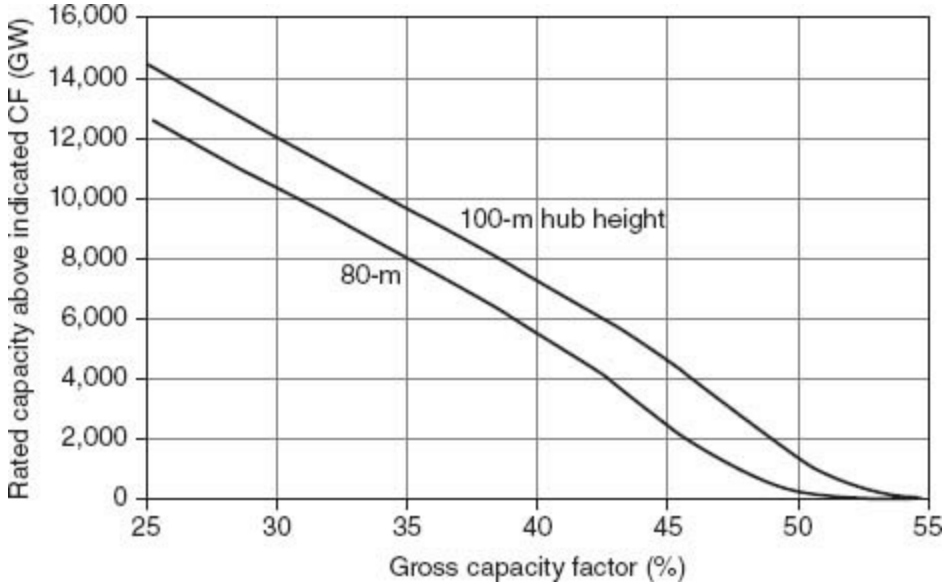
Unless it is a single wind turbine for a particular site, such as an off-grid home in the

country, most often when a good wind site has been found it makes sense to install a large number of wind turbines in what is often called a *wind farm* or a *wind plant*. Obvious advantages result from clustering wind turbines together at a windy site. Reduced site development costs, simplified connections to transmission lines, and more centralized access for operation and maintenance, all are important considerations.

7.8.1 Onshore Wind Power Potential

Questions naturally arise as to whether there are sufficient wind resources to supply a significant fraction of electricity demand and whether the land areas required to do so might be excessive. To help address the first question, the National Renewable Energy Laboratory (NREL) began developing maps of U.S. wind resources back in the 1980s, including the 50-m hub-height map shown in Figure 7.29. With these maps as the starting point, NREL has attempted to estimate the nation's total wind potential on lands outside of wilderness areas, parks, urban areas, and other regions unlikely to be developed. Figure 7.36 shows the potential gigawatts of rated capacity that could be installed on land as a function of the gross (without turbine wake losses, etc.) CF at 80-m and 100-m hub heights.

FIGURE 7.36 The onshore potential gigawatts of rated capacity above a given gross capacity factor (without losses) at hub heights of 80-m and 100-m for the contiguous 48 states. From NREL website, 2012.



Example 7.11 Wind Potential for the United States. Compare the current 4 billion MWh of U.S. electricity demand with the total onshore wind potential at 80-m for turbines having a 35% CF and again for 100-m turbines with 40% CF. Assume 10% rotor wake losses between turbines.

Solution. From Figure 7.36 the 80-m height can provide about 8000 GW of power at 35% CF. Including wake losses, that works out to

$$\text{Available (80-m, 35\%)} = 0.35 \times 8760\,\text{h} \times 8000\,\text{GW} \times (1 - 0.10)$$
$$= 22.1 \times 10^6\,\text{GWh/yr} = 22.1 \times 10^9\,\text{MWh/yr}$$

which is more than five times as much electricity as is now being used.

At 100-m it looks like about 7500 GW of power can be provided at 40% CF, which would provide

$$\text{Available (100-m, 40\%)} = 0.40 \times 8760\,\text{h} \times 7500\,\text{GW} \times (1 - 0.10)$$
$$= 23.6 \times 10^6\,\text{GWh/yr} = 23.6 \times 10^9\,\text{MWh/yr}$$

This is almost six times the total electricity being used today.

Clearly, wind resources are sufficient to have a major impact on current and future electricity demands. A recent NREL report (Denholm et al., 2009) presents results of a major study of actual area requirements for a large number of wind projects in the United States. To organize their study, they distinguish between direct and indirect land uses. Direct land uses consist of permanent disturbances such as access roads and turbine pads that will remain in place over the life of the project, and areas that are affected during construction but which can revert to other uses after project completion. Indirect-use areas are mostly those required for turbine spacing and other boundary considerations. Their study concluded that typical projects have permanent direct-use areas of about 0.74 acres per MW of installed capacity, most of which is for roads, plus another 1.7 ac/MW of temporary direct use. Both values have very large uncertainties associated with them. These areas do not include turbine spacing, which can be on the order of 5–10 rotor diameters between towers, depending on the array configuration, plus other buffer areas.

Example 7.12 Permanently Disturbed Land Area. Estimate the permanently disturbed area of land needed to provide half of the 4-billion MWh/yr of U.S. electricity demand. Assume turbines are located in sites with 7.5 m/s average wind speed and assume NREL's permanent direct-use area of 0.74 ac/MW.

Solution. Using Equation 7.68, with 7.5-m/s average wind speed, the capacity factor could be

$$\text{CF} = 0.0435\bar{V} = 0.0435 \times 7.5 = 0.326$$

The rated power of all those wind turbines would be

$$P_R = \frac{0.5 \times 4 \times 10^9\,\text{MWh/yr}}{8760\,\text{h/yr} \times 0.326} = 0.70 \times 10^6\,\text{MW}$$

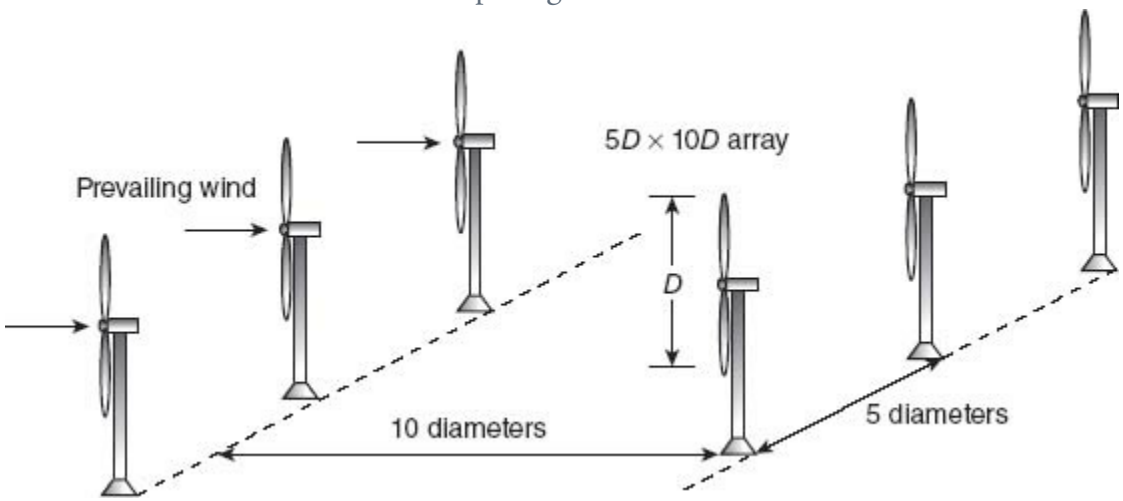
At 0.74 ac/MW of installed capacity, the permanently affected area needed would be

$$A = 0.74\,\text{ac/MW} \times 0.70 \times 10^6\,\text{MW}$$
$$= 520{,}000\,\text{ac} = 810\,\text{mi}^2 = 2100\,\text{km}^2$$

That is less than 0.2% of the 300 million AC of cropland harvested each year in the United States.

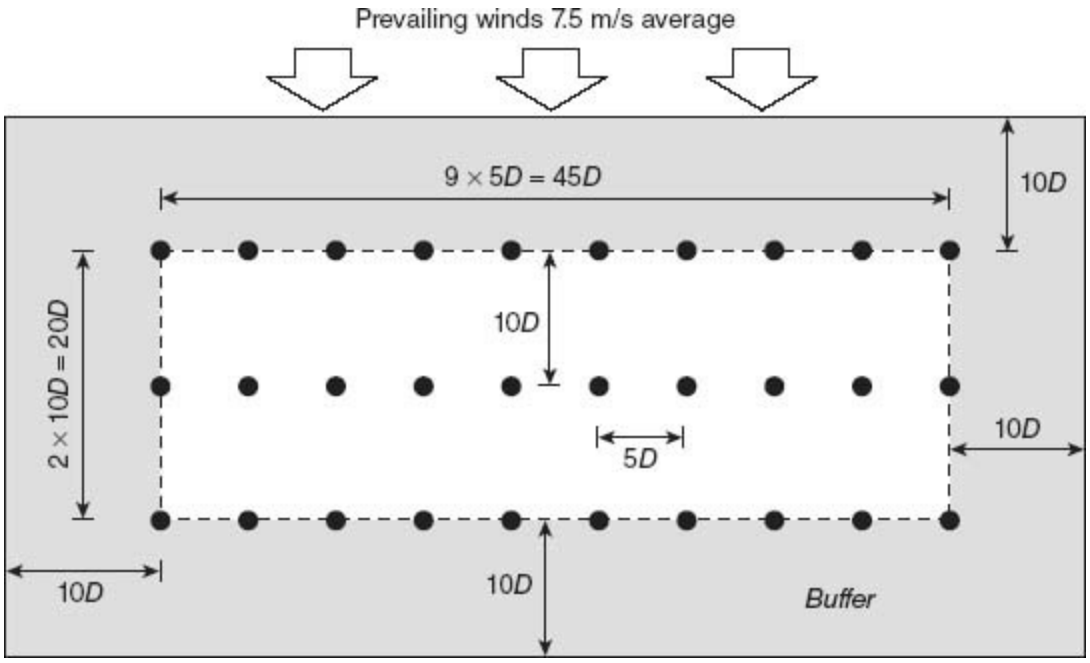
The above example calculated the area of land permanently affected by turbine pads, roads, and grid interfaces, but it does not include necessary spaces between turbines as well as buffers around the entire wind farm. Certainly wind turbines located too close together will result in upwind turbines interfering with the wind received by those located downwind. As energy is extracted by rotors, the wind slows down, which reduces the power available to downwind machines. After about ten rotor diameters of distance behind a turbine, however, wind speed can recover to nearly its undisturbed value, which means in principle another row of turbines could be put in place. Depending on rotor spacing, rotor wake losses from one row to another may need to be accounted for. Actually laying out a wind farm requires careful evaluation of prevailing wind directions, irregular terrain considerations, access roads, transmission and grid connection facilities, current and projected land use for areas between towers, and so forth. Those constraints, at least for land-based projects, frequently result in long strings of turbines or clusters of turbines without regular row-and-column regularity. When rows and columns are appropriate, side-by-side spacing along a row perpendicular to the prevailing winds are often on the order of five rotor diameters, while row-to-row spacing is more like 10 diameters. That layout would be described as a $5D \times 10D$ array (Fig. 7.37).

FIGURE 7.37 A common $5D \times 10D$ spacing of towers for a flat terrain.



The total area required, direct and indirect, including buffer areas, for a large number of real projects in the United States has been found to be around 85 ± 50 ac/MW, or about 7.5 MW/mi^2 of land on average (Denholm et al., 2009). An example of an array with a buffer zone is shown in Figure 7.38.

FIGURE 7.38 An example array based on a $5D \times 10D$ array with a $10D$ buffer.



Example 7.13 Total Area Required for a Wind Farm. Estimate the array area required for a wind farm consisting of thirty 2-MW, 90-m turbines arranged in three rows of 10 turbines using a $5D \times 10D$ tower spacing. Then add an additional $10D$ of buffer space around the entire turbine array and find the total area required. Also find their power density ratio.

Solution. The turbine-corner to turbine-corner area of this array will be

$$\begin{aligned}\text{Array area} &= (9 \times 5D) \cdot (2 \times 10D) = 900D^2 \\ &= 900 \cdot (90)^2 = 7.29 \times 10^6\ \text{m}^2\end{aligned}$$

On a per unit of power basis, this is

$$\text{Array power density} = \frac{60\ \text{MW}}{7.29 \times 10^6\ \text{m}^2} \times \frac{2.59 \times 10^6\ \text{m}^2}{\text{mi}^2} = 21.3\ \text{MW/mi}^2$$

This, by the way, is a little over 8 W/m^2 of land, which is considerably less than the solar insolation that could be captured by photovoltaics.

The total area including the buffer zone around the array is

$$\begin{aligned}\text{Total area} &= (9 \times 5 + 20)D \cdot (2 \times 10 + 20)D = 2600D^2 \\ &= 2600 \times (90)^2 = 21.06 \times 10^6\ \text{m}^2\end{aligned}$$

The power density for the full array and buffer is now

$$\begin{aligned}\text{Total power density} &= \frac{60 \times 10^6\ \text{W}}{21.06 \times 10^6\ \text{m}^2} \\ &= 2.85\ \text{W/m}^2 = 7.4\ \text{MW/mi}^2 = 2.9\ \text{MW/km}^2\end{aligned}$$

This turns out to be about the same as the 7.5 MW/mi^2 that the NREL (Denholm et al., 2009) report said is average for the country.

In the above examples, less than 1% of the total area is turbine-pads, roads, and other permanent land disturbances. The turbine array itself covers about one-third of the total area while the remaining two-thirds are buffer zones. For perspective, to supply half of U.S. electricity at a 33% CF would require about 700, 000 MW of wind turbines. Using assumptions in the above examples, the permanently disturbed land area would be about 800 mi^2. Including turbine spacing, the array area itself would span 33, 000 mi^2, which is less than 1% of the land area in the coterminous 48 states. The total area, two-thirds of which is a buffer zone, would be about 100, 000 mi^2, which is about the size of Wyoming. Figure 7.39 shows these on a map.

FIGURE 7.39 Estimated area required to meet half of U.S. electricity demand with wind turbines.



With 99% of the total wind farm area potentially available for compatible conventional farming or ranching, opportunities for mutually beneficial land uses are abundant. Farmers are unlikely to want to own and operate a wind farm, but they can derive a significant revenue stream by leasing their land to a wind project developer. Annual payments can be based on a per-acre or per-turbine basis, or they may be shared revenues based on the MWh of energy generated. The following example explores those options.

Example 7.14 Comparing Revenue Streams for a Wind Farm. Suppose you are the landowner of the 5200-ac (21.06×10^6 m^2) wind farm described in Example 7.13. The developers offer you the following revenue choices in exchange for being able to locate their plant on your land.

a. 0.35 ¢ for each kWh generated

b. $100/yr per acre

c. A flat $9000/yr per MW of installed capacity.

Assuming 7-m/s average wind speed and 10% rotor wake losses between turbines, compare the three options.

Solution. These are 2-MW, 90-m turbines in 7 m/s winds, so from Equation 7.63:

$$\mathrm{CF} = 0.087\bar{V} - \frac{P_R}{D^2} = 0.087 \times 7.0 - \frac{2000}{90^2} = 0.362$$

Including 10% losses, those thirty 2-MW turbines will generate about

$$\mathrm{kWh/yr} = 60{,}000\,\mathrm{kW} \times 8760 \times 0.362 \times (1 - 0.10) = 171.24 \times 10^6\,\mathrm{kWh/yr}$$

a. Land-owner revenue if s/he accepts the 0.35 ¢/kWh option will be

$$171.24 \times 10^6\,\mathrm{kWh/yr} \times \$0.0035/\mathrm{kWh} = \$599{,}340/\mathrm{yr}$$

b. On a per-acre basis, the revenue based on 0.35 ¢/kWh would be

$$\text{Per acre revenue} = \frac{\$599{,}340/\mathrm{yr}}{5200\,\mathrm{ac}} = \$115.26/\mathrm{ac}$$

So $0.0035/kWh is a better deal than the $100/yr per acre option.

c. Revenue per MW under the 0.35 ¢/kWh option would be

$$\text{Per MW revenue} = \frac{\$599{,}340/\mathrm{yr}}{30\,\text{turbines} \times 2\,\mathrm{MW/turbine}} = \$9989/\mathrm{yr/MW}$$

This, too, is better than the $9000/yr the plant owner is offering in the per MW deal.

So, if the turbines produce as hoped the land owner would be better off taking the 0.35 ¢/kWh option rather than either the per acre or the per MW offer. However, the winds may not be as strong as predicted and the turbines may not perform as well as hoped, so there would be greater risk with the per kWh option. It is the usual tradeoff—greater risk leads to greater reward potential.

The land leasing computation in the above example illustrates an important point. Wind farms are quite compatible with conventional farming, especially cattle ranching, and the added revenue a farmer can receive by leasing land to a wind park is often more than the value of the crops harvested on that same land. As a result, ranchers and farmers are becoming some of the strongest proponents of wind power, since it helps them stay in their primary business while earning higher profits.

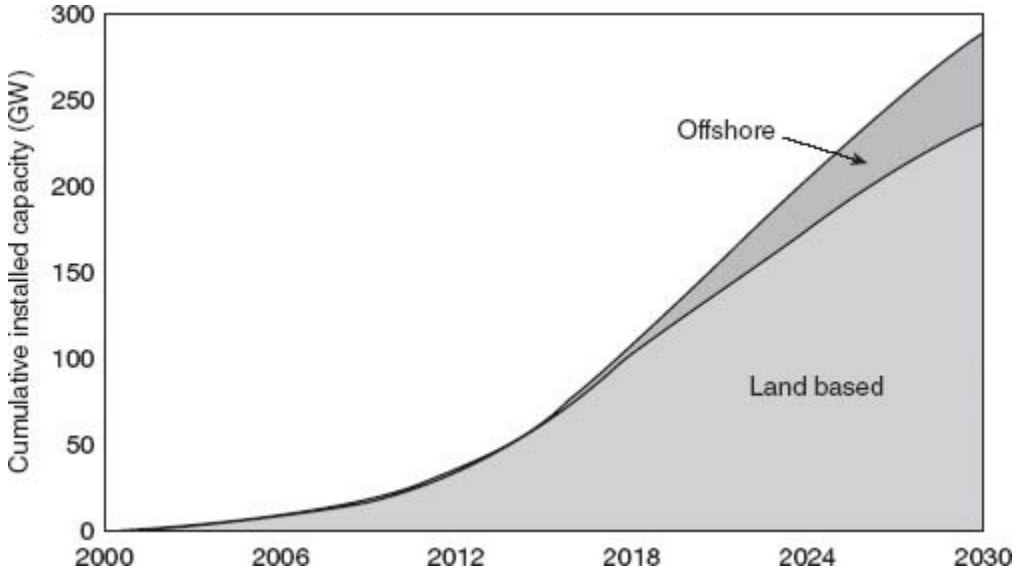
7.8.2 Offshore Wind Farms

While onshore wind farms have been the dominant source of wind power globally, the now small, but rapidly growing, offshore market has considerable potential for the future. The advantages inherent to offshore wind include closer access to large, coastal metropolitan load centers, which can avoid transmission costs and constraints. In fact, over half of the nation's population lives in counties adjacent to the oceans, or the Great Lakes, and states with coastal boundaries use three-fourths of U.S. electricity. Moreover, the price of electricity tends to be higher in coastal areas, so the economic competitiveness of wind is improved. Offshore winds also tend to be stronger, steadier, and less turbulent, and they frequently blow in the afternoon, when power is most valuable. If located far enough from the shore, visual and audible noise impacts can be less of an issue than they are for land-

based wind farms. On the other hand, the marine environment is harsh, access for maintenance purposes can be difficult, and costs are considerably higher than land-based installations. NREL (Musial and Ram, 2010), for example, suggests the levelized cost of offshore wind power is about double that of onshore wind farms.

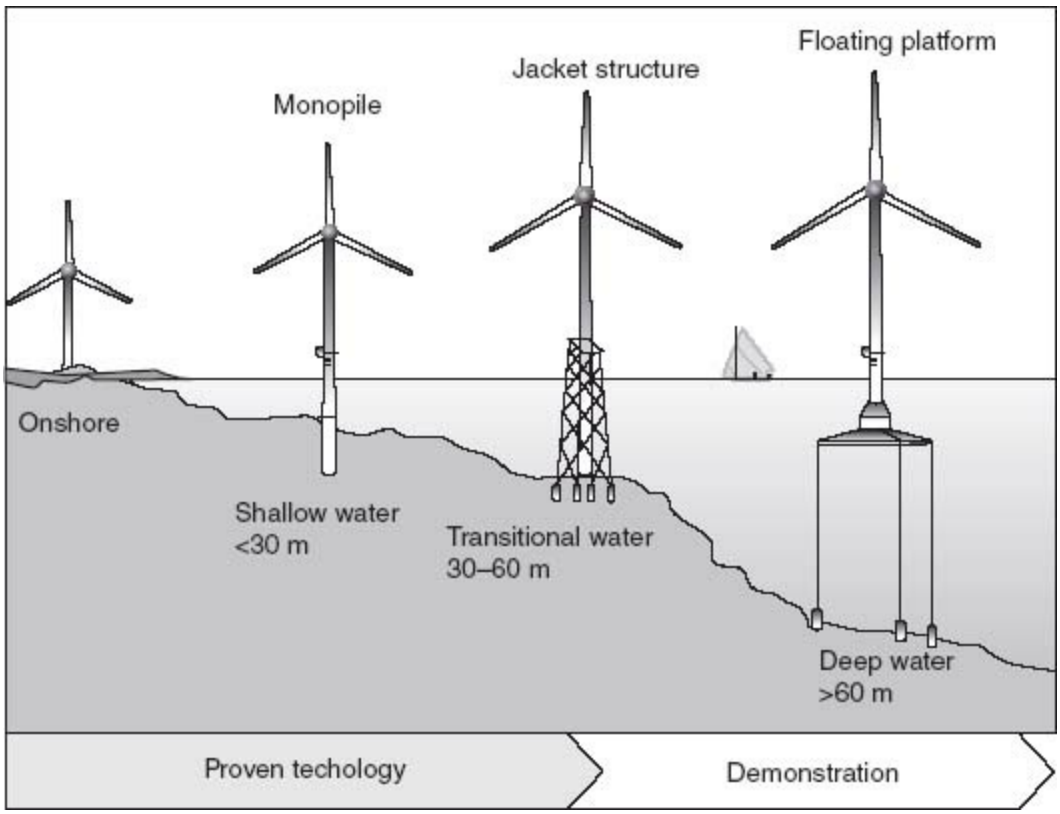
As of 2012, the United States had no offshore wind in place, but NREL's least-cost optimization model for a 20% wind supply by 2030 found over 50 GW of capacity could by then come from offshore wind (Fig. 7.40). Meanwhile, most of the global installed capacity has been in Northern Europe, especially in Denmark and the United Kingdom. European goals include increasing the installed capacity from the 10 GW in place in 2012 to 150 GW by 2030.

FIGURE 7.40 Cumulative wind generation capacity for a U.S. 20% wind, 2030 scenario. From: DOE, 2008.



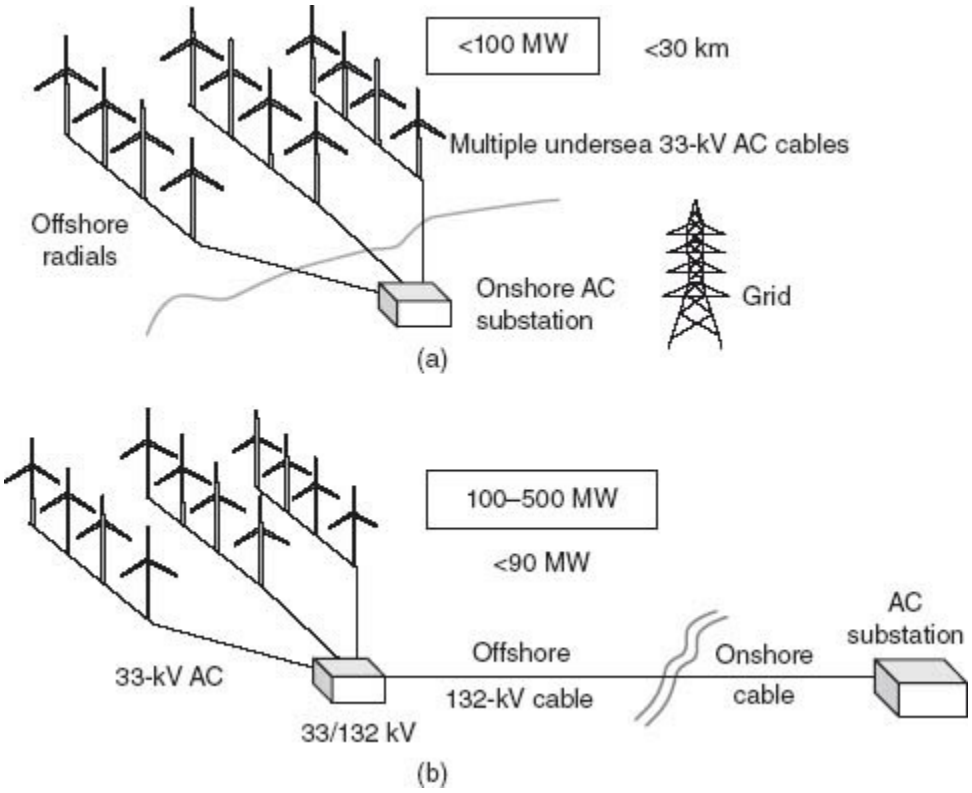
The developable offshore wind resource depends not only on wind speed, but also on water depth and distance from the shore. More subtle constraints include wave, ocean current, and storm intensity as well as the potential to interfere with shipping lanes and traditional fishing grounds. Most existing installations are in waters less than 30 m deep, which allows individual turbines to be mounted on a tower that is supported by a single large steel tube driven deep into the seabed. In those shallow depths, prestressed concrete gravity-base designs are also being used. For what are referred to as transitional waters, 30–60-m deep, jacket (lattice) structures similar to those developed by the oil and gas industry are being used, as well as multipile versions of the simple monopile substructure used in shallower waters. Still being developed are floating substructures that are decoupled from the bottom, such as the one sketched in Figure 7.41.

FIGURE 7.41 Offshore wind energy technologies. Redrawn from NREL (Musial and Ram, 2010).



Not only is water depth an issue, distance from the shore also provides design challenges. To help reduce transmission losses, within each turbine tower transformers and switchgear convert generator voltages from approximately 690 V to 30–36 kV. As shown in Figure 7.42a, for relatively small arrays located within about 30 km of shore, that voltage is sufficient to allow multiple undersea AC cables to connect strings of turbines directly to a shore-based substation. For larger arrays and longer distances, those strings are routed to offshore transformers that raise the voltage from typically 33 kV to 132 kV (Fig. 7.42b).

FIGURE 7.42 Small systems, close to shore, may run multiple undersea AC cables from strings of turbines to shore (a). Larger systems further out use offshore transformers to boost voltages before transmission to shore (b).



Transmission from offshore-transformers to substations on shore is provided by three-phase submarine cables such as the one shown in Figure 7.43. Since the individual conductors in these cables are so close together, they have much more inherent shunt capacitance than typical overhead lines on shore. While overhead lines are inherently inductive, and hence absorb reactive power, three-phase submarine cables create reactive power (VARs). To compensate, special reactive power compensation equipment is required both on the offshore platform and the on-shore substation. Three-phase undersea cables act very much like elongated capacitors, which have to be charged and discharged with each cycle. That charging current reduces the real current that can be delivered to loads, which means there are limits to the practical length of submarine cables.

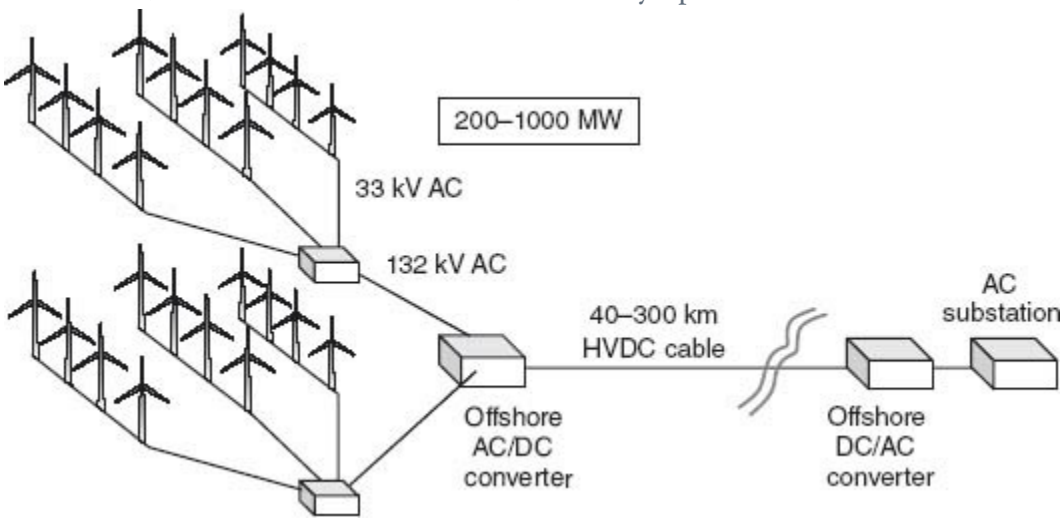
FIGURE 7.43 A cutaway view of a Vattenfall 132-kV submarine cable.



For large wind farms located beyond about 50 km offshore, high voltage DC transmission (HVDC) becomes a viable option; beyond about 100 km, it is the only

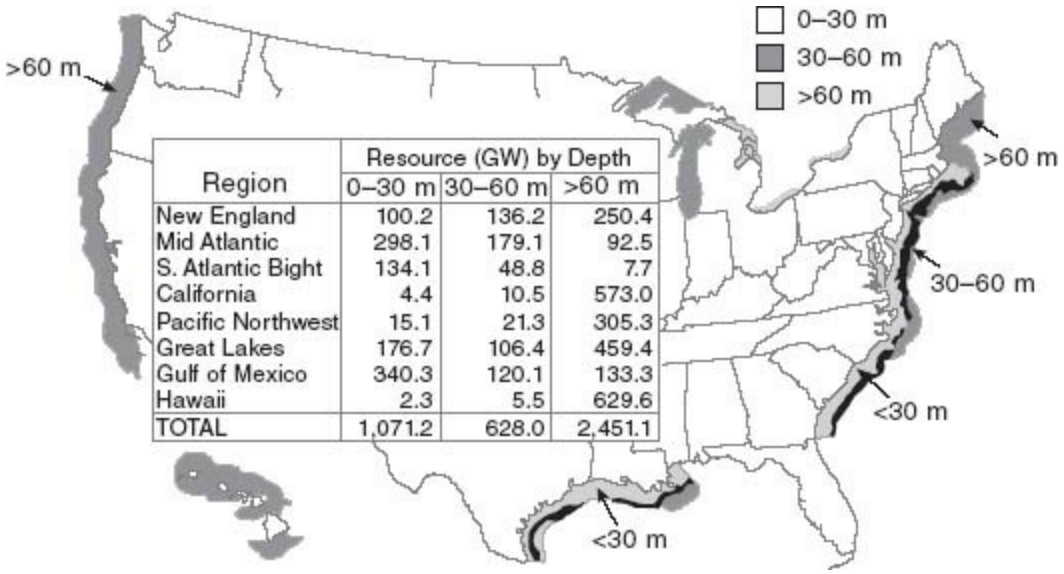
option. That means an offshore, AC-to-DC converter is needed along with an onshore DC-to-AC converter to connect the substation there (Fig. 7.44). While this extra equipment increases system complexity and cost, there are some inherent advantages to DC transmission. For one, it allows variable speed turbines to seamlessly connect to the fixed-frequency grid. It also reduces transmission losses to almost negligible amounts even for long distances. Also, since cables can carry more DC current than AC, cables now being used for a medium-sized AC wind farm could later be used for a much larger wind farm by adding a converter. Finally, the power electronics in the converters allow greater control of active and reactive power, much like conventional synchronous generators powered by steam turbines.

FIGURE 7.44 For larger systems located farther offshore, high-voltage DC transmission becomes a viable, and in some circumstances, necessary option.



NREL (Musial and Ram, 2010) has tried to estimate the total resource potential for offshore wind along the coasts of the United States as well as within large bodies of water such as the Great Lakes. The gross resources were quantified based on water depth, distance from shore, and wind speed in a band extending out 100 km from the coastline. As shown in Figure 7.45, the total resource is estimated at more than 4000 GW, which is about four times the current total generation capacity for all electric power plants in the United States. Unfortunately, most of that is at depths greater than 60 m. California, for example, has tremendous wind resources, but the sea bottom drops off rapidly along most of its shoreline. The prime areas with strong winds and shallow depths are along the eastern seaboard and the coastlines of Texas and Louisiana.

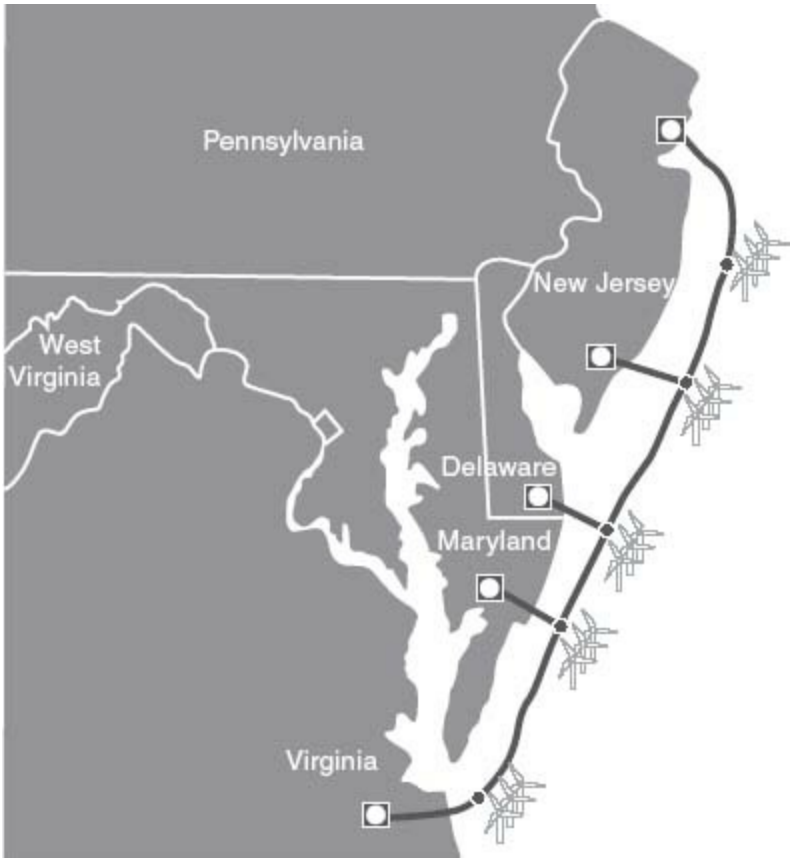
FIGURE 7.45 United States offshore wind resource by region and depth for annual average wind speed sites above 7.0 m/s. Total current U.S. generation is currently about 1000 GW. From NREL (Musial and Ram, 2010).



Region	Resource (GW) by Depth		
	0–30 m	30–60 m	>60 m
New England	100.2	136.2	250.4
Mid Atlantic	298.1	179.1	92.5
S. Atlantic Bight	134.1	48.8	7.7
California	4.4	10.5	573.0
Pacific Northwest	15.1	21.3	305.3
Great Lakes	176.7	106.4	459.4
Gulf of Mexico	340.3	120.1	133.3
Hawaii	2.3	5.5	629.6
TOTAL	1,071.2	628.0	2,451.1

The relatively shallow waters in the outer continental shelf in the Mid-Atlantic region of Figure 7.45 extend miles out to sea, which offers the potential for extensive wind development far from the densely populated shoreline. One project, called the Atlantic Wind Connection (AWC), proposes a transmission backbone that includes a limited number of landfall points to minimize the environmental impacts of multiple onshore grid-connection points (Fig. 7.46). Offshore power hubs would connect via undersea HVDC transmission lines, which have the added advantage of allowing easier integration and control of multiple wind farms.

FIGURE 7.46 Proposed Atlantic Wind Connection transmission backbone for offshore wind farms.



A very carefully done study of the wind potential for the East Coast concludes that about one-third of total U.S. electricity, equivalent to all of the Florida to Maine electricity demand, can be provided with that Atlantic coast offshore resource. Moreover, since these offshore winds are well timed to meet peak demands, with the exception of summer, all peak-time demand from Virginia to Maine could be satisfied with offshore wind energy in the waters off those states (Dvorak et al., 2012).

Example 7.15 Estimating the Shallow Water Wind Resource. Using the NREL assumptions of one 5-MW turbine placed on every square kilometer of water with an annual average wind speed above 7 m/s, estimate the area and energy-generation potential in waters less than 30 m deep.

Solution. From Figure 7.45, the total U.S. resource in waters less than 30-m deep is estimated to be 1071.2 GW. Since that estimate is for winds that blow at least at an average of 7 m/s, we can make a conservative calculation using 7 m/s in Equation 7.68 to find

$$\mathrm{CF} = 0.0435\bar{V} = 0.0435 \times 7 = 0.305$$

$$\text{Annual generation} = 0.305 \times 8760\,\text{h/yr} \times 1071.2\,\text{GW} = 2.86 \times 10^6\,\text{GWh/yr}$$

Current total generation in the United States is about 4 million GWh/yr, so the shallow water resource could be sufficient for more than half of that total.

At 5 MW per turbine:

$$\text{Number of turbines} = \frac{1071.2\,\text{GW}}{5\,\text{MW/turbine}} \times \frac{1000\,\text{MW}}{\text{GW}} = 214{,}000\,\text{turbines}$$

And at one turbine per square kilometer they would span an area of about 214, 000 km^2 (82, 000 mi^2).

7.9 WIND TURBINE ECONOMICS

Wind technology has evolved rapidly over the past three decades. Turbines have gotten much bigger, CFs have increased, and system costs have declined substantially. Wind has become the most cost-effective renewable energy technology available today and projections suggest that within just a few years it will provide power, without special incentives, as cheaply as any conventional source.

The economics of wind power depend on a number of key factors, including:

- The capital cost of the complete system, which includes the complete turbine (blades, generator, tower, and foundation), construction, grid connections, and initial project engineering and permitting costs. These account for about 80% of the levelized cost of energy (LCOE) from wind (Blanco, 2009).
- Variable costs, mostly operation and maintenance, but also annual costs of insurance, taxes, land leasing, and ongoing management and administration. These make up most of the remaining 20% of LCOE.
- Location, primarily whether it is a land-based or offshore system. Offshore systems cost about double that of onshore systems.
- Capacity factor, which depends on the wind resource, hub height, and ratio of generator rated power to swept area.
- Incentives, which may be in such forms as production or investment tax credits, utility rebates, renewable energy credits, and accelerated depreciation benefits.
- Financing, which includes the mix of debt and equity, as well as the structure of the investment recovery system.

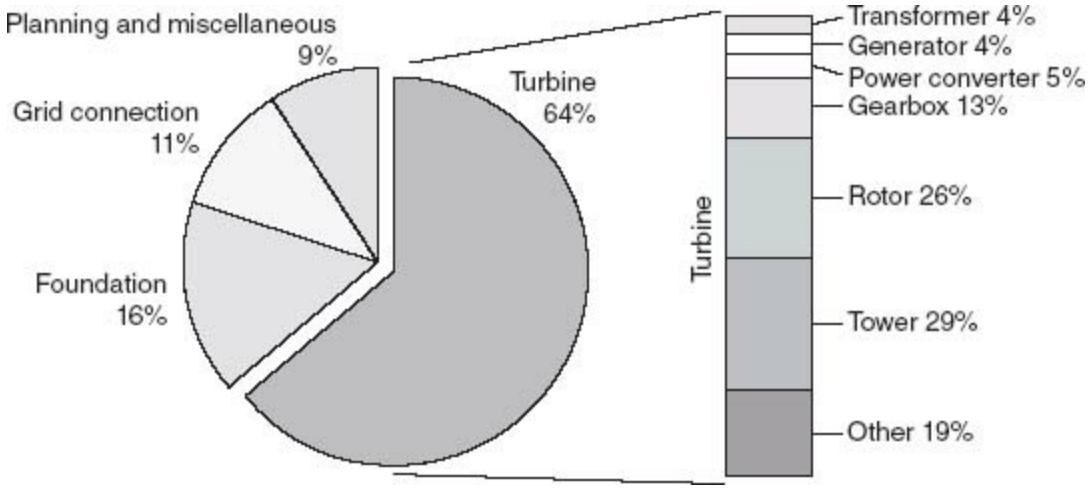
7.9.1 Annualized Cost of Electricity from Wind Turbines

For the first two decades of significant wind power activity, the price of turbines seemed to follow a typical learning curve, decreasing in price by about 10% for every doubling of cumulative installed capacity. But costs bottomed out and began to rise in 2003, mostly due to a sudden increase in commodity prices, especially copper and steel, which affected the entire conventional electric power industry, not just wind. Both of these essential materials tripled in cost within a decade. Added to that were supply-chain bottlenecks caused by new technological advances, coupled with surges in demand. Turbine prices peaked in 2009 after a doubling in cost compared to 2003, but in the ensuing years they began to resume their downward trend.

Figure 7.47 shows a breakdown of the capital costs of an onshore wind system, for which nearly two-thirds is the turbine itself. Half of the turbine cost is the rotor and tower. For offshore systems, given the additional costs of foundations and transmission, the portion of total cost that is the turbines themselves, drops to about half of the capital cost.

FIGURE 7.47 A breakdown of the capital costs of a wind system. Based on Blanco (2009)

and EWEA (2007).



To find a levelized cost estimate for energy delivered by wind turbines, we need to divide annual costs by annual energy delivered. To find annual costs, we need to spread the capital cost over the investment term using an appropriate factor and then add in an estimate of annual operations and maintenance costs. We introduced this approach in Section 6.4.2 in the context of photovoltaic systems, but now let us apply it as an example of a simple way to begin the analysis of wind turbines.

To the extent that a wind project is financed by debt, we can annualize the capital costs using an appropriate capital recovery factor (CRF) that depends on the interest rate and loan term. The annual payments on such a loan would be

$$A = P \cdot \mathrm{CRF}(i, n) \tag{7.69}$$

where A represents annual payments ($/yr), P is the principal borrowed ($), i is the interest rate (decimal fraction: e.g., 0.10 for a 10% interest rate), n is the loan term (years) and CRF(i, n) is the following

$$\mathrm{CRF}(i, n) = \frac{i(1+i)^n}{(1+i)^n - 1} \tag{7.70}$$

The capital recovery factor has units of per year as long as both interest and the loan term are expressed on a yearly basis.

As a start to making annualizing costs, Table 7.6 presents data on several representative wind energy systems. The data for the 2002 and the 2009 systems correspond to turbines installed during the years when historically their costs were their lowest and their highest, respectively. The 2013 data show two turbines with the same nameplate power ratings, but with different blade diameters and hub heights corresponding to turbines designed for standard winds versus ones designed specifically for low wind-speed conditions. The losses shown are estimates of the impact of rotor wakes on wind farms and electrical losses. Additional losses may be appropriate in the future due to the likelihood of increased wind curtailment during instances in which available wind power exceeds the grid's need for power.

TABLE 7.6 Representative Costs for an LCOE Wind Analysis

Characteristics	2002	2009	2013 Turbine Pricing	
Technology Type	Standard	Standard	Standard	Low Wind
Rated power (MW)	1.5	1.5	1.62	1.62
Hub height (m)	65	80	80	100
Rotor diameter (m)	70.5	77	82.5	100
Installed capital cost ($/kW)	1300	2150	1600	2025
Operating cost ($/kW/yr)	60	60	60	60
Losses (%)	15	15	15	15
Financing (nominal) (%)	9	9	9	9

Source: Wiser et al. (2012).

Example 7.16 A Simple Levelized Cost Estimate. Using data from Table 7.6, estimate the annual cost of the 2013 "standard" turbine in a wind regime that is characterized as having 7 m/s average wind speed at 50-m elevation (the beginning of Class IV winds, e.g., Table 7.4). Assume a 20-year "book" life for the system and the usual 1/7th wind-shear factor.

Solution. First we need to estimate the average wind speed at 80 m. From Equation 7.18:

$$\bar{V}_{80} = \bar{V}_{\text{Ref}} \left(\frac{H}{H_{\text{Ref}}} \right)^{\alpha} = 7 \cdot \left(\frac{80}{50} \right)^{1/7} = 7.49\,\text{m/s}$$

We will use Equation 7.63 to estimate CF (being careful to use the appropriate units):

$$\text{CF} = 0.087\bar{V} - \frac{P_{\text{R}}}{D^2} = 0.087 \times 7.49 - \frac{1620}{82.5^2} = 0.413$$

The annual energy delivered, accounting for 15% losses, would be

$$\text{Energy} = 0.413 \cdot (1 - 15\%) \cdot 8760\,\text{h/yr} \cdot 1620\,\text{kW} = 4.98 \times 10^6\,\text{kWh/yr}$$

Now we need to find annual costs. Using Equation 7.70

$$\text{CRF}(9\%, 20) = \frac{0.09(1 + 0.09)^{20}}{(1 + 0.09)^{20} - 1} = 0.1095/\text{yr}$$

The capital cost of the system is \$1600/kW × 1620 kW = \$2, 592, 000. Amortizing that using the above CRF gives an annual cost of

$$A = \$2{,}592{,}000 \times 0.1095/\text{yr} = \$283{,}944/\text{yr}$$

Adding the O&M cost at \$60/kW/yr

$$\text{O\&M} = \$60/\text{kW/yr} \times 1620\,\text{kW} = \$97{,}200/\text{yr}$$

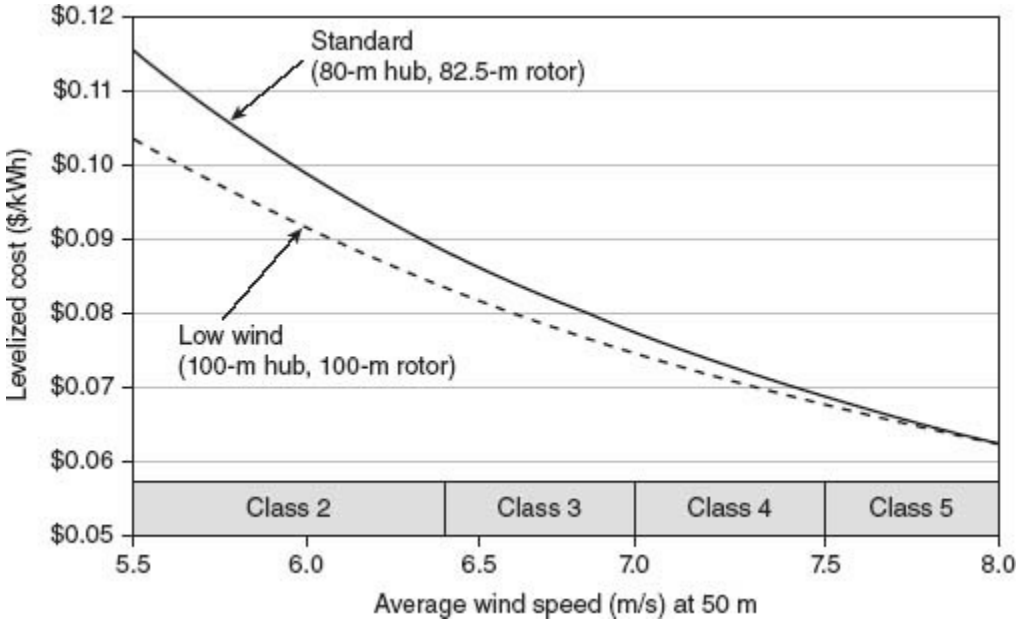
The levelized cost per kWh is therefore

$$\text{Levelized cost} = \frac{\$283{,}944 + \$97{,}200/\text{yr}}{4.98 \times 10^6\,\text{kWh/yr}} = \$0.076/\text{kWh}$$

A wind-speed sensitivity analysis comparing the standard 2013 turbine in Example 7.16

with the 2013 low-wind turbine in Table 7.6 is shown in Figure 7.48. Both turbines have the same generator rated power, but the low wind-speed turbine has a larger rotor, a higher hub height, and it costs more to build. With turbines now being designed with options for low wind sites, much more of the planet's wind resource can be economically captured than previously forecasted.

FIGURE 7.48 Levelized cost sensitivity analysis for the 2013 Standard turbine in Table 7.6 compared with the low wind-speed turbine.



7.9.2 LCOE with MACRS and PTC

The simple analysis that led to Figure 7.48 ignored several economic incentives that have been established to encourage the development of the renewable energy industry. It also ignores the somewhat complex realities of how these systems are financed. Both of these factors have been subject to the whims of Congress, so the descriptions here will likely continue to change over time. In addition to financial incentives, various states have enacted Renewable Portfolio Standards (RPS) that require retail power suppliers to provide a certain minimum percentage of electricity from specified renewable power sources, including wind power. These have been a powerful motivator behind the rapid growth of wind and solar energy systems.

The key tax incentives for wind energy systems in the United States have offered a choice between a production tax credit (PTC) and an investment tax credit (ITC). The PTC was originally created as part of the Energy Policy Act of 1992. At the time it provided an inflation-adjustable 1.5 ¢/kWh income tax credit for the first 10 years of production. As of 2012, the PTC rate was 2.2 ¢/kWh. Over time the PTC has been extended, usually for just a few years at a time, and all too often Congress has allowed it to completely expire before taking action to renew it. Needless to say, this uncertainty has had a tendency to periodically wreak havoc within the industry. The alternative to the PTC has been a 30% ITC, which at times Congress has allowed to be paid as an upfront cash payment delivered when the project is placed in service.

Another tax incentive for businesses is the right to use a rapid depreciation schedule

called the Modified Accelerated Cost Recovery System (MACRS), which was introduced in Section 6.4.6. Table 7.7 shows how valuable MACRS can be for an example $1, 000, 000 installed system cost. Using a corporate tax rate of 38.9%, and a 9% discount rate to account for the time value of money, MACRS saves a bit more than 30% on the equivalent capital cost of the system.

TABLE 7.7 Showing the Impact of MACRS

System cost			$1,000,000	
Corporate tax rate			38.9%	
Corporate discount rate			9%	
Year	MACRS	Depreciation	Depreciation Tax Savings	Present Value of Tax Savings
1	20.00%	$200,000	$77,800.00	$71,376.15
2	32.00%	$320,000	$124,480.00	$104,772.33
3	19.20%	$192,000	$74,688.00	$57,672.84
4	11.52%	$115,200	$44,812.80	$31,746.52
5	11.52%	$115,200	$44,812.80	$29,125.25
6	5.76%	$57,600	$22,406.40	$13,360.20
			Total	$308,053.28
			Net system cost	$691,946.72

Table 7.8 presents a similar present-value calculation to describe the impact of 10 years' worth of PTCs. As shown, for every million kWh per year generated, the present value of the PTC tax savings is $141, 188 (ignoring any inflationary impact on the PTC).

TABLE 7.8 Showing the Impact of the PTC

Annual kWh Generated Production Tax Credit (PTC) Corporate discount rate	($/kWh)	1, 000, 000 $0.022 9%
Year	PTC	Present Value of Tax Savings
1	$22, 000	$20, 183
2	$22, 000	$18, 517
3	$22, 000	$16, 988
4	$22, 000	$15, 585
5	$22, 000	$14, 298
6	$22, 000	$13, 118
7	$22, 000	$12, 035
8	$22, 000	$11, 041
9	$22, 000	$10, 129
10	$22, 000	$9, 293
	Tax savings per 10^6 kWh	$141, 188

Example 7.17 Levelized Cost of Power Including Tax Benefits. The wind system of

Example 7.16 has an installed cost of $2, 592, 000 with an annual O&M cost of $97, 200. It delivers 4.98 million kWh/yr. The corporate tax rate is 38.9% and their discount rate is 9%. Find the levelized cost of electricity including the MACRS and the 2.2 ¢/kWh PTC impacts.

Solution. Let us begin with MACRS. From Table 7.7, for every $1, 000, 000 of installed cost, MACRS saves $308, 053 in taxes, so for this system the present value of those tax savings is

$$\text{MACRS tax savings} = \frac{\$308{,}053}{\$1{,}000{,}000} \times \$2{,}592{,}000 = \$798{,}474$$

For the PTC, for every million kWh/yr generated there is a present value savings of $141, 188. So

$$\text{PTC tax savings} = \frac{\$141{,}188}{10^6\,\text{kWh/yr}} \times 4.98 \times 10^6\,\text{kWh/yr} = \$703{,}116$$

The present value cost of the system, with MACRS and PTC savings is

$$\begin{aligned}\text{Net total cost} &= \text{Installed cost} - \text{MACRS} - \text{PTC}\\ &= \$2{,}592{,}000 - \$798{,}474 - \$703{,}116 = \$1{,}120{,}440\end{aligned}$$

Annualizing that with the CRF(9%, 20 yr) = 0.1095/yr derived in Example 7.16 gives

$$\text{Annualized first cost} = \$1{,}120{,}440 \times \$0.1095/\text{yr} = \$122{,}688/\text{yr}$$

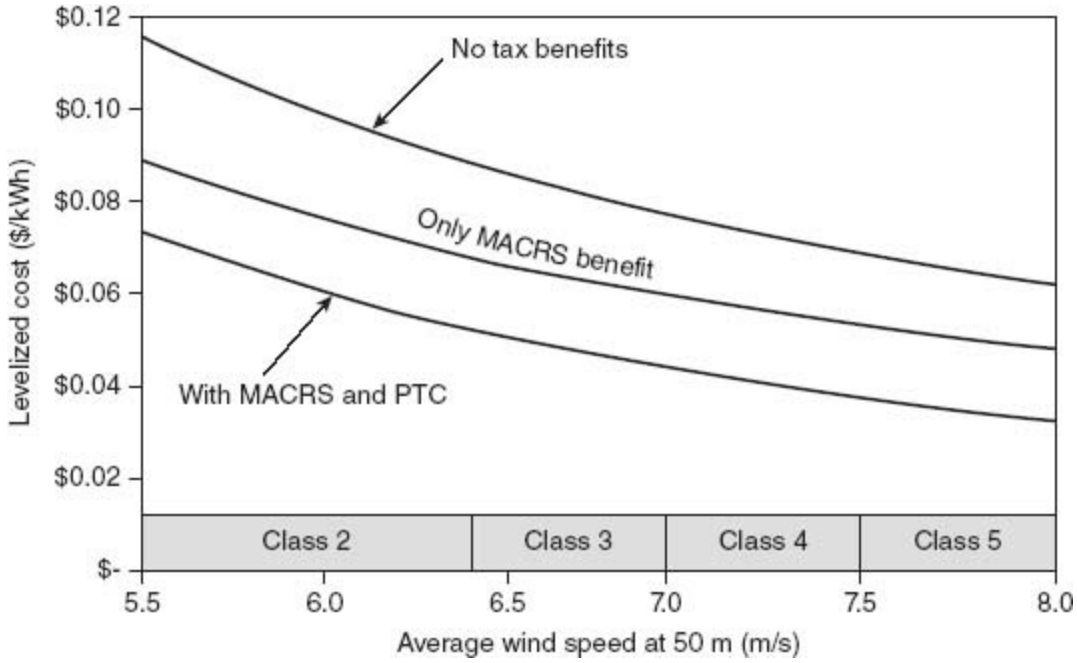
Adding the $97, 200/yr O&M cost and dividing by the kWh/yr generated yields a levelized cost of electricity of

$$\text{LCOE} = \frac{\$122{,}688/\text{yr} + \$97{,}200/\text{yr}}{4.98 \times 10^6\,\text{kWh/yr}} = \$0.044/\text{kWh}$$

So, the LCOE has dropped from 7.6 ¢/kWh to 4.4 ¢/kWh due to MACRS and PTC.

Figure 7.49 presents an LCOE sensitivity analysis for the 2013 Standard wind energy system with curves for no tax benefits, only the MACRS benefit, and with both MACRS and PTC working together.

FIGURE 7.49 LCOE for the 2013 Standard wind turbine in Table 7.6 (1620 kW, 80-m hub, 82.5-m rotor, $1600/kW) with and without tax benefits.



The LCOE approach is most appropriate for policy studies comparing one energy system with another. However, for renewable energy systems, it misses some important subtleties, such as the fact that renewables in general are not dispatchable, which means they cannot be easily varied to follow constantly changing demands. Dispatchable technologies are more valuable than less-flexible renewables, which makes for a somewhat misleading comparison when the LCOE of say, wind, is compared to the LCOE of a more traditional gas turbine. Nonetheless, the levelized cost of wind, when tax benefits are included, has crossed the threshold of economic competitiveness with every nonrenewable energy system.

7.9.3 Debt and Equity Financing of Wind Energy Systems

The economic viability of most large wind projects these days is based on power purchase agreements (PPAs) between an owner–investor group and a utility that agrees to buy power from the project. PPAs for wind systems are similar to those that were introduced in Section 6.4.7 for photovoltaics. Basically, a contract includes an agreed-upon PPA base rate, which may then be adjusted on an hour-by-hour basis using time of delivery (TOD) factors such as the ones shown in Table 6.10.

Projects are usually financed with a combination of equity provided by the owners and debt provided by a lending agency, such as a bank. Owners take more risks with their equity investments than do lenders, so they require a higher rate of return. Lenders take less risk, but want verification that annual operating income before counting depreciation, interest deductions, and other accounting tricks will always be significantly higher than debt payments. The starting point in analyzing such a deal is a detailed year-by-year cash flow. If the owners have a significant tax appetite, the analysis can be relatively straightforward since they can take advantage of all of those early tax benefits. Table 7.9 shows an example of spreadsheet based 75% debt and 25% equity financing for the same 2013 Standard turbine that we have been working with. After 20 years of cash flows, the investors earn a healthy 22.8% internal rate of return.

TABLE 7.9 PPA Cash-Flow Analysis with Debt and Equity Resulting 22.8% IRR for the Equity Investors Over

the First 20 Years (data correspond to the 2013 Standard wind turbine in Table 7.6)

Inputs	Value	Comments
Single turbine rated power (kW)	1620	2013 "Standard"
Turbine diameter (m)	82.5	Enter
Hub height (m)	80	Enter
Average 50-m wind speed (m/s)	7	Enter
Avg wind speed at hub (m/s)	7.486	V = V50 (Hub/50)^(1/7)
Estimated turbine CF	0.4133	CF = 0.087*V_{avg} – P/D^2
Wind farm losses (%)	15%	Enter
Generation (kWh/h)	4,985,172	CF × 8760 × Rated power × (1 – loss)
Installed cost ($/kW)	$1600	Enter
Installed cost ($)	2,592,000	$/kW × Total rated power
Equity fraction (%)	75%	Enter
Equity	$1,944,000	Fraction × Installed cost
Debt	$648,000	Installed Cost – Equity
Debt interest (%)	8%	Enter
Debt term (yrs)	15	Enter
Debt CRF (i,n)/yr	0.11683	$i(1 + i)^n/((1 + i)^n - 1)$
Debt payments ($/yr)	$75,706	Debt × CRF
O&M expense at t = 0 ($/kW/yr)	$60	Enter
O&M base at t = 0	$97,200	O&M $/kw/yr × rated kW
O&M escalation rate (%)	1.5%	Enter
Owner tax rate (%)	38.9%	Enter
PTC ($/kWh)	$0.022	Enter good for 10 yrs
PPA year = 0 Price ($/kWh)	$0.100	Enter
PPA value at t = 0	$498,517	PPA $/kWh × kWh/yr
PPA escalation rate (%/yr)	2%	Enter

Year	0	1	2	3	...	20
Operating revenue (PPA)		$508,488	$518,657	$529,030	...	$740,770
O&M expenses		$98,658	$100,138	$101,640	...	$130,914
Operating income		$409,830	$418,519	$427,390	...	$609,856
Debt payment		$75,706	$75,706	$75,706	...	–
Debt payment interest		$51,840	$49,931	$47,869	...	$0
Debt balance	$648,000	$624,134	$598,360	$570,523	...	$0
Depreciation (5-yr MACRS)		$518,400	$829,440	$497,664	...	–
Taxable income		($160,410)	($460,851)	($118,142)	...	$609,856
Income taxes (w/o PTC)		($62,400)	($179,271)	($45,957)	...	$237,234
PTC		($109,674)	($109,674)	($109,674)	...	–
Income tax l		($172,073)	($288,945)	($155,631)	...	$237,234
After tax net equity cash flow	($1,944,000)	$506,197	($631,759)	$507,316	...	$372,622
Cumulative IRR (%)		–74%	–28.5%	–7.9%	...	22.8%
	20-yr IRR = 22.8%					

If investors cannot take immediate advantage of the tax benefits associated with loan interest, depreciation, and tax credits, they may opt for any of a number of clever ownership arrangements. One of the most popular of these arrangements is to share the ownership between a "tax investor" and a "sponsor" in what is called a strategic investor flip (Cory and Schwabe, 2009). During roughly the first 10 years when MACRS and PTC are delivering major tax benefits, the tax investor owns almost all of the company. After the tax investor has reaped as many of those tax benefits as are necessary to meet his/her goals, the ownership flips and the sponsor takes over as the major owner. For the remaining life of the system, the sponsor then takes almost all of the profits.

7.10 ENVIRONMENTAL IMPACTS OF WIND TURBINES

Wind systems have negative as well as positive impacts on the environment. The negative ones relate to bird kills, noise, construction disturbances, aesthetic impacts, and pollution associated with imbedded energy. The positive impacts result from wind displacing other, more polluting, energy systems.

Birds do collide with wind turbines, just as they collide with cars, cell-phone towers, glass windows, and high voltage power lines. While the rate of deaths caused by wind turbines is miniscule compared to these other obstacles that humans put into their way, it is still an issue that can cause concern. A number of European studies have concluded that birds almost always modify their flight paths well in advance of encountering a turbine, and very few deaths are reported. In the earlier days at Altamont pass in California, there were reports of raptor deaths, especially when a solid row of fast-spinning turbines blocked their way, but modern large turbines spin so slowly that birds now more easily avoid them. Studies of eider birds and offshore wind parks in Denmark concluded that the eiders avoided the turbines even when decoys to attract them were placed nearby. They also noted no change in the abundance of nearby eiders when turbines were purposely shut down to study their behavior.

People's perceptions of the aesthetics of wind farms are important in siting the machines. A few simple considerations have emerged, which can make them much more acceptable. Arranging same-size turbines in simple, uniform rows and columns seems to help, as does painting them a light grey color to blend with the sky. Larger turbines rotate more slowly, which makes them somewhat less distracting.

Noise from a wind turbine or a wind farm is another potentially objectionable phenomenon and modern turbines have been designed specifically to control that noise. It is difficult to actually measure the sound level caused by turbines in the field because the ambient noise caused by the wind itself masks their noise. At a distance of only a few rotor diameters away from a turbine, the sound level is comparable to a person whispering.

The air quality advantages of wind are pretty obvious. Other than the very modest imbedded energy, wind systems emit none of the SO_x, NO_x, CO, VOCs or particulate matter associated with fuel-fired energy systems. And, of course, since there are virtually no greenhouse gas emissions, wind economics will get a boost if and when carbon-emitting sources begin to be taxed.

REFERENCES

Blanco MI. The economics of wind energy. Renewable and Sustainable Energy Reviews 2009; 13(6–7):1372–1382.

Cavallo AJ, Hock M, Smith DR. Wind energy: Technology and economics. In: Burnham L, editor. *Renewable Energy, Sources for Fuels and Electricity.* Washington, DC: Island Press; 1993.

Cory K, Schwabe P. Wind levelized cost of energy: a comparison of technical and financing

input variables.2009 October. NREL/TP-6A2-46671.

Denholm P, Hand M, Jackson M, Ong S. Land-use requirements of modern wind power plants in the United States. 2009. NREL/TP-6A2-45834.

DOE. 20% wind energy by 2030: increasing wind energy's contribution to U.S. electricity supply.2008 July. DOE/GO-102008-2567.

Dvorak MJ, Corcoran B, Ten Hoeve J, McIntyre N, Jacobson M. *US East Coast offshore wind energy resources and their relationship to peak-time electricity demand*. Wind Energy, Wiley Online Library; 2012. DOI:10.1002/we.1524.

Elliott DL, Holladay CG, Barhett WR, Foote HP, Sandusky WF. *Wind Energy Resource Atlas of the United States.* Golden, CO: Solar Energy Research Institute, U.S. Department of Energy; 1987. DOE/CH 100934.

EWEA. *Wind Directions.* Brussels: European Wind Energy Agency; 2007.

Jacobson MZ, Masters GM. Exploiting wind versus coal. Science 2001;293:1438.

Johnson, GL. *Wind Energy Systems.* Englewood Cliffs, NJ: Prentice Hall; 1985.

IRENA. Renewable energy technologies: cost analysis series, Volume 1. International Renewable Energy Agency; 2012 June.

Musial W, Ram B. Large-scale offshore wind power in the United States: assessment of opportunities and barriers. National Renewable Energy Laboratory; 2010 September. NREL/TP-500-40745.

Wiser R, Bolinger M. 2011 wind technologies market report. Lawrence Berkeley National Laboratory; 2012.

Wiser R, Lantz E, Bolinger M, Hand M. Recent developments in the levelized cost of energy from U.S. wind power projects. National Renewable Energy Laboratory; 2012 February.

Wu B, Lang Y, Zargari N, Kouro S. *Power Conversion and Control of Wind Energy Systems.* Hoboken, NJ: Wiley IEEE Press; 2011.

PROBLEMS

7.1 A horizontal-axis wind turbine with a 20-m diameter rotor is 30% efficient in 10 m/s winds at 1 atm of pressure and 15°C temperature.

a. How much power would it produce in those winds?

b. Estimate the air density on a 2500-m mountaintop at 10°C?

c. Estimate the power the turbine would produce on that mountain with the same wind speed assuming its efficiency is not affected by air density.

7.2 An anemometer mounted 10 m above a surface with crops, hedges, and shrubs, shows a wind speed of 5 m/s. Assuming 15°C and 1 atm pressure, determine the following for a wind turbine with hub height 80 m and rotor diameter of 80 m:

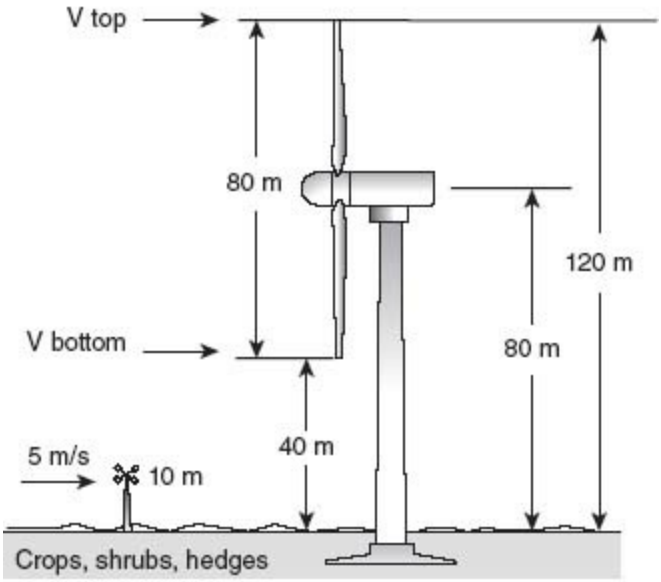


FIGURE P7.2

a. Estimate the wind speed and the specific power in the wind (W/m^2) at the highest point that the rotor blade reaches. Assume no air density change over these heights.

b. Repeat (a) at the lowest point at which the blade falls.

c. Compare the ratio of wind power at the two elevations using results of (a) and (b) and compare that with the ratio obtained using Equa-tion 7.20.

d. What would the power density be at the highest tip of the blade if we include the impact of elevation on air density? Assume the temperature is still 15°C. Does air density change seem worth considering in the above analysis?

7.3 The analysis of a tidal power facility is similar to that for a normal wind turbine. That is, we can still write $P = 1/2\ \rho\ A\ v^3$ but now ρ = 1000 kg/m^3 and v is the speed of water rushing toward the turbine. The following graphs assume sinusoidally varying water speed, with amplitude V_{max}. We assume the turbine can accept flows in either direction (as the tide ebbs and floods) so it is only the magnitude of the tidal current that matters.

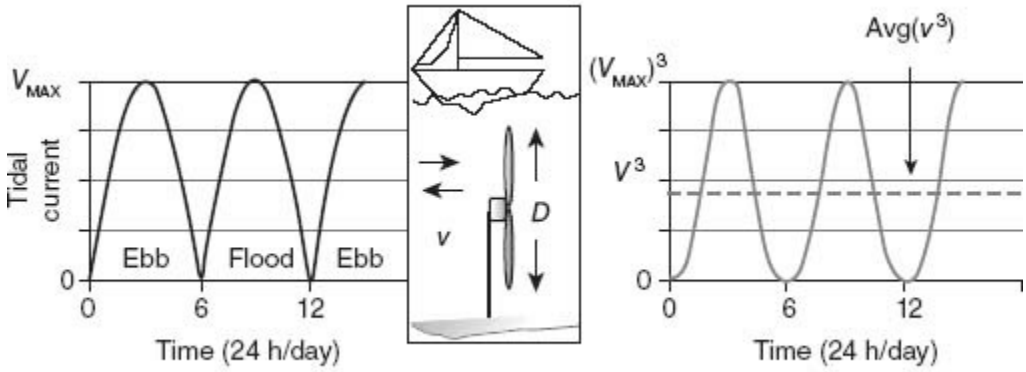


FIGURE P7.3

For a sinusoidal tidal flow with V_{max} = 2 m/s,

a. What is the average power density (W/m^2) in the tidal current? A bit of calculus

gives us the following helpful start:

$$(v^3)_{\text{avg}} = \text{avg}(V_{\max} \sin v)^3 = V_{\max}^3 \frac{\int_0^{\pi/2} \sin^3 v \, dv}{\pi/2} = \frac{4}{3\pi} V_{\max}^3$$

b. If a 600-kW turbine with 20-m diameter blades has a system efficiency of 30%, how many kWh would it deliver per year in these tides?

7.4 Consider an 82-m (diameter), 1.65-MW wind turbine with a rated wind speed of 13 m/s.

a. At what rpm does the rotor turn when it operates with a TSR of 4.8 in 13 m/s winds? How many seconds per rotation is that?

b. What is the tip speed of the rotor in those winds (m/s and mph)?

c. What gear ratio is needed to match the rotor speed to an 1800 rpm generator when the wind is blowing at the rated wind speed?

d. What is the efficiency of the complete wind turbine (blades, gearbox, generator) in 13 m/s winds?

7.5 An early prototype 10-kW Makani Windpower system consisted of two 5-kW wind turbines mounted on a wing that flies in somewhat vertical circles (like a kite) several hundred meters above ground. A tether attached to the "kite" carries power from the turbines down to the ground. Since the speed of the kite-turbines moving through the air is much faster than the wind speed, much smaller turbine blades can be used than those on conventional ground-mounted wind turbines. Also with no need for a tower, the cost of materials is far lower than for a conventional system.

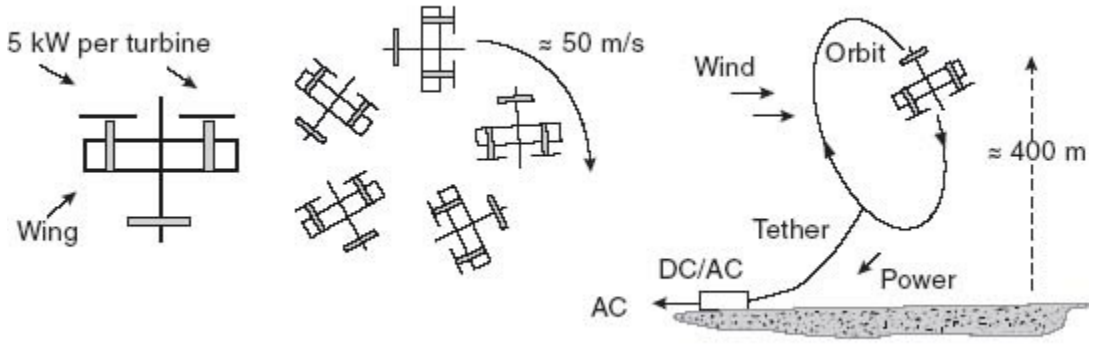


FIGURE P7.5

Suppose each wing/turbine is moving through the air at 50 m/s and suppose the overall efficiency is half that of the Betz limit, what blade diameter would be required to deliver 5 kW of power per turbine. Do not bother to correct air density for this altitude.

7.6 Consider the following probability density function for wind speed:

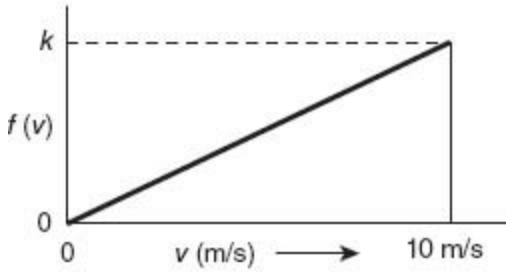


FIGURE P7.6

a. What is an appropriate value of k for this to be a legitimate pdf?

b. What is the average power in these winds (W/m^2) under standard temperature and pressure conditions (1 atm, 15°C)?

7.7 Suppose a wind turbine has a cut-in wind speed of 5 m/s and a furling wind speed of 25 m/s. If the winds the turbine sees have Rayleigh statistics with an average wind speed of 9 m/s,

a. For how many hours per year will the turbine be shut down because of excessively high-speed winds?

b. For how many hours per year will the turbine be shut down because winds are too low?

c. If this is a 1-MW turbine, how much energy (kWh/yr) would be produced for winds blowing at or above the rated wind speed of 12 m/s?

7.8 The table below shows a portion of a discretized estimate of the energy delivered by a Siemens 2300-kW, 101-m diameter wind turbine (Table 7.5) exposed to Rayleigh winds with average speed 6 m/s. For example, for winds blowing around 4 m/s ($3.5 \le v \le 4.5$), the turbine produces 100 kW of power and in a year's time, a Rayleigh pdf predicts it delivers 107, 841 kWh.

TABLE P7.8

P (MW)	2300	
v avg	6	m/s
v (m/s)	kW	kWh/yr
0	0	–
1	0	–
2	0	–
3	0	–
4	100	107,841
5	?	?
etc		

a. How many kWh/yr would be generated for winds blowing at 5 m/s winds? Do this by hand.

b. Create your own spreadsheet (similar to Example 7.9) and find the annual energy delivered by this turbine in these winds.

c. Compare your answer in (b) to the energy predicted by using the simplified capacity

factor Equation 7.63.

7.9 Continue Problem 7.8 to see how well the correlation in Equation 7.63 matches the Rayleigh probability spreadsheet approach over a range of average wind speeds. Plot capacity factors for the Rayleigh estimate and the one from Equation 7.63 versus average wind speed (similar to Fig. 7.33) using average wind speeds of 5, 6, 7, 8, and 9 m/s.

7.10 The 101-m Siemens turbines in Table 7.5 come with either a 2300 or a 3000 kW generator. Using the approach based on Equation 7.63:

a. Find the energy (kWh/yr) each will deliver in an area with 5.7 m/s average wind speed.

b. Determine the optimum generator size for these winds. Check to be sure it does better than the standard size generators.

c. At what wind speed would the 3000 kW generator begin to outperform the 2300 kW generator? Check to see that the two generator outputs are the same at that wind speed.

7.11 Consider the design of a home-built wind turbine using a 350-W permanent magnet DC motor used as a generator. The goal is to deliver 70 kWh in a 30-day month.

a. What capacity factor would be needed for the machine?

b. If the average wind speed is 5 m/s, and Rayleigh statistics apply, what should the rotor diameter be if the CF correlation of Equation 7.63 is used?

c. How fast would the wind have to blow to cause the turbine to put out its full 0.35 kW if the machine is 20% efficient at that point?

d. If the TSR is assumed to be 4, what gear ratio would be needed to match the rotor speed to the generator if the generator needs to turn at 600 rpm to deliver its rated 350 W?

7.12 Consider the perspective of a landowner being offered the following three choices by a wind developer. Compare the options.

a. A flat $20, 000/yr per turbine

b. 0.5¢ for each kWh generated

c. $500/yr per acre (4047 m^2/acre) of array (turbine corner to turbine corner) plus $100/yr per acre of buffer zone.

The proposal is for thirty 1.6-MW, 80-m turbines with 3D (side-by-side) and 10D (row-to-row) spacing plus a 5D buffer zone. Winds are modeled with Rayleigh assumptions at an average wind speed of 7 m/s. Wind-farm losses (wake loss, interconnects, blade bugs) are estimated at 15%.

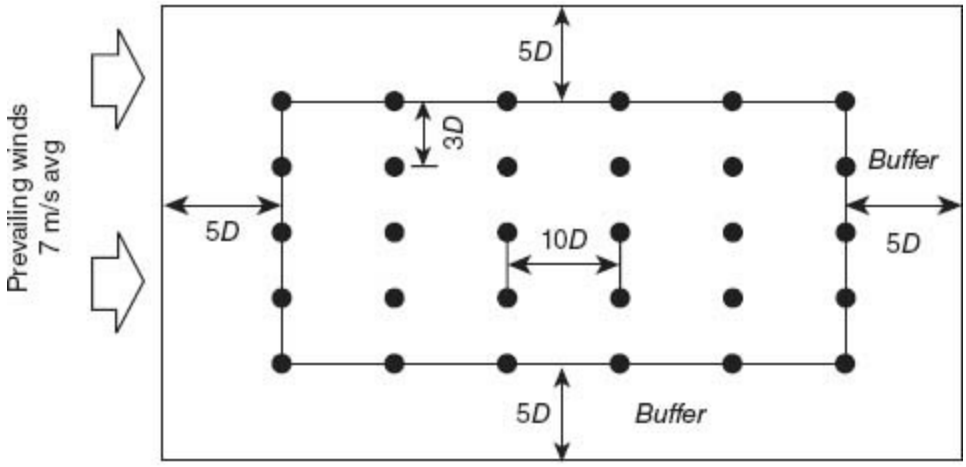


FIGURE P7.12

7.13 The 2013 "low wind" turbine pricing in Table 7.6 uses a 1.62 MW turbine with an installed cost of $2025/kW with a 100-m rotor diameter.

a. At a site with 6 m/s Rayleigh winds at 50-m, estimate the energy this turbine would deliver at a hub height of 100 m assuming the usual 1/7th wind-shear factor. Assume 15% losses.

b. Assuming a nominal 9% financing charge with a 20-year term along with annual O&M costs of $60/kW, find the levelized cost of electricity. Does it agree with Figure 7.48?

7.14 A wind turbine with a capital cost of $3 million delivers 5 million kWh/yr. Assuming a 35% corporate tax rate and a nominal 9% discount factor find the following:

a. The present value of the 5-year MACRS depreciation assuming it starts at the end of the first year of operation.

b. The present value of the production tax credit (PTC) assuming a 10-year PTC at a fixed 2.2¢/kWh first paid at the end of the initial year of operation.

c. What is the net capital cost if we subtract the present values of its MACRS and PTC payments?

d. Assuming the above net cost is amortized using a 20-year, 9% CRF, what is the levelized cost of electricity for this turbine? Compare it to the LCOE without MACRS and PTC.

CHAPTER 8

MORE RENEWABLE ENERGY SYSTEMS

8.1 INTRODUCTION

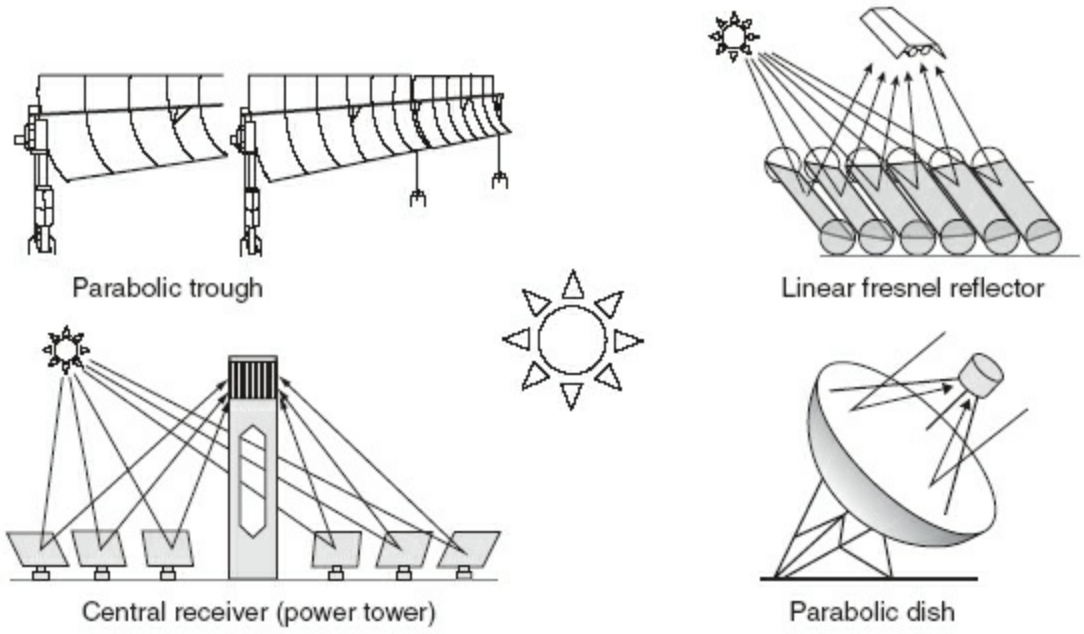
This book has focused on the most aggressively pursued renewable energy systems, which are those based on wind and photovoltaic (PV) technologies, but there are other small and large systems that are also beginning to contribute to the renewables mix. Concentrating solar–thermal power systems, tidal and wave power, hydroelectric, biomass, and geothermal power are conversion technologies in which there is growing interest.

8.2 CONCENTRATING SOLAR POWER SYSTEMS

Most electricity around the globe is generated in power plants that convert heat into mechanical work. A heat source boils water to make high temperature, high pressure steam, which expands through a turbine to spin a generator. The special attribute of concentrating solar power (CSP) plants is they get that heat from sunlight rather than from fossil or nuclear fuels. Just to keep the nomenclature clear, CSP systems convert thermal energy into electricity, while concentrating photovoltaic (CPV) systems convert photons into electricity.

There are four competing CSP design approaches: linear parabolic troughs, central receivers (power towers), linear Fresnel reflectors (LFRs), and parabolic dish systems using Stirling engines (Fig. 8.1). They share the common advantage of using solar energy as their fuel, and they share common challenges that all heat engines have of creating a high temperature source and a low-temperature sink and of doing so in the most economical fashion. In this section, we begin by addressing these commonalities and end with a comparison of the ability of these technologies to meet those challenges.

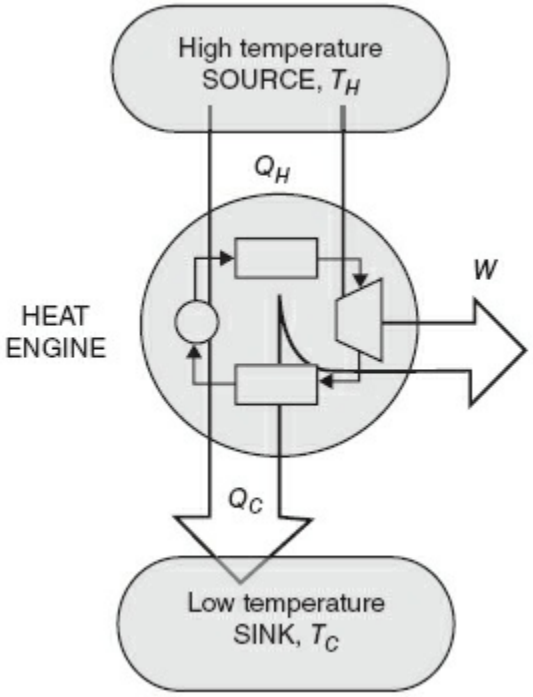
FIGURE 8.1 The four approaches to concentrating solar–thermal power systems.



8.2.1 Carnot Efficiency for Heat Engines

Very simply, a heat engine extracts heat Q_H from a high temperature source, such as a boiler, converts part of that heat into work W, usually in the form of a rotating shaft, and rejects the remaining heat Q_C into a low temperature sink such as the atmosphere or a local body of water. Figure 8.2 provides a general model describing such engines.

FIGURE 8.2 A heat engine converts some of the heat extracted from a high temperature reservoir into work, rejecting the rest into a low temperature sink.



The thermal efficiency of a heat engine is the ratio of work done to input energy provided by the high temperature source:

$$\text{Thermal efficiency} = \frac{\text{Net work output}}{\text{Total heat input}} = \frac{W}{Q_H} \tag{8.1}$$

Since energy is conserved

$$Q_H = W + Q_C \tag{8.2}$$

which leads to another expression for efficiency:

$$\text{Thermal efficiency} = \frac{Q_H - Q_C}{Q_H} = 1 - \frac{Q_C}{Q_H} \tag{8.3}$$

The most efficient heat engine that could possibly operate between a hot and cold thermal reservoir was first described back in the 1820s by the French engineer Sadi Carnot. To sketch out the basis for his famous equation, which links the maximum possible efficiency of a heat engine to the temperatures of the hot and cold reservoirs, we need to introduce the concept of *entropy*.

As is often the case in thermodynamics, the definition of this extremely important quantity is not very intuitive. It can be described as a measure of molecular disorder or molecular randomness. At one end of the entropy scale is a pure crystalline substance at absolute zero temperature. Since every atom is locked into a predictable place, in perfect order, its entropy is defined to be zero. In general, substances in the solid phase have more ordered molecules and hence lower entropy than liquid or gaseous substances. When we burn some coal, there is more entropy in the gaseous end products than in the solid lumps we burned. That is, unlike energy, entropy is not conserved in a process. In fact for every real process that occurs, disorder increases and the total entropy of the universe increases.

The concept of ever-increasing entropy is enormously important. It tells us that in any isolated system (e.g., the universe) in which the total energy cannot change, the only processes that can occur spontaneously are ones that result in an increase in the entropy of the system. The implications of that include the requirement that heat flows naturally from warm objects to cold ones, and not the other way around. It also dictates the direction of certain chemical reactions.

When we started the analysis of the heat engine mentioned in Figure 8.2, we began by tabulating energy flows. The first law of thermodynamics treats energy in the form of heat transfer on an equal basis with energy that shows up as work done by the engine. For an entropy analysis, that is not the case. Work is considered to be an idealized process in which no increase in disorder occurs, and hence it has no accompanying entropy transfer. This is a key distinction. Processes involve heat transfer and work. Heat transfer is accompanied by entropy transfer, but work is entropy free.

Obviously, to be a useful analysis tool, entropy must be described with equations as well as mental images. Going back to the heat engine, if an amount of heat Q is removed from a "large" thermal reservoir at temperature T (large enough that the temperature of the reservoir does not change as a result of this heat loss), the loss of entropy ΔS from the reservoir is defined as

$$\Delta S = \frac{Q}{T} \tag{8.4}$$

where T is an absolute temperature measured using either the Kelvin or Rankine scale. Equation 8.4 suggests that entropy goes down as temperature goes up. We know that high temperature heat is more useful than the same amount at lower temperature, which reminds us that entropy is not such a good thing. Less is better!

If we apply Equation 8.4 to a heat engine, along with the requirement that entropy must increase during its operation, we can easily determine the maximum possible efficiency of such a machine. Since there is no entropy change associated with the work done, the requirement that entropy must increase (or, at best break even) tells us that the entropy added to the low temperature sink must exceed the entropy removed from the high temperature reservoir:

$$\frac{Q_C}{T_C} \geq \frac{Q_H}{T_H} \tag{8.5}$$

Rearranging Equation 8.5 and substituting it into Equation 8.3 tells us that the maximum possible efficiency of a heat engine is given by

$$\eta_{max} = 1 - \frac{T_C}{T_H} \tag{8.6}$$

This is the classical result described by Carnot. One immediate observation that can be made from Equation 8.6 is that the maximum possible heat engine efficiency increases as the temperature of the hot reservoir increases or the temperature of the cold reservoir decreases. In fact, since neither infinitely high temperatures nor absolute zero temperatures are possible, we must conclude that no real engine can convert thermal energy into mechanical energy with 100% efficiency—there will always be waste heat rejected to the environment.

CSP technologies convert sunlight into thermal energy to run a heat engine to power a generator. With the environment providing the cold temperature sink, the maximum efficiency of a heat engine is directly related to how hot the high temperature source can be made. Without concentration, sunlight cannot provide high enough temperatures to make the thermodynamic efficiency of a heat engine worth pursuing. But with concentration, it is an entirely different story. There are four successfully demonstrated approaches to concentrating sunlight that have been pursued with some vigor: linear parabolic-trough systems, central receivers with mirrors reflecting sunlight onto a power tower, linear Fresnel concentrators, and parabolic dish systems with Stirling engines. The power system for the first three of these are based on relatively conventional Rankine-cycle heat engines, which means they have the potential to include thermal storage that can be used to extend the hours of operation, help meet peak demands, and smooth out some of their variability as clouds drift by. They can also be hybridized with a fossil-fuel system to produce steam when the sun is not shining, which increases their economic viability.

8.2.2 Direct Normal Irradiance

While thermal storage can give CSP an economic advantage over PV systems, realize that the ability to concentrate solar energy, both for solar thermal and PV systems, depends on the ability to focus sunlight onto a receiver. Focusing the beam portion of total irradiation

is quite straightforward, but that is not the case for the diffuse and reflected portions. A sizeable fraction of incoming radiation is therefore unusable for CSP, which offsets some of its storage advantages.

Concentrating solar–thermal power systems typically utilize either single-axis tracking along a north–south horizontal array or they use two-axis tracking that tracks the sun's path throughout the day. Since both of these approaches work with just the direct normal irradiance (DNI) portion of the total, it is interesting to estimate the resulting insolation penalty. Table 8.1 shows irradiance data for five cities that represent locations with some of the highest radiation levels in the country. For each, the total irradiance is given for horizontal collectors, south-facing fixed arrays with tilt equal to latitude, and for two-axis trackers. For the DNI, a comparison is made between horizontal single-axis collectors and those that can continuously track the sun

TABLE 8.1 Comparison of Solar Irradiation Incident on Various Collector Orientations for Five Very Sunny Locations

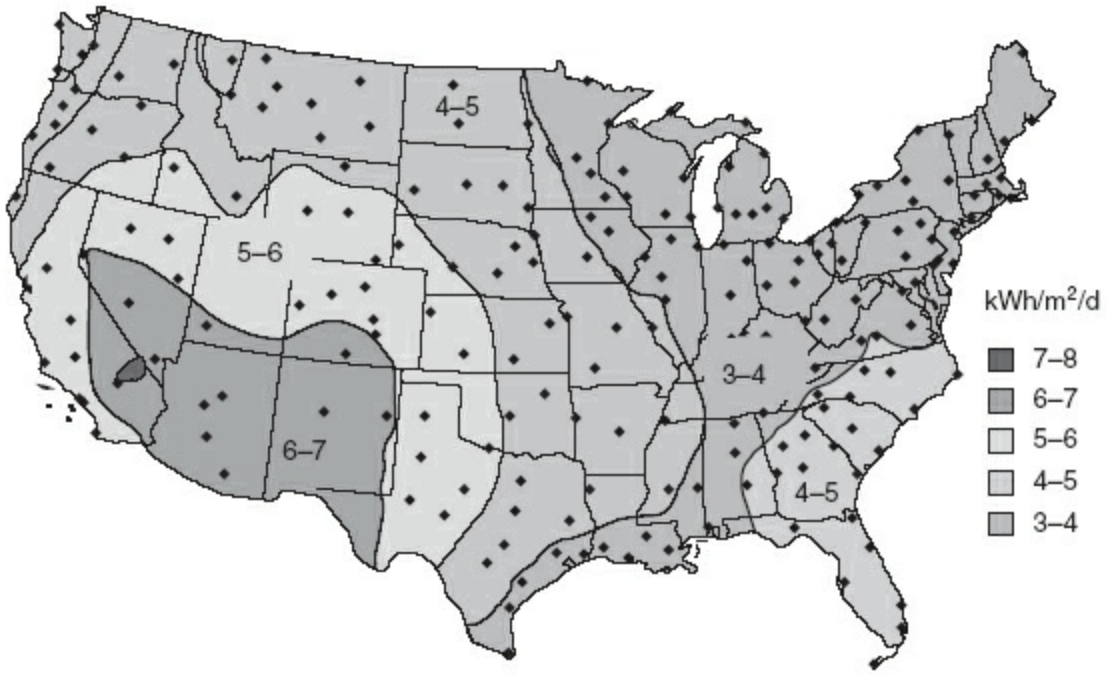
Irradiance (kWh/m^2/d)	Daggett, CA	Tucson, AZ	Las Vegas, NV	EI Paso, TX	Albuquerque, NM
Total horizontal	5.8	5.7	5.7	5.7	5.6
Total south fixed tilt = Lat	6.6	6.5	6.5	6.5	6.4
Total 2-axis tracking	9.4	9.0	9.1	8.9	8.8
DNI 1-axis horiz N–S axis	6.6	6.2	6.2	6.0	5.9
DNI 1-axis tracking	7.5	7.0	7.1	6.7	6.7
Ratios					
(Total 2-axis)/(DNI 2-axis)	125%	129%	128%	133%	131%
DNI (2-axis)/(1-axis horiz)	114%	113%	115%	112%	114%

Source: Data from NREL's Redbook.

From Table 8.1, it can be seen that in these very sunny areas, per unit of collector area a dual-axis tracking, non-concentrating photovoltaic array has 25–33% more radiation to work with than a dual-axis CSP. Comparing the DNI radiation numbers, it appears that a dual-axis concentrator sees 12–15% more radiation than its single-axis, horizontal counterparts.

The disadvantages of being able to focus only the direct beam portion of the available radiation suggests that CSP systems need to be located in the very sunniest locations to be competitive. Figure 8.3 shows a map of those locations in the United States, which are, not unexpectedly, concentrated in the hot, dry, sunny southwestern portion of the country. Globally, suitable areas for CSP include North Africa, the Middle East, Southern Africa, Australia, and the western side of South America. With relatively limited geographic regions where CSP seems likely to be installed, natural questions include whether there is sufficient area and solar resource, close enough to load centers to allow CSP to become a major supplier of electric power without significant new investment in transmission infrastructure.

FIGURE 8.3 Direct normal irradiance (DNI) on two-axis tracking concentrating collectors (from NREL).

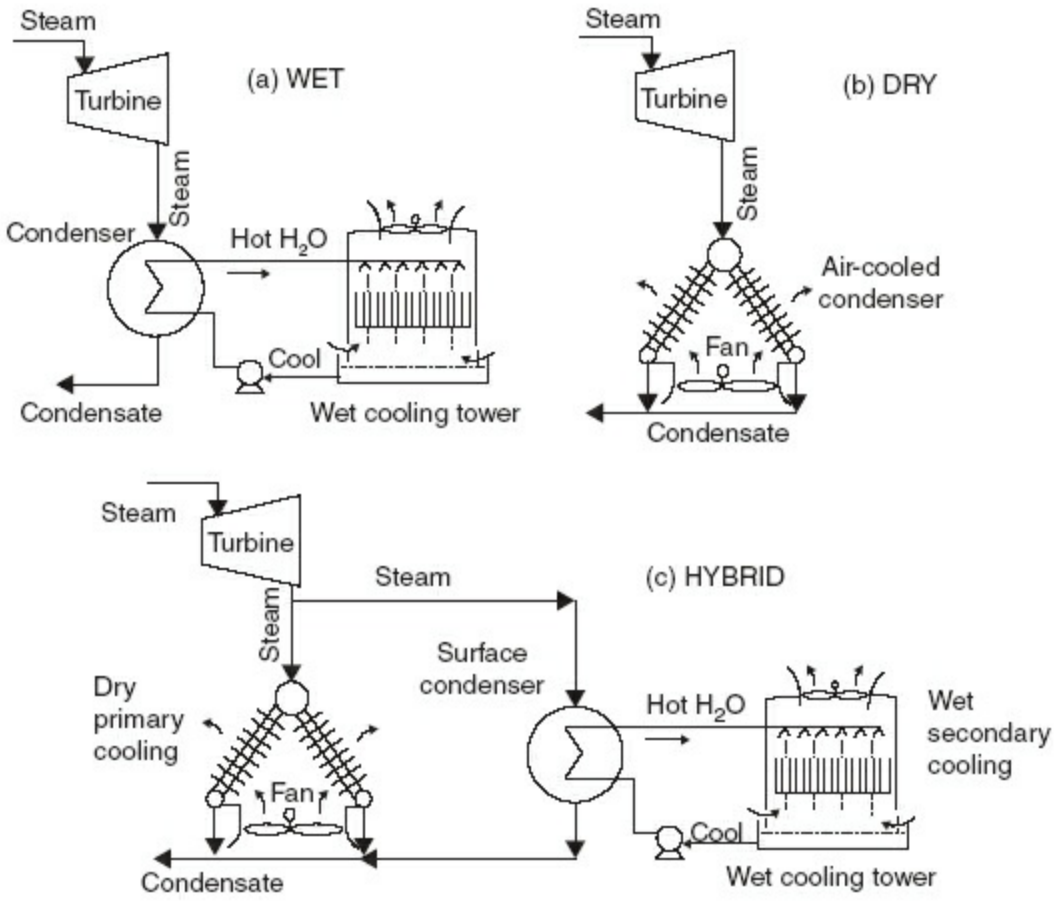


The results of one resource assessment indicates that CSP projects covering less than 1% of the southwestern land area could generate over four times the current electric power demand in the United States (Stoddard NREL, 2006). These would be on nonsensitive lands that have no primary use today and which have a solar resource of at least 6.75 kWh/m^2/d. The estimates were based on 5 ac/MW and a 27% capacity factor.

8.2.3 Condenser Cooling for CSP Systems

Parabolic trough, linear Fresnel, and central receiver CSP systems use thermal energy to power a Rankine steam cycle, which means there is a condenser in the system that needs to cool the working fluid before it returns to the steam generator. The condenser can be either water-cooled or air-cooled, or a hybrid combination of both (Fig. 8.4). Since these plants are likely to be located in desert areas, the availability of adequate water supplies for water-cooling can be problematic. Dry cooling methods avoid that constraint, but they have higher capital costs, higher auxiliary operating power requirements, and since they do not cool to as low a temperature, especially on hot days when peak power is most needed, their Carnot efficiency is decreased.

FIGURE 8.4 Three approaches to CSP condensers: (a) recirculating evaporative cooling; (b) dry cooling with an air-cooled condenser; and (c) hybrid combination.



The simplest way to extract heat is with "once-through" cooling in which a large volume of water ($\approx$25, 000 gal/MWh), usually from a nearby river or ocean, flows through the condenser. With most CSP plants likely to be located in desert regions, once-through cooling will probably not be a viable option. Instead, the most common way for a CSP plant to reject heat is with a recirculating, evaporative cooling system. Cooling water that has been heated in the condenser is sprayed into a mechanical-draft cooling tower. A fan blows air through the descending water droplets, which encourages evaporation. The cooled water collected at the bottom of the tower is then returned to the condenser. In addition to evaporative losses, cooling towers periodically have to flush accumulated salts, which means additional water is need to make up for those losses. And finally mirrors in all CSP systems have to be periodically washed to maintain their reflectance.

Dry cooling systems avoid almost all of that water loss by transferring heat directly to the air through fan-cooled heat exchangers. Rather than passing spent steam from the turbine to a conventional water-cooled condenser, exhaust steam is routed directly through an array of air-cooled heat-exchange tubes. The fan power required to blow air over those tubes is considerable and the temperature of the condensed steam is higher than that for wet cooling systems. Moreover, their performance drops off when ambient temperatures rise, so on the hottest days when power is most needed, their ability to deliver that power is compromised.

Hybrid cooling systems offer a compromise between controlling water loss and managing performance. The system shown in Figure 8.4c has both a wet- and a dry cooling system, which operate in parallel. The dry cooling system is the primary heat rejection system and is

normally the only system in operation. On the hottest days, however, a portion of the steam from the turbine is routed to the wet cooling system, thereby reducing the load on the dry system. With reduced load, the dry system can perform well even on those hot days. To the extent that the wet system is used, however, there is a water loss penalty. By reducing the size of the air system, hybrid cooling can be less expensive than an all-air system.

The consumptive water requirement of CSP depends on the solar technology being used as well as the type of cooling system. Higher steam temperatures lead to greater plant efficiency, which means more power is delivered as electricity and less is lost to the cooling system. Central receiver technology achieves higher solar concentrations and higher temperatures, so they need less cooling per MWh. Table 8.2 summarizes the combination of attributes of water use, performance penalties, and cost penalties associated with cooling technologies for central receivers and parabolic troughs.

TABLE 8.2 Water, Cost, and Performance Attributes Associated with Different CSP Cooling Systems

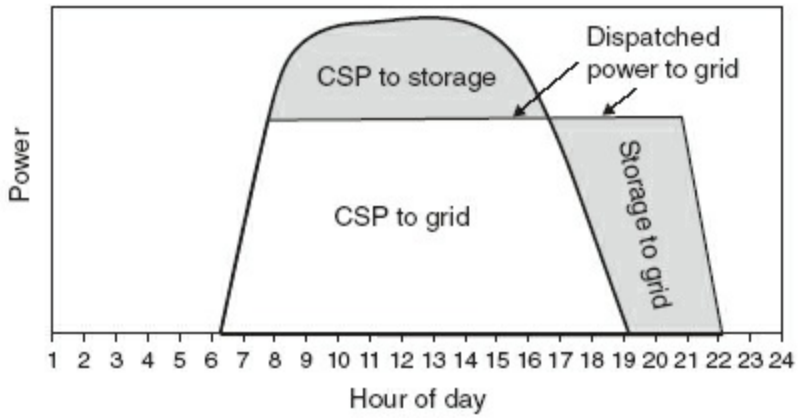
System	Criterion	Recirculating Evaporative	Air Cooling	Hybrid
Parabolic trough	Water consumption (gal/MWh)	800	78	100–450
	Performance penalty (%)	0%	4.5–5%	1–4%
	Cost penalty (%)	0%	2–9%	8%
Power tower	Water consumption (gal/MWh)	500–750	90	90–250
	Performance penalty (%)	0%	1–3%	1–3%
	Cost penalty (%)	0%		5%

Source: U.S. Department of Energy (2010).

8.2.4 Thermal Energy Storage for CSP

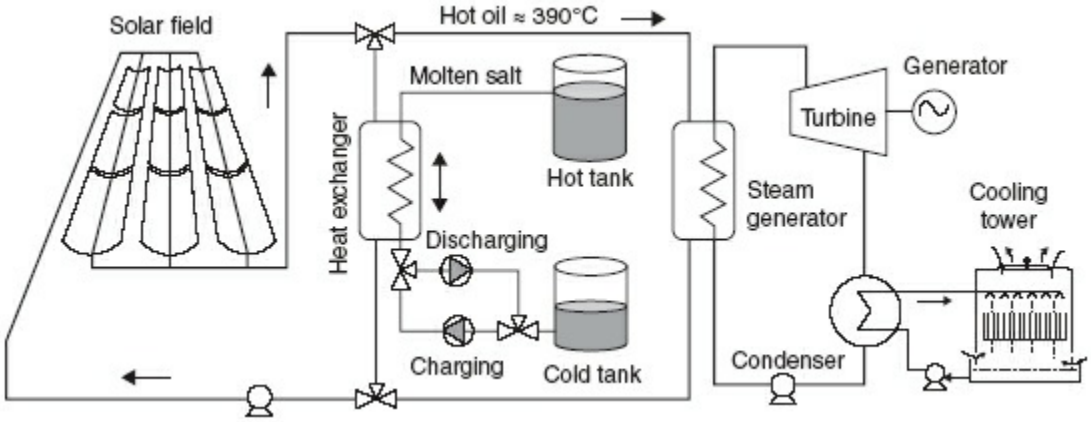
A key advantage of solar–thermal CSP over nondispatchable solar systems is the potential to include thermal energy storage (TES). Thermal storage can not only provide smoothing of the output as clouds drift by, but it can also make it possible to extend the hours during which the plant can guarantee that it will be fully operational. By storing energy during periods of low grid demand and delivering it later during high demand hours, storage can increase the economic value of the kWh sold, which helps offset the cost of storage. Figure 8.5 illustrates the concept. With storage, CSP can qualify as firm capacity, which is a category of grid resource having the ability to control when they generate power.

FIGURE 8.5 Energy storage makes it possible to shift the time of delivery of power. From Stoddard (NREL 2006).



TES systems have focused on molten nitrate salts as the storage media, and possibly as the heat transfer fluid (HTF) as well. One formulation of a molten salt consists of a binary combination of potassium nitrate and sodium nitrate, while another includes calcium nitrate. Molten salts offer several advantages over currently available high temperature oils. They allow for higher storage temperatures, which reduces the volume of storage needed, they are cheaper, and their nonflammable, nontoxic properties make them more environmentally friendly. They are highly efficient, with potential round-trip charging/discharging cycle efficiencies over 98% and standby thermal losses of about 0.03%/h (Sioshansi and Denholm, 2010). They are liquid at atmospheric pressure, but their melting temperature is much higher than the boiling point of water, which means they may have to be kept hot overnight to avoid system complications that can arise if they are ever allowed to freeze back to their solid state. This freeze problem is avoided with an indirect design scheme in which heat-transfer oil collects thermal energy from the solar array and transfers it to the molten-salt storage unit through a heat exchanger. The system in Figure 8.6 shows an indirect system powered by a solar trough collector array, but the same system could be fired by a power tower.

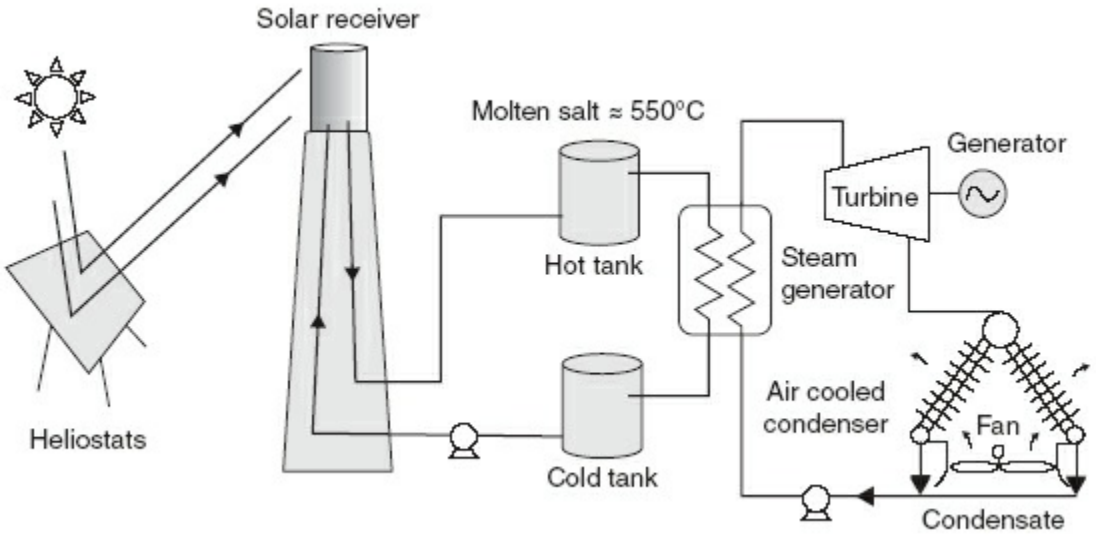
FIGURE 8.6 An indirect system with two-tank molten salt storage and hot-oil solar-field heat transfer fluid.



A disadvantage with indirect systems is that the maximum temperature of an oil-based HTF is relatively low, on the order of 400°C, which limits the molten salt storage temperature. That, in turn, means a larger volume and extra costs. In a direct thermal storage approach, molten salt serves both as the HTF in the collector system and as the thermal medium in the storage tank, which eliminates the need for the expensive heat

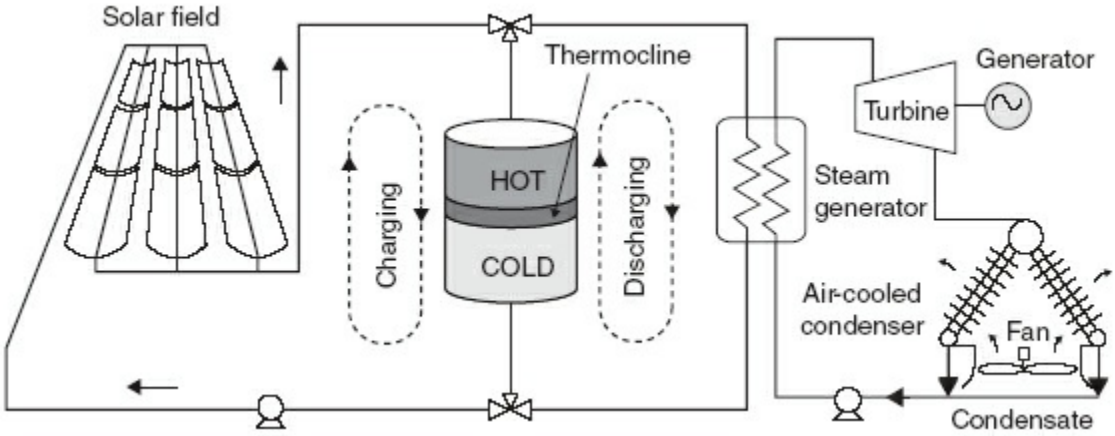
exchanger. In addition to the efficiency gained by eliminating heat-exchange losses, a direct system can operate at a considerably higher temperature, which also improves efficiency. Figure 8.7 shows a direct system, this time with a solar receiver (power tower) and an air-cooled condenser.

FIGURE 8.7 A direct system with molten salt as both the heat transfer fluid and the storage medium.



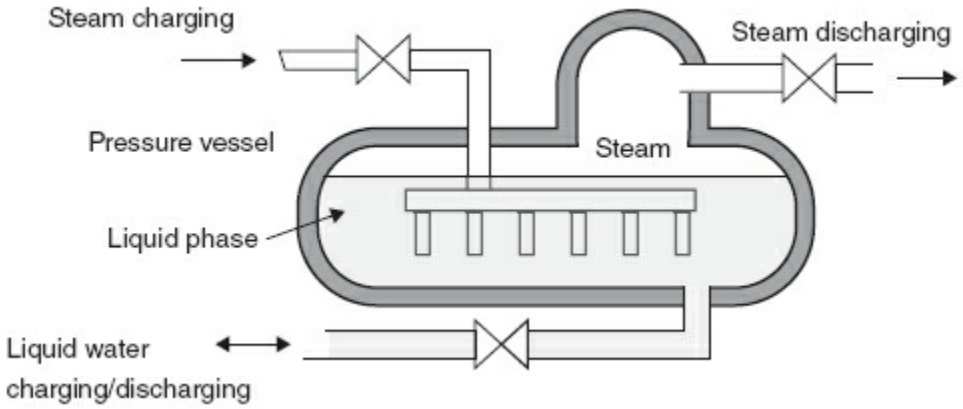
Finally, a design option for the future would utilize just a single storage tank that would contain both the hot and cold fluids instead of the standard two-tank approach (Fig. 8.8). A single-tank system would take advantage of the thermal buoyancy that occurs when a less-dense hot liquid floats on top of a colder, denser bottom layer. This stratification is a phenomenon most of us have experienced when diving down from warm surface waters toward the cold bottom waters in a pond or lake. The region between the two stratified layers in which the temperature rapidly transitions from hot to cold is called the thermocline, so these systems are referred to as providing single-tank thermocline storage. In addition to the molten salt, a low cost filler material such as quartzite rock in combination with silica sand would occupy much of the volume. The filler acts to inhibit vertical mixing of the layers while it reduces the fluid volume required.

FIGURE 8.8 A direct, single-tank, thermocline, molten salt storage system.



Finally, for modest systems and short-term storage (minutes), there is a relatively simple single-tank energy storage scheme based on saturated steam and pressurized hot water. These are called Ruths accumulators and Figure 8.9 shows how they work.

FIGURE 8.9 A Ruths accumulator can provide short-term, single-tank energy storage in the form of a mix of saturated steam and pressurized liquid water.



8.2.5 Linear Parabolic Trough Systems

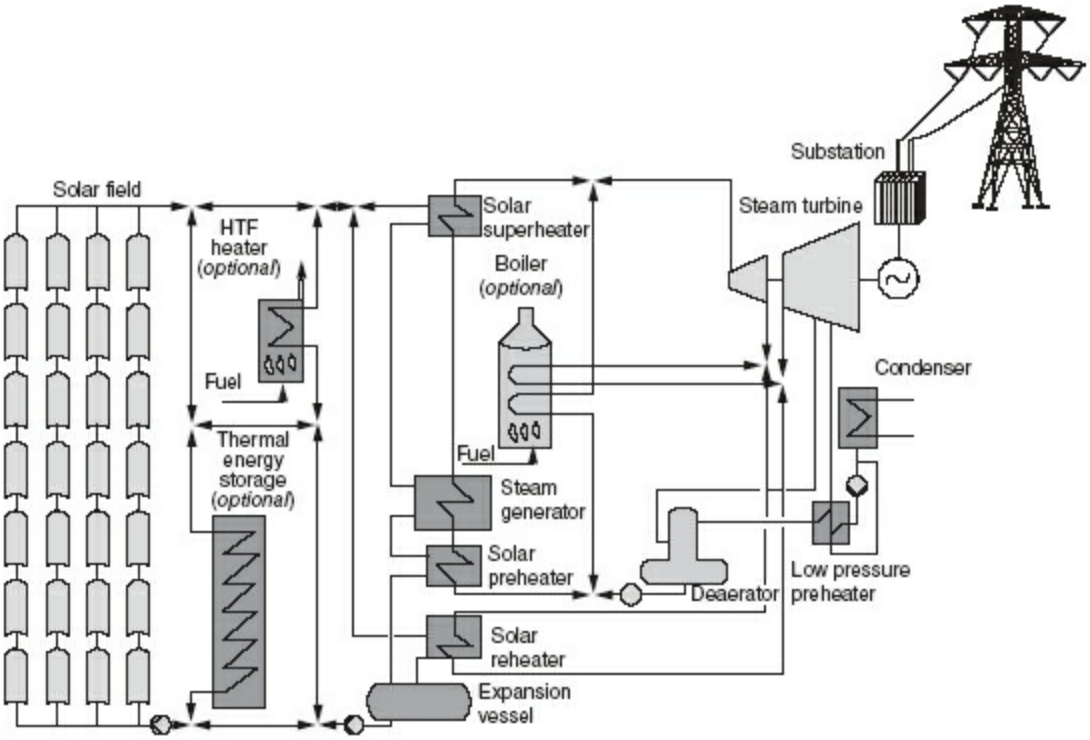
For several decades, the world's largest solar power plant was the 354-MW parabolic-trough facility located in the Mojave Desert near Barstow, California, called the Solar Electric Generation System (SEGS). SEGS consists of nine large arrays made up of rows of parabolic-shaped mirrors that reflect and concentrate sunlight onto linear receivers located along the foci of the parabolas. The receivers, or heat collection elements (HCEs), consist of stainless steel absorber tubes surrounded by a glass envelope with a vacuum drawn between the two to reduce heat losses. A heat transfer fluid circulates through the receivers, delivering the collected solar energy to a somewhat conventional steam turbine/generator to produce electricity. The SEGS collectors, with over 2 million m^2 of surface area, run along a north–south axis and rotate from east to west to track the sun throughout the day.

The first plant, SEGS I, is a 13.4-MW facility built in 1985, while the final plant, SEGS IX, produces 80 MW and was completed in 1991. SEGS I was designed with a few hours of thermal storage using a highly flammable mineral oil called Caloria. Unfortunately, an accident in 1999 set the storage unit on fire and it was destroyed. Later SEGS plants have not included storage but have been designed to operate as hybrids with backup energy supplied by fossil fuels to run the steam/turbine when solar power is not available. As of 2012, the Kramer Junction SEGS plant was still the largest in the world, but Spain, with over 1500 MW has become the country with the greatest total solar-trough generating capacity, including the 150-MW Andasol power station consisting of three 50-MW blocks, each with 7.5 h of thermal storage.

Figure 8.10 presents an overall system diagram that suggests many of the design variations possible for a parabolic trough power plant. In this case, the HTF is heated to approximately 400°C in the receiver tubes along the parabola foci. The HTF passes through a series of heat exchangers to generate high pressure superheated steam for the turbine. The system shown includes the possibility for thermal storage as well as fossil-fuel-based auxiliary heat to run the plant when solar power is insufficient. One option shown

for hybrid operation is based on a natural-gas-fired HTF heater in parallel with the solar array. The other is an optional gas boiler to generate steam for the turbine, which makes it virtually the same as a complete, conventional steam-cycle power plant with an auxiliary solar unit.

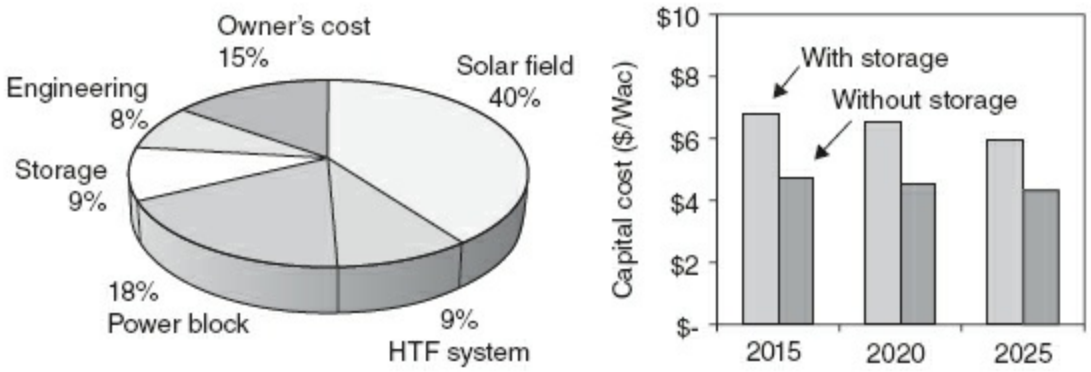
FIGURE 8.10 Solar-trough system coupled with a steam turbine/generator, including optional heat storage and two approaches to fossil-fuel hybridization. From NREL website.



Just as the capacity factor of a wind turbine can be raised by simply increasing blade diameter, a trough system's capacity factor can be increased by expanding the collector array size. There is a parameter called the *solar multiple* that is often used to characterize the relative size of a trough array and the rated power of the generator. The solar multiple is the ratio of the actual size of the solar array to the size that would be required to just reach the rated electrical capacity under ideal conditions. The usual multiple for systems without storage is about 1.4, which results in capacity factors around 28%. Larger multiples are appropriate for systems with storage but there is an economic tradeoff between increasing capital costs for larger arrays with more hours of storage versus the increased revenue that will result from greater production of dispatchable power. One study suggests that for a 6-h storage system, a multiple of 2.1 resulting in a 40% capacity factor is optimal. For 12 h of storage, a multiple of 3.0 will increase that capacity factor to about 57% (IRENA, 2012).

Of all the CSP technologies, solar troughs have the most established track record. Over decades of operation, solar troughs have been proven reliable and current systems have become cost competitive with conventional electricity. As Figure 8.11 indicates, capital costs of parabolic trough plants are projected to decline to around $6/W, including storage in the near future, which translates to a levelized cost of electricity of $115/MWh assuming just the permanent 10% investment tax credit (Stoddard, NREL, 2006). As to the resource base, the same NREL study estimates parabolic troughs in California alone could generate 1.6 million GWh/yr, which is about 40% of current U.S. electricity consumption.

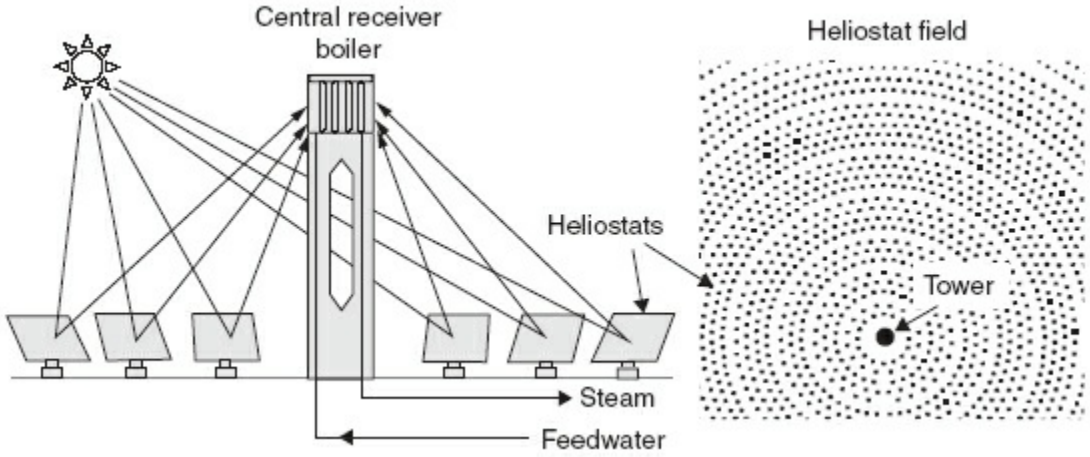
FIGURE 8.11 Distribution of capital costs of parabolic trough CSP systems in 2010, with projections to 2025. From Stoddard (NREL 2006).



8.2.6 Solar Central Receiver Systems (Power Towers)

Another approach to achieve the concentrated sunlight needed for solar thermal power plants is based on a system of computer-controlled mirrors, called *heliostats*, which bounce sunlight onto a receiver mounted on top of a tower (Fig. 8.12). These systems are referred to as central receivers, or more loosely, as power towers.

FIGURE 8.12 One version of a central receiver system (CRS) with heliostats to reflect sunlight onto a boiler.



The evolution of power towers began in 1976 with the establishment of the National Solar Thermal Test Facility at Sandia National Laboratories in Albuquerque, New Mexico. That soon led to the construction of number of test facilities around the world, the largest of which was a 90-m tall, 10-MW power tower, called *Solar One*, built near Barstow, California. In Solar One, water was pumped up to the receiver where it was turned into steam that was brought back down to a steam turbine/generator. Steam could also be diverted to a large, thermal storage tank filled with oil, rock, and sand to test the potential for continued power generation during marginal solar conditions or after the sun had set.

Solar One operated from 1982 to 1988, after which time it was dismantled and parts of it, including the 1818 heliostats and the tower itself, were reused in another 10-MW test facility called *Solar Two*. While Solar One used water as the heat-exchange medium with an oil/rock storage tank, Solar Two used a two-tank, molten salt, thermal storage unit capable

of delivering the full 10-MW output for an extra 3 h past sunset. After operating for 3 years, Solar Two was decommissioned in 1999.

Both Solar One and Solar Two were test facilities, not designed to produce commercial power. The first power tower to actually sell power is the Planta Solar (PS10) 11-MW plant near Seville, Spain. The first commercial central receiver with thermal storage is the 20-MW Gemasolar plant (first known as Solar Tres), also in Spain. Completed in 2011, the plant uses molten salt as both the HTF and the energy storage medium. Its molten salt storage system is capable of 15 h of operation without sunlight.

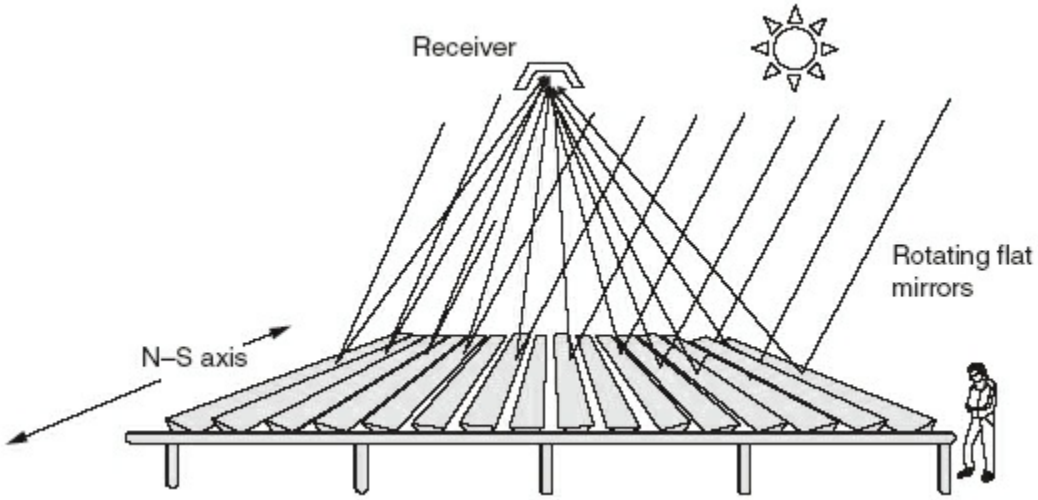
As of 2013, the world's largest central receiver is a 370-MW system consisting of three 140-m towers surrounded by a total of over 300, 000 heliostats, located on 3500 AC in Ivanpah Dry Lake, California. The power block is based on a specially adapted steam turbine, but with an air-cooled condenser that reduces water use to about 30 gal/MWh (vs. 850 gal/MWh for a wet-cooling trough system).

There are several arguments that suggest power towers may have an edge over parabolic troughs. With greater concentrations of sunlight on their boilers, they can achieve higher temperatures and pressures, which lead to greater power-block efficiencies. They do not have miles of absorber tubes circulating HTFs, which means less pumping power and reduced thermal losses. Flat heliostat mirrors are cheaper and easier to install than the curved reflectors used in troughs. Moreover, heliostats are less sensitive to modest variations in the terrain since each independently controlled heliostat is mounted on its own pedestal, which translates into less grading and land disturbance during construction. On the other hand, heliostat spacing requirements result in more gross land area needed per MW of power output. As to costs, a 2012 analysis comparing troughs to towers concluded their capital costs are virtually the same (Black and Veatch, 2012).

8.2.7 Linear Fresnel Reflectors

Linear Fresnel reflectors (LFRs) represent somewhat of an evolution of parabolic trough reflectors. The difference being the use of independently controlled, long, flat glass mirrors mounted along a horizontal axis in place of the more traditional curved parabolic reflectors. Parallel lines of mirrors reflect sunlight onto a fixed receiver mounted above the reflectors as suggested in Figure 8.13. Receivers can accommodate a number of HTFs, including thermal oils, molten salt, or water vaporized in the receiver tubes to create steam that can be routed directly to a steam turbine. Direct steam conversion creates other application opportunities including seawater desalination, solar absorption cooling, or steam for other industrial processes.

FIGURE 8.13 One module in a linear Fresnel reflector array.



LFRs offer several advantages over their parabolic trough counterparts. With their receivers fixed in place, LFRs have simpler piping systems that avoid the complications associated with flexible junctions in troughs. They can use cheaper flat-glass mirrors and their support structure is lighter and simpler, which makes them easier to install. By being closer to the ground and almost horizontal, wind loads are reduced, resulting in better structural stability, less mirror-glass breakage, and more consistent focusing. Since arrays of Fresnel reflectors can be more tightly spaced than troughs, land area requirements are reduced. Moreover, in some climates, crops that would wither under the sun can be grown, with less irrigation, in the shade provided by the mirrors.

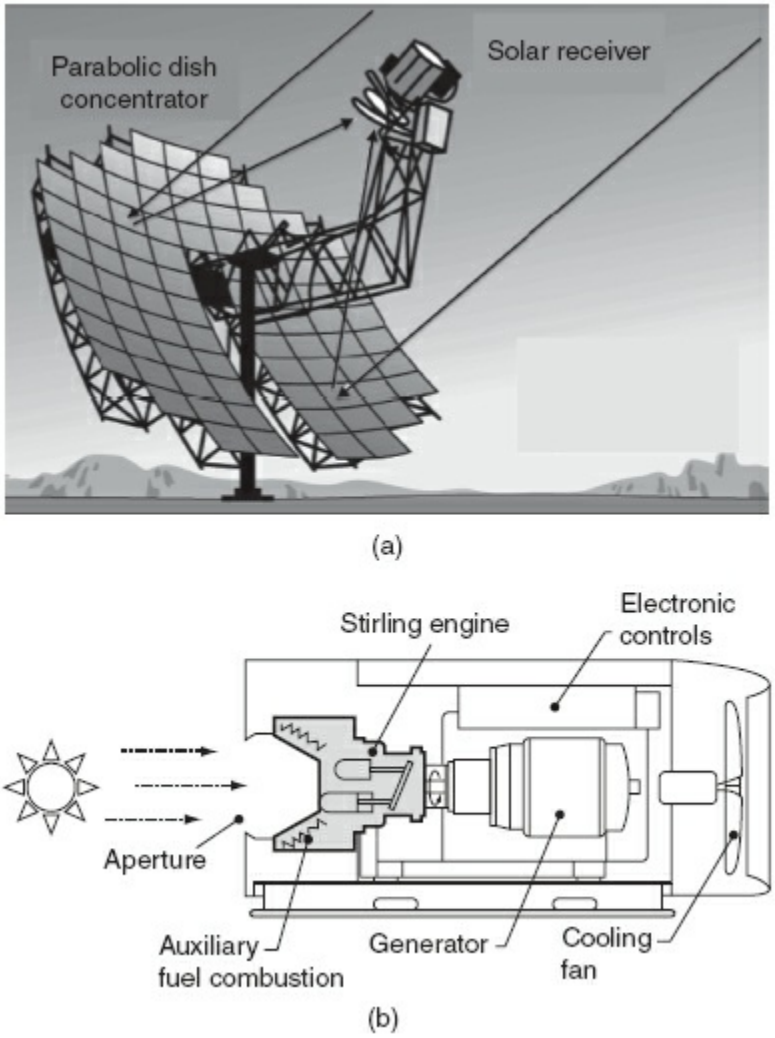
Earlier Fresnel reflector designs produced relatively low temperature steam, but newly developed solar boilers with vacuum absorber tubes generate high pressure, superheated steam greatly improving efficiencies. There are not many systems in place, so available cost trends are minimal. In fact, the first commercial power generation using LFRs began in 2009 at the Puerto Errado 1.4-MW thermosolar power plant in Spain. A second adjacent plant, this one rated at 30 MW, went online in 2012. They generate 500°C steam directly without a thermal oil HTF, which is significantly higher than the typical 390°C steam from troughs. They use air-cooled condensers and have their own innovative glass cleaning systems that minimize water consumption. Individual control units consisting of an array with 128 reflector units covering a rectangular area 17-m wide by 45-m long dimensions produce 270 kW AC each. By stacking up control units in rows and columns, virtually any size power plant can be created.

8.2.8 Solar Dish Stirling Power Systems

Dish Stirling systems use a concentrator made up of multiple reflective mirrors that approximate a parabolic dish (Fig. 8.14). The dish tracks the sun and focuses the DNI with far greater concentrations than can be achieved in troughs, Fresnel reflectors, or power towers. Focused sunlight is absorbed by a thermal receiver, which creates a very high temperature source that can be used to generate steam, but more often is used to power a special type of heat engine, called a Stirling engine. The receiver can be made up of a bank of tubes containing a heat transfer medium, usually helium or hydrogen, which also serves as the working fluid for the engine. Another approach is based on heat pipes in which the

boiling and condensing of an intermediate fluid is used to transfer heat from the receiver to the Stirling engine. The cold side of the Stirling engine is maintained using a water-cooled, fan-augmented radiator system similar to that in an ordinary automobile. Being an air-cooled closed system, very little make-up water is required other than what is needed to wash the mirrors.

FIGURE 8.14 (a) Sketch of a dish-Stirling tracking collector. (b) The receiver with engine, generator, and cooling fan. From Florida A&M University.



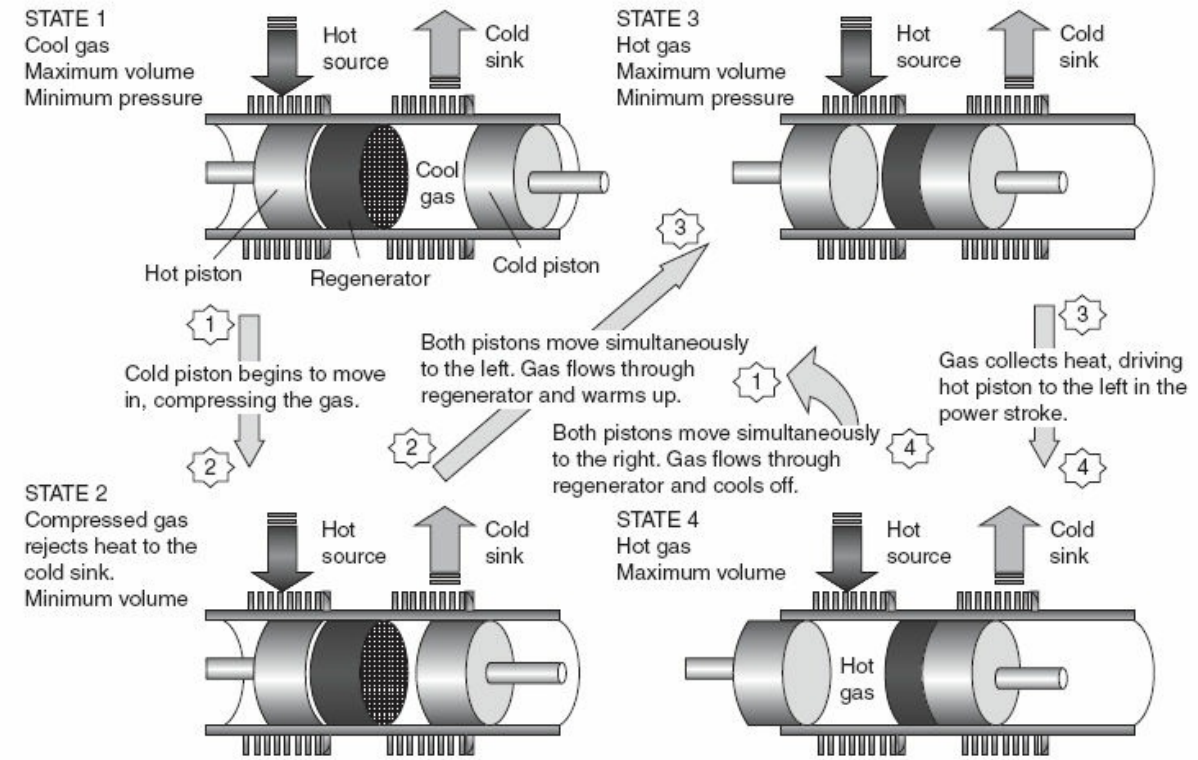
Stirling engines are very different from conventional spark-ignition and diesel-cycle reciprocating internal combustion engines. A Stirling-cycle engine is an example of a piston-driven, reciprocating engine that relies on external rather than internal combustion. As such, it can run on virtually any source of heat, such as conventional fuel combustion or concentrated sunlight. When combustion is the heat source, the fuel burns slowly and constantly with no explosions. This makes these engines inherently very quiet, which makes them especially attractive for submarines. In fact, their development for submarines has helped stimulate their potential application in solar dish systems.

Stirling-cycle engines were patented in 1816 by a minister in the Church of Scotland, Robert Stirling. He was apparently motivated in part, by concern for the safety of his parishioners, who were at some risk from poor-quality steam engines that had a tendency,

in those days, to violently and unexpectedly explode. His engines had no such problem since they were designed to operate at relatively low pressures. The first known application of a Stirling engine was in 1872 by John Ericsson, a British-American inventor. Thereafter, Stirling engines were used quite extensively until the early 1900s, at which point advances in steam and spark-ignition engines, with higher efficiencies and greater versatility, pretty much eliminated them from the marketplace. If dish concentrators can make it into the marketplace, Stirling engines will certainly enjoy a well-deserved comeback.

The basic operation of a Stirling engine is explained in Figure 8.15. In this case, the engine consists of two pistons in the same cylinder—one on the hot side of the engine, the other on the cold side—separated by a "short-term" thermal energy storage device called a *regenerator*. Unlike an internal combustion engine, the gas, which may be just air, but is more likely to be nitrogen, helium, or hydrogen, is permanently contained in the cylinder. The regenerator may be just a wire or ceramic mesh or some other kind of porous plug with sufficient mass to allow it to maintain a good thermal gradient from one face to the other. It also needs to be porous enough to allow gas in the cylinder to be pushed through it first in one direction, then the other. As the gas passes through the regenerator, it either picks up heat or drops it off, depending on which way the gas is moving.

FIGURE 8.15 The four states and transitions of the Stirling cycle.



As shown, the space on the left side of the regenerator is kept hot with some source of heat, which might be a continuously burning flame or, in this case, concentrated sunlight. On the right side, the space is kept cold by radiative cooling or active cooling with a circulating heat-exchange fluid. If it is actively cooled, that rejected heat becomes a potential source of useful heat for cogeneration of heat and power, for example, in an off-grid home power system.

The Stirling cycle consists of four states and four transitions between those states. As

shown in Figure 8.15, the cycle starts with the hot piston up against the hot face of the regenerator while the cold piston is fully extended away from the cold face of the regenerator. In this State "1, " essentially all of the gas is cool (there is an insignificant amount stored within the pores of the regenerator), the pressure is at its lowest and the gas volume is the highest it will ever be in the cycle. The following describes the transitions from one state to another:

① → ② The hot piston remains stationary while a camshaft moves the cold piston to the left, compressing the gas while transferring heat to the cold sink. Ideally, this is an isothermal process; that is, the temperature of the gas remains constant at T_C.

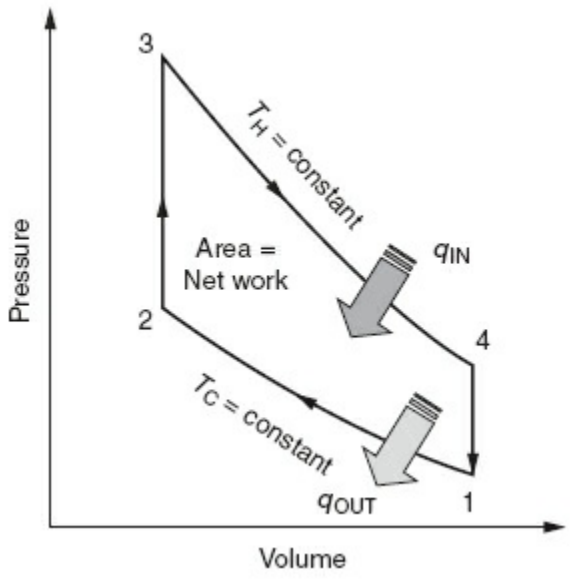
② → ③ Both pistons now move simultaneously to the left at the same rate and by the same amount. The gas passing through the regenerator into the hot space picks up heat in the regenerator, increasing the temperature and pressure of the gas while its volume remains constant.

③ → ④ The gas in the hot space absorbs energy from the hot source and isothermally expands, pushing the hot piston to the left. This is the power stroke.

④ → ① Both pistons now move simultaneously to the right while maintaining a constant volume. The gas passing through the regenerator into the cold space transfers heat to the regenerator while the gas temperature and pressure drop.

The idealized pressure-volume diagram shown in Figure 8.16 may make it easier to understand the states and transitions in the above Stirling cycle. In thermodynamics, P–V diagrams, such as this one, greatly enhance intuition, especially since the area contained within the process curves represents the net work produced during the cycle.

FIGURE 8.16 Pressure–volume diagram for an ideal Stirling cycle.



Stirling engines are classic heat engines operating between a hot source and a cold sink. As such their efficiency is constrained by the Carnot-cycle limit (interestingly, Carnot did not develop his famous relationship until well after Stirling's patent). With the receiver absorber reaching temperatures around 750°C and the air-cooled radiator at 30°C, Equation 8.6 constrains the efficiency to

$$\eta < 1 - \frac{T_C}{T_H} = 1 - \frac{273 + 30\ \text{K}}{273 + 750\ \text{K}} = 0.70 = 70\% \tag{8.7}$$

In practice, the Stirling engine itself has an efficiency about half that of the Carnot limit, around 35%. Including losses at the reflector, receiver, gear box, and generator plus parasitic power needed to operate the system, the overall efficiency is over 20%, which is considerably higher than any of the other CSP technologies. In good locations, with these efficiencies, the land area required is lower than other CSPs at about 4 ac/MW of capacity. On the downside, with a fair number of moving parts in multiple relatively small receivers suggests maintenance could become an issue. Accurate dual-axis tracking is also a challenge, especially with its relatively heavy engines out on a long connecting structure. And, without storage, they lose the value of dispatchability, so their main competition is with PVs that have cost and investor confidence advantages.

Dish Stirling systems can be relatively small stand-alone power plants that do not need access to fuel lines or sources of cooling water. Relative to troughs and towers, an individual dish is economically optimal in kilowatt sizes rather than tens or hundreds of megawatts, which means that multiple generations of designs can be built, tested, and modified before scaling them up in fields with hundreds or thousands of units. Manufacturing would be similar to a small automobile factory. Their small scale and their ability to be installed on uneven terrain could be an advantage in rural electrification projects. Large-scale installations could be easier to finance since the time from project design to delivered power could be very short, with the first units coming online almost immediately. Short lead times mean capacity can be added incrementally as needed to follow load growth, avoiding the periods of oversupply that characterize large-scale generation facilities.

8.2.9 Summarizing CSP Technologies

Table 8.3 summarizes some of the main characteristics of troughs, towers, linear Fresnel, and dish Stirling systems. Most of these have been explored in previous sections, but perhaps an overall assessment might be helpful.

TABLE 8.3 CSP Technology Assessment

Measure	Parabolic Trough	Solar Tower	Linear Fresnel	Dish Stirling
Maturity of technology (2012)	Commercially proven	Pilot commercial projects	Pilot projects	Demonstration projects
Typical capacity (MW)	10–300	10–200	10–200	0.01–0.025
Collector concentration	70–80 suns	>1000 suns	>60 suns	>1300 suns
Operating temperature (°C)	350–550	250–565	390–500	550–750
Plant peak efficiency (%)	14–20	23	18	30
Annual solar-to-kWh efficiency (net) (%)	11–16	7–20	13	12–25
Annual capacity factor (%)	25–28 (no TES) 29–43 (7-h TES)	55 (10-h TES)	22–24	25–28
Maximum slope of solar field (%)	<1–2	<2–4	<4	10% or more
Water requirement (m^3/MWh)	3 (wet cooling) 0.3 (dry)	2–3 (wet) 0.25 (dry)	3 (wet) 0.2 (dry)	0.05–0.1 (mirror washing)
Land occupancy	Large	Medium	Medium	Small
Storage system	Molten salt	Molten salt	Pressurized steam	No storage
Maturity of technology (2012)	Commercially proven	Pilot commercial projects	Pilot projects	Demonstration projects

Modified from IRENA (2012).

Parabolic troughs are the most mature CSP technology, but they still have considerable room for improvement. Most of the earlier plants do not have thermal storage, most operate at relatively low steam temperatures, and most still use wet cooling for heat rejection. Their long receiver heat-collection runs require flat terrains and result in more pumping power and increased thermal losses from the receivers. They are the only CSP technology with a long record of operational experience, which gives them a significant edge in the risk-averse financial community.

Power towers have higher solar concentration ratios, higher steam temperatures, and higher solar-to-electricity efficiencies than troughs. Without long runs of receiver plumbing, they do not need to use synthetic oils as their HTF, which means they can more easily take advantage of more efficient, direct-steam or molten-salt technologies. Higher temperatures translate to lower cost thermal storage, and thermal storage is likely to be crucial to the future success of CSP.

LFRs offer some cost advantages over linear troughs. Cheaper mirrors, lower wind loads leading to simpler structural support systems, and a higher ratio of cheap reflector to expensive receivers all make them a promising alternative. Their optical efficiency is limited, however, which reduces performance and their current steam-generating receivers are less easily adapted to thermal storage. But, their simplicity can make them a contender.

Finally, dish Stirling systems may carve out their own niche in the CSP world. Being small, modular units, they lend themselves to mass production manufacturing and quick, simple installations in irregular terrain. Their concentration ratios are the highest in the industry, giving them the best peak and annual efficiencies. They are inherently air cooled without special add-on equipment, so they work well in dry desert conditions. They are still in the demonstration project stage of development, which means final levelized cost

estimates are preliminary at best. Their major disadvantage is they are not compatible with conventional thermal storage.

Another measure of the potential for CSP to meet a significant fraction of U.S. electricity demands just on suitable land in California alone is presented in Table 8.4. As shown there, both terrain matters and efficiency translate into the total resource base available. Parabolic dish technology, with the highest efficiency and variable terrain capability, could ultimately provide enough energy for the entire country, while power towers could provide only one-third. For comparison, CPV can provide more than either troughs or towers.

TABLE 8.4 Resource Assessment for CSP in California Alone

	Solar Resource Land Area (mi^2)	Capacity Potential (GW)	Generation Potential (10^6 GWh/yr)
Parabolic trough, no storage, <1% slope	5,900	661	1.61
Parabolic trough, 6-h storage, <1% slope	5,900	471	1.64
Power tower, 6-h storage, <1% slope	5,900	342	1.23
Parabolic dish, <3% slope	11,600	1,480	3.37
Parabolic dish, <5% slope	14,400	1,837	4.20
Concentrating PV, <3% slope	11,600	1,235	2.86
Concentrating PV, <5% slope	14,400	1,534	3.56
Total U.S. Capacity and Demand (2012)		1,070	3.90

Source: Stoddard (NREL 2006).

Concentrating solar–thermal power technologies were the first large-scale renewable energy systems installed anywhere in the world. With decades of actual operating history, the original parabolic troughs have clearly demonstrated these can be robust, reliable power sources, but early versions of the other CSP technologies never stopped being anything more than just demonstration projects until very recently. Just as more CSP technologies have begun to move into commercial reality, they have encountered stiff competition from suddenly-low-cost, utility-scale PV systems. PVs are not only cost competitive, they are also perceived by the financial community to be much less risky investments than CSPs. Moreover, PVs do not face the same water challenges that are inherent to most CSP technologies. On the other hand, the principal advantage that most CSPs have is their potential to incorporate thermal storage into their designs. And that is a major advantage.

8.3 WAVE ENERGY CONVERSION

There are a number of technologies currently being explored to tap into the enormous potential for the oceans to provide electrical power. These include wave energy conversion (WEC), tidal energy both in the form of ocean currents and tidal basins, ocean thermal energy conversion (OTEC), and salinity gradients. Of these, the most promising near-term options are wave energy and ocean current energy, both of which are currently in the demonstration phase of development.

8.3.1 The Wave Energy Resource

Solar energy creates uneven temperatures and pressures across the globe, which results in winds that blow from high pressure to low pressure areas. Winds, in turn, create waves as they skim across the surface of the ocean. So, in that sense we can think of wave power as another form of solar energy. It has similar issues to other renewables, including its variability and predictability. Obviously, the output power from a WEC system would be highly variable, but that variability is somewhat predictable within a time frame of several days. Waves created by a storm in the eastern Pacific will make their way to the west coast of North America a few days later. This delay provides a far greater lead-time for scheduling generation assets on the grid than is possible with either solar or wind resources. In fact, a compelling case has been made for combining offshore wind with wave power since they are somewhat complementary in terms of their timing (Stoutenburg et al., 2010).

Storms generate complex and irregular waves that eventually form relatively smooth swells that can travel thousands of miles with relatively modest energy loss. As those swells approach land, they interact with the sea bottom, which causes wave heights to increase while the period between waves decreases. The power in idealized sinusoidal waves can be derived from first principles (e.g., Twiddell and Weir, 2006) resulting in

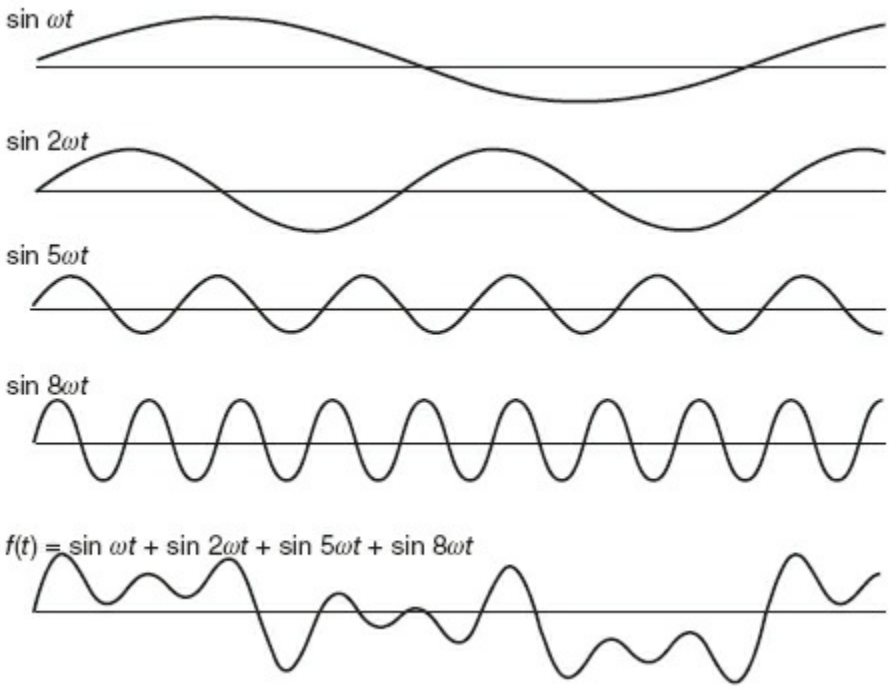
$$P = \frac{\rho g^2 H^2 T}{32\pi} \tag{8.8}$$

where P is power per meter of distance along the ridge of the wave (W/m), ρ is the density of sea water (1025 kg/m^3), g is gravitational acceleration (9.8 m/s^2), H is the trough-to-crest wave height (m), and T is the period between waves (s). For example, a series of sinusoidal, 3-m waves with a period of 8 s would have power equal to

$$P = \frac{\rho g^2 H^2 T}{32\pi} = \frac{1}{32\pi} \cdot 1025 \frac{\text{kg}}{\text{m}^3} \cdot \left(\frac{9.8\ \text{m}}{\text{s}^2}\right)^2 \cdot (3\ \text{m})^2 \cdot 8\ \text{s}$$
$$= 70{,}500 \frac{\text{J/s}}{\text{m}} = 70.5\ \text{kW/m}$$

Actual waves in the ocean, however, are a complex mix of waves having many different wavelengths instead of the single simple smooth waveform used to derive Equation 8.8. For example, consider the waveforms that result when four simple sinusoids of different frequencies are added together, as shown in Figure 8.17.

FIGURE 8.17 Combining four waves into a complex wave.



So, given the complex waveforms that characterize real waves, how can an equation like (8.8) that applies to just a single-frequency wave be modified to account for this complexity? What should be used for H and how can we characterize T? These issues are obviously of great importance in designing ships, so they have been addressed for a long time (e.g., Michel, 1968). As to wave height, it has been common practice for sailors recording their observations to ignore the smaller waves, so one measure that has evolved is based on the trough-to-crest height of just the highest one-third of the waves ($H_{1/3}$). A more scientific version based on the statistics of buoy measurements is called the significant wave height, H_S, which turns out to be quite close to $H_{1/3}$.

As to the period of a complex mix of waves, again there have been various approaches. One is based on counting the number of upward crossings through the mean water level. Another, called the peak wave period T_P, is based on the peak value of a spectral distribution of wavelengths. With real buoy data, that spectrum can be measured, but for scoping purposes it is handy to assume a spectral distribution function. With a commonly used Pierson–Moskowitz spectrum, along with the use of H_S to characterize wave heights, the result is the following

$$P = 0.42\,(H_S)^2\,T_P \tag{8.9}$$

where P is average power per meter of length along the wave crest (W/m), H_S is the significant wave height (m), and T_P is the peak wave period (s). The 0.86 factor accounts for the difference between two methods of determining the wave period (Paasch et al., 2012). When the constants are plugged in to Equation 8.9, the following simple relationship for power (kW/m) is found

$$P = 0.42\,(H_S)^2\,T_P \tag{8.10}$$

For example, if the significant wave height is 3 m and the peak wave period is 8 s, using

Equation 8.10, the estimated average power in those waves would be

$$P = 0.42 \times 3^2 \times 8 = 30.2 \text{ kW/m}$$

These two parameters, H_S and T_P are part of the valuable data sets, called scatter diagrams which buoys have long provided. For example, the scatter diagram for a deep-water San Francisco buoy (National Data Buoy Center, NDBC 46026) shown in Table 8.5 tells us hours per year for each sea-state condition.

TABLE 8.5 An Example Scatter Diagram of Hours per Year for Each Sea State[a]

	Peak Wave Period T_P (s)													
H_S (m)	3	4	5	6	7	8	9	10	11	12	14	17	20	Tot h
5.5	0	0	0	0	0	0	1	1	0	1	4	6	1	14
5.0	0	0	0	0	0	1	1	2	2	2	8	13	3	32
4.5	0	0	0	0	0	3	2	3	4	6	14	19	4	55
4.0	0	0	0	0	1	6	6	5	7	13	38	32	8	116
3.5	0	0	0	0	5	21	16	17	18	38	85	53	12	265
3.0	0	0	0	3	13	62	39	36	47	97	161	76	23	557
2.5	0	0	0	12	47	139	82	82	110	200	253	105	38	1068
2.0	0	0	4	41	126	272	165	168	226	325	302	132	51	1812
1.5	0	3	21	127	212	367	263	292	301	338	308	195	52	2479
1.0	2	18	35	97	117	255	224	210	213	246	387	264	37	2105
0.5	2	4	3	7	11	37	26	25	22	37	62	20	1	257
0.125	0	0	0	0	0	0	0	0	0	0	0	0	0	0
													Total	8760

[a]San Francisco buoy NDBC 46026.
Source: Previsic et al. (2004).

A sea-state scatter diagram such as the one shown in Table 8.5 is the starting point for wave energy calculations. For example, if we ask how much energy is available per meter of wave width at the above San Francisco buoy with a significant wave height of 3 m and an 8-s peak wave period, Table 8.5 tells us there are 62 h with heights between 2.75 and 3.25 m, and wave periods between 7.75 and 8.25 s. Using the midpoints of each in Equation 8.10 gives us

$$\text{Energy} \approx 0.42 \times 3^2 \times 8 \text{ kW/m} \times 62 \text{ h/yr} = 1875 \text{ kWh/yr/m}$$

Repeating this simple calculation for the full table leads to an estimate for the entire annual energy available at this buoy. For this particular buoy, Table 8.6 indicates a total resource of 173 MWh/yr per meter of wave distance along the crest. Averaging that out over 8760 h/yr suggests a wave resource at this buoy of 19.7 kW/m. This is a far greater resource flux density than either solar or wind could possibly provide.

TABLE 8.6 San Francisco Annual Wave-Energy Scatter Diagram (kWh/m/yr) Based on Equation 8.10 for Buoy 46026

	Peak Wave Period T_P (s)													
H_S (m)	3	4	5	6	7	8	9	10	11	12	14	17	20	Tot kWh/yr
5.5	0	0	0	0	0	0	114	127	0	152	711	1296	254	2655
5.0	0	0	0	0	0	84	95	210	231	252	1176	2321	630	4998
4.5	0	0	0	0	0	204	153	255	374	612	1667	2747	680	6693
4.0	0	0	0	0	47	323	363	336	517	1048	3575	3656	1075	10,940
3.5	0	0	0	0	180	864	741	875	1019	2346	6123	4636	1235	18,018
3.0	0	0	0	68	344	1875	1327	1361	1954	4400	8520	4884	1739	26,471
2.5	0	0	0	189	864	2919	1937	2153	3176	6300	9298	4686	1995	33,516
2.0	0	0	34	413	1482	3656	2495	2822	4176	6552	7103	3770	1714	34,217
1.5	0	11	99	720	1402	2775	2237	2759	3129	3833	4075	3133	983	25,156
1.0	3	30	74	244	344	857	847	882	984	1240	2276	1885	311	9975
0.5	1	2	2	4	8	31	25	26	25	47	91	36	2	299
0.13	0	0	0	0	0	0	0	0	0	0	0	0	0	–
													Total	172,939

Calculations similar to the ones just described have led to estimates of the average annual wave energy resource for coastal areas around the United States. As shown in Figure 8.18, the total wave energy resource on just the western coast is about 440 TWh/yr, which at a conversion efficiency of just 10% is 10 times the nations current total electricity demand of 4 TWh/yr. So the resource is substantial.

FIGURE 8.18 A wave energy resource estimate for sites with a wave power flux of at least 10 kW/m. From Bedard et al. (2004).

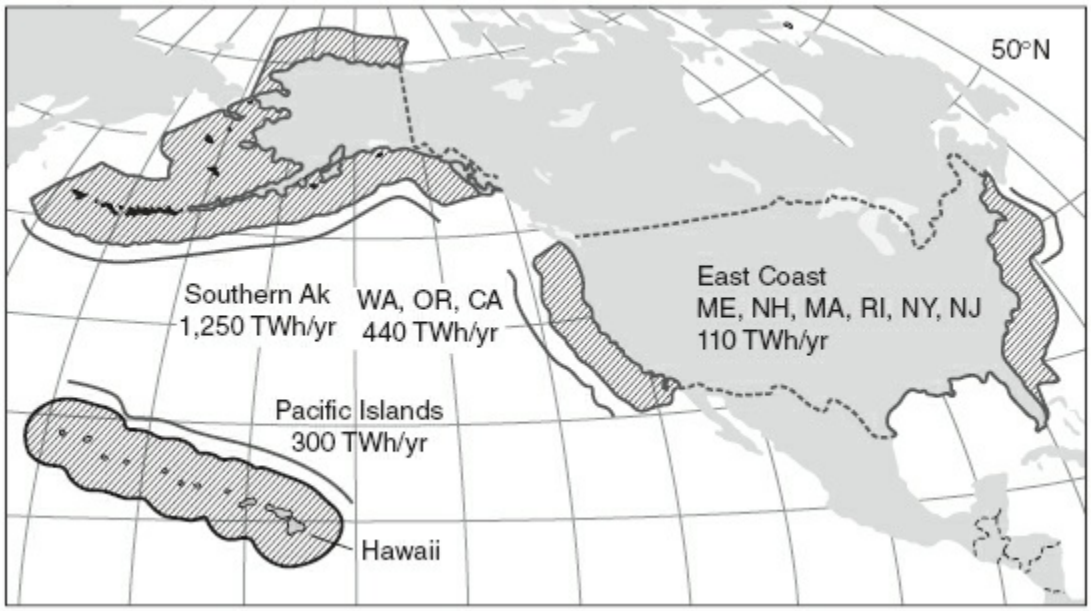
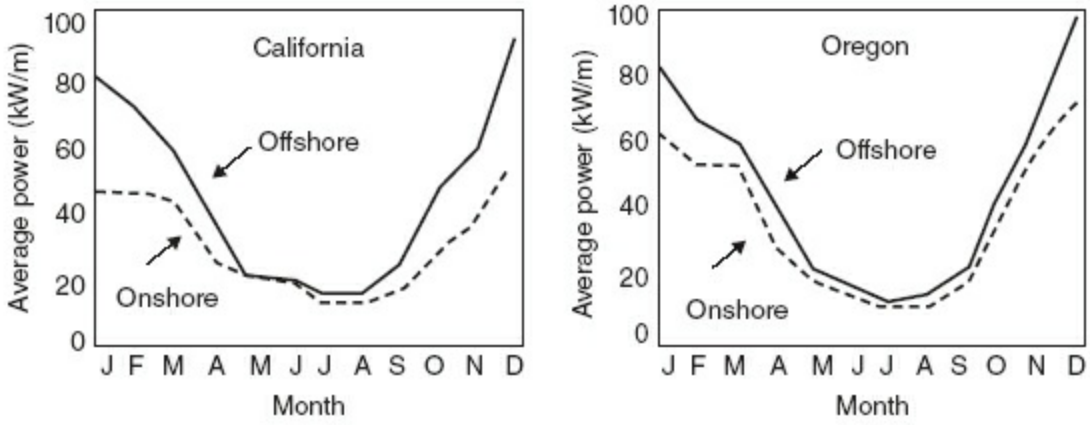


Figure 8.19 shows the dramatic seasonal variation in wave energy resources for representative sites in California, Oregon, Alaska, and Hawaii. Unfortunately, because ocean storms are less common in the summer, wave resources drop during the months when power is most needed. Similarly, the near-shore resources, which are the most likely to be developed, are considerably below those offshore as well. Nonetheless, even in summer, near-shore power flux along the west coast is upward of 20 kW/m, which is still

significant.

FIGURE 8.19 Average wave power at selected buoys in California and Oregon. Redrawn from Paasch et al. (2012).

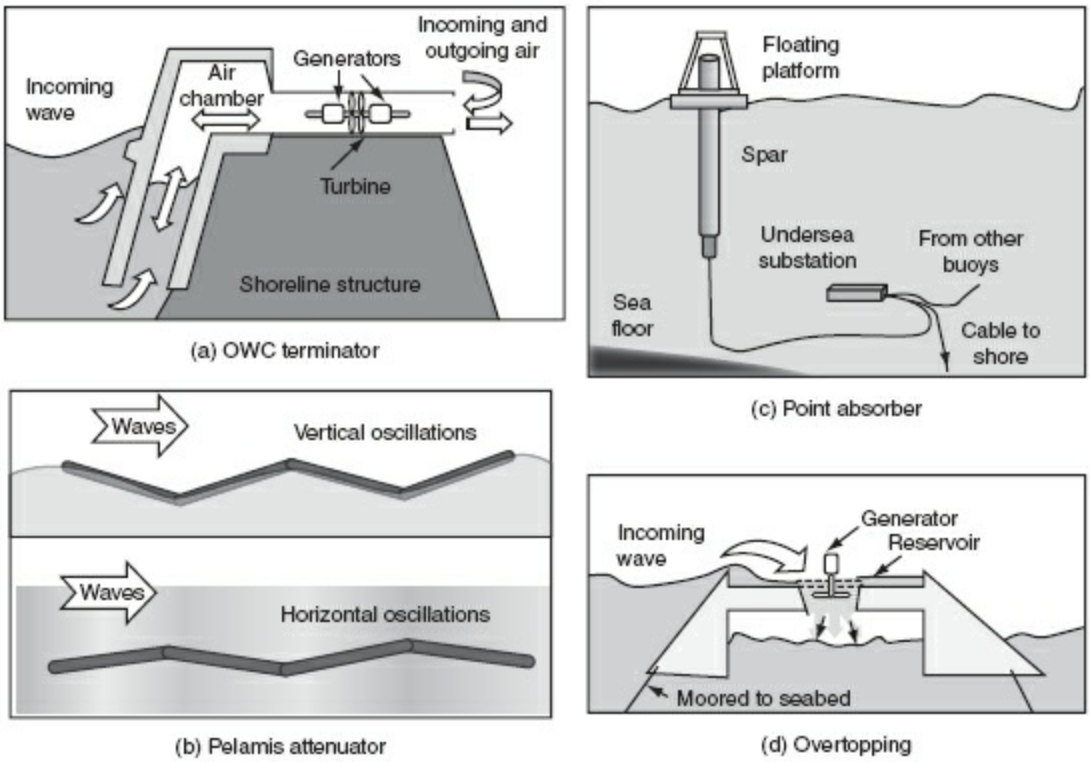


8.3.2 Wave Energy Conversion Technology

The WEC industry is in its infancy, so new technologies and modifications to the existing ones are highly likely. At this early point, four quite distinct categories of WEC technology have emerged: terminators, attenuators, point absorbers, and overtopping devices.

- *Terminators* are partially submerged structures that are aligned perpendicular to the direction of wave travel so that water flows into the device. One version of a terminator, called an oscillating water column (OWC), is designed so that incoming wave action compresses air trapped inside a chamber above the water column. Expanding air from the chamber spins a turbine to generate electricity. Onshore or in shallow water, these may be mounted on the sea floor, or they can be anchored, floating platforms. A sketch of one is shown in Figure 8.20a.
- *Attenuators* are long, multi-segment floating structures that look something like a floating snake. They are aligned so that their front end points into the oncoming wave. The joints connecting segments allow flexing to occur vertically and horizontally from one segment to another as a wave passes by. Hydraulic pumps can be used to convert that flexing into shaft power for a generator. One version, called the Pelamis (named after a species of sea snake), consists of four 30-m long cylindrical pontoons hinged together (Fig. 8.20b)
- *Point absorbers* are floating platforms tethered to the ocean floor that utilize the rise and fall of an incoming wave to provide mechanical power for a generator. In one version, the PowerBuoy (Fig. 8.20c), wave action causes the floating portion to move up and down relative to a cylindrical tube anchored to the ocean floor. A rack and pinion system converts that up and down motion into power that spins a generator.
- *Overtopping* devices are somewhat similar to land-based hydroelectric plants in that they consist of a reservoir that drains water through a hydroelectric turbine. In fact, they may be located onshore or they can be built with moored offshore platforms. In either case, wave crests cause water to flow over the top of their open reservoir structure. As water is released from the reservoir, it spins a low head hydropower turbine (Fig. 8.20d).

FIGURE 8.20 Four categories of wave power technologies.



8.3.3 Predicting WEC Performance

Buoy bin data providing hours per month or year of significant wave height H_S and peak wave period T_P establish the resource base for whatever technology might be under consideration. Coupling buoy data with binned WEC energy performance data, also presented as a scatter diagram, allows us to estimate likely energy delivered.

Table 8.7 presents performance data for a 1-MW Energetech oscillating-wave-column WEC system. Values in the table are power converted from wave power to mechanical power at the turbine shaft, but does not include generator efficiency. If this system were to be located near San Francisco NBDC Buoy 46026, we can use that buoy's scatter diagram from Table 8.5 along with the Energetech performance data in Table 8.7 to develop an estimate of annual energy that might be delivered. For example, suppose a particular sea state is characterized as having 3-m, 8-s waves. From Table 8.5, that sea state occurs 62 h/yr and from Table 8.7 during which time this system would deliver 344 kW of turbine shaft power.

$$\text{Energy(3-m, 8-s)} = 344\ \text{kW} \times 62\ \text{h/yr} = 21{,}328\ \text{kWh/yr}$$

TABLE 8.7 Scatter Diagram for Power Delivered by a 1-MW Wave Generator[a] (kW)

	Peak Wave Period T_P (s)												
H_S(m)	3	4	5	6	7	8	9	10	11	12	14	17	20
8.5	60	137	195	259	308	364	444	555	700	860	1000	1000	1000
8.0	64	146	207	275	327	387	471	589	742	913	1000	1000	1000
7.5	67	154	218	290	345	409	498	622	784	965	1000	1000	1000
7.0	71	162	229	305	363	429	523	653	824	1000	1000	1000	1000
6.5	74	168	239	317	378	447	544	680	857	1000	1000	1000	1000
6.0	76	173	246	326	388	459	560	699	882	1000	1000	1000	1000
5.5	76	174	248	329	393	464	566	708	891	1000	1000	1000	1000
5.0	78	174	247	327	389	462	561	699	885	1000	1000	1000	1000
4.5	91	171	244	315	375	448	548	674	864	1000	1000	1000	1000
4.0	133	170	229	304	360	422	511	643	814	988	1000	1000	1000
3.5	100	165	232	293	340	401	486	601	754	916	1000	1000	1000
3.0	120	179	230	268	303	344	411	509	643	781	911	926	1000
2.5	73	118	163	196	231	269	325	401	500	596	699	652	652
2.0	58	93	125	151	173	199	237	285	348	413	455	444	776
1.5	44	67	86	101	110	120	132	164	183	226	317	332	234
1.0	25	37	47	53	50	57	64	105	132	140	152	122	3
0.5	12	16	18	23	11	15	24	4	7	8	23	10	13
0.125	0	1	2	3	4	5	6	7	8	9	10	11	12

Energetech OWC WEC; Previsic et al. (2004).

Table 8.8 reproduces the above calculation for every sea state at this buoy. Total generation is estimated to be 2698 MWh/yr of shaft energy. The EPRI study from which these data have been obtained assume a 95% availability factor, an 85% directionality factor, and a 90% generator efficiency. Putting these together suggests an annual output of electrical energy would be

$$\text{Energy} = 2698\ \text{MWh/yr} \times 0.95 \times 0.85 \times 0.90 = 1961\ \text{MWh/yr}$$

TABLE 8.8 Annual Energy Expected (MWh/yr) from the Turbine in Table 8.7 Located Near San Francisco Buoy 46026

	Peak Wave Period T_P (s)													Total
H_S (m)	3	4	5	6	7	8	9	10	11	12	14	17	20	MWh
5.5	0.0	0.0	0.0	0.0	0.0	0.0	0.6	0.7	0.0	1.0	4.0	6.0	1.0	13.3
5.0	0.0	0.0	0.0	0.0	0.0	0.5	0.6	1.4	1.8	2.0	8.0	13.0	3.0	30.2
4.5	0.0	0.0	0.0	0.0	0.0	1.3	1.1	2.0	3.5	6.0	14.0	19.0	4.0	50.9
4.0	0.0	0.0	0.0	0.0	0.4	2.5	3.1	3.2	5.7	12.8	38.0	32.0	8.0	105.7
3.5	0.0	0.0	0.0	0.0	1.7	8.4	7.8	10.2	13.6	34.8	85.0	53.0	12.0	226.5
3.0	0.0	0.0	0.0	0.8	3.9	21.3	16.0	18.3	30.2	75.8	146.7	70.4	23.0	406.4
2.5	0.0	0.0	0.0	2.4	10.9	37.4	26.7	32.9	55.0	119.2	176.8	68.5	24.8	554.4
2.0	0.0	0.0	0.5	6.2	21.8	54.1	39.1	47.9	78.6	134.2	137.4	58.6	39.6	618.1
1.5	0.0	0.2	1.8	12.8	23.3	44.0	34.7	47.9	55.1	76.4	97.6	64.7	12.2	470.8
1.0	0.1	0.7	1.6	5.1	5.9	14.5	14.3	22.1	28.1	34.4	58.8	32.2	0.1	218.0
0.5	0.0	0.1	0.1	0.2	0.1	0.6	0.6	0.1	0.2	0.3	1.4	0.2	0.0	3.8
0.125	0.0	0.0	0.0	0.0	0.0	0.0	0.0	0.0	0.0	0.0	0.0	0.0	0.0	0.0
													Total	2698

The average electrical power output would be

$$\text{Average power} = \frac{1961\ \text{MWh/yr}}{8760\ \text{h/yr}} = 0.224\ \text{MW} = 224\ \text{kW}$$

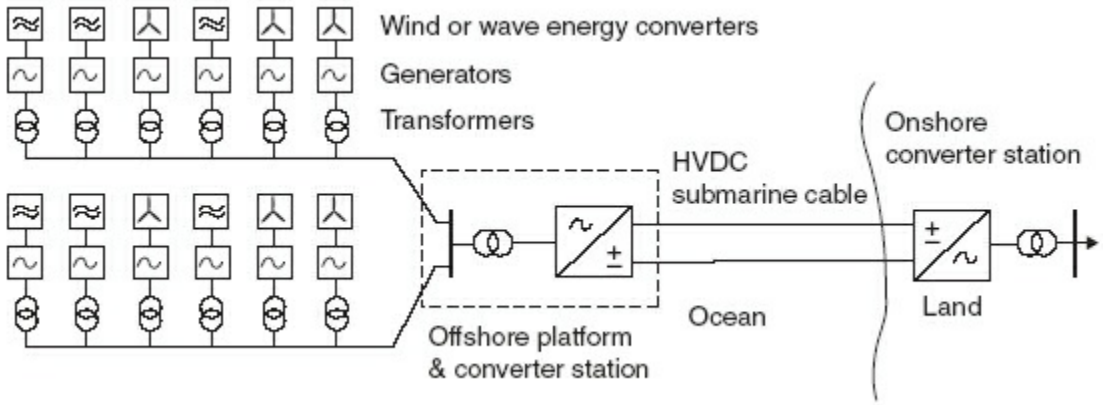
8.3.4 A Future for Wave Energy

With so few machines in operation, and such a variety of technological approaches to consider, the economics of wave power are not very well established. A 2012 study by Black & Veatch sketched out a series of scenarios for future deployment rates, estimated learning rates (the percent drop in cost for each doubling of installed capacity), and impacts associated with facilities located at the best sites first so that later installations eventually have increased costs (Black & Veatch, 2012). Their base case estimate for the capital cost of the first plants in 2015 is $9240/kW, with two-thirds of that being the hydrodynamic absorber and the power takeoff equipment. Their base case estimate drops to $4000/kW by 2045.

Their base case scenario suggests 5 GW of wave generation installed by 2050 could result in a 17¢/kWh cost of electricity. Their optimistic scenario, with faster learning and deployment rates and lower capital costs, brings that cost estimate down to 9¢/kWh in 2050.

One way to make wave power even more cost-effective is to colocate it with offshore wind power. Clearly, there would be significant benefits associated with sharing the costs of connecting offshore resources to onshore grid facilities (Fig. 8.21). In addition, since concerns about protecting the marine environment are challenges faced by both technologies, siting both on the same stretch of shoreline increases the likelihood of finding acceptable locations. Moreover, since it is easier to construct wave facilities in deeper water, the same shore connection could accommodate near-shore wind and farther-offshore WECs.

FIGURE 8.21 Colocated offshore wind and wave converters could share transmission costs. Redrawn from Stoutenburg and Jacobson (2011).



In addition, colocating wave and wind converters can have synergistic operational advantages as well. When the winds slow down, sometime later the waves will decrease, and vice versa. The better forecasting ability for wave power can offset some of the operational uncertainty inherent with variable wind power. Also, there may be complementarity in the timing of the resources. The winds may increase at night while the waves calm down. In one study, for example, there was a significant reduction in hours of no power with a

combination of wind (75%) and wave (25%) energy farms (Stoutenburg et al., 2010). The number of no power hours for 100% wind was 1330 h/yr and 242 h/yr for 100% wave, but with a 25% wave, 75% wind combination, the no-power hours dropped to only 70 h/yr.

8.4 TIDAL POWER

The history of tidal power began centuries ago when Europeans created tidal storage dams (called barrages) that created storage ponds filled by the incoming tide. Water wheels powered by releases from storage could then be used for such purposes as grinding grain. A bit more than a half-century ago, the first large tidal power system (240 MW) began operation in the La Rance River estuary in France. In the more recent past, several other large plants have been built, including a 254 MW plant in South Korea completed in 2011. Several MW-scale plants are being proposed in the Philippines, Russia, England, and South Korea. As encouraging as these developments may be, it is difficult to envision this approach to utilize tidal power playing much of a role in our global energy future. Not only are there relatively few locations where the resource and the geography are appropriate, but the costs and environmental impacts of building large impoundment projects on sensitive coastal shorelines pose formidable challenges for the future.

8.4.1 Tidal Current Power

The future of tidal power seems to lie in what is now referred to as tidal in-stream energy conversion (TISEC). Submerged turbines, some of which bear close resemblance to conventional wind turbines, can tap into the power of tidal currents that flow back and forth in naturally constrained passageways.

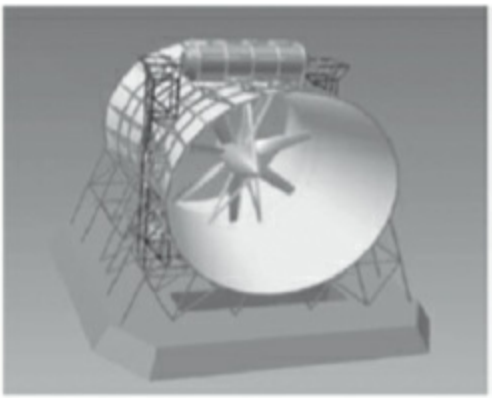
Tidal currents are similar to most other renewable resources in that the resource is highly variable in nature, which poses challenges for large-scale implementation. On the other hand, the variability of tidal resources is completely predictable, which greatly increases its value. In modern power markets, a resource does not need to be constant to be valuable; in fact, in some cases, plants that are unable to vary their outputs as loads change can cause problems of their own. Tidal resources with variable, but entirely predictable, generation can easily be matched with other generation technologies to meet changes in demand.

Tidal in-stream technologies are still in their infancy, with most installations being first-of-their-kind demonstrations. A number of options are still being tested and refined, which can be briefly categorized in several ways. Most turbines are horizontal axis, three-bladed turbines with various approaches being taken to deal with the changing direction of tidal currents. In some, the rotors swing around a vertical axis during slack-water intervals. Others have two rotors, each facing in opposite directions. It is also possible to rotate the pitch of the rotors to allow a single rotor to work in ebb and flood tides. Rotor performance can be enhanced with a shroud to accelerate the flow of water through the turbine (Fig. 8.22b). Vertical axis turbines are also being developed, which have the advantage of always facing into the current without any special controls.

FIGURE 8.22 Examples of horizontal axis tidal current turbines.



(a) Rolls-Royce



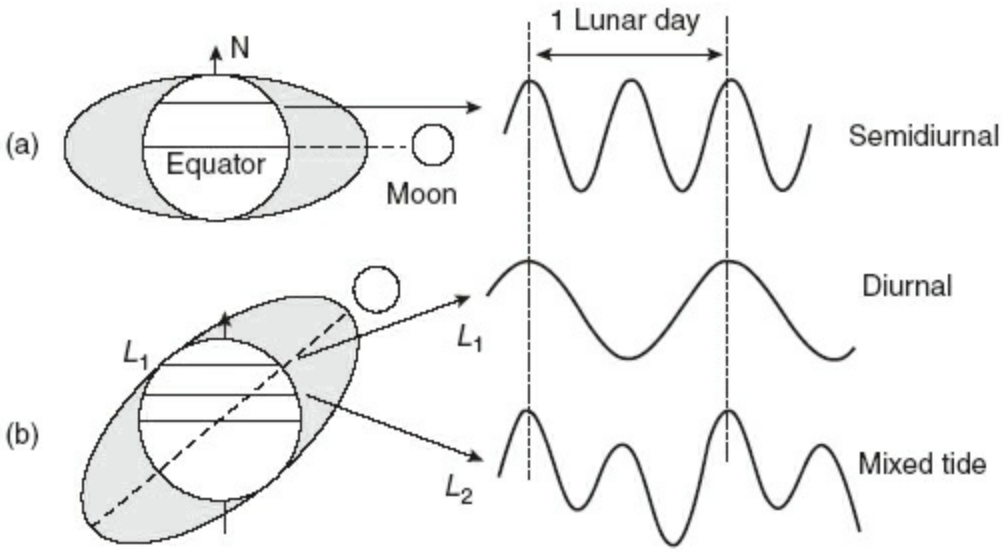
(b) Lunar energy

Support structures may be designed to sit on the bottom with a vertical connection to a turbine tower as suggested in Figure 8.22a. These are completely submerged as opposed another approach in which a monopole tower is drilled deep into the sea floor, extending up through the water surface to provide easy access for installation and maintenance. A cross-arm can make it possible to mount several turbines on a single tower. It is also possible to create a floating platform with multiple towers, each with its own turbine, extending down into the tidal flow.

8.4.2 Origin of the Tides

Tidal changes are the result of gravitational forces exerted mostly by the moon and partially by the sun. Figure 8.23 presents a simple model involving just the moon and the earth meant to provide some intuition into tidal variations at different locations on earth during different seasons. In Figure 8.23a, the moon is on the ecliptic plane of the earth's orbit, which means that it circles the earth directly above the equator. This will occur around the time of the March and September equinoxes. The gravitational force exerted on an unrestricted ocean surrounding the earth converts an otherwise spherical ocean into a more elliptical shape. If we imagine being at some location on the spinning earth in Figure 8.23a, we would experience two relatively equal tidal cycles during a single lunar day: high tide, low tide, high tide, low tide. This is called a semidiurnal tidal cycle.

FIGURE 8.23 A simple model showing tidal bulges when the moon is over the equator, resulting in a semidiurnal cycle (a). In (b), with the moon to the north, a single diurnal tidal cycle will occur at latitude L_1, while other latitudes will experience a mixed cycle. The figure is greatly exaggerated to clarify the concepts.



In Figure 8.23b, the moon is sitting above a much higher latitude (exaggerated for emphasis). Far to the north, at latitude L_1 there will be only one tidal cycle per day, which is called a diurnal cycle. At other latitudes, however, there will be two high tides per day, but one will be higher than the other. Of course in reality, tides at a given location are heavily influenced by local geographical features, so this picture is greatly oversimplified.

Figure 8.24 introduces the influence of the sun, which exerts its own gravitational force on the earth. Although the sun has far greater mass, it is so far away that its tidal impact is only about 45% that of the moon. Since a lunar day is 24.84 h and a solar day is 24 h, the solar and lunar tides are usually out of phase with each other, which introduces the notion of spring tides and neap tides. During a full moon and a new moon, the sun and the moon are in phase with each other, their impacts are additive and tidal swings are the greatest. These are called *spring tides*, not because they occur in the spring, but because the word derives the German *springen,* which means to leap. When the solar and lunar cycles are 90° out of phase with each other, as occurs during a first- and third-quarter moon, high tides are lower and low tides are higher. Figure 8.25 shows an example of the potential impacts of neap and spring tides on tidal currents.

FIGURE 8.24 Showing the creation of spring tides when the moon and sun are in phase, and neap tides when they are 90° out of phase.

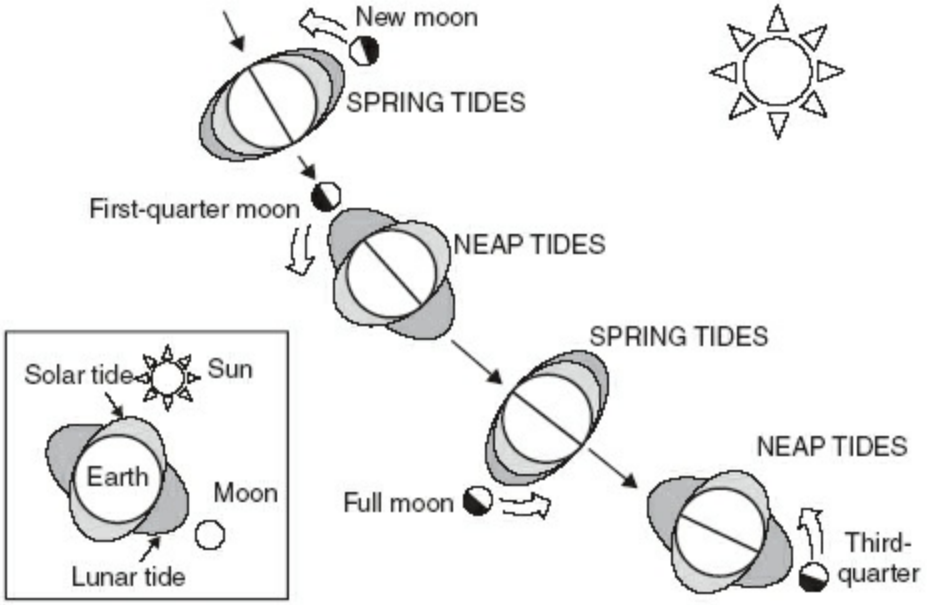
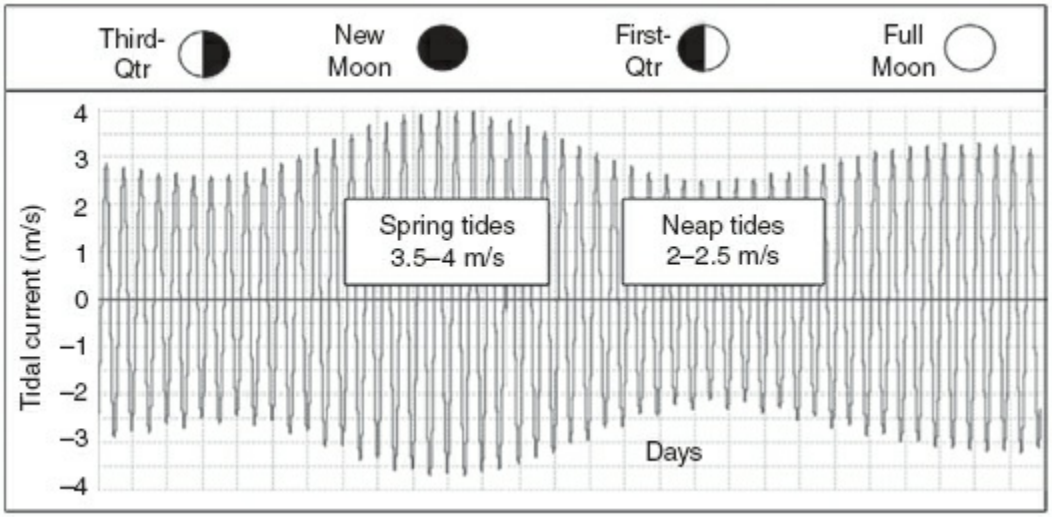


FIGURE 8.25 An example of the impact of spring and neap tides on tidal current.



8.4.3 Estimating In-Stream Tidal Power

Near-shore tidal changes can induce strong currents, especially between islands or up and down long inlets. Technologies that tap into that power can be quite similar to wind power systems, and in fact, power calculations are analogous to those presented for wind in Chapter 7.

Using the same approach that was taken in deriving Equation 7.7 for wind, the fundamental equation for tidal currents is exactly the same:

$$P = \frac{1}{2}\rho A v^3 \tag{8.11}$$

where P is tidal power (watts), ρ is water density (1025 kg/m^3), A is swept area (m^2), and v is stream speed normal to the converter area (m/s). The big difference between this

equation for wind versus water is the density of seawater, which is 837 times that of air (1025/1.225 = 837). The other difference, of course, is tidal speeds, which are usually considerably lower. For example, for equal power density, a modest 1 m/s tidal current is the same as a brisk 9.4 m/s wind (both provide 513 W/m^2).

Similar to wind, for an unshrouded turbine, the Betz maximum extraction efficiency of 16/27 (59.3%) occurs when the turbine slows the current to one-third of its upstream velocity.

Example 8.1 A Tidal Current Generator. A horizontal-axis, 3-bladed turbine with 5-m blade diameter is operating in a current running at 2 m/s (3.89 knots, 4.47 mph). Find the power in the water and, assuming the following efficiencies, find its overall efficiency and expected power delivered:

Turbine = 75% of the Betz limit
Drive train = 96%
Generator = 95%
Power conditioning = 98%

If the turbine is designed to spin at 40 rpm, what would be the rotor tip speed and tip-speed ratio (TSR = rotor-blade tip speed/fluid flow speed)?

Solution. Using Equation 8.11, tidal power to the turbine is

$$p = \frac{1}{2} \times 1025 \frac{\text{kg}}{\text{m}^3} \times \frac{\pi}{4} (5\ \text{m})^2 \times (2\ \text{m/s})^3 = 80{,}503\ \text{W}$$

The turbine efficiency is 0.75 × 59.3% = 44.48%.

Including the other losses, the overall efficiency would be

$$\text{Efficiency} = 0.4448 \times 0.96 \times 0.95 \times 0.98 = 39.7\%$$

Power delivered under these conditions would be

$$P = 0.397 \times 80.503\ \text{kW} = 31.96\ \text{kW}$$

The tip speed at 40 rpm would be

$$\text{Tip speed} = \frac{40\ \text{rev/min} \times (\pi 5)\ \text{m/rev}}{60\ \text{s/min}} = 10.47\ \text{m/s}\ (23.4\ \text{mph})$$

And the tip-speed-ratio would be

$$\text{TSR} = \frac{10.47\ \text{m/s}}{2\ \text{m/s}} = 5.2$$

Again, this is quite similar to the TSR for a wind turbine.

The above example predicts power delivery under a single tidal speed. Under variable tidal conditions, we cannot, of course, just insert average tidal speed into Equation 8.11 and expect to get average value of power. To find that important quantity, we need to go through some of the same steps that were developed in Chapter 8 for wind power. Begin by expressing the average power starting with the fundamental relationship given in Equation

8.11:

$$P_{\text{avg}} = \left(\frac{1}{2}\rho A v^3\right)_{\text{avg}} = \frac{1}{2}\rho A \left(v^3\right)_{\text{avg}} \tag{8.12}$$

To keep things simple, let us begin by assuming tidal currents are smooth semidiurnal sinusoids, which we can express as

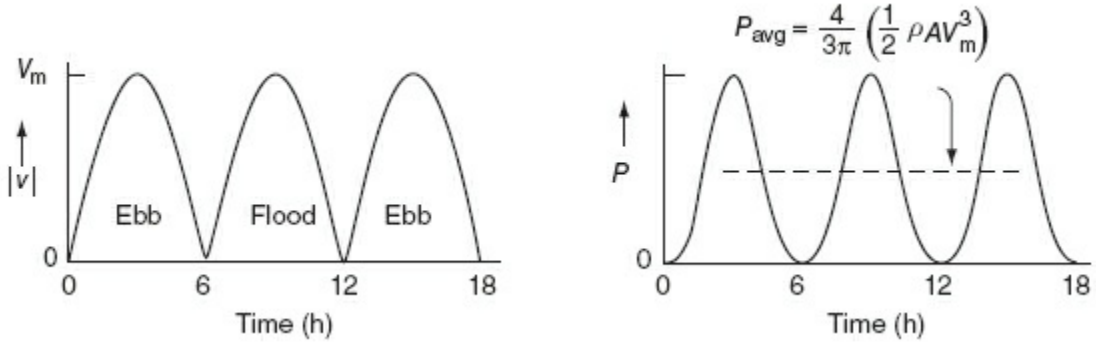
$$v = V_{\text{m}} \sin(\omega t) \tag{8.13}$$

We will also assume that the turbine works equally well in both directions of tidal flow. The average value of the cube of a half-cycle of a sinusoid is given by

$$(v^3)_{\text{avg}} = \frac{1}{T}\int_0^T f(t)\text{d}t = \frac{1}{\pi}\int_0^\pi (V_{\text{m}} \sin t)^3\, dt = \frac{4}{3\pi}V_{\text{m}}^3 \tag{8.14}$$

Figure 8.26 shows the magnitude of the tidal current as two, positive, half-cycles, and the power that results when we cube those speeds.

FIGURE 8.26 Deriving the average value of v^3 for a sinusoidal tidal current.



Substituting Equation 8.14 into Equation 8.13 results in the following expression for average power in sinusoidal tidal current:

$$P_{\text{avg}} = \frac{1}{2}\rho A \frac{4}{3\pi} V_{\text{m}}^3 = \frac{2}{3\pi}\rho A V_{\text{m}}^3 \tag{8.15}$$

Example 8.2 Average Power Generated by Tidal Current. Compare the average power delivered to a 5-m (diameter) turbine during sinusoidal spring tides with maximum speed 4 m/s versus neap tides with 2.5 m/s maximum speeds (similar to those shown in Figure 8.25).

Solution. Using Equation 8.15 for each current:

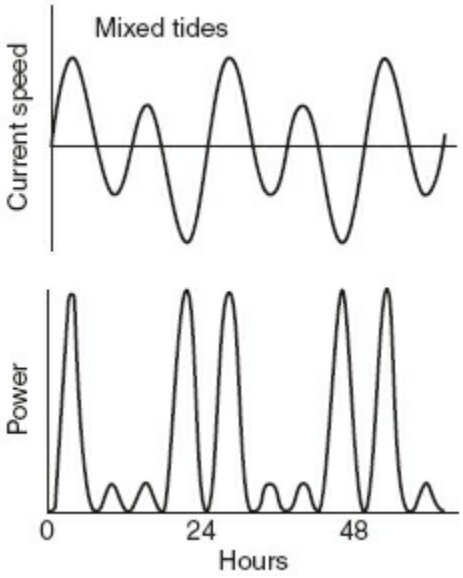
$$P_{\text{avg}}(\text{spring}) = \frac{2}{3\pi} \times 1025 \times \frac{\pi}{4} \times 5^2 \times 4^3 = 273.3 \times 10^3 \text{ W}$$

$$P_{\text{avg}}(\text{neap}) = \frac{2}{3\pi} \times 1025 \times \frac{\pi}{4} \times 5^2 \times 2.5^3 = 66.7 \times 10^3 \text{ W}$$

So, just over four times as much power is generated in those spring tides.

The impact of power being proportional to the cube of current speed is greatly magnified for mixed tidal conditions, which on a given day have a mix of high peaks and lower peaks. These are the most common tidal conditions. Figure 8.27 illustrates how looking at power can translate that cubic into two nice high power peaks in a row followed by two much lower peaks in a row.

FIGURE 8.27 For common mixed-tidal conditions, the power in tidal current can show dramatic differences in a single day.



8.4.4 Estimating Tidal Energy Delivered

Tidal energy calculations follow a very similar procedure used for wind turbines. We need a power curve for the tidal turbine and we need some statistical evaluation of the currents available at the site.

Figure 8.28 shows an example power curve, identifying the cut-in tidal current speed, the rated power of the generator and the rated current speed at which rated power will be delivered. Figure 8.29 shows a statistical analysis of currents in the Tacoma Narrows, Washington. A spreadsheet combination of the two is presented in Table 8.9. To demonstrate one of the rows, the probability that the current speed is 1.9 m/s is given as 0.063. At that speed, the turbine/generator is predicted to deliver 600 kW. So, the expected energy to be delivered while currents are 1.9 m/s would be

$$\text{Energy} = 0.063 \times 8760\ \text{h/yr} \times 600\ \text{kW} = 331{,}128\ \text{kWh/yr}$$

TABLE 8.9 Estimating the Energy Delivered by a Tidal Current Plant[a]

Tidal Speed (m/s)	Probability	h/yr @ speed	Power (kW)	Energy (kWh/yr)
0.0	0	0	0	0
0.1	0.075	657	0	0
0.3	0.080	701	0	0
0.5	0.088	771	0	0
0.7	0.094	823	20	16,469
0.9	0.093	815	55	44,807
1.1	0.091	797	98	78,122
1.3	0.083	727	170	123,604
1.5	0.078	683	270	184,486
1.7	0.072	631	410	258,595
1.9	0.063	552	600	331,128
2.1	0.051	447	800	357,408
2.3	0.040	350	980	343,392
2.5	0.034	298	1000	297,840
2.7	0.025	219	1000	219,000
2.9	0.017	149	1000	148,920
3.1	0.010	88	1000	87,600
3.3	0.005	44	1000	43,800
3.5	0.001	9	1000	8760
			Total	2,543,930

[a]Plant is the 1000-kW turbine in Figure 8.28 with tidal currents shown in Figure 8.29.

FIGURE 8.28 An example power curve for a tidal turbine/generator.

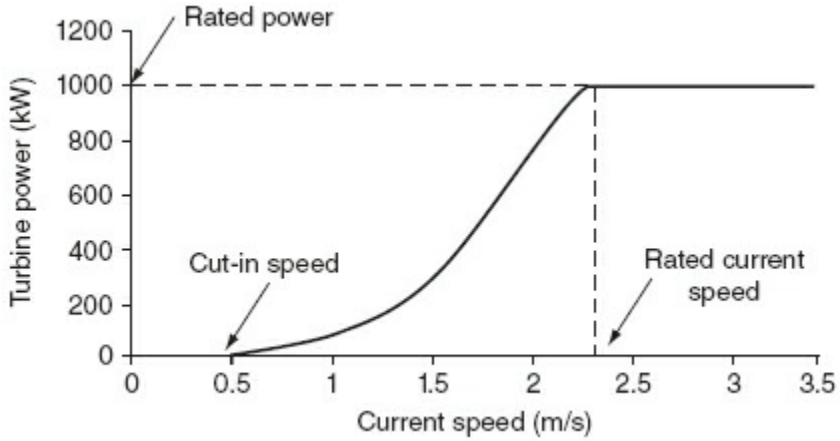
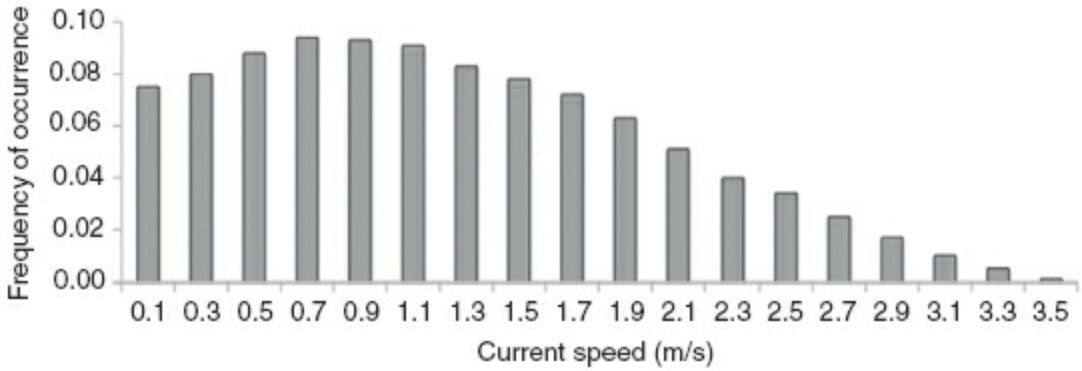


FIGURE 8.29 Surface tidal current speed probability distribution for the Tacoma Narrows, Washington. From Hagerman et al. (2006).



The total energy for this set up is 2.54×10^6 kWh/yr, which says the capacity factor for this turbine would be

$$\text{Capacity factor} = \frac{2.54 \times 10^6 \text{ kWh/yr}}{1000 \text{ kW} \times 8760 \text{ h/yr}} = 0.29 = 29\%$$

This estimate was based on currents at the surface of the Tacoma Narrows, so a more careful analysis would require data on currents at the expected depths. A fine reference for making such calculations is the EPRI report by Hagerman and Polagye (2006).

8.5 HYDROELECTRIC POWER

Hydropower is a very significant source of electricity with close to 1 TW of capacity delivering 16.5% (3400 TWh) of the total global supply. In more than two dozen countries, hydropower supplies more than 90% of their electricity. Most of the new hydro facilities are being installed in Asia (led by China) and Latin America (led by Brazil). In fact, the two largest hydro plants are in China (Three Gorges, 22.4 GW) and Brazil (Itaipu, 14 GW). China has by far the greatest installed capacity (210 GW) and is aggressively pursuing new projects. Hydropower generates 8% of U.S. electricity, which may sound modest, but it is still considerably more than the other renewable sources combined. The focus in the United States and most other Organisation for Economic Co-operation and Development (OECD) countries, where the best sites have already been developed, has shifted from developing new sites to improving existing facilities and adding generation capabilities to existing nonpowered dams. Hydroelectric power is an established, mature technology, but there is some attention being paid to developing cheaper and better technologies for small-capacity and low head applications.

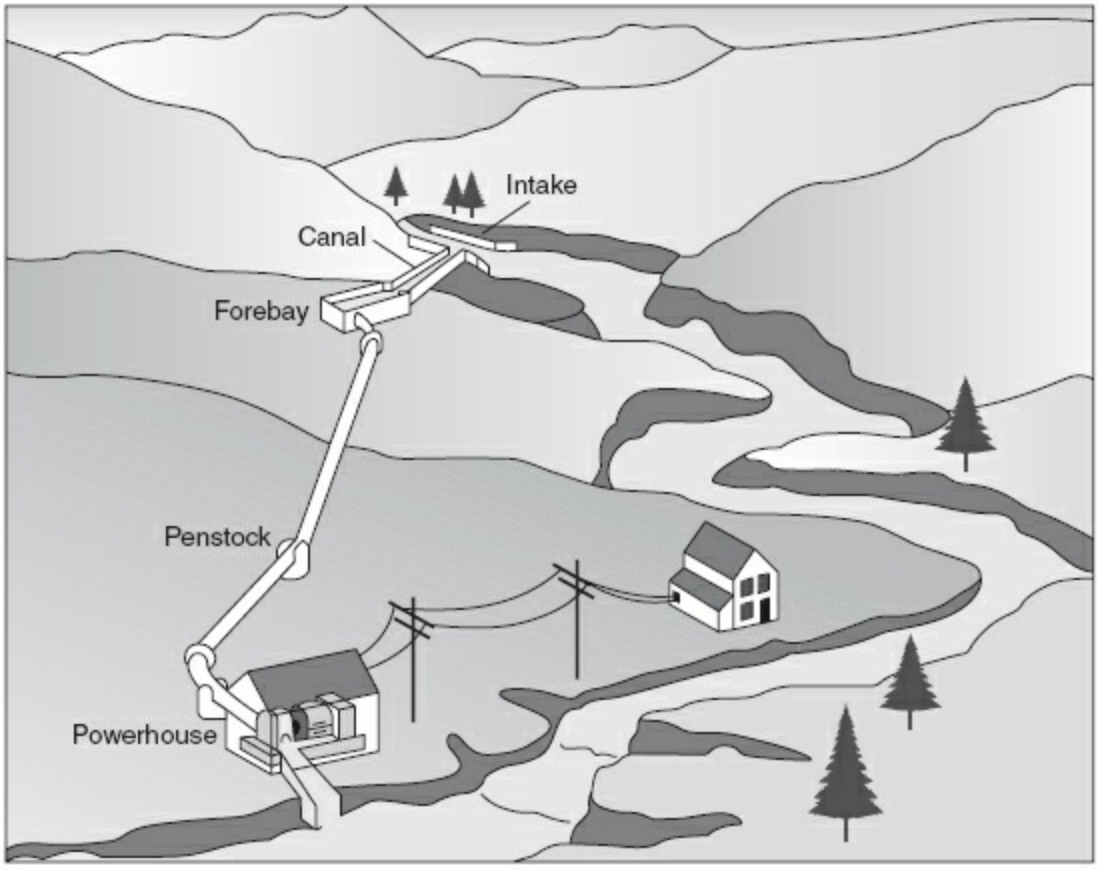
Hydroelectric power has a distinct advantage over most other renewable technologies in that it is a far more flexible source of power. It can provide baseload power, peaking power, spinning reserve, and energy storage. It can meet minute-by-minute load fluctuations faster, and with greater range and flexibility, than conventional power plants. With storage it is an ideal complement to variable and unpredictable renewables.

8.5.1 Hydropower Configurations

One way to classify hydroelectric plants is by the way they interact with their resource.

Run-of-the-river plants have little or no storage capacity. Without significant civil works involved, they do not cause nearly the ecosystem disruption of their dams and reservoir counterparts. An example of a run-of-the-river system is shown in Figure 8.30. A portion of the river is diverted into a forebay that provides modest storage. From there, water travels in a pipeline, called a *penstock*, that delivers water under pressure to a hydraulic turbine/generator in a powerhouse located at some elevation below the intake. If this is a very small, off-grid system, the powerhouse may also contain a battery bank to help provide for peak demands that exceed the average generator output.

FIGURE 8.30 A micro-hydropower system in which water is diverted into a penstock and delivered to a powerhouse below.



Conventional hydro systems with storage are the most common hydroelectric plants. Such facilities frequently serve multiple purposes besides power generation, including urban water supply, flood control, irrigation, and recreation. The obvious and important advantage of storage is its role in decoupling the timing of precipitation and snowmelt from the constantly varying load that the grid must satisfy. The benefits and costs associated with impoundments on local economies and environment are closely related to the size of projects. Small projects can provide enormous social benefits to local communities with minimal ecological impacts. Moreover, local communities share benefits and costs somewhat equitably, which is not the case for large hydro plants. The Three Gorges dam in China, for example, displaced over one million people, but will contribute significant power that will benefit the entire country.

There is an interesting debate underway in the United States about whether large hydroelectric facilities will be counted as renewable energy systems under individual state-

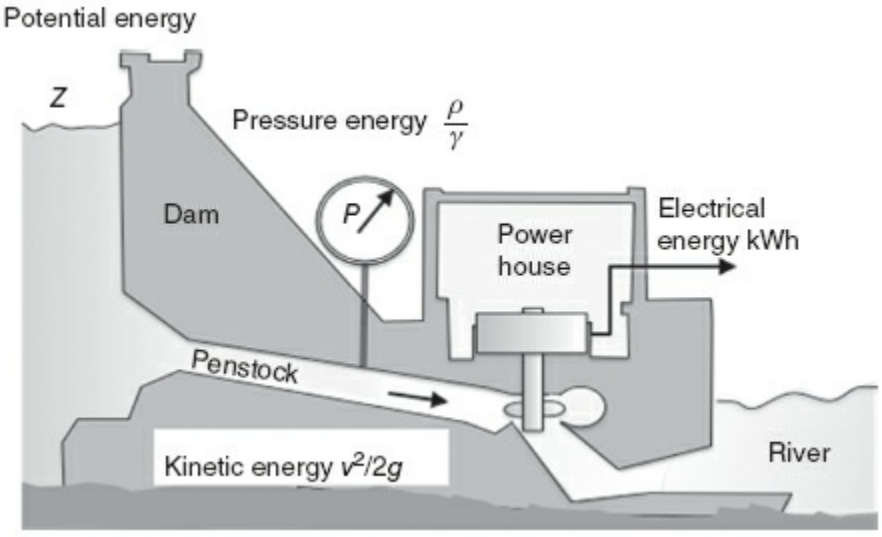
by-state Renewable Portfolio Standards (RPS) frameworks. Some of the debate relates to whether a state can really count on future precipitation patterns to continue as global warming progresses. Some raise concerns about impacts on the environment and whether dams will eventually silt up and cease to function. Most states with RPS goals allow only small hydropower systems to count, but the definition of that threshold is highly variable.

The third category of hydroelectric systems is pumped hydro, in which a reservoir serves mainly to supply peaking power for the grid. Water from a lower elevation source is pumped uphill during off-peak times to the storage reservoir. When power is needed, water spins a generator as it flows back to the lower body of water. Round-trip efficiencies above 80% for this cycle are not uncommon. Not only does pumped hydro provide grid stability services in general, it can also be the easiest way to integrate variable renewables into the grid. In fact, in the right geographical circumstances, it seems reasonable to imagine sending power directly from renewables to a pumped hydro facility, rather than to the grid itself.

8.5.2 Basic Principles

The energy associated with water manifests itself in three ways: as potential energy, pressure energy, and kinetic energy. The energy in a hydroelectric system starts out as potential energy by virtue of its height above some reference level—in this case, the height above the powerhouse. Water under pressure in the penstock is able to do work when released, so there is energy associated with that pressure as well. Finally, as water flows there is the kinetic energy that is associated with any mass that is moving. Figure 8.31 suggests the transformations between these forms of energy as water flows from a reservoir, through a penstock, to a turbine.

FIGURE 8.31 Transformations of energy in a hydroelectric system.



It is convenient to express each of these three forms of energy on a per unit of weight basis, in which case energy is referred to as *head* and has dimensions of length, with units such as "feet of head, " or "meters of head." The total energy is the sum of the potential, pressure, and kinetic head, and is given by

$$\text{Energy head} = z + \frac{p}{\gamma} + \frac{v^2}{2g}$$

(8.16)

where

z	=	elevation above a reference height (m) or (ft)
p	=	pressure (N/m^2) or (lb/ft^2)
γ	=	specific weight (N/m^3) or (lb/ft^3)
v	=	average velocity (m/s) or (ft/s)
g	=	gravitational acceleration (9.81 m/s^2) or (32.2 ft/s^2)

In working with hydropower systems, especially in the United States, mixed units are likely to be incurred, so Table 8.10 is presented to help sort them out.

TABLE 8.10 Useful Conversions for Water

	American	SI
1 cubic foot =	7.4805 gal	0.02832 m^3
1 foot per second =	0.6818 mph	0.3048 m/s
1 cubic footper second =	448.8 gal/min(gpm)	0.02832 m^3/s
Water density =	62.428 lb/ft^3	1000 kg/m^3
1 pound per square inch =	2.307 ft of water	6896 N/m^2
1 kW =	737.56 ft-lb/s	1000 N-m/s

Example 8.3 Mixed Units in the American System. Suppose a 4-in diameter penstock delivers 150 gal/min of water through an elevation change of 100 ft. The pressure in the pipe is 27 psi when it reaches the turbine. What fraction of the available head is lost in the pipe? What power (kW) is delivered to the turbine?

Solution. From Equation 8.16:

$$\text{Pressure head} = \frac{p}{\gamma} = \frac{27\ \text{lb/in}^2 \times 144\ \text{in}^2/\text{ft}^2}{62.428\ \text{lb/ft}^3} = 62.28\ \text{ft}$$

To find velocity head, we need to use $Q = vA$, where Q is flow rate, v is velocity, and A is cross-sectional area:

$$v = \frac{Q}{A} = \frac{150\ \text{gpm}}{(\pi/4) \cdot (4/12\ \text{ft})^2 \times 60\ \text{s/min} \times 7.4805\ \text{gal/ft}^3} = 3.83\ \text{ft/s}$$

So, from Equation 8.16, the velocity head is

$$\text{Velocity head} = \frac{v^2}{2g} = \frac{(3.83\ \text{ft/s})^2}{2 \times 32.2\ \text{ft/s}^2} = 0.228\ \text{ft}$$

The total head available for the turbine is the sum of the velocity and pressure head, or

62.28 + 0.228 ft = 62.51 ft. This is called the net head, H_N.

$$H_N = 62.28 + 0.228 \text{ ft} = 62.51 \text{ ft of head}$$

Note that the velocity head is negligible.
Since we started with 100 ft of head, pipe losses are 100 – 62.51 ft = 37.49 ft, or 37.49%.
Using conversions from Table 8.10, while carefully checking to see that units properly cancel, the power delivered to the turbine by a flow of 150 gal/min at a head of 62.51 ft is

$$P = \frac{150 \text{ gpm} \times 62.428 \text{ lb/ft}^3 \times 62.51 \text{ ft}}{60 \text{ s/min} \times 7.4805 \text{ gal/ft}^3} \times \frac{\text{kW}}{737.56 \text{ ft-lb/s}} = 1.77 \text{ kW}$$

If there are no losses in the piping, the power theoretically available from a site is determined by the difference in elevation between the surface of the source and the turbine, called the *gross head* H_G, and the rate at which water flows from one to the other, Q. Using a simple dimensional analysis, we can write

$$\text{Power} = \frac{\text{Energy}}{\text{Time}} = \frac{\text{Weight}}{\text{Volume}} \times \frac{\text{Volume}}{\text{Time}} \times \frac{\text{Energy}}{\text{Weight}} = \gamma Q H \quad (8.17)$$

Substituting appropriate units in both the SI and American systems results in the following key relationships for idealized (without losses) power:

$$P \text{ (kW)} = \frac{Q \text{ (gpm)} \cdot H_G \text{(ft)}}{5300} \quad (8.18)$$

and

$$P \text{ (kW)} = 9.81 Q \text{ (m}^3\text{/s)} \cdot H_G \text{ (m)} \quad (8.19)$$

While Equations 8.18 and 8.19 make no distinction between a site with high head and low flow and one with the opposite characteristics, the differences in physical facilities are considerable. With a high head site, lower flow rates translate into smaller diameter piping, which is more readily available and a lot easier to work with, as well as smaller, less-expensive turbines.

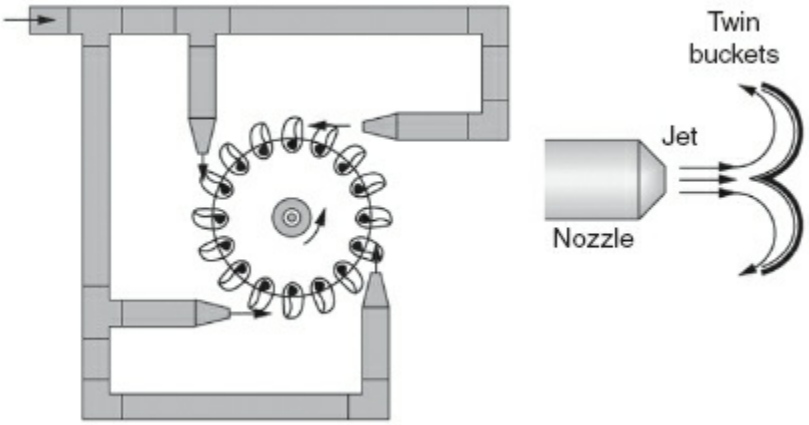
8.5.3 Turbines

Just as energy in water manifests itself in three forms—potential, pressure, and kinetic head—there are also three different approaches to transform that waterpower into the mechanical energy needed to rotate the shaft of an electrical generator. *Impulse turbines* capture the kinetic energy of high speed jets of water squirting onto buckets along the circumference of a wheel. In contrast, water velocity in a *reaction turbine* plays only a modest role and instead it is mostly the pressure difference across the runners, or blades, of these turbines that creates the desired torque. Generally speaking, impulse turbines are most appropriate in high head, low flow circumstances, while the opposite is the case for reaction turbines. And, finally, the slow-moving, but powerful, traditional overshot *waterwheel* converts potential energy into mechanical energy. The slow rotational rates of waterwheels

are a poor match to the high speeds needed by generators so they are not used for electric power.

Impulse turbines are most commonly used in small systems. The original impulse turbine was developed and patented by Lester Pelton in 1880 and its modern counterparts continue to carry his name. In a *Pelton wheel*, water squirts out of nozzles onto sets of twin buckets attached to the rotating wheel. The buckets are carefully designed to extract as much of the water's kinetic energy as possible, while leaving enough energy in the water to enable it to leave the buckets without interfering with the incoming water. A diagram of a four-nozzle Pelton wheel is shown in Figure 8.32. These turbines have efficiencies typically in the range of 70–90%.

FIGURE 8.32 A four-nozzle Pelton impulse turbine.



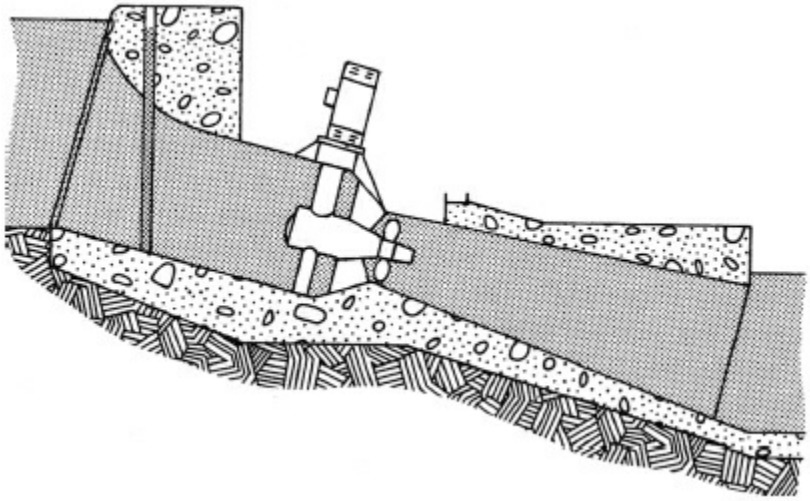
The efficiency of the original Pelton design suffers somewhat at higher flow rates because water trying to leave the buckets tends to interfere with the incoming jet. Another impulse turbine, called a *Turgo wheel*, is similar to a Pelton. However, the runner has a different shape and the incoming jet of water hits the blades somewhat from one side, allowing exiting water to leave from the other, which greatly reduces the interference problem. The Turgo design also allows the jet to spray several buckets at once, which spins the turbine at a higher speed than a Pelton, which makes it somewhat more compatible with generator speeds.

There is another impulse turbine called a *cross-flow* turbine, which is especially useful in low-to-medium head situations (5–20 m). This turbine is also known as a Banki, Mitchell, or Ossberger turbine—names that reflect its inventor, principal developer, and current manufacturer. These turbines are especially simple to fabricate, which makes them popular in developing countries, where they can be built locally.

For low head installations with large flow rates, reaction turbines are the ones most commonly used. Rather than having the runner be shot at by a stream of water, as is the case with impulse turbines, reaction turbine runners are completely immersed in water and derive their power from the mass of water moving through them rather than the velocity. Most reaction turbines used in micro-hydro installations have runners that look like an outboard motor propeller. The propeller may have anywhere from three to six blades, which for small systems are usually fixed pitch. Larger units that include variable-pitch blades and other adjustable features are referred to as Kaplan turbines. They are widely used in low head situations ($\approx$2–40 m). An example of a right-angle-drive system in which a

bulb contains the gearing between the turbine and an externally mounted generator is shown in Figure 8.33. For the largest systems, another very versatile reaction turbine (≈ 10–350 m head), called a Francis, is the most widely used.

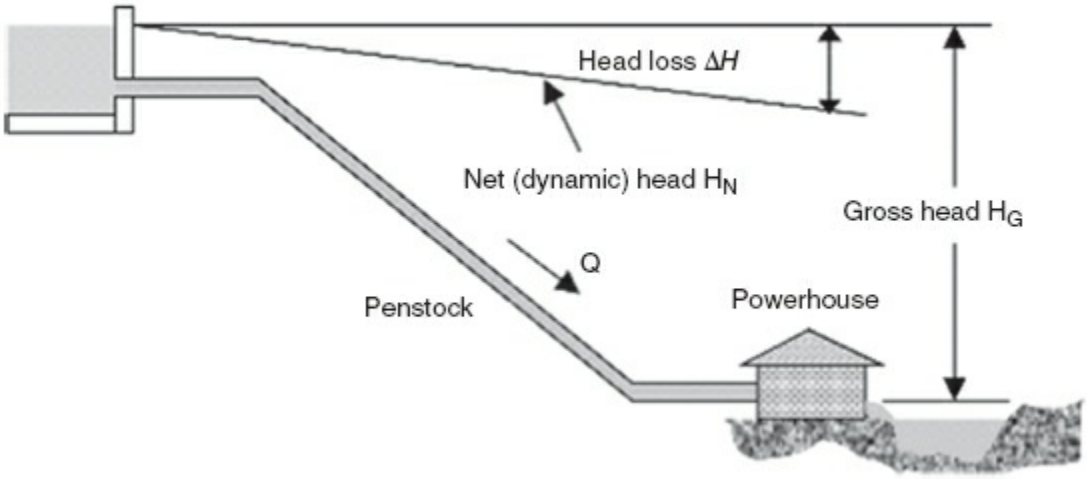
FIGURE 8.33 A right-angle-drive propeller, reaction turbine.



8.5.4 Accounting for Losses

Equations 8.18 and 8.19 do not account for friction losses in the penstock, nor do they account for turbine and generator inefficiencies. Begin with penstock losses. The net head, H_N, is the gross head (the actual elevation difference) minus the head loss in the piping. The net head is also called the *dynamic head*. Those losses are a function of the pipe diameter, the flow rate, the length of the pipe, how smooth the pipe is, and how many bends, valves, and elbows the water has to pass through on its way to the turbine. Section 6.6.3 addressed these issues in the context of PV-powered water pumping. Figure 8.34 illustrates the difference between gross and net head.

FIGURE 8.34 Net head is what remains after pipe losses are accounted for.



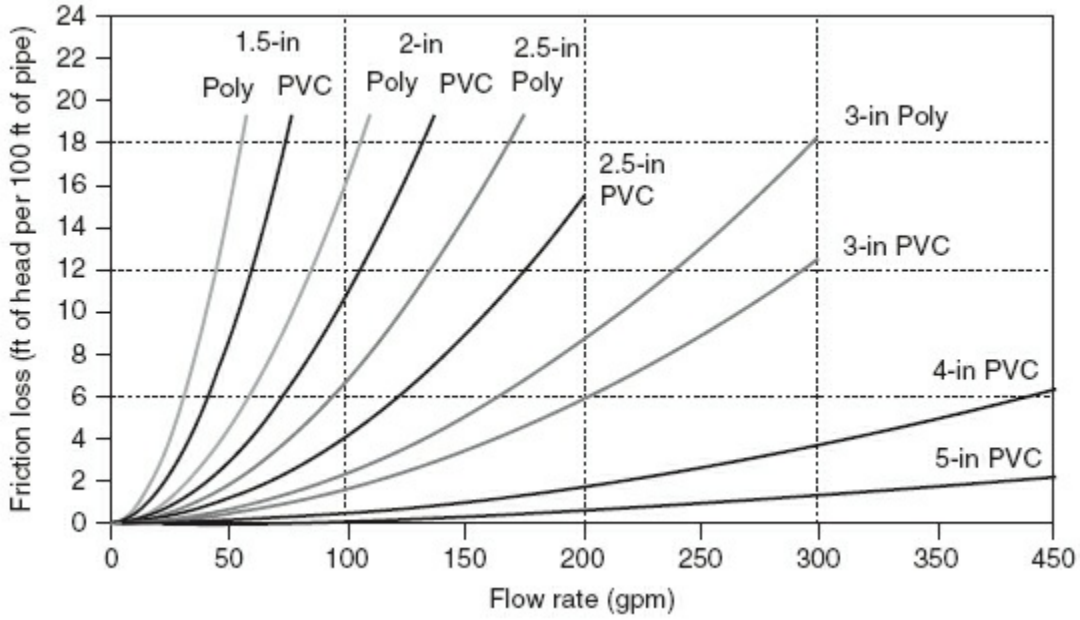
To be useful, Equations 8.18 and 8.19 need to be rewritten in terms of net head H_N, rather than gross head H_G, and since the goal is to estimate actual electrical power delivered

by the system, we should also include an efficiency η to account losses in the turbine and the generator itself.

$$P_{\text{delivered}}\ (\text{kW}) = \frac{\eta Q\ (\text{gpm}) H_{\text{N}}(\text{ft})}{5300} = 9.81 \eta Q\ (\text{m}^3/\text{s}) H_{\text{N}}(\text{m}) \quad (8.20)$$

As an example of how to estimate penstock losses, let us consider calculations for a micro-hydro system. Figure 8.35 shows the friction loss, expressed as feet of head per 100 ft of pipe, for PVC and for polyethylene (poly) pipe of various diameters. PVC pipe has lower friction losses and it is also less expensive than poly pipe, but small-diameter poly may be easier to install since it is somewhat flexible and can be purchased in rolls from 100 to 300 ft long. Larger diameter poly comes in shorter lengths that can be butt-welded on site. Both need to be protected from sunlight, since ultraviolet exposure makes these materials brittle and easier to crack.

FIGURE 8.35 Friction head loss, in feet of head per 100 ft of pipe, for 160-psi PVC piping and for polyethylene, SDR pressure-rated pipe.



Example 8.4 Power from a Micro-Hydro Plant. Suppose 150 gal/min of water is taken from a creek and delivered through 1000 feet of 3-in-diameter polyethylene pipe to a turbine 100 ft lower than the source. Assuming 80% efficiency for the turbine/generator, estimate the energy delivered in a 30-day month.

Solution. From Figure 8.35, at 150 gal/min, 3-in poly loses about 5 ft of head for every 100 ft of length. Since we have 1000 ft of pipe, the friction loss is

$$1000\ \text{ft} \times 5\ \text{ft}/100\ \text{ft} = 50\ \text{ft of head loss}$$

The net head available to the turbine is

$$\text{Net head} = \text{Gross head} - \text{Friction head} = 100\ \text{ft} - 50\ \text{ft} = 50\ \text{ft}$$

Using a 70% turbine/generator efficiency in Equation 8.20 suggests delivered power would

be

$$P_{\text{delivered}}\ (\text{kW}) = \frac{\eta\ Q\ (\text{gpm})H_{\text{N}}(\text{ft})}{5300} = \frac{0.80 \times 150 \times 50}{5300} = 1.13\ \text{kW}$$

The monthly electricity supplied would be 24 h × 30 d/mo × 1.13 kW = 815 kWh, which is roughly the average electrical energy used by a typical U.S. household.

Example 8.4 would be a poor design since half of the power potentially available is lost in the piping. Larger diameter pipe will reduce losses and increase power delivered, so bigger is better from an energy perspective. But, large pipe costs more, especially when the cost of larger valves and other fittings is included, and it is more difficult to work with. Since the cost of the piping is often a significant fraction of the total cost of a micro-hydro project, an economic analysis should be used to decide upon the optimum pipe diameter. Keeping flow rates less than about 5 ft/s and friction losses less than 20% seem to be good design guidelines for high-head micro-hydro systems. Coupled with an 80%-efficient turbine/generator package suggests an overall efficiency of about 60% as a target for a small hydro system. Large hydro systems with minimal penstock losses can have efficiencies above 90%.

8.5.5 Measuring Flow for a Micro-Hydro System

Obviously, a determination of the available water flow is essential to planning and designing a system. In some circumstances, the source may be so abundant and the demand so low that a very crude assessment may be all that is necessary. If, however, the source is a modest creek, or perhaps just a spring, especially if it is one whose flow is seasonal, much more careful observations and measurements may be required before spending any money. In those circumstances, regular measurements taken over at least a full year should be made.

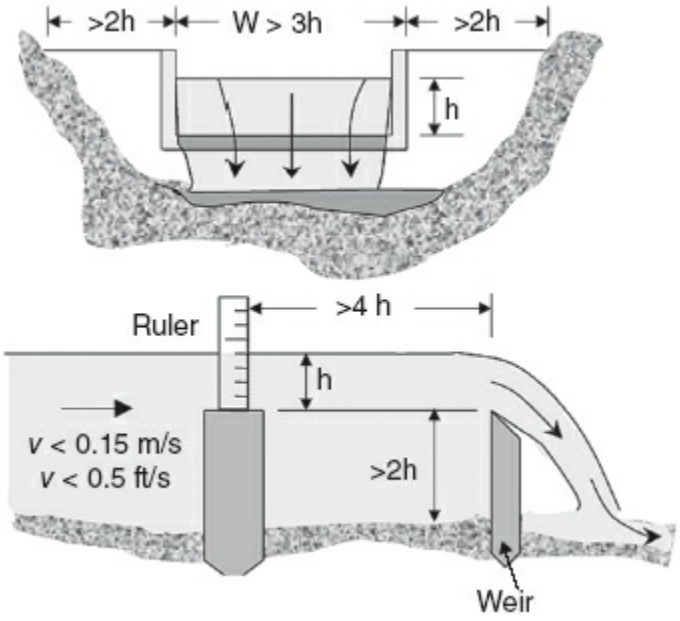
Methods of estimating stream flow vary from the very simplest float-and-stopwatch approach to more sophisticated approaches, including one in which stream velocity measurements are made across the entire cross-section of the creek using a propeller-or-cup-driven current meter. For micro-hydro systems, oftentimes the best approach involves building a temporary wall of plywood, concrete, or metal, called a weir, across the creek. The height of the water as it flows through a notch in the weir can be used to determine flow.

The notch in the weir may have a number of different shapes, including rectangular, triangular, and trapezoidal. It needs to have a sharp edge to it so the water drops off immediately as it crosses the weir. For accuracy, it must create a very slow moving pool of water behind it so that the surface is completely smooth as it approaches the weir, and a ruler of some sort needs to be set up so that the height of the water upstream can be measured. When the geometric relationships for the rectangular weir shown in Figure 8.36 are followed, and height h is more than about 5 cm, or 2 in, the flow can be estimated from the following:

$$Q = 1.8\,(W - 0.2h)h^{1.5} \quad \text{with } Q\ (\text{m}^3/\text{s}),\ h\ (\text{m}),\ W\ (\text{m}) \tag{8.21}$$

$$Q = 2.9\,(W - 0.2h)h^{1.5} \quad \text{with } Q\ (\text{gpm}),\ h\ (\text{in}),\ W\ (\text{in}) \tag{8.22}$$

FIGURE 8.36 A rectangular weir used to measure flows. Based on Inversin (1986).



Example 8.5 Designing a Weir. Design a weir to be able to measure flows expected to be between 100 and 500 gal/min.

Solution. At the 100-gal/min low flow rate, we will use the suggested minimum water surface height above the notch of 2 in. From Equation 8.22,

$$W \leq \frac{Q}{2.9h^{1.5}} + 0.2h = \frac{100}{2.9 \times 2^{1.5}} + 0.2 \times 2 = 12.6 \text{ in}$$

For the high flow rate expected, we have to adapt a trial-and-error approach to solve Equation 8.22. Let us make $W = 12$ in and try $h = 6$ in.

$$Q = 2.9(12 - 0.2 \times 6)6^{1.5} = 460 \text{ gpm}$$

The 6-in notch is a little short for our 500 gal/min goal. At 7 in, the flow could be 570 gal/min. That suggests a notch roughly 12 × 7 in would probably work just fine.

8.5.6 Electrical Aspects of Small-Scale Hydro

Large hydroelectric systems are used as a source of AC power that is fed directly into utility lines using conventional synchronous generators and grid interfaces. Since the output frequency is determined by the rpm of the generator, very precise speed controls are necessary. While mechanical governors and hand-operated control valves have been traditionally used, modern systems have electronic governors controlled by microprocessors.

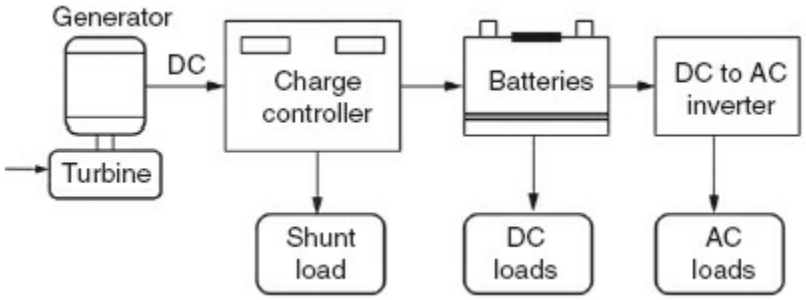
On the other end of the scale, micro-hydro systems usually generate DC, which is used to charge batteries. An exception would be the case in which utility power is conveniently available, in which case a grid-connected system in which the meter spins in one direction when demand is less than the hydro system provides, and the other way when it does not, would be simpler and cheaper than the battery-storage approach. The electrical details of

grid-connected systems, as well as stand-alone systems with battery storage, are covered in some detail in Chapter 6.

The battery bank in a stand-alone micro-hydro system allows the hydro system, including pipes, valves, turbine, and generator, to be designed to meet just the average daily power demand, rather than the peak, which means everything can be smaller and cheaper. Loads vary throughout the day of course, as appliances are turned on and off, but the real peaks in demand are associated with the surges of current needed to start the motors in major appliances and power tools. Batteries handle that with ease. Since daily variations in water flow are modest, micro-hydro battery storage systems can be sized to cover much shorter outages than weather-dependent PV systems must handle. Two days of storage is considered reasonable.

A diagram of the principal electrical components in a typical battery-based micro-hydro system is given in Figure 8.37. To keep the batteries from being damaged by overcharging, the system shown includes a charge controller that diverts excess power from the generator to a shunt load, which could be, for example, the heating element in an electric water-heater tank. Other control schemes are possible, including use of regulators that either adjust the flow of water through the turbine or modulate the generator output by adjusting the current to its field windings. As shown, batteries can provide DC power directly to some loads, while other loads receive AC from an inverter.

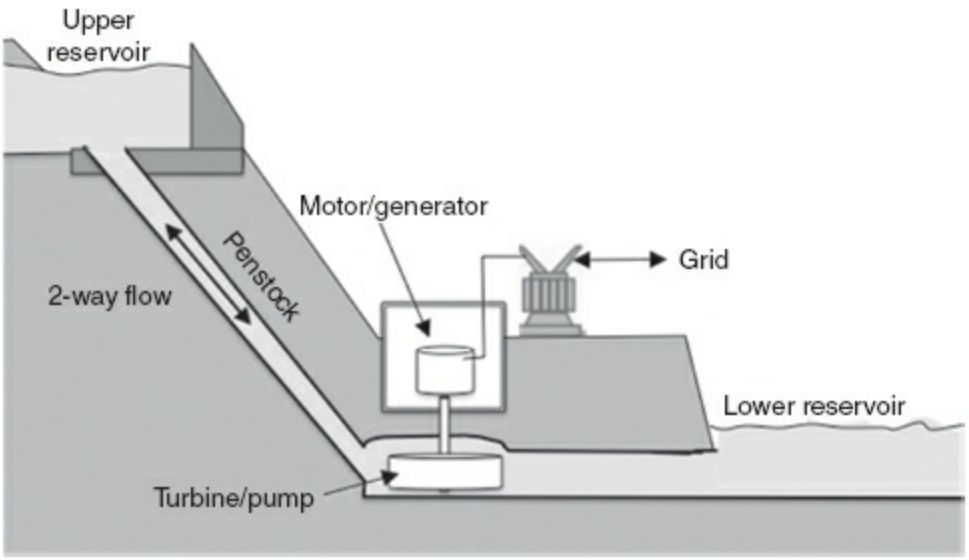
FIGURE 8.37 Electrical block diagram of a battery-based micro-hydro system.



8.6 PUMPED-STORAGE HYDRO

Large-scale pumped-storage hydroelectric (PSH) power is a fully commercialized technology that globally provides close to 130 GW of storage, which is 99% of all grid electricity storage on the planet. In the United States, pumped storage represents 2.2% of all generation capacity, while in Japan, it is 18% and in Australia 19% (IRENA, 2012). Most commercial-scale systems use a reversible Francis pump/turbine unit that is connected to a motor/generator so that the same equipment is used to pump water uphill as is used to generate power when it comes back down (Fig. 8.38). With typical round-trip efficiencies of 75–85%, it is currently the most cost-effective way to provide large-scale bulk electricity storage. The penalties associated with those pumping losses are easily offset by the financial gains that can be realized by topping off the upper reservoir during off-peak times and selling that power back during peak demand periods.

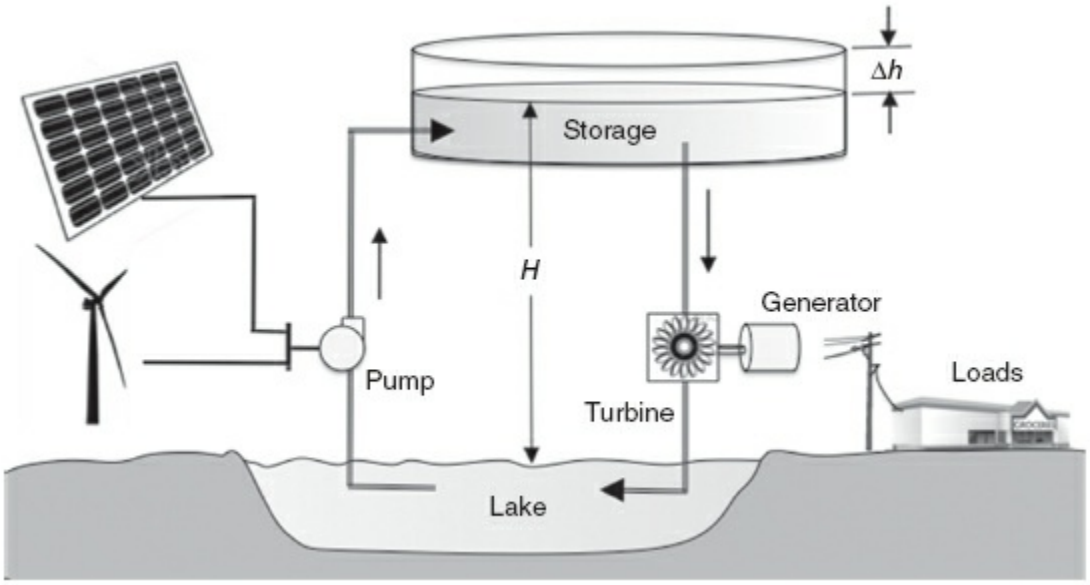
FIGURE 8.38 Essence of a pumped-storage hydroelectric plant.



Pumped-storage offers a number of desirable attributes in addition to providing peaking power. They can start up and shut down in a matter of just a few minutes and they can switch from pump mode to generation mode in less than half an hour. Their quick responsiveness to varying loads makes them ideal for load following, grid stabilization, and as providers of nonpolluting spinning reserves. In terms of large-scale, bulk grid storage, pumped hydro is currently more cost-effective than any of its emerging competitors (Fig. 9.9). Its main competition is conventional large hydropower with storage, which is the first choice for any good site.

As renewables become more prevalent on the grid, pumped-storage can not only provide backup power when wind or solar drops, but it may also be able to help avoid curtailment from those sources when excess power is being generated. An intriguing prospect for village-scale power suggests using a two-penstock system design in which uphill pumping power is provided directly by renewables while loads are satisfied by downhill releases from the storage reservoir (Fig. 8.39). Storage provides the decoupling between renewables and loads, both of which are variable and uncertain.

FIGURE 8.39 A two-penstock pumped-hydro system with dedicated renewables.



The energy available in the upper reservoir, relative to the lower one, is given by

$$E = \frac{\rho A g \Delta h H}{3.6 \times 10^6} \tag{8.23}$$

where E is the energy (kWh), ρ is the density of water (1000 kg/m^3), A is the surface area of the upper reservoir (m^2), Δh is the allowable change in the surface level (m), g is gravitational acceleration (9.81 m/s^2), H is the average difference in elevation of the two reservoirs (m), and the 3.6 million converts J to kWh.

Example 8.6 A Two-Penstock Pumped Storage System. The system in Figure 8.39 needs to supply a small village that has a 100-kW average load. A storage pond will be built at an elevation of 250 m above an existing lake. The pond will be 3-m deep but only the top 2 m can be used for variable storage. Assuming each penstock has an efficiency of 90% and the pump and turbine each have 85% efficiency, how big should the pond be to provide 2 days of storage during which time the renewables are unable to produce power?

Solution. Energy that needs to be delivered during those two days is

$$E = 100 \text{ kW} \times 24 \text{ h/d} \times 2 \text{ d} = 4800 \text{ kWh to the village}$$

Including inefficiencies, the tank needs to provide

$$E \text{ (from tank)} = \frac{4800 \text{ kWh}}{0.90 \times 0.85} = 6274.5 \text{ kWh}$$

Using Equation 8.23 gives

$$E \text{ (kWh)} = \frac{1000 \left(\text{kg/m}^3\right) A \left(\text{m}^2\right) 9.81 \left(\text{m/s}^2\right) \Delta h \text{ (m)} \, H \text{ (m)}}{3.6 \times 10^6 \text{ (J/kWh)}}$$

$$A = \frac{3.6 \times 10^6 \times 6274.5}{1000 \times 9.81 \times 2 \times 250} = 4432 \text{ m}^2$$

That is about the size of an American football field.

8.7 BIOMASS FOR ELECTRICITY

Biomass energy systems utilize solar energy that has been captured and stored in plant material during photosynthesis. While the overall efficiency of conversion of sunlight to stored chemical energy is low, plants have already solved the two key problems associated with all solar energy technologies, that is, how to collect the energy when it is available, and how to store it for use when the sun is not shining. Plants have also very nicely dealt with the greenhouse problem since the carbon released when they use that stored energy for respiration is the same carbon they extracted in the first place during photosynthesis. That is, they get energy with no net carbon emissions.

While there is already a sizeable agricultural industry devoted to growing crops specifically for their energy content, it is almost entirely devoted to converting plant material into alcohol fuels for motor vehicles. Growing crops for fuel competes with food crops for farmland and usually results in no net reduction in carbon emissions compared with gasoline. In fact, in one study, converting biomass into electricity that powers electric vehicles was found to deliver an average of 80% more miles of transportation per acre of crops than using ethanol in internal combustion engines. In addition, crops-to-electricity-to-electrified transportation would provide double the greenhouse gas offsets (Campbell et al., 2009).

Rather than growing special biomass energy crops, biomass for electricity production is essentially all waste residues from agricultural and forestry industries and, to some extent, municipal solid wastes. Since it is based on wastes that must be disposed of anyway, biomass feedstock for electricity production may have low cost, no-cost, or even negative-cost advantages.

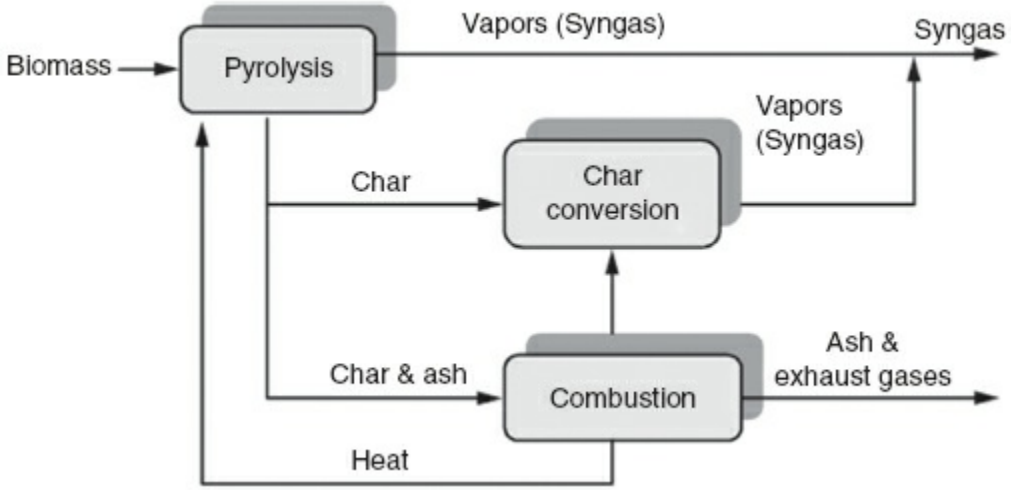
Currently, about 11 GW of biomass-powered generation supplies about 1.4% of U.S. electricity. Most of these plants operate on a conventional steam Rankine cycle, but some newer plants use combined-cycle technology. Since transporting their rather disbursed fuel sources over any great distances could be prohibitively expensive, biomass power plants tend to be small and located near their fuel source, so they are not able to take advantage of the economies of scale that go with large steam plants. To offset the higher cost of smaller plants, lower grade steel and other materials are often used, which requires lower operating temperatures and pressures and hence lower efficiencies. Moreover, biomass fuels tend to have high water content and are often wet when burned, which means wasted energy goes up the stack as water vapor. The net result is that existing biomass plants tend to have rather low efficiencies—typically less than 20%. Even though the fuel may be very inexpensive, those low efficiencies translate to reasonably expensive electricity, which is currently around 10 ¢/kWh. About two-thirds of existing biomass power plants cogenerate both electricity and useful heat, which can nearly double their usable energy output and, by crediting the value of exported heat, cut their net cost of electricity generation by about one-third.

An alternative approach to build small, inefficient plants dedicated to biomass power production is to burn biomass along with coal in slightly modified, conventional steam-

cycle power plants. Called co-firing, this method is an economical way to utilize biomass fuels in relatively efficient plants. Since biomass burns cleaner than coal, overall emissions are correspondingly reduced in co-fired facilities.

New, combined-cycle power plants do not need to be large to be efficient, so it is interesting to contemplate a new generation of biomass power plants based on gas turbines rather than steam. The problem is, however, that gas turbines cannot run directly on biomass fuels since the resulting combustion products would damage the turbine blades, so an intermediate step would have to be introduced. By gasifying the fuel first and then cleaning the gas before combustion, it would be possible to use biomass with gas turbines. A two-step process for gasifying biomass fuels is illustrated in Figure 8.40. In the first step, the raw biomass fuel is heated, causing it to undergo a process called *pyrolysis*, in which the volatile components of the biomass are vaporized. As the fuel is heated, moisture is first driven off; then at a temperature of about 400°C, the biomass begins to break down, yielding a product gas, or *syngas*, consisting mostly of hydrogen, carbon monoxide, methane, carbon dioxide, and nitrogen (N_2), as well as tar. The solid byproducts of pyrolysis are char (fixed carbon) and ash. In the second step, char heated to about 700°C reacts with oxygen, steam, and hydrogen to provide additional syngas. The heat needed to drive both steps comes from the combustion of some of the char.

FIGURE 8.40 Biomass gasification process.



Another technology for converting biomass to energy is based on the anaerobic (without oxygen) decomposition of organic materials by microorganisms to produce a biogas consisting primarily of methane and carbon dioxide. The biochemical reactions taking place are extremely complex, but in simplified terms they can be summarized as

(8.24)
$$C_nH_aO_bN_cS_d + H_2O + \text{bacteria} \rightarrow CH_4 + CO_2 + NH_3 + H_2S + \text{new cells}$$

where $C_nH_aO_bN_cS_d$ is meant to represent organic matter, and the equation is obviously not chemically balanced. The technology is conceptually simple, consisting primarily of a closed tank, called a digester, in which the reactions can take place in the absence of oxygen. The desired end product is methane, which is typically between 55% and 75% of the resulting gas.

Anaerobic digesters are fairly common in municipal wastewater treatment plants, where

their main purpose is to transform sewage sludge into innocuous, stabilized end products that can be easily disposed of in landfills, or sometimes, recycled as soil conditioners. Anaerobic digesters can be used with other biomass feedstock including food processing wastes, various agricultural wastes, municipal solid wastes, bagasse, and aquatic plants such as kelp and water hyacinth. When the biogas is treated to remove its sulfur, the resulting gas can be used in fuel cells or burned in reciprocating engines to produce electricity and usable waste heat.

8.8 GEOTHERMAL POWER

Geothermal energy is abundant, but dispersed. It does not vary with time, the way other renewables do, so when it can be developed, it can provide baseload power with very high capacity factors. Its origin lies deep within the earth where radioactive decay continuously heats the core to temperatures in excess of 6000°C. Heat from the core at the center of the earth works its way toward the surface through the mantle, which is at about 1000°C. Heat flow from the mantle through the earth's 30-km-thick crust delivers an energy flux of only about 0.06 W/m^2, which is far, far lower than the solar, wind, tidal, and wave flux densities we see on the earth's surface. Such small fluxes are completely impractical to exploit, so it is the enormous energy that has been accumulated over eons that we are extracting. At a given site, the rate of extraction can exceed the rate of heat regeneration and the local resource may diminish over time, so some question whether this abundant resource should actually be referred as being renewable.

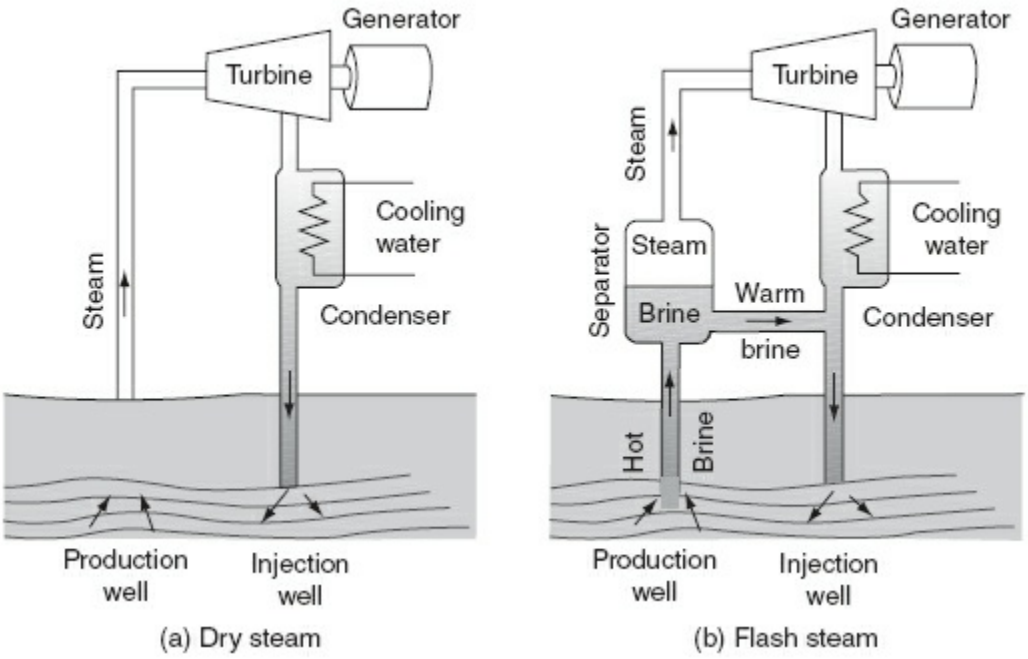
The temperature gradient through the earth's mantle averages about 30°C/km, but near tectonic plate boundaries, where most geothermal plants have been built, the gradient is typically above 80°C/km. At present, most geothermal wells are no more than 3-km deep, which in normal 30°C/km sites would yield temperatures of perhaps 100°C—adequate for industrial process heat or district heating of buildings, but far too low for efficient generation of electricity. The best geothermal regions are characterized by water that has percolated its way down to form deep, high-temperature/high-pressure aquifers that contain dry steam, or a mixture of vapor and liquid, or pressurized hot water. Natural channels may lead from these deep aquifers back to the surface, creating well-loved hot springs and geysers. These natural convective *hydrothermal regions* are the prime areas for geothermal power generation, but they are fairly unusual.

Sources of hot dry rock (HDR) are much more widespread than are the more easily exploited hydrothermal regions. Granite and other poorly conducting, impermeable rocks, buried deep beneath the surface, have had millions of years to accumulate thermal energy. Beneath a significant portion of the world's landmass, these HDRs can have temperatures considerably above 200°C. A new type of enhanced geothermal system (EGS) based on fracturing that rock is being developed to exploit this vast resource. By pumping high pressure cold water down an injection well, natural cracks in the rocks can be enhanced, increasing their permeability. After the initial fracturing, water pumped down injection wells works its way through the hot rock and is collected at about 250°C by an array of shallower return boreholes. Compared with hydrothermal resources, it has been estimated that EGS in the United States may increase the geothermal resource base a 1000-fold. As of 2012, there were only a few, small EGS plants operating in Europe, and the first large-scale

project was still under development in Australia.

First-generation geothermal plants made direct use of hot dry steam generated in hot aquifers in very special locations typically identified by local geysers. Dry steam, typically above 230°C, brought to the surface through extraction wells is piped directly to a steam turbine as shown in Figure 8.41a. Exhaust steam from the turbine is usually passed through a condenser and the condensate is then reinjected into the ground or back into the aquifer. Simpler, cheaper, but less-efficient systems may use a noncondensing turbine, also known as a back-pressure turbine, in which the steam can be released to the atmosphere or used for local thermal loads.

FIGURE 8.41 Illustrating dry steam (a) and flash steam (b) geothermal plants.

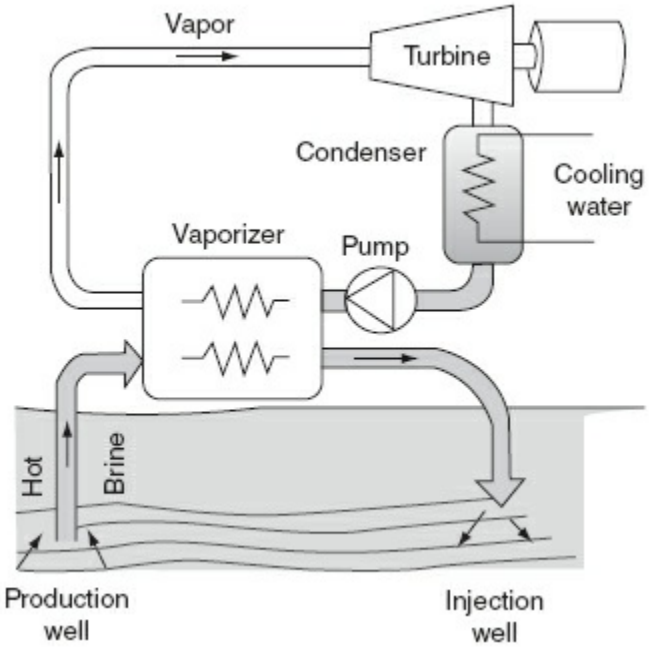


Unfortunately, aquifers providing hot dry steam are rare. It is much easier to find aquifers containing superheated water at high pressure with temperatures exceeding 175°C. Under pressure, the boiling point of water increases, so it can remain as liquid at temperatures well above 100°C. When the pressure is reduced, the water flashes to steam. Figure 8.41b shows a flash-steam plant in which extracted superheated water from the aquifer passes through a pressure reducing separator, or flash tank, and the released steam then drives the turbine. Most existing geothermal plants use these flash generators.

The third type of geothermal plant uses a binary cycle in which extracted hot water transfers its heat through a heat exchanger to a second loop containing a working fluid with a lower boiling point than water (Fig. 8.42). The working fluid, which is usually ammonia or an organic compound such as butane, pentane, or isopentane, vaporizes in the heat exchanger and the vapor then spins a turbine in either a conventional Rankine cycle system or a Kalina cycle. The advantage of these binary plants is they can generate power from resources that have temperatures that are too low (100–175°C) for conventional steam plants. This ability to generate power from lower quality resources expands their areas in which geothermal power can be economically extracted and used. These systems have the added advantage that the contaminants associated with extracted aquifer water or steam

never come in contact with the turbine loop. About 11% of existing geothermal capacity are binary plants, but most new plants being planned will use this technology.

FIGURE 8.42 A binary-cycle geothermal plant.



Where sources of high-temperature hydrothermal resources are available, geothermal power plants have proven to be reliable and cost-effective, with generation costs in the range of 50–100 $/MWh. Currently the 3.1 GW of geothermal power in the United States provides about 0.4% of total electricity demand, and the identified hydrothermal resource base is estimated to be only about 7 GW. Undiscovered hydrothermal resources may increase that to 30 GW, which is still modest (Augustine et al., 2010). But with coming HDR technologies, that resource base could be increased 1000 fold. Worldwide, in 2010, the 10.7 GW of geothermal capacity generated about 67.3 TWh of electricity, which means they operated with a quite high average capacity factor of 72%. A recent IEA study suggests that by 2050, geothermal electricity generation could provide around 1400 TWh/yr, or about 3.5% of global electricity plus an equivalent amount of thermal energy for space heating, cooling, and industrial processes (IEA, 2011). Most of the added capacity after 2030 would rely on enhanced geothermal systems in hot dry rocks.

REFERENCES

Augustine C, Young K, Anderson A. Updated U.S. geothermal supply curve. Presented at Stanford Geothermal Workshop. Golden, CO: National Renewable Energy Laboratory; 2010 Feb. NREL/CP-6A-47458.

Bedard R, Hagerman G, Previsic M, Siddiqui O, Thresher R, Ram B. Offshore wave power feasibility demonstration project, final report. Palo Alto, CA: EPRI; 2005. E21 EPRI Global WP009-US Rev 2.

Black & Veatch Cost and performance data for power generation technologies. Prepared for the National Renewable Energy Laboratory (NREL), Golden, CO:NREL; 2012 Feb.

Campbell JE, Lobell DB, Field CB. Greater transportation energy and GHG offsets from bioelectricity than ethanol. Science 2009;324:1055–1057.

Hagerman G, Polagye B, Bedard R, Previsic M. Methodology for estimating tidal current energy resources and power production by tidal in-stream energy conversion (TISEC) devices. Palo Alto, CA: EPRI; 2006 June.

IEA Technology roadmap, Geothermal heat and power. Paris: International Energy Agency; 2011.

Inversin AR. *Micro-Hydropower Sourcebook*. Arlington, VA: National Rural Electrification Cooperative Association; 1986.

IRENA Renewable energy technologies: cost analysis series, Volume 1: Power sector, issue 3/5, hydropower. Bonn, Germany: International Renewable Energy Agency; 2012 June.

Kelly B. Nexant parabolic trough solar power plant systems analysis; task 2 comparison of wet and dry rankine cycle heat rejection. Golden, CO: National Renewable Energy Laboratory; 2006. NREL/SR-550-40163.

Michel WH *Sea spectra simplified*. Washington, DC: Marine Technology; 1968.

Paasch R, Ruehl K, Hovland J, Meicke S. Wave energy: a Pacific perspective. Philosophical Transactions of the Royal Society A 2012;370: 481–501.

Previsic M, Bedard R, Hagerman G, Siddiqui O. System level design, performance and costs for San Francisco California Pelamis offshore wave power plant. Palo Alto, CA: EPRI. 2004.

Sioshansi R, Denholm P. *The value of concentrating solar power and thermal energy storage*. Golden, CO: NREL; 2010. NREL-TP-6A2-45833.

Stoddard L, Abiercunas J, O'Connell R. Economic, energy, and environmental benefits of concentrating solar power in California. Golden, CO: NREL; 2006. NREL/SR-550-39291.

Stoutenburg E., Jenkins N, Jacobson M. Power output variations of colocated offshore wind turbines and wave energy converters in California. Renewable Energy 2010; 35(12):2781–2791.

Stoutenburg ED, Jacobson MZ. Reducing offshore transmission requirements by combining offshore wind and wave farms. IEEE Journal of Oceanic Engineering 2011; 99.

Twiddell J, Weir T. *Renewable Energy Resources*. 2nd ed., London: Taylor & Francis; 2006.

U.S. Department of Energy. Concentrating solar power commercial application study: reducing water consumption of concentrating solar power electricity generation. Report to Congress. 2010.

U.S. Department of Energy. Report to Congress on the potential environmental effects of marine and hydrokinetic energy technologies. Energy Efficiency and Renewable Energy; 2009 December.

PROBLEMS

8.1 A perfect Carnot heat engine receives 1000 kJ/s of heat from a high temperature

source at 600°C and rejects heat to a cold temperature sink at 20°C.

a. What is the thermal efficiency of this engine?

b. What is the power delivered by the engine in watts?

c. At what rate is heat rejected to the cold temperature sink?

d. What are the entropy changes of the source and the sink?

8.2 Suppose an ocean thermal energy conversion system uses the difference in temperature between 25°C water at the ocean's surface and 5°C water several hundred meters below the surface to power a Rankine cycle engine.

a. What is the maximum theoretical efficiency of the system?

b. If the system runs at 40% of the Carnot efficiency, what flow rate of water through the system would be needed to generate 1 MW of electrical power (the density of seawater is 10^3 kg/m^3 with a specific heat of 4.2×10^3 J/kg/K)?

8.3. A solar pond consists of a thin layer of fresh water floating on top of a denser layer of salt water. When the salty layer absorbs sunlight, it warms up and much of that heat is held there by the insulating effect of the fresh water above it (without the fresh water, the warm salt water would rise to the surface and dissipate its heat to the atmosphere).

a. What is the maximum efficiency of a heat engine operating between the 90°C salty layer of a pond and the 20°C freshwater layer?

b. If a real engine is able to achieve 20% of the efficiency of a Carnot engine, how many kilowatt-hours of electricity could be generated per day from a 100 × 100 m pond that captures and stores 30% of the 6 kWh/m^2 solar radiation striking the surface?

8.4 A portion of the WEC performance (kW) of the 750-kW Pelamis system is shown in Figure P8.4. Suppose this machine is located in the vicinity of a buoy having the wave scatter diagram shown in Table 8.5.

	Peak Wave Period T_P(s)												
H_S (m)	3	4	5	6	7	8	9	10	11	12	14	17	20
3.0	0	91	180	246	402	424	417	369	343	331	229	144	93
2.5	0	7	93	171	279	342	351	320	274	230	174	100	65
2.0	0	0	66	109	199	219	225	205	195	162	112	64	41
1.5	0	0	26	62	112	141	143	129	110	91	63	36	23
1.0	0	0	11	27	50	62	64	57	49	41	28	0	0
0.5	0	0	0	0	0	0	0	0	0	0	0	0	0

FIGURE P8.4

a. What is the energy available (kWh/m/yr) in the waves at that location that have a 2-m significant wave height and an 8-s peak wave period?

b. Assuming power take-off losses of 25%, how much energy (kWh/yr) would be delivered by the Pelamis machine from those same 2-m, 8-s waves?

c. This Pelamis (sea snake) is 180-m long. What fraction of the energy in the waves that impact this machine is actually delivered?

8.5 The following table (P8.5) is an hours-per-month wave scatter diagram for the month

of August for the same buoy described in Table 8.5 in the chapter.

TABLE P8.5

	Peak Wave Period T_P(s)												
H_S (m)	3	4	5	6	7	8	9	10	11	12	14	17	20
3.0	0	0	0	0	0	2	1	0	0	0	0	0	0
2.5	0	0	0	0	3	9	3	2	0	0	0	0	0
2.0	0	0	0	4	19	42	12	7	4	2	1	0	0
1.5	0	0	2	24	52	74	32	19	9	6	9	15	1
1.0	1	4	10	30	37	68	42	28	16	16	47	40	5
0.5	1	1	1	3	3	9	5	3	2	5	9	4	0
0.0	0	0	0	0	0	0	0	0	0	0	0	0	0

a. Compare the average power (kW/m) in waves with 3-m significant wave height versus 2-m height if both have a peak wave period of 9 s.

b. How much energy (kWh/m) would waves with significant wave heights between 2.25 and 2.75 m have during this month?

c. How much energy would the 1-MW turbine in Table 8.7 deliver in this month for those 2.5-m waves? Assume 95% availability, an 85% directionality factor, and a 90%-efficient generator.

8.6 An in-stream tidal power system consisting of an underwater 11-m-diameter, horizontal-axis turbine delivers its rated power of 300 kW in 2.4 m/s currents.

a. What is the efficiency of this system at that current speed?

b. In those currents what will be the blade rpm and the blade tip speed (m/s and mph) if it operates with a TSR = 5.0?

c. If placed in a region with sinusoidal current oscillations with peak speed of 2.5 m/s, what would be the average power that the water would provide to this turbine?

d. If we assume the average turbine efficiency is 60% of its value at rated power, how much energy would the turbine deliver and what would be its capacity factor?

8.7 Suppose a 300-kW tidal power system is located in the current regime described below (Fig. P8.7). Also shown are data for the power curve of the turbine.

TABLE P8.7

Tidal Speed (m/s)	Probability	Power (kW)
0.0	0.000	0
0.5	0.243	0
1.0	0.278	25
1.5	0.222	90
2.0	0.150	220
2.5	0.077	300
3.0	0.030	300
3.5	0.000	300

a. Estimate the annual energy that would be delivered by 1.5 m/s tidal speeds (actually, between 1.25 and 1.75 m/s).

b. Estimate the total annual energy delivered and the overall capacity factor for the turbine.

8.8 Suppose 200 gal/min of water is taken from a creek and delivered through 800 ft of 3-in diameter PVC pipe to a turbine 100 ft lower than the source. If the turbine/generator has an efficiency of 40%

a. Find the electrical power that would be delivered by the generator.

b. What diameter pipe would be needed to keep the flow speed around 5 ft/s or less?

c. Assuming locally available PVC pipe comes in 1-in diameter increments (2-in, 3-in, etc.), pick a pipe size closest to the above suggested diameter and find the power delivered by the generator with this pipe.

8.9 Equations 8.21 and 8.22 for a rectangular weir are based on water height h above the notch being at least 2 in while the notch width W must be at least $3h$. Design a notch (width and height) that will be able to measure the maximum flow when the minimum flow is estimated to be 200 gal/min. What maximum flow rate could be accommodated?

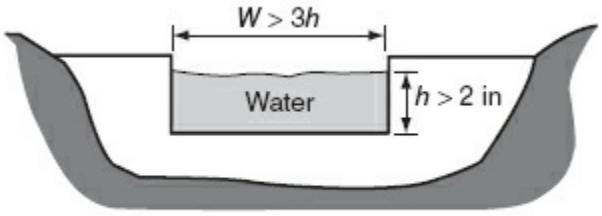


FIGURE P8.9

8.10 Suppose 300-m of elevation separate the upper and lower reservoirs of a pumped-hydro system. Each has an average surface area of 10 ha (100, 000 m^2) and their surfaces are allowed to vary in elevation by 1 m. If the penstock efficiency is 90% and the turbine/generator efficiency is 80% what is the average power that could be delivered over a 12-h period?

8.11 Consider the design of an off-grid, pumped-hydro system for a PV-powered small cabin located next to a pond. Suppose the demand is estimated to be 10 kWh/d with a peak demand of 3 kW. A tank will be placed on a nearby hilltop 100 ft above the turbine/generator. Connecting pipe runs to and from the tank are each 800 ft.

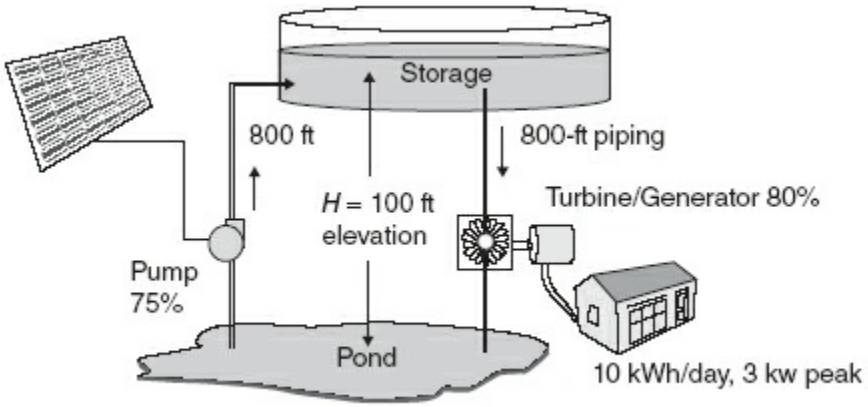


FIGURE P8.11

a. Assuming an average of 15% head losses in the pipeline and 80% conversion efficiency for the turbine/generator, how many gallons of water needs to flow from the upper tank to the pond in a day's time?

b. Size the upper storage tank (gallons) to provide a full day's worth of back-up energy when the renewables do not supply any power. Assume maximum allowed tank drainage is 75%.

c. Assuming piping losses are 20% during peak demand, what flow rate from the tank would be needed to supply the 3-kW peak?

d. Using the choices given in Figure 8.35, what size pipe would keep losses to around 20% at peak demand?

e. How much energy would a PV system have to provide to meet the average daily demand for energy? Assume 15% piping losses in each piping run and a 75%-efficient pump.

f. In an area with 5.5 kWh/m^2/d insolation, size a PV system to supply the 10 kWh/d needed by the household. Assume a derate factor of 0.75.

CHAPTER 9

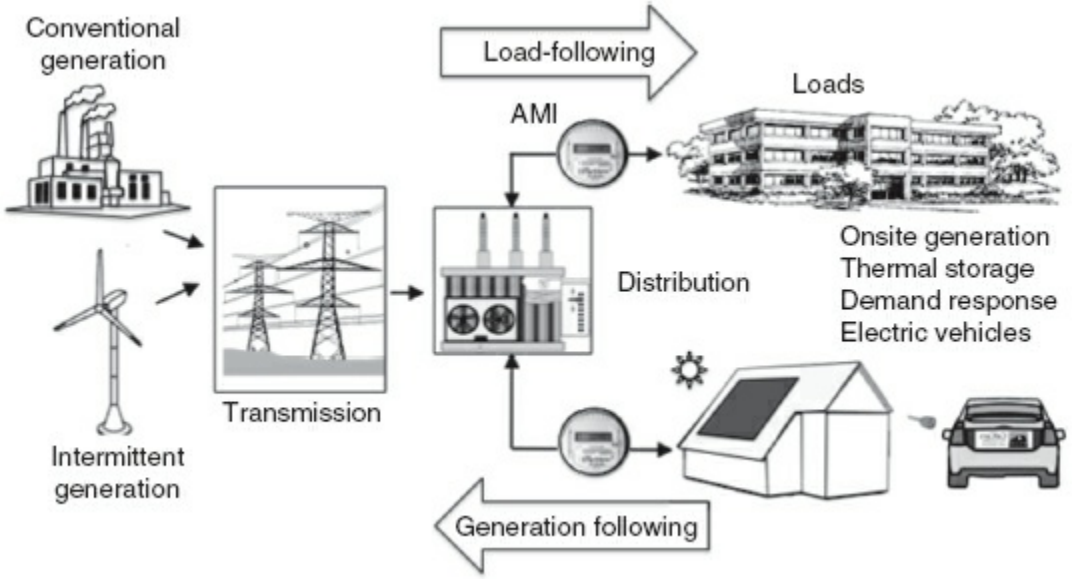
BOTH SIDES OF THE METER

9.1 INTRODUCTION

The electric power industry is in the midst of a dramatic paradigm shift. It has been amazingly effective at providing as much power as its customers want, whenever they want it, at a reasonable cost, and with almost complete reliability. But it has had control of, and been responsible for, only the supply side of the supply-and-demand equation; that is, their side of the meter. With modern communication technologies, sensors and the advent of smart meters, that paradigm is beginning to shift toward managing the demand side as well.

This chapter will begin on the supply side with an introduction to the coming smart grid, but its focus will be on the other side of the meter. With three-fourths of the U.S. electricity being consumed in buildings, mostly for lighting, air conditioning, and plug loads, new technologies and management systems in our homes and offices can have a major impact on the grid. And, as we electrify our vehicle fleet, managing those new loads and perhaps taking advantage of the electricity storage that they may be able to supply for the grid will be challenging. The potential for onsite generation, which might include photovoltaics, fuel cells, and perhaps vehicle-to-grid (V2G) power, suggests currents may flow in either direction within the distribution system. Instead of the grid following the load, loads can use demand response (DR) and onsite generation to follow variations in supply (Fig. 9.1).

FIGURE 9.1 With onsite generation and demand response, loads can follow variations in supply, instead of the traditional load-following by generation.



9.2 SMART GRID

The National Academy of Engineering named electrification the greatest engineering achievement of the twentieth century. But it is an aging grid whose basic structure has changed little since the times of Edison and Westinghouse. While information technology (IT) has transformed so much of our lives in the twenty-first century, the electric power industry has yet to tap into the full potential that IT offers.

While the definition of "smart grid" is still somewhat ambiguous, it usually contains components that include the following features.

- Enables numerous automated transmission and distribution system attributes that allow systems to be observable, controllable, and able to adapt and self-heal automatically.
- Accommodates and facilitates renewable energy sources, distributed generation, combined heat and power (CHP) systems, and energy storage on both sides of the meter.
- Enables and encourages demand response and demand-side management (DSM) through the integration of smart meters, smart appliances, and customer information and incentive programs.
- Anticipates and encourages electric vehicle charging protocols to enable smart charging schedules and possible two-way vehicle-to-grid power flows.
- With an increased reliance on computers, intelligent electronic devices, software, and communication technologies, assuring cybersecurity for the smart grid must be an essential part of its development.

9.2.1 Automating Distribution Systems

After safety, reliability is the number one priority for utilities. And, indeed, their record is quite an exceptional 99.97% availability. Power outages cost the American economy roughly $80–160 billion per year, which translates to 2–4 ¢/kWh for customers nationwide (GTM,). Weather events, animals, vehicle interactions, and other causes are not under the control of the utilities, but they are responsible for proper equipment maintenance and for grid management to avoid overloads. A smarter grid can reduce the number of customers affected by an outage and shorten the response times for those who are. A smarter grid can also help avoid brownouts and blackouts by appropriate power management on the utility side of the meter along with the facilitation of timely demand response among its customers.

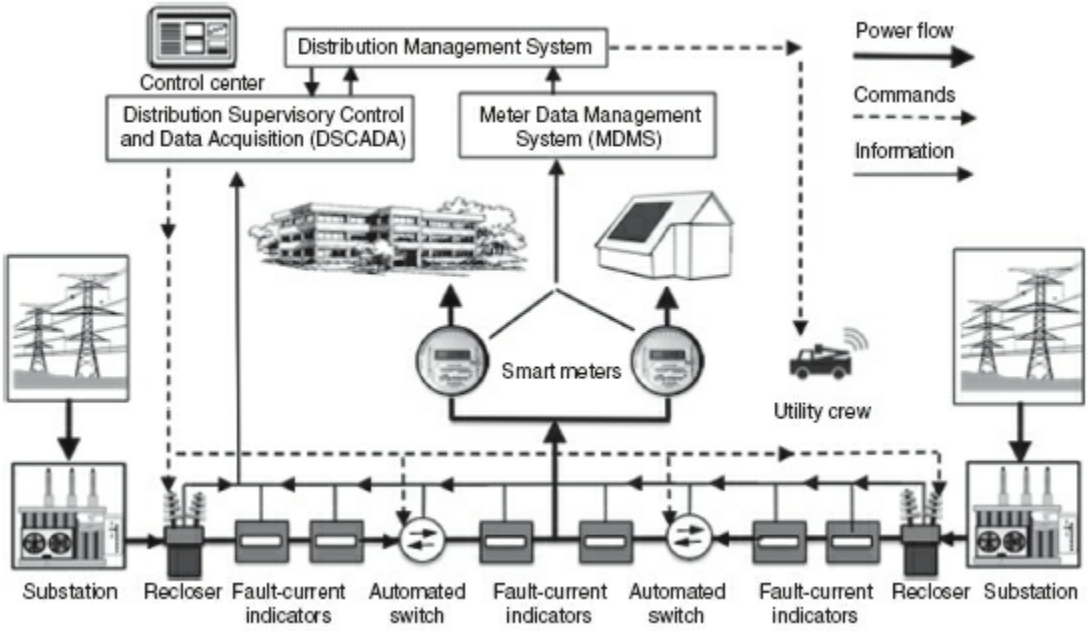
It may be surprising to learn that many utilities still rely on customers calling in about power outages before the utility realizes there has been a fault in a line somewhere. The addresses of those trouble calls help determine where the fault has occurred, so work crews can be sent out to drive along the affected lines to visually locate the actual fault. Workers then manually flip switches to isolate the fault and restore power to as many customers as they can. After all of that, crews can then begin to make repairs.

With a smarter grid, that process can be shortened by sensors that indicate when an outage has occurred and new controls, called fault detection, isolation and restoration (FDIR) systems, which can automatically isolate the fault so that repair crews can safely

work as soon as they arrive on the scene. Automatic alerts and updates can then be sent to the affected customers via phone or email. More communication between customers and utilities along with shorter outage periods can improve an often contentious relationship between the two.

Figure 9.2 suggests some of the technologies and controls that make this all happen. Two pathways, among many that may be possible, are shown by which power can flow from substations to customers. When a fault occurs in one of those pathways, fault-current indicators send an alert to a supervisory control and data acquisition (SCADA) system, which then sends commands to automated switches that isolate the line. After repairs are made the SCADA system commands reclosers to reactivate the line.

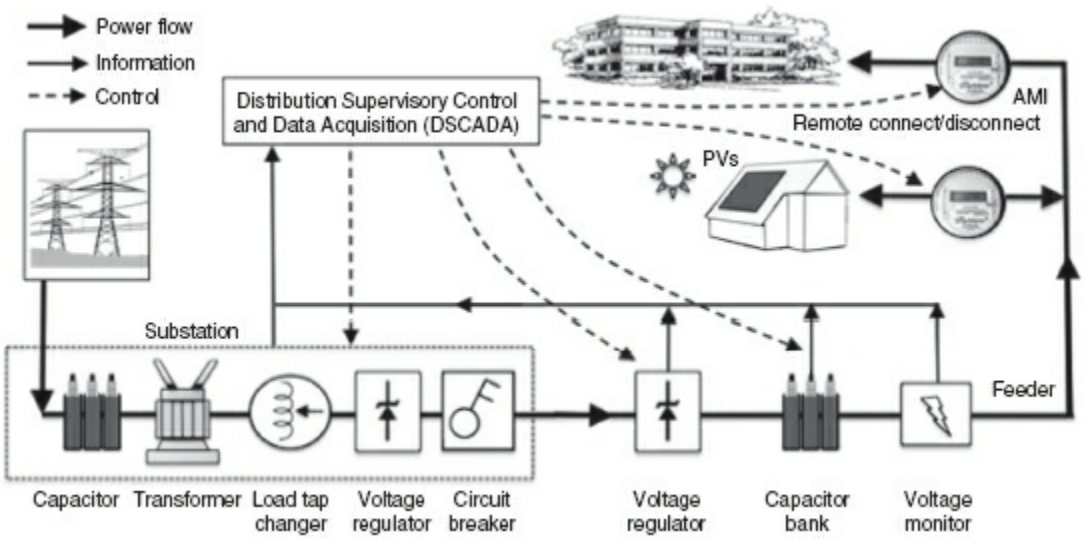
FIGURE 9.2 Distribution system outage restoration architecture. Based on GTM (2008).



9.2.2 Volt/VAR Optimization

During normal operation, slight imbalances in supply and demand show up as frequency changes, which generators automatically respond to by adjusting their output voltages and power factors. When the grid is stressed, it is also possible at the substation level to slightly decrease feeder voltages by changing the taps on transformers and by adjusting capacitor banks to reduce wasteful reactive power. With a smarter grid, that process could be automated using what is referred to as Volt/VAR optimization. Conservation voltage reductions have the potential to reduce power demand by a few percent without affecting customers as long as the voltage remains above the minimum mandated 114 V. While it can be done now within substations, operators have to be cautious about voltages out at the ends of feeders, so it is a less effective option than it could be. With a smarter grid supplying intelligence and control capabilities, Volt/VAR optimization could be extended along feeder lines and therefore be considerably more effective (Fig. 9.3).

FIGURE 9.3 Distribution-control-center-based Volt/VAR optimization architecture.



The need for Volt/VAR optimization will become even more important with a growth in rooftop photovoltaics and other on-site power generation systems. Those variable inputs to the distribution grid have the potential to play havoc with the voltages along feeder lines as power begins to flow in both directions.

With the advent of smart meters and advanced metering infrastructure (AMI) capable of remotely connecting and disconnecting customers, new response options in the case of system emergencies are possible. Today, when an emergency such as an earthquake or a storm knocks out a power plant and generation falls below demand, the only way to keep the system in balance is to drop entire feeder lines. As suggested in Figure 9.3, with smart meters, it would be possible to control individual loads along a feeder line so that critical services such as police stations, hospitals, and emergency shelters could remain connected, while less critical customers could be dropped.

9.2.3 Better Control of the Grid

Most blackouts are short-term and affect just a local distribution system, as when distractions cause someone to drive into a power pole, causing our lights to go out for a while. Some are predictable, as in the rolling blackouts that California had to endure during its ill-fated experiment with deregulation in 2000–2001. The big ones that have enormous impacts are those unexpected overloads or short circuits that occur on the transmission system itself. Examples include the great blackout that hit the Midwest and the Northeastern parts of the United States, as well as Ontario, Canada, in August 2003. That blackout caused 50 million people to be without power, some for as long as four days, and cost the United States roughly $4–10 billion. The world's largest blackout, which occurred in 2012 in India, left half a billion people without power.

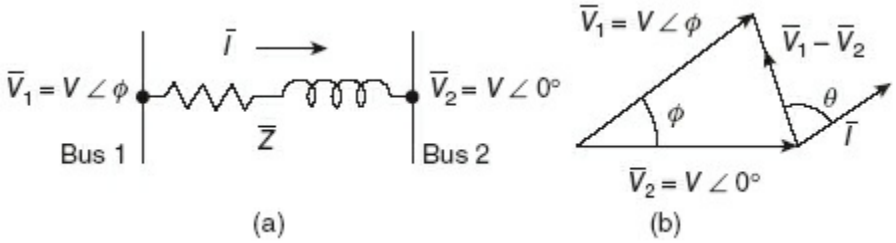
Most often, major blackouts occur when the grid is running at near capacity, which for most of the United States occurs during the hottest days of summer when the demand for air conditioning is at its highest. Perhaps surprisingly, one of the most common triggers for blackouts on those hot days results from insufficient attention having been paid to the simple management of tree growth within transmission-line rights-of-way. Line temperatures increase as they carry more current, and on hot, windless days they can expand and sag enough to short out to underlying vegetation. It was just such an event that

triggered the 2003 northeastern blackout. A power line in a rural area that came in contact with overgrown trees caused a power plant, miles away, to trip offline. It was a hot day and the northeastern grid was already running at near capacity. Lacking adequate diagnostic support, grid operators were slow to understand and control what was happening and the cascading effect of the original fault ultimately triggered the shutdown of more than 100 power plants.

While small variations in grid frequency are routine, large deviations can cause the rotational speed of generators to fluctuate, leading to vibrations that can damage turbine blades and other equipment. Significant imbalances can lead to automatic shutdowns of portions of the grid, which can affect thousands of people. When parts of the grid shut down, especially when that occurs without warning, the power that surges around the outage can potentially overload other parts of the grid causing those sections to go down as well.

A major potential of the emerging smart grids is the ability to ascertain the status of the grid in real time using new devices called phasor measurement units (PMUs). We are used to thinking about currents flowing from high voltage toward low voltage, but they can also flow between points that have exactly the same voltage magnitudes but are out of phase with each other (Fig. 9.4). The phase shift along a long line can help the line deliver power, but too much phase difference can limit its ability to do so. PMUs use clock signals from satellites to provide synchronized phase angle measurements, so the measured phasors are often referred to as synchrophasors. System operators currently gather information about power flows throughout their control regions, but their ability to monitor real-time conditions, including phase angles between voltage and current has been limited.

FIGURE 9.4 Showing how power can be delivered between two busbars having the same voltage. Out-of-phase voltages (a) and phasor diagram (b).



Synchrophasor-based transmission monitoring offers the promise of better control of the stability of the grid. With generation and load centers often being at a considerable distance from each other, oscillations, in which power sloshes back and forth as operators try to keep the system balanced, are a frequent occurrence. These oscillations can create damaging voltages or power flows that can trigger automatic shutdown systems to protect equipment. Existing transmission monitoring technologies report system status every 4 s, but that often is not fast enough to allow an effective response to instabilities. Synchrophasors, on the other hand, can measure power system parameters much faster, which provides more time to respond to emergencies. In fact, a Department of Energy study of the 2003 northeast power failure suggested synchrophasor transmission monitoring could have given operators sufficient time to isolate the problem and prevent the cascading of power failures that eventually occurred.

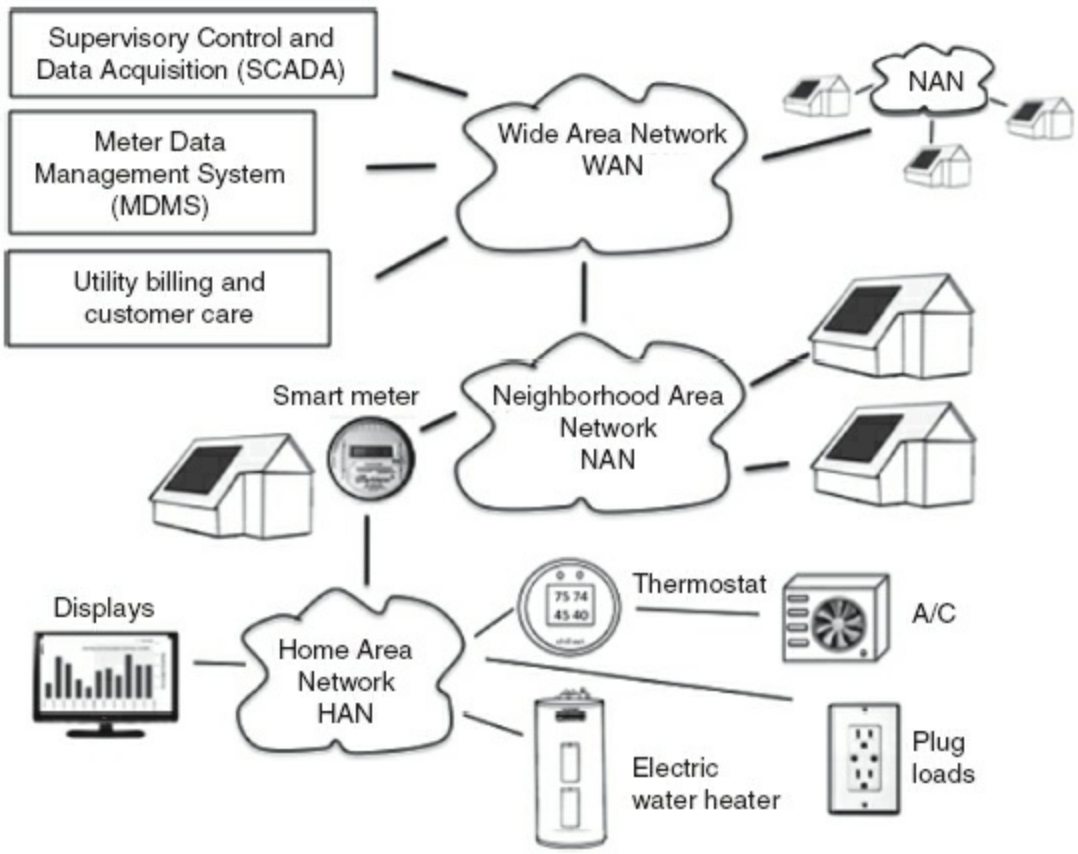
9.2.4 Advanced Metering Infrastructure

The heart of advanced metering infrastructure (AMI) is smart meters themselves, but AMI also includes technologies that enable the two-way flow of information and controls between customers and utilities. The meters themselves are an advance on conventional electromechanical meters in that they can measure and report power demands in near real time rather than the traditional once-a-month, meter-reader, data collection. The attributes of smart meters include

- Remote collection of meter data transmitted to the utility, typically with 15-min intervals, over the power line itself or by a neighborhood radio link. The simplest economic justification for smart meters is the cost savings associated with eliminating manual collection of meter data.
- Remote connect and disconnect signals that allow the utility to transfer account billing when household ownership changes. This would also make possible selective shedding of loads in emergencies. In appropriate situations, it might enable pay-as-you-go utility rates in which customers pay in advance for a certain number of kilowatt hours.
- The ability to collect almost real-time data makes possible new rate structures that can be designed to encourage customers to respond to the varying costs of generation that the utility itself faces. Smart meters make it easier to offer conventional time-of-use rates, which are typically set up with predetermined, fixed prices that depend on the hour of day, day of the week, and season of the year. A more aggressive option is real-time pricing in which the price of electricity more accurately reflects the instantaneous cost of electricity no matter when, and by how much, those costs vary with time. Something in between are critical-peak-pricing schemes in which the utility offers a reduced cost flat-rate or time-of-use schedule for all but a few hours per day, and days per year. On those special days, which are announced on the day before the critical peak price applies, a much higher rate is charged.
- Two-way communication that allows the meter to interact with the household as well as with the utility. Instead of receiving a once-a-month bill that arrives weeks later, customers would be provided with real time information to help encourage efficiency and load management.

Figure 9.5 suggests a framework in which smart meters communicate with the utility through neighborhood area networks (NAN) that are linked to a wide area network (WAN). The WAN connects users to the substation and to the utility. On the other side of the meter, we can envision home area networks (HAN) within households that might enable automatic controls on loads like air conditioners, electric water heaters, smart power strips, and pool pumps. Shedding only a few percent of building loads during peak demand periods can avoid building and operating a significant fraction of expensive peaking generation.

FIGURE 9.5 Smart-metering communication networks.



9.2.5 Demand Response

Smart meters and home area networks make possible new opportunities for managing customer loads. With the ability to remotely turn individual loads on or off, combined with almost real-time price signals or other incentives from the utilities, it is easy to imagine programs that would encourage load shifting away from peaks. Decisions about when to run the dishwasher or do the laundry can be influenced by displays that show the impact on utility bills.

Loads with significant thermal mass change temperature very slowly, so delaying when a water heater, refrigerator, or air conditioner turns on will make little difference to consumers. Delaying or cycling those loads, driven by price signals, can be automated easily. The thermal mass effect can also be put to use as an energy storage option. Chilling a building down a little more than usual during the morning before a coming hot afternoon can be very effective. Curtailment of excess wind power is already an issue in some parts of the country and will become more so as the fraction of renewables on the grid increases. Rather than curtailing renewables, thermostats on electric water heaters can be automatically adjusted to allow elevated storage temperatures.

The largest drivers of peak demand are summer afternoon lighting and cooling loads in buildings. In California, they are responsible for almost all of the diurnal variation in summer demand (Fig. 1.17). Fortunately, major advances in lighting efficiency and controls associated with the development of light-emitting diodes (LEDs) are beginning to reach commercial reality. LED lighting is now more efficient than fluorescents, they last about ten times as long, have no issues with mercury, and they are much more amenable to

dimming. Sensors allow individual fixtures to be dimmed in response to incoming natural daylight or demand response (DR) signals. Waste heat from lighting in commercial buildings adds to the cooling load, so more efficient and controllable lighting can also reduce air conditioner demands.

A recent study by the Electric Power Research Institute (EPRI) evaluated the realistically achievable summer peak demand savings from DR and energy-efficiency measures (EPRI, 2008). They conclude that across the United States these measures can be expected to offset 37% of the electricity load growth and 40% of summer peak demand growth between 2008 and 2030. Stated differently, the expected savings from energy efficiency programs in 2030 is 8.5% of the total electricity load and demand response programs would offset 14% of the summer peak demand. These savings are in addition to what will be achieved through market-driven efficiency, appliance/equipment standards, building codes, and energy legislation.

9.2.6 Dynamic Dispatch

Demand response (DR) refers to load shedding during peak demand periods, which means it is not used that often and when it is, can be viewed as somewhat of an inconvenience. A new concept, called *demand dispatch*, is similar to DR in that it involves turning loads on and off, but it does so almost continuously at all times of the day and at all times of the year. Demand dispatch is analogous to the continuous dispatching of generation assets on the utility side of the meter. Both are meant to balance the generation/load equation. Momentarily turning off a load has the same impact as momentarily increasing the supply. Both generation dispatch and demand dispatch can provide the ancillary service called regulation, or frequency regulation, introduced in Section 1.4.2.

As described by Brooks et al. (2010), demand dispatch takes advantage of the scheduling flexibility of some kinds of loads. For example, a plug-in electric vehicle could have a flexible charging schedule based on the simple goal of assuring the vehicle is fully charged by next morning's departure. Criteria for loads that might be good candidates for demand dispatch include

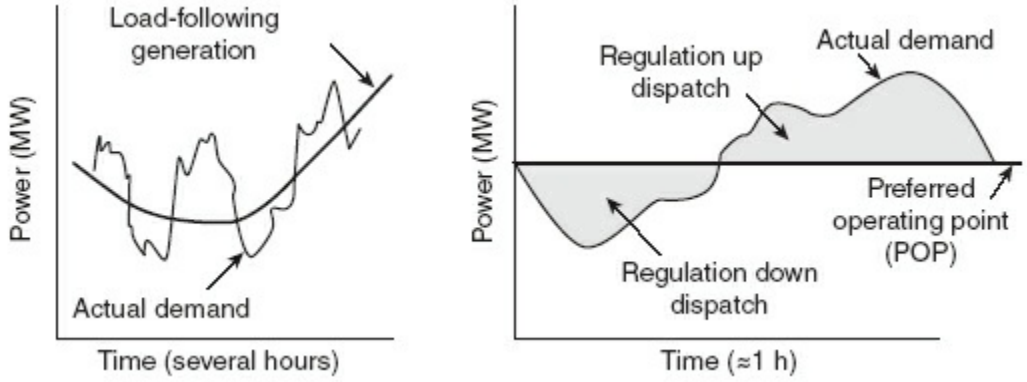
- Energy needed over the next day or so is reasonably well known.
- Power does not need to be drawn continuously to meet that goal.
- Turn-on time is not critical to the consumer; rather, the main goal is to draw the needed energy within a specified time frame.

Good candidates for demand dispatch include dishwashers, washers and dryers, electric water heaters, battery chargers for consumer electronics, defrost cycles on refrigerators, and plug-in electric vehicles. The thought is that in the near future many such devices will have built-in two-way communication capabilities that could allow grid operators to influence when those devices consume energy. Turning one refrigerator on or off would have little value, but if a large number of such dispatchable loads could be aggregated there would be a real potential to address some of the key problems operators face in trying to maintain supply and demand balance on the grid. When a cloud passes over a large collector array, for example, aggregated dispatchable loads could quickly and easily be turned off for a short while without anyone ever noticing a change in their appliance performance.

An even more interesting target for demand dispatch is frequency regulation. Figure 9.6

is a reminder of the difference between the roles played by load-following plants and those that provide regulation services. Most plants can be slowly ramped up and down to track the relatively smooth, predictable diurnal changes in load. It is the constant fine-tuning of load balancing that regulation services provide. Regulation services, which are dispatched at 4-s intervals, can provide *regulation up* power, which means they increase power when necessary, and/or *regulation down* power, which means they decrease power to follow decreasing loads. The key indicator of supply and demand imbalance is the deviation from the desired 60-Hz frequency. When demand exceeds supply, frequency drops; when supply exceeds demand, frequency rises.

FIGURE 9.6 Regulation provides quick-response services to keep generation and load in balance.



Many loads could have the potential to automatically provide regulation down services if they had built-in frequency-sensing capabilities that could adjust power demand during frequency droops. No dispatch signal would be needed. Better control, however, would be realized if loads could be aggregated and controlled by an outside entity. An especially interesting prospect is to imagine aggregating fleets of electric vehicles to provide demand-dispatch services to a utility or grid operator. The vehicle itself, when first plugged in, would provide information to the aggregator about location, battery status, and recharge power capabilities of the charge station. The driver would provide information about the number of miles of range needed and when the charging must be completed. The aggregator would employ algorithms to optimize the provision of services among the many vehicles currently plugged in. The fee for charging would be related to how flexible the vehicle owner is about their charge requirement. In the usual circumstance, someone arrives home in the early evening, plugs in, and needs a few hours of charging by the next morning. The fee for charging would be minimal compared to a midday charge that must be completed while the owner has lunch.

The aggregator, with many vehicles under its control, would respond to load-dispatch commands coming from the grid operator. The aggregator then determines which connected vehicles should be charged for the next few seconds to comply with the operator's command. Realize that regulation services are required 24 h a day, so this regulation service is valuable overnight as well as during peak periods. Providers of regulation services are paid a fee which would go to the aggregator. An example would be something on the order of $35/MW per hour, which could work out to several cents per kWh (Brooks et al., 2010). That is enough to offset a sizable fraction of the cost of vehicle charging.

As electric vehicle charging becomes ever more important, demand dispatch could encourage shifting the preferred operating point (POP in Fig. 9.7) to minimize the need for regulation up and maximize the use of EV demand dispatch. This could spread EV charging over the entire 24-h day without increasing the peak demand for electricity. A Google simulation applying EV demand dispatch to the PJM regional transmission organization indicated the potential to supply 10 kWh/d to 3.2 million vehicles, which is enough for each of them to be driven about 30 mi/d. PJM serves 50 million people, so 3.2 million plug-in vehicles might represent about one-fifth of their fleet. It will be a long time before we have that many EVs on the road.

Calculations by University of Delaware Professor Willett Kempton show electric vehicles selling regulation services 18 h/d could earn significant revenues. Even after accounting for hook-up fees and accelerated battery replacements, they estimate net revenues for owners could easily exceed the cost of electricity to charge those vehicles (Kempton and Tomic, 2005).

9.3 ELECTRICITY STORAGE

As growth in wind, solar, and other renewables progresses, maintaining grid balance will become ever more challenging. With modest penetration rates and better forecasting, the variability in supply when the wind slows or clouds drift over solar plants can be met with a combination of fast-ramping supply options, such as gas turbines and hydroelectric plants. The quest for large-scale stationary electricity storage to supplement those options is well underway. In addition, there is also considerable potential for battery-powered vehicles to provide not only regulation services but also grid storage.

9.3.1 Stationary Battery Storage

As a load management technique, storage allows utilities to shave their power demand peaks and fill the valleys, as is suggested in Figure 9.8. Some of these storage systems would not only help the grid by providing power during times of peak demand but they may also provide ancillary services to the grid including quick-response "spinning" reserves, voltage stability, frequency regulation, and reactive power support.

FIGURE 9.7 Shifting the load-following generation upward increases the potential for regulation-down dispatch to supply plug-in vehicle charging.

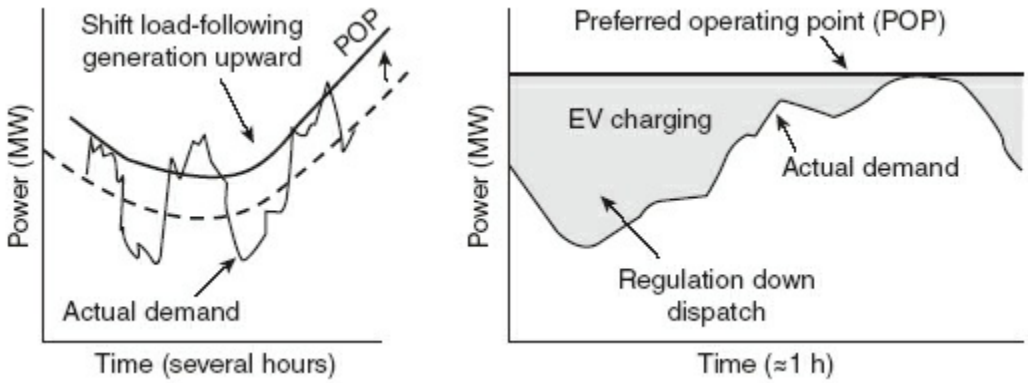
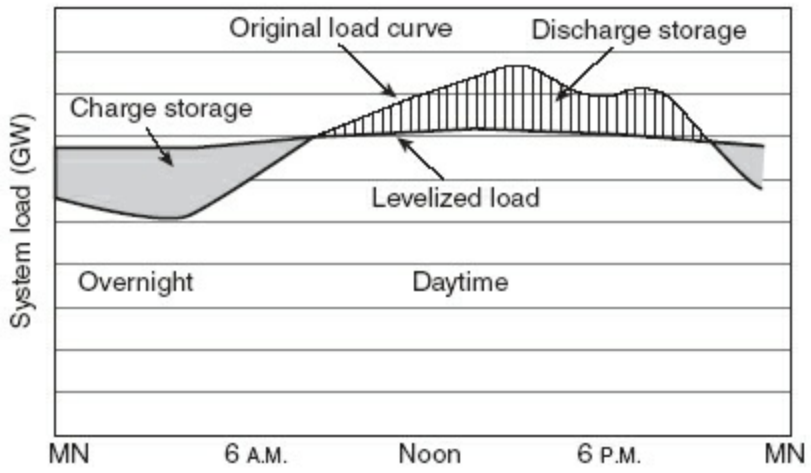
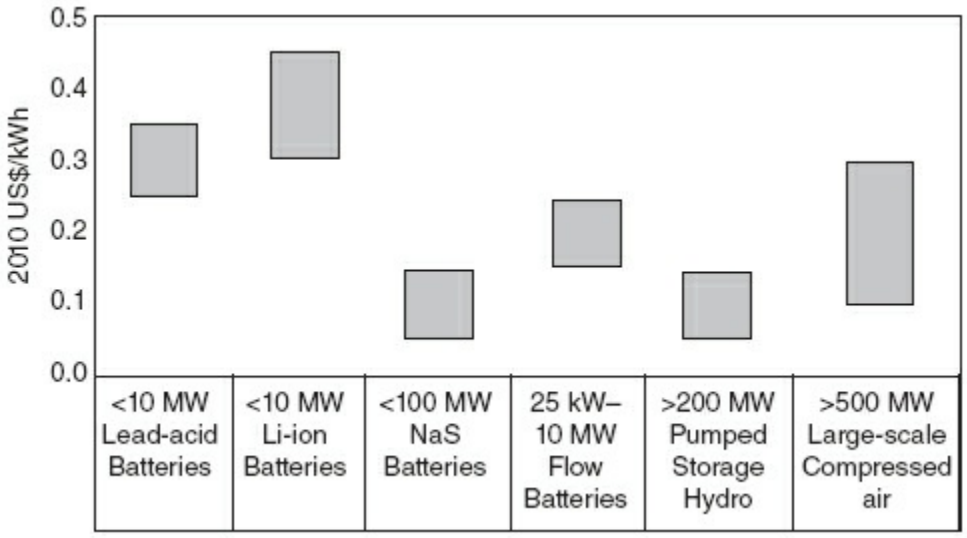


FIGURE 9.8 Storage can absorb power during periods of low demand in order to provide it during peak periods.



Until recently, the only way to provide grid storage has been with conventional hydroelectric dams sometimes augmented with facilities that allow water to be pumped uphill into another reservoir when demand is low, and then running it back down through turbines when demand is high. These pumped-storage systems are difficult to site and have only been cost-effective in large systems, but they are quite efficient (75–85%). New storage options being developed include battery systems, flywheels, ultracapacitors, compressed air energy storage, and reversible electrolyzer/fuel-cells with hydrogen storage. An economic comparison of some of these in terms of cost of per kWh of energy storage is presented in Figure 9.9.

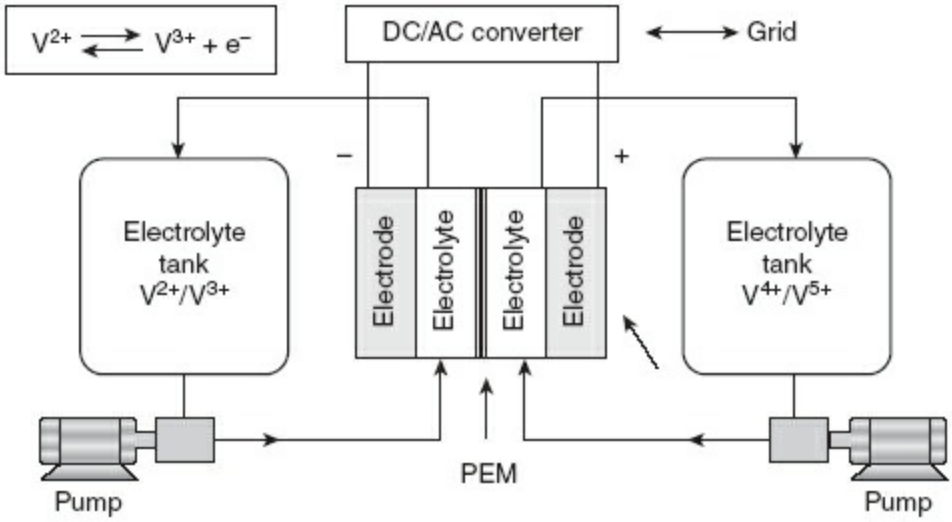
FIGURE 9.9 Comparison of the lifecycle cost of bulk energy storage systems. From IRENA (2012).



An example of a promising battery for stationary applications is the vanadium redox energy system shown in Figure 9.10. This is an example of what is called a *flow battery*, so named because electrolytes stored in large plastic tanks are continuously circulated through the battery cells where the reactions actually take place. Increasing the volume of the tanks increases the energy stored, while increasing the number of cell stacks increases the power

that the system can deliver.

FIGURE 9.10 A vanadium redox flow battery energy storage system.

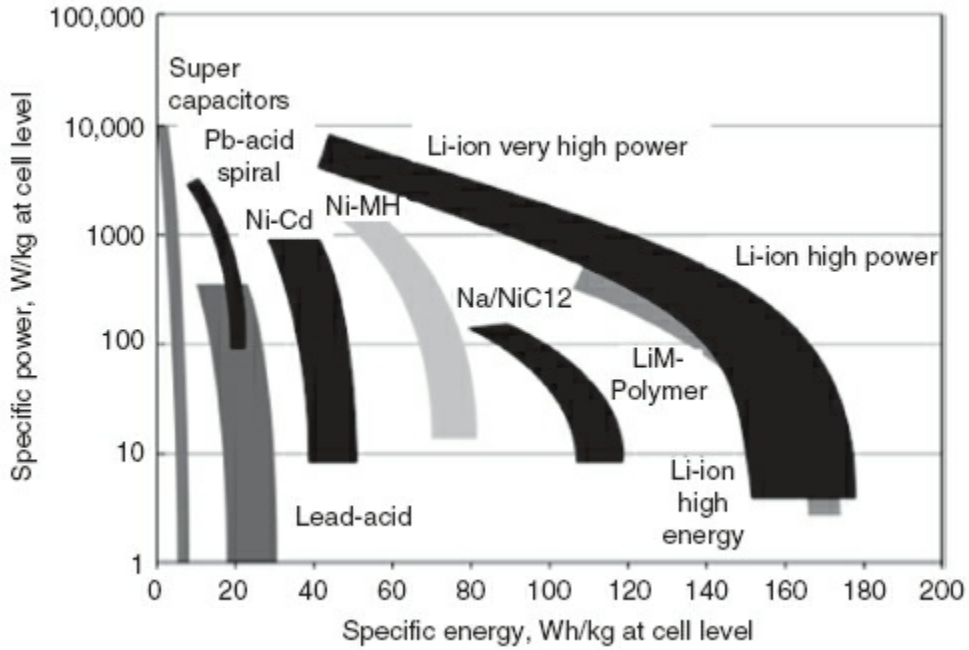


Sodium–sulfur (NaS) is another example of a promising new battery technology tailored to larger-scale grid applications. These batteries have a high energy density, high round-trip efficiencies (89–92%), long cycle life, and their fabrication takes advantage of inexpensive materials. On the downside, these are molten metal batteries that usually operate at very high temperatures (300–350°C). Liquid sodium is corrosive and highly flammable when exposed to air and moisture and there have been several significant fires in early installations. New technologies under development seem likely to allow operation at temperatures below 100°C.

9.3.2 Electric Vehicles and Mobile Battery Storage

There are a number of important attributes of battery systems including cost, weight, volume, cycle lifetime, kWh of storage, and kW of power. Figure 9.11 points out the difference between two key measures, specific power (W/kg) and specific energy (Wh/kg), for a number of battery types. For stationary grid-support systems, weight and volume are less important, but for vehicles both are critical.

FIGURE 9.11 Specific power and specific energy for a number of battery types. Based on data from Johnson Control and SAFT.



Batteries for vehicles need to be small and light. Perhaps it is no surprise to realize that the incredible progress made in laptop and cell phone batteries, where such concerns are of paramount importance, has been found to be transferable to vehicles. The most promising battery technology for vehicles is based on an electrochemical reaction involving lithium ions. As shown in Figure 9.11, lithium-ion batteries have an energy density roughly double that of nickel–metal-hydride (NiMH), quadruple the density of nickel–cadmium (NiCd), and ten times that of conventional lead–acid batteries.

Lithium-ion batteries are actually a family of technologies. The first successful generation had a lithium-carbon anode and a lithium-cobalt-oxide (Li_xCoO_2) cathode. The basic reactions describing their operation in which one electron transfers from anode to cathode during discharge are

$$\begin{aligned} &\text{Anode } (-): \quad LiC \rightarrow Li^+ + e^- + C \\ &\text{Cathode } (+): \quad Li^+ + e^- + Li_xCoO_2 \rightarrow Li_{1+x}CoO_2 \end{aligned} \tag{9.1}$$

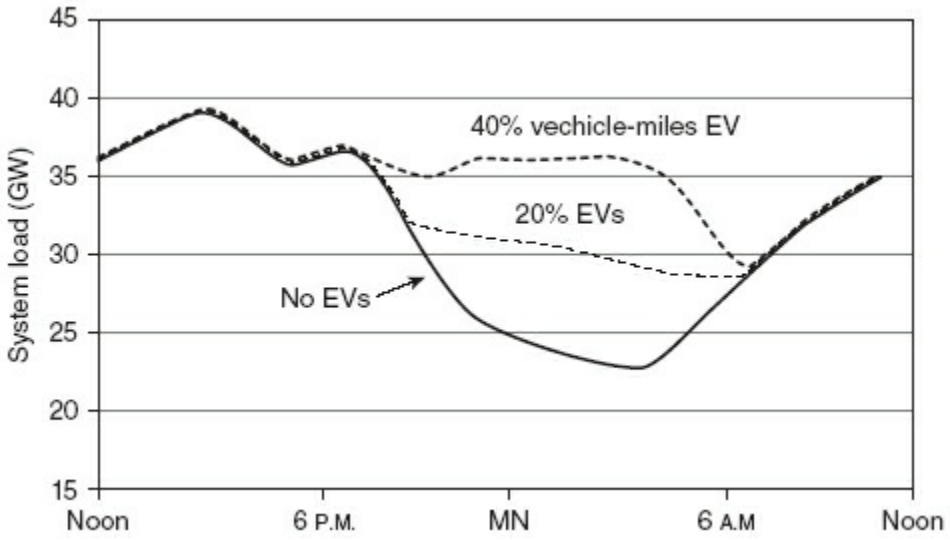
The reactions shown in Equation 9.1 show the cathode using a cobalt oxide, but other materials are in use including lithium iron phosphate ($LiFePO_4$), lithium nickel oxide ($LiNiO_2$), and lithium manganese oxide ($LiMn_2O_4$). The specific energy for these various materials ranges from about 0.15 to 0.25 kWh/kg. Work on other Li-ion technologies suggests the potential to transfer two, or even three, electrons per cathode reaction, which greatly reduces the amount of heavy cathode material required and greatly increases their potential for future improvements in energy density.

With the development of these new lightweight, powerful batteries, the dream of electric vehicles has become a reality, and with that reality comes new attention to possible interactions between vehicles and the grid. Two versions of electric-drive vehicles have emerged. A plug-in hybrid electric vehicle (PHEV) is basically a conventional hybrid-electric vehicle with extra batteries added to extend the number of miles that can be driven on electricity before the backup internal combustion engine (ICE) has to kick in. Their competition are all-electric battery-powered vehicles (BEVs) that eliminate most of the

complexities that go with PHEVs, but which do not have the added comfort of a having a gas tank. Together these are often just described as plug-in vehicles or electric-drive vehicles. The advantages of electric-drive vehicles include helping to reduce our dependence on oil, which is of enormous importance as an economic and national security issue, improved air quality and health benefits, and reducing overall climate-changing carbon emissions.

Ideally, for either PHEVs or BEVs, batteries would be charged from the grid at night, when demand and prices are low, and discharged during the day while the vehicle is in use. Figure 9.12 shows a simple analysis of what this "valley-filling" might look like. It has been estimated that the idle capacity of the U.S. grid could supply nearly three-fourths of the energy needs of today's light-vehicle fleet as electrics without needing new capacity or transmission (Kintner-Meyer, 2007).

FIGURE 9.12 Impacts of night charging for electric vehicles in California in the spring. Based on 3 mi/kWh and 280 billion vehicle/mi/yr.



The impacts of EVs on the grid extend beyond the concern for raising peak demand. Their power requirement during charging is also important. Table 9.1 shows representative values of power draw for various levels of charge rate. Level I charging is ordinary 120-V household power, Level II includes charging power up to 14.4 kW, and anything above that is often referred to as Level III. The table shows how many miles of range could be achieved per hour of charging under the assumption that each kWh of power delivered to the batteries will provide 3 mi of driving range.

TABLE 9.1 Examples of Charge Rates for Plug-in Vehicles[a]

Level	Typical Location	Voltage	Current (A)	Power (kW)	Miles per Hour of Charging
Level I	Residential	120	15	1.8	5.4
Level II	Residential	240	30	7.2	22
Level II	City street	240	60	14.4	43
DC fast charge	Highway	500	120	60	180

[a]Assumes 3 mi/kWh.

With each EV drawing about 7 kW while being charged at home on a 240-V circuit, there can be significant near-term issues with their impact on local feeders. Suppose the power draw along a typical residential feeder line averages something like 7 kW per household. That means each new EV charging at 240 V is like adding another household to the line. Feeder lines typically have individual transformers that serve about 6–12 houses. If a cluster of homes, each being fed by the same transformer on a nearby power pole, adds a few EVs all being charged at the same time, the transformer could be inadequate and fail.

It is interesting to contemplate the implications of EVs not only buying power, but also delivering power to the grid. Realize that a typical car is used only about 1 h/d, so it is parked somewhere almost all of the time. Plugged into an ordinary 240-V, 30-A home circuit, an EV could potentially sell or buy about 7 kW of power to or from the grid. If each of the 130 million households in the United States had one EV, their total power capacity would be comparable to the entire U.S. grid. Such vehicle-to-grid (V2G) systems would not be used for baseload power since it is much cheaper to provide that with conventional generators, but properly organized and controlled V2G could provide large amounts of quick-response, high value grid services.

9.4 DEMAND SIDE MANAGEMENT

In the 1980s, regulators began to recognize that energy conservation could be treated as a "source" of energy that could be directly compared with traditional supply sources. If utilities could help customers be more efficient in their use of electricity, delivering the same energy service with fewer kilowatt-hours, and if they could do so at a lower cost than supplying energy, then it would be in the public's interest to encourage that to occur. What emerged is a process called *integrated resource planning* (IRP), or as it is sometimes referred to, *least-cost planning* (LCP).

The new and defining element of IRP was the incorporation of utility programs that were designed to control energy consumption on the customer's side of the electric meter. These are known as demand-side management (DSM) programs. While DSM most often refers to programs designed to save energy, it has been defined in a broader sense to refer to any program that attempts to modify customer energy use. As such it includes

- *Conservation/energy efficiency programs* that have the effect of reducing consumption during most or all hours of customer demand.
- *Load management programs* that have the effect of reducing peak demand or shifting electric demand from the hours of peak demand to non-peak time periods.
- *Fuel substitution programs* that influence a customer's choice between electric or natural gas service from utilities. For example, the electricity needed for air conditioning can be virtually eliminated by replacing a compressive refrigeration system with one based on absorption cooling.

DSM programs have included a wide range of strategies such as energy information programs, including energy audits; utility rebates on energy-efficient appliances and other devices; incentives to help energy service companies (ESCOs) reduce commercial and industrial customer demand; load control programs to remotely control customer appliances such as water heaters and air conditioners; and tariffs designed to shift or reduce

loads (time-of-use rates, demand charges, real-time pricing, interruptible rates).

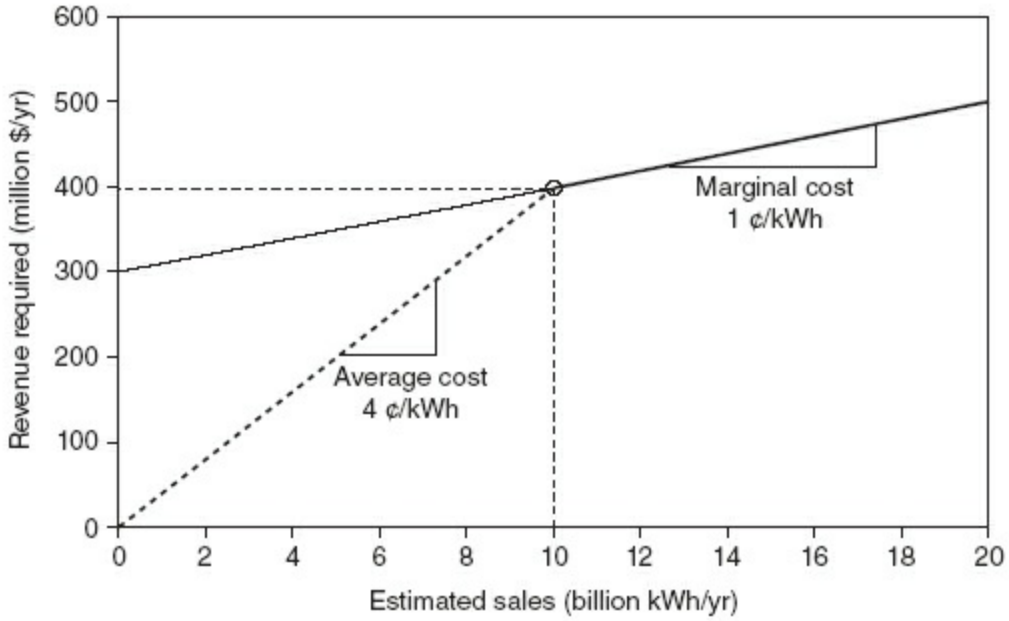
9.4.1 Disincentives Caused by Traditional Ratemaking

Electric utilities have traditionally made their money by selling kilowatts of power and kilowatt-hours of energy, so the question arises as to how they could possibly find it in their best interests to sell less, rather than more, electricity? To understand that challenge, we need to explore the role of state-run public utility commissions (PUCs) in determining the rates and profits investor-owned utilities (IOUs) have traditionally been allowed to earn.

A fairly common ratemaking process is based on utilities providing evidence for the costs and the expected demand to their PUC in what is usually referred to as a general rate case. General rate cases often focus only on the nonfuel component of utility costs (depreciation of equipment, taxes, nonfuel operation and maintenance costs, return-on-investment, and general administrative expenses). Dividing these revenue requirements by expected energy sales results in a base case ratepayer cost per kWh. Fuel costs, which may change more rapidly than the usual schedule of general rate case hearings, may be treated in separate proceedings. In general, changes in fuel costs are simply passed on to the ratepayers as a separate charge in their bills.

To understand how this process encourages sales of kWh, and discourages DSM, consider the simple graph of (nonfuel) revenue requirements versus expected energy sales shown in Figure 9.13 (similar to Fig. 1.29). In this example, the utility has a fixed annual revenue requirement of $300 million needed to recover capital costs of equipment along with other fixed costs, plus an additional amount that depends on how many kilowatt-hours are generated. In this example, each additional kilowatt-hour of electricity generated costs an additional amount of one cent. That 1 ¢/kWh is called the *short-run marginal cost*, which means it is based on operating existing capacity longer. There is also *long-run marginal cost*, which applies when the additional power needed triggers an expansion of the existing power plants, transmission lines, or distribution system.

FIGURE 9.13 Estimated sales of 10 billion kWh would require $400 million in revenue, so the (nonfuel) base rate would be 4 ¢/kWh.



If the utility in Figure 9.13 projects that it will sell 10 billion kWh/yr, then annual revenue of $400 million would be needed. The ratio of the two is an average base rate of 4 ¢/kWh, which is what the utility would be allowed to charge until the next general rate case is heard.

Consider now the perverse incentives that would encourage this utility to sell more kWh than the 10 billion estimated in Figure 9.13. Having established a price of 4 ¢/kWh, any sales beyond the estimated 10 billion kWh/yr would yield revenues of 4¢ for each extra kWh sold. Since each extra kWh generated has a marginal cost of only 1¢, and it is being sold at 4¢, there will be a net 3¢ profit for each extra kWh that can be sold.

Note too, that the example utility loses money if it sells less than 10 billion kWh. Generating one fewer kWh reduces costs by 1¢, but reduces revenue by 4¢. In other words, this rather standard practice of ratemaking not only encourages utilities to want to sell more energy, it also strongly discourages conservation that would reduce those sales.

9.4.2 Necessary Conditions for Successful DSM Programs

As the above example illustrates, traditional ratemaking has tended to reward energy sales and penalize energy conservation, no matter what the relative costs of supply- and demand-side options might be. During the 1980s and early 1990s, energy planners and utility commissions grappled with the problem of finding fair and equitable ratemaking procedures that would reverse these tendencies, allowing cost-effective energy efficiency to compete. Three conditions were found to be necessary for DSM to be successful:

- Decoupling utility sales from utility profits.
- Recovery of DSM program costs to allow utilities to earn profits on DSM.
- Incentives to encourage utilities to prefer DSM over generation.

While there are several approaches that regulators have taken to decouple utility profits from sales, the *electric rate adjustment mechanism* (ERAM) is a good example of one that works quite effectively. ERAM simply incorporates any revenue collected above or below one year's forecasted amount into the following year's authorized base rate revenue, thereby

eliminating incentives to sell more kWh and removing disincentives to reduce kWh sales. Clearly, decoupling is a necessary condition for DSM to work, but it is not sufficient.

The second condition allows utilities to earn profits on demand-side programs just as they do on supply-side investments. Recovery of DSM program costs can be accomplished by including them in the rate base alongside capital costs of power plants and other utility infrastructure. In this way, supply-side and demand-side investments would both earn whatever rate of return the regulators would allow. Alternatively, DSM costs might be included as an expense that is simply passed along to the ratepayer.

Experience has shown that just decoupling sales and profits, along with rate-basing or expensing DSM costs, does not provide sufficient encouragement for utilities to actively pursue customer energy efficiency. Additional incentives for the utilities and their stockholders seem to be needed. Shared savings programs have emerged in which shareholders are allowed to keep some fraction of the net savings that DSM programs provide. The following example illustrates this idea.

Example 9.1 A Shared Savings Program. Suppose a utility offers a $2 rebate on 18-W, 8000-h, compact fluorescent lamps (CFLs) that produce as much light as the 75-W incandescents they are intended to replace. Suppose it costs the utility an additional $1 per CFL to administer the program. The utility has a marginal cost of electricity of 3 ¢/kWh and 1 million customers are expected to take advantage of the rebate program.

If a shared savings program allocates 15% of the net utility savings to shareholders and 85% to ratepayers, what would be the DSM benefit to each?

Solution

Energy savings = (75 – 18) W/CFL × 8 kh × $0.03/kWh × 10^6 CFL = $13.68 million

Program cost = ($2 + $1)/CFL × 10^6 CFL = $3 million

Net savings to utility = $13.68 – $3 million = $10.68 million

Shareholder benefit = 15% × $10.68 million = $1.60 million

Ratepayer savings = 85% × $10.68 million = $9.08 million

In the above example, it was quite easy to calculate the energy savings associated with replacing 75-W incandescents with 18-W CFLs, assuming their rated 8000-h lifetime is realized. For many other efficiency measures, however, the savings are less easy to calculate with such confidence. Exactly how much air conditioning will be saved by upgrading the insulation in someone's home, for example, is not at all easy to predict.

Further complicating load reduction estimates are the problems of *free riders* and *take backs*. Free riders are customers who would have purchased their energy efficiency devices even if the utility did not offer an incentive. In the above example, it was assumed that all 1 million rebates went to customers who would not have purchased CFLs without them. Take backs refer to customers who change their behavior after installing energy-efficiency devices. For example, after insulating a home, a user may be tempted to turn down the thermostat in the summer—thereby negating some fraction of the energy savings. While free riders, take backs, and uncertainties in estimating energy savings may result in less DSM value to the utility than anticipated, one can argue that these are more than offset by the environmental advantages of not generating unneeded electricity. Some utilities have, in

fact, tried to incorporate environmental externalities into the avoided-cost benefits of DSM.

9.4.3 Cost-Effectiveness Measures of DSM

The goal of integrated resource planning is to minimize the cost to customers of reliable energy services by suitably incorporating supply-side and demand-side resources. A proper measure of cost-effectiveness on the demand side, unfortunately, is largely in the eyes of the beholder; that is, the most cost-effective DSM strategy for stockholders may be different from the best strategy as seen by utility customers. In fact, utility customers can also see things differently depending on whether the customer is someone who takes advantage of the conservation incentives or whether it is a customer who either cannot, or will not, take advantage of the benefit (e.g., they already purchased the most efficient refrigerator on their own before an incentive was offered). To account for such differences of perspective, a number of standardized DSM cost-effectiveness measures have been devised.

The *ratepayer impact measure* (RIM) test is primarily a measure of what happens to utility rates as a result of the DSM program. For a DSM program to be cost-effective using the RIM test, utility rates must not increase. That is, even nonparticipants must not see an increase in their electric bills (or at least a lower increase than they would have seen without DSM), which is why this is sometimes referred to as the *no-losers test*. Clearly, this is a difficult test to pass.

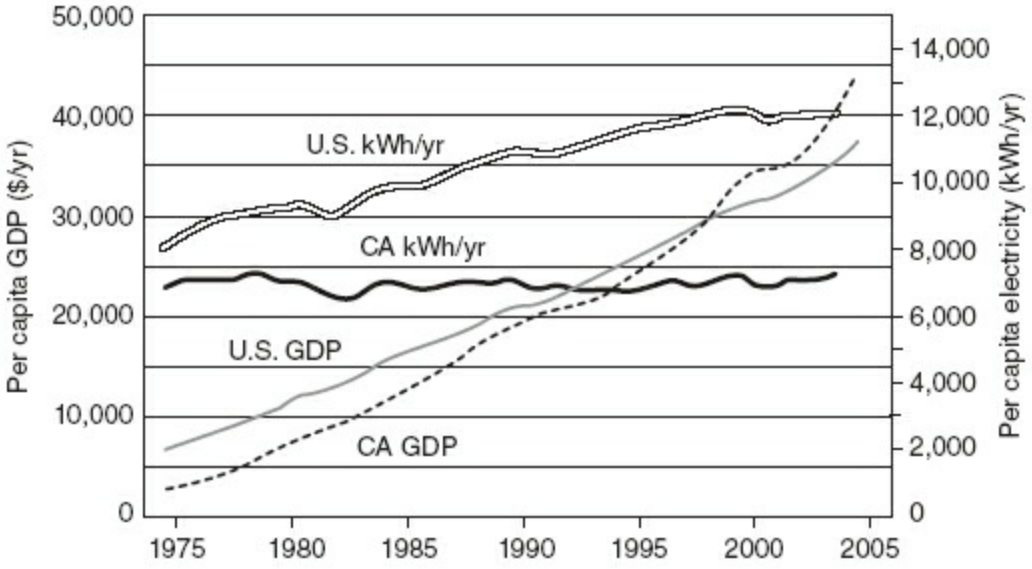
The *total resource cost* (TRC) test asks whether society as a whole is better off with DSM. It is again a cost–benefit calculation in which benefits result from reduced costs of fuel, operation, maintenance, and transmission losses, as well as a potential reduction in the needed power plant capacity, as before. Total costs are somewhat different since they include not only the DSM administrative costs incurred by the utility but they also add any extra cost the customer pays when purchasing the more efficient product. For measures passing the TRC test, utility *rates* may go up or down, but the average utility *bills* will decrease. Nonparticipants may see an increase in their bills, but the savings by those that participate must at least offset that increase. The TRC test is the most commonly used measure of DSM cost-effectiveness. A variation on the TRC test is called the *societal test*, the difference being that it includes quantified impacts of environmental externalities in the cost and benefit calculations.

The *utility cost test* (UCT) is similar to the TRC test in that it compares the costs and benefits of DSM, but it does so only from the perspective of the utility itself. Since this is a utility perspective, the cost of DSM includes both the rebate and the administrative costs. If UCT is satisfied, total energy bills go down, rates may go up or down so nonparticipants may see higher bills. Participants will see lower energy bills but, after paying for more expensive equipment, may end up paying more for the same energy service (e.g., illumination).

Perhaps the most persuasive demonstration of the impact of efficiency programs on the customer's side of the meter is shown in Figure 9.14. California led the way on decoupling of utility profits from sales, adopting least-cost planning methods to allow energy efficiency to compete with energy supply, and encouraging cost-effective DSM with additional incentives to shareholders. Those utility programs, along with aggressive appliance and building efficiency standards, has kept its per capita electricity demand almost constant for

3 decades during which time it continued to grow throughout most of the rest of the country. And it did so with a greater rate of per capita GDP growth as well.

FIGURE 9.14 A comparison of California's per capita electricity demand and GDP with the rest of the nation. From California Energy Commission.



9.5 ECONOMICS OF ENERGY EFFICIENCY

Two approaches have evolved to describe the potential economic impact of energy efficiency programs. Energy conservation supply curves demonstrate the cumulative impact of multiple efficiency measures, with results expressed in terms of how much it costs to save a kilowatt-hour. The *cost of conserved energy* (CCE, $/kWh) is directly analogous and comparable to the $/kWh cost of generation. The second approach uses CCE to evaluate the cost of using efficiency as a way to reduce greenhouse gas (GHG) emissions.

9.5.1 Energy Conservation Supply Curves

By converting all of the costs of an energy efficiency measure into a uniform series of annual costs and dividing that by the annual energy saved, a convenient and persuasive measure of the value of saved energy can be found. The resulting cost of conserved energy (CCE), which has units of $/kWh, is also sometimes referred to as the cost of saved energy (CSE).

$$\text{CCE} = \frac{\text{Annualized cost of conservation (\$/yr)}}{\text{Annual energy saved (kWh/yr)}} \tag{9.2}$$

When the only cost of the conservation measure is the extra initial capital cost, the annualized cost of conservation in the numerator is easy to obtain using an appropriate capital recovery factor (CRF). In more complicated situations, it may be necessary to do a levelized cost analysis in which the present value of all future costs is obtained, and then that is annualized using CRF and a fuel-savings levelizing factor.

Example 9.2 CCE for a Lighting Retrofit Project. Suppose it costs $60 in parts and labor to put in new lamps and replace burned-out ballasts in a conventional 4-lamp fluorescent fixture. For $75, more efficient ballasts and lamps can be used in the replacement, which will maintain the same illumination but will decrease the power needed by the fixture from 150 to 100 W. For an office in which the lamps are on 3000 h/yr, what is the CCE for the better system if it is financed with a 10-year, 6% loan assuming the new components last at least that long? Electricity from the utility costs 10 ¢/kWh.

Solution. The extra cost is $75 – $60 = $15. From Equation 1.7 the CRF is

$$\text{CRF}\ (6\%, 10\ \text{yr}) = \frac{i(1+i)^n}{(1+i)^n - 1} = \frac{0.06(1.06)^{10}}{(1.06)^{10} - 1} = 0.13587/\text{yr}$$

The annualized cost of the improvement is

$$A = P \times \text{CRF}\ (i, n) = \$15 \times 0.13587/\text{yr} = \$2.038/\text{yr}$$

The annual energy saved is

$$\text{Saved energy} = \frac{(150 - 100)\ \text{W} \times 3000\ \text{h/yr}}{1000\ \text{W/kW}} = 150\ \text{kWh/yr}$$

The cost of conserved energy is

$$\text{CCE} = \frac{\$2.038/\text{yr}}{150\ \text{kWh/yr}} = \$0.0136/\text{yr} = 1.36\ ¢/\text{kWh}$$

The choice is therefore to spend 10¢ to purchase 1 kWh for illumination or to spend 1.36¢ to avoid the need for that kWh. In either case, the amount of illumination is the same. Note, too, that there will also be a reduction in demand charges with the more efficient system.

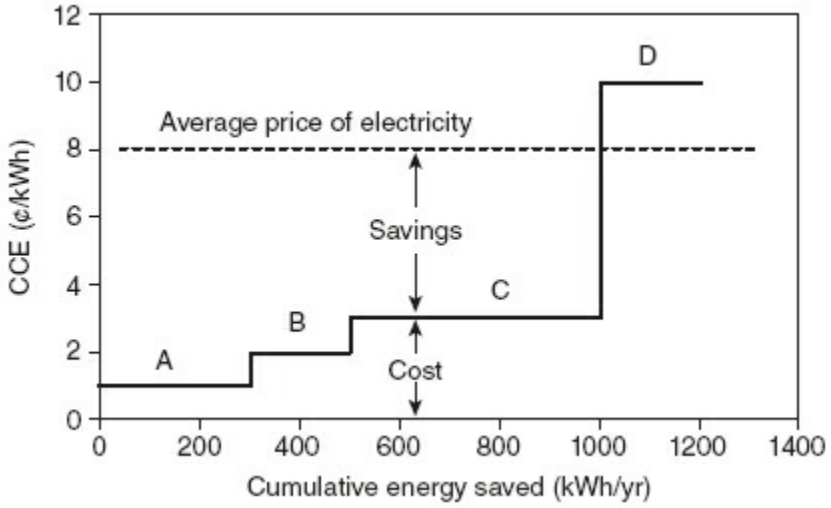
While CCE provides a straightforward measure of the economic benefits of a single efficiency improvement for an individual or corporation, it has greater application as a policy tool for energy forecasters. By analyzing a number of efficiency measures and then graphing their potential cumulative savings, policy makers can estimate the total energy reduction that might be achievable at a cost less than that of purchased electricity.

To illustrate the procedure, consider four hypothetical conservation measures A, B, C, and D. Suppose they have individual costs of conserved energy and individual annual energy savings values as shown in Table 9.2. If we do measure A, 300 kWh/yr will be saved at a cost of 1 ¢/kWh. If we do A and B another 200 kWh/yr will be saved (assuming these are independent measures for which the energy savings of one does not affect the savings of the other) for a total of 500 kWh/yr saved. Similarly total costs can be added up, so, for example, doing all four measures will save 1200 kWh/yr at total cost of 4200 ¢/yr. That is an average cost of 3.5 ¢/kWh. A plot of the marginal CCE (¢/kWh) versus the cumulative energy saved (kWh/yr) is called an *energy conservation supply curve*. Such a curve for the above example is presented in Figure 9.15.

TABLE 9.2 Hypothetical Example of Four Independent Conservation Measures

Conservation Measure	CCE (¢/kWh)	Saved Energy (kWh/yr)	Cumulative Energy Saved (kWh/yr)	Cumulative Cost (¢/yr)	Average Cost (¢/kWh)
A	1	300	300	300	1
B	2	200	500	700	1.4
C	3	500	1000	2200	2.2
D	10	200	1200	4200	3.5

FIGURE 9.15 Energy conservation supply curve for the example in Table 9.2.

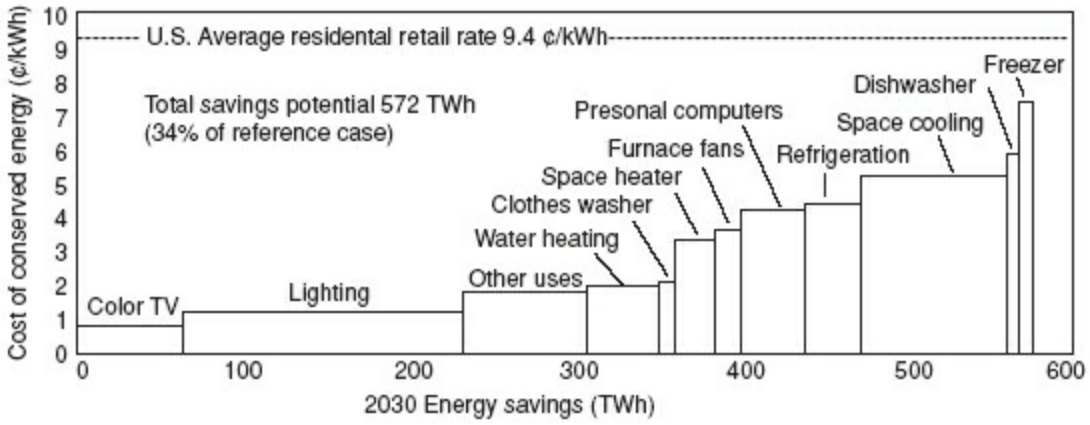


One of the important advantages of these energy conservation supply curves is their derivation does not depend upon any assumptions about the cost of competing generation technologies. Having derived the curve it can now be used to compare it with whatever utility rates or generation technologies are locally important.

Continuing the example, suppose the cost of electricity for this customer is 8 ¢/kWh as shown in Figure 9.15. Measures A, B, and C each save energy at less than that cost, and so it would be cost-effective to implement those three, saving a total of 1000 kWh/yr. Measure D, which costs 10 ¢/kWh, is not cost-effective since it would be cheaper to purchase utility electricity at 8¢. But, what if we did all four measures at the same time? A total of 1200 kWh/yr would be saved at a total cost of 4200 ¢/yr, for an *average* CCE of 3.5 ¢/kWh. On the one hand, it might be argued that when the marginal cost of an efficiency measure is above the cost of purchased electricity it should not be implemented. On the other hand, the full package of measures still saves money at today's cost of electricity; purchased electricity will likely cost more in the future, and the cost of externalities that society must pay has been ignored. The point is both arguments will be encountered, so it is important to be clear about whether assertions about cumulative energy efficiency potential are based on marginal CCE or average CCE.

An example of a real conservation supply curve is shown in Figure 9.16. The biggest single target, lighting, could be reduced in 2030 by an estimated 169 billion kWh at a cost of 1.2 ¢ per kWh of saved energy. An overall investment in lighting of $2 billion would save $14 billion at today's residential retail rate of 9.4 ¢/kWh. In this study, if all of the measures shown in the figure were deployed, for an investment of $5.2 billion they could save 572 billion kWh/yr in 2030, which is 30% of their baseline demand.

FIGURE 9.16 U.S. residential electric savings potential for 2030. Combined savings would reduce 2030 demand by 572 TWh/yr. From Brown et al. (2008).



9.5.2 Greenhouse Gas Abatement Curves

An energy conservation supply curve can be flipped over to form the basis for a very persuasive way to present the cost of greenhouse gas (GHG) abatement. CCE tells us what it would cost to save energy. The difference between a CCE value and the energy cost that would have been incurred if the measure were not adopted is a nice measure of the dollar savings that the efficiency measure provides (Fig. 9.15). If we then attach a carbon emission rate to those energy savings, we can get a cost of carbon abatement. This is often a negative number. Negative-cost abatements that efficiency offers can often help offset the positive costs of other clean technologies such as wind and solar power.

Example 9.3 GHG Abatement Cost. A lighting retrofit for a large commercial building has a total project cost of $3.2 million, financed with a simple 5%, 30-year note. It is projected to save 4.5 million kWh/yr. The local utility charges $0.12/kWh and it has an overall carbon emission factor of 0.5 kg CO_2/kWh (about half that of a coal plant).

Ignoring other potential financial incentives, find the CCE and the cost of carbon abatement.

Solution. From Equation 1.7, the amortized cost is

$$A = P \cdot \text{CRF}(5\%, 30\text{ yr}) = \$3.2 \times 10^6 \left[\frac{0.05(1.05)^{30}}{(1.05)^{30} - 1}\right] = \$208,165/\text{yr}$$

Savings on the electricity bill will be

$$\text{Savings} = 4.5 \times 10^6\ \text{kWh/yr} \times \$0.12/\text{kWh} = \$540,000/\text{yr}$$

The cost of conserved energy will be

$$\text{CCE} = \frac{\$208,165/\text{yr}}{4.5 \times 10^6\ \text{kWh/yr}} = \$0.046/\text{kWh}$$

Annual net cost will be

$$\text{Net cost} = \$208{,}165/\text{yr} - \$540{,}000/\text{yr} = -\$331{,}835/\text{yr}$$

Carbon savings will be

$$4.5 \times 10^6 \text{ kWh/yr} \times 0.5 \text{ kg } CO_2/\text{kWh} = 2.25 \times 10^6 \text{ kg } CO_2/\text{yr}$$

At 1000 kg per metric ton (t), that is a carbon reduction of 2250 t/yr.

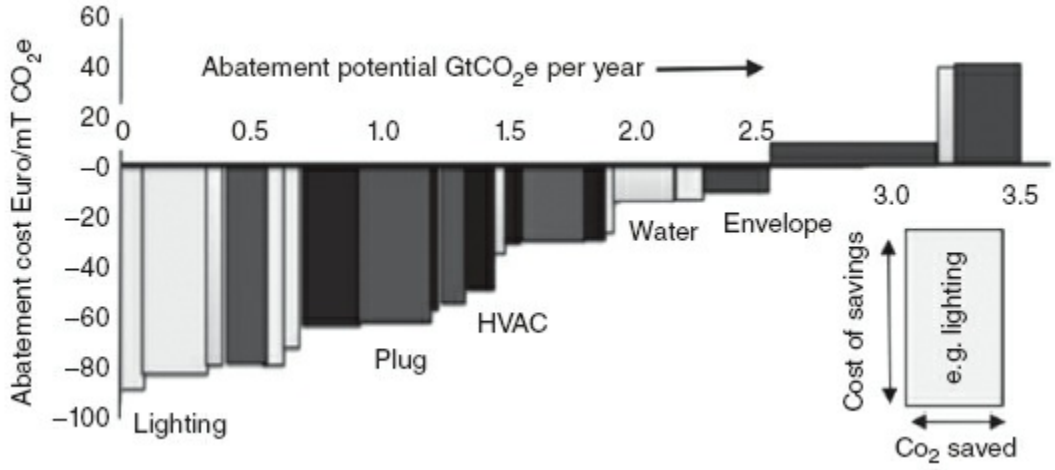
Cost of carbon abatement will be

$$\text{Abatement cost} = \frac{-\$331{,}835/\text{yr}}{2250 \text{ t } CO_2/\text{yr}} = -\$147.5/\text{t } CO_2$$

Yes, that is a minus sign. And these are actual data from a real project in San Francisco.

Just as it is useful to create a figure that shows the cumulative effects of increasing energy efficiency with an energy conservation supply curve (e.g., Fig. 9.16), a similar approach can be taken for cumulative abatement costs of GHGs. By stacking rectangles, each representing a particular abatement technique, with width being the annual gigatons (Gt) of CO_2e saved (the e means GHG equivalents) and its height being the cost in Euros per metric ton, a cost of carbon abatement curve is created. McKinsey & Company has produced a number of these very influential abatement curves. Figure 9.17 shows their graph of the global GHG abatement potential for the building sector in 2030. Their estimated reduction below their baseline scenario for the building sector could total 3.5 Gt CO_2e/yr at an average negative cost of –32 Euros per metric ton.

FIGURE 9.17 Global greenhouse gas abatement curve for the buildings sector, 2030. Redrawn from McKinsey & Company (2009).



The 2009 McKinsey global carbon abatement analysis for all sectors concludes there is potential by 2030 to reduce GHG emissions by 35% compared with 1990 levels, which would be sufficient to have a good chance of holding global warming below the 2°C threshold that the Intergovernmental Panel on Climate Change (IPCC) believes is necessary if we are to avoid very serious climate change impacts. They estimate the annual costs to accomplish this goal at 200–350 billion Euros, which is less than 1% of forecasted global GDP in 2030.

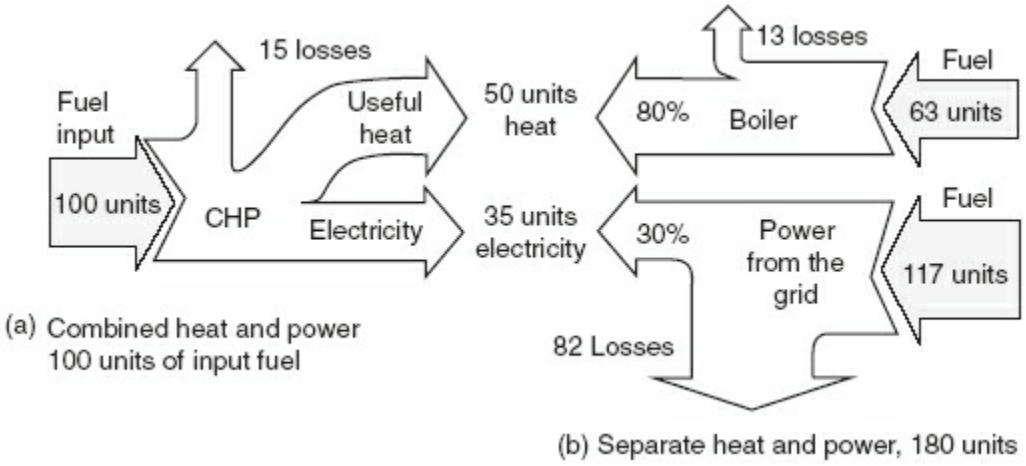
9.6 COMBINED HEAT AND POWER SYSTEMS

The analysis of heat engines that leads to the Carnot efficiency limit (Section 8.2.1) assumes the only output that is useful is the work or electricity produced by the engine. While there is nothing wrong with that analysis, it ignores the potential benefits associated with capturing and using the heat rejected by the engine. Such waste heat can be used for water heating, space heating of buildings, or process heat for industry. It can also be used to cool buildings. Systems that produce both electricity and useful thermal energy in a sequential process from a single source of fuel used to be mostly referred to as *cogeneration* systems, but they now are more often called *combined-heat-and-power* (CHP) systems.

9.6.1 CHP Efficiency Measures

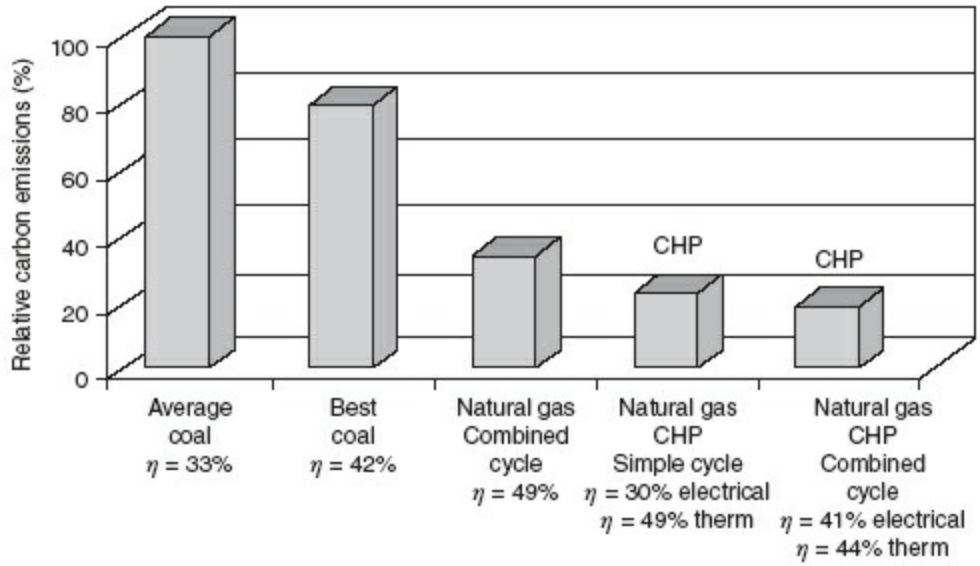
A representative example of the efficiency benefit associated with CHP systems is shown in Figure 9.18. In this example, a CHP system with 100 units of input energy delivers 35 units of electricity and 50 units of useful waste heat, for an overall efficiency of 85%. If the same 35 units of electricity were to be delivered from a 30%-efficient utility grid, and a separate 80%-efficient boiler delivers the same 50 units of useful heat, a total of 180 units of fuel would be needed.

FIGURE 9.18 In this example, the combined heat and power (CHP) system needs only 100 units of fuel to deliver the same electricity and useful heat as 180 units from the grid and a boiler.



Burning a fuel to generate electricity and then capturing and utilizing waste heat can reduce primary energy demand by something like 40% compared to separate grid electricity and fuel-fired boilers. Those efficiency gains translate into GHG reductions as well. Figure 9.19 makes that point by comparing carbon emissions from conventional power plants with emissions from simple-cycle and combined-cycle plants designed for CHP. As shown there, replacing a conventional coal-fired power plant with a natural-gas-fired combined-cycle CHP plant reduces carbon emissions by over 80%.

FIGURE 9.19 Comparing carbon emissions for plants with and without combined heat and power (CHP). Waste heat is assumed to displace an 83%-efficient boiler.



Higher temperature heat is more versatile since it can be used in a variety of applications such as process steam, absorption cooling, and space heating, while simple water heating may be the only application of low temperature heat. Distance from generator to load is also important since transporting heat more than a few hundred meters can be costly and wasteful. Finding applications where the timing and magnitude of electric and thermal demands are aligned can greatly affect the economics of cogeneration. For example, if the thermal application is for space heating alone, then the heat may have no value all summer long, whereas if it is used for space heating and cooling, it may be useful all year round. Applications to steady heat demands in industrial processing are prime targets for cogeneration. And finally, if the waste heat is displacing the need to purchase an expensive fuel, such as propane or electricity, rather than inexpensive natural gas, the overall economics are obviously enhanced.

9.6.2 Economics of Combined Heat and Power

With combined heat and power, it is a little tricky to allocate the costs and benefits of the plant since the value of a unit of electricity is so much higher than a unit of thermal energy, yet both will be produced with the same fuel source. This dilemma requires some creative accounting.

The simplest approach to describe the efficiency of a cogeneration plant is to simply divide the total output energy (electrical plus thermal) by the total thermal input, remembering to use the same units for each quantity.

$$\text{Overall thermal efficiency} = \frac{\text{Electrical} + \text{Thermal output}}{\text{Thermal input}} \tag{9.3}$$

While this measure is often used, it does not distinguish between the value of recovered heat and electrical output. For example, the overall efficiency of the CHP system in Figure 9.18 is 85%, while the efficiency of separate grid and boiler system is just 57%. Another measure is called the overall energy savings, which is defined as

$$\text{Overall energy savings} = 1 - \frac{\text{Thermal input with CHP}}{\text{Thermal input without CHP}} \tag{9.4}$$

where, of course, the two approaches (with and without CHP) must deliver the same electrical and thermal outputs. For the example in Figure 9.18,

$$\text{Overall energy savings} = 1 - \frac{100}{63 + 117} = 0.444 = 44.4\%$$

While the above measures illustrate the overall energy (or fuel) savings for society gained by cogeneration, a different perspective is often taken by industrial facilities when considering CHP. Under the assumption that the facility needs heat anyway, say for process steam, the extra thermal input needed to generate electricity using cogeneration can be described using a quantity called the *energy chargeable to power* (ECP).

$$\text{ECP} = \frac{\text{Total thermal input} - \text{Displaced thermal input}}{\text{Electrical output}} \tag{9.5}$$

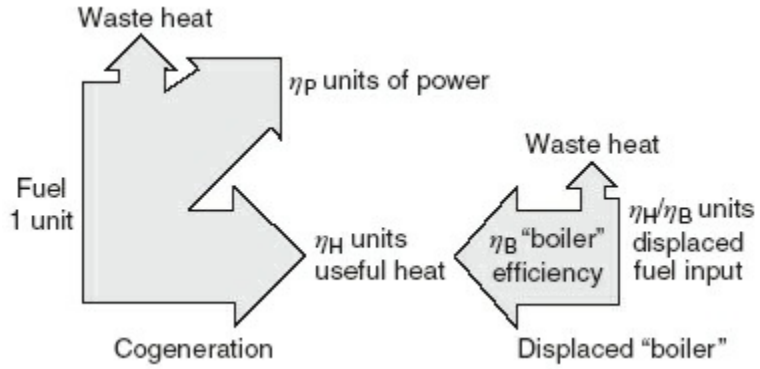
where the displaced thermal input is based on the efficiency of the boiler or other source of heat that would have been used instead of CHP. The units of ECP are the same as would be found for the heat rate of a conventional power plant, that is, Btu/kWh or kJ/kWh. Heat recovery is important to the economics since, in a sense, it helps subsidize the cost of the more important output—electricity—so we should look more carefully at the role it plays.

The ECP defined in Equation 9.5 can be expressed more generally in terms of electrical and boiler efficiency. Referring to Figure 9.20, we can write per unit of fuel input

$$\text{ECP} = \frac{1}{\eta_P}\left(1 - \frac{\eta_H}{\eta_B}\right) \tag{9.6}$$

where η_P is the CHP fuel to power efficiency, η_H is the CHP fuel to heat efficiency, and η_B is the efficiency of the source of heat if CHP is not used.

FIGURE 9.20 Finding the fuel for a boiler (or furnace or steam generator) displaced by a cogeneration plant.



To use Equation 9.5 with our two sets of units based on 3412 Btu/kWh and 3600 kJ/kWh we can write

$$\text{ECP (Btu/kWh)} = \frac{3412}{\eta_P}\left(1 - \frac{\eta_H}{\eta_B}\right) \tag{9.7}$$

$$\text{ECP (kJ/kWh)} = \frac{3600}{\eta_P}\left(1 - \frac{\eta_H}{\eta_B}\right) \tag{9.8}$$

Heat recovery is important to the economics of CHP. When the ECP is modified to account for the cost of fuel, a simple, and important measure of the added cost of electricity with CHP is called the *cost chargeable to power* (CCP).

$$\text{CCP} = \text{ECP} \times \text{Unit cost of energy} \tag{9.9}$$

Its units are \$/kWh, which makes it easy to compare CHP with other generation alternatives.

Example 9.4 Cost of Electricity from a Fuel Cell. A 10-kW fuel cell has an electrical efficiency of 35%, a thermal efficiency of 50%, and it operates with a 90% capacity factor. The after-incentives capital cost of \$50, 000 is financed with a 5%, 20-year loan having annual loan payments of \$4012. It runs on natural gas that costs $\$8/10^6$ Btu and its thermal output displaces gas for an existing 80%-efficient boiler that provides hot water to an apartment house.

Using Figure 9.20 as a guide, work out the power flows for the system, then find the following:

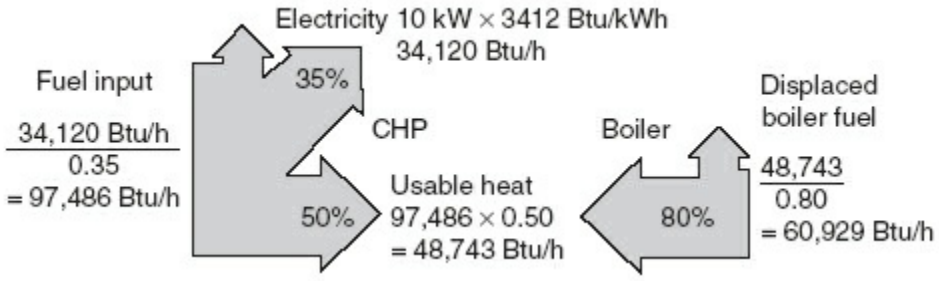
a. Energy chargeable to power (ECP, Btu/kWh)

b. Fuel cost chargeable to power (CCP, \$/kWh)

c. The total cost of electricity (fuel cost + amortized fuel cell, \$/kWh)

d. How many gallons of water per day could be heated from 60°F to 120°F?

Solution. Using the figure as a guide, start with the 10 kW output, find the CHP fuel input, then the CHP usable heat, then the boiler fuel energy input.



a. Using the above figure and Equation 9.5, the energy chargeable to power is

$$\text{ECP} = \frac{\text{Total thermal input} - \text{Displaced thermal input}}{\text{Electrical output}}$$

$$= \frac{(97{,}486 - 60{,}929)\ \text{Btu/h}}{10\ \text{kW}} = 3656\ \text{Btu/kWh}$$

Or, with less intuition, we can use Equation 9.7

$$\text{ECP} = \frac{3412}{\eta_P}\left(1 - \frac{\eta_H}{\eta_B}\right) = \frac{3412}{0.35}\left(1 - \frac{0.50}{0.80}\right) = 3656 \text{ Btu/kWh}$$

This is far less than the 10, 500 Btu/kWh typical for a thermal plant.

b. The fuel cost chargeable to power is

$$\text{CCP} = 3656 \text{ Btu/kWh} \times \$8/10^6 \text{ Btu} = \$0.0292/\text{kWh}$$

c. With a 90% capacity factor, the annual electricity delivered will be

$$\text{Electricity} = 10 \text{ kW} \times 8760 \text{ h/yr} \times 0.90 = 78{,}840 \text{ kWh/yr}$$

The annual fuel cost to generate electricity will be

$$\text{Fuel} = 78{,}840 \text{ kWh/yr} \times \$0.0292/\text{kWh} = \$2306/\text{yr}$$

The annual cost of electricity (fuel + amortization) is

$$\text{Cost} = \frac{\text{Fuel} + \text{Amortization}}{\text{kWh generated}} = \frac{\$2306/\text{yr} + \$4012/\text{yr}}{78{,}840 \text{ kWh/yr}} = \$0.080/\text{kWh}$$

d. The energy delivered to hot water while the unit is running at full power is

$$\text{Hot water} = \frac{48{,}743 \text{ Btu/h} \times 24 \text{ h/d}}{8.34 \text{ lb/gal} \times 1 \text{ Btu/lb}\,^\circ\text{F} \times (120 - 60)\,^\circ\text{F}} = 2338 \text{ gal/d}$$

9.7 COGENERATION TECHNOLOGIES

CHP systems can often save close to half of the fuel and emissions compared with providing these services separately. Most CHP is fueled with natural gas, which is far cleaner than the coal the world burns today, so it is well worth promoting. As Figure 9.19 indicates, displacing coal with natural-gas-fired cogeneration can easily cut carbon emissions by three-fourths. And, CHP can also be fueled by renewable energy sources such as biomass or even solar (e.g., capturing waste heat from water used to cool concentrating photovoltaic systems).

9.7.1 HHV and LHV

Before describing some of the emerging technologies for distributed generation, we need to sort out a subtle distinction having to do with the way power plant efficiencies are often presented. When a fuel is burned, some of the energy released ends up as latent heat in the water vapor produced (about 1060 Btu/lb of vapor, or 2465 kJ/kg). Usually that water vapor, along with the latent heat it contains, exits the stack along with all the other combustion gases, and its heating value is, in essence, lost. In some cases, however, that is not the case. For example, the most fuel-efficient, modern furnaces used for space heating homes achieve their high efficiencies (over 90%) by causing the combustion gases to cool enough to condense the water vapor before it leaves the stack. Whether the latent heat in water vapor is included or not leads to two different values of what is called the *heat of*

combustion for a fuel. The *higher heating value* (HHV), also known as the *gross heat of combustion*, includes the latent heat while the *lower heating value* (LHV), or *net heat of combustion*, does not.

Examples of HHV and LHV for various fuels, along with the LHV/HHV ratios, are presented in Table 9.3. Since natural gas is a combination of methane, ethane, and other gases, which varies depending on the source, the values given for HHV and LHV in the table are meant to be just representative, or typical, values. For natural gas, the difference between HHV and LHV is about 10%.

TABLE 9.3 Higher Heating Value (HHV) and Lower Heating Value (LHV) for Various Fuels[a]

	HHV		LHV		
Fuel	(Btu/lb)	(kJ/kg)	(Btu/lb)	(kJ/kg)	LHV/HHV
Methane	23,875	55,533	21,495	49,997	0.9003
Propane	21,669	50,402	19,937	46,373	0.9201
Natural gas	22,500	52,335	20,273	47,153	0.9010
Gasoline	19,657	45,722	18,434	42,877	0.9378
No. 4 oil	18,890	43,938	17,804	41,412	0.9425

[a]The gases are based on dry, 60°F, 30-in Hg conditions. Natural gas is a representative value.
Source: Based on Babcock and Wilcox (1992) and Petchers (2002).

Since the efficiency of a power plant is output power divided by fuel energy input, the question becomes which fuel value should be used, HHV or LHV? Unfortunately, both will be encountered. For large power stations, efficiency is almost always based on HHV, but for the most common distributed generation technologies such as microturbines and reciprocating engines, it is usually based on LHV. When it is important to reconcile the two, the following relationship may be used:

$$\frac{\text{HHV Thermal efficiency}}{\text{LHV Thermal efficiency}} = \text{Fuel (LHV/HHV ratio)} \tag{9.10}$$

where the LHV/HHV ratio can be found from Table 9.3.

Example 9.5 Microturbine Efficiency. A microturbine has a natural gas input of 13, 700 Btu (LHV) per kWh of electricity generated. Find its LHV efficiency and its HHV efficiency.

Solution. Using the energy conversion 3412 Btu/kWh, the LHV efficiency will be

$$\text{LHV efficiency} = \frac{3412 \text{ Btu/kWh}}{13{,}700 \text{ Btu/kWh}} = 0.249 = 24.9\%$$

Using the LHV/HHV ratio of 0.9010 for natural gas (Table 9.3) in Equation 9.10 gives the HHV efficiency for this turbine

$$\text{HHV Efficiency} = 24.9\% \times 0.901 = 22.4\%$$

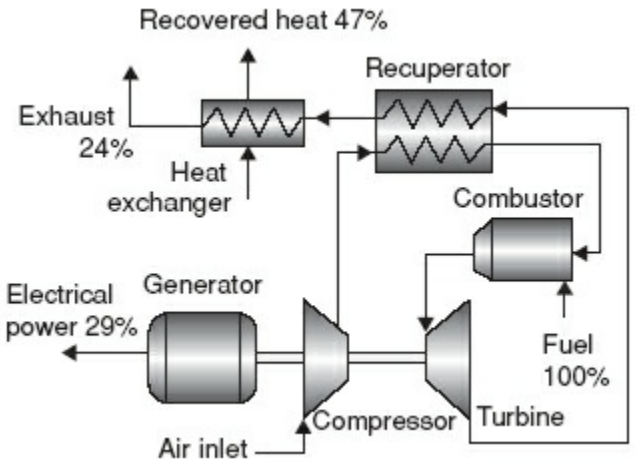
9.7.2 Microturbines

Microturbines are small combustion turbines with individual units that generate roughly 25 kW to several hundred kW of electricity along with sizeable amounts of waste heat. They tend to be fueled with conventional natural gas, but also may operate with lower quality biogas from landfills or wastewater treatment plants, propane, hydrogen, or diesel. The technology is scalable, which means multiple units can be ganged together for larger loads.

Microturbines can be either fairly conventional simple-cycle gas turbines or they may be recuperated machines with internal heat exchangers that transfer some of the exhaust heat into the incoming air stream before it enters the compressor. Simple-cycle unrecuperated turbines have lower capital costs and somewhat better reliability, but their electrical efficiency is quite low, on the order of 15%. They do, however, provide abundant waste heat at higher temperatures than their recuperated counterparts. For either type, cogeneration is provided by a heat exchanger operating from the turbine exhaust.

Figure 9.21 shows a sketch of a recuperated microturbine. While the electrical efficiency of recuperators is still somewhat modest, around 25–30%, when waste heat is captured and utilized, their overall efficiency can still be well over 80%. The economic advantage of microturbines is closely tied to the value of that heat, which for recuperated turbines tends to be relatively low temperature 50–80°C hot water. Good candidates for microturbines include applications that can use as much of the waste heat as possible, all year around. Water heating loads in hotels, laundromats, apartment houses, and swimming pools, if they are heated all year long, are good examples. Figure 9.21 shows a microturbine system that incorporates a heat recuperator to boost turbine efficiency and a heat exchanger to capture waste heat.

FIGURE 9.21 Microturbine with recuperator and waste heat cogeneration. Representative lower heating value (LHV) efficiencies are shown.



The economics of microturbines are quite favorable as the following example suggests.

Example 9.6 Economics for a Microturbine. A natural-gas-fired 60-kW microturbine costing $120, 000 operates with an 80% capacity factor. It has 30% electrical efficiency and 40% conversion efficiency to useful heat that displaces fuel for a 75%-efficient boiler. Operations and Maintenance (O&M) costs are $0.015/kWh. The factory in which it is

used pays \$0.10/kWh for purchased electricity, a demand charge of \$10/mo per peak kW, and \$8/10^6 Btu for natural gas.

Find the initial return on investment (ROI); that is, the ratio of the first year's savings to the initial investment.

Solution. Total electricity generated is

$$\text{Generation} = 60\ \text{kW} \times 8760\ \text{h/yr} \times 0.80 = 420{,}480\ \text{kWh/yr}$$

Annual fuel and O&M costs for the microturbine are

$$\text{Fuel cost} = \frac{1}{0.30} \cdot 420{,}480 \frac{\text{kWh}}{\text{yr}} \cdot 3412 \frac{\text{Btu}}{\text{kWh}} \cdot \frac{\$8}{10^6\ \text{Btu}} = \$38{,}258/\text{yr}$$

$$\text{O\&M} = 420{,}480\ \text{kWh/yr} \cdot \$0.015/\text{kWh} = \$6307/\text{yr}$$

$$\text{Total cost} = \$38{,}258 + \$6307 = \$44{,}565/\text{yr}$$

Savings for electricity and demand charges (assuming the turbine drops peak demand by 60 kW) are

$$\text{Electricity savings} = 420{,}480\ \text{kWh/yr} \times \$0.10/\text{kWh} = \$42{,}048/\text{yr}$$

$$\text{Demand charge savings} = 60\ \text{kW} \times 12\ \text{mo/yr} \times \$10/\text{mo/kW} = \$7{,}200/\text{yr}$$

The thermal energy delivered by the turbine is

$$\text{Thermal} = 40\% \times \frac{420{,}480\ \text{kWh/yr} \times 3412\ \text{Btu/kWh}}{0.30} = 1.913 \times 10^9\ \text{Btu/yr}$$

so the value of fuel saved by not burning it in that 75%-efficient boiler is

$$\text{Boiler fuel savings} = \frac{1.913 \times 10^9\ \text{Btu/yr}}{0.75} \times \frac{\$8}{10^6\ \text{Btu}} = \$20{,}404/\text{yr}$$

$$\text{Total savings} = \$42{,}048 + \$7200 + \$20{,}404 = \$69{,}652/\text{yr}$$

$$\text{Net cost minus savings} = \$44{,}565 - \$69{,}652 = -\$25{,}087/\text{yr}$$

So the initial return on the \$120, 000 investment is

$$\text{ROI} = \frac{\text{First year's net savings}}{\text{Initial cost}} = \frac{\$25{,}087}{\$120{,}000} = 0.209 = 20.9\%$$

In other words, it has about a 5-year simple payback.

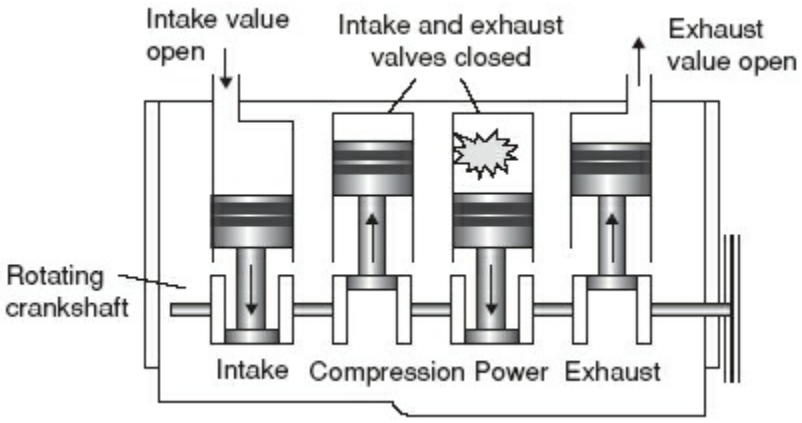
9.7.3 Reciprocating Internal Combustion Engines

Distributed generation today is dominated by installations that utilize reciprocating, that is, piston-driven, internal combustion engines (ICEs) connected to constant-speed AC generators. They are readily available in sizes that range from 0.5 kW to 6.5 MW, with electrical efficiencies in the vicinity of 37–40% (LHV basis). They can be designed to run on a number of fuels, including gasoline, natural gas, kerosene, propane, fuel oil, alcohol,

waste-treatment plant digester gas, and hydrogen. They are the least expensive of the currently available DG technologies and when burning natural gas they are relatively clean. Reciprocating engines make up a large fraction of the current market for CHP.

Most of these engines are conventional, four-stroke, reciprocating engines very much like the ones found in automobiles and trucks. The four-stroke cycle, as illustrated in Figure 9.22, consists of an intake stroke, a compression stroke, a power stroke, and an exhaust stroke. During the intake stroke, the piston moves downward. The partial vacuum created draws in air, or a mixture of air and vaporized fuel, through the open intake valve. During the compression stroke, the piston moves upward with both the intake and exhaust valves closed. The gases are compressed and heated and near the top of the stroke, combustion is initiated. The hot, expanding gases drive the piston downward in the power stroke forcing the crankshaft to rotate. In the final stroke, the rising piston forces the hot exhaust gases to exit via the now-open exhaust valve, completing the cycle.

FIGURE 9.22 Basic four-stroke, internal combustion engine.



An alternative to the four-stroke engine is one in which every other stroke is a power stroke. In these two-stroke engines, as the piston approaches its lowest point in the power stroke, an exhaust port opens allowing exhaust gases to escape while the intake port opens to allow fresh fuel and air to enter. Both close at the start of the compression stroke. Two-stroke engines have greater power for their size, but because neither intake nor exhaust functions are particularly effective, their efficiency is not as good as four-stroke engines and they produce much higher emissions. Since air quality is so often a critical constraint in siting distributed generation, two-stroke engines have limited potential.

There are two important variations on the four-stroke engine: *spark ignition* (Otto cycle) and *compression ignition* (diesel cycle). Spark-ignited engines burn gasoline or other easily ignitable fuels such as natural gas or propane. Combustion is initiated by an externally timed spark, which ignites the air–fuel mixture that entered the cylinder during the intake stroke and compressed during the subsequent compression stroke.

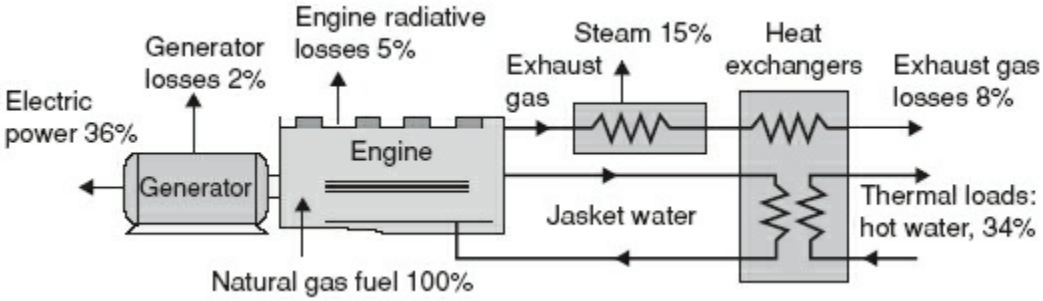
In contrast, compression-ignition engines burn heavier petroleum distillates such as diesel or fuel oil. These fuels are not premixed with air, but instead are injected under high pressure directly into the cylinder toward the end of the compression cycle. Self-ignited, diesel engines have much higher compression ratios than spark-ignited engines, which means during the compression stroke, the air is heated to much higher temperatures. As the pressure increases, so does the temperature until a point is reached at which spontaneous

combustion causes the fuel to explode, initiating the power stroke. In addition to having higher compression ratios, diesel engines also experience much more sudden fuel ignition—more of an explosive "bang" than occurs in the slower burning air–fuel mixture of a spark-ignited engine. Both of these factors mean diesel engines must be built to be stronger and heavier than their spark-ignited counterparts. Despite these more severe material requirements, diesel engines tend to have higher efficiencies, which means for the same output they can be physically smaller in size and somewhat less expensive. Generally speaking, they require more maintenance than spark-ignition engines and their emissions are more problematic, making them more difficult to site in areas where air quality is an issue.

The efficiency of ICEs can be increased by pressurizing the air, or air–fuel mixture, before it is enters the cylinder (called *charged aspiration*). This can be done with a turbocharger, which is a small turbine driven by the exhaust gases, or a supercharger, which is mechanically driven by an auxiliary shaft from the engine. Thermal efficiencies (from fuel to horsepower) as high as 41% (38% HHV) using gasoline for spark-ignited engines, and 46% LHV (44% HHV) for diesel-cycle engines have been achieved. An added benefit of charged aspiration is it allows the engine to run with a leaner air–fuel mixture, which helps lower combustion temperature and hence lowers NO_x emissions.

For CHP applications, waste heat from reciprocating engines can be tapped mainly from cooling water that circulates around cylinders in the engine jacket and from exhaust gases, with additional potential from oil and turbo coolers. While engine exhaust and cooling water each provide about half of the useful thermal energy in a reciprocating engine cogeneration system, the exhaust is at a much higher temperature (around 450°C vs. 100°C) and hence is more versatile. Figure 9.23 shows an example heat balance for a reciprocating engine cogeneration system utilizing a heat recovery steam generator (HRSG) for steam along with other heat exchangers to provide lower temperature energy for such loads as absorption air conditioning, hot water, and boiler heat. The conversion efficiency from fuel to electricity (36%) and usable heat (49%) gives an overall thermal efficiency of 85%.

FIGURE 9.23 Heat balance for an example reciprocating engine, cogeneration system with overall efficiency of 85%. Based on data from Petchers (2002).



9.8 FUEL CELLS

I believe that water will one day be employed as a fuel, that hydrogen and oxygen, which constitute it, used singly or together, will furnish an inexhaustible source of heat

and light.

Jules Verne, *Mysterious Island*, 1874

The portion of the above quote in which Jules Verne describes the joining of hydrogen and oxygen to provide a source of heat and light is a remarkably accurate description of how a fuel cell actually works. It misses the mark, however, when it suggests that water itself will be the fuel. While water can be electrolyzed to yield hydrogen and oxygen, the energy to do so far exceeds the energy that would be returned when these gases are recombined in a fuel cell. It is more accurate to consider a fuel cell as a sort of battery that delivers electricity (and heat) as long as it receives a continuous supply of energy-rich fuel (usually hydrogen).

There are several potential advantages of fuel cells compared to other energy conversion systems. Because they convert chemical energy directly into electrical power, they avoid the traditional intermediate steps of converting fuel into heat, heat into mechanical motion, and mechanical energy into electricity. Since they are not heat engines, they are not constrained by the Carnot limits and fuel-to-electricity efficiencies as high as 65% are likely, which gives fuel cells the potential to be roughly twice as efficient as the average central power station operating today.

Moreover, the usual combustion products, such as SO_x, CO, particulates, and assorted partially burned hydrocarbons, are totally eliminated. For most fuel cells, NO_x emissions are either eliminated or greatly reduced. If the original fuel is a hydrocarbon, such as natural gas, there will still be carbon emissions, but if fuel cells are powered by hydrogen obtained by electrolysis of water using renewable energy systems such as wind, hydroelectric, or photovoltaics, they would have no GHG emissions at all.

Since fuel cells are vibration-free, quiet, and emit little pollution, they can be located very close to their loads—for example, in the basement of a building. Being close to the load not only avoids transmission and distribution system losses, but its waste heat can be used to cogenerate electricity and useful heat for applications such as space heating, hot water, and even air conditioning. As a CHP system, fuel cells can have overall efficiencies of over 80%.

9.8.1 Historical Development

While fuel cells are only now beginning to reach commercial reality, it is worth noting that they were first developed more than 170 years ago. Sir William Grove, the English scientist credited with the invention of the original galvanic cell battery, published his original experiments on what he called a "gaseous voltaic battery" in 1839. He described the effects caused by his battery as follows: "A shock was given which could be felt by five persons joining hands, and which when taken by a single person was painful."

Grove's battery depended upon a continuous supply of rare and expensive gases, and corrosion problems were expected to result in a short cell lifetime, so the concept was not pursued. Fifty years later, Mond and Langer picked up on Grove's work and developed a 1.5-W cell with 50% efficiency, which they named a "fuel cell". After another half century of little progress, Francis T. Bacon, a descendant of the famous seventeenth century scientist, began work in 1932 that eventually resulted in what is usually thought to be the first practical fuel cell. By 1952, Bacon was able to demonstrate a 5-kW alkaline fuel cell (AFC) that powered, among other things, a 2-ton capacity fork-lift truck. In the same year, Allis Chalmers demonstrated a 20-hp fuel-cell-powered tractor.

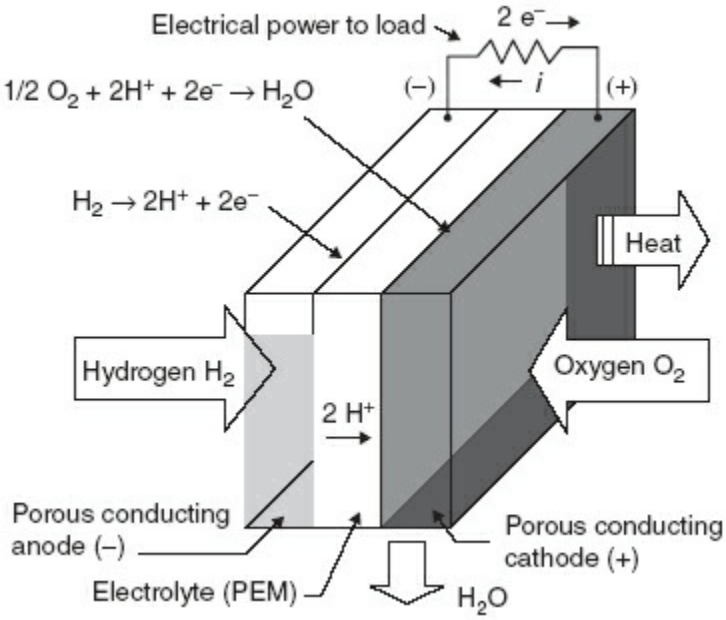
Fuel cell development was greatly stimulated by NASA's need for onboard electrical power for spacecraft. The Gemini series of earth-orbiting missions used fuel cells that relied on permeable membrane technology, while the later Apollo manned lunar explorations and subsequent space shuttle flights have used advanced versions of the AFCs originally developed by Bacon. Fuel cells not only provide electrical power, their by-product is pure water, which has been used by astronauts as a drinking water supply.

Fuel cells for terrestrial use were the subject of intense development toward the end of the twentieth century, with most of the emphasis at that time being devoted to hydrogen-powered fuel cells for electric vehicles. Competition from battery-powered EVs, however, has made fuel-cell cars less likely to become a reality. Instead, fuel cells for stationary applications seem to be a viable market.

9.8.2 Basic Operation of Fuel Cells

There are many variations on the basic fuel cell concept, but a common configuration looks something like Figure 9.24. As shown there, a single cell consists of two porous gas diffusion electrodes separated by an electrolyte. It is the choice of electrolyte that distinguishes one fuel cell type from another.

FIGURE 9.24 Basic configuration of a proton exchange membrane (PEM) fuel cell.



The electrolyte in Figure 9.24 consists of a thin membrane that is capable of conducting positive ions but not electrons or neutral gases. Guided by flow field plates, fuel (hydrogen) is introduced on one side of the cell while an oxidizer (oxygen) enters from the opposite side. The entering hydrogen gas has a slight tendency to dissociate into protons and electrons as follows:

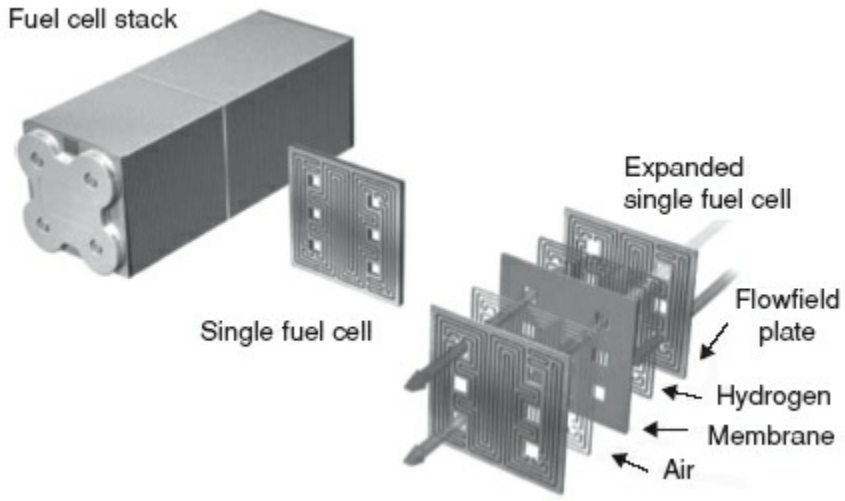
$$H_2 \leftrightarrow 2H^+ + 2e^- \tag{9.11}$$

This dissociation can be encouraged by coating the electrodes or membrane with catalysts to help drive the reaction to the right. Since the hydrogen gas releases protons in the vicinity of the electrode on the left (the anode), there will be a concentration gradient

across the membrane between the two electrodes. That gradient will cause protons to diffuse through the membrane leaving electrons behind. As a result, the cathode takes on a positive charge with respect to the anode. Those electrons that had been left behind are drawn toward the positively charged cathode, but since they cannot pass through the membrane they must find some other route. If an external circuit is created between the electrodes, the electrons will take that path to get to the cathode. The resulting flow of electrons through the external circuit delivers energy to the load (remember conventional current flow is opposite to the direction that electrons move, so current i "flows" from cathode to anode).

A single cell, such as that shown in Figure 9.24, typically produces on the order of 1 V or less under open-circuit conditions, and about 1/2 V under normal operating conditions. To build up the voltage, cells need to be stacked in series with appropriate flow passageways created to allow hydrogen and air to interact with each cell (Fig. 9.25).

FIGURE 9.25 A fuel cell stack consists of multiple cells arranged in series to increase the voltage. From www.ballard.com.



9.8.3 Fuel Cell Thermodynamics: Enthalpy

The way that the fuel cell shown in Figure 9.24 works is summarized by the following pair of half-cell reactions:

$$\text{Anode:} \quad H_2 \rightarrow 2H^+ + 2e^- \tag{9.12}$$

$$\text{Cathode:} \quad 1/2O_2 + 2H^+ + 2e^- \rightarrow H_2O \tag{9.13}$$

When combined, Equations 9.12 and 9.13 result in the same equation that we would write for ordinary combustion of hydrogen:

$$H_2 + \frac{1}{2}O_2 \rightarrow H_2O \tag{9.14}$$

The reaction described in Equation 9.14 is *exothermic*, that is, it liberates heat (as opposed to *endothermic* reactions, which need heat to be added to make them occur). Since Equation 9.14 is exothermic, it will occur spontaneously—the hydrogen and oxygen want

to combine to form water. Their eagerness to do so provides the energy that the fuel cell uses to deliver electrical energy to its load. The questions, of course, are how much energy is liberated in the reaction and how much of that can be converted to electrical energy. To answer those questions, we need to describe three quantities from thermodynamics: *enthalpy*, *free energy*, and *entropy*. Unfortunately, the precise definitions of each of these quantities tend not to lend themselves to easy, intuitive interpretation. Moreover, they have very subtle properties that are beyond our scope here, and there are risks in trying to present a simplified introduction, so we will proceed with some caution.

The enthalpy of a substance is defined as the sum of its *internal energy* U, and the product of its volume V and pressure P:

(9.15) Enthalpy $H = U + PV$

The internal energy U of a substance refers to its microscopic properties, including the kinetic energies of molecules and the energies associated with the forces acting between molecules, between atoms within molecules, and within atoms. The total energy of that substance is the sum of its internal energy plus the observable, macroscopic forms such as its kinetic and potential energies. The units of enthalpy are usually kJ of energy per mole of substance.

Molecules in a system possess energy in various forms such as *sensible* and *latent* energy, which depend on temperature and state (solid, liquid, and gaseous), *chemical energy* (associated with the molecular structure), and *nuclear energy* (associated with the atomic structure). For a discussion of fuel cells, it is changes in chemical energy that are of interest and those changes are best described in terms of enthalpy.

As is usually the case for discussions about energy, it is changes in energy, or in this case, enthalpy, rather than absolute values that are of interest. For example, we can talk about the potential energy of an object as being its weight times its height above some reference elevation. Our choice of reference elevation does not matter as long as we are only interested in the change in potential energy as an object is raised against gravity from one elevation to another. The same concept applies for enthalpy. We need to describe it with respect to some arbitrary reference conditions.

In the case of enthalpy, a reference temperature of 25°C and a reference pressure of 1 atm (standard temperature and pressure, STP) are assumed. It is also assumed that the reference condition for the chemically stable form of an element at 1 atm and 25°C is zero. For example, the stable form of oxygen at STP is gaseous O_2, so the enthalpy for O_2 (g) is zero, where (g) just means it is in the gaseous state. On the other hand, since atomic oxygen (O) is not stable, its enthalpy is not zero (it is, in fact, 247.5 kJ/mol). Note that the state of a substance at STP matters. Mercury, for example, at 1 atm and 25°C is a liquid, so the standard enthalpy for Hg (l) is zero, where (l) means the liquid state.

One way to think about enthalpy is that it is a measure of the energy that it takes to form that substance out of its constituent elements. The difference between the enthalpy of the substance and the enthalpies of its elements is called the *enthalpy of formation*. It is in essence the energy stored in that substance due to its chemical composition. A short list of enthalpies of formation at STP conditions appears in Table 9.4. To remind us that a particular value of enthalpy (or other thermodynamic properties such as entropy and free energy) is at STP conditions, a superscript "o" is used (e.g., H^o). Table 9.4 also includes

two other quantities, the absolute entropy S^o and the Gibbs free energy G^o, which will be useful when we try to determine the maximum possible fuel cell efficiency. Note that when a substance has negative enthalpy of formation, it means that the chemical energy in that substance is less than that of the constituents from which it was formed. That is, during its formation, some of the energy in the reactants did not end up as chemical energy in the final substance.

TABLE 9.4 Enthalpy of Formation H^o, Absolute Entropy S^o, and Gibbs Free Energy G^o at 1 atm, 25°C for Selected Substances

Substance	State	H^o (kJ/mol)	S^o (kJ/mol K)	G^o (kJ/mol)
H	gas	217.9	0.114	203.3
H_2	gas	0	0.130	0
O	gas	247.5	0.161	231.8
O_2	gas	0	0.205	0
H_2O	liquid	−285.8	0.0699	−237.2
H_2O	gas	−241.8	0.1888	−228.6
C	solid	0	0.006	0
CH_4	gas	−74.9	0.186	−50.8
CO	gas	−110.5	0.197	−137.2
CO_2	gas	−393.5	0.213	−394.4
CH_3OH	liquid	−238.7	0.1268	−166.4

In chemical reactions, the difference between the enthalpy of the products and the enthalpy of the reactants tells us how much energy is released or absorbed in the reaction. When there is less enthalpy in the final products than in the reactants, heat is liberated; that is, the reaction is exothermic. When it is the other way around, heat is absorbed and the reaction is endothermic.

If we analyze the reaction in Equation 9.14, the enthalpies of H_2 and O_2 are zero so the enthalpy of formation is simply the enthalpy of the resulting H_2O. Note that in Table 9.4, the enthalpy of H_2O depends on whether it is liquid water or gaseous water vapor.

$$H_2 + \frac{1}{2}O_2 \rightarrow H_2O(l) \quad \Delta H = -285.8 \text{ kJ} \tag{9.16}$$

When the resulting product is water vapor,

$$H_2 + \frac{1}{2}O_2 \rightarrow H_2O(g) \quad \Delta H = -241.8 \text{ kJ} \tag{9.17}$$

The negative signs for the enthalpy changes in Equations 9.16 and 9.17 tell us these reactions are exothermic; that is, heat is released. The difference between the enthalpy of liquid water and gaseous water vapor is 44.0 kJ/mol. Therefore, that amount is the familiar latent heat of vaporization of water. Recall that latent heat is what distinguishes the HHV of a hydrogen-containing fuel and the LHV. The HHV includes that 44.0 kJ/mol of latent heat in the water vapor formed during combustion, while the LHV does not.

Example 9.7 The HHV for Methane. Find the HHV of methane CH_4 in kJ/mol and

kJ/kg when it is oxidized to CO_2 and liquid H_2O.

Solution. The reaction is written below, and beneath it are enthalpies taken from Table 9.4. Note that the equation must be balanced so we know how many moles of each constituent are involved.

$$\begin{array}{lllll} CH_4\,(g) + 2O_2\,(g) & \rightarrow & CO_2\,(g) + 2H_2O(l) \\ (-74.9) \quad 2 \times (0) & & (-393.5) \quad 2 \times (-285.8) \end{array}$$

Note too that we have used the enthalpy of liquid water to find the HHV.

The difference between the total enthalpy of the reaction products and the reactants is

$$\begin{aligned} \Delta H &= [(-393.5) + 2 \times (-285.8)] - [(-74.9) + 2 \times (0)] \\ &= -890.2 \text{ kJ/mol of } CH_4 \end{aligned}$$

Since the result is negative, it is exothermic and heat will be released. The HHV is the absolute value of ΔH, which is 890.2 kJ/mol.

Since there are $12 + 4 \times 1 = 16$ g/mol of CH_4, the HHV can also be written as

$$\text{HHV} = \frac{890.2 \text{ kJ/mol}}{16 \text{ g/mol}} \times 1000 \text{ g/kg} = 55{,}638 \text{ kJ/kg}$$

9.8.4 Entropy and the Theoretical Efficiency of Fuel Cells

While the enthalpy change tells us how much energy is released in a fuel cell, it does not tell us how much of that energy can be converted directly into electricity. To figure that out, we need to review another thermodynamic quantity, *entropy*. Entropy has already been introduced in the context of heat engines in Section 8.2.1, where it was used to help develop the Carnot efficiency limit. In a similar fashion, the concept of entropy will help us develop the maximum efficiency of a fuel cell.

To begin, let us note that all energy is not created equal. That is, for example, 1 J of energy in the form of electricity or mechanical work is much more useful than a joule of heat. We can convert that joule of electricity or work into heat with 100% conversion efficiency, but we cannot get back the joule of electricity or work from just a single joule of heat. What this suggests is that there is a hierarchy of energy forms, with some being "better" than others. Electricity and mechanical energy (doing work) are of the highest quality. In theory, we could go back and forth between electricity and mechanical work with 100% conversion efficiency. Heat energy is of much lower quality, with low temperature heat being of lower quality than high temperature heat. So, where does chemical energy fit into this hierarchy? It is better than thermal, but worse than mechanical and electrical. Entropy will help us figure out just where it stands.

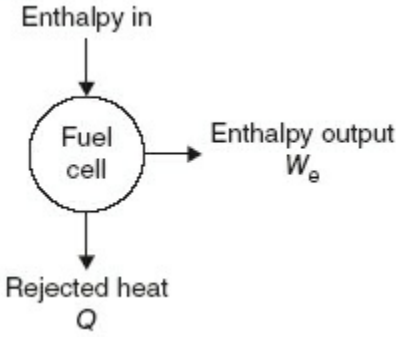
Recall that when an amount of heat Q is removed from a thermal reservoir large enough that its temperature T does not change during the process (i.e., the process is isothermal), the loss of entropy ΔS from the reservoir is defined to be

$$\Delta S = \frac{Q}{T} \tag{9.18}$$

With Q measured in kilojoules (kJ) and T in kelvins (K = °C + 273.15), the unit of entropy is kJ/K. Recall too that entropy is only associated with heat transfer and that electrical or mechanical work is perfect so these forms have zero entropy. And, finally, remember that in any real system, if we carefully add up all of the entropy changes, the second law of thermodynamics requires that there be an overall increase in entropy. Now let us apply these ideas to a fuel cell.

Consider Figure 9.26, which shows a fuel cell converting chemical energy into electricity and waste heat. The fuel cell reactions (Eqs. 9.16 and 9.17) are exothermic, which means their enthalpy changes ΔH are negative. Working with negative quantities leads to awkward nomenclature, which we can avoid by saying those reactions act as a source of enthalpy H that can be converted to heat and work as Figure 9.26 implies.

FIGURE 9.26 The energy balance for a fuel cell.



The cell generates an amount of electricity W_e and rejects an amount of thermal energy Q to its environment. Since there is heat transfer, and it is a real system, there must be an increase in entropy. We can use that requirement to determine the minimum amount of rejected heat and therefore the maximum amount of electric power that the fuel cell will generate. To do so, we need to carefully tabulate the entropy changes occurring in the cell:

$$H_2 + \frac{1}{2}O_2 \rightarrow H_2O + Q \tag{9.19}$$

where we have included the fact that heat Q will be released. The entropy of the reactants H_2 and O_2 will disappear, but new entropy will appear in the H_2O that is formed plus the entropy that appears in the form of heat Q. As long as the process is isothermal, which is a reasonable assumption for a fuel cell, we can write the entropy appearing in the rejected heat as

$$\Delta S = \frac{Q}{T} \tag{9.20}$$

What about the entropy associated with the work done, W_e? Since there is no heat transfer in electrical (or mechanical) work, that entropy is zero.

To make the necessary tabulation, we need values of the entropy of the reactants and products. And, as usual, we need to define reference conditions. It is conventional practice to declare that the entropy of a pure crystalline substance at zero absolute temperature is

zero (the "third law of thermodynamics"). The entropy of a substance under other conditions, referenced to the zero base conditions, is called the *absolute entropy* of that substance and those values are tabulated in a number of places. Table 9.4 gives absolute entropy values, S^{o}, for several substances under STP conditions (25°C, 1 atm).

The second law of thermodynamics requires that in a real fuel cell, there be a net increase in entropy (an ideal cell will release just enough heat to make the increase in entropy be zero). Therefore, we can write that the entropy that shows up in the rejected heat and the product water (liquid water) must be greater than the entropy contained in the reactants (H_2 and O_2):

$$\text{Entropy gain} \geq \text{Entropy loss} \tag{9.21}$$

$$\frac{Q}{T} + \sum S_{\text{products}} \geq \sum S_{\text{reactants}} \tag{9.22}$$

which leads to

$$Q \geq T\left(\sum S_{\text{reactants}} - \sum S_{\text{products}}\right) \tag{9.23}$$

Equation 9.23 tells us the minimum amount of heat that must appear in the fuel cell. That is, we cannot convert all of the fuel's energy into electricity—we are stuck with some thermal losses. At least our thermal losses are going to be less than if we tried to generate electricity with a heat engine.

We can now easily determine the maximum efficiency of the fuel cell. From Figure 9.26, the enthalpy supplied by the chemical reaction H equals the electricity produced W_e plus the heat rejected Q:

$$H = W_e + Q \tag{9.24}$$

Since it is the electrical output that we want, we can write the fuel cell's efficiency as

$$\eta = \frac{W_e}{H} = \frac{H - Q}{H} = 1 - \frac{Q}{H} \tag{9.25}$$

To find the maximum efficiency, all we need to do is plug in the theoretical minimum amount of heat Q from Equation 9.23.

Example 9.8 Maximum Efficiency of a Fuel Cell (Entropy Analysis). Suppose a fuel cell that operates at 25°C (298 K) and 1 atm forms liquid water (i.e., we are working with the HHV of the hydrogen fuel):

$$H_2 + \frac{1}{2}O_2 \rightarrow H_2O(l) \qquad \Delta H = -285.8 \text{ kJ/mol of } H_2$$

a. Find the minimum amount of heat rejected per mole of H_2

b. What is the maximum efficiency of the fuel cell?

Solution

a. From the reaction, 1 mol of H_2 reacts with 1/2 mol of O_2 to produce 1 mol of liquid H_2O. The loss of entropy by the reactants per mole of H_2 is found using values given in Table 9.4:

$$\sum S_{\text{reactants}} = 0.130\frac{\text{kJ}}{\text{mol}\cdot\text{K}} \times 1 \text{ mol } H_2 + 0.205\frac{\text{kJ}}{\text{mol}\cdot\text{K}} \times \frac{1}{2}\text{mol } O_2$$
$$= 0.2325 \text{ kJ/K}$$

The gain in entropy in the product water is

$$\sum S_{\text{product}} = 0.0699\frac{\text{kJ}}{\text{mol}\cdot\text{K}} \times 1 \text{ mol } H_2O(l) = 0.0699 \text{ kJ/K}$$

From Equation 9.23, the minimum amount of heat released during the reaction is therefore

$$Q_{\min} = T\left(\sum S_{\text{reactants}} - \sum S_{\text{products}}\right)$$
$$= 298 \text{ K}(0.2335 - 0.0699) \text{ kJ/K} = 48.45 \text{ kJ per mole } H_2$$

b. From Equation 9.16, the enthalpy made available during the formation of liquid water from H_2 and O_2 is H = 285.8 kJ/mol of H_2. The maximum efficiency possible occurs when Q is a minimum, thus from Equation 9.25

$$\eta_{\max} = 1 - \frac{Q_{\min}}{H} = 1 - \frac{48.45}{258.8} = 0.830 = 83.0\%$$

9.8.5 Gibbs Free Energy and Fuel Cell Efficiency

The chemical energy released in a reaction can be thought of as consisting of two parts: an entropy-free part, called *free energy* ΔG, that can be converted directly into electrical or mechanical work plus a part that must appear as heat Q. The "G" in free energy is in honor of Josiah Willard Gibbs (1839–1903) who first described its usefulness, and the quantity is usually referred to as Gibbs free energy. The free energy G is the enthalpy H created by the chemical reaction, minus the heat that must be liberated $Q = T\,\Delta S$ to satisfy the second law.

The Gibbs free energy ΔG corresponds to the maximum possible, entropy-free, electrical (or mechanical) output from a chemical reaction. It can be found at STP using Table 9.4 by taking the difference between the sum of the Gibbs energies of the reactants and the products:

$$\Delta G = \sum G_{\text{products}} - \sum G_{\text{reactants}} \quad (9.26)$$

This means the maximum possible efficiency is just the ratio of the Gibbs free energy to the enthalpy change ΔH in the chemical reaction

$$\eta_{\max} = \frac{\Delta G}{\Delta H} \quad (9.27)$$

Example 9.9 Maximum Fuel Cell Efficiency Using Gibbs Free Energy. What is the maximum efficiency at STP of a proton exchange membrane (PEM) fuel cell based on the HHV of hydrogen?

Solution. The HHV corresponds to liberated water in the liquid state so that the appropriate reaction is

$$H_2 + \frac{1}{2}O_2 \rightarrow H_2O(l) \qquad \Delta H = -285.8 \text{ kJ/mol of } H_2$$

From Table 9.4, the Gibbs free energy of the reactants H_2 and of O_2 are both zero, and that of the product, liquid water is –237.2 kJ. Therefore, from Equation 9.26,

$$\Delta G = -237.2 - (0 + 0) = -237.2 \text{ kJ/mol}$$

So, from Equation 9.27,

$$\eta_{max} = \frac{\Delta G}{\Delta H} = \frac{-237.2 \text{ kJ/mol}}{-285.8 \text{ kJ/mol}} = 0.830 = 83.0\%$$

This is the same answer that we found in Example 9.8 using entropy.

9.8.6 Electrical Output of an Ideal Cell

The Gibbs free energy ΔG is the maximum possible amount of work or electricity that a fuel cell can deliver. Since work and electricity can be converted back and forth without loss, they are referred to as reversible forms of energy. For an ideal fuel cell, the maximum possible electrical output is therefore equal to the magnitude of ΔG. From Table 9.4, for a fuel cell producing liquid water, the maximum electrical output at STP is equal to

$$W_e = |\Delta G| = 237.2 \text{ kJ per mole of } H_2 \qquad (9.28)$$

To use Equation 9.28, we just have to adjust the units so that the electrical output W_e will have the conventional electrical units of volts, amperes, and watts. To do so, let us introduce the following nomenclature along with appropriate physical constants:

q = charge on an electron = 1.6×10^{-19} coulombs

N = Avogadro's number = 6.022×10^{23} molecules/mol

v = volume of 1 mole of ideal gas at STP = 22.4 L/mol

n = rate of flow of hydrogen into the cell (mol/s)

I = current (amperes), where 1 ampere = 1 coulomb/s

V_R = ideal (reversible) voltage across the two electrodes (volts)

P = electrical power delivered (watts)

For each mole of H_2 into an ideal fuel cell, two electrons will pass through the electrical load (see Fig. 9.24). We can therefore write that the current flowing through the load will be

$$I(\mathrm{A}) = n\frac{\mathrm{mol}}{\mathrm{s}} \cdot 6.022 \times 10^{23}\frac{\mathrm{molecules\ H_2}}{\mathrm{mol}} \cdot \frac{2\ \mathrm{electrons}}{\mathrm{molecule\ H_2}} \cdot 1.602 \times 10^{-19}\frac{\mathrm{coulombs}}{\mathrm{electron}}$$

$$I(\mathrm{A}) = 192{,}945\ n \tag{9.29}$$

Using Equation 9.28, the ideal power (watts) delivered to the load will be the 237.2 kJ/mol of H_2 times the rate of hydrogen use:

$$P(\mathrm{W}) = 237.2\frac{\mathrm{kJ}}{\mathrm{mol}} \times n\frac{\mathrm{mol}}{\mathrm{s}} \times 1000\frac{\mathrm{J}}{\mathrm{kJ}} \times \frac{1\ \mathrm{W}}{\mathrm{J/s}} = 237{,}200\ n \tag{9.30}$$

And the voltage produced across the terminals of this ideal fuel cell will be

$$V_\mathrm{R} = \frac{P(\mathrm{W})}{I(\mathrm{A})} = \frac{237{,}200\ n}{192{,}945\ n} = 1.229\ \mathrm{V} \tag{9.31}$$

Note that the voltage does not depend on the input rate of hydrogen. It should also be noted that the ideal voltage decreases with increasing temperature, so at the more realistic operating temperature of a PEM cell of about 80°C, V_R is closer to 1.18 V.

We can now easily find the hydrogen that needs to be supplied to this ideal fuel cell per kWh of electricity generated.

$$\mathrm{H_2\ rate} = \frac{n\ \mathrm{mol/s} \times 2\ \mathrm{g/mol} \times 3600\ \mathrm{s/h}}{237{,}200\ n\ (\mathrm{W}) \times 10^{-3}\ \mathrm{kW/W}} = 30.35\ \mathrm{g\ H_2/kWh} \tag{9.32}$$

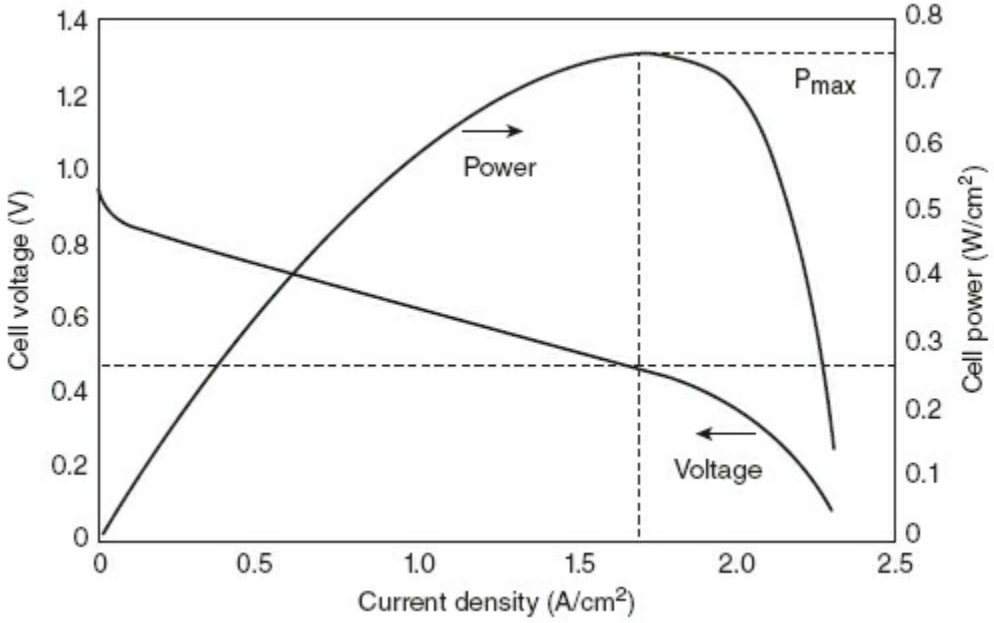
9.8.7 Electrical Characteristics of Real Fuel Cells

Just as real heat engines do not perform nearly as well as a perfect Carnot engine, and real wind turbine blades do not begin to match the Betz limit, real fuel cells do not deliver the full Gibbs free energy either. *Activation* losses result from the energy required by the catalysts to initiate the reactions. The relatively slow speed of reactions at the cathode, where oxygen combines with protons and electrons to form water, tends to limit fuel cell power. *Ohmic* losses result from current passing through the internal resistance posed by the electrolyte membrane, electrodes, and various interconnections in the cell. Another loss, referred to as *fuel crossover*, results from fuel passing through the electrolyte without releasing its electrons to the external circuit. And finally, *mass transport* losses result when hydrogen and oxygen gases have difficulty reaching the electrodes. This is especially true at the cathode if water is allowed to build up, clogging the catalyst. For these and other reasons, real fuel cells, in general, generate only about 60–70% of the theoretical maximum.

Figure 9.27 shows the relationship between current and voltage for a typical PEM fuel cell. Note that the open-circuit voltage (zero current) is a little less than 1 V, which is about 25% lower than the theoretical value of 1.229 V. Also shown is the product of voltage and current, which is power. Since power at zero current, or at zero voltage, is zero, there must be a point somewhere in between at which power is a maximum. This should look very

familiar since it is quite analogous to photovoltaic *I–V* curves. As shown in the figure, that maximum corresponds to operation of the fuel cell at around 0.5 V per cell, at which point it will deliver about 0.75 W/cm^2.

FIGURE 9.27 The voltage–current curve for a typical fuel cell. Also shown is the power delivered, which is the product of voltage and current.



Over most of the fuel cell *I–V* graph, voltage drops linearly as current increases. That suggests a simple equivalent circuit consisting of a voltage source in series with some internal resistance. Fitting the *I–V* curve in the linear region for the fuel cell shown in Figure 9.27 yields the following approximate relationship:

$$V = 0.85 - \frac{0.25}{A(\text{cm}^2)} I \tag{9.33}$$

where V is cell voltage, I is current (A), and A is the cell area (cm^2).

Example 9.10 Rough Parameters of a Home-Scale Fuel Cell Stack. A 1-kW fuel cell operating on a continuous basis would provide all of the electrical needs of a typical U.S. house. If such a fuel cell stack generates 48 V DC with cells operating at 0.5 V each, how many cells of the type described by Equation 9.33 would be needed and what should be the membrane area of each cell?

Solution. With 0.5 V cells all wired in series, 48/0.5 = 96 cells would be needed to generate 48 V DC. The current that needs to flow through each cell is

$$I = \frac{P}{V} = \frac{1000 \text{ W}/96 \text{ cells}}{0.5 \text{ V/cell}} = 20.83 \text{ A}$$

Using Equation 9.33 to find the area of each cell yields

$$A = \frac{0.25I}{0.85 - V} = \frac{0.25 \times 20.83}{0.85 - 0.5} = 14.8 \text{ cm}^2$$

9.8.8 Types of Fuel Cells

To this point in this chapter, the fuel cell reactions and explanations have been based on the assumption that hydrogen H_2 is the fuel; Equations 9.12 and 9.13 describe the reactions, and the electrolyte passes protons from anode to cathode through a membrane. While it is true that these are the most likely candidates for vehicles and small, stationary power systems, there are competing technologies that use other electrolytes and which have other distinctive characteristics that may make them more suitable in some applications.

Polymer Electrolyte Fuel Cells (PEMs): Originally known as *solid polymer electrolyte* (SPE) fuel cells, and often now called *proton exchange membrane* fuel cells, these are among the furthest along in their development, in part because of the early stimulus provided by the Gemini space program, and more recently since they are the leading candidates for use in electric vehicles. They have the highest power density of all the fuel cell categories. They operate at low temperatures and can be quickly started and stopped, which makes them ideally suited for portable applications, especially vehicles.

Typical PEM cells generate over 0.5 W/cm^2 of membrane at around 0.65 V per cell and a current density of 1 A/cm^2. To control water evaporation from the membranes, these cells require active cooling to keep temperatures in the desired operating range of 50–80°C. With such low temperatures, waste heat cogeneration is restricted to simple water or space heating applications, which is fine for residential power systems. One limitation of PEM cells is their need for very pure hydrogen as their fuel source. Hydrogen reformed from hydrocarbon fuels such as methanol (CH_3OH) or methane CH_4 often contains carbon monoxide (CO), which can lead to CO poisoning of the catalyst. When CO adsorbs onto the surface of the anode catalyst, it diminishes the availability of sites where the hydrogen reactions need to take place. Minimizing CO poisoning, managing water and heat in the cell stack, and developing lower cost materials and manufacturing techniques are current challenges for PEM cells.

Direct Methanol Fuel Cells (DMFCs): These cells use the same polymer electrolytes as PEM cells do, but they offer the significant advantage of being able to utilize a liquid fuel, methanol (CH_3OH), instead of gaseous hydrogen. Liquid fuels are much more convenient for portable applications such as motor vehicles as well as small, portable power sources for everything from cell phones and laptop computers to replacements for diesel-engine generators.

The chemical reactions taking place at the anode and cathode are as follows:

$$CH_3OH + H_2O \rightarrow CO_2 + 6H^+ + 6e^- \quad \text{(Anode)} \tag{9.34}$$

$$\frac{1}{2}O_2 + 2H^+ + 2e^- \rightarrow H_2O \quad \text{(Cathode)} \tag{9.35}$$

for an overall reaction of

$$CH_3OH + \frac{3}{2}O_2 \rightarrow CO_2 + 2H_2O \qquad \text{(Overall)} \tag{9.36}$$

Significant technical challenges remain, including control of excessive fuel crossover through the membrane and reducing catalyst poisoning by CO and other methanol reaction products, but the advantages of portability and simplified fuel handling make them a potentially very attractive technology.

Phosphoric Acid Fuel Cells (PAFCs): These fuel cells were introduced into the marketplace in the 1990s and there are hundreds of 200-kW units currently in operation. Their operating temperature is higher than that of PEM fuel cells (close to 200°C), which makes the waste heat more usable for absorption air conditioning as well as water and space heating in buildings.

The electrochemical reactions taking place in a PAFC are the same ones that occur in a PEM cell, but the electrolyte in this case is phosphoric acid rather than a proton exchange membrane. These cells tolerate CO better than PEM cells, but they are quite sensitive to H_2S. Although there are already a number of PAFCs in use, their future will be closely tied to whether higher production levels will be able to reduce manufacturing costs to the point where they will be competitive with other cogeneration technologies.

Alkaline Fuel Cells (AFCs): These highly efficient and reliable fuel cells were developed for the Apollo and Space Shuttle programs. Their electrolyte is potassium hydroxide (KOH) and the charge carrier is OH^- rather than H^+ ions. The electrochemical reactions are as follows:

$$H_2 + 2OH^- \rightarrow 2H_2O + 2e^- \qquad \text{(Anode)} \tag{9.37}$$

$$\frac{1}{2}O_2 + H_2O + 2e^- \rightarrow 2OH^- \qquad \text{(Cathode)} \tag{9.38}$$

The major problem with AFCs is their intolerance for exposure to CO_2, even at the low levels found in the atmosphere. Since air is the source of O_2 for the cathodic reactions, it is unlikely that these will be used in terrestrial applications.

Molten-Carbonate Fuel Cells (MCFCs): These fuel cells operate at very high temperatures, on the order of 650°C, which means the waste heat is of high enough quality that it can be used to generate additional power in accompanying steam or gas turbines. At this high temperature, there is the potential for the fuel cell waste heat to be used to convert, or *reform*, a hydrocarbon fuel, such as methane, into the hydrogen needed by the fuel cell itself. Moreover, the usual accompanying CO in fuel reforming does not poison the catalyst, and in fact, becomes part of the fuel. Efficiencies of 50–55% are projected for internal-reforming MCFCs. With combined-cycle operation, electrical efficiencies of 65% are projected and cogeneration efficiencies approaching 90% are possible.

In an MCFC, the conducting ion is carbonate CO_3^{2-} rather than H^+ and the electrolyte is molten lithium, potassium, or sodium carbonate. At the cathode, CO_2 and O_2 combine to form carbonate ions, which are conducted through the electrolyte to the anode where they combine with hydrogen to form water and carbon dioxide as shown in the following electrochemical reactions:

(9.39) $$H_2 + CO_3^{2-} \rightarrow H_2O + CO_2 + 2e^- \quad \text{(Anode)}$$

(9.40) $$\frac{1}{2}O_2 + CO_2 + 2e^- \rightarrow CO_3^{2-} \quad \text{(Cathode)}$$

Note that the overall reaction is the same as that described earlier for a "generic" fuel cell

(9.41) $$H_2 + \frac{1}{2}O_2 \rightarrow H_2O \quad \text{(Overall)}$$

MCFCs operate in a very corrosive environment and the challenges associated with devising appropriate materials that will operate with suitably long lifetimes are significant.

Solid Oxide Fuel Cells (SOFCs): SOFCs and MCFCs have been competing for the future large power station market. Both operate at such high temperatures (MCFC, 650°C; SOFC, 750–1000°C) that their waste heat can be used for combined-cycle steam or gas turbines and both can take advantage of those temperatures to do internal fuel reforming. The SOFC is physically smaller than an MCFC for the same power and it may ultimately have greater longevity. It also has been the first to be commercially successful.

The electrolyte in an SOFC is a solid ceramic material made of zirconia and yttria, which is very unlike the liquids and solid polymers used in every other type of fuel cell. The charge carrier that is transported across the electrolyte is the oxide O^{2-} ion, which is formed at the cathode when oxygen combines with electrons from the anode. At the anode, the oxide ion combines with hydrogen to form water and electrons, as shown below:

(9.42) $$H_2 + O^{2-} \rightarrow H_2O + 2e^- \quad \text{(Anode)}$$

(9.43) $$\frac{1}{2}O_2 + 2e^- \rightarrow O^{2-} \quad \text{(Cathode)}$$

The first commercially successful SOFC uses 25-W, 100 cm × 100 cm, cells in 1-kW stacks to create 25-kW modules that are assembled into 100- or 200-kW systems (Bloomenergy). The systems can be configured into even larger power plants. While it is normally fueled by natural gas, which is internally converted to hydrogen, other biofuel sources are possible.

Example 9.11 Economics of a 200-kW Solid Oxide Fuel Cell. Assuming the following cost and performance features for an SOFC

Natural gas consumption is 1.32 million Btu/h to generate 200 kW (AC).

Natural gas costs $8 per million Btu.

Displaced electricity saves $0.10/kWh and $10/mo/kW of demand.

O&M cost is $0.02/kWh.

Capacity factor is 0.90.

a. What is the overall efficiency of the system?

b. What would the capital cost of the system need to be if it is to have no more than a 10-year simple payback period?

Solution

a. The efficiency from natural gas to electricity would be

$$\eta = \frac{\text{Output}}{\text{Input}} = \frac{200\ \text{kW} \times 3412\ \text{Btu/kWh}}{1.32 \times 10^6\ \text{Btu/h}} = 0.517 = 51.7\%$$

The fuel plus O&M costs would be

$$\text{Fuel} + \text{O\&M} = \frac{1.32 \times 10^6\ \text{Btu/h}}{200\ \text{kW}} \times \frac{\$8}{10^6\ \text{Btu}} + \$0.02/\text{kWh} = \$0.0728/\text{kWh}$$

The annual cost of fuel and O&M with a 90% capacity factor is

$$\text{Operation} = 200\ \text{kW} \times 8760\ \text{h/yr} \times 0.90 \times \$0.0728/\text{kWh} = \$114{,}791/\text{yr}$$

The savings on electricity by avoiding purchasing utility power would be

$$\text{Savings} = 200\ \text{kW} \times 8760\ \text{h/yr} \times 0.90 \times \$0.10/\text{kWh} = \$157{,}680/\text{yr}$$

Demand savings assuming the full 200 kW is online during peaks

$$\text{Demand savings} = 200\ \text{kW} \times \$10/\text{mo/kW} \times 12\ \text{mo/yr} = \$24{,}000/\text{yr}$$

Net annual operational savings from the fuel cell

$$\text{Net savings} = \$157{,}680 + \$24{,}000 - \$114{,}791 = \$66{,}889/\text{yr}$$

For a 10-year simple payback, the fuel cell would have to cost no more than

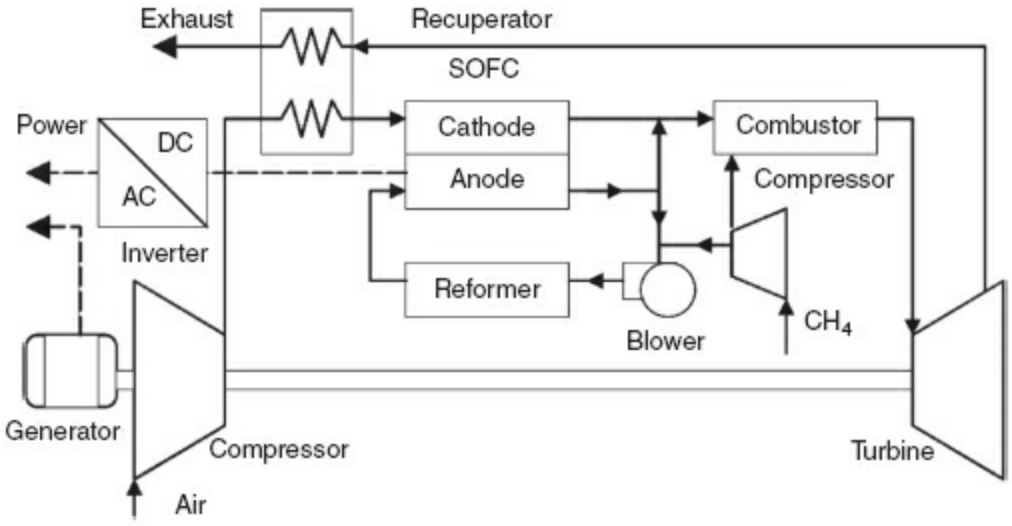
$$\text{Payback} = \frac{\text{Investment cost}}{\text{1st year's savings}} = \frac{P(\$)}{\$66{,}889/\text{yr}} = 10\ \text{yrs}$$

$$\text{Capital cost} = \$668{,}890$$

For this 200-kW system that works out to \$3.34/W.

The efficiency of 52% calculated in Example 9.11 is for a fuel cell system that does not capture waste heat. Development has been underway for some time to combine an SOFC with a microturbine to achieve even higher electrical efficiencies (Fig. 9.28). Efficiencies in the range of 60–73% seem possible with this configuration (EPRI, 2003).

FIGURE 9.28 Gas turbines with pressurized solid oxide fuel cells (SOFCs) may be capable of efficiencies exceeding 70%.



9.8.9 Hydrogen Production

With the exception of DMFCs, fuel cells require a source of hydrogen H_2 for the anodic reactions. For those that operate at higher temperatures (MCFCs and SOFCs), methane may be reformed to yield hydrogen as part of the fuel cell system itself, but in general, obtaining a supply of hydrogen of sufficient purity and at a reasonable cost is a major hurdle that must be dealt with before large-scale commercialization of fuel cells will be achieved.

Hydrogen as a fuel has many desirable attributes. When burned, it yields only small amounts of NO_X created when combustion temperatures are high enough to cause the nitrogen and oxygen in air to combine. For hydrogen used in fuel cells, however, the only end product is water. Given its low density, it readily escapes from confined environments so it is less likely to concentrate into dangerous pools the way gasoline fumes, for example, do. It is, however, not an energy source. It is, like electricity, a high quality energy carrier that is not naturally available in the environment. It must be manufactured, which means an energy investment must be made to create the desired hydrogen fuel.

The main technologies currently in use for hydrogen production are steam reforming of methane (SMR), partial oxidation (POX), and electrolysis of water. More exotic methods of production in the future may include photocatalytic, photoelectrochemical, or biological production of hydrogen using sunlight as the energy source.

Methane Steam Reforming (MSR): About 5% of U.S. natural gas is already converted to hydrogen for use in ammonia production, oil refining, and a variety of other chemical processes. Almost all of that is done with steam methane reformers. After some gas cleanup, especially to remove sulfur, a mixture of natural gas and steam is passed through a catalyst at a very high temperature (700–850°C), producing a synthesis gas, or syngas, consisting of CO and H_2:

$$CH_4 + H_2O \rightarrow CO + 3H_2 \quad (9.44)$$

The above reaction is endothermic, that is, heat must be added, which may be provided in part by burning some of the methane as fuel.

The hydrogen concentration in the syngas is then increased using a water-gas shift reaction:

$$CO + H_2O \rightarrow CO_2 + H_2 \quad (9.45)$$

This reaction is exothermic, which means some of the heat released can be used to drive Equation 9.44. The resulting syngas in Equation 9.45 is 70–80% H_2, with most of the remainder being CO_2 plus small quantities of CO, H_2O, and CH_4. Final processing includes removal of CO_2 and conversion of remaining CO into methane in a reverse of reaction Equation 9.44. The overall energy efficiency of SMR hydrogen production is typically 75–80%, but higher levels are achievable.

Partial Oxidation (POX): These systems are based on methane (or other hydrocarbon fuels) being partially oxidized in the following exothermic reaction.

$$CH_4 + \frac{1}{2}O_2 \rightarrow CO + 2H_2 \quad (9.46)$$

Since Equation (9.46) is exothermic, it produces its own heat, which makes it potentially simpler than the MSR process since it can eliminate the MSR heat exchanger required to transfer heat from Equation 9.45 to Equation 9.44. After the partial oxidation step, a conventional shift reaction can be used to concentrate the H_2 in the resulting syngas.

Gasification of Biomass, Coal, or Wastes: As mentioned in Section 8.7, gasification of biomass or other solid fuels such as coal or municipal wastes by high temperature pyrolysis can be used to produce hydrogen. In fact, that was the primary method of hydrogen production before natural gas become so widely available. With the likelihood of relatively inexpensive technology to remove CO_2 from the resulting syngas, there is growing interest in coal gasification for hydrogen production.

Electrolysis of Water: In reactions that are the reverse of conventional fuel cells, electrical current forced through an electrolyte can be used to break apart water molecules, releasing hydrogen and oxygen gases.

$$2H_2O \rightarrow 2H_2 + O_2 \quad (9.47)$$

In fact, the same membranes that are used in PEM cells can be used in low temperature electrolyzers. Similarly, solid oxide electrolytes can be used for high temperature electrolysis.

A sketch of an electrolysis cell that uses a proton exchange membrane is shown in Figure 9.29. Deionized water introduced into the oxygen side of the cell dissociates into protons, electrons, and oxygen. The oxygen is liberated, the protons pass through the membrane, and the electrons take the external path through the power source to reach the cathode where they reunite with protons to form hydrogen gas. Overall efficiency can be as high as 85%.

Hydrogen produced by electrolysis has the advantage of being highly purified, so the problems of catalytic CO poisoning that some fuel cells are subject to is not a concern. When the electricity for electrolysis is generated using a renewable energy system, such as wind, hydro, or photovoltaic power, hydrogen is produced without emission of any GHGs. And, as Figure 9.30 suggests, when the resulting hydrogen is subsequently converted back to electricity using fuel cells, the ultimate goals of carbon-free electricity, available whenever

it is needed, whether or not the sun is shining or the wind is blowing, without depleting scarce nonrenewable resources, can become an achievable reality.

FIGURE 9.29 A proton exchange membrane used to electrolyze water.

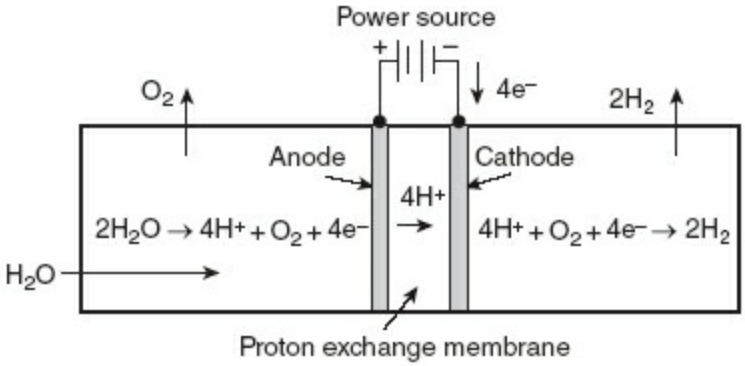
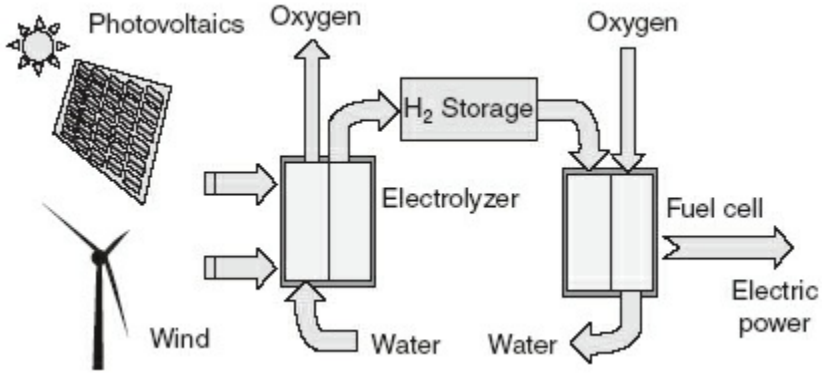


FIGURE 9.30 Renewable energy sources coupled with fuel cells can provide electric power where and when it is required, cleanly, efficiently, and sustainably.



REFERENCES

Babcock and Wilcox 1992. *Steam*. 40th ed., Babcock & Wilcox, Barberton, OH.

Brooks A, Lu E, Reicher D, Spirakis C, B. Weihl 2010. Demand Dispatch: using real-time control of demand to help balance generation and load. *IEEE Power & Energy Magazine*, vol. 10, pp. 1540–7977.

Brown R, Borgeson S, and J. Koomey 2008. Building-sector efficiency potential based on the clean energy futures study. In: *Think Efficiency*. American Physical Society.

EPRI 2003. Demonstration of a high-efficiency solid oxide fuel cell-microturbine hybrid power system. Electric Power Research Institute.

EPRI 2008. *U.S. Potential for Energy Efficiency and Demand Response in a Carbon-Constrained Future*. Palo Alto, CA: Electric Power Research Institute.

GTM. *Foundations for Tomorrow's Smart Grid: Optimizing the Distribution Grid to Address Present and Future Challenges*. Ventyx: GreenTech Media.

IRENA 2012. *Renewable Energy Technologies: Cost Analysis Series—Hydropower*. Vol. 1: Power Sector, Issue 3/5. International Renewable Energy Agency, Jun.

Kempton W, and J. Tomic 2005. Vehicle-to-grid power fundamentals: Calculating capacity and net revenue, *Journal of Power Sources*, vol. 144, pp. 268–279.

Kintner-Meyer M. 2007. Regional PHEV demonstration: A grid perspective. Pacific Northwest National Laboratory. PNNL-SA-55212.

McKinsey & Company 2009. Pathways to a Low-Carbon Economy, Version 2 of the Global Greenhouse Gas Abatement Cost Curve.

Petchers N. 2002. *Combined Heating, Cooling and Power: Technologies and Applications*. The Fairmont Press, Lilburn, GA.

PROBLEMS

9.1 Consider the possibility of sending power from one line to another even though they have the same voltage, but are out of phase with each other. Suppose a link with j 5-Ω-reactance connects two 10 kV lines out of phase with each other by 10°. Find real power P and reactive power Q delivered from one line to the other.

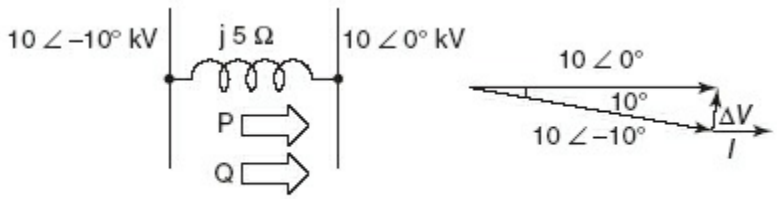


FIGURE P9.1

9.2 The rate structure for an office building includes an energy charge of \$0.07/kWh and a summer demand charge of \$9/mo per peak kW. As a money saving strategy, during the 21 d/mo that the office is occupied, it has been decided to shed 10 kW of load for an hour during the period of peak demand in the summer.

a. How much energy (kWh/mo) will be saved?

b. By what amount will their bill be reduced (\$/mo) during those months?

c. What is the value of the energy saved in dollars per kWh?

9.3 Consider the following energy conservation supply curve:

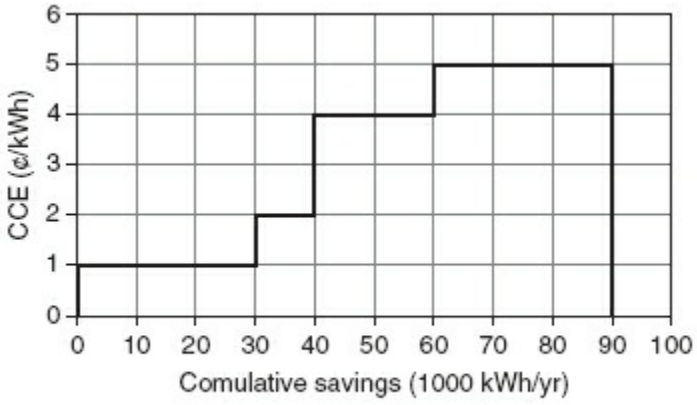


FIGURE P9.3

How much energy can be saved at an average cost of less than 3 ¢/kWh?

9.4 The following are CCE data taken from Figure 9.16 for simple efficiency improvements that can easily be adopted into U.S. homes.

TABLE P9.4

	CCE	Savings Potential
Household Item	(¢/kWh)	(Million kWh/yr)
TV	0.8	60, 000
Lighting	1.3	170, 000
Misc plug loads	1.8	60, 000
Computers	4.3	40, 000
Refrigerators	4.6	30, 000

If all of these were to be done together

a. What is the average CCE (¢/kWh)?

b. Find the average net-cost of carbon abatement ($/t CO_2) if the average electricity carbon intensity is 0.4 kg CO_2/kWh and the average retail price of residential electricity displaced is 9.4 ¢/kWh.

9.5 Four measures are being proposed for a small industrial facility to reduce its need to purchase utility electricity. The following table describes each measure and gives its capital cost and annual kWh savings. The owner uses a CRF of 0.06/yr.

TABLE P9.5

	Suggested Measure	Capital Cost ($)	Savings (kWh/yr)
A.	Better lighting system	100,000	150,000
B.	High efficiency motors	20,000	120,000
C.	More efficient chiller	180,000	180,000
D.	Photovoltaic system	150,000	60,000

a. Compute the CCE for each measure and plot an appropriate energy conservation supply curve.

b. How much energy can be saved (kWh/yr) if the criterion is that each measure must have a CCE of no more than 6 ¢/kWh?

c. How much energy can be saved (kWh/yr) if the criterion is that the average cost of energy saved is no more than 6 ¢/kWh?

9.6 In Example 9.3, a $3.2 million lighting retrofit saved 4.5 million kWh/yr with a CCE of 4.63 ¢/kWh and a carbon abatement cost of negative $147.48/t CO_2. Suppose you combine that retrofit with a $3 million photovoltaic project that delivers 825, 000 kWh/yr.

TABLE P9.6

Utility rate	$0.12	$/kWh
Term	30	years
Interest	5%	
CRF (i, n)	0.0651	per year
Carbon rate	0.50	kg CO_2/kWh

	Cost 10^6 $/yr	Avoided 10^6 kWh/yr	Utility Savings 10^3 $/yr	System Cost 10^3 $/yr	Net Cost 10^3 $/yr	CCE (¢/kWh)	Carbon Savings (t/yr)	CO_2 Abatement ($/t)
Lighting	$3.20	4.500	$540.00	$208.16	$(331.84)	4.63	2250	$(147.48)
Solar	$3.00	0.825						
Hybrid	$6.20							

a. For the PV project, what is its CCE ($/kWh) and carbon abatement cost ($/t CO_2)? Table P9.6 may help organize your results.

b. With both projects done at the same time (hybrid system) find the overall CCE ($/kWh) and carbon abatement cost ($/t CO_2).

c. Draw a "McKinsey" GHG abatement curve for these two investments, like the one shown in Figure 9.17.

9.7 A natural-gas-fired 65-kW microturbine has 28% electrical efficiency, 52% conversion efficiency to useful heat, and it runs with an 85% capacity factor. That heat displaces natural gas used in an 80%-efficient boiler. Its $220, 000 capital cost for an installed system is amortized with a 0.08/yr CRF.

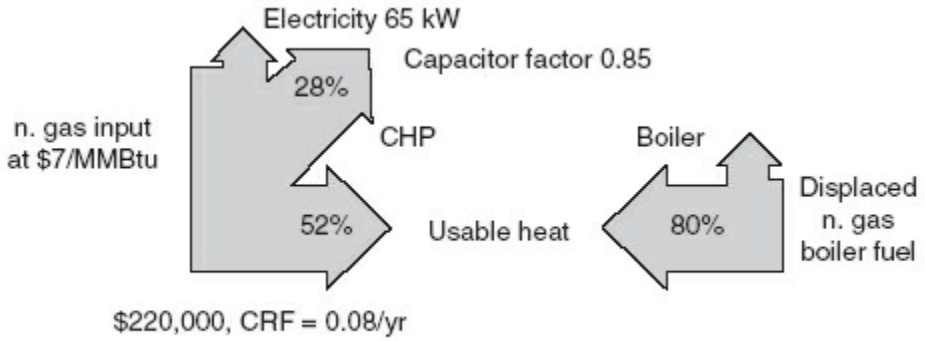


FIGURE P9.7

a. Work out the power flows for a diagram like that shown in Example 9.4.

b. Find the energy chargeable to power (ECP, Btu/kWh).

c. Find the fuel cost chargeable to power (CCP, $/kWh).

d. Find the cost of electricity generated ($/kWh).

e. Compare the overall efficiency of the CHP system to the efficiency of a separate gas boiler for heat, coupled with electricity from a gas-fired power plant having a heat rate of 9000 Btu/kWh, and 8% transmission losses to the site.

9.8 One way to design a CHP system is to size it based on a steady demand for heat and then net meter the system just like what is commonly done for PV systems. Consider a laundromat that needs 6000 gal/d of water heated from 60°F to 120°F (recall water

density 8.34 lb/gal and the 3412 Btu/kWh conversion). Suppose PEM fuel cells convert 40% of their input energy into heating water and 34% into generation of electricity.

a. How many kW (output electrical capacity) of fuel cells should the laundromat install to have the CHP waste heat meet its hot water demand (as long as the fuel cell is running at full output)?

b. By how much would their energy bill (gas and electricity) decrease ($/yr) if the laundry pays $0.13/kWh for its electricity and $1.20 per therm (100, 000 Btu) of gas burned in their 80%-efficient boiler? Assume an annual capacity factor of 85%.

c. If the after-incentives fuel cell cost of $4/kW is amortized with a 10-year, 5% loan for which the interest portion is tax deductible using a 35% marginal tax bracket, what is the net cash flow for the first year's operation of the system?

9.9 A fuel cell company claims their CHP unit delivers 5 kW of electricity, 20, 000 Btu/h of usable heat (e.g., for hot water), while burning 1/2 therm of natural gas per hour (1 therm = 100, 000 Btu), all the while cutting carbon emissions by 41%.

a. What is the overall efficiency of the unit as it converts gas into electricity and useful heat?

b. What is the overall efficiency savings by using the CHP unit instead an 85%-efficient boiler for hot water and our conventional 33%-efficient grid?

c. Assuming CO_2 emissions from the grid average 0.6 kg CO_2/kWh while emissions from natural gas are 5 kg/therm, what percent carbon emission savings would this CHP provide?

d. What would the after-tax-credits cost of this system have to be if the goal is to get a simple payback of 10 years? Assume electricity costs $0.15/kWh, natural gas costs $1.10/therm, and the system runs with a capacity factor of 0.9.

9.10 What percentage reduction in carbon emissions do the following natural-gas-fired CHP systems provide compared to the specified separately generated electricity and heat systems? For carbon emissions, assume natural gas emits 53 g CO_2/MJ, and for average grid emissions assume 0.6 kg CO_2/kWh. The joule equivalent of 1 kWh of electricity is 3.6 MJ.

a. CHP with 36% electrical efficiency and 40% thermal efficiency versus an 85%-efficient gas boiler for heat and the above average grid for electricity.

b. CHP with 50% electrical efficiency and 20% thermal efficiency versus a 33%-efficient, 1.0 kg CO_2/kWh, coal-fired power plant for electricity and an 80%-efficient gas-fired boiler for heat.

9.11 Whether an electric vehicle has a carbon advantage over an internal combustion engine (ICE) depends on the source of EV electricity as well as the fuel efficiency of the car to which it is being compared. Assuming a well-to-wheels emission rate of 11.2 kg CO_2/gal of gasoline for an ICE and 3.0 mi/kWh efficiency for an EV find the following:

a. What fuel efficiency (mi/gal) would conventional ICE vehicles have to achieve to be as clean as EVs powered by natural-gas combined-cycle power plants that emit 0.45 kg CO_2/kWh?

b. What carbon emission rate (kg CO_2/kWh) would the grid have to achieve to be as

clean as a 50 –mi/gal ICE vehicle (for comparison, the U.S. grid averages 0.6 kg CO_2/kWh)?

c. Which is cleaner, an EV powered by electricity from a coal-fired power plant that emits 1.0 kg CO_2/kWh or a new car that meets the 2016 corporate average fuel economy (CAFE) standard of 35.5 mi/gal?

9.12 Under the assumptions given in Problem 9.11

a. What price of gasoline ($/gal) for an ICE vehicle getting 35.5 mi/gal would be equivalent to off-peak electricity at $0.06/kWh for the EV?

b. Size a photovoltaic system (kWp and m^2) to supply 10, 000 electric vehicle mi/yr in an area with 5.5 kWh/m^2/d of insolation. Assume a 0.75 derate factor and 18%-efficient photovoltaics.

c. Suppose the PV system just designed costs $4/Wp, it is financed with a 4%, 30-year loan, with tax-deductible interest and the owner is in a 25% marginal tax bracket. Compare the first-year $/mi cost of PV electricity for the EV versus $4/gal gasoline for a 35.5 mi/gal ICE.

APPENDIX A

ENERGY ECONOMICS TUTORIAL

There are many ways to calculate the economic viability of distributed generation and energy efficiency projects. The capital cost of equipment, the operation and maintenance costs, along with fuel costs, must be combined in some manner so that a comparison may be made with the costs of not doing the project. The treatment presented here, although somewhat superficial, is intended to provide a reasonable start to the financial evaluation—enough at least to know whether the project deserves further, more careful, analysis.

A.1 SIMPLE PAYBACK PERIOD

One of the most common ways to evaluate the economic value of a project is with a simple payback analysis. This is just the ratio of the extra first cost, ΔP, to the annual savings, S:

$$\text{Simple payback (yr)} = \frac{\text{Extra first cost } \Delta P(\$)}{\text{Annual savings } S(\$/\text{yr})} \tag{A.1}$$

For example, an energy-efficient air conditioner that costs an extra $1000 and which saves $200/yr in electricity would have a simple payback of 5 years.

Simple payback has the advantage of being the easiest to understand of all economic measures, but it has the unfortunate problem of being one of the least convincing ways to present the economic advantages of a project. Surveys consistently show that individuals and corporations alike demand very short payback periods—on the order of only a few years—before they are willing to consider an energy investment. The 5-year payback in the above example would probably be too long for most decision makers, yet, for example, if the air conditioner lasts for 10 years the extra cost is equivalent to an investment that earns a tax-free annual return of over 15%. Almost anyone with some money to invest would jump at the chance to earn 15%, but most would not choose to put it into a more efficient air conditioner.

Simple payback is also one of the most misleading measures since it does not include anything about the longevity of the system. Two air conditioners may both have 5-year payback periods, but even though one lasts for 20 years and the other one falls apart after 5, the payback period makes absolutely no distinction between the two.

A.2 INITIAL (SIMPLE) RATE OF RETURN

The initial (or simple) rate of return is just the inverse of the simple payback period. That

is, it is the ratio of the annual savings to the extra initial investment:

$$\text{Initial (simple) rate of return} = \frac{\text{First-yr savings } S(\$)}{\text{Extra first cost } \Delta P(\$)} \tag{A.2}$$

Just as the simple payback period makes an investment look worse than it is, the initial rate of return does the opposite and makes it look too good. For example, if an efficiency investment with a 20% initial rate of return, which sounds very good, lasts only 5 years, then just as the device finally pays for itself, it dies and the investor has earned nothing. On the other hand, if the device has a long lifetime, the simple return on investment is a good indicator of the true value of the investment as will be shown in the next section.

Even though the initial rate of return may be misleading, it does often serve a useful function as a convenient "minimum threshold" indicator. If the investment has an initial rate of return that falls below the threshold, there is no need to proceed any further.

A.3 THE TIME VALUE OF MONEY AND NET PRESENT VALUE

The simple payback period and rate of return are just that—too simple. Any more serious analysis involves taking into account the time value of money, that is, the fact that having one dollar 10 years from now is not as good as having one dollar in your pocket today. To account for these differences, a present worth analysis in which all future costs are converted into an equivalent *present value* or *present worth* (the terms are used interchangeably) is often required.

Begin by imagining an investment today of P into an account earning interest, i. After 1 year the account will have earned interest iP, so it will then be worth $P + iP = P(1+i)$; after two years it will have $P(1+i)^2$, and so forth. That says the future amount of money F in an account that starts with P, which earns annual interest i over a period of n years, will be

$$F = P(1+i)^n \tag{A.3}$$

Rearranging Equation A.3 gives us a relationship between a future amount of money F and what it should be worth to us today P:

$$P = \frac{F}{(1+i)^n} \tag{A.4}$$

When converting a future value F into a present value P, the interest term i in Equation A.4 is usually referred to as a *discount rate*, d. The discount rate can be thought of as the interest rate that could have been earned if the money had been put into the best alternative investment. For example, if an efficiency investment is projected to save $1000 in fuel in the fifth year, and the best alternative investment is one that would have earned 10%/yr interest, the present worth of that $1000 would be

$$P = \frac{F}{(1+d)^n} = \frac{\$1000}{(1+0.10)^5} = \$620.92 \tag{A.5}$$

That is, a person with a discount rate of 10% should be neutral about the choice between having $620.92 in his or her pocket today, and having $1000 in 5 years. Or stated differently, that person should be willing to spend $620.92 today in order to save $1000 worth of energy 5 years from now. Note that the higher the discount rate, the less valuable a future payoff becomes. For instance, with a 20% discount rate, that $1000 in 5 years is equivalent to only $401.87 today. A high discount rate implies you do not care much about returns very far into the future.

When viewed from the perspective of a neutral decision—that is, would someone be just as happy with P now or F later, the discount rate takes on added meaning and may not refer to just the best alternative investment. Ask people without significant financial resources, for instance college students, about the choice between $621 today or $1000 in 5 years and chances are high that they would much prefer the $621 today. In 5 years, college students anticipate having a lot more money so $1000 then would not mean nearly as much as $621 today when they are so strapped for cash. That is, their personal discount rate is probably much higher than 10%. Similarly, if there is significant risk in the proposition, then factoring in the probability that there will be no F in the future, means the discount rate would need to be much higher than would be suggested by the interest that a conventional alternative investment might earn. Deciding just what is an appropriate discount rate for an investment in energy efficiency or distributed generation is often the most difficult, and critical, step in a present value analysis.

Frequently, a distributed generation or efficiency investment will deliver financial benefits year after year. To find the present value P of a stream of annual cash flows A, for n years into the future, with a discount rate d, we can introduce a conversion factor called the *present value function* (PVF):

$$P = A \cdot \mathrm{PVF}(d, n) \tag{A.6}$$

For a series of n annual $1 amounts that start 1 year from the present, PVF is the summation of the present values:

$$\mathrm{PVF}(d, n) = \frac{1}{1+d} + \frac{1}{(1+d)^2} + \cdots \frac{1}{(1+d)^n} \tag{A.7}$$

A series analysis of Equation A.7 yields the following:

$$\mathrm{PVF}(d, n) = \frac{(1+d)^n - 1}{d(1+d)^n} \tag{A.8}$$

With all of the variables expressed in annual terms, the units of PVF will be years.

The present value of all costs, present and future, for a project is called the *life-cycle cost* of the system under consideration.

When a choice is to be made between two investments, the net present value (NPV) of the savings can be found by

$$\mathrm{NPV} = \Delta A \times \mathrm{PVF}(d, n) - \Delta P \tag{A.9}$$

where ΔP is the extra capital cost of the more efficient product, and ΔA is the extra annual energy savings associated with purchasing the better product.

Example A.1 NPV of an Energy-Efficient Motor. Two 100-hp electric motors are being considered—call them "cheap" and "premium." The cheap motor draws 79 kW and costs $2400; the premium motor draws 75 kW and costs $2900. The motors run 1600 h/yr with electricity costing $0.08/kWh. Over a 20-year life, find the NPV of the premium motor when a discount rate of 10% is assumed.

Solution. The annual electricity savings for the premium motor is

$$\Delta A = (79 - 75)\mathrm{kW} \times 1600\ \mathrm{h/yr} \times \$0.08/\mathrm{kWh} = \$512/\mathrm{yr}$$

The present value factor for a 20-year cash flow with a 10% discount rate is

$$\mathrm{PVF}(d, n) = \frac{(1+d)^n - 1}{d(1+d)^n} = \frac{(1+0.10)^{20} - 1}{0.10(1+0.10)} = 8.5136\ \mathrm{yr}$$

The present value of 20 years of electricity savings for the premium motor is

$$\mathrm{PV(savings)} = \Delta \mathrm{A} \times \mathrm{PVF}(d, n) = \$512/\mathrm{yr} \times 8.5136\ \mathrm{yr} = \$4359$$

The premium motor costs an additional $500 so the NPV of the savings is

$$\mathrm{NPV} = \$4359 - \$500 = \$3859$$

What does this really mean? It means if you buy the cheap motor, you make extra electricity payments of $512/yr to the utility. If you buy the premium motor, you can go to the bank, take out a 20-year, 10% loan for $4359 and make the same annual payments of $512, but now it is to the bank instead of the utility. Use $500 of that $4359 to pay the extra cost of the better motor. Put the other $3859 into your pocket on day 1. Do with it what you like. The NPV is $3859.

A.4 INTERNAL RATE OF RETURN

The *internal rate of return* (IRR) is perhaps the most persuasive measure of the value of an energy-efficiency or distributed-generation project. It is also the trickiest to compute. The IRR allows the energy investment to be directly compared with the return that might be obtained for any other competing investment. IRR is the discount rate that makes the NPV of the energy investment equal to zero. In the simple case of a first-cost premium, ΔP, for the more efficient product, which results in an annual fuel savings ΔA, it is the discount rate that makes the NPV in Equation A.9 be zero:

$$\mathrm{NPV} = \Delta A \times \mathrm{PVF}(\mathrm{IRR}, n) - \Delta P = 0 \tag{A.10}$$

Rearranging Equation A.10, and realizing that $\Delta P/\Delta A$ is just the simple payback period introduced earlier, gives the following convenient relationship for finding the IRR:

$$\text{PVF}(\text{IRR}, n) = \frac{\Delta P}{\Delta A} = \text{Simple payback period} \quad \text{(A.11)}$$

Solving Equation A.11 is not straightforward and if you are doing it by hand requires making trial-and-error estimates of the discount rate (IRR) until the equation balances. Most spreadsheet programs, and most pocket calculators, will also do the calculation automatically. If the calculation is to be done by hand, it helps to have precalculated values for the PVF, such as those presented in Table A.1. To use Table A.1, enter the table in the row corresponding to the project lifetime and move across until the simple payback period $\Delta P/\Delta A$ is reached. The IRR is the interest rate at the top of that column of the table. Some interpolation may be called for if you want the exact answer.

TABLE A.1 Simple Payback to Help Estimate IRR[a]

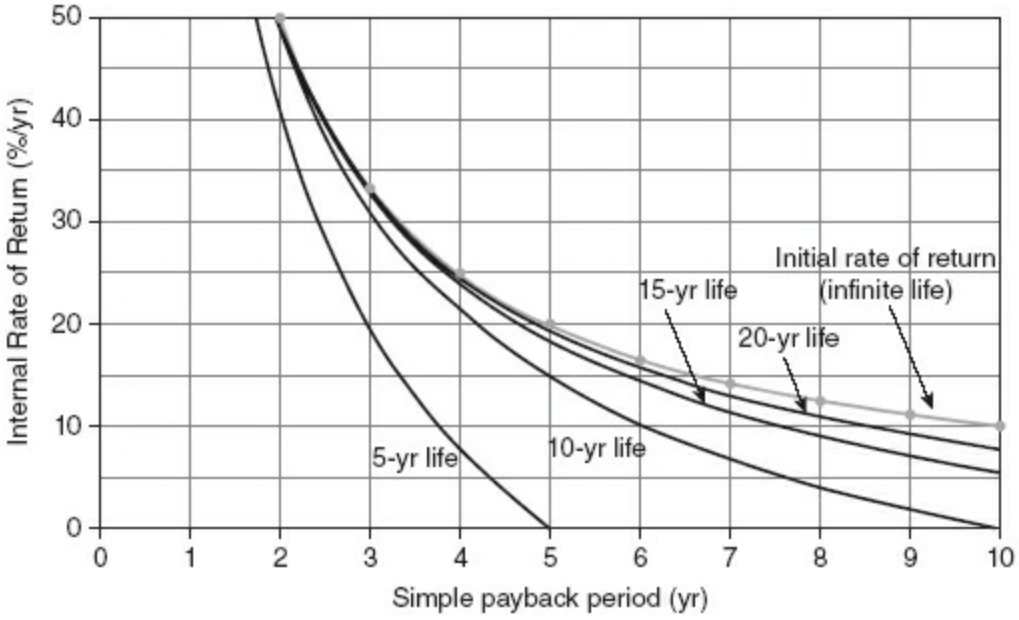
	Internal Rate of Return (%)													
Life (yr)	3%	4%	5%	6%	7%	8%	9%	10%	12%	14%	16%	18%	20%	22%
5	4.58	4.45	4.33	4.21	4.10	3.99	3.89	3.79	3.60	3.43	3.27	3.13	2.99	2.86
6	5.42	5.24	5.08	4.92	4.77	4.62	4.49	4.36	4.11	3.89	3.68	3.50	3.33	3.17
7	6.23	6.00	5.79	5.58	5.39	5.21	5.03	4.87	4.56	4.29	4.04	3.81	3.60	3.42
8	7.20	6.73	6.46	6.21	5.97	5.75	5.53	5.33	4.97	4.64	4.34	4.08	3.84	3.62
9	7.79	7.44	7.11	6.80	6.52	6.25	6.00	5.76	5.33	4.95	4.61	4.30	4.03	3.79
10	8.53	8.11	7.72	7.36	7.02	6.71	6.42	6.14	5.65	5.22	4.83	4.49	4.19	3.92
11	9.25	8.76	8.31	7.89	7.50	7.14	6.81	6.50	5.94	5.45	5.03	4.66	4.33	4.04
12	9.95	9.39	8.86	8.38	7.94	7.54	7.16	6.81	6.19	5.66	5.20	4.79	4.44	4.13
13	10.63	9.99	9.39	8.85	8.36	7.90	7.49	7.10	6.42	5.84	5.34	4.91	4.53	4.20
14	11.30	10.56	9.90	9.29	8.75	8.24	7.79	7.37	6.63	6.00	5.47	5.01	4.61	4.26
15	11.94	11.12	10.38	9.71	9.11	8.56	8.06	7.61	6.81	6.14	5.58	5.09	4.68	4.32
20	14.88	13.59	12.46	11.47	10.59	9.82	9.13	8.51	7.47	6.62	5.93	5.35	4.87	4.46
25	17.41	15.62	14.09	12.78	11.65	10.67	9.82	9.08	7.84	6.87	6.10	5.47	4.95	4.51
30	19.60	17.29	15.37	13.76	12.41	11.26	10.27	9.43	8.06	7.00	6.18	5.52	4.98	4.53

[a]Enter the row with project life, move across to values close to your simple payback, move up to read IRR. A 15-year project with a 5-year simple payback has an IRR a bit over 18%.

For example, from the table a project with a 15-year lifetime and a 5-year simple payback would have an IRR of a bit over 18% (actual value is 18.4%). Table A.1 can also be used to determine the IRR when the decision maker wants a simple energy payback within a certain number of years. For example, if management wants projects with an estimated 30-year lifetime to have no more than a 7-year simple payback, they are in essence requiring an IRR of 14%. That is a great investment.

Since it is so common for the simple payback period to be used to judge a project, and it is so often misleading, it may be handy to use Figure A.1 to translate payback into the more persuasive IRR. Note that for long-lived projects, the initial rate of return is a good approximation to IRR.

FIGURE A.1 Internal rate of return (IRR) as a function of the simple payback period, with project life as a parameter.



A.5 NET PRESENT VALUE WITH FUEL ESCALATION

Chances are that the cost of fuel in the future will be higher than it is today, which means the annual amount of money saved by an efficiency measure or a renewable energy system could increase with time. To account for that potential, it is handy to have a way to include a fuel price escalation factor in the present worth analysis.

Begin by rewriting Equation A.7 so that it is the sum of present values for an annual amount that is worth \$1 at time $t = 0$, but becomes $\$(1 + e)$ at $t = 1$ year, and escalates to $\$(1 + e)^n$ in the nth year

$$\mathrm{PVF}(d, e, n) = \frac{1+e}{1+d} + \frac{(1+e)^2}{(1+d)^2} + \cdots \left(\frac{1+e}{1+d}\right)^n \quad \text{(A.12)}$$

where d is the discount rate and e is the escalation rate of the annual savings. A comparison of Equation A.7 with Equation A.12 lets us write an equivalent discount rate d' when there is fuel savings escalation, e

$$\frac{1}{1+d'} = \frac{1+e}{1+d} \quad \text{(A.13)}$$

Solving

$$\text{Equivalent discount rate with fuel escalation } d' = \frac{d-e}{1+e} \tag{A.14}$$

Using Equation A.14 in the PVF gives

$$\text{PVF}(d, e, n) = \text{PVF}(d', n) = \frac{(1+d')^n - 1}{d'(1+d')^n} \tag{A.15}$$

Note for the special case when $d = e$, so that $d' = 0$, then from Equation A.12 PVF = n.

The equivalent discount rate d' given in Equation A.14 can be used in all of the present value relationships, including Equations A.5, A.8, A.9, and A.11.

Example A.2 NPV of Premium Motor with Fuel Escalation. The premium motor in Example A.1 costs an extra \$500 and saves \$512/yr at today's price of electricity. If electricity rises at an annual rate of 3%/yr, find the NPV of the premium motor if the best alternative investment earns 10%.

Solution. Using Equation A.14, the equivalent discount rate with fuel escalation is

$$d' = \frac{d-e}{1+e} = \frac{0.10 - 0.03}{1 + 0.03} = 0.06796$$

From Equation A.15, the PVF for 20 years of escalating savings is

$$\text{PVF}(d', n) = \frac{(1+d')^n - 1}{d'(1+d')^n} = \frac{(1.06796)^{20} - 1}{0.06796(1.0.06796)^{20}} = 10.764 \text{ yr}$$

From Equation A.9, the NPV associated with purchasing the premium motor is

$$\text{NPV} = \Delta A \cdot \text{PVF}(d', n) = \$512/\text{yr} \times 10.764 \text{ yr} - \$500 = \$5011$$

Without fuel escalation, the NPV was \$3859.

A.6 IRR WITH FUEL ESCALATION

To find the IRR when there is fuel escalation, the present value of the escalating series of annual savings must equal the extra initial principal:

$$\text{NPV} = \Delta A \times \text{PVF}(d', n) - \Delta P = 0 \tag{A.16}$$

$$\text{PVF}(d', n) = \frac{\Delta P}{\Delta A} = \text{Simple payback period} \tag{A.17}$$

Comparing Equation A.16 to Equation A.11, we can see that d' will be the same as the internal rate of return that is found without fuel escalation, which we will call IRR_0. Replacing d' with IRR_0 in (A.14) gives

$$d' = \frac{d - e}{1 + e} = \text{IRR}_0 \tag{A.18}$$

The discount rate d is the new IRR with fuel escalation, which we will call IRR_e:

$$\text{IRR}_e = d = \text{IRR}_0(1 + e) + e \tag{A.19}$$

Example A.3 IRR for a Photovoltaic System with Fuel Escalation. A 2-kW rooftop photovoltaic system that costs $3/Wp (after incentives) generates 3200 kWh/yr. It displaces the need to buy utility power that now costs $0.12/kWh. If utility power escalates at 3%/yr, and the system lasts 25 years, what is the IRR on the investment?

Solution. The system costs $6000 and saves $384/yr ($0.12 × 3200), so it has a simple payback period of:

$$\text{Simple payback} = \frac{\$6000}{\$384/\text{yr}} = 15.62 \text{ yr}$$

From Table A.1 with a lifetime of 25 years and simple payback of 15.62, the IRR with no fuel escalation is 4%. From Equation A.19 the IRR including fuel escalation is

$$\text{IRR}_e = \text{IRR}_0(1 + e) + e = 0.04(1 + 0.03) + 0.03 = 0.071 = 7.1\%$$

That is a significant increase, making the system economically better than almost any alternative safe investment.

A.7 ANNUALIZING THE INVESTMENT

In many circumstances the extra capital required for an energy investment will be borrowed from a lending company, obtained from investors who require a return on their investments, or taken from one's own accounts. In all of these circumstances, the economic analysis can be thought of as a loan that converts the capital cost into a series of equal annual payments that eventually pay off the loan with interest. Even if the money is not actually borrowed, the same approach can be used to annualize the cost of the energy investment, which has many useful applications. The key equation is

$$A = P \times \text{CRF}(i, n) \tag{A.20}$$

where

A = Annual loan payments ($/yr)

P = Principal borrowed ($)

i = interest rate (e.g., 10% corresponds to i = 0.10/yr)

n = loan term (yr)

and

$$\text{CRF}(i, n) = \text{Capital recovery factor } (\text{yr}^{-1}) = \frac{i(1+i)^n}{(1+i)^n - 1} \tag{A.21}$$

Note the capital recovery factor (CRF) is just the inverse of the PVF. Since we are treating the first cost of the investment as a loan, we have gone back to using an interest rate i rather than a discount rate d.

A short table of values for the CRF is given in Table A.2.

TABLE A.2 Capital Recovery Factors

	Loan Interest Rate (%)										
Term (yrs)	2%	3%	4%	5%	6%	7%	8%	9%	10%	11%	12%
5	0.2122	0.2184	0.2246	0.2310	0.2374	0.2439	0.2505	0.2571	0.2638	0.2706	0.2774
10	0.1113	0.1172	0.1233	0.1295	0.1359	0.1424	0.1490	0.1558	0.1627	0.1698	0.1770
15	0.0778	0.0838	0.0899	0.0963	0.1030	0.1098	0.1168	0.1241	0.1315	0.1391	0.1468
20	0.0612	0.0672	0.0736	0.0802	0.0872	0.0944	0.1019	0.1095	0.1175	0.1256	0.1339
25	0.0512	0.0574	0.0640	0.0710	0.0782	0.0858	0.0937	0.1018	0.1102	0.1187	0.1275
30	0.0446	0.0510	0.0578	0.0651	0.0726	0.0806	0.0888	0.0973	0.1061	0.1150	0.1241

Equations A.20 and A.21 were written as if the loan payments are made only once each year. They are easily adjusted to find monthly payments by dividing the annual interest rate i by 12 and multiplying the loan term n in years by 12, leading to the following:

$$\text{CRF}(i, n) = \frac{(1/12)[1 + (1/12)]^{12n}}{[1 + (1/12)]^{12n} - 1} \text{ per mo} \tag{A.22}$$

Example A.4 Comparing Annual Costs to Annual Savings. The photovoltaic system in Example A.3 that costs \$6000 and generates 3200 kWh/yr is to be added to a 4%, 30-year home mortgage. It displaces electricity costing \$0.12/kWh, which works out to \$384/yr. Find the annual monetary savings and find the cost of electricity from the system.

Solution. From (A.21) the CRF will be

$$\text{CRF}(4\%,\ 30\text{ yr}) = \frac{i(1+i)^n}{(1+i)^n - 1} = \frac{0.04(1.04)^{30}}{(1.04)^{30} - 1} = 0.05783/\text{yr}$$

The annual loan payments will be

$$\text{A} = \text{P} \times \text{CRF}(i,n) = \$6000 \times 0.05783/\text{yr} = \$347/\text{yr}$$

So the system saves \$384 – \$347 = \$37 in the first year. That is an immediate positive cash flow for the buyer, which is a far more optimistic way to think about the purchase than calling it a system with a 15.6-year payback period.

The cost of electricity from the system is

$$\text{Electricity cost} = \frac{\$347/\text{yr}}{3200\text{ kWh/yr}} = \$0.1084/\text{kWh} = 10.84\ ¢/\text{kWh}$$

which is a little bit cheaper than the current price of electricity from the utility. As utility

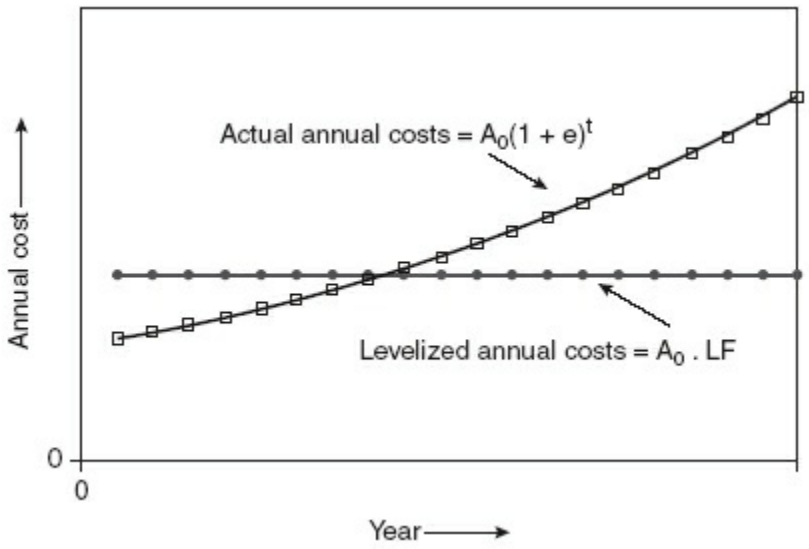
prices rise, the investment will look even better over time.

A.8 LEVELIZED BUSBAR COSTS

To do an adequate comparison of cost per kilowatt-hour from a renewable energy system versus that for a fossil-fuel-fired power plant, the potential for escalating future fuel costs must be accounted for. To ignore that key factor is to ignore one of the key advantages of renewable energy systems; that is, their independence from the uncertainties associated with future fuel costs.

The cost of electricity per kilowatt-hour for a power plant has two key components—an up-front, fixed cost to build the plant plus an assortment of costs that will be incurred in the future. In the usual approach to a levelized cost estimation, a present value calculation is first performed to find an equivalent initial cost, and then that amount is spread out into a uniform series of annual costs. The ratio of the equivalent annual cost ($/yr) to the annual electricity generated (kWh/yr) is called the *levelized, busbar* cost of power (the "busbar" refers to the wires as they leave the plant boundaries). Figure A.2 illustrates the concept.

FIGURE A.2 Levelizing annual costs when there is fuel escalation.



In the first step, the present value of all future costs must be found. To keep things simple, we will assume the annual costs today are A_0, and that they escalate due to fuel prices, O&M, and other factors at the rate e. The present value of these escalating annual costs over a period of n years is given by:

$$\text{PV(annual costs)} = A_0 \cdot \text{PVF}(d', n) \tag{A.23}$$

With d being the nominal discount rate (without escalation) and e being the escalation in future costs, the equivalent discount rate d' including fuel escalation was given in Equation A.14 as:

$$d' = (d - e)/(1 + e) \tag{A.14}$$

Having found the present value of those future costs, we now want to find an equivalent annual cost using the CRF:

$$\text{Levelized annual costs} = A_0[\text{PVF}(d', n) \cdot \text{CRF}(d, n)] \tag{A.24}$$

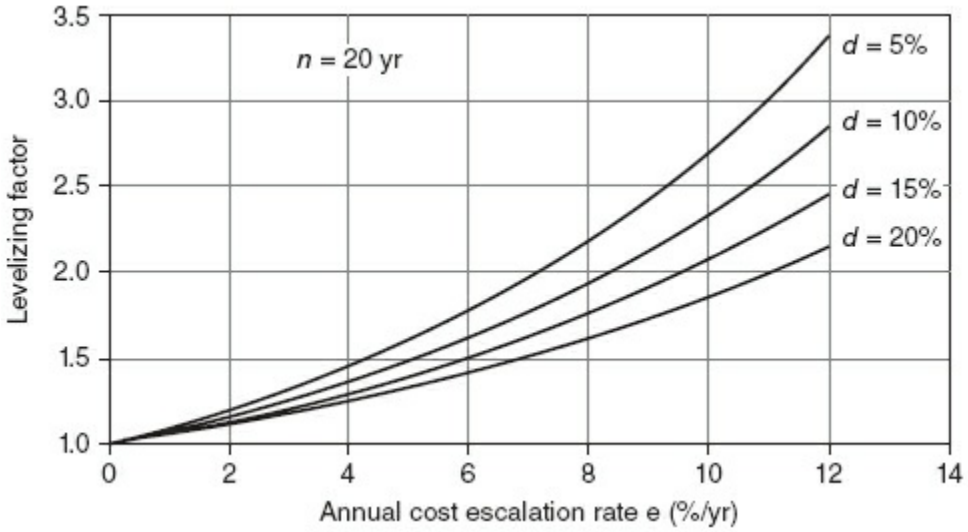
The product in the brackets, called the *levelizing factor*, is a multiplier that converts the escalating annual fuel and O&M costs into a series of equal annual amounts.

$$\text{Levelizing factor (LF)} = \left[\frac{(1+d')^n - 1}{d'(1+d')^n}\right] \cdot \left[\frac{d(1+d)^n}{(1+d)^n - 1}\right] \tag{A.25}$$

Note that when there is no escalation ($e = 0$), then $d' = d$ and the levelizing factor is just unity.

The impact of the levelizing factor can be very high, as is illustrated in Figure A.3. For example, if fuel prices increase at 5%/yr for an owner with a 10% discount rate, the levelizing factor is 1.5.

FIGURE A.3 Levelizing factor of a function of the escalation rate of annual costs e, with the owner's discount rate d as a parameter. With a discount rate of 10%/yr and fuel escalation rate of 5%/yr, the 20-year levelized cost of fuel is 1.5 times the initial cost.



We can do a levelized cost of energy (LCOE) for a conventional steam plant by using the heat rate of the plant (Btu/kWh), the initial fuel cost ($/Btu), the per kWh O&M costs and the levelizing factor:

$$\text{Levelized annual cost (\$ /kWh)} = \left[\text{Heat rate}\left(\frac{\text{Btu}}{\text{kWh}}\right) \times \text{Fuel}\left(\frac{\$}{\text{Btu}}\right) + \text{O\&M}\left(\frac{\$}{\text{kWh}}\right)\right] \times \text{LF} \tag{A.26}$$

Just as the future cost of fuel and O&M needs to be levelized, so does the capital cost of the plant. To do so, it is handy to combine the CRF with other costs that depend on the capital cost of the plant into a quantity called the *fixed charge rate* (FCR). The FCR covers costs that are incurred even if the plant does not operate, including depreciation, return on investment, insurance and taxes. FCRs vary depending on plant ownership and current

costs of capital, but tend to be in the range of 10–18%/yr (see Section 1.6.1). The governing equation that annualizes capital costs is then:

$$\text{Levelized fixed cost (\$ /kWh)} = \frac{\text{Capital cost (\$/kW)} \times \text{FCR (1/yr)}}{8760\ \text{h/yr} \times \text{Capacity factor}} \quad \text{(A.27)}$$

Table 1.4 in Chapter 1 provides estimates for some of the key variables in Equations A.26 and A.27.

Example A.5 Cost of Electricity from a Diesel Generator. An efficient diesel generator system is characterized by the following parameters. Find its levelized ($/kWh) cost of electricity.

Plant cost = $ 500/kW, Plant life = 20 yr

Diesel fuel = ($3.90/gal)/(130,000 Btu/gal) = $30/$10^6$ Btu

Heat rate = 9300 Btu/kWh

Capacity factor = 0.70

Variable O& M cost = $0.05/kWh

Fixed charge rate = 0.12/yr

Owner discount rate = 0.10/yr

Annual fuel and O& M cost escalation rate = 4%/yr

Solution. From Equation A.27, the levelized fixed cost is

$$\text{Levelized fixed cost} = \frac{\$500/\text{kW} \times 0.12/\text{yr}}{8760\ \text{h/yr} \times 0.70} = \$0.0098/\text{kWh}$$

The initial annual cost for fuel and O&M is

$$A_0 = 9300\frac{\text{Btu}}{\text{kWh}} \times \frac{\$30}{10^6\ \text{Btu}} + \frac{\$0.05}{\text{kWh}} = \$0.329/\text{kWh}$$

This needs to be levelized to account for the future rise in costs. From Equation A.14, the inflation-adjusted discount rate d′ would be

$$d' = \frac{d-e}{1+e} = \frac{0.10-0.04}{1+0.04} = 0.05769$$

From Equation A.25, the levelizing factor for annual costs is

$$\text{Levelizing factor (LF)} = \left[\frac{(1.05769)^{20}-1}{0.05769(1.05769)^{20}}\right] \cdot \left[\frac{0.10(1.10)^{20}}{(1.10)^{20}-1}\right] = 1.373$$

The levelized annual cost is therefore

$$\text{Levelized annual cost} = A_0\ \text{LF} = \$0.329/\text{kWh} \times 1.373 = \$0.452/\text{kWh}$$

The LCOE (fixed plus annual) is

$$\text{LCOE} = \$0.0098/\text{kWh} + \$0.452/\text{kWh} = \$0.462/\text{kWh}$$

Note the capital cost of the plant is a negligible part of the total.

A.9 CASH-FLOW ANALYSIS

One of the most flexible and powerful ways to analyze an energy investment is with a cash-flow analysis. This technique easily accounts for complicating factors such as fuel escalation, tax-deductible interest, depreciation, periodic maintenance costs, and disposal or salvage value of the equipment at the end of its lifetime.

Figure A.4 shows an example of cash-flow analysis for a $1000, 6%, 10-year loan used to pay for a conservation measure that, at the time of loan initiation, saves a homeowner $150/yr in electricity. That savings in the electric bill is expected to increase 5%/yr. The homeowner has a personal discount factor of 10%. Since this is a home loan, any interest paid on the loan will qualify as a tax deduction and the homeowner's federal (and perhaps state) income taxes will go down accordingly. Let us work our way through the spreadsheet.

FIGURE A.4 Cash-flow analysis for a $1000, 6%, 10-year loan, showing fuel escalation and income tax savings on loan interest. The cash flow is always positive even though this energy saving investment has an uninspiring simple payback of 6.67 years.

Loan Principal ($)	1000.00	Energy Savings (kWh/yr)	1500
Interest	0.06	Price at t = 0 ($/kWh)	0.10
Loan term (yrs)	10	Savings at t = 0 ($/yr)	150
CRF (i, n) per yr	0.135868	Escalating at (%/yr)	5
Payments ($/yr)	135.87		
Tax bracket	0.305	Personal discount rate (yr^{-1})	0.10

End of Year	Loan Payment	Interest	Delta Principal	Loan Balance	Tax Savings	Loan Cost	Electric Savings	Net Savings	PV Savings	Cum PV Savs
0	0.00	0.00	0.00	1000.00	0.00	0.00	0.00	0.00	0.00	0.00
1	135.87	60.00	75.87	924.13	18.30	117.57	157.50	39.93	36.30	36.30
2	135.87	55.45	80.42	843.71	16.91	118.96	165.38	46.42	38.36	74.66
9	135.87	14.95	120.92	128.18	4.56	131.31	232.70	101.39	43.00	369.75
10	135.87	7.69	128.18	0.00	2.35	133.52	244.33	110.81	42.72	412.48

Begin with the loan payments. From Equation A.21, the CRF (0.06, 10) can easily be found to be 0.13587/yr. Since the loan is for $1000 it means 10 annual payments of $135.87 must be made. At time t = 0, the $1000 loan begins and the borrower has use of that money for a full year before making the first payment. That means, with 6% interest, 0.06 × $1000 = $60 in interest is owed at the end of the first year, which comes out of the first $135.87 payment. The difference $135.87 – $60 = $75.87 is applied to the loan balance, bringing it down from $1000 to $924.13 at time t = 1 year. In the next year, 0.06

× $924.13 = $55.45 pays the interest, and $135.87 – $55.45 = $80.42 is applied to the principal. Very nicely, when the tenth payment is made, the loan is completely paid off.

Figure A.4 includes the tax advantages that go with home loan interest being tax deductible. In this case, the homeowner is shown to be in 30.5% marginal tax bracket, which means every dollar of interest saves $0.305 in taxes. Table 6.5 in Chapter 6 shows 2012 federal marginal tax brackets for 2012. Having teased out the interest in each year's payments for the example loan in Figure A.4, we can now determine the income tax advantages associated with that interest. When the first payment of $135.87 was made on the loan, $60 was tax-deductible interest. That means the taxpayer's net income (net income = gross income – tax deductions) will be reduced by that $60 deduction. With the taxpayer in the 30.5% tax bracket, that buyer's income taxes in the first year will be reduced by $60 × 0.305 = $18.30. Therefore, the loan in that first year really only costs the homeowner $135.87 – $18.30 = $117.57.

The spreadsheet shown in Figure A.4 also includes an electricity savings associated with the efficiency measure worth $150/yr at $t = 0$. That rises by 5% each year, so by the time the first payment is made the fuel savings is 1.05 × $150 = $157.50. The total savings at the time of that first annual payment is therefore

$$\begin{aligned}\text{First year savings} &= \$157.50\ (\text{electricity}) + \$18.30\ (\text{taxes}) - \$135.87\ (\text{loan}) \\ &= \$39.93\end{aligned}$$

This homeowner has a personal discount rate of 10%, so the first year's savings has a present value of $39.93/(1.10) = $36.30. Continuing through the 10 years, and adding up the cumulative present values of each year's savings results in a total NPV of $412.48. If the system lasts longer than 10 years, the benefits would be even greater.

APPENDIX B

USEFUL CONVERSION FACTORS

LENGTH

1 inch	= 2.540 cm
1 foot	= 0.3048 m
1 yard	= 0.9144 m
1 mile	= 1.6093 km
1 meter	= 3.2808 ft
	= 39.37 in
1 kilometer	= 0.6214 mi

AREA

1 square inch	= 6.452 cm^2
	= 0.0006452 m^2
1 square foot	= 0.0929 m^2
1 acre	= 43, 560 ft^2
	= 0.0015625 sq mi
	= 4046.85 m^2
	= 0.404685 ha
1 square mile	= 640 acre
	= 2.604 km^2
	= 259 ha
1 square meter	= 10.764 ft^2
1 hectare	= 2.471 acre
	= 0.00386 sq mi
	= 10, 000 m^2

VOLUME

1 cubic foot	= 0.03704 cu yd
	= 7.4805 gal (US)
	= 0.02832 m^3
	= 28.32 L

1 acre-foot	= 43, 560 ft^3
	= 1233.49 m^3
	= 325, 851 gal (US)
1 gallon (US)	= 0.134 ft^3
	= 0.003785 m^3
	= 3.785 L
1 cubic meter	= 8.11 × 10^{-4} ac-ft
	= 35.3147 ft^3
	= 264.172 gal (US)
	= 1000 L
	= 10^6 cm^3

LINEAR VELOCITY

1 foot per second	= 0.6818 mph
	= 0.3048 m/s
1 mile per hour	= 1.467 ft/s
	= 0.4470 m/s
	= 1.609 km/h
1 meter per second	= 3.280 ft/s
	= 2.237 mph

MASS

1 pound (avoirdupois)	= 0.453592 kg
1 kilogram	= 2.205 lb (avoirdupois)
	= 35.27396 oz (avoirdupois)
1 ton (short)	= 2000 lb (avoirdupois)
	= 907.2 kg
	= 0.9072 ton (metric)
1 ton (metric)	= 1000 kg
	= 2204.622 lb (avoirdupois)
	= 1.1023 ton (short)

FLOW RATE

1 cubic foot per second	= 0.028316 m^3/s
	= 448.8 gal (US)/min (gpm)
1 cubic foot per minute	= 4.72 × 10^{-4} m^3/s
	= 7.4805 gpm
1 gallon (US) per minute	= 6.31 × 10^{-5} m^3/s

1 million gallons per day	= 0.0438 m^3/s
1 million acre feet per year	= 39.107 m^3/s
1 cubic meter per second	= 35.315 ft^3/s (cfs)
	= 2118.9 ft^3/min (cfm)
	= 22.83×10^6 gal/d
	= 70.07 ac-ft/d

DENSITY

1 pound per cubic foot	= 16.018 kg/m^3
1 pound per gallon	= 1.2×10^5 mg/L
1 kilogram per cubic meter	= 0.062428 lb/ft^3
1 gram per cubic centimeter	= 62.427961 lb/ft^3

CONCENTRATION

1 milligram per liter in water	=1.0 ppm
(specific gravity = 1.0)	
	= 1000 ppb
	= 1.0 g/m^3
	= 8.34 lb per million gal

PRESSURE

1 atmosphere	= 76.0 cm Hg
	= 14.696 lb/in^2 (psia)
	= 29.921 in of Hg (32°F)
	= 33.8995 ft of H_2O (32°F)
	= 101.325 kPa
1 pound per square inch	= 2.307 ft of H_2O
	= 2.036 in Hg
	= 0.06805 arm
1 Pascal (Pa)	= 1 N/m^2
	= 1.45×10^{-4} psia
1 inch of mercury (32°F)	= 3386.4 Pa
(60°F)	= 3376.9 Pa

ENERGY

1 British Thermal Unit	= 778 ft-lb
	= 252 cal
	= 1055 J

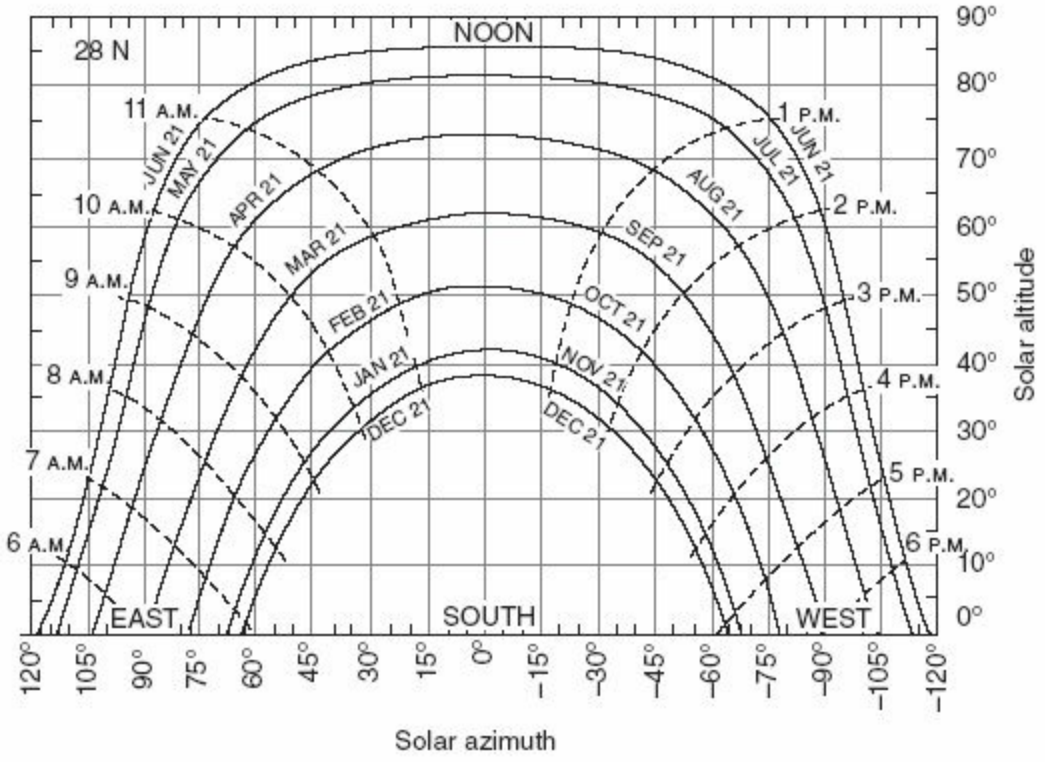
	= 0.2930 Wh
1 quadrillion Btu	= 10^{15} Btu
	= 1055×10^{15} J
	= 2.93×10^{11} kWh
	= 172×10^{6} barrels (42 gal) of oil equivalent
	= 36.0×10^{6} metric tons of coal equivalent
	= 0.93×10^{12} cubic feet of natural gas equivalent
1 joule	= 1 N m
	= 9.48×10^{-4} Btu
	= 0.73756 ft-lb
1 kilowatt-hour	= 3600 kJ
	= 3412 Btu
	= 860 kcal
1 kilocalorie	= 4.185 kJ

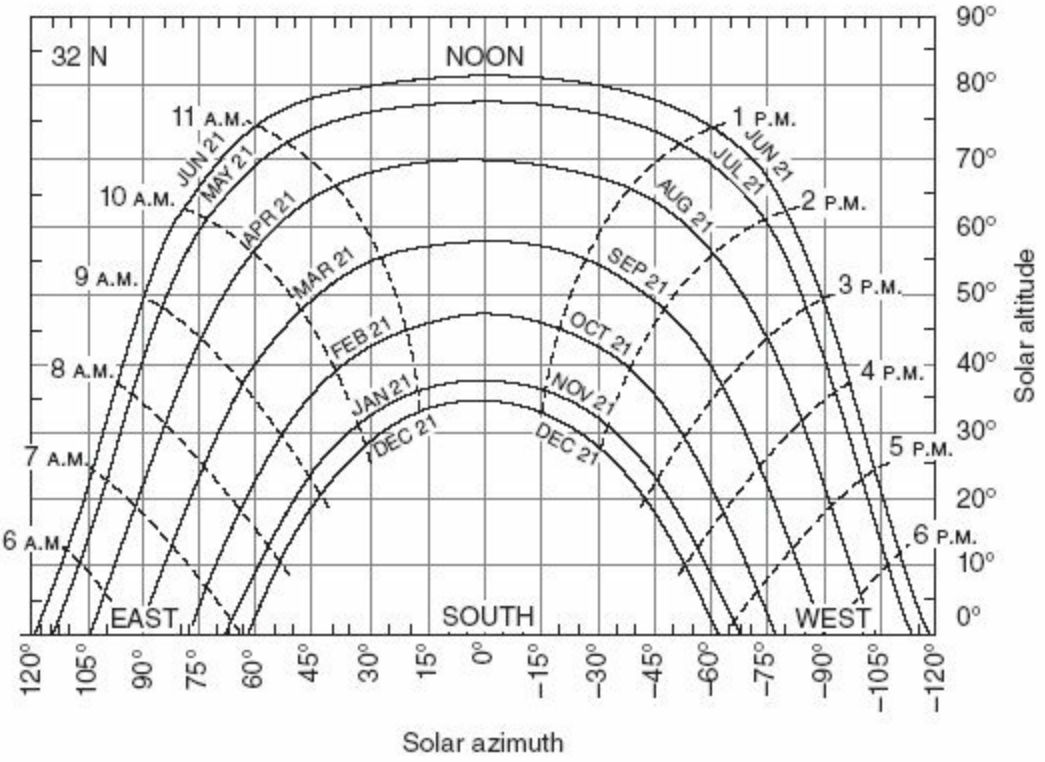
POWER

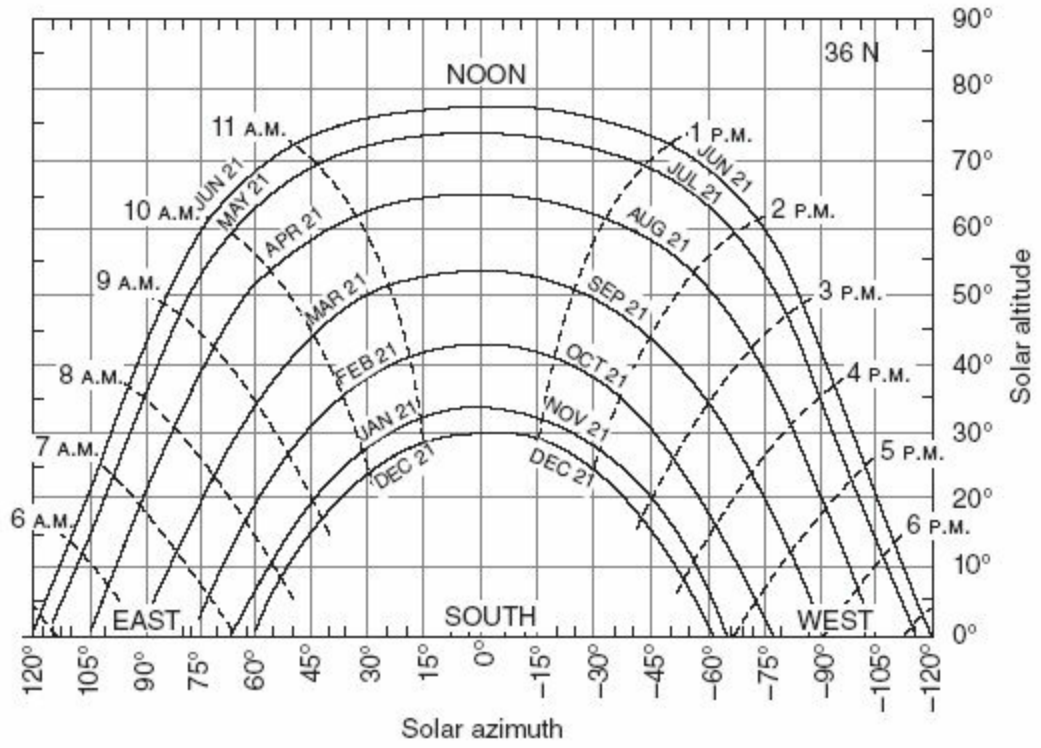
1 kilowatt	= 1000 J/s
	= 3412 Btu/h
	= 1.340 hp
1 horsepower	= 746 W
	= 550 ft-lb/s
1 quadrillion Btu per year	= 0.471 million barrels of oil per day
	= 0.03345 TW

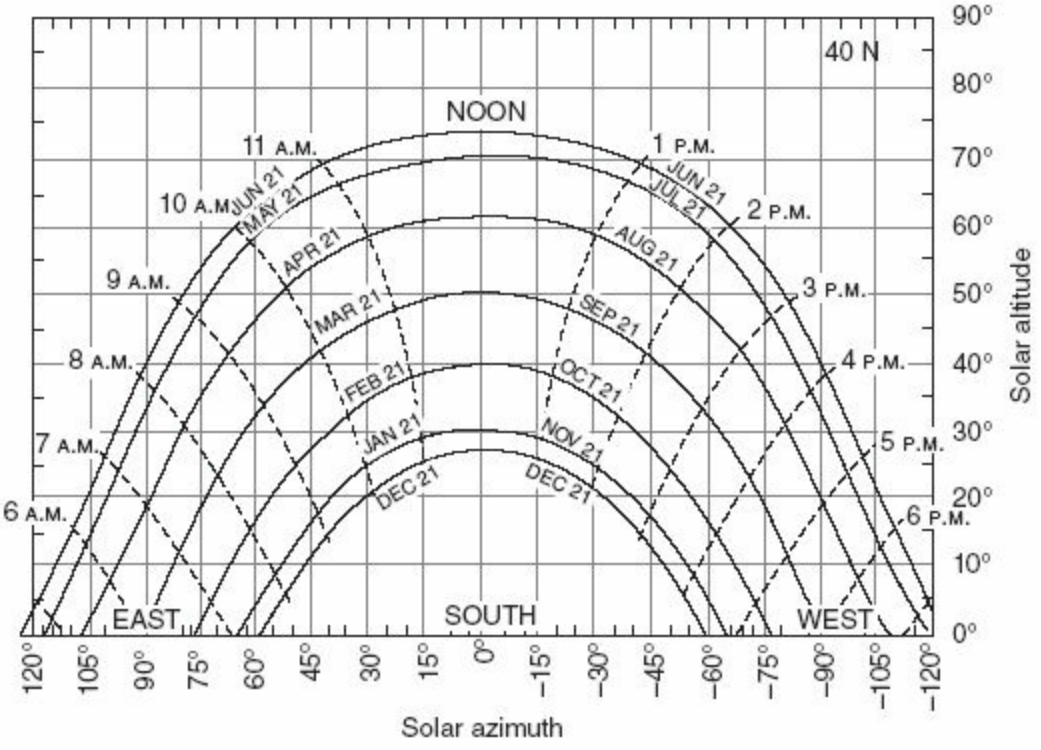
APPENDIX C

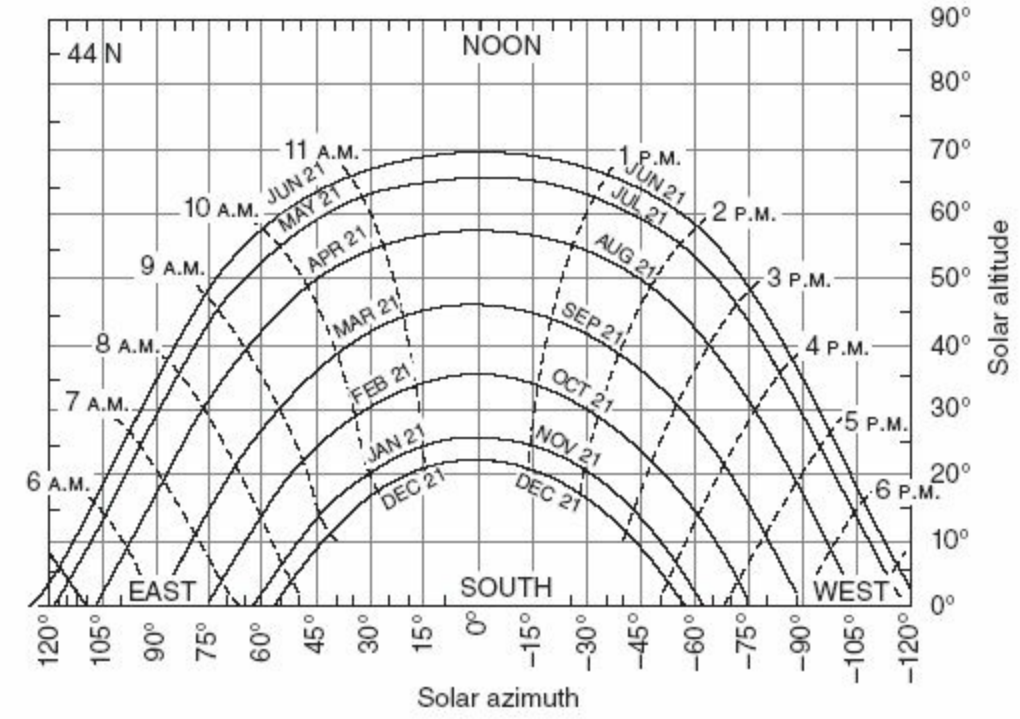
SUN-PATH DIAGRAMS

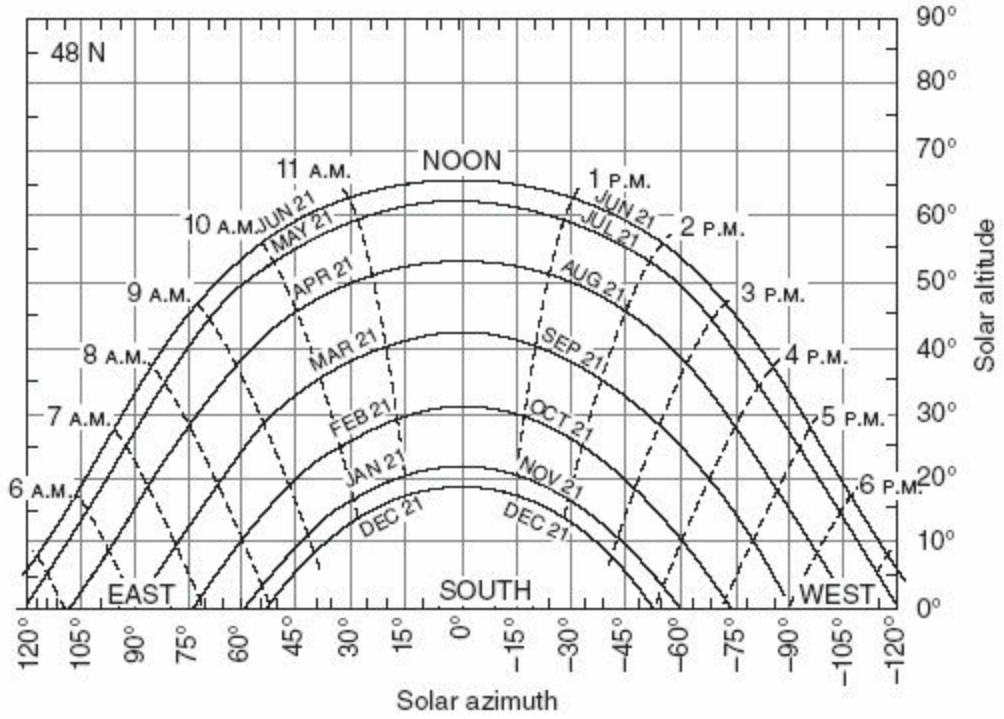

28 N
NOON
11 A.M.
10 A.M.
9 A.M.
8 A.M.
7 A.M.
6 A.M.
1 P.M.
2 P.M.
3 P.M.
4 P.M.
5 P.M.
6 P.M.
JUN 21
MAY 21
APR 21
MAR 21
FEB 21
JAN 21
DEC 21
JUL 21
AUG 21
SEP 21
OCT 21
NOV 21
DEC 21
EAST
SOUTH
WEST
90°
80°
70°
60°
50°
40°
30°
20°
10°
0°
Solar altitude
120° 105° 90° 75° 60° 45° 30° 15° 0° −15° −30° −45° −60° −75° −90° −105° −120°
Solar azimuth


32 N
NOON
11 A.M.
10 A.M.
9 A.M.
8 A.M.
7 A.M.
6 A.M.
1 P.M.
2 P.M.
3 P.M.
4 P.M.
5 P.M.
6 P.M.
JUN 21
MAY 21
APR 21
MAR 21
FEB 21
JAN 21
DEC 21
JUL 21
AUG 21
SEP 21
OCT 21
NOV 21
DEC 21
EAST
SOUTH
WEST
90°
80°
70°
60°
50°
40°
30°
20°
10°
0°
Solar altitude
120° 105° 90° 75° 60° 45° 30° 15° 0° −15° −30° −45° −60° −75° −90° −105° −120°
Solar azimuth


36 N
NOON
11 A.M.
1 P.M.
10 A.M.
2 P.M.
9 A.M.
3 P.M.
8 A.M.
4 P.M.
7 A.M.
5 P.M.
6 A.M.
6 P.M.
JUN 21
JUL 21
MAY 21
AUG 21
APR 21
SEP 21
MAR 21
OCT 21
FEB 21
NOV 21
JAN 21
DEC 21
DEC 21
EAST
SOUTH
WEST
90°
80°
70°
60°
50°
40°
30°
20°
10°
0°
120° 105° 90° 75° 60° 45° 30° 15° 0° −15° −30° −45° −60° −75° −90° −105° −120°
Solar azimuth
Solar altitude


40 N
NOON
11 A.M.
1 P.M.
10 A.M.
2 P.M.
9 A.M.
3 P.M.
8 A.M.
4 P.M.
7 A.M.
5 P.M.
6 A.M.
6 P.M.
JUN 21
JUL 21
MAY 21
AUG 21
APR 21
SEP 21
MAR 21
OCT 21
FEB 21
NOV 21
JAN 21
DEC 21
DEC 21
EAST
SOUTH
WEST
90°
80°
70°
60°
50°
40°
30°
20°
10°
0°
120° 105° 90° 75° 60° 45° 30° 15° 0° −15° −30° −45° −60° −75° −90° −105° −120°
Solar azimuth
Solar altitude


44 N
NOON
11 A.M.
10 A.M.
9 A.M.
8 A.M.
7 A.M.
6 A.M.
1 P.M.
2 P.M.
3 P.M.
4 P.M.
5 P.M.
6 P.M.
JUN 21
MAY 21
APR 21
MAR 21
FEB 21
JAN 21
DEC 21
JUL 21
AUG 21
SEP 21
OCT 21
NOV 21
DEC 21
EAST
SOUTH
WEST
90°
80°
70°
60°
50°
40°
30°
20°
10°
0°
Solar altitude
120° 105° 90° 75° 60° 45° 30° 15° 0° −15° −30° −45° −60° −75° −90° −105° −120°
Solar azimuth


48 N
NOON
11 A.M.
10 A.M.
9 A.M.
8 A.M.
7 A.M.
6 A.M.
1 P.M.
2 P.M.
3 P.M.
4 P.M.
5 P.M.
6 P.M.
JUN 21
MAY 21
APR 21
MAR 21
FEB 21
JAN 21
DEC 21
JUL 21
AUG 21
SEP 21
OCT 21
NOV 21
DEC 21
EAST
SOUTH
WEST
90°
80°
70°
60°
50°
40°
30°
20°
10°
0°
Solar altitude
120° 105° 90° 75° 60° 45° 30° 15° 0° −15° −30° −45° −60° −75° −90° −105° −120°
Solar azimuth

APPENDIX D

HOURLY CLEAR-SKY INSOLATION TABLES

Clear-Sky Insolation: Beam + Diffuse										Latitude 20°N									
Solar	Tracking		Tilt Angles Latitude 20°							Solar	Tracking		Tilt Angles Latitude 20°						
Time	1-Axis	2-Axis	0	20	30	40	50	60	90	Time	1-Axis	2-Axis	0	20	30	40	50	60	90
			JANUARY 21 (W/m²)										DECEMBER 21 (W/m²)						
7, 5	341	359	58	103	122	138	149	156	151	7, 5	235	252	35	72	87	100	110	118	118
8, 4	786	828	303	418	459	486	499	498	409	8, 4	738	794	269	393	439	473	492	497	428
9, 3	923	973	525	670	715	739	740	721	540	9, 3	887	955	486	645	697	729	740	729	572
10, 2	983	1037	696	860	905	923	914	878	624	10, 2	951	1025	654	832	886	914	915	889	660
11, 1	1010	1067	804	978	1023	1037	1021	975	673	11, 1	980	1057	760	949	1003	1027	1021	985	711
12	1018	1076	841	1018	1063	1076	1057	1007	689	12	988	1066	796	988	1042	1065	1057	1017	728
kWh/day	9.10	9.60	5.61	7.08	7.51	7.72	7.70	7.46	5.48	kWh/day	8.57	9.23	5.20	6.77	7.27	7.55	7.61	7.45	5.71
			FEBRUARY 21 (W/m²)										NOVEMBER 21 (W/m²)						
7, 5	523	530	121	162	176	185	189	188	154	7, 5	299	315	54	94	110	124	134	140	135
8, 4	856	867	381	460	479	486	478	456	318	8, 4	755	795	296	407	446	472	484	483	398
9, 3	973	986	610	710	730	728	705	662	425	9, 3	900	948	515	657	701	724	726	707	531
10, 2	1028	1043	786	901	919	910	875	814	499	10, 2	964	1017	685	845	889	907	899	864	616
11, 1	1053	1069	897	1020	1037	1024	981	908	545	11, 1	993	1049	792	962	1006	1020	1005	960	665
12	1061	1078	935	1061	1078	1063	1017	940	560	12	1002	1058	828	1002	1045	1059	1041	992	682
kWh/day	9.93	10.07	6.53	7.57	7.76	7.73	7.47	7.00	4.44	kWh/day	8.82	9.31	5.51	6.93	7.35	7.55	7.53	7.30	5.37
			MARCH 21 (W/m²)										OCTOBER 21 (W/m²)						
7, 5	630	630	193	203	199	190	177	158	81	7, 5	456	461	112	148	161	169	172	171	141
8, 4	881	881	456	481	474	452	418	373	182	8, 4	808	818	368	443	462	468	461	441	311
9, 3	983	983	684	724	712	680	629	559	266	9, 3	937	949	593	690	709	708	686	645	419
10, 2	1034	1034	860	910	896	855	790	702	331	10, 2	997	1012	766	877	895	888	854	796	494
11, 1	1060	1059	970	1027	1011	965	892	792	371	11, 1	1026	1042	875	995	1012	1000	958	889	539
12	1067	1067	1008	1067	1051	1003	926	823	385	12	1035	1051	912	1035	1051	1038	994	921	554
kWh/day	10.24	10.24	7.34	7.76	7.63	7.29	6.74	5.99	2.85	kWh/day	9.48	9.62	6.34	7.34	7.53	7.50	7.26	6.81	4.36
			APRIL 21 (W/m²)										SEPTEMBER 21 (W/m²)						
6, 6	84	86	14	8	8	7	7	6	4	6, 6	0	0	0	0	0	0	0	0	0
7, 5	654	673	258	223	196	164	128	90	32	7, 5	569	569	187	194	190	181	168	150	78
8, 4	847	871	510	476	439	389	330	261	41	8, 4	833	833	445	467	458	437	404	360	176
9, 3	937	962	727	700	657	595	516	423	88	9, 3	945	945	668	703	691	659	609	542	259
10, 2	986	1011	893	874	827	756	663	552	141	10, 2	1002	1002	840	886	870	830	767	681	322
11, 1	1013	1036	998	984	934	858	756	633	175	11, 1	1030	1030	947	1000	983	938	866	769	362
12	1022	1043	1034	1022	971	892	788	661	187	12	1039	1039	984	1039	1022	975	900	799	376
kWh/day	10.06	10.32	7.84	7.55	7.09	6.43	5.59	4.59	1.15	kWh/day	9.80	9.80	7.16	7.54	7.41	7.07	6.53	5.80	2.77
			MAY 21 (W/m²)										AUGUST 21 (W/m²)						
6, 6	205	222	50	24	23	22	21	19	13	6, 6	65	67	12	8	7	7	6	6	4
7, 5	625	677	292	225	183	136	86	57	38	7, 5	607	627	251	217	192	162	128	91	36
8, 4	787	850	528	456	400	334	259	178	47	8, 4	809	833	498	465	429	381	323	257	48
9, 3	870	936	731	662	599	519	425	320	51	9, 3	905	931	711	684	642	581	505	415	91
10, 2	919	984	886	822	754	665	558	435	53	10, 2	959	984	874	854	807	738	648	540	142
11, 1	946	1009	984	923	853	759	643	509	55	11, 1	988	1011	976	961	912	837	739	619	175
12	958	1017	1017	958	887	790	672	534	55	12	998	1020	1011	998	948	871	770	646	187
kWh/day	9.66	10.37	7.96	7.18	6.51	5.66	4.66	3.57	0.57	kWh/day	9.66	9.93	7.65	7.38	6.93	6.28	5.47	4.50	1.18
			JUNE 21 (W/m²)										JULY 21 (W/m²)						
6, 6	229	255	64	31	29	28	26	24	16	6, 6	188	204	48	25	24	23	21	19	13
7, 5	599	666	300	224	176	125	71	61	41	7, 5	600	652	288	223	181	136	87	60	40
8, 4	752	833	528	443	382	311	232	147	50	8, 4	765	829	521	449	395	330	256	176	50
9, 3	833	918	723	640	571	486	388	280	55	9, 3	851	918	720	652	590	511	419	316	55
10, 2	881	967	873	793	719	625	514	389	57	10, 2	901	968	874	810	743	655	549	428	58
11, 1	909	992	967	891	814	714	594	459	58	11, 1	930	994	970	909	840	746	632	500	59
12	921	1000	999	924	846	745	622	483	59	12	943	1003	1003	943	873	778	660	525	59
kWh/day	9.33	10.26	7.91	6.97	6.23	5.32	4.27	3.20	0.61	kWh/day	9.41	10.13	7.84	7.08	6.42	5.58	4.59	3.52	0.61

Clear-Sky Insolation: Beam + Diffuse										Latitude 25°N									
Solar	Tracking		Tilt Angles Latitude 25°							Solar	Tracking		Tilt Angles Latitude 25°						
Time	1-Axis	2-Axis	0	20	30	40	50	60	90	Time	1-Axis	2-Axis	0	20	30	40	50	60	90
			JANUARY 21 (W/m²)										DECEMBER 21 (W/m²)						
7, 5	185	195	25	50	61	71	78	83	84	7, 5	59	64	6	16	20	24	27	29	30
8, 4	735	774	251	367	411	442	461	466	402	8, 4	673	723	213	334	381	417	441	452	407
9, 3	894	943	464	621	674	706	718	710	562	9, 3	853	918	421	588	648	688	708	708	585
10, 2	962	1015	629	811	867	898	902	880	664	10, 2	927	998	582	776	841	880	894	881	693
11, 1	993	1048	733	928	987	1015	1014	983	724	11, 1	960	1034	684	893	959	997	1006	985	755
12	1002	1058	769	969	1027	1055	1052	1018	744	12	970	1045	719	932	999	1037	1044	1020	775
kWh/day	8.54	9.01	4.97	6.52	7.03	7.32	7.40	7.26	5.62	kWh/day	7.91	8.52	4.53	6.15	6.70	7.05	7.19	7.13	5.72
			FEBRUARY 21 (W/m²)										NOVEMBER 21 (W/m²)						
7, 5	454	460	95	133	147	157	162	163	140	7, 5	149	157	21	42	51	58	64	68	68
8, 4	827	838	343	429	455	467	466	451	334	8, 4	700	737	244	355	396	426	444	449	388
9, 3	955	968	564	679	708	717	704	671	463	9, 3	869	916	455	607	658	690	702	693	550
10, 2	1013	1028	733	869	900	904	882	834	553	10, 2	941	993	618	795	850	880	885	863	653
11, 1	1041	1056	840	989	1020	1022	993	935	609	11, 1	974	1028	721	912	969	997	996	966	713
12	1049	1065	877	1029	1061	1061	1031	969	627	12	984	1039	756	952	1009	1037	1034	1001	733
kWh/day	9.63	9.76	6.03	7.23	7.52	7.59	7.45	7.08	4.82	kWh/day	8.25	8.70	4.87	6.37	6.86	7.14	7.21	7.08	5.48
			MARCH 21 (W/m²)										OCTOBER 21 (W/m²)						
7, 5	613	613	183	196	195	189	178	162	91	7, 5	384	388	85	118	130	138	143	144	124
8, 4	869	869	436	473	471	457	429	389	212	8, 4	776	786	330	411	435	447	446	433	323
9, 3	973	973	656	714	712	690	648	588	316	9, 3	916	928	546	658	686	694	683	652	453
10, 2	1025	1025	825	899	898	870	817	740	395	10, 2	981	995	713	845	875	879	858	813	544
11, 1	1051	1051	932	1016	1014	983	923	836	445	11, 1	1012	1027	818	962	993	994	967	912	599
12	1059	1059	968	1056	1054	1022	959	869	462	12	1021	1037	854	1002	1033	1034	1004	946	617
kWh/day	10.12	10.12	7.03	7.65	7.64	7.40	6.95	6.30	3.38	kWh/day	9.16	9.28	5.84	6.99	7.27	7.34	7.20	6.85	4.70
			APRIL 21 (W/m²)										SEPTEMBER 21 (W/m²)						
6, 6	139	143	25	16	13	12	11	10	7	6, 6	0	0	0	0	0	0	0	0	0
7, 5	664	683	267	237	212	181	147	108	33	7, 5	553	553	177	187	186	179	168	153	86
8, 4	847	871	510	489	457	413	358	293	62	8, 4	820	820	425	458	456	440	413	375	204
9, 3	935	960	719	712	678	624	553	467	143	9, 3	934	934	641	694	691	668	627	568	305
10, 2	983	1007	880	885	849	789	707	604	210	10, 2	992	992	806	875	872	844	792	717	383
11, 1	1009	1032	981	994	958	894	804	691	253	11, 1	1021	1021	910	989	986	954	895	810	431
12	1017	1039	1015	1032	995	930	838	721	267	12	1030	1030	946	1028	1024	992	930	842	448
kWh/day	10.17	10.43	7.78	7.70	7.33	6.76	6.00	5.07	1.68	kWh/day	9.67	9.67	6.86	7.43	7.40	7.16	6.72	6.09	3.27
			MAY 21 (W/m²)										AUGUST 21 (W/m²)						
6, 6	282	306	76	42	32	31	28	26	17	6, 6	112	116	23	15	13	12	11	10	7
7, 5	645	698	314	251	210	163	112	60	39	7, 5	617	637	260	230	207	178	145	109	37
8, 4	794	857	541	481	431	369	297	217	47	8, 4	809	834	498	477	446	404	350	288	65
9, 3	872	938	737	686	632	559	472	371	51	9, 3	903	928	703	695	661	609	540	456	143
10, 2	919	984	887	846	789	710	610	494	81	10, 2	955	980	860	864	829	770	690	590	208
11, 1	945	1008	981	947	889	805	699	573	119	11, 1	983	1007	959	971	935	872	785	675	249
12	956	1016	1013	981	923	838	730	600	132	12	993	1015	993	1007	971	907	817	704	264
kWh/day	9.87	10.60	8.08	7.49	6.89	6.11	5.17	4.08	0.84	kWh/day	9.75	10.02	7.60	7.51	7.15	6.60	5.86	4.96	1.68
			JUNE 21 (W/m²)										JULY 21 (W/m²)						
6, 6	307	342	95	52	39	37	35	32	21	6, 6	263	286	75	43	33	31	29	27	18
7, 5	622	691	327	253	206	154	99	63	42	7, 5	621	674	310	248	208	162	113	62	41
8, 4	761	842	546	473	416	349	272	188	51	8, 4	772	836	534	475	425	364	293	215	51
9, 3	837	923	734	669	608	530	437	333	55	9, 3	853	921	727	676	622	551	464	365	55
10, 2	883	968	879	822	758	673	569	449	57	10, 2	902	969	875	833	777	698	600	486	80
11, 1	910	993	969	919	853	764	653	524	70	11, 1	930	994	968	933	875	792	687	563	117
12	922	1001	1000	952	886	795	682	550	83	12	941	1002	999	966	908	824	717	590	130
kWh/day	9.56	10.52	8.10	7.33	6.65	5.81	4.81	3.73	0.67	kWh/day	9.62	10.36	7.98	7.38	6.79	6.02	5.09	4.03	0.86

Clear-Sky Insolation: Beam + Diffuse										Latitude 30°N									
Solar	Tracking		Tilt Angles Latitude 30°							Solar	Tracking		Tilt Angles Latitude 30°						
Time	1-Axis	2-Axis	0	20	30	40	50	60	90	Time	1-Axis	2-Axis	0	20	30	40	50	60	90
			JANUARY 21 (W/m²)										DECEMBER 21 (W/m²)						
7, 5	31	33	3	7	9	11	13	14	14	7, 5	0	0	0	0	0	0	0	0	0
8, 4	666	701	197	310	354	387	410	421	380	8, 4	584	627	155	266	310	346	372	388	365
9, 3	858	904	399	564	623	664	685	686	572	9, 3	808	869	351	523	587	635	663	672	584
10, 2	936	987	556	752	819	861	878	869	693	10, 2	896	964	505	711	784	834	860	860	713
11, 1	971	1024	656	870	940	982	995	979	764	11, 1	934	1006	602	827	905	955	978	972	786
12	981	1035	690	909	981	1023	1035	1016	787	12	945	1018	636	866	945	996	1018	1009	810
kWh/day	7.90	8.33	4.31	5.92	6.47	6.83	7.00	6.95	5.64	kWh/day	7.39	7.95	3.86	5.52	6.12	6.54	6.76	6.79	5.71
			FEBRUARY 21 (W/m²)										NOVEMBER 21 (W/m²)						
7, 5	369	373	68	101	113	123	129	132	118	7, 5	17	18	2	4	5	6	7	8	8
8, 4	791	802	302	394	424	441	447	439	343	8, 4	628	661	190	296	338	369	391	401	362
9, 3	932	944	512	641	679	697	695	672	493	9, 3	830	874	390	549	606	645	666	667	557
10, 2	995	1009	674	830	872	889	880	845	600	10, 2	913	963	546	736	801	842	858	850	679
11, 1	1025	1040	776	948	993	1009	995	952	664	11, 1	950	1003	644	852	921	962	975	960	750
12	1034	1049	811	988	1034	1049	1034	988	686	12	961	1014	677	892	961	1003	1014	996	773
kWh/day	9.26	9.39	5.48	6.81	7.20	7.37	7.32	7.07	5.12	kWh/day	7.64	8.05	4.22	5.77	6.30	6.65	6.81	6.77	5.49
			MARCH 21 (W/m²)										OCTOBER 21 (W/m²)						
7, 5	592	592	170	188	189	185	176	163	99	7, 5	296	300	59	85	96	103	108	111	99
8, 4	853	853	412	460	464	456	435	401	239	8, 4	736	745	288	374	402	419	424	417	328
9, 3	960	960	622	698	706	693	661	610	361	9, 3	890	902	495	619	655	672	670	649	479
10, 2	1014	1014	784	881	892	876	836	771	454	10, 2	960	974	654	804	845	861	853	820	585
11, 1	1040	1040	885	996	1009	992	946	872	513	11, 1	994	1008	754	920	963	979	966	925	650
12	1048	1048	920	1035	1048	1031	983	907	533	12	1004	1018	789	959	1004	1019	1004	961	672
kWh/day	9.97	9.97	6.67	7.48	7.57	7.44	7.09	6.54	3.87	kWh/day	8.76	8.88	5.29	6.56	6.92	7.09	7.05	6.80	4.95
			APRIL 21 (W/m²)										SEPTEMBER 21 (W/m²)						
6, 6	193	199	38	25	18	17	16	14	10	6, 6	0	0	0	0	0	0	0	0	0
7, 5	670	690	273	248	226	197	164	127	33	7, 5	532	532	165	179	179	175	166	153	93
8, 4	845	868	505	497	472	433	383	323	99	8, 4	804	804	402	445	448	439	417	385	229
9, 3	930	955	705	717	692	648	585	506	197	9, 3	920	920	608	677	683	670	638	588	347
10, 2	977	1002	858	888	864	816	744	651	276	10, 2	979	979	766	856	865	849	808	745	438
11, 1	1002	1026	955	996	973	922	845	743	327	11, 1	1009	1009	865	969	979	961	916	844	496
12	1010	1033	988	1033	1010	959	880	775	345	12	1018	1018	899	1007	1018	999	952	877	515
kWh/day	10.24	10.51	7.66	7.77	7.50	7.03	6.35	5.50	2.23	kWh/day	9.50	9.50	6.51	7.26	7.33	7.19	6.84	6.31	3.72
			MAY 21 (W/m²)										AUGUST 21 (W/m²)						
6, 6	348	377	103	62	40	38	35	32	21	6, 6	161	166	35	24	18	17	16	15	10
7, 5	662	716	333	275	235	189	139	85	40	7, 5	624	644	266	242	220	193	161	126	37
8, 4	798	861	550	503	458	400	332	256	48	8, 4	806	831	494	485	460	423	374	315	99
9, 3	872	938	737	705	659	595	514	419	80	9, 3	897	923	690	700	675	632	570	494	194
10, 2	917	982	880	863	817	748	658	549	149	10, 2	949	974	840	867	843	795	725	635	271
11, 1	942	1006	970	962	917	845	750	633	194	11, 1	976	1001	934	972	949	899	823	724	321
12	951	1013	1001	997	951	879	781	662	210	12	985	1009	966	1008	985	934	857	755	338
kWh/day	10.03	10.77	8.15	7.74	7.20	6.51	5.64	4.61	1.27	kWh/day	9.81	10.09	7.48	7.59	7.32	6.85	6.20	5.37	2.20
			JUNE 21 (W/m²)										JULY 21 (W/m²)						
6, 6	372	414	127	76	48	45	42	38	25	6, 6	327	356	102	63	41	39	36	33	22
7, 5	641	712	350	281	235	184	128	69	43	7, 5	638	692	329	272	233	188	139	86	43
8, 4	767	849	560	499	447	384	310	229	51	8, 4	777	841	543	496	451	395	328	252	51
9, 3	838	924	740	693	639	569	482	383	55	9, 3	854	921	727	695	649	585	506	412	79
10, 2	882	968	877	843	790	715	619	506	102	10, 2	900	967	869	850	804	736	647	540	146
11, 1	908	991	964	939	886	808	707	586	145	11, 1	927	991	957	948	903	832	737	622	190
12	919	999	993	972	919	839	737	613	159	12	936	999	987	981	936	864	768	650	206
kWh/day	9.74	10.72	8.23	7.63	7.01	6.25	5.31	4.24	1.00	kWh/day	9.78	10.53	8.04	7.63	7.10	6.41	5.55	4.54	1.27

Clear-Sky Insolation: Beam + Diffuse										Latitude 35°N									
Solar	Tracking		Tilt Angles Latitude 35°							Solar	Tracking		Tilt Angles Latitude 35°						
Time	1-Axis	2-Axis	0	20	30	40	50	60	90	Time	1-Axis	2-Axis	0	20	30	40	50	60	90
			JANUARY 21 (W/m^2)										DECEMBER 21 (W/m^2)						
7, 5	0	0	0	0	0	0	0	0	0	7, 5	0	0	0	0	0	0	0	0	0
8, 4	572	602	142	244	286	319	343	357	338	8, 4	456	490	97	188	226	257	282	298	293
9, 3	810	853	331	498	562	609	638	649	568	9, 3	748	804	279	449	515	567	602	619	563
10, 2	902	951	479	685	760	812	841	844	709	10, 2	855	920	424	636	716	775	811	823	716
11, 1	942	994	573	801	882	936	963	961	791	11, 1	901	969	516	751	838	900	935	943	802
12	954	1006	605	840	923	978	1004	1001	818	12	914	984	547	790	879	942	976	983	830
kWh/day	7.41	7.81	3.65	5.30	5.90	6.33	6.57	6.62	5.63	kWh/day	6.83	7.35	3.18	4.84	5.47	5.94	6.24	6.35	5.58
			FEBRUARY 21 (W/m^2)										NOVEMBER 21 (W/m^2)						
7, 5	265	268	42	67	77	85	91	94	88	7, 5	0	0	0	0	0	0	0	0	0
8, 4	746	755	258	353	386	408	419	417	343	8, 4	529	557	135	229	268	298	321	334	315
9, 3	903	915	456	596	642	669	676	664	515	9, 3	779	820	322	483	543	588	616	627	549
10, 2	973	986	609	781	835	863	867	845	637	10, 2	877	924	469	668	741	791	819	822	691
11, 1	1005	1019	706	897	955	985	985	957	711	11, 1	920	970	561	783	861	914	940	939	773
12	1015	1029	739	937	996	1026	1026	995	736	12	932	983	593	822	902	956	981	978	800
kWh/day	8.80	8.92	4.88	6.33	6.79	7.05	7.10	6.95	5.32	kWh/day	7.14	7.52	3.57	5.15	5.73	6.14	6.37	6.42	5.46
			MARCH 21 (W/m^2)										OCTOBER 21 (W/m^2)						
7, 5	566	566	156	176	180	178	172	161	105	7, 5	194	197	33	52	59	65	69	72	67
8, 4	834	834	384	442	452	450	435	408	263	8, 4	686	694	244	332	362	383	393	391	323
9, 3	944	944	583	674	692	689	667	625	401	9, 3	858	869	439	572	615	641	648	636	496
10, 2	1000	999	735	854	877	874	846	793	508	10, 2	935	948	589	754	805	833	836	816	618
11, 1	1027	1027	831	967	993	990	959	899	575	11, 1	971	985	684	868	924	952	953	926	691
12	1035	1035	864	1005	1033	1030	997	935	598	12	982	996	717	907	964	993	993	964	716
kWh/day	9.78	9.77	6.24	7.23	7.42	7.39	7.15	6.71	4.30	kWh/day	8.27	8.38	4.70	6.06	6.50	6.74	6.79	6.65	5.11
			APRIL 21 (W/m^2)										SEPTEMBER 21 (W/m^2)						
6, 6	243	250	52	36	27	21	20	18	12	6, 6	0	0	0	0	0	0	0	0	0
7, 5	674	694	276	257	238	212	180	144	33	7, 5	506	506	151	168	170	168	161	150	97
8, 4	840	863	496	500	482	449	405	349	134	8, 4	783	783	375	427	435	432	416	390	250
9, 3	923	948	685	716	701	666	612	541	248	9, 3	902	902	569	654	669	665	642	601	384
10, 2	969	994	830	883	872	835	775	692	340	10, 2	963	963	719	829	849	845	817	765	488
11, 1	994	1018	921	989	980	942	878	788	399	11, 1	994	994	813	939	963	959	927	868	554
12	1002	1025	952	1025	1017	979	913	821	419	12	1003	1003	845	977	1002	997	964	903	576
kWh/day	10.29	10.56	7.47	7.79	7.61	7.23	6.65	5.89	2.75	kWh/day	9.30	9.30	6.10	7.01	7.17	7.13	6.89	6.45	4.12
			MAY 21 (W/m^2)										AUGUST 21 (W/m^2)						
6, 6	404	437	130	84	58	44	41	37	25	6, 6	207	214	48	35	27	22	21	19	13
7, 5	674	729	348	297	259	214	165	111	41	7, 5	628	648	269	251	232	207	177	142	37
8, 4	800	863	554	520	481	429	365	292	48	8, 4	801	826	485	488	469	438	394	340	133
9, 3	870	936	730	718	681	625	552	463	135	9, 3	890	916	670	698	683	648	595	526	243
10, 2	913	979	866	872	838	780	700	600	215	10, 2	940	966	812	861	849	813	754	673	331
11, 1	937	1001	951	970	937	878	794	687	268	11, 1	967	992	902	965	955	918	855	767	389
12	945	1008	980	1003	971	912	826	717	286	12	976	1000	932	1000	991	954	889	799	408
kWh/day	10.14	10.90	8.14	7.92	7.48	6.85	6.06	5.10	1.75	kWh/day	9.84	10.12	7.31	7.59	7.42	7.04	6.48	5.73	2.70
			JUNE 21 (W/m^2)										JULY 21 (W/m^2)						
6, 6	426	474	158	102	70	51	48	44	29	6, 6	382	416	129	85	60	46	42	39	26
7, 5	656	729	370	307	263	212	157	98	44	7, 5	651	706	344	294	257	213	164	112	43
8, 4	771	853	568	520	475	416	346	268	51	8, 4	779	843	547	513	474	423	360	288	51
9, 3	838	924	738	710	666	603	523	430	93	9, 3	851	919	722	708	671	615	543	455	132
10, 2	880	966	869	858	816	750	664	559	168	10, 2	896	963	855	859	825	767	688	589	211
11, 1	904	988	951	951	911	844	754	642	218	11, 1	921	986	939	955	923	864	780	675	262
12	913	995	979	983	943	876	785	671	235	12	930	994	967	988	956	897	812	704	280
kWh/day	9.86	10.86	8.29	7.88	7.34	6.63	5.77	4.75	1.44	kWh/day	9.89	10.66	8.04	7.82	7.37	6.75	5.97	5.02	1.73

Clear-Sky Insolation: Beam + Diffuse										Latitude 40°N									
Solar	Tracking		Tilt Angles Latitude 40°							Solar	Tracking		Tilt Angles Latitude 40°						
Time	1-Axis	2-Axis	0	20	30	40	50	60	90	Time	1-Axis	2-Axis	0	20	30	40	50	60	90
			JANUARY 21 (W/m²)										DECEMBER 21 (W/m²)						
7, 5	0	0	0	0	0	0	0	0	0	7, 5	0	0	0	0	0	0	0	0	0
8, 4	439	462	87	169	204	232	254	269	266	8, 4	271	292	43	99	123	144	161	172	178
9, 3	744	784	260	424	489	540	575	593	544	9, 3	663	712	205	364	429	481	519	542	516
10, 2	857	903	397	609	689	749	788	803	708	10, 2	799	860	339	551	634	699	744	766	699
11, 1	905	954	485	722	811	876	915	927	801	11, 1	855	920	425	665	758	828	874	895	799
12	919	968	515	761	852	919	958	968	832	12	871	937	454	703	799	871	918	937	831
kWh/day	6.81	7.17	2.97	4.61	5.24	5.71	6.02	6.15	5.47	kWh/day	6.05	6.51	2.48	4.06	4.69	5.18	5.51	5.69	5.21
			FEBRUARY 21 (W/m²)										NOVEMBER 21 (W/m²)						
7, 5	146	147	19	34	39	44	48	50	49	7, 5	0	0	0	0	0	0	0	0	0
8, 4	687	696	211	306	341	367	382	386	332	8, 4	392	412	80	154	184	210	229	242	239
9, 3	866	877	396	544	596	630	646	644	526	9, 3	709	746	251	407	469	517	550	567	520
10, 2	944	957	539	725	787	827	842	833	663	10, 2	828	873	388	591	668	726	763	777	686
11, 1	980	993	629	838	907	949	963	950	747	11, 1	880	927	474	704	789	852	890	901	780
12	990	1004	660	876	947	990	1005	989	775	12	894	942	504	742	830	894	932	943	811
kWh/day	8.24	8.35	4.25	5.77	6.29	6.62	6.77	6.71	5.41	kWh/day	6.51	6.86	2.89	4.45	5.05	5.50	5.80	5.92	5.26
			MARCH 21 (W/m²)										OCTOBER 21 (W/m²)						
7, 5	534	534	140	163	168	168	164	156	108	7, 5	87	88	13	21	25	28	30	31	30
8, 4	809	809	352	419	435	438	429	409	282	8, 4	622	629	198	283	315	338	352	355	307
9, 3	924	924	538	644	671	677	665	633	435	9, 3	816	827	379	518	567	599	615	612	502
10, 2	982	982	681	819	853	862	847	807	554	10, 2	903	915	520	696	756	793	808	799	639
11, 1	1010	1010	771	928	968	979	962	916	629	11, 1	943	956	608	807	873	914	928	915	721
12	1019	1019	801	966	1007	1019	1001	953	655	12	955	968	638	845	913	955	968	954	749
kWh/day	9.54	9.54	5.76	6.91	7.19	7.27	7.13	6.79	4.67	kWh/day	7.70	7.80	4.07	5.50	5.98	6.30	6.43	6.38	5.15
			APRIL 21 (W/m²)										SEPTEMBER 21 (W/m²)						
6, 6	288	297	65	47	37	25	24	22	14	6, 6	0	0	0	0	0	0	0	0	0
7, 5	674	694	277	264	247	224	194	160	39	7, 5	475	475	135	154	158	158	153	145	99
8, 4	832	856	482	499	487	461	422	372	169	8, 4	757	757	344	404	417	419	410	389	266
9, 3	913	938	659	708	702	677	632	570	296	9, 3	881	881	526	624	647	652	639	607	416
10, 2	959	984	794	870	871	846	798	726	399	10, 2	944	944	666	794	825	832	816	776	531
11, 1	983	1007	880	973	977	954	903	826	465	11, 1	975	975	754	901	937	946	928	882	604
12	991	1015	909	1008	1014	991	939	860	488	12	985	985	784	938	975	985	966	919	629
kWh/day	10.29	10.56	7.22	7.73	7.66	7.36	6.88	6.21	3.25	kWh/day	9.05	9.05	5.63	6.69	6.95	7.00	6.86	6.52	4.46
			MAY 21 (W/m²)										AUGUST 21 (W/m²)						
6, 6	450	488	155	107	78	48	45	41	27	6, 6	249	257	62	46	37	27	25	23	15
7, 5	684	740	360	316	281	238	190	137	41	7, 5	629	649	270	257	241	218	190	157	42
8, 4	799	862	552	532	500	454	395	326	78	8, 4	793	818	472	486	474	448	411	362	165
9, 3	866	932	718	724	697	650	585	503	188	9, 3	880	905	645	690	684	658	614	553	288
10, 2	906	972	844	874	852	805	735	645	279	10, 2	929	955	778	848	848	823	775	705	388
11, 1	929	994	924	969	950	903	831	735	338	11, 1	955	980	861	948	952	928	877	802	452
12	937	1001	951	1001	983	937	864	766	359	12	964	989	890	983	987	964	912	835	474
kWh/day	10.21	10.98	8.06	8.05	7.70	7.13	6.43	5.54	2.26	kWh/day	9.83	10.12	7.06	7.54	7.46	7.17	6.70	6.04	3.17
			JUNE 21 (W/m²)										JULY 21 (W/m²)						
6, 6	471	524	188	128	93	57	53	48	32	6, 6	428	466	154	107	80	51	47	43	29
7, 5	668	742	386	330	289	240	185	126	45	7, 5	661	717	357	313	278	237	189	137	44
8, 4	772	855	572	538	498	445	380	305	51	8, 4	778	843	547	526	493	447	389	321	77
9, 3	835	921	731	722	686	632	560	473	147	9, 3	847	914	710	714	687	640	575	495	185
10, 2	875	961	853	865	834	780	703	607	233	10, 2	889	957	834	861	838	792	722	633	273
11, 1	898	982	929	956	928	874	795	693	288	11, 1	913	979	913	954	935	888	816	722	331
12	906	989	955	987	960	906	826	723	308	12	921	986	940	986	968	921	849	752	351
kWh/day	9.94	10.96	8.27	8.06	7.62	6.96	6.18	5.23	1.90	kWh/day	9.95	10.74	7.97	7.94	7.59	7.03	6.33	5.45	2.23

Clear-Sky Insolation: Beam + Diffuse										Latitude 45°N									
Solar	Tracking		Tilt Angles Latitude 45°							Solar	Tracking		Tilt Angles Latitude 45°						
Time	1-Axis	2-Axis	0	20	30	40	50	60	90	Time	1-Axis	2-Axis	0	20	30	40	50	60	90
			JANUARY 21 (W/m²)										DECEMBER 21 (W/m²)						
7, 5	0	0	0	0	0	0	0	0	0	7, 5	0	0	0	0	0	0	0	0	0
8, 4	248	261	37	85	106	124	138	148	153	8, 4	45	48	5	14	18	22	25	27	30
9, 3	651	686	187	338	401	451	489	512	491	9, 3	536	576	131	265	322	369	406	431	429
10, 2	795	837	313	521	604	670	715	740	683	10, 2	720	774	252	453	536	603	652	682	651
11, 1	854	900	393	633	727	799	848	872	790	11, 1	792	852	330	566	661	737	791	822	768
12	871	918	420	670	768	843	893	916	825	12	812	874	357	604	703	782	837	868	806
kWh/day	5.97	6.29	2.28	3.82	4.44	4.93	5.27	5.46	5.06	kWh/day	5.00	5.37	1.79	3.20	3.78	4.24	4.58	4.79	4.56
			FEBRUARY 21 (W/m²)										NOVEMBER 21 (W/m²)						
7, 5	36	36	4	7	9	10	11	12	12	7, 5	0	0	0	0	0	0	0	0	0
8, 4	610	618	163	253	288	315	333	341	308	8, 4	201	212	31	70	87	101	113	121	125
9, 3	818	829	332	484	540	581	605	611	524	9, 3	610	642	179	320	378	425	460	482	462
10, 2	907	919	464	659	729	778	804	807	676	10, 2	762	802	303	502	581	643	687	710	656
11, 1	948	960	547	768	847	901	928	928	768	11, 1	825	869	383	613	703	773	820	843	764
12	959	973	575	805	887	942	970	969	800	12	843	888	410	650	744	816	864	887	799
kWh/day	7.60	7.70	3.59	5.15	5.71	6.11	6.33	6.37	5.38	kWh/day	5.64	5.94	2.20	3.66	4.24	4.70	5.02	5.20	4.81
			MARCH 21 (W/m²)										OCTOBER 21 (W/m²)						
7, 5	496	496	123	147	153	156	154	148	108	7, 5	11	11	1	2	3	3	3	4	4
8, 4	779	779	318	391	411	421	418	403	295	8, 4	539	545	150	229	260	283	299	306	276
9, 3	899	899	489	608	642	657	654	632	462	9, 3	763	773	316	457	509	547	569	574	494
10, 2	960	959	620	775	820	841	838	810	593	10, 2	861	872	445	629	695	742	766	769	646
11, 1	989	989	703	881	932	957	953	922	675	11, 1	906	918	527	737	811	862	888	888	737
12	998	998	731	917	971	996	993	960	703	12	920	932	555	773	850	903	929	929	768
kWh/day	9.24	9.24	5.24	6.52	6.89	7.06	7.03	6.79	4.97	kWh/day	7.08	7.17	3.43	4.88	5.41	5.78	5.98	6.01	5.08
			APRIL 21 (W/m²)										SEPTEMBER 21 (W/m²)						
6, 6	327	337	78	59	47	34	27	24	16	6, 6	0	0	0	0	0	0	0	0	0
7, 5	672	692	274	268	254	234	207	175	57	7, 5	437	437	118	139	144	145	143	136	98
8, 4	822	845	464	493	487	468	436	391	201	8, 4	726	726	310	376	394	401	397	382	277
9, 3	901	925	627	693	697	682	646	593	341	9, 3	854	854	478	588	618	631	627	604	439
10, 2	946	971	752	849	862	849	812	752	454	10, 2	919	919	607	751	792	810	805	777	566
11, 1	969	994	831	948	966	956	918	854	526	11, 1	952	952	688	854	901	923	918	886	646
12	977	1001	858	981	1001	992	954	889	551	12	962	962	716	889	939	961	956	923	673
kWh/day	10.25	10.53	6.91	7.60	7.63	7.44	7.05	6.47	3.74	kWh/day	8.74	8.74	5.12	6.30	6.64	6.78	6.73	6.49	4.73
			MAY 21 (W/m²)										AUGUST 21 (W/m²)						
6, 6	489	529	179	129	99	67	49	45	30	6, 6	287	296	74	57	47	35	28	26	17
7, 5	690	747	369	332	300	261	214	163	42	7, 5	627	647	268	261	247	227	202	171	58
8, 4	796	859	546	540	514	474	421	357	117	8, 4	782	807	454	480	474	454	423	379	195
9, 3	859	925	699	725	707	669	612	539	240	9, 3	866	892	614	676	678	662	627	574	330
10, 2	898	964	816	868	857	822	764	683	340	10, 2	915	941	737	828	838	825	788	729	439
11, 1	919	985	889	959	953	920	860	776	405	11, 1	941	966	814	924	940	929	891	828	510
12	927	992	914	990	986	953	893	808	428	12	949	974	840	957	974	964	927	862	534
kWh/day	10.23	11.01	7.91	8.10	7.85	7.38	6.73	5.93	2.78	kWh/day	9.78	10.07	6.76	7.41	7.42	7.23	6.85	6.28	3.63
			JUNE 21 (W/m²)										JULY 21 (W/m²)						
6, 6	508	565	216	155	118	79	57	52	35	6, 6	467	507	179	130	101	70	52	47	31
7, 5	677	751	399	351	313	266	213	155	46	7, 5	668	725	366	329	298	258	213	162	44
8, 4	772	854	570	550	517	470	410	339	84	8, 4	776	840	541	533	507	468	415	351	115
9, 3	830	916	717	727	701	656	592	512	200	9, 3	840	907	691	715	696	658	602	529	235
10, 2	868	954	830	864	845	802	736	649	295	10, 2	880	948	807	856	844	809	750	671	333
11, 1	889	975	900	952	937	895	828	737	356	11, 1	903	970	879	945	938	904	845	761	396
12	896	981	924	981	968	927	859	768	377	12	910	977	904	976	970	937	877	793	418
kWh/day	9.98	11.01	8.19	8.18	7.83	7.26	6.53	5.66	2.41	kWh/day	9.98	10.77	7.83	7.99	7.74	7.27	6.63	5.84	2.73

Clear-Sky Insolation: Beam + Diffuse — Latitude 50°N

Solar	Tracking		Tilt Angles Latitude 50°						
Time	1-Axis	2-Axis	0	20	30	40	50	60	90
			JANUARY 21 (W/m²)						
7, 5	0	0	0	0	0	0	0	0	0
8, 4	30	32	3	9	12	14	16	18	19
9, 3	512	539	114	239	291	336	371	394	396
10, 2	705	743	226	420	501	567	616	647	626
11, 1	782	824	298	530	625	701	757	790	750
12	803	846	323	567	666	746	803	837	790
kWh/day	4.86	5.12	1.60	2.96	3.52	3.98	4.32	4.54	4.37
			FEBRUARY 21 (W/m²)						
7, 5	0	0	0	0	0	0	0	0	0
8, 4	507	514	115	193	225	251	269	280	264
9, 3	754	764	266	416	474	518	548	561	505
10, 2	858	870	385	584	659	716	751	765	672
11, 1	905	917	460	689	774	838	876	889	773
12	919	931	486	724	814	879	919	931	807
kWh/day	6.97	7.06	2.93	4.49	5.08	5.52	5.81	5.92	5.24
			MARCH 21 (W/m²)						
7, 5	450	450	104	129	136	140	140	136	105
8, 4	742	742	280	358	383	396	399	390	301
9, 3	868	868	435	564	605	629	634	622	481
10, 2	932	932	554	723	778	809	818	802	621
11, 1	963	963	630	824	887	923	933	916	709
12	973	973	655	858	924	962	973	955	740
kWh/day	8.88	8.88	4.66	6.05	6.50	6.76	6.82	6.69	5.17
			APRIL 21 (W/m²)						
6, 6	361	372	90	70	58	44	30	27	18
7, 5	666	686	269	270	259	241	217	187	75
8, 4	808	831	442	482	483	470	444	405	230
9, 3	885	910	590	672	685	679	653	609	381
10, 2	929	954	704	820	844	843	819	770	502
11, 1	953	978	775	914	945	948	924	873	580
12	960	985	800	946	979	984	960	909	607
kWh/day	10.17	10.45	6.54	7.40	7.53	7.43	7.13	6.65	4.18
			MAY 21 (W/m²)						
6, 6	521	564	202	152	121	87	52	48	32
7, 5	694	751	374	346	317	281	237	187	42
8, 4	791	854	535	543	524	490	444	385	155
9, 3	850	916	674	718	710	681	634	569	289
10, 2	887	953	780	854	855	832	785	715	397
11, 1	907	973	847	941	948	928	881	809	467
12	914	980	870	971	980	961	914	841	492
kWh/day	10.21	11.00	7.69	8.08	7.93	7.56	6.98	6.27	3.26
			JUNE 21 (W/m²)						
6, 6	538	599	241	181	143	103	60	55	37
7, 5	683	758	408	369	334	290	239	183	46
8, 4	769	851	563	558	532	491	437	371	125
9, 3	823	909	697	725	709	673	618	546	251
10, 2	858	944	799	856	848	817	762	685	353
11, 1	878	964	864	939	937	908	853	774	420
12	885	970	886	967	967	939	885	805	443
kWh/day	9.98	11.02	8.03	8.22	7.97	7.50	6.82	6.03	2.90

Solar	Tracking		Tilt Angles Latitude 50°						
Time	1-Axis	2-Axis	0	20	30	40	50	60	90
			DECEMBER 21 (W/m²)						
7, 5	0	0	0	0	0	0	0	0	0
8, 4	0	0	0	0	0	0	0	0	0
9, 3	337	363	59	147	185	218	244	264	275
10, 2	599	644	164	339	413	475	524	557	556
11, 1	699	751	233	452	543	619	676	714	698
12	726	780	257	490	586	666	726	764	743
kWh/day	4.00	4.29	1.17	2.37	2.87	3.29	3.61	3.83	3.80
			NOVEMBER 21 (W/m²)						
7, 5	0	0	0	0	0	0	0	0	0
8, 4	14	14	1	4	5	6	7	8	9
9, 3	464	489	107	219	266	307	338	359	360
10, 2	666	701	217	400	475	537	584	613	592
11, 1	748	787	288	509	599	671	724	756	717
12	771	811	313	546	640	716	771	803	758
kWh/day	4.56	4.79	1.54	2.81	3.33	3.76	4.08	4.27	4.11
			OCTOBER 21 (W/m²)						
7, 5	0	0	0	0	0	0	0	0	0
8, 4	429	434	101	168	195	216	232	241	227
9, 3	693	701	250	387	440	480	507	520	468
10, 2	807	817	367	552	623	675	708	721	635
11, 1	859	870	441	656	736	796	832	844	735
12	874	885	466	691	775	837	874	886	769
kWh/day	6.45	6.53	2.78	4.22	4.76	5.17	5.43	5.54	4.90
			SEPTEMBER 21 (W/m²)						
6, 6	0	0	0	0	0	0	0	0	0
7, 5	393	393	100	121	127	129	128	124	94
8, 4	687	687	273	343	365	376	377	368	282
9, 3	820	820	426	544	581	602	605	592	455
10, 2	889	889	543	700	749	777	783	767	590
11, 1	924	923	617	798	855	888	896	877	676
12	934	934	642	831	892	926	934	915	706
kWh/day	8.36	8.36	4.56	5.84	6.25	6.47	6.51	6.37	4.90
			AUGUST 21 (W/m²)						
6, 6	319	330	86	69	57	45	32	29	19
7, 5	622	641	263	262	252	234	211	182	74
8, 4	768	792	432	469	469	456	430	392	222
9, 3	850	875	578	655	666	658	633	589	368
10, 2	897	923	689	799	820	818	793	745	485
11, 1	923	948	759	890	918	920	896	845	560
12	931	956	783	922	952	955	931	880	586
kWh/day	9.69	9.98	6.40	7.21	7.32	7.22	6.92	6.45	4.04
			JULY 21 (W/m²)						
6, 6	499	542	201	152	122	90	55	50	34
7, 5	672	729	371	343	315	278	235	186	45
8, 4	770	834	531	536	517	483	437	378	152
9, 3	831	898	667	708	699	670	623	558	282
10, 2	869	936	772	842	842	818	771	702	388
11, 1	890	958	838	927	933	912	865	793	457
12	897	964	860	956	964	944	897	825	480
kWh/day	9.96	10.76	7.62	7.98	7.82	7.45	6.87	6.16	3.19

Clear-Sky Insolation: Beam + Diffuse										Latitude 55°N									
Solar	Tracking		Tilt Angles Latitude 55°							Solar	Tracking		Tilt Angles Latitude 55°						
Time	1-Axis	2-Axis	0	20	30	40	50	60	90	Time	1-Axis	2-Axis	0	20	30	40	50	60	90
			JANUARY 21 (W/m^2)										DECEMBER 21 (W/m^2)						
7, 5	0	0	0	0	0	0	0	0	0	7, 5	0	0	0	0	0	0	0	0	0
8, 4	0	0	0	0	0	0	0	0	0	8, 4	0	0	0	0	0	0	0	0	0
9, 3	293	308	46	120	152	180	202	219	230	9, 3	56	60	6	21	28	33	38	42	46
10, 2	566	596	139	301	371	430	476	508	514	10, 2	400	430	78	199	252	298	335	362	378
11, 1	672	708	201	410	499	572	629	667	663	11, 1	548	589	136	315	392	458	510	547	560
12	701	739	223	447	541	619	679	719	710	12	588	632	157	353	438	509	565	605	616
kWh/day	3.76	3.96	0.99	2.11	2.58	2.98	3.29	3.51	3.52	kWh/day	2.60	2.79	0.60	1.42	1.78	2.09	2.33	2.51	2.58
			FEBRUARY 21 (W/m^2)										NOVEMBER 21 (W/m^2)						
7, 5	0	0	0	0	0	0	0	0	0	7, 5	0	0	0	0	0	0	0	0	0
8, 4	366	371	67	127	151	172	188	198	195	8, 4	0	0	0	0	0	0	0	0	0
9, 3	666	675	197	337	394	439	472	491	462	9, 3	241	254	40	100	127	149	168	182	190
10, 2	792	802	302	498	575	636	679	701	646	10, 2	520	547	130	279	342	396	438	468	473
11, 1	847	858	369	598	688	758	805	829	756	11, 1	631	664	192	387	470	538	591	627	622
12	864	875	392	632	726	799	848	873	793	12	662	697	214	423	512	585	641	678	670
kWh/day	6.21	6.29	2.26	3.75	4.34	4.81	5.14	5.31	4.91	kWh/day	3.45	3.63	0.94	1.96	2.39	2.75	3.04	3.23	3.24
			MARCH 21 (W/m^2)										OCTOBER 21 (W/m^2)						
7, 5	395	395	85	108	116	121	122	121	97	7, 5	0	0	0	0	0	0	0	0	0
8, 4	695	695	239	320	347	365	373	370	300	8, 4	283	286	55	101	120	136	148	156	153
9, 3	829	829	377	513	560	590	604	601	489	9, 3	596	604	182	306	357	397	426	443	417
10, 2	897	897	484	663	725	766	785	781	637	10, 2	733	742	285	465	536	592	630	651	600
11, 1	930	930	551	758	830	878	900	896	731	11, 1	794	804	351	563	647	711	756	778	710
12	940	940	574	790	866	916	939	935	764	12	812	822	374	597	684	752	798	821	746
kWh/day	8.43	8.43	4.05	5.51	6.02	6.36	6.51	6.47	5.27	kWh/day	5.63	5.70	2.12	3.47	4.00	4.42	4.72	4.88	4.51
			APRIL 21 (W/m^2)										SEPTEMBER 21 (W/m^2)						
6, 6	390	402	101	81	68	54	39	29	19	6, 6	0	0	0	0	0	0	0	0	0
7, 5	658	677	262	268	260	246	225	198	91	7, 5	341	341	81	101	107	111	111	109	86
8, 4	791	814	415	467	473	466	447	415	256	8, 4	639	639	234	306	330	345	350	346	278
9, 3	866	890	547	644	666	669	652	618	415	9, 3	779	778	369	493	535	562	574	569	460
10, 2	909	934	649	783	818	828	815	779	544	10, 2	851	851	474	640	696	733	749	744	603
11, 1	932	957	713	871	914	930	919	882	626	11, 1	888	888	540	732	798	841	860	855	694
12	940	965	735	901	947	965	955	918	655	12	899	899	562	764	833	878	898	893	725
kWh/day	10.03	10.31	6.11	7.13	7.35	7.35	7.15	6.76	4.56	kWh/day	7.89	7.89	3.96	5.31	5.77	6.06	6.19	6.14	4.97
			MAY 21 (W/m^2)										AUGUST 21 (W/m^2)						
6, 6	547	592	222	173	142	108	71	50	33	6, 6	347	359	98	80	68	55	40	31	21
7, 5	696	752	376	356	331	298	257	210	43	7, 5	613	632	256	261	253	238	218	192	90
8, 4	783	845	520	541	529	502	461	408	191	8, 4	751	774	407	454	459	451	432	400	246
9, 3	838	903	643	705	706	687	649	593	334	9, 3	829	855	536	627	646	648	631	596	399
10, 2	873	939	738	833	845	833	798	739	449	10, 2	876	902	636	762	794	803	789	752	523
11, 1	892	958	798	914	934	926	893	833	524	11, 1	901	927	699	848	887	901	890	852	603
12	899	965	818	942	964	958	925	866	549	12	909	935	720	877	919	935	924	887	631
kWh/day	10.16	10.95	7.41	7.98	7.94	7.67	7.18	6.53	3.70	kWh/day	9.54	9.83	5.98	6.94	7.13	7.13	6.92	6.53	4.39
			JUNE 21 (W/m^2)										JULY 21 (W/m^2)						
6, 6	563	626	264	206	168	127	83	57	38	6, 6	525	571	221	174	143	110	74	53	35
7, 5	686	762	413	383	352	312	264	209	46	7, 5	673	731	373	353	329	296	255	208	45
8, 4	763	845	552	560	541	507	459	399	164	8, 4	762	826	515	534	522	495	454	402	187
9, 3	814	899	671	718	711	684	638	574	298	9, 3	819	885	637	695	695	676	638	582	326
10, 2	846	932	762	840	844	823	780	714	408	10, 2	855	922	731	821	832	819	783	725	439
11, 1	865	951	820	918	928	912	870	803	478	11, 1	875	942	790	901	919	910	876	817	511
12	871	957	839	945	957	943	901	834	502	12	881	949	810	928	949	942	908	848	536
kWh/day	9.95	10.99	7.80	8.19	8.05	7.67	7.09	6.35	3.37	kWh/day	9.90	10.70	7.34	7.88	7.83	7.55	7.07	6.42	3.62

Clear-Sky Insolation: Beam + Diffuse										Latitude 60° N									
Solar	Tracking		Tilt Angles Latitude 60°							Solar	Tracking		Tilt Angles Latitude 60°						
Time	1-Axis	2-Axis	0	20	30	40	50	60	90	Time	1-Axis	2-Axis	0	20	30	40	50	60	90
			JANUARY 21 (W/m²)										DECEMBER 21 (W/m²)						
7, 5	0	0	0	0	0	0	0	0	0	7, 5	0	0	0	0	0	0	0	0	0
8, 4	0	0	0	0	0	0	0	0	0	8, 4	0	0	0	0	0	0	0	0	0
9, 3	19	20	2	7	9	11	13	14	15	9, 3	0	0	0	0	0	0	0	0	0
10, 2	332	349	56	154	198	236	267	290	306	10, 2	81	87	9	35	46	56	65	71	78
11, 1	490	516	106	264	333	392	440	475	493	11, 1	283	304	46	141	183	220	251	274	294
12	534	562	124	300	377	443	496	534	551	12	345	370	61	180	233	279	316	345	367
kWh/day	2.22	2.33	0.45	1.15	1.46	1.72	1.93	2.09	2.18	kWh/day	1.07	1.15	0.17	0.53	0.69	0.83	0.95	1.04	1.11
			FEBRUARY 21 (W/m²)										NOVEMBER 21 (W/m²)						
7, 5	0	0	0	0	0	0	0	0	0	7, 5	0	0	0	0	0	0	0	0	0
8, 4	178	181	25	55	68	79	88	94	97	8, 4	0	0	0	0	0	0	0	0	0
9, 3	539	546	128	247	297	338	370	390	384	9, 3	6	7	1	2	3	4	4	5	5
10, 2	696	705	218	399	474	535	580	609	586	10, 2	279	294	49	131	168	199	225	244	258
11, 1	765	775	275	494	583	655	708	741	707	11, 1	441	464	97	239	300	353	396	427	443
12	785	795	295	526	620	696	752	785	747	12	485	511	115	275	344	404	451	485	501
kWh/day	5.14	5.21	1.59	2.91	3.46	3.91	4.24	4.45	4.29	kWh/day	1.94	2.04	0.41	1.02	1.29	1.52	1.70	1.84	1.91
			MARCH 21 (W/m²)										OCTOBER 21 (W/m²)						
7, 5	330	330	65	86	94	99	101	101	85	7, 5	0	0	0	0	0	0	0	0	0
8, 4	636	635	197	277	306	326	338	339	289	8, 4	106	107	16	34	41	48	53	57	58
9, 3	778	778	316	454	505	541	562	566	484	9, 3	459	465	114	214	256	291	318	335	330
10, 2	851	851	409	593	662	710	739	746	639	10, 2	628	636	202	364	430	485	525	550	530
11, 1	888	887	467	682	761	818	851	860	737	11, 1	703	712	258	457	538	604	652	681	650
12	899	898	487	712	795	855	890	899	771	12	725	734	278	489	574	644	695	725	690
kWh/day	7.86	7.86	3.40	4.90	5.45	5.84	6.07	6.12	5.24	kWh/day	4.52	4.57	1.46	2.62	3.11	3.50	3.79	3.97	3.83
			APRIL 21 (W/m²)										SEPTEMBER 21 (W/m²)						
6, 6	414	426	111	92	79	64	48	31	21	6, 6	0	0	0	0	0	0	0	0	0
7, 5	646	665	251	263	259	248	230	206	106	7, 5	281	281	62	80	86	89	91	90	74
8, 4	770	792	385	446	458	457	444	418	277	8, 4	578	578	192	263	288	305	314	315	265
9, 3	842	866	500	610	639	651	644	618	442	9, 3	725	725	310	435	481	513	530	533	452
10, 2	885	909	589	738	782	804	802	778	576	10, 2	803	803	401	570	632	676	701	706	600
11, 1	907	932	644	820	873	901	904	880	662	11, 1	842	841	458	656	729	781	810	816	695
12	915	940	663	848	904	935	938	915	692	12	853	853	477	686	762	816	847	853	728
kWh/day	9.84	10.12	5.62	6.78	7.08	7.18	7.08	6.78	4.86	kWh/day	7.31	7.31	3.32	4.69	5.19	5.54	5.74	5.77	4.90
			MAY 21 (W/m²)										AUGUST 21 (W/m²)						
6, 6	569	616	239	193	163	128	91	52	35	6, 6	371	383	108	90	78	64	49	33	22
7, 5	694	750	374	363	342	313	275	231	68	7, 5	601	620	246	256	251	240	222	199	103
8, 4	773	834	499	533	528	508	474	428	225	8, 4	729	751	377	433	443	442	428	403	265
9, 3	824	888	607	685	695	686	657	610	374	9, 3	804	829	490	592	619	629	620	595	424
10, 2	856	922	690	803	826	826	802	755	495	10, 2	850	875	577	717	758	777	774	749	553
11, 1	874	940	742	878	910	915	894	848	573	11, 1	874	900	632	797	846	872	872	848	636
12	880	946	759	904	939	946	926	880	600	12	882	908	650	824	877	904	906	882	665
kWh/day	10.06	10.85	7.06	7.82	7.87	7.70	7.31	6.73	4.14	kWh/day	9.34	9.62	5.51	6.59	6.87	6.95	6.84	6.54	4.67
			JUNE 21 (W/m²)										JULY 21 (W/m²)						
6, 6	584	649	284	229	192	151	106	59	40	6, 6	547	594	239	194	164	130	93	55	37
7, 5	687	762	414	394	367	331	286	234	51	7, 5	672	729	371	360	340	310	273	229	68
8, 4	755	837	535	557	545	518	477	423	200	8, 4	752	815	495	527	521	501	467	420	220
9, 3	801	886	639	703	705	688	651	597	342	9, 3	804	870	602	676	685	674	645	598	365
10, 2	831	917	719	816	831	822	790	735	457	10, 2	837	904	683	792	813	812	787	740	483
11, 1	848	935	769	888	911	907	878	823	530	11, 1	856	923	735	866	895	899	878	831	559
12	854	940	786	913	938	937	908	854	556	12	862	930	752	891	923	929	909	862	585
kWh/day	9.87	10.91	7.51	8.09	8.04	7.77	7.29	6.60	3.80	kWh/day	9.80	10.60	7.00	7.72	7.76	7.58	7.19	6.61	4.05

APPENDIX E

MONTHLY CLEAR-SKY INSOLATION TABLES

Daily Clear-Sky Insoation (kWh/m^2)														Latitude 20° N							
Azimuth:		South						SE, SW						East, West						Tracking	
Tilt:	0	20	30	40	50	60	90	20	30	40	50	60	90	20	30	40	50	60	90	1-Axis	2-Axis
Jan	5.61	7.08	7.51	7.72	7.70	7.46	5.48	7.85	7.52	7.06	6.45	5.73	3.18	7.57	7.17	6.67	6.10	5.47	3.41	9.10	9.60
Feb	6.53	7.57	7.76	7.73	7.47	7.00	4.44	7.32	7.19	6.90	6.46	5.89	3.61	6.73	6.40	6.01	5.54	5.01	3.22	9.93	10.07
Mar	7.34	7.76	7.63	7.29	6.74	5.99	2.85	6.30	6.41	6.34	6.13	5.77	3.95	5.39	5.15	4.85	4.51	4.13	2.73	10.24	10.24
Apr	7.84	7.55	7.09	6.43	5.59	4.59	1.15	5.02	5.29	5.41	5.40	5.25	3.98	3.90	3.73	3.56	3.33	3.08	2.09	10.06	10.32
May	7.96	7.18	6.51	5.66	4.66	3.57	0.57	3.95	4.31	4.56	4.68	4.67	3.85	2.79	2.71	2.58	2.47	2.29	1.62	9.66	10.37
Jun	7.91	6.97	6.23	5.32	4.27	3.20	0.61	3.56	3.95	4.23	4.40	4.43	3.78	2.39	2.34	2.24	2.15	2.00	1.44	9.33	10.26
July	7.84	7.08	6.42	5.58	4.59	3.52	0.61	7.85	7.52	7.06	6.45	5.73	3.18	7.57	7.17	6.67	6.10	5.47	3.41	9.41	10.13
Aug	7.65	7.38	6.93	6.28	5.47	4.50	1.18	7.32	7.19	6.90	6.46	5.89	3.61	6.73	6.40	6.01	5.54	5.01	3.22	9.66	9.93
Sept	7.16	7.54	7.41	7.07	6.53	5.80	2.77	6.30	6.41	6.34	6.13	5.77	3.95	5.39	5.15	4.85	4.51	4.13	2.73	9.80	9.80
Oct	6.34	7.34	7.53	7.50	7.26	6.81	4.36	5.02	5.29	5.41	5.40	5.25	3.98	3.90	3.73	3.56	3.33	3.08	2.09	9.48	9.62
Nov	5.51	6.93	7.35	7.55	7.53	7.30	5.37	3.95	4.31	4.56	4.68	4.67	3.85	2.79	2.71	2.58	2.47	2.29	1.62	8.82	9.31
Dec	5,7.0	6,77	7,77	7,55	7,61	7,45	5,71	3,56	3,95	4,73	4,40	4,43	3,78	7,39	7,34	7,74	7,15	7,00	1,44	8.57	9.23
kWh/m^2/yr	2522	2650	2603	2483	2292	2041	1065	2067	2108	2098	2038	1930	1359	1750	1672	1576	1465	1336	882	3469	3615

Daily Clear-Sky Insoation (kWh/m^2)														Latitude 25° N							
Azimuth:		South						SE, SW						East, West						Tracking	
Tilt:	0	20	30	40	50	60	90	20	30	40	50	60	90	20	30	40	50	60	90	1-Axis	2-Axis
Jan	4.97	6.52	7.03	7.32	7.40	7.26	5.62	6.00	6.26	6.34	6.23	5.98	4.31	4.74	4.53	4.26	3.93	3.59	2.32	8.54	9.01
Feb	6.03	7.23	7.52	7.59	7.45	7.08	4.82	6.79	6.91	6.83	6.56	6.17	4.12	5.76	5.50	5.15	4.76	4.32	2.78	9.63	9.76
Mar	7.03	7.65	7.64	7.40	6.95	6.30	3.38	7.35	7.26	6.96	6.51	5.92	3.57	6.70	6.34	5.91	5.43	4.87	3.04	10.12	10.12
Apr	7.78	7.70	7.33	6.76	6.00	5.07	1.68	7.62	7.27	6.75	6.13	5.36	2.86	7.39	6.99	6.50	5.92	5.26	3.21	10.17	10.43
May	8.08	7.49	6.89	6.11	5.17	4.08	0.84	7.58	7.07	6.42	5.69	4.86	2.36	7.68	7.27	6.73	6.10	5.43	3.27	9.87	10.60
Jun	8.10	7.33	6.65	5.81	4.81	3.73	0.67	7.47	6.91	6.21	5.45	4.61	2.14	7.70	7.27	6.72	6.08	5.41	3.22	9.56	10.52
July	7.98	7.38	6.79	6.02	5.09	4.03	0.86	7.47	6.97	6.32	5.60	4.78	2.32	7.58	7.16	6.63	6.01	5.35	3.21	9.62	10.36
Aug	7.60	7.51	7.15	6.60	5.86	4.96	1.68	7.43	7.09	6.58	5.97	5.22	2.79	7.22	6.82	6.34	5.76	5.12	3.11	9.75	10.02
Sept	6.86	7.43	7.40	7.16	6.72	6.09	3.27	7.15	7.05	6.75	6.30	5.72	3.44	6.54	6.19	5.76	5.28	4.73	2.94	9.67	9.67
Oct	5.84	6.99	7.27	7.34	7.20	6.85	4.70	6.56	6.68	6.60	6.34	5.95	3.98	5.58	5.32	4.97	4.59	4.16	2.65	9.16	9.28
Nov	4.87	6.37	6.86	7.14	7.21	7.08	5.48	5.86	6.11	6.19	6.08	5.83	4.20	4.65	4.43	4.17	3.83	3.50	2.25	8.25	8.70
Dec	4.53	6.15	6.70	7.05	7.19	7.13	5.72	5.60	5.90	6.03	5.98	5.77	4.26	4.31	4.11	3.87	3.55	3.25	2.09	7.91	8.52
kWh/m^2/yr	2424	2608	2591	2502	2341	2116	1175	2521	2477	2370	2215	2011	1226	2308	2189	2039	1864	1673	1037	3413	3558

Daily Clear-Sky Insoation (kWh/m^2)														Latitude 30° N							
Azimuth:		South						SE, SW						East, West						Tracking	
Tilt:	0	20	30	40	50	60	90	20	30	40	50	60	90	20	30	40	50	60	90	1-Axis	2-Axis
Jan	4.31	5.92	6.47	6.83	7.00	6.95	5.64	5.38	5.68	5.82	5.79	5.63	4.22	4.11	3.91	3.71	3.43	3.15	2.06	7.90	8.33
Feb	5.48	6.81	7.20	7.37	7.32	7.07	5.12	6.35	6.53	6.53	6.36	6.04	4.22	5.24	5.02	4.73	4.38	4.01	2.63	9.26	9.39
Mar	6.67	7.48	7.57	7.44	7.09	6.54	3.87	7.13	7.11	6.90	6.53	6.01	3.79	6.36	6.04	5.63	5.21	4.70	2.98	9.97	9.97
Apr	7.66	7.77	7.50	7.03	6.35	5.50	2.23	7.65	7.37	6.93	6.36	5.64	3.16	7.29	6.90	6.44	5.89	5.26	3.27	10.24	10.51
May	8.15	7.74	7.20	6.51	5.64	4.61	1.27	7.77	7.32	6.72	6.03	5.21	2.65	7.75	7.33	6.80	6.18	5.51	3.36	10.03	10.77
Jun	8.23	7.63	7.01	6.25	5.31	4.24	1.00	7.72	7.20	6.56	5.82	4.98	2.43	7.82	7.38	6.83	6.19	5.52	3.32	9.74	10.72
July	8.04	7.63	7.10	6.41	5.55	4.54	1.27	7.66	7.21	6.62	5.93	5.12	2.60	7.65	7.23	6.70	6.09	5.43	3.29	9.78	10.53
Aug	7.48	7.59	7.32	6.85	6.20	5.37	2.20	7.46	7.19	6.75	6.18	5.49	3.06	7.12	6.74	6.28	5.73	5.11	3.16	9.81	10.09
Sept	6.51	7.26	7.33	7.19	6.84	6.31	3.72	6.93	6.90	6.68	6.31	5.80	3.64	6.21	5.89	5.49	5.06	4.56	2.88	9.50	9.50
Oct	5.29	6.56	6.92	7.09	7.05	6.80	4.95	6.12	6.29	6.28	6.11	5.80	4.05	5.05	4.84	4.55	4.20	3.84	2.50	8.76	8.88
Nov	4.22	5.77	6.30	6.65	6.81	6.77	5.49	5.25	5.54	5.67	5.64	5.48	4.10	4.02	3.83	3.62	3.34	3.07	2.00	7.64	8.05
Dec	3.86	5.52	6.12	6.54	6.76	6.79	5.71	4.97	5.31	5.50	5.53	5.42	4.19	3.69	3.52	3.34	3.11	2.86	1.90	7.39	7.95
kWh/m^2/yr	2310	2545	2555	2497	2368	2172	1289	2445	2423	2341	2207	2025	1280	2200	2088	1951	1790	1613	1015	3346	3489

Daily Clear-Sky Insoation (kWh/m^2)																						Latitude 35° N
Azimuth:		South						SE, SW						East, West						Tracking	
Tilt:	0	20	30	40	50	60	90	20	30	40	50	60	90	20	30	40	50	60	90	1-Axis	2-Axis
Jan	3.65	5.30	5.90	6.33	6.57	6.62	5.63	4.76	5.11	5.31	5.37	5.29	4.15	3.50	3.36	3.20	3.00	2.77	1.89	7.41	7.81
Feb	4.88	6.33	6.79	7.05	7.10	6.95	5.32	5.84	6.08	6.15	6.07	5.83	4.26	4.67	4.49	4.26	3.95	3.66	2.45	8.80	8.92
Mar	6.24	7.23	7.42	7.39	7.15	6.71	4.30	6.84	6.90	6.77	6.48	6.04	3.96	5.96	5.68	5.32	4.94	4.50	2.92	9.78	9.77
Apr	7.47	7.79	7.61	7.23	6.65	5.89	2.75	7.61	7.41	7.04	6.53	5.89	3.46	7.12	6.76	6.32	5.81	5.22	3.31	10.29	10.56
May	8.14	7.92	7.48	6.85	6.06	5.10	1.75	7.90	7.50	6.98	6.31	5.53	2.93	7.74	7.32	6.81	6.20	5.55	3.42	10.14	10.90
Jun	8.29	7.88	7.34	6.63	5.77	4.75	1.44	7.90	7.43	6.85	6.14	5.32	2.71	7.87	7.43	6.88	6.25	5.58	3.39	9.86	10.86
July	8.04	7.82	7.37	6.75	5.97	5.02	1.73	7.79	7.40	6.87	6.21	5.44	2.87	7.64	7.23	6.72	6.12	5.47	3.36	9.89	10.66
Aug	7.31	7.59	7.42	7.04	6.48	5.73	2.70	7.42	7.22	6.86	6.35	5.71	3.35	6.96	6.60	6.17	5.66	5.08	3.20	9.84	10.12
Sept	6.10	7.01	7.17	7.13	6.89	6.45	4.12	6.64	6.69	6.54	6.25	5.82	3.80	5.82	5.54	5.19	4.81	4.36	2.81	9.30	9.30
Oct	4.70	6.06	6.50	6.74	6.79	6.65	5.11	5.60	5.83	5.88	5.80	5.57	4.06	4.49	4.30	4.08	3.77	3.48	2.31	8.27	8.38
Nov	3.57	5.15	5.73	6.14	6.37	6.42	5.46	4.63	4.96	5.16	5.21	5.13	4.03	3.42	3.28	3.12	2.93	2.70	1.83	7.14	7.52
Dec	3.18	4.84	5.47	5.94	6.24	6.35	5.58	4.30	4.68	4.93	5.04	5.01	4.07	3.06	2.96	2.81	2.66	2.46	1.71	6.83	7.35
kWh/m^2/yr	2178	2462	2500	2470	2372	2207	1393	2350	2349	2292	2182	2024	1326	2078	1977	1853	1708	1547	992	3271	3412

Daily Clear-Sky Insoation (kWh/m^2)																						Latitude 40° N
Azimuth:		South						SE, SW						East, West						Tracking	
Tilt:	0	20	30	40	50	60	90	20	30	40	50	60	90	20	30	40	50	60	90	1-Axis	2-Axis
Jan	2.97	4.61	5.24	5.71	6.02	6.15	5.47	4.08	4.47	4.72	4.86	4.85	4.00	2.87	2.79	2.67	2.55	2.37	1.69	6.81	7.17
Feb	4.25	5.77	6.29	6.62	6.77	6.71	5.41	5.26	5.56	5.69	5.69	5.53	4.21	4.08	3.91	3.74	3.51	3.26	2.23	8.24	8.35
Mar	5.76	6.91	7.19	7.27	7.13	6.79	4.67	6.49	6.62	6.57	6.36	6.01	4.14	5.51	5.28	4.98	4.64	4.27	2.84	9.54	9.54
Apr	7.22	7.73	7.66	7.36	6.88	6.21	3.25	7.51	7.38	7.10	6.65	6.07	3.74	6.89	6.55	6.16	5.70	5.16	3.34	10.29	10.56
May	8.06	8.05	7.70	7.13	6.43	5.54	2.26	7.96	7.62	7.17	6.55	5.82	3.24	7.66	7.25	6.76	6.18	5.55	3.47	10.21	10.98
Jun	8.27	8.06	7.62	6.96	6.18	5.23	1.90	8.02	7.61	7.09	6.41	5.64	2.99	7.85	7.41	6.87	6.26	5.61	3.45	9.94	10.96
July	7.97	7.94	7.59	7.03	6.33	5.45	2.23	7.85	7.52	7.06	6.45	5.73	3.18	7.57	7.17	6.67	6.10	5.47	3.41	9.95	10.74
Aug	7.06	7.54	7.46	7.17	6.70	6.04	3.17	7.32	7.19	6.90	6.46	5.89	3.61	6.73	6.40	6.01	5.54	5.01	3.22	9.83	10.12
Sept	5.63	6.69	6.95	7.00	6.86	6.52	4.46	6.30	6.41	6.34	6.13	5.77	3.95	5.39	5.15	4.85	4.51	4.13	2.73	9.05	9.05
Oct	4.07	5.50	5.98	6.30	6.43	6.38	5.15	5.02	5.29	5.41	5.40	5.25	3.98	3.90	3.73	3.56	3.33	3.08	2.09	7.70	7.80
Nov	2.89	4.45	5.05	5.50	5.80	5.92	5.26	3.95	4.31	4.56	4.68	4.67	3.85	2.79	2.71	2.58	2.47	2.29	1.62	6.51	6.86
Dec	2.48	4.06	4.69	5.18	5.51	5.69	5.21	3.56	3.95	4.23	4.40	4.43	3.78	2.39	2.34	2.24	2.15	2.00	1.44	6.05	6.51
kWh/m^2/yr	2029	2352	2415	2410	2342	2208	1471	2231	2249	2216	2130	1997	1357	1938	1848	1738	1612	1467	960	3167	3305

Daily Clear-Sky Insoation (kWh/m^2)																						Latitude 45° N
Azimuth:		South						SE, SW						East, West						Tracking	
Tilt:	0	20	30	40	50	60	90	20	30	40	50	60	90	20	30	40	50	60	90	1-Axis	2-Axis
Jan	2.28	3.82	4.44	4.93	5.27	5.46	5.06	3.33	3.73	4.02	4.19	4.25	3.67	2.21	2.17	2.11	2.03	1.90	1.41	5.97	6.29
Feb	3.59	5.15	5.71	6.11	6.33	6.37	5.38	4.64	4.97	5.16	5.23	5.15	4.08	3.46	3.34	3.20	3.04	2.83	1.99	7.60	7.70
Mar	5.24	6.52	6.89	7.06	7.03	6.79	4.97	6.07	6.27	6.29	6.17	5.90	4.26	5.02	4.83	4.60	4.30	4.00	2.74	9.24	9.24
Apr	6.91	7.60	7.63	7.44	7.05	6.47	3.74	7.33	7.28	7.08	6.71	6.21	3.98	6.60	6.30	5.95	5.54	5.05	3.35	10.25	10.53
May	7.91	8.10	7.85	7.38	6.73	5.93	2.78	7.94	7.68	7.29	6.73	6.07	3.53	7.52	7.12	6.65	6.11	5.51	3.51	10.23	11.01
Jun	8.19	8.18	7.83	7.26	6.53	5.66	2.41	8.06	7.73	7.26	6.63	5.92	3.29	7.76	7.33	6.81	6.22	5.59	3.48	9.98	11.01
July	7.83	7.99	7.74	7.27	6.63	5.84	2.73	7.84	7.58	7.19	6.63	5.97	3.46	7.44	7.05	6.57	6.04	5.43	3.45	9.98	10.77
Aug	6.76	7.41	7.42	7.23	6.85	6.28	3.63	7.15	7.09	6.88	6.50	6.01	3.84	6.46	6.15	5.80	5.39	4.91	3.23	9.78	10.07
Sept	5.12	6.30	6.64	6.78	6.73	6.49	4.73	5.88	6.06	6.06	5.93	5.66	4.05	4.90	4.71	4.47	4.17	3.87	2.63	8.74	8.74
Oct	3.43	4.88	5.41	5.78	5.98	6.01	5.08	4.40	4.71	4.88	4.94	4.86	3.85	3.30	3.18	3.04	2.88	2.67	1.87	7.08	7.17
Nov	2.20	3.66	4.24	4.70	5.02	5.20	4.81	3.20	3.57	3.84	4.00	4.05	3.49	2.13	2.09	2.02	1.94	1.82	1.33	5.64	5.94
Dec	1.79	3.20	3.78	4.24	4.58	4.79	4.56	2.76	3.13	3.42	3.60	3.68	3.27	1.73	1.68	1.65	1.57	1.48	1.08	5.00	5.37
kWh/m^2/yr	1866	2216	2299	2317	2273	2167	1514	2088	2124	2111	2046	1938	1362	1782	1704	1610	1499	1372	915	3027	3160

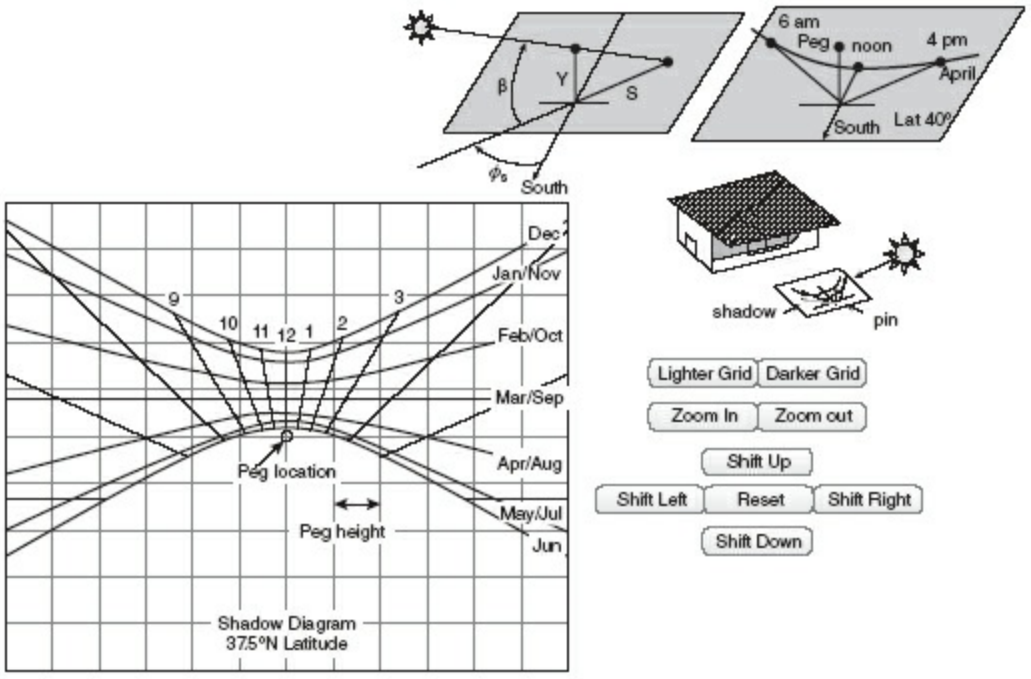
Daily Clear-Sky Insoation (kWh/m^2)																						Latitude 50° N
Azimuth:		South						SE, SW						East, West						Tracking	
Tilt:	0	20	30	40	50	60	90	20	30	40	50	60	90	20	30	40	50	60	90	1-Axis	2-Axis
Jan	1.60	2.96	3.52	3.98	4.32	4.54	4.37	2.54	2.91	3.19	3.38	3.47	3.14	1.56	1.53	1.51	1.45	1.39	1.04	4.86	5.12
Feb	2.93	4.49	5.08	5.52	5.81	5.92	5.24	3.98	4.34	4.60	4.72	4.71	3.91	2.84	2.78	2.68	2.58	2.42	1.78	6.97	7.06
Mar	4.66	6.05	6.50	6.76	6.82	6.69	5.17	5.58	5.85	5.94	5.91	5.72	4.32	4.48	4.34	4.18	3.95	3.70	2.62	8.88	8.88
Apr	6.54	7.40	7.53	7.43	7.13	6.65	4.18	7.09	7.11	7.00	6.70	6.28	4.21	6.26	6.00	5.68	5.34	4.92	3.34	10.17	10.45
May	7.69	8.08	7.93	7.56	6.98	6.27	3.26	7.86	7.68	7.36	6.85	6.26	3.81	7.31	6.93	6.50	6.00	5.44	3.53	10.21	11.00
Jun	8.03	8.22	7.97	7.50	6.82	6.03	2.90	8.04	7.78	7.38	6.80	6.14	3.58	7.60	7.18	6.69	6.14	5.53	3.51	9.98	11.02
July	7.62	7.98	7.82	7.45	6.87	6.16	3.19	7.76	7.58	7.25	6.75	6.15	3.73	7.23	6.86	6.42	5.93	5.36	3.47	9.96	10.76
Aug	6.40	7.21	7.32	7.22	6.92	6.45	4.04	6.91	6.92	6.79	6.49	6.07	4.05	6.12	5.86	5.54	5.19	4.77	3.22	9.69	9.98
Sept	4.56	5.84	6.25	6.47	6.51	6.37	4.90	5.41	5.64	5.71	5.66	5.46	4.09	4.37	4.23	4.06	3.82	3.57	2.50	8.36	8.36
Oct	2.78	4.22	4.76	5.17	5.43	5.54	4.90	3.75	4.08	4.31	4.43	4.42	3.66	2.69	2.63	2.53	2.44	2.28	1.66	6.45	6.53
Nov	1.54	2.81	3.33	3.76	4.08	4.27	4.11	2.41	2.75	3.02	3.19	3.27	2.96	1.50	1.46	1.44	1.38	1.32	0.98	4.56	4.79
Dec	1.17	2.37	2.87	3.29	3.61	3.83	3.80	2.00	2.33	2.60	2.79	2.90	2.72	1.15	1.14	1.13	1.09	1.06	0.80	4.00	4.29
kWh/m^2/yr	1692	2059	2157	2194	2169	2089	1520	1928	1978	1982	1937	1851	1343	1618	1552	1473	1380	1272	866	2863	2990

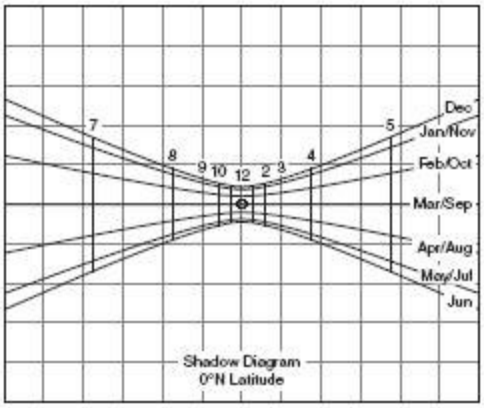
Daily Clear-Sky Insoation (kWh/m^2)														Latitude 55° N							
Azimuth:		South						SE, SW						East, West						Tracking	
Tilt:	0	20	30	40	50	60	90	20	30	40	50	60	90	20	30	40	50	60	90	1-Axis	2-Axis
Jan	0.99	2.11	2.58	2.98	3.29	3.51	3.52	1.77	2.08	2.34	2.53	2.64	2.52	0.98	0.99	0.98	0.97	0.95	0.74	3.76	3.96
Feb	2.26	3.75	4.34	4.81	5.14	5.31	4.91	3.28	3.66	3.94	4.12	4.17	3.62	2.21	2.19	2.16	2.10	2.01	1.54	6.21	6.29
Mar	4.05	5.51	6.02	6.36	6.51	6.47	5.27	5.04	5.35	5.51	5.56	5.45	4.30	3.92	3.81	3.71	3.56	3.36	2.46	8.43	8.43
Apr	6.11	7.13	7.35	7.35	7.15	6.76	4.56	6.77	6.88	6.84	6.62	6.28	4.42	5.86	5.65	5.39	5.10	4.75	3.32	10.03	10.31
May	7.41	7.98	7.94	7.67	7.18	6.53	3.70	7.70	7.60	7.35	6.93	6.40	4.05	7.03	6.68	6.29	5.84	5.33	3.53	10.16	10.95
Jun	7.80	8.19	8.05	7.67	7.09	6.35	3.37	7.95	7.77	7.42	6.93	6.32	3.84	7.38	6.98	6.52	6.01	5.44	3.52	9.95	10.99
July	7.34	7.88	7.83	7.55	7.07	6.42	3.62	7.61	7.50	7.25	6.82	6.29	3.97	6.97	6.62	6.22	5.77	5.26	3.47	9.90	10.70
Aug	5.98	6.94	7.13	7.13	6.92	6.53	4.39	6.60	6.68	6.63	6.41	6.07	4.24	5.73	5.51	5.25	4.95	4.60	3.19	9.54	9.83
Sept	3.96	5.31	5.77	6.06	6.19	6.14	4.97	4.86	5.14	5.28	5.30	5.18	4.05	3.82	3.71	3.60	3.44	3.23	2.34	7.89	7.89
Oct	2.12	3.47	4.00	4.42	4.72	4.88	4.51	3.04	3.38	3.64	3.79	3.83	3.32	2.07	2.04	2.01	1.94	1.85	1.40	5.63	5.70
Nov	0.94	1.96	2.39	2.75	3.04	3.23	3.24	1.64	1.93	2.16	2.34	2.44	2.33	0.92	0.93	0.92	0.91	0.88	0.68	3.45	3.63
Dec	0.60	1.42	1.78	2.09	2.33	2.51	2.58	1.17	1.41	1.62	1.77	1.87	1.85	0.59	0.59	0.59	0.59	0.57	0.44	2.60	2.79
kWh/m^2/yr	1511	1878	1984	2034	2026	1965	1477	1749	1808	1826	1799	1732	1293	1447	1393	1330	1255	1165	811	2664	2784

Daily Clear-Sky Insoation (kWh/m^2)														Latitude 60° N							
Azimuth:		South						SE, SW						East, West						Tracking	
Tilt:	0	20	30	40	50	60	90	20	30	40	50	60	90	20	30	40	50	60	90	1-Axis	2-Axis
Jan	0.45	1.15	1.46	1.72	1.93	2.09	2.18	0.94	1.15	1.32	1.46	1.55	1.56	0.45	0.45	0.46	0.46	0.45	0.36	2.22	2.33
Feb	1.59	2.91	3.46	3.91	4.24	4.45	4.29	2.50	2.87	3.15	3.34	3.43	3.12	1.58	1.58	1.58	1.55	1.52	1.20	5.14	5.21
Mar	3.40	4.90	5.45	5.84	6.07	6.12	5.24	4.42	4.77	5.00	5.11	5.08	4.19	3.32	3.27	3.20	3.13	2.97	2.27	7.86	7.86
Apr	5.62	6.78	7.08	7.18	7.08	6.78	4.86	6.39	6.57	6.61	6.48	6.22	4.58	5.41	5.25	5.06	4.81	4.54	3.28	9.84	10.12
May	7.06	7.82	7.87	7.70	7.31	6.73	4.14	7.48	7.45	7.28	6.94	6.47	4.30	6.69	6.38	6.03	5.64	5.20	3.52	10.06	10.85
Jun	7.51	8.09	8.04	7.77	7.29	6.60	3.80	7.80	7.67	7.40	6.99	6.44	4.09	7.10	6.71	6.30	5.85	5.33	3.51	9.87	10.91
July	7.00	7.72	7.76	7.58	7.19	6.61	4.05	7.40	7.36	7.17	6.83	6.36	4.20	6.64	6.32	5.97	5.58	5.13	3.46	9.80	10.60
Aug	5.51	6.59	6.87	6.95	6.84	6.54	4.67	6.22	6.37	6.40	6.25	5.99	4.38	5.29	5.12	4.93	4.68	4.40	3.15	9.34	9.62
Sept	3.32	4.69	5.19	5.54	5.74	5.77	4.90	4.26	4.57	4.76	4.85	4.80	3.92	3.23	3.18	3.09	3.01	2.85	2.14	7.31	7.31
Oct	1.46	2.62	3.11	3.50	3.79	3.97	3.83	2.26	2.58	2.82	2.99	3.07	2.78	1.44	1.43	1.43	1.39	1.35	1.05	4.52	4.57
Nov	0.41	1.02	1.29	1.52	1.70	1.84	1.91	0.83	1.02	1.17	1.29	1.37	1.37	0.41	0.41	0.41	0.41	0.40	0.31	1.94	2.04
Dec	0.17	0.53	0.69	0.83	0.95	1.04	1.11	0.42	0.53	0.63	0.71	0.76	0.79	0.17	0.18	0.18	0.18	0.18	0.14	1.07	1.15
kWh/m^2/yr	1327	1670	1774	1828	1830	1780	1366	1552	1612	1635	1620	1569	1195	1273	1228	1179	1119	1046	743	2404	2514

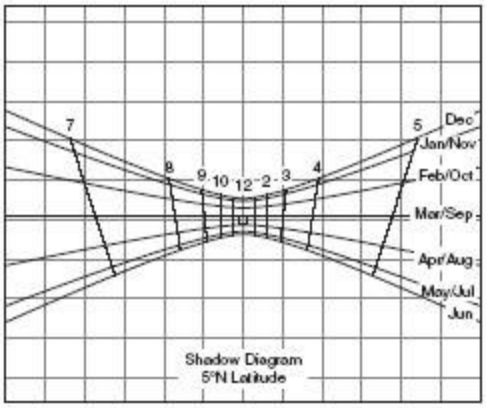
APPENDIX F

SHADOW DIAGRAMS

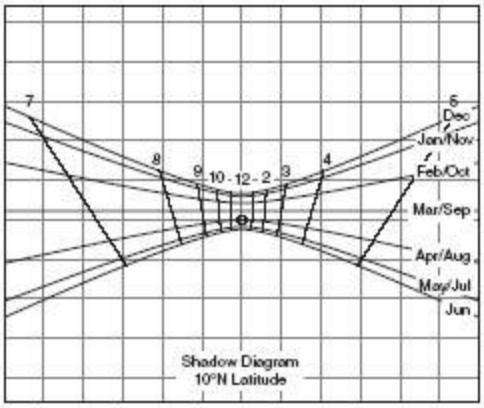




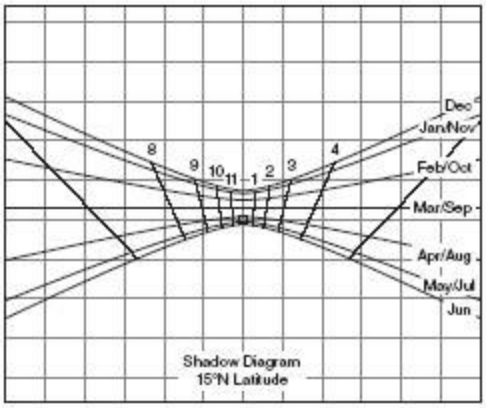
Shadow Diagram
0°N Latitude



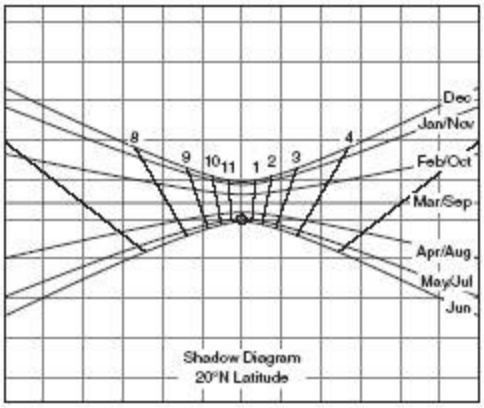
Shadow Diagram
5°N Latitude



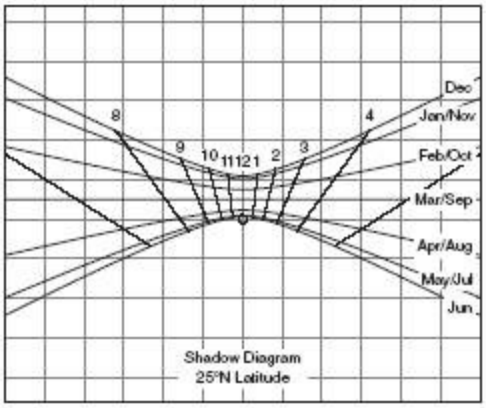
Shadow Diagram
10°N Latitude



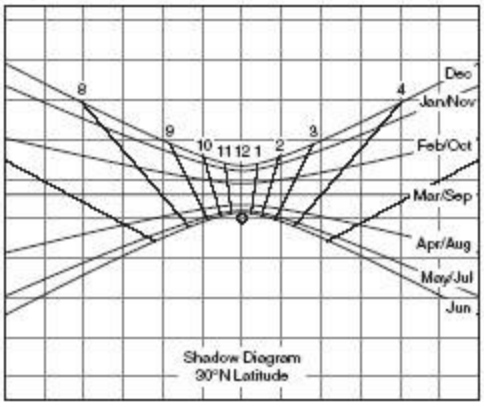
Shadow Diagram
15°N Latitude



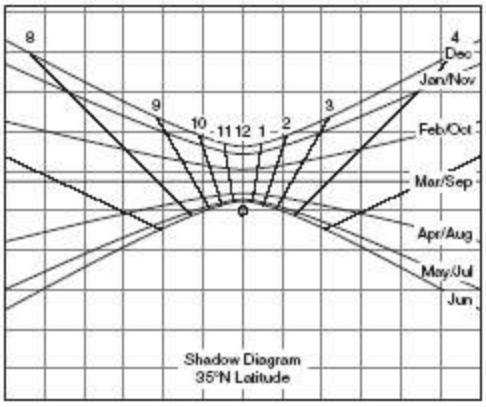
Shadow Diagram
20°N Latitude



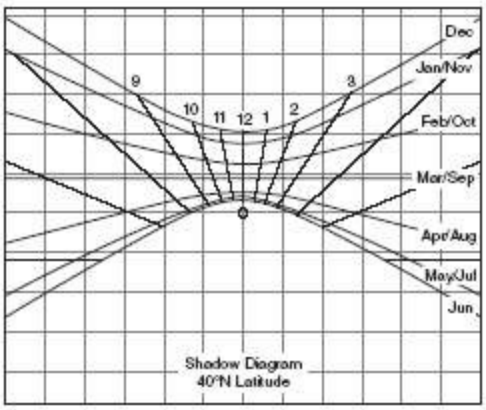
Shadow Diagram
25°N Latitude

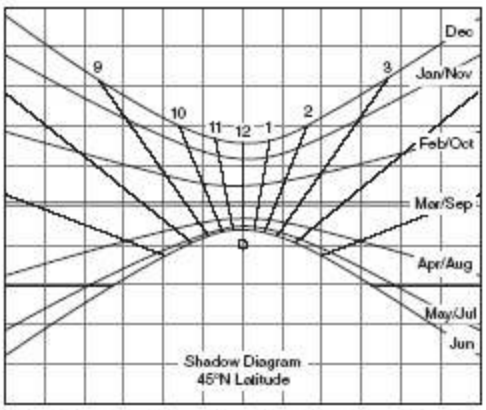


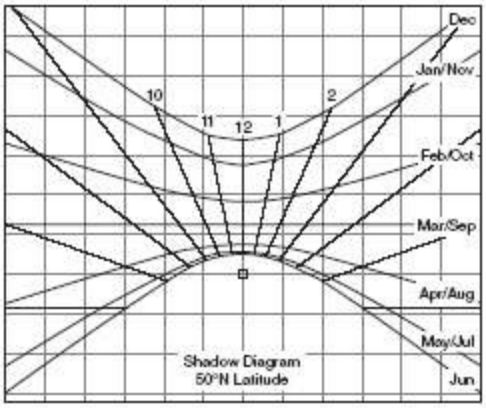
Shadow Diagram
30°N Latitude

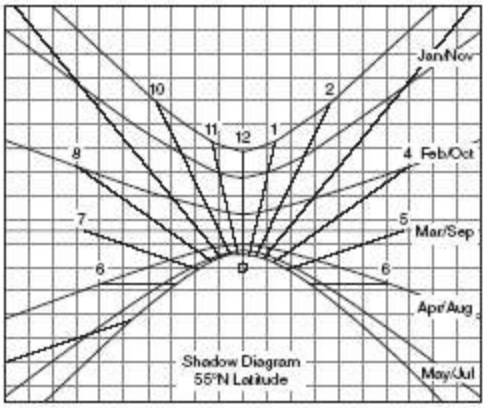


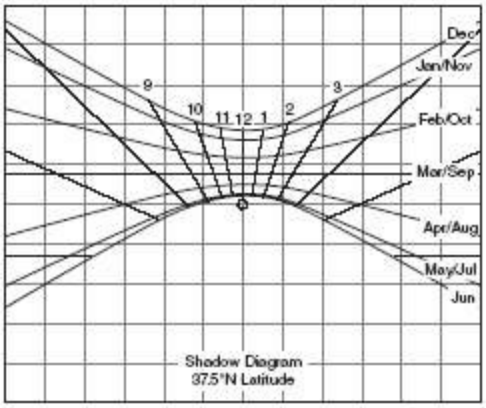
Shadow Diagram
35°N Latitude

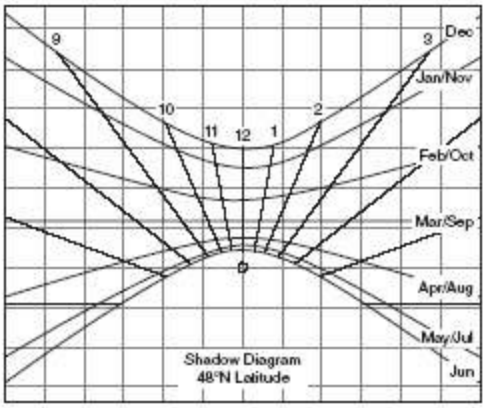

Dec
Jan/Nov
Feb/Oct
Mar/Sep
Apr/Aug
May/Jul
Jun
9
10
11
12
1
2
3
Shadow Diagram
40°N Latitude

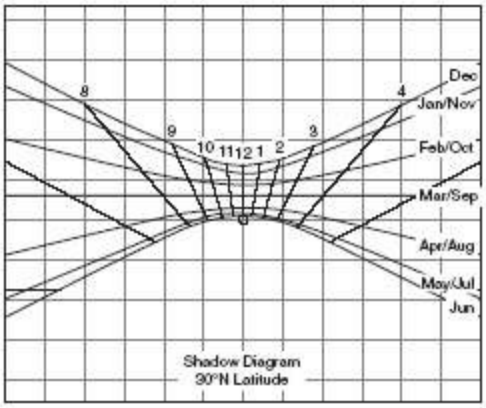

Dec
Jan/Nov
Feb/Oct
Mar/Sep
Apr/Aug
May/Jul
Jun
9
10
11
12
1
2
3
Shadow Diagram
45°N Latitude

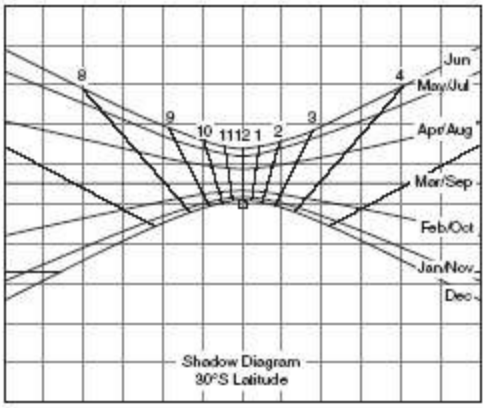

Dec
Jan/Nov
Feb/Oct
Mar/Sep
Apr/Aug
May/Jul
Jun
10
11
12
1
2
Shadow Diagram
50°N Latitude


Jan/Nov
Feb/Oct
Mar/Sep
Apr/Aug
May/Jul
10
11
12
1
2
9
7
6
4
5
6
Shadow Diagram
55°N Latitude


Dec
Jan/Nov
Feb/Oct
Mar/Sep
Apr/Aug
May/Jul
Jun
9
10
11
12
1
2
3
Shadow Diagram
37.5°N Latitude


Dec
Jan/Nov
Feb/Oct
Mar/Sep
Apr/Aug
May/Jul
Jun
9
10
11
12
1
2
3
Shadow Diagram
48°N Latitude


Dec
Jan/Nov
Feb/Oct
Mar/Sep
Apr/Aug
May/Jul
Jun
8
9
10
11
12
1
2
3
4
Shadow Diagram
30°N Latitude


Jun
May/Jul
Apr/Aug
Mar/Sep
Feb/Oct
Jan/Nov
Dec
8
9
10
11
12
1
2
3
4
Shadow Diagram
30°S Latitude

APPENDIX G

SOLAR INSOLATION TABLES BY CITY

	Fairbanks, AK						Latitude 64.82° N						
Tilt	Jan	Feb	Mar	Apr	May	Jun	July	Aug	Sept	Oct	Nov	Dec	Year
Lat − 15	0.7	2.2	4.5	5.6	5.7	5.7	5.4	4.5	3.4	1.9	1.0	0.2	3.4
Lat	0.7	2.4	4.7	5.6	5.3	5.2	4.9	4.2	3.4	2.0	1.1	0.3	3.3
Lat + 15	0.8	2.5	4.7	5.3	4.6	4.5	4.3	3.8	3.2	2.0	1.1	0.3	3.1
90	0.8	2.5	4.5	4.9	4.1	3.9	3.7	3.3	3.0	2.0	1.1	0.3	2.8
1-Axis (Lat)	0.8	2.7	5.8	7.7	8.0	8.0	7.4	5.8	4.4	2.3	1.2	0.3	4.5
Temp. (°C)	−18.7	−13.8	−4.6	5.0	15.2	21.2	22.4	19.1	12.7	0.0	−11.7	−16.8	2.5

	Montgomery, AL					Latitude 32.30°N							
Tilt	Jan	Feb	Mar	Apr	May	Jun	July	Aug	Sept	Oct	Nov	Dec	Year
Lat − 15	3.4	4.2	5.0	5.9	6.2	6.3	6.0	5.9	5.3	4.9	3.8	3.3	5.0
Lat	3.8	4.6	5.2	5.8	5.8	5.8	5.6	5.7	5.4	5.3	4.3	3.7	5.1
Lat + 15	4.0	4.7	5.1	5.4	5.2	5.1	4.9	5.2	5.2	5.4	4.5	4.0	4.9
90	3.5	3.7	3.4	2.9	2.3	2.1	2.2	2.6	3.2	4.0	3.8	3.5	3.1
1-Axis (Lat)	4.5	5.5	6.5	7.5	7.6	7.5	7.0	7.1	6.7	6.5	5.1	4.4	6.3
Temp. (°C)	13.5	16.0	20.3	24.7	28.3	31.9	32.8	32.4	30.6	25.7	20.4	15.7	24.3

South-facing, fixed or tracking; kWh/m^2/day. Average daily maximum temperature (°C).

	Phoenix, AZ						Latitude 33.43° N						
Tilt	Jan	Feb	Mar	Apr	May	Jun	July	Aug	Sept	Oct	Nov	Dec	Year
Lat − 15	4.4	5.4	6.4	7.5	8.0	8.1	7.5	7.3	6.8	6.0	4.9	4.2	6.4
Lat	5.1	6.0	6.7	7.4	7.5	7.3	6.9	7.1	7.0	6.5	5.6	4.9	6.5
Lat + 15	5.5	6.2	6.6	6.9	6.6	6.3	6.0	6.4	6.7	6.7	5.9	5.3	6.3
90	4.9	5.0	4.5	3.7	2.7	2.3	2.4	3.1	4.2	5.1	5.1	4.8	4.0
1-Axis (Lat)	6.2	7.5	8.7	10.3	10.7	10.8	9.6	9.6	9.3	8.4	6.8	5.8	8.6
Temp. (°C)	18.8	21.5	24.2	29.2	34.2	39.7	41.1	39.8	36.8	31.2	23.8	19.0	29.9

	Tucson, AZ						Latitude 32.12° N						
Tilt	Jan	Feb	Mar	Apr	May	Jun	July	Aug	Sept	Oct	Nov	Dec	Year
Lat − 15	4.6	5.5	6.4	7.5	7.8	7.8	6.9	6.6	6.6	6.1	5.0	4.3	6.3
Lat	5.4	6.2	6.7	7.3	7.3	7.1	6.4	6.6	6.8	6.6	5.8	5.1	6.5
Lat + 15	5.9	6.4	6.6	6.8	6.4	6.1	5.6	6.0	6.6	6.8	6.2	5.6	6.3
90	5.2	5.1	4.4	3.5	2.5	2.1	2.2	2.8	4.0	5.1	5.3	5.1	3.9
1-Axis (Lat)	6.7	7.8	9.0	10.4	10.7	10.6	8.8	9.1	9.1	8.6	7.3	6.2	8.7
Temp. (°C)	17.7	19.9	22.7	27.3	32.2	37.6	37.4	36.0	34.1	29.1	22.6	17.9	27.9

	Daggett, CA						Latitude 34.87° N						
Tilt	Jan	Feb	Mar	Apr	May	Jun	July	Aug	Sept	Oct	Nov	Dec	Year
Lat − 15	4.6	5.4	6.5	7.5	7.9	8.1	7.8	7.6	7.1	6.2	5.0	4.4	6.5
Lat	5.3	6.0	6.8	7.4	7.4	7.4	7.2	7.3	7.3	6.8	5.8	5.2	6.6
Lat + 15	5.7	6.2	6.7	6.8	6.5	6.3	6.2	6.6	7.0	6.9	6.2	5.6	6.4
90	5.2	5.1	4.7	3.8	2.8	2.4	2.5	3.3	4.4	5.4	5.4	5.2	4.2
1-Axis (Lat)	6.5	7.5	9.0	10.3	10.9	11.2	10.7	10.6	10.1	8.8	7.2	6.3	9.1
Temp. (°C)	15.9	18.9	21.4	25.6	30.8	36.6	39.9	38.6	34.3	28.2	20.8	15.8	27.2

	Fresno, CA						Latitude 36.77° N						
Tilt	Jan	Feb	Mar	Apr	May	Jun	July	Aug	Sept	Oct	Nov	Dec	Year
Lat − 15	2.8	4.1	5.5	6.8	7.6	7.8	7.9	7.5	6.8	5.5	3.6	2.5	5.7
Lat	3.1	4.4	5.7	6.7	7.1	7.2	7.3	7.3	6.9	6.0	4.1	2.8	5.7
Lat + 15	3.2	4.5	5.6	6.2	6.3	6.1	6.3	6.6	6.7	6.1	4.2	3.0	5.4
90	2.8	3.7	4.0	3.6	3.0	2.6	2.7	3.5	4.4	4.8	3.7	2.6	3.4
1-Axis (Lat)	3.4	5.2	7.2	8.9	10.1	10.5	10.8	10.3	9.2	7.4	4.7	3.1	7.6
Temp. (°C)	12.3	16.5	19.2	23.9	29.0	33.7	37.0	35.9	32.3	26.5	18.2	12.1	24.7

	Los Angeles, CA						Latitude 33.93° N						
Tilt	Jan	Feb	Mar	Apr	May	Jun	July	Aug	Sept	Oct	Nov	Dec	Year
Lat − 15	3.8	4.5	5.5	6.4	6.4	6.4	7.1	6.8	5.9	5.0	4.2	3.6	5.5
Lat	4.4	5.0	5.7	6.3	6.1	6.0	6.6	6.6	6.0	5.4	4.7	4.2	5.6
Lat + 15	4.7	5.1	5.6	5.9	5.4	5.2	5.8	6.0	5.7	5.5	5.0	4.5	5.4
90	4.1	4.1	3.8	3.3	2.5	2.2	2.4	3.0	3.6	4.2	4.3	4.1	3.5
1-Axis (Lat)	5.1	6.0	7.1	8.2	7.8	7.7	8.7	8.4	7.4	6.6	5.6	4.9	7.0
Temp. (°C)	18.7	18.8	18.6	19.7	20.6	22.2	24.1	24.8	24.8	23.6	21.3	18.8	21.3

South-facing, fixed or tracking; kWh/m^2/day. Average daily maximum temperature (°C).

	San Diego, CA						Latitude 32.73° N						
Tilt	Jan	Feb	Mar	Apr	May	Jun	July	Aug	Sept	Oct	Nov	Dec	Year
Lat − 15	4.1	4.8	5.6	6.4	6.3	6.3	6.8	6.7	6.0	5.3	4.5	3.9	5.6
Lat	4.7	5.3	5.8	6.3	5.9	5.8	6.4	6.5	6.1	5.7	5.1	4.6	5.7
Lat + 15	5.1	5.5	5.7	5.9	5.2	5.1	5.6	5.9	5.8	5.8	5.4	5.0	5.5
90	4.5	4.3	3.9	3.2	2.4	2.1	2.2	2.9	3.6	4.4	4.6	4.5	3.5
1-Axis (Lat)	5.7	6.5	7.4	8.2	7.5	7.4	8.4	8.4	7.7	7.1	6.2	5.5	7.2
Temp. (°C)	18.8	19.2	19.1	20.2	20.6	22.0	24.6	25.4	25.1	23.7	21.1	18.9	21.6

	Santa Maria, CA						Latitude 34.90° N						
Tilt	Jan	Feb	Mar	Apr	May	Jun	July	Aug	Sept	Oct	Nov	Dec	Year
Lat − 15	4.0	4.7	5.7	6.6	7.0	7.2	7.4	7.1	6.3	5.4	4.4	3.9	5.8
Lat	4.6	5.2	5.9	6.5	6.6	6.6	6.9	6.9	6.4	5.8	5.0	4.5	5.9
Lat + 15	4.9	5.4	5.8	6.0	5.8	5.7	6.0	6.2	6.2	6.0	5.3	4.9	5.7
90	4.4	4.4	4.0	3.4	2.7	2.3	2.5	3.2	3.9	4.6	4.6	4.5	3.7
1-Axis (Lat)	5.5	6.4	7.5	8.6	8.8	9.0	9.2	8.9	8.2	7.3	6.0	5.4	7.6
Temp. (°C)	17.7	18.2	17.9	19.4	19.9	21.7	22.9	23.4	23.8	23.3	20.4	17.9	20.6

	Alamosa, CO						Latitude 37.45° N						
Tilt	Jan	Feb	Mar	Apr	May	Jun	July	Aug	Sept	Oct	Nov	Dec	Year
Lat − 15	4.7	5.5	6.2	6.9	7.1	7.4	7.0	6.8	6.5	5.9	4.9	4.4	6.1
Lat	5.5	6.2	6.5	6.8	6.6	6.8	6.5	6.5	6.7	6.4	5.6	5.2	6.3
Lat + 15	6.0	6.5	6.4	6.3	5.8	5.7	5.6	5.9	6.4	6.5	6.0	5.7	6.1
90	5.7	5.6	4.7	3.7	2.9	2.5	2.6	3.2	4.3	5.2	5.5	5.5	4.3
1-Axis (Lat)	6.8	7.9	8.7	9.6	9.8	10.3	9.5	9.2	9.1	8.4	7.0	6.3	8.5
Temp. (°C)	0.7	4.4	9.3	14.8	20.0	25.4	27.8	26.2	22.6	16.9	8.6	1.9	14.9

	Boulder, CO						Latitude 40.02° N						
Tilt	Jan	Feb	Mar	Apr	May	Jun	July	Aug	Sept	Oct	Nov	Dec	Year
Lat − 15	3.8	4.6	5.4	6.1	6.2	6.6	6.6	6.3	5.9	5.1	4.0	3.5	5.4
Lat	4.4	5.1	5.6	6.0	5.9	6.1	6.1	6.1	6.0	5.6	4.6	4.2	5.5
Lat + 15	4.8	5.3	5.6	5.6	5.2	5.2	5.3	5.5	5.8	5.7	4.8	4.5	5.3
90	4.5	4.6	4.3	3.6	2.8	2.6	2.7	3.2	4.0	4.6	4.4	4.3	3.8
1-Axis (Lat)	5.2	6.2	7.2	8.0	8.1	8.8	8.7	8.4	7.9	7.1	5.5	4.9	7.2
Temp. (°C)	6.2	8.1	11.2	16.6	21.6	27.4	31.2	29.9	24.9	19.1	11.4	6.9	17.9

	Grand Junction, CO						Latitude 39.12° N						
Tilt	Jan	Feb	Mar	Apr	May	Jun	July	Aug	Sept	Oct	Nov	Dec	Year
Lat − 15	3.8	4.7	5.5	6.5	7.0	7.5	7.3	7.0	6.5	5.4	4.1	3.6	5.7
Lat	4.4	5.2	5.7	6.4	6.6	6.8	6.7	6.7	6.6	5.9	4.6	4.1	5.8
Lat + 15	4.7	5.4	5.6	6.0	5.8	5.8	5.8	6.1	6.4	6.0	4.9	4.5	5.6
90	4.4	4.7	4.2	3.7	3.0	2.7	2.8	3.5	4.4	4.8	4.4	4.3	3.9
1-Axis (Lat)	5.2	6.4	7.3	8.7	9.3	10.1	9.8	9.4	9.0	7.5	5.6	4.9	7.8
Temp. (°C)	1.9	7.4	13.1	18.8	24.4	30.9	34.2	32.5	27.3	19.8	10.8	3.7	18.8

South-facing, fixed or tracking; kWh/m^2/day. Average daily maximum temperature (°C).

	Daytona Beach, FL						Latitude 29.18° N						
Tilt	Jan	Feb	Mar	Apr	May	Jun	July	Aug	Sept	Oct	Nov	Dec	Year
Lat − 15	3.8	4.5	5.5	6.4	6.4	6.0	5.9	5.8	5.2	4.7	4.1	3.6	5.2
Lat	4.3	4.9	5.7	6.3	6.0	5.5	5.5	5.6	5.3	5.0	4.6	4.1	5.2
Lat + 15	4.6	5.1	5.6	5.9	5.4	4.8	4.9	5.1	5.1	5.1	4.8	4.4	5.1
90	3.9	3.8	3.6	2.9	2.1	1.8	1.9	2.4	3.0	3.6	4.0	3.9	3.1
1-Axis (Lat)	5.2	6.0	7.2	8.3	7.9	7.1	7.1	7.0	6.5	6.1	5.5	4.9	6.6
Temp. (°C)	20.0	20.8	23.8	26.7	29.2	31.1	32.1	31.7	30.4	27.5	24.2	21.3	26.6

	Miami, FL						Latitude 25.80° N						
Tilt	Jan	Feb	Mar	Apr	May	Jun	July	Aug	Sept	Oct	Nov	Dec	Year
Lat − 15	4.1	4.7	5.5	6.2	5.9	5.5	5.7	5.6	5.1	4.7	4.2	3.9	5.1
Lat	4.7	5.2	5.7	6.1	5.6	5.1	5.4	5.5	5.1	5.1	4.7	4.5	5.2
Lat + 15	5.0	5.4	5.6	5.7	5.0	4.5	4.8	5.0	4.9	5.1	4.9	4.9	5.1
90	4.1	3.9	3.4	2.6	1.9	1.6	1.7	2.1	2.7	3.5	3.9	4.1	3.0
1-Axis (Lat)	5.7	6.4	7.2	7.8	7.2	6.3	6.7	6.7	6.2	6.1	5.6	5.4	6.5
Temp. (°C)	24.0	24.7	26.2	28.0	29.6	30.9	31.7	31.7	31.0	29.2	26.9	24.8	28.2

	Tallahassee, FL						Latitude 30.38° N						
Tilt	Jan	Feb	Mar	Apr	May	Jun	July	Aug	Sept	Oct	Nov	Dec	Year
Lat − 15	3.6	4.3	5.2	6.1	6.2	6.0	5.7	5.6	5.3	5.0	4.1	3.4	5.0
Lat	4.0	4.7	5.4	6.0	5.9	5.6	5.4	5.4	5.3	5.4	4.6	4.0	5.1
Lat + 15	4.3	4.9	5.3	5.6	5.2	4.9	4.7	4.9	5.1	5.5	4.8	4.2	5.0
90	3.6	3.7	3.4	2.9	2.2	1.9	2.0	2.4	3.1	4.0	4.0	3.7	3.1
1-Axis (Lat)	4.8	5.8	6.7	7.8	7.7	7.1	6.8	6.8	6.6	6.7	5.5	4.6	6.4
Temp. (°C)	17.2	19.1	23.1	26.9	30.2	32.7	32.9	32.8	31.4	27.5	22.8	18.8	26.3

	Atlanta, GA						Latitude 33.65° N						
Tilt	Jan	Feb	Mar	Apr	May	Jun	July	Aug	Sept	Oct	Nov	Dec	Year
Lat − 15	3.4	4.2	5.1	6.0	6.2	6.3	6.1	5.9	5.3	4.9	3.8	3.2	5.0
Lat	3.8	4.6	5.3	5.8	5.8	5.8	5.7	5.7	5.4	5.2	4.2	3.7	5.1
Lat + 15	4.1	4.7	5.1	5.4	5.2	5.1	5.0	5.2	5.1	5.3	4.9	3.9	4.9
90	3.5	3.7	3.5	3.0	2.4	2.2	2.2	2.7	3.2	4.0	3.8	3.5	3.1
1-Axis (Lat)	4.5	5.5	6.6	7.6	7.7	7.6	7.3	7.2	6.7	6.4	5.0	4.3	6.4
Temp. (°C)	10.2	12.8	17.9	22.6	26.4	29.9	31.1	30.6	27.7	22.6	17.4	12.2	21.8

	Savannah, GA						Latitude 32.13° N						
Tilt	Jan	Feb	Mar	Apr	May	Jun	July	Aug	Sept	Oct	Nov	Dec	Year
Lat − 15	3.5	4.3	5.2	6.1	6.2	6.1	6.0	5.6	5.1	4.8	3.9	3.4	5.0
Lat	4.0	4.7	5.4	6.0	5.8	5.7	5.6	5.4	5.1	5.1	4.4	3.9	5.1
Lat + 15	4.3	4.8	5.3	5.6	5.2	4.9	4.9	5.0	4.9	5.2	4.6	4.2	4.9
90	3.7	3.8	3.6	3.0	2.3	2.0	2.1	2.5	3.0	3.8	3.9	3.7	3.1
1-Axis (Lat)	4.8	5.7	6.8	7.9	7.7	7.4	7.1	6.8	6.3	6.3	5.3	4.5	6.4
Temp. (°C)	15.4	16.9	21.2	25.3	28.9	31.6	32.8	32.1	29.6	25.3	21.1	16.8	24.7

South-facing, fixed or tracking; kWh/m^2/day. Average daily maximum temperature (°C).

	Honolulu, HI						Latitude 21.33° N						
Tilt	Jan	Feb	Mar	Apr	May	Jun	July	Aug	Sept	Oct	Nov	Dec	Year
Lat − 15	4.3	5.0	5.6	5.9	6.3	6.4	6.5	6.5	6.1	5.3	4.5	4.1	5.5
Lat	4.9	5.5	5.8	5.9	5.9	5.9	6.0	6.2	6.2	5.7	5.1	4.8	5.7
Lat + 15	5.3	5.8	5.8	5.5	5.3	5.1	5.3	5.7	6.0	5.8	5.4	5.2	5.5
90	4.2	4.0	3.2	2.2	1.5	1.4	1.4	1.8	2.8	3.7	4.1	4.3	2.9
1-Axis (Lat)	6.1	7.0	7.5	7.7	8.0	8.1	8.3	8.5	8.2	7.3	6.2	5.9	7.4
Temp. (°C)	26.7	26.9	27.6	28.2	29.3	30.3	30.8	31.5	31.4	30.5	28.9	27.3	29.1

	Boise, ID						Latitude 43.57° N						
Tilt	Jan	Feb	Mar	Apr	May	Jun	July	Aug	Sept	Oct	Nov	Dec	Year
Lat − 15	2.5	3.5	4.7	5.9	6.7	7.1	7.6	7.1	6.3	4.9	2.9	2.3	5.1
Lat	2.8	3.8	4.9	5.8	6.2	6.5	7.0	6.8	6.5	5.2	3.2	2.6	5.1
Lat + 15	2.9	3.9	4.8	5.4	5.5	5.5	6.0	6.2	6.2	5.3	3.3	2.8	4.8
90	2.7	3.4	3.7	3.6	3.2	3.0	3.3	3.8	4.6	4.5	3.0	2.6	3.5
1-Axis (Lat)	3.1	4.5	6.2	7.8	9.0	9.6	10.7	9.9	8.8	6.6	3.7	2.9	6.9
Temp. (°C)													

	Indianapolis, IN						Latitude 39.73° N						
Tilt	Jan	Feb	Mar	Apr	May	Jun	July	Aug	Sept	Oct	Nov	Dec	Year
Lat − 15	2.8	3.6	4.3	5.2	5.9	6.3	6.2	5.9	5.2	4.2	2.8	2.3	4.6
Lat	3.1	3.9	4.4	5.1	5.6	5.8	5.8	5.7	5.3	4.5	3.1	2.6	4.6
Lat + 15	3.3	4.0	4.3	4.7	4.9	5.0	5.1	5.2	5.1	4.5	3.2	2.7	4.3
90	3.0	3.5	3.2	3.0	2.7	2.6	2.7	3.1	3.5	3.6	2.8	2.5	3.0
1-Axis (Lat)	3.6	4.6	5.3	6.5	7.4	7.9	7.8	7.5	6.7	5.5	3.5	2.9	5.8
Temp. (°C)	0.9	3.5	10.5	17.4	23.2	28.2	29.7	28.7	25.3	18.8	11.1	3.6	16.7

	Dodge City, KS						Latitude 37.77° N						
Tilt	Jan	Feb	Mar	Apr	May	Jun	July	Aug	Sept	Oct	Nov	Dec	Year
Lat − 15	4.0	4.8	5.5	6.3	6.5	7.0	7.1	6.6	5.9	5.2	4.0	3.6	5.5
Lat	4.6	5.3	5.8	6.2	6.1	6.4	6.5	6.4	6.0	5.6	4.6	4.2	5.6
Lat + 15	5.0	5.5	5.7	5.8	5.4	5.5	5.7	5.8	5.7	5.7	4.8	4.6	5.4
90	4.6	4.6	4.2	3.5	2.7	2.5	2.7	3.2	3.9	4.5	4.3	4.3	3.7
1-Axis (Lat)	5.6	6.5	7.4	8.3	8.4	9.0	9.2	8.7	7.8	7.0	5.5	5.0	7.4
Temp. (°C)	5.3	8.5	13.7	20.0	24.6	30.6	33.9	32.6	27.4	21.5	12.9	6.6	19.8

	Lake Charles, LA						Latitude 30.12° N						
Tilt	Jan	Feb	Mar	Apr	May	Jun	July	Aug	Sept	Oct	Nov	Dec	Year
Lat − 15	3.3	4.1	4.9	5.5	6.0	6.2	5.9	5.7	5.4	5.0	3.9	3.2	4.9
Lat	3.7	4.5	5.1	5.4	5.6	5.7	5.5	5.6	5.4	5.4	4.3	3.7	5.0
Lat + 15	3.9	4.6	4.9	5.1	5.0	5.0	4.9	5.1	5.2	5.4	4.6	3.9	4.8
90	3.2	3.5	3.2	2.6	2.1	1.9	2.0	2.4	3.1	3.9	3.7	3.4	2.9
1-Axis (Lat)	4.3	5.4	6.2	6.9	7.2	7.5	7.0	7.0	6.8	6.6	5.2	4.3	6.2
Temp. (°C)	15.4	17.4	21.5	25.5	28.9	31.7	32.7	32.7	30.4	26.8	21.6	17.4	25.2

South-facing, fixed or tracking; kWh/m^2/day. Average daily maximum temperature (°C).

	Boston, MA						Latitude 42.37° N						
Tilt	Jan	Feb	Mar	Apr	May	Jun	July	Aug	Sept	Oct	Nov	Dec	Year
Lat − 15	3.0	3.8	4.6	5.2	5.7	6.0	6.0	5.7	5.0	4.1	2.8	2.5	4.5
Lat	3.4	4.2	4.7	5.0	5.3	5.5	5.6	5.5	5.1	4.3	3.1	2.9	4.6
Lat + 15	3.6	4.3	4.6	4.7	4.7	4.8	4.9	5.0	4.9	4.4	3.3	3.1	4.4
90	3.4	3.9	3.7	3.1	2.8	2.6	2.8	3.1	3.5	3.6	3.0	2.9	3.2
1-Axis (Lat)	3.9	5.0	5.9	6.5	7.1	7.4	7.5	7.1	6.4	5.2	3.6	3.2	5.7
Temp. (°C)	2.1	3.1	7.7	13.3	19.2	24.6	27.7	26.6	22.7	17.1	11.2	4.7	15.0

	Caribou, ME						Latitude 46.87° N						
Tilt	Jan	Feb	Mar	Apr	May	Jun	July	Aug	Sept	Oct	Nov	Dec	Year
Lat − 15	2.9	3.9	5.0	5.1	5.3	5.6	5.6	5.2	4.3	3.1	2.2	2.2	4.2
Lat	3.3	4.3	5.2	5.0	4.9	5.1	5.2	4.9	4.3	3.3	2.4	2.5	4.2
Lat + 15	3.5	4.5	5.2	4.7	4.4	4.5	4.6	4.5	4.1	3.3	2.5	2.7	4.0
90	3.4	4.2	4.6	3.7	2.9	2.8	2.9	3.0	3.2	2.8	2.3	2.7	3.2
1-Axis (Lat)	3.7	5.1	6.5	6.5	6.7	7.1	7.2	6.6	5.6	3.9	2.7	2.8	5.4
Temp. (°C)	−7.0	−5.0	1.3	8.2	16.5	22.2	24.7	23.1	17.8	11.1	3.1	−4.4	9.3

	Columbia, MO						Latitude 38.82° N						
Tilt	Jan	Feb	Mar	Apr	May	Jun	July	Aug	Sept	Oct	Nov	Dec	Year
Lat − 15	3.3	4.0	4.7	5.6	6.0	6.4	6.6	6.2	5.3	4.5	3.2	2.8	4.9
Lat	3.8	4.4	4.9	5.5	5.6	5.9	6.1	5.9	5.4	4.9	3.6	3.2	4.9
Lat + 15	4.0	4.5	4.8	5.1	5.0	5.1	5.3	5.4	5.1	4.9	3.8	3.4	4.7
90	3.7	3.9	3.5	3.2	2.7	2.5	2.7	3.1	3.5	3.9	3.3	3.2	3.3
1-Axis (Lat)	4.4	5.2	6.0	7.1	7.6	8.1	8.4	7.9	6.9	6.0	4.2	3.7	6.3
Temp. (°C)	2.6	5.2	11.8	18.7	23.4	28.2	31.4	30.4	26.0	19.8	12.0	4.6	17.8

	Glascow, MT						Latitude 48.22° N						
Tilt	Jan	Feb	Mar	Apr	May	Jun	July	Aug	Sept	Oct	Nov	Dec	Year
Lat − 15	2.7	3.7	4.8	5.4	5.8	6.4	6.8	6.4	5.2	4.1	2.8	2.3	4.7
Lat	3.1	4.1	5.0	5.3	5.5	5.9	6.3	6.1	5.3	4.3	3.1	2.6	4.7
Lat + 15	3.3	4.2	4.9	4.9	4.8	5.0	5.5	5.5	5.0	4.4	3.3	2.8	4.5
90	3.2	3.9	4.2	3.6	3.2	3.1	3.4	3.8	3.9	3.8	3.1	2.8	3.5
1-Axis (Lat)	3.5	4.8	6.3	7.2	7.7	8.6	9.4	8.7	6.9	5.3	3.6	3.0	6.3
Temp. (°C)	−6.7	−2.7	4.3	13.6	19.6	25.3	29.3	28.6	21.3	14.8	4.2	−3.9	12.3

	Cape Hatteras, NC						Latitude 35.27° N						
Tilt	Jan	Feb	Mar	Apr	May	Jun	July	Aug	Sept	Oct	Nov	Dec	Year
Lat − 15	3.3	4.1	5.1	6.0	6.1	6.2	6.1	5.8	5.3	4.6	3.7	3.2	5.0
Lat	3.8	4.5	5.2	5.9	5.8	5.7	5.7	5.6	5.4	4.9	4.2	3.6	5.0
Lat + 15	4.0	4.6	5.2	5.5	5.1	5.0	5.0	5.1	5.1	4.9	4.5	3.9	4.8
90	3.6	3.7	3.6	3.1	2.5	2.2	2.3	2.7	3.3	3.8	3.9	3.6	3.2
1-Axis (Lat)	4.5	5.4	6.6	7.7	7.6	7.6	7.4	7.2	6.7	6.0	5.0	4.3	6.3
Temp. (°C)	11.3	11.9	15.3	19.4	23.6	27.1	29.2	29.3	27.1	22.4	18.2	13.8	20.7

South-facing, fixed or tracking; kWh/m^2/day. Average daily maximum temperature (°C).

	Raleigh, NC						Latitude 35.87° N						
Tilt	Jan	Feb	Mar	Apr	May	Jun	July	Aug	Sept	Oct	Nov	Dec	Year
Lat − 15	3.4	4.1	5.0	5.8	6.0	6.2	6.0	5.7	5.1	4.6	3.7	3.1	4.9
Lat	3.8	4.5	5.2	5.7	5.7	5.7	5.6	5.5	5.2	4.9	4.1	3.6	5.0
Lat + 15	4.1	4.6	5.1	5.3	5.0	4.9	4.9	5.0	5.0	5.0	4.3	3.8	4.8
90	3.6	3.8	3.6	3.1	2.5	2.3	2.4	2.8	3.3	3.8	3.7	3.5	3.2
1-Axis (Lat)	4.5	5.5	6.5	7.5	7.4	7.5	7.2	6.9	6.4	6.0	4.9	4.2	6.2
Temp. (°C)	9.4	11.4	16.7	22.1	25.9	29.4	31.1	30.4	27.3	22.0	17.0	11.5	21.2

	Bismarck, ND						Latitude 46.77° N						
Tilt	Jan	Feb	Mar	Apr	May	Jun	July	Aug	Sept	Oct	Nov	Dec	Year
Lat − 15	3.1	4.0	5.0	5.6	6.1	6.5	6.8	6.4	5.3	4.2	2.9	2.6	4.9
Lat	3.5	4.4	5.2	5.5	5.7	5.9	6.3	6.1	5.4	4.5	3.2	3.0	4.9
Lat + 15	3.7	4.5	5.1	5.1	5.1	5.1	5.5	5.5	5.1	4.5	3.4	3.2	4.7
90	3.7	4.2	4.3	3.7	3.3	3.1	3.4	3.7	3.9	3.9	3.2	3.1	3.6
1-Axis (Lat)	4.0	5.2	6.4	7.3	8.0	8.6	9.2	8.5	7.0	5.5	3.7	3.3	6.4
Temp. (°C)	−18.7	−14.9	−7.9	−0.6	5.7	10.9	13.6	12.2	6.2	0.3	−7.9	−15.9	−1.4

	Omaha, NE						Latitude 41.37° N						
Tilt	Jan	Feb	Mar	Apr	May	Jun	July	Aug	Sept	Oct	Nov	Dec	Year
Lat − 15	3.3	4.0	4.7	5.5	6.0	6.5	6.5	6.1	5.2	4.4	3.2	2.7	4.9
Lat	3.8	4.4	4.9	5.3	5.6	6.0	6.0	5.8	5.3	4.7	3.5	3.2	4.9
Lat + 15	4.1	4.6	4.8	5.0	5.0	5.2	5.3	5.3	5.1	4.7	3.7	3.4	4.7
90	3.9	4.1	3.8	3.2	2.8	2.7	2.8	3.2	3.6	3.9	3.3	3.2	3.4
1-Axis (Lat)	4.5	5.3	6.1	7.0	7.5	8.3	8.3	7.8	6.7	5.7	4.1	3.6	6.3
Temp. (°C)	−1.3	1.7	8.7	16.9	22.7	28.0	30.3	28.9	23.8	17.8	8.7	0.5	15.6

	Albuquerque, NM						Latitude 35.05° N						
Tilt	Jan	Feb	Mar	Apr	May	Jun	July	Aug	Sept	Oct	Nov	Dec	Year
Lat − 15	4.6	5.4	6.3	7.3	7.7	7.8	7.4	7.2	6.6	5.9	4.8	4.3	6.3
Lat	5.3	6.0	6.5	7.2	7.2	7.1	6.9	6.9	6.8	6.5	5.5	5.0	6.4
Lat + 15	5.8	6.2	6.5	6.6	6.3	6.1	6.0	6.3	6.5	6.6	5.9	5.5	6.2
90	5.2	5.1	4.5	3.7	2.8	2.4	2.5	3.2	4.2	5.1	5.2	5.1	4.1
1-Axis (Lat)	6.5	7.5	8.6	9.9	10.3	10.4	9.5	9.3	9.0	8.3	6.8	6.1	8.5
Temp. (°C)	8.2	11.9	16.3	21.6	26.5	32.2	33.6	31.7	27.7	21.7	14.1	8.6	21.2

	Ely, NV						Latitude 39.28° N						
Tilt	Jan	Feb	Mar	Apr	May	Jun	July	Aug	Sept	Oct	Nov	Dec	Year
Lat − 15	4.0	4.7	5.5	6.3	6.6	7.2	7.2	6.9	6.6	5.5	4.1	3.6	5.7
Lat	4.6	5.2	5.7	6.2	6.2	6.6	6.6	6.6	6.7	6.0	4.7	4.3	5.8
Lat + 15	5.0	5.5	5.6	5.7	5.5	5.6	5.7	6.0	6.5	6.1	5.0	4.7	5.6
90	4.8	4.8	4.3	3.6	2.9	2.6	2.8	3.4	4.4	4.9	4.5	4.5	4.0
1-Axis (Lat)	5.5	6.5	7.4	8.4	8.9	9.9	9.9	9.5	9.2	7.7	5.6	5.1	7.8
Temp. (°C)	4.3	6.4	9.1	13.9	19.6	25.7	30.6	29.1	24.0	17.5	9.6	4.8	16.2

South-facing, fixed or tracking; kWh/m^2/day. Average daily maximum temperature (°C).

	LAS Vegas, NV						Latitude 36.08° N						
Tilt	Jan	Feb	Mar	Apr	May	Jun	July	Aug	Sept	Oct	Nov	Dec	Year
Lat − 15	4.4	5.3	6.4	7.5	7.8	8.1	7.7	7.5	7.1	6.1	4.8	4.2	6.4
Lat	5.1	5.9	6.7	7.4	7.3	7.4	7.1	7.2	7.2	6.6	5.5	4.9	6.5
Lat + 15	5.6	6.1	6.6	6.8	6.5	6.3	6.2	6.5	7.0	6.8	5.9	5.4	6.3
90	5.0	5.1	4.7	3.9	3.0	2.6	2.6	3.4	4.5	5.3	5.2	5.0	4.2
1-Axis (Lat)	6.2	7.3	8.8	10.2	10.6	11.1	10.4	10.3	9.8	8.6	6.7	5.9	8.8
Temp. (°C)	14.1	17.4	20.4	25.3	31.0	37.9	41.1	39.6	34.8	27.8	19.7	14.2	26.9

	Albany, NY						Latitude 42.75° N						
Tilt	Jan	Feb	Mar	Apr	May	Jun	July	Aug	Sept	Oct	Nov	Dec	Year
Lat − 15	2.7	3.6	4.4	5.0	5.5	5.8	6.0	5.5	4.8	3.7	2.4	2.1	4.3
Lat	3.0	3.9	4.5	4.9	5.1	5.4	5.5	5.2	4.8	3.9	2.6	2.4	4.3
Lat + 15	3.2	4.1	4.4	4.5	4.6	4.6	4.8	4.8	4.6	3.9	2.7	2.5	4.1
90	3.1	3.7	3.5	3.1	2.7	2.6	2.8	3.0	3.3	3.2	2.4	2.4	3.0
1-Axis (Lat)	3.5	4.6	5.5	6.3	6.8	7.2	7.5	6.9	6.0	4.6	2.9	2.6	5.4
Temp. (°C)	−11.7	−10.1	−4.2	1.7	7.4	12.6	15.3	14.3	9.7	3.7	−0.7	−7.7	2.6

	New York City, NY						Latitude 40.78° N						
Tilt	Jan	Feb	Mar	Apr	May	Jun	July	Aug	Sept	Oct	Nov	Dec	Year
Lat − 15	2.9	3.7	4.6	5.3	5.8	6.0	6.0	5.7	5.0	4.1	2.9	2.4	4.5
Lat	3.2	4.0	4.8	5.2	5.4	5.5	5.6	5.5	5.0	4.4	3.2	2.8	4.6
Lat + 15	3.4	4.1	4.6	4.8	4.8	4.8	4.9	5.0	4.8	4.4	3.3	3.0	4.3
90	3.2	3.6	3.5	3.1	2.7	2.6	2.7	3.0	3.4	3.6	3.0	2.7	3.1
1-Axis (Lat)	3.7	4.7	5.8	6.6	6.9	7.2	7.2	6.9	6.2	5.3	3.7	3.1	5.6
Temp. (°C)	3.1	4.6	10.0	16.2	22.1	26.7	29.6	28.7	24.6	18.5	12.2	5.8	16.8

	Burns, OR						Latitude 43.58° N						
Tilt	Jan	Feb	Mar	Apr	May	Jun	July	Aug	Sept	Oct	Nov	Dec	Year
Lat − 15	2.8	3.7	4.7	5.8	6.5	6.9	7.5	7.0	6.3	4.8	2.8	2.4	5.1
Lat	3.1	4.0	4.9	5.7	6.1	6.3	6.9	6.8	6.4	5.2	3.1	2.7	5.1
Lat + 15	3.3	4.1	4.8	5.3	5.4	5.4	6.0	6.1	6.1	5.2	3.3	2.9	4.8
90	3.2	3.7	3.8	3.6	3.2	3.0	3.3	3.8	4.5	4.4	2.9	2.8	3.5
1-Axis (Lat)	3.5	4.8	6.1	7.6	8.7	9.4	10.5	9.8	8.7	6.5	3.6	3.1	6.9
Temp. (°C)	0.9	4.2	8.7	13.6	18.7	23.6	29.5	28.5	23.1	16.6	7.3	1.8	14.7

	Eugene, OR						Latitude 44.12° N						
Tilt	Jan	Feb	Mar	Apr	May	Jun	July	Aug	Sept	Oct	Nov	Dec	Year
Lat − 15	1.8	2.6	3.8	4.8	5.6	6.0	6.7	6.3	5.4	3.6	1.9	1.4	4.2
Lat	2.0	2.7	3.8	4.7	5.3	5.5	6.2	6.0	5.5	3.8	2.1	1.6	4.1
Lat + 15	2.0	2.8	3.7	4.3	4.6	4.8	5.4	5.5	5.2	3.8	2.1	1.6	3.8
90	1.8	2.3	2.9	3.0	2.8	2.7	3.1	3.5	3.9	3.2	1.8	1.5	2.7
1-Axis (Lat)	2.1	3.1	4.6	5.9	7.1	7.8	9.1	8.4	7.1	4.6	2.3	1.7	5.3
Temp. (°C)	8.0	10.8	13.3	15.8	19.5	23.4	27.6	27.7	24.6	18.1	11.3	7.9	17.3

South-facing, fixed or tracking; kWh/m^2/day. Average daily maximum temperature (°C).

	Medford,OR						Latitude 42.37° N						
Tilt	Jan	Feb	Mar	Apr	May	Jun	July	Aug	Sept	Oct	Nov	Dec	Year
Lat − 15	2.1	3.2	4.5	5.7	6.6	7.1	7.7	7.2	6.3	4.5	2.3	1.7	4.9
Lat	2.3	3.5	4.6	5.6	6.2	6.5	7.1	6.9	6.4	4.8	2.4	1.9	4.9
Lat + 15	2.4	3.5	4.5	5.2	5.5	5.6	6.2	6.3	6.2	4.8	2.5	2.0	4.5
90	2.2	3.0	3.4	3.5	3.1	2.9	3.2	3.8	4.4	4.0	2.2	1.8	3.1
1-Axis (Lat)	2.6	4.0	5.6	7.3	8.7	9.5	10.7	9.9	8.6	5.9	2.7	2.0	6.5
Temp. (°C)	7.6	11.8	14.7	18.1	22.7	27.8	32.5	32.2	28.2	20.8	11.4	6.8	19.6

	Portland, OR						Latitude 45.60° N						
Tilt	Jan	Feb	Mar	Apr	May	Jun	July	Aug	Sept	Oct	Nov	Dec	Year
Lat − 15	1.7	2.5	3.6	4.6	5.4	5.8	6.3	5.9	5.1	3.4	1.9	1.4	4.0
Lat	1.9	2.6	3.7	4.5	5.0	5.3	5.8	5.6	5.1	3.6	2.1	1.6	3.9
Lat + 15	1.9	2.7	3.5	4.1	4.4	4.6	5.1	5.1	4.9	3.6	2.1	1.6	3.6
90	1.8	2.3	2.8	2.9	2.8	2.7	3.1	3.4	3.7	3.0	1.9	1.5	2.6
1-Axis (Lat)	2.0	3.0	4.3	5.5	6.5	7.2	8.1	7.5	6.5	4.3	2.2	1.7	4.9
Temp. (°C)	7.4	10.6	13.3	15.9	19.5	23.3	26.6	26.8	23.7	17.8	11.4	7.6	17.0

	Redmond, OR						Latitude 44.27° N						
Tilt	Jan	Feb	Mar	Apr	May	Jun	July	Aug	Sept	Oct	Nov	Dec	Year
Lat − 15	2.6	3.5	4.8	5.9	6.6	7.0	7.6	7.1	6.3	4.7	2.9	2.4	5.1
Lat	3.0	3.8	4.9	5.7	6.2	6.4	7.0	6.9	6.4	5.1	3.2	2.7	5.1
Lat + 15	3.1	3.9	4.8	5.3	5.5	5.5	6.1	6.2	6.1	5.1	3.3	2.9	4.8
90	2.9	3.4	3.8	3.7	3.3	3.1	3.4	3.9	4.5	4.3	3.0	2.7	3.5
1-Axis (Lat)	3.4	4.4	6.2	7.7	8.8	9.5	10.6	9.9	8.6	6.3	3.6	3.0	6.9
Temp. (°C)	5.1	8.4	11.5	15.1	19.6	24.8	29.6	28.8	24.1	17.9	9.4	5.4	16.7

	Pittsburgh, PA						Latitude 40.50° N						
Tilt	Jan	Feb	Mar	Apr	May	Jun	July	Aug	Sept	Oct	Nov	Dec	Year
Lat − 15	2.4	3.2	4.1	4.9	5.5	5.9	5.9	5.5	4.8	3.8	2.4	1.9	4.2
Lat	2.6	3.4	4.2	4.8	5.2	5.4	5.5	5.3	4.8	4.1	2.6	2.1	4.2
Lat + 15	2.7	3.5	4.1	4.4	4.6	4.7	4.8	4.8	4.6	4.1	2.7	2.2	3.9
90	2.5	3.0	3.1	2.9	2.6	2.5	2.6	2.9	3.2	3.3	2.3	2.0	2.7
1-Axis (Lat)	2.9	3.9	5.0	6.0	6.6	7.2	7.2	6.8	6.0	4.8	2.9	2.3	5.1
Temp. (°C)	0.9	2.7	9.4	15.7	21.4	26.1	28.1	27.1	23.5	16.9	10.2	3.7	15.5

	Guam, PI						Latitude 13.55° N						
Tilt	Jan	Feb	Mar	Apr	May	Jun	July	Aug	Sept	Oct	Nov	Dec	Year
Lat − 15	4.3	4.8	5.4	5.8	5.7	5.5	5.1	4.9	4.8	4.6	4.3	4.1	4.9
Lat	5.0	5.2	5.7	5.7	5.4	5.1	4.8	4.7	4.9	4.9	4.9	4.8	5.1
Lat + 15	5.3	5.4	5.6	5.3	4.9	4.5	4.3	4.4	4.7	4.9	5.1	5.1	5.0
90	3.8	3.3	2.6	1.7	1.5	1.5	1.5	1.5	2.0	2.8	3.5	3.8	2.5
1-Axis (Lat)	6.1	6.4	7.1	7.3	7.0	6.6	6.0	5.7	6.0	5.9	5.9	5.8	6.3
Temp. (°C)	28.7	28.6	29.2	29.9	30.4	30.5	30.2	29.9	30.1	29.9	29.6	29.0	29.7

South-facing, fixed or tracking; kWh/m^2/day. Average daily maximum temperature (°C).

	San Juan, PR						Latitude 18.43° N						
Tilt	Jan	Feb	Mar	Apr	May	Jun	July	Aug	Sept	Oct	Nov	Dec	Year
Lat − 15	4.5	5.1	5.8	6.1	5.7	6.0	6.0	6.0	5.6	5.0	4.5	4.1	5.4
Lat	5.1	5.6	6.1	6.1	5.4	5.5	5.6	5.8	5.7	5.4	5.1	4.8	5.5
Lat + 15	5.5	5.8	6.0	5.7	4.9	4.8	5.0	5.3	5.5	5.5	5.4	5.2	5.4
90	4.2	3.9	3.1	2.0	1.5	1.5	1.5	1.7	2.5	3.3	3.9	4.1	2.8
1-Axis (Lat)	6.3	6.9	7.7	7.8	6.9	7.2	7.3	7.4	7.1	6.7	6.1	5.7	6.9
Temp. (°C)	28.4	28.7	29.1	29.9	30.7	31.4	31.4	31.5	31.6	31.3	29.9	28.8	30.2

	Charleston, SC						Latitude 32.90° N						
Tilt	Jan	Feb	Mar	Apr	May	Jun	July	Aug	Sept	Oct	Nov	Dec	Year
Lat − 15	3.5	4.3	5.3	6.2	6.2	6.1	6.0	5.6	5.1	4.8	3.9	3.4	5.0
Lat	4.0	4.7	5.5	6.1	5.8	5.6	5.6	5.4	5.2	5.2	4.5	3.9	5.1
Lat + 15	4.3	4.9	5.4	5.7	5.2	4.9	4.9	4.9	5.0	5.2	4.7	4.2	4.9
90	3.7	3.9	3.6	3.1	2.4	2.1	2.2	2.5	3.1	3.9	4.0	3.8	3.2
1-Axis (Lat)	4.8	5.8	6.9	8.0	7.7	7.3	7.2	6.8	6.4	6.3	5.3	4.6	6.4
Temp. (°C)	14.3	16.1	20.3	24.3	28.2	30.9	32.3	31.7	29.4	25.1	20.8	16.4	24.2

	Nashville, TN						Latitude 36.12° N						
Tilt	Jan	Feb	Mar	Apr	May	Jun	July	Aug	Sept	Oct	Nov	Dec	Year
Lat − 15	3.1	3.9	4.7	5.7	6.0	6.4	6.2	5.9	5.2	4.6	3.3	2.8	4.8
Lat	3.5	4.2	4.8	5.6	5.7	5.9	5.8	5.7	5.3	4.9	3.6	3.1	4.9
Lat + 15	3.7	4.3	4.7	5.2	5.0	5.1	5.1	5.2	5.0	5.0	3.8	3.4	4.6
90	3.3	3.5	3.3	3.1	2.5	2.3	2.4	2.9	3.3	3.9	3.3	3.0	3.1
1-Axis (Lat)	4.1	5.0	6.0	7.2	7.5	7.8	7.5	7.3	6.5	6.0	4.2	3.6	6.1
Temp. (°C)	7.7	10.4	16.2	21.6	26.0	30.3	31.9	31.3	28.1	22.5	15.8	10.1	21.0

	Brownsville, TX						Latitude 25.90° N						
Tilt	Jan	Feb	Mar	Apr	May	Jun	July	Aug	Sept	Oct	Nov	Dec	Year
Lat − 15	3.2	4.0	4.8	5.4	5.7	6.2	6.4	6.0	5.4	4.9	3.9	3.1	4.9
Lat	3.6	4.3	5.0	5.3	5.4	5.7	5.9	5.8	5.5	5.3	4.4	3.6	5.0
Lat + 15	3.8	4.4	4.9	5.0	4.8	5.0	5.2	5.3	5.3	5.4	4.6	3.8	4.8
90	3.0	3.2	3.0	2.3	1.8	1.6	1.7	2.1	2.9	3.7	3.6	3.1	2.7
1-Axis (Lat)	4.2	5.2	6.1	6.6	6.8	7.6	7.9	7.7	7.0	6.6	5.3	4.1	6.3
Temp. (°C)	20.5	22.3	25.8	28.9	31.0	32.8	34.1	34.2	32.4	29.6	25.7	22.1	28.3

	El Paso, TX						Latitude 31.80° N						
Tilt	Jan	Feb	Mar	Apr	May	Jun	July	Aug	Sept	Oct	Nov	Dec	Year
Lat − 15	4.6	5.6	6.6	7.4	7.8	7.7	7.2	6.9	6.4	5.9	4.9	4.4	6.3
Lat	5.3	6.2	7.0	7.3	7.3	7.1	6.7	6.7	6.6	6.4	5.7	5.1	6.5
Lat + 15	5.8	6.5	6.9	6.8	6.4	6.0	5.8	6.1	6.3	6.6	6.1	5.6	6.2
90	5.1	5.2	4.6	3.5	2.5	2.1	2.2	2.8	3.8	4.9	5.2	5.1	3.9
1-Axis (Lat)	6.5	7.9	9.2	10.1	10.4	10.2	9.2	9.0	8.7	8.2	7.0	6.3	8.6
Temp. (°C)	13.4	16.8	21.1	25.9	30.6	35.8	35.6	34.2	30.6	25.8	19.1	14.2	25.3

South-facing, fixed or tracking; kWh/m^2/day. Average daily maximum temperature (°C).

	Fort Worth, TX						Latitude 32.83° N						
Tilt	Jan	Feb	Mar	Apr	May	Jun	July	Aug	Sept	Oct	Nov	Dec	Year
Lat − 15	3.8	4.5	5.3	5.9	6.2	6.7	6.9	6.5	5.7	5.0	4.0	3.5	5.3
Lat	4.3	4.9	5.5	5.7	5.8	6.2	6.4	6.3	5.8	5.4	4.5	4.1	5.4
Lat + 15	4.6	5.1	5.4	5.3	5.2	5.3	5.7	5.6	5.7	5.5	4.8	4.4	5.2
90	4.0	4.0	3.6	2.9	2.3	2.1	2.3	2.8	3.4	4.1	4.1	4.0	3.3
1-Axis (Lat)	5.1	6.0	6.9	7.4	7.7	8.4	8.8	8.5	7.4	6.7	5.5	4.9	6.9
Temp. (°C)	12.3	14.9	19.9	24.6	28.3	33.3	35.8	35.7	31.0	25.8	19.3	14.2	24.6

	Midland, TX						Latitude 31.93° N						
Tilt	Jan	Feb	Mar	Apr	May	Jun	July	Aug	Sept	Oct	Nov	Dec	Year
Lat − 15	4.3	5.1	6.2	6.8	7.0	7.1	6.9	6.6	5.9	5.5	4.6	4.1	5.8
Lat	5.0	5.7	6.5	6.7	6.5	6.5	6.4	6.4	6.0	6.0	5.3	4.8	6.0
Lat + 15	5.4	5.9	6.4	6.2	5.8	5.6	5.5	5.8	5.8	6.1	5.6	5.2	5.8
90	4.7	4.7	4.2	3.2	2.4	2.0	2.2	2.7	3.5	4.5	4.8	4.7	3.6
1-Axis (Lat)	6.1	7.1	8.4	9.0	9.0	9.1	9.0	8.7	7.8	7.6	6.5	5.8	7.9
Temp. (°C)	13.6	16.4	21.8	26.6	30.8	34.1	35.2	34.5	29.7	25.2	19.0	14.7	25.1

	San Antonio, TX						Latitude 29.53° N						
Tilt	Jan	Feb	Mar	Apr	May	Jun	July	Aug	Sept	Oct	Nov	Dec	Year
Lat − 15	3.7	4.5	5.2	5.7	5.9	6.5	6.7	6.6	5.8	5.1	4.1	3.5	5.3
Lat	4.3	4.9	5.4	5.6	5.6	6.0	6.3	6.3	5.9	5.5	4.6	4.1	5.4
Lat + 15	4.5	5.0	5.3	5.2	5.0	5.2	5.5	5.8	5.7	5.6	4.9	4.4	5.2
90	3.8	3.8	3.4	2.7	2.1	1.9	2.0	2.6	3.3	4.0	4.0	3.8	3.1
1-Axis (Lat)	5.1	6.0	6.8	7.0	7.1	7.9	8.4	8.3	7.5	6.9	5.6	4.8	6.8
Temp. (°C)	16.0	18.7	23.1	26.8	29.6	33.2	35.0	35.2	31.8	27.6	22.2	17.5	26.4

	Salt Lake City, UT						Latitude 40.77° N						
Tilt	Jan	Feb	Mar	Apr	May	Jun	July	Aug	Sept	Oct	Nov	Dec	Year
Lat − 15	2.9	4.0	5.0	5.9	6.6	7.2	7.3	7.0	6.3	5.0	3.3	2.5	5.2
Lat	3.2	4.3	5.2	5.8	6.2	6.6	6.7	6.7	6.4	5.4	3.7	2.9	5.3
Lat + 15	3.4	4.4	5.1	5.4	5.5	5.6	5.8	6.1	6.1	5.5	3.9	3.1	5.0
90	3.2	3.9	3.9	3.5	3.0	2.8	2.9	3.6	4.3	4.5	3.5	2.9	3.5
1-Axis (Lat)	3.7	5.1	6.5	7.7	8.7	9.6	9.8	9.4	8.6	6.8	4.3	3.3	7.0
Temp. (°C)	2.4	6.4	11.2	16.3	22.2	28.2	33.4	31.9	26.2	18.9	10.4	3.2	17.6

	Sterling, VA						Latitude 38.95° N						
Tilt	Jan	Feb	Mar	Apr	May	Jun	July	Aug	Sept	Oct	Nov	Dec	Year
Lat − 15	3.1	3.9	4.7	5.4	5.8	6.1	6.0	5.7	5.0	4.3	3.2	2.7	4.7
Lat	3.5	4.2	4.8	5.3	5.5	5.7	5.6	5.5	5.1	4.6	3.6	3.1	4.7
Lat + 15	3.7	4.3	4.7	4.9	4.8	4.9	4.9	5.0	4.9	4.6	3.7	3.3	4.5
90	3.4	3.7	3.5	3.1	2.6	2.5	2.6	2.9	3.3	3.7	3.3	3.0	3.1
1-Axis (Lat)	4.0	5.0	6.0	6.8	7.1	7.4	7.2	6.9	6.3	5.6	4.2	3.5	5.8
Temp. (°C)	4.5	6.6	12.6	18.4	23.5	28.2	30.6	29.7	26.1	19.8	13.7	7.2	18.4

South-facing, fixed or tracking; kWh/m^2/day. Average daily maximum temperature (°C).

	Burlington, VT						Latitude 44.47° N						
Tilt	Jan	Feb	Mar	Apr	May	Jun	July	Aug	Sept	Oct	Nov	Dec	Year
Lat − 15	2.6	3.6	4.5	5.0	5.6	5.9	6.1	5.6	4.7	3.5	2.2	1.9	4.3
Lat	2.9	3.9	4.7	4.9	5.3	5.4	5.6	5.3	4.8	3.7	2.4	2.1	4.3
Lat + 15	3.1	4.1	4.6	4.5	4.6	4.7	4.9	4.8	4.5	3.7	2.4	2.2	4.0
90	3.0	3.8	3.9	3.2	2.9	2.7	2.9	3.2	3.4	3.1	2.2	2.2	3.0
1-Axis (Lat)	3.3	4.6	5.8	6.3	7.0	7.4	7.7	7.1	6.0	4.4	2.6	2.4	5.4
Temp. (°C)	−3.8	−2.5	4.1	12.0	19.6	24.3	27.3	25.5	20.6	13.9	6.7	−0.9	12.2

	Seattle, WA						Latitude 47.45° N						
Tilt	Jan	Feb	Mar	Apr	May	Jun	July	Aug	Sept	Oct	Nov	Dec	Year
Lat − 15	1.5	2.3	3.5	4.6	5.4	5.7	6.1	5.6	4.7	3.0	1.7	1.3	3.8
Lat	1.6	2.5	3.6	4.4	5.1	5.2	5.7	5.4	4.7	3.2	1.8	1.4	3.7
Lat + 15	1.7	2.5	3.5	4.1	4.5	4.5	4.9	4.9	4.5	3.2	1.8	1.4	3.5
90	1.5	2.2	2.8	3.0	3.0	2.8	3.1	3.4	3.4	2.7	1.7	1.3	2.6
1-Axis (Lat)	1.8	2.8	4.3	5.5	6.7	7.0	7.9	7.2	5.9	3.7	2.0	1.5	4.7
Temp. (°C)	7.2	9.7	11.5	14.0	17.7	21.1	24.0	24.0	20.7	15.4	10.3	7.3	15.2

	Madison, WI						Latitude 43.13° N						
Tilt	Jan	Feb	Mar	Apr	May	Jun	July	Aug	Sept	Oct	Nov	Dec	Year
Lat − 15	3.0	3.9	4.5	5.1	5.8	6.2	6.2	5.7	4.8	3.8	2.5	2.3	4.5
Lat	3.4	4.3	4.7	5.0	5.5	5.7	5.8	5.5	4.8	4.0	2.8	2.6	4.5
Lat + 15	3.6	4.4	4.6	4.6	4.8	4.9	5.0	5.0	4.6	4.0	2.9	2.8	4.3
90	3.5	4.0	3.7	3.2	2.9	2.8	2.9	3.2	3.4	3.3	2.6	2.7	3.2
1-Axis (Lat)	3.9	5.0	5.8	6.4	7.3	7.8	7.7	7.1	6.0	4.8	3.2	3.0	5.7
Temp. (°C)	−4.0	−1.1	5.3	13.7	20.5	25.7	28.0	26.4	21.9	15.5	6.7	−1.2	13.1

	Lander, WY						Latitude 42.82° N						
Tilt	Jan	Feb	Mar	Apr	May	Jun	July	Aug	Sept	Oct	Nov	Dec	Year
Lat − 15	3.7	4.8	5.7	6.2	6.5	7.0	7.0	6.8	6.1	5.1	3.8	3.4	5.5
Lat	4.3	5.3	6.0	6.1	6.1	6.4	6.5	6.5	6.2	5.5	4.3	4.0	5.6
Lat + 15	4.6	5.6	5.9	5.7	5.4	5.5	5.6	5.9	6.0	5.6	4.6	4.3	5.4
90	4.5	5.1	4.8	4.0	3.2	2.9	3.1	3.6	4.3	4.7	4.3	4.3	4.1
1-Axis (Lat)a	5.0	6.5	7.6	8.3	8.5	9.4	9.5	9.3	8.3	6.9	5.2	4.6	7.4
Temp. (°C)	−0.4	2.8	7.6	13.2	18.9	25.2	30.1	28.8	22.4	15.4	5.8	0.1	14.2

[a] The 1-axis tracker is south-facing at a tilt angle equal to its latitude.

Source: NREL (1994). *Solar Radiation Data Manual for Flat-Plate and Concentrating Collectors.*

INDEX

active stall control
AC-to-DC Conversion
advanced metering infrastructure
air conditioning demand
air density
air mass ratio
alkaline fuel cells (AFCs)
Altamont Pass
altitude angle of the sun
AM 1.5 (air-mass ratio 1.5)
amorphous silicon
amortizing costs
anaerobic digestors
ancillary services
Andasol power station
anemometers
apparent power, s
appliance energy consumption
area required for wind farms
Atlantic wind connection
attenuators, wave power
automated distribution systems
automatic generation control (AGC)
average power in the wind
azimuth angle of the sun

back-to-back voltage-source converters
balancing authorities
band-gap energy
  and PV efficiency
  in tandem cells
Banki turbine
batteries
  flow batteries
  for grid storage
  i-v curves
  lead-acid batteries
  lithium batteries

sizing, off grid
sodium-sulfur batteries
for vehicles
Betz efficiency
binary cycle, geothermal
biomass for electricity
biomass gasification
bipolar junction transistors
blackbody radiation
blackouts
boost converters
Brayton cycle
buck-boost converters
buck converter
building energy efficiency
buoy data
bypass diodes and blocking diodes

cadmium telluride (CdTe)
california energy
AB 1890
conservation achievements
deregulation
summer load profile
California solar initiative
capacitive reactance
capacitors
idealized
for power factor correction
capacity factors
for concentrating solar power
for photovoltaics
for tidal power
for wind
capital recovery factor
carbon emissions
abatement curves
costs and emissions
emission rates
Carnot efficiency
cash flow analysis
central receiver systems

centrifugal pumps
choppers
CIS, copper indium selenium cells
clearness index
clear sky insolation
  beam radiation
  calculator
  equation summary
  hour-by-hour
  monthly
clock (civil) time
coal-fired steam power plants
cogeneration, *see* combined heat and power
combined-cycle power plants
combined heat and power
  biomass
  economics
  efficiency measures
  fuel cells
  microturbines
  reciprocating engines
combiner box
combustion turbines
complex algebra
concentrating solar power systems (CSP)
  central receiver systems
  comparison
  cooling systems
  dish-Stirling power systems
  levelized cost of energy
  linear fresnel reflectors
  parabolic trough systems
  resource assessment
  thermal energy storage
conversion factors (Appendix B)
converters
  AC - DC
  back-to-back
  DC - DC
copper indium gallium selenide (CIGS)
Coulomb efficiency
critical peak pricing

crystalline silicon PV technologies
cumulative distribution function
current gulps
cut-in and cut-out windspeed
Czochralski process

Darrieus rotor
day numbers
DC-to-AC Inverters
DC-to-DC converters
debt and equity financing
declination
delta-connected 3-phase systems
demand charges
demand dispatch
demand response (DR)
demand side management (DSM)
  cost-effectiveness measures
  disincentives by traditional ratemaking
  necessary conditions for success
depletion region
derating factors for PVs
deregulation
DFIG (doubly-fed induction generator)
diesel generators
diffuse horizontal irradiance (DHI)
diffuse radiation
diffuse sky factor
diodes
  blocking diodes
  bypass diodes
  ideal
  p-n junction diode
  in rectifiers
  Shokley equation
direct band-gap materials
direct methanol fuel cells (DMFCs)
direct normal irradiance (DNI)
dirt on PVs
discount rate
dish-Stirling power systems
dispatching

distributed generation
distribution systems
DNI direct-normal irradiance
doubly-fed induction generator
dry cooling
duty cycle of switches
dynamic head, water

economics of energy systems
  combined heat and power
  conventional generation
  diesel generators
  energy efficiency
  fuel cells
  geothermal systems
  photovoltaic grid systems
  photovoltaic stand-alone systems
  retail prices of electricity
  wave energy systems
  wind systems
eddy current losses
Edison, Thomas Alva
electricity milestones
electric rate adjustment mechanism (ERAM)
electric vehicles
  charging
  for frequency response
electrolysis of water
electromagnetism
electromotive force (mmf)
electron drift velocity
end-use energy
Energetech oscillating WEC system
energy chargeable to power
energy economics tutorial (Appendix A)
energy Policy Act of 1992 (EPAct)
energy service companies (ESCOs)
enhanced geothermal systems
Enron
enthalpy
entropy
environmental impacts of wind

equation of time
equinox
equivalent circuits for PV cells
exempt wholesale generators
experience curves
extraterrestrial solar flux

Faraday's law of magnetic induction
faults
federal energy regulatory commission (FERC)
feed-in tariffs
fill factor
financial calculations
  capital recovery factor
  cash flow analysis
  fixed charge rate
  flip financing of wind
  fossil fuel costs
  fuel escalation, npv
  initial rate of return
  internal rate of return (irr)
  levelized cost of energy (lcoe)
  MACRS
  marginal tax brackets
  net present value (NPV)
  rate structures
  tutorial (Appendix A)
  weighted average cost of capital
firm capacity
fixed charge rate
flip financing of wind
flow batteries
fossil fuel costs
Fourier series analysis
Francis turbine
frequency regulation
friction loss in pipes
fuel cells
  economics
  electrical characteristics
  thermodynamics
  types of fuel cells

fuel escalation, NPV
furling windspeed

gallium arsenide cells (GaAs)
gas turbines
general rate case
generators
  circuit models
  doubly fed induction (DFIG)
  fixed-speed synchronous
  induction
  permanent magnet, synchronous
  squirrel-cage induction
  variable-speed synchronous
geothermal power
GE wind turbine
Gibbs free energy
Gildea anniversary
global horizontal irradiance (GHI)
greenhouse gas abatement curves
grid-connected PV systems
grid stability
ground-cover ratio
ground-fault interrupter (GFI)

harmonics
  gulps of current
  overloaded neutrals
  total harmonic distortion
  transformers impacts
heat engines
heat rates
heat transfer fluid
heliostats
high heating value of fuel (HHV)
high-voltage DC (HVDC)
hill-climbing algorithm
hole-electron pairs
home area networks (HAN)
horizontal axis wind turbines
hot dry rock
hour angle
hourly clear-sky insolation tables

household electrical loads
hybrid cooling systems
hybrid electric vehicles
hybrid PV modules
hydraulic system curves
hydroelectric power
hydrogen production
hydrothermal regions
hysteresis losses

IEC 61400-1 Wind classifications
IGBT transistors
impedance
impulse turbines
incremental conductance algorithm
independent power producers (IPPs)
independent system operators (ISOs)
indirect band-gap materials
inductance
inductive reactance
inductors, idealized
initial rate of return
instant costs
Insull, Samuel
integrated gasification combined cycle (IGCC)
integrated resources planning (IRP)
internal combustion engines
internal rate of return (IRR)
inverters
  derating factors
  electronic systems
  microinverters
investor owned utilities (IOUs)
islanding of PV systems
isolation transformers
Ivanpah central receiver

Kaplan turbines
Kempton, Willett
Kirchhoff's current and voltage laws

La Rance River tidal plant
LCOE of concentrating solar power

LCOE of wind turbines
lead-acid batteries
learning rates
least-cost planning
Lenz's law
levelized cost of energy (LCOE)
levelizing factor for fuel escalation
light-emitting diodes (LEDs)
linear fresnel reflectors
linear power supplies
line voltages
lithium batteries
load duration curves
low heating value of fuel (LHV)

MACRS Modified accelerated cost recovery system
magnetic fields and flux density
magnetomotive force (mmf)
Makani windpower
marginal tax brackets
maximum power point
maximum power point trackers
McKinsey GHG abatement curves
merchant power plants
metallurgic-grade silicon
methane steam reforming
micro-hydro power
microinverters
microturbines
Milankovitch oscillations
mixed tides
modified accelerated cost recovery system (MACRS)
module mismatch factors
molten-carbonate fuel cells (MCFCs)
molten salt storage
monthly clear-sky insolation tables
MOSFET transistors
motor dc I-V curves
MPPT controllers
multicrystalline silicon
multijunction solar cells

national solar radiation data base (NSRDB)

natural gas combined cycle
neap tides
neighborhood area networks (NAN)
net metering
net present value (NPV)
nominal operating cell temperature (NOCT)
north american electric reliability corporation (NERC)
North American power grid
Northeast power blackout
nuclear power

off-grid PV systems
offshore cables
offshore wind farms
once-through cooling
one-line diagrams
onshore wind potential
optical depth
optimum band gap
overnight costs
overtopping devices, wave power

parabolic dish reflectors
parabolic trough systems
partial oxidation
peak-hours approach to PV performance
peak-hours for stand alone systems
peak-wave period
Pelamis wave converter
Pelton wheel
permanent magnet synchronous generator
phase voltages
phasor measurement units (PMUs)
phasors
phosphoric acid fuel cells (PAFCs)
photon energy
photovoltaic materials and characteristics
  equivalent circuits
  I-V curves
  materials
  module performance data
  parallel and series leakage resistance
  semiconductor physics

shading impacts
temperature impacts
photovoltaic systems
grid-connected system sizing
off-grid systems with battery storage
predicting performance
system economics, behind the meter
utility system economics
water pumping
physics of shading
pico-scale PV systems
Pierson-Moskowitz spectrum
piping friction loss
pitch-controlled wind turbines
Planck's constant
Planta Solar, Seville, Spain
plug-in hybrid electric vehicles (PHEVs)
p-n junctions
point absorbers, wave power
polycrystalline silicon
polymer electrolyte fuel cells (PEMs)
positive-displacement pumps
power conditioning unit
power electronics
power factor
power factor correction
power purchase agreements (PPAs)
power quality
power towers
power triangle
present value calculations
pressure-volume diagram
probability density functions (pdfs)
production tax credit (PTC)
proton exchange membrane (PEM) fuel cells
publicly owned utilities (POUs)
public utilities commissions
public utility holding company act (PUHCA)
public utility regulatory policies act (PURPA)
Puerto Erado linear fresnel system
pulse-width modulation
pumped storage hydro

pump hydraulic and I-V curves
PVUSA test conditions
PVWATTS
pyranometer
pyrheliometer
pyrolysis

qualifying facilities (QFs)
Q volt-amps reactive

ramp rates
Rankine cycle
rare earth elements
rated windspeed
rate structures
Rayleigh probability density function
reactance
reaction turbines
reactive power, Q
real power, W
real-time pricing
rear-contact solar cell
reciprocating engines
rectifiers
reflected radiation
regional transmission organizations (RTOs)
regulation services
renewable portfolio standards (RPS)
residential wiring
reverse saturation current
ripple
root mean square (rms)
Rosenfelds, the unit
rotating magnetic field
rotor spacing, wind farms
roughness classifications
Ruths accumulator

SCADA (Supervisory control and data acquisition)
screening curves
sea state scatter diagrams
second law of thermodynamics
self-regulating modules

semiconductor physics
shading analysis
  derate factors
  impacts on I-V curves
  losses in PV systems
  maximum power point trackers
  shadow diagrams
  sun path diagrams
shared savings program
Shockley diode equation
Shockley-Queisser efficiency limit
Siemens wind turbine
significant wave height
simple payback period
single-axis trackers
single-phase residential power
slip speed
smart grid
smart meters
sodium-sulfur batteries
solar advisor model
solar angles summary
solar declination
solar electric generating system (SEGS)
solar irradiation
  average monthly, by city
  clear sky calculations
  equations summary
  hourly clear sky tables
  measurements
  monthly clear sky tables
  NREL radiation data manual
solar one and solar two
solar spectrum
solar time and clock time
SolFocus concentrators
solid oxide fuel cells (SOFCs)
solstice
sonic anemometers
sonic detection and ranging (SODAR)
spring tides
squirrel-cage induction generator

stall-controlled wind turbines
standard test conditions (STCs) for PVs
standby power
state of charge
Stefan-Boltzmann law of radiation
stirling engines
storage battery, grid
storage, pumped hydro
storage thermal, grid
submarine cables
sun path diagrams
sunrise and sunset times
Sunshot Program
sunspots
supervisory control and data acquisition (SCADA)
Suzlon wind turbine
switch mode converters
synchronous generators
synchrophasors
syngas

Tacoma Narrows, WA tides
temperature derating of PVs
tandem solar cells
terminators, wave power
thermal energy storage for CSP
thermal stratification
Three Gorges dam
three-phase rectifiers
three-phase systems
  balanced, wye-connected
  delta-connected
  overloaded neutrals
  rectifiers
tidal in-stream energy conversion
tides, origin
tilt angle impact on PVs
time of delivery factors (TOD)
time of use (TOU) rate structure
tip-speed-ratio (TSR)
total harmonic distortion
tracking systems

transformers
  battle over AC vs DC
  harmonics
  idealized
  isolation
  magnetization losses
transmission systems
  AC - DC links
  FERC Order 888
  HVDC
  losses
  North American grid
  offshore wind and wave farms
  reactive power in T&D
  voltage loss
transparent conducting oxide (TCO)
turgo wheel
typical meterological year (TMY) data

utility rate structures
  commercial-building rates
  critical peak pricing
  feed-in tariffs
  ratemaking disincentives
  real-time pricing
  residential rate structures
  time of use (TOU)

vampire loads
vanadium redox batteries
variable-speed synchronous generators
vehicle to grid (V2G)
Vergnet wind turbine
Vestas wind turbine
voltage loss in transmission lines
volt-amps reactive (VARS)
volt/VAR optimization

water pumping PV systems
wave energy conversion systems
  predicting performance
  resource assessment
  scatter diagrams

technologies
Weibull probability density function
weighted average cost of capital
western electricity coordinating council
Westinghouse, George
wet cooling
wide area networks (WAN)
Wien's displacement rule
wind power systems
economics
environmental impacts
estimating capacity factors
generators
historical development
IEC classifications
offshore wind farms
rotors
turbine power curves
turbine specifications
with wave power
wind resources
air density
measuring the wind
onshore wind potential
probability density functions
windshear exponent
windspeed classifications
wire losses
wound-rotor induction generator
wound-rotor synchronous generator
wye connected 3-phase power